University of Alberta

MUDGASES GEOCHEMISTRY AND FACTORS CONTROLLING THEIR VARIABILITY

Volume 1

by

DANIELA VLAD

A thesis submitted to the Faculty of Graduate Studies and Research
in partial fulfillment of the requirements for the degree of

Doctor of Philosophy

Department of Earth and Atmospheric Sciences

Spring 2010
Edmonton, Alberta

Examining Committee

Karlis Muehlenbachs, Earth and Atmospheric Sciences

Murray Gingras, Earth and Atmospheric Sciences

Ben Rostron, Earth and Atmospheric Sciences

Sirish L. Shah, Chemical and Materials Engineering

Frank W. Schwartz, Ohio State University

For my daughter

ABSTRACT

Carbon isotope analyses of gases extracted from drilling muds while drilling in the Western Canada Sedimentary Basin (WCSB) can be used to create carbon isotopic depth profiles. These profiles provide essentially continuous data through the stratigraphic section, offering a unique opportunity to study the in-situ gases in various rock matrices. Carbon isotope and molecular compositions of Jurassic - Cretaceous mud gases have been examined from ten depth profiles in the undisturbed WCSB.

The isotopic profiles are surprisingly complex, showing numerous inflections and deviations towards increasing and decreasing carbon isotope values ($\delta^{13}C$) and wetness index with depth that suggest a correlation with the stratigraphic framework and can be explained in terms of the origin and alteration of the gases. However, the gas isotope geochemistry must be incorporated and applied in a multidisciplinary approach in order to gain a better understanding of causes of variations.

The discernible degree of correlativity of carbon isotope trends between the WCSB wells are likely to be related to the presence of major gas compartments bounded by stratigraphic surfaces, compartmentalization of the gas being strongly influenced by stratigraphic variations. The majority of these boundaries act as effective barriers to gas migration. Mudgas geochemistry is best employed in conjunction with petrophysical analysis and conversion into mineralogy, for defining details of transition zones and reservoir compartments.

Combined evidence suggests that isotopic variability of WCSB gases is only partly induced by source maturity at one single location. The main shifts of carbon isotope ratios are likely to be related to the physical properties of the rocks, differences

between organic precursors (type II versus type III kerogen), total organic carbon (TOC) content, gas biodegradation and mixing.

The present thesis demonstrates that the carbon isotopic mud gas profiles represent a powerful tool that provide information about the compartmentalization of the gas, the effectiveness of low permeability barriers, the origin, alteration and maturity of gases, and the regional gas dynamics. Mudgas geochemistry proves to be one part of the puzzle in the investigation of regional gas dynamics, and should be integrated with geological information, lithostratigraphic-, and sequence stratigraphic information, petrographic information and geophysical data.

ACKNOWLEDGEMENTS

The author expresses her gratitude to her supervisor, Dr . Karlis Muehlenbachs for his help, guidance, and understanding. Furthermore, Karlis Muehlenbachs is due a special note of appreciation for his exceptional character as a scientist and as a human being, and for introducing me into the fascinating and never-ending story of the stable carbon isotopes of natural gases. I am also grateful to Dr. Murray Gingras, and Dr. Ben Rostron for their helpful comments and suggestions.

Beyond moral support, this study was made possible by financial support from the Canadian Association of Petroleum Producers, which sustained the collection and analyses of the gas samples used in this study.

Dr. József Tóth is acknowledged for many helpful discussions and suggestions. Stephan Bachu and Karsten Michael from the Alberta Geological Survey, Edmonton are gratefully acknowledged for their help in understanding the hydrological regime in the Alberta basin.

I would like to thank Alton Brown, a brilliant and independent consultant, whose research interests include petroleum migration, carbonate sedimentology and diagenesis, basin analysis and gas geochemistry. Alton Brown has given me significant support, and generously shared his knowledge in discussions and comments.

I am also grateful to Prof. Dr. Michael Whiticar, from the University of Victoria, British Columbia for his valuable suggestions regarding information on the generation pathways of hydrocarbon gases and their migrational or post-genetic history. His strong confidence that the isotopic fractionation of natural gases during migration does not exist in nature made me explore as much as I could into this subject. Dr. John H. Doveton from Kansas Geological Survey kindly provided matrix algebra solution assistance while completion of the fifth Chapter of the thesis. My gratitude for his helpful comments! Observations from Barbara Tilley – University of Alberta, helped to greatly improve this manuscript during all these years.

Once again I would like to thank my husband Florin and my daughter Diana for their enormous patience all these years, for their love and support.

Finally, thanks God for giving me the power to keep going onto a slender *trail* of this ambiguous and somewhat unpredictable science, which is geology.

TABLE OF CONTENTS

Chapter **Page**

CHAPTER ONE: INTRODUCTION

1.1. Background …………………………………………………..…………..… 1

1.2. Mudgas isotope analysis while drilling ………………………………….……. 3

1.3. Reasoning and objectives of the study ……………………………….....… 5

1.4. Study areas ………………………………………………………..…….. 9

1.5. Previous work …………………………………………………..…. 14

1.6. Methods …………………………………………………………………. 16

1.6.1. Sequence stratigraphic framework ………………………………. 17

1.6.2. Geochemical interpretation of mudgas data …………………….. 19

1.6.3. Multilog quantification and mineralogical inversions ……..……. 20

1.6.4. Regional hydrogeology – gas geochemistry …………………….. 20

1.7. Sampling and measuring …………..…………………………..…..……. 21

1.7.1. Gas compositions ……………………………………...……. 23

1.7.2. Carbon stable isotope analysis of hydrocarbon gases ………..….. 23

1.7.3. Data reliability and uncertainties ……………………………..…. 24

CHAPTER TWO: SEQUENCE STRATIGRAPHIC FRAMEWORK

2.1. Introduction …………………………………………………...……. 26

2.1.1. Methods ………………………………………………………. 27

2.2. Sequence stratigraphic approach ………………………………………….. 30

2.3. Core descriptions and facies associations ………………………………… 32

2.4. Foothills region ……………………………………………………………… 75

2.4.1. Geological setting ……………………………………………….. 75

2.4.2. Geophysical log correlations …………………………………… 77

2.4.2.1. Fernie and Mannville groups ………………………….. 79

2.4.2.2. Colorado Group ……………………………………….. 80

2.4.2.3. Belly River Group and Lea Park Formation ………….. 85
2.4.2.4. Edmonton Group and Bearpaw Formation ……………. 93
2.4.2.5. Scollard and Paskapoo formations …………………….. 95
2.5. Lloydminster region …………………………………………………… 96
2.5.1. Geological setting …………………………………………… 96
2.5.2. Geophysical log correlations …………………………………… 99
2.5.2.1. Methodology ……………………………………….. 99
2.5.2.2. Results …………………………………………….… 102

CHAPTER THREE: CARBON ISOTOPE SIGNATURES OF MUDGASES AND THEIR STRATIGRAPHIC DETERMINATION
3.1. Introduction ……………………………………………………... 106
3.2. Foothills region ………………………………………..……... 109
3.2.1. Results …………………………………………………..... 109
3.2.2. Discussion ………………………………………………… 121
3.3. Lloydminster region ……………………………………………… 135
3.3.1. Results ……………………………………………………. 135
3.3.1.1. Regional sequence stratigraphic surfaces and their relatioship with the stable carbon isotopic trends ……... 136
3.3.1.2. Lithology influence ……………………………………152
3.4. Conclusions ……………………………………………………… 154

CHAPTER FOUR: MUDGASES DISTRIBUTION, ORIGIN AND MIGRATION
4.1. Introduction ……………………………………………………… 156
4.1.1. Controls on mudgas composition ……………………………… 157
4.1.2. Primary controls on stable carbon isotope ratio of mudgases ……………………………………………………. 160
4.1.3. Post-generation controls on stable carbon isotope ratio of mudgases ………………………………………………. 168
4.1.3.1. Migration and mixing ………………………………… 168
4.1.3.2. Bacterial alteration …………………………………….. 170

4.2. Results – Foothills region ………………………………………………….. 172
4.2.1. Compositional variations ……………………………………… 172
4.2.2. $\delta^{13}C$ variations ………………………………………………… 177
4.2.3. Combination of gas composition and stable carbon isotope ratios ……………………………………………….. 184
4.2.4. Discussion ………………………………………………….. 199
4.3. Results – Lloydminster region …………………………………….. 204
4.3.1. Compositional variations ……………………………………… 204
4.3.2. $\delta^{13}C$ variations …………………………………………………. 207
4.3.3. Combination of gas composition and stable carbon isotope ratios ……………………………………………….. 209
4.3.4. Discussion ………………………………………………….. 228

CHAPTER FIVE: FORMATION COMPARTMENTALIZATION USING ISOTOPIC FINGERPRINTS OF MUDGASES AND MULTILOG QUANTIFICATION

5.1. Introduction ………………………………………………………… 235
5.2. Methodology ……………………………………………………….. 236
5.2.1. Examination of inflections in the multi-component geochemical depth profiles ……………………………………. 236
5.2.2. Matrix algebra compositional log analysis …………………….. 237
5.2.2.1. Mineral identification through crossplots ……………. 237
5.2.2.2. Matrix algebra compositional log analysis - calculations …………………..………… 241
5.2.3. X-Ray diffractometry analysis (XRD) ………………………... 249
5.3. Results ……………………………………………………………… 254
5.3.1. Foothills region ………………………………………………… 256
5.3.2. Lloydminster region …………………………………………… 261
5.4. Well logs – qualitative uses in mudgas geochemistry …………………... 270
5.5. Discussion ………………………………………………………… 272

CHAPTER SIX: HYDRODYNAMICS, FLOW SYSTEMS AND GAS MIGRATION PATHWAYS

6.1. Introduction ………………………………………………………………… 275

6.2. Foothills region ……………………………………………………………. 277

6.2.1. Flow of formation waters ……………………………………… 277

6.2.2. Gas migration mechanisms and pathways in the Foothills region ……………………………………….. 279

6.3. Lloydminster region ………………………………………………………. 294

6.3.1. Flow of formation waters ……………………………………… 294

6.3.2. Gas migration mechanisms and pathways in the Lloydminster region …………………………………….. 295

6.4. Discussion ………………………………………………………………. 306

6.4.1. Foothills region ………………………………………………… 306

6.4.2. Lloydminster region …………………………………………… 309

CHAPTER SEVEN: THE SCV SOURCE DETECTION

7.1. Introduction ……………………………………………………………… 312

7.2. Surface gas migration and the application of carbon isotopic mud logs for remediation leaking wells ……………………………………...… 312

7.2.1. The SCV source detection in the Foothills area ……………….. 313

7.2.2. The SCV source detection in the Lloydminster area ……….…. 324

7.3. Environmental implications …………………………………………….. 344

CHAPTER EIGHT: SUMMARY AND RELATIONSHIPS BETWEEN FOOTHILLS AND HEAVY OIL STUDY AREAS

8.1. Stable isotopes results and discussion…………………………………… 361

8.1.1. δ ^{13}C of Methane ……………………………………………….. 362

8.1.1.1. Regional variations …………………………………...… 366

8.1.1.2. Mixing of thermogenic and bacteriogenic methane ….. 368

8.1.2. δ ^{13}C of C2+ hydrocarbons …………………………………...… 369

8.1.2.1. Maturity trends versus source effects versus biodegradation ………………………………………………...…. 372
8.1.2.2. Carbon isotope fractionation ……………………..…..….. 382
8.1.2.3. Mixing of thermogenic and bacteriogenic ethane …..… 384
8.1.3. Regional migration vs. indigenous sources ……………………. 386
8.2. Isotopic complexity: insights from the stratigraphic framework …..…….. 390
8.2.1. Downhole variations …………………………………………… 391
8.2.2. Isotopic shifts and stratigraphic variations ………………..…….393
8.3. Conclusions ……………………………………………………………. 397

CHAPTER NINE: CONCLUSIONS
9.1. Conclusions …………………………………………………………… 401
9.2. Future work …………………………………………………………… 412

BIBLIOGRAPHY ………………………………………………………..……. 414

ADDENDUM A
Diffractograms for nine shale samples taken from the Shell Paradise 10-25-047-3W4 core (Figures 5-9 to 5-21)……………….……………..….………… 435

*****

APPENDICES
Appendix A: Photographs of cores (Plates 1-122) and their log signatures
- Figures A-1 to A-40 ………………………………………………....… 449
- Plates (1-122) ...…………………………………………………….…….. 489

Appendix B: Well log cross-sections and Composite diagrams ……………... 735
- Appendix I (I-1 to I-5): Foothills region – well log cross-sections …. 735
- Appendix II (II-1 to II-8): Lloydminster region – well log cross-sections ……………………………………………………………. 740
- Appendix III (III-1 to III-7): Composite diagrams: mudlogs–compositional profiles ……………………………………..…….. 748

LIST OF TABLES

Table **Page**

2-1 Sedimentary facies of the Cretaceous section (Mannville Gp., Joli Fou, Viking, Cardium, Lea Park, Belly River formations) ………… 33

***

3-1 The average carbon isotope ratios for the Ardley coal seam ………….. 114

3-2 Carbon isotope signatures of key stratigraphic surfaces and depositional facies within the foreland basin fill of the west-central Alberta. Note that the isotope trends in the section are described from top to bottom ………………………………………………………. 132

3-3 Carbon isotope signature along Mannville/Colorado boundary in the Lloydminster region. Transitions are from Colorado to Mannville …….. 137

3-4 Carbon isotope signature along regional sequence stratigraphic surfaces for Husky C3-30-47-4W4 profile. The transition is recorded downward ………………………………………………………….… 138

3-5 Carbon isotope signature along regional sequence stratigraphic surfaces for Husky A9-15-51-23W3 profile. The transition is recorded downward …………………………………………………………..… 139

3-6 Carbon isotope signature along regional sequence stratigraphic surfaces for Petrovera 10-17-47-27W3 profile. The transition is recorded downward ….………………………………………………………… 140

3-7 Carbon isotope signature along regional sequence stratigraphic surfaces for Lindbergh 13-9-56-6W4 profile. The transition is recorded downward ………………………………………………………………. 141

3-8 Carbon isotope signature along regional sequence stratigraphic surfaces for Petrovera 1D-25-55-5W4 profile. The transition is recorded downward ………………………………………………………...….. 142

***

4-1 Wetness index exceeding 10 %, in descending order – Foothills region ………………………………………………………… 173

4-2 Ranges per formation for average isotopic composition for mudgases collected from the three locations of the carbon isotope mud gas depth profiles – Foothills region ……………………………………………….….. 177

LIST OF FIGURES

Figure **Page**

1-1 Carbon isotopic mud gas depth profile ………………………………….. 4

1-2 Carbon isotopic composition of gases from three mudlogs in west-central Alberta. Note: the isotope profiles for butane are not displayed in this figure for simplicity reasons …………………………………………..…. 7

1-3 Sketch map with study areas locations in west-central Alberta and Lloydminster region …………………………………………………….. 10

1-4 Locations of the carbon isotope mud gas depth profiles from the Foothills region, west-central Alberta …………………………………………..…. 11

1-5 Locations of the carbon isotope mud gas depth profiles from the Heavy oil region, east-central Alberta and west-central Saskatchewan ………..…. 12

1-6 Data availability map, showing the location of the ten carbon isotope depth profiles, the well log cross-section locations used to build the sequence stratigraphic framework, and the control core data represented by yellow stars …………………………………………………………… 13

1-7 Sketch diagram showing the integrated methodology applicable throughout the present study ……………………………………..………………. 17

1-8 Schematic geological cross-section illustrating the simplified sequence stratigraphic framework within the study areas, showing the main depositional environments, and key stratigraphic boundaries …................... 18

1-9 Principle of mud circulation during drilling and sampling. Gas samples are collected with gas 'bags' or bottles at the degassing line in the mudlogging unit ………………………………………………………… 22

***

2-1 Legend of symbols used in lithologs. ………………………………….….. 36

2-2 Litholog for the 06-04-42-4W5 core, annotated with main contacts (discussed in text) and facies interpretation. Legend for the litholog is given in Figure 2-1 37

2-3 Litholog for the 02/06-09-46-9W5 core, annotated with main contacts (discussed in text) and facies interpretation. Legend for the litholog is given in Figure 2-1 38

2-4 Litholog for the 08-02-43-05W5 core, annotated with main contacts (discussed in text) and facies interpretation. Legend for the litholog is given in Figure 2-1 39

2-5 Litholog for the 09-10-44-09W5 core, annotated with main contacts (discussed in text) and facies interpretation. Legend for the litholog is given in Figure 2-1. 40

2-6 Litholog for the 10-04-49-11W5 core, annotated with main contacts (discussed in text) and facies interpretation. Legend for the litholog is given in Figure 2-1. 41

2-7 Litholog for the 14-28-42-05W5 core, annotated with main contacts (discussed in text) and facies interpretation. Legend for the litholog is given in Figure 2-1. 42

2-8 Litholog for the 16-11-045-07W5 core, annotated with main contacts (discussed in text) and facies interpretation. Legend for the litholog is given in Figure 2-1. 43

2-9 Litholog for the 08-25-042-05W5 core, annotated with main contacts (discussed in text) and facies interpretation. Legend for the litholog is given in Figure 2-1. 44

2-10 Litholog for the 02-33-47-07W5 core, annotated with main contacts (discussed in text) and facies interpretation. Legend for the litholog is given in Figure 2-1. 45

2-11 Litholog for the 06-12-048-11W5 core, annotated with main contacts (discussed in text) and facies interpretation. Legend for the litholog is given in Figure 2-1. 46

2-12 Litholog for the 08-14-042-06W5 core, annotated with main contacts (discussed in text) and facies interpretation. Legend for the litholog is given in Figure 2-1. …………………………………………..………… 47

2-13 Litholog for the 06-26-048-11W5 core, annotated with main contacts (discussed in text) and facies interpretation. Legend for the litholog is given in Figure 2-1. ……………………………………………..……… 48

2-14 Litholog for the 06-33-048-11W5 core, annotated with main contacts (discussed in text) and facies interpretation. Legend for the litholog is given in Figure 2-1. ……………………………………………..……… 49

2-15 Litholog for the 09-32-043-07W5 core, annotated with main contacts (discussed in text) and facies interpretation. Legend for the litholog is given in Figure 2-1. ……………………………………………..……… 50

2-16 Litholog for the 10-11-43-09W5 core, annotated with main contacts (discussed in text) and facies interpretation. Legend for the litholog is given in Figure 2-1. ………………………………………………..…… 51

2-17 Litholog for the 10-14-044-09W5 core, annotated with main contacts (discussed in text) and facies interpretation. Legend for the litholog is given in Figure 2-1. …………………………………………..………… 52

2-18 Litholog for the 10-16-042-09W5 core, annotated with main contacts (discussed in text) and facies interpretation. Legend for the litholog is given in Figure 2-1. …………………………………………..………… 53

2-19 Litholog for the 10-23-043-09W5 core, annotated with main contacts (discussed in text) and facies interpretation. Legend for the litholog is given in Figure 2-1. ………………………………………..…………….. 54

2-20 Litholog for the 10-26-045-09W5 core, annotated with main contacts (discussed in text) and facies interpretation. Legend for the litholog is given in Figure 2-1. ………………………………………………..…….. 55

2-21 Litholog for the 11-30-045-09W5 core, annotated with main contacts (discussed in text) and facies interpretation. Legend for the litholog is given in Figure 2-1. …………………………………………………..…. 56

2-22 Litholog for the 12-03-042-09W5 core, annotated with main contacts (discussed in text) and facies interpretation. Legend for the litholog is given in Figure 2-1. ……………………………………………………..….. 57

2-23 Litholog for the 02/14-01-042-07W5 core, annotated with main contacts (discussed in text) and facies interpretation. Legend for the litholog is given in Figure 2-1. …………………………………………………..…… 58

2-24 Litholog for the 14-06-047-09W5 core, annotated with main contacts (discussed in text) and facies interpretation. Legend for the litholog is given in Figure 2-1. …………………………………………………..…… 59

2-25 Litholog for the 16-16-047-10W5 core, annotated with main contacts (discussed in text) and facies interpretation. Legend for the litholog is given in Figure 2-1. ………………………………………………..……… 60

2-26 Litholog for the 06-22-042-09W5 core, annotated with main contacts (discusse d in text) and facies interpretation. Legend for the litholog is given in Figure 2-1 …………………………...………………………… 61

2-27 Litholog for the 04-10-042-09W5 core, annotated with main contacts (discussed in text) and facies interpretation. Legend for the litholog is given in Figure 2-1 …………………………………………………..…… 62

2-28 Litholog for the 10-10-042-09W5 core, annotated with main contacts (discussed in text) and facies interpretation. Legend for the litholog is given in Figure 2-1 ……………………………………………...………. 63

2-29 Litholog for the 06-12-045-07W5 core, annotated with main contacts (discussed in text) and facies interpretation. Legend for the litholog is given in Figure 2-1 ……………………………………………………...…. 64

2-30 Litholog for the 07-06-042-07W5 core, annotated with main contacts (discussed in text) and facies interpretation. Legend for the litholog is given in Figure 2-1………………………………………………….……... .. 65

2-31 Litholog for the 07-08-042-07W5 core, annotated with main contacts (discussed in text) and facies interpretation. Legend for the litholog is given in Figure 2-1. ………………………………………………..……… 66

2-32 Litholog for the 08-11-042-07W5 core, annotated with main contacts (discussed in text) and facies interpretation. Legend for the litholog is given in Figure 2-1. ………………………………………………..……… 67

2-33 Litholog for the 10-17-042-04W5 core, annotated with main contacts (discussed in text) and facies interpretation. Legend for the litholog is given in Figure 2-1. ………………………………………..……………… 68

2-34 Litholog for the 03/13-13-042-05W5 core, annotated with main contacts (discussed in text) and facies interpretation. Legend for the litholog is given in Figure 2-1. …………………………………………………..…… 69

2-35 Litholog for the 03-13-043-05W5 core, annotated with main contacts (discussed in text) and facies interpretation. Legend for the litholog is given in Figure 2-1. …………………………………………………..…… 70

2-36 Litholog for the 10-32-048-06W5 core, annotated with main contacts (discussed in text) and facies interpretation. Legend for the litholog is given in Figure 2-1. ……………………………………………………..…. 71

2-37 Litholog for the 08-02-43-05W5 core, annotated with main contacts (discussed in text) and facies interpretation. Legend for the litholog is given in Figure 2-1. ……………………………………………..…..…….. 72

2-38 Litholog for the 16-11-045-07W5 core, annotated with main contacts (discussed in text) and facies interpretation. Legend for the litholog is given in Figure 2-1. …………………………………………………..…… 73

2-39 Litholog for the 10-25-047-03W4 core, annotated with main contacts (discussed in text) and facies interpretation. Legend for the litholog is given in Figure 2-1. Red numbers: XRD samples (see Chapter five for discussion). ……………………………………………………………. 74

2-40 Generalized stratigraphic chart for Jurassic – Cretaceous of west-central Alberta. (Compiled from Leckie and Smith, 1993; Poulton et al., 1994; Hayes et al., 1994; Leckie et al., 1994; Dawson et al., 1994; Hamblin et Lee, 1997) …………………………………………………. 76

2-41 Base map showing the database of the study within the Foothill region: locations where well logs were used are shown with different well symbols, whereas mudlog locations are shown with yellow circles. Locations of the five regional cross-sections 1-1' through 5-5' are also shown. Township locations are shown on

the right border, and range locations along the bottom ……………………..…… 79
2-42 Typical geophysical log signature of Ferrier, Mannville and Colorado groups and bounding surfaces in Pembina-Ferrier-Gilby area. Horizontal black lines in the depth column indicate thick coal seams …….. 81
2-43 Typical vertical profile for two shallow-marine coarsening-upward sequences along with their gamma-ray and resistivity well-log responses. Viking Formation - 07-06-042-07W5 core. Legend for the litholog is given in Figure 2-1. ……………….……………………………..…………… 83
2-44 Typical vertical profile for a shallow-marine coarsening-upward sequence along with its gamma-ray and resistivity well-log responses. Viking Formation - 03/13-13-042-05W5 core. Legend for the litholog is given in Figure 2-1. …………………………..………………………… 84
2-45 Typical vertical profile for three shallow-marine coarsening-upward sequences along with their gamma-ray well-log response. Cardium Formation - 06-26-048-11W5 core. Legend for the litholog is given in Figure 2-1. ……..………………………………………….………. 86
2-46 Typical vertical profile for two shallow-marine coarsening-upward sequences along with their gamma-ray and resistivity well-log responses. Cardium Formation – 10-26-045-09W5 core. Legend for the litholog is given in Figure 2-1. ………………………………..………………… 87
2-47 Typical geophysical log signature of Belly River Group and bounding formations in Ferrier-Gilby area. Horizontal red lines in the depth column indicate thick coal seams …………………………………………. 88
2-48 Typical vertical profile of a channel-fill deposit along with its gamma-ray well-log response. Belly River Formation - 02/06-09-46-9W5 core. Legend for the litholog is given in Figure 2-1….. 91
2-49 Typical vertical profile of a channel-fill deposit along with its gamma-ray well-log response. Belly River Formation – 10-04-49-11W5 core. Legend for the litholog is given in Figure 2-1. ..….. 92
2-50 Typical geophysical log signature of Bearpaw – Edmonton Gp. Horizontal red lines in the depth column indicate thick coal seams ……… 94

2-51 Stratigraphic chart for Upper Devonian - Cretaceous, Lloydminster area (compiled from Leckie and Smith, 1993; Gregor, 1997) ……………. 97

2-52 Gamma-ray log signature calibrated against the litholog for the 10-25-047-03W4 core. Legend for the litholog is given in Figure 2-1, and facies summaries in Table 2-1. Red numbers: XRD samples. ………………………………………………………… 100

2-53 Base map showing the database of the study within Lloydminster basin: locations where well logs were used are shown with different well symbols, whereas mudlog locations are shown with open squares. Locations of the eight regional cross-sections 1-1' through 8-8' are shown with different colors; 4th – Fourth Meridian. Township locations are shown on the right border, and range locations along the bottom ………………………………………………………………… 101

***

3-1 Carbon isotopic composition and wetness of gases from three mudlogs in west-central Alberta ………………………………………………... 107

3-2 Carbon isotopic composition and wetness of gases from two mudlogs in the heavy oil region ………………………………………………... 108

3-3 Mudgas isotopic depth profile from Petro-Canada Ferrier 14-3-042-09W5 and its relationship with the regional stratigraphy ……………………..… 111

3-4 Mudgas isotopic depth profile from Petro-Canada Gilby 15-16-42-04W5 and its relationship with the regional stratigraphy ……………………….. 112

3-5 Mudgas isotopic depth profile from IORL Pembina 11-04-049-11W5 and its relationship with the regional stratigraphy ………………………. 113

3-6 Litholog for the 10-04-49-11W5 core, annotated with main contacts and facies interpretation. Core porosity and permeability data is also shown, as reported in the core analysis report from IHS Energy public database. Legend for the litholog is given in Figure 2-1…………………………… 116

3-7 Litholog for the 08-02-43-5W5 core, annotated with main contacts and facies interpretation. Core porosity and permeability data is also shown, as reported in the core analysis report from IHS Energy public database. Legend for the litholog is given in Figure 2-1…………………………… 117

3-8 Variations of carbon isotope ratios for methane with stratigraphic position, Foothills region. Major shifts in carbon isotope ratios tend to occur at sequence boundaries and maximum flooding surfaces ……… 123

3-9 Variations of carbon isotope ratios for ethane with stratigraphic position, Foothills region. Major shifts in carbon isotope ratios tend to occur at sequence boundaries and maximum flooding surfaces ………... 124

3-10 Variations of carbon isotope ratios for propane with stratigraphic position, Foothills region. Major shifts in carbon isotope ratios tend to occur at sequence boundaries and maximum flooding surfaces ………. 125

3-11 Litholog for the 03-13-43-5W5 core, annotated with main contacts and facies interpretation. Core porosity and permeability data is also shown, as reported in the core analysis report from IHS Energy public database. Legend for the litholog is given in Figure 2-1………………………..… 127

3-12 Litholog for the 02-33-47-7W5 core, annotated with main contacts and facies interpretation. Core porosity and permeability datais also shown, as reported in the core analysis report from IHS Energy public database. Legend for the litholog is given in Figure 2-1………………………….……. 128

3-13 Litholog for the 10-14-44-9W5 core, annotated with main contacts and facies interpretation. Core porosity and permeability data is also shown, as reported in the core analysis report from IHS Energy public database. Legend for the litholog is given in Figure 2-1…………………………….. 129

3-14 Litholog for the 04-10-42-9W5 core, annotated with main contacts and facies interpretation. Core porosity and permeability data is also shown, as reported in the core analysis report from IHS Energy public database. Legend for the litholog is given in Figure 2-1…………………………….. 130

3-15 Stable carbon isotope ratios for co-genetic ethane and propane in a natural gas (Maturity line after Faber, 1987; Whiticar, 1990.) ………….. 131

3-16 Carbon isotopic composition of mudgases from Lindbergh

00/13-09-56-6W4 in relationship with stratigraphy ………………………. 143
3-17 Carbon isotopic composition of mudgases from Husky
A9-15-51-23W3 in relationship with stratigraphy ……………………….. 144
3-18 Carbon isotopic composition of mudgases from Husky
C3-30--47-4W4 in relationship with stratigraphy …………………….….145
3-19 Carbon isotopic composition of mudgases from Petrovera
1D-25-55-5W4 in relationship with stratigraphy …………………………. 146
3-20 Carbon isotopic composition of mudgases from Petrovera
112/01-04-48-22W3 in relationship with stratigraphy …………………… 147
3-21 Carbon isotopic composition of mudgases from Petrovera Golden Lake
11/09-30-47-22W3 in relationship with stratigraphy ……………………. 148
3-22 Carbon isotopic composition of mudgases from Petrovera
10-17-47-27W3 in relationship with stratigraphy ……………………….. 149

***

4-1 Relative yields of hydrocarbon and nonhydrocarbon gases with increasing pyrolysis temperature for sapropelic (Type II) and humic (Type III) organic matter. These generation curves exclude non-organic mechanisms of H2S, CO2 and N2 production such as sulphate reduction (after Hunt, 1996) …………………………………………….……158
4-2 Natural gas diagram (Bernard diagram) distinguishing bacterial from thermogenic gases on the basis of molecular composition and carbon isotope ratio of methane. The arrow indicates compositional and isotopic alteration of bacterial gas induced by microbial oxidation (after Bernard, 1977 and Whiticar, 1999) …………………………………..161
4-3 Variation in $\delta^{13}C$ of methane and C_{2+} concentration for generated hydrocarbons as a function of increasing organic maturity (after Schoell, 1980 and Schoell, 1983) …………………………………….162
4-4 Genetic classification of gases defined by Schoell (1983) on the basis of methane $\delta^{13}C$ and the abundance of ethane and higher alkanes ………..163

4-5 Genetic classification of natural gases defined by Schoell (1983) on the basis of methane $\delta^{13}C$ and ethane $\delta^{13}C$ …………………..………. 164

4-6 James diagram (1983) relating the separation of carbon isotope ratios between C1 – C5 alkanes to various maturity parameters indicated on the *x*-axis: %Ro, TAI and LOM (the level of organic maturity) ……………………………………………………… 166

4-7 Clayton diagram for the genetic characterization of natural gases. The *y*-axis indicates the difference between the carbon isotope ratios of methane and the presumed source kerogen …………………………..… 167

4-8 Idealized "natural gas plot" of gaseous hydrocarbons (after Chung et al., 1988) ……………………………………………….… 171

4-9 Combined depth profile of wetness index for three mudlogs in west-central Alberta …………………………………………………... 174

4-10 In depth distribution of the wetness index for mudgases sampled in the Foothills region ……………………………………………………. 175

4-11 Methane concentration (a), and total abundance of gas components (b) at Ferrier and Gilby locations – west-central Alberta ……………….. 176

4-12 Composite depth profile for $\delta^{13}C$ for methane sampled in the Foothills region ………………………………………………………… 179

4-13 Composite depth profile for $\delta^{13}C$ for ethane sampled in the Foothills region …………………………………………………….… 180

4-14 Composite depth profile for $\delta^{13}C$ for propane sampled in the Foothills region …………………………………………………..…. 180

4-15 In-depth carbon isotope mud profiles for mudgases sampled in the Foothills region ………………………………………………….... 182

4-16 C2/C3 versus C2/iC4 diagram showing the possible biodegradation of hydrocarbon gases (Prinzhofer, 2000) - Gilby 15-16-42-4W5 ………… 183

4-17 Bernard diagram showing the distribution of Cretaceous gases, west-central Alberta: a) Pembina 11-04-49-11W5, and b) Ferrier 14-03-42-9W5. Mixtures of bacterial and thermogenic gases appear to be developed in majority of Colorado, Lea Park and Belly River gases, with a strong migrational component for shallower gases: Paskapoo, Scollard, and Horseshoe Canyon gases …………………………………… 185

4-18 Bernard diagram showing the distribution of Cretaceous, and sub-Cretaceous gases for Gilby 15-16-42-4W5. Mixtures of bacterial and thermogenic gases appear to be developed in majority of Colorado, and post Colorado gases; Mannville and sub-Cretaceous gases display a strong thermogenic signature …………………………………………………………….... 186

4-19 Distribution of Cretaceous mudgases relative to the genetic Classification defined by Schoell (1983) on the basis of $\delta^{13}C$ of methane and the relative abundance of C2+ alkanes. Gilby 15-16-42-4W4, west-central Alberta ………………………………. 188

4-20 Distribution of Cretaceous mudgases relative to the genetic classification defined by Schoell (1983) on the basis of $\delta^{13}C$ of methane and the relative abundance of C2+ alkanes. Ferrier 14-3-42-9W5, west-central Alberta ………………………………………………………………….. 189

4-21 Distribution of Cretaceous mudgases relative to the genetic classification defined by Schoell (1983) on the basis of $\delta^{13}C$ of methane and the relative abundance of C2+ alkanes. Pembina 11-4-49-11W5, west-central Alberta ……………………………………………………………………190

4-22 James diagram showing the distribution of the Paskapoo – Scollard mudgases (a), and Edmonton Group mudgases (b) - Gilby 15-16-42-9W5. Maturities less than 0.5 to approximately 1% vitrinite reflectance are indicated using optimal fit between the ethane - propane pair …………192

4-23 James diagram showing the distribution of the Paskapoo - Scollard mudgases for Gilby 15-16-42-9W5 profile. Maturities less than 0.6% vitrinite reflectance are indicated, and as well the possible bacterial oxidation of methane …………………………………………..193

4-24 James diagram showing the distribution of the Horseshoe Canyon and Bearpaw mudgases for Gilby 15-16-42-9W5 profile. Isotopic separations indicate that the majority of these gases were generated at low levels of maturities ……………………………………….193

4-25 James diagram showing the distribution of the Horseshoe Canyon mudgases for Pembina 11-4-49-11W5 profile. Isotopic separations indicate gases were generated at LOM's of 6-12 ……………………..….. 194

4-26 James diagram showing the distribution of the Belly River mudgases for Ferrier 14-3-42-4W5 profile. Majority of the gases were generated within the oil window; some of the gases indicate a thermogenic signature based on the optimal fit between the ethane, propane and butane …………195

4-27 Natural gas plots for a selection of Belly River gas samples from the Ferrier 14-3-42-4W5 profile, showing linear relationships between isotope ratios and their inverse carbon numbers …….……………196

4-28 James diagram showing the distribution of the Belly River – Lea Park mudgases for Gilby 15-16-42-9W5 profile. Isotopic separations between gas components indicate a wide range of maturities, from less than 5 LOM and up to 12 LOM ………196

4-29 James diagram showing the distribution of the Belly River mudgases for Pembina 11-4-49-11W5 profile. Maturities higher than 0.5 to approximately 0.7% vitrinite reflectance are indicated using optimal fit between the ethane-propane pair ………………………………………. 197

4-30 James diagram showing the distribution of the Colorado mudgases (a) Ferrier 14-3 -42-9W4, and (b) - Gilby 15-16-42-9W5. Maturities ranging from 6 LOM to 12 LOM are indicated using optimal fit between the ethane-propane pair …………………………………………...198

4-31 James diagram showing the distribution of Mannville, Fernie and Pekisko mudgases on the Gilby 15-16-42-9W5 profile. As indicated by the isotopic separations between gas components, these gases were generated within the oil window ………………………….……………….. 199

4-32 The overall organic maturity trend in the central part of the Alberta basin for Mannville strata. The values for the mean maximum vitrinite reflectance are from isomaturity maps of Bustin (1991) …….….…………..201

4-33 Stable carbon isotope ratios for co-genetic ethane and propane in mudgases from (a) Ferrier and (b) Gilby (After Faber, 1987;

Whiticar, 1990.) 202

4-34 The relative ethane concentration plotted against depth for mudgases from Ferrier and Gilby 203

4-35 The relative propane concentration plotted against depth for mudgases from Ferrier and Gilby 204

4-36 In depth and spatial distribution for the wetness index - Heavy oil region, east-central Alberta and west-central Saskatchewan 206

4-37 Plots of propane $\delta^{13}C$ versus ethane $\delta^{13}C$ for Colorado and Mannville gases in the heavy oil region 208

4-38 Bernard diagram showing the distribution of Cretaceous gases at Lindbergh 13-9-56-6W4 location, heavy oil region. Mixtures of bacterial and thermogenic gases appear to be developed in majority of the mudgases 209

4-39 Bernard diagram showing the distribution of Cretaceous gases at Petrovera 1D-25-55-5W4 location, heavy oil region. Mixtures of bacterial and thermogenic gases appear to be developed in majority of the mudgases 210

4-40 Bernard diagram showing the distribution of Cretaceous gases at Husky 3C-30-47-4W4 location, heavy oil region. Mixtures of bacterial and thermogenic gases appear to be developed in majority of the mudgases 211

4-41 Bernard diagram showing the distribution of Cretaceous gases at Husky 9-15-51-22W3 location, heavy oil region. Mixtures of bacterial and thermogenic gases appear to be developed in majority of the mudgases 211

4-42 Bernard diagram showing the distribution of Cretaceous gases at Petrovera 1-4-48-22W3 location, heavy oil region. Mixtures of bacterial and thermogenic gases appear to be developed in majority of the mudgases, with a strong shift towards the bacteriogenic gas field 212

4-43 Distribution of Cretaceous gases relative to the genetic classification defined by Schoell (1983) on the basis of $\delta^{13}C$ of methane and

the relative abundance of C2+ alkanes. Lindbergh
4C-16/13-09-56-6W4 ………………………………………………….. . 213

4-44 Distribution of Cretaceous gases relative to the genetic classification defined by Schoell (1983) on the basis of $\delta^{13}C$ of methane and the relative abundance of C2+ alkanes: a) Petrovera 1D-25-55-5W4; b) Husky 3C-30-47-4W4 ………………………………………………. 214

4-45 Distribution of Cretaceous gases relative to the genetic classification defined by Schoell (1983) on the basis of $\delta^{13}C$ of methane and the relative abundance of C2+ alkanes: a) Petrovera 1-4-48-22W3; b) Husky 9-15-51-23W3 ……………………………………………… 215

4-46 James diagram showing the distribution of the Colorado mudgases: (a) Lindbergh 13-9-56-6W6, b) Petrovera 1D-25-55-5W4. The majority of Colorado gases appear to have been generated at low levels of maturity ……………………………………………….. 217

4-47 James diagram showing the distribution of the Colorado mudgases; Husky 3C-30-47-4W4 ……………………………………………….. 218

4-48 Natural gas plot for the Husky 3C-30-47-4W4 well, showing representative gas samples from the Second White Speckled Shale Formation. The predicted source composition varies between –25% and ~-29‰ ……………………………….………… 219

4-49 James diagram showing the distribution of the Colorado mudgases; Petrovera 10-17-47-27W3 …………………………………………….….. 219

4-50 Natural gas plots for a selection of representative gas samples from the Colorado Group; Petrovera 10-17-47-27W3 …………………………… 220

4-51 James diagram showing the distribution of the Colorado mudgases; Petrovera A9-30-47-22W3 …………………………………………….. 221

4-52 James diagram showing the distribution of the Colorado mudgases: (a) Husky 9-15-51-23W3, b) Petrovera 1-4-48-22W3. The majority of Colorado gases appear to have been generated at low levels of maturity. Gases sampled at 330.2m and 281.2m (b) represent exceptions; they are biodegraded and thus cannot indicate a reliable maturity level ……………222

4-53 Natural gas plots for a selection of Colorado gas samples from the Petrovera A9-30-47-22W3 profile, showing non-linear relationships between isotope ratios and their inverse carbon numbers ……………...… 223

4-54 Natural gas plots for a selection of Colorado gas samples from the Petrovera 1-4-48-22W3 profile, showing non-linear relationships between isotope ratios and their inverse carbon numbers ………………………….. 223

4-55 Isotopic differences of methane, ethane and propane for the Colorado gases sampled in the heavy oil region, east-central Alberta and west-central Saskatchewan ……………..…………………………... 224

4-56 James diagram showing the distribution of the Mannville mudgases: (a) Lindbergh 13-9-56-6W6, b) Petrovera 10-17-47-27W3. The majority of Mannville gases appear to have been generated at high levels of maturity, within the oil window ………….…………………………….. 226

4-57 James diagram showing the distribution of the Mannville mudgases: (a) Petrovera 1D-25-55-5W4, b) Husky C3-30-47-4W4. The majority of Mannville gases have the n-butane $\delta^{13}C$ values plotted high above the calculated maturation line ……………….…………………………….. 227

4-58 "Natural gas plot" for a selection of Mannville gas samples from the Lindbergh 13-9-56-6W4 profile, showing quasi-linear relationships between C2-C4 isotope ratios and their inverse carbon numbers. These gas samples originate from coals or coaly shales …….…………………….228

4-59 "Natural gas plot" for a selection of Mannville gas samples from the Lindbergh 13-9-56-6W4 profile, showing quasi-linear relationships between C2-C4 isotope ratios and their inverse carbon numbers. These linear trends are indicative of a thermogenic, single sourced gas from kerogen Type III ………………………..………….……… 230

4-60 "Natural gas plots" for a selection of Colorado gas samples from the Petrovera 10-17-47-22W3 profile, showing isotopic reversals between the $\delta^{13}C_3$ and $\delta^{13}C_4$ values ………..……………………………. 231

4-61 "Natural gas plots" for a selection of gas samples from the Lindbergh A9-13-56-6W4 profile, showing isotopic reversals between the $\delta^{13}C_3$ and $\delta^{13}C_4$ values ………………………………………….………….... 232

4-62 "Natural gas plots" for two gas samples from the Petrovera 10-17-47-27W3 profile, showing isotopic similarity between Colorado and Mannville gases …………………………………………….. 232

4-63 Stable carbon isotope ratios for co-genetic ethane and propane in Colorado mudgases from Petrovera 10-17-47-27W3 (after Faber, 1987; Whiticar, 1990.) ………………………………….…… 233

***

5-1 Neutron – density crossplot for the Mannville Group at Husky A9-15-51-23W3 well location, Lloydminster region …………………… 238

5-2 M – N plot for mineral identification applicable to Mannville Group at Petrovera 1D-25-55-22W3 well location, heavy oil region - Alberta ……………………………………………………... 239

5-3 ROMA - UMA crossplot for lithology identification. Scollard Formation, well Pembina 11-4-49-11W5, Foothills region, Alberta ……... 240

5-4 Example of compositional profile, calculated by a matrix algebra solution …………………….……………………………………….……… 242

5-5 Shale point defined on a neutron – sonic crossplot. Values are from the Colorado Group, Gilby 15-16-42-4W4, west-central Alberta ………………….……………………………………….. 245

5-6 Matrix algebra solution for Colorado Group in Gilby 15-16-42-4W5 well, west-central Alberta. The result is shown as a graphic lithology log of the system porosity-shale-quartz ………………………………….…... 246

5-7 Shale point defined on a neutron – density crossplot. Values are from the Mannville Group, Gilby 15-16-42-4W4, west-central Alberta ….. 247

5-8 Matrix algebra solution for the Mannville Group in Husky 3C-30-47-4W4 well, Lloydminster region. The result is shown as a graphic lithology log of the system porosity-shale-quartz-coal ……… 248

5-9 The resultant diffractogram of sample #2 (538.5m depth) - Shell

Paradise 10-25-047-3W4 core. 436
5-10 The resultant diffractogram of sample #1 (538.9m depth) - Shell Paradise 10-25-047-3W4 core. 437
5-11 The resultant diffractogram of sample #3 (546m depth) - Shell Paradise 10-25-047-3W4 core 438
5-12 The resultant diffractogram of sample #4 (567.4m depth) - Shell Paradise 10-25-047-3W4 core 439
5-13 The resultant diffractogram of sample #5 (576.5m depth) - Shell Paradise 10-25-047-3W4 core 440
5-14 The resultant diffractogram of sample #6 (636m depth) - Shell Paradise 10-25-047-3W4 core 441
5-15 The resultant diffractogram of sample #6 (636m depth) - Shell Paradise 10-25-047-3W4 core – larger intensity scale 442
5-16 The resultant diffractogram of sample &7 (654.2m depth) - Shell Paradise 10-25-047-3W4 core 443
5-17 The resultant diffractogram of sample #7 (654.2m depth) - Shell Paradise 10-25-047-3W4 core - larger intensity scale 444
5-18 The resultant diffractogram of sample #8 (670m depth) - Shell Paradise 10-25-047-3W4 core 445
5-19 The resultant diffractogram of sample #8 (670m depth) - Shell Paradise 10-25-047-3W4 core - larger intensity scale 446
5-20 The resultant diffractogram of sample #9 (682m depth) - Shell Paradise 10-25-047-3W4 core 447
5-21 The resultant diffractogram of sample #9 (682m depth) - Shell Paradise 10-25-047-3W4 core - larger intensity scale 448
5-22 Matrix algebra solution for the Joli Fou - Mannville section in Shell Paradise 10-25-47-3W4 well, Lloydminster region. The result is shown as a graphic lithology log of the system porosity-quartz-shale-smectite 251
5-23 Matrix algebra solution for the Joli Fou - Mannville section in Shell Paradise 10-25-47-3W4 well, Lloydminster region.

The result is shown as a graphic lithology log of the system porosity-quartz-shale-illite. Note: the quartz- dominated sample #5 from 576.5m depth is also shown in red …………………………………... 252

5-24 Matrix algebra solution for the Joli Fou - Mannville section in Shell Paradise 10-25-47-3W4 well, Lloydminster region. The result is shown as a graphic lithology log of the system porosity-quartz-shale-siderite ……...…………………………………...… 253

5-25 Wireline data plus mineralogical interpretation for Husky 3C-30-47-4W4 profile …….……………………………………………..255

5-26 "Natural gas plot" showing some of the Paskapoo gases, Ferrier 14-3-42-9W5, Foothills region …………………………………………… 256

5-27 "Natural gas plot" showing some of the Paskapoo - Scollard gases, Ferrier 14-3-42-9W5, Foothills region …………………………….... 257

5-28 "Natural gas plot" for some of the Horseshoe Canyon gases, indicating a single thermogenic generation of the gas and a single sub-compartment bounded by two effective shale-rich barriers. Ferrier 14-3-42-9W5, west-central Alberta ……………………………….. 258

5-29 "Natural gas plot" showing two different gases separated by a quartz-rich shale barrier. Scollard Formation, Ferrier 14-3-42-9W5, west-central Alberta ……………………………………………………..259

5-30 "Natural gas plot" of the Manville gases from the Gilby profile ………… 260

5-31 C2/C3 diagram for Gilby profile showing $\delta^{13}C2 - \delta^{13}C3$ (‰) versus C2/C3 distinguishes gases generated from the primary cracking of kerogen, the secondary cracking of oil, and the tertiary cracking of the wet portion of the gases (after Lorant et al, 1998) ……… 261

5-32 "Natural gas plot" for Colorado gases from Petrovera 1D-25-55-5W4, showing the difference between two gas sub-compartments separated by an effective montmorillonite-rich shale barrier ……….……………….. 262

5-33 Stable carbon isotopic profile and the conversion into mineralogy, Husky 9-15-51-23W3 ……………………………………………………….. 263

5-34 Stable carbon isotopic profile and the conversion into mineralogy,

Petrovera 1D-25-55-5W4 ………………………………………………….. 264
5-35 "Natural gas plot" showing two different gas compartments (Joli Fou gases and Colony Gases) Husky C3-30-47-4W4 separated by an effective montmorillonite-rich shale barrier …………….. 265
5-36 "Natural gas plot" showing some Middle Mannville gases confined in a single gas sub-compartment at Husky C3-30-47-4W4 profile by two effective barriers: an upper quartz-cemented band and a lower shale-rich layer ……………………………………………..….266
5-37 "Natural gas plot" for Colorado gases from Husky 9-15-51-23W3, showing the slight difference between two gas sub-compartments separated by a partial effective montmorillonite-rich shale barrier ………. 267
5-38 "Natural gas plot" for Second White Speckled Shales gases from Husky C3-30-47-4W4, showing the slight difference between two gas sub-compartments separated by a partial effective montmorillonite-rich shale barrier ………………………………………… 268

***

6-1 C_2/C_1 versus methane $\delta^{13}C$ diagrams showing the basic principle of their use. Modified from Prinzhofer et al. (2000) ………………………. 277
6-2 Flow patterns (indicated by arrows) in the coal-bearing Upper Cretaceous-Tertiary strata of the Alberta basin: (a) Scollard-Paskapoo aquifer; (b) Edmonton aquifer; c) Belly River aquifer. Modified from Bachu and Michael, 2003. Note: the grey squares indicate the Foothills area in the present study …………………………………….. 278
6-3 The distribution of the isotopic composition of methane and physico-chemical parameters of the Scollard gases in the different mudlog locations in the Foothills region. Only the mean values are shown ……………………………………………………. 281
6-4 The distribution of the isotopic composition of methane and physico-chemical parameters of the Horseshoe Canyon gases

in the different mudlog locations in the Foothills region. Only the mean values are shown …………………………………………………282

6-5 Combination plot of $\delta^{13}C_{CO2}$ and $\delta^{13}C_{CH4}$ with isotope fractionation lines (Ec). Methanogenesis by carbonate reduction has a larger $CO_2 - CH_4$ isotope separation than by methyl-type fermentation (freshwater region), or methane consumption (modified after Whiticar, 1999) …………………………………………. 283

6-6 Combination plot of $\delta^{13}C_{CO2}$ and $\delta^{13}C_{CH4}$ with isotope fractionation lines (Ec) for the Paskapoo Formation gases (after Whiticar, 1999) ……. 284

6-7 The overall organic maturity trend in the Ferrier-Gilby area, and Lloydminster area for Mannville strata. The values for the mean maximum vitrinite reflectance are from isomaturity maps of Bustin (1991) ………………………………………………….. 285

6-8 The distribution of the isotopic composition of methane and physico-chemical parameters of the Upper Belly River gases in the different mudlog locations in the Foothills region. Only the mean values are shown ………………………………………………..287

6-9 C2/C3 diagram showing δ^{13} C2 – δ^{13}C3 versus C2/C3 distinguishing gases generated from the primary cracking of kerogen, the secondary cracking of oil, and the tertiary cracking of the wet portion of the gases for Ferrier and Gilby profiles (after Lorant et al, 1998) ……………………289

6-10 C2/C3 versus C2/iC4 diagram showing the possible biodegradation of hydrocarbon gases (Prinzhofer, 2000). Ferrier 14-3-42-9W5 ……………………………………………………………… 290

6-11 C2/C3 versus C2/iC4 diagram showing the possible biodegradation of hydrocarbon gases (Prinzhofer, 2000). Gilby 15-16-42-4W5 ……………………………………………………….290

6-12 The pattern of ethane δ^{13}C change with depth in the Scollard Formation, Foothills region ………………………………………………...291

6-13 The pattern of ethane δ^{13}C change with depth in the Horseshoe Canyon Formation, Foothills region …………………………..…… 291

6-14 The pattern of ethane $\delta^{13}C$ change with depth in the Belly River Group, Foothills region ………………………………………………… 294

6-15 In depth variation of the total abundance of hydrocarbon gases in the Horseshoe Canyon Formation, Foothills region ………………………….. 293

6-16 Spatial distribution of the methane content in Colorado shales, Lloydminster region ……………………………………………………..…295

6-17 Methane concentration (in vol. %) variability with depth in five mudlog profiles within the Lloydminster region ……….………….. 296

6-18 Depth profiles of methane $\delta^{13}C$ from gases sampled in Lower Mannville reservoirs, Lloydminster area ……………………………………………298

6-19 The distribution of the isotopic composition of methane and physico-chemical parameters of the Sparky sand gases in the different mudlog locations in the Lloydminster region. Only the mean values are shown ……………………………………………299

6-20 The distribution of the isotopic composition of methane and physico-chemical parameters of the Lloydminster sand gases in the different mudlog locations in the Lloydminster region. Only the mean values are shown ………………………..………………300

6-21 The distribution of the isotopic composition of methane and physico-chemical parameters of the Mannville Group gases in the different mudlog locations in the Lloydminster region. Only the mean values are shown ……………………………………………301

6-22 The distribution of the isotopic composition of methane and physico-chemical parameters of the Colorado Group gases in the different mudlog locations in the Lloydminster region. Only the mean values are shown ………...……………………………302

6-23 Gas wetness distribution within the Lloydminster region ….……………... 303

6-24 Gases from Sparky sandstone plotted on a C1-C2 diagram in linear scale, showing a trend of segregative migration ……………………. 304

6-25 Gases from Lloydminster sandstone plotted on a C1-C2 diagram in logarithmic scale, showing a trend of segregative migration ………………305

6-26 Inferred migration trend of the gas phase through the carrier sandstone beds of the Mannville Group, Lloydminster region ……………………….. 305

6-27 Stable carbon isotope ratios for co-genetic methane and ethane in a natural gas (After Faber, 1987; Whiticar, 1990.) …………….…………..307

***

7-1 Isotope ratios of eight SCV gases superimposed on the mudgas isotopic depth profile from Petro-Canada Ferrier 14-03-042-9W5. Legend for SCV gases is provided in Figure 7-2 ……………………... 315

7-2 SCV gases from Figure 7-1 and their presumable sources. Petro-Canada Ferrier 14-03-042-9W5…………………………………………….... 316

7-3 Isotope ratios of five SCV gases superimposed on the mudgas isotopic depth profile from Petro-Canada Ferrier 14-03-042-9W5. Legend for SCV gases is provided in Figure 7-4………………… …… 317

7-4 SCV gases from Figure 7-3 and their presumable sources. Petro-Canada Ferrier 14-03-042-9W5………………………………………… …… 318

7-5 Isotope ratios of thirteen SCV gases superimposed on the mudgas isotopic depth profile from PC Gilby 15-16-42-04W5. Legend for SCV gases is provided in Figure 7-6…………………………. 319

7-6 SCV gases from Figure 7-5 and their presumable sources. PC Gilby 15-16-42-04W5……………………………………..……….. 320

7-7 Isotope ratios of two SCV gases superimposed on the mudgas isotopic depth profile from IORL Pembina 11-04-049-11W5. Legend for SCV gases is provided in Figure 7-8…………………..…… 321

7-8 SCV gases from Figure 7-7 and their presumable sources. IORL Pembina 11-04-049-11W5…………………………….………… 322

7-9 Chung diagram for 8-24-42-7W5 SCV gas in the Ferrier- Gilby area …..… 322

7-10 Location of wells affected by gas migration (blue dots), which best matched the Ferrier mudlog. Presumable SCV sources are indicated… …. 323

7-11 Location of wells affected by gas migration (blue dots), which best

matched the Gilby mudlog. Presumable SCV sources are indicated……… 323
7-12 Location of wells affected by gas migration (blue dots), which best matched the Pembina mudlog. Presumable SCV source is indicated…….. 324
7-13 Isotope ratios of twelve SCV gases superimposed on the mudgas isotopic depth profile from Lindbergh 13-9-056-06W4.
Legend for SCV gases is provided in Figure 7-14……………………… .. 325
7-14 SCV gases from Figure 7-13 and their presumable sources.
Lindbergh 13-09-056-06W4…………………………………………… 326
7-15 Isotope ratios of twelve SCV gases superimposed on the mudgas isotopic depth profile from Lindbergh 13-09-056-06W4.
Legend for SCV gases is provided in Figure 7-16………………………. . 327
7-16 SCV gases from Figure 7-15 and their presumable sources.
Lindbergh 13-09-056-06W4…………………………….…………….. 328
7-17 Isotope ratios of ten (10) SCV gases superimposed on the mudgas isotopic depth profile from Lindbergh 13-9-056-06W4.
Legend for SCV gases is provided in Figure 7-18,
and a close-up view in Figure 7-19…………………………………… 329
7-18 SCV gases from Figure 7-17 and their presumable sources.
Lindbergh 13-09-056-06W4…………………………………………… 330
7-19 Close-up view of SCV gases from Figure 7-17.
Lindbergh 13-09-056-06W4 …………………………………… …….. 330
7-20 Isotope ratios of thirteen SCV gases superimposed on the mudgas isotopic depth profile from Lindbergh 13-9-056-06W4
Legend for SCV gases is provided in Figure 7-21. ………………………. 331
7-21 SCV gases from Figure 7-19 and their presumable sources.
Lindbergh 13-9-056-06W4……………………………………………….. 332
7-22 Isotope ratios of thirteen SCV gases superimposed on the mudgas isotopic depth profile from Petrovera 1D-25-55-5W4.
Legend for SCV gases is provided in Figure 7-23, and a close-up view of the SCV gases presumably related to the Viking Fm. in Figure 7-24………. 333
7-23 SCV gases from Figure 7-22 and their presumable sources.

Petrovera 1D-25-55-5W4…………………………………………….... 334
7-24 SCV gases from Figure 7-22 and their presumable sources ……………….. 334
7-25 Isotope ratios of fifteen SCV gases superimposed on the mudgas isotopic depth profile from Petrovera 1D-25-55-5W4.
Legend for SCV gases is provided in Figure 7-26………………..……. 335
7-26 SCV gases from Figure 7-25 and their presumable sources.
Petrovera 1D-25-55-5W4……………………………………………..336
7-27 Isotope ratios of fifteen SCV gases superimposed on the mudgas isotopic depth profile from Petrovera 1D-25-55-5W4.
Legend for SCV gases is provided in Figure 7-28 ……………………….. 337
7-28 SCV gases from Figure 7-27 and their presumable sources.
Petrovera 1D-25-55-5W4………………………………………………… 338
7-29 Isotope ratios of nine SCV gases superimposed on the mudgas isotopic depth profile from Husky C3-30-47-4W4.
Legend for SCV gases is provided in Figure 7-30……………………... 339
7-30 SCV gases from Figure 7-29 and their presumable sources.
Husky C3-30-47-4W4…………………………………………………. 340
7-31 Isotope ratios of eight SCV gases superimposed on the mudgas isotopic depth profile from Husky C3-30-47-4W4.
Legend for SCV gases is provided in Figure 7-32……………………….. 341
7-32 SCV gases from Figure 7-31 and their presumable sources.
Husky C3-30-47-4W4…………………………………………………. 342
7-33 Isotope ratios of nine SCV gases superimposed on the mudgas isotopic depth profile from Husky C3-30-47-4W4.
Legend for SCV gases is provided in Figure 7-34………………………… 343
7-34 SCV gases from Figure 7-33 and their presumable sources.
Husky C3-30-47-4W4……………………………………….………. 344
7-35 Isotope ratios of nine SCV gases superimposed on the mudgas isotopic depth profile from Husky C3-30-47-4W4.
Legend for SCV gases is provided in Figure 7-36………………………… 345
7-36 SCV gases from Figure 7-35 and their presumable sources.

Husky C3-30-47-4W4…………………………………………………….…….. 346

7-37 Isotope ratios of sixteen SCV gases superimposed on the mudgas isotopic depth profile from Petrovera 10-17-47-27W3.
Legend for SCV gases is provided in Figure 7-38…………………...……. 347

7-38 SCV gases from Figure 7-37 and their presumable sources.
Petrovera 10-17-47-27W3………………………………………………… 348

7-39 Isotope ratios of thirteen SCV gases superimposed on the mudgas isotopic depth profile from Petrovera 112-/01-04-48-22W3.
Legend for SCV gases is provided in Figure 7-40……………………….. 349

7-40 SCV gases from Figure 7-39 and their presumable sources.
Petrovera 112-/01-04-48-22W3…………………………………………… 350

7-41 Isotope ratios of seventeen SCV gases superimposed on the mudgas isotopic depth profile from Petrovera 112-/01-04-48-22W3.
Legend for SCV gases is provided in Figure 7-42……………………….. 351

7-42 SCV gases from Figure 7-41 and their presumable sources.
Petrovera 112-/01-04-48-22W3………………………………… …….. 352

7-43 Isotope ratios of fourteen SCV gases superimposed on the mudgas isotopic depth profile from Husky A9-15- 51-23W3.
Legend for SCV gases is provided in Figure 7-44……………………… 353

7-44 SCV gases from Figure 7-43 and their presumable sources.
Petrovera 112-/01-04-48-22W3………………………………………….. 354

7-45 Base map showing the location of the carbon isotope mud gas depth profiles from the heavy oil region, and the presumable sources for the SCV gases in their vicinity. The most prevalent source is indicated with a yellow star beside………………………………………………………………………. 357

7-46 Frequency of presumable sources for the SCV gases in the vicinity of:
a) Lindbergh 13-9-56-6W4 well, and b) Petrovera 1d-25-55-5W4 well …..358

7-47 Frequency of presumable sources for the SCV gases in the vicinity of:
a) Husky A9-15-51-23W3 well, and b) Husky C3-30-47-4W4 well ……... 359

7-48 Frequency of presumable sources for the SCV gases in the vicinity of:
a) Petrovera 1-4-48-27W3 well, and b) Petrovera 10-17-47-27W3 well … 360

***

8-1 Locations of ten carbon isotope mud gas depth profiles in the WCSB …... 361

8-2 Schematic geological cross-section illustrating the relative positions of Ferrier, Gilby, Husky 3C-30, and Lindbergh 13A-9 profiles. Thermal maturity of the foreland basin strata in the study areas is represented after Bustin, 1991. Isolines represent vitrinite reflectance Romax%. The location of the line of cross section (A-A') is shown in Figure 8-1……………………………………………………………...… 363

8-3 Plots of: (a) Depth - $\delta^{13}C$ values for CH_4; (b) Depth – Wetness index profiles in the WCSB. The data used is derived from the four carbon isotope mudgas profiles plotted along the geological cross section from Figure 8-2. ………………………………………………………………… 365

8-4 Bernard diagram showing the distribution of mudgases from four isotopic mudgas profiles plotted along the geological cross section A-A' from Figure 8-1. Mixtures of bacterial and thermogenic gases appear to be developed in majority of the gases, with a strong migrational component for shallower gases: Paskapoo and Scollar, in the Ferrier profile………..… 367

8-5 Plot of wetness vs. methane $\delta^{13}C$ of the mud gas data of the four isotope depth profiles in Figure 8-2. ……………………………………………..…. 368

8-6 Plot of methane $\delta^{13}C$ vs. ethane $\delta^{13}C$ of the mud gas data of the four isotope depth profiles in Figure 8-2. Published data indicate that cogenetic gases have 5‰< (δ^{13}Cethane - δ^{13}C methane) < 18‰. Mixing with isotopically light bacteriogenic methane shifts gas compositions outside the cogenetic field in the direction shown by the arrow……………………………………… 370

8-7 Plot of ethane $\delta^{13}C$ vs. methane $\delta^{13}C$ of the mud gas data of the four isotope depth profiles in Figure 8-2. Two main clusters are shown: foothills-, and heavy oil gases. Position of the vitrinite reflectance curve for type II kerogen: after Faber (1987), and Whiticar (1990)……………..….. 371

8-8 C2/C3 versus C2/iC4 diagram showing the possible biodegradation of some of the Colorado hydrocarbon gases from the Lloydminster heavy oil area (after Prinzhofer, 2000) …………………………………… 373

8-9 Combination plot of $\delta^{13}C_{CO2}$ and $\delta^{13}C_{CH4}$ with isotope fractionation lines (Ec) for the Paskapoo Formation gases in the foothills area (after Whiticar, 1999). …………………………………………………… 374

8-10 Plot of ethane $\delta\ ^{13}C$ vs. propane $\delta\ ^{13}C$ of the mud gas data of the four isotope depth profiles in Figure 8-2. The maturity relation (red line) is taken from Faber (1987), and Whiticar (1990)…………………… …. 376

8-11 Plot of ethane $\delta\ ^{13}C$ vs. propane $\delta\ ^{13}C$ of the mud gas data of the four isotope depth profiles in Figure 8-2. Apart from Figure 8-9, here gases are grouped by stratigraphic unit (from oldest to youngest): Sub-Cretaceous (red symbols), Cretaceous Mannville (green symbols), Cretaceous Colorado (blue symbols), Cretaceous Lea Park (purple symbols), Cretaceous Belly River (dark yellow symbols), and Cretaceous-Tertiary Edmonton Gp to Paskapoo (yellow symbols). Two apparent maturity trends are shown: the red dashed line in the foothills area, and the green dashed line in the heavy oil area……………………………………………......... 377

8-12 Graph of ethane $\delta\ ^{13}C$ vs. propane $\delta\ ^{13}C$ for mudgas samples from the Lea Park-, Horseshoe Canyon-, Scollard, and Paskapoo formations – foothills region. Lea Park sediments are dominated by Type III organic matter ((Schröder-Adams et al., 1997), and Horseshoe Canyon – Paskapoo formations contain coal beds throughout. Maturity curves: after Berner and Faber (1996)………………………………………………… 378

8-13 Plot of propane concentration vs. propane $\delta\ ^{13}C$ of the mud gas data of the four isotope depth profiles in Figure 8-2. As in Figure 8-10, effects of maturation and oxidation are distinguished…………………………...… 380

8-14 Plot of ethane concentration vs. ethane $\delta\ ^{13}C$ of the mud gas data of the four isotope depth profiles in Figure 8-2. Arrows indicate maturation trends, and distribution of mixed gases (bacteriogenic and migrated)……. 381

8-15 Carbon isotopic difference between propane and ethane vs. that between ethane and methane for mudgas data of the four isotope depth profiles in Figure 8-2. Maturation arrows are based on the models of James (1983) (black arow), and Sundberg and Bennet (1983) (red arrow)…………….. 383

8-16 Plot of ethane $\delta^{13}C$ vs. Bernard parameter [C1/(C2+C3)] for the Colorado mudgases in Husky 3C-30-47-4W4 and Lindbergh 13A-9-56-6W5……. 384

8-17 Plot of ethane $\delta^{13}C$ vs. propane $\delta^{13}C$ of the Colorado Group mud gas data of the three isotope depth profiles in Figure 8-2. The maturity relation (red line) is taken from Faber (1987), and Whiticar (1990). The deviation of ethane isotopes in sediments above the Second White Specks Shale Fm. in the heavy oil region towards values that indicate an enrichment of ^{12}C can be explained by an admixture of near-surface bacterial ethane to "incipient" (low temperature thermogenic) gases. ……………………………………. 385

8-18 "C1-C2" diagram showing segregative migration among a) Lea Park gases, and b) Colorado gases from Ferrier, Gilby, and Husky – Lindbergh (after Prinzhofer and Pernaton, 1997)……………………………………… 388

8-19 "C1-C2" diagram showing two distinct clusters among Mannville mudgases from Gilby (foothills area), and Husky – Lindbergh (heavy oil area). After Prinzhofer and Pernaton, 1997……………………………………… 389

8-20 Variations in wetness, methane d13C, and ethane d13C in mudgases from the foothills region ……………………………………………………….. 392

8-21 SW to NE stratigraphic cross -section showing carbon isotope depth profiles from four wells across the two study areas in the Western Canada Sedimentary Basin. Datum is Sea Level. The stratigraphic units used in the study are correlated across the four wells. Each well includes isotope profiles for methane, ethane, propane; normal-, and isobutane are added for the two Lloydminster wells…………………………………………………….. 394

8-22 Lindbergh 13A-09-56-6W4 isotopic depth profile plotted together with: a) gas compartments identified using the multilog quantification approach; and b) the simplified litholog of the stratigraphic section, showing main sandstone bodies, siderite concretion , and shale-rich layers. Legend for key stratigraphic surfaces is same as in Figure 8-21 ……………………… 395

8-23 Carbon isotope depth profile for Pembina 11-04-49-11W5 plotted together with a simplified litholog of the stratigraphic section. The arrows on the left side of the profile represent gas compartment boundaries as resulted from the multilog quantification approach. Many inflections on the simplified lithologs appear at the same stratigraphic level as the effective barriers identified using the multilog quantification. The black arrows on the right side of the profile points towards some of the isotopic inflections most probably and most reliably related to physico-chemical contrasts at the shale/sand contacts. Suggested bentonite influence on the isotopic variations is represented with blue circles…………………………………………… 400

LIST OF APPENDICES

Appendix A: Photographs of cores (Plates 1-122) and their log signatures (Figures A-3 to A-40)

Page

Figure A-1 Location map of the Foothills region, showing the core control used in this study …………………………………………………………...……. 449

Figure A-2 Location of the cored well from the heavy - oil region, which penetrates the entire Mannville Group in the Lloydminster area ……… 450

Figure A-3 Core from the Belly River Formation (06-04-042-04W5/0 well) with accompanying wireline log signatures …………………………….…….. 451

Figure A-4 Core from the Lea Park - Belly River formations (02/06-09-046-09W5/0 well) with accompanying wireline log signatures …... 452

Figure A-5 Core from the Lea-Park - Belly River formations (08-02-043-05W5/0 well) with accompanying wireline log signatures …..…. 453

Figure A-6 Core from the Lea-Park - Belly River formations (09-10-044-09W5/0 Well) with accompanying wireline log signatures …….. 454

Figure A-7 Core from the Belly River formation (10-04-049-11W5/0 well) with accompanying wireline log signatures ……………………………..455

Figure A-8 Core from the Lea-Park - Belly River formations (14-28-042-04W5/0 well) with accompanying wireline log signatures …..….. 456

Figure A-9 Core from the Belly River formation (16-11-045-07W5/0 well) with accompanying wireline log signatures …………………...…….. 457

Figure A-10 Core from the Lea-Park - Belly River formations (08-25-042-05W5/0 well) with accompanying wireline log signatures …..….. 458

Figure A-11 Core from the Cardium Formation (02-33-047-07W5/0 well) with accompanying wireline log signatures …………………………..…. 459

Figure A-12 Core from the Cardium Formation (06-12-048-11W5/0 well) with accompanying wireline log signatures ……………………………. 460

Figure A-13 Core from the Cardium Formation (06-14-042-06W5/0 well) with accompanying wireline log signatures ………………...……….. 461

Figure A-14. Core from the Cardium Formation (06-26-048-11W5/0 well) with accompanying wireline log signatures …………………...….…. 461

Figure A-15. Core from the Cardium Formation (06-33-048-11W5/0 well) with accompanying wireline log signatures …………………………… 463

Figure A-16. Core from the Cardium Formation (09-32-043-07W5/0 well) with accompanying wireline log signatures …………………………..…. 464

Figure A-17. Core from the Cardium Formation (10-11-043-09W5/0 well) with accompanying wireline log signatures ……………………….…. 465

Figure A-18. Core from the Cardium Formation (10-14-044-09W5/0 well) with accompanying wireline log signatures ……………………………. 466

Figure A-19. Core from the Cardium Formation (10-16-042-09W5/0 well) with accompanying wireline log signatures ……………………..…………. 467

Figure A-20. Core from the Cardium Formation (10-23-043-09W5/0 well) with accompanying wireline log signatures …………………………… 468

Figure A-21. Core from the Cardium Formation (10-26-045-09W5/0 well) with accompanying wireline log signatures …………………………..…. 469

Figure A-22. Core from the Cardium Formation (11-30-045-09W5/0 well) with accompanying wireline log signatures ……………………………. 470

Figure A-23. Core from the Cardium Formation (12-03-042-09W5/0 well) with accompanying wireline log signatures ……………………………. 471
.

Figure A-24. Core from the Cardium Formation (14-01-042-07W5/0 well) with accompanying wireline log signatures ……………………….…… 472

Figure A-25. Core from the Cardium Formation (14-06-047-09W5/0 well) with accompanying wireline log signatures ………………………………….. 473

Figure A-26. Core from the Cardium Formation (16-16-047-10W5/0 well) with accompanying wireline log signatures ……………………….…… 474

Figure A-27. Core from the Colorado Group (06-22-042-09W5/0 well) with accompanying wireline log signatures …………………...…….. 475

Figure A-28. Core from the Cardium Formation (04-10-042-09W5/2 well) with accompanying wireline log signatures ……………………………. 476

Figure A-29. Core from the Belly River Formation (10-10-042-09W5/0 well) with accompanying wireline log signatures ……………………………. 477

Figure A-30. Core from the Viking Formation (06-12-045-07W5/0 well) with accompanying wireline log signatures ……………………………..…. 478

Figure A-31. Core from the Viking Formation (07-06-042-07W5/0 well) with accompanying wireline log signatures …………………...……….. 479

Figure A-32. Core from the Viking Formation (07-08-042-05W5/0 well) with accompanying wireline log signatures …………………………..… 480

Figure A-33. Core from the Viking Formation (08-11-042-07W5/0 well) with accompanying wireline log signatures ……………………………. 481

Figure A-34. Core from the Viking Formation (10-17-042-04W5/0 well) with accompanying wireline log signatures ……………………………. 482

Figure A-35. Core from the Viking Formation (03/13-13-045-05W5/0 well) with accompanying wireline log signatures ……………………………. 483

Figure A-36. Core from the Joli Fou – Mannville contact (03-13-043-05W5/0 well) with accompanying wireline log signatures ……… 484

Figure A-37. Core from the Joli Fou – Mannville contact (10-32-048-06W5/0 well) with accompanying wireline log signatures …..…. 485

Figure A-38. Core from the Joli Fou - Mannville contact (02/11-15-045-07W5/0 well) with accompanying wireline log signatures …... 486

Figure A-39. Core from the Joli Fou – Mannville contact (16-11-045-07W5/0 well) with accompanying wireline log signatures ……… 487

Figure A-40. Core from the Joli Fou – Mannville section (10-25-047-03W4/0 well) with accompanying wireline log signatures ……... 488

PLATES ……………………………………………………………… 490

Appendix B

Page

Appendix I

I-1 Along-dip regional well-log cross-section – Foothills region: Section 1-1’ ……… 735

I-2 Along-strike regional well-log cross-section – Foothills region: Section 2-2’ …....736

I-3 Along-dip regional well-log cross-section – Foothills region: Section 3-3’ ……… 737

I-4 Along-dip regional well-log cross-section – Foothills region: Section 4-4’ ……… 738

I-5 Along-strike regional well-log cross-section – Foothills region: Section 5-5’ …... 739

Appendix II

II-1 Along-dip regional well-log cross-section – Lloydminster region: Section 1-1’ 740

II-2 Along-dip regional well-log cross-section – Lloydminster region: Section 2-2’ …741

II-3 Along-dip regional well-log cross-section – Lloydminster region: Section 3-3’ …742

II-4 Along-dip regional well-log cross-section – Lloydminster region: Section 4-4’ …743

II-5 Along-strike regional well-log cross-section
- Lloydminster region: Section 5-5’ ……………………………………..……....744

II-6 Along-strike regional well-log cross-section
- Lloydminster region: Section 6-6’ ……………………………………..…………745

II-7 Along-strike regional well-log cross-section
- Lloydminster region: Section 7-7’ ……………………..……………………...… 746

II-8 Along-strike regional well-log cross-section
- Lloydminster region: Section 8-8’ ………………………… ………………….. 747

Appendix III

III-1 Composite diagram showing the compositional profile for Ferrier 14-3-42-9W5 together with data that result from the isotope ratio mass spectrometry ……………………………………………………………………..…748

III-2 Composite diagram showing the compositional profile for Gilby 15-16-42-4W5 together with data that result from the isotope ratio mass spectrometry …………………………………………………………………….….. 749

III-3 Composite diagram showing the compositional profile for Pembina

11-4-49-11W5 accompanied by data that result from the isotope ratio mass spectrometry 750
III-4 Composite diagram showing the compositional profile for Lindbergh 4C-16/13-09-56-6W4 together with data that result from the isotope ratio mass spectrometry 751
III-5 Composite diagram showing the compositional profile for Petrovera 1D-25-55-5W4 together with data that result from the isotope ratio mass spectrometry 752
III-6 Composite diagram showing the compositional profile for Husky C3-30-47-4W4 together with data that result from the isotope ratio mass spectrometry 753
III-7 Composite diagram showing the compositional profile for Husky A9-15-51-23W5 together with data that result from the isotope ratio mass spectrometry 754

CHAPTER ONE
INTRODUCTION

1.1. Background

Natural gases are omnipresent elements of sedimentary basins, being ubiquitously detected in the subsurface either as traces, or as accumulations in oil and gas reservoirs. Generated throughout the entire organic maturation process, these gases consist predominantly of methane, with lesser concentrations of higher alkanes and nonhydrocarbon species including carbon dioxide (CO_2), nitrogen (N_2), hydrogen sulfide (H_2S), and helium (He). Natural gases are significant target of hydrocarbon exploration activity owing both to their inherent value as fuels and chemical raw materials, as well as their common occurrence with petroleum. Being considerably more mobile than petroleum hydrocarbon fractions, natural gas occurrences may also be indicative of nearby oil and condensate accumulations (Reitsema et al., 1980). Geochemical methods have been successfully employed in oil-oil and oil-rock correlations. The most reliable correlation approaches have combined compositional and isotopic measurements of refractory biomarker fractions in both oils and sedimentary organic matter to establish a genetic link between them (Schoell et al., 1992; Murray et al., 1994; Schoell et al., 1994).

In comparison with bitumen and oils, natural gases contain fewer components and therefore have a smaller chemical diversity contrast, no analogous compositional and isotopic approach existing for gas-gas and/or gas –source correlations. Owing to both the mobility and reactivity of natural gas constituents, correlation of reservoired gases with possible source rocks is inherently more difficult, but not impossible (James, 1983). However, the molecular and isotopic composition of natural gases is sufficiently large in range, relatively specific and predictable to provide diagnostic information on their origin and history (Whiticar, 1994). A variety of geochemical tools and techniques are available to the scientist to characterize them. In many cases, the combination of gas concentration and molecular and isotopic compositions can help to ascertain the kerogen type or thermal maturity of the source rock from which the natural gas was derived. Gas can be effectively correlated with other gases, oils, and their source rocks. The ability to carry out gas-gas correlations allows mapping the suite of hydrocarbons that can be related back to a site of active source rock using gas-source correlations (James, 1983, 1990; Whiticar, 1994).

Dominated by a few low-molecular weight gaseous hydrocarbons, natural gas is compositionally and isotopically simple. As a result of limited molecular complexity, important genetic and post-genetic information is commonly obtained from stable carbon isotope compositions. Stable carbon isotope ratios in hydrocarbon gases provide a fingerprint technique, which can be used to assess the nature and thermal maturity of potential source beds, the pathways by which gas migration occurred, and the presence of mixed-source gases.

Combining gas geochemistry and stable isotope measurements on the $C_1 - C_4$ hydrocarbons allows a better characterization of such parameters as indices of maturity, type of source (primary versus secondary cracking), efficiency of hydrocarbon accumulations, and traces of bacterial alteration.

Until the last decade, genetic models for natural gases were based primarily on field data collected for different gas types. These includes shallow, low-temperature bacterial gases (Claypool and Kaplan, 1974; Schoell, 1977; Jenden and Kaplan, 1986; Coleman et al., 1988; Rice, 1992), higher temperature thermogenic gases, often associated with oil (Galimov et al., 1970; Stahl and Carey, 1975; Schoell, 1980; Jenden and Kaplan, 1989), and coalbed and shale-hosted gases (Colombo et al., 1970; Smith et al., 1985; Rice, 1993; Martini et al., 1996; Rowe and Muehlenbachs, 1999). Papers attempting to synthesize this knowledge (Stahl, 1977; Bernard, 1978; Schoell, 1983; James, 1983; Whiticar et al., 1986; Chung et al., 1988; Schoell, 1988) still provide the backbone of most natural gas interpretations carried out in the oil and gas industry. These models and empirical schemes are not without problems, however. Models developed for one type of gases or for one type of basin often do not work for another, some schemes are contradictory (Jenden et al., 1988; Lorant et al., 1998; James, 1983; Prinzhofer et al., 2000b), and a given data set may give rise to very different interpretations, particularly when post-generative processes such as diffusive fractionation are invoked (Jenden et al., 1993; Prinzhofer and Huc, 1995; Prinzhofer and Pernaton, 1997).

1.2. Mudgas isotope analysis while drilling

Isotope analysis can be performed on mudgases that are collected in the mud-logging unit during drilling of a well. A *mudgas carbon isotope depth profile* represent carbon isotope analyses of gases (containing light hydrocarbon gases - C_1, C_2, C_3, C_4, C_5 – and other gases), extracted from drilling muds during drilling of a new well.

The recent development of *continuous flow/gas chromatograph/isotope ratio mass spectrometry* (CF/GC/IRMS) technique has lowered sample size requirements by several orders of magnitude and enabled the analysis of trace amounts of higher hydrocarbon homologues recovered from drilling fluids. Results are reliable for concentrations of C_{2+} components in the order of 100 parts per million (ppm) and in some cases as low as a few parts per million (ppm). Enabling carbon isotopic analyses of traces of higher hydrocarbon homologues in very dry gases, this new technique proved to be ideally suited for the isotopic study of in situ hydrocarbon gases from mud-loggers of oil and gas wells.

The gases retained within the drilling muds are analyzed for $^{13}C/^{12}C$ composition. Stable isotopic fractionations are measured relative to a standard. In the case of carbon the standard is a fossil belemnite from Pee Dee Formation in South Carolina (the PDB standard). Isotopic fractionations are normally small and so values are measured in parts per thousand (‰) and expressed as $\delta^{13}C$ values as follows:

$$\delta^{13}C ‰ = [(^{13}C/^{12}C\text{sample} - {}^{13}C/^{12}C\text{standard}) / (^{13}C/^{12}C\text{standard})] * 1000$$

These values are used then to create carbon isotopic depth profiles or mudlogs (Figure 1-1). Depths for each gas sample are calculated accounting for the lag time explained below. Carbon isotope ratios for C_1, C_2, C_3 and n-C_4 of each gas sample (expressed in delta notation) are plotted against the depth of each sample to create the carbon isotope mud gas depth profile shown in Figure 1-1. Each horizontal set of squares (C1), circles (C2) and triangles (C3) represents analyses from one gas sample.

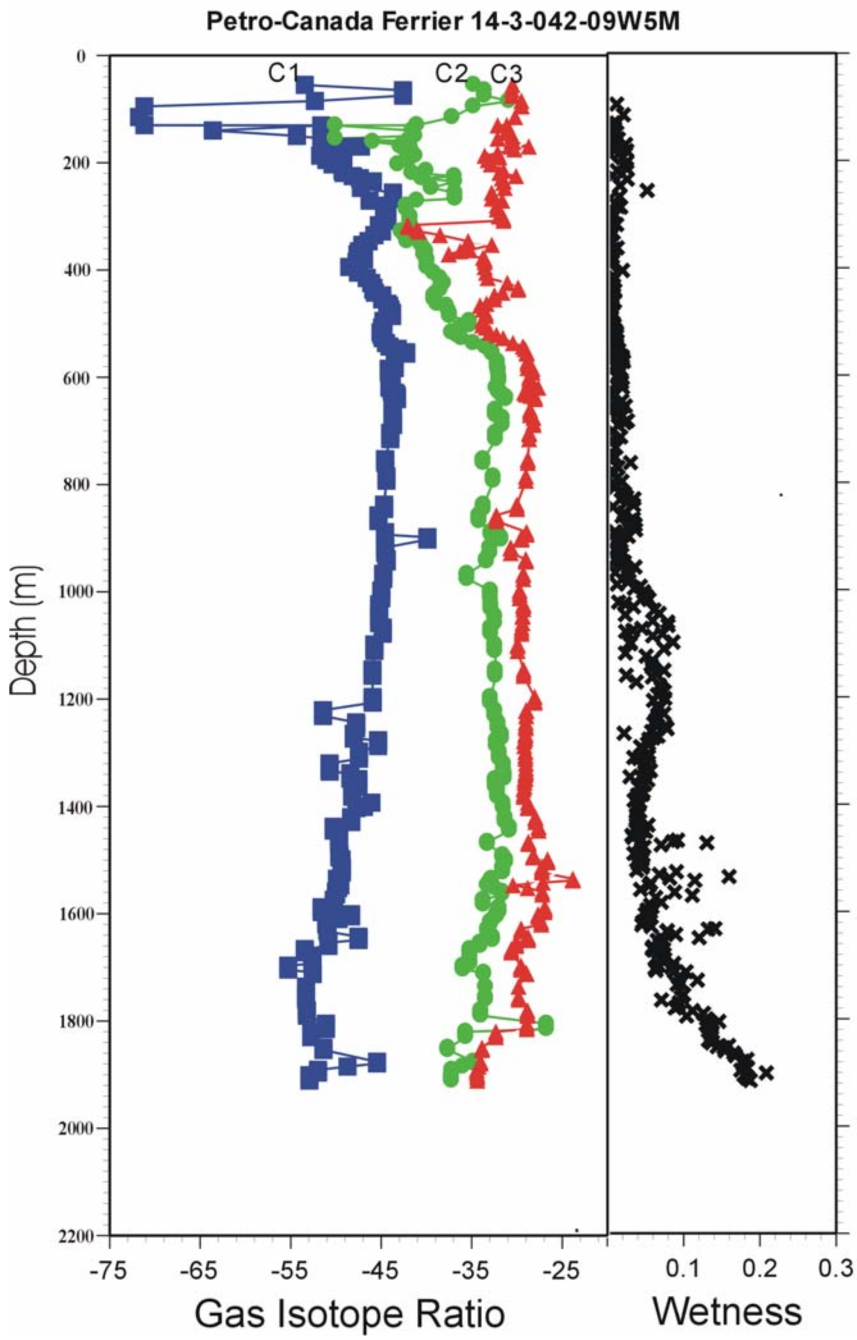

Figure 1-1 Carbon isotopic mud gas depth profile

Natural gas hydrocarbons are all enriched in the light isotopes (^{12}C) relative to the standard and so have negative δ values. Because δ values can be negative, such terms as isotopically more negative, isotopically more positive, isotopically heavier, isotopically lighter, heavy isotopic composition, light isotopic composition, and so on are commonly used. These all are used to describe a relative situation pertaining to the amount of heavy isotope in a sample. Isotopically more positive or more negative describe which δ values (or group of δ values) represent samples that have more or less of the heavy isotope, respectively. When comparing the isotopic compositions of samples, the terms *lighter* or *heavier* indicate relative enrichment in the light or heavy isotope respectively, and are equivalent to isotopically more negative or isotopically more positive.

More negative values (to the left on the graph in Figure 1-1) indicate more ^{12}C; more positive values indicate an increase in ^{13}C. Since ^{12}C bonds are broken more easily than ^{13}C bonds, the general maturation trend is toward increasing ^{13}C, i.e. carbon isotope ratios move towards the right on the graph. So for a simple situation of gases increasing in maturity as depth increases, there should be a gentle slope towards the right. Small portions of the curves have this trend, but the situation is much more complicated and surprisingly complex (as can be seen in Figure 1-1).

1.3. Reasoning and objectives of the study

Canada is one of the world's largest natural gas producers and exporter in the world, with the vast majority of it coming from the Western Canada Sedimentary Basin (WCSB). The WCSB is estimated to have 424 trillion cubic feet (12,000 km^3) of resource base remaining (discovered and undiscovered), which represents about two thirds of Canadian gas reserves (Natural Resources Canada – Energy Sector, 2009 report). In January 2009 *Oil and Gas Journal* (OGJ) reported that Canada had 57.9 trillion cubic feet (Tcf) of proven natural gas reserves.

The Western Canada Sedimentary Basin will likely continue to be the main gas supply area in Canada for many years, new gas reserves in the WCSB likely coming from unconventional sources. Natural gas is pervasive throughout the WCSB at all stratigraphic levels, but published work concerning its origins, maturity, migration and alteration is limited. Despite prolific gas reservoirs, and over a century of interest in their exploration and exploitation [since the 1883 Langevin Siding (now Alderson) discovery in Alberta], little attempt has been made to establish the source and migration-induced factors controlling gas composition and distribution in the subsurface.

One of the biggest advantages of carbon isotope mud gas depth profiles is that they provide essentially continuous gas samples from the surface down to the total well depth, through potential production horizons and the intervening shales, silts and coals. One can therefore look at the variation of gases within a reservoir, across the overlying and underlying potential seal rocks (which may also be gas sources) and into the next successive reservoir rocks. With this information we can observe sharp transitions in isotopic ratios at some formation boundaries (effective seals/baffles), no change in isotope ratios across other formation boundaries (ineffective seals/baffles), or mixing trends of carbon isotope ratios across a seal (partially effective seal/baffle). Within each gas package (including those separated by seals and those within the seals themselves) we can gain information about the source, maturation, alteration, and mixing of gases. By looking at the results from the entire stratigraphic section one can make general inferences about the regional gas dynamics.

The existing stable carbon isotope ratios ($\delta^{13}C$) of the various production gases (light hydrocarbons) are quite variable across the Western Canada Sedimentary Basin (WCSB). Also, at any given place where a new oil and gas well is drilled, one will detect large isotopic differences with depth in the gases recovered from drilling mud, the so-called mudgases [Rowe and Muehlenbachs, 1999(a); Rowe and Muehlenbachs, 1999(b); Tilley and Muehlenbachs, 2006].

The isotope ratios in the mud gas depth profiles do not generally increase monotonically with depth. In only a few profiles is the gas isotope signal smoothly varying. In most cases various inflections and shifts of isotope ratio with depth are observed (Figure 1-2). These isotopic differences are marked and have been largely exploited to fingerprint problem gases leaking into the environment (Rowe and Muehlenbachs, 1999b).

The cause of much of this variation in gas carbon isotope values can be understood in terms of known geochemical source, as well as processes accompanying gas biogenesis, thermogenesis, and catagenesis. Also revealed in the isotopic signal is bioalteration of the gas as seen in the heavy oil fields (Rowe and Muehlenbachs, 1999b). This knowledge in itself does not explain the isotopic complexity observed in both the production and mudlog gases. Therefore, the principal motivation for undertaking this

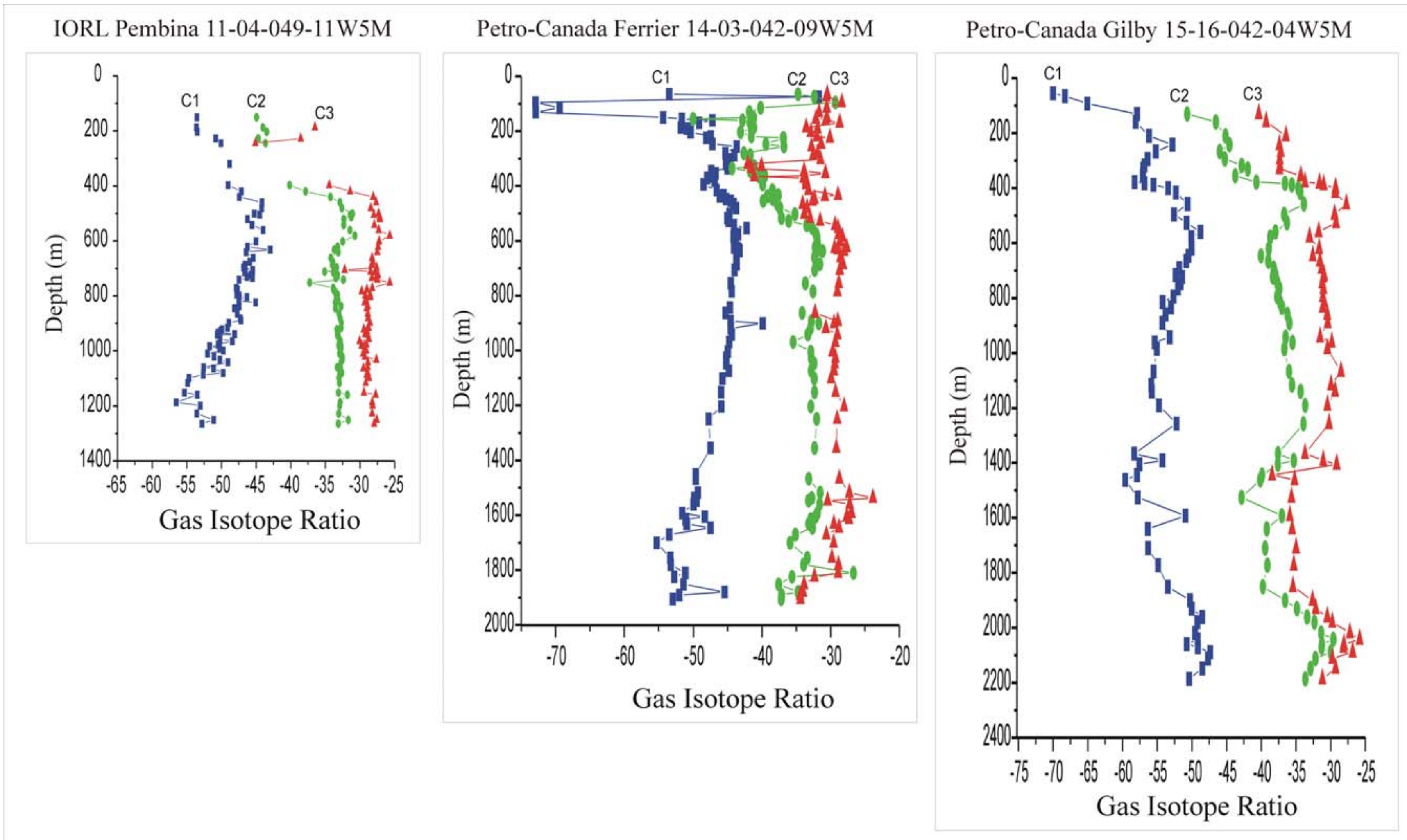

Figure 1-2 Carbon isotopic composition and wetness of gases from three mudlogs in west-central Alberta. Note: the isotope profiles for butane are not displayed in this figure for simplicity reasons.

project was the need for a better understanding of the isotopic complexity observed in mud log gases. The question was simple: What causes isotopic variations in light hydrocarbon gases dissolved in drilling mud? The answer, as it will be shown, is complicated.

As already mentioned, the present thesis focuses not only on assessing the degree of correlation between gas isotope geochemistry and stratigraphy in the Western Canada Sedimentary Basin (foothills and heavy oil regions in Alberta and Saskatchewan), but also concentrates on the evaluation of the gas compartments and migration pathways, as it can be inferred from the isotopic depth profiles.

Therefore, another goal of the present study was to find if the observed isotopic gas stratification in the mudlogs is controlled by major sequence stratigraphic boundaries and determine if these surfaces correlate regionally existing gas isotope mudlogs (with implications in reservoir compartmentalization, effectiveness of regional seals, and gas dynamics).

By taking an in-depth characterization of the carbon isotope and molecular compositions of mud gases, the purpose of this thesis is to contribute as well to a better understanding of the origin, maturity, mixing, alteration, and migration of gases in WCSB, and to show that consideration of the carbon isotope depth profiles by themselves can contribute significantly to the geological understanding of a region, and therefore, that carbon isotope depth profiles can be extremely valuable geological tools, particularly for evaluating the effectiveness of potential seal rocks.

The study also concentrates on the effects of migration from one field to another and/or within the same formation on the stable isotopic signature of migrating gases. A better understanding of the processes that affect the carbon stable isotopic composition of migrating gases would enable us to trace their sources in different geological settings. Integrated with lithofacial-, and hydrogeological information, the isotopic and molecular compositions of mudgases will help us also to better understand the formation of hydrodynamic and possibly physical barriers, as well as the relationship between the flow of formation water and gas migration within the study areas. Thus, results from this study are of interest to both the public and the oil and gas industry in western Canada.

Finally, it is the objective of this thesis to show that an accurate understanding of both regional and local geological pictures has a definite interdisciplinary nature, and should involve a complex integration of geoscience's disciplines.

1.4. Study areas

This study was conducted within two different regions located within the Western Canada Sedimentary Basin: foothills region (Pembina – Gilby – Ferrier area) and heavy oil region (Lloydminster area).

The first study area in the Western Canada Sedimentary Basin (WCSB) is located in west-central Alberta, 130 km southwest from Edmonton (or ~ 65 Km northwest from Red Deer), close to the approximate limit of Foothills deformation (Figure 1-3).

The second study area is confined to an area of approximately 12,000 km^2 in the Interior Plains of east-central Alberta and west-central Saskatchewan, approximately centered on the border town of Lloydminster in Twp. 50 (Figure 1-5). Both study areas were defined on the basis of isotopic fingerprints locations (small black dots in Figure 1-3). A total of ten carbon isotope mud gas depth profiles were used in the present study.

Figure 1-4 shows the detailed locations of the three carbon isotope mud gas depth profiles in west-central Alberta, Canada, while Figure 1-5 shows the detailed locations of the seven carbon isotope mud gas depth profiles in the heavy oil region of east-central Alberta and west-central Saskatchewan. In the foothills area the three isotope depth profiles are from wells at Ferrier, Pembina, and Gilby fields. The Lower Cretaceous in the Ferrier well is within the active gas generation zone. The other two lie within the present oil window for the Lower Cretaceous sediments. In the heavy-oil area, all of the seven isotope depth profiles lie outside the oil window for the Lower Cretaceous sediments. Figure 1-6 synthesizes the data availability map, showing the location of the ten carbon isotope depth profiles, the well log cross-section locations used to build the sequence stratigraphic framework, and the control core data represented by the yellow stars.

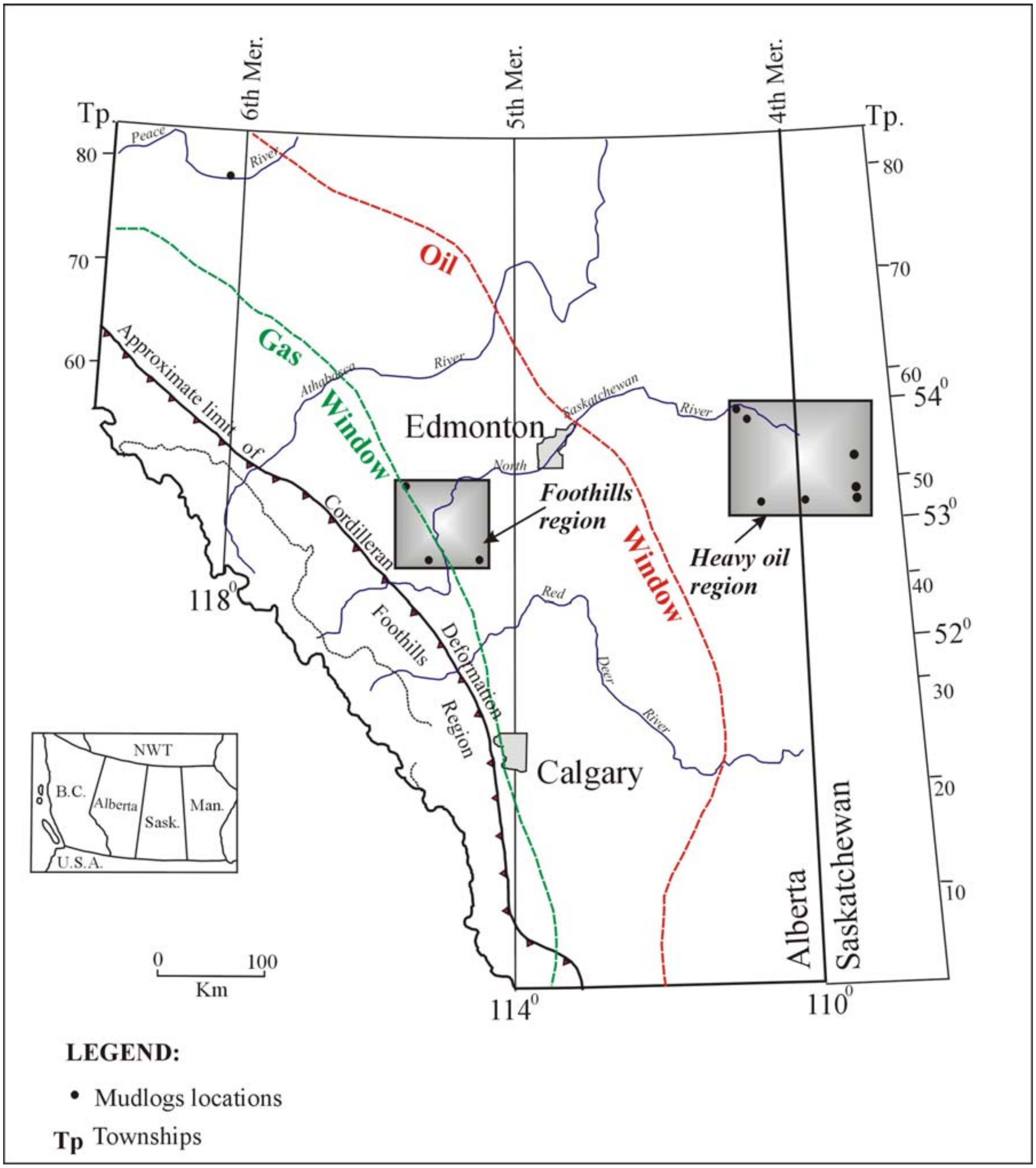

Figure 1-3 Sketch map with study areas locations in west-central Alberta and Lloydminster region.

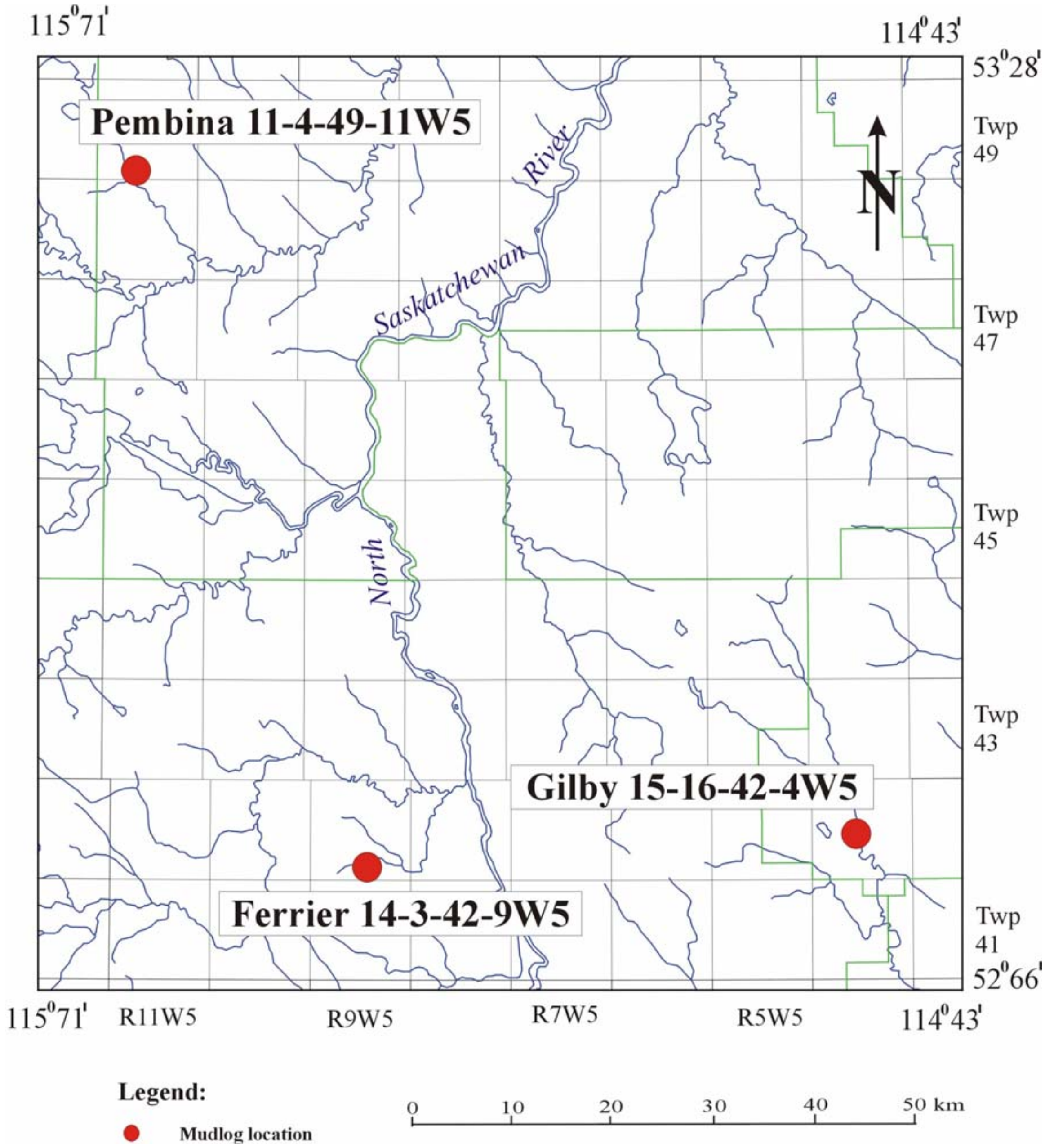

Figure 1-4 Locations of the carbon isotope mud gas depth profiles from the Foothills region, west-central Alberta

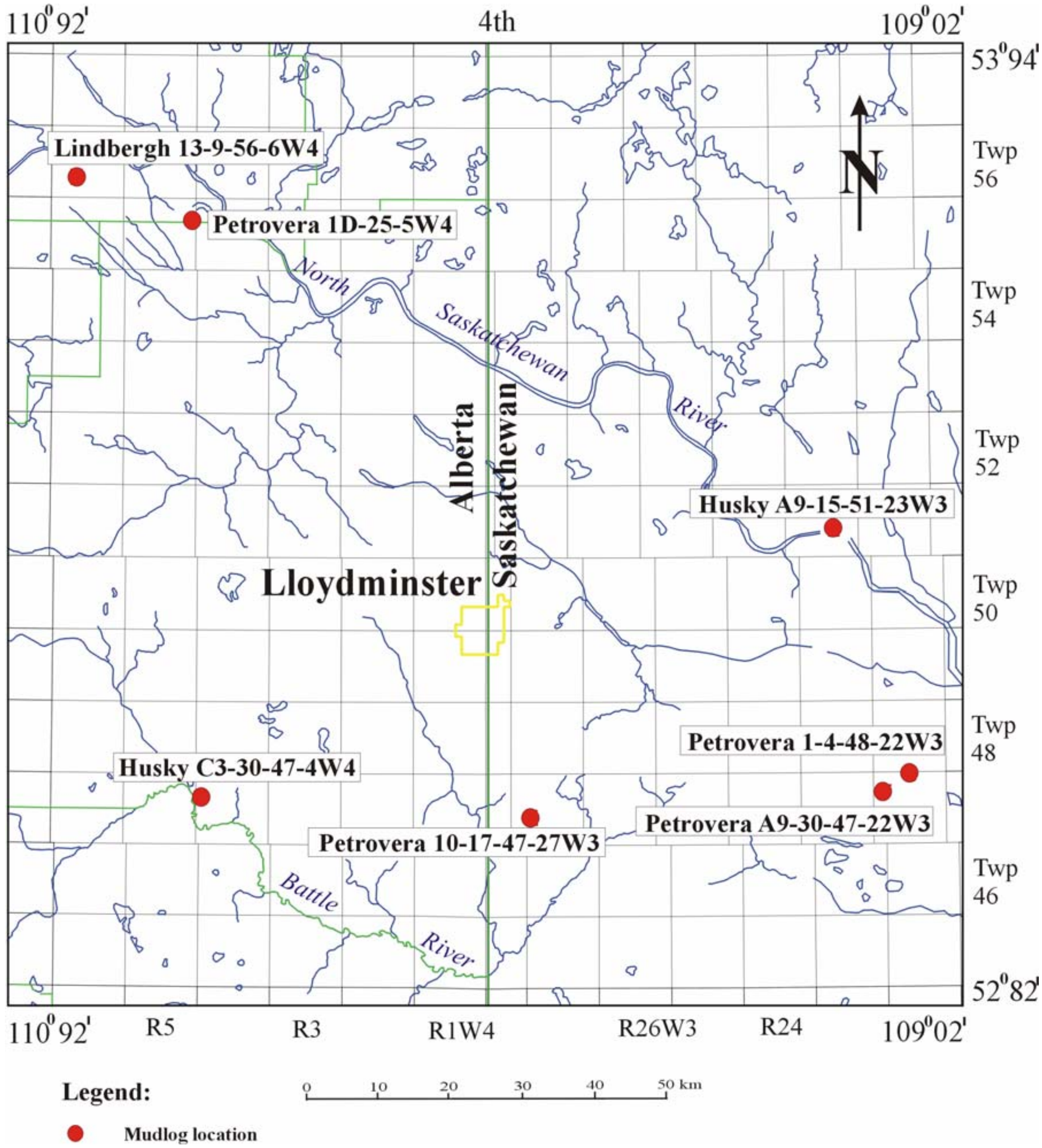

Figure 1-5 Locations of the carbon isotope mud gas depth profiles from the heavy oil region, east-central Alberta and west-central Saskatchewan.

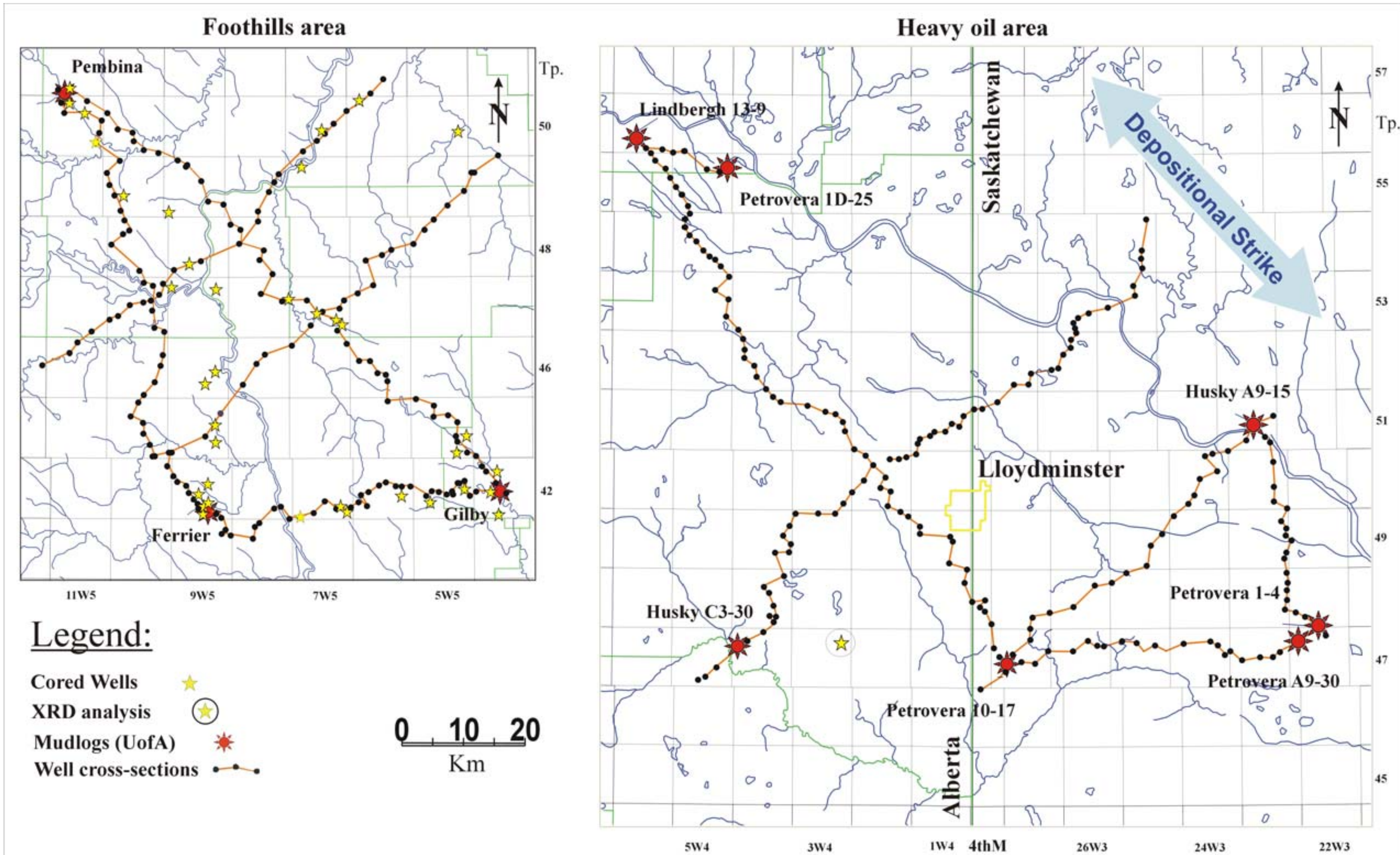

Figure 1-6 Data availability map, showing the location of the ten carbon isotope depth profiles, the well log cross-section locations used to build the sequence stratigraphic framework, and the control core data represented by yellow stars.

1.5. Previous work

Previous studies of the carbon isotope composition of natural gases (James, 1983; James and Burns, 1984; Chung et al., 1988; James 1990; Jenden et al., 1993) have relied on broad scale sampling of production gases, thereby limiting information about the origin, alteration, and migration of gases to the production horizons. Carbon isotope analyses of gases extracted from drilling muds during the drilling of a new well (carbon isotope mud gas depth profiles) provide a unique view of the variation of gases throughout a stratigraphic section at one well location. The advantage of carbon isotope mud gas depth profiles is that they provide essentially continuous gas samples from the surface down to the total well depth, through production horizons and the intervening shales, silts and coals. One can therefore look at the variation of gases within a reservoir, across the overlying and underlying potential barrier or seal rocks (which may also be gas sources) and into the next successive reservoir rocks. Within each gas package (including those separated by seals and those within the seals themselves) one can gain information about the source, maturation, and alteration (bacterial contamination and/or mixing) of gases. By looking at the results from the entire stratigraphic section one can make general inferences about the regional gas dynamics, migration mechanisms and pathways, and the effectiveness of potential seal rocks (Jenden et al., 1993).

This study represents part of an ongoing environmental project that uses the isotopic profiles as templates to fingerprint the source depths of gases that leak to surface (Rowe and Muehlenbachs, 1999b). The original technique for the identification of surface casing vent (SCV) gas sources was developed at the University of Alberta (Rich, 1995; Rowe, 1998). This technique is based upon a correlation between the carbon stable isotopic compositions of leaking natural gas and mud gases collected during drilling close to the leaky wells (Rowe and Muehlenbachs, 1999b). The technique involves an automated procedure for separating natural gas constituents (e.g. methane - CH_4, ethane - C_2H_6; propane - C_3H_8, butane – C_4H_{10}, and carbon dioxide - CO_2) by a gas chromatography followed by an oxidation of hydrocarbons to CO_2, and their subsequent analysis in a mass spectrometer (for more details see Rowe, 1998).

Isotopic studies of leaking gas have demonstrated the following:

- SCV gases are mostly thermogenic gases sourced in formations located at much shallower depths than the production horizons (Rowe, 1998).
- Some of the SCV gases are extremely immature – a discovery which has extended substantially the known lower temperature limits of thermogenic gas generation (e.g. < 60°C) and has cast a doubt on models which imply that high-temperature kinetic reactions are the sole pathway to hydrocarbon generation (Rowe and Muehlenbachs, 1999a).
- It was also found that the stable isotopic composition of methane is often non-diagnostic to the origin of leaking gas due to a possible mixing with bacterial methane (Rowe, 1998). Instead, carbon stable isotopic ratios of C_2+ components were found to be useful for correlating SCV gases.

The implementation of stable isotope analysis for identifying gas leak sources has dramatically improved SCV flow remediation in Alberta and Saskatchewan (Rowe and Muehlenbachs, 1999b). Attempts to determine the sources of migrating soil gases by correlating their carbon stable isotopic compositions with these of mud gas profiles have been successful in only a handful of cases, however. In addition, the interpretation of the stable isotopic composition of migrating natural gas in areas where steam or fire flooding has been used for heavy oil recovery has also proved challenging (Rowe, 1998). Problems with the interpretation of the stable isotopic results in the above mentioned cases have been attributed to alteration of carbon stable isotope composition of soil gases subjected to bio-mediated oxidation, which in steamed areas have most likely been augmented by thermal pollution.

Isotopic fingerprints techniques were subsequently applied to natural gas seeps and gas occurrences across Alberta in combination with an evaluation of the regional petroleum hydrogeology to determine the origin of the hydrocarbons (Letourneau et al., 2002).

Beside their applications in assessing the origin of natural gas deposits and to fingerprint shallow gases for remediation of leaking gas wells, the detailed carbon isotope mud profiles led to studies of compartmentalization of gas reservoirs on both local and more regional scales. The carbon stable isotopic ratios of mud gases have successfully been applied as tool for correlating gas-charged sedimentary horizons throughout west-central Alberta (Tilley et al., 2001), and more recently carbon isotope and molecular compositions of Mississippian to Upper Cretaceous mud gases have been examined from four isotope depth profiles and correlated across the Western Canada Sedimentary Basin in several different tectonic settings to provide insights into gas maturity and alteration trends (Tilley and Muehlenbachs K., 2006).

Carbon stable carbon isotopic analyses in central WCSB showed that individual geological formations may have related gases with unique and distinguishing signatures, and that Colorado Group contain low-temperature thermogenic gases (Rowe and Muehlenbachs, 1999a).

1.5. Methods

There are at least four main factors, which may lead to the complex trend and to variable gas proportions and isotopic compositions (Galimov, 1973; Schoell, 1983):

- the degree of maturity of the source rocks;
- kerogen type (genetic potential of the source rock);
- migration pathways of the individual hydrocarbon gases;
- biodegradation and mixing.

Information on the maturities of source rocks, mixing and biodegradation effects can be deduced from the chemical analyses of the gases. The other two factors are strongly dependent on geological factors, and information about them can only be deduced using a multidisciplinary approach, as consequently was undertaken in this study. Therefore, the interpretation derived from the geochemical analyses of mudgases is integrated within a sequence stratigraphic framework, with the wireline logs quantifications and petrophysical approach, and the regional flow of formation waters (Figure 1-7).

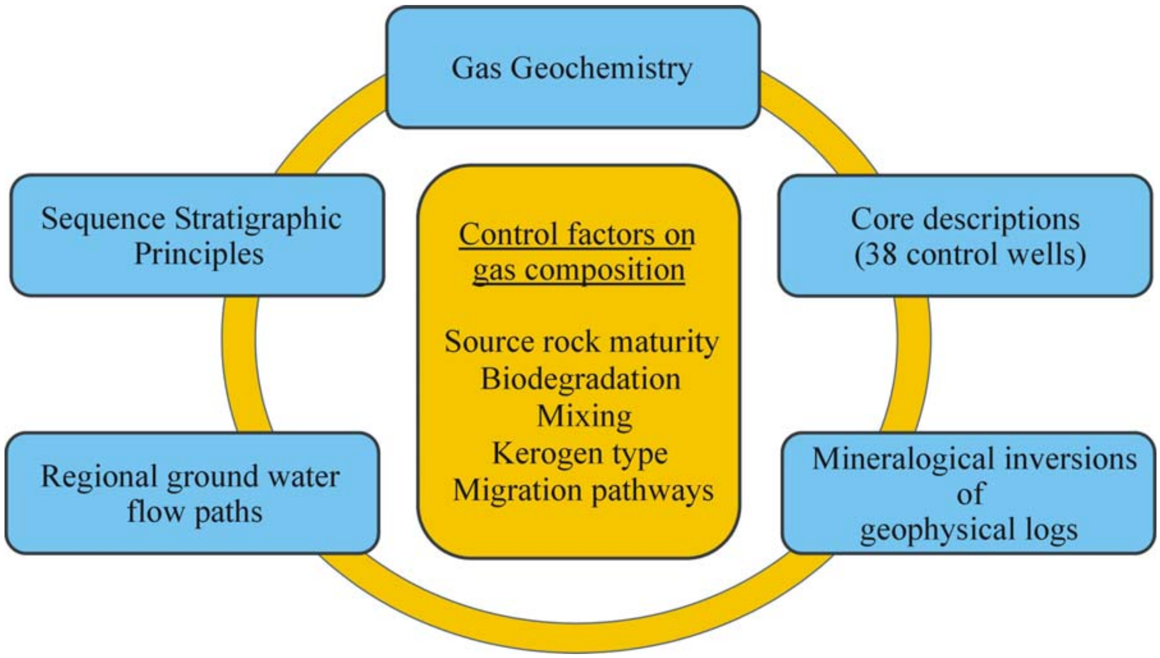

Figure 1-7 Sketch diagram showing the integrated methodology applicable throughout the present study

1.5.1. Sequence stratigraphic framework

Chapter Two of the thesis considers the well-log correlations throughout the entire foreland basin succession, in order to provide “significant” stratigraphic horizons and sedimentological trends that will lead to standard interpretation of mud gas isotope data. Sequence stratigraphic principles applied to geochemical data in Chapter three better explain the mudgas signatures in relationship with significant sequence stratigraphic surfaces.

The sedimentologic and stratigraphic analysis of the Western Canada Cretaceous stratigraphic section is based primarily on regional well-log cross-sections, core control, and basin-wide interpretations from literature. Correlations between sections were accomplished by matching significant stratigraphic surfaces: subaerial unconformities, maximum flooding surfaces, ravinement surfaces, maximum regressive surfaces. The type section shown in Figure 1-8 link the foothills with the heavy oil area through a well situated at the Holmberg field. The section consists essentially from Cretaceous-Tertiary

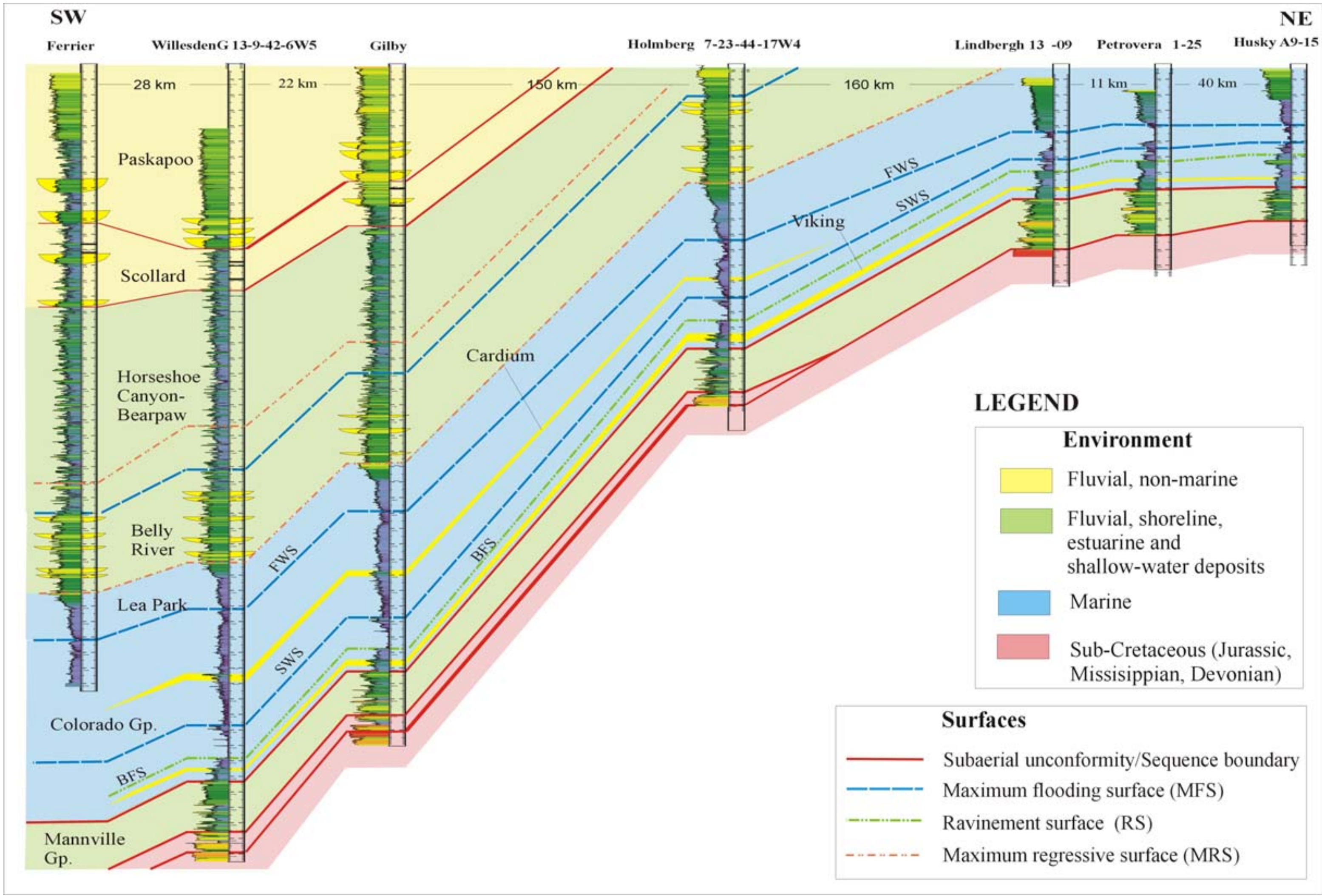

Figure 1-8 Schematic geological cross-section illustrating the simplified sequence stratigraphic framework within the study areas, showing the main depositional environments, and key stratigraphic boundaries.

strata underlain by Sub-Cretaceous sediments, and is divided into several depositional successions. The Mannville Group, the depositional response to the Columbian orogeny, consists of fluvial and estuarine valley-fill sediments, and sheet sands and shales deposited by repeated marine transgressive-regressive events. The Colorado Group was deposited during a quiet period in tectonic plate convergence when the basin was subject to a widespread marine transgression. Colorado strata consist predominantly of thick shales that form aquitards, within which there are isolated, thin, sandy units that form aquifers. Some of the sandstones, like the Viking and Cardium formations, are laterally extensive.

Post Colorado Cretaceous–Tertiary in the foothills area comprises a succession of terrigenous clastics divided from the base upward into the following: the Belly River Formation, the Bearpaw Formation, the Edmonton Group, the Scollard Formation, which includes the Ardley Coal Zone (ACZ) and the Paskapoo Formation. The succession is characterized by a complex depositional history within a largely fluvial setting. The entire post-Colorado stratigraphic section comprises mostly nearshore and continental deposits – an alternation of shales, silts, sandstones, conglomerates, and coals. The presence of coals within the Belly River, Horseshoe Canyon and Scollard formations is considered to be important in controlling the compositional changes observed in shallow mudgases.

1.5.2. Geochemical interpretation of mudgas data

Chapter Four of the thesis considers mudgases, their origin, occurrences, and history (relative migration, postsourcing alteration, mixed sources). The main goals of the geochemical analysis are:

- classify mud gases (genetic classification of mudgases);
- estimate maturity levels;
- identify gas source rocks types;
- assess biodegradation;
- investigate mixing/migration possibilities.

As a basis for geochemical interpretation, this study used several geochemical models that have been constructed based on experiments and observations. The approach particularly follows the models described by Schoell (1983), James (1983), Chung et al. (1988), Whiticar (1990, 1994), Berner and Faber (1996), and Prinzhofer and Pernaton (1997).

1.5.3. Multilog quantification and mineralogical inversions

Chapter Five provides an in-depth study of the gas compartments, and the nature of the boundaries that separate them. To assess the degree of compartmentalization throughout a stratigraphic section at one well location, the approach resumed looking essentially at interrelationships between isotopic fingerprints and information derived from geophysical wireline quantification. The wireline data (gamma-ray, sonic, density, litho-density, photoelectric factor, and neutron porosity logs) have been used to derive mineral fractions and porosity, using methods outlined by Doveton (1994) and Hearst and Nelson (1985). The methodology included a very close and detailed inspection of every gas sample along every profile. The isotopic gas signatures, their molecular composition, in addition to their post-generation history of migration and alteration were integrated with the compositional profiles calculated with matrix algebra solution. The result is the identification of several gas packages, with distinct isotopic and molecular composition, and with distinctive biodegradation and/or mixing signatures.

1.5.4. Regional hydrogeology – gas geochemistry

Chapter Six turns attention to the hydrogeological aspects, and discusses the combination of regional hydrogeology and isotope geochemistry in order to outline lateral migration pathways for mudgases. The essence of the chapter is an attempted correlation, by visual assessment, of regional trends of changes in geochemical parameters of natural gases, on the one hand, with regional directions of groundwater flow paths, on the other hand. The approach resumed by considering two major assumptions, several geochemical parameters indicating the direction of natural gas migration, and basin scale flow models. The assumptions state that:

- the molecular compositions of natural gases as well as the isotope ratios in the hydrocarbons seem to be controlled by the process of lateral migration;
- methane content distribution suggests a linkage to other processes (such as groundwater recharge) that might affect the total composition of the gas.

According with some authors, (Stahl, 1977; Shamsuddin and Khan, 1991; Leythaeuser et al., 1983; Prinzhofer et al., 2000) there are several *geochemical parameters* indicating the direction of natural gas migration. The distance of migration would be negatively correlated with $\delta^{13}C_1$, volume % C2+, wetness index, and C2/C1, and positively correlated with volume % C1 and ($\delta^{13}C_2$ - $\delta^{13}C_1$) values. In other words, methane $\delta^{13}C$, C2+, C2/C1 ratio and the wetness index all decrease – indicating the migration directions and pathways. The methane concentration and the isotopic difference between methane $\delta^{13}C$ and ethane $\delta^{13}C$, on the other hand, increase away from the presumed source.

The contribution of this study is therefore the interpretation of basin-scale gas geochemistry within a sequence stratigraphic framework - interpretation enhanced by innovative methodology combining geochemical-, and stratigraphic data with mineralogical inversions as derived from wireline logs. This integrated approach can potentially be developed into a new methodology for regional-scale geological characterization

1.6. Sampling and measuring of carbon isotope ratios

Each mud gas depth profile consists of over 150 carbon isotope analyses and over 175 compositional analyses. Gas samples, taken at more or less frequent intervals (< 5m to >30m), encompass the depth range of < 50m to 650 meters in the Heavy oil area and 55 to 2185 meters in the Foothills area, and include Upper Cretaceous through Mississippian sequences (Foothills region) and through Devonian strata (Heavy oil region).

Gas samples were collected during drilling from a commercial online mudlogging unit at the well site. As the drilling fluid/cuttings mixture returned to the surface through the annulus surrounding the drill pipe, it was degassed and entered the mud logging unit (Figure 1-9). After the gas had passed through a gas detector, a sample was withdrawn using a syringe and then injected into a glass or plastic sealed bottle. Sample depths were calculated as a function of the time required for the mud to travel from the bit to the sampling point, the bit depth and the circulation rate.

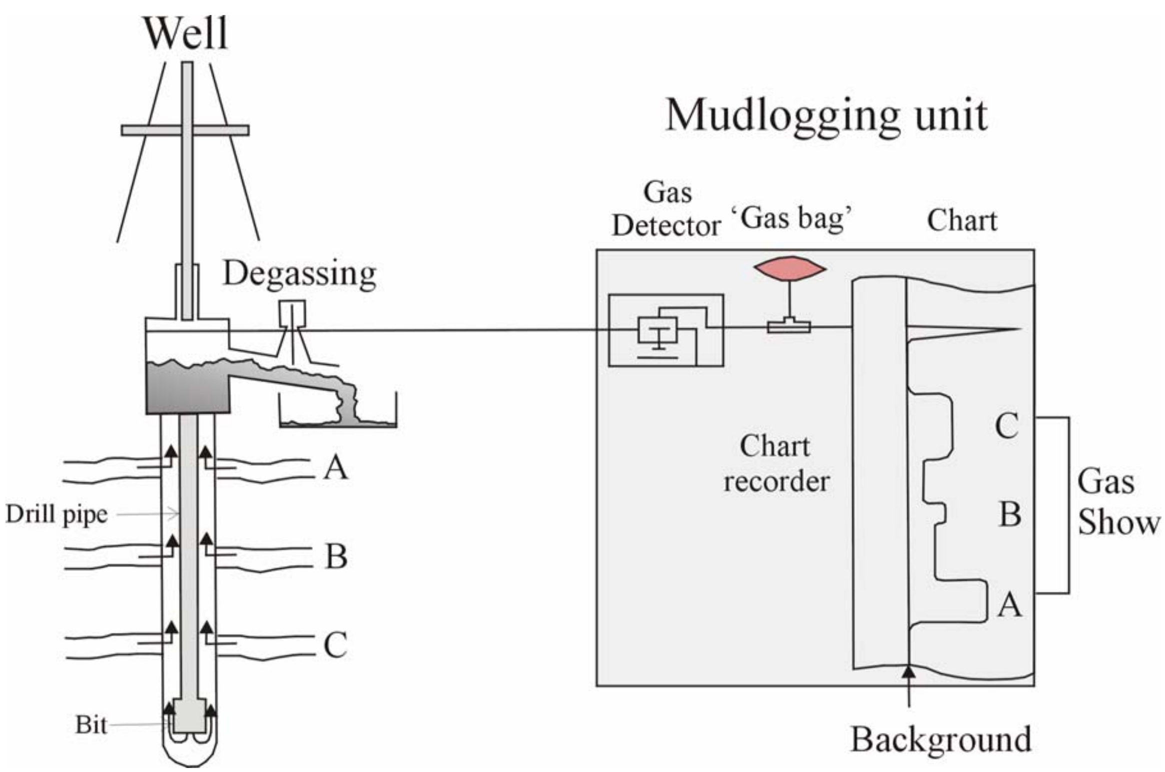

Figure 1-9 Principle of mud circulation during drilling and sampling. Gas samples are collected with gas 'bags' or bottles at the degassing line in the mudlogging unit.

The mudgas sampling technique is described in more detail in Rowe (1998). In short, the manual procedure developed specifically for these types of gases consist in the following: "Gases contained within the shale/rock matrix at depth were mixed with loosened material and drilling fluid (fresh water) as the bit penetrated the subsurface (wells were drilled overbalanced). This matrix/fluid mixture (mud) traveled up to annulus surrounding the drill stem at a constant velocity determined by the drilling fluid circulation rate. The time required for the mud to travel from the bit to the sampling point was a function of bit depth and circulation rate, allowing samples to be collected at known depth intervals." (Rowe, 1998)

1.6.1. Gas compositions

Molecular compositions and concentrations of light hydrocarbons were measured by Brian Szatkowski (G-Chem Environmental Ltd., Lloydminster, Alberta), using a Hewlett Packard 5890 Series II gas chromatograph configured for low detection, equipped with a GC Alumina 30 m x 0.53 mm ID column (Scientific Instrument Services, Inc.) and a FID detector, using He as carrier gas. Reproducibility for all species is better than ±5 %. The lower detection limit of light hydrocarbon gases is 5 ppb.

1.6.2. Carbon stable isotope analysis of hydrocarbon gases

Carbon isotope ratios were obtained at the University of Alberta with a Finnigan-MAT 252 GC-C CF-IRMS system. The gas chromatograph was equipped with a PLOT fused silica capillary column (27.5 m x 0.45 mm, 0.32 mm (I.D.), helium carrier gas). Gases extracted directly from the sealed bottles were injected into a liquid nitrogen cooled cryogenic trap. The cryogenic trap was then instantaneously heated to 180 ºC and the gaseous sample was introduced onto the GC column. The column was held at 30 ºC for 7 min, ramped at 40 ºC /min to 80 ºC and held for 1 min, ramped at 20 ºC /min to 200 ºC and then held for 11 min.

Isotopic values were calculated by integrating the m/z 44, 45, and 46 ion currents of the CO_2 peaks resulting from on-line (continuous flow) combustion of chromatographically separated compounds (Brand, 1996). Laboratory CO_2 pulses admitted directly into the mass spectrometer were used as reference. Carbon isotope compositions are reported as $\delta^{13}C$ values in ppt ($^{o}/_{oo}$) with respect to the PDB standard.

Reproducibility of the $\delta^{13}C$ values was ±0.1 $^{o}/_{oo}$ for methane, and ±0.2 $^{o}/_{oo}$ for the C_{2+} components (ethane, propane and butane) (Tilley and Muehlenbachs, 2006).

From the three wells in the Foothills region, a number of approximately 250 gas samples were collected from depths of 50 to 2200 metres, which span the range from Upper Cretaceous down through Jurassic sediments. Several gas samples in the Mississippian Pekisko Formation were also analyzed.

The detailed carbon isotope mud profiles obtained in the Lloydminster heavy-oil area represent carbon isotopic analyses of about 350 gas samples extracted from mud during the drilling of each well. The mud-gases were collected from the surface down to the pre-Cretaceous unconformity ~ 3-12 m depth intervals. Isotope ratios of mudgases provided an isotopic depth profile (or 'fingerprint') for each of the seven wells sampled and used in this study.

1.6.3. Data reliability and uncertainties

Before interpreting the data of the carbon isotope mudgas depth profiles, it is necessary to determine that the mud gases are actually representative of the gases at depth. Several factors indicate that the carbon isotope analyses are likely to be representative of the in situ gases:

- the definite trends of carbon isotope values with depth indicate that the results are not random;
- the presence of sharp inflections in depth trends suggests that there is little mixing of gases during the upward ascent of drilling fluid;
- the correspondence of several significant inflections with stratigraphic boundaries (identified from gamma ray logs, and discussed in more detail in the following chapters) implies that the calculated depths are accurate to at least within a few metres.

A further factor to consider is random measurement error in all the parameters that enter the model. Thus, the key question is how much error in gas concentration and carbon isotopic values is introduced by random and systematic deviations. Critical for the use of the light alkanes concentrations and their carbon isotope ratios are measurements with sufficient accuracy and precision on small samples. As already mentioned, the gas samples used in this study were determined in the G-Chem Environmental Ltd., Lloydminster, Alberta. For successful carbon isotope measurements, concentrations of at least 150 ppm v/v methane (CH_4), 10 ppm v/v ethane (C_2H_6), 5 ppm v/v propane (C_3H_8), and 2 ppm v/v n-butane (n-C_4H_{10}) are required (Szatkowski et al., 2002). The majority of methane concentrations of the mudgas samples used in this study are in the order of thousands of ppm (1000 ppm to > 500,000 ppm), therefore the methane carbon isotope values are considered relatively accurate. Regarding ethane and propane concentrations, with very few exceptions in the Paskapoo Formation (foothills area), and Lea Park Formation (heavy oil area), majority of the samples recovered >10 ppm v/v ethane, and >5 ppm v/v propane.

Uncertainties in the reported $\delta^{13}C$ values are not indicated throughout the text. Instead, based on pooled data for sample duplicates reported by Rowe (1998), Arkadakskiy (2006) and Tilley and Muehlenbachs (2006), uncertainties that apply to the entire thesis are provided as follows: ± 0.2 ‰ ($\delta^{13}C_1$), ± 0.5 ‰ ($\delta^{13}C_2$), ± 0.25 ‰ ($\delta^{13}C_3$), ± 0.5 ‰ ($\delta^{13}iC_4$), ± 0.7 ‰ ($\delta^{13}nC_4$), ± 0.9 ‰ ($\delta^{13}iC_5$), and ± 0.8 ‰ ($\delta^{13}nC_5$).

CHAPTER TWO
SEQUENCE STRATIGRAPHIC FRAMEWORK

2.1. Introduction

As a new application of stable isotope analyses of natural gases, the mud gas isotopic and compositional profiles interpretation first require an accurate and fundamental understanding of the data and their significance. Fundamental factors such as the integrity of isotope data in a complex drilling mud system, the effect of drilling conditions/parameters and the geological factors play an important role in the release of gases from the cuttings into the drilling mud. To start to investigate one of the factors – stratigraphic/rock properties – represent one of the main purpose of this study. The best way to decipher the effects of these "geological" controls is within a sequence stratigraphic framework.

Sequence stratigraphy uses the three-dimensional arrangement of key bounding surfaces to reveal genetically related packages of rocks (Bohacs, 1993). This approach allows the recognition and mapping of coeval depositional sedimentary environments and facies, and enables the construction of predictive models based on understanding the depositional processes.

Based on this framework, it is possible to predict rock property variations from standard input geological data. Acquisition and compilation of geophysical logs, in conjunction with description of conventional cores can therefore reveal "significant" stratigraphic horizons and sedimentological trends and will lead to standard interpretation of mud gas isotope data. As a result, one of the research objectives was to examine the large-scale stratigraphic pattern within the two different regions: foothills (Pembina – Gilby – Ferrier area) and heavy oil (Lloydminster area) - Western Canada Sedimentary Basin, through the use of regional well-log cross-sections.

2.1.1. Methods

The sedimentologic and stratigraphic analysis of the Western Canada Cretaceous stratigraphic section is based primarily on regional well-log cross-sections, and descriptions of conventional cores tied as close as possible to the examination of well logs. A total of 38 control wells were examined and integrated in this study. Their location is shown in Figure A-1 and Figure A-2 (Appendix A). Based on their availability, core descriptions were carried out on sections of the Cretaceous Foreland basin (foothills region) and on the entire stratigraphic sequence of the Mannville Group in one well (heavy-oil region). A list of all of the examined wells with cores within the study areas is presented below:

1. 06-04-42-04W5	20. 11-30-45-09W5
2. 06-09-46-09W5	21. 12-03-42-09W5
3. 08-02-43-05W5	22. 14-01-42-07W5
4. 09-10-44-09W5	23. 14-06-47-09W5
5. 10-04-49-11W5	24. 16-16-47-10W5
6. 14-28-42-04W5	25. 06-22-42-09W5
7. 16-11-45-07W5	26. 04-10-42-09W5
8. 08-25-42-05W5	27. 06-12-45-07W5
9. 02-33-47-07W5	28. 07-06-42-07W5
10. 06-12-48-11W5	29. 07-08-42-05W5
11. 06-14-42-06W5	30. 08-11-42-07W5
12. 06-26-48-11W5	31. 10-17-42-04W5
13. 06-33-48-11W5	32. 13-13-42-05W5
14. 09-32-43-07W5	33. 03-13-43-05W5
15. 10-11-43-09W5	34. 10-32-48-06W5
16. 10-14-44-09W5	35. 11-15-45-07W5
17. 10-16-42-09W5	36. 16-11-45-07W5
18. 10-23-43-09W5	37. 10-10-42-09W5
19. 10-26-45-09W5	38. 10-25-47-03W4

The core descriptions (facies associations and type of bounding discontinuities) are presented in detail, in section 2.3. of Chapter Two, and in Appendix “A” in the form of a collection of plate photographs.

The subdivision of the Upper Cretaceous sediments as derived from the study of cores was integrated with a suite of well-log cross sections, as the formations were correlated throughout the study areas. The reliability and precision of log interpretation of the Upper Cretaceous strata was evaluated as the two databases were compared and contrasted. Core interpretation has been utilized to supplement interpretations based on log response, and cross-sections were correlated using the examined cored wells and their particular well log signatures as a guide.

Initiated to elucidate the stratigraphic control on the carbon isotope geochemistry, the idea of cross-section correlations is:

- first, to understand and develop a regional facies distribution and thickness, and to reveal a series of key bounding surfaces, and
- secondly, to compare and contrast regionally existing gas isotope mudlogs (foothills vs. heavy oil regions).

The subsurface study of the foreland basin fill is assisted by the presence of regionally recognizable characteristics of its well-log signature, which allows analysis of the regional framework of the section. The concept of sequence stratigraphy was applied to the foreland section in order to subdivide it into major order sequences or cycles, bounded by significant and regionally recognizable sequence stratigraphic surfaces. Some major erosional surfaces are present within some cycles that can be determined accurately by the lithologies described in cores, and in some cases by ichnofossils. The significant sequence stratigraphical surfaces were used in our approach to better understand and demonstrate their relationship with geochemical depth profiles.

The shallowest gases have lower carbon isotope values than the deepest (Schoell, 1980) but the increases are not monotonic with depth. The mudlogs show numerous inflections and variations in the trends of the carbon isotope values. As already mentioned (Galimov, 1973; Schoell, 1983), the unexpected trends of these isotopic depth profiles are primarily due to a multitude of factors influencing the carbon isotope values (e.g. type of source material, biological processes, thermal alteration, mixing, migration), but all these factors are part of a much larger panorama, which is the rock framework.

By presenting the carbon isotopic signatures of gases in relationship with the general stratigraphy and depositional trends in the basin, the present thesis will try to set up some preliminary principles for mud logs interpretation based on sequence stratigraphic correlations.

A subsurface data set comprised of approximately 180 wire-line logs for the Foothills study area and approximately 200 wire-line logs for the Lloydminster study area form the foundation of the sequence stratigraphic approach. The results of the regional correlations are presented in the form of structural cross-sections (Appendix “B”: Appendices I-II). The first study area is represented by a number of five structural well log cross-sections with lengths varying between ~ 50 km and 150 km. Three of the five cross-sections within the Foothills area link the three carbon isotopic mud gas profiles: Pembina (1300 m deep), Ferrier (1950 m deep), and Gilby (2185 m deep).

The stratigraphic framework of the second study area is represented by eight structural well log cross-sections with lengths varying between ~ 18 km and 70 km.

Correlations were constructed on the framework of mainly gamma-ray, resistivity, sonic and density logs. Following the drafting of the cross-sections, only one digitized log (gamma-ray, Sp or resistivity) for each well was selected for the final graphic representations from Appendix “B”: Appendices I-1 to I-5 (Foothills region) and Appendices II-1 to II-8 (Lloydminster region).

Once again, the aim of this work was to provide a basic grid of stratigraphic cross-sections to be a reference framework and context for understanding the lateral and vertical distribution of facies comprising the Western Canada Foreland Basin in the two study areas. This reference framework forms the stratigraphic skeleton upon which subsequent, more detailed analyses of the sequence stratigraphy, sedimentology, paleogeography, and tectonic history of the Western Canada foreland basin may possibly be based. A detailed verification of regional unconformities and other significant sequence stratigraphic surfaces would require the examination of all the available core data over the entire study area, as well as closer grid spacing, well beyond the scope of the present study.

2.2. Sequence stratigraphic approach

The sequence stratigraphic approach resumes to looking at the geological record as composed of rock packages bounded by physical surfaces formed by distinct events. The stacking of the depositional environments, along with the physical attributes of the surfaces separating the environments, reveals the sequence stratigraphic framework. The foreland basin section was analyzed and correlated a regional scale in an attempt to both gain a much better understanding of lateral and vertical changes in the layers making up the foreland basin fill and to disclose the critical significance of sequence stratigraphic surfaces on carbon isotope ratios. The key bounding surfaces that reveal geochemically significant rock packages (as it will be further discussed and shown) are the unconformable portions of the sequence boundaries (subaerial unconformities and/or ravinement surfaces, which have eroded through a subaerial unconformity), ravinement surfaces, and the maximum flooding surfaces.

The key stratigraphic surfaces identified and used on the wireline log data in order to separate various facies successions on a large scale within the foreland sedimentary basin are briefly defined below.

The subaerial unconformity (SU) is a surface created during times of relative sea-level fall by subaerial processes (Sloss et al., 1949). In area of channeling, this surface may be expressed as a *subaerial erosional surface* (Nummedal and Swift, 1987), whereas in interfluves it may be expressed as a *subaerial exposure surface*. This surface may be difficult to recognize from well data alone. It requires the recognition of a facies dislocation: the superposition of a proximal on a significantly more distal facies without the preservation of the intermediate facies.

The maximum flooding surface (MFS) is the surface that forms at the turnaround point between transgression and subsequent regression (Posamentier et al., 1988; Van Wagoner et al., 1988; Galloway, 1989). It separates retrograding units below from overlying prograding units. On well logs, a consistently correlative point of maximum gamma-ray and lowest resistivity, indicating the most clay rich shale, marks this surface. In marine successions, the maximum flooding surface is commonly associated with condensed intervals. These may have a distinctive log response, such as a gamma-ray peak, a resistivity trough, or a density maximum.

The maximum regressive surface (MRS) (Embry, 1993) can be recognized in proximal locations as the surface between a prograding unit and an overlying retrograding unit. Where these units show a gradual upward increase in gamma and a gradual decrease in gamma respectively, the maximum regressive surface may be a gamma-ray minimum.

The ravinement surface (RS) represents a low-relief erosional surface cut by wave processes associated with erosional shoreface retreat during transgression. This surface is analogous to the marine erosion surface of Nummedal and Swift (1987), the high-energy flooding surface of Pemberton and MacEachern (1995), or the transgressive surface of erosion (TSE) of others (Bhattacharya and Walker, 1991; MacEachern et al., 1992). Generally, ravinement surfaces are mantled by a conglomeratic lag and/or transgressive sheet sandstone, trending up to shelf mudstones. According to MacEachern and Hobbs (2004), these types of erosional surfaces are possibly the most abundantly represented stratigraphic discontinuity in Cretaceous strata of the WCSB. They are particularly well developed in the Viking Formation (MacEachern et al., 1992), in the Bluesky Formation, Falher Members, the Dunvegan Formation, and the Cardium Formation.

The regressive surface of marine erosion (RSE) (Bruun, 1962; Plint, 1988; Dominguez and Wanless, 1991; Plint and Nummedal, 2000) represents a scoured surface cut by waves in an attempt to re-establish an equilibrium profile during the forced regression of a shoreline accompanying a fall in base-level. It usually separates underlying deeper marine strata from overlying shallower marine strata.

In addition to the key sequence stratigraphic surfaces mentioned above, allostratigraphic facies contacts may also have distinctive log signature where they mark sharp lithological changes. An example of such facies contact is the change from sandstone (either transgressive or regressive) to overlying marine shales, which is termed “flooding surface” (FS) and interpreted to correspond to an abrupt water deepening (Van Wagoner et al., 1990).

In coastal settings, a relative rise in sea-level could flood the interfluve areas generating accommodation space, and causing the shoreline to transgress rapidly. As a result, many interfluves are characterized by sharp erosion surfaces, which are the products of ravinement processes.

It should be noted that for every key bounding surface there is a contrast in permeability and porosity. Thus, it is to be expected that in the subsurface, these surfaces would affect if not control the *in situ* gas geochemistry.

The wireline log responses (see Figs. A3 to A40 in the Appendix A) of these key stratigraphic surfaces were correlated with the examined drill core data.

2.3. Core descriptions and facies associations

Conventional cores were examined and logged at the AEUB Core Research Centre in Calgary, Alberta. The cores were divided into major depositional units, which are part of a sequence stratigraphic framework developed for the study areas.

The vast number of facies seen in the cores has been additionally grouped into facies associations (Table 2-1), representing a vertical succession with gradational contacts between successive facies. Each facies association is bounded above and/or below by either sequence boundaries, transgressive surface of erosion, amalgamated sequence boundary and transgressive surface of erosion, regressive surface of marine erosion, or marine flooding surfaces.

The rocks have been subdivided using both the individual facies and the depositional discontinuities. These surfaces can be traced on log sections, where they form mappable, regionally extensive bounding discontinuities characterized in core by abrupt juxtaposition of facies, grain size breaks, and chert pebbles. The facies are interpreted on the basis of their own characteristics and their relationships to each other and to the bounding discontinuities.

Table 2-1 Sedimentary facies of the Cretaceous section (Mannville Gp., Joli Fou, Viking, Cardium, Lea Park, Belly River formations)

Facies Associations	**Description**	**Interpretation**	**Examples in wells**
CL	Light and dark banded coal with shale partings.	Peat	16-11-045-07W5 (Fig. 2-38) 09-10-44-09W5 (Fig. 2-5)
MR	Coaly shale, abundant plant debris, with root traces	Marsh	03-13-043-05W5 (Fig. 2-35)
FP	Carbonaceous siltstone with thin, interbedded rippled sandstone. Mild pedogenesis. Coal stringers, root traces, plant fragments and convolute bedding locally abundant.	Floodplain	06-04-42-4W5 (Fig. 2-2)
LN	Dark carbonaceous shale, massive to laminated, with lag of organic debris (e.g. well preserved ostracodes), and interbeds of coal, siltstone (ripple cross-laminated) and very fine sandstone. Local siderite, wood fragments, soft sediment deformation.	Lacustrine or lagoon, with initial flooding phase and upwards shoaling	08-25-042-05W5 (Fig. 2-9) 08-02-43-05W5 (Fig. 2-4)
CS	One or more sharp-based, fining upwards units of siltstone and fine-grained, ripple to planar-laminated sandstone (10-50 cm thick), overlain by bioturbated mudstone (1-5 cm thick). *Glossifungites*	Crevasse splay	09-10-044-09W5 (Fig. 2-5) 16-11-045-07W5 (Fig. 2-8)
BF	Sharp-based, coarsening upwards unit, 2-8 m thick. Mudstone with syneresis cracks, organic debris, siderite and pyrite nodules, bivalves, and abundant *Helminthopsis* and *Chondrites*. Grades upwards into interbedded sandstone with planar- and ripple-lamination, moderate bioturbation (*Planolites, Rosselia, Teichichnus, Palaeophycus, Asterosoma* ?). Top contact rooted or overlain by coal.	Brackish bay fill with upwards increasing marine influence	07-06-042-07W5 (Fig. 2-30) 16-11-045-07W5 (Fig. 2-38)
CH	Sharp-based, conglomeratic to medium- and fine-grained sandstone, fining-upward, up to 10 m thick. Structures include cross-bedding, parallel-bedding and ripples, roots near top. May contain a basal lag of pebbles, mud- and coal-intraclasts.	Channel	16-11-045-07W5 (Fig. 2-8) 03-13-043-05W5 (Fig. 2-35)

Table 2-1 Sedimentary facies of the Cretaceous section (Mannville Gp., Joli Fou, Viking, Cardium, Lea Park, Belly River formations)

Facies Associations	Description	Interpretation	Examples in wells
VFd	Interbedded bioturbated silty shales, muddy sandstones and sharp based fine-grained sandstones (ripple laminated, cross-bedded, or structureless). Irregular mudstone laminations. Monotypic ichnologic character (mixed *Skolithos - Cruziana* ichnofacies). Sandier upward appearance.	Bay Head delta – Flood tidal delta	07-06-042-07W5 (Fig.2-30)
VFc	Clast-rich cross-bedded sandstones (medium and coarser-grained), with silty shales, and minor bioturbation; rippled sandstones interbedded with shale layers also present. Mud drapes on top of ripples (tidal action).	Tidal channel	13-13-042-05W5 (Fig. 2-34)
CP	Carbonaceous siltstone with thin, interbedded rippled sandstone. Coaly beds, root traces, plant fragments and horizontal burrowing locally abundant.	Coastal plain	10-25-047-03W4 (Fig. 2-39)
ST	Interbedded sandstones and shales. Wavy and ripple laminated bedding, micro-faulting, slump structures, and minor bioturbation within the shale dominant interval. The fine to medium grained sandstone dominated beds are characterized by wavy laminations, flaser bedding, and lenticular bedding and show evidence of synaeresis cracking. Abundance of organic laminae. Significant bioturbation by small, horizontal trace makers.	Progradational shallow marine subtidal to intertidal sequence	10-25-047-03W4 (Fig. 2-39)
F	Fine-grained sandstone with massive to low-angle parallel bedding, plant debris. Intense bioturbation (*Macaronichnus segregates*) 2-4 m below top surface. Rooted upper surface.	Foreshore	02/06-09-46-9W5 (Fig. 2-3) 10-23-043-09W5 (Fig. 2-19)
US	Fine-grained to medium grained sandstone with planar-tabular and through cross-bedding, sets up to 40 cm thick.	Upper shoreface	06-26-048-11W5 (Fig. 2-13) 10-26-045-09W5 (Fig. 2-20)

Table 2-1 Sedimentary facies of the Cretaceous section (Mannville Gp., Joli Fou, Viking, Cardium, Lea Park, Belly River formations)

Facies Associations	Description	Interpretation	Examples in wells
PZ	Very fine-grained sandstone, with *Palaeophycus* bioturbation zone	Middle shoreface	14-28-42-05W5 (Fig. 2-7)
LS	Very fine to fine grained sandstone (10 cm to several metres in thickness) with amalgamated HCS/SCS. The beds show sharp bases and tops; wave-ripple cross-lamination may occur towards tops. In the more distal areas, sandstone beds are thinner and alternate with silty mudstones (2 – 5 cm thick). Rare isolated burrows, with no significant bioturbation.	Lower shoreface	06-12-048-11W5 (Fig. 2-11) 08-14-042-06W5 (Fig. 2-12) 09-32-043-07W5 (Fig. 2-15)
UOS	Very fine- to fine grained sandstones (30-80%), centimetre thick, interbedded with siltstones and mudstones; pervasive bioturbation (*Cruziana* ichnofacies).	Upper Offshore	06-12-048-11W5 (Fig. 2-11) 16-16-047-10W5 (Fig. 2-25)
LOS	Marine shales (dark grey to black) with thin interbeds of very-fine grained sandstone with HCS and rarely, wave ripples. In the more distal areas a few thin very fine-grained sandstone laminae are partially preserved or may show sediment deformation. Moderate to intense bioturbation (churned appearance).	Lower Offshore	02-33-047-07W5 (Fig. 2-10) 09-32-043-07W5 (Fig. 2-15) 16-16-047-10W5 (Fig. 2-25)
TL	Coarse conglomerate (clast-supported, matrix-supported, and thin stringers within mudstones) or coarse to granular sandstone; few centimetres-tens of centimetres in thickness.	Transgressive lag	06-12-048-11W5 (Fig. 2-11)
TS	Coarse conglomerate (clast-supported, matrix-supported, and thin stringers within mudstones) or coarse to granular sandstone; up to 2m in thickness.	Transgressive shoreface	02-33-47-07W5 (Fig. 2-10) 10-16-042-09W5 (Fig. 2-18) 10-10-42-09W5 (Fig. 2-28)

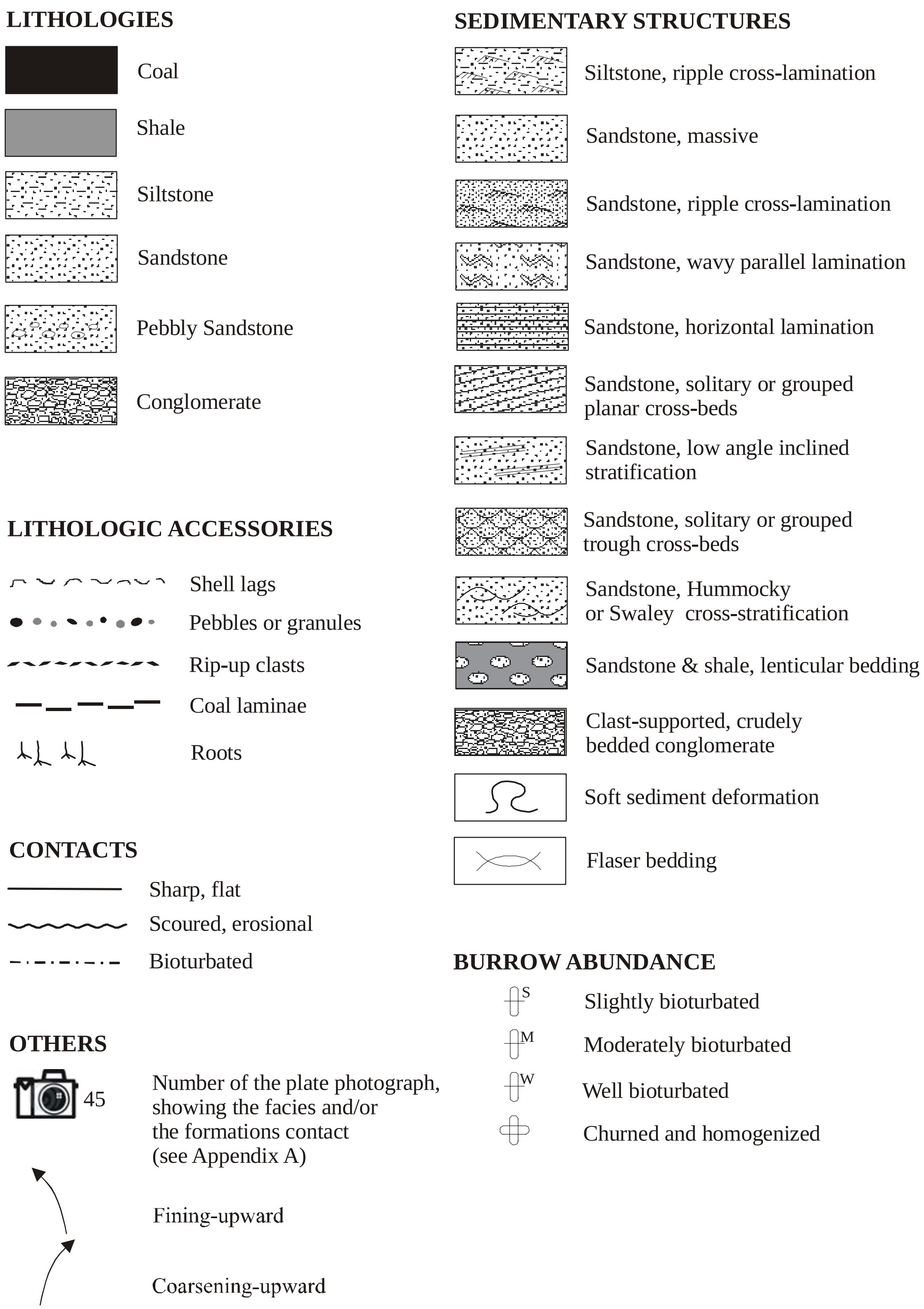

Figure 2-1 Legend of symbols used in lithologs.

The succession of facies associations and discontinuity surfaces in the study areas are summarized in 38 representative lithologs (Figures 2-2 to 2-39). Along with the core box photographs (see Appendix "A") from each of the fields, these lithologs illustrate the variable succession of facies associations in the study areas.

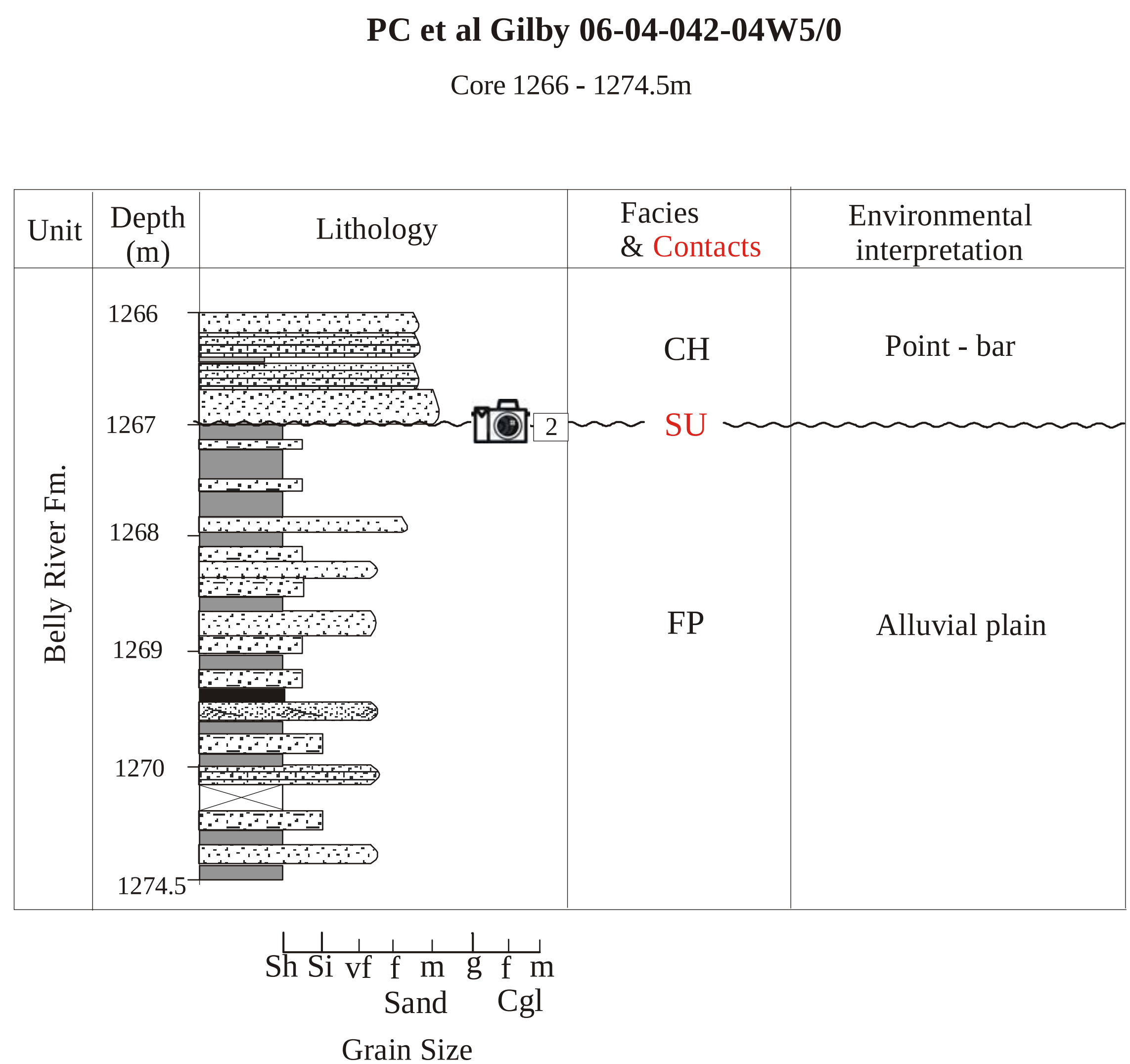

Figure 2-2 Litholog for the 06-04-42-4W5 core, annotated with main contacts (discussed in text) and facies interpretation. Legend for the litholog is given in Figure 2-1.

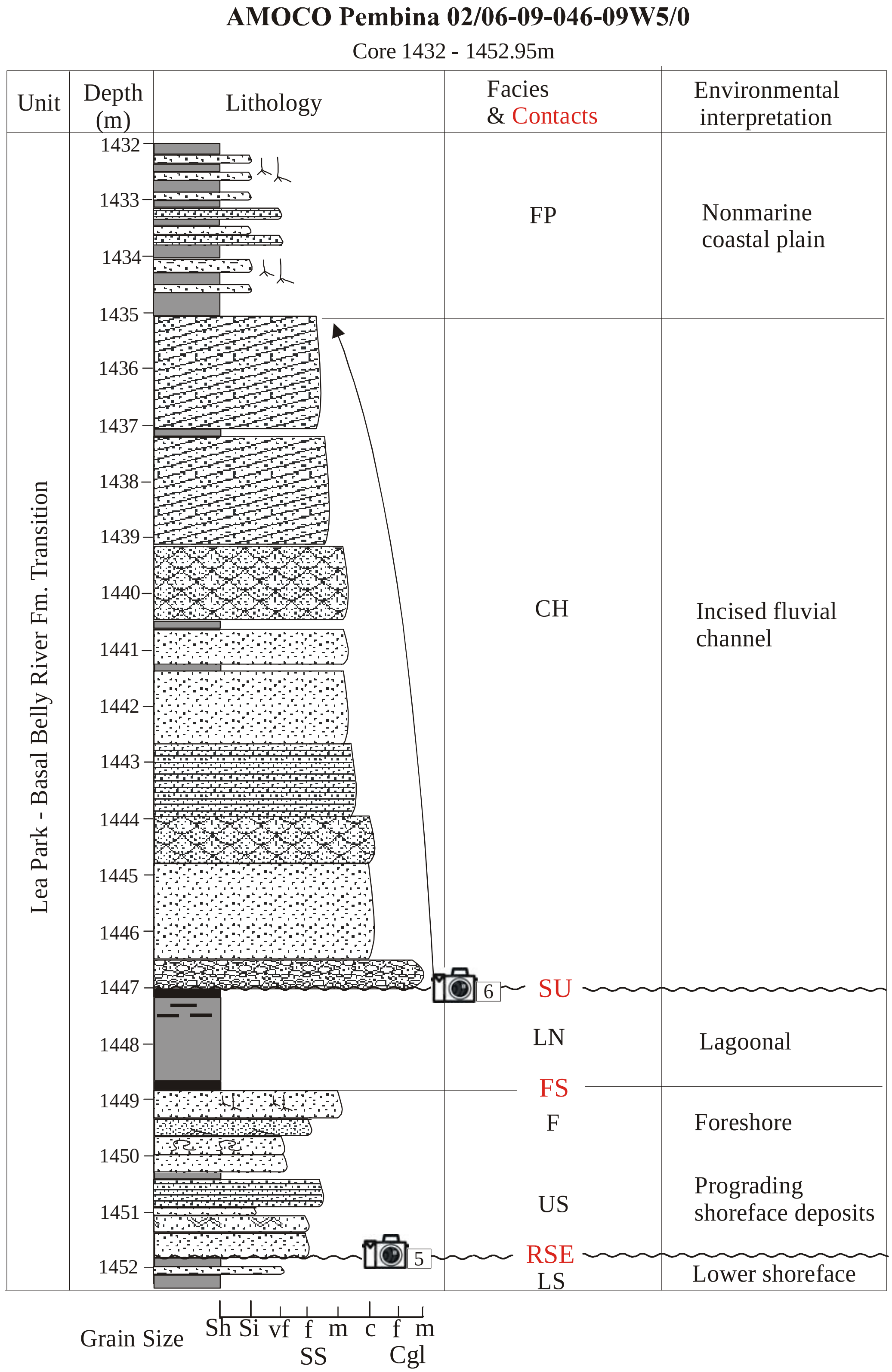

Figure 2-3 Litholog for the 02/06-09-46-9W5 core, annotated with main contacts (discussed in text) and facies interpretation. Legend for the litholog is given in Figure 2-1.

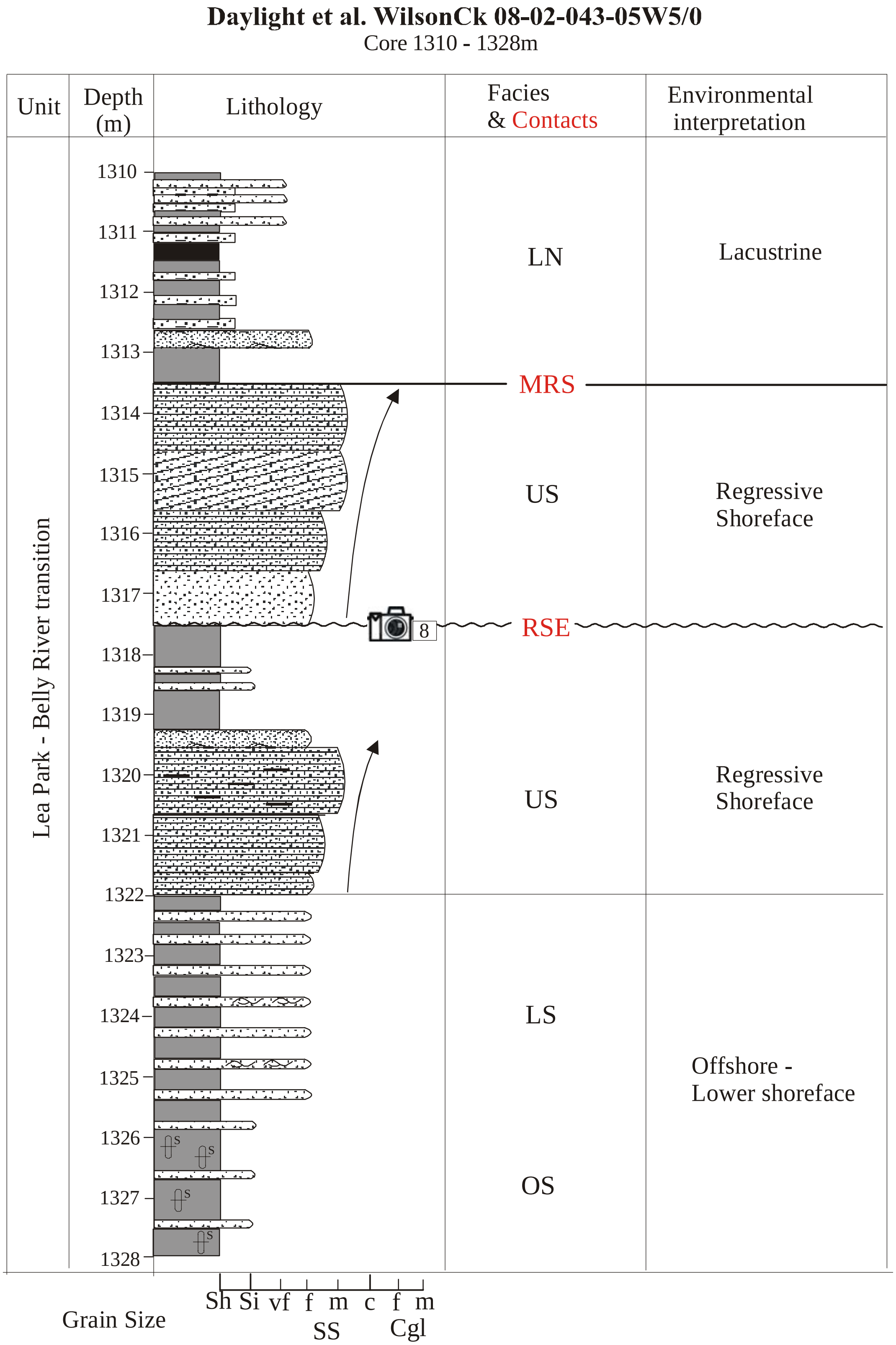

Figure 2-4 Litholog for the 08-02-43-05W5 core, annotated with main contacts (discussed in text) and facies interpretation. Legend for the litholog is given in Figure 2-1.

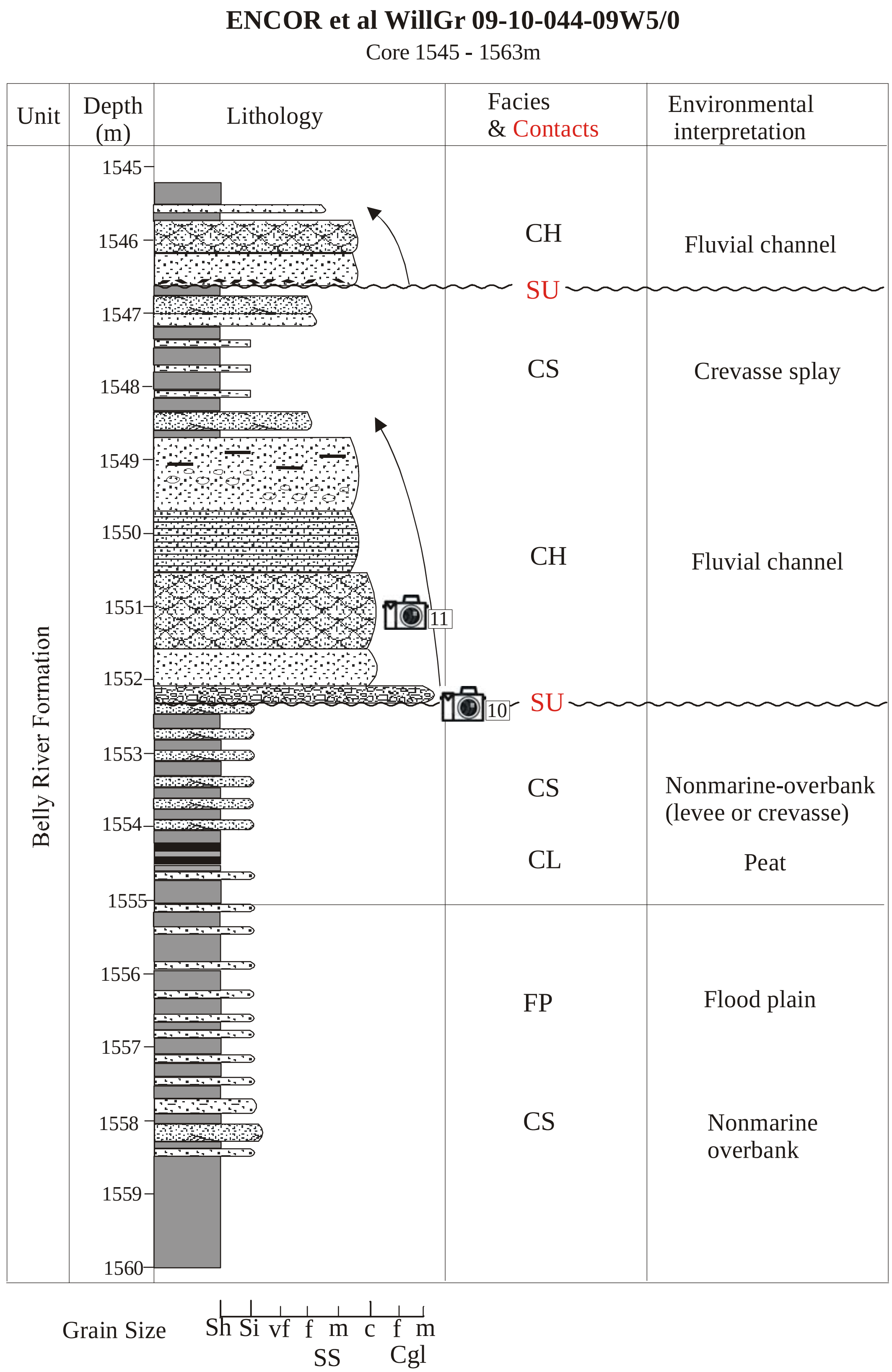

Figure 2-5 Litholog for the 09-10-44-09W5 core, annotated with main contacts (discussed in text) and facies interpretation. Legend for the litholog is given in Figure 2-1.

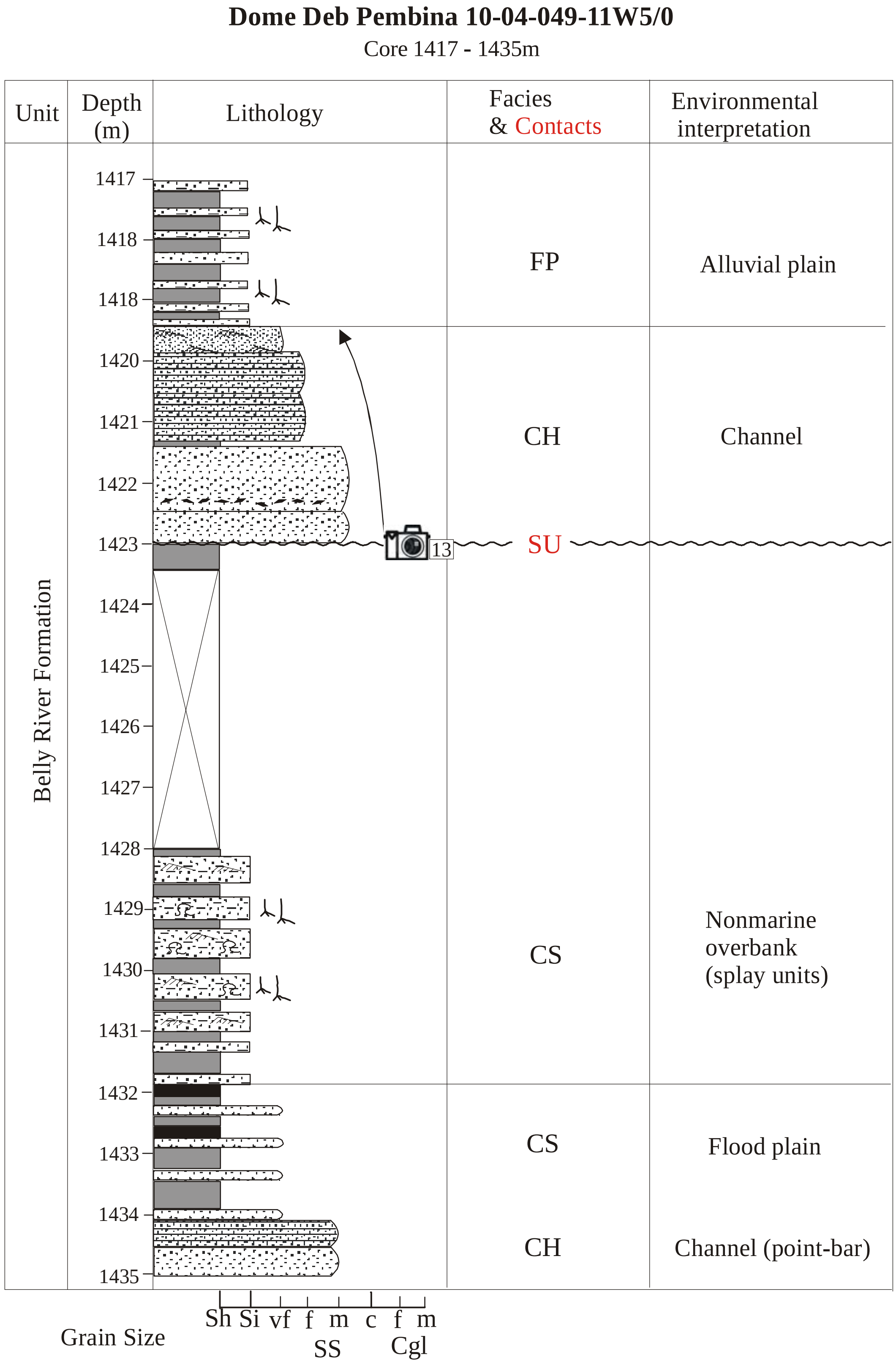

Figure 2-6 Litholog for the 10-04-49-11W5 core, annotated with main contacts (discussed in text) and facies interpretation. Legend for the litholog is given in Figure 2-1.

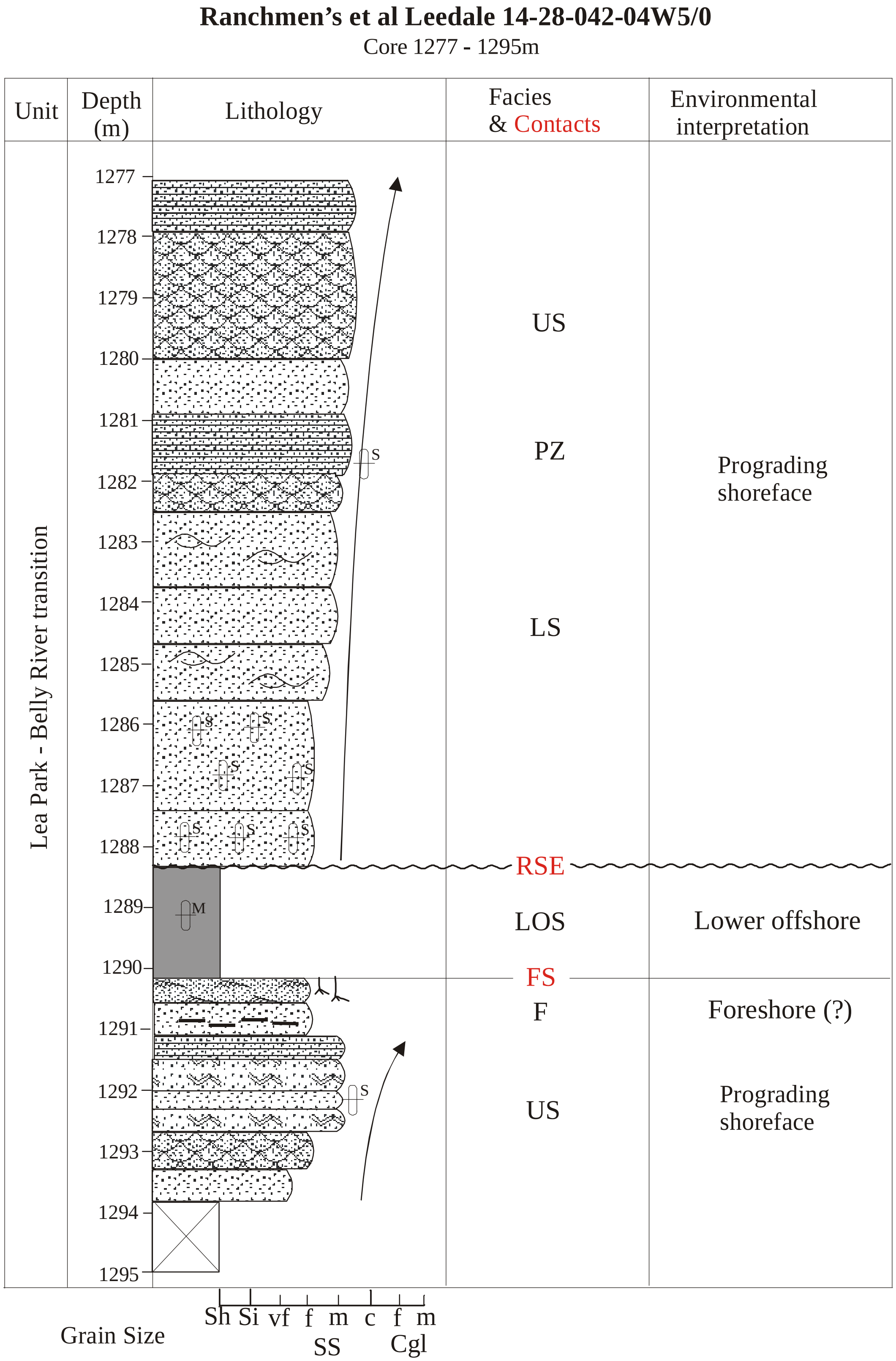

Figure 2-7 Litholog for the 14-28-42-05W5 core, annotated with main contacts (discussed in text) and facies interpretation. Legend for the litholog is given in Figure 2-1.

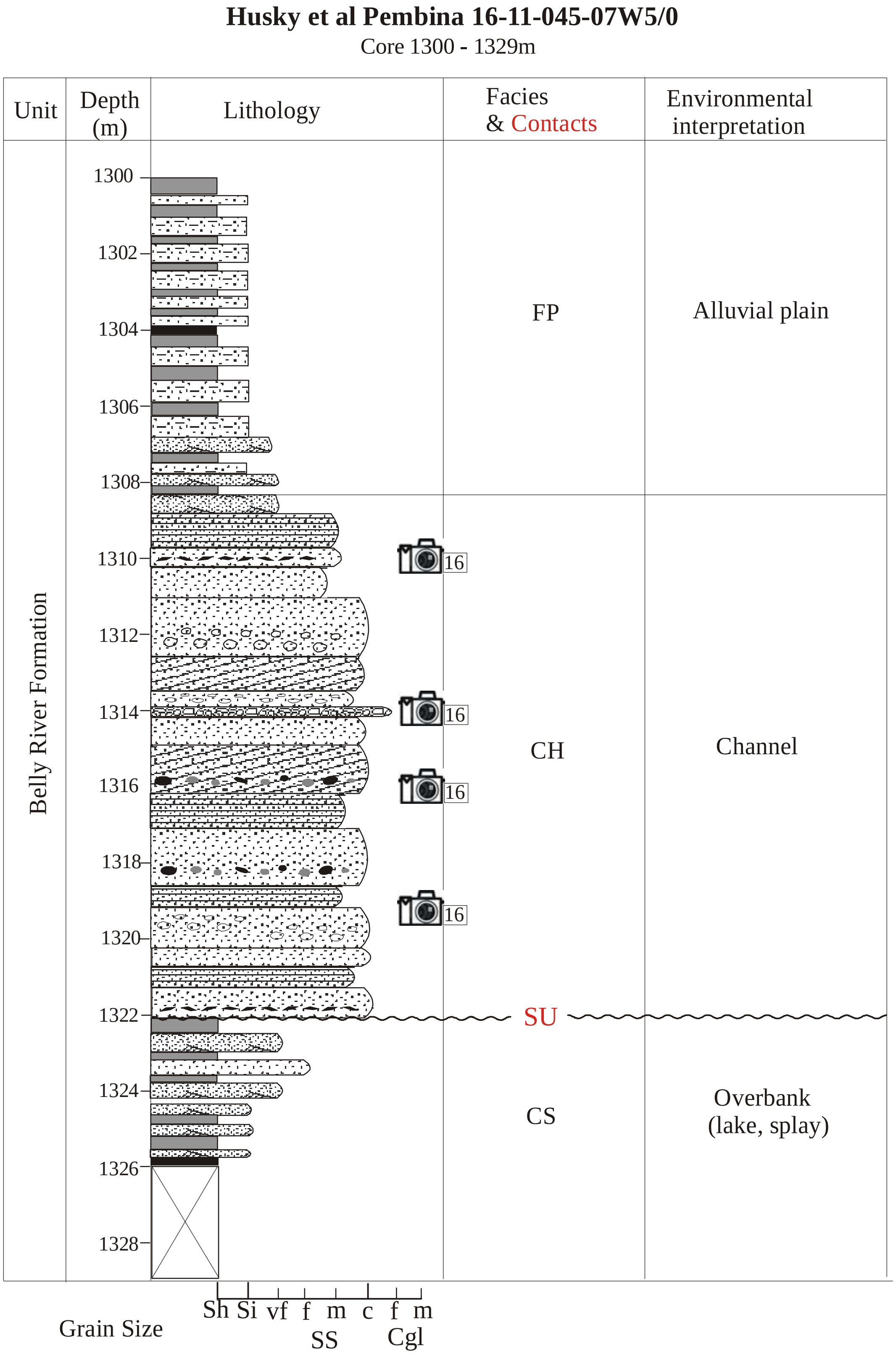

Figure 2-8 Litholog for the 16-11-045-07W5 core, annotated with main contacts (discussed in text) and facies interpretation. Legend for the litholog is given in Figure 2-1.

PW Gas Wilsonck 08-25-042-05W5/0
Core 1312 - 1324m

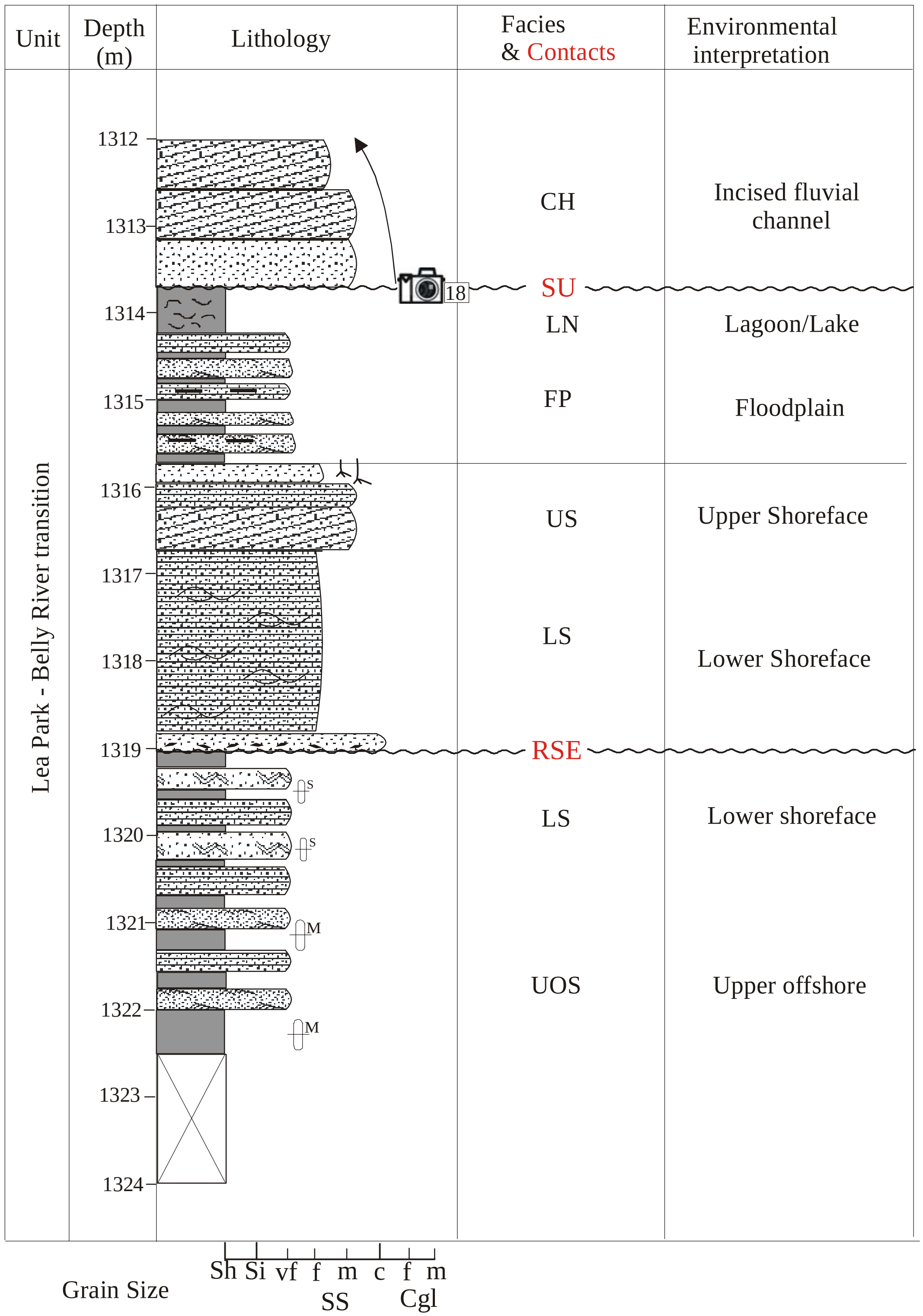

Figure 2-9 Litholog for the 08-25-042-05W5 core, annotated with main contacts (discussed in text) and facies interpretation. Legend for the litholog is given in Figure 2-1.

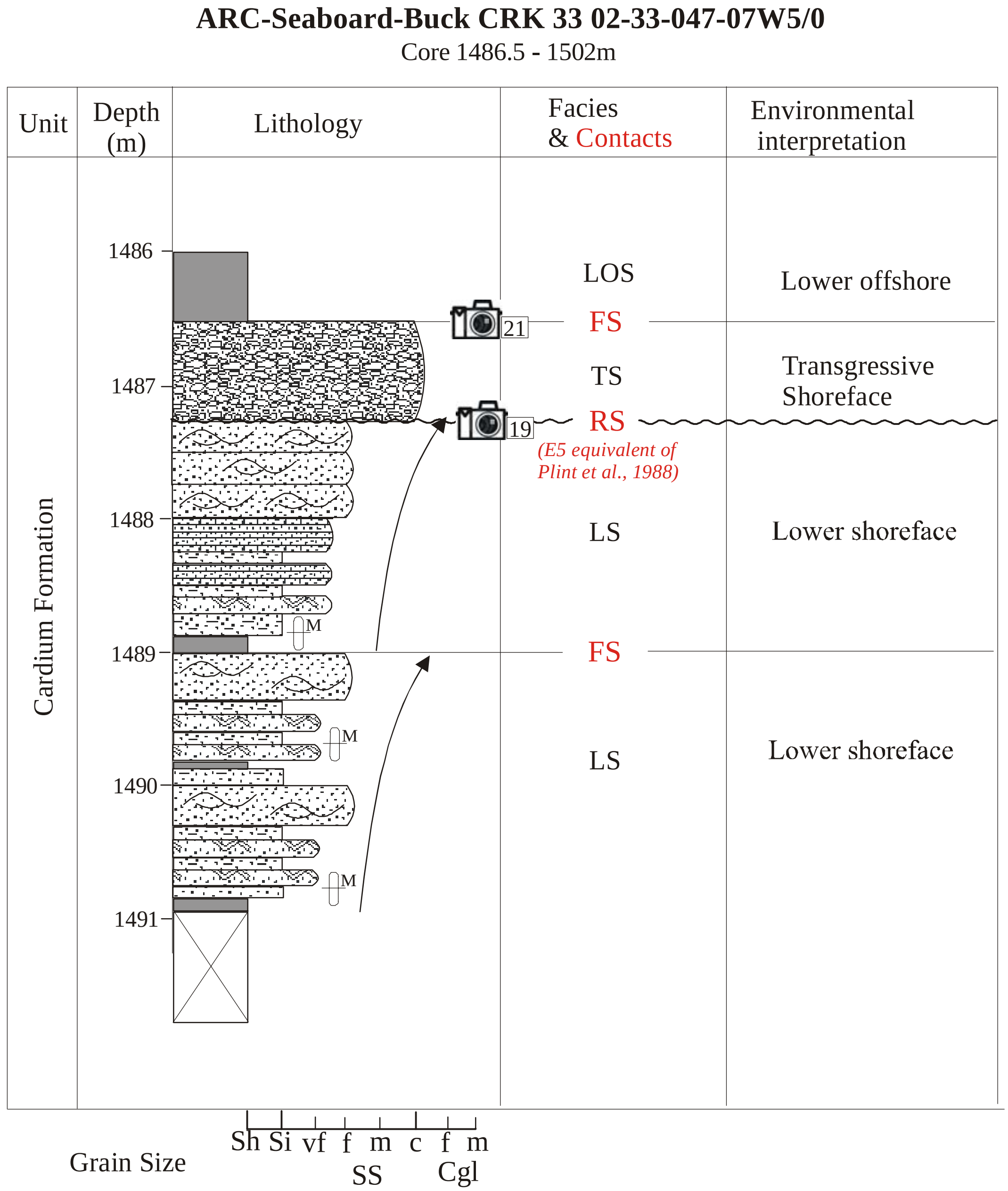

Figure 2-10 Litholog for the 02-33-47-07W5 core, annotated with main contacts (discussed in text) and facies interpretation. Legend for the litholog is given in Figure 2-1.

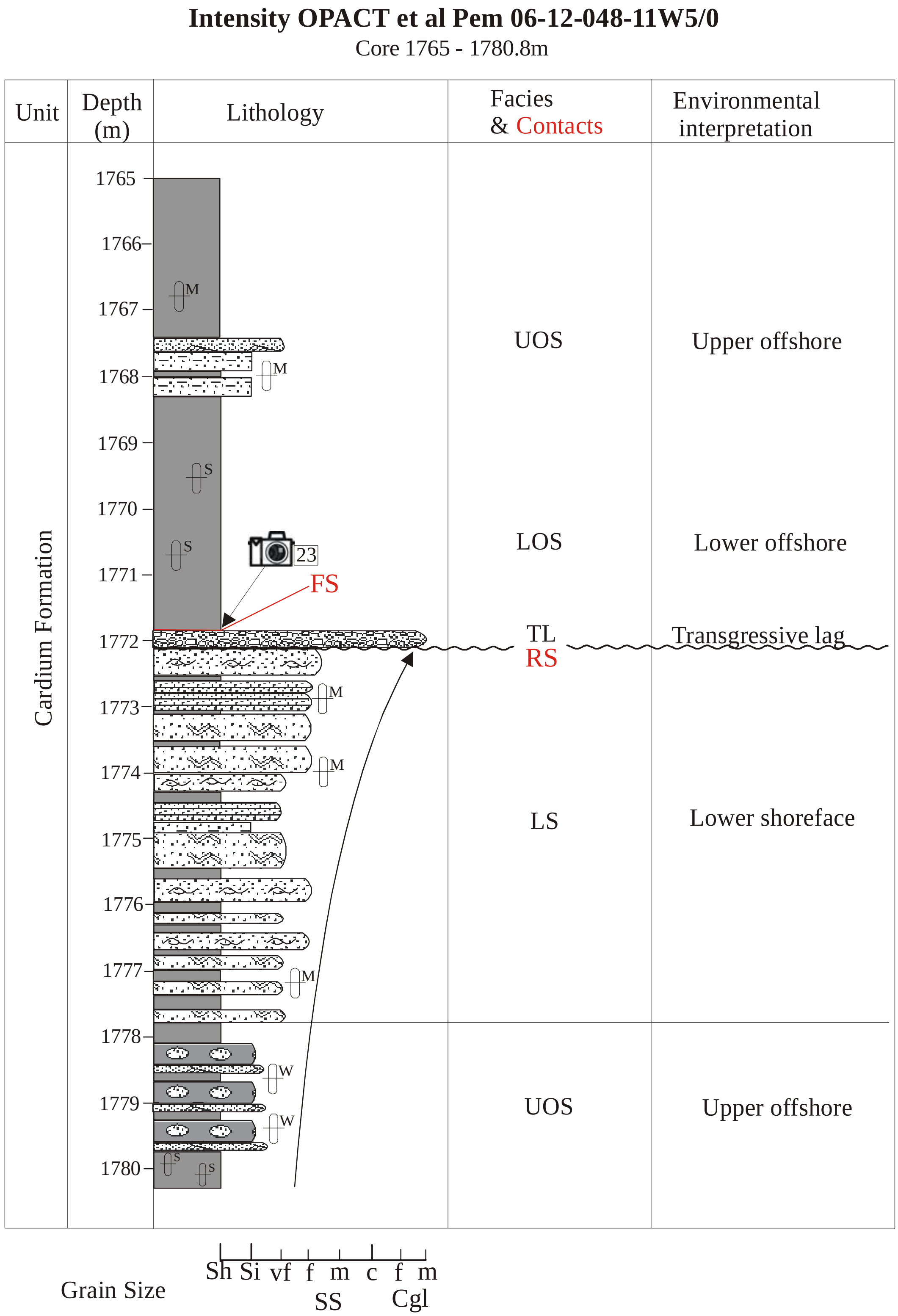

Figure 2-11 Litholog for the 06-12-048-11W5 core, annotated with main contacts (discussed in text) and facies interpretation. Legend for the litholog is given in Figure 2-1.

Penn West et al WillGr 06-14-042-06W5/0
Core 1907.4 - 1916.6m

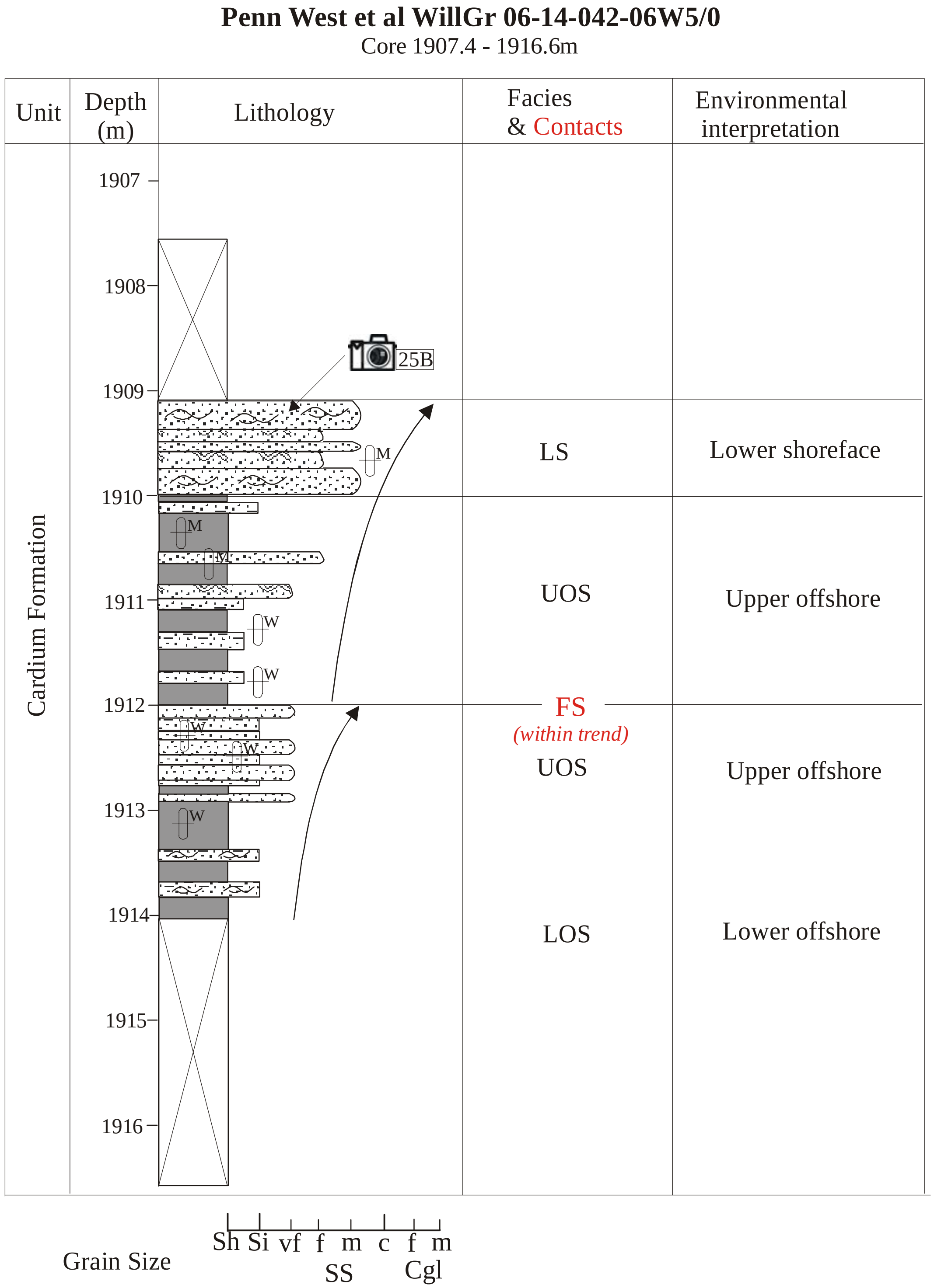

Figure 2-12 Litholog for the 08-14-042-06W5 core, annotated with main contacts (discussed in text) and facies interpretation. Legend for the litholog is given in Figure 2-1.

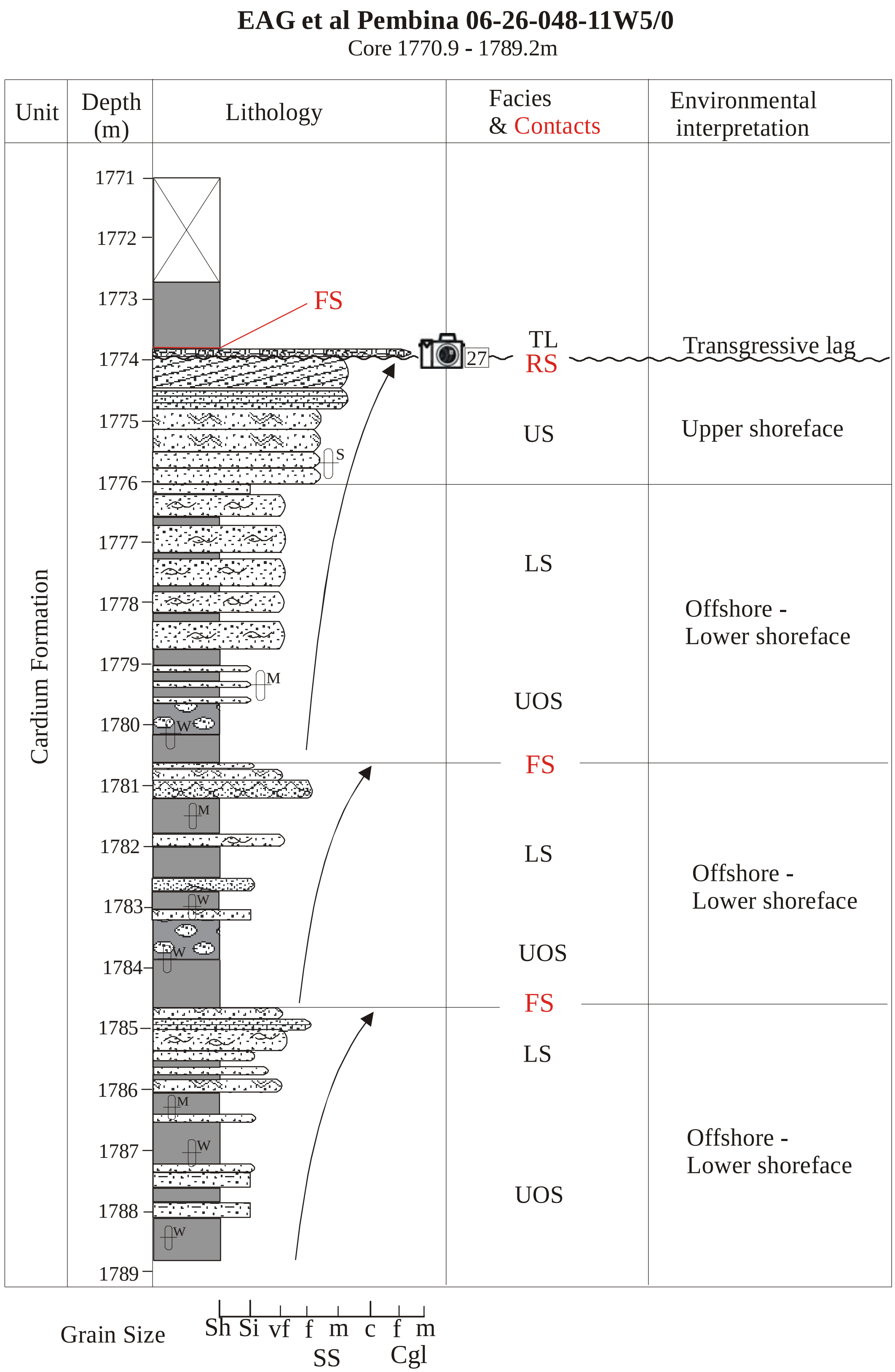

Figure 2-13 Litholog for the 06-26-048-11W5 core, annotated with main contacts (discussed in text) and facies interpretation. Legend for the litholog is given in Figure 2-1.

Amoco Pembina 06-33-048-11W5/0

Core 1760.5 - 1778.8m

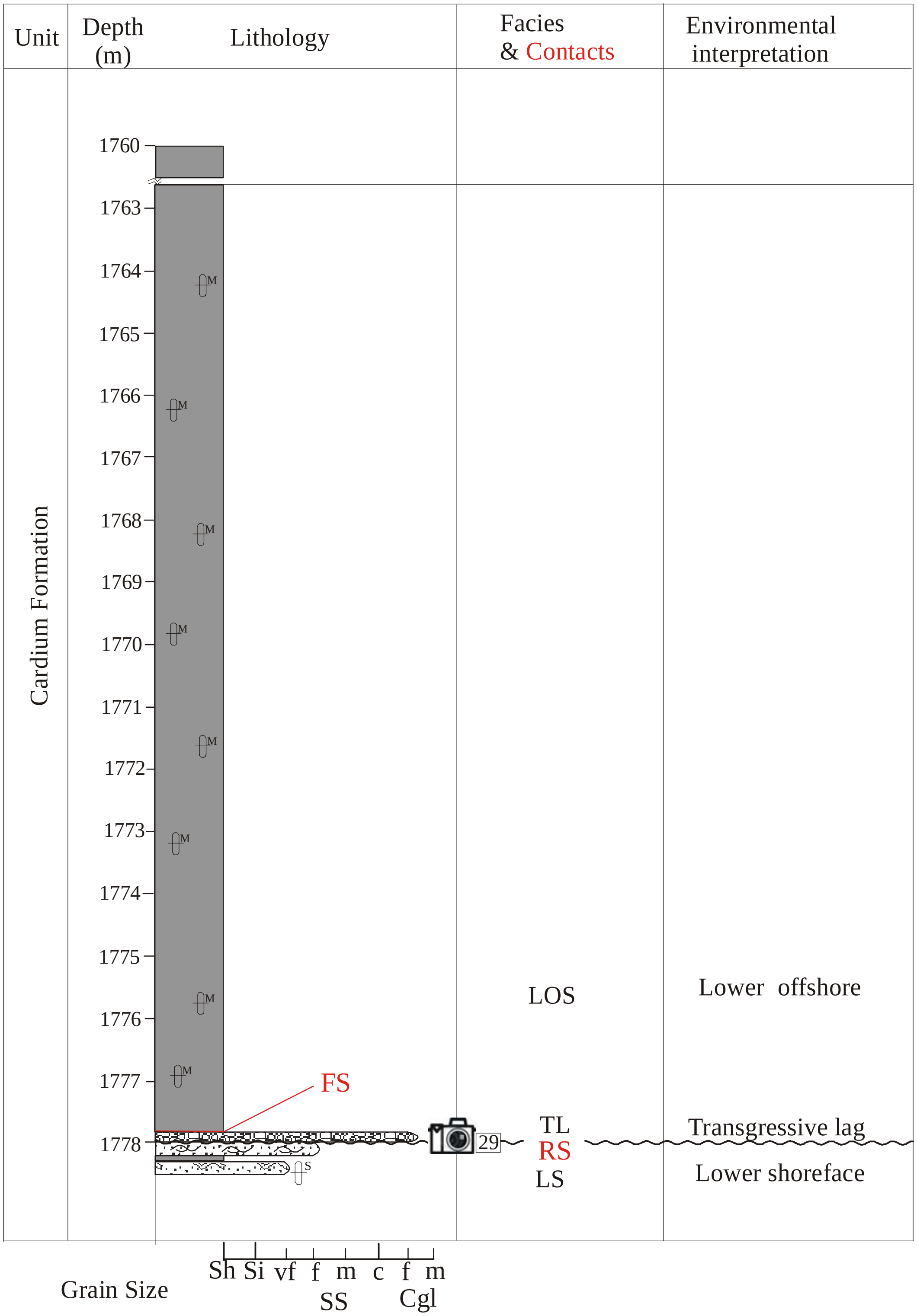

Figure 2-14 Litholog for the 06-33-048-11W5 core, annotated with main contacts (discussed in text) and facies interpretation. Legend for the litholog is given in Figure 2-1.

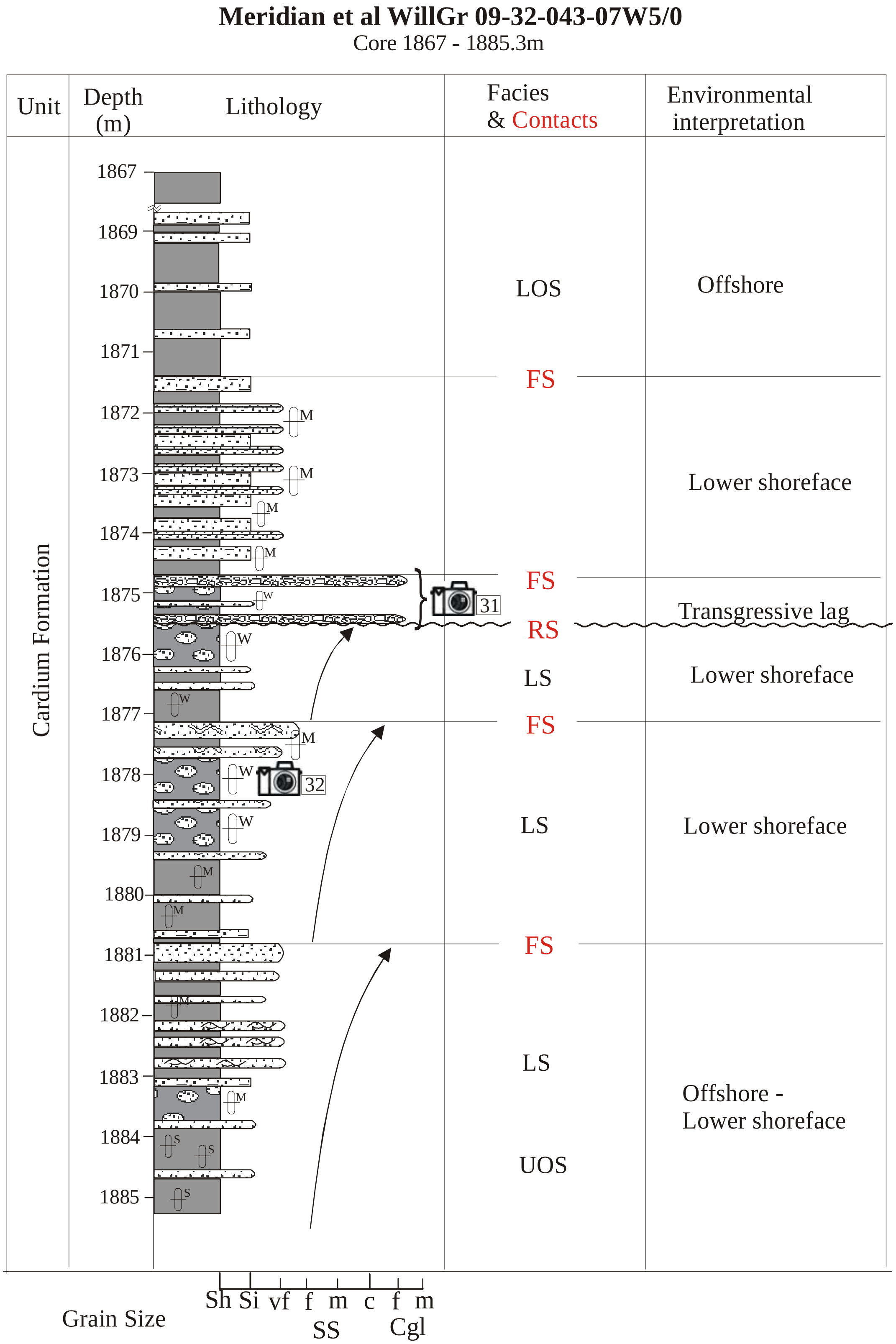

Figure 2-15 Litholog for the 09-32-043-07W5 core, annotated with main contacts (discussed in text) and facies interpretation. Legend for the litholog is given in Figure 2-1.

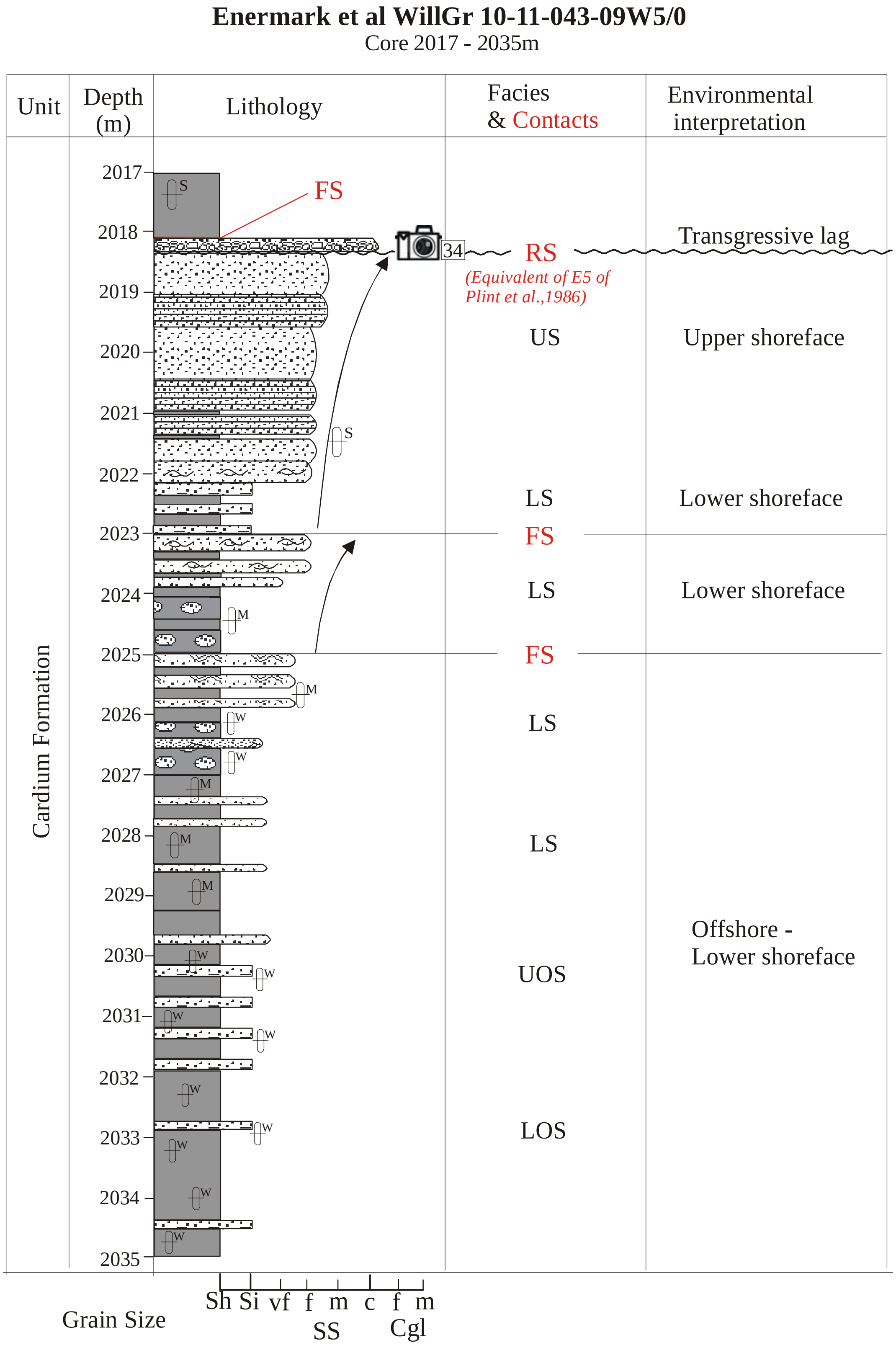

Figure 2-16 Litholog for the 10-11-43-09W5 core, annotated with main contacts (discussed in text) and facies interpretation. Legend for the litholog is given in Figure 2-1.

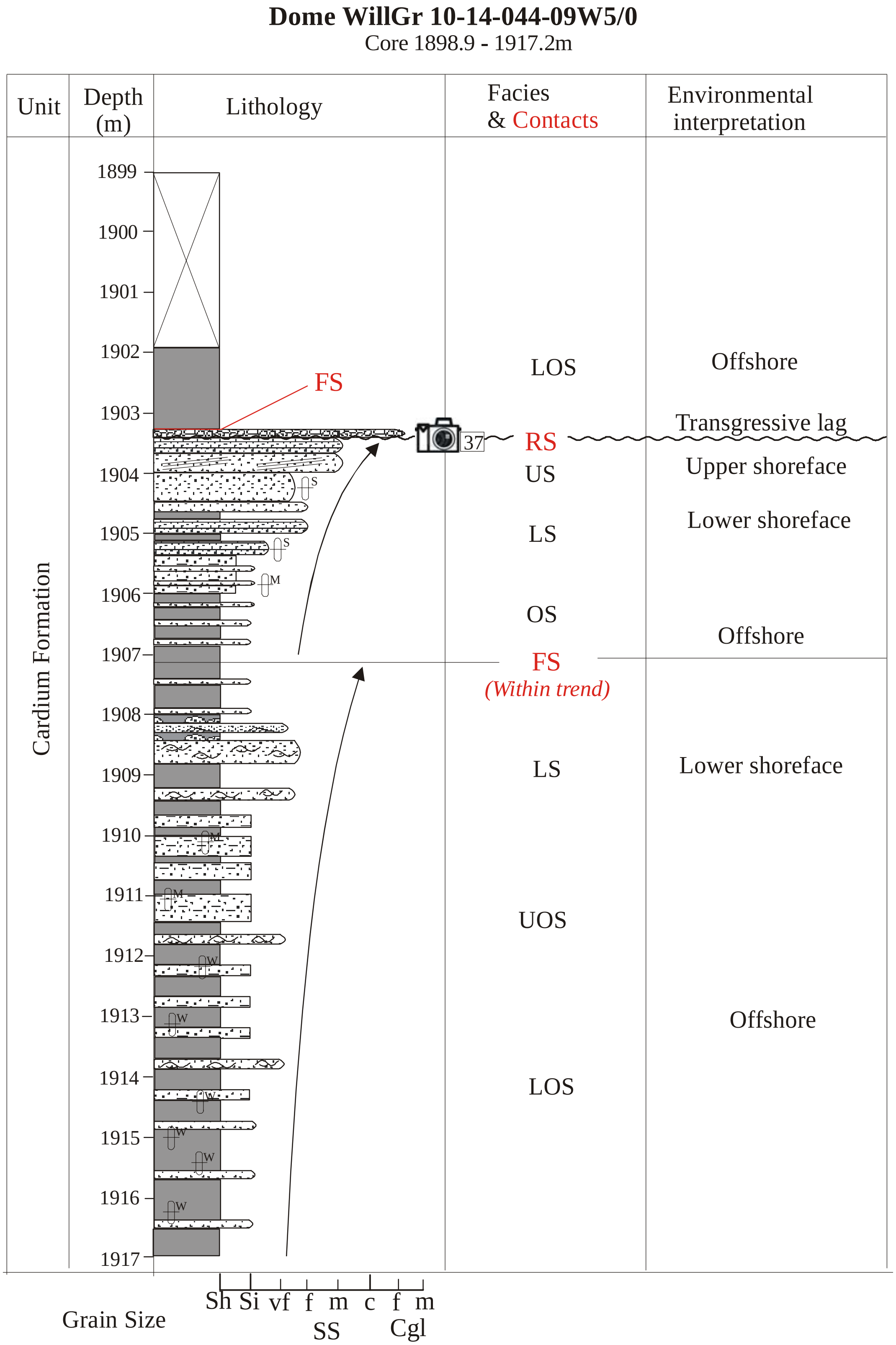

Figure 2-17 Litholog for the 10-14-044-09W5 core, annotated with main contacts (discussed in text) and facies interpretation. Legend for the litholog is given in Figure 2-1.

PC et al Ferrier 10-16-042-09W5/0
Core 2077 - 2093m

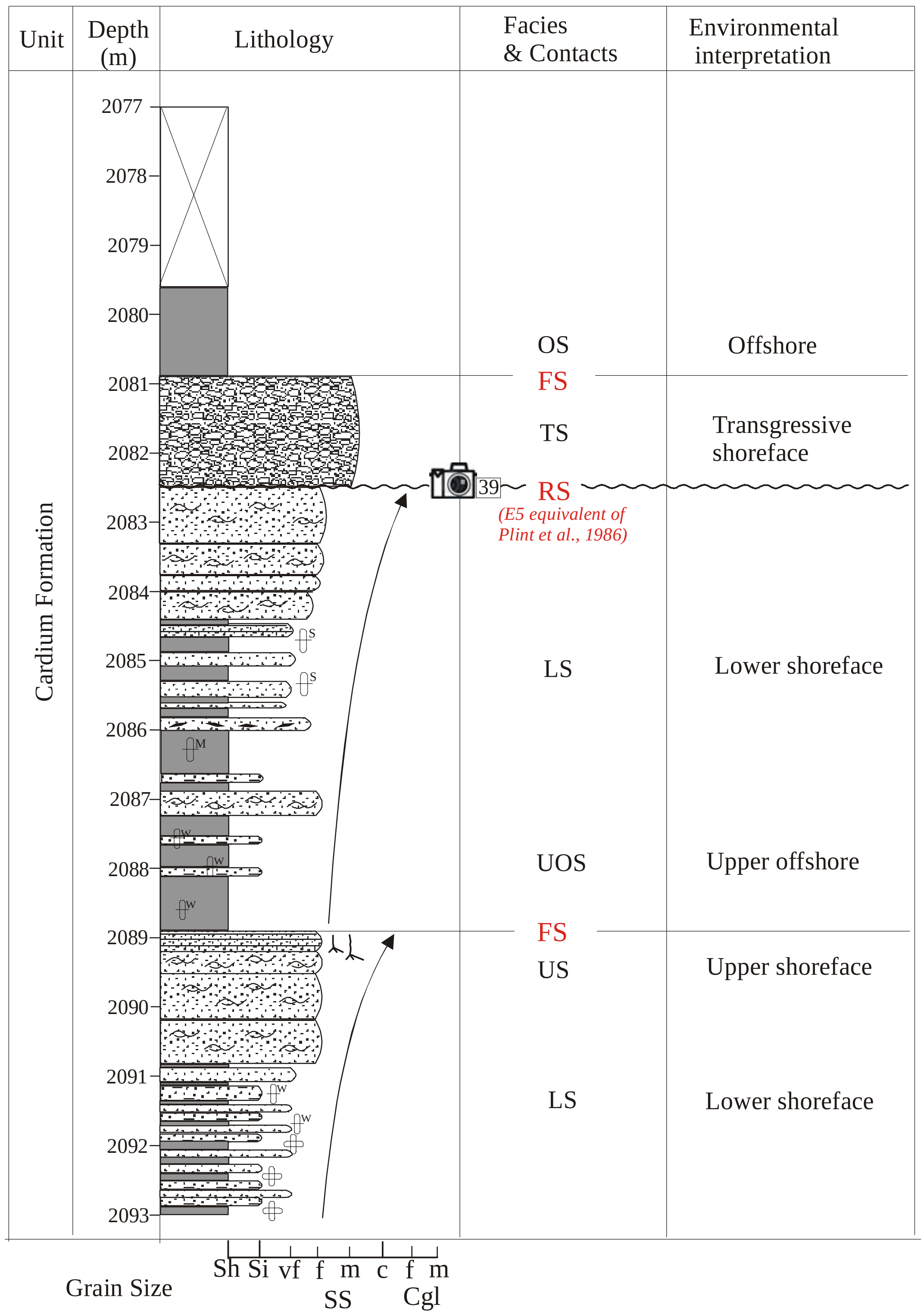

Figure 2-18 Litholog for the 10-16-042-09W5 core, annotated with main contacts (discussed in text) and facies interpretation. Legend for the litholog is given in Figure 2-1.

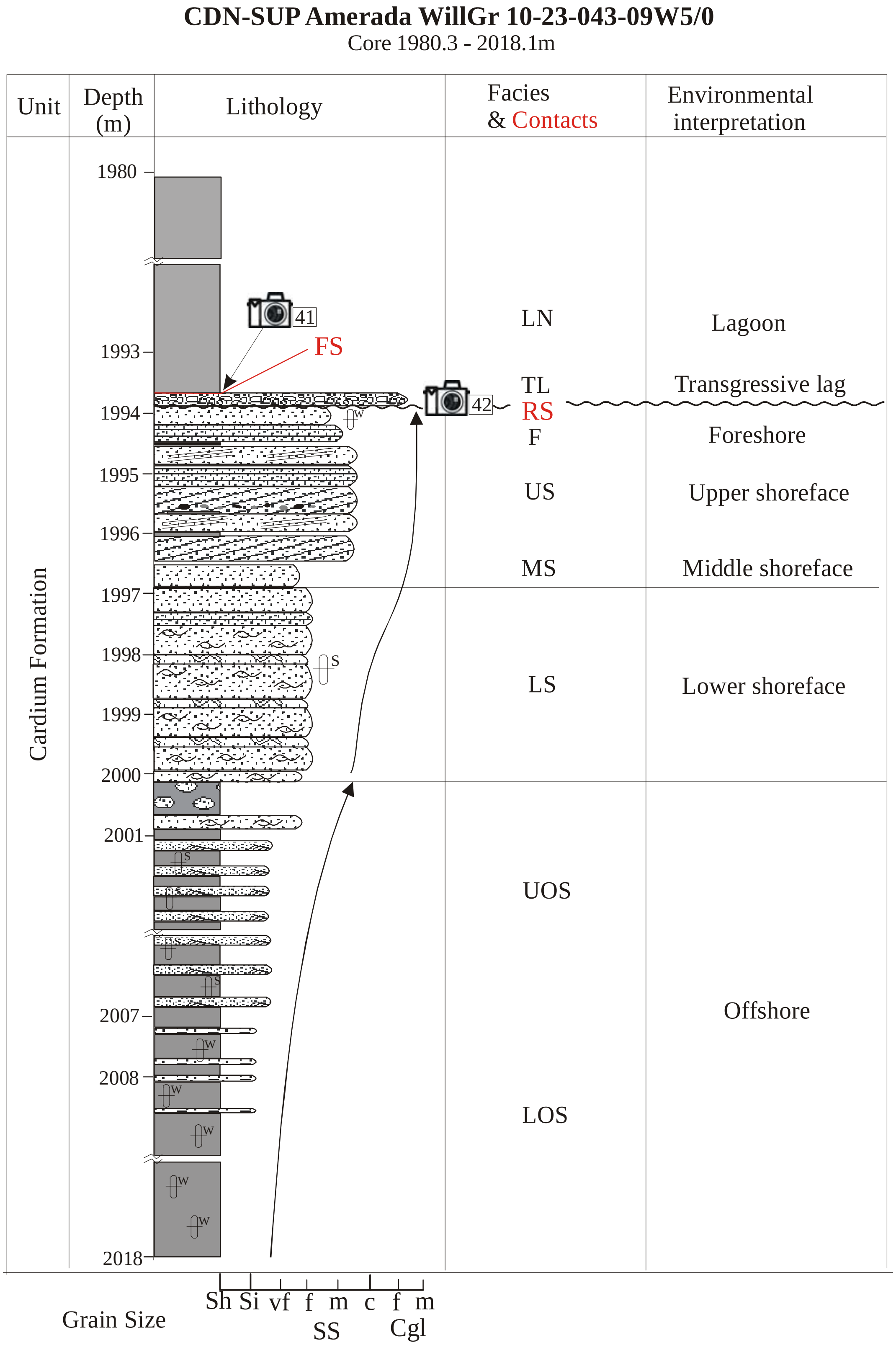

Figure 2-19 Litholog for the 10-23-043-09W5 core, annotated with main contacts (discussed in text) and facies interpretation. Legend for the litholog is given in Figure 2-1.

Dome Alder Flats 10-26-045-09W5/0

Core 1743.8 - 1762m

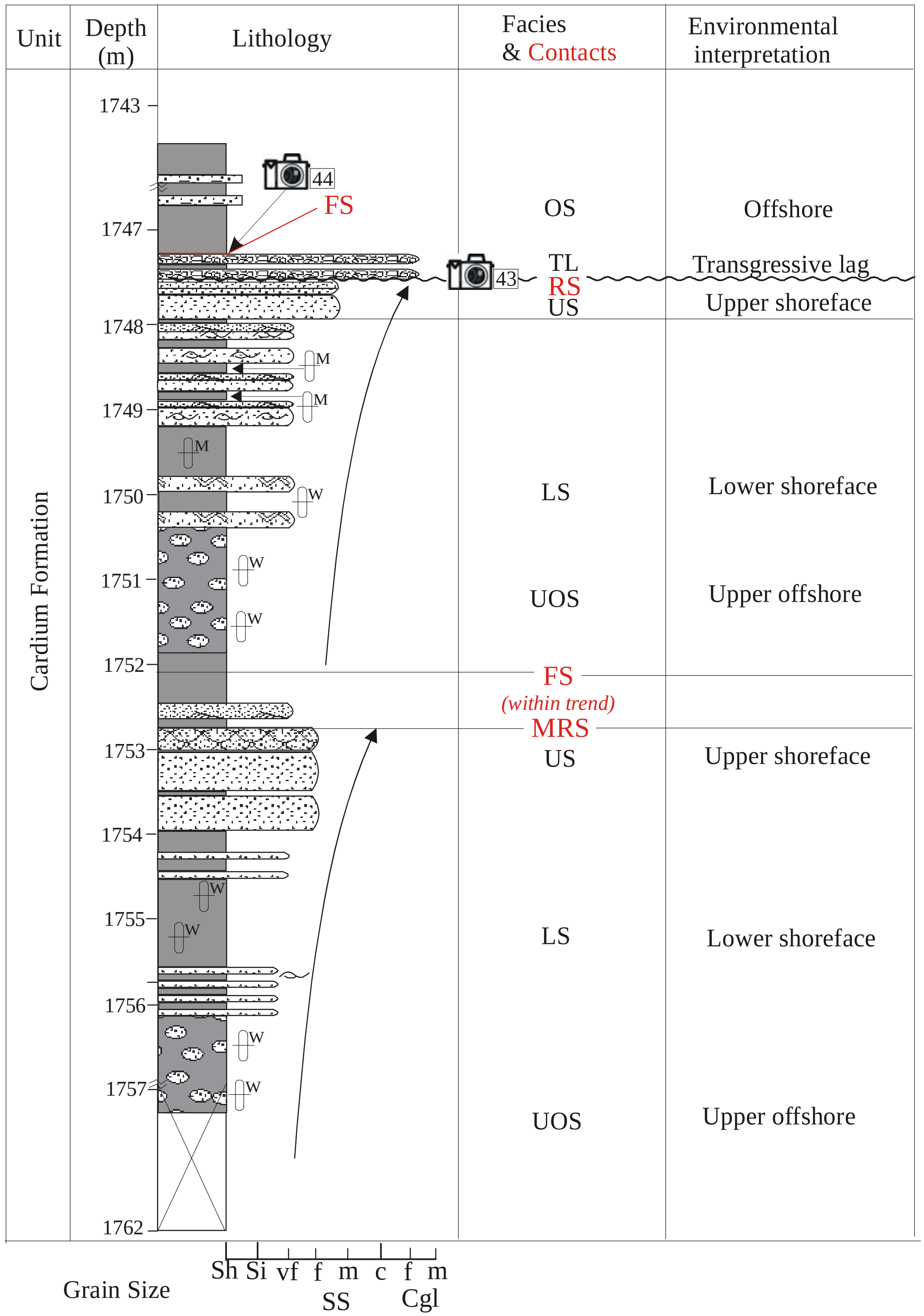

Figure 2-20 Litholog for the 10-26-045-09W5 core, annotated with main contacts (discussed in text) and facies interpretation. Legend for the litholog is given in Figure 2-1.

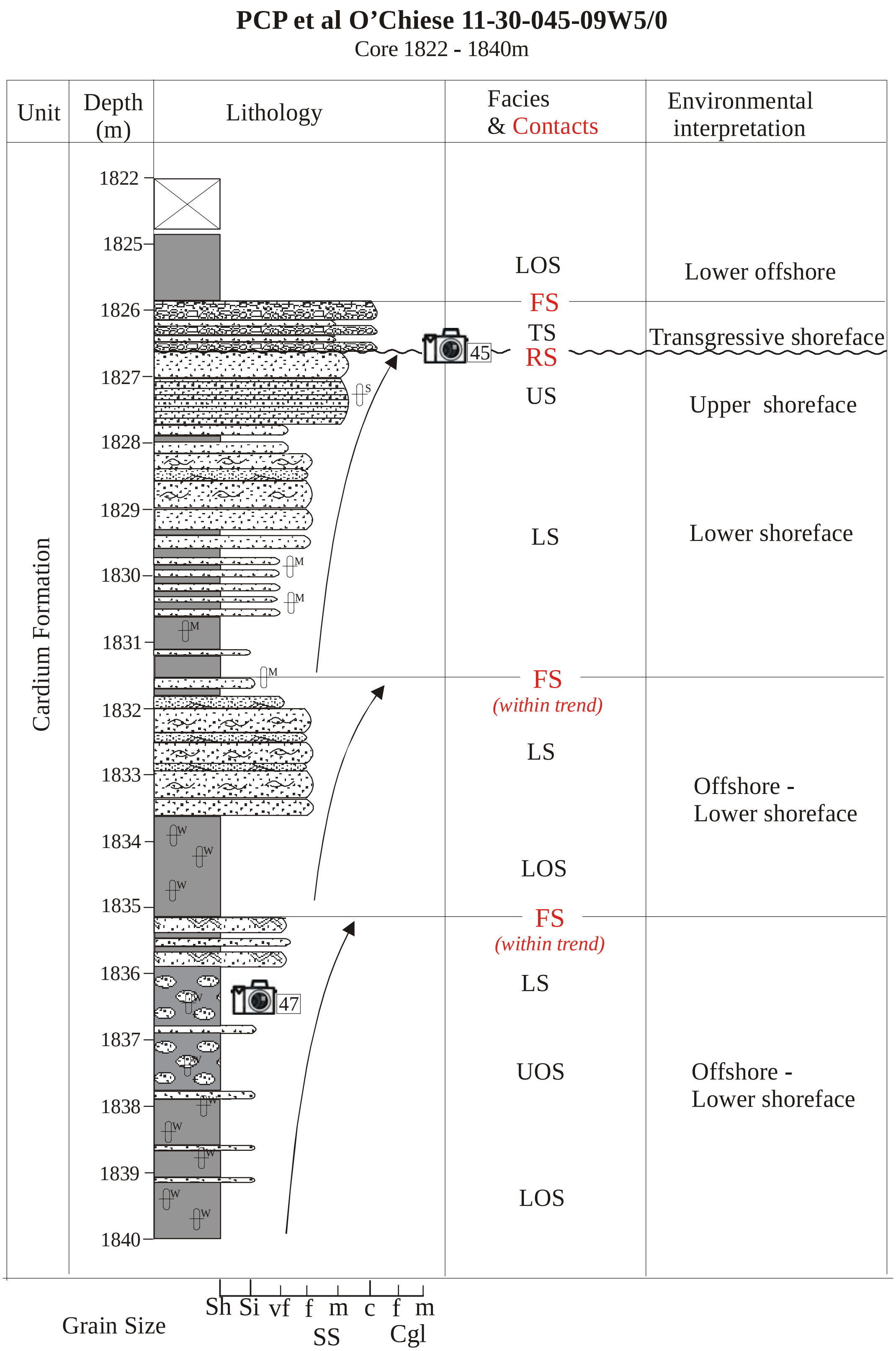

Figure 2-21 Litholog for the 11-30-045-09W5 core, annotated with main contacts (discussed in text) and facies interpretation. Legend for the litholog is given in Figure 2-1.

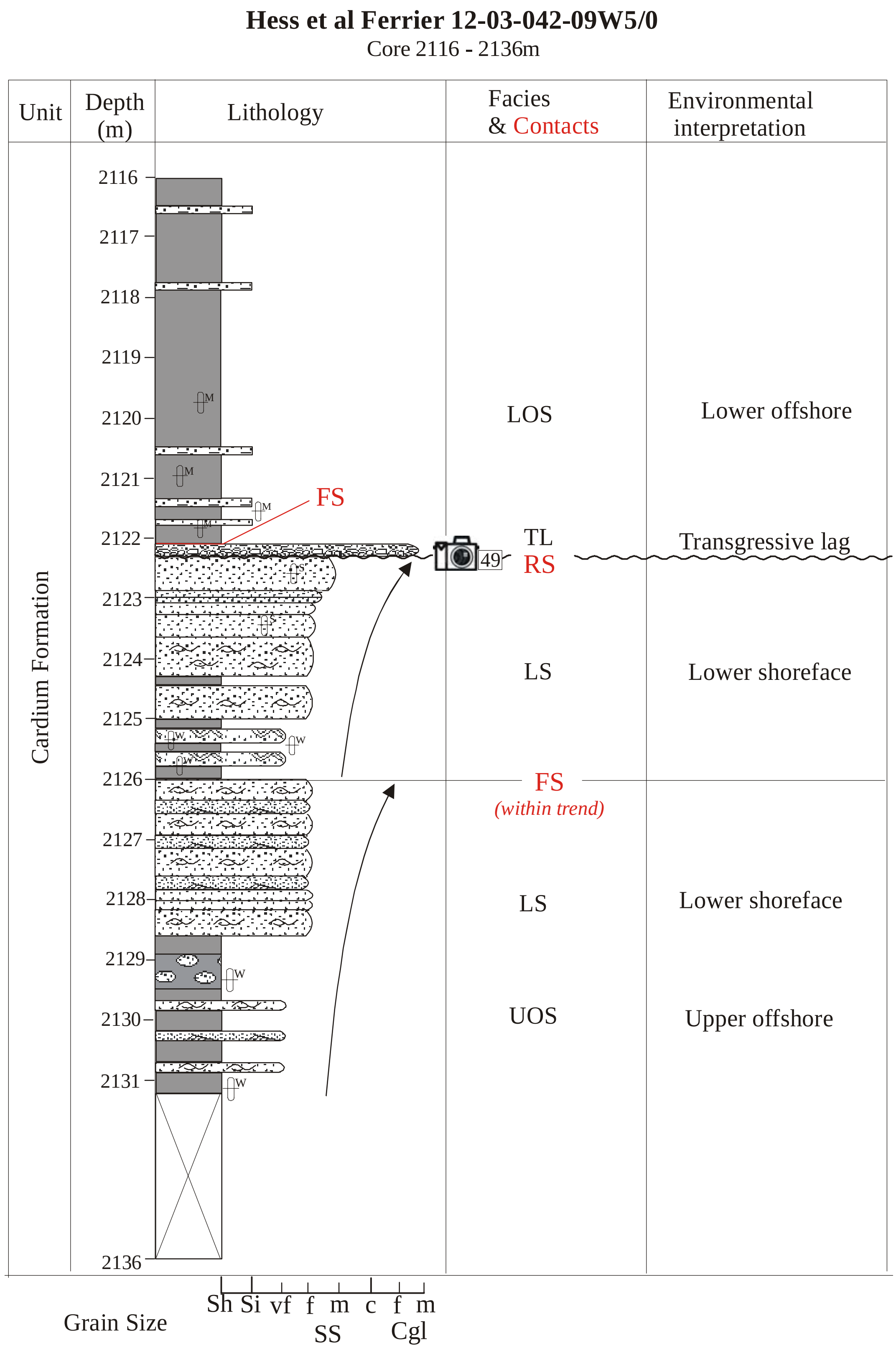

Figure 2-22 Litholog for the 12-03-042-09W5 core, annotated with main contacts (discussed in text) and facies interpretation. Legend for the litholog is given in Figure 2-1.

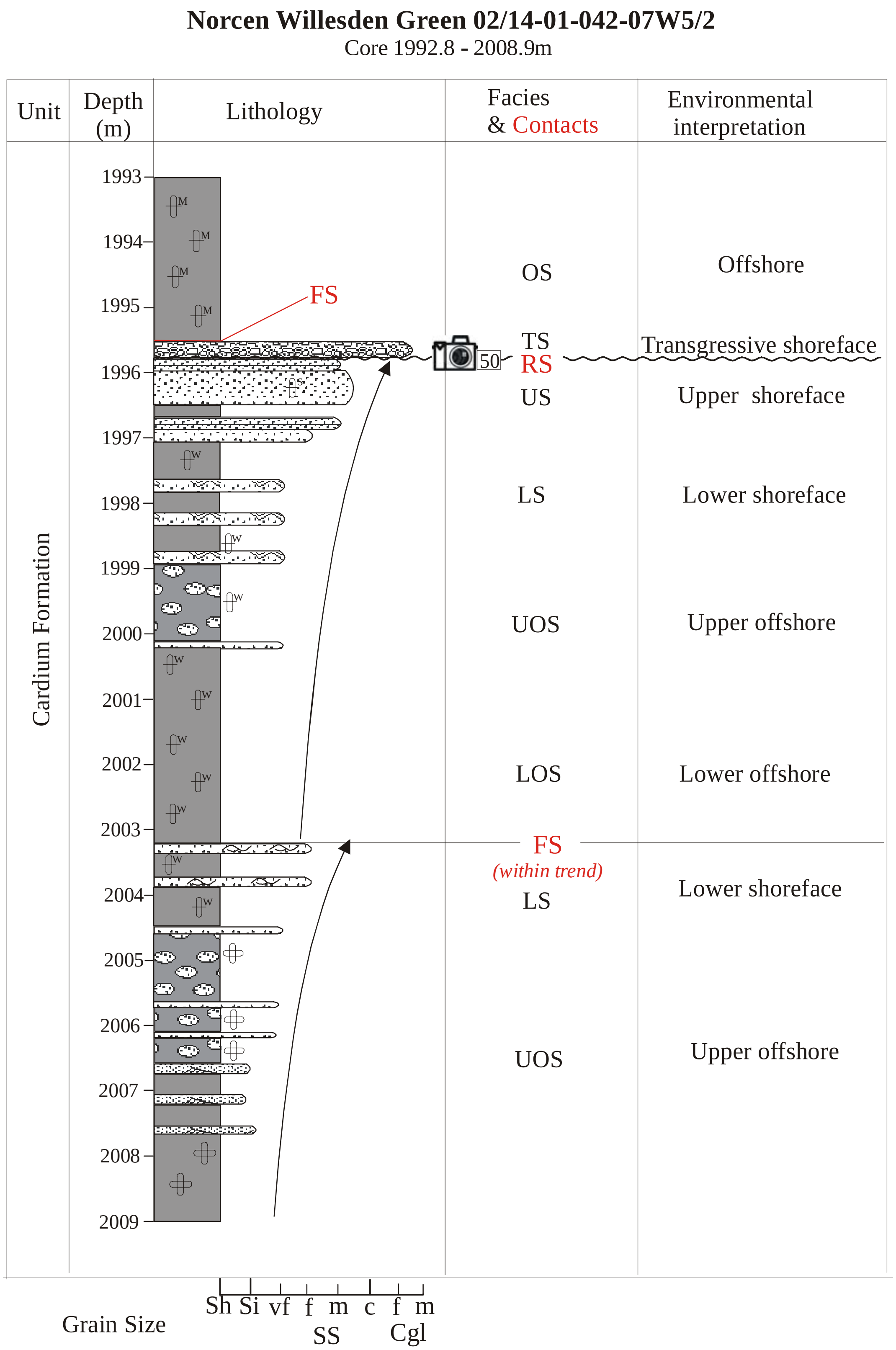

Figure 2-23 Litholog for the 02/14-01-042-07W5 core, annotated with main contacts (discussed in text) and facies interpretation. Legend for the litholog is given in Figure 2-1.

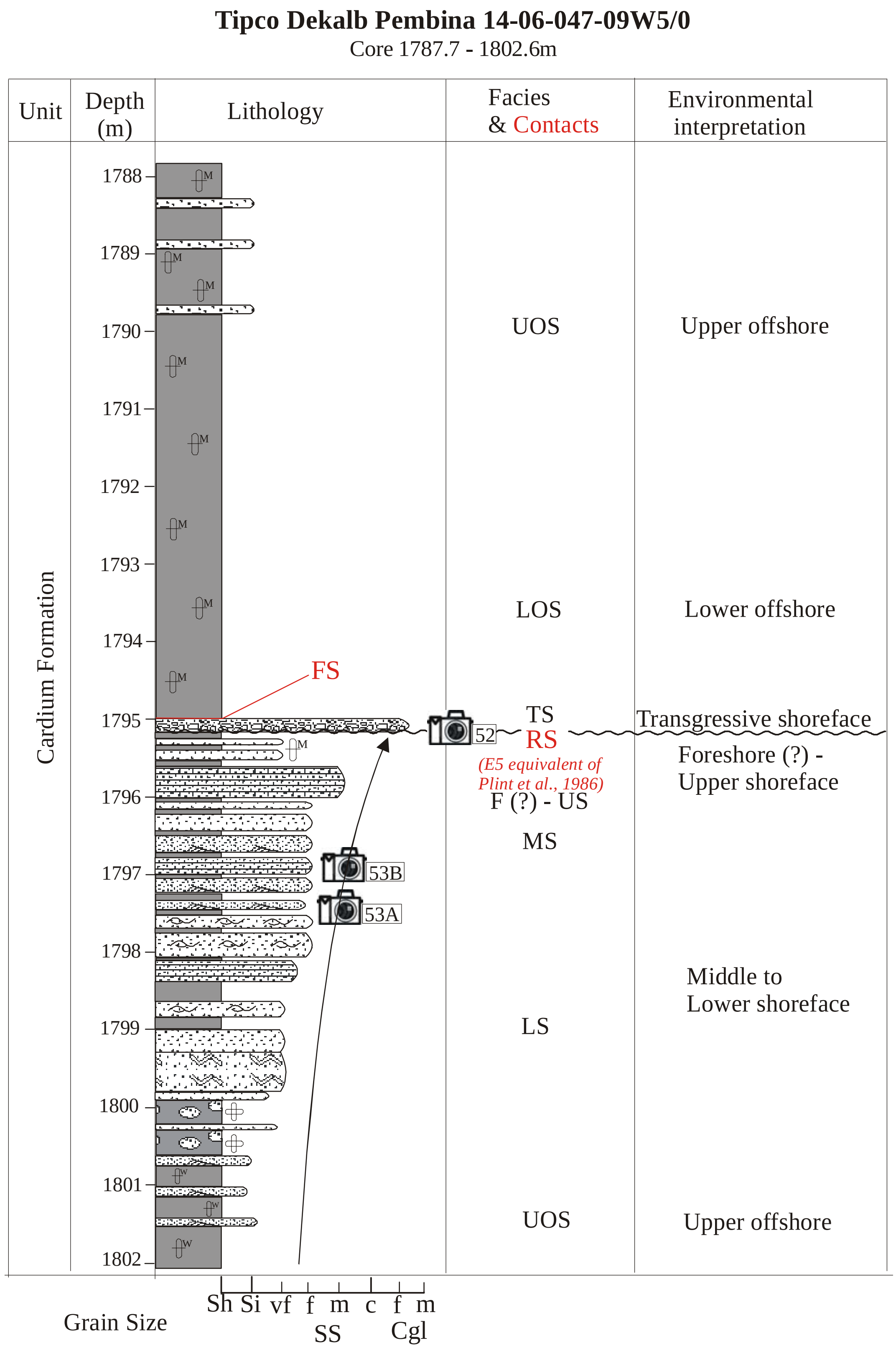

Figure 2-24 Litholog for the 14-06-047-09W5 core, annotated with main contacts (discussed in text) and facies interpretation. Legend for the litholog is given in Figure 2-1.

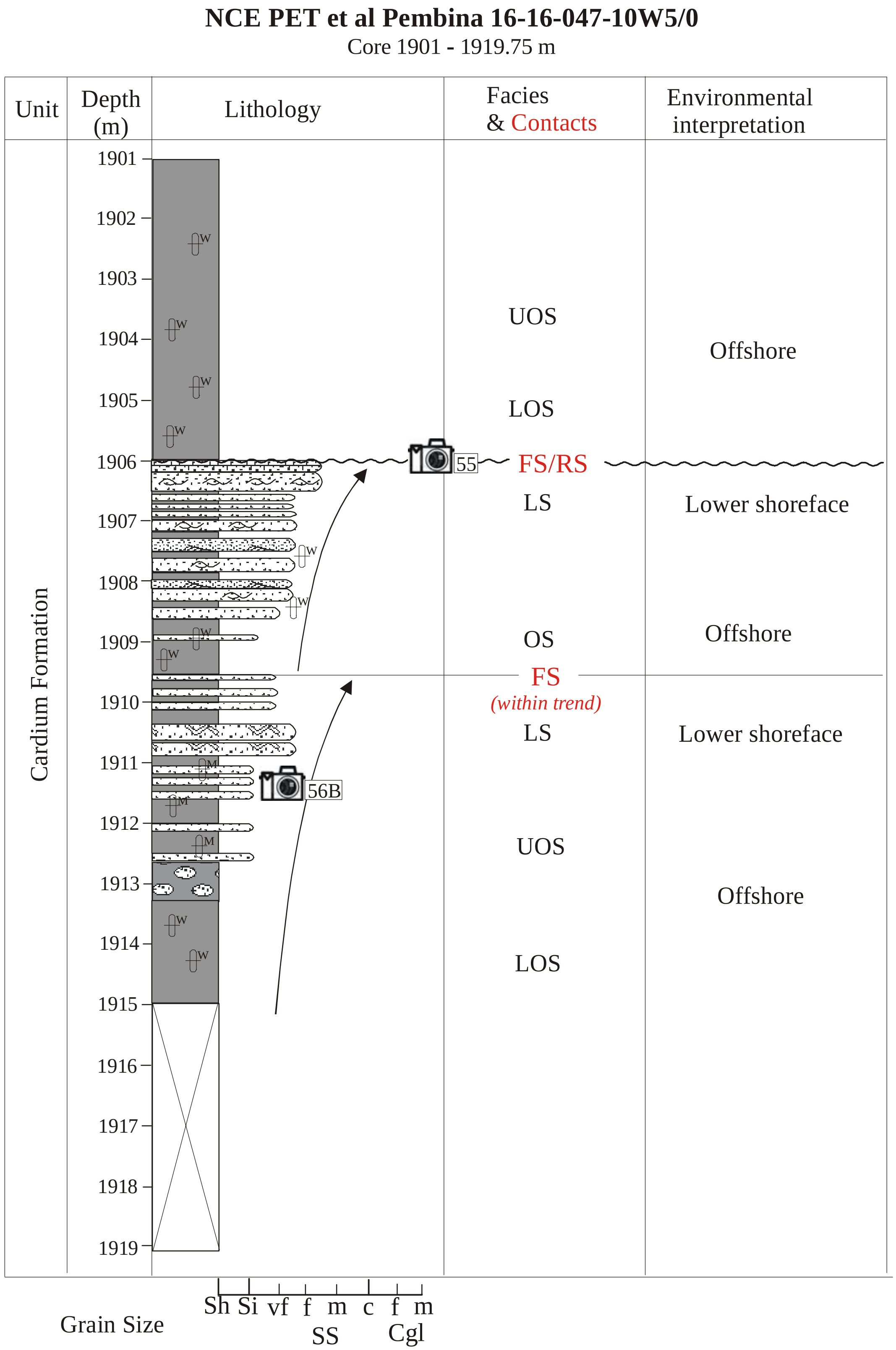

Figure 2-25 Litholog for the 16-16-047-10W5 core, annotated with main contacts (discussed in text) and facies interpretation. Legend for the litholog is given in Figure 2-1.

Hess CDN-SUP Crimson 06-22-042-09W5/0

Core 2074.5 - 2089.7m

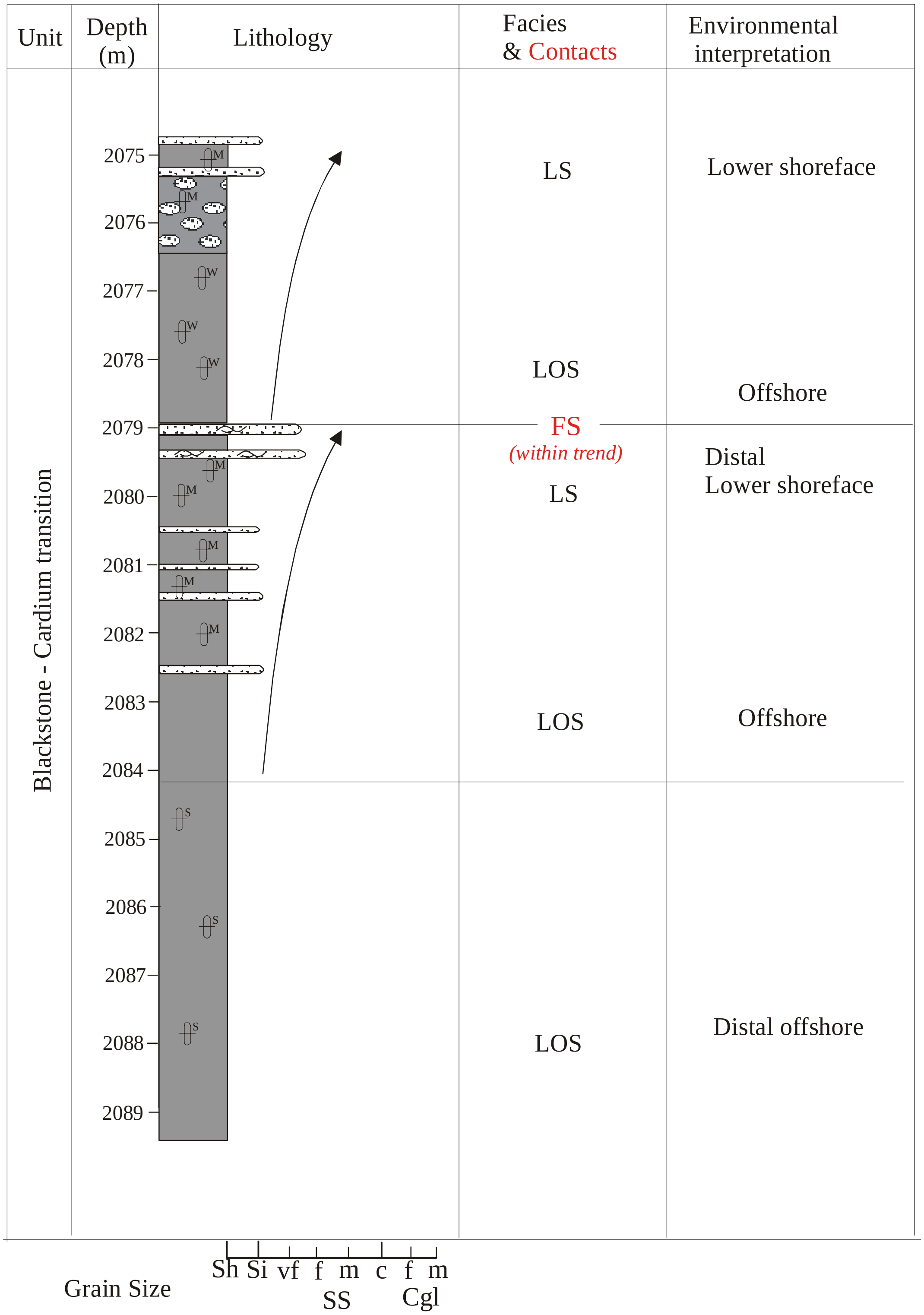

Figure 2-26 Litholog for the 06-22-042-09W5 core, annotated with main contacts (discussed in text) and facies interpretation. Legend for the litholog is given in Figure 2-1.

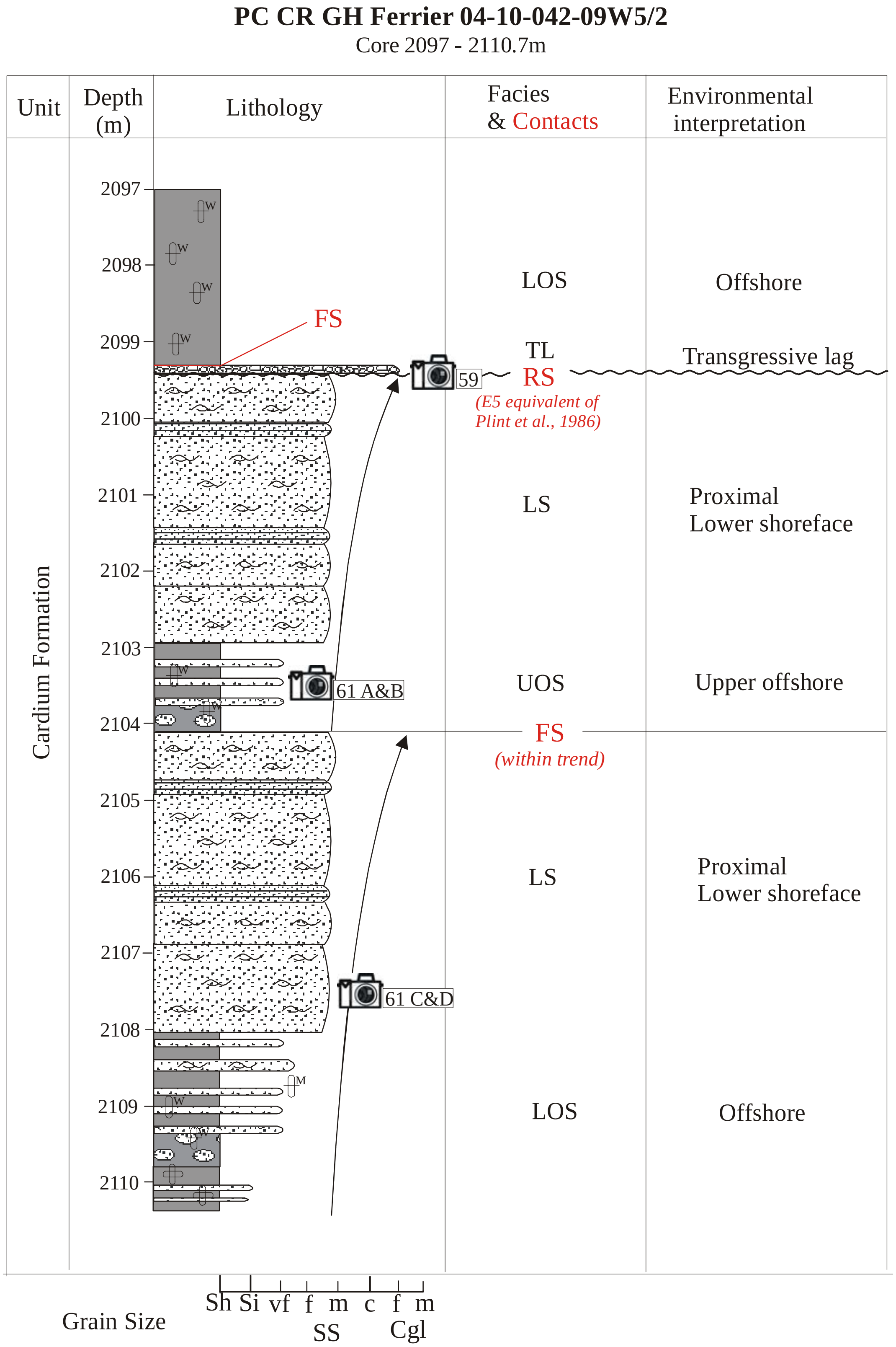

Figure 2-27 Litholog for the 04-10-042-09W5 core, annotated with main contacts (discussed in text) and facies interpretation. Legend for the litholog is given in Figure 2-1.

PC CR EX Crimson 10-10-042-09W5/0

Core 2058.3- 2073.3m

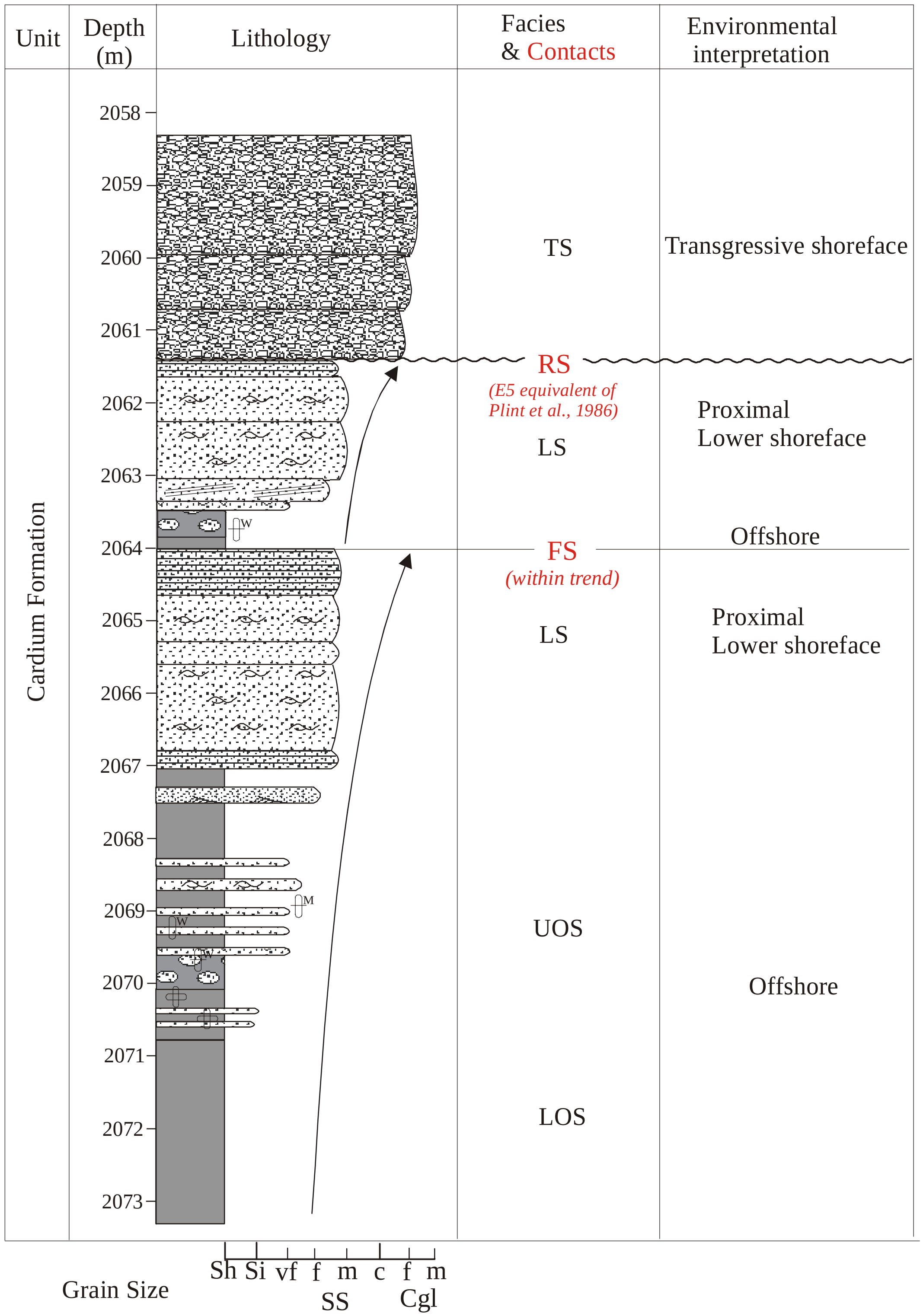

Figure 2-28 Litholog for the 10-10-042-09W5 core, annotated with main contacts (discussed in text) and facies interpretation. Legend for the litholog is given in Figure 2-1.

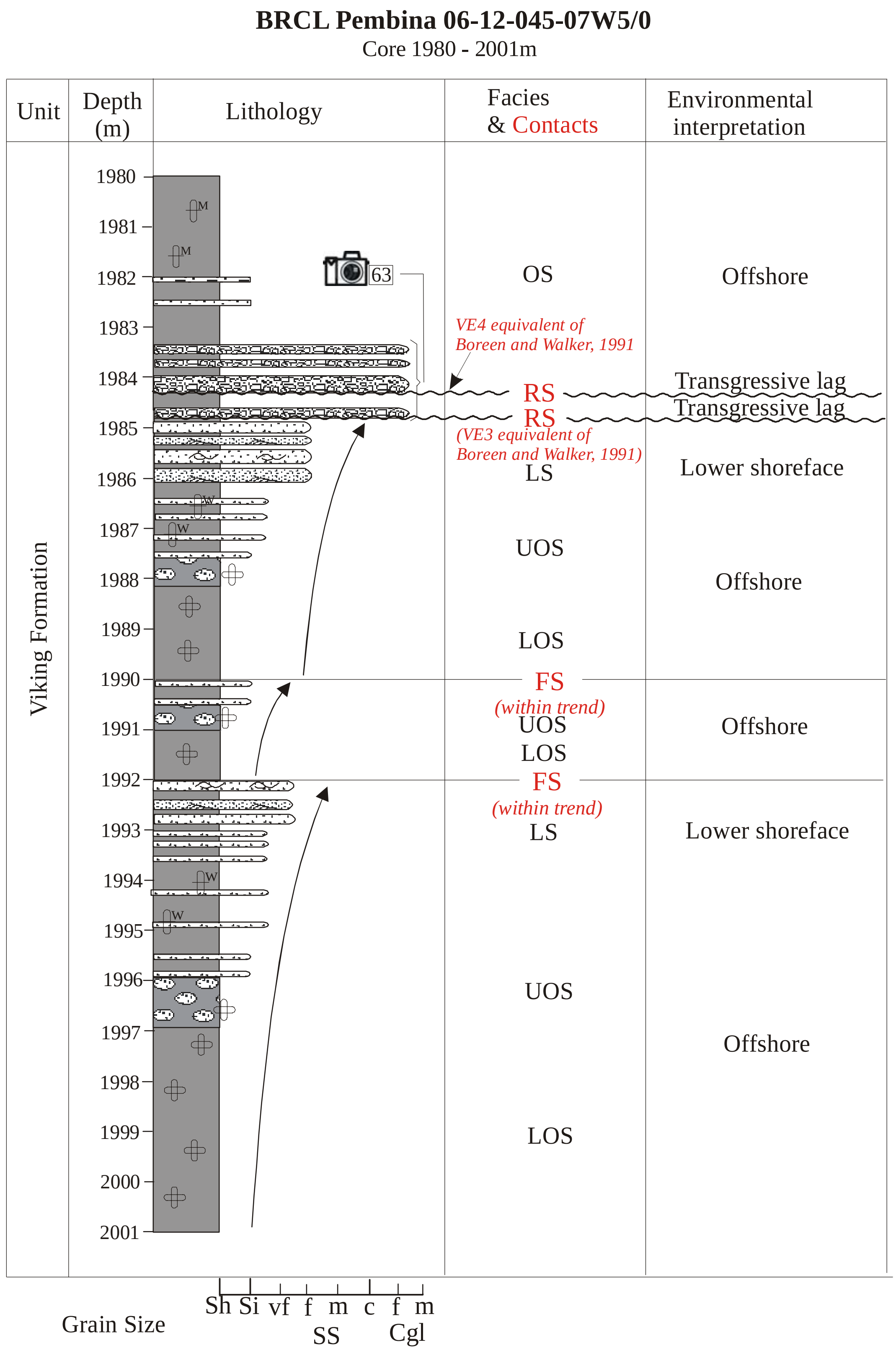

Figure 2-29 Litholog for the 06-12-045-07W5 core, annotated with main contacts (discussed in text) and facies interpretation. Legend for the litholog is given in Figure 2-1.

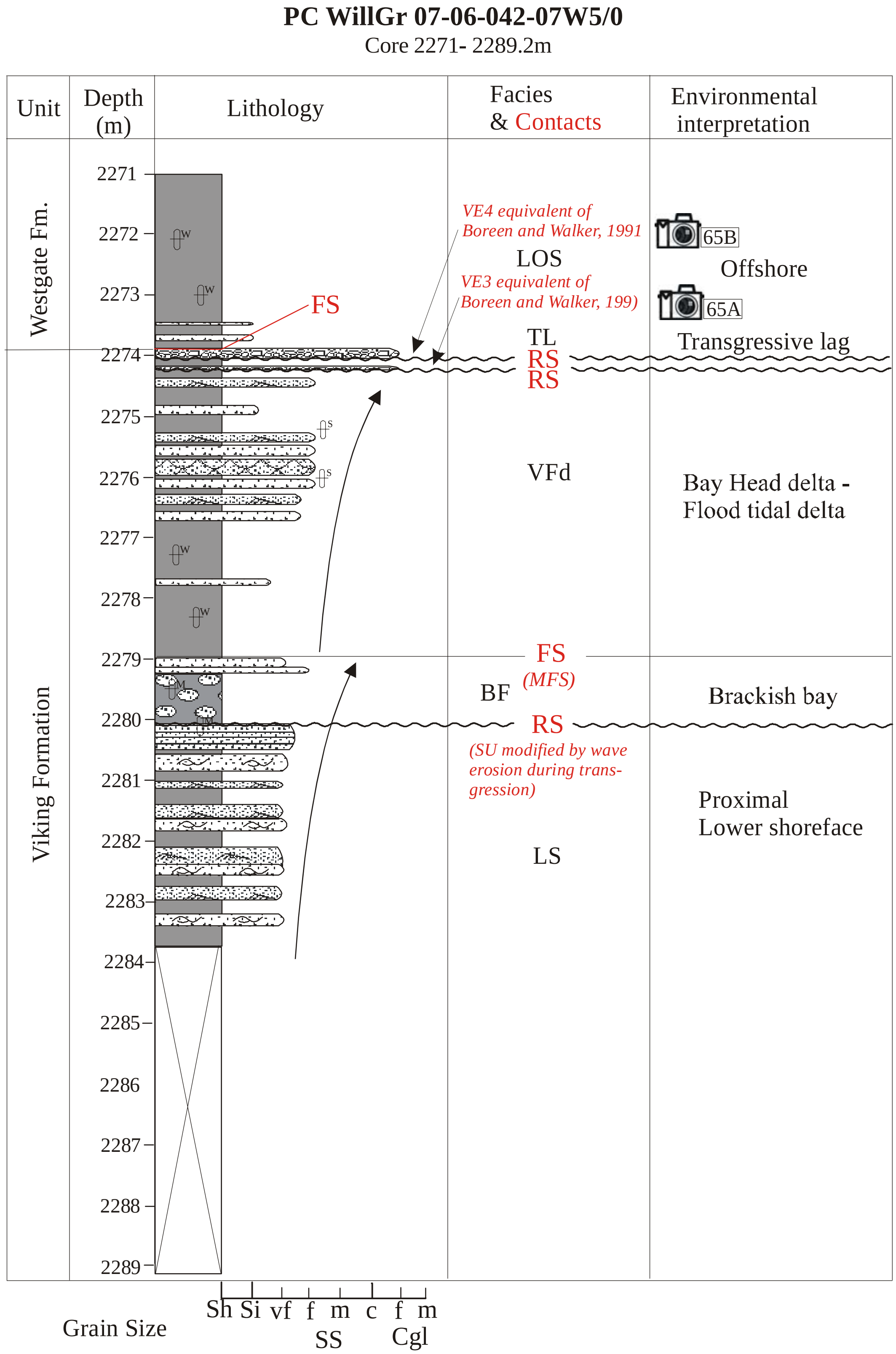

Figure 2-30 Litholog for the 07-06-042-07W5 core, annotated with main contacts (discussed in text) and facies interpretation. Legend for the litholog is given in Figure 2-1.

ACL WillGr 07-08-042-05W5/0

Core 2051- 2069m

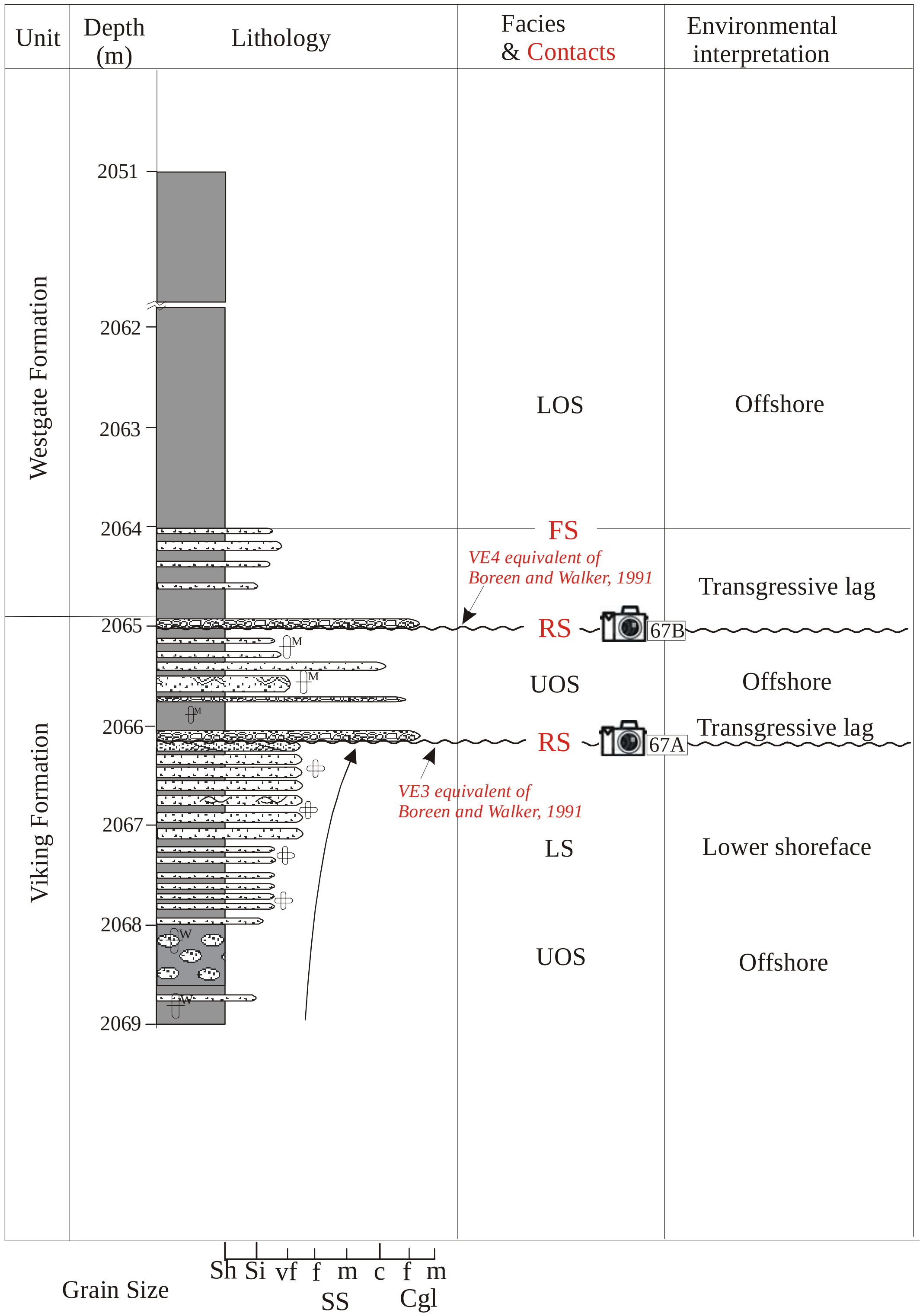

Figure 2-31 Litholog for the 07-08-042-07W5 core, annotated with main contacts (discussed in text) and facies interpretation. Legend for the litholog is given in Figure 2-1.

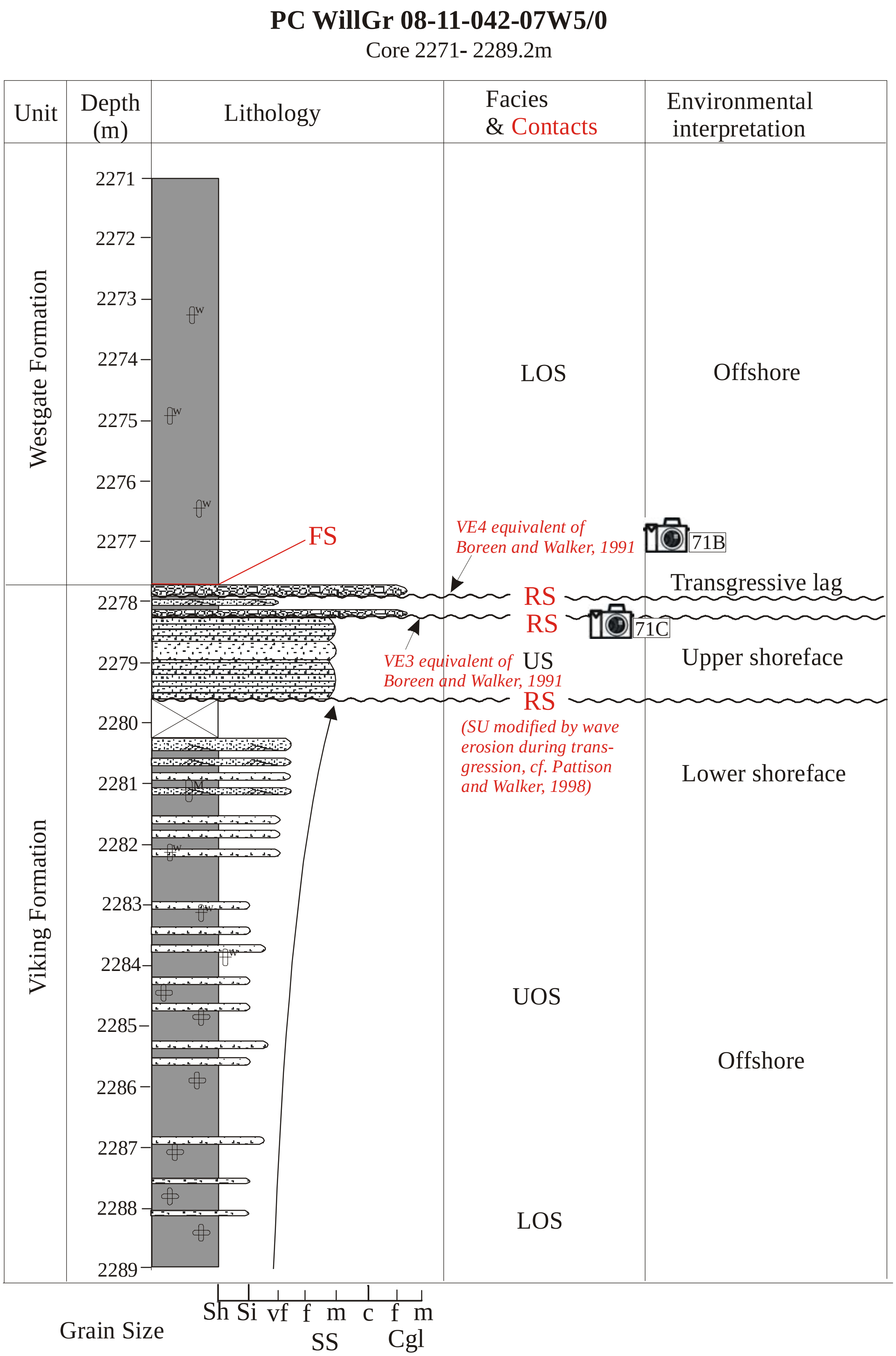

Figure 2-32 Litholog for the 08-11-042-07W5 core, annotated with main contacts (discussed in text) and facies interpretation. Legend for the litholog is given in Figure 2-1.

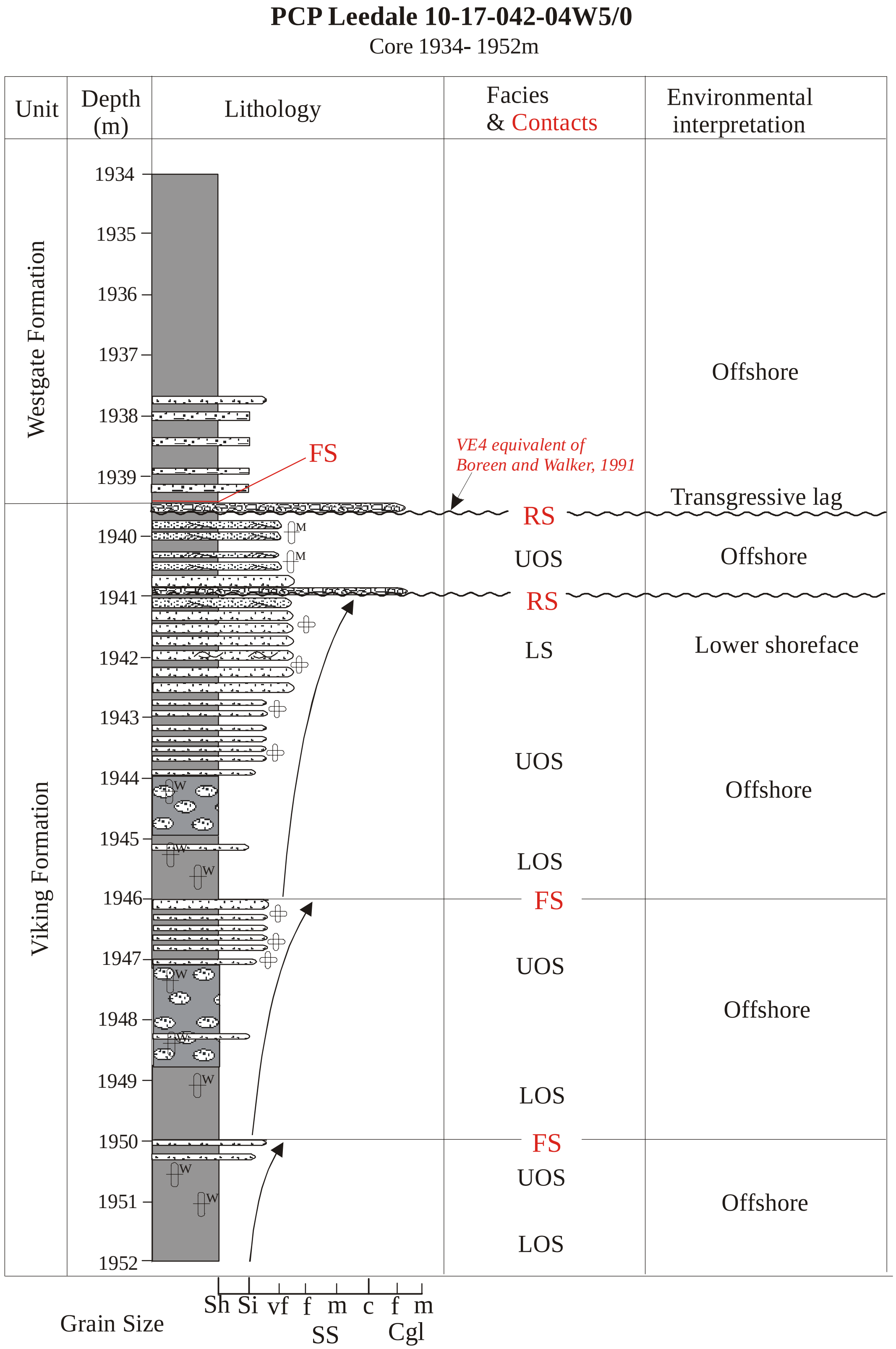

Figure 2-33 Litholog for the 10-17-042-04W5 core, annotated with main contacts (discussed in text) and facies interpretation. Legend for the litholog is given in Figure 2-1.

ESSO Open Creek 03/13-13-042-05W5/0

Core 1974 - 1980.5m

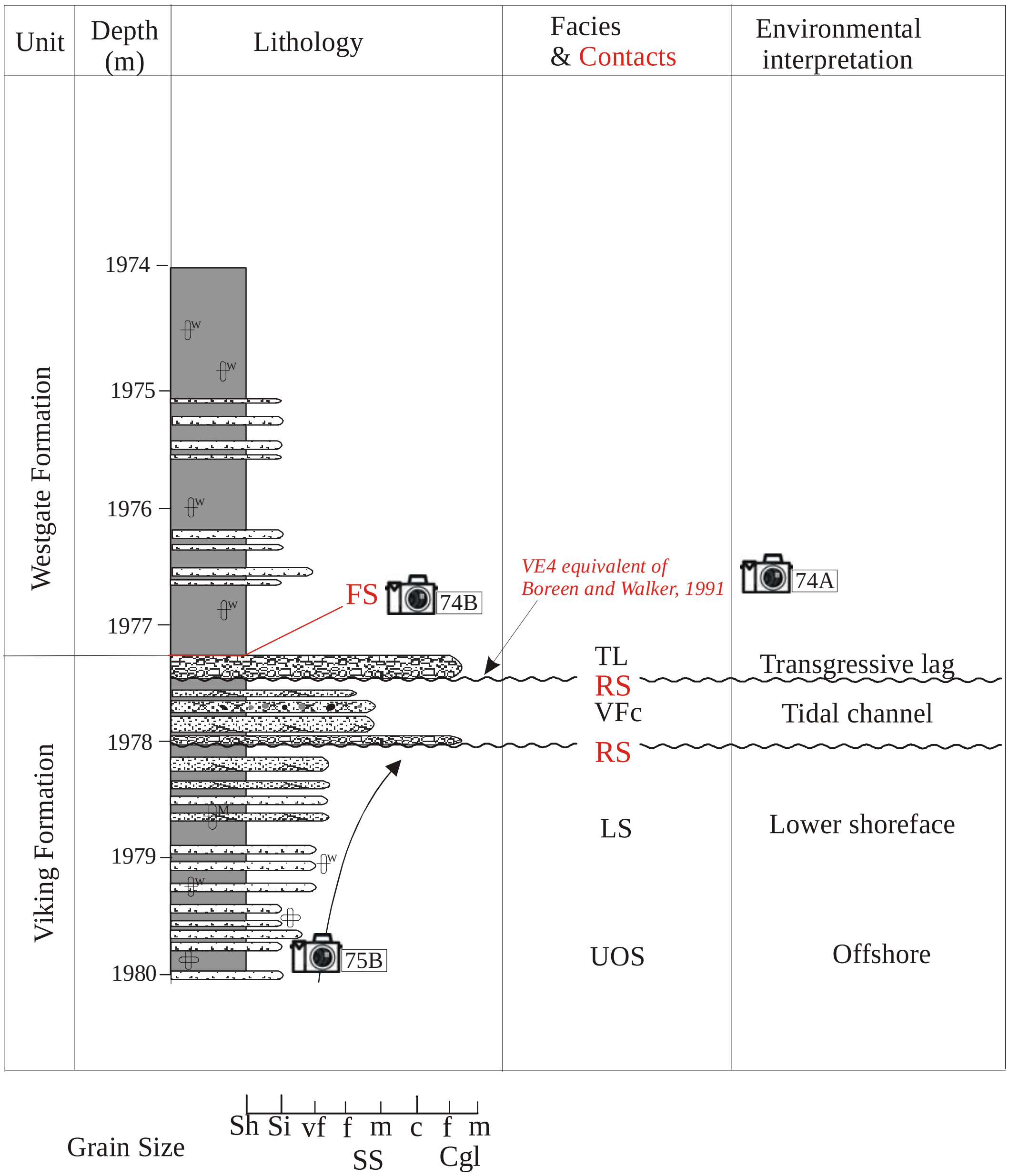

Figure 2-34 Litholog for the 03/13-13-042-05W5 core, annotated with main contacts (discussed in text) and facies interpretation. Legend for the litholog is given in Figure 2-1.

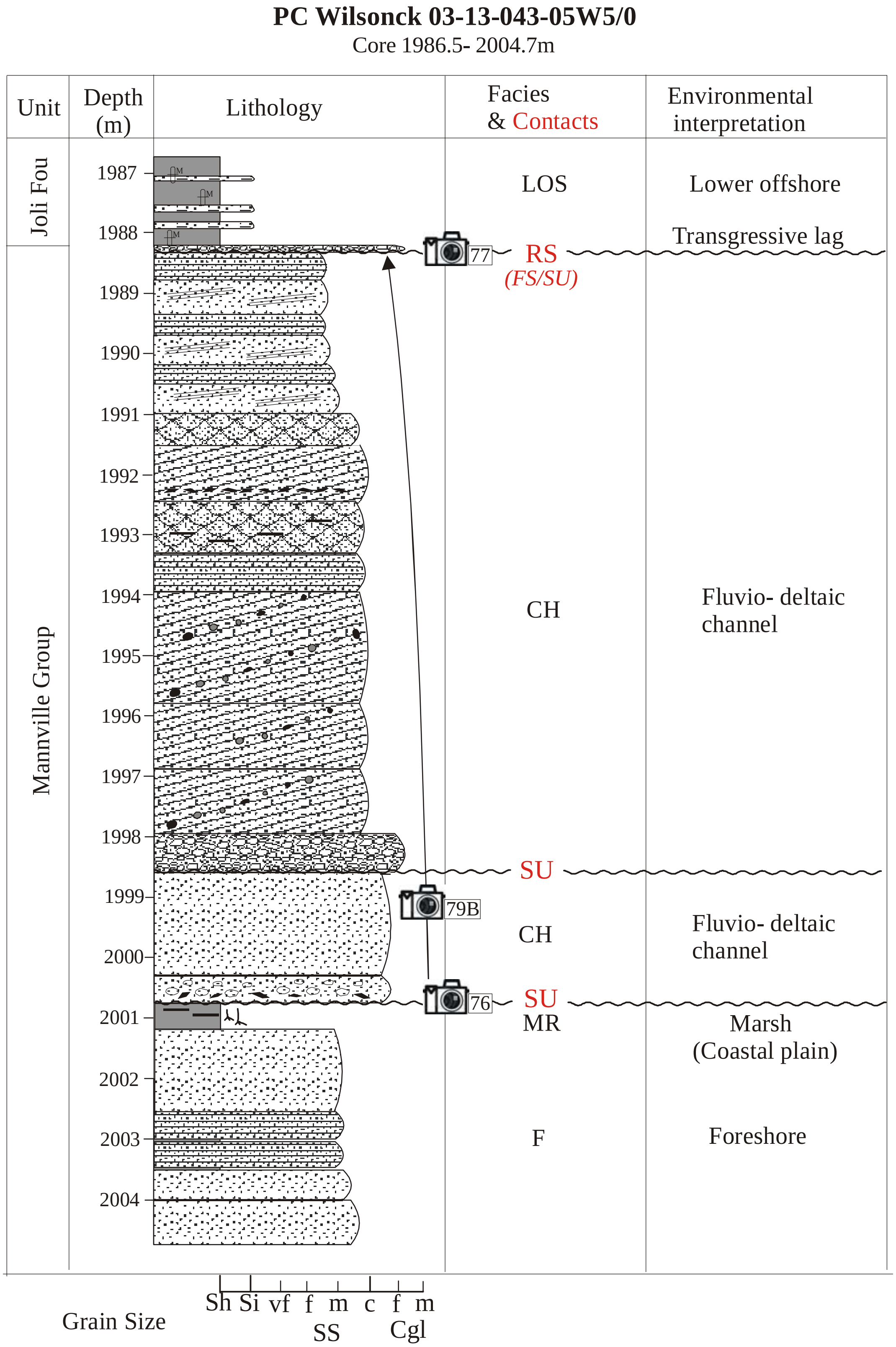

Figure 2-35 Litholog for the 03-13-043-05W5 core, annotated with main contacts (discussed in text) and facies interpretation. Legend for the litholog is given in Figure 2-1.

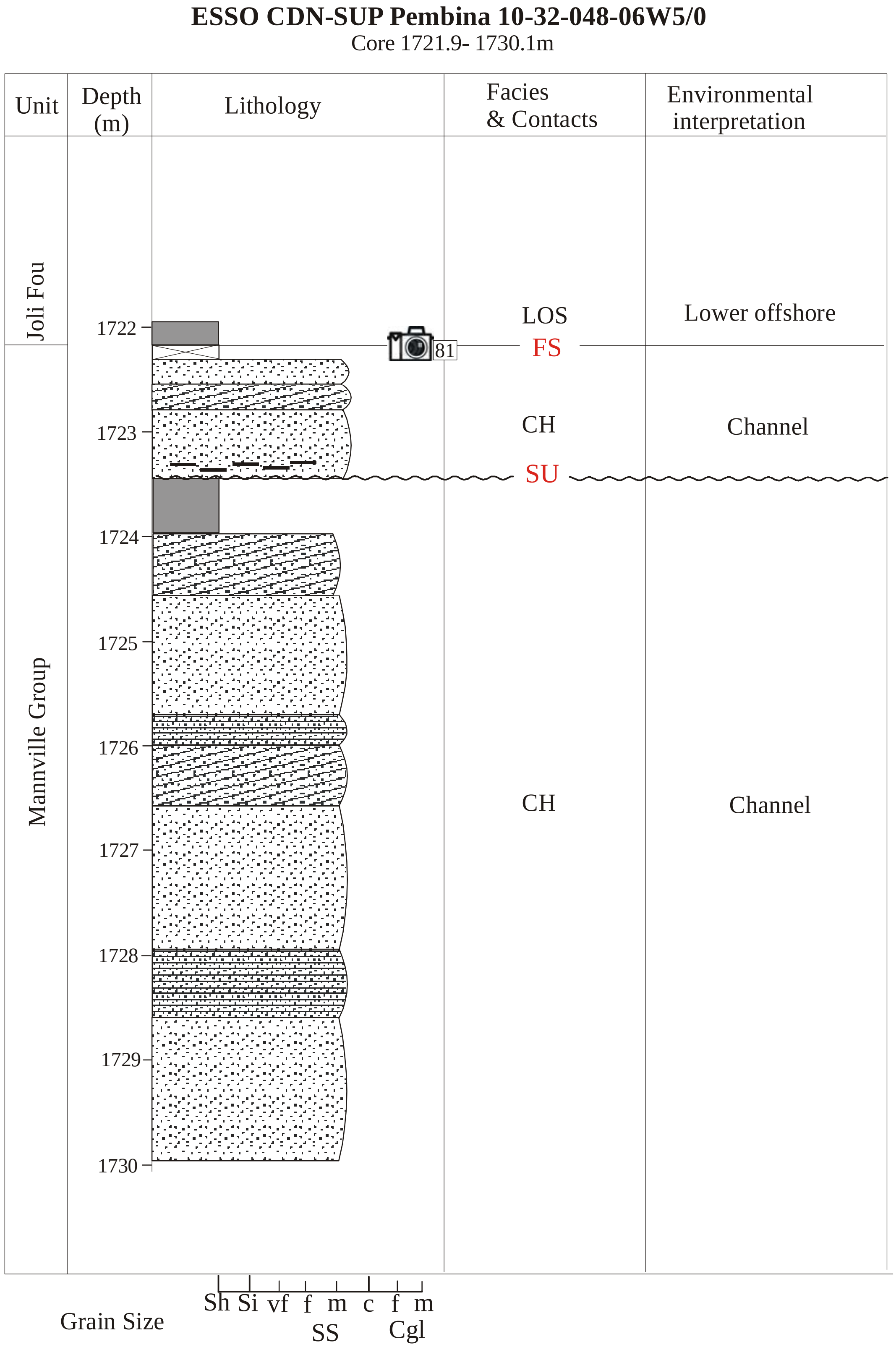

Figure 2-36 Litholog for the 10-32-048-06W5 core, annotated with main contacts (discussed in text) and facies interpretation. Legend for the litholog is given in Figure 2-1.

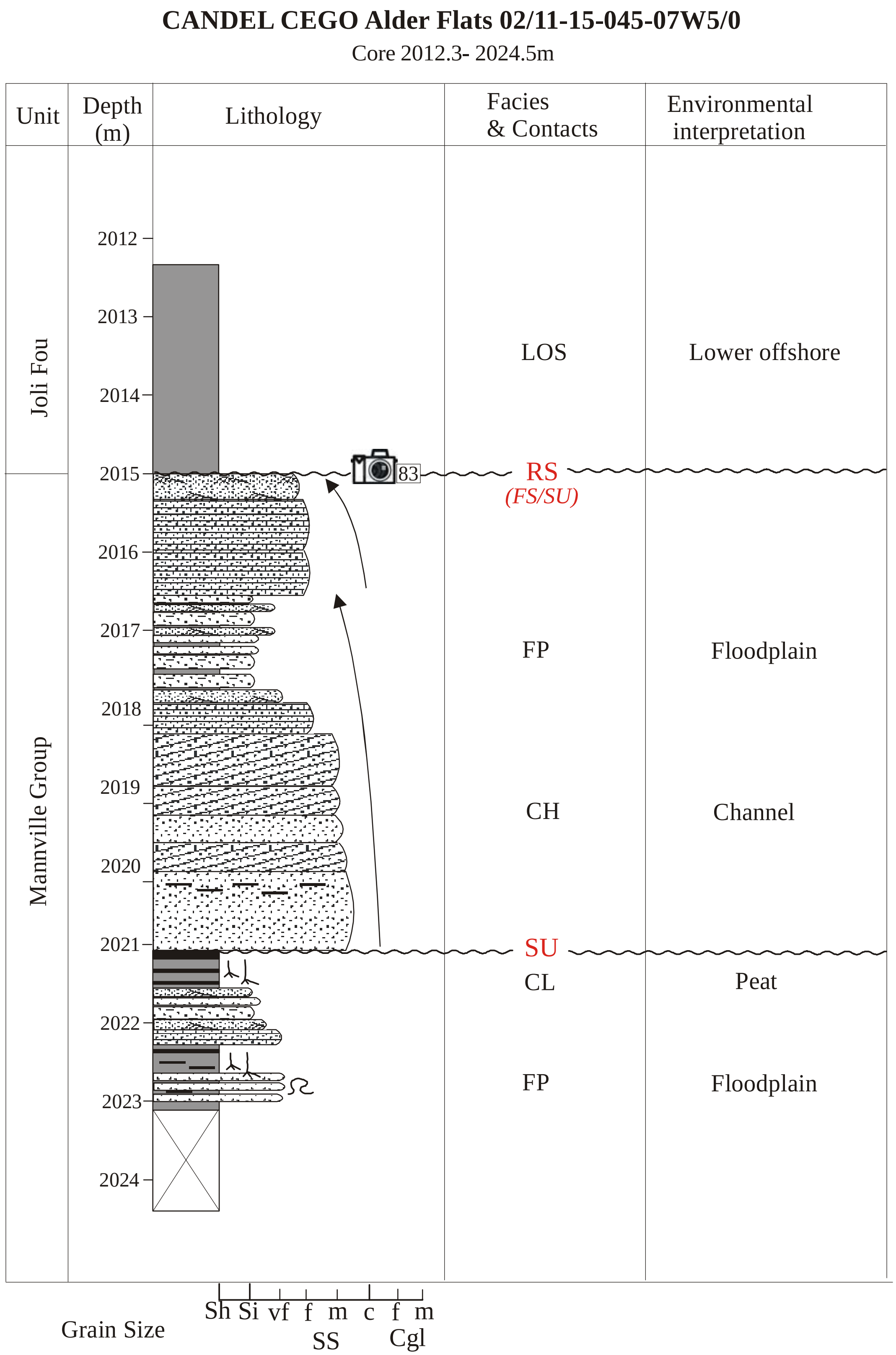

Figure 2-37 Litholog for the 08-02-43-05W5 core, annotated with main contacts (discussed in text) and facies interpretation. Legend for the litholog is given in Figure 2-1.

Husky et al Pembina 16-11-045-07W5/0
Core 2015- 2028.75m

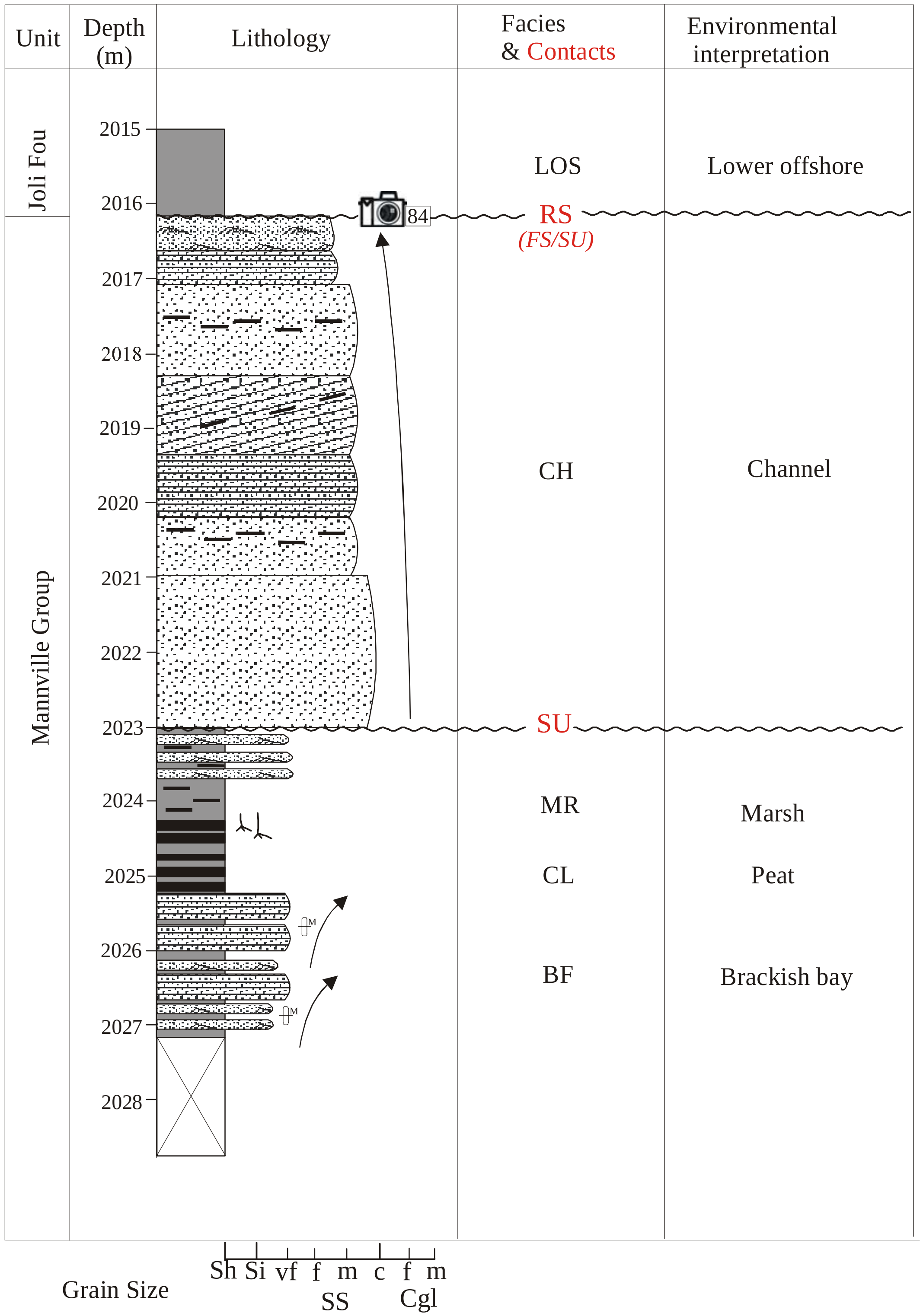

Figure 2-38 Litholog for the 16-11-045-07W5 core, annotated with main contacts (discussed in text) and facies interpretation. Legend for the litholog is given in Figure 2-1.

Shell Husky Paradise 10-25-047-03W4/0

Core 538- 699m

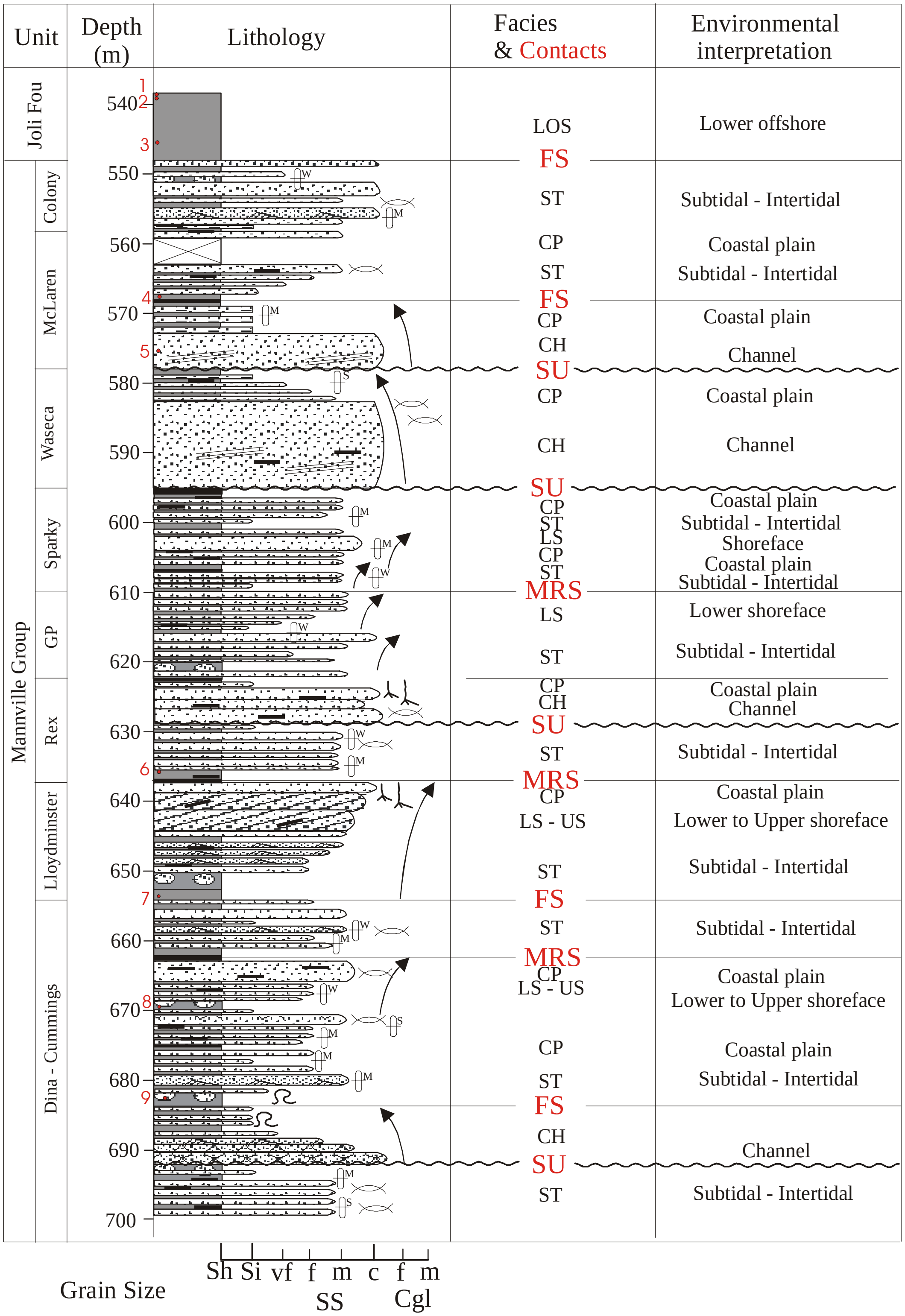

Figure 2-39 Litholog for the 10-25-047-03W4 core, annotated with main contacts (discussed in text) and facies interpretation. Legend for the litholog is given in Figure 2-1. Red numbers: XRD samples (see Chapter Five for discussion).

2.4. Foothills region

2.4.1. Geological setting

The stratigraphic interval in the subsurface covered by cross-sections ranges in thickness between 2000 and 2800 m, with a regional thickening towards the west and northwest.

The generalized stratigraphy of the basin used here (Figure 2-40) is derived from the reviews of many authors (Macqueen and Leckie, 1992; Caldwell and Kauffman, 1993; Stott and Aitken, 1993, and Mossop and Shetsen (compls.), 1994) but correspond largely to the summary of Cant and Stockmal (1989) - representative of the Western Canada Sedimentary Basin (WCSB) in western to central Alberta. The names used for stratigraphic units are the most common subsurface designations.

According with the results of the geological data compiled in a geological atlas (Mossop and Shetsen, 1994), the Paleozoic sediments of the WCSB are separated by a basin-scale angular unconformity from the Upper Jurassic to early Cenozoic foreland basin fill. Paleozoic sediments are regarded as passive preexisting underlying strata to the foreland basin. The foreland basin achieved its greatest lateral extent during the Early Cretaceous (Barremian-Aptian) transgression of the Clearwater Sea (Kauffman and Caldwell, 1993). The sandstones of the (Aptian) Lower Mannville in central Alberta were overlain by the basal Upper Mannville, which is marked by the (Albian) Glauconitic sandstone and equivalent strata in the Clearwater Formation.

The Mannville Group represents a complex succession of marine and non-marine clastic strata, which records a major episode of uplift and erosion in the ancestral Cordillera. It has an unconformable base and an unconformable top (Leckie et al., 1996).

In west-central Alberta, the Mannville Group comprises a complex succession of non-marine, and brackish-restricted marine sandstones and shales (Ellerslie-Ostracode-Glauconitic strata), which are locally dissected by deep, narrow incised valley-fill channels (Leckie et al., 1996) of the uppermost Mannville coal-bearing strata.

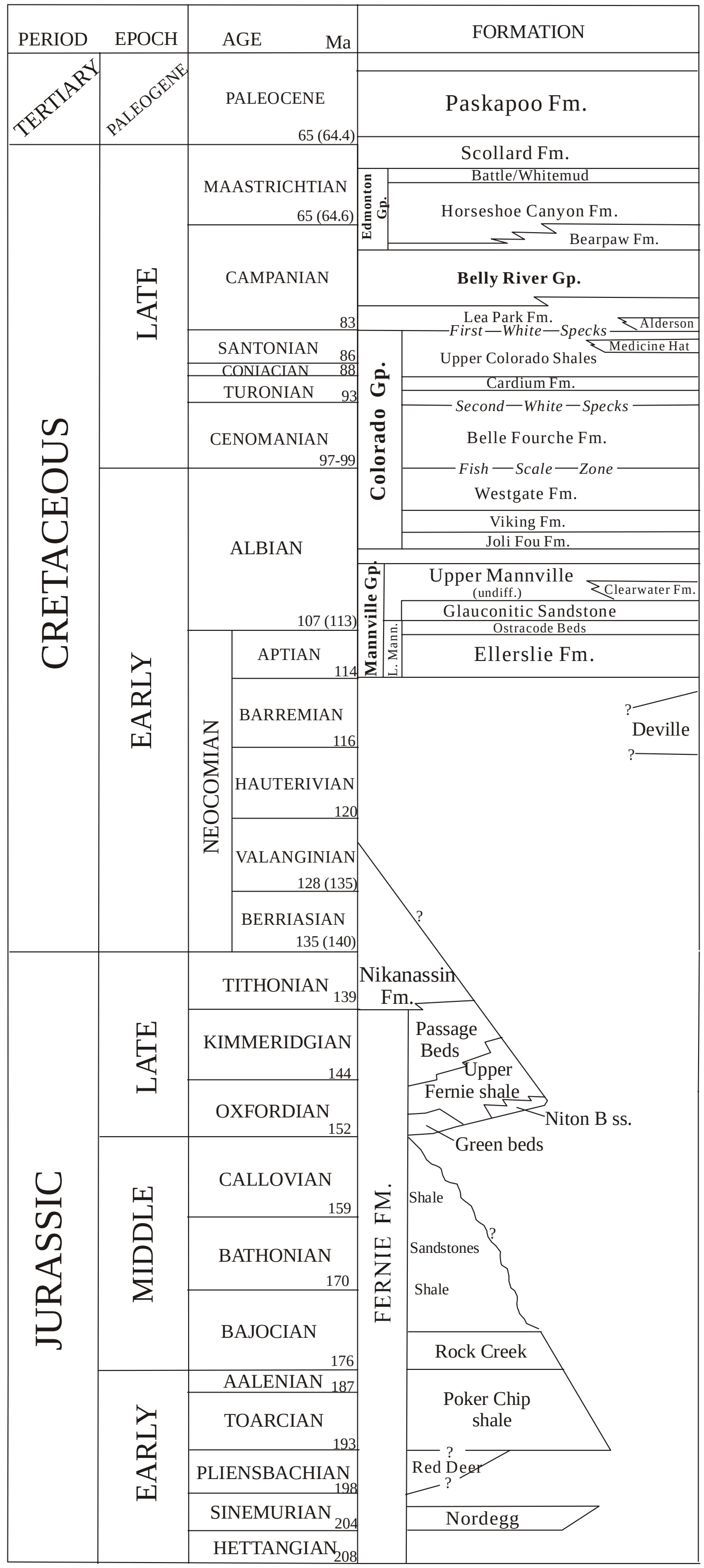

Figure 2-40 Generalized stratigraphic chart for Jurassic - Cretaceous of west-central Alberta. (Compiled from Leckie and Smith, 1993; Poulton et al., 1994; Hayes et al., 1994; Leckie et al., 1994; Dawson et al., 1994; Hamblin et Lee, 1997). Formation ages are from Leckie et al., 1994.

The Early Cretaceous Viking Formation is underlain by shales of the Joli Fou Formation and overlain by shales of the Colorado Group. It is made of a number of coarsening-upward sequences representing shallow marine or shoreline sedimentation, which resulted from a relative base level fall. A similar genesis is now thought to apply to the Cardium Formation (Walker and Plint, 1992).

The post-Colorado portion of the Zuni sequence (Sloss, 1963) in the Plains represents an eastward-thinning prism originally 2.5 Km or more, which extended into Manitoba (Dawson et al., 1994). It was later partly eroded as crustal extension began in the Eocene (Price, 1994), leaving only erosional remnants over the plains. Post-Colorado strata form an overall coarsening-upward succession (Jerzykiewicz, 1985) divided in our study area into four main clastic wedges related to orogenic pulses. These are: (a) Belly River Group: fluvial, shoreline, estuarine and shallow-water deposits; (b) Edmonton Group: fluvial, estuarine, shoreline and shallow-water marine deposits; (c) Scollard Formation: fluvial deposits; and (d) Paskapoo Formation: fluvial deposits.

The Paskapoo Formation represents the last preserved response to the Laramide Orogeny, which likely culminated in the Paleocene. Deposition occurred in a subsiding foreland basin with greater rates of subsidence to the west, as shown by the greater thickness of strata to the west.

2.4.2. Geophysical log correlations

In this study, correlation of the various sedimentary units was primarily based upon geophysical well-log signatures, various interpretations drawn from the literature, and the extrapolation to well logs of the lithologies described in the examined cores. One reference well was selected from every township and all reference wells were then correlated with this reference well. In correlating various sedimentary units, particular attention was paid to the general stratigraphic position of the unit and its sandstone thickness. Coal beds were particularly useful in defining boundaries of sedimentary units.

As already mentioned, this study relies heavily on subsurface data in the form of geophysical logs of 180 wells in ~35 townships. The geophysical logs used for this section are conventional oil and gas logs and they are from the Alberta Geological Survey database and from the International Datashare Corporation (GeoDesk exploration software database).

An attempt was made to collect a minimum of 6-9 wells/township from the oil and gas well logs. Wells were selected on the basis of their geographic distribution, the availability and quality of the logs (gamma-ray, resistivity, sonic, density, spontaneous potential). Locations of the 180 wells used in the database are shown in Figure 2-41.

Observations from the well logs led to general interpretation of depositional environments in the basin. However, the larger scale regional characteristics and implications of the rock units, rather than detailed sedimentology are the focus of this paper. Moreover, in a study of this kind only the largest scale units are useful, so in many cases details of local rock units could be neglected.

Examination of the cross-section(s) helps to understand facies changes that occur, to construct the regional stratigraphic framework in this area and to establish some preliminary principles for mudlog interpretation.

In the Foothills region five well-log cross-sections of approximately 50–150 km in length (between Ferrier, Pembina and Gilby oil fields) were completed. These cross-sections link the three carbon isotopic mud logs from Pembina-Ferrier-Gilby oil field area (Figure 2-41). The conventional oil and gas well logs used have depths of about 2200-2800m, presenting the general foreland basin geometry and stratigraphy in this region.

The first structural geological cross-section (Section 1-1’, Ferrier-Gilby) is located southeast from Edmonton, trending west to east from Township 42 Range 9W5 to Township 42 Range 4W5 (Appendix I_1). The second cross-section (Section 2-2’, Pembina – Gilby), is trending NW – SE, from Township 49 Range 11W5 to Township 42 Range 4W5 (Appendix I_2). Pembina and Ferrier profiles are connected through Section 5-5’ (Appendix I-5). The other two well log cross-sections (Section 3-3’ and Section 4-4’) were oriented in a southwest – northeast trend, constructed parallel to the paleo-slope (see Appendix I_3, and Appendix I_4). The present sea level is used as a datum.

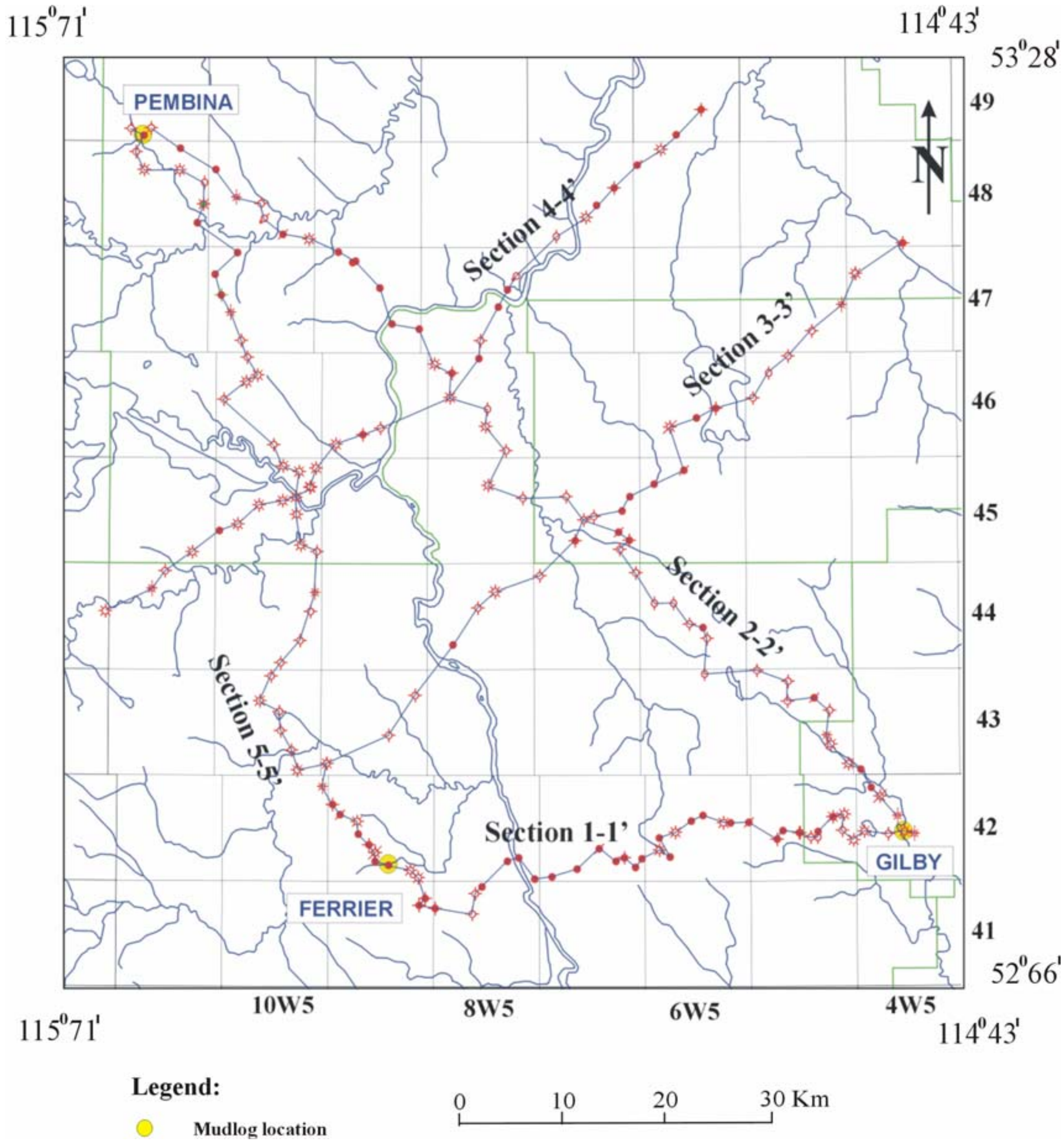

Figure 2-41 Base map showing the database of the study within the Foothill region: locations where well logs were used are shown with different well symbols, whereas mudlog locations are shown with yellow circles. Locations of the five regional cross-sections 1-1' through 5-5' are also shown. Township locations are shown on the right border, and range locations along the bottom.

2.4.2.1. Fernie and Mannville groups

The lowermost clastic wedge of the foreland basin - Fernie Group – is deposited on an unconformity cut into the older passive margin sequence and shows some coarsening- and shallowing-upward successions.

Lying on the sub-Cretaceous unconformity at the top of the Fernie Group, the dominantly fine-grained Mannville fluvial succession is interrupted only by the brackish Ostracod Beds and the shallow-marine deposits of the Glauconitic Sandstone. These marine- to marginal marine sediments are commonly less than 30 m thick, but are laterally extensive. The Upper Mannville interval consists predominantly of fluvial sediments, containing very thick and laterally extensive coal beds.

2.4.2.2. Colorado Group

Shales of the Colorado Group are intercalated with numerous sandstones that reflect sea-level changes within the WCSB. In this study area these are the Viking and Cardium formations.

The Viking Formation is made up of three to four coarsening-upward sequences (Boreen and Walker, 1991; Reinson et al., 1994). The middle and uppermost cycles are capped by “clean” sandstones or interbedded sandstone-mudstones, both interpreted as shoreface-incipient bar deposits (Reinson et al., 1994). According with the existing lithostratigraphic schemes, the base of the Viking Formation is defined by the first resistivity and/or gamma-ray well log deflection above the Joli Fou shales; the top is taken at the log deflection indicating the last coarse grained sandstone above the “main sand body”; the upper boundary of the Viking Formation is usually easy to pick up on logs because there is a sharp break in lithology from sandstone or sandy siltstone to shale. The reference geophysical log from Figure 2-42 has been included to show the various surfaces, formation picks, nomenclature and typical log response within the Fernie, Mannville, and Colorado groups.

On well logs the most recognizable marker is lying at the top of the so-called “Viking sandstone” in the subsurface. This marker is an erosion surface that was probably cut subaerially (the VE4 surface of Boreen and Walker, 1991); subsequent transgression modified this surface forming a *ravinement surface*. This same surface can be correlated landward where it is expressed as an E/T surface (erosion/transgression of

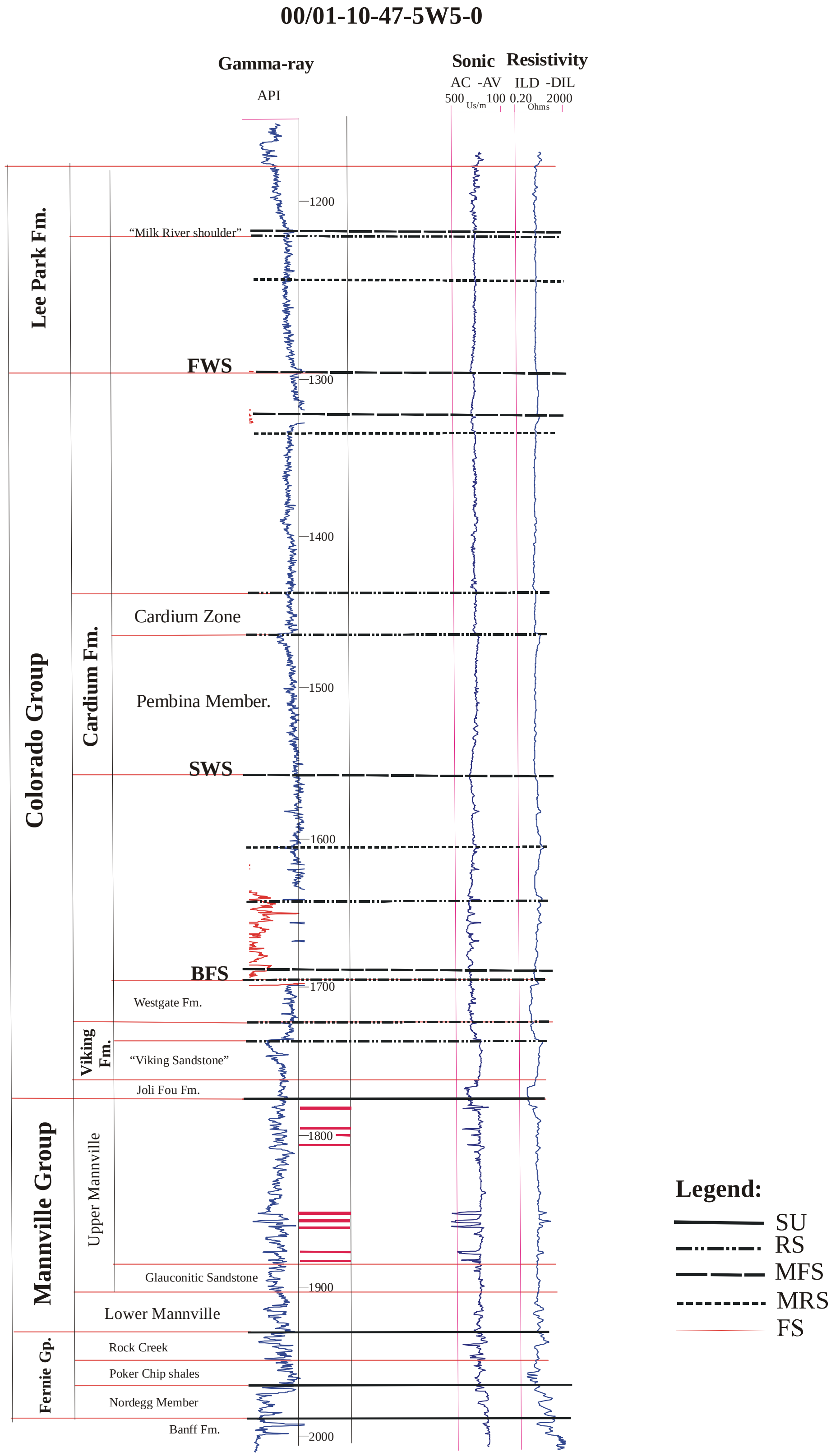

Figure 2-42 Typical geophysical log signature of Ferrier, Mannville and Colorado groups and bounding surfaces in Pembina-Ferrier-Gilby area. Horizontal red lines in the depth column indicate thick coal seams.

Plint et al., 1988) or a flooding surface merged with a sequence boundary or unconformity (FS/SB).

The top of the Viking Formation in Pembina-Gilby-Ferrier area represents also a transgressive surface reflecting erosive shoreface retreat, amalgamated with subaerial exposure surface (FS/SB) (Pattison, 1991). A typical wireline expression (gamma-ray and resistivity) for the uppermost part of the Viking Formation (including at least one ravinement surface as defined in this thesis) is represented in Figure 2-43 and Figure 2-44. As can be observed, the sharp break in lithology can be picked on both gamma-ray and resistivity logs. A close-up view of the two lag conglomerates at the top of the Viking Formation in the Willesden Green area (between Ferrier and Gilby) can be seen as well in Plate no.71 (Appendix A). Continued transgression blanketed the coarser Viking sediments with the widespread Colorado shales. Inclusive in this interval are the regionally extensive Base of Fish Scales and Second White Specks Shale wireline markers.

The wireline expression of the "Base of Fish Scales" (BFS) is a sharp increase in the gamma-ray and resistivity responses and an abrupt, but lower magnitude decrease in sonic transit time. This boundary represents a sharp lithological contact, typically expressed as a thin, parallel- or cross-laminated sandstone or pebble layer with abundant disarticulated fish and other vertebrate remains overlying shale (Bloch et al., 1999).

Although not so regionally persistent as that at the base of Fish Scale, and with a different composition, the same kind of conglomerate occurs at the base of Second White Speckled Formation. The sharp basal lithological contact, the occurrence of bioclastic conglomerate and the abrupt disappearance of agglutinated species (the absence of the *Textularia alcesensis* Zone over the broad area of the WCSB – Bloch et al., 1993) suggest a period of marine erosion at both the Albian-Cenomanian boundary and the Cenomanian-Turonian boundary. Therefore, the base of the Base of Fish Scale and the base of the Second White Speckled Shales could be regarded as *ravinement surfaces* – expressed on wireline logs by an increase in resistivity and radioactivity.

PC WillGr 07-06-042-07W5/0

Core 2271- 2289.2m

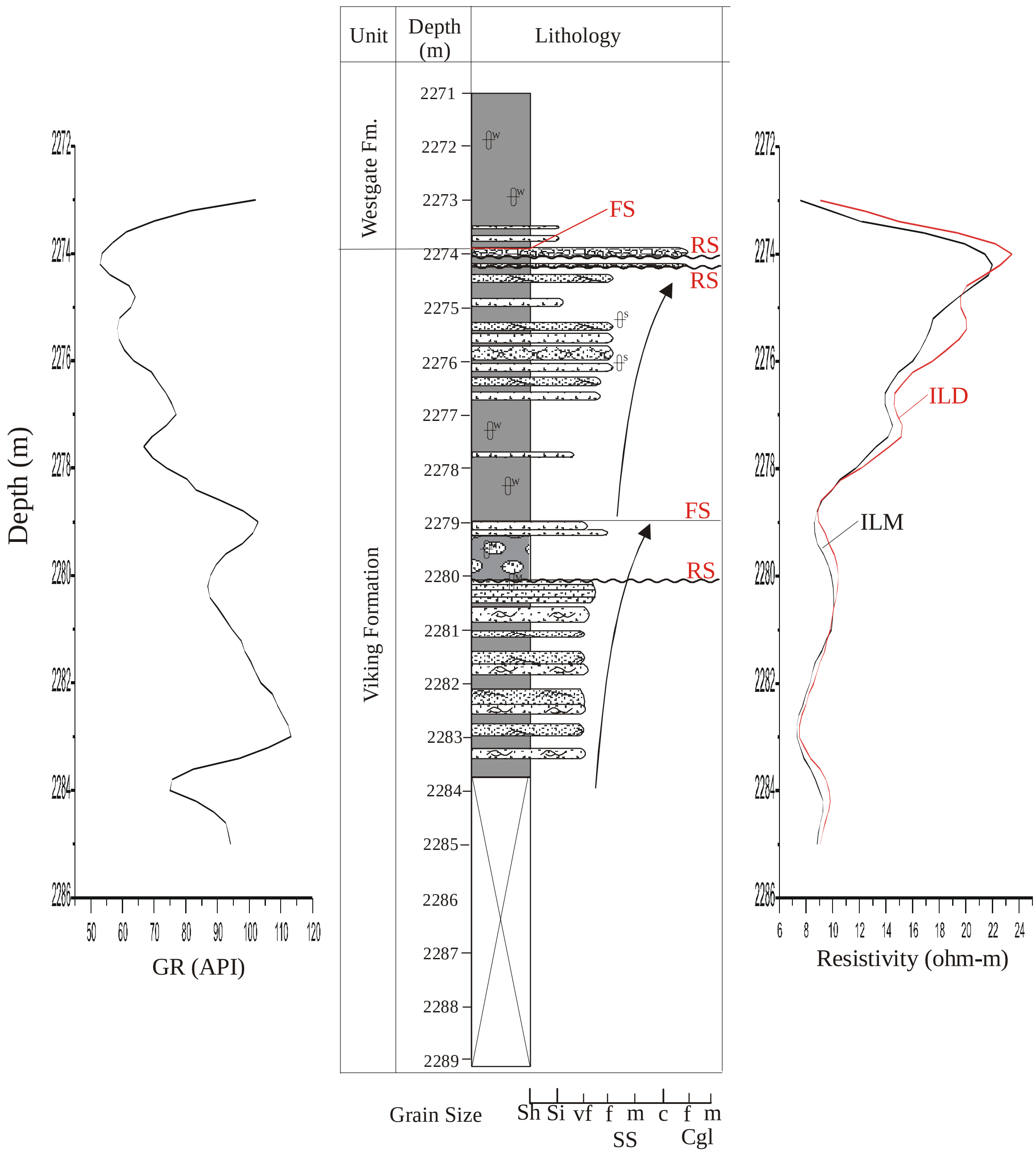

Figure 2-43 Typical vertical profile for two shallow-marine coarsening-upward sequences along with their gamma-ray and resistivity well-log responses. Viking Formation - 07-06-042-07W5 core. Legend for the litholog is given in Figure 2-1.

ESSO Open Creek 03/13-13-042-05W5/0

Core 1974 - 1980.5m

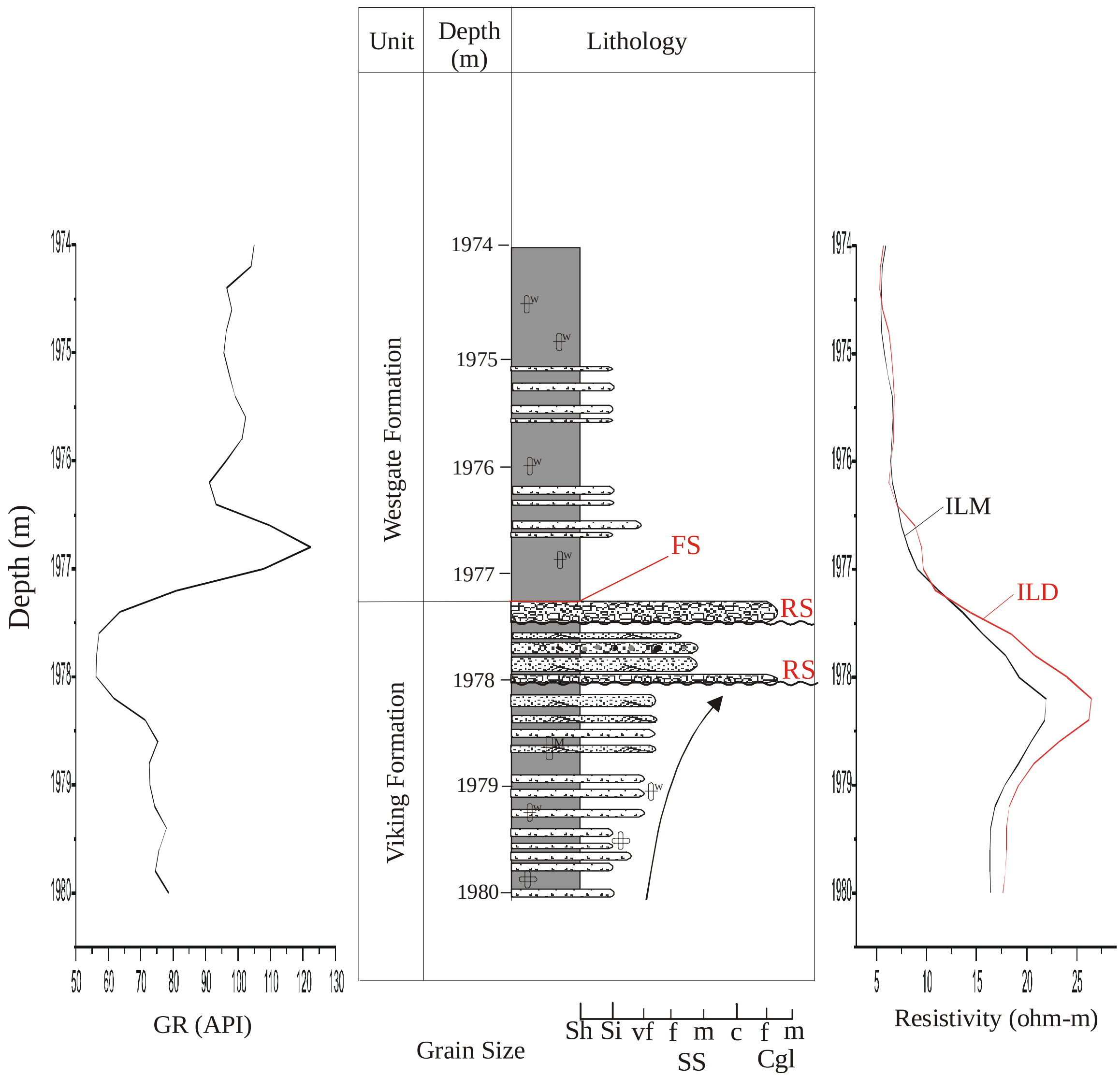

Figure 2-44 Typical vertical profile for a shallow-marine coarsening-upward sequence along with its gamma-ray and resistivity well-log responses. Viking Formation - 03/13-13-042-05W5 core. Legend for the litholog is given in Figure 2-1.

During the Early Cenomanian and the latest Cenomanian to early Turonian, sea level in the Western Interior Seaway reached a maximum (Caldwell and Kauffmann, 1993). These two transgressions are associated, one with the Fish Scale Formation, and the other one with the Second White Speckled Formation. The maximum gamma-ray peaks and the correlative major resistivity inflections at the formations tops are interpreted in our log cross-sections as *maximum flooding surfaces*.

Above the Second White Speckled Shales, a basin-wide sea-level fall culminated in the deposition of Cardium sandstones and conglomerates. Two lithostratigraphic units characterize the Cardium Formation in the subsurface of west-central Alberta: the Pembina River Member below and the Cardium Zone Member above (Krause and Nelson, 1984). We identified the major inflection on gamma-ray log within the Cardium Formation with the top of Pembina River Member (correlative with the Raven River Member of Plint et al., 1986). This inflection apparently appears on the well logs as a maximum regressive surface (low gamma-ray reading, high resistivity, capping overall shallowing-upward sequences), but corresponds with an erosional unconformity, interpreted as a *ravinement surface (RS)*. This erosion surface is identified with the E4 (Cardium "B sand") and/or E5 (Cardium "A sand") of Plint et al. (1988). According to Pemberton and MacEachern (1995), this particular surface within the Cardium Formation may reflect either a sequence boundary overlain by a forced regression conglomeratic shoreface, or a sequence boundary modified by subsequent transgression (FS/SB). A typical gamma-ray expression for the Cardium Formation (including the erosional surface related to ravinement processes) is represented in Figure 2-45. Another example of log-core correlation for the Cardium Formation is given in Figure 2-46.

2.4.2.3. Belly River Group and Lea Park Formation

Figure 2-47 illustrates the internal stratigraphic subdivisions of the Belly River Group, and also the bounding surfaces; distinctive gamma-ray/resistivity/sonic log characteristics of the component parts are shown. A brief description of each subdivision and marker is given starting from the base to the top.

Within the Lea Park Formation there is a very distinctive pick over the entire cross-section, known as "the Milk River Formation pick". This pick is distinguished on most logs by an abrupt increase in resistivity, which tend to form a kind of shoulder on

EAG et al Pembina 06-26-048-11W5/0

Core 1770.9 - 1789.2m

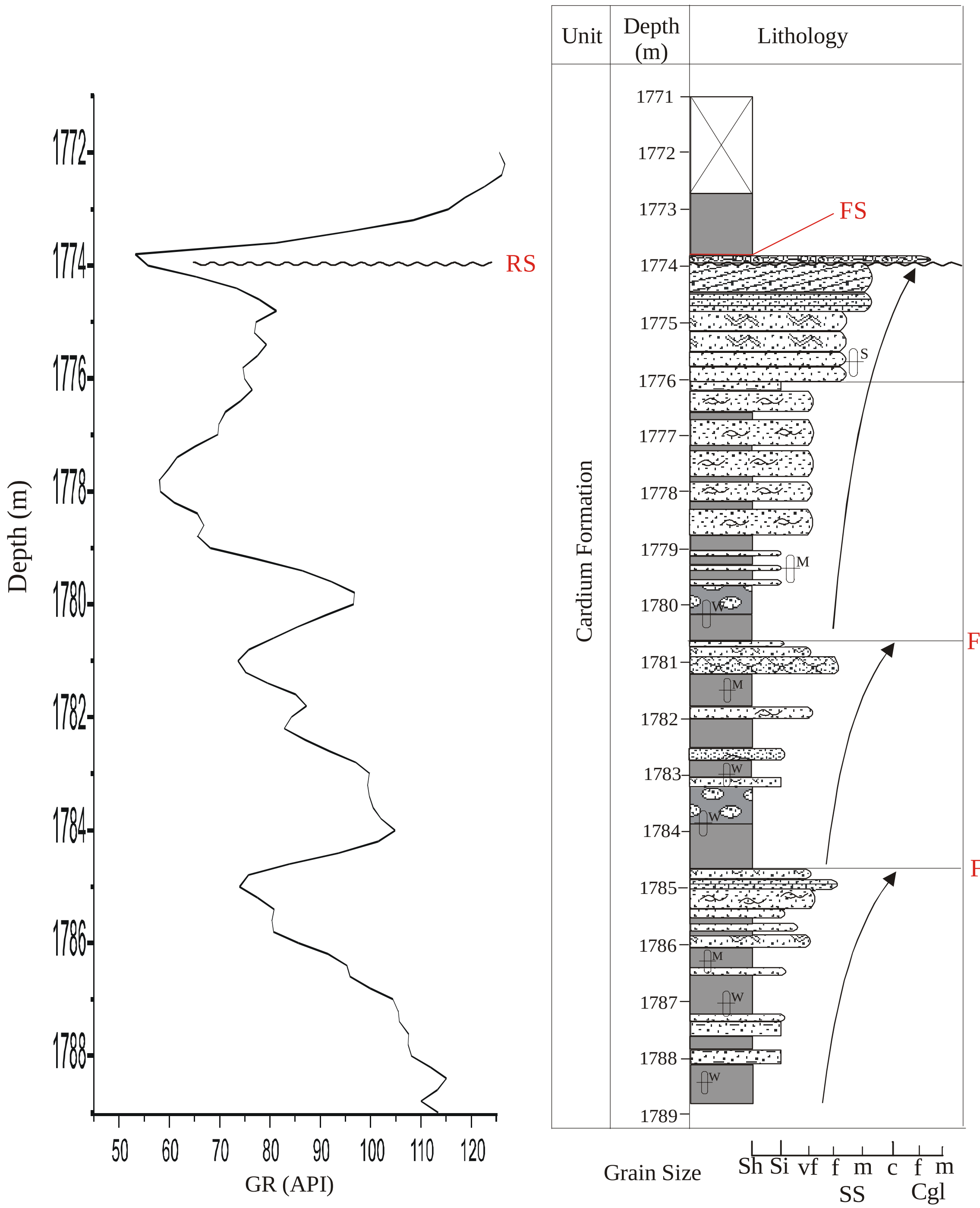

Figure 2-45 Typical vertical profile for three shallow-marine coarsening-upward sequences along with their gamma-ray well-log response. Cardium Formation - 06-26-048-11W5 core. Legend for the litholog is given in Figure 2-1.

Dome Alder Flats 10-26-045-09W5/0

Core 1743.8 - 1762m

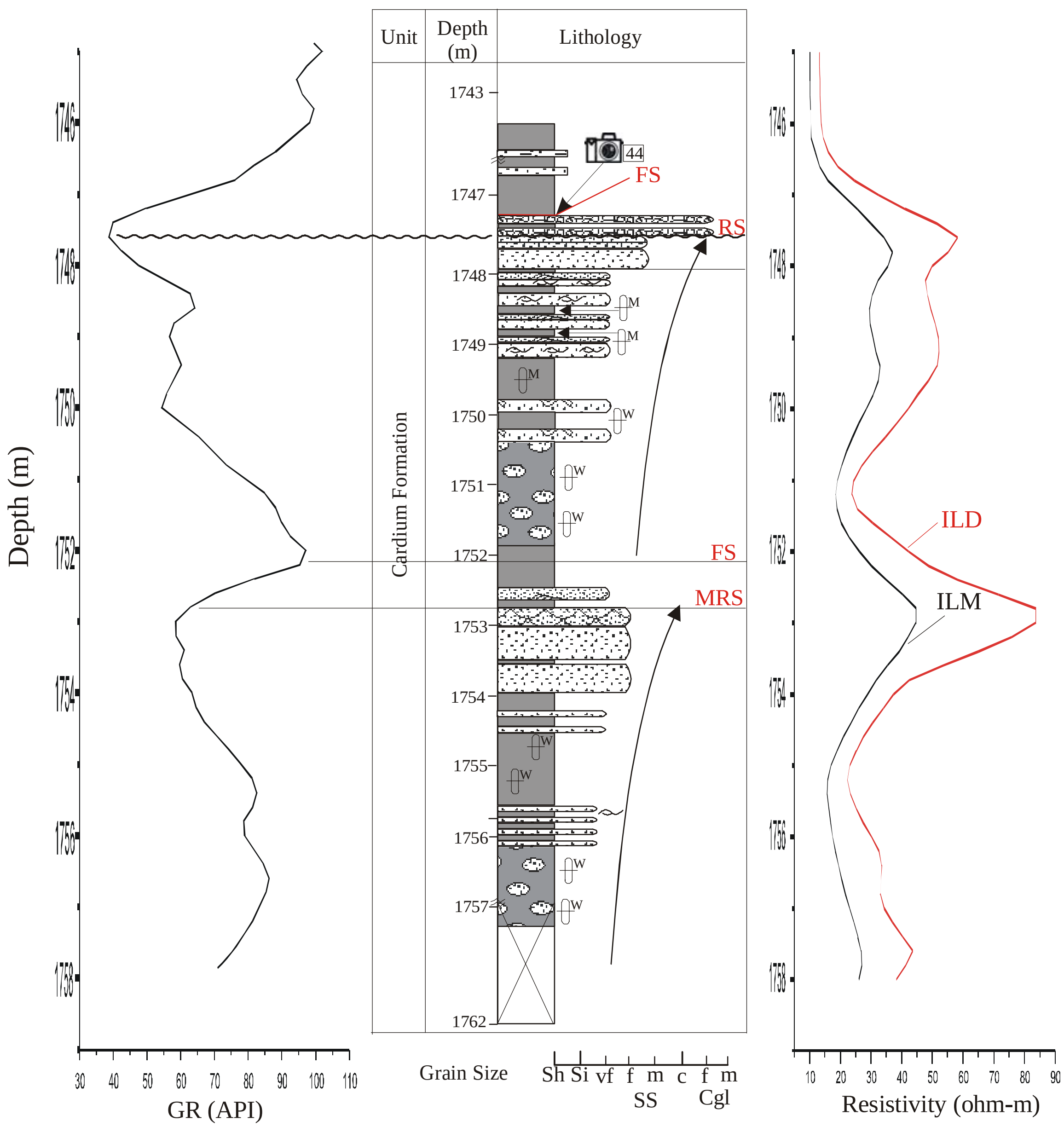

Figure 2-46 Typical vertical profile for two shallow-marine coarsening-upward sequences along with their gamma-ray and resistivity well-log responses. Cardium Formation - 10-26-045-09W5 core. Legend for the litholog is given in Figure 2-1.

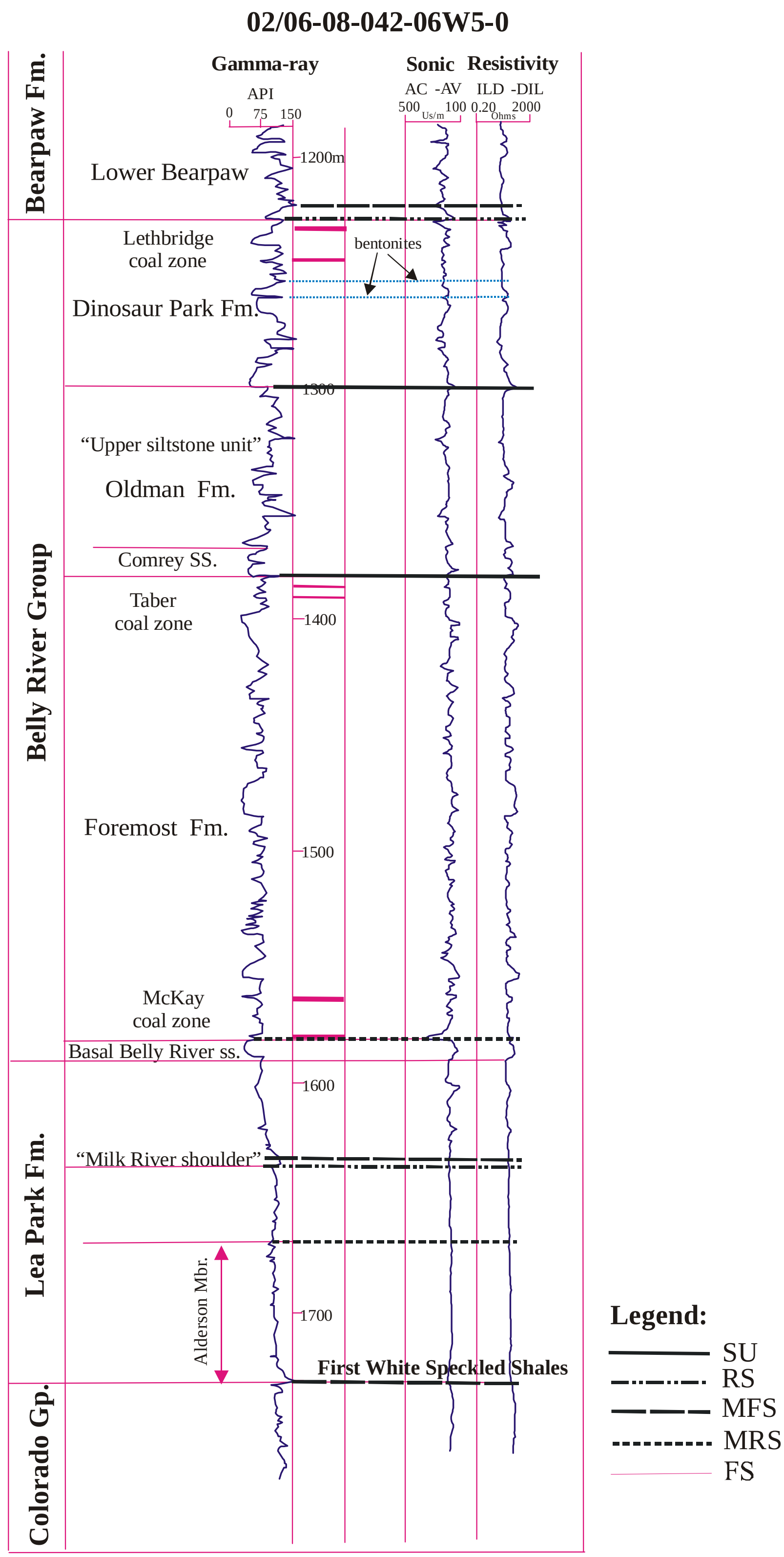

Figure 2-47 Typical geophysical log signature of Belly River Group and bounding formations in Ferrier-Gilby area. Horizontal red lines in the depth column indicate thick coal seams.

the resistivity log, and a sharp decrease in the gamma-ray log at the contact. In our area, this pick marks the contact between the last shallowing-upward marine succession of the Alderson Member (the basinward equivalent member of the Milk River Formation – Meijer Drees and Myhr, 1981) and the marine shales of the Pakowki Member/Lea Park Formation. This contact is marked over large areas by a thin, chert-pebble bed (Glass, 1990). Paleontological and stratigraphic evidence (Braman and Sweet, 1990) suggest this surface may be a regional disconformity. Therefore, we interpreted it as a *ravinement surface*.

Within the Alderson Member there is an additional representative surface, corresponding with a *maximum regressive surface*, which caps one of the shallowing-upward marine successions of the Alderson Member.

The McKay coal zone defines the base of the Belly River clastic wedge sequence. This zone generally overlies a very thick (25-30 m) upward-coarsening sequence within the Lea Park Formation, with the lowest coal seam sitting on the Basal Belly River shoreline sandstone (see Figure 2-6 for Basal Belly River facies in the Ferrier area). McKay coal zone is interpreted as aggradational floodplain deposits deposited during the subsequent base level rise and transgression, which ended the deposition of the last progradational succession beginning with Lea Park Formation.

The Taber coal zone marks the middle of the Belly River Gp. (or top of the Foremost Formation in central-southern Alberta).

The Oldman sandstones (Comrey Member of the Oldman Formation) are quite clearly discernible as zones of low gamma-ray radioactivity in the middle portion of the Belly River Group, gradationally overlying a variable thickness of the Taber coal zone (very poorly developed throughout the section) in most locations. These sandstones are overlain by higher gamma-ray radioactivity siltstones of the “upper siltstone” member (Hamblin, 1995), which in turn is sharply overlain by the distinctive low gamma-ray signature of the Dinosaur Park Formation.

The thickness of the Comrey sandstone is quite variable (see Appendices I-1 to I-5), with thick sharp-based, narrow sand-rich bodies separated by relatively wide areas with somewhat lower sandstone/siltstone ratios. On logs, the Comrey sandstone unit is commonly a composite of several stacked sandstone subunits, each of which is typically manifest as a fining-upward channel unit. These sandy units form a more or less continuous “sheet” over the cross-section. In addition, the overlying “upper siltstone” is present and the level of erosion beneath the downcut base of the Dinosaur Park Formation primarily determines its thickness variation. A typical vertical profile of a Belly River channel-fill deposit along with its gamma-ray well-log signature is shown in Figures 2-48 and 2-49.

The discontinuity (Eberth and Hamblin, 1993) at the base of the Dinosaur Park Formation is placed on geophysical logs at the first major leftward gamma-ray deflection following a maximum gamma-ray peak or a series of peaks between the Taber and Lethbridge coal zones. The discontinuity is traced over our cross-sections as a subaerial unconformity.

The strata below the Lethbridge coal zone (or the upper part of the Dinosaur Park Formation) consist of a predominantly fine-grained unit with minor interbedded sandstones and at least two-three distinctive bentonitic ash layers. These bentonites are very distinctive on the induction log and stand out as distinct spikes to the left. This “bentonitic zone” is 20 to 30 m thick and is also recognized as a zone of relatively high natural gamma-ray responses on geophysical logs (Figure 2-47).

The top of the Belly River Group was identified based on the recognition of either a marine sequence separating the Horseshoe Canyon Formation from the Belly River Group and/or the presence of the Lethbridge coal zone. In spite of increasing difficulty of recognizing marine sequences overlying the Belly River Group north of about township 40 (Macdonald et al., 1987), the marine sequences (Bearpaw Formation) are identified by low resistivity flat responses and/or gamma-ray upward coarsening sequences. A coal or a coal zone at about the stratigraphic level of the Lethbridge coal zone is, however, very widespread throughout Pembina-Gilby-Ferrier area.

The nonmarine sediments of the upper Belly River are overlain sharply by the Bearpaw Formation, which form the base of the next clastic wedge, the Edmonton Group. The contact between the Belly River Group and the Bearpaw Formation is in fact represented by a *ravinement surface* underlying a very thin transgressive succession. This succession is capped by a *maximum flooding surface* grading to a number of 2-3 sandy coarsening upward sequences. The maximum flooding surface was defined at a

AMOCO Pembina 02/06-09-046-09W5/0

Core 1432 - 1452.95m

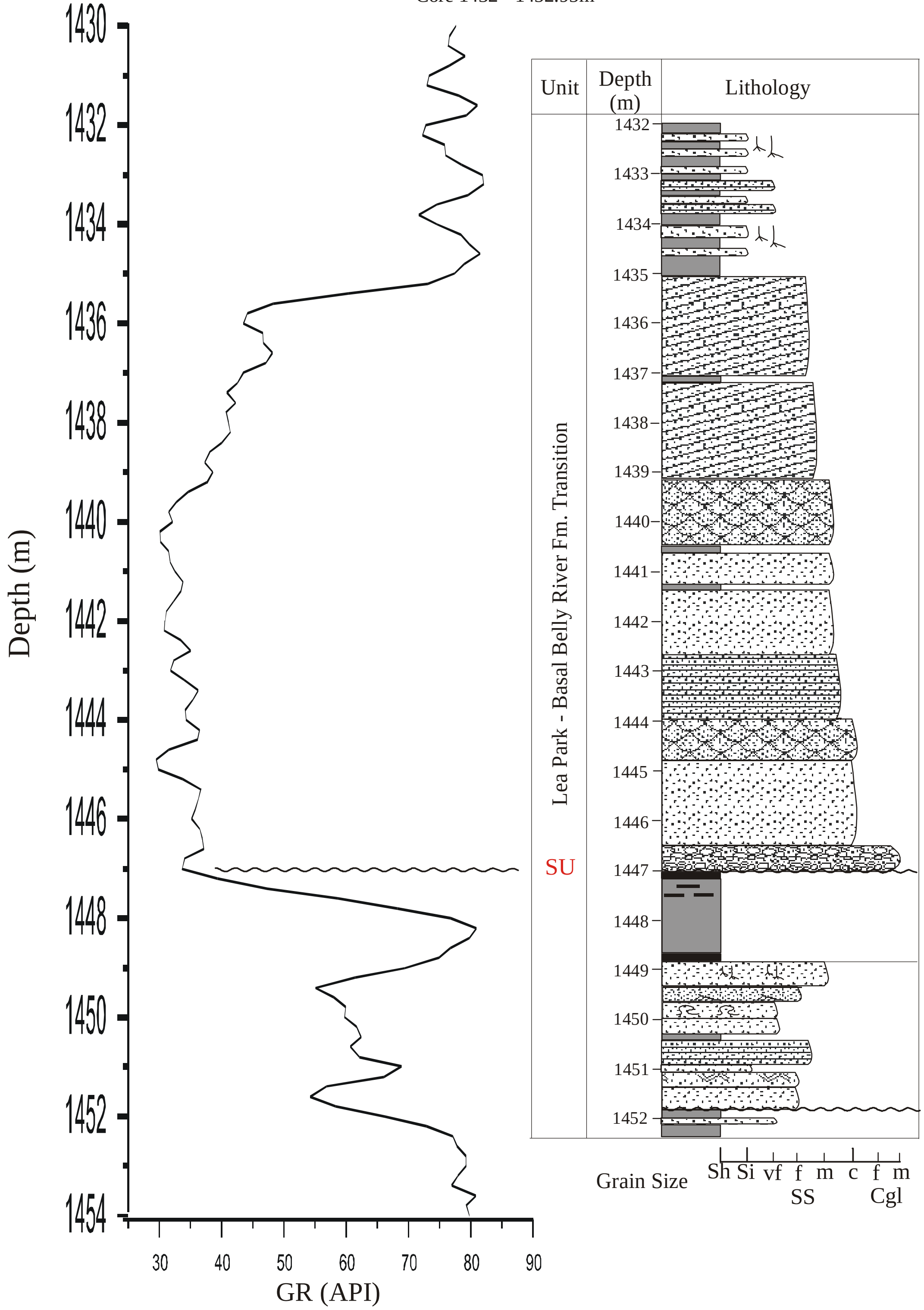

Figure 2-48 Typical vertical profile of a channel-fill deposit along with its gamma-ray well-log response. Belly River Formation - 02/06-09-46-9W5 core. Legend for the litholog is given in Figure 2-1.

Dome Deb Pembina 10-04-049-11W5/0

Core 1417 - 1435m

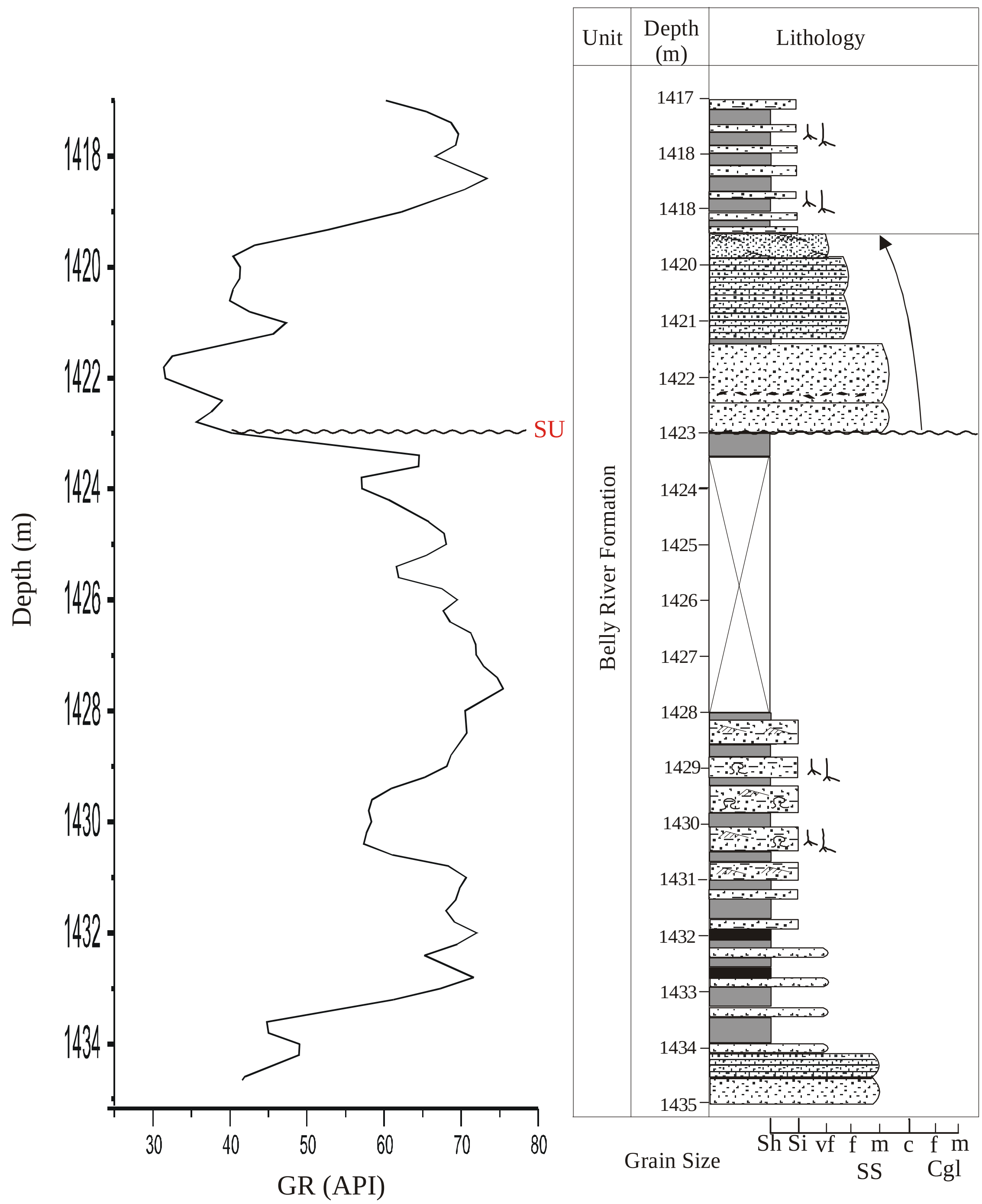

Figure 2-49 Typical vertical profile of a channel-fill deposit along with its gamma-ray well-log response. Belly River Group - 10-04-49-11W5 core. Legend for the litholog is given in Figure 2-1.

prominent high gamma-ray and resistivity log deflection that corresponded to the base of the first prominent upward-coarsening facies succession that forms Lower Bearpaw Formation in this area.

2.4.2.4. Edmonton Group and Bearpaw Formation

The Bearpaw Formation and the lower Horseshoe Canyon Formation have an interfingering relationship, with marine strata to the east laterally equivalent to terrestrial /transitional strata in the west. The Bearpaw Formation in our case consists of two parts: Lower Bearpaw Formation and Upper Bearpaw Formation. Between these two formations there is a more or less extensive zone known as the "Lower tongue" (McCabe et al., 1989) or *Basal coal zone* of the Horseshoe Canyon Formation. This zone was identified based on the stratigraphic position and on the geophysical log response: relatively high resistivity and variable natural gamma-ray response, with low natural gamma-ray response at coal zones (Figure 2-50).

The Basal coal zone of the Horseshoe Canyon Formation varies in thickness from 10 to 40 m. This zone is recognized as a coal-bearing interval underlying a series of coarsening upward sequences.

One to two major coarsening upward sequences are recognized just above the Basal coal zone of the Horseshoe Canyon Formation. These successions - representing the Upper Bearpaw Formation - progressively migrate upwards and to the east reflecting the eastward shift of shoreline positions through time. In general, these coarsening upward sequences are capped by coal seams, which can be correlated with a high degree of confidence over distances of 5-6 km. The limited lateral continuity of coal seams over the entire along dip cross-section Ferrier – Gilby (Section 1-1', Appendix I-1) is due to the west-east orientation (approximately perpendicular to paleoshoreline trend).

In all well log cross-sections, the upper Horseshoe Canyon strata consists largely of alluvial plain deposits with thin discontinuous coal seams, whereas thicker and more laterally extensive coal seams (Drumheller zone) are contained within the lower

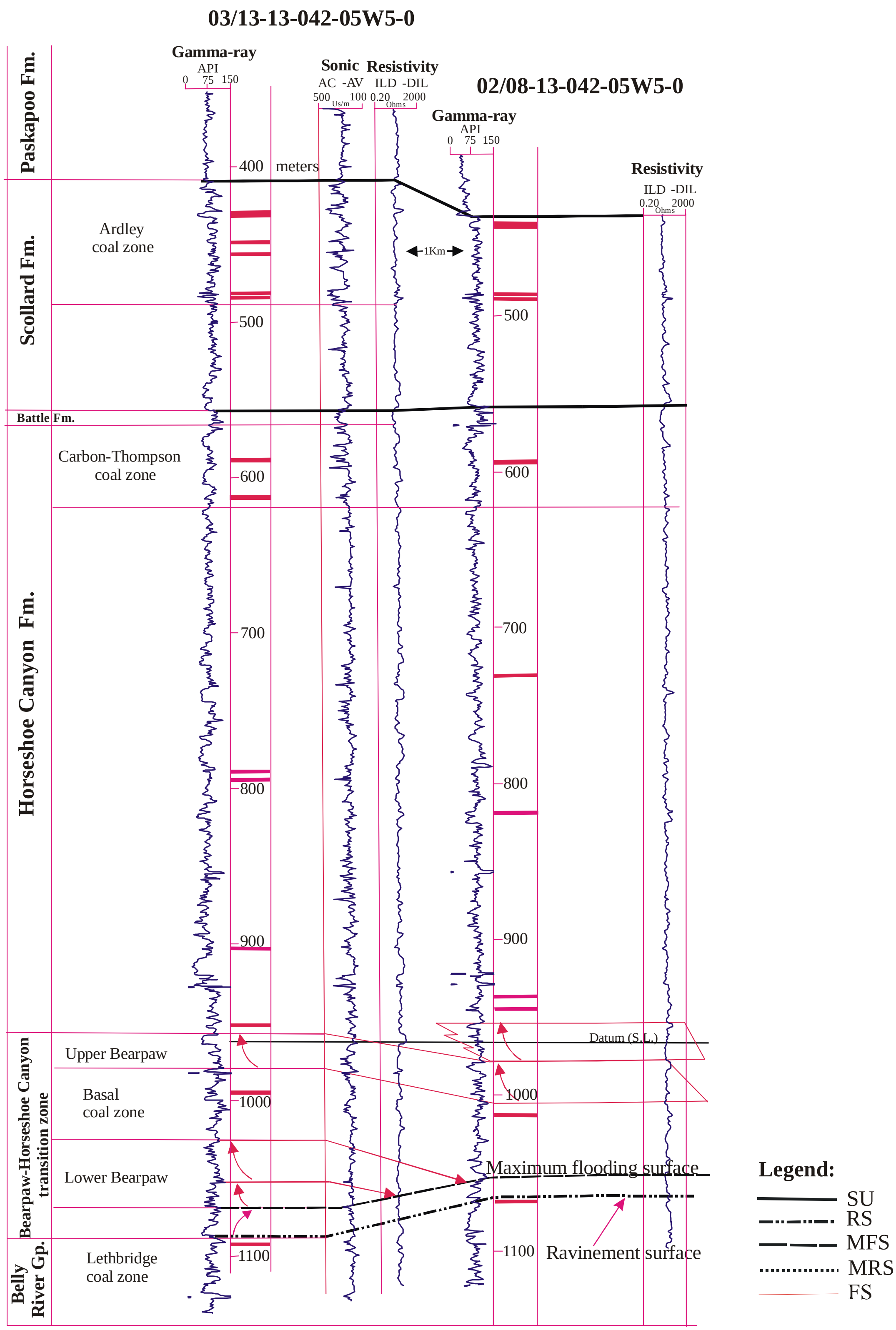

Figure 2-50 Typical geophysical log signature of Bearpaw - Edmonton Gp. Horizontal red lines in the depth column indicate thick coal seams.

Horseshoe Canyon Formation and in the uppermost part of the Horseshoe Canyon Formation.

In the uppermost part of the Horseshoe Canyon Formation there is coal zone known as *the Carbon-Thompson coal zone*. Coal seams are generally thin, but they are grouped into relatively continuous coaly beds in our log cross-sections (Appendix I-2). Some seams formed closely spaced pairs that could be correlated with a high degree of confidence. High resistivity response, variable natural gamma-ray response and very low velocity on sonic logs at coaly beds characterize this zone.

In the subsurface cross-section fining-upward sandstone beds with sharp basal contacts were noted on geophysical logs within the Carbon-Thompson coal zone. The number of sandstone bodies, their thickness and their grain size generally increase from the base to the top of the coal zone. The sandstones tend to be isolated and enclosed by finer grained sediments

Capping the Edmonton Group, the Battle Formation was recognized as an 8 to 20 m thick zone displaying a very low resistivity, a relatively high natural gamma-ray and high apparent porosity responses.

2.4.2.5. Scollard and Paskapoo formations

In the area covered by this section, the Scollard Formation is approximately 100 m thick and can be divided into a lower, non-coaly interval and an upper coaly interval. The base of the Scollard Formation (or Battle/Scollard contact) has been regarded as unconformable (Russell, 1983) on the basis of faunal differences between the uppermost Horseshoe Canyon Formation and lower Scollard Formation. The base of the Scollard Formation has been traced at the first major inflection to the left on the gamma-ray logs following the thin sequence of bentonitic mudstones of Battle Formation. This major inflection represents a regional subaerial unconformity the base of the sandstone marker horizon of the lower Scollard Formation.

The sandstone units occur normally as thin to thick lenticular beds but, in places, form individual sandstone sheets up to 10-15 m thick near the base of the formation.

Individual channels, identified on geophysical logs, are separated by erosional bounding surfaces and are typically 2 to 5 m thick.

One of the outstanding characteristics of the Ardley coal zone is that some of the seams are laterally persistent over long distances. Our cross-section runs through a well defined trend of thick cumulative coal and a corresponding trend with seams 3 m or more thick (5 m in the case of coal Nr. 14 – Ardley coal).

The major subaerial unconformity defined by Lerbekmo et al. (1992) between the Scollard and Paskapoo formations is placed on geophysical logs at the first major leftward gamma-ray deflection above the Ardley coal zone, at the base of “the first prominent thick sandstone unit above the uppermost major coal seam of the Ardley coal zone” (Gibson, 1977). This massive sandstone marker probably represents a large blanket or major channel sandstone of fluvial origin, which has eroded and removed some of the underlying Scollard strata.

2.5. Lloydminster region

2.5.1. Geological setting

The Mannville-, and the Colorado groups, together with the Lea Park – Belly River transition zone represent the regional stratigraphy (Figure 2-51). The Mannville Group consists of heavy-oil bearing sands with interbedded shales, siltstones and fine-grained sandstones. Above the Mannville Group lies the Upper Cretaceous Colorado Group – a sequence of marine shales. Shales of the Colorado Group are intercalated with several sandstone and conglomerate units. In our study area these are (in ascending order): the Spinney Hill sandstone, the Viking sandstone and the St. Walburg sandstone.

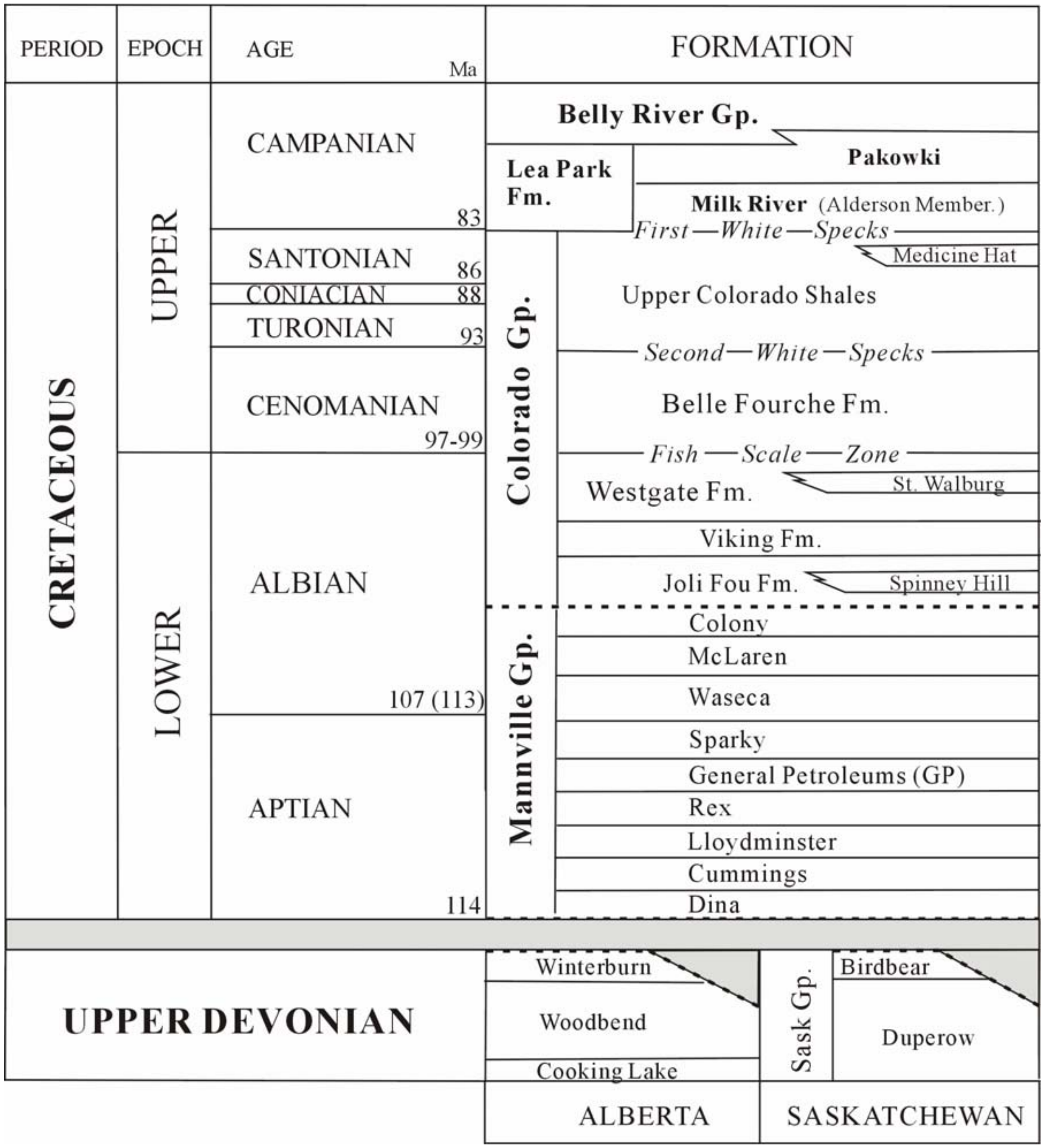

Figure 2-51 Stratigraphic chart for Upper Devonian - Cretaceous, Lloydminster area (compiled from Leckie and Smith, 1993; Gregor, 1997)

The Lower Cretaceous stratigraphy, represented by the Mannville Group, can be thought of as representing deposition under initially transgressive and later regressive conditions (Putnam, 1982).

Within the Lloydminster study area, an average thickness of 180 metres of Lower Cretaceous Mannville Group sediments was deposited on the sub-Cretaceous unconformity. Following deposition of the Mannville Group, marine conditions prevailed over most of the Western Canada Basin as the transgressing Joli Fou Sea flooded over the final remnants of Upper Mannville sedimentation. Due to the transgressive nature of this flooding surface, its unconformable nature is only apparent in areas more distal to marine influence during Upper Mannville times (Tompkins, 1989).

In the present study we kept the informal subdivision of the Mannville sequence: the Lower, Middle and Upper Mannville sub-groups based on genetic similarity between units (Jackson, 1984). The Lower Mannville is depositionally related to the initial marine transgression whereas the Upper Mannville incorporates the progradational deposition related to a regressional phase of sedimentation. The Middle Mannville reflects the change from a transgressive, marine dominated succession to a regressive phase of sedimentation (Jackson, 1984).

Sandstones of the Lloydminster Formation consist of relatively thin, widespread sheet sandstones, as do most of the Middle Mannville sandstones (Putnam, 1982). The Lloydminster interval is characterized by the classic progradational sequence.Various ribbon shaped channel deposits cross- cutting the sheet sandstones have been assigned either tidal channel origin (Fuglem, 1970), or fluvial-distributary channel origin associated with the switching of delta lobes. Overlying the Lloydminster Formation are the less predictable Rex, GP, and Sparky formations.

Sparky coal is an areally extensive marker horizon present over much of the Lloydminster sub-basin (Smith et al., 1984). Within the Sparky Formation, multiple cycles consist of a basal restricted marine shale followed by cyclical shoreface sandstones and marine siltstones, randomly interrupted by sandstone and siltstone channelling related to the downcutting of distributary or tidal channels.

The Upper Mannville formations of the Lloydminster area were deposited in a series of progradational pulses dissected by numerous tidal and fluvial channels in an overall shallow water, nearshore marine setting (Jackson, 1984). The Upper Mannville, (composed of the Waseca, McLaren, and Colony formations), is usually between 43 and 61 metres thick, consisting of a variable sequence of lithic sandstones, siltstones, shales, and coals (Vigrass, 1977). Most of the sandstones bodies are lenticular, with very limited areal extent (Putnam, 1982).

Within the study area, recognition of the three upper Mannville formations (Waseca, McLaren and Colony) can be very problematic. As a result, a genetic grouping of these units into the Upper Mannville (Putnam, 1982a, 1982b) has been followed.

The complete Mannville cored section in the area (see Fig. 2-38 of the cored well 10-25-47-3W4) has been used as a calibration point (Figure 2-52).

The Mannville Group is overlain by the marine shales of the Joli Fou Formation (Colorado Group). These dark marine shales overlie the Colony Formation except where a tongue of glauconitic Spinney Hill sandstone enters the area from the northeast (see Appendices II-2 and II-3). The Spinney Hill is a transgressive, deltaic sandstone that forms the basal part of the Colorado Group in central and east-central Saskatchewan.

2.5.2. Geophysical log correlations

The main objective of this study was to resolve the regional stratigraphy of the subsurface Cretaceous section within Lloydminster sub-basin, in order to better understand the relationship between the isotopic composition of C1-C4 alkanes in hydrocarbon mudgases sampled from Lower and Upper Cretaceous strata and the framework geology.

2.5.2.1. Methodology

This study used mainly gamma-ray and sonic/resistivity well log pairs (where available) for stratigraphic correlations. The emphasis has been placed on the use of well log interpretation to delineate formational boundaries and paleo- environmental interpretations. In some cases gamma-ray logs are not recorded above the top of the First White Speckled Formation (FWS) regional marker. In other cases they are completely missing. Moreover, in some locations only SP and conductivity logs were available from wells that fully penetrated the Cretaceous section.

Shell Husky Paradise 10-25-047-03W4/0

Core 538- 699m

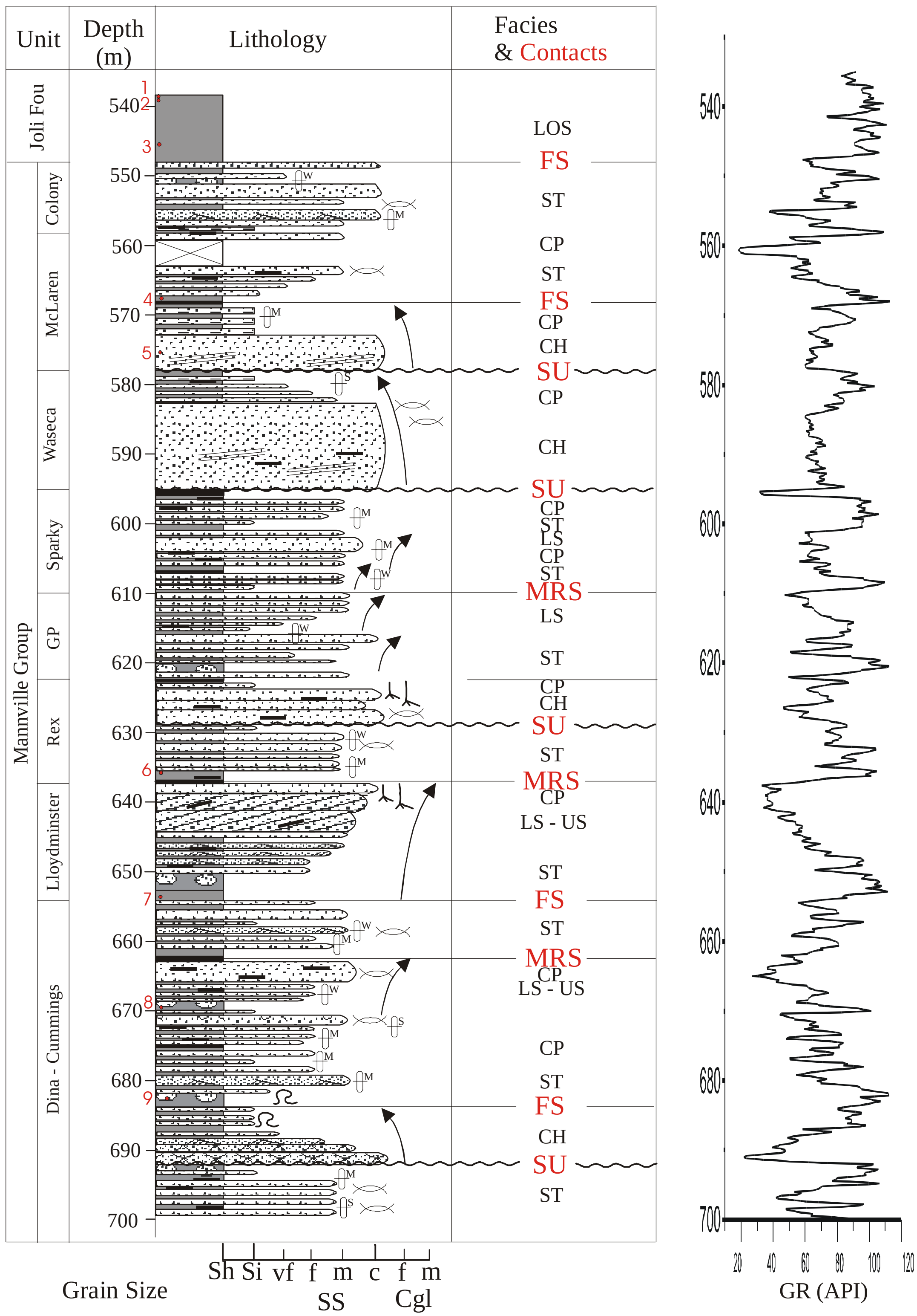

Figure 2-52 Gamma-ray log signature calibrated against the litholog for the 10-25-047-03W4 core. Legend for the litholog is given in Figure 2-1, and facies summaries in Table 2-1. Red numbers: XRD samples.

To accurately identify markers and formations log signatures, the SP, resistivity and conductivity logs were compared one against other and against available gamma-ray logs. When ambiguity existed, the correlations were plotted with a question mark symbol. Locations of the 200 wells used in the database are shown in Figure 2-53.

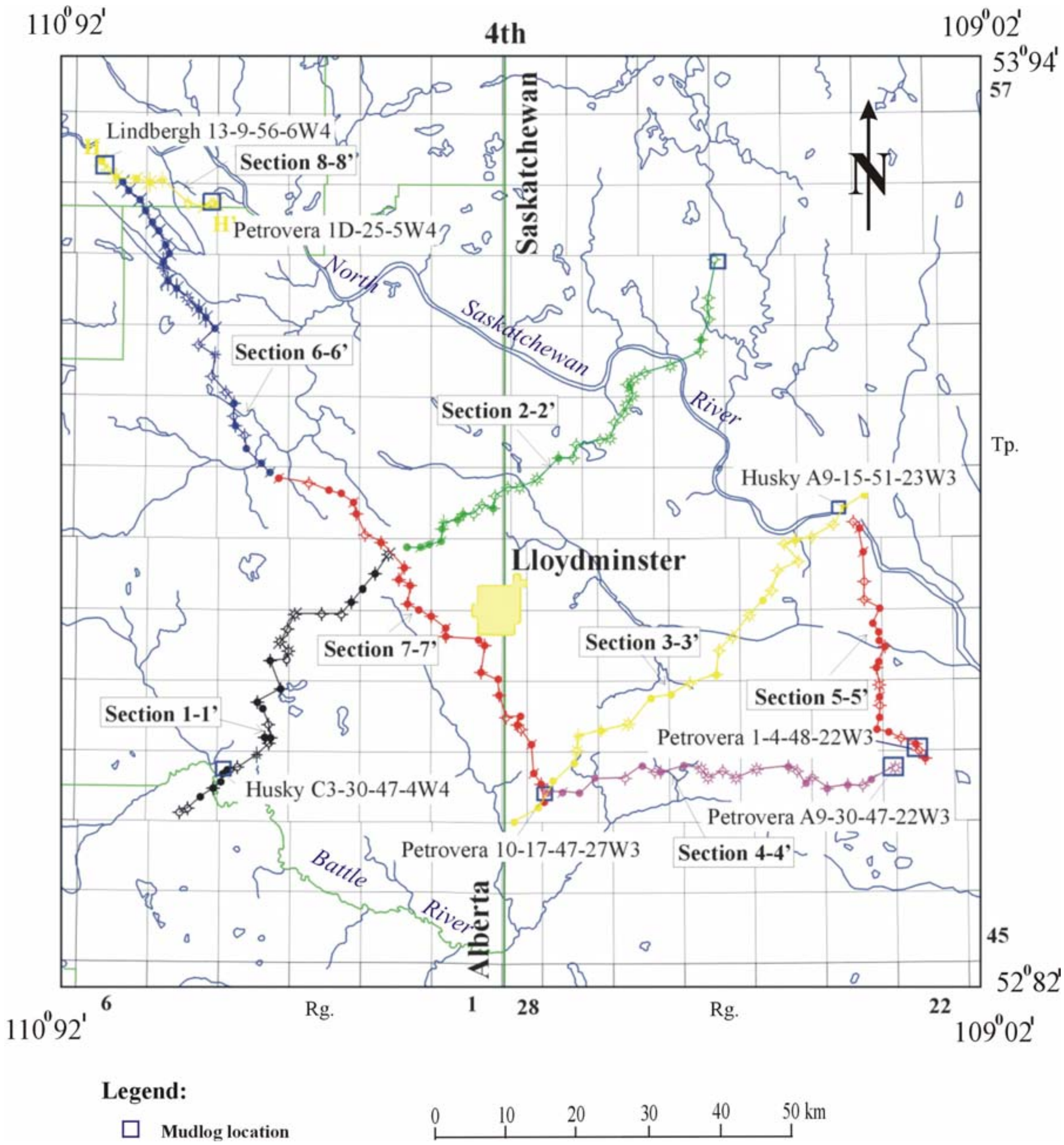

Figure 2-53 Base map showing the database of the study within Lloydminster basin: locations where well logs were used are shown with different well symbols, whereas mudlog locations are shown with open squares. Locations of the eight regional cross-sections 1-1' through 8-8' are shown with different colors; 4th - Fourth Meridian. Township locations are shown on the right border, and range locations along the bottom.

Unfortunately, a large number of wells have no wireline logs above the so-called "Milk River shoulder", making the interpretation difficult.

For the purpose of the present study, for every key stratigraphic surface identified with a combination of logs (gamma-ray, neutron porosity, density porosity, resistivity, and conductivity) a small yellow-filled circle was used in the corresponding appendices (Appendix B, II-1 to II-8).

Lithology determination was made by overlaying porosity logs and viewed together with gamma-ray log. The method is a process of simple pattern recognition, and gives immediate indications of the lithology of logged units (Doveton, 1986).

Knowing that integration of well log data with detailed core analysis can produce a superior understanding of the stratigraphy, the subdivision of the Mannville sediments as derived from the study of well logs was integrated with a suite of well-log cross sections and core study (Tompkins, 1989) throughout the Lloydminster sub-basin. The reliability and precision of our log interpretation of the Mannville strata was evaluated as the two databases were compared and contrasted.

The Upper Mannville above the Sparky Member was correlated in less detail.

2.5.2.2. Results

Regional well-log cross-sections constructed across the area (Appendix B, II-1 to II-8) show the relatively undisturbed pattern of sedimentation and a slightly eastward thinning of the formations. In this part of the Alberta basin, after the significant reduction of the shale permeability, and after uplift and erosion, the principal direction of fluid migration become stratigraphically controlled – particularly through the interbedded permeable beds. The stratigraphic well-log correlations within the area point out the availability of such permeable beds as an important factor in controlling the direction of fluid migration, and consequently the direction of gas migration.

The Lower Cretaceous Mannville Group of the Western Canada Basin unconformably overlies a major erosional surface that has developed on Mississippian and Devonian strata within the Lloydminster area and is overlain by thick marine shales of the Lower Cretaceous Colorado Group. Lower Cretaceous sediments of the study area consist of a complex, interbedded sequence of sandstones, shales, siltstones, mudstones, and coals deposited in a shallow marine to nearshore, deltaic, tidal flat setting with abundant evidence of channelling (fluvial and/or tidal and/or estuarine) throughout the sequence (Tompkins, 1989).

The undifferentiated Dina-Cummings Formation reflects an interval, which is more accurately correlated within the sub-basin. It also is more in line with the nature of the remaining Mannville formations, which represent correlatable, time-stratigraphic cycles of sedimentation. This concept is essential for deciphering the basin framework and identifying both channeling and shoreline sandstones.

The Lloydminster, Rex, G.P., and Sparky formations (the Middle Mannville) were deposited in marine to nearshore environments. Their cyclic nature reflects transgressive/regressive phases. The sand bodies in this interval are dominantly sheet sandstones (5-10 m in thickness). Some of them (like Lloydminster or Sparky sandstones) are traceable over tens of kilometres. Where the sandstone bodies are not laterally extensive, they are separated by low permeability lagoonal or deep-water sediments (Tompkins, 1989). In addition to lateral facies changes, these sandstone bodies are commonly interrupted by thick ribbon-shaped sand and/or shale deposits (up to 40-50m). These ribbons can be estuarine channels, tidal inlet channels, or distributary type channels. Each sandstone body has to be studied individually to infer the depositional environment, but this is not the purpose of the present study.

In the Upper Mannville (Waseca, McLaren and Colony formations) ribbon sand bodies are more abundant than in the Middle Mannville, and sheet sandstones are not as regionally continuous (see Appendices II-1 to II-8).

Within the Colorado Group, the First and Second White Specks Formation, and the Fish Scale Zone are more radioactive than the rest of the shales. They are basin-wide markers, in the meantime representing important sequence stratigraphic boundaries. The top of the Second White Specks Formation (referred in this paper to as SWS) is easily picked on geophysical logs. The formation consists of calcareous siltstone, calcareous mudstone and claystone, sandstone and bentonite (Ridgley, 1998).

The erosional surface at the base of the Second White Specks Formation interpreted as being a ravinement surface in our stratigraphic cross-sections represents a lithologic break between the non-calcareous sediments of the underlying Belle Fourche Formation and the Second White Specks Formation (Shurr et al., 2002). Near the Cenomanian-Turonian (Belle Fourche Fm./Second White Specks Fm.) boundary lays the so-called X-bentonite, a basin-wide stratigraphic marker (Cadrin et al., 1995). This bentonite led marks a strong right-deflection on gamma-ray logs within calcareous sediments of the Second White Specks Formation.

The unconformity found above SWS (see Appendix II-8) could be interpreted as marking the last Turonian regression and is interpreted as an erosional ravinement surface. This is consistent with the interpretation of a major unconformity at the base of the equivalent Morden Formation in east-central Saskatchewan (Bloch et al., 2002).

It is well known that aquitard thicknesses can play an important role in fluid migration. Where overlying aquitards are less thick due to facies changes (as is the case of Colorado shales west of third meridian, which are interrupted by the presence of the St. Walburg and Spinney Hill sandstones), the regional scale lateral up-dip fluid migration could became vertically ascending.

In the deeper part of the Cretaceous section (Mannville Group), the high proportion of coalesced sandstone bodies provides effective hydraulic conduits that are able to transmit the fluid. Within the Colorado Group, Viking sandstone and St. Walburg sandstone (where present below the Base of Fish Scale Zone) are playing the same role.

The Lea Park – Belly River transition zone represents a succession of shales, siltstones and sandstones, interrupted by regional unconformities (especially within Milk River Formation), and arranged in progradational sequences, which downlap (Hamblin and Lee, 1997) in a north-northeastern direction onto a regional disconformity (Braman and Sweet, 1990) known as “Milk River Shoulder”.

Above the “Milk River shoulder”, the shoreline successions are arranged in regressive/transgressive series that offlap also north - northeastward, as can be seen on regional cross-sections (Appendices II-1 to II-8). This interpretation is consistent with some other interpretations in southern and central Alberta (see Hamblin and Abrahamson, 1994; Power and Walker, 1996). Two of the most developed shoreline sandstones within the Lloydminster sub-basin are know as the Ribstone Creek -, and the Victoria members.

Based on the wire-line log response, at least two unconformities were identified in the Milk River Formation. They are named “Milk River markers” on the regional cross-sections; Shurr et al. (2002) also documented these unconformities.

Shallow marine sandstones, having thicknesses of < 1m, and up to 25 m in Basal Belly River are laterally discontinuous, pinching out within finer sediments of the Pakowki/Lea Park Formation. The overlying nonmarine, fine-grained deposits of the Belly River Formation (where still present, and not removed by erosion), and the thin marine shale tongues that separate the shoreline-related sandstone tongues within the coarsening-upward sequences of the transition zone may form the vertical seals for stratigraphic traps.

CHAPTER THREE
CARBON ISOTOPE SIGNATURES OF MUDGASES AND THEIR STRATIGRAPHIC DETERMINATION

3.1. Introduction

In general, sequence stratal units and their bounding surfaces directly control the distributional trends, external geometry and internal heterogeneity of fluid/hydrocarbon-bearing reservoirs in formations. From an exploration point of view, the highly prospective trends appear to occur at sequence boundaries (erosional subaerial unconformities, and/or ravinement surfaces, which have eroded through a subaerial unconformity), or other related bounding surfaces (Reinson et al., 1994).

The same kind of parameters influence or control the carbon isotopic mudgas profiles in the ten studied isotopic depth profiles from Western Canada Sedimentary Basin. Therefore, paleoenvironmental conditions and depositional processes could also control the stratigraphic and lateral variation of the isotopic signature of mudgases.

The aim of this part of the project will be to answer the question: Do the major sequence stratigraphic surfaces correlate with regionally existing gas isotope mudlogs or not?

The principal intention is to compare the trends observed in the isotopic mudlogs with significant key bounding surfaces identified in Chapter Two, and to see if their variations can be correlated regionally within the stratigraphic framework, i.e. to interpret those, possibly existing trends.

As can be observed from a simple visual examination of the carbon isotopic depth profiles (Figure 3-1 and Figure 3-2), there are numerous variations with depth for $\delta^{13}C_1$, $\delta^{13}C_2$, $\delta^{13}C_3$, and $\delta^{13}nC_4$ values, materialized by the presence of sharp inflections, doglegs and crossovers. For the most part, these trends are mirrored in part by changes of both the concentration of hydrocarbons and wetness index (defined as C_2+C_3+C_4 abundance divided by the total abundance of C_1 to C_4 gas components).

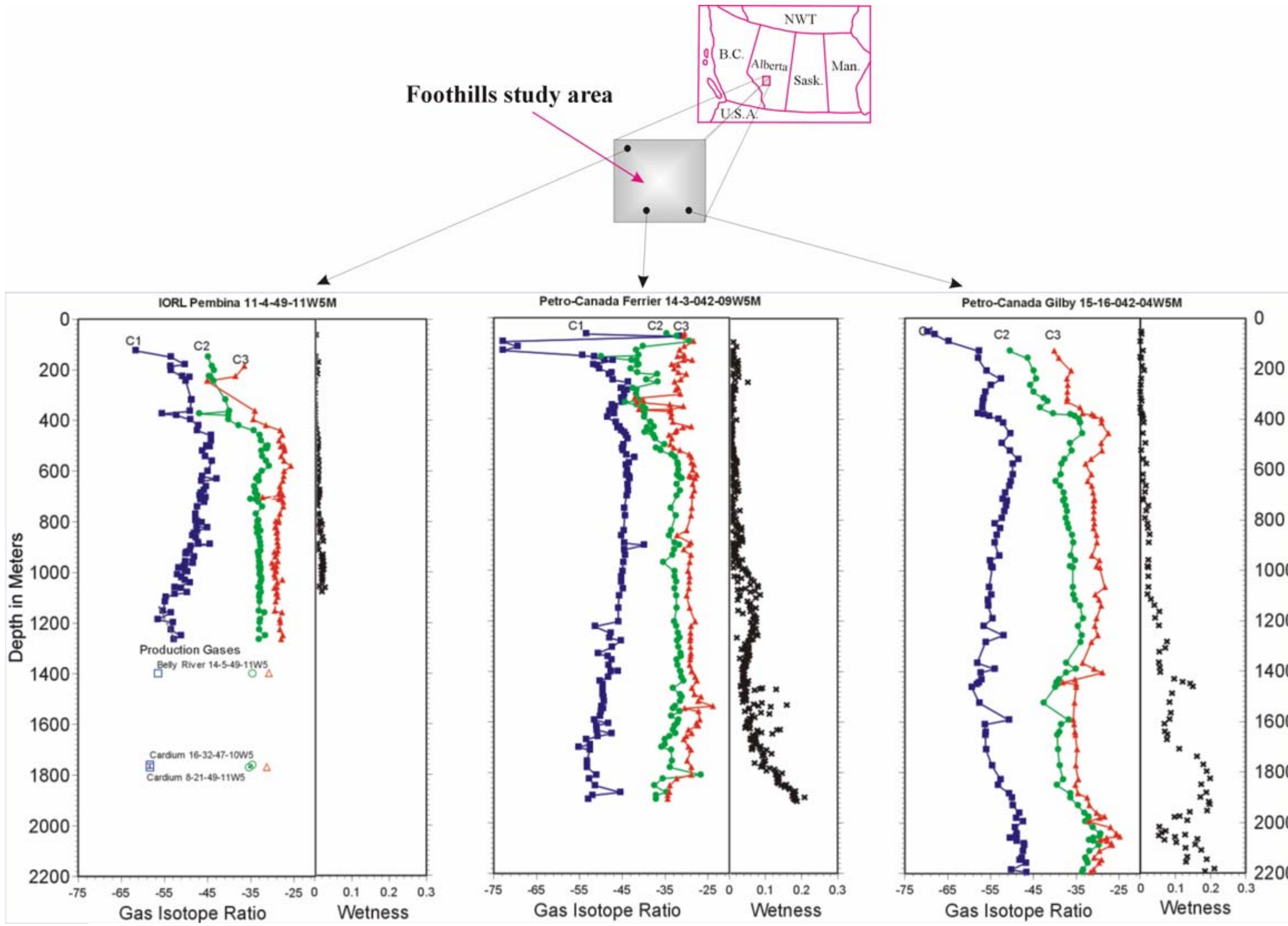

Figure 3-1 Carbon isotopic composition and wetness of gases from three mudlogs in west-central Alberta. Note: the isotope profiles for butane are not displayed in this figure for simplicity reasons.

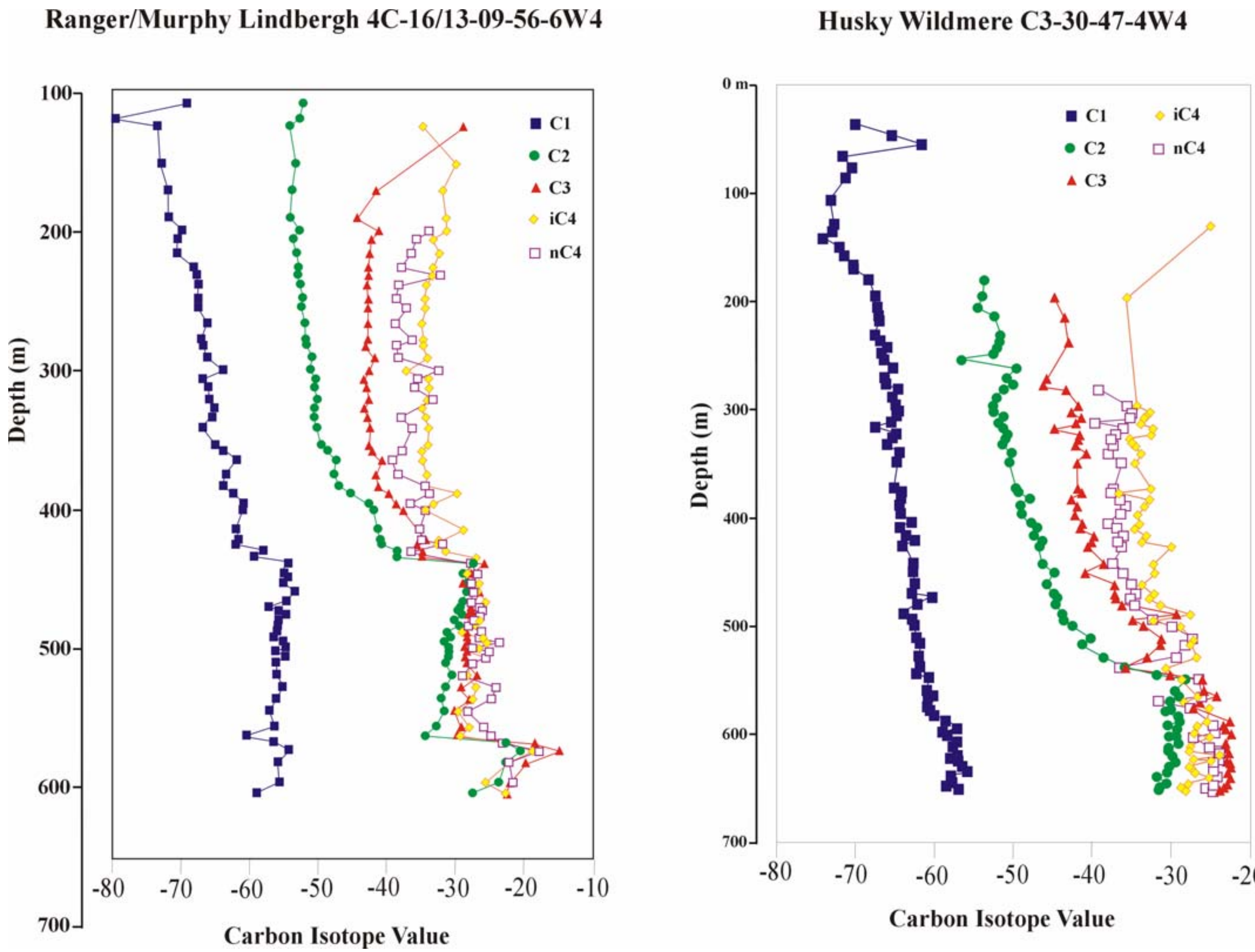

Figure 3-2 Carbon isotopic composition and wetness of gases from two mudlogs in the heavy oil region.

These inflections and deviations towards increasing and decreasing values with depth are named isotopic boundaries and they correlate in part (as it will be shown) with the regional stratigraphy. They can also be explained in terms of the origin and post-generation history of the gases (both biodegradation and mixing of gases cause deviations in the isotopic trends).

The strong correlation between isotopic and stratigraphic boundaries indicates that compartmentalization of the gas is strongly influenced by stratigraphic variations. This implies that the majority of stratigraphic boundaries act as effective barriers to gas migration so that one can say that each gas package retains its distinct isotopic character.

3.2. Foothills region

3.2.1. Results

The detailed carbon isotope mud profiles obtained in the Pembina-Ferrier-Gilby oil fields of west-central Alberta (Figure 3-1) represent carbon isotopic analyses of over 250 gas samples extracted from mud during the drilling of each well. The mud-gases were collected from the surface down to the Belly River Formation (Pembina), to the Colorado Group (Ferrier), and to the Fernie Group (Gilby) at ~ 5-10m depth intervals. Isotope ratios of mudgases provided an isotopic depth profile (or 'fingerprint') for each of the wells sampled.

As expected (Schoell, 1980), the shallowest gases have lower carbon isotope values than the deepest but the increases are not monotonic with depth. The mud gas profiles show numerous inflections and variations in the trends of the carbon isotope values and the wetness index (C_2+C_3+C_{i4}/C_1+C_2+C_3+C_4) with depth. Some of these inflections correspond with regional unconformities in terms of formation boundaries, indicating a lack of cross-formational flow (Figures 3-3, 3-4, and 3-5). Other inflections occur within formations suggesting intra formational compartmentalization of the gas.

In general, there is a remarkable degree of correlativity of carbon isotope trends between the three wells. Normally geologists go from bottom to top but because the mudgas profiles are finished at different depths, they are described and interpreted in this thesis from top to bottom.

In descending order, a first distinctive inflection occurs at the boundary between Paskapoo Formation and Scollard Formation in all three mudlogs. This boundary marks a sharp facies change from the overlying massive sandstone of the Paskapoo Formation to the underlying silty and sandy shales of the upper Scollard Formation.

The thick amalgamated channel sandstones of the Lower Paskapoo represent the first 20-50 metres above the boundary. In the Ferrier and Gilby mudgas profiles there is a slight change in the C_2 and C_3 values from top to the bottom of this coarse grained deposit. In the Ferrier mudgas profile the C_2 isotope ratio is increasing in the upper half of the sandstone body from –37.41‰ to -35.21‰; the lower half of the sandstone body shows a decreasing trend of the C_2 values (from -35.21‰ to –37.18‰) (Figure 3-3).

The Gilby profile (Figure 3-4) shows a similar trend for the C_2 isotopic ratio within the basal sandstone body of the Paskapoo Formation: increasing from –42.62‰ to –41.76‰ in the upper half- and then decreasing from –41.76‰ to –43.56‰ in the lower half of the body. The same profile shows an increasing for the $\delta^{13}C_{C3}$ values from –37.11‰ to –34.13‰ within the basal sandstone of the Paskapoo Formation, from top towards bottom.

The Pembina mudgas profile (Figure 3-5) shows the following values for the carbon isotope ratios of gases sampled in the basal sandstone of the Paskapoo Formation:

- –49.05‰ for $\delta\ ^{13}C_{C1}$;
- –40.18‰ for $\delta\ ^{13}C_{C2}$, and
- –34.46‰ for $\delta^{13}C_{C3}$

Below the Paskapoo - Scollard boundary, a very distinctive inflection of the C_1, C_2 and C_3 isotope ratios trend towards higher values occurs in an 80-120 m thick zone. This regionally occurring, apparently overmature zone partially corresponds with the Ardley coal zone of the Scollard Formation. Within this zone, the coal Nr. 14 of the Scollard Formation (Ardley coal) appears to have the greatest values of the isotope ratios (Table 3-1).

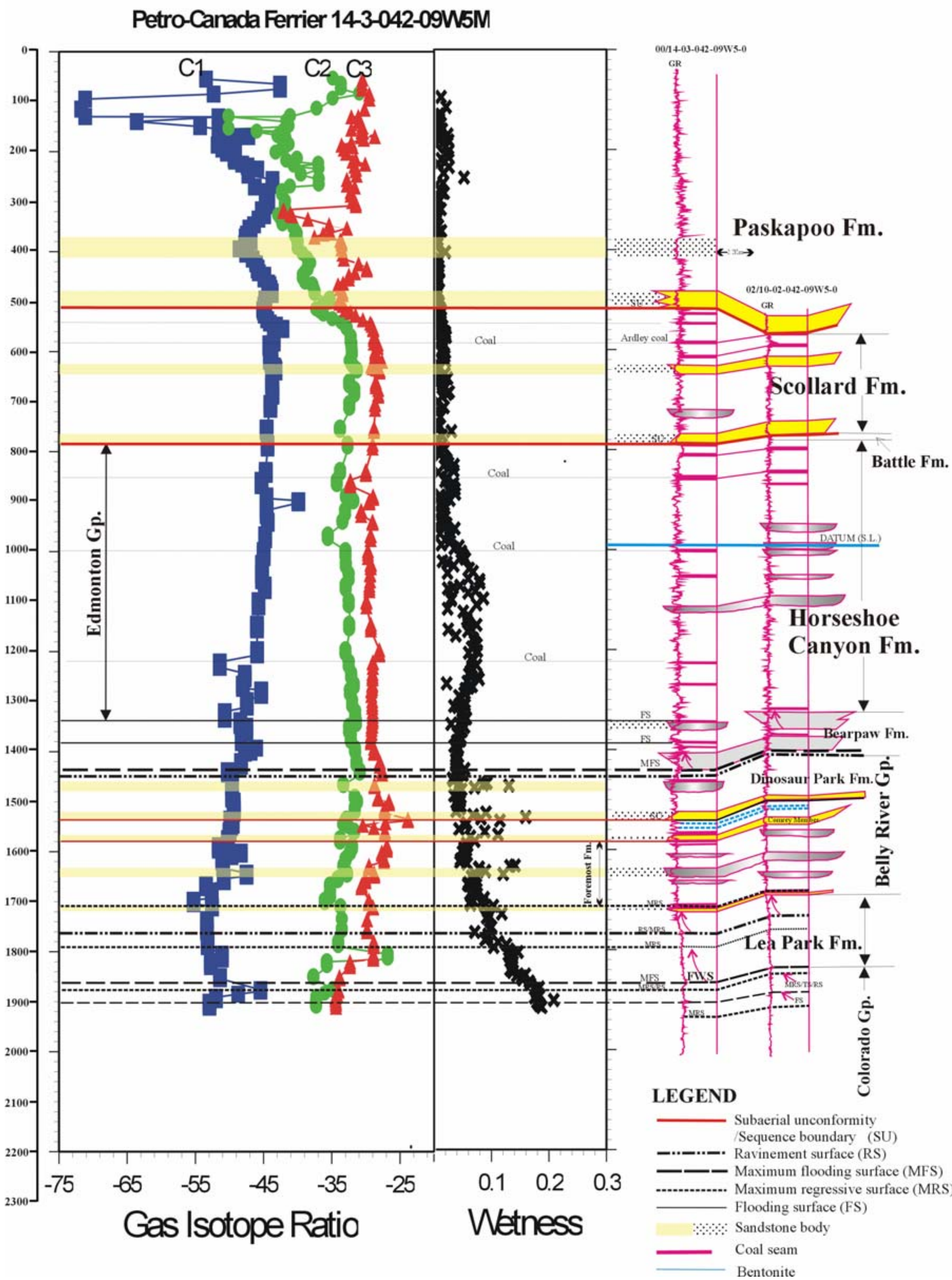

Figure 3-3 Mudgas isotopic depth profile from Petro-Canada Ferrier 14-3-042-09W5 and its relationship with the regional stratigraphy.

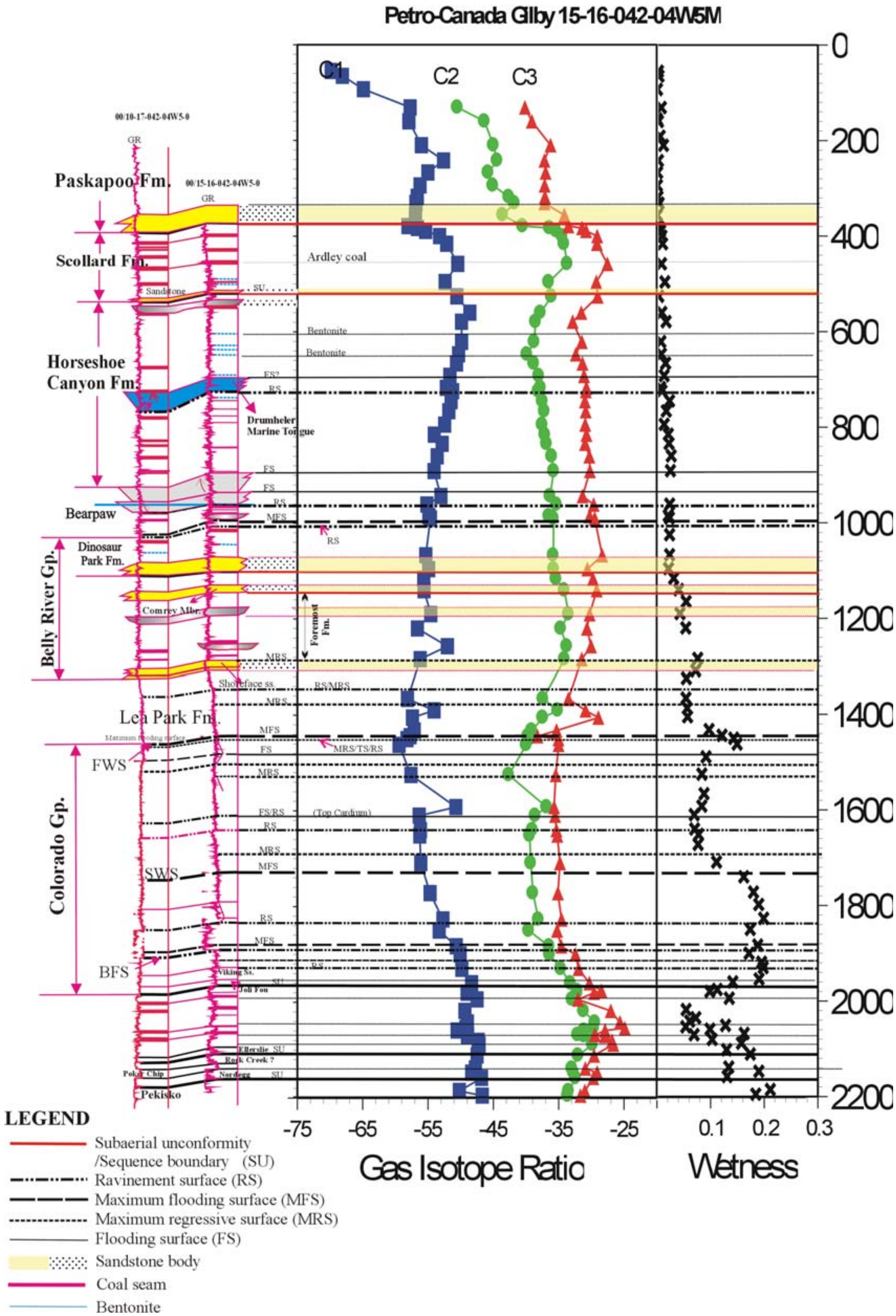

Figure 3-4 Mudgas isotopic depth profile from Petro-Canada Gilby 15-16-42-04W5 and its relationship with the regional stratigraphy.

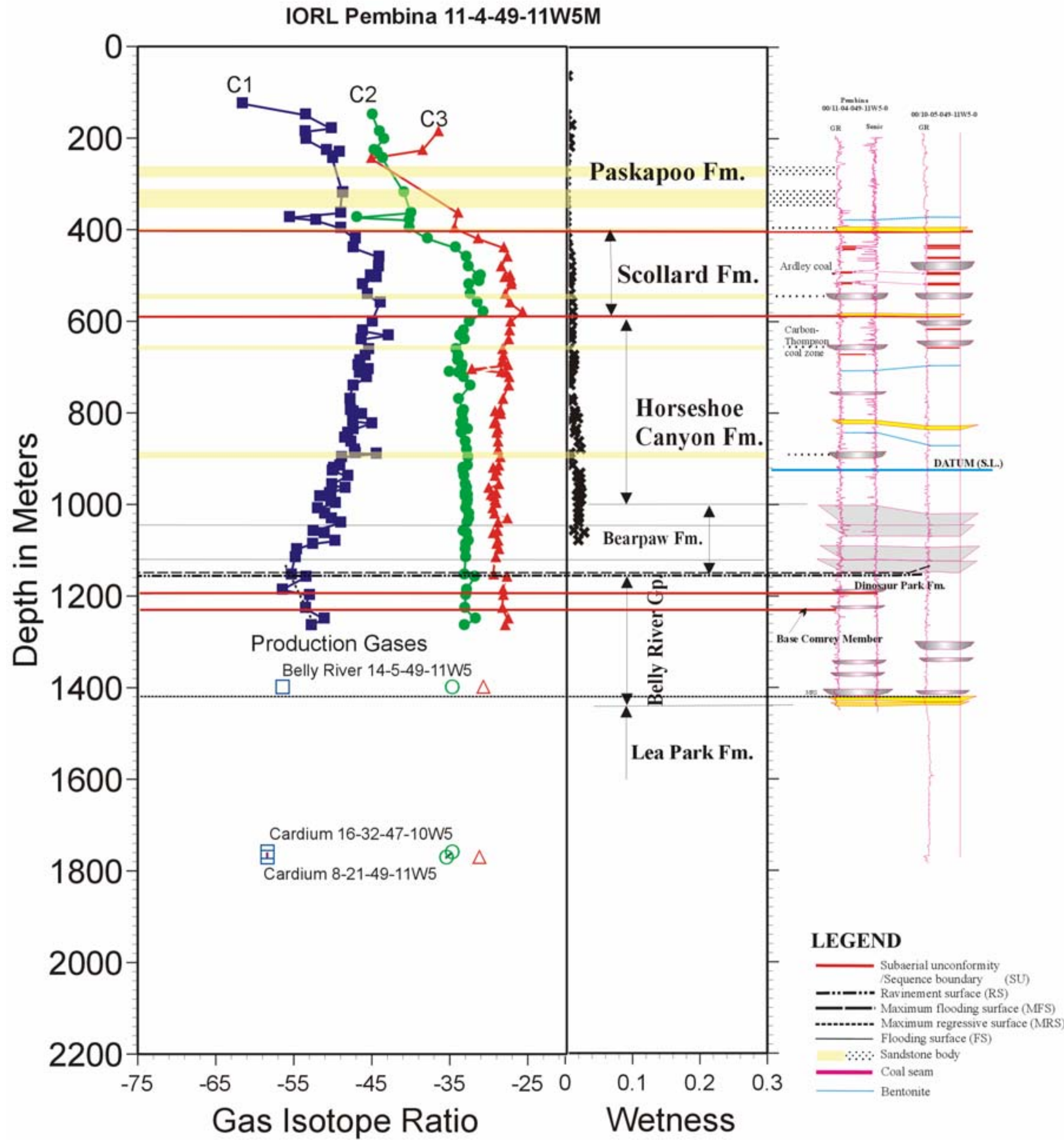

Figure 3-5 Mudgas isotopic depth profile from IORL Pembina 11-04-049-11W5 and its relationship with the regional stratigraphy.

Table 3-1 The average carbon isotope ratios for the Ardley coal seam

	Pembina	**Ferrier**	**Gilby**
$\delta^{13}C_{C1}$	-45.25‰	-44.17‰	-50.44‰
$\delta^{13}C_{C2}$	-31.09‰	-32.02‰	-33.68‰
$\delta^{13}C_{C3}$	-27.33‰	-28.30‰	-27.55‰

The lower half of the Scollard Formation is dominated by thick, multistoried, erosively based, fluvial channel sandstones up to 8 m thick (Gibson, 1977; Jerzykiewicz and Sweet, 1988). The fluvial sheet sandstone near the base of the Scollard shows the same increasing trend of the carbon isotope ratios from top to bottom.

Fluvial sands tend to be deposited continuously during valley-fill, providing an effective reservoir for migrating fluids (hydrocarbons). The overlying and interbedded nonmarine, fine-grained strata deposits within these two clastic wedges of fluvial strata - Paskapoo and Scollard – constitute the vertical seals in fluvial channel stratigraphic traps. The source of gases may be the coals of the underlying Horseshoe Canyon Formation (in the Scollard case), or the coal-bearing strata of the upper Scollard.

Below the apparently overmature zone there is a relatively continuous trend of decreasing methane (C1) values, accompanied by a trend of slightly increasing ethane (C2) values down to the top of the Belly River Group (for Pembina and Ferrier mudgas profiles) and the top of the Upper Bearpaw Formation (for Gilby mudgas profile). Within this trend (stratigraphically comprising the Edmonton Group and the transition zone between the Horseshoe Canyon Formation and the Bearpaw Formation) there are some minor inflections corresponding with within-trend flooding surfaces and coal beds at the tops of the progradational sequences of the Upper Bearpaw Formation. Except for the uppermost progradational sequence of the Upper Bearpaw Formation in the Gilby well, the presence of these minor flooding surfaces suggests a decrease with depth for the C1 isotope ratio (from –47.52‰ to –49.65‰ – Ferrier profile, and from –53.02‰ to –55.17‰ – Gilby profile) and an increase with depth for the C2 isotope ratio (from –32.35‰ to -31‰, Ferrier profile; from –36.31‰ to –35.32‰, Gilby profile), and C3 isotope ratio (from –29.17‰ to -28‰, Ferrier profile; from –31.34‰ to –29.65‰, Gilby profile). The presence of the coal beds (associated with these flooding surfaces) seams to "move" the carbon isotope signatures toward more positive values.

The overlying nonmarine, fine-grained deposits of the lower Horseshoe Canyon Formation, and the thin marine shale tongues that separate the shoreline-related sandstone tongues within the coarsening-upward sequences of the Upper Bearpaw Formation form the vertical seals for stratigraphic traps.

The *ravinement surface* that marks the boundary between the Bearpaw Formation and the underlying Belly River Group shows a distinct increase in the wetness index from 0.04% to 0.09% (Ferrier mudgas profile), accompanied by a relatively strong deflection towards more negative values for C_2 and C_3 isotope ratios: -33.21‰ for $\delta^{13}C_{C2}$, and –28.74‰ for $\delta^{13}C_{C3}$. Moreover, in the Ferrier mudgas profile, where there is much more detailed data, a decreasing trend with depth for C_2-C_3 can be observed within the thin transgressive unit of the Bearpaw Formation, from the maximum flooding surface downward, in the direction of the ravinement surface. In this case there is an apparent increase in maturity near the maximum flooding surface.

The same deflection towards more negative values for C_2 and C_3 isotope ratios can be observed in the Pembina mudgas profile: -33.12 to –31.82‰ for $\delta^{13}C_{C2}$, and –29.45 to –27.74‰ for $\delta^{13}C_{C3}$ (Figure 3-5).

The Belly River Group shows a puzzling trend of decreasing and increasing carbon isotope values. Stratigraphic surfaces within the Belly River Group on Figure 3-3 mark these minor inflections, and they suggest compartmentalization of the Belly River Formation into several gas zones – the stratigraphic traps and corresponding seals. Belly River core porosity and permeability data from two of the 38 control cores previously described confirm the rock properties variability (Figures 3-6 and 3-7).

The base of the Dinosaur Formation is marked by a regional discontinuity, with localized erosion, and it is characterized by thick, multistoried channel-fill of medium to coarse-grained sandstone enclosed in inter-channel siltstone (Eberth and Hamblin, 1993). Moderate gas reserves are contained in this unit (Hamblin and Lee, 1997). Their source could be the adjacent Bearpaw shales (toward east), or the under- and overlying coals.

The overlying fine-grained unit ("Upper silty unit") provides the vertical seal for the gases contained in Comrey sandstone bodies of the Oldman Formation, creating many

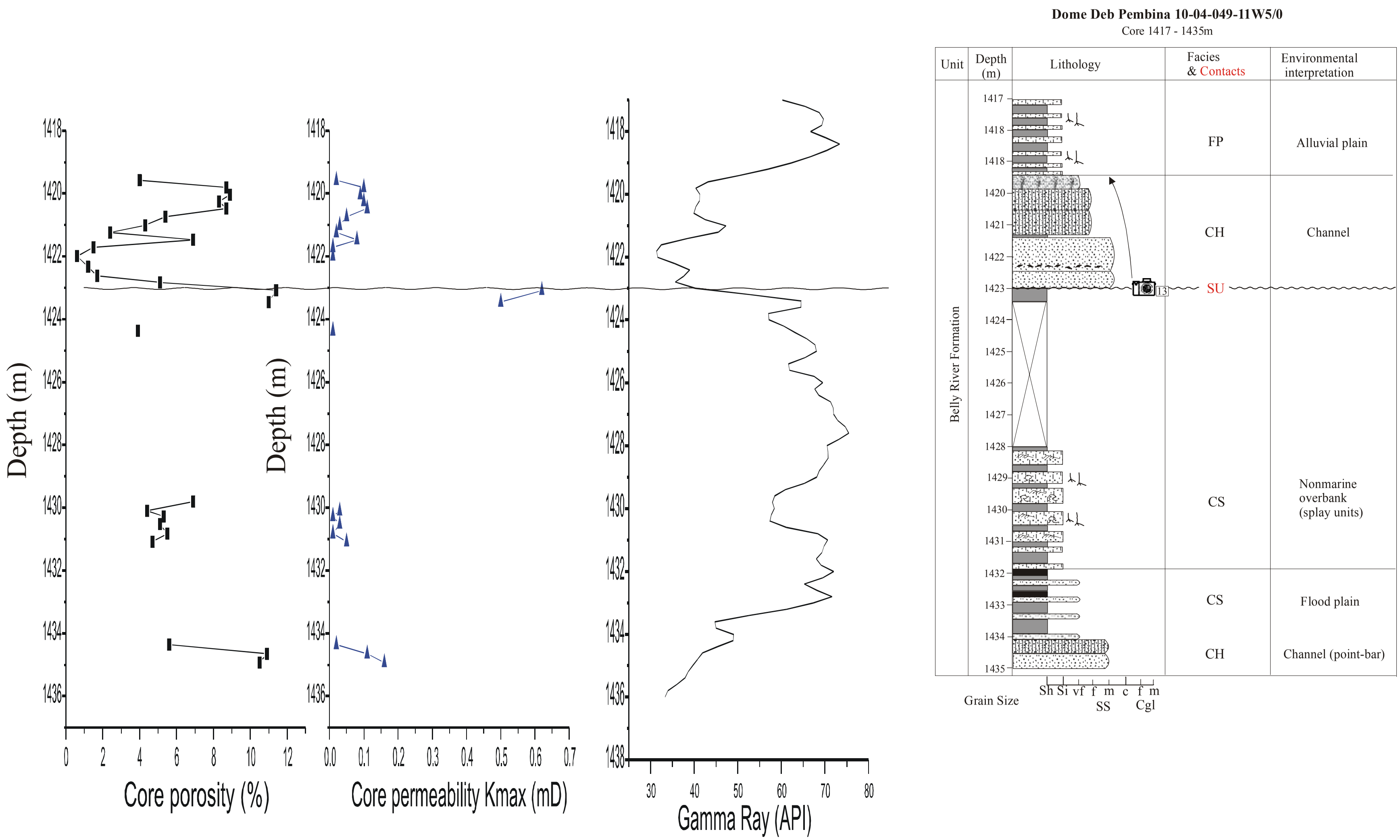

Figure 3-6 Litholog for the 10-04-49-11W5 core, annotated with main contacts and facies interpretation. Core porosity and permeability data is also shown, as reported in the core analysis report from IHS Energy public database. Legend for the litholog is given in Figure 2-1.

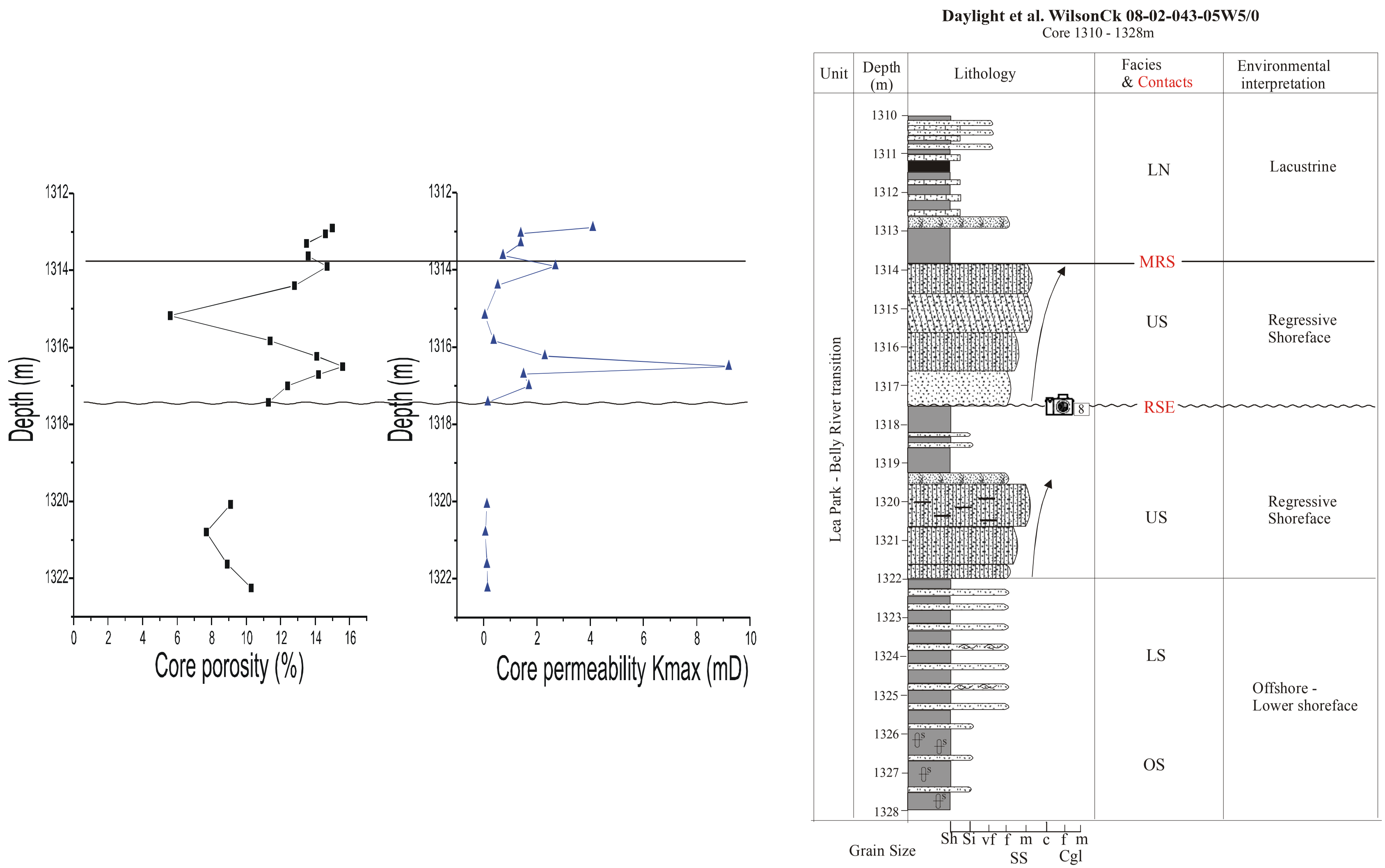

Figure 3-7 Litholog for the 08-02-43-5W5 core, annotated with main contacts and facies interpretation. Core porosity and permeability data is also shown, as reported in the core analysis report from IHS Energy public database. Legend for the litholog is given in Figure 2-1.

stratigraphic traps. The source of hydrocarbons may be the adjacent and interbedded coal seams.

In all of the sandstone bodies with more or less lateral extent, the wetness index values tend to decrease downwards.

The two subaerial discontinuities - at the base of the Dinosaur Park Formation and at the base of the Comrey Member - appear to significantly influence the carbon isotope trends (the subaerial unconformity at the base of the channel, Figure 3-6). Going down into the Gilby profile, the first discontinuity (1116 m depth) marks a transition toward more positive values for C_2 (from –35.38 to –34.17‰), and C_3 (from –29.75 to –29.18‰) isotope ratios, the latter (~ 1150 m depth) toward more negative values of the C_3 isotope ratios (from –29.18 to –30.27‰), (Figure 3-4). In the case of the Ferrier and (partially) Pembina profiles, both discontinuities seem to mark transitions towards more positive values of the C_2 and C_3 isotope ratios below the discontinuity. For example, the subaerial discontinuity at the base of the Dinosaur Park Formation in the Ferrier profile marks transition towards from –33.23 to –31.60‰ for $\delta^{13}C_{C2}$, and from –30.45 to –27.41‰ for $\delta^{13}C_{C2}$. The difference could be due to fewer mudgas samples in the case of the Gilby profile. In the case of the Pembina profile, being the shortest mudgas profile, the correlation had to stop at the base of the Dinosaur Park Formation.

The transition toward more positive values below the discontinuities could be due to the discontinuity itself and/or because of the presence of the coals (Taber coal zone in the case of the unconformity at the base of the Oldman Formation).

Thick, channel-sandstone bodies, encased in mudstones, characterize the nonmarine portion of the Foremost Formation. Large gas reserves are contained in this composite unit (Hamblin and Lee, 1997). The interbedded, nonmarine, fine-grained deposits provide vertical seal for the pools contained in channel and crevasse splay sandstone bodies, creating many stratigraphic traps.

Within those prominent channel sandstone bodies (with thickness more than 3-5 metres, recognized on logs with a fair degree of confidence) can be observed an inflection of the carbon isotope ratios towards more positive values, beginning with the top of the sandstones.

The carbon isotope values in the Basal Belly River decrease with depth starting from the maximum regressive surface (MRS), which caps the clean sandstone of the prograding nearshore and shoreface facies.

The Lea Park Formation in the Ferrier (and Gilby?) profile has an upper zone with relatively uniform isotope values, and a lower zone with C_2 and C_3 values that decrease with depth (Figure 3-3). The upper zone corresponds in part with the marine sequence of the Pakowki Formation/Upper Lea Park Formation. The lower part represents the last progradational cycle within the Alderson Member (Figure 3-3, Ferrier profile, between 1775 – 1800m depth, and Figure 2-3). The bounding surface that caps this cycle represents a *ravinement surface* ("Milk River shoulder").

Within the lower shallow-marine sequence of the Lea Park Formation (Alderson Member of the Milk River Formation) there is a strong inflection toward more positive values of the C_1-C_2 isotope ratios across a surface that caps another major progradational cycle; this surface was identified on our log cross-section with a *maximum regressive surface*.

The top of the Colorado Group (FWS) shows a distinct increase in the wetness index accompanied by a continuing trend of decreasing C_1 and C_2 values. With further depth, the C_1 and C_2 values increase and then decrease.

The *maximum flooding surface* represented by the top of the First White Specks Formation marks a strong inflection within both the Ferrier and Gilby profiles (Figures 3-3 and 3-4) toward more positive values of the carbon isotope ratios. Downward from this level the carbon isotope ratios decrease rapidly within an up to 10 metres thick interval - until a surface that represents a *maximum regressive surface* on our cross-section. This maximum regressive surface could represent the top of the Medicine Hat shoreline sandstone, which caps one of the progradational cycles within the uppermost Colorado shales across the Alberta basin.

Gilby profile

The mudgas profile for the Colorado Group shows a relatively continuous trend of increasing methane (C_1) values, accompanied by a trend of slightly increasing ethane (C_2) and propane (C_3) values for more than 500 m down to the top of the Mannville Group

(Figure 3-4). Within this broad trend are minor inflections corresponding with different bounding surfaces.

Within the Upper Colorado Shales appear two distinctive inflections, which correspond: the lower one (Figure 3-4, at 1615 m depth) with a presumable major flooding surface/sequence boundary (FS/SB) following the Cardium Formation deposition, and the upper one (Figure 3-4, 1530 m depth) with a maximum regressive surface.

The Cardium Formation is identified on the mudgas profile by its smaller wetness index values. The small inflection at the regionally marine erosion surface, which caps the Pembina River Member, suggests compartmentalization of the gas in the Cardium in two zones: one with more negative isotope ratios values (Pembina River Member) and the other one with more positive isotope ratios values (Cardium Zone Member).

Below the Cardium Formation and the Second White Speckled Shale (SWS), Colorado shales show a continuous trend of increasing C_1, accompanied by relatively uniform C_2 and C_3 values. Inflection in the wetness index at the top of the SWS (1730 m depth, Figure 3-4) corresponds with the maximum flooding surface associated with the formation.

At the Base of Fish Scales (BFS), there is a break in the slope of the C_2 and C_3 trend toward more rapidly increasing values (Figure 3-4, ~1900 m depth). These trends continue through the Viking Formation, both in Ferrier and Gilby profiles, with a break in the wetness index at the top of the "Viking Sandstone" (ravinement surface).

A zone of lower C_1-C_3 values separates the SWS and BFS: the Belle Fourche Formation (Bloch et al., 1999). Within these Lower Colorado shales, the lower isotope ratios for the Belle Fourche Formation could also be related to the change from type II organic matter of the SWS and BFS to type II+III organic matter of the Belle Fourche Formation (Schröder-Adams et al., 1996).

In Figure 3-4, the Mannville Group shows a puzzling trend of decreasing and increasing C_2 and C_3 isotope ratio values, having, from top to the bottom, three zones of decreased C_2 and C_3 values separated by two zones of higher C_2 and C_3 values. The latter ones could be related to the presence of the upper coal zone within the Upper Mannville and to the presence of the Glauconitic Sandstone, respectively.

According to Leckie et al. (1996) the regional Glauconitic Sandstone in this area includes several porous marine sandstones, which have a sheet-like geometry. These marine sandstones comprise prolific reservoirs in stratigraphic traps, where the Upper Mannville channels dissect the porous sandstones.

Within the lowermost group of the foreland succession in this area – Fernie Group - the Poker Chip shales and overlying unit (Rock Creek Formation) seem to play a seal role for the gases trapped into the Nordegg Member. The two small inflections at the top and base of the Nordegg Member correspond to regional *unconformities*, indicating a lack of cross-formational flow.

The Pekisko Formation shows a continuous trend of C_1, C_2 and C_3 values towards slightly decreasing values with depth.

3.2.2. Discussion

Sediments respond mainly to the physical energy levels in the system relative to their grain size, with only a slight influence of flow depth (Southard, 1971). Therefore, their physical properties reflect the energy level of deposition. For example, a high-energy environment (wave-dominated shoreline, alluvial fan or proximal braided fluvial system) tends to produce well-sorted or coarse-grained deposits with better porosity and permeability and low organic matter concentration. If porosity is preserved, these rocks can serve as reservoirs. In opposition, low-energy environments (in slowly moving-, or unmoving waters) are sites for accumulation of fine-grained sediments having lower permeabilities. These environments tend to have higher concentrations and better preservation of organic matter and may become petroleum source rocks or reservoir seals.

The physical energy levels (and often oxygenation states) do change in repeated patterns, bounded by significant physical surfaces that can be used to decipher the sequence stratigraphy within each basin. Giving insights into the relation of depositional processes to resultant lithofacies packages, these preserved sediment-fluid interfaces were used in our approach to better understand and demonstrate their relationship with geochemical depth profiles.

Sequence boundaries are obvious as facies dislocations (an upward jump to a significantly more proximal facies), and abrupt upward decreases in gamma-ray reading. Within fluvial systems, sequence boundaries are recognized by abrupt changes of facies associations (Richards, 1996), e.g. a change in grain size (from fine grained to coarse grained) in response to increased stream power and sediment load. This is mainly the case of the subaerial unconformities marking the base of sand in fluvial successions (e.g. base of Dinosaur-, Scollard-, and Paskapoo formations).

Sequence boundaries also often mark an abrupt upward change from a progradational well log signature to an aggradational or retrogradational well log signature, whenever they are represented by ravinement surfaces, which have eroded through subaerial unconformities.

The grain size and facies change that occur across subaerial unconformities (sequence boundaries) typically result in permeability contrasts (Reynolds, 1996), and therefore, in flow unit boundaries and inflection marks along the isotopic mudgas profiles.

In general, according with the results presented in this thesis, the presence of the subaerial unconformities on the mudgas profiles seems to mark a transition from more positive values (within underlying deposits) to more negative values (within overlying deposits) of the carbon isotope ratios. The coarse grained deposits above the unconformity present in general a slight downward increase of the carbon isotope ratios. Major shifts in carbon isotope ratios tend to occur at sequence boundaries and maximum flooding surfaces (Figures 3-8 to 3-10).

The marine flooding surfaces are recognized as abrupt upward increases in shale content (Emery et al., 1996), and hence porosity and permeability decreases. These shales form numerous intraformational seals in paralic successions. Maximum flooding surfaces have great extent. They form regional seals that control the long-distance migration of fluids in the subsurface, and form major barriers within fields (Emery et al., 1996).

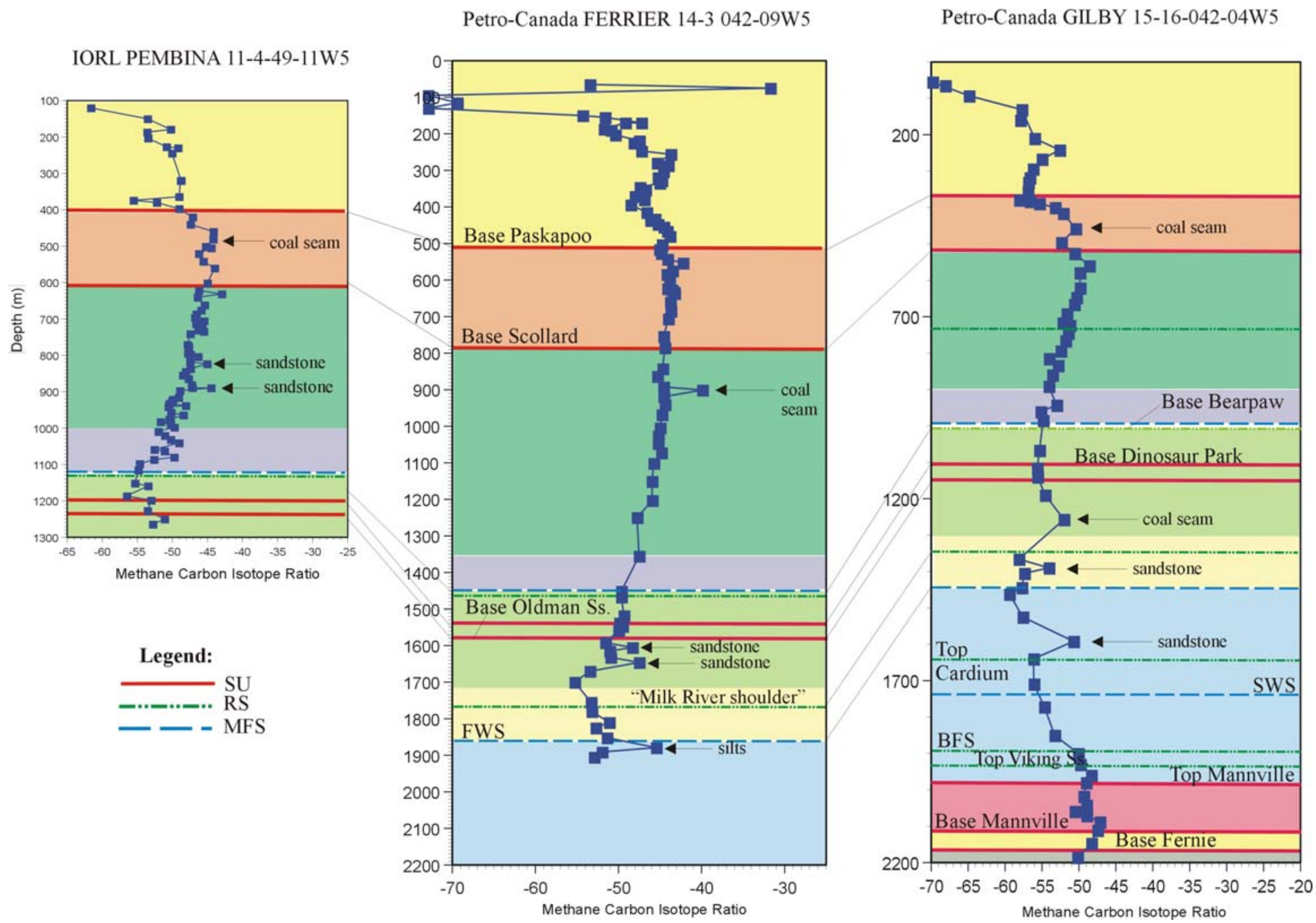

Figure 3-8 Variations of carbon isotope ratios for methane with stratigraphic position, Foothills region. Major shifts in carbon isotope ratios tend to occur at sequence boundaries and maximum flooding surfaces.

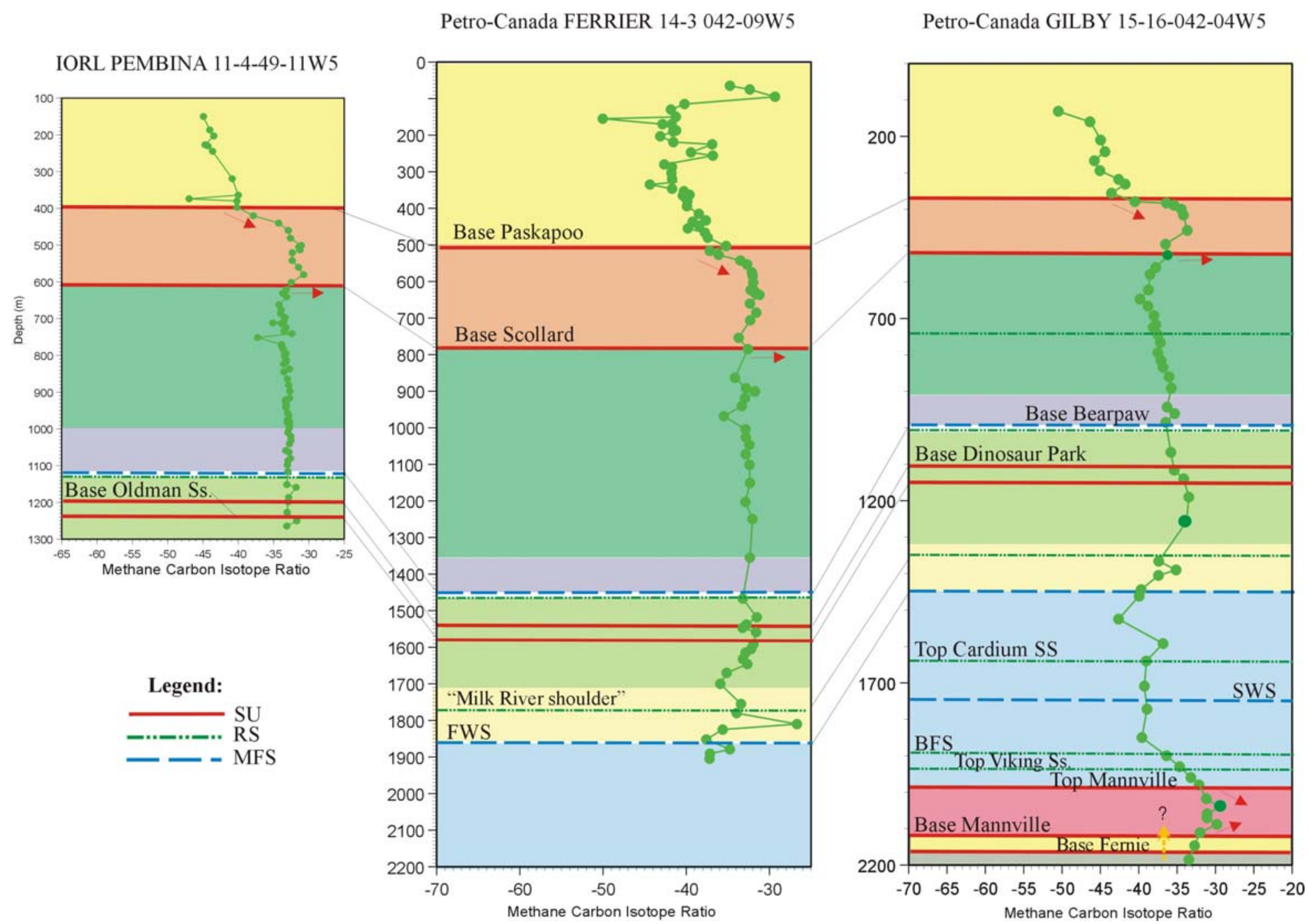

Figure 3-9 Variations of carbon isotope ratios for ethane with stratigraphic position, Foothills region. Major shifts in carbon isotope ratios tend to occur at sequence boundaries and maximum flooding surfaces.

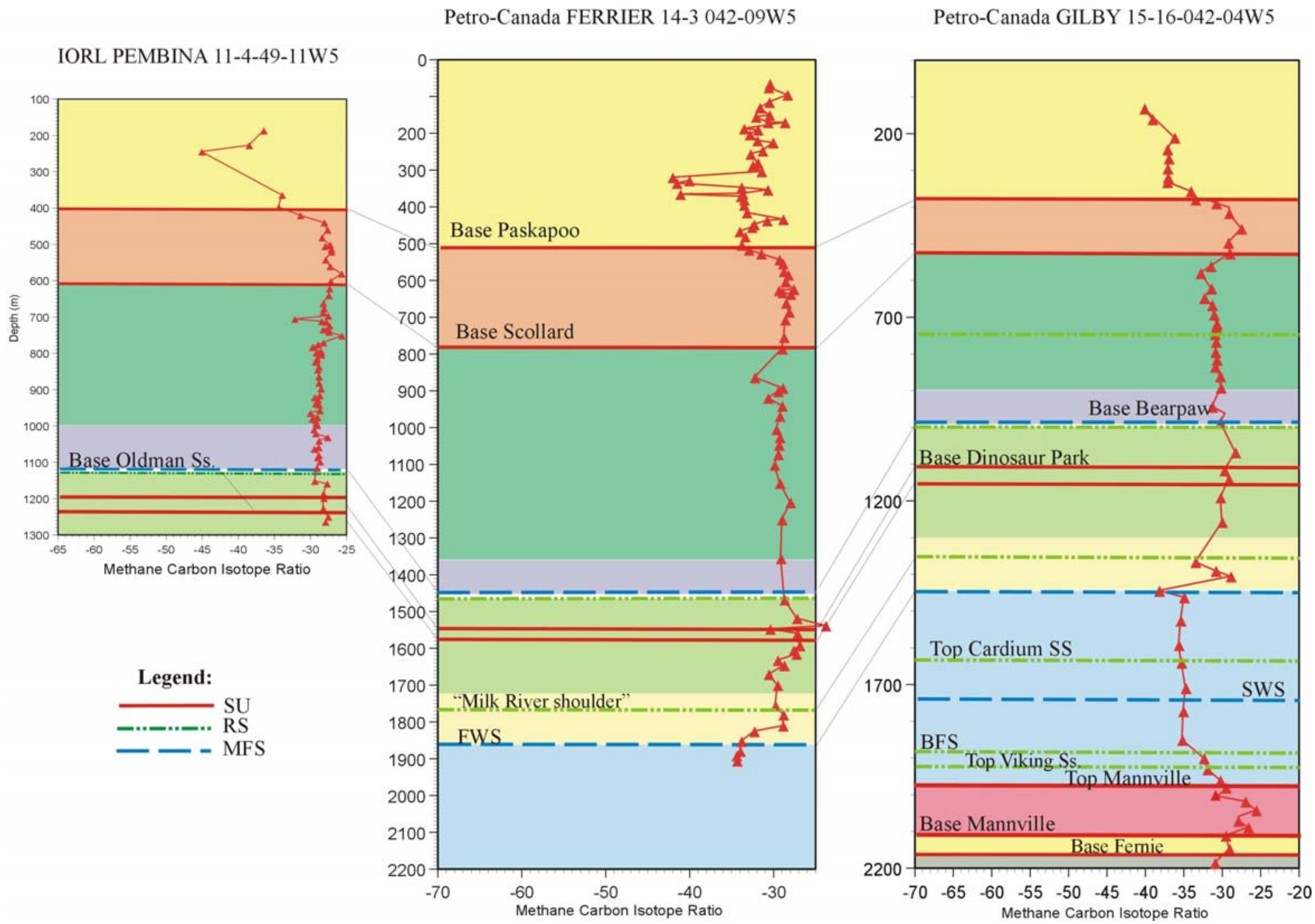

Figure 3-10 Variations of carbon isotope ratios for propane with stratigraphic position, Foothills region. Major shifts in carbon isotope ratios tend to occur at sequence boundaries and maximum flooding surfaces.

On the three foothills mud log profiles, the presence of maximum flooding surfaces seems to mark a transition from overlying isotopically more negative gases (immature gases?) toward isotopically more positive underlying gases (more mature?). The profile for C2 and C3 especially crosses over at these flooding surfaces and within the thin transition zone between the seal (shales and/or coals) above, and the corresponding reservoir, below.

In general, reworking of underlying sands by ravinement or transgressive erosion may produce transgressive sands of good reservoir quality. The uppermost deposits of the transgressive sequence tend to become shaly with good sealing properties. On Pembina, Gilby, and Ferrier mudlog profiles, the carbon isotope signature associated with this kind of sequence shows a quite rapidly increase from the ravinement surface below, to the maximum flooding surface above (an apparent maturity near the maximum flooding surface).

Widely recognized in marine succession is the cleaning-up well log motif, where the shale content decreases upwards, whereas primary porosity and bed thickness may increase upwards. Within the prograding units (prograding shoreface successions) below the ravinement surfaces, vertical permeability barriers exist, and are most common in the lower parts of the successions. In contrast, extensive vertical permeability barriers exist throughout the overlying transgressive deposits (Cattaneo and Steel, 2003). These deposits consist of predominantly horizontally bedded sediments (mostly shales and thin sandstone beds) deposited in an offshore setting (see lithologs from Figures 2-10 to 2-34, Chapter Two). The shale beds generally act as local permeability barriers. They could be partially or totally effective as barriers to fluid migration, depending on the nature of depositional processes (the existence or not of the intercalated sandstone beds, as a result of storm events).

Depending on the nature of stratal architecture, the ravinement surfaces could serve as partially effective hydrodynamic isolation, influencing the carbon isotope ratio trends in mudgas profiles by inflecting them towards isotopically more negative values.
In short, every key bounding surface contrasts permeability and porosity between overlying and underlying rock units due to facies and grain size changes. Figures 3-11 to 3-14 show several examples where core porosity and permeability values change across

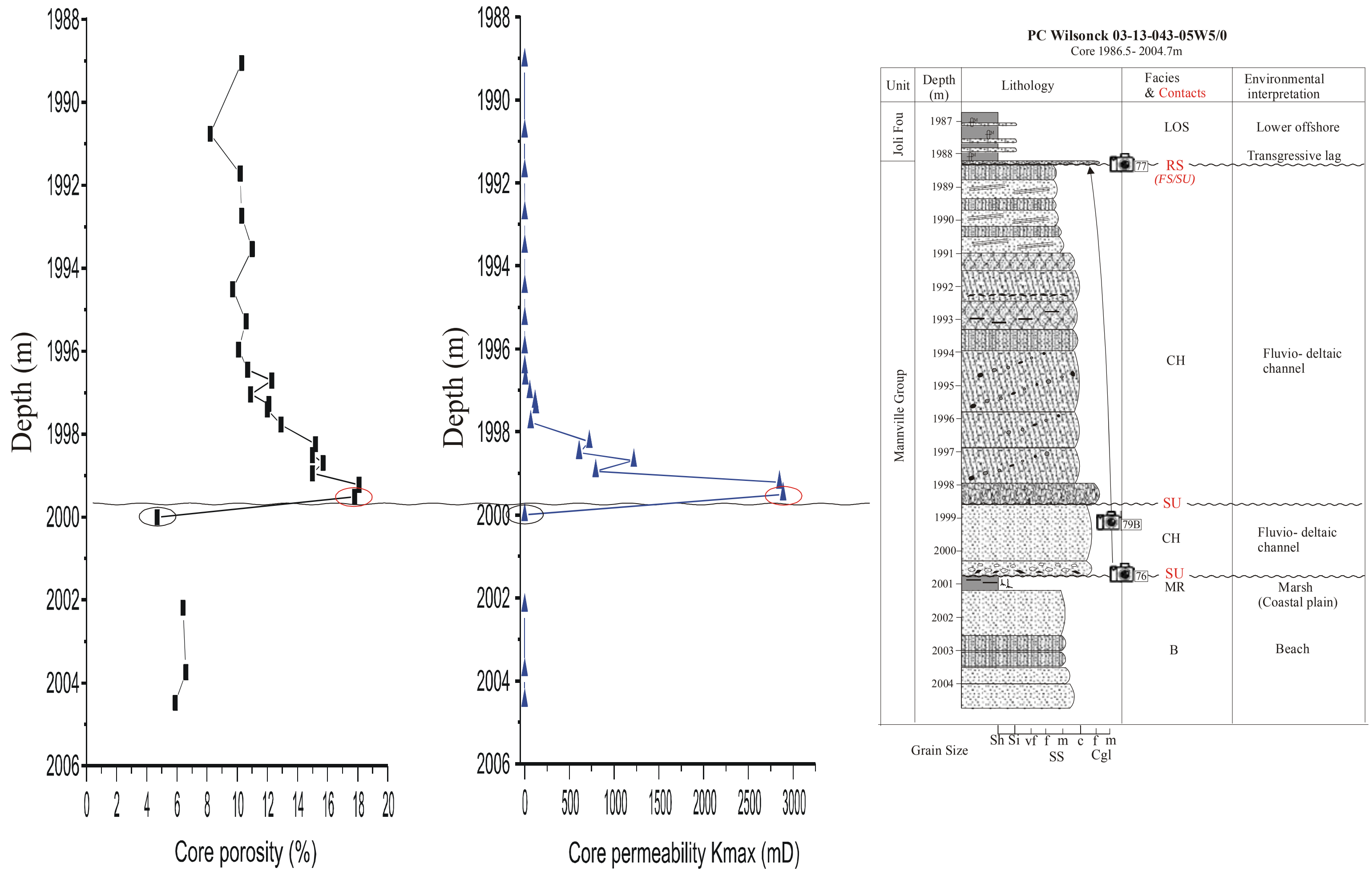

Figure 3-11 Litholog for the 03-13-43-5W5 core, annotated with main contacts and facies interpretation. Core porosity and permeability data is also shown, as reported in the core analysis report from IHS Energy public database. Legend for the litholog is given in Figure 2-1.

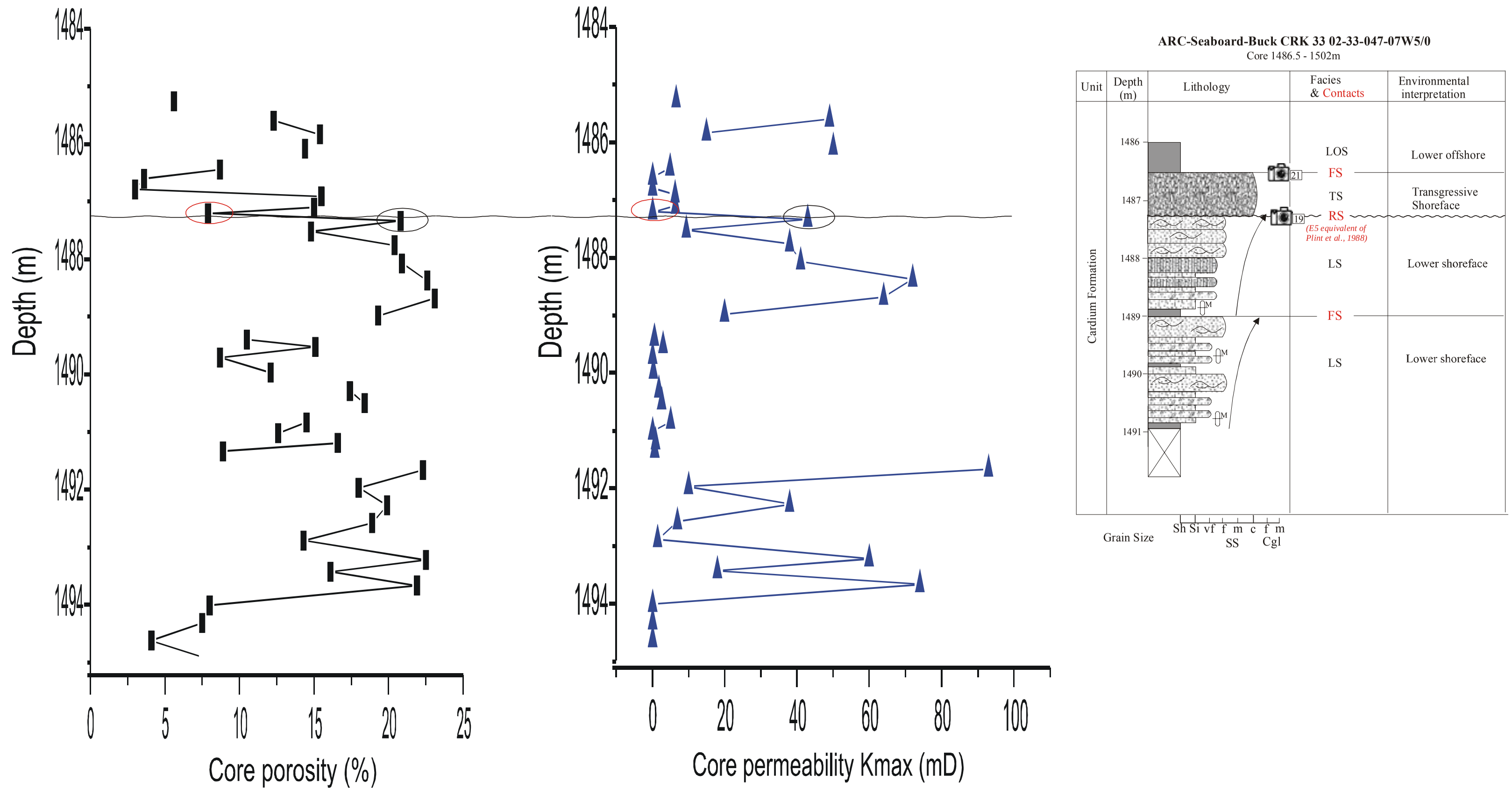

Figure 3-12 Litholog for the 02-33-47-7W5 core, annotated with main contacts and facies interpretation. Core porosity and permeability data is also shown, as reported in the core analysis report from IHS Energy public database. Legend for the litholog is given in Figure 2-1.

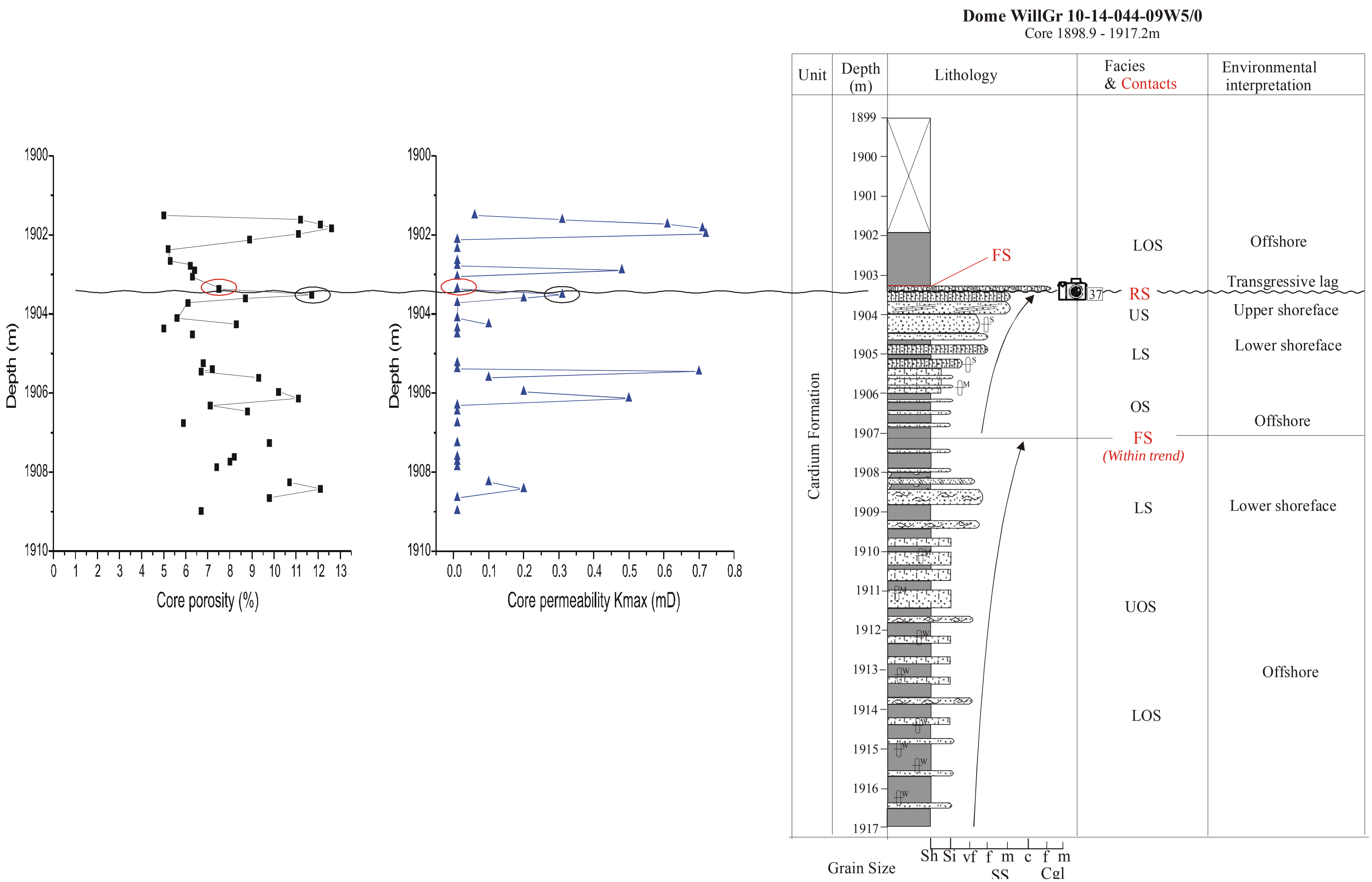

Figure 3-13 Litholog for the 10-14-44-9W5 core, annotated with main contacts and facies interpretation. Core porosity and permeability data is also shown, as reported in the core analysis report from IHS Energy public database. Legend for the litholog is given in Figure 2-1.

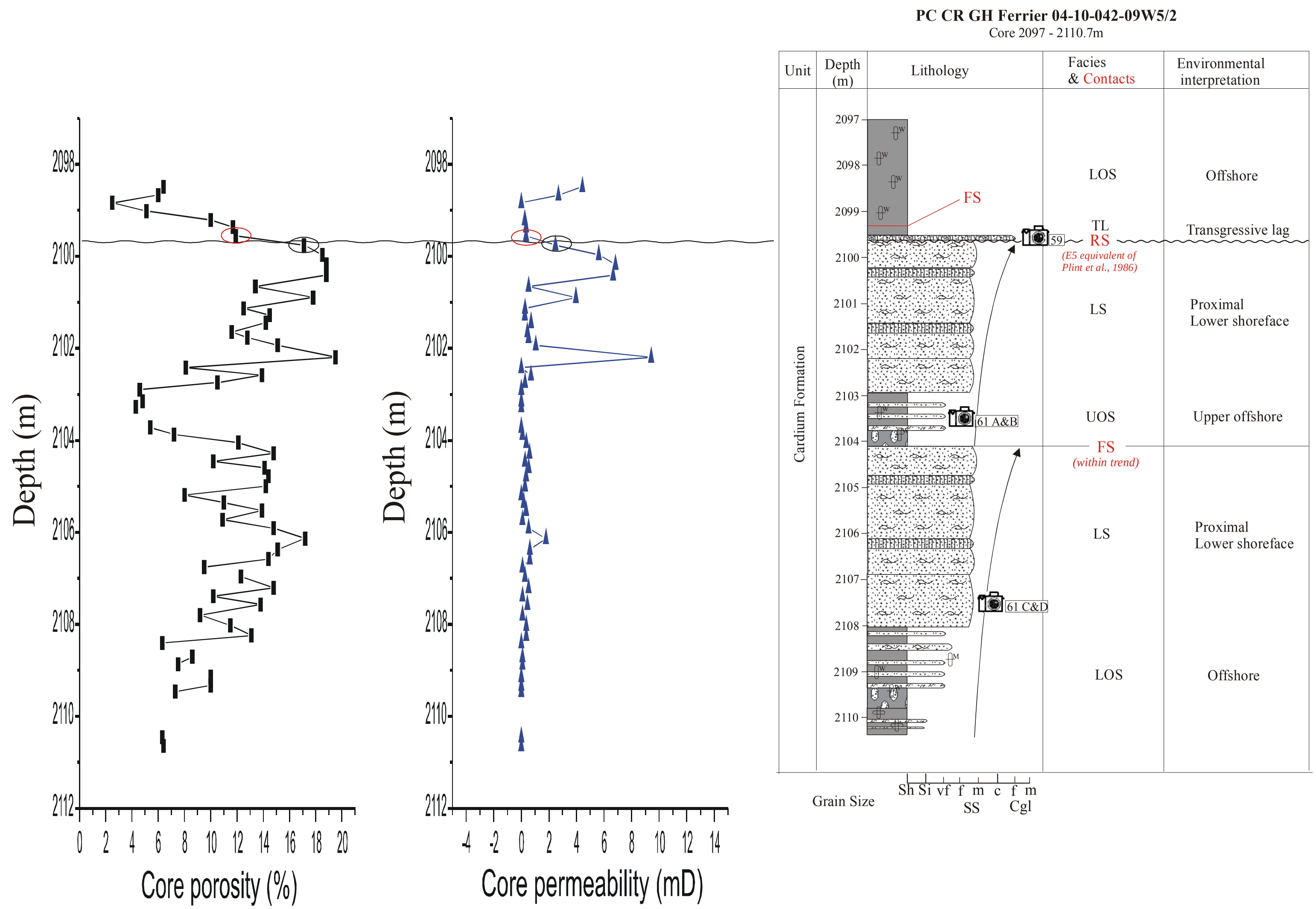

Figure 3-14 Litholog for the 04-10-42-9W5 core, annotated with main contacts and facies interpretation. Core porosity and permeability data is also shown, as reported in the core analysis report from IHS Energy public database. Legend for the litholog is given in Figure 2-1.

key stratigraphic surfaces. The four examples relate to control cores previously described in the area (see Chapter Two).

The regional stratigraphic surfaces identified in the Foothills study area, as well as some relevant depositional facies within the foreland basin fill of the west-central Alberta, and their corresponding carbon isotope signatures are presented in Table 3-2.

Ethane $\delta^{13}C$ values of gases from the Cardium Formation in the Gilby mud gas profile indicate lower (less mature) than the ethane $\delta^{13}C$ values of Belly River mud gases (Figure 3-15). Using the above argument, Tilley et al. (2001) suggested that early more mature gas migrated out of the Cardium and was replaced by later less mature gas during uplift. Gases in the Belly River Formation may be a mixture of (a) less mature gas migrated upwards from the Cardium or other more local, immature sources and (b) older, more mature gases preserved in less permeable Belly River units. This aspect will be further discussed in the following chapters, and especially the summary chapter.

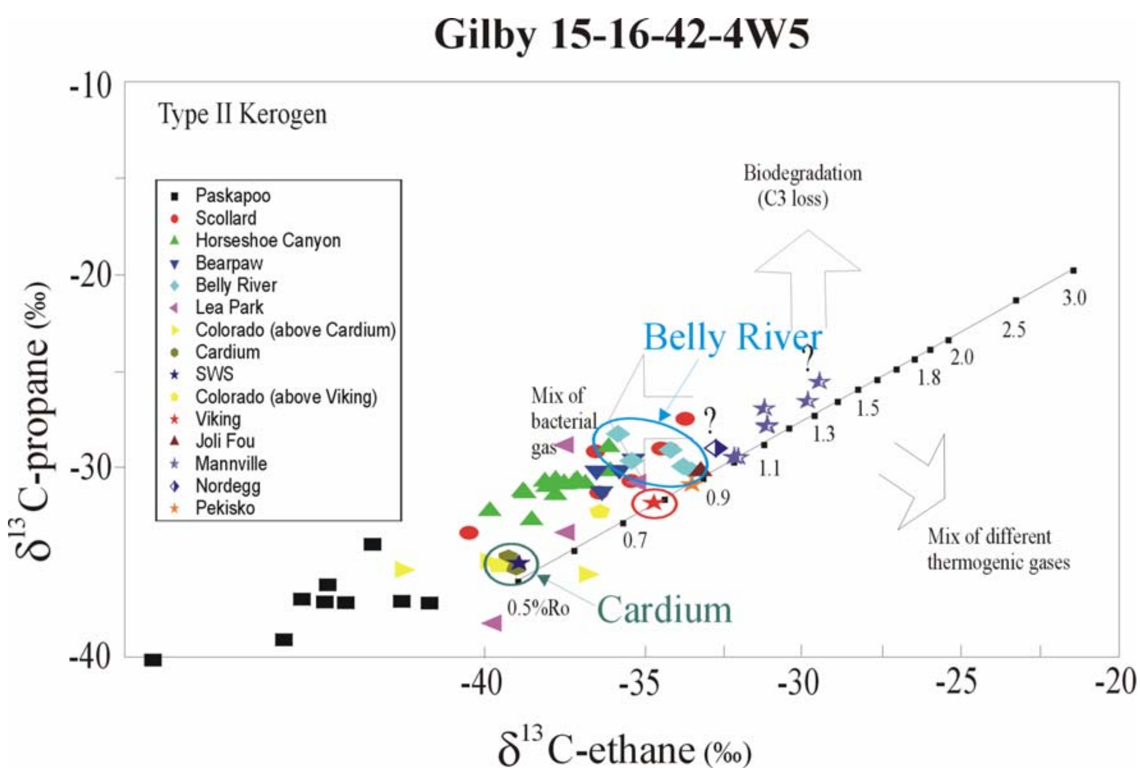

Figure 3-15 Stable carbon isotope ratios for co-genetic ethane and propane in a natural gas. (Gas maturity line after Faber, 1987; Whiticar, 1990.)

Table 3-2 Carbon isotope signatures of key stratigraphic surfaces and depositional facies within the foreland basin fill of the west-central Alberta. Note that the isotope trends in the section are described from top to bottom.

Carbon isotope ratios						
SURFACES	**1. Subaerial unconformities (SU)**	*Paskapoo Fm. /Scollard Fm. unconformity*	Isotope ratio increase downward: -49.05 to –47.15 (Pembina), -45.07 to –44.85 (Ferrier) and decrease: -56.91 to –58.06 (Gilby)	Transition towards more positive values: -37.18 to –36.12 (Ferrier), -43.56 to –40.51 (Gilby), -40.18 to –37.87 (Pembina).	Marks transition towards more positive values (-33 to –31.53 for Ferrier; -34.13 to –33.52 for Gilby); -34.46 to –31.43 (Pembina)	0.02
		Scollard Fm. /Edmonton Gp. unconformity	Slight inflection towards more positive values: -44.56 to -44.42 (Ferrier); -52.38 to –50.58 (Gilby); -47 to –46 (Pembina).	Transition towards more positive values: -33.7 to –32.58 (Ferrier) -36.52 to –36.10 (Gilby) -30.75 to –32.5 (Pembina)	Transition towards more negative (-25.72 to –27.25 (Pembina), and more positive (-29.25 to –29.04 (Gilby)	0.01 - 0.02
		Within Belly River Gp. unconformities	Mark transitions towards more negative values (-49.5 to -50 – Ferrier; -55 to -56 – Gilby)	Mark transition towards more positive values: >-33, -36 (base Dinosaur Park Fm.); >-34 (base Comrey Mbr.)	Mark transitions towards more positive values (except for that at the base of the Comrey Mbr., Gilby profile	0.02 – 0.04 (pre Dinosaur Park Fm.) 0.04 – 0.07 (pre Comrey Mbr.)
		Top Mannville Group unconformity	Transition towards more negative values (-48.32 to –49.02)	Marks transition towards more positive values: -33.2 to -32.14	Transition towards more positive values (-30.3 to –29.57)	0.14
		Pre-Cretaceous unconformity	-48.3 to –50.2	Marks transition towards more negative values: < -33	Transition towards more negative values: < -30	0.18
	2. Maximum flooding surface (MFS)	*Within Bearpaw*	- Inflection towards more negative values (Ferrier and Pembina)	- Inflection towards more positive values: -31 (Ferrier) - Transition towards more negative values	Transition towards more positive values (Pembina, Ferrier, Gilby)	0.02 - 0.04 (within Bearpaw Fm.) 0.10 - 0.18 (FWS) 0.16 (SWS, Gilby)
		FWS	- Inflection towards more positive values (- 45, Ferrier; and -57, Gilby) - Isotope ratio decrease towards surface: -53 to -45 (Ferrier); -59 to -57 (Gilby)	- Inflection towards more positive values: -35 (Ferrier); -39 (Gilby) - Transition towards more negative values	- Inflection towards more negative values: -39 (Gilby) - Slight decrease (Ferrier)	
		SWS	• undeterminable	• undeterminable	• undeterminable	
		Associated with BFS	• Inflection towards more positive values (Gilby)	- Inflection towards more positive values: -37 (Gilby) - Transition towards more negative values	- Transition towards more positive values	

Table 3-2 Continued

Carbon isotope ratios						
SURFACES	**3. Ravinement surfaces (RS)**	*Top Belly River*	• Inflection towards more positive values (Pembina)	Slight inflection towards more negative values (-33 to –34) m.; -37 to -39: within FWS	Transition towards more negative values	Inflection towards greater values (0.14 – 0.2)
		"Milk River shoulder"	Slight inflection towards more positive values (Ferrier)	Slight inflection towards more negative values: -34 (Ferrier)	Transition towards more positive values (-29 to –30, Ferrier)	
		Top "Cardium Sandstone"	Isotope ratio increase towards surface	Slight inflection towards more negative values: -39 (Gilby)	-35	
		Within Lower Colorado shales	Isotope ratio increase towards surface	Transition towards more negative values: (-38 to –40)	Transition towards more negative values (-35 to – 36, Gilby)	
		BFS	Isotope ratio increase towards surface	Slight inflection towards more negative values: -37 (Gilby)	Transition towards more positive values (-35 to –33, Gilby)	
	4. Maximum regressive surfaces (MRS)	*Top "Viking Sandstone"*	• Isotope ratio increase towards surface	Isotope ratio increase towards surface	Transition towards more positive values (Gilby)	
		Top Basal Belly River	• Transition towards more positive values: -53 (Ferrier)	Inflection towards more positive values: -33.5	No change (Ferrier)	0.08 – 0.10 (top Basal Belly River) 0.06 – 0.14 (Alderson Mbr.)
		Alderson Member	• Transition towards more positive values: -51 (Ferrier), -54 (Gilby)	• Inflection towards more positive values: (-27, Ferrier; -35, Gilby)	Transition towards more positive values: Gilby	
		Upper Colorado shales	• Transition towards more positive values	• Inflection towards more negative (?) values: within "Upper Colorado shales", Gilby Transition towards more positive (?) values: "Upper Colorado shales", Gilby	Undeterminable	

Table 3-2 Continued

Carbon isotope ratios						
FACIES	**1. Sandstone bodies**	*Fluvial sandstones*	• Decrease with depth: basal Paskapoo sandstone • Increase with depth: basal Scollard sandstone, Upper Scollard • Overall increase, with small exceptions: Belly River Gp.	• Increase followed by decrease: basal Paskapoo sandstone (both profiles) • Increase: -34 to -33 (Ferrier), and -37.5 to -37 (Gilby) - basal Scollard sandstone • Decrease: Belly River Gp. (Ferrier) • Increase: -35.5 to -34, Comrey sandstone (Gilby)	• Increase with depth: Paskapoo sandstones, Scollard sandstones, basal Dinosaur Park sandstone (only C3, Ferrier profile), Comrey sandstone (Gilby) • Decrease with depth: lower part of the Belly River sandstones (Ferrier)	• Strong inflection toward greater values: 0.16 (basal Dinosaur Park sandstone, Ferrier), 0.12 (Foremost Fm. sandstone sheet, Ferrier) • 0.04: Foremost Fm. sandstone sheet, Gilby
		Shoreface sandstones	• Decrease with depth (-53 to -54, Basal Belly River) Increase with depth: -49 to -47, Glauconitic Sandstone (Gilby)	~ -33 to -34	Decrease with depth (-27 to -28 for C3, Ferrier)	Greater values than over- and underlying deposits (0.07 - 0.12)
	2. Coal seams		• Inflection towards <u>more positive</u> values: -42 (Ardley coal, Ferrier); -52.13 to –50.44 (Ardley coal, Gilby); -47 (Ardley coal, Pembina); -51 to -53 (McKay zone coals). • Inflections towards <u>more negative</u> values: -44.2 to –45.25 (Pembina); -43.5 to –44.17 (Ferrier)	-33: Ardley coals, Lethbridge Zone coals –34.18 to -33.68 Inflection towards <u>more positive</u> values: -32.62 to -31.09 (Pembina); -34.18 to –33.68 (Gilby); -32.12 to –32.02 (Ferrier)	Inflection towards <u>more positive</u> values: -29.15 to –27.55 (Gilby); -28.45 to –27.33 (Pembina); -28.93 to –28.84 (Ferrier). Inflections towards <u>more negative</u> (?) values: Carbon-Thompson coal zone (Ferrier and Gilby); coal zone above Glauconitic Sandstone (Gilby profile)	0 – 0.02: Ardley coal zone 0 – 0.04: Carbon-Thompson coal zone 0.10: Lethbridge coals (Ferrier profile) 0.14 – 0.16: Upper Mannville coals (Gilby profile)

Significant portions of the profiles (e.g. top Edmonton Group – base Belly River Group) show a puzzling trend of decreasing C1 values (apparent decreasing maturity) with depth. C2 values for this interval suggest very slight increasing maturity with depth. Low C1 values are commonly associated with bacterial activity at shallow depths (e.g. top part of these profiles), but the consistency and gradational nature of the C1 trends here do not seem consistent with this mechanism alone. The anomalous isotope trends may be due, according with Tilley et al. (2001), to a combination of the effects of the burial history of this part of the Western Canada Sedimentary Basin and the fact that the gases comprising the profile have been extracted from a variety of lithologies including sands and conglomerates, shales and coals. Maximum burial occurred during the early Eocene when temperatures in the Basal Belly River in this area reached 75-90^{0}C (Nurkowski, 1984; Hacquebard, 1977). Uplift and erosion began at about 48 Ma (Kalkreuth and McMechan, 1984) and resulted in removal of about 1700 m in this area (Issler et al., 1999). It is possible that the analyzed gases reflect a complicated suite and mixture of (a) gases that evolved at higher temperatures during the time of maximum burial and (b) gases that evolved at lower temperatures during the more recent period of uplift and erosion (Tilley et al., 2001).

3.3. Lloydminster region

3.3.1. Results

In each of the carbon isotopic mud gas depth profiles in the Lloydminster region, the Colorado/Mannville stratigraphic boundary is mirrored by a distinct change in isotopic signature. Mannville Group gases are enriched in ^{13}C relative to the Colorado gases (in some cases as much as 20‰), and can be easily identified from $\delta^{13}C_{C2}$ alone. The isotopic partitioning between C_{2+} components (i.e. ($\delta^{13}C_{C3}$ -$\delta^{13}C_{C2}$ or $\delta^{13}C_{nC4}$-$\delta^{13}C_{C3}$) shows a definite depth trend. Isotopic separations gradually increase from ~2-5‰ at the Mannville/Colorado boundary, to differences of 10‰ or more in very shallow samples.

These isotopic signatures reflect the different genetic histories of the Colorado and Mannville Group gas deposits (see discussion in Chapter four).

3.3.1.1. Regional sequence stratigraphic surfaces and their relationship with the stable carbon isotopic trends

The regional stratigraphic surfaces identified in the Lloydminster study area and their corresponding carbon isotope signatures are presented in Tables 3-3 to 3-8 (where the red arrows indicate an increase for the isotopic values, and the blue arrows a decrease, respectively; Petrovera A9-30-47-22W3 and Petrovera Golden Lake 112/01-04-48-22W3 are not included in the discussion since they represent hot well bores in the heavily steamed Golden Lake area). The carbon isotope ratio variations for C_1-C_4 with stratigraphic position are shown in Figures 3-16 through 3-22. Major shifts in geochemical signature appear at the boundary between Mannville Group and Colorado Group (see Table 3-3), and are also related to the presence of some horizons with sealing properties (high shale content and/or low porosity).

One of the purposes integrating mudgas geochemistry with stratigraphy is to try recognizing compartments within which reservoirs have similar properties, including gas content, and gas composition. The boundary between Mannville and Colorado groups is clearly one of the boundaries of such compartments (Figures 3-16 to 3-22). There is an obvious decrease in the carbon isotope composition above the top of the Mannville Group (see Table 3-3), with some exceptions, suggesting an unconformable relationship between the two major groups (although in some places Joli Fou aquitard may be weaker than in others: i.e. Petrovera 10-17-47-27W3, allowing Mannville gases to migrate vertically into the Colorado shales; see discussion in Chapter Four). The same relationship between the isotopic composition of the alkane gases within Colorado and Mannville groups has been reported by Rowe (1998), Rowe and Muehlenbachs (1999b), and Szatkowski et al. (2002).

Table 3-3 Carbon isotope signature along Mannville/Colorado boundary in the Lloydminster region. Transitions are from Colorado to Mannville.

		Carbon isotope ratio				
		δ^{13}C1	**δ^{13}C2**	**δ^{13}C3**	**δ^{13}iC4**	**δ^{13}nC4**
Well	Husky C3 -30-47-4W4	-62.16/-61.98 ↑	-38.62/-35.84 ↑	-33.04/-35.91 ↓	26.82/-30.75 ↓	-29.43/-36.53 ↓
	Husky A9 -15-51-23W3	-64.85/-66.4 ↓	-40.97/-45.55 ↓	?/-38.58	?/-33.43	-
	Petrovera 10 -17-47-27W3	-62.6/-62.38 ↑	-34.03/-34.03	-29.2/-29.09 ↑	-28.41/-28.42	-28.88/-30.36 ↓
	Lindbergh 13 -9-56-6W4	-59.32/-54.33 ↑	-38.38/-27.82 ↑	-34.82/-25.79 ↑	-26.96/-25.7 ↑	?/-27.69
	Petrovera 1D-25-55-5W4	-58.14/-53.26 ↑	-31.37/-28.59 ↑	-30.78/-25.4 ↑	?/-27.29	-30.51/-32.6 ↓

↑ increase in isotopic ratio from Colorado to Mannville; ↓ decrease in isotopic ratio from Colorado to Mannville

Table 3-4 Carbon isotope signature along regional sequence stratigraphic surfaces for Husky C3-30-47-4W4 profile. The transition is recorded downward.

	Well	**Husky C3 -30-47-4W4**				
Surfaces	**Carbon isotope ratio**	**δ^{13}C1**	**δ^{13}C2**	**δ^{13}C3**	**δ^{13}iC4**	**δ^{13}nC4**
Maximum flooding surfaces	FWS	-65.58/ -65.12 ↑	-52.23/-52.73 Slight decrease	-43.41/-41.83 ↑	?/-34.48	-39.34/-35.65 ↑
	SWS	-64.46/-63.17 ↑	-49.02/-47.7 ↑	-42.26/-41.24 ↑	-34.24/-33.99 ↑	-36.4/-38.03 ↓
	Top Cummings	-58.01/-**57.8** ↑	-31.82/-**30.6** ↑	-22.6/-**22.95** ↓	-25.14/-**27.76** ↓	-24.25/-**24.71** ↓
Ravinement surfaces	Base SWS	-62.58/-64.26 ↓	-46.36/-46.81 ↓	-40.11/-40.58 ↓	-33.71/-30.01 ↑	-36.74/-36.35 Slight increase
	BFS	-62.81/-62.89 Slight decrease	-46.35/-44.82 ↑	-38.6/-40.95 ↓	-32.29/-32.12 Slight increase	-37.46/-36.11 ↑
	Top Viking	-62.32/-64.01 ↓	-44.71/-43.78 ↑	-36.3/-29.42 ↑	-31.36/-27.66 ↑	-

↑ increase in isotopic value; ↓ decrease in isotopic value

Table 3-5 Carbon isotope signature along regional sequence stratigraphic surfaces for Husky A9-15-51-23W3 profile. The transition is recorded downward.

	Well	Husky A9 -15-51-23W3				
Surfaces	**Carbon isotope ratio**	**C1**	**C2**	**C3**	**iC4**	**nC4**
Maximum flooding surfaces	FWS	-71.36/-69.46 ↑	-51.49/-50.83 ↑	-41.87/-42.32 ↓	-31.79/-34.65 ↓	?/-37.34
	SWS	-67.62/-68.83 ↓	-49.85/-49.12 Slight increase	-42.15/-41.64 ↑	-34.69/-35.11 ↓	-36.36/-37.19 ↓
	Top Cummings	No available data				
Ravinement surfaces	Base SWS	-68.15/-68.83 Slight decrease	-48.8/-49.12 ↓	-40.91/-41.64 ↓	-33.76/-35.11 ↓	-36.22/-37.19 ↓
	BFS	-67.9/-67.66 Slight increase	-45.2/-47.4 ↓	-26.52/-33.88 ↓	-34.13/-34.1 ↑	-34.95/?
	Top Viking	-65.89/-65.1 Slight increase	-44.51/-42.41 ↑	-37.27/-35.87 ↑	-32.32/-31.15 ↑	-36.9/?

↑ increase in isotopic value; ↓ decrease in isotopic value

Table 3-6 Carbon isotope signature along regional sequence stratigraphic surfaces for Petrovera 10-17-47-27W3 profile. The transition is recorded downward.

	Well	**Petrovera 10 -17-47-27W3**				
Surfaces	**Carbon isotope ratio**	**δ^{13}C1**	**δ^{13}C2**	**δ^{13}C3**	**δ^{13}iC4**	**δ^{13}nC4**
Maximum flooding surfaces	FWS	-60.94/-62.74 ↓	-46.07/-43.56 ↑	-37.6/-41.09 ↓	?/-36.72	?/-39/21
	SWS	-62.49/-62.96 Slight decrease	-41.21/-40.65 ↑	-39.16/-38.52 ↑	-34.51/-34.99 Slight decrease	-37.33/-36.13 ↑
	Top Cummings	-59.59/-61.5 ↓	-29.5/-30.29 ↓	-20.72/?	-27.26/-27.04	-27.41/-27.65
Ravinement surfaces	Base SWS	-62.95/-62.18 Slight increase	-39.82/-40.07 ↓	-36.88/-37.01 ↓	-33.68/-33.68 No change	-37.13/-36.38 ↑
	BFS	-61.93/-61.89 Slight increase	-39.61/-38.25 ↑	-35.19/-33.48 ↑	-32.72/-31.43 ↑	-35.67/-33.98 ↑
	Top Viking	-59.81/-61.35 ↓	-36.29/-34.59 ↑	-30.78/-30.73 Slight increase	-29.53/-31.75 ↓	-30.66/-32.93 ↓

↑ increase in isotopic value; ↓ decrease in isotopic value

Table 3-7 Carbon isotope signature along regional sequence stratigraphic surfaces for Lindbergh 13-9-56-6W4 profile. The transition is recorded downward.

	Well	**Lindbergh 13 -9-56-6W4**				
Surfaces	**Carbon isotope ratio**	**δ^{13}C1**	**δ^{13}C2**	**δ^{13}C3**	**δ^{13}iC4**	**δ^{13}nC4**
Maximum flooding surfaces	FWS	-70.5/-68.15 ↑	-53.12/-52.83 ↑	-42.49/-42.68 ↓	-32.26/-33.22 ↓	-36.42/-37.75 ↓
	SWS	-66.78/-65.97 ↑	-50.33/-50.39 Slight decrease	-43.3/-42.95 ↑	-33.8/-33.73 Slight increase	-32.45/-35.9 ↓
	Top Cummings	-57.04/-56.39 ↑	-31.52/-32.65 ↓	-30.15/-29.11 ↑	-29.61/-27.89 ↑	-28.18/-25.83 ↑
Ravinement surfaces	Base SWS	-65.95/-65.24 Slight increase	-50.07/-50.49 Slight decrease	-42.62/-43.21 ↓	-34.05/-34.76 Slight decrease	-33.29/?
	BFS	-66.86/-65.04 ↑	-50.14/-49.52 ↑	-42.36/-42.58 Slight decrease	-33.86/-34 ↓	-
	Top Viking	-63.83/-62.37 ↑	-46.91/-45.22 ↑	-41.2/-39.67 ↑	-34.23/-29.76 ↑	-34.31/-33.74 ↑

↑ increase in isotopic value; ↓ decrease in isotopic value

Table 3-8 Carbon isotope signature along regional sequence stratigraphic surfaces for Petrovera 1D-25-55-5W4 profile. The transition is recorded downward.

	Well	**Petrovera 1D-25-55-5W4**				
Surfaces	**Carbon isotope ratio**	**δ^{13}C1**	**δ^{13}C2**	**δ^{13}C3**	**δ^{13}iC4**	**δ^{13}nC4**
Maximum flooding surfaces	FWS	-68.74/-67.11 ↑	-53.13/-53.05 Slight increase	-41.43/-43 ↓	-32.32/-35.47 ↓	-43.28/-38.42 ↑
	SWS	-66.29/-65.97 ↑	-51.78/-50.1 ↑	-43.58/-44.19 ↓	-35.76/-34.65 ↑	-38.51/-37.35 ↑
	Top Cummings	-55.58/-57.84 ↓	-30.72/-36.81 ↓	-21.68/-21.24 Slight increase	-21.47/-21.86 Slight decrease	-27.54/-28.72 ↓
Ravinement surfaces	Base SWS	Insufficient data				
	BFS	-63.90/-63.83 Slight increase	-49.52/-48.95 ↑	-42.23/-41.55 ↑	-34.5/-33.9 ↑	-36.63/-34.54 ↑
	Top Viking	-62.78/-60.27 ↑	-44.38/-39.18 ↑	-38.23/-34.66 ↑	-33.41/-32.16 ↑	-36.01/-35.22 ↑

↑ increase in isotopic value; ↓ decrease in isotopic value

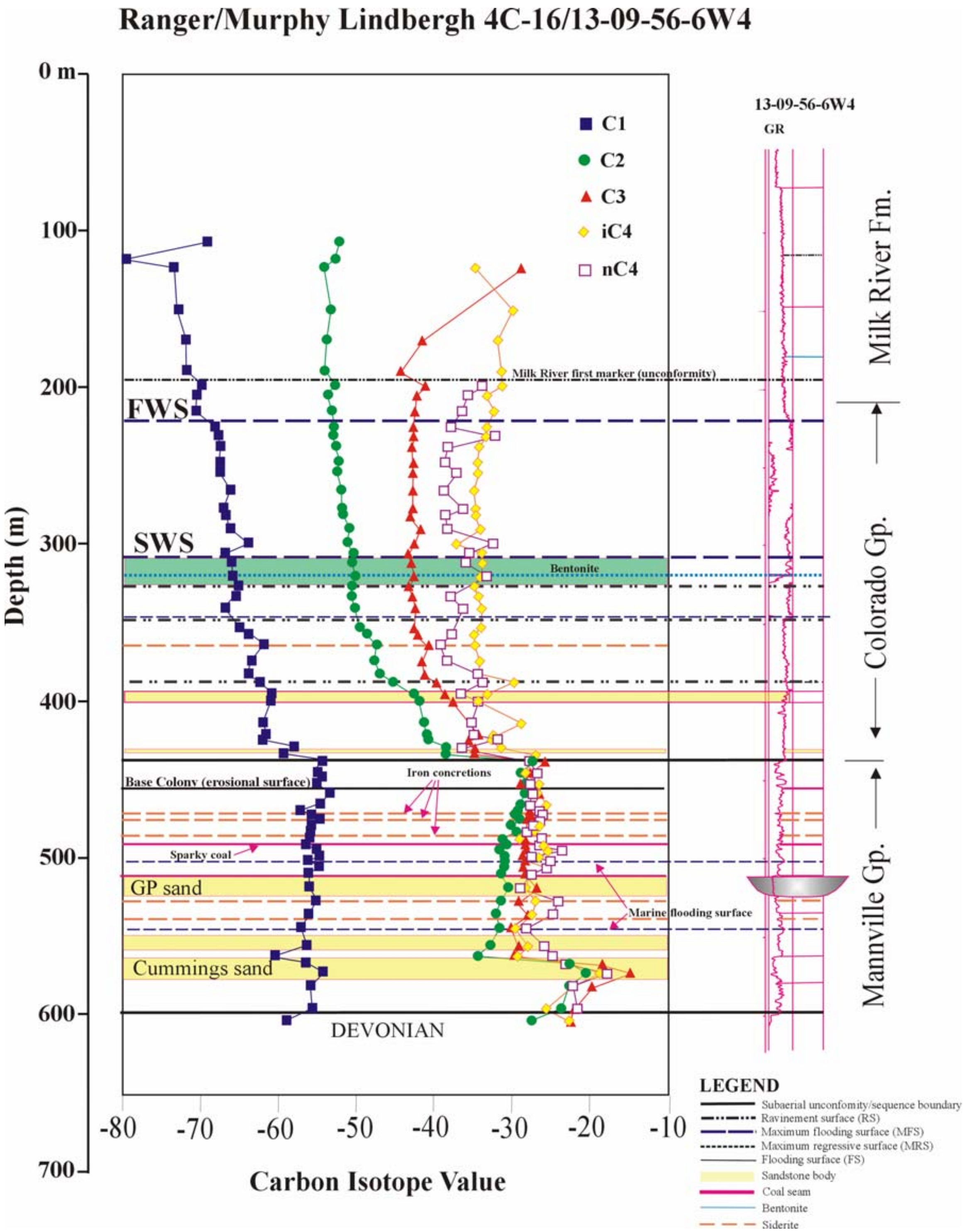

Figure 3-16 Carbon isotopic composition of mudgases from Lindbergh 00/13-09-56-6W4 in relationship with stratigraphy.

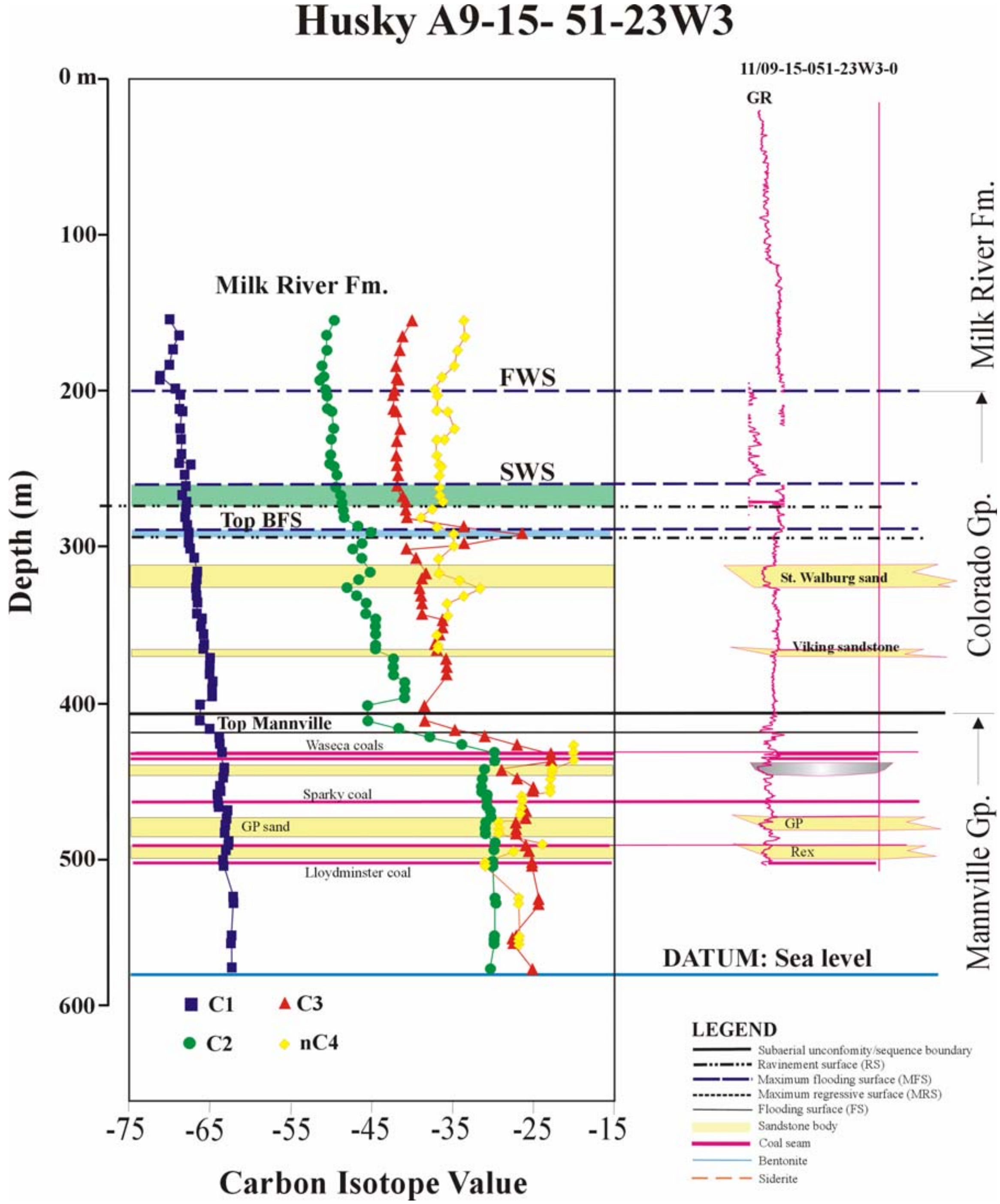

Figure 3-17 Carbon isotopic composition of mudgases from Husky A9-15-51-23W3 in relationship with stratigraphy.

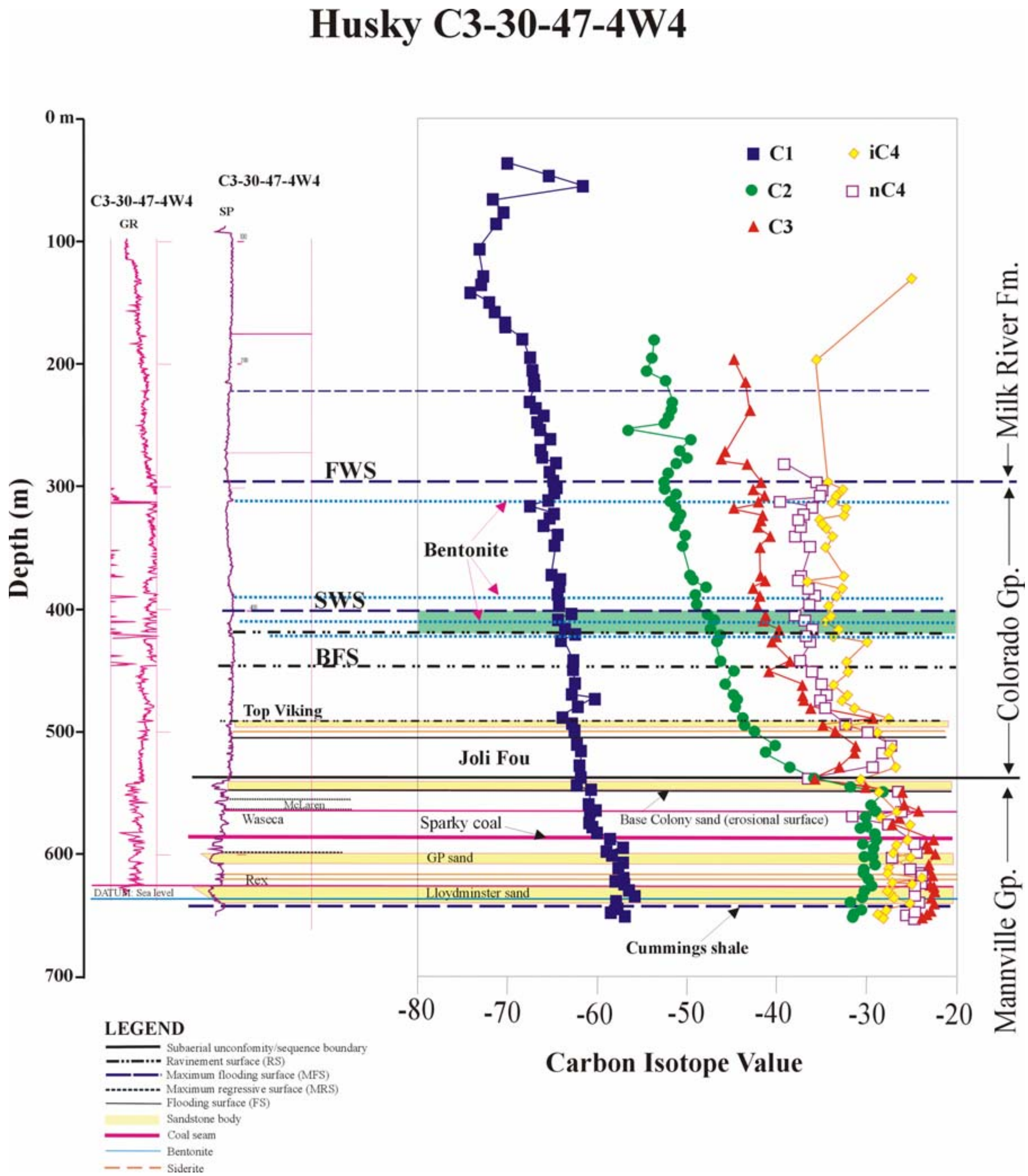

Figure 3-18 Carbon isotopic composition of mudgases from Husky C3-30--47-4W4 in relationship with stratigraphy

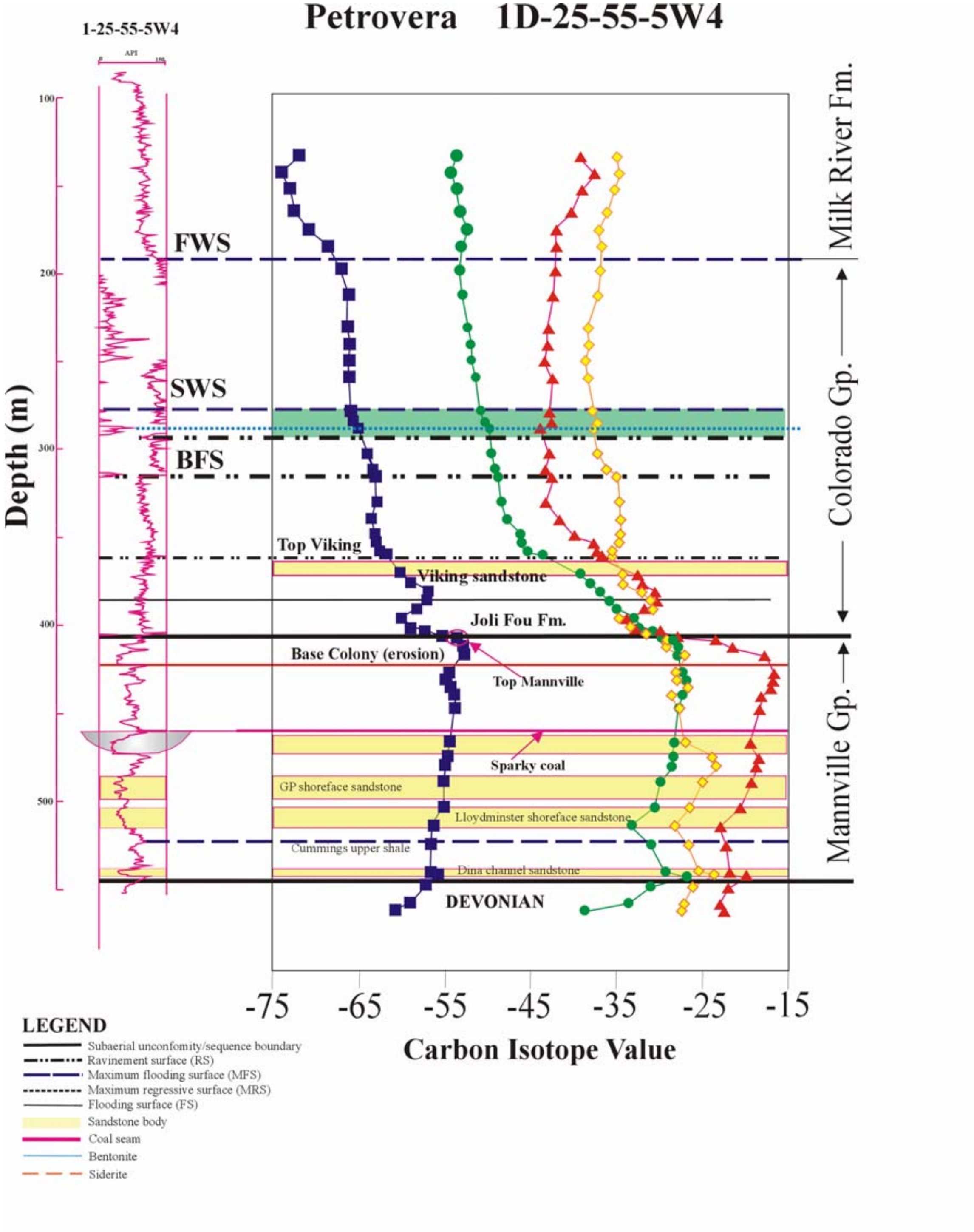

Figure 3-19 Carbon isotopic composition of mudgases from Petrovera 1D-25-55-5W4 in relationship with stratigraphy.

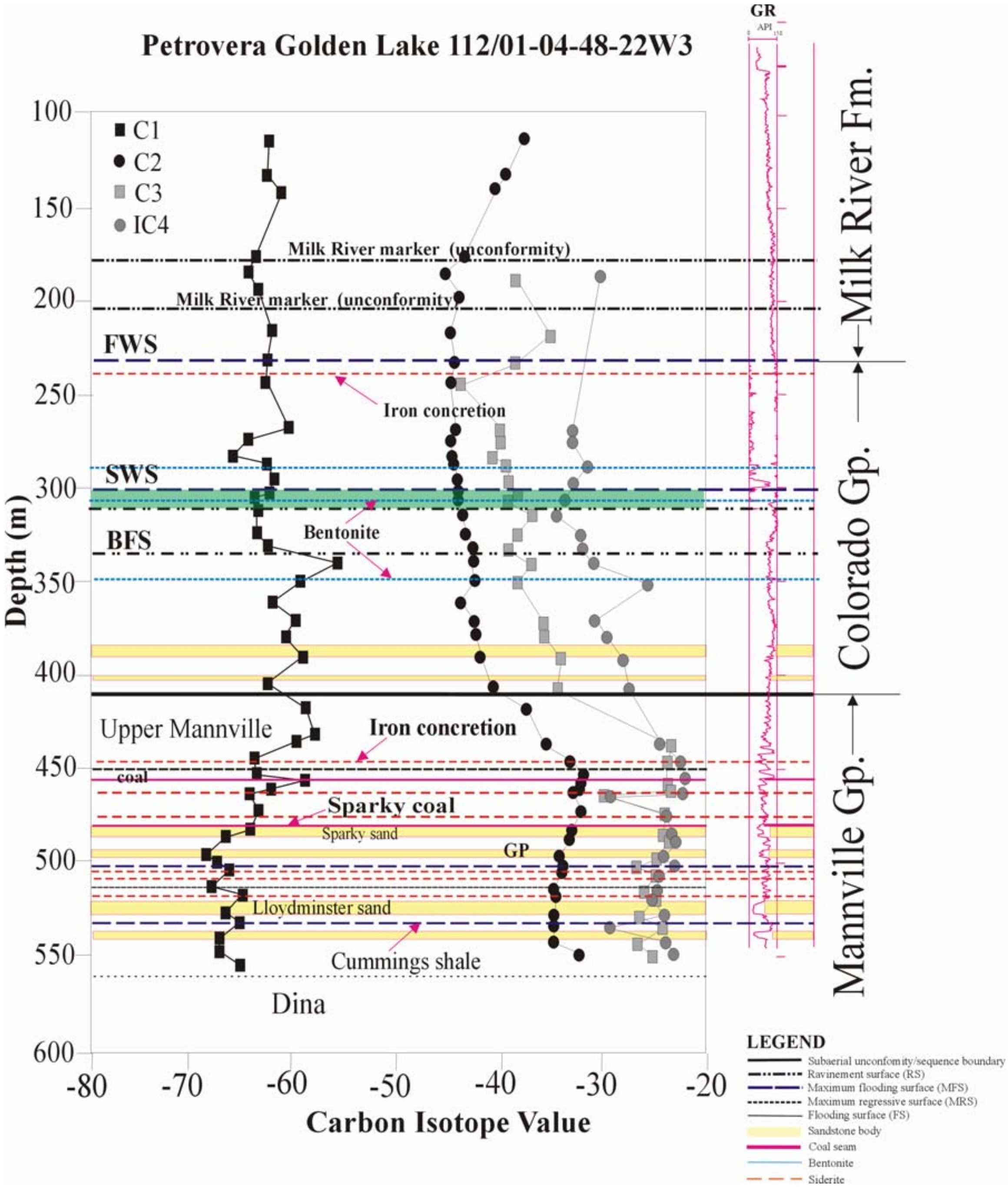

Figure 3-20 Carbon isotopic composition of mudgases from Petrovera 112/01-04-48-22W3 in relationship with stratigraphy.

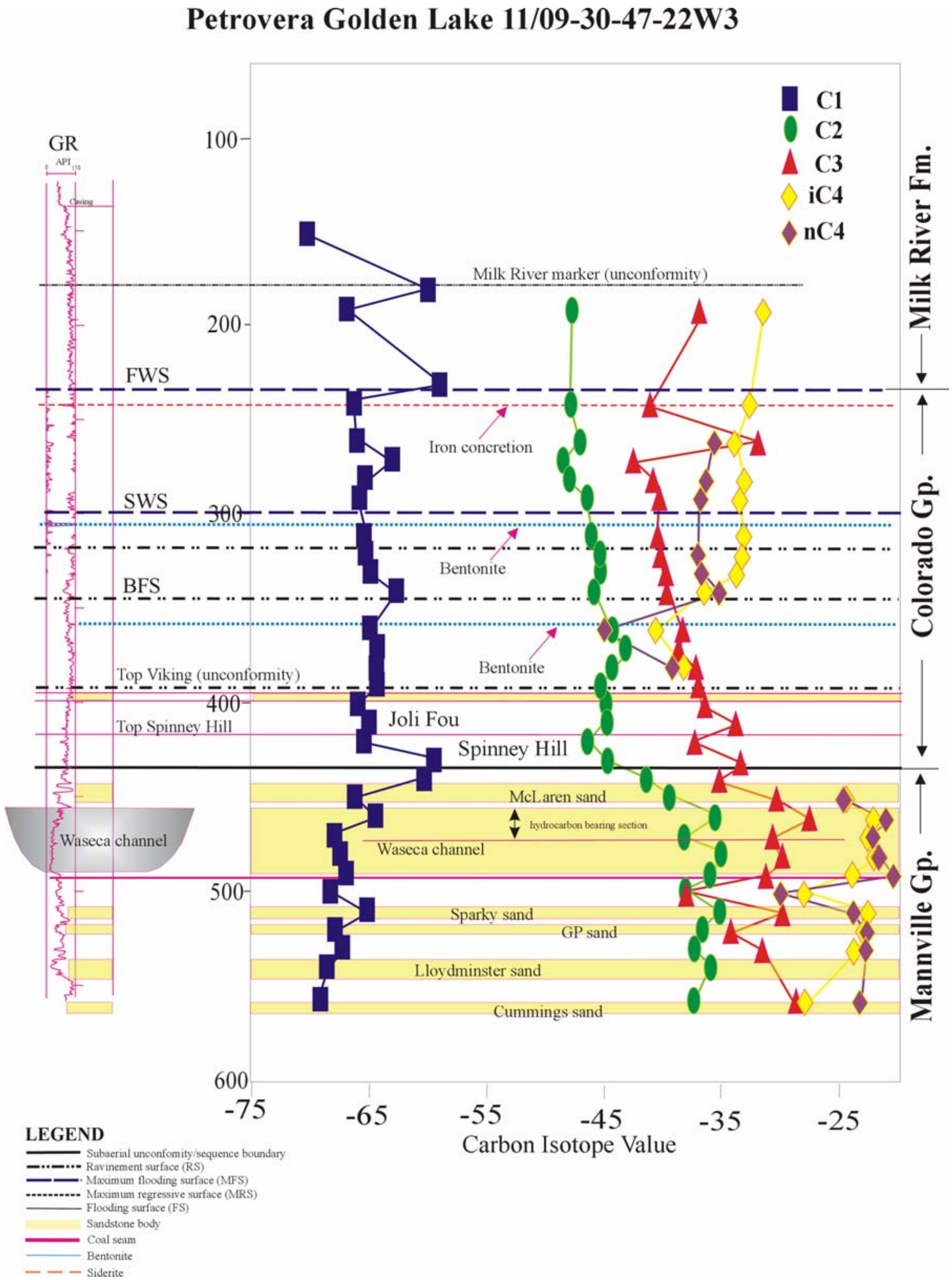

Figure 3-21 Carbon isotopic composition of mudgases from Petrovera Golden Lake 11/09-30-47-22W3 in relationship with stratigraphy.

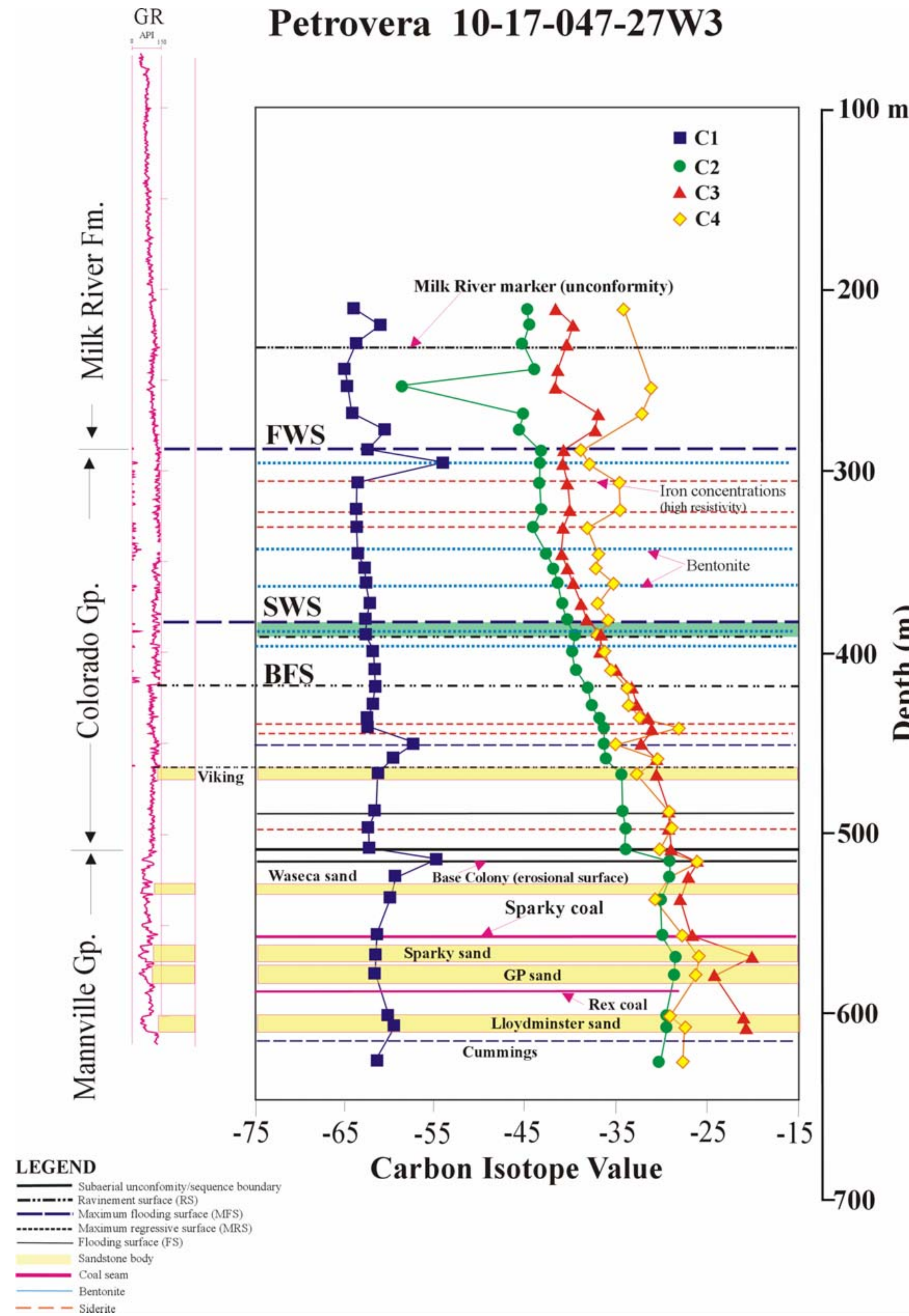

Figure 3-22 Carbon isotopic composition of mudgases from Petrovera 10-17-47-27W3 in relationship with stratigraphy

Erosional truncations commonly result in flow boundaries that compartmentalize reservoirs. Difference in facies above or below erosional truncations (unconformities recognized as truncations of underlying sedimentary intervals) can form flow unit boundaries reflected in permeability differences. A good example of such boundary is the base of the Colony member at Petrovera 10-17-47-4W4 (Figure 3-22) and at Lindbergh 13-9-56-6W4 (Figure 3-16), thought to be a downcutting erosional surface. Above this surface the mudgas isotopic composition is decreasing rapidly (gentle slope), meanwhile below it the trend is towards more positive values (^{13}C enrichment).

In the Foothills study region, the maximum flooding surface represented by the top of the First White Specks Formation marks a strong inflection within both the Ferrier and Gilby profiles toward more positive values of the carbon isotope ratios. In the heavy oil region, its effect seems do not be so obvious; nonetheless, the surface marks a general decrease for the methane and ethane carbon isotope ratios across the boundary (see Tables 3-4 to 3-9). On the other hand, the isotope ratio of the C_3 component above the FWS is characterized by more positive values, suggesting a microbial alteration (probably due to the presence of bacteriogenic gas within the Milk River Formation).

Bacterial alteration of Mannville gases has led to characteristic isotopic reversals between the $\delta^{13}C_{C3}$ and $\delta^{13}C_{nC4}$ values and fairly positive propane $\delta^{13}C$ values (Rowe and Muehlenbachs, 1999).

Gas moving less easier in rocks with low permeability and porosity, and ^{13}C being less mobile than ^{12}C, one should expect (at least theoretically) an enrichment in ^{13}C along/or within those shales related to maximum flooding surfaces.

The maximum flooding surface associated with the transgressional event, which marked the end of the Cummings deposition (a basin-wide shale with a distinct resistivity signature) shows an obvious inflection towards more positive values for ethane stable isotope ratio (in two of the profiles where its behaviour is more relevant: Lindbergh 13-9-56-6W4 and Husky C3-30-47-4W4). But the trends for C_1, C_3 and C_4 are opposite in the two locations: enrichment in ^{12}C for Lindbergh (Table 3-8), and enrichment in C13 for Husky C3-30-47-4W4 (Table 3-4). This could be related to different sealing properties of the shales, as it will be further related in Chapter Five.

The maximum flooding surface at the top of the Second White Specks Shale Formation (SWS) seems to form an overall regional seal that controls the long-distance migration of fluids in the subsurface, and forms a major barrier within Lloydminster sub-basin, at least within Colorado Group; as can be observed in Tables 3-4 to 3-9, this surface marks transition from overlying isotopically more negative (immature?), towards isotopically more positive (more mature?) underlying gases (as is also the case in the Foothills region). To illustrate this statement, in Figures 3-16, 3-19, 3-22 one can better observe that the zone above SWS (between SWS and FWS) displays a relatively uniform isotope value trend, whereas below SWS, there is a relatively continuous trend of increasing methane (C1)-, ethane (C2)-, and propane (C3) values, down to the top of the Mannville Group. The suggestion that SWS maximum flooding surface may act as a major isotopic boundary within the Western Canada Sedimentary Basin will be further mentioned in Chapter Nine.

Flooding surfaces formed during transgression are evidence of shoreface erosion and abrupt deepening. Erosion events can remove up to 10-20 metres of strata and downcut through previous unconformities. These transgressive lag sediments may cap a flooding surface and diagenetic alternation frequently occurs below the lag, forming permeability flow barriers.

Depending on the nature of stratal architecture, the ravinement surfaces could serve as partially effective hydrodynamic isolation, influencing the carbon isotope ratios of methane in mudgas profiles by inflecting them towards more negative values: see Husky C3-30-47-4W4: top Viking and base of the Second White Specks (SWS); Husky A9-15-51-23W3: base Second White Specks; Petrovera A9-30-47-23W3: top Viking and base Fish Scale (BFS). On the other hand, with very few exceptions (see Husky A9-15-51-23W3), the transition across this type of bounding surface is exemplified by a downward increase in the carbon isotope value for ethane and propane, contrary on what it is observed in the Foothills region, where the ravinement surfaces mark inflections towards more negative values (Table 3-2).

3.3.1.2. Lithology influence

Bentonite beds, which are composed of montmorillonitic clays derived from volcanic ash, are excellent seals for gas accumulations. On our mudlog profiles, their presence marks a change from more negative towards more positive carbon isotope values. In Figure 3-22 (Petrovera 10-17-47-27W3), beneath bentonite layers of the Upper Colorado shales, the C_1 and C_2 components show an ^{13}C enrichment; above these beds the isotopic concentrations are more negative (with some exceptions when the isotopic value for C_2 are more positive above bentonite layers; also for Husky C3-30-47-4W4, the lowermost two bentonite layers within Colorado Group, have more negative isotope values for C_1, C_2 and C_3 below them).

In order to further explain the suggestion that bentonites layers might have a fractionation effect on gas isotopes, the adsorption process on sedimentary organic matter should be considered, for both shales and coals. Their sorption capacity is a function of the total organic content (TOC), and the pore structure (Ross and Bustin, 2007). Relative to organic-rich shales and coals, organic-poor shales (bentonites) have a low sorption capacity. The low sorption capacities of shales relate to the affinity of water to their negatively charged surfaces (Chiou and Rutherford, 1997). Hydrophobic layers (e.g. bentonites) will pass methane, while hydrophilic ones will pass water more easily. Thus, molecular sizes, as well as polarity of the shale layer are critical. For example, a bentonite layer not 100% water saturated, will be able to absorb some ^{12}C hydrocarbon gases, will pass others, and the majority of the ^{13}C hydrocarbon gases will concentrate in a free state below the seal (bentonite layer), within the rock matrix.

Another trapping mechanism (seal) is the formation of early diagenetic cements as either layers or concretions, obviously the layers being more effective traps.

Interbedded bentonite and shales beds reduce permeability to gas migration. Their selective permeability effect can be more or less effective, in that manner that the isotopic values of the mudgases can be inflected or not towards more positive values across these layers.

As documented by Mathison (1988) in the Upper Mannville strata, sideritic nodules are common throughout the shales; also, sideritized silty shales are present on top of conglomerate or sand channels. Such of sealing horizons were identified on the mud log profiles as having low gamma-ray readings, low neutron-, and density porosity units and decimetre thicknesses. They are named “iron concretions” on Figures 3-16 through 3-22.

The coal seems within the Mannville Group represent a potential source of isotopically enriched organic matter. The isotopic values are obviously more positive at the coal stratigraphic levels (see Figure 3-16 – Sparky coal, Figure 3-17 – Waseca coals, Sparky coal, and the coal seam above the Rex channel; Figures 3-18 to 3-21 – Sparky coals).

Most coal beds are self-sourcing reservoirs. However, these coalbeds (reservoirs) may contain self-sourced or migrated thermogenic gas, or biogenic gas, or some mixtures of these (Rice, 1993). In cases where coal beds are self-sourcing reservoirs for thermogenic gas, migration does not occur (Rice, 1993). In other cases, however, coal beds trap (adsorb) gas migrating from other source rocks, or they may adsorb gas generated by microbes (secondary biogenic gas) at the coal cleat-water interface. Southeast of our study area (Holysh, 1989), microbes carrying waters were found to move downward into underpressured Mannville sands.

In some cases, the $\delta^{13}C$ of methane appears with depletion in the heavier ^{13}C isotope at coal stratigraphic levels. This situation could also be explained by the presence of secondary biogenic gas due to downward flow of fresh groundwaters.

After thermogenic gas charged the Mannville reservoirs, the basin was uplifted and several hundreds metres of overburden were removed (Nurkowski, 1984; Kalkreuth and McMechan, 1988). This cooling event may has caused the beds be undersaturated in place (Scott et al., 1994). If the above reasoning is valid, the following scenario is proposed: along the cropped edges of the strata, incursion of fresh water may have repressured the coal and supplied microbes that generated carbon dioxide and secondary biogenic methane (that in places resaturated the coal).

The results presented in Chapter Four and further work may enable to understand the true nature of the gases found within the Mannville sediments.

On the profile Petrovera A9-30-47-22W3 (Figure 3-21), within Waseca channel sandstone, there is an obvious increase in δ^{13} C above a limit, which defines the base of the hydrocarbon (heavy oil) bearing section on resistivity log. This may be another evidence that stable carbon isotopes trend is influenced by the framework porosity, a decrease in porosity being accompanied by an increase in carbon isotope values.

3.4. Conclusions

Sequence stratigraphic principles can give new insights into geochemical data from mudlogged wells of the Western Canada Foreland Basin. Carbon isotope values and composition of hydrocarbon gases extracted from drilling muds while drilling do not vary monotonically as might be expected if the gases reflected increasing maturity with depth (Schoell, 1983). The mudlogs show numerous inflections and variations in carbon isotope and gas composition that are correlatable over 150 km in both Foothills-, and Lloydminster areas. Some of these inflections correspond with regional unconformities, indicating lateral but not cross-formational flow. Other inflections occur within formations suggesting intra formational compartmentalization of the gas. Boundaries to such compartments are often the sequence stratigraphic surfaces identified from geophysical logs (see Figures 3-3 to 3-5, and Figures 3-16 to 3-22). Intra formational compartmentalization of the gas will be further show in the following chapters.

In the 6,500 sq km (Foothills region) and ~13,000 sq km respectively (Lloydminster region) study areas, subaerial unconformities mark on mudgas profiles a general downward transition from negative towards more positive carbon isotope values. This is the obvious case of the Mannville-Joli Fou boundary in both study areas, as well as the major subaerial unconformity between the Paskapoo, and Scollard formations within the Foothills area. Maximum flooding surfaces mark a transition from overlying immature, towards more mature underlying gases. Ravinement surfaces have higher concentrations of heavier hydrocarbons, and mark inflections towards more negative carbon isotope values for ethane and propane. Every key bounding surfaces contrasts permeability and porosity between overlying and underlying rock units due to facies and grain size changes. From an exploration point of view, highly prospective trends may be at erosional subaerial unconformities, or other related bounding surfaces. Consequently, such surfaces will be the loci preferential fluid flow and will appear as anomalies in geochemical depth profiles. Stable isotopes of carbon seem to be a promising tool in stratigraphic studies. Individual geological formations may have related gases that have unique and distinguishing carbon isotope compositions. Records of strong positive and/or negative carbon-isotope inflections should provide a potential marker for the recognition and correlation of stratigraphic intervals, whose timing could be determined from the consistent relationship between the carbon-isotope record and biostratigraphic indicators documented in fossiliferous successions elsewhere.

CHAPTER FOUR
MUDGASES DISTRIBUTION, ORIGIN AND MIGRATION

4.1. Introduction

Interest in gas geochemical signatures has been recently developed and they are now considered to be an essential criterion for the understanding of hydrocarbon history and behavior in sedimentary basins (James, 1983, 1990; Clayton, 1991; Whiticar, 1994; Rooney et al., 1995; Cramer et al., 1999; Littke et al, 1999; Prinzhofer et al., 2000a; Prinzhofer et al., 2000b). The general use of relatively new methods of chemical and isotopic analysis of the whole range of C1–C5 gas molecules has enabled the development of new concepts and models concerning the genesis and evolution of hydrocarbons.

Stable carbon isotope ratios in hydrocarbon gases provide a fingerprint technique, which can be used to assess the nature and thermal maturity of potential source beds, the pathways by which gas migration occurred, and the presence of mixed-source gases.

Combining gas geochemistry and stable isotope measurements on the C_1 – C_4 hydrocarbons allows a better characterization of such parameters as indices of maturity, type of source (primary versus secondary cracking), efficiency of hydrocarbon accumulations, and traces of bacterial alteration.

Until the last decade, genetic models for natural gases were based primarily on field data collected for different gas types. These includes shallow, low-temperature bacterial gases (Claypool and Kaplan, 1974; Schoell, 1977; Jenden and Kaplan, 1986; Coleman et al., 1988; Rice, 1992), higher temperature thermogenic gases, often associated with oil (Galimov et al., 1970; Stahl and Carey, 1975; Schoell, 1980; Jenden and Kaplan, 1989), and coalbed and shale-hosted gases (Colombo et al., 1970; Smith et al., 1985; Rice, 1993; Martini et al., 1996; Rowe and Muehlenbachs, 1999). Papers attempting to synthesize this knowledge (Stahl, 1977; Bernard, 1978; Schoell, 1983; James, 1983; Whiticar et al., 1986; Chung et al., 1988; Schoell, 1988) still provide the backbone of most natural gas interpretations carried out in the oil and gas industry. These models and empirical schemes are not without problems, however. Models developed for one type of gases or for one type of basin often do not work for another, some schemes are contradictory (Jenden et al., 1988; Lorant et al., 1998; James, 1983; Prinzhofer et al., 2000b), and a given data set may give rise to very different interpretations, particularly when post-generative processes such as diffusive fractionation are invoked (Jenden et al., 1993; Prinzhofer and Huc, 1995; Prinzhofer and Pernaton, 1997).

With important interpretive principles derived from the above syntheses, this chapter attempts to discuss the mudgas molecular and isotope compositions within the Western Canada Sedimentary Basin.

4.1.1. Controls on mudgas composition

The relative abundance of C_{2+} alkanes are controlled by a number of factors associated with both the primary generation of hydrocarbons, as well as post-generation processes including gas migration, mixing, bacterial methylotrophy, and dissolution (Stahl, 1977; Schoell, 1983, 1988; Tissot and Welte, 1984; Galimov, 1988; Clayton, 1991; Whiticar, 1994; Hunt, 1996) .

One of the main factors influencing the hydrocarbon gas composition is the mechanism of gas generation. Hydrocarbon gases may be generated by one of two principal mechanisms, either bacteriogenic or thermogenic (Schoell, 1988). Bacteriogenic gas generation begins during sedimentation and diagenesis once anaerobic conditions have been achieved. This generation mechanism is mediated by methanogenesis, which metabolize either CO_2 or acetate to produce methane according to the one of the following reactions:

$$CO_2 + 4H_2 \rightarrow CH_4 + 2H_2O \qquad (4.1.)$$

or

$$CH_3COOH \rightarrow CH_4 + CO_2 \qquad (4.2.)$$

Gas produced by bacterial metabolism is characterized by a wetness index of approximately zero, being comprised almost of CH_4. Oremland et al. (1988) have also demonstrated bacterial ethane production in sediment slurries, although only in trace amounts. Bacterial methanogenesis is the dominant mechanism of gas generation up to a maximum temperature on the order of 70^{0}C (Hunt, 1996), above which the abiotic production of methane becomes dominant. Thermogenic production of hydrocarbon gases from kerogen and larger carbon number hydrocarbons begins at temperature of 50^{0}C (Hunt, 1996). The onset of thermogenic generation is characterized by dominant methane production with significant proportions of C_2 and higher alkanes generated at temperatures above 65-70^{0}C (Hunt, 1996).

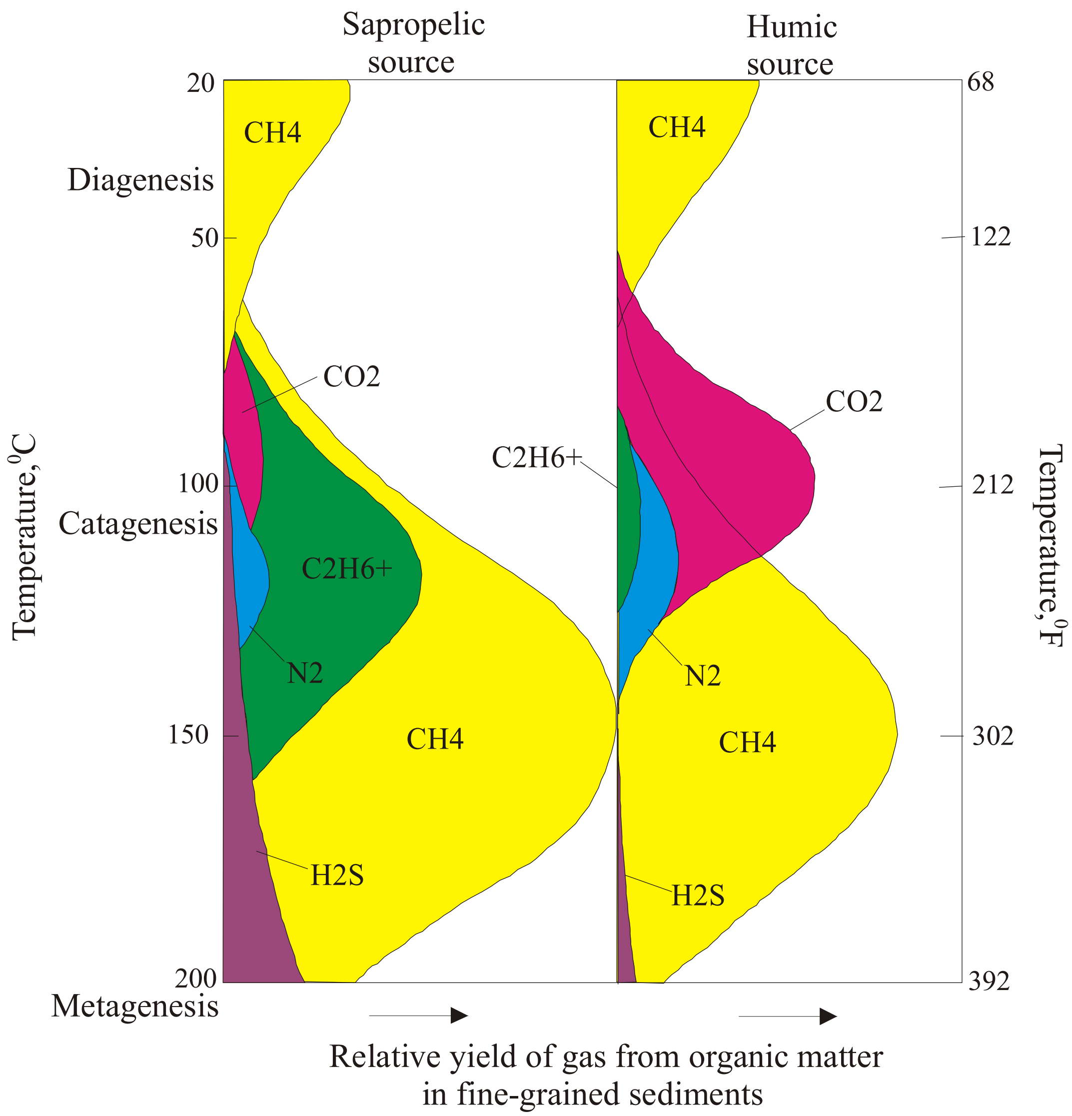

Figure 4-1 Relative yields of hydrocarbon and nonhydrocarbon gases with increasing pyrolysis temperature for sapropelic (Type II) and humic (Type III) organic matter. These generation curves exclude non-organic mechanisms of H_2S, CO_2 and N_2 production such as sulphate reduction (modified after Hunt, 1996).

A second factor influencing the relative abundance of C_{2+} alkanes is the composition of the source kerogen. Sapropelic, type II kerogen is characterized by generation of a higher proportion of wet gas components for a given time-temperature exposure than are humic type III kerogens (Figure 4-1).

The isotopic composition of insoluble sedimentary organic matter (kerogen) varies from –15 to -35‰, but most kerogen show a narrower range of –23 to -32‰.

Regarding the post-generation mechanisms affecting the gas composition, one of these processes is gas migration. Previous studies (Leythaeuser et al., 1980; Leythaeuser et al., 1984) have described the compositional fractionation of gases resulting through gas expulsion from source rocks and subsequent migration to reservoirs. During these processes, alkanes are separated in a process analogous to chromatographic separation, with the distance for each component from source to migration front increasing in direct proportion to the diffusion coefficient and, correspondingly, inverse proportional to molecular weight. Thus, methane would tend to migrate further from the source than ethane, which in turn will diffuse further than propane, and so on. Graphical representation of the wetness index would represent the effect of such a process as a pattern of decreasing gas wetness away from the presumed gas source.

Gas mixing may also influence the observed spatial pattern of gas wetness. Thermogenic gas with a high relative abundance of C_{2+} alkanes generated at depth may undergo mixing with dry gases generated by bacterial metabolism in shallower systems (Jenden et al., 1988; Jenden and Kaplan, 1989). Similarly, in systems containing a juxtaposition of humic and sapropelic kerogens, gases from both sources may mix to produce intermediate dry gas index pools. Such mixing processes may complicate the pattern of gas composition observed on a regional scale.

Bacterial methylotrophy constitute a third process by which gas composition may be altered following generation (Bernard et al., 1978; Schoell, 1983; Whiticar, 1994, 1998). Some genera of microbes utilize CH_4 and higher carbon number alkanes as electron acceptors in their metabolic processes. Of these, the microbiology of aerobic methane oxidizers is best understood and evidence of their effect on gas composition best characterized. Compositional and isotopic evidence of methane oxidation by aerobic bacteria to produce CO_2 has been reported in diverse systems including laboratory cultures, surface water columns, freshwater and marine sediments and soils (Barker and Fritz, 1981; Coleman et al., 1981; Whiticar and Faber, 1986). More equivocal is the mechanism for anaerobic oxidation of CH_4 to produce CO_2. Rosenfeld (1947) first reported the anaerobic oxidation of hydrocarbons by sulfate reducing bacteria, a process later refuted by Sorokin (1957). It is possible that the oxidation observed in the former study arose as a consequence of its use of impure bacterial cultures (Davis and Yarborough, 1966). Davis and Yarborough (1966) reported the anaerobic oxidation of methane by *Desulfovibrio desulfuricans*, a sulfate reducing bacterium. In an experiment, ^{14}C-labeled methane and ethane were oxidized by pure cultures of sulfate reducing bacteria to produce $^{14}CO_2$, although the rate of oxidation was slow and that amount of hydrocarbon reduced was small. The influence of anaerobic hydrocarbon oxidation on natural gas composition has not yet been resolved.

An additional process by which the composition of a hydrocarbon gas may be altered is dissolution (Clayton, 1991; Zheng and Yapa, 2002). Alkanes coexisting with-, or having been generated in conjunction with oils are subject to dissolution into the liquid phase. Alkanes solubility in liquid hydrocarbons increases with increasing chain length. As a consequence of this relationship between carbon number and solubility, it is expected that areas in which dissolution occurs would be characterized by relative decreases in the wetness index, as C2+ fractions would preferentially partition into the liquid phase (Clayton, 1991). Conversely, where significant volumes of formation waters occur in conjunction with gaseous alkanes, a decrease in the relative proportion of gaseous methane would be expected (Clayton, 1991). This pattern reflects the decreasing aqueous solubility of alkanes with increasing carbon number.

4.1.2. Primary controls on stable carbon isotope ratio of mudgases

Owing to the numerous combination of processes that could lead to a given gas composition, resolution of gas source and post-generation effects on gas composition cannot rely on the basis on gas composition alone. Integration of stable carbon isotopic data is fundamental to solve these influences on gas composition.

The preferential utilization of ^{12}C by methanogenic bacteria to produce ^{13}C-enriched methane has long been recognized and forms the basis for a number of methods of distinguishing bacteriogenic from thermogenic methane.

One dependable method of differentiating gas generation mechanism was described by Bernard et al. (1977) and relies on the graphical representation of gas composition using two parameters. The first one is the $^{13}C/^{12}C$ ratio of methane, reported in the delta notation. This parameter is plotted against the dimensionless ***Bernard parameter***, which is the ratio of methane concentration to the sum of the ethane and propane concentrations $\{CH_4/(C_2H_6+ C_3H_8)\}$.

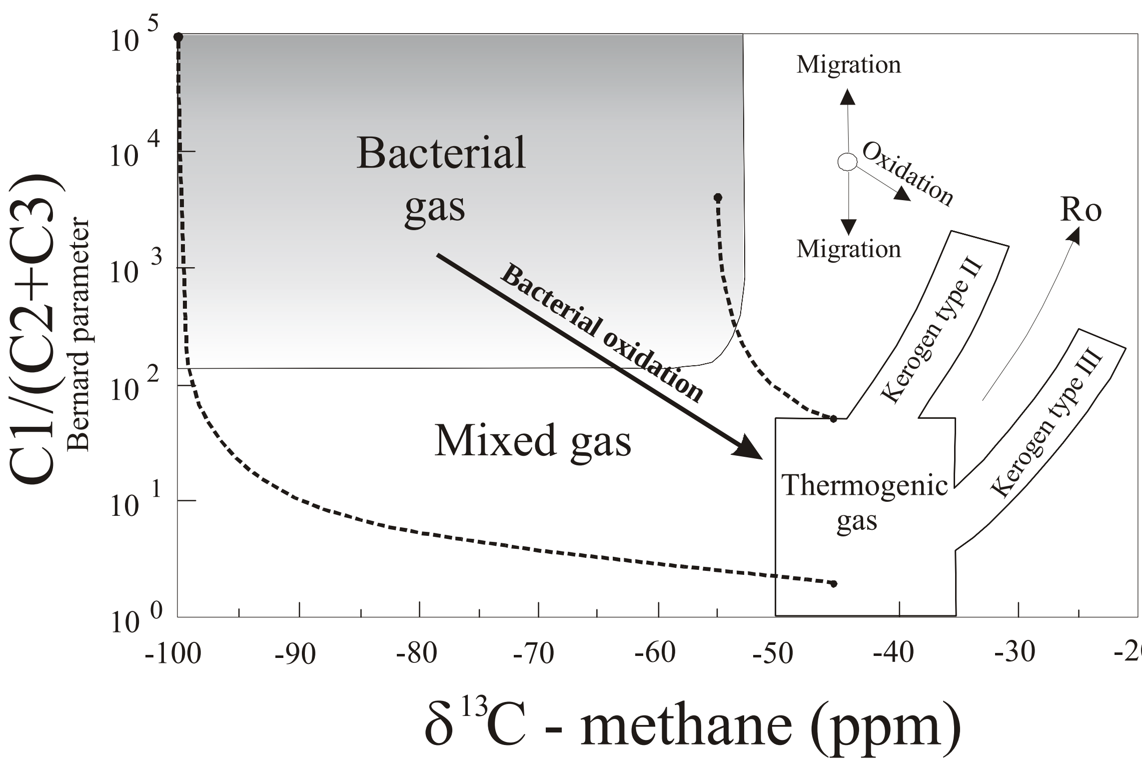

Figure 4-2 Natural gas diagram (Bernard diagram) distinguishing bacterial from thermogenic gases on the basis of molecular composition and carbon isotope ratio of methane. The arrow indicates compositional and isotopic alteration of bacterial gas induced by microbial oxidation (after Bernard, 1977 and Whiticar, 1999).

Bacterial and thermogenic gas fields have been defined using empirical data on the basis of these two parameters, as illustrated in Figure 4-2. As is shown in this figure, bacterial gases are characterized by higher ratios of methane to C_2 and C_3 components, as well as ^{13}C-depleted methane. It should be noted that the distribution of reservoired gas compositions on a Bernard diagram might not strictly represent primary effects on gas compositions. Microbial oxidation of methane may increase gas wetness and enrich residual methane in the ^{13}C isotope, thereby moving bacterial gases toward the realm of thermogenic gases on the diagram (Figure 4-2).

Maturation effects may also be resolved on the basis of $^{13}C/^{12}C$ ratios. Schoell (1980) developed a summary of the carbon isotopic variation and C_{2+} fraction as a function of vitrinite reflectance (%Ro). These isotopic and compositional fields are represented in Figure 4-3. In general, Figure 4-3 reveals a trend toward increasingly less negative $\delta^{13}C$ for methane generated from increasingly mature organic sources. This enrichment pattern has been reported by more recent studies (James, 1983; Clayton, 1991) and will be further discussed.

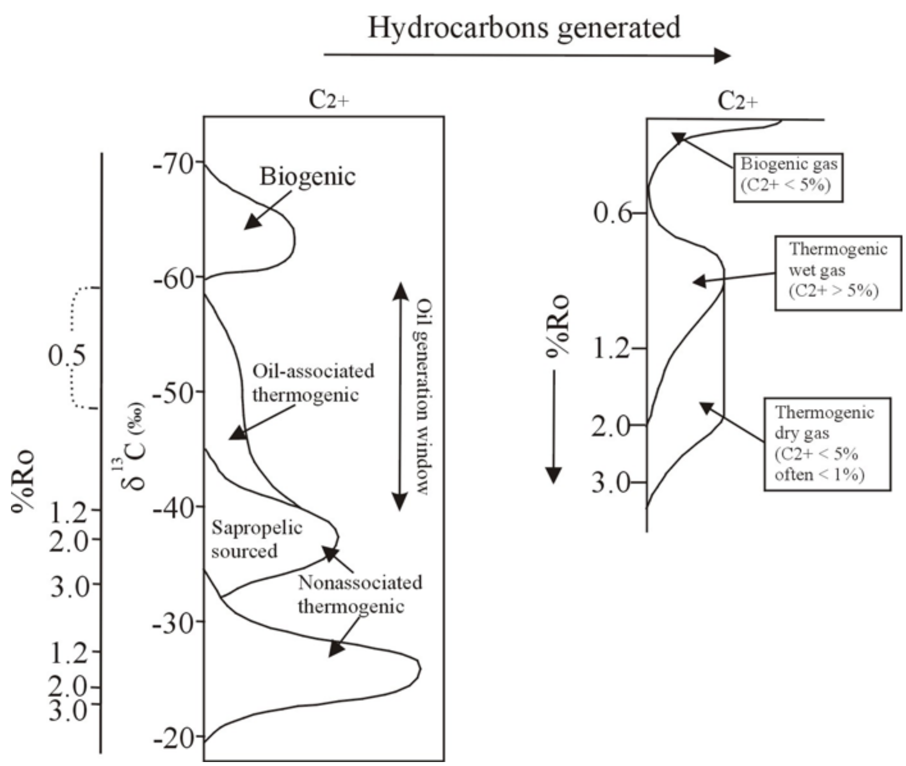

Figure 4-3 Variation in $\delta^{13}C$ of methane and C_{2+} concentration for generated hydrocarbons as a function of increasing organic maturity (after Schoell, 1980 and Schoell, 1983).

These source-related compositional and isotopic effects have been combined in a number of more sophisticated gas typing procedures. One means for the genetic characterization gases relies on the comparison of compositional and isotopic data for sampled gases with established ranges for natural gases from other basins. Schoell (1980, 1983) defined a suite of genetic classes on the basis of gas composition and isotope ratios for cogenerated gases from North America and European basins. Specifically, the compositional data on which this approach relies is the volume percentage of C2+ alkanes in reservoired gases.

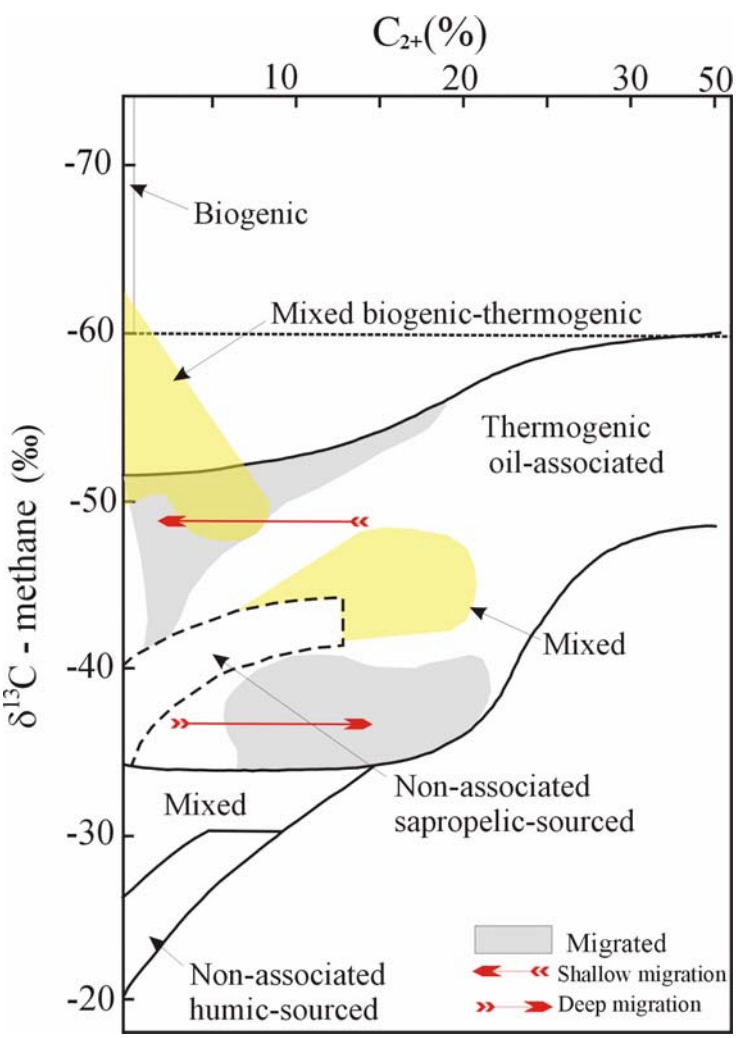

Figure 4-4 Genetic classification of gases defined by Schoell (1983) on the basis of methane $\delta^{13}C$ and the abundance of ethane and higher alkanes. Deep migration: deep dry gases migrate into shallower less mature zones and gain C_{2+} hydrocarbons; shallow migration: associated gases migrate and are stripped of their C_{2+} hydrocarbons.

Isotopic data used in this method comprise the $\delta^{13}C$ values of CH_4 and C_2H_6, as well as the δD of CH_4. Cross-plots of (1) $\delta^{13}C_{CH4}$, versus $\Sigma C2+$ (Figure 4-4), (2) $\delta^{13}C_{CH4}$ versus $\delta^{13}C_{C2H6}$ (Figure 4-5) are used to define five genetic classes. The first of these is biogenic gas, characterized by $\delta^{13}C_{CH4}$ more negative than -58 to -60 per mil and $\Sigma C2+$ concentrations of 1-2 volume%. The second and third of these are oil- and condensate associated gases, respectively. These are characterized by $\delta^{13}C_{CH4}$ values between –52 and -34‰, with condensate-associated gases tending towards the more positive end of this range. $\Sigma C2+$ concentrations may range up to 50 volume% or more for these associated gases. Nonassociated gases from humic and sapropelic kerogens constitute the fourth and fifth compositional fields, respectively. Sapropelic-sourced nonassociated gases are characterized by $\delta^{13}C_{CH4}$ values ranging from -45 to -30‰ and $\Sigma C2+$ less than 15 volume %. Nonassociated gases from a humic source have $\delta^{13}C_{CH4}$ between -35 and -20‰ and $\Sigma C2+$ less than 10 volume %.

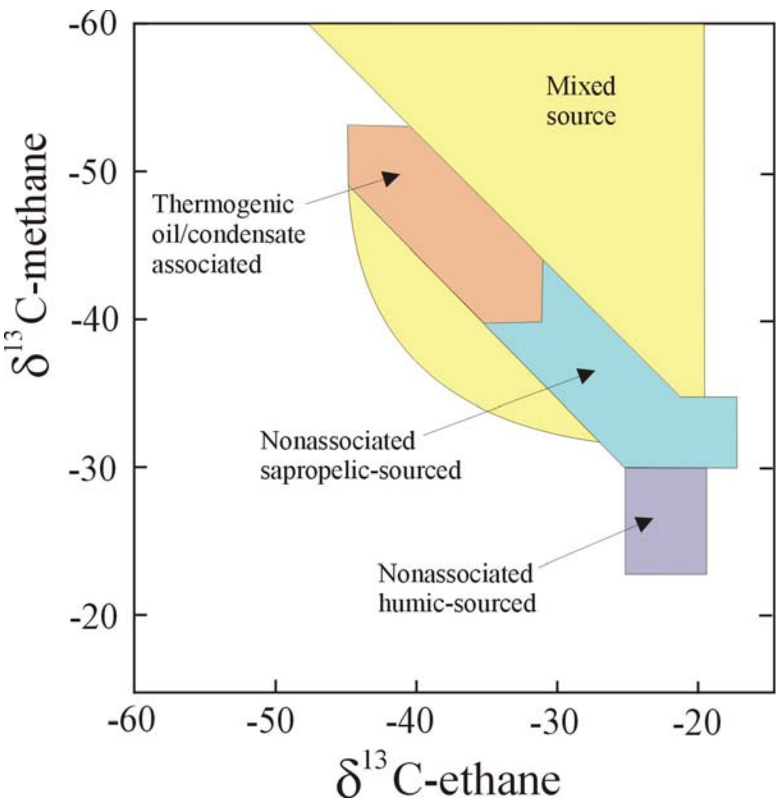

Figure 4-5 Genetic classification of natural gases defined by Schoell (1983) on the basis of methane $\delta^{13}C$ and ethane $\delta^{13}C$.

With respect to these compositional fields, *associated* and *nonassociated* gases have a genetic connotation, their meanings differing from standard petroleum geology usage. Associated gases are those generated together with oil or condensates within the "oil window", whereby nonassociated gases are generated at maturities exceeding the range over which oil generation occurs. The term associated in petroleum geology indicates gases, which coexist with oil in a reservoir, whereas nonassociated gases are reservoired in the absence of oil.

Although the empirical-range approach described by Schoell (1980, 1983) is useful as a first approximation of gas source, it suffers from a number of limitations, which preclude its use as a precise determinant of gas type (Gűrgey et al., 2005). One of the fundamental limitations of this method lies in the relatively restricted dataset on which it is based. Deviation of a given hydrocarbon system from the isotopic and compositional ranges employed by Schoell may contribute to erroneous classification of reservoired gases (Clayton, 1991). Such deviations may be attributable to a diversity of factors, including differences in source isotopic composition and maturity between the gas of interest, and that on which the empirical ranges are based. Furthermore, the proportion of the gas generation potential realized for a given source may influence the isotopic composition of a reservoired gas, thereby resulting in a deviation from classifications based on empirical data.

A second approach used for the genetic classification of natural gases is *the partition function approach* (James, 1983). This method relates the difference in $\delta^{13}C$ values of cogenerated hydrocarbons to source maturity. By considering the $\delta^{13}C$ values of C1 – C5 alkanes relative to one another rather than relative to the source kerogen, this method attempts to counteract any erroneous results arising from variability in source $\delta^{13}C$ values. James (1983) notes two maturity-related effects. Firstly, a regular progression toward increasingly positive $\delta^{13}C$ values is noted with increasing carbon number. This arises owing to the relationship of the mass difference between the ^{12}C and ^{13}C isotopes with the mass of the alkane molecule. For lower carbon number alkanes the 1 amu mass difference between the two isotopes represents a greater proportion of the molecular mass. Hence, it is expected that a mass-discriminating process will be more greatly affected by the mass difference between the two isotopes when lighter molecules are involved, with a corresponding increase in isotopic separation of alkanes relative to the source kerogen is noted.

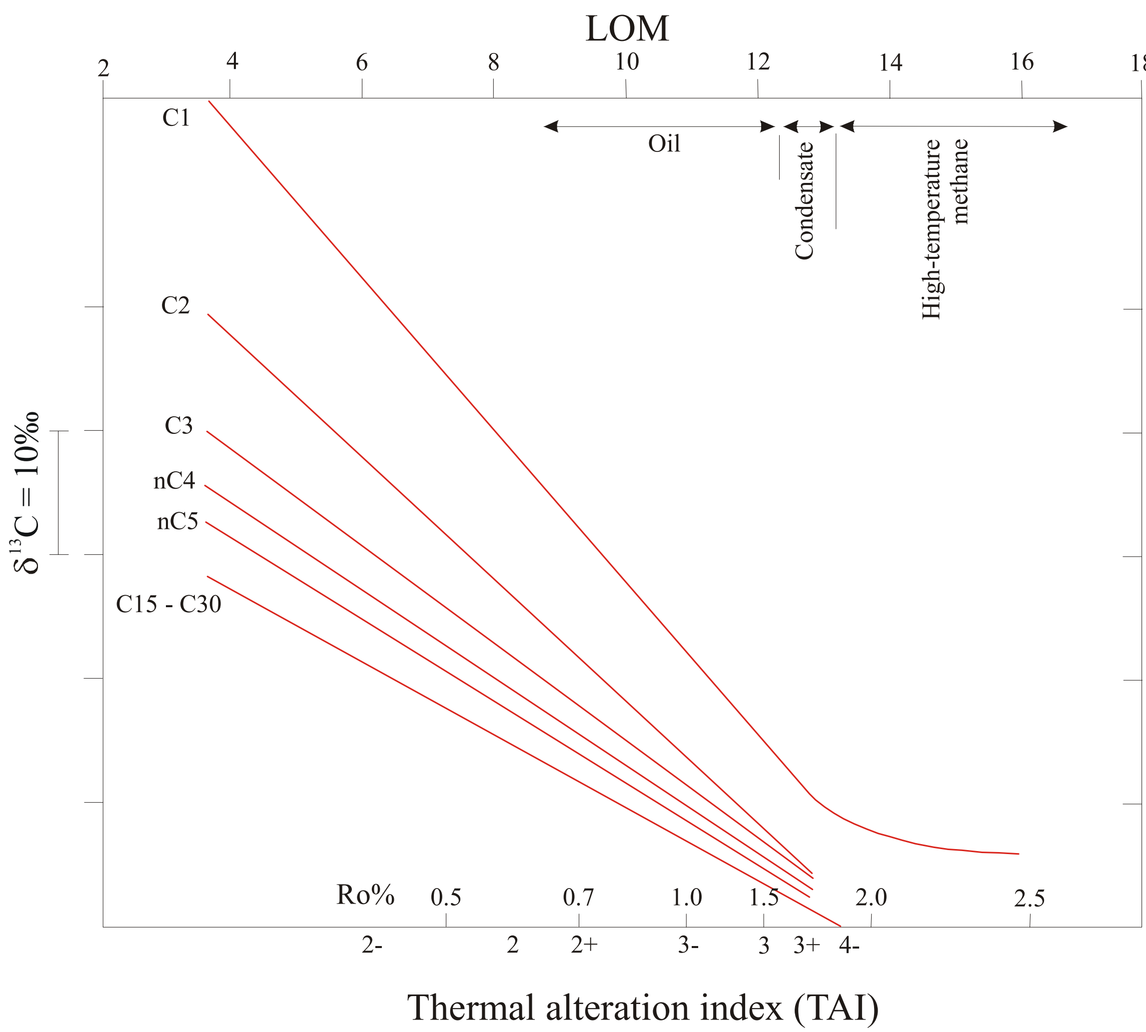

Figure 4-6 James diagram (1983) relating the separation of carbon isotope ratios between C1 – C5 alkanes to various maturity parameters indicated on the *x*-axis: %Ro, TAI and LOM (the level of organic maturity).

Maturity-related effects on the isotopic composition of C1- C5 alkanes have been summarized by James (1983) through the diagram depicted in Figure 4-6. The *y*-axis of this diagram employs a sliding $\delta^{13}C$ scale rather than the fixed $\delta^{13}C$ ranges used in the empirical approach. On the *x*-axis are shown three maturity parameters: (1) level of organic metamorphism – LOM (Hood et al. 1975), (2) Thermal Alteration Index – TAI

(Staplin, 1969), and (3) vitrinite reflectance - %Ro (Van Krevelen, 1961). The five lines shown on this diagram represent calculated isotopic separations for increasing maturity. The relative order of these lines from the top of the diagram downward reflects the increasing ^{13}C enrichment for higher carbon number alkanes previously discussed. Convergence of the five lines toward the right side of the diagram reflects decreasing fractionation with increasing time-temperature exposure of the source organic matter.

Maturity ranges for condensate and oil generation are also shown, as is the maturity range for methane generation through the cracking of higher carbon number alkanes.

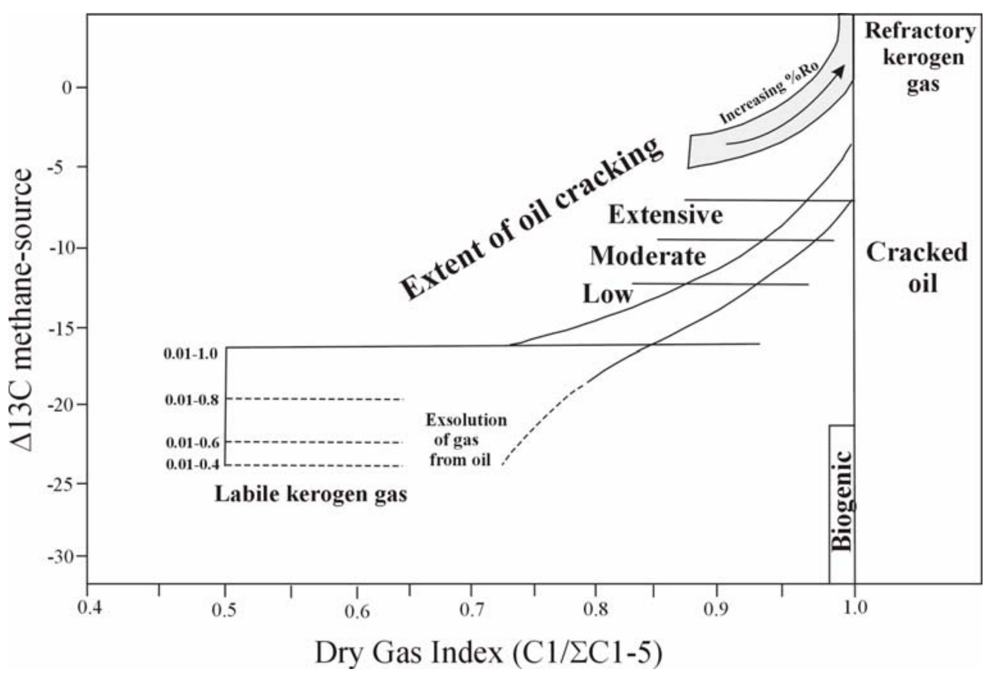

Figure 4-7 Clayton diagram for the genetic characterization of natural gases. The *y*-axis indicates the difference between the carbon isotope ratios of methane and the presumed source kerogen.

A more recently developed means of classifying natural gases on the basis of $\delta^{13}C$ and compositional data has been described by Clayton (1991). This approach is advantageous in that it employs elements of both the empirical and partition function approaches, and accounts for the limitations inherent in each. As with both of the methods previously discussed, genetic characterization of gases in this approach employs a summary diagram (Figure 4-7) with which data may be compared. In similarity to the Schoell (1983) model, the $\delta^{13}C$ versus dry gas index (DGI) summary diagram, of Clayton

(1991) utilizes a fixed $\delta^{13}C$ scale. However, the latter makes no estimation of source $\delta^{13}C$, instead requiring an independent determination of carbon isotope ratios for the source kerogen. The abbreviation GGI appearing in the compositional and isotopic field for labile kerogen-sourced gas denotes the Gas Generation Index, a parameter defined by Clayton (1991) to describe the fraction of the gas generating potential of a given kerogen that has been realized. The result of increasing GGI therefore parallels increased source maturity, insofar as the $\delta^{13}C$ signature of generated methane begins to approach the kerogen $\delta^{13}C$.

The degree of maturation of the hydrocarbon gases, and indirectly the time of generation, can be evaluated by measuring the isotope composition of the methane and its homologues. Bonds of ^{12}C to ^{13}C and ^{13}C to ^{13}C present in the kerogen structure are stronger than ^{12}C to ^{12}C bonds and, therefore, they break at higher temperature or in a longer time than ^{12}C to ^{12}C bonds. Consequently, hydrocarbons rich in the heavy isotope can be interpreted as the ultimate products generated by mature kerogen.

4.1.3. Post-generation controls on stable carbon isotope ratio of mudgases

4.1.3.1. Migration and mixing

The effect of gas migration and mixing on the isotopic signatures of hydrocarbon gases has been a topic of considerable controversy in the past. First proposed by Ingerson (1953) isotopic fractionation of gases during migration was invoked by Colombo et al. (1966, 1969) in order to explain observed patterns of $\delta^{13}C$ and wetness variation in natural gas fields of southern Italy and Sicily. These authors noted a correlation between the proportion of methane in a reservoired gas and the $\delta^{13}C$ value of methane, whereby gases containing greater proportions of C2+ alkanes were characterized by more positive values for the associated methane. These authors attributed this compositional and isotopic variation to migration distances from the presumed gas source. Later work (Fuex, 1980), using both experimental data and mathematical modeling of the gas migration process, indicated that under the steady-state generation and migration of natural gas, fractionation is negligible for both the carbon and hydrogen isotopes of methane. Following this point of view, Whiticar (1994) reiterated that no convincing evidence has been found since Fuex (1980) to indicate that isotopic fractionation accompanies the compositional fractionation associated with migration.

However, recently, Prinzhofer et al., (2000) indicate that the ratio $^{13}C/^{12}C$ of methane is subject to fractionation due to migration, on the other hand noting that chemical and biological processes may obscure the origin of the fractionation. According with this point of view, for the carbon isotopes, the lighter isotope moves faster and is enriched in the area the most distal from the source.

The debate about the existence or the importance of isotopic and chemical fractionation of light hydrocarbons during migration will be further discussed in the following chapters.

Isotopic fractionation of hydrocarbon gases associated with microbial oxidation has been the focus of a number of studies. Barker and Fritz (1981) report fractionation factors between substrate CH_4 and CO_2 produced by methane oxidation by *Methanomas methanooxidans*, an aerobic bacterium. It was found that bacterial selectivity favors the ^{12}C isotope, thereby enhancing the residual methane in ^{13}C and producing ^{12}C-enriched CO_2. In all cases, the product CO_2 was isotopically lighter than the residual CH_4, although considerable variability was noted in the fractionation factor between CO_2 and CH_4. Fractionation factors of 1.0313 to 1.0052 were reported. Coleman et al. (1981) reported a similar range of carbon isotope fractionation factors for mixed cultures containing methane oxidizers. Those authors also determined fractionation factors of 1.103 to 1.325 for hydrogen isotopes in the methane oxidation process. Thus, it can be concluded that the progression of methane oxidation will serve to enrich residual methane in ^{13}C and ^{2}H, while producing ^{12}C-enriched CO_2.

Isotopic fractionation associated with dissolution of methane into coexisting liquid fluids has been reported in laboratory studies by Colombo et al. (1966) and Fuex (1980). The earlier study involved the dissolution of pure methane into n-heptane, water, and crude oil solvents at pressure approximately two times atmospheric. The pressure was subsequently decreased in a stepwise manner, allowing gas exsolution to occur. Aliquots of the exsolved gas were sampled and their $\delta^{13}C$ values measured. It was found that the maximum fractionation was developed when n-heptane and oil were used as solvents. In these cases, the earliest exsolved gases differed from the last aliquot sampled by 1.5 per mil, with the latter being isotopically heavier. Dissolution and exsolution of methane using an aqueous solvent did not impart a measurable isotopic fractionation. This finding was supported by Fuex (1980), who inferred on the basis of similar experiments that the dissolution of methane in water and its subsequent exsolution are unlikely to impart a carbon isotopic fractionation in excess of 1 per mil. On the basis of these two studies and findings, it appears that dissolution of alkanes in coexisting or cogenerated fluids is unlikely to affect significantly the isotopic composition of reservoired gases.

4.1.3.2. Bacterial alteration

Recognition of gas biodegradation can be readily achieved using a comprehensive assemblage of chemical and isotopic characteristics. These types of gases can be recognized by their greater $\Delta\delta^{13}C$ (C_2 - C_1) and $\Delta\delta^{13}C$ ($C_3 - C_2$) values, elevated C_2/C_3 and iC_4/nC_4 ratios (Pallasser, 2000).

An indicator of bacterial degradation in the gas phase is isotopically heavy propane. Bacteria preferentially attack the wet gas components (ethane to butanes), leaving dry gases (James and Burns, 1984; Zengler et al. 1999; Boreham et al., 2001). Of the wet gas components, the propane appears to be the most readily metabolized (acetyl-pathway?), with the weaker ^{12}C-^{12}C bond being preferentially broken, leaving the residual propane enriched in ^{13}C, and hence isotopically heavier. A plot of the stable carbon isotope values of the individual gas components readily identifies a dry gas resulting from bacterial processes from one derived from coal gas or bacteriogenic methane, since the characteristically isotopic reversals between the $\delta^{13}C_{propane}$ and $\delta^{13}C_{butane}$ values are very easily recognized. Microbial alteration can cause selective enrichment of ^{13}C not only in propane, but also in n-butane (James and Burns, 1984).

Furthermore, biodegraded gases often co-occur with biodegraded oils (Dimitrakopoulos and Muehlenbachs, 1987).

Natural gas plots (Chung, 1988) are used in this study as a tool to distinguish the origin and alteration of the various gas packages. On a natural gas plot (Figure 4-8), the carbon isotope ratios of individual gaseous hydrocarbons are plotted as a function of the inverse of the carbon numbers of their molecules. The premise is that the thermal cracking of isotopically homogeneous parent molecules produces a gas with $\delta^{13}C_1$, $\delta^{13}C_2$, $\delta^{13}C_3$ and $\delta^{13}nC4$ carbon isotope ratios that plot as a straight line on the natural gas plot. Deviations from a true linear relationship indicate either a heterogeneous source material or alteration of the gas. The slope of the line indicates the level of maturity of the gas where the shallower the slope the more mature the gas. Extension of the line to 1/Cn = 0 can be used to predict the isotopic composition of the source material of that gas.

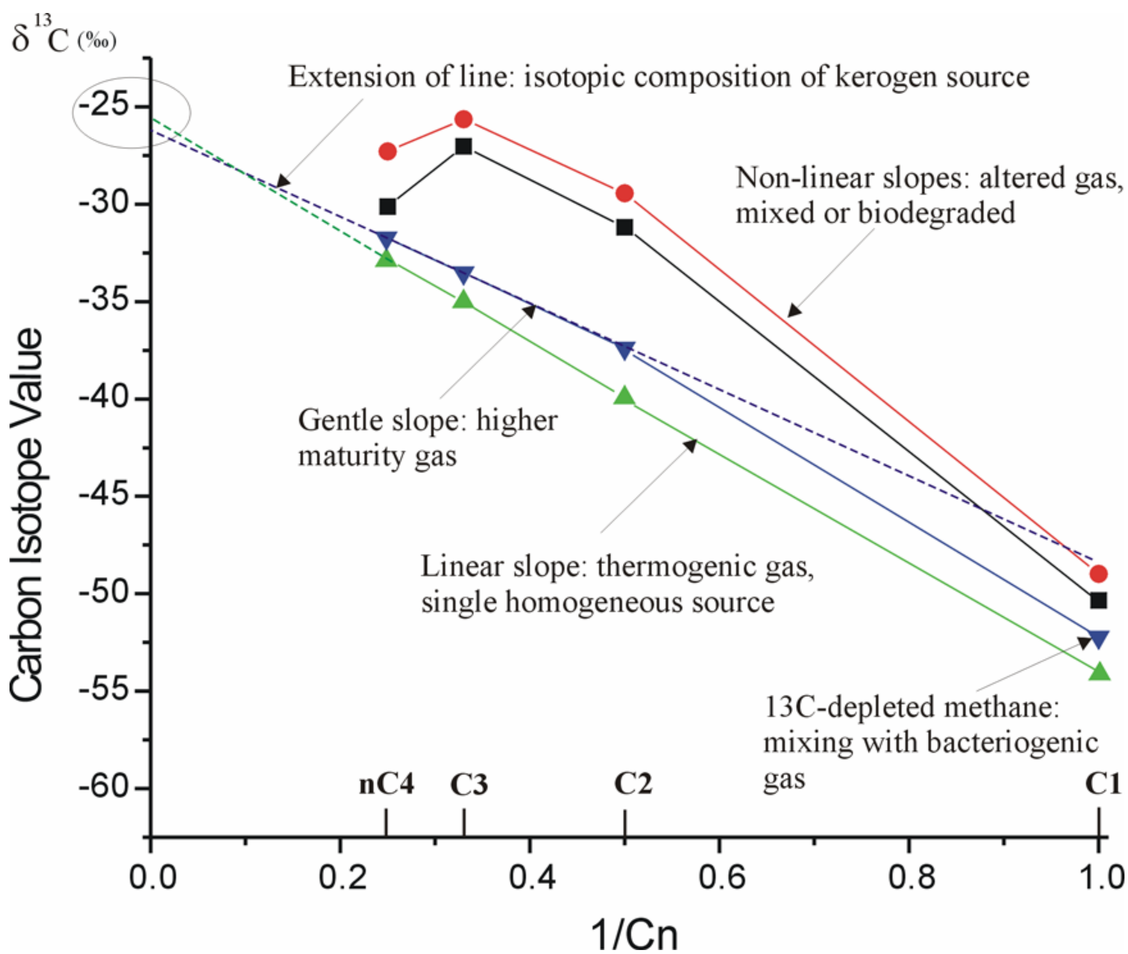

Figure 4-8 Idealized “natural gas plot” of gaseous hydrocarbons (after Chung et al., 1988).

4.2. Results – Foothills region

4.2.1. Compositional variations

Regional variations of the relative abundance of C1 through C4 alkanes are expressed in terms of *wetness index* (C_2+C_3+C_4 abundance divided by the total abundance of C_1 to C_4 gas components). Wetness indices for mudgases vary from 0.0008 (Paskapoo Formation, Gilby) to 0.33 (Belly River Formation, Gilby).

The highest wetness values observed in the study area are developed within the Upper Belly River Formation at both Ferrier and Gilby locations. These mudgases were sampled from coal and/or coaly shale beds. The other wet gases, with wetness index higher than 0.1, are developed mostly within the Lea Park - Colorado Group shales, as it can be seen in Table 4-1.

The hydrocarbon gases within the Foothills region include mainly methane, ethane and heavier hydrocarbons (including iso-, and n-pentane). The heavy hydrocarbon gases (C2+) range from less than 1% (as low as 0.08% to 0.5% for Paskapoo, Scollard, and Horseshoe Canyon gases) to more than 33% by volume (Upper Belly River gases, at both Ferrier and Gilby locations).

Figure 4-9 depicts the depth distribution of the wetness index for all three locations in the first study area – west central Alberta: Ferrier, Gilby and Pembina. As it is shown in this figure, gases sampled at shallower depth (down to ~ 1100m depth) are marked by wetness indexes of 0.001 to approximately 0.026 indicating a predominance of methane.

An abrupt shift in wetness index appears at about 1120m depth - Upper Belly River Formation at Gilby location and at about 1100m depth – Horseshoe Canyon Formation, at Ferrier location.

Table 4-1 Wetness index exceeding 10 %, in descending order – Foothills region.

Wetness Index	Sample depth (m)	Group/Formation	Field
0.33	1257	Upper Belly River	Gilby
0.31	1646	Upper Belly River	Ferrier
0.22	2098.5	Colorado Gp	Ferrier
0.21	2185.4	Pekisko	Gilby
0.20	1930	Viking	Gilby
0.20	2147	Fernie Gp. - Nordegg	Gilby
0.18	1772	Colorado Gp - SWS	Gilby
0.18	1900	Colorado Gp. – Westgate shales	Gilby
0.18	1891	Colorado Gp	Ferrier
0.18	1850	Colorado Gp.	Gilby
0.17	2111	Fernie Gp. – Rock Creek	Gilby
0.17	1905	Colorado Gp.	Ferrier
0.17	1879	Colorado Gp.	Ferrier
0.16	2088.3	Lower Mannville	Gilby
0.15	1462	Colorado Gp.	Gilby
0.15	1960	Joli Fou	Gilby
0.14	1852	Lea Park	Ferrier
0.14	1632	Upper Belly River	Ferrier
0.13	1825	Lea Park	Ferrier
0.13	1444	Lea Park	Gilby
0.12	1810	Lea Park	Ferrier
0.11	1709	Colorado Gp.	Gilby
0.10	2059	Upper Mannville Coal	Gilby
0.10	1980	Upper Mannville coal	Gilby
0.10	1755	Lea Park	Ferrier

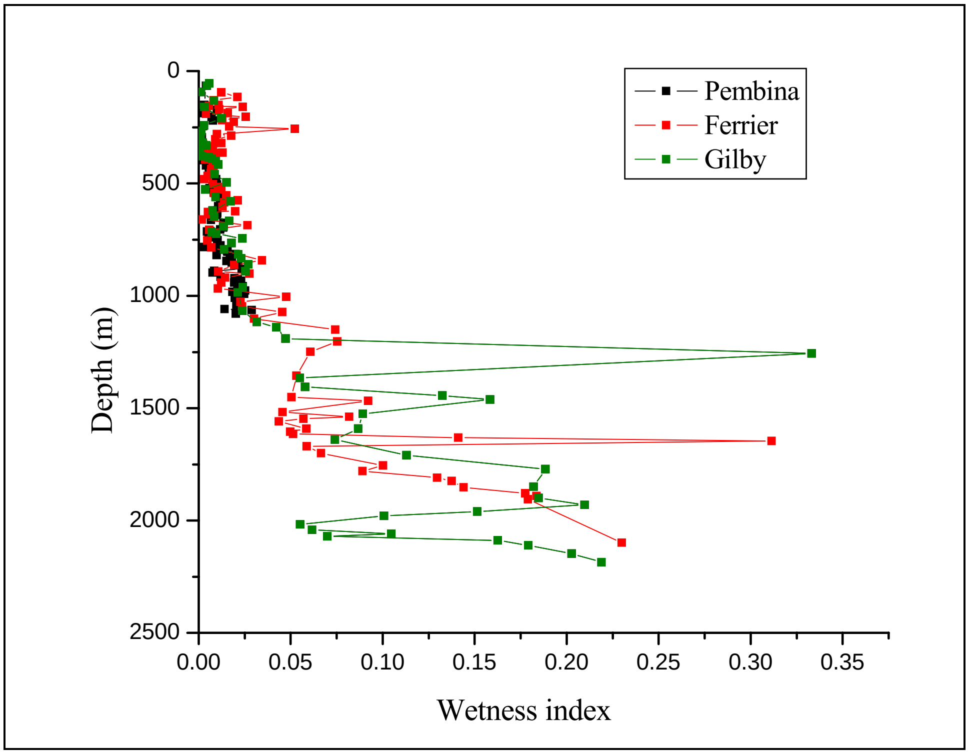

Figure 4-9 Combined depth profile of wetness index for three mudlogs in west-central Alberta.

It should be noted that, overall, mudgases sampled at Gilby location seem to be slightly wetter (with the exception of the very first 250 metres) than those sampled at Ferrier and Pembina locations. However, looking at the wetness index variations formation by formation (Figure 4-10), a different distribution is observed. Increasingly wetness values are developed toward the southwestern limit of the study area, with peaks observed at both Ferrier and Gilby locations. The wettest gas occurrence is located at Ferrier, and not at Gilby (as it could be suggested from Figure 4-9); the wetness distribution exhibit a pattern of increasing values from east to west, and from southeast to northwest. This spatial variation in wetness index parallels both increasing depth and thickness of the sedimentary cover.

In a graphic columnar representation (Figure 4-11) used to compare the magnitudes of frequencies distribution of the methane concentration and the gas abundance for both Ferrier and Gilby locations, it can be easily observed the higher abundance of gas recovered at Ferrier location. The methane concentration is also generally higher at Ferrier location, suggesting that there are likely gas sources here.

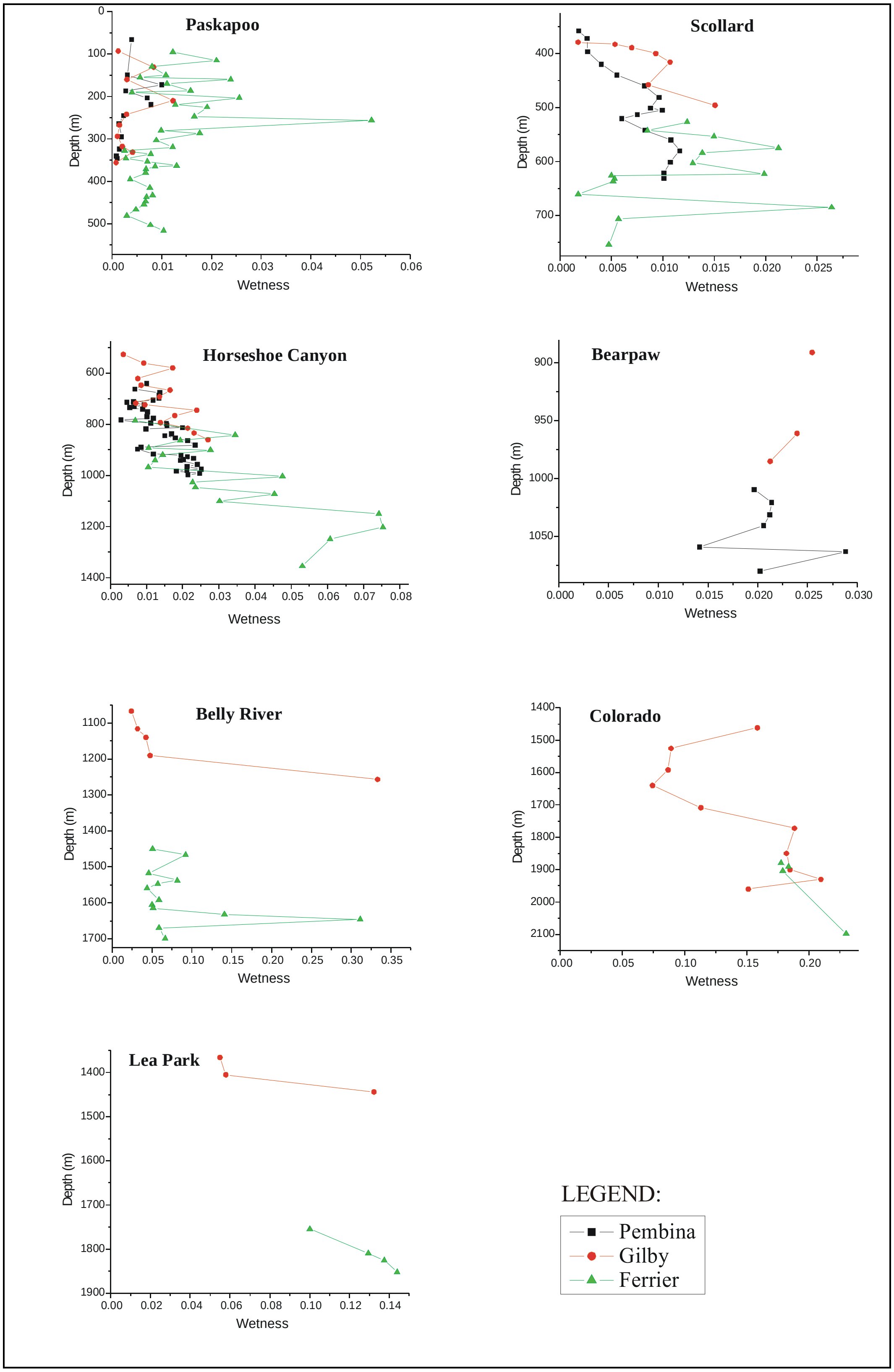

Figure 4-10 In depth distribution of the wetness index for mudgases sampled in the Foothills region

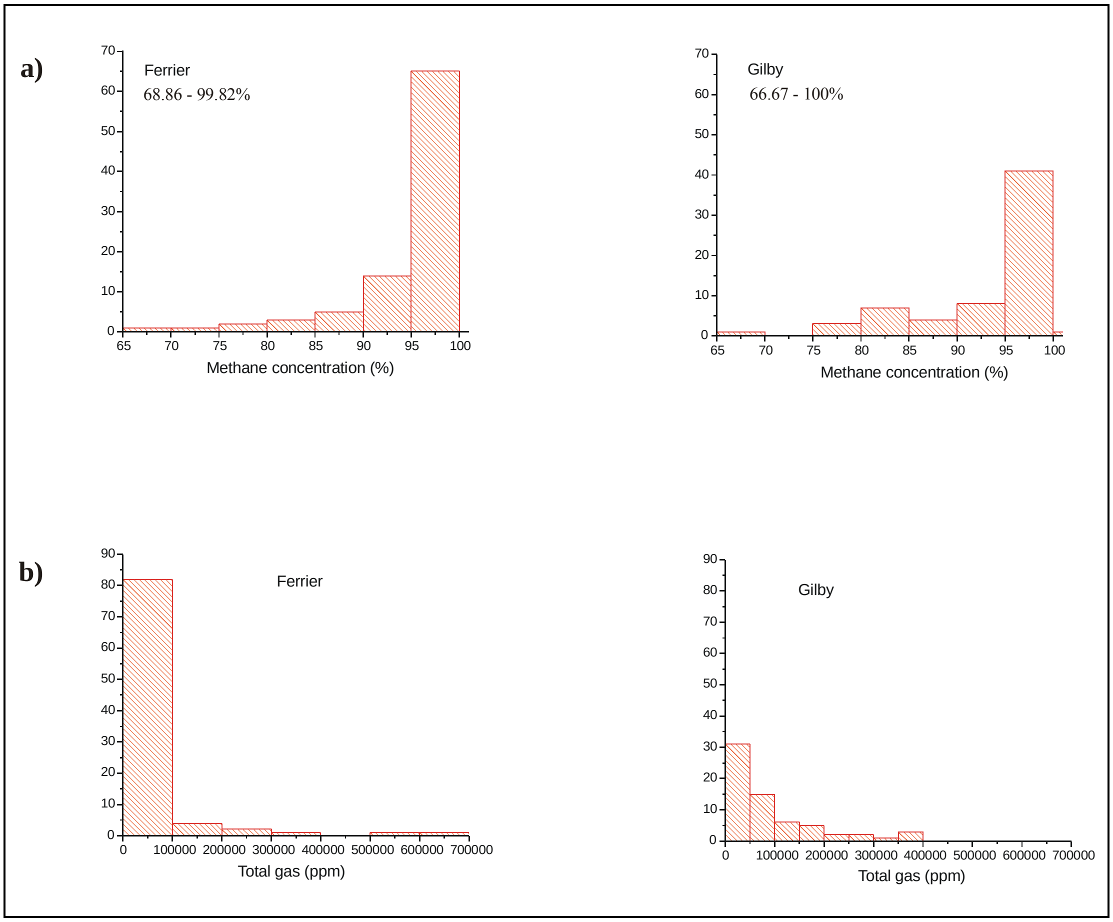

Figure 4-11 Methane concentration (a), and total abundance of gas components (b) at Ferrier and Gilby locations – west-central Alberta

Measured compositional data for mudgases sampled within the Foothills region, as well as the isotopic concentration data of C_1 to C_5 alkanes were acquired from the University of Alberta database. Gases were collected from the drilling mud while drilling the following wells:

1. Pembina 00/11-04-049-11W5-0
2. Ferrier 00/14-03-042-09W5-0
3. Gilby 00/15-16-042-04W5-0

4.2.2. $\delta^{13}C$ variations

Ranges of carbon isotopic ratios for hydrocarbons in different formations, for each mudlog location (Ferrier, Pembina and Gilby) are summarized in Table 4-2.

Table 4-2 Ranges per formation for average isotopic composition for mudgases collected from the three locations of the carbon isotope mud gas depth profiles – Foothills region

Formation	$\delta^{13}C$ (‰ vs. PDB)									
	CH4		C2H6		C3H8		iC4H10		nC4H10	
Paskapoo	F	-48.99	F	-40.11	F	-33.05	F	-29.50	F	-30.58
	P	-51.73	P	-44.16	P	-40.06	P		P	-33.97
	G	-59.05	G	-45.00	G	-37.25	G	-30.03	G	-33.79
Scollard	F	-43.78	F	-32.52	F	-28.85	F	-27.68	F	-28.81
	P	-45.38	P	-32.58	P	-27.84	P	-26.78	P	-28.90
	G	-54.03	G	-35.97	G	-30.11	G	-28.81	G	-30.67
Horseshoe Canyon	F	-45.04	F	-32.87	F	-29.51	F	-28.20	F	-28.07
	P	-47.68	P	-33.40	P	-28.68	P	-28.41	P	-29.97
	G	-51.40	G	-37.72	G	-31.07	G	-29.04	G	-31.14
Bearpaw	P	-51.80	P	-32.85	P	-28.96	P	-28.35	P	-29.78
	G	-54.28	G	-35.96	G	-30.37	G	-29.23	G	-30.6
Belly River	F	-50.47	F	-33.02	F	-28.16	F	-28.40	F	-27.00
	P	-53.69	P	-32.67	P	-28.20	P	-26.89	P	-27.96
	G	-54.63	G	-34.51	G	-29.51	G	-29.15	G	-30.36
Lea Park	F	-52.34	F	-33.45	F	-30.76	F	-30.41	F	-29.48
	G	-56.82	G	-37.41	G	-32.89	G	-28.25	G	-29.83
Colorado	F	-50.21	F	-35.95	F	-33.03	F	-31.32	F	-31.10
	G	-53.61	G	-38.04	G	-34.13	G	-31.89	G	-33.46
Mannville	G	-49	G	-30.79	G	-27.45	G	-28.39	G	-29.19
Fernie	G	-47.89	G	-32.36	G	-29.34	G	-28.61	G	-29.21
Pekisko	G	-50.2	G	-33.47	G	-30.99	G	-32.09	G	-29.95

Note: F: Ferrier, P: Pembina, G: Gilby

Mudgases are relatively variable in their isotopic composition; methane $\delta^{13}C$ values range from about –72.91 to –39.9 ‰; ethane $\delta^{13}C$ values range from –50.49 to -26.69 ‰, propane $\delta^{13}C$ values range from –45.11 to -23.84 ‰, iso-butane $\delta^{13}C$ values range from –35.34 to -21.06 ‰, normal-butane $\delta^{13}C$ values range from –37.06 to -22.21 ‰. The apparent conclusion from Table 4-2 regarding the $\delta^{13}C_{CH4}$ values from the ten main formations/groups conceals significant differences in the carbon isotope composition especially between the Belly River, Bearpaw, Horseshoe Canyon, Scollard and Paskapoo formations. These differences are revealed in a plot of $\delta^{13}C_{CH4}$ versus depth below surface (Figure 4-12). In this diagram several separations of the $\delta^{13}C_{CH4}$ data are observed:

- at depths below 1500 m, Belly River gases tend to be characterized by $\delta^{13}C_{CH4}$ values less negative than those of the majority of Colorado methanes at equivalent depths;
- at depths below ~ 900 m, some of the Horseshoe Canyon gases (Ferrier location) are characterized by $\delta^{13}C_{CH4}$ values less negative than those of the majority of Bearpaw methanes at equivalent depths;
- at depths below 500 m, Scollard gases are more positive (heavier) than the Horseshoe Canyon gases at equivalent depths.

Although some degree of overlap in the $\delta^{13}C_{CH4}$ values exist among the three formations (Belly River, Horseshoe Canyon and Scollard), the data tend to be distributed such that $\delta^{13}C_{CH4Belly\ River} < \delta^{13}C_{CH4Horseshoe\ Canyon} < \delta^{13}C_{CH4Scollard}$. Thus, the $\delta^{13}C$ of methane seems to have a relatively strong stratigraphic control, with increasing depletion in the heavier ^{13}C isotope downward in the uppermost part of the stratigraphic section (Belly River – Paskapoo). However, at deeper depths, an opposite trend is observed: increasing enrichment in the heavier ^{13}C isotope downward. In the lowermost part of the section the data seems to be distributed such that $\delta^{13}C_{CH4Lea\ Park} < \delta^{13}C_{CH4Colorado} < \delta^{13}C_{CH4Mannville,}$ a trend which is the normal trend of enrichment in the heavier ^{13}C isotope with increasing depth.

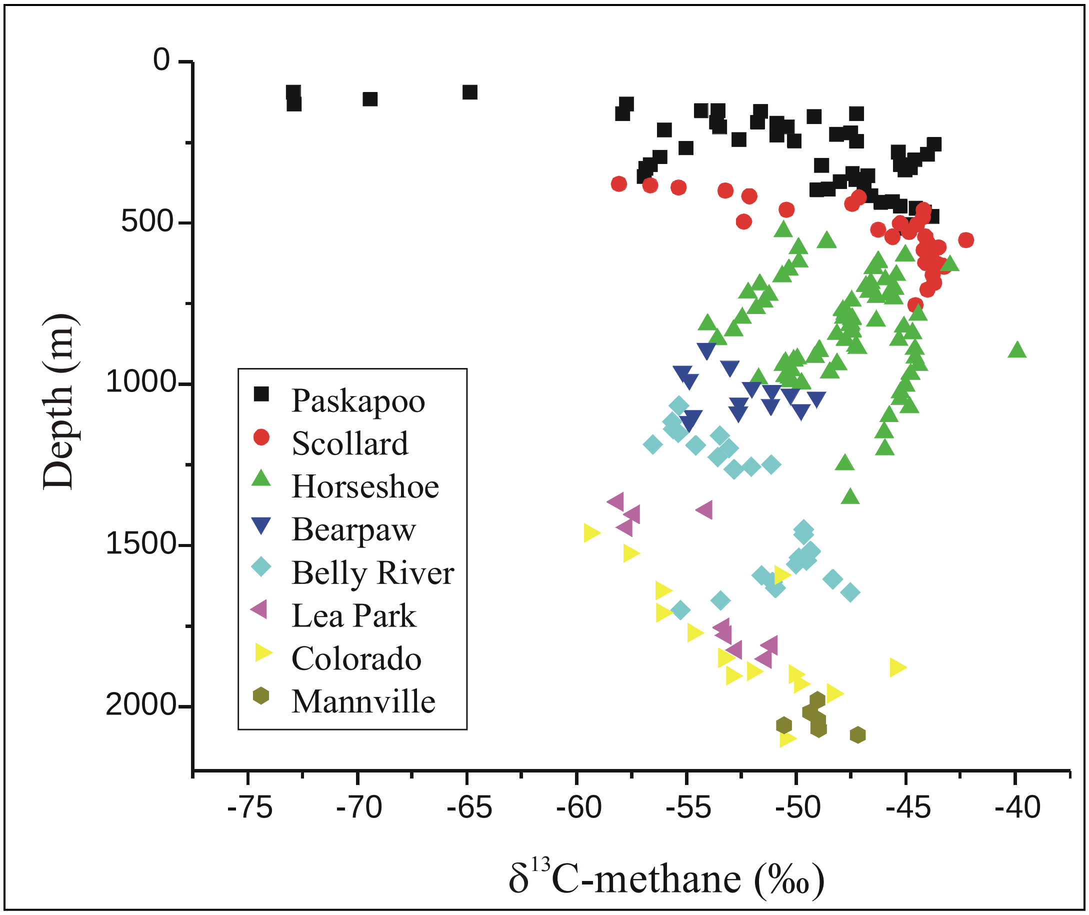

Figure 4-12 Composite depth profile for $\delta^{13}C$ for methane sampled in the Foothills region.

Consideration of the depth relationship for $\delta^{13}C$ values of C2 and higher alkanes reveals the same variation in the carbon isotope composition: a stratigraphic interval comprising Belly River, Horseshoe Canyon and Scollard formations, which tend to be characterized by $\delta^{13}C$ values more positive than the normal values for the considered depth (Figures 4-13 and 4-14).

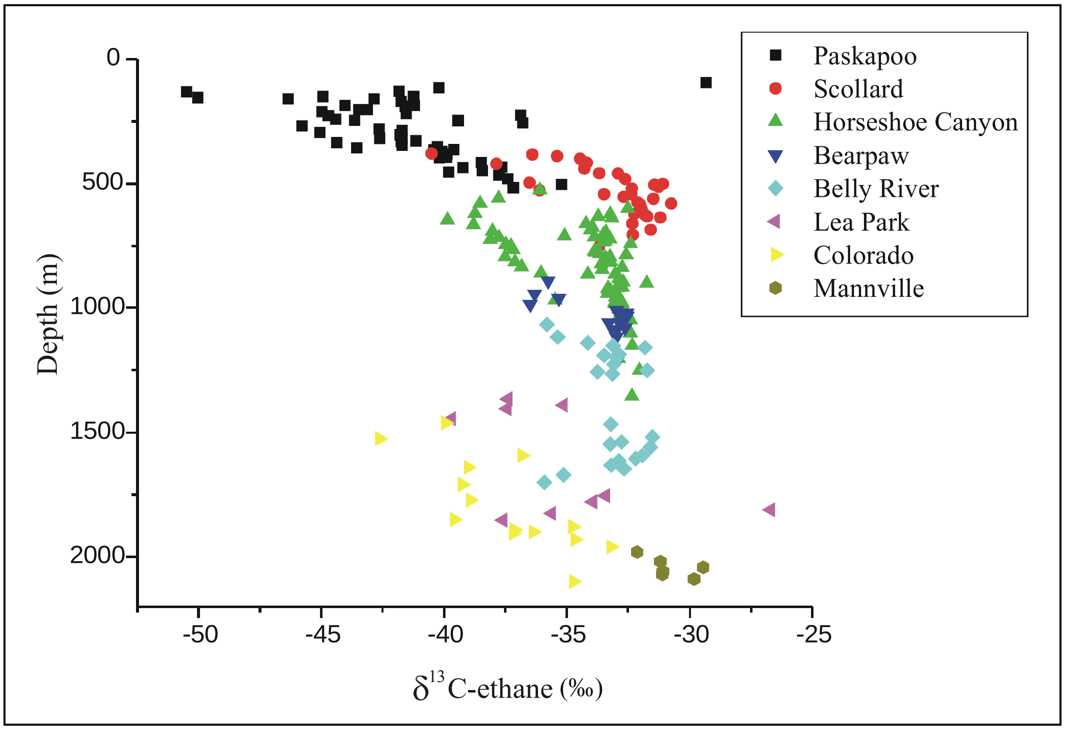

Figure 4-13 Composite depth profile for $\delta^{13}C$ for ethane sampled in the Foothills region

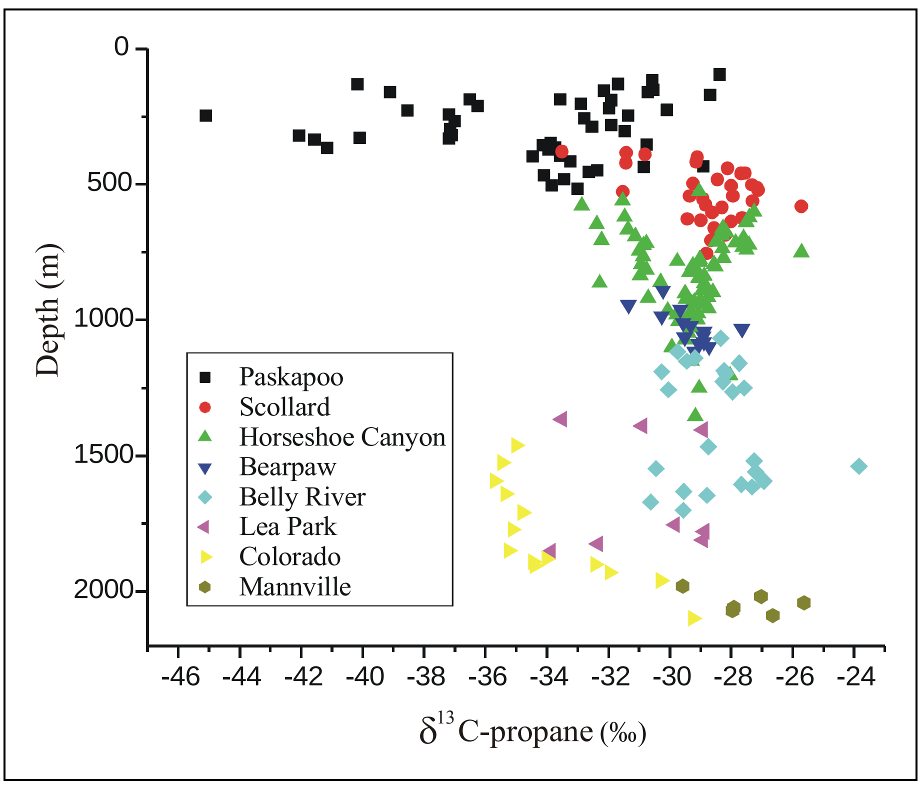

Figure 4-14 Composite depth profile for $\delta^{13}C$ for propane sampled in the Foothills region

In general, $\delta^{13}C$ values of methane, ethane and propane seem to increase with increasing depth below the First White Specks Shale (below ~1460 m – Ferrier, and below ~1870 m – Gilby). This depth-related variation also appears as increased $\delta^{13}C$ values approaching the western limit of the study area (Figure 4-15).

Overall, the carbon isotope data within the Foothills region appear to follow two different major patterns: one approximately linear trend towards increasing values with increasing depth, and another one with no systematic variation in $\delta^{13}C$ with increasing depth. The trend towards $\delta^{13}C$ increasing values refers to the Colorado – Mannville stratigraphic interval. The other pattern, with noticeable shifts toward increasing enrichment in the ^{13}C isotope refers mainly to the Belly River – Scollard stratigraphic interval.

These very distinctive inflections of the C1 – C3 isotope ratios trend towards higher values (apparently greater maturity) occurs in the following depth ranges:

- in the ~540 to ~860 m (Scollard-Horseshoe Canyon) and ~1420 to ~1640 m ranges (Belly River) - Ferrier mudlog profile;
- in the ~380 to ~660 m (Scollard-Horseshoe Canyon) and ~1100 to ~1300 m ranges (Belly River) – Gilby mudlog profile;
- in the ~400 to ~ 800 m range (Scollard-Horseshoe Canyon) – Pembina mudlog profile.

As already described above, the shallower part of the stratigraphic section (Belly River – Paskapoo) deviates somewhat from this trend. This depth-related variation does not appear to coincide with any systematic maturity trend, and needs further explanations.

The entire post-Colorado stratigraphic section comprises mostly nearshore and continental deposits – an alternation of shales, silts, sandstones, conglomerates, and coals. The presence of coals within the Belly River, Horseshoe Canyon and Scollard formations is considered to be important in controlling the compositional changes observed in shallow mudgases.

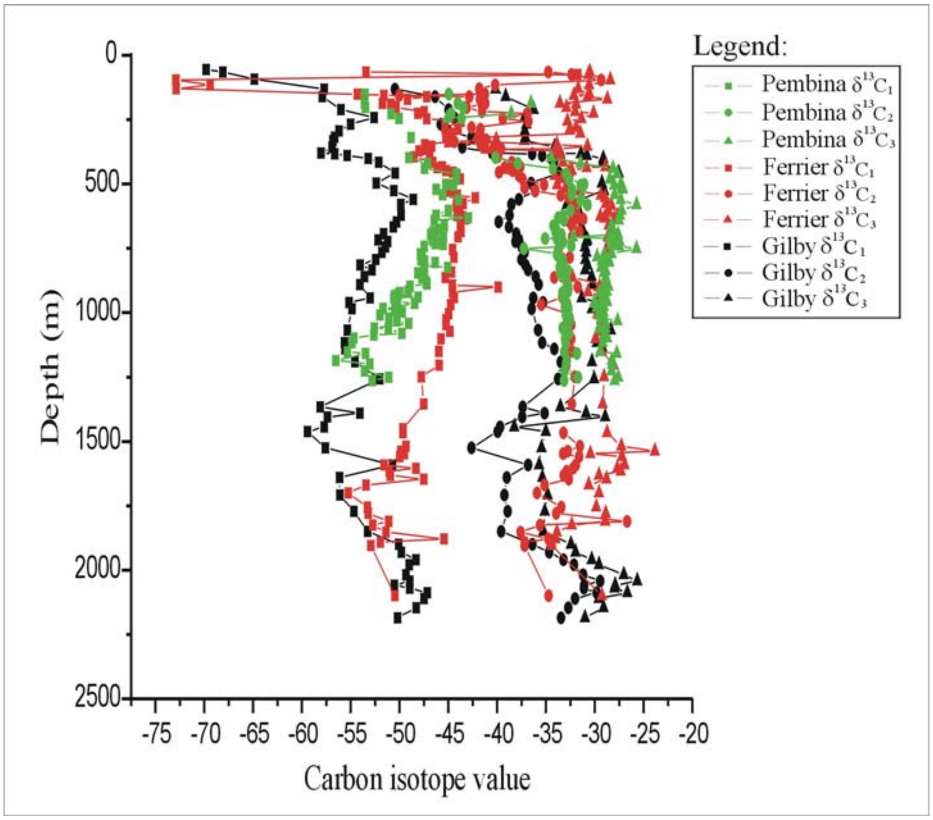

Figure 4-15 In-depth carbon isotope mud profiles for mudgases sampled in the Foothills region

Biogenic gas can occur in coals and coal-bearing strata over a wide range of ranks. Biogenic gas generated from all types of coals consists mainly of methane (Rice and Claypool, 1981; Schoell, 1983; Rice, 1992). The presence of heavier hydrocarbon gases with biogenic methane indicates the overprint of late-stage biogenic methane in coals that have already generated thermogenic hydrocarbons.

In contrast to biogenic gases, thermogenic coalbed gases are characterized by (1) common presence of heavier hydrocarbons (C_{2+} values can be several percent or greater), (2) enrichment of heavy isotope ^{13}C in methane and ethane with increasing rank (methane $\delta^{13}C$ values more positive than –55 ‰ and ethane $\delta^{13}C$ values more positive than –33 ‰) (Rice, 1993). As can be observed in Figure 4-12 and Figure 4-13, most of the Scollard, Horseshoe Canyon and Belly River gases have methane $\delta^{13}C$ values more than –55 ‰, and ethane $\delta^{13}C$ values more than –33 ‰.

Another process to be taken into consideration is the *bacterial alteration of the wet gas components*. At shallow depths, coal beds are commonly aquifers where microorganisms can flourish. Aerobic bacteria are capable of preferentially attacking the wet gas components (C_{2+}) resulting in the destruction of most of the wet gases (James and Burns, 1984). As a result of the alteration, the $\delta^{13}C$ values of the residual propane and other wet gases could be much heavier than expected. Bacterial alteration of the wet gas components could explain the molecular compositional changes observed in the shallower part of the stratigraphic section, above the Colorado Group gases (Belly River, Bearpaw, Horseshoe Canyon, Scollard, and Paskapoo formations).

These gases (affected by biodegradation, as indicated also in Figure 4-16, could be misinterpreted as over-mature because they are very dry (the wetness index ranges between 0.0017 for Scollard and 0.02 for Horseshoe Canyon) and have high $\delta^{13}C$ values.

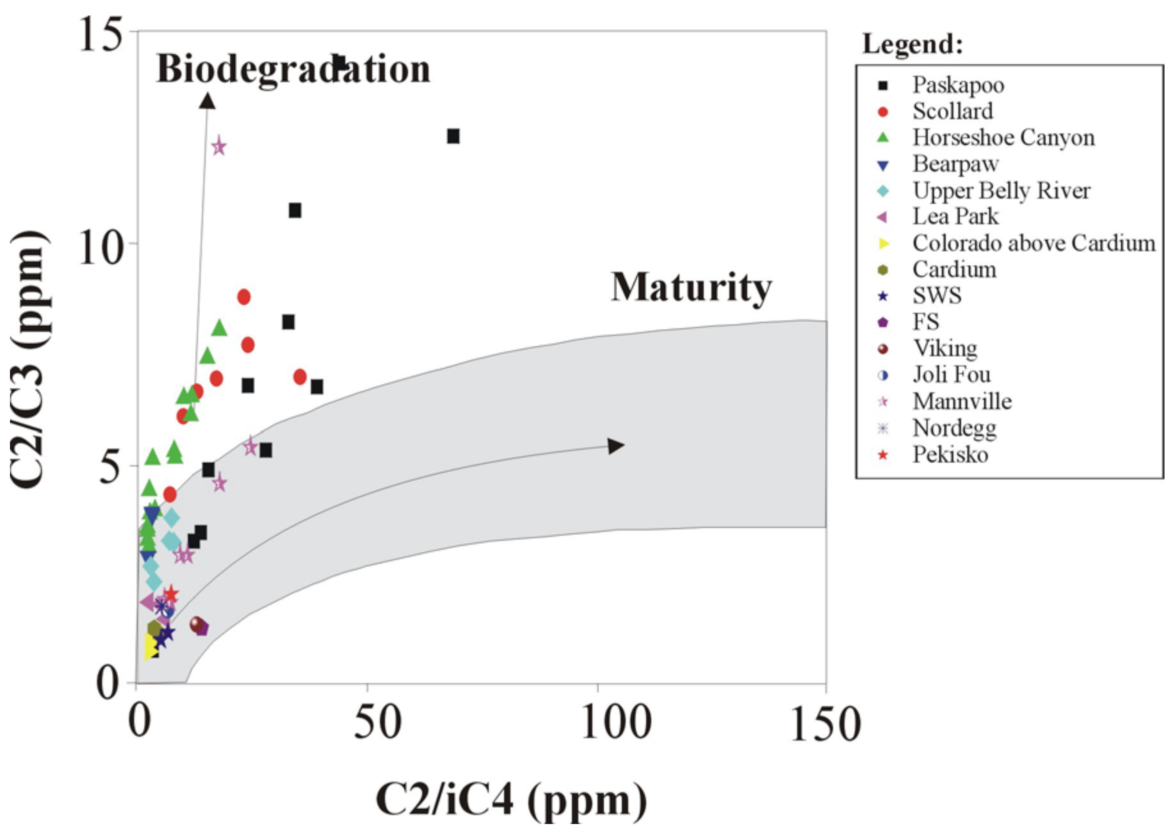

Figure 4-16 C2/C3 versus C2/iC4 diagram showing the possible biodegradation of hydrocarbon gases (Prinzhofer, 2000) - Gilby 15-16-42-4W5.

4.2.3. Combination of gas composition and stable carbon isotope ratios

Consideration of gas composition and carbon isotope data for mudgases with empirically derived genetic classification of gases permits greater insight into the factors controlling the compositional and isotopic variations described. As discussed earlier, a relatively simple method of gas typing relies on the composition of gases with the fields defined by Bernard (1977). Figure 4-17 illustrates the distribution of Jurassic-Cretaceous mudgases collected in the Foothills region on such Bernard diagram. As it is evident from this distribution, mudgases within the Bearpaw, Edmonton, Scollard, and Paskapoo formations at the Pembina location fall into the mixed gas field, with some of the Bearpaw and Edmonton samples lying on the border between the thermogenic-, and mixed gas fields on the basis of their relatively ^{13}C-depleted carbon isotope ratios.

Of the post-Colorado samples collected at Ferrier location, several Belly River-, Horseshoe Canyon-, Scollard-, and Paskapoo gases occur within the thermogenic gas range, with the remainder falling distinctly within the mixed biogenic-thermogenic gas field (Figure 4-17b). Although most of the samples have δ^{13}C1 values characteristic for thermogenic methane, they occur in the mixing region owing to their high abundances of methane relative to C2 and higher carbon number alkanes. All of these samples were collected in the uppermost part of the stratigraphic section.

A similar combination of gas occurrences within both the thermogenic gas field and mixed biogenic-thermogenic fields is noted for Gilby mudgases (Figure 4-18). Lower Colorado (including Fish Scale), Mannville, Fernie and Pekisko mudgases fall within the thermogenic gas field of gas composition and methane δ^{13}C signatures, as well as on the border between the thermogenic and mixed fields (five samples).

For Upper Colorado samples (including Cardium and Second White Specks formations), as well as for the Lea Park and Belly River samples, their occurrence in the mixing field is attributable to relatively ^{13}C–depleted methane. Edmonton, Scollard and Paskapoo samples occur in the mixed gas range on the basis of their higher Bernard parameter values, as some of their δ^{13}C values are characteristic of a thermogenic origin.

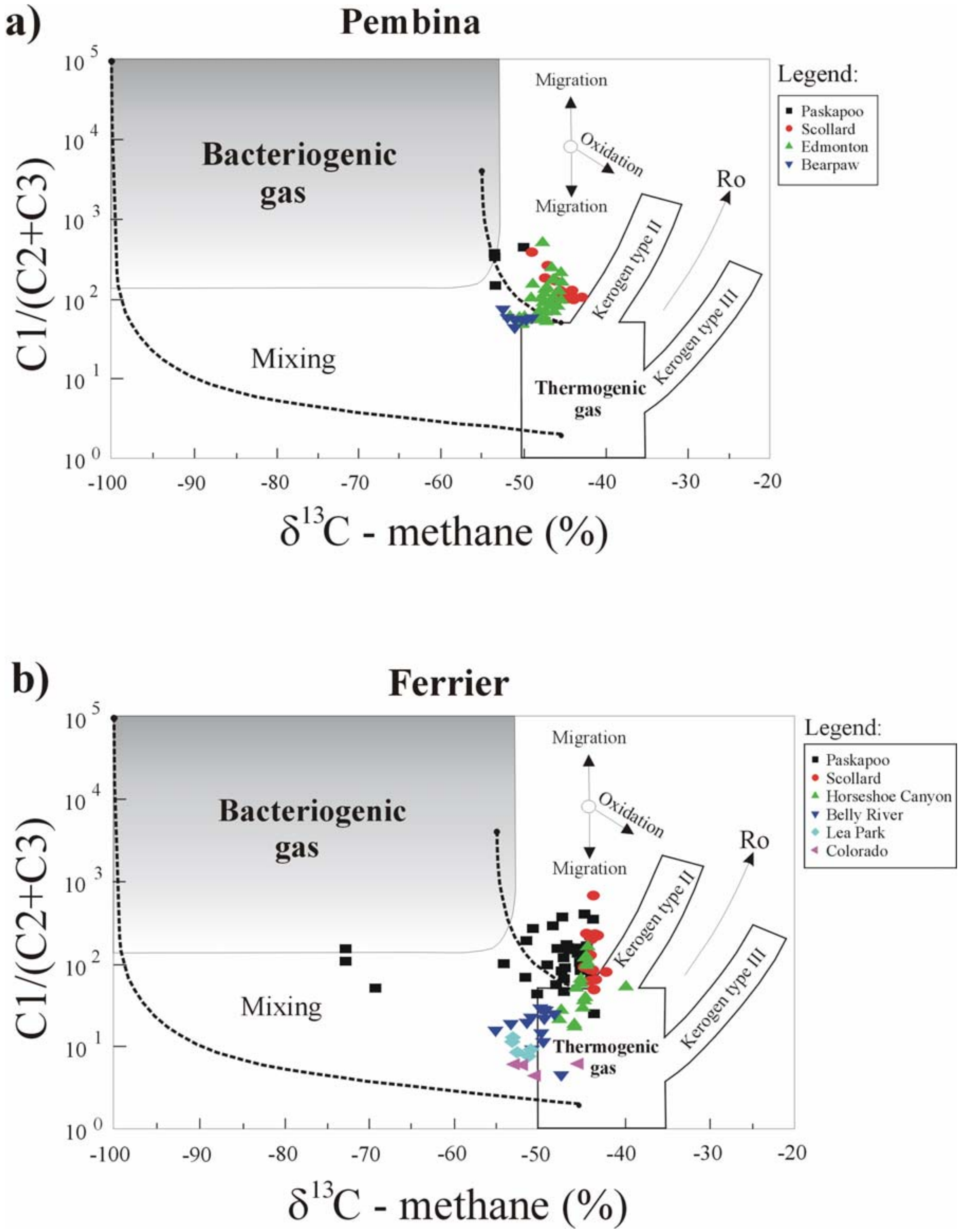

Figure 4-17 Bernard diagram showing the distribution of Cretaceous gases, west-central Alberta: a) Pembina 11-04-49-11W5, and b) Ferrier 14-03-42-9W5. Mixtures of bacterial and thermogenic gases appear to be developed in majority of Colorado, Lea Park and Belly River gases, with a strong migrational component for shallower gases: Paskapoo, Scollard, and Horseshoe Canyon gases.

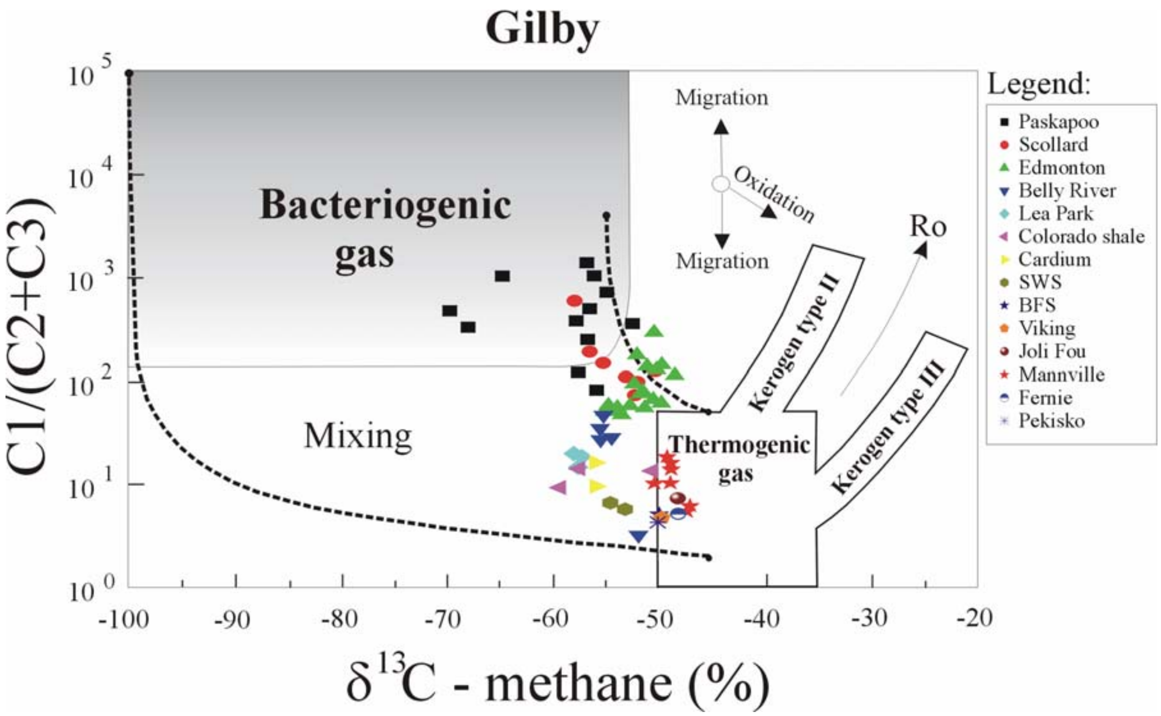

Figure 4-18 Bernard diagram showing the distribution of Cretaceous, and sub-Cretaceous gases for Gilby 15-16-42-4W5. Mixtures of bacterial and thermogenic gases appear to be developed in majority of Colorado, and post Colorado gases; Mannville and sub-Cretaceous gases display a strong thermogenic signature.

Applying the more rigorous genetic characterizations of gases as defined by Schoell (1983) confirms the possibility of mixing between thermogenic and biogenic gases. Figure 4-19 illustrates the distribution of Gilby mudgases on the Schoell $\delta^{13}C_{CH4}$ versus C_{2+} abundance diagram. As compared with the Bernard approach, this Schoell diagram indicates a number of Mannville gases that may have a degree of bacterial input. Three of the Mannville mudgases shown on this diagram fall into the region of overlap between the thermogenic oil-associated and the mixed thermogenic-biogenic fields. Contrary of how they fall on the Bernard diagram (where they fall within the mixing field), mudgases from the Second White Speck Formation (SWS) appear to be thermogenic oil-associated on the Schoell diagram.

The implication for this discrepancy will be discussed below.

As compared with the Bernard diagram, the Schoell diagram confirms the possibility of migration for the shallower gases from Horseshoe Canyon, Scollard and Paskapoo formations, for both Ferrier (Figure 4-20) and Pembina (Figure 4-21) locations.

The majority of the Horseshoe Canyon samples at Ferrier location (Figure 4-20) fall into the thermogenic oil-associated field, with a migrational component, as indicated on the Bernard diagram also. Only two Horseshoe Canyon samples indicate the possibility of bacterial gas mixture on the Schoell diagram, and these two samples are collected within the lowermost part of the Horseshoe Canyon Formation, towards the boundary with the Belly River Formation.

Comparison of the same data in the Bernard and Schoell diagrams in Figure 4-17b and Figure 4-20 respectively shows that a cross-plot of molecular versus carbon isotopic composition allows differentiation of gases of various origins. Specific problems of mixing and migration are more readily solved using the Schoell diagram – the plot of variations of molecular composition in natural gases versus the isotope variations in methane. For example, the Paskapoo, Scollard and Horseshoe Canyon mudgases can be recognized as migrated associated gases at Ferrier location (Figure 4-20) on such a Schoell diagram, whereas the compositional change in the molecular composition of these gases during migration does not indicate a precise genetic source of such migrated gases in the Bernard diagram (Figure 4-17b).

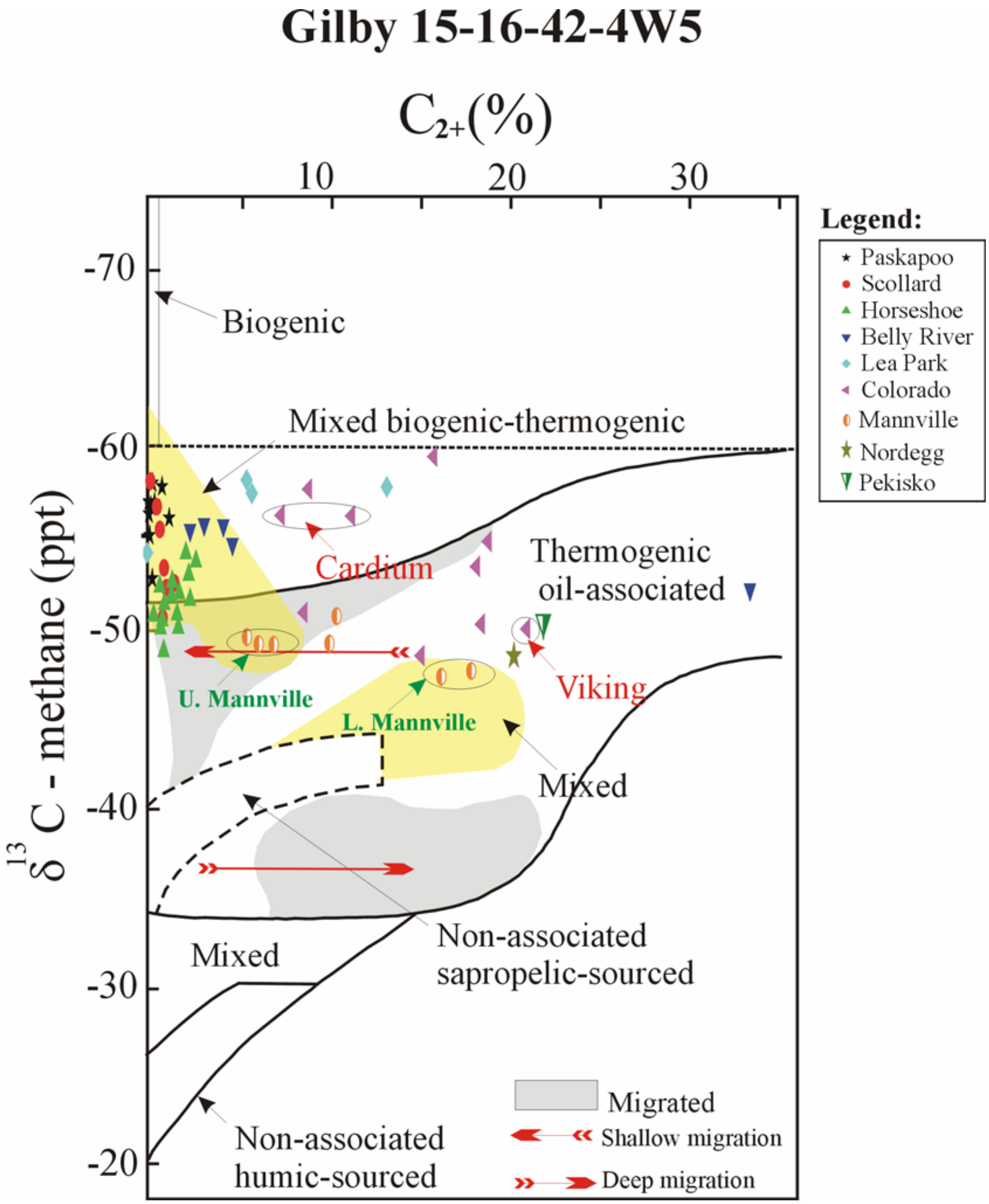

Figure 4-19 Distribution of Cretaceous mudgases relative to the genetic classification defined by Schoell (1983) on the basis of $\delta^{13}C$ of methane and the relative abundance of C2+ alkanes. Gilby 15-16-42-4W4, west-central Alberta.

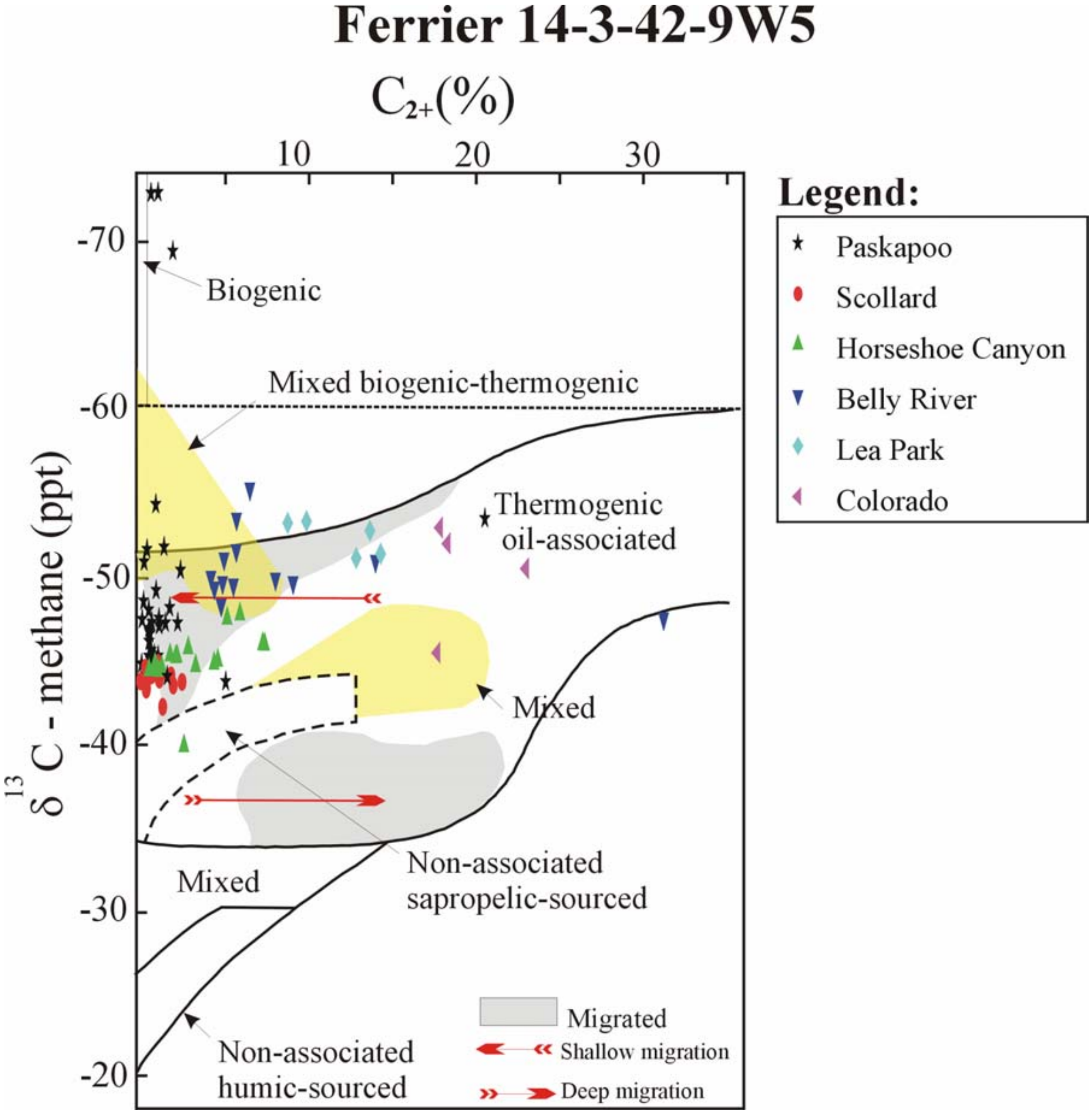

Figure 4-20 Distribution of Cretaceous mudgases relative to the genetic classification defined by Schoell (1983) on the basis of $\delta^{13}C$ of methane and the relative abundance of C2+ alkanes. Ferrier 14-3-42-9W5, west-central Alberta.

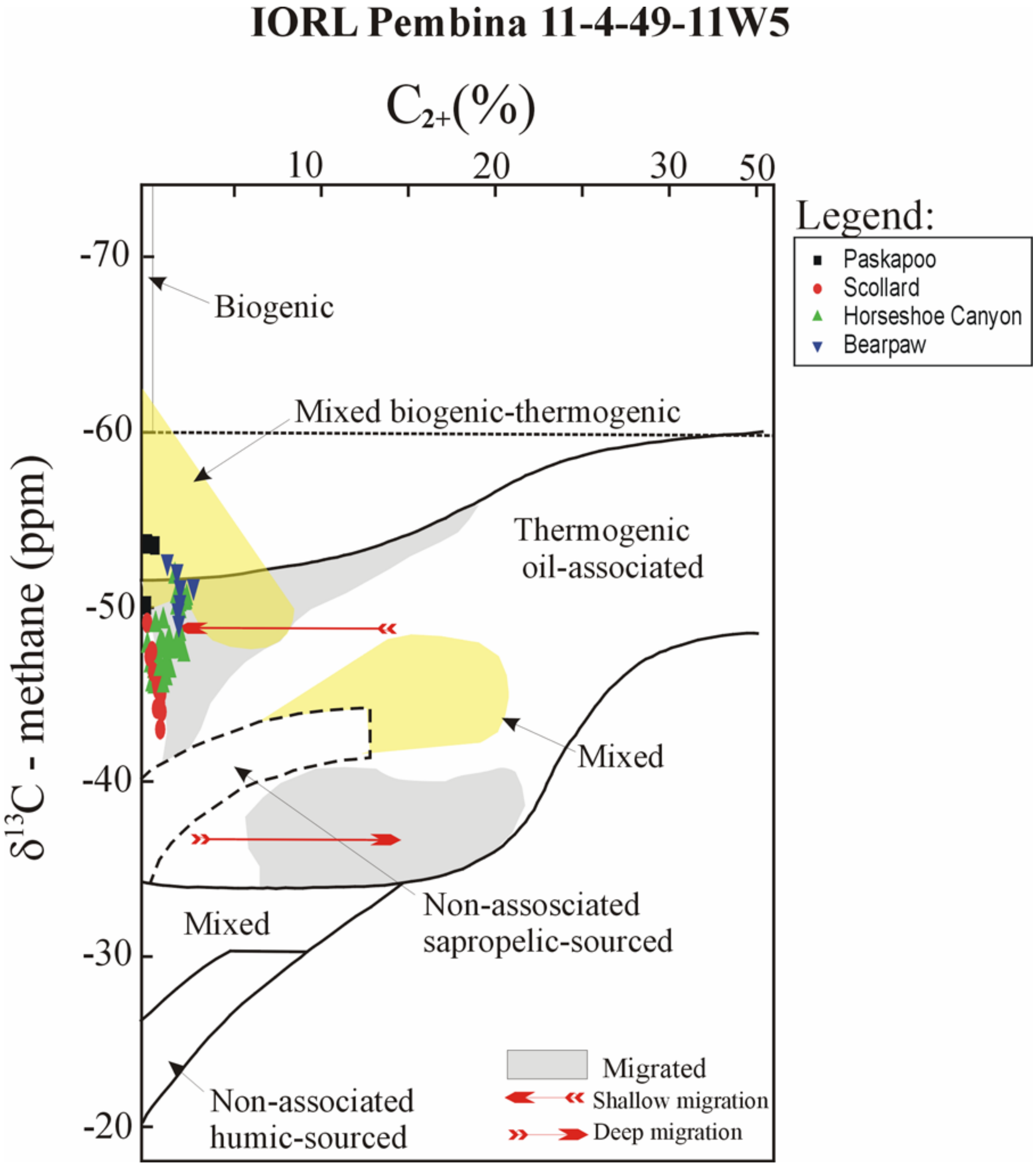

Figure 4-21 Distribution of Cretaceous mudgases relative to the genetic classification defined by Schoell (1983) on the basis of $\delta^{13}C$ of methane and the relative abundance of C2+ alkanes. Pembina 11-4-49-11W5, west-central Alberta.

Given the equivocal nature of some of the results obtained using the empirical range approaches of gas classification set forth by Bernard (1977), and Schoell (1983) the partition function approach described by James (1983) was applied to the data obtained in the present study. Figures 4-22 through 4-31 illustrate the distribution of isotopic data from Ferrier, Gilby and Pembina locations relative to the calculated isotopic separations of James (1983). As per the method described therein, data were moved across the diagram to produce the best fit possible relative to the calculated curves while maintaining isotope measured isotope separations. In cases where isotopic data for all species from C_1 to C_4 did not fit the curves precisely, an optimum fit between C_2H_6 (ethane) and C_3H_8 (propane) $\delta^{13}C$ values was selected. This is consistent with the recommendation of James (1983), who noted superior fit of empirical C_2-C_3 pairs from several localities to the calculated curves.

Placement of measured $\delta^{13}C$ values for Scollard – Horseshoe Canyon mudgases on a James diagram (Figure 4-22a) indicates that the maturity range over which these gases were generated extends from approximately 0.6 to ~1.2 vitrinite reflectance. This range falls within the oil generation window and is not entirely consistent with the present thermal maturity range observed for these rocks [Bustin (1991) indicates maturities lower than ~0.71%Ro for Campanian-Maastrichtian strata in this region]. Only the majority of the Horseshoe Canyon samples at Gilby location fall into a very low maturity range on James diagram, with vitrinite reflectance values of considerably less than 0.55% (Figure 4-24).

The majority of Belly River, Lea Park and Colorado mudgases contain methane that is considerably ^{13}C-depleted relative to the isotope composition predicted by the partition function model upon which the James diagram is based. This discrepancy is evidenced by the distribution of a number of methane data points above the line describing the predicted carbon isotopic composition of methane. Maturity estimates derived using the carbon isotope ratios of Colorado mudgases are also valid, with a resultant range of less than 0.7 to ~1.1 %vitrinite reflectance (Figure 4-30).

Some of the Paskapoo-Scollard, and even Horseshoe Canyon samples contain methane that is enriched relative to predicted isotope compositions – suggesting bacterial oxidation (Figures 4-22 to 4-25).

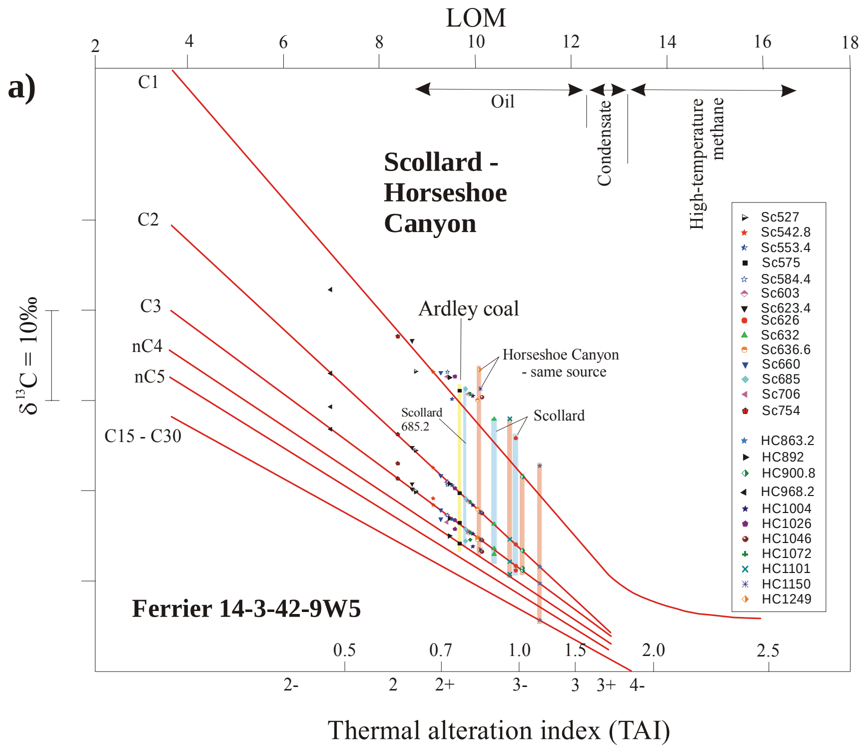

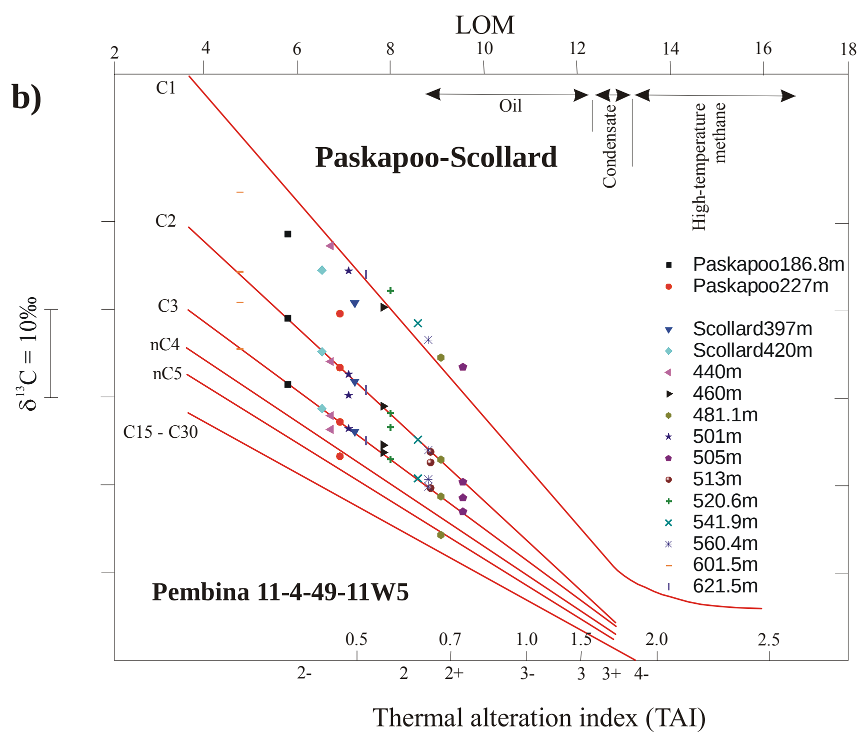

Figure 4-22 James diagram showing the distribution of the Paskapoo - Scollard mudgases (a), and Edmonton Group mudgases (b) - Gilby 15-16-42-9W5. Maturities less than 0.5 to approximately 1% vitrinite reflectance are indicated using optimal fit between the ethane - propane pair.

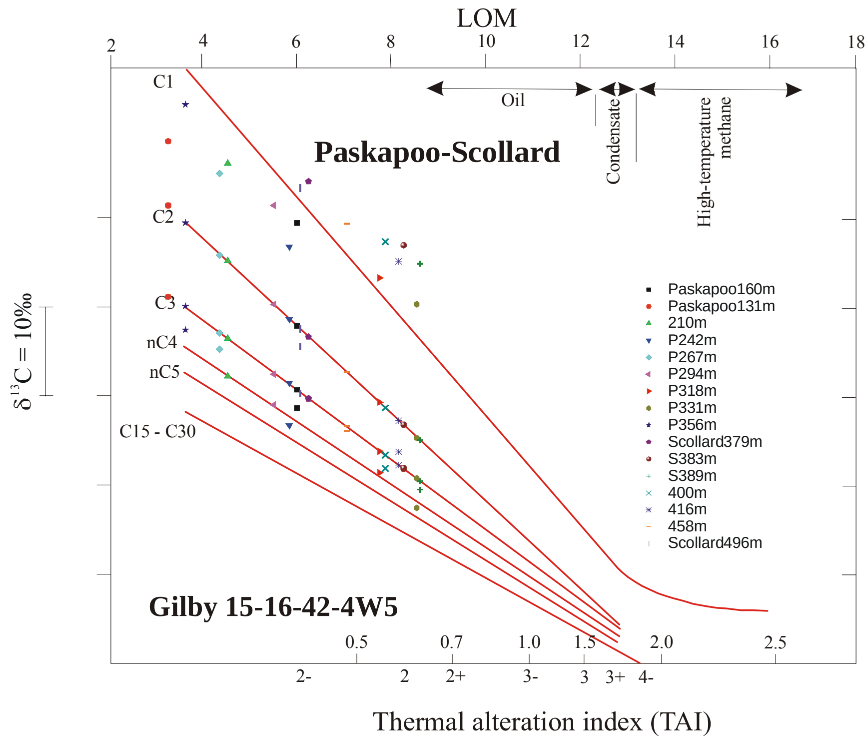

Figure 4-23 James diagram showing the distribution of the Paskapoo - Scollard mudgases for Gilby 15-16-42-9W5 profile. Maturities less than 0.6% vitrinite reflectance are indicated, and as well the possible bacterial oxidation of methane.

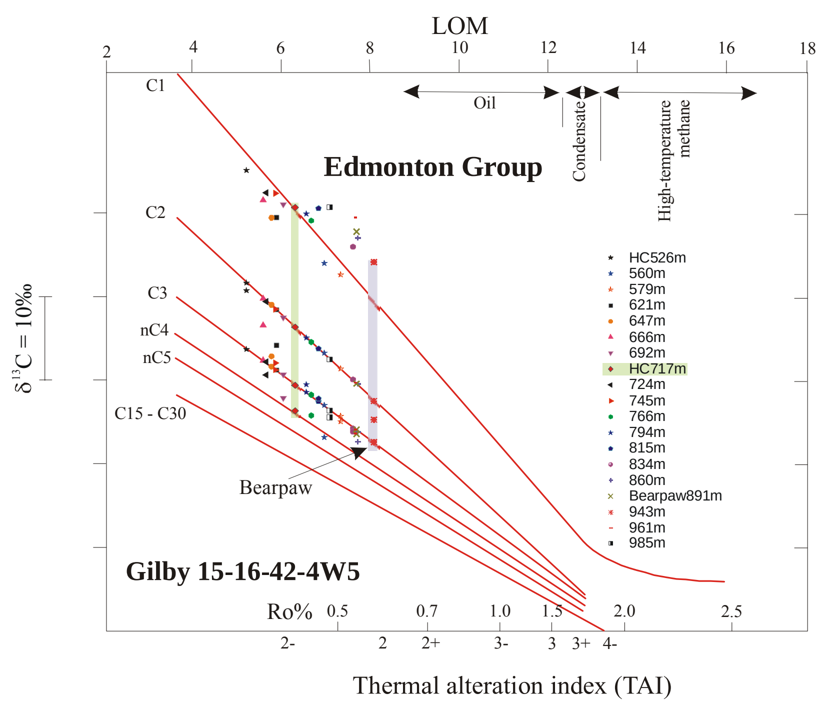

Figure 4-24 James diagram showing the distribution of the Horseshoe Canyon and Bearpaw mudgases for Gilby 15-16-42-9W5 profile. Isotopic separations indicate that the majority of these gases were generated at low levels of maturities.

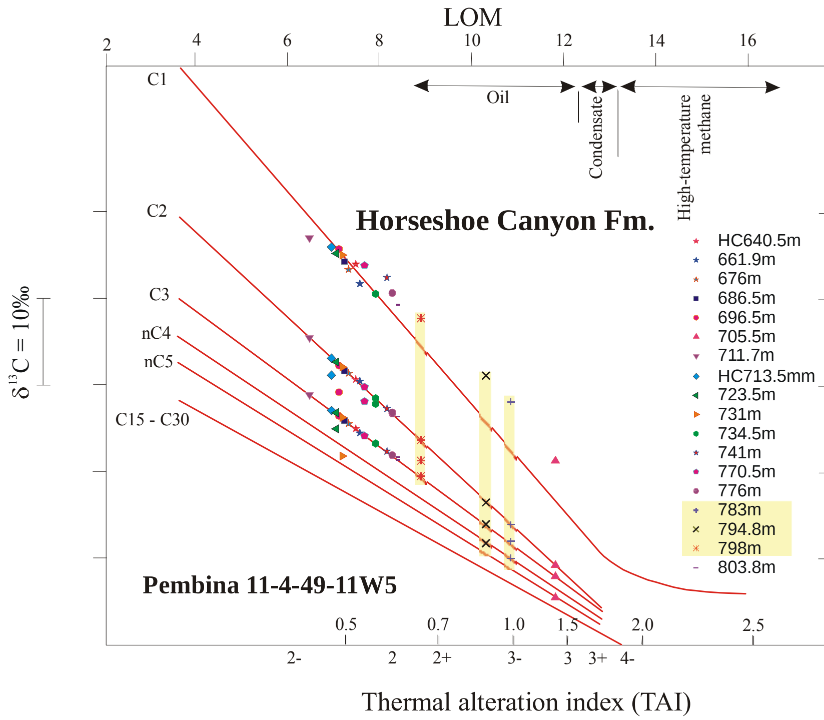

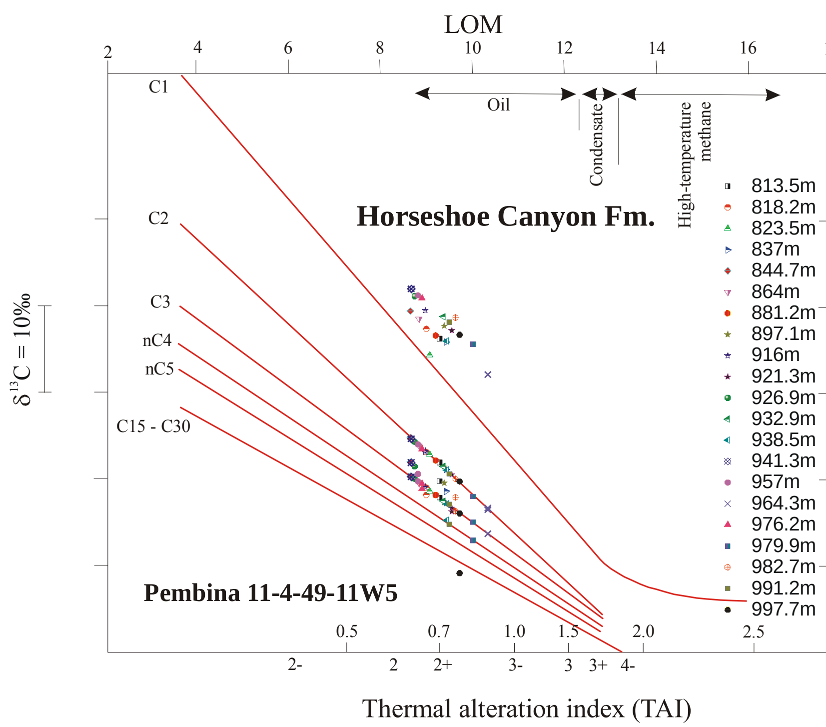

Figure 4-25 James diagram showing the distribution of the Horseshoe Canyon mudgases for Pembina 11-4-49-11W5 profile. Isotopic separations indicate gases were generated at LOM's of 6-12.

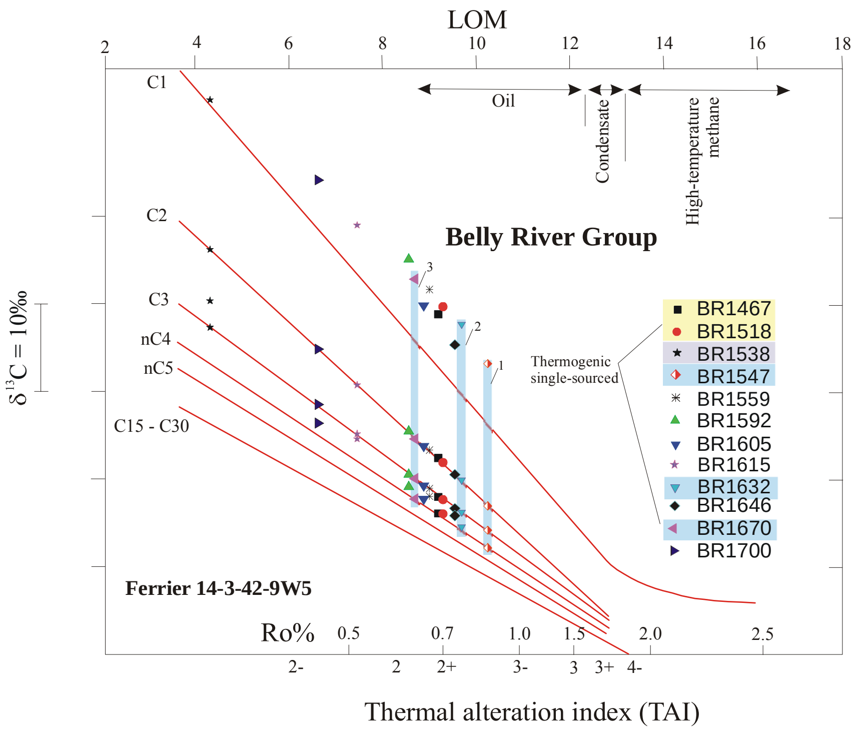

Figure 4-26 James diagram showing the distribution of the Belly River mudgases for Ferrier 14-3-42-4W5 profile. Majority of the gases were generated within the oil window; some of the gases indicate a thermogenic signature based on the optimal fit between the ethane, propane and butane.

In Figure 4-27 three Belly River gases are shown, to highlight their linear trends on a Chung diagram ("natural gas plot"). Slopes of $\delta^{13}C_{C2+}$ versus 1/n increase with depth indicating that the maturity of gases decrease with depth. The data are distributed such as the gas from 1547m depth is more mature than the gas from 1632m depth, and the gas from 1632m depth is more mature than the gas from 1670m depth. This relationship could be interpreted as being the result of a vertical and /or lateral migration process.

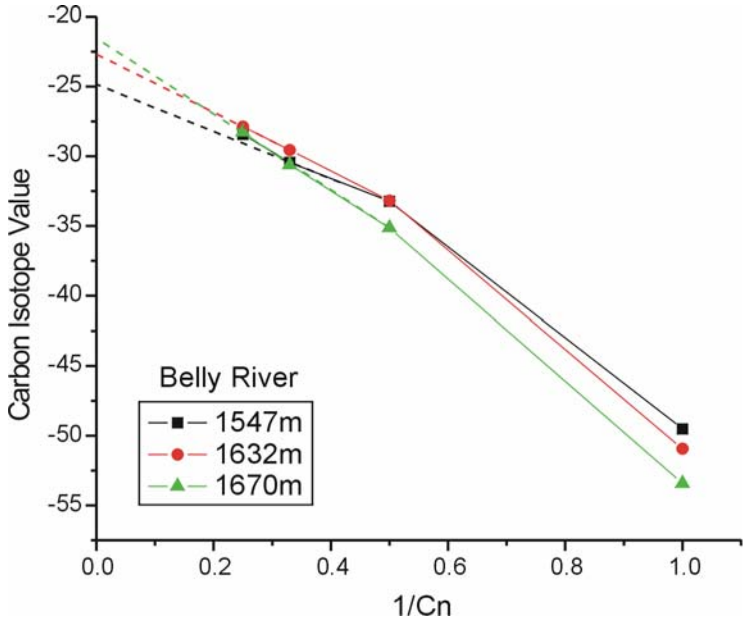

Figure 4-27 Natural gas plots for a selection of Belly River gas samples from the Ferrier 14-3-42-4W5 profile, showing linear relationships between isotope ratios and their inverse carbon numbers.

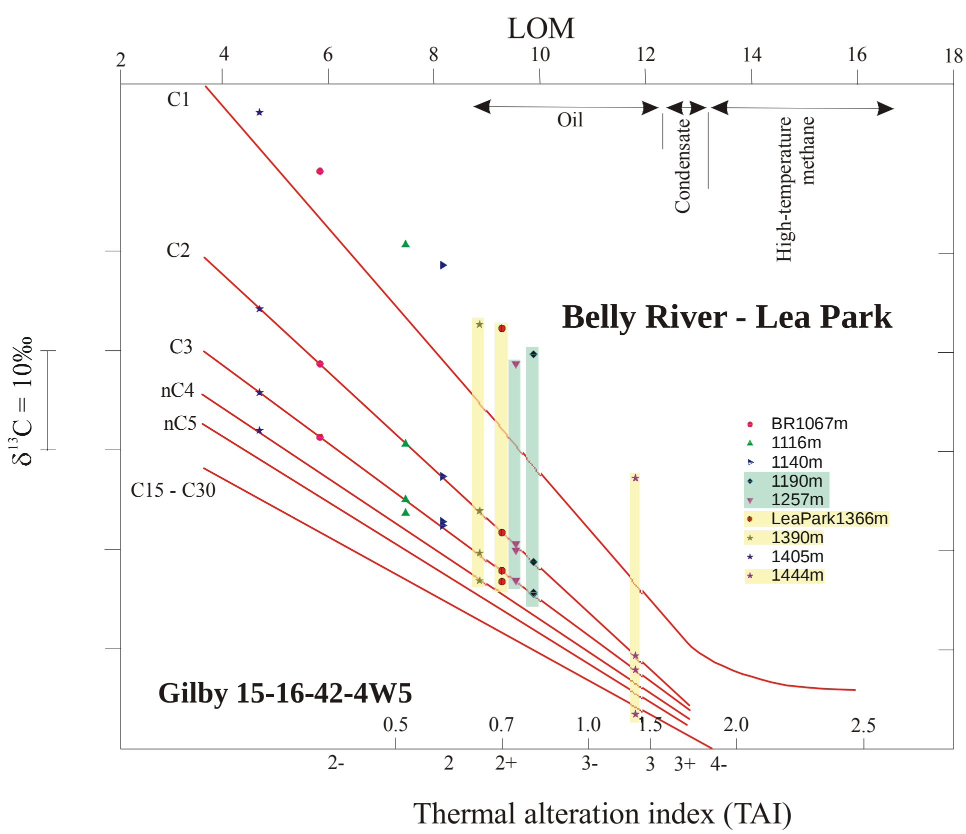

Figure 4-28 James diagram showing the distribution of the Belly River – Lea Park mudgases for Gilby 15-16-42-9W5 profile. Isotopic separations between gas components indicate a wide range of maturities, from less than 5 LOM and up to 12 LOM.

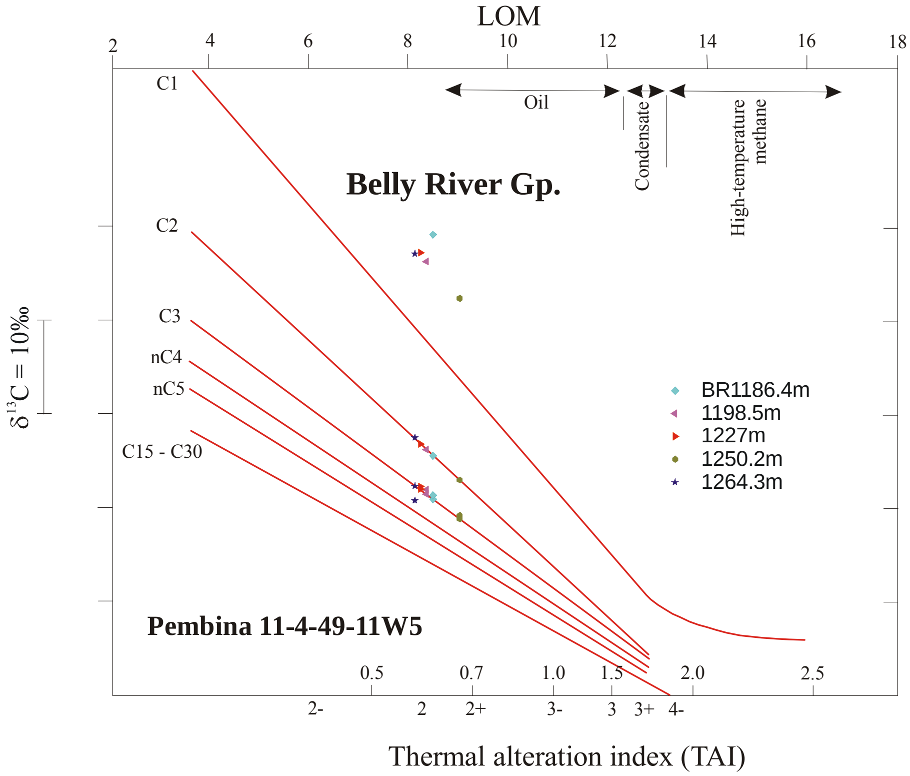

Figure 4-29 James diagram showing the distribution of the Belly River mudgases for Pembina 11-4-49-11W5 profile. Maturities higher than 0.5 to approximately 0.7% vitrinite reflectance are indicated using optimal fit between the ethane-propane pair.

Mannville samples also provide a reasonable fit to the James diagram (Figure 4-31), indicating a maturity range of 0.7 to ~1% vitrinite reflectance for generation of the majority of samples. In all Mannville gases methane is ^{13}C-depleted relative to the composition predicted by the partition functions, and isotopic reversals are observed between propane δ^{13}C and n-butane δ^{13}C values.

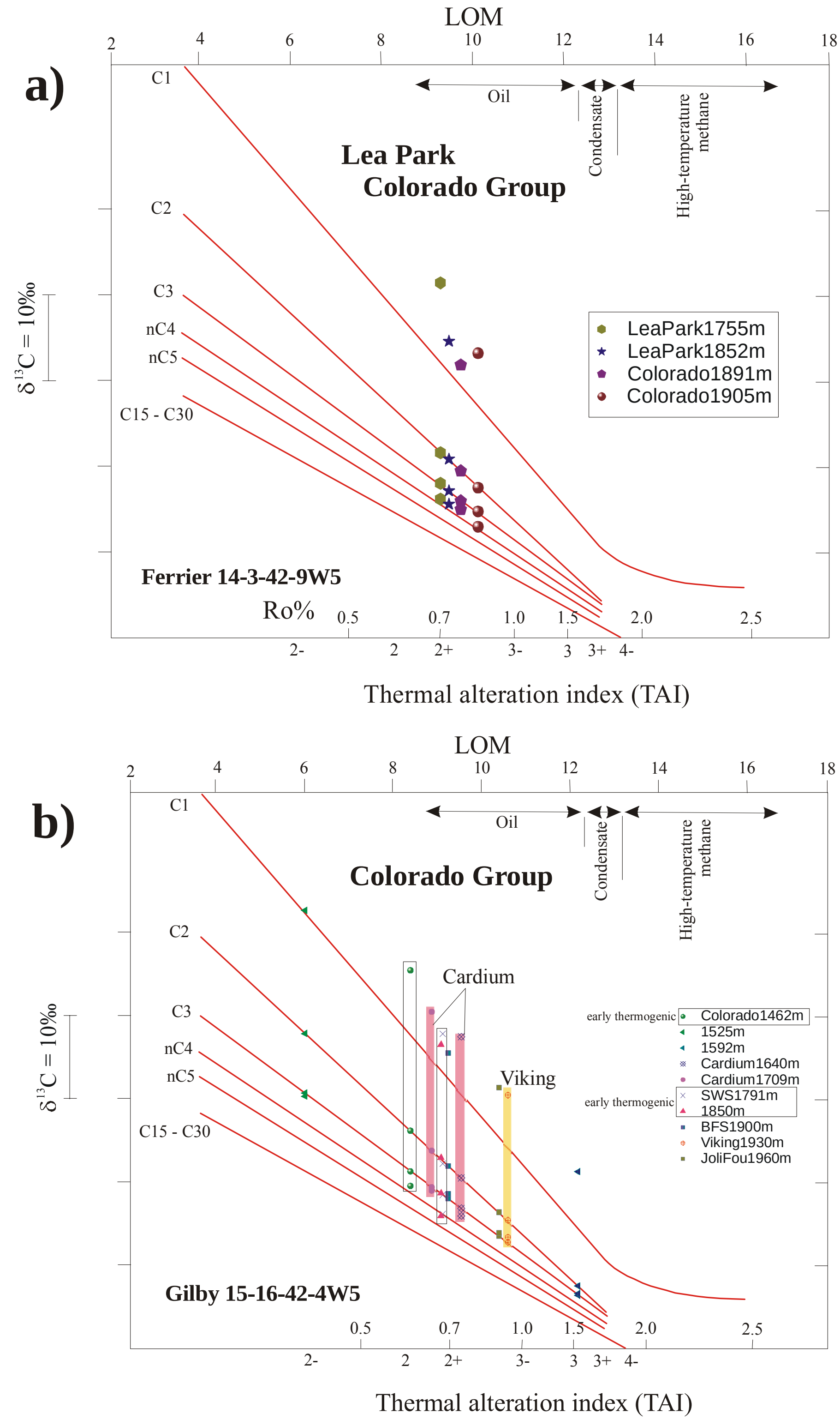

Figure 4-30 James diagram showing the distribution of the Colorado mudgases (a) Ferrier 14-3 - 42-9W4, and (b) - Gilby 15-16-42-9W5. Maturities ranging from 6 LOM to 12 LOM are indicated using optimal fit between the ethane-propane pair.

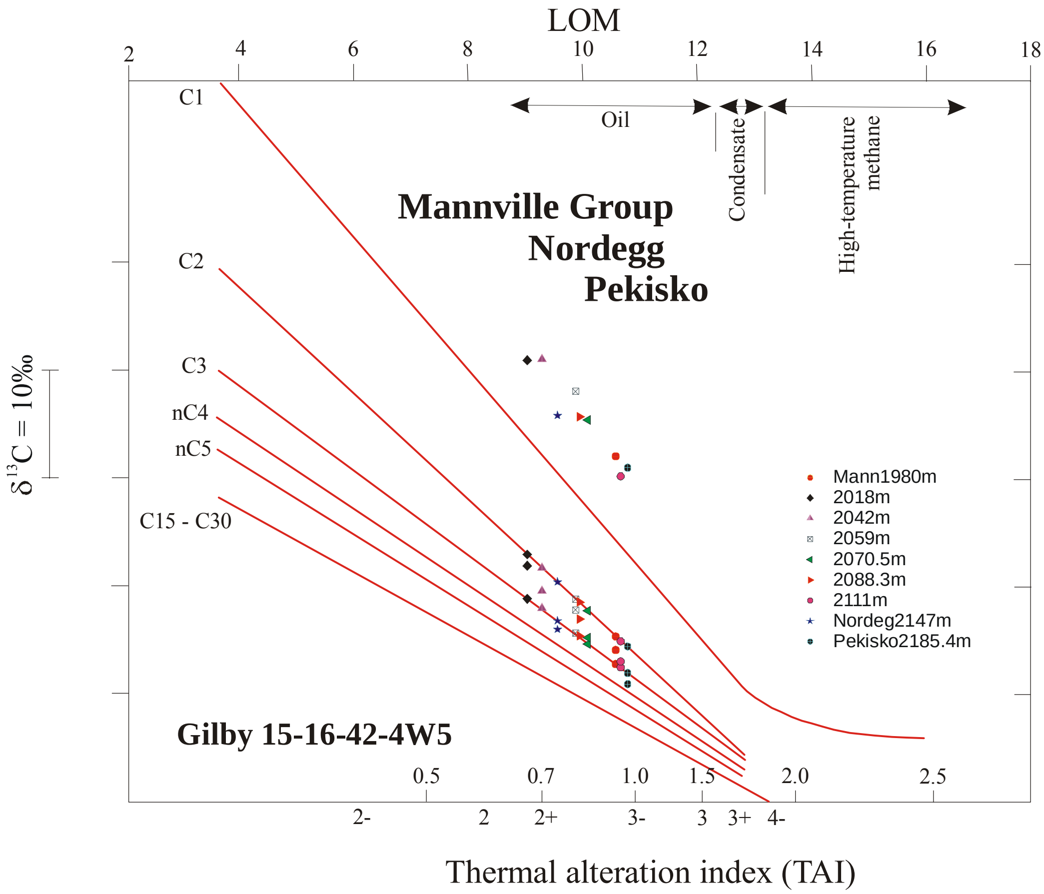

Figure 4-31 James diagram showing the distribution of Mannville, Fernie and Pekisko mudgases on the Gilby 15-16-42-9W5 profile. As indicated by the isotopic separations between gas components, these gases were generated within the oil window.

4.2.4. Discussion

The overall westward increase (from Gilby to Ferrier location) in the proportion of methane, as well as the total abundance of the light hydrocarbons (C_1 to C_4) might be attributable to one of two processes, either migration and/or mixing. In both scenarios, the observed wetness index highs in the Ferrier location are believed to be indicative of active thermogenic gas generation. This contention is supported by both the compositional and isotopic data reported in the present study. For example, methane $\delta^{13}C$ data for Scollard, Horseshoe Canyon, Belly River, and Lea Park formations, as well as for Colorado Group are indicative of a thermogenic origin for methane in the western part of the Foothills study area. As indicated in Figures 4-12 and 4-15, methane sampled in this part of the study area has the most ^{13}C- enriched isotopic composition, relative to the remainder of the study area (at the only two available locations, at Gilby and Pembina), with $\delta^{13}C$ values of > -40‰ in the Horseshoe Canyon Formation (Ferrier), >-42‰ in the Scollard Formation (Ferrier), >43‰ in the Scollard Formation (Pembina). The distribution of these gases on the Bernard and Schoell diagrams indicates that a thermogenic source is likely for these gases. Gilby mudgases have methane $\delta^{13}C$ values of > -48‰.

Schoell diagrams for the Ferrier and Pembina mudgases (Figure 4-20 and Figure 4-21) indicate that the majority of the gases from Scollard, Horseshoe Canyon, and Belly River formations were generated in conjunction with liquid hydrocarbons in the oil-window of source maturity. This result is also supported by the application of the James (1983) partition approach, which also indicates generation of these gases in the oil window (see Figures 4-22, 4-25, 4-26 and 4-29).

Maturities estimated by use of the James diagram are not entirely consistent with present-day maturities of the foreland basin strata reported by Bustin (1991) in the study area. For example, Ferrier mudgases from Paskapoo, Scollard and Horseshoe Canyon formations indicate a much higher level of thermal maturity than that of the present-day.

This disagreement between estimated and reported source maturities lends further confidence to the argument that gas migration is an existing process at least through the uppermost part of the foreland basin succession. Suitable source maturities and higher organic matter contents are present in the foreland-basin petroleum source rocks in the area – Fernie Group shales, Mannville Group coals and shales, Colorado Group shales, and post Colorado shales and coals – thus suggesting that gases are likely sourced internally within the interval of interest in the present study and that vertical or horizontal migration of hydrocarbons from underlying strata need to be invoked.

Depth-related variation in the carbon isotopic signatures of light hydrocarbons (C_1 to C_3) for Ferrier and Gilby profiles parallel the increase in source maturity depicted in Figure 4-32 (Bustin, 1991), whereby both source maturity and the $\delta^{13}C$ values increase westward (from Gilby to Ferrier location). This likely indicates a causative relationship between the two parameters, in which the isotopically heavier hydrocarbons are generated at greater source maturities. As previously discussed and illustrated in the

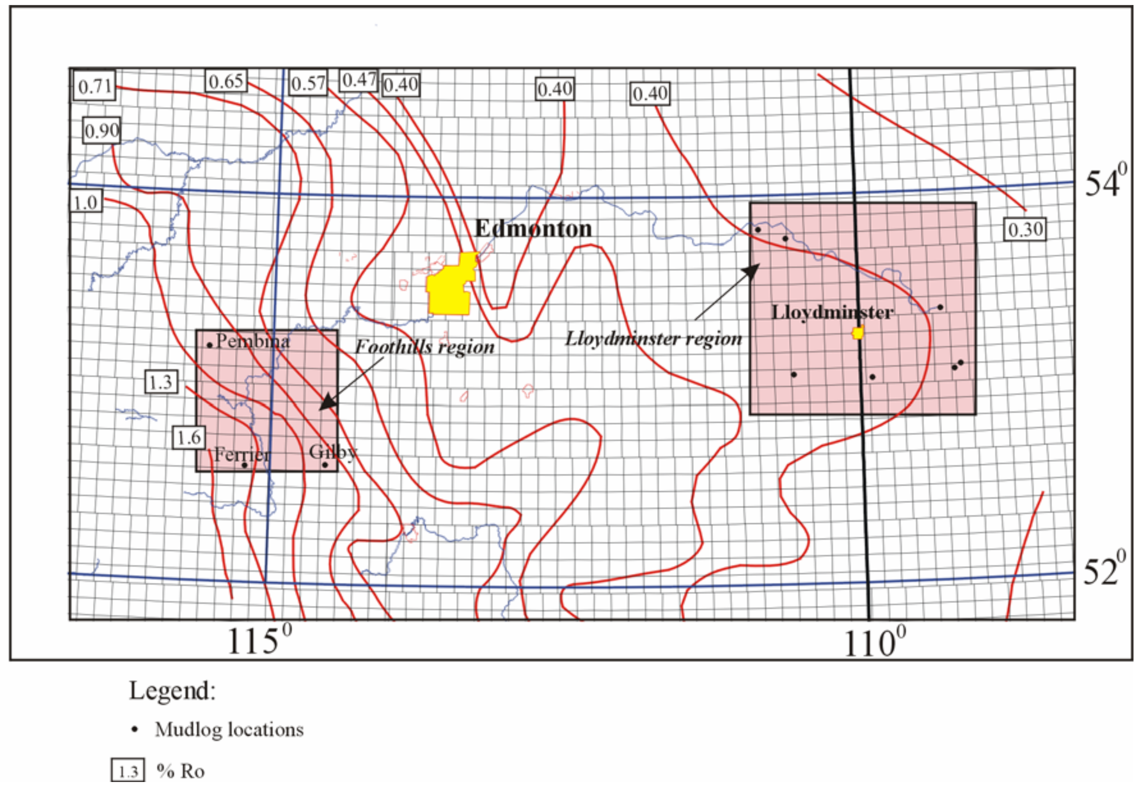

Figure 4-32 The overall organic maturity trend in the central part of the Alberta basin for Mannville strata. The values for the mean maximum vitrinite reflectance are from isomaturity maps of Bustin (1991).

James diagram (Figure 4-6), gases generated at increased source maturities are characterized by preferential incorporation of the heavier isotope. Given the relatively small temperature gradient observed for the strata of interest, it is likely that this progressive enrichment ^{13}C westward is not attributable to temperature effects on the degree of isotopic fractionation. Rather, a more reasonable explanation is that progressive ^{13}C enrichment is a consequence of a Rayleigh distillation effect, whereby preferential generation of ^{12}C-enriched hydrocarbons during early stages of maturation leaves the residual organic matter ^{13}C-enriched, and imparts a heavier isotopic composition in later-generated gas (Clayton, 1990; Whiticar, 1999). This carbon isotope mass balance is commonly described by the distillations functions of Rayleigh (1896).

A plot of propane $\delta^{13}C$ versus ethane $\delta^{13}C$ suggests also that gases from Ferrier field are generated at higher levels of maturity than gases from Gilby field (Figure 4-33).

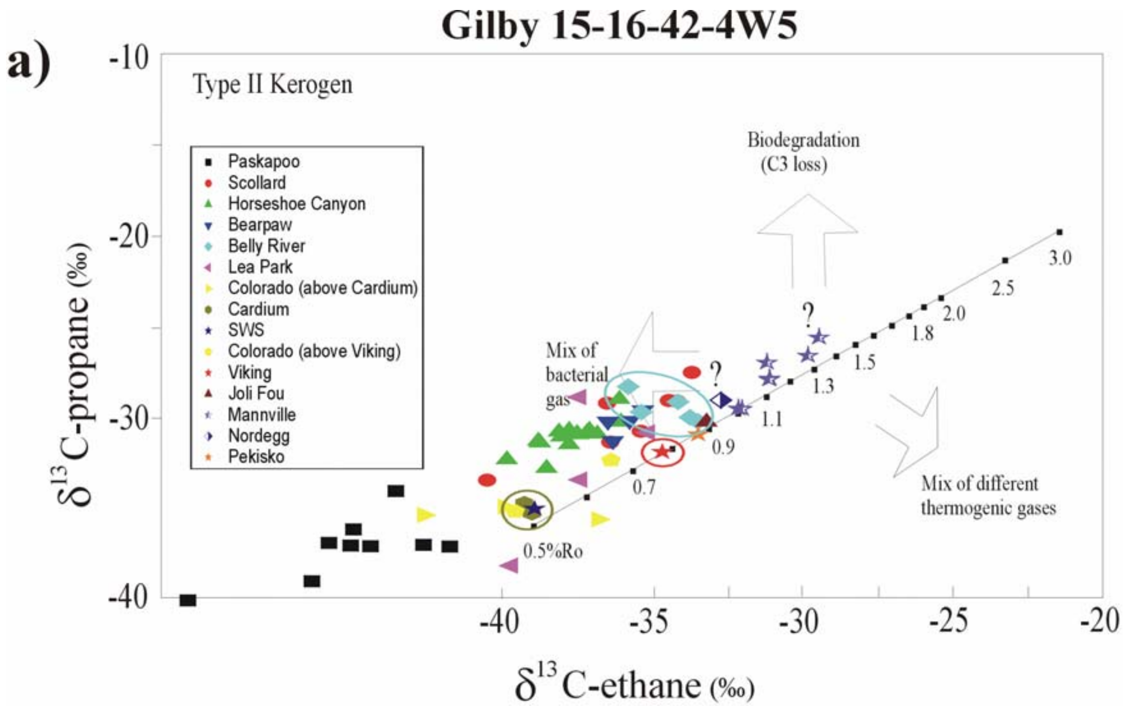

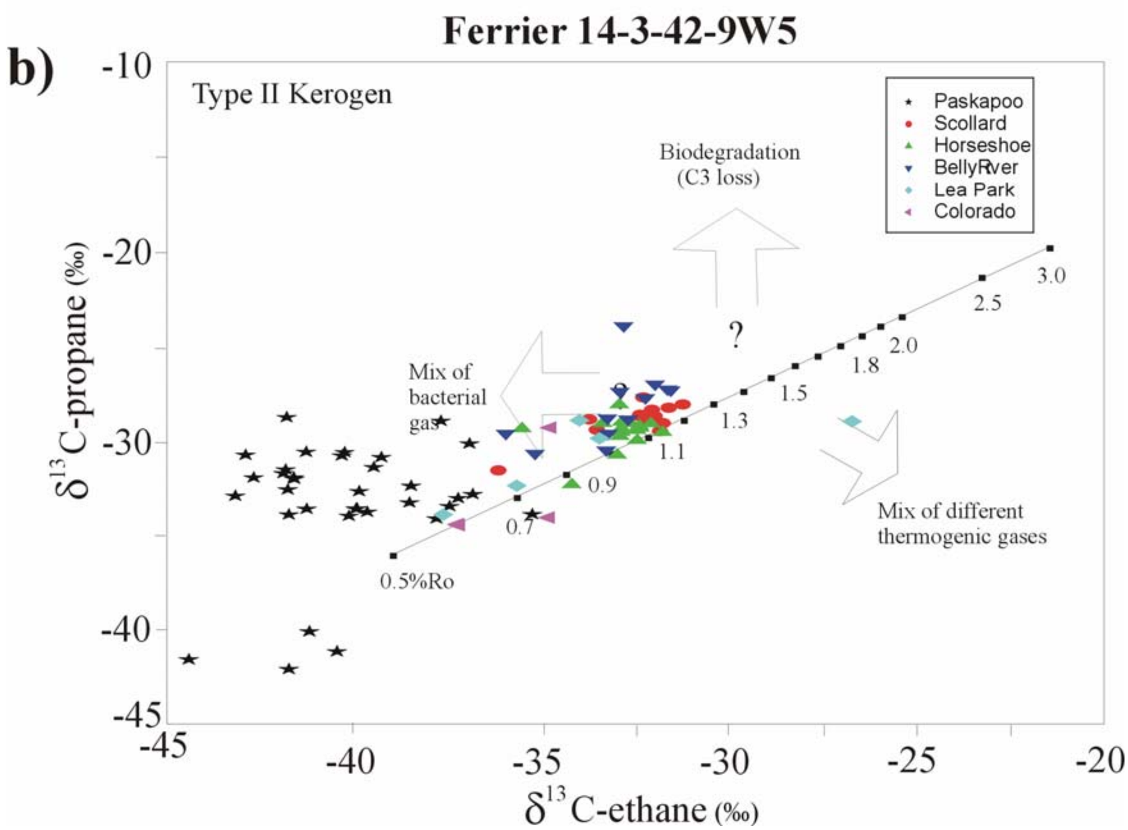

Figure 4-33 Stable carbon isotope ratios for co-genetic ethane and propane in mudgases from (a) Ferrier and (b) Gilby (After Faber, 1987; Whiticar, 1990.)

Moreover, since the ethane and propane concentrations decrease with increasing maturation of the organic precursors (Berner and Faber, 1987), this parameter observed at both Ferrier, and Gilby profiles support higher level of maturity for gases generated at Ferrier location (Figure 4-34 and 4-35).

Another explanation for the more positive wet-gas components at Ferrier location would probably be the different carbon isotopic composition of the source rocks, these sources being enriched in ^{13}C relative to the those related to Gilby profile (Rayleigh distillation processes).

Highly mature gases become dry (due to cracking of the C_{2+} compounds) and, depending on the source, have δ values of -40 to -30‰ (for associated gas and nonassociated gas of sapropelic-liptinitic origin) and of -30 to -20‰ (for nonassociated gas of humic origin). With the exception of few Paskapoo samples, all the mudgases sampled within the Foothills region have methane $\delta^{13}C$ values in the range of -40‰ to – 58‰, indicating relatively mature sources and/or kerogen type III sources (University of Alberta database).

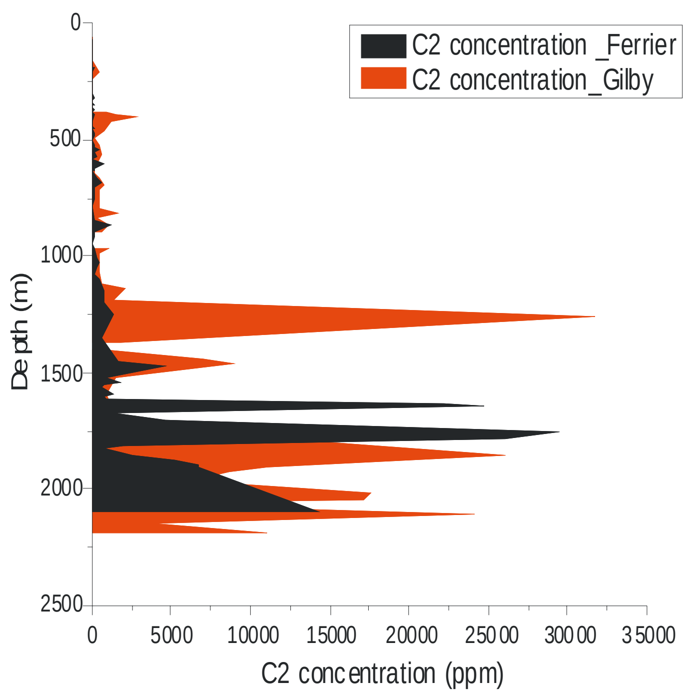

Figure 4-34 The relative ethane concentration plotted against depth for mudgases from Ferrier and Gilby.

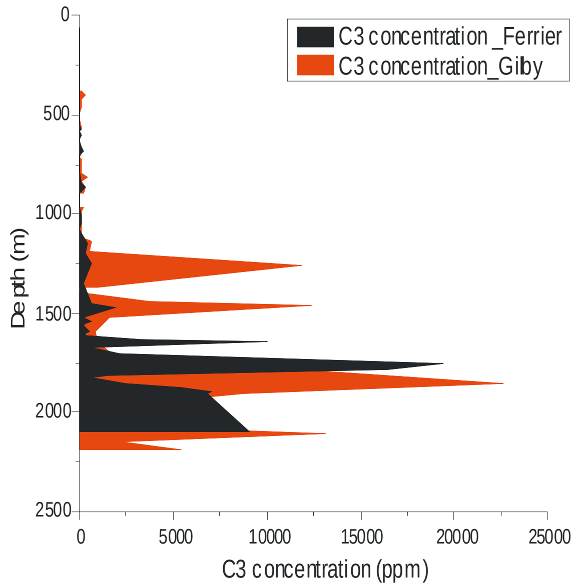

Figure 4-35 The relative propane concentration plotted against depth for mudgases from Ferrier and Gilby.

4.3. Results – Lloydminster region

4.3.1. Compositional variations

Measured compositional data for mudgases sampled within the Lloydminster region, as well as the isotopic concentration data of C_1 to C_5 alkanes were acquired from the University of Alberta database. Gases were collected from drilling mud while drilling the following wells:

1. Petrovera 00/01-25-055-05W4-0
2. Husky C0/03-30-047-04W4-0
3. Husky 11/09-15-051-23W3-0
4. Lindbergh 00/13-09-056-06W4-0
5. Petrovera 11/10-17-047-27W3-1
6. Petrovera 1A1-04-048-22W3-0
7. Petrovera 11/09-30-047-22W3-1

The hydrocarbon gases within the Lloydminster region include mainly methane, ethane and heavier hydrocarbons (including iso-, and n-pentane). The heavy hydrocarbon gases (C_{2+}) range from less than 1% (the bulk majority) to more than 18% by volume (University of Alberta database).

The wettest gases are developed within the marine shales of the Cummings Formation – at Husky C3-30-47-4W4, at the Wildmere field. In the Cummings Formation, the percentage of C_{2+} alkanes varies from 13.10% to 18.19% (Figure 4-36). Consequently, methane concentration varies between 81.80% and 86.89%, and the wetness index varies between 0.13 and 0.18, respectively.

The overall methane content varies between 81.80% (Husky Wildmere) and 99.86% (Petrovera Golden Lakes). Only 11 samples however, were found with methane content less than 95%. Majority of the mudgases, in the entire Cretaceous section are characterized by an excessive dryness, with more than 96% methane.

The wetness index varies from 0.0013 (Lea Park Formation, Petrovera Golden Lakes 1-4-48-22W3) to 0.18 (Cumming shales, Husky 3C-30-47-4W4).

Other wet gases are found within the sandstone bodies of the Lower Mannville Group (GP, Rex, Lloydminster) at Husky C3-30-47-4W4, Lindbergh 13A-9-56-6W4, and Petrovera 1D-25-55-5W4. Here, the methane percentage varies between 90.96% and 96.75%.

The spatial and in depth variation in wetness index within the three main stratigraphical units in this study area is summarized in Figure 4-36.

The driest gases are developed at a very shallow depths - at both Husky C3-30-47-4W4, in the Wildmere field, and Petrovera 1-4-48- 22W3 (Golden Lakes) – within the Lea Park Formation. The methane percentage varies between 99.83% and 99.86%. The wetness index of these shallow gases varies between 0.0013 and 0.0016 (Figure 4-36).
Other formations with a high methane concentration are found also at the two mentioned locations – in the southern part of the study area:

- within the Westgate shales (366.2m depth and 369.2m depth - Petrovera 1-4-48-22W3), above the Viking Formation;
- within the basal shoreline sand of the Basal Belly River Formation (106m depth - Husky C3-30-47-4W4)

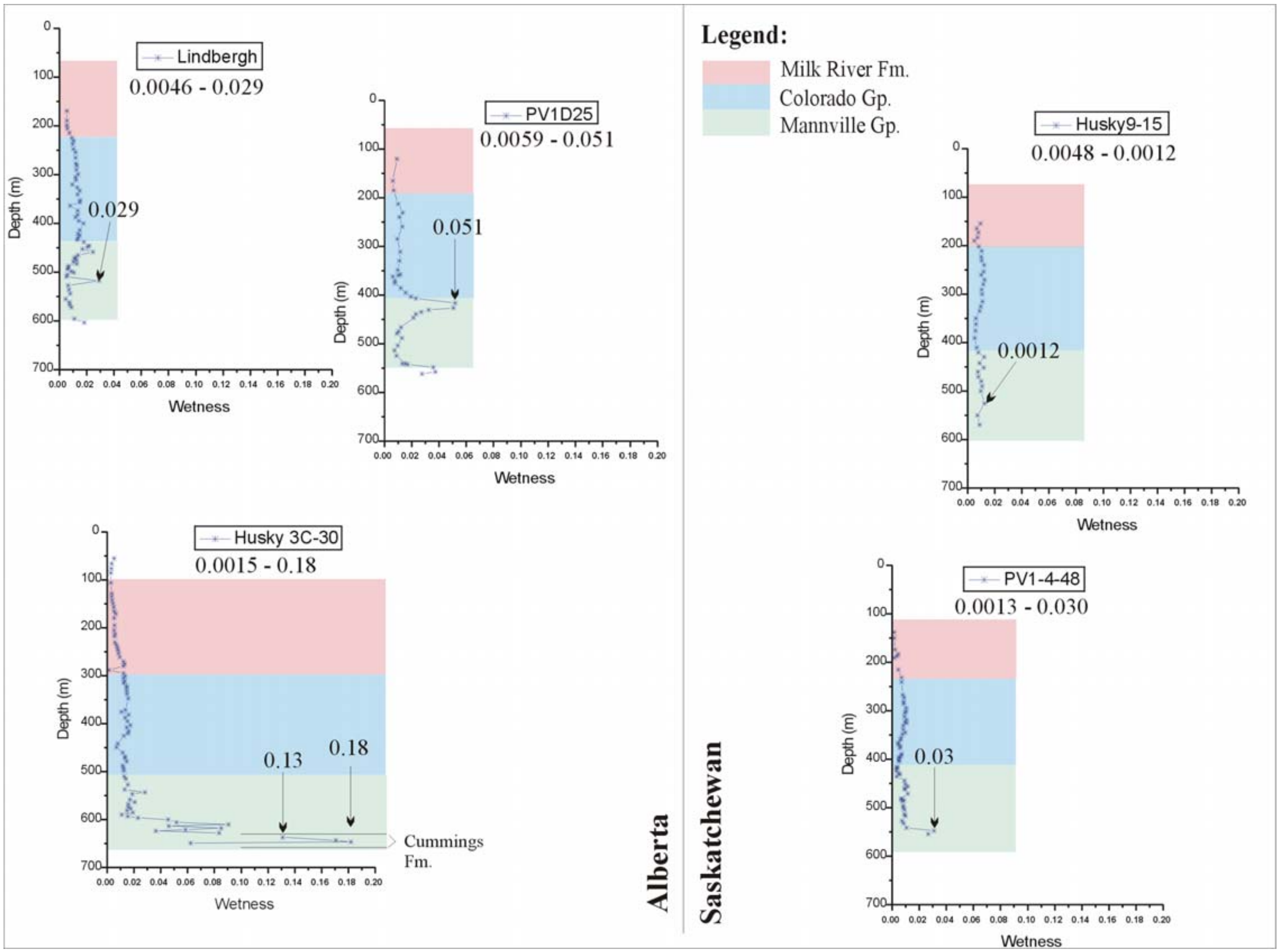

Figure 4-36 In depth and spatial distribution for the wetness index - Heavy oil region, east-central Alberta and west-central Saskatchewan.

- within some of the Upper Mannville sandstone bodies (419.6m, 435.4m - Petrovera 1-4-48- 22W3)
- within the Spinney Hill Sandstone (99.47% - 99.50% methane - Petrovera 1-4-48-22W3)

4.3.2. $\delta^{13}C$ variations

Isotopic depth profiles from across the heavy oil study area reveal a marked difference in the isotopic signature of gases contained within the two major stratigraphic units: Mannville and Colorado groups. $\delta^{13}C$ values of ethane indicate that the Colorado ($\delta^{13}C_2$ = -53.05 to –31.37‰) and Mannville groups ($\delta^{13}C_2$ = -45.55 to –20.47‰) contain, with few exceptions, two very different types of gases. This contrasting isotopic composition is also revealed on a plot of propane $\delta^{13}C$ versus ethane $\delta^{13}C$ for each isotopic depth profile within the heavy oil region (Figure 4-37).

Gases from each of the Mannville formations were found to have a wide range of stable carbon isotopic composition:

- $\delta^{13}C_{C1}$ from –52.83‰ to –77.97‰;
- $\delta^{13}C_{C2}$ from –20.47‰ to – 45.55‰;
- $\delta^{13}C_{C3}$ from –14.91‰ to –38.58‰;
- $\delta^{13}C_{nC4}$ from –17.87‰ to –36.53‰.

For Colorado Group $\delta^{13}C_{C1}$ values range from -54‰ to –69.46‰, $\delta^{13}C_{C2}$ values range from –31.37‰ to –53.05‰ and $\delta^{13}C_{C3}$ values range from –26.52‰ to –42.68‰.

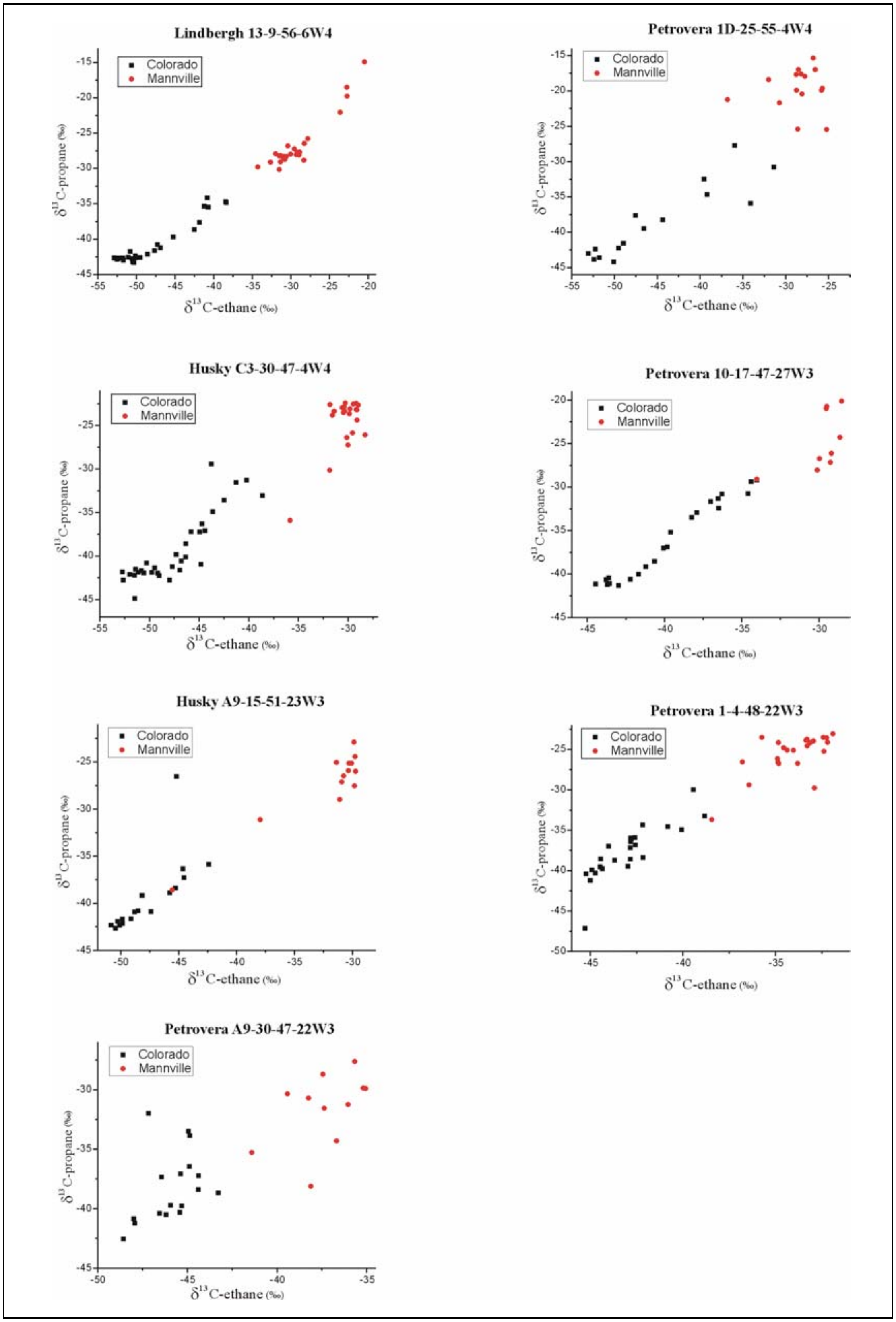

Figure 4-37 Plots of propane δ^{13}C versus ethane δ^{13}C for Colorado and Mannville gases in the heavy oil region.

4.3.3. Combination of gas composition and stable carbon isotope ratios

As for the Foothills mudgases, a relatively simple method of gas typing relies on the composition of gases with the fields defined by Bernard (1977). Figures 4-38 through 4-42 illustrate the distribution of Cretaceous mudgases collected in the heavy-oil region on such Bernard diagrams. As it is evident from these distributions, the majority of mudgases fall into the mixed gas field, with some of the Lower Mannville (Figure 4-39), Colorado shales (Figures 4-40, 4-41, 4-42), Viking (Figures 4-39, 4-42), Upper Mannville (Figure 4-42), and Lea Park (Figures 4-38 through 4-42) samples lying on the border between the thermogenic-, and mixed gas fields on the basis of their relatively ^{13}C-depleted carbon isotope ratios.

The occurrence of the majority of the mudgas samples in the mixing field is attributable to relatively ^{13}C–depleted methane, as well as to higher Bernard parameter values.

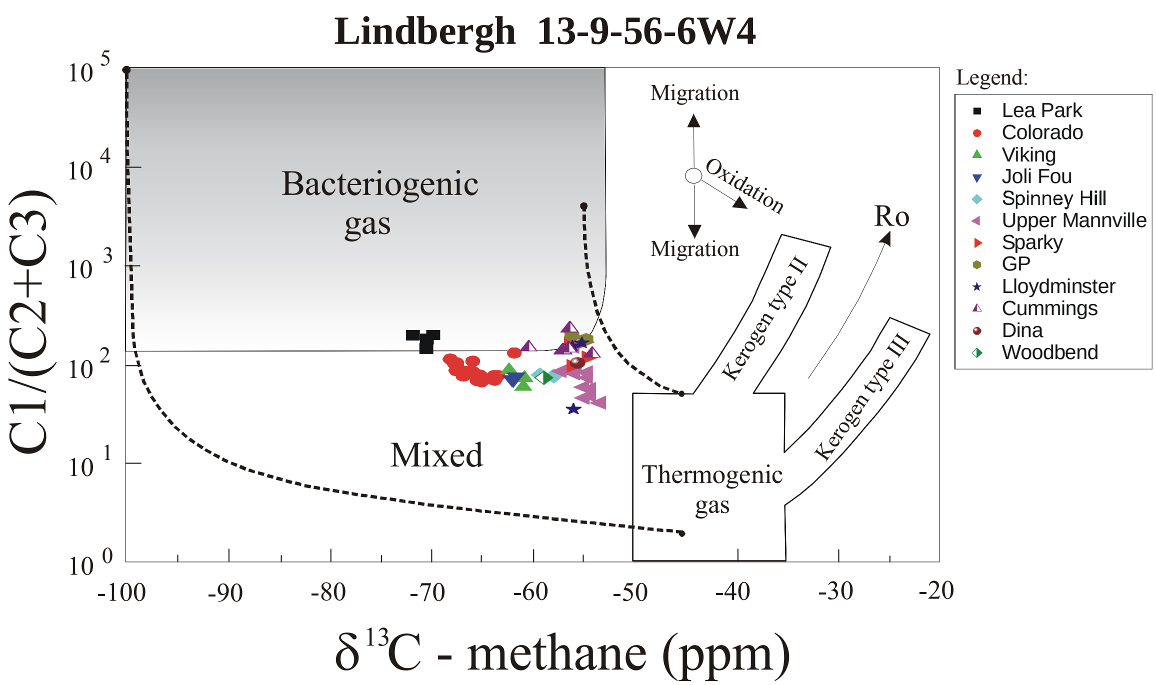

Figure 4-38 Bernard diagram showing the distribution of Cretaceous gases at Lindbergh 13-9-56-6W4 location, heavy oil region. Mixtures of bacterial and thermogenic gases appear to be developed in majority of the mudgases.

The majority of the post-Colorado samples (Lea Park Formation) collected throughout the Lloydminster heavy oil region, occur within the biogenic gas range – as indicated on Bernard diagrams.

The Bernard approach for characterizing mudgases emphasizes a higher degree to which bacterial gas input is contributing to mudgases sampled in the eastern part of the study area: Petrovera 1-4-48-22W3 and Husky 9-15-51-23W3. As can be observed in Figure 4-42, with the exception of the Dina samples, most of the other mudgases are strongly shifted towards the bacterial gas field.

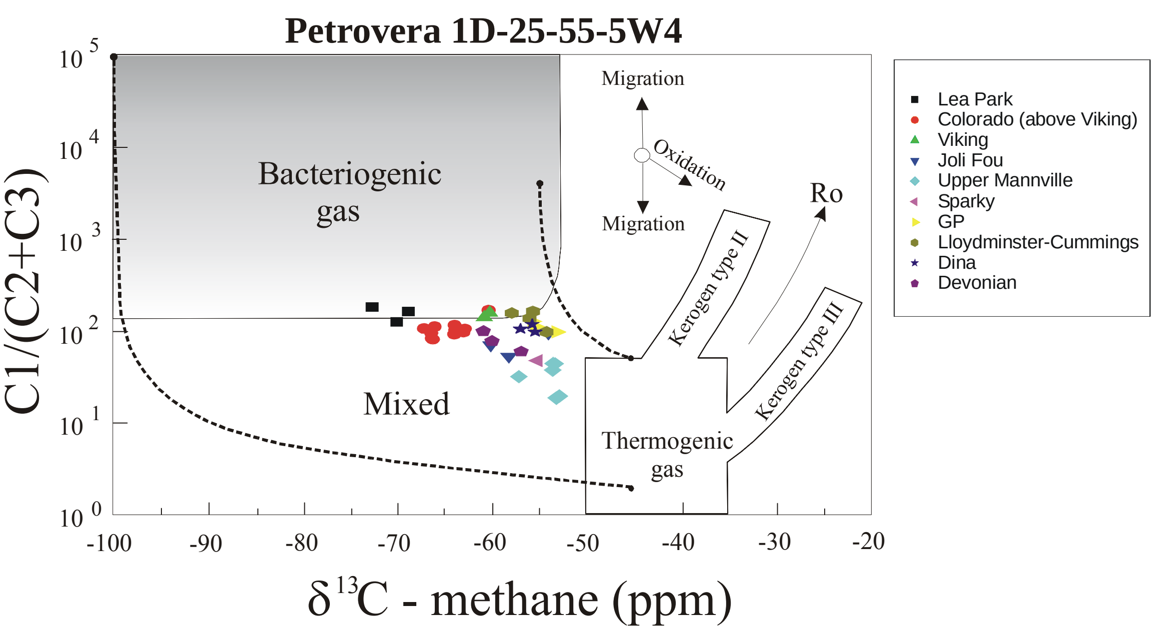

Figure 4-39 Bernard diagram showing the distribution of Cretaceous gases at Petrovera 1D-25-55-5W4 location, heavy oil region. Mixtures of bacterial and thermogenic gases appear to be developed in majority of the mudgases.

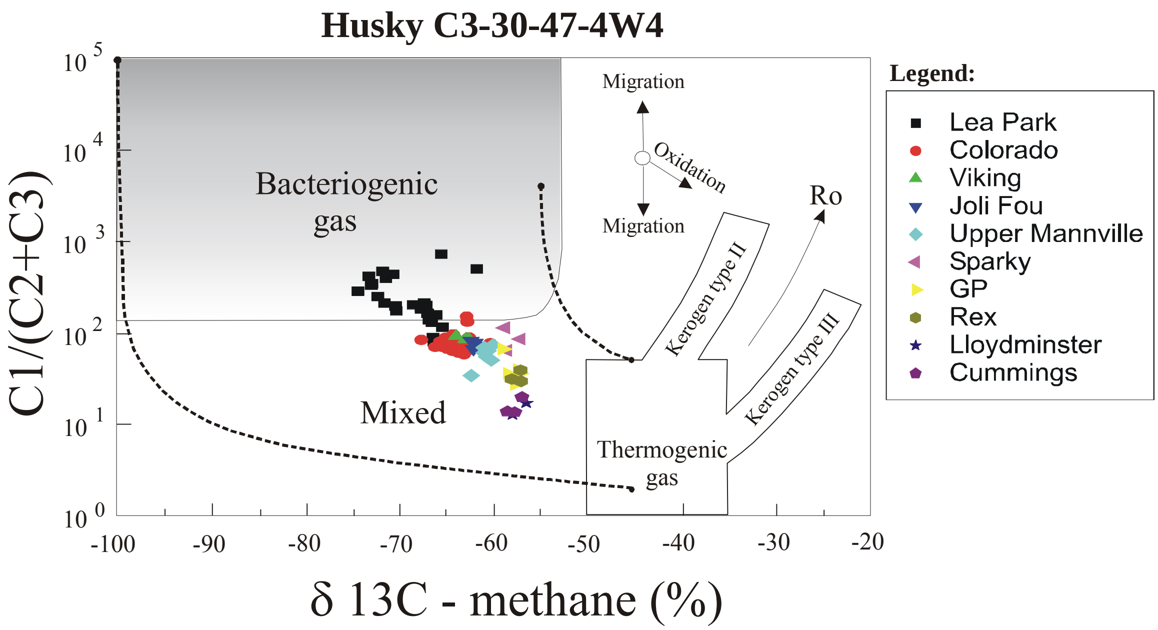

Figure 4-40 Bernard diagram showing the distribution of Cretaceous gases at Husky 3C-30-47-4W4 location, heavy oil region. Mixtures of bacterial and thermogenic gases appear to be developed in majority of the mudgases.

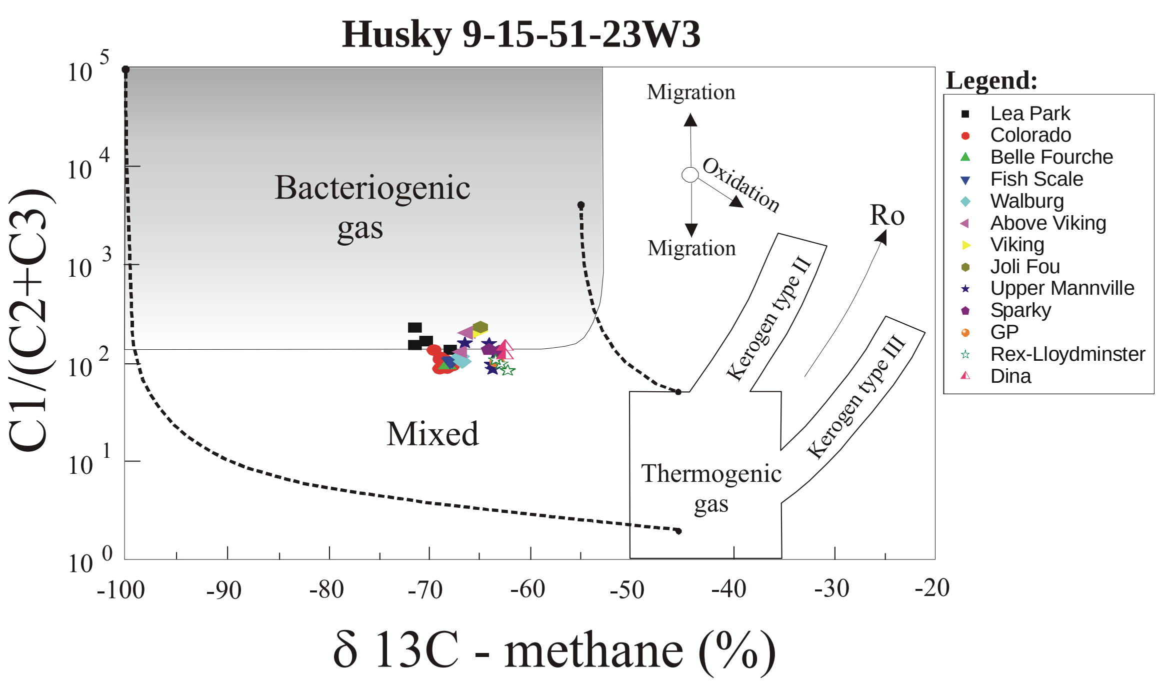

Figure 4-41 Bernard diagram showing the distribution of Cretaceous gases at Husky 9-15-51-22W3 location, heavy oil region. Mixtures of bacterial and thermogenic gases appear to be developed in majority of the mudgases.

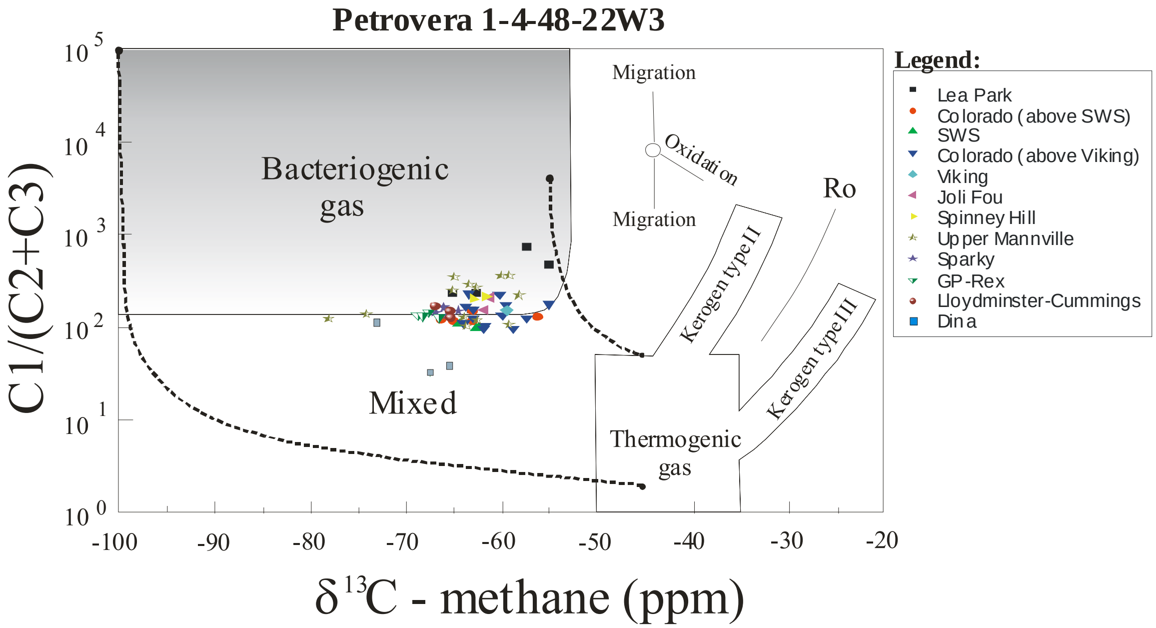

Figure 4-42 Bernard diagram showing the distribution of Cretaceous gases at Petrovera 1-4-48-22W3 location, heavy oil region. Mixtures of bacterial and thermogenic gases appear to be developed in majority of the mudgases, with a strong shift towards the bacteriogenic gas field.

The genetic characterization of gases as defined by Schoell (1983) confirms the possibility of mixing between thermogenic and biogenic gases for the heavy oil region. Figure 4-43 illustrates the distribution of Lindbergh mudgases on the Schoell $\delta^{13}C_{CH4}$ versus C_{2+} abundance diagram. As compared with the Bernard approach, this Schoell diagram indicates a great number of Colorado gases that, instead of falling into the mixed biogenic-thermogenic gas field, occur in the region intermediate between the biogenic gas and mixed biogenic-thermogenic gas fields.

As compared with the Bernard diagram, the Schoell diagrams confirm the possibility of mixing for the majority of the Mannville gases within the heavy oil region. However, contrary of how they fall on the Bernard diagram (where they fall within the bacteriogenic field), some mudgases from the Lower Mannville Formation (i.e. GP and Lloydminster formations gases) appear to be mixed biogenic-thermogenic on the Schoell diagram at Lindbergh location (Figure 4-43). The same patterns indicate the Viking and Lloydminster formations mudgases at Petrovera 1D-25-55-5W4 location (Figure 4-44a). Despite the fact that they fall within the bacteriogenic gas field on the Bernard diagram, they appear to be obviously mixed on the Schoell diagram.

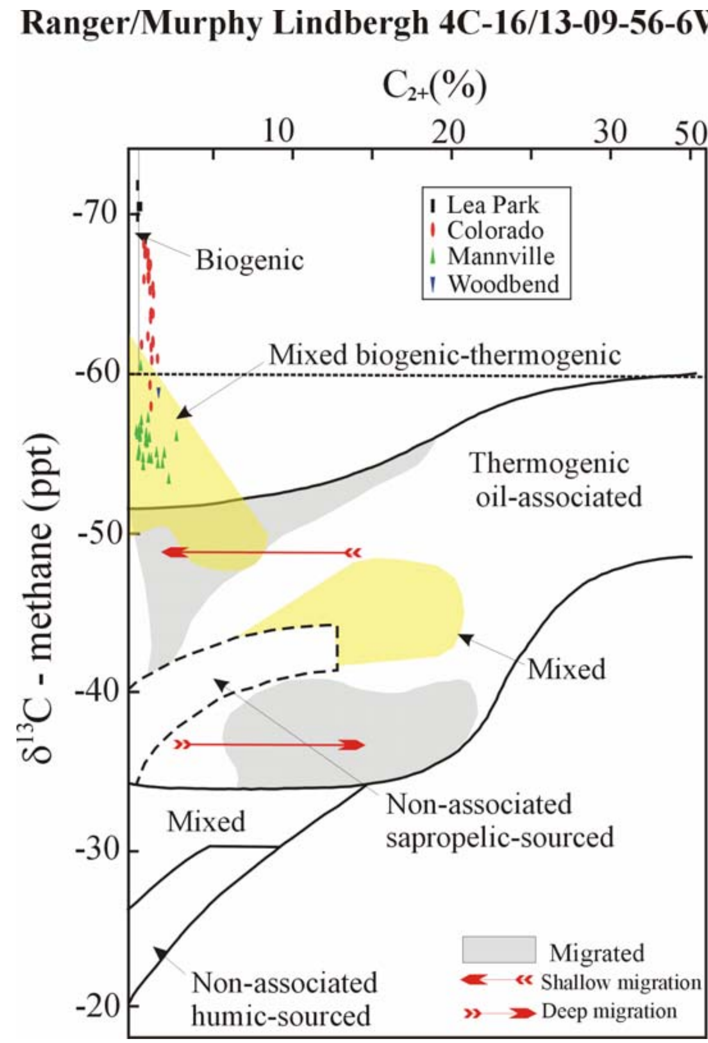

Figure 4-43 Distribution of Cretaceous gases relative to the genetic classification defined by Schoell (1983) on the basis of $\delta^{13}C$ of methane and the relative abundance of C_{2+} alkanes. Lindbergh 4C-16/13-09-56-6W4.

In the Husky 3C-30-47-4W4 well case, the Schoell diagram yet indicate that the lower Mannville gases become wetter with increasing depth, and that some of the Colorado gases with isotopically very light $\delta^{13}C_{methane}$ values, but with a certain percentage of C_{2+} alkanes plot in the region intermediate between the biogenic gas and mixed biogenic-thermogenic gas fields. In the same region intermediate between the biogenic gas and mixed biogenic-thermogenic gas fields on the Schoell diagram fall most of the samples at Petrovera 1-4-48-22W3 (Figure 4-45a) and Husky 9-15-51-23W3 (Figure 4-45b).

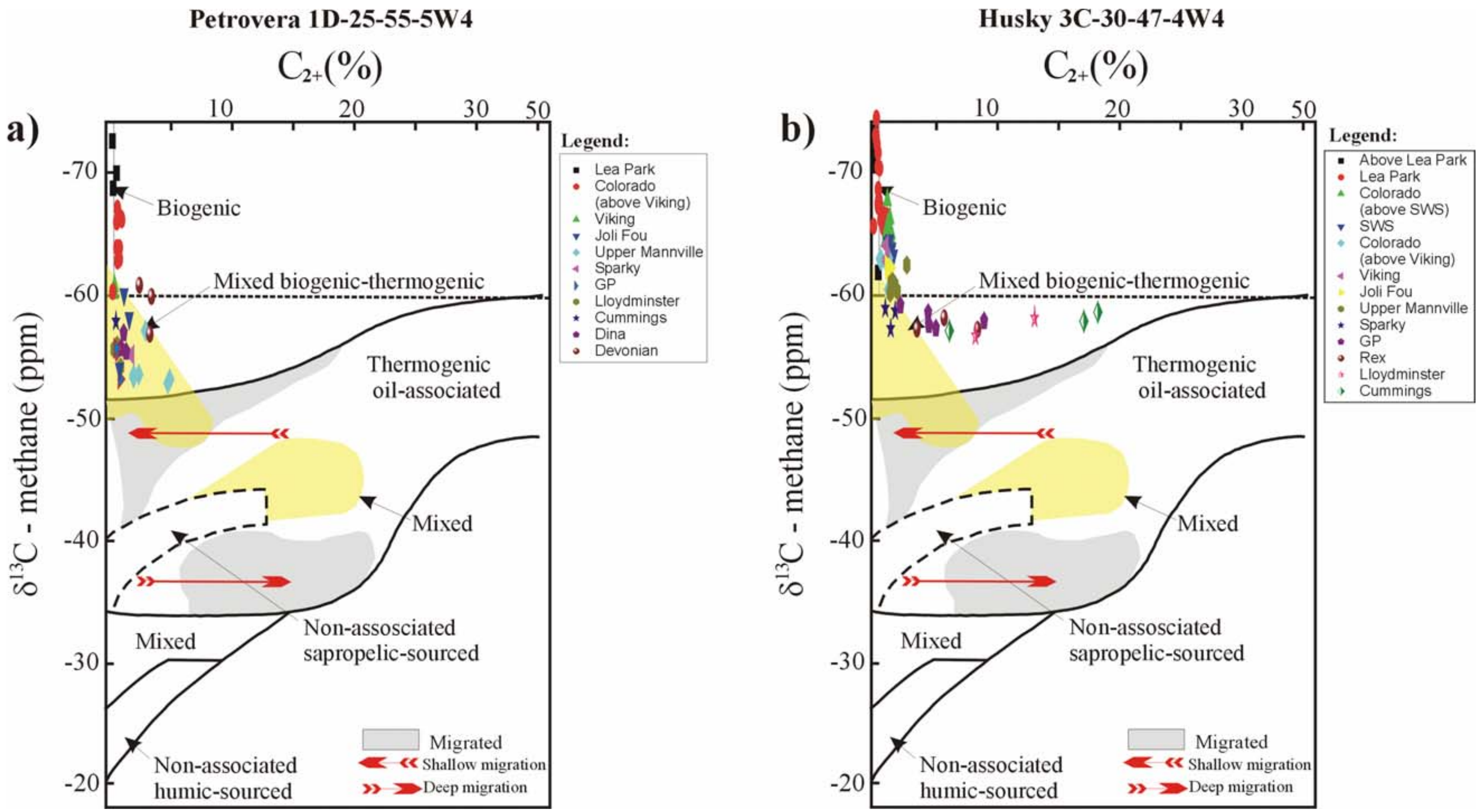

Figure 4-44 Distribution of Cretaceous gases relative to the genetic classification defined by Schoell (1983) on the basis of δ^{13}C of methane and the relative abundance of C2+ alkanes: a) Petrovera 1D-25-55-5W4; b) Husky 3C-30-47-4W4.

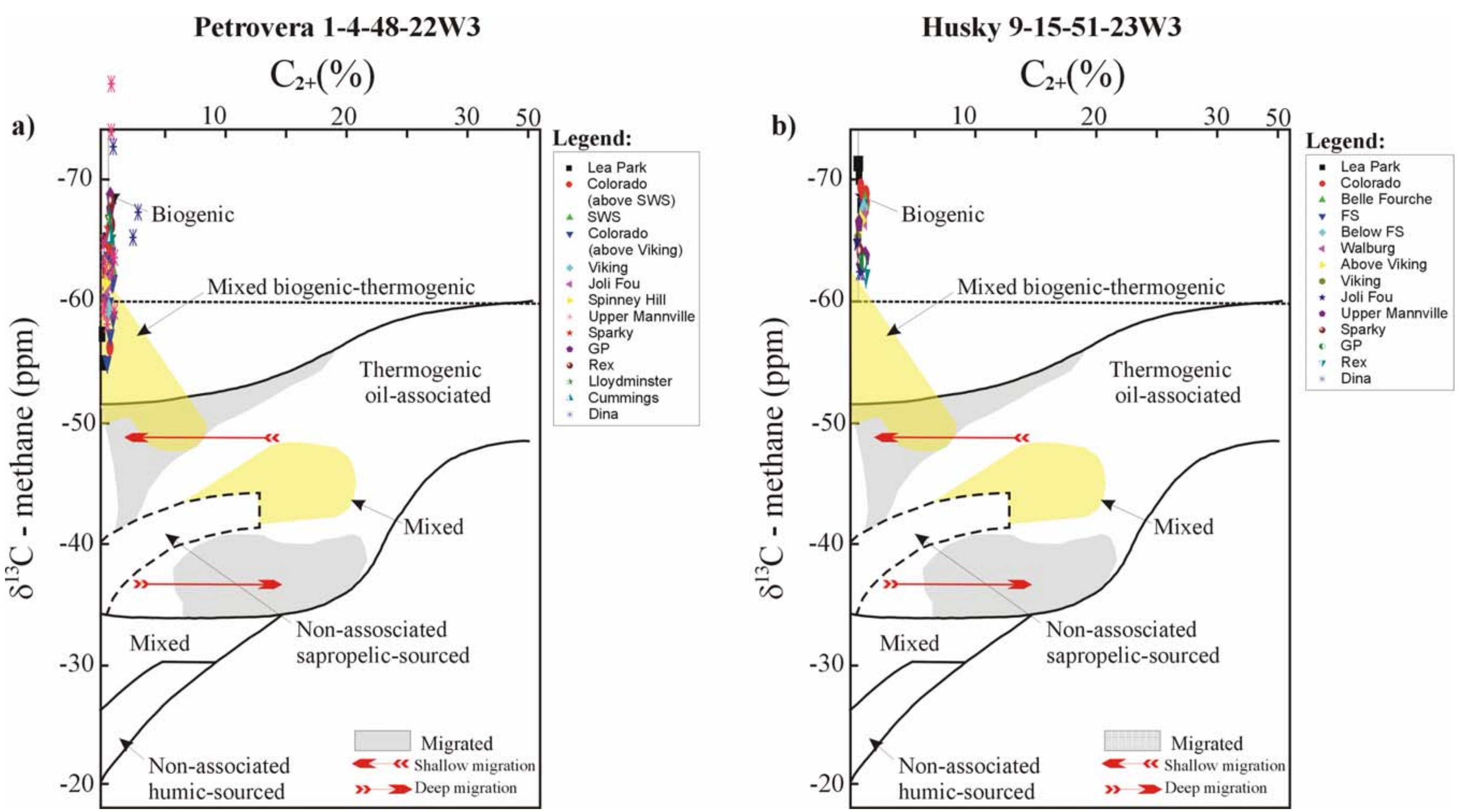

Figure 4-45 Distribution of Cretaceous gases relative to the genetic classification defined by Schoell (1983) on the basis of $\delta^{13}C$ of methane and the relative abundance of C2+ alkanes: a) Petrovera 1-4-48-22W3; b) Husky 9-15-51-23W3.

Obviously, in some cases, different methods/plots give different results. A simple explanation for all these discrepancies would be the reality that, in fact they are empirical-range approaches and the databases on which they are based are rather restricted. Comparison of the same data in the Bernard and Schoell diagrams respectively shows that a cross-plot of molecular versus carbon isotopic composition allows differentiation of gases of various origins. Once more it is shown that specific problems of mixing and migration are more readily solved using the Schoell diagram – the plot of variations of molecular composition in natural gases versus the isotope variations in methane.

For example, the mudgases sampled in the eastern part of the study area can be recognized as very dry gases at Husky 9-15-51-23W3 and Petrovera 1-4-48-22W3 locations on such of Schoell diagram, and even likely sources of biogenic gas, whereas the compositional change in the molecular composition of these gases does not indicate a precise genetic source of such mixed gases in the Bernard diagram.

Following James (1983), carbon isotopic separations between gas components were plotted along the vertical axis using a sliding scale that is the difference (in ppt) between the $\delta^{13}C$ values of gas components. The Colorado gas data were moved across the diagram to produce the best fit possible relative to the calculated curves while maintaining isotope measured isotope separations. In cases where isotopic data for all species from C_1 to C_4 did not fit the curves precisely, an optimum fit between C_2H_6 (ethane) and C_3H_8 (propane) $\delta^{13}C$ values was selected. This is consistent with the recommendation of James (1983), who noted superior fit of empirical C_2-C_3 pairs from several localities to the calculated curves.

Placement of measured $\delta^{13}C$ values for mudgases sampled in the western side of the study area (Lindbergh 9-13-56-6W4, Petrovera 1D-25-55-4W4, and Husky 3C-30-47-4W4) on a James diagram (Figure 4-46 and Figure 4-47) indicates that the maturity range over which the Colorado gases were generated extends from approximately 2 to 7 LOM (equivalent with a vitrinite reflectance less than 0.5%). This range falls outside the oil generation window. The only samples apparently indicating a higher level of maturity are

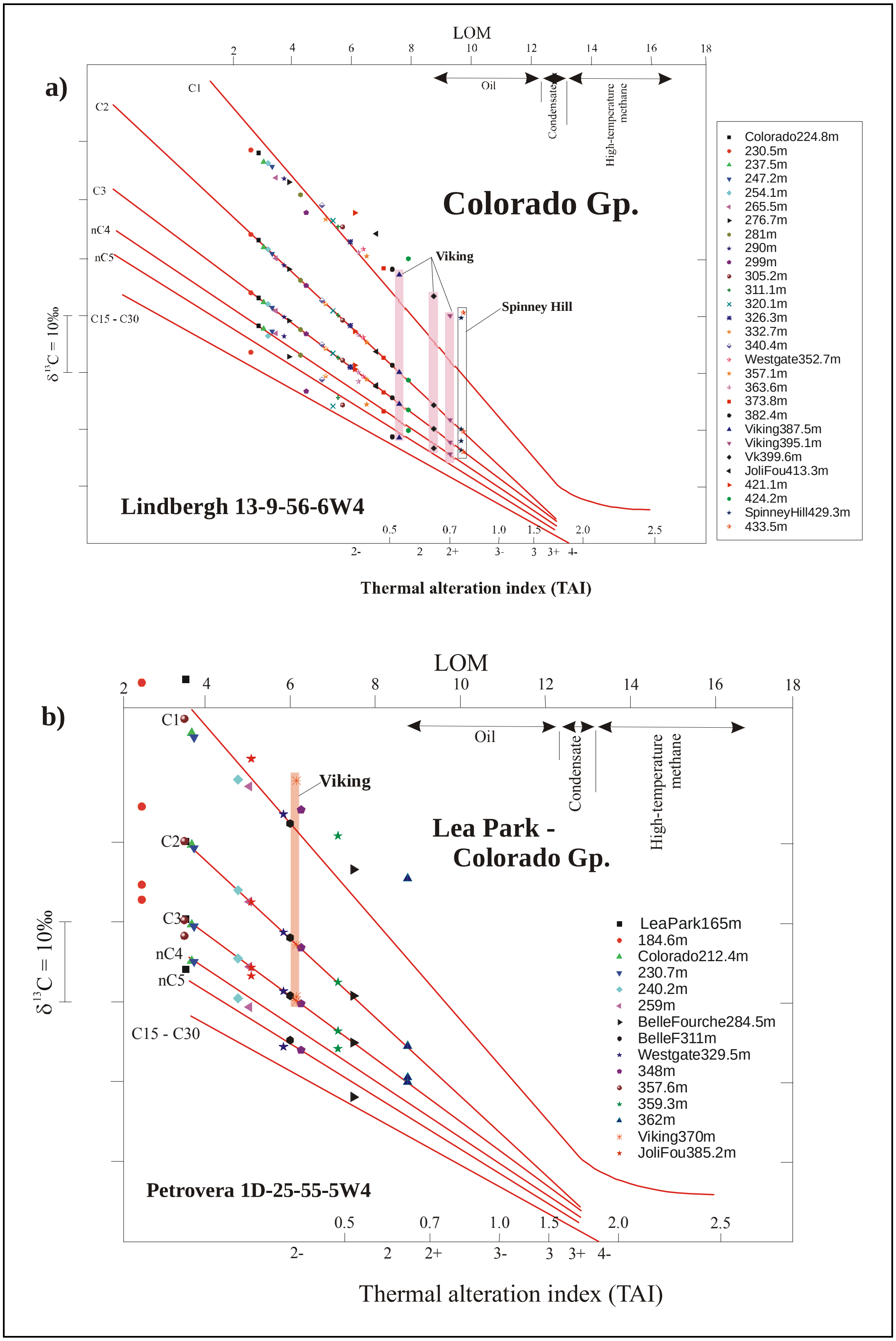

Figure 4-46 James diagram showing the distribution of the Colorado mudgases: a) Lindbergh 13-9-56-6W6, b) Petrovera 1D-25-55-5W4. The majority of Colorado gases appear to have been generated at low levels of maturity.

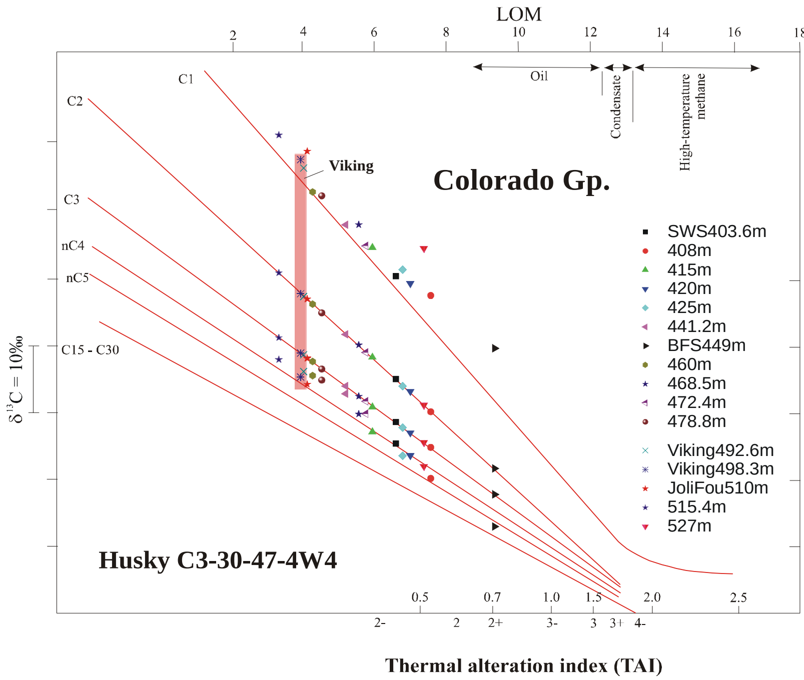

Figure 4-47 James diagram showing the distribution of the Colorado mudgases; Husky 3C-30-47-4W4.

the Viking and Spinney Hill samples (Lindbergh well), and one Fish Scale Formation gas sample (Husky 3C-30-47-4W4).

The majority of mudgases contain methane that is considerably ^{13}C-depleted relative to the isotope composition predicted by the partition function model upon which the James diagram is based. This disagreement is evidenced by the distribution of a number of methane data points above the line describing the predicted carbon isotopic composition of methane, suggesting gas mixing (bacteriogenic-thermogenic).

Figure 4-47 shows that the majority of the Second White Specks Shale gases fit the calculated curves quite well. As indicated as well on the "natural gas plot" (Figure 4-48) these gases illustrate the linear trend that is indicative of a thermogenic, single source gas. The predicted source composition varies between –25‰ and ~-29‰ (a marine source, consistent with Type II kerogen).

At Petrovera 10-17-47-27W3, Colorado gases from shallower than 400 m (290 – 400m depth interval) appear to have been generated within the oil window, indicating a high level of maturity (Figure 4-49). This is obviously not the case, for the reason that, as indicated on the" natural gas plot" of these gases (Figure 4-50), there are no linear

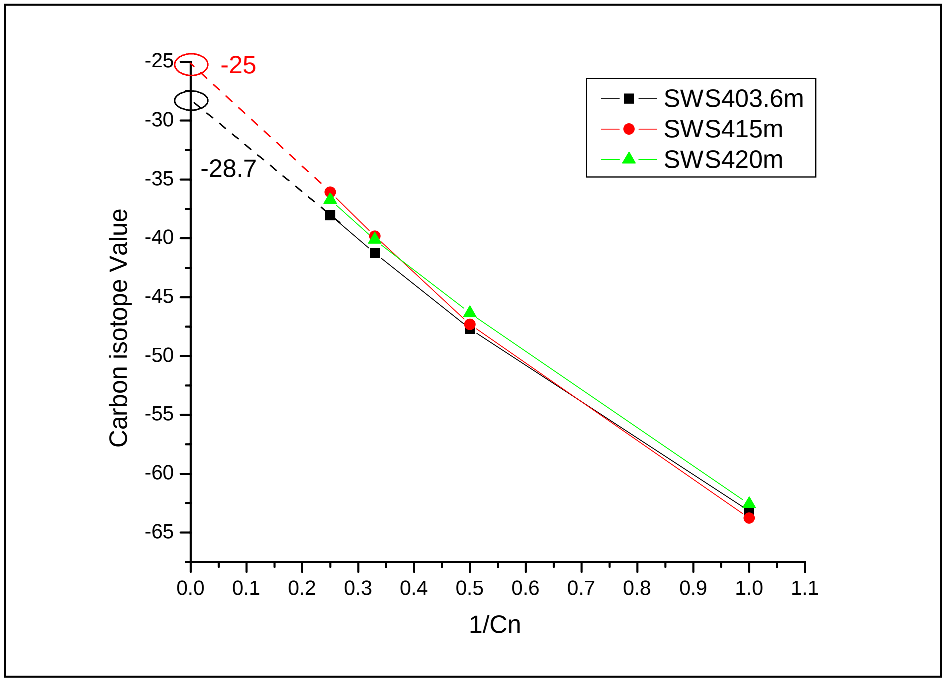

Figure 4-48 "Natural gas plot" for the Husky 3C-30-47-4W4 well, showing representative gas samples from the Second White Specks Shale Formation. The predicted source composition varies between –25‰ and ~-29‰.

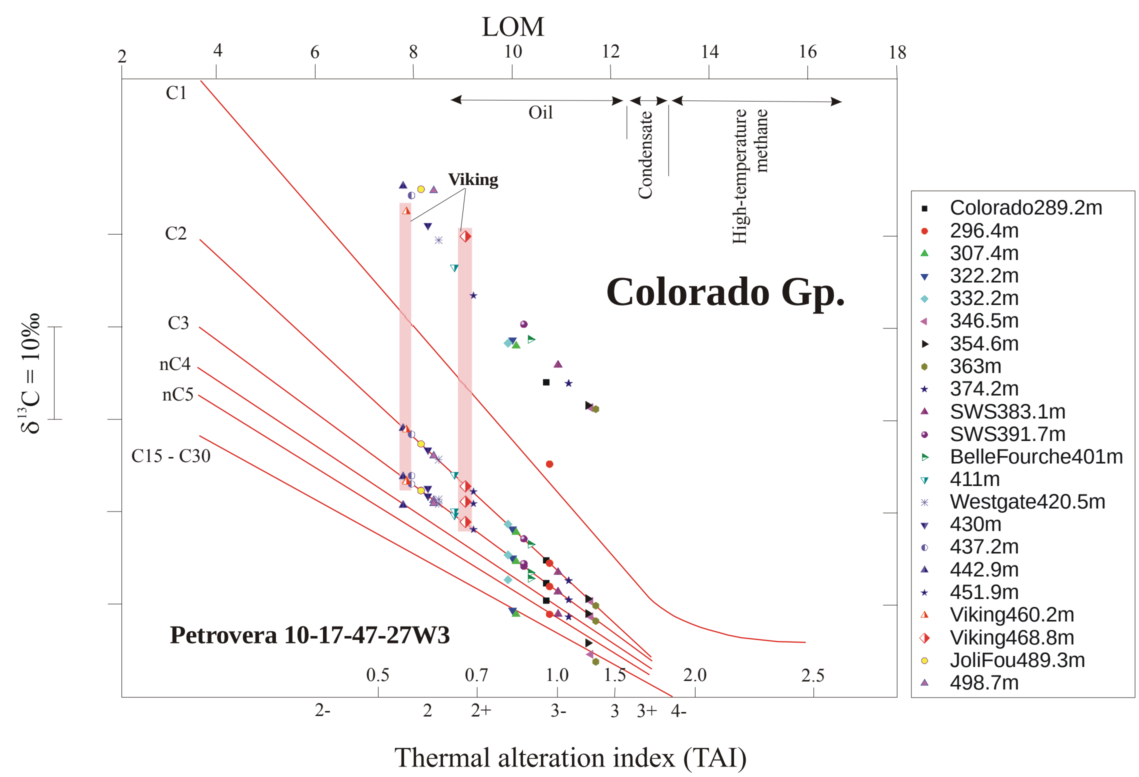

Figure 4-49 James diagram showing the distribution of the Colorado mudgases; Petrovera 10-17-47-27W3.

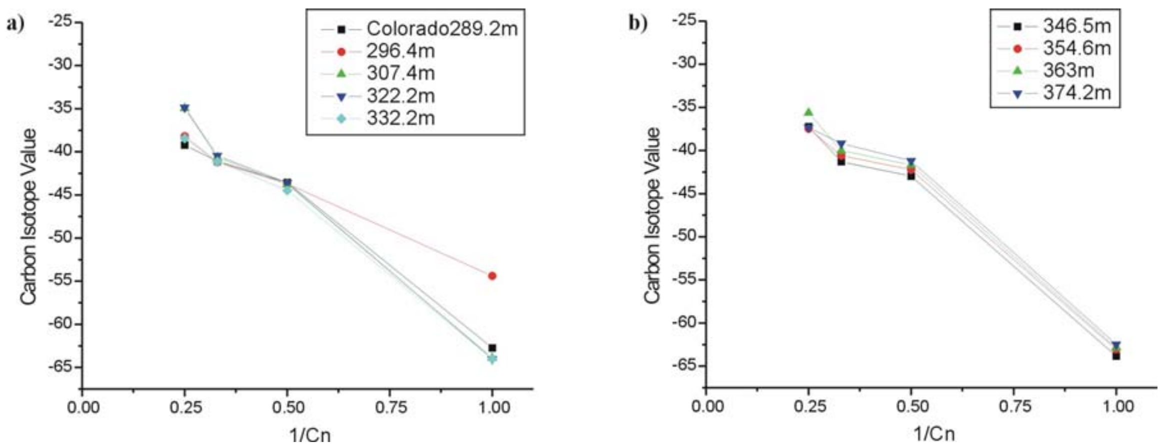

Figure 4-50 "Natural gas plots" for a selection of representative gas samples from the Colorado Group; Petrovera 10-17-47-27W3.

relationships between the isotope ratios and their inverse carbon numbers. These gases seem to be altered, either mixed or biodegraded, or they can be migrated.

Placement of measured $\delta^{13}C$ values for mudgases sampled in the eastern side of the study area (Husky A9-15-51-23W3, Petrovera 1-4-48-22W3, and Petrovera A9-30-47-22W3) on a James diagram (Figure 4-51 and Figure 4-52) indicates that the maturity range over which the Colorado gases were apparently generated extends considerably from approximately 2 to ~10 LOM.

In Figure 4-51, some of the Upper Colorado shales, including the Belle Fourche shales, fit the calculated curves extremely well. They appear to be potential thermogenic gas sources, as demonstrated as well by their linear slopes on "natural gas plots" (Figure 4-53).

In the Golden Lake field (Petrovera 1-4-48-22W3 and Petrovera A9-30-47-22W3), most likely due to the effects of bacterial alteration (Rowe and Muehlenbachs, 1999a), some of the Colorado gases display a variety of non-linear slopes (Figure 4-54); these gases could be misinterpreted as being generated at higher levels of maturity.

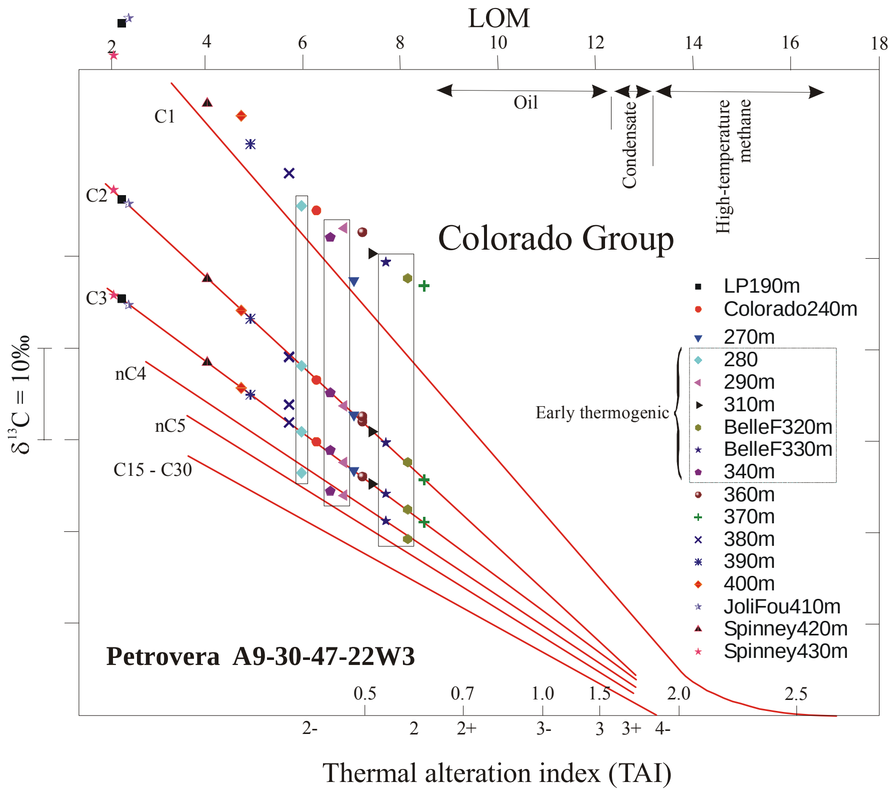

Figure 4-51 James diagram showing the distribution of the Colorado mudgases; Petrovera A9-30-47-22W3

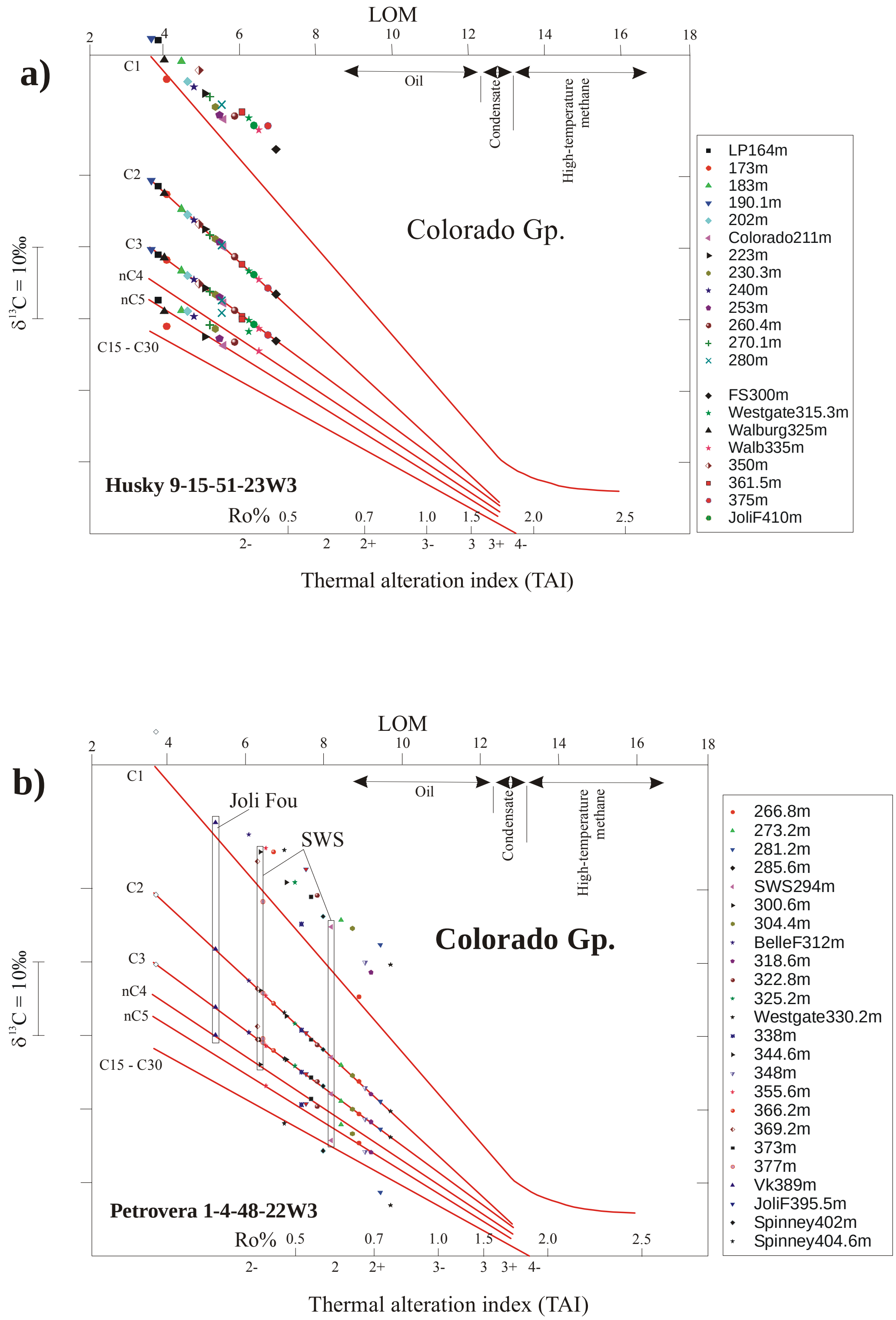

Figure 4-52 James diagram showing the distribution of the Colorado mudgases: a) Husky 9-15-51-23W3, b) Petrovera 1-4-48-22W3. The majority of Colorado gases appear to have been generated at low levels of maturity. Gases sampled at 330.2m and 281.2m (b) represent exceptions; they are biodegraded and thus cannot indicate a reliable maturity level.

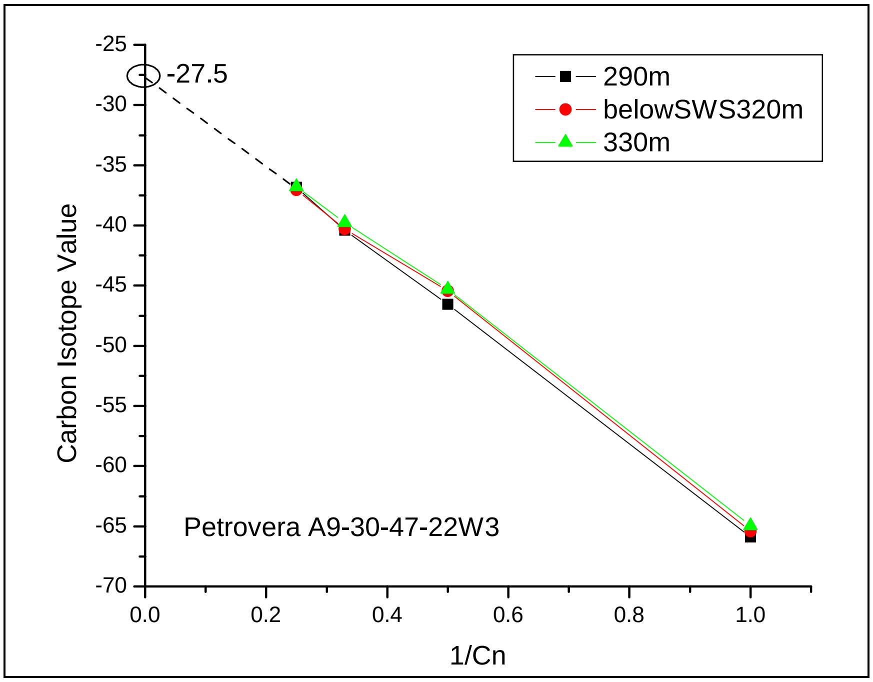

Figure 4-53 "Natural gas plots" for a selection of Colorado gas samples from the Petrovera A9-30-47-22W3 profile, showing linear relationships between isotope ratios and their inverse carbon numbers.

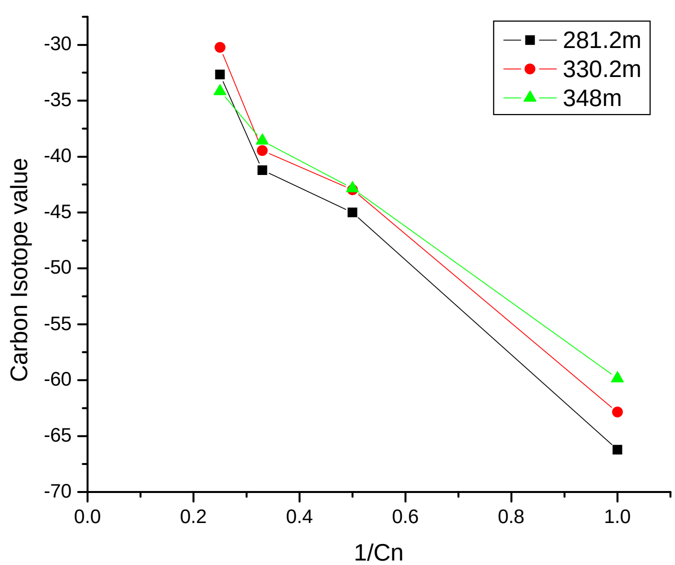

Figure 4-54 "Natural gas plots" for a selection of Colorado gas samples from the Petrovera 1-4-48-22W3 profile, showing non-linear relationships between isotope ratios and their inverse carbon numbers.

Figure 4-55 is an example for the isotopic differences of methane, ethane and propane for all the Colorado gases sampled in the heavy oil region. As can be seen on this diagram, data shows a considerable scatter, suggesting that $\delta^{13}C$ isotope differences, and thus the gaseous components are not essentially controlled by the source maturity.

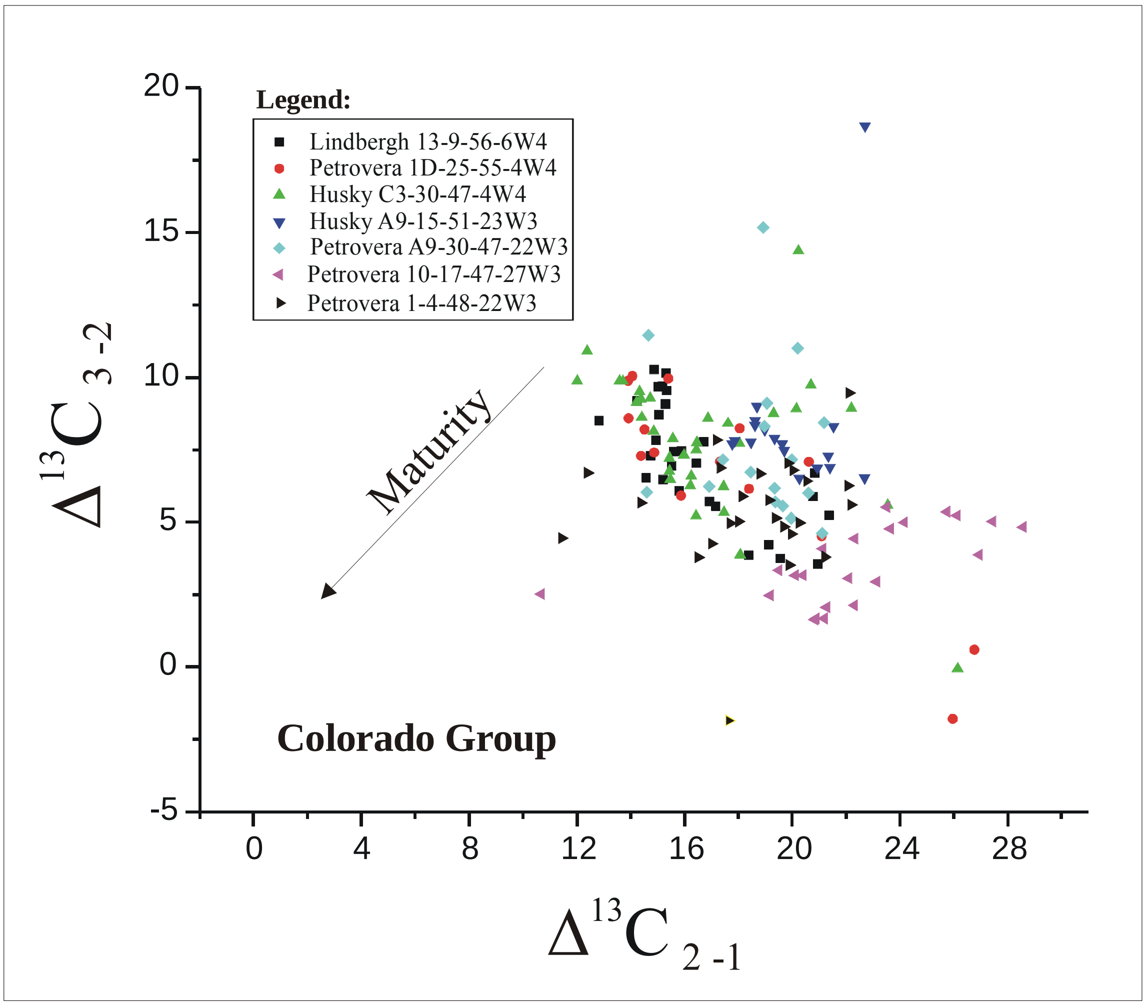

Figure 4-55 Isotopic differences of methane, ethane and propane for the Colorado gases sampled in the heavy oil region, east-central Alberta and west-central Saskatchewan.

Mannville samples from the heavy oil region do not provide a reasonable fit to the James diagram. As already specified, Mannville gases are mixtures of thermogenic and microbial gas and should not be expected to fit. However, plotting Mannville gases on James diagrams reveal the following characteristics:

1. isotopic reversals between the $\delta^{13}C_3$ and $\delta^{13}C_4$ values (Figure 4-56);
2. $\delta^{13}C_4$ values often plot quite high above the maturation line, indicating biodegradation (Figure 4-56a)
3. uncommon large isotopic separations;
4. some of the samples fall into a very high maturity range, with vitrinite reflectance values of considerably high than 1.35% (Lindbergh 16-9-56-6W4, Figure 4-56a; Husky 3C-30-47-4W4, Figure 4-57b; Petrovera 10-17-47-23W3, Figure 4-56b);
5. some of the Mannville gases at Lindbergh well location (Figure 4-56a) indicate a good fit to the James diagram: Colony gas (469.2m), Waseca gas (487m) and Sparky gas (490.8m); plotted also on a Chung diagram, these gases form essentially linear trends for C_2, C_3 and nC_4, suggesting a thermogenic origin, but the $\delta^{13}C_1$ ratios are distinctly more negative than the linear trend predicts (Figure 4-58);
6. Upper Mannville gases appear to be more mature than the Lower Mannville gases: Colony and McLaren gases indicates maturities of ~12 LOM, while Cummings gases have maturities less than 9 LOM (Figure 4-56, Figure 4-57a);
7. Within all Mannville gases methane is ^{13}C-depleted relative to the composition predicted by the partition functions.

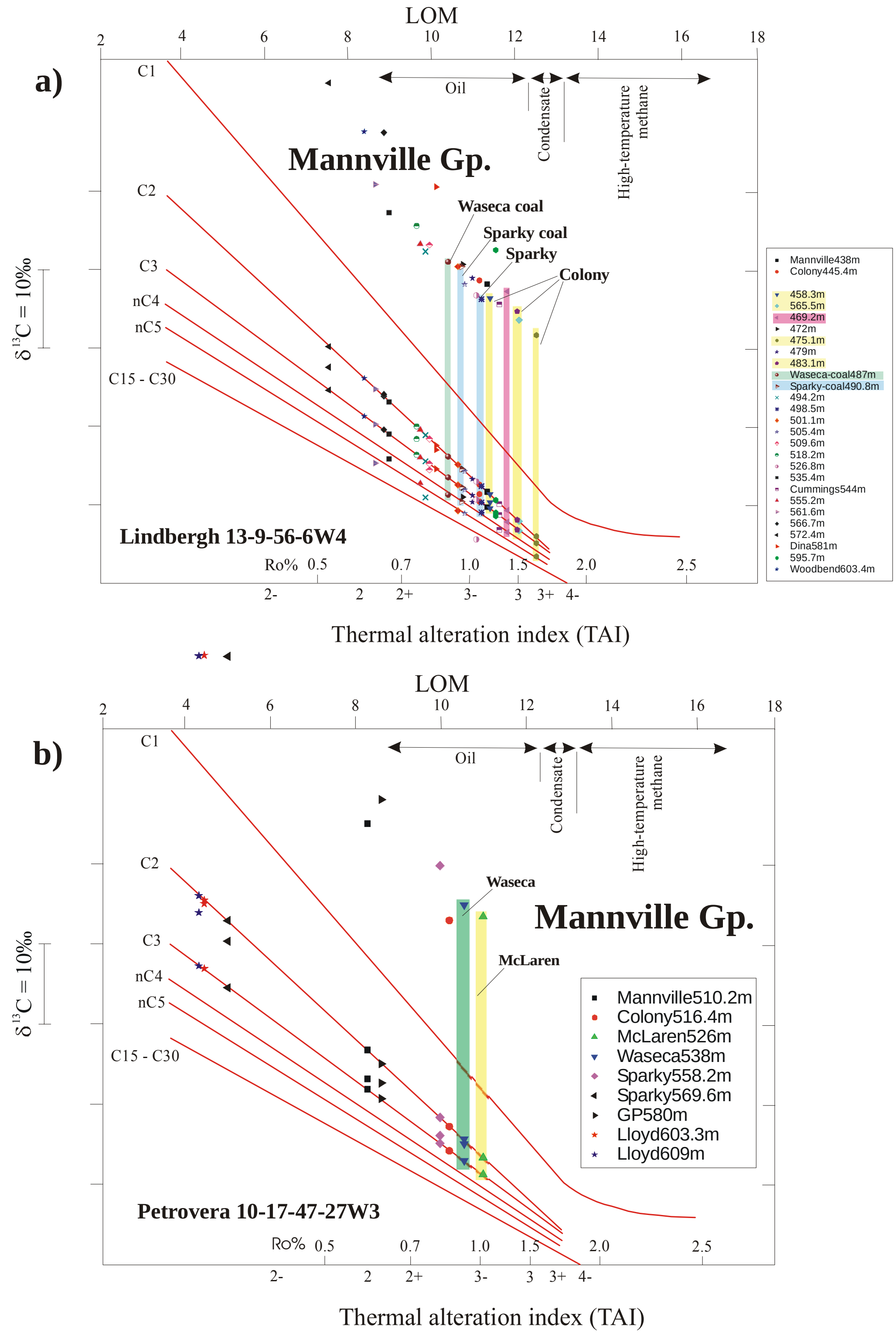

Figure 4-56 James diagram showing the distribution of the Mannville mudgases: a) Lindbergh 13-9-56-6W6, b) Petrovera 10-17-47-27W3. The majority of Mannville gases appear to have been generated at high levels of maturity, within the oil window.

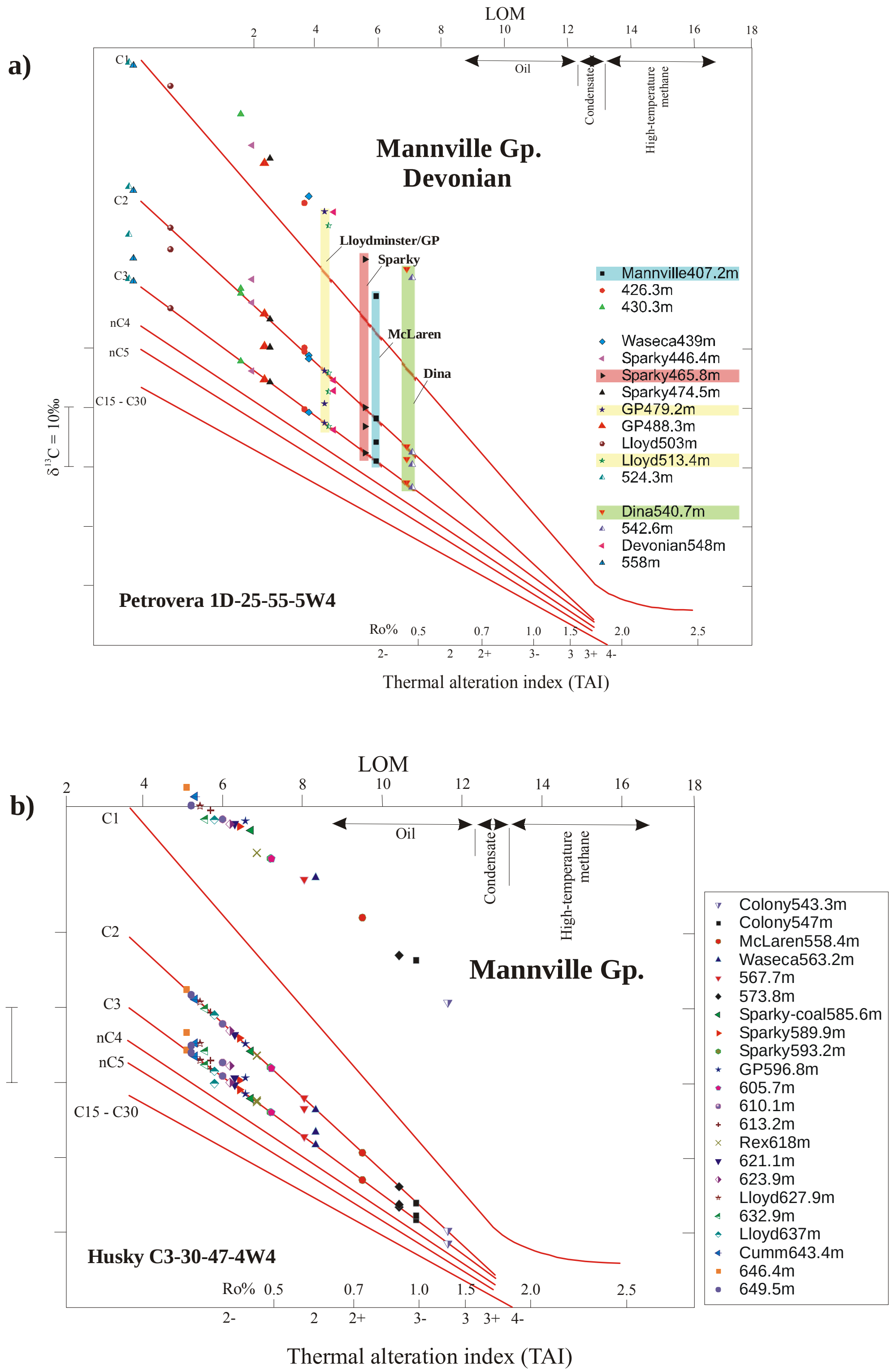

Figure 4-57 James diagram showing the distribution of the Mannville mudgases: a) Petrovera 1D-25-55-5W4, b) Husky C3-30-47-4W4. The majority of Mannville gases have the n-butane $\delta^{13}C$ values plotted high above the calculated maturation line.

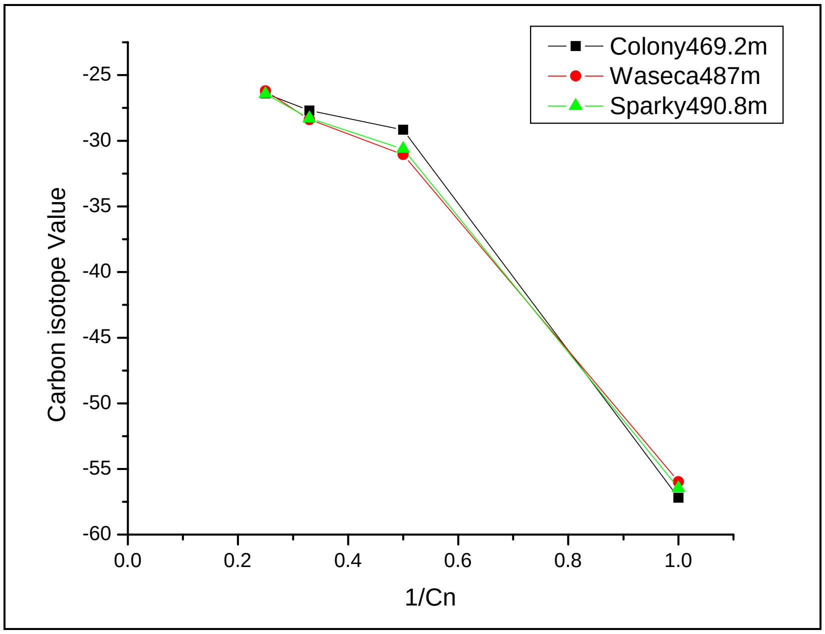

Figure 4-58 "Natural gas plot" for a selection of Mannville gas samples from the Lindbergh 13-9-56-6W4 profile, showing quasi-linear relationships between C2-C4 isotope ratios and their inverse carbon numbers. These gas samples originate from coals or coaly shales.

4.3.4. Discussion

Geochemical analyses of mudgases in the Lloydminster heavy oil study area suggest three main factors controlling the variations in gas composition:

1. different kerogen composition,
2. different gas generation mechanisms, and
3. biodegradation.

Gas chromatograms of Mannville oils in the Lloydminster area show that they are extensively biodegraded, possibly during up-dip migration from deeper basin, resulting in the existing giant heavy oil deposits (Deroo et al., 1977) situated at the northeastern edge of the basin. Carbon isotope ratios of these gases associated with heavy oils also show the effects of biodegradation (Figures 4-53 and 4-54): the $\delta^{13}C_{nC4}$ values are commonly less negative than the $\delta^{13}C_{C3}$ values, a result of microbial alteration (James, 1990).

Lower Cretaceous Mannville gases associated with the heavy oils have migrated long distances, and biodegradation has significantly altered their isotope ratios from the patterns established in deeper, unaltered gases. Bacterial alteration of Mannville gases has led to characteristic isotopic reversals between the $\delta^{13}C_{C3}$ and $\delta^{13}C_{nC4}$ values and fairly positive propane $\delta^{13}C$ values. In addition, Mannville gases have apparently mixed with large amounts of bacterial methane, which accounts for very negative $\delta^{13}C_{C1}$ values (-77.97‰ to -60‰).

A high number of butane $\delta^{13}C$ values plotted between the ethane and propane lines on James diagrams. The values are reversed from the theoretical separations. Such reversals indicate that the source effect is overriding the maturity effect on which James' plot is based. According to James, these reversals occur more frequently with heavier hydrocarbons and gases from Type III kerogen.

On the basis of the presented data we can conclude that the Mannville gases are extremely dry gases, highly biodegraded, and mixed. They resulted from intra-reservoir bacterial degradation (association with the heavy oil leg), and possibly from the coal source rocks of the Mannville Group. Coaly organic matter from the Mannville Group seems to be able to generate early thermogenic gas in sufficient quantities to count up for the recovered gas abundance in the western part of the Lloydminster study area: e.g. Lindbergh location. Some gas samples from the Mannville Group at Lindbergh location (as presented also in Figure 4-58) illustrate the linear trend, which is indicative of a thermogenic, single sourced gas from kerogen Type III (Figure 4-59). The most likely cause of low methane $\delta^{13}C$ value is an influx of biogenic methane mixed with the thermogenic gas. Admixture of bacterial gas seems to constitute also a reasonable explanation that account for the extreme dryness of the Mannville gases.

The Colorado gases fit the calculated curves quite well, with measured data essentially defining the ethane, propane and butane curves. In most of the gases the methane values are considerably higher than the calculated lines predict. This could be due to mixing with isotopically light biogenic methane (James, 1983).

The isotopic separations between Colorado gas components indicate that the majority of the gases was generated at LOM's of 6-8, although several gases appear to be considerably less mature (LOM's ranging from ~ 2-5), and others considerably more mature (LOM's ranging from ~ 9-10).

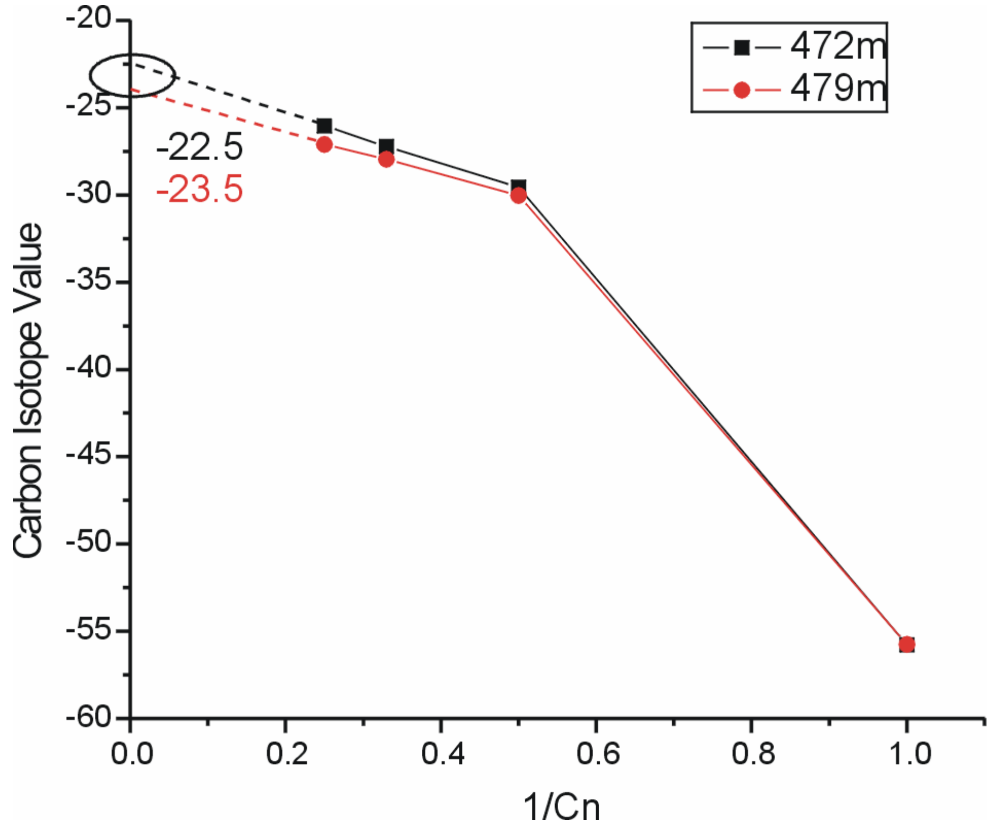

Figure 4-59 "Natural gas plot" for a selection of Mannville gas samples from the Lindbergh 13-9-56-6W4 profile, showing quasi-linear relationships between C_2-C_4 isotope ratios and their inverse carbon numbers. These linear trends are indicative of a thermogenic, single sourced gas from kerogen Type III.

With the exception of the more mature gases, which are located mostly within Viking and Spinney Hill sandstone (Figure 4-46a, Lindbergh), and which are supposed to represent migrated gases, the majority of Colorado gases are, as reported also by Rowe and Muehlenbachs (1999a) some of the most immature thermogenic gases ever reported.

In the light of these findings, two models on the generation of the gas in the Colorado Group remain bacterial gas generation and early thermogenic gas generation.

Depending on the effectiveness of the permeability barriers, the C_{2+} components of the Colorado gases in the Western Canadian sedimentary basin could have migrated from deeper formations (i.e. Mannville Group). The hypothesis that the gases in the Mannville Group had migrated vertically into the Colorado shale Group – at least locally, is sustained by the fact that, even the isotope ratios of C_{2+} in both groups are not very similar, isotopic reversals between C_3 and C_4 components, as well as between C_2 and C_3 components of mudgases do occur in the Colorado Group shales gases too (Petrovera 10-17-47-27W3: the majority of the gases sampled below the Second White Specks Formation - 411 to 468.8 m depth interval – present isotopic reversals between the $\delta^{13}C_3$ and $\delta^{13}C_4$ values, as can be seen in Figure 4-60; Lindbergh A9-13-56-6W4: samples from Westgate shales and Spinney Hill show isotopic reversals between $\delta^{13}C_2$ and $\delta^{13}C_3$ values; Figure 4-61).

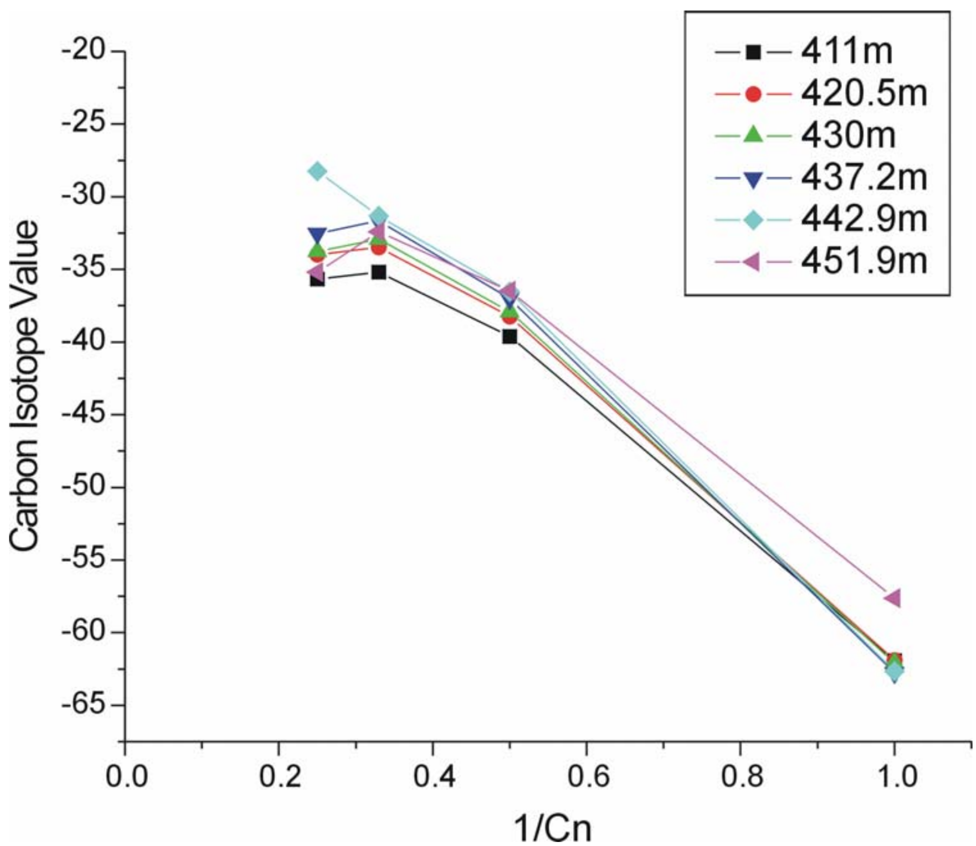

Figure 4-60 "Natural gas plots" for a selection of Colorado gas samples from the Petrovera 10-17-47-22W3 profile, showing isotopic reversals between the $\delta^{13}C_3$ and $\delta^{13}C_4$ values.

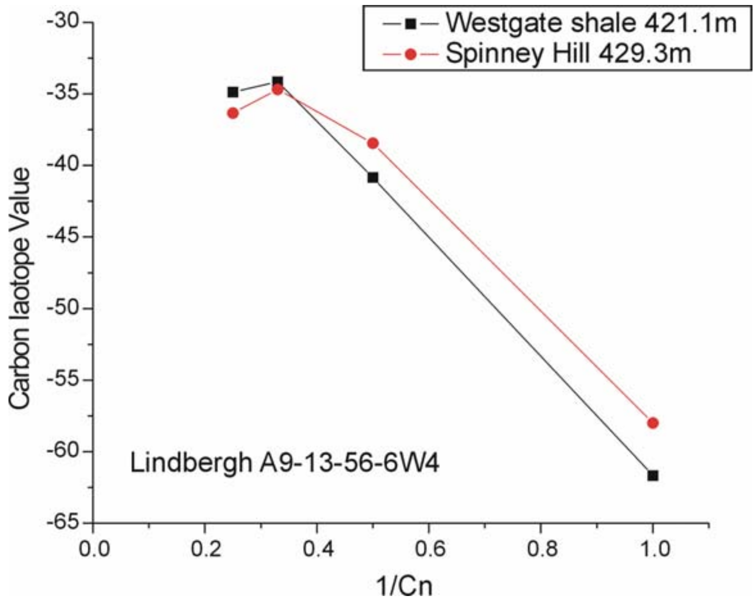

Figure 4-61 "Natural gas plots" for a selection of gas samples from the Lindbergh A9-13-56-6W4 profile, showing isotopic reversals between the $\delta^{13}C_3$ and $\delta^{13}C_4$ values.

Moreover, as can be seen in Figure 4-62, the Joli Fou sample from 498.7 m depth and the Mannville sample from 510.2 m depth at Petrovera 10-17-47-27W3 have practically the same isotopic composition.

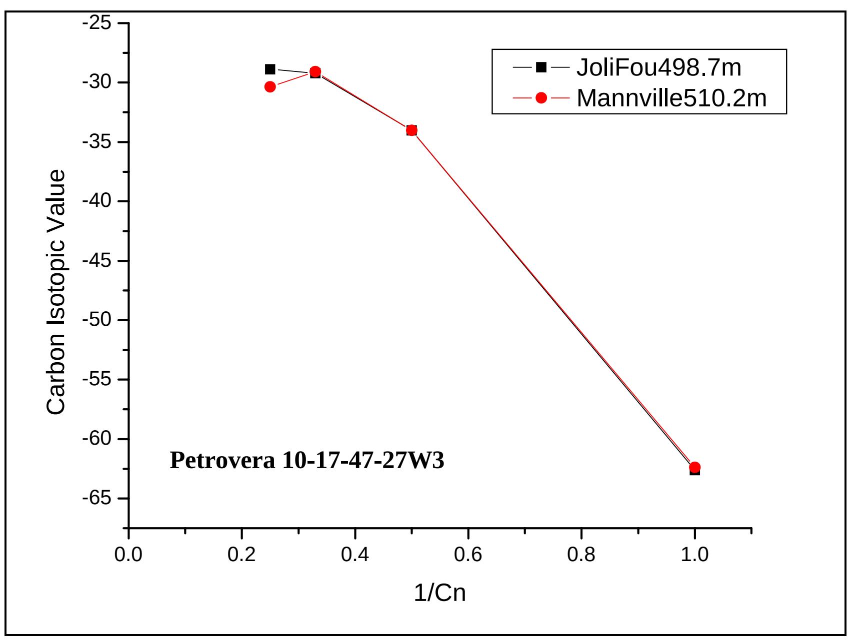

Figure 4-62 "Natural gas plots" for two gas samples from the Petrovera 10-17-47-27W3 profile, showing isotopic similarity between Colorado and Mannville gases.

Another aspect that should be taken into consideration is the fact that, by placing the measured $\delta^{13}C$ values for some Colorado mudgases on James' diagrams (Figure 4-6) the maturity range over which these gases were generated indicates the oil generation window (in some cases up to 1.4% Ro). This is not consistent with the present thermal maturity range observed for these rocks in this area (Figure 4-32, from Bustin, 1991). Even plotted on a diagram ethane $\delta^{13}C$ versus propane $\delta^{13}C$, some of the Colorado gases indicate 0.7% up to 0.9% Ro for vitrinite reflectance (Figure 4-63).

The conclusion is that the post-generation history of the gases from Western Canadian Sedimentary Basin is much more complicated that it was thought before.

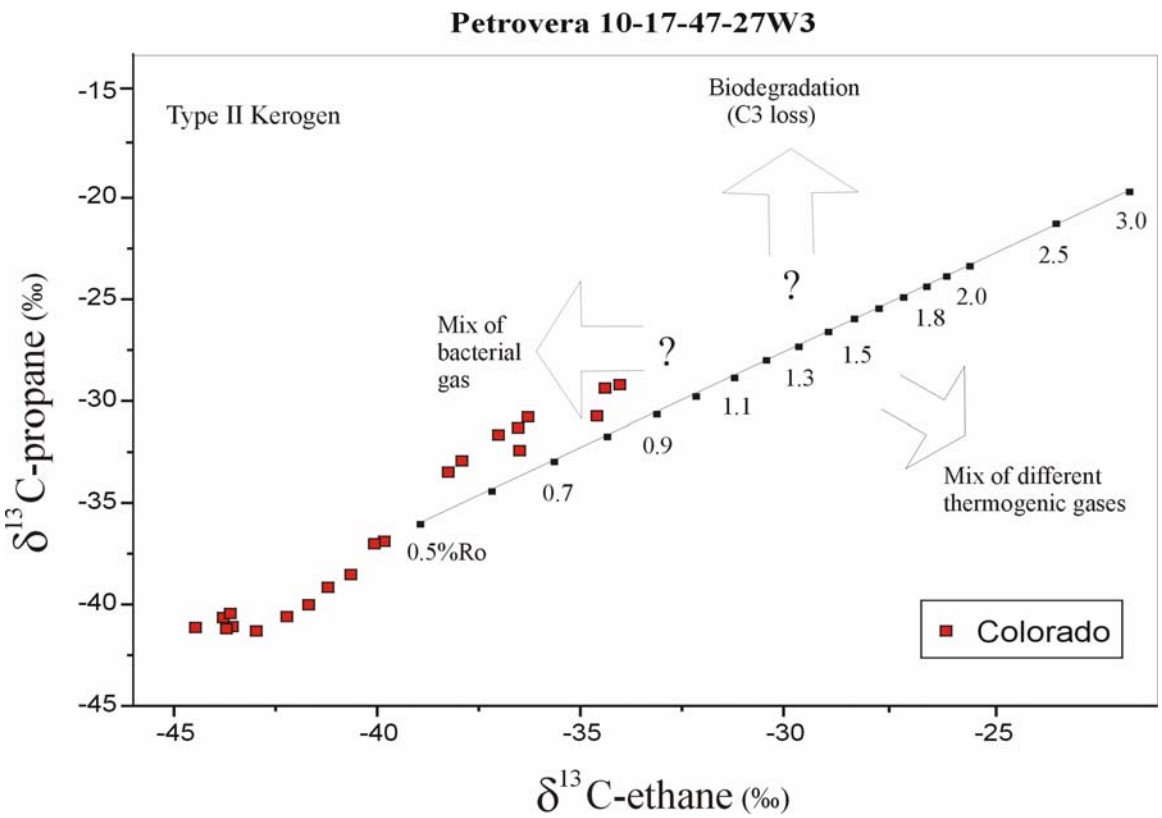

Figure 4-63 Stable carbon isotope ratios for co-genetic ethane and propane in Colorado mudgases from Petrovera 10-17-47-27W3. Position of the vitrinite reflectance curve for type II kerogen after Faber (1987), and Whiticar (1990).

Application of the partition function methodology of James (1983) to the Colorado data in the Lloydminster region indicate that gas generation took place generally over maturities of 2 and 7 LOM (less than 0.5%Ro): Lindbergh 9-15-56-6W4, Husky 3C-30-47-4W4, Petrovera 1D-25-55-5W4, Husky 9-15-51-23W3. The only exception is represented by the Colorado data from Petrovera 10-17-47-22W3, where James diagram indicates gas source maturities ranging between 8-12 LOM, and entering the oil generation window. The other two-mudlog locations, within the Golden Lakes field (Petrovera 1-4-48-22W3 and Petrovera A9-30-47-22W3) show maturity up to 9 LOM for Colorado gases. It should be noted that several of the methane samples (especially in the western limit of the study area) exhibit considerably greater depletions in the ^{13}C isotope than is predicted by the partition functions for thermogenic gas production. Such a pattern would be expected in the case of admixture of isotopically light methane (such as bacterial methane) with thermogenic gas.

It has to be noted that in the Golden Lakes region some reservoirs have been steamed for decades to produce heavy oil. These hot well bores seem to influence the isotopic composition of hydrocarbon gases obtained from mud-gases in this region.

According to Rowe (1998), the increased maturity in such of steamed wells (Petrovera A9-30-47-22W3 and Petrovera 1-4-48-22W3) may be a direct result of the steam injection operations. The high temperatures (greater than 100^0C) may be facilitating in-situ gas generation around the wellbores. Subsurface temperatures greater than 100^0C can be achieved during steamflooding, essentially "cooking" the organic materials that surround the wellbores, liberating gaseous hydrocarbons. The coal seems within the Mannville Group represent a potential source of isotopically enriched organic matter.

University of Alberta

MUDGASES GEOCHEMISTRY AND FACTORS CONTROLLING THEIR VARIABILITY

Volume 2

by

DANIELA VLAD

A thesis submitted to the Faculty of Graduate Studies and Research
in partial fulfillment of the requirements for the degree of

Doctor of Philosophy

Department of Earth and Atmospheric Sciences

Spring 2010
Edmonton, Alberta

TABLE OF CONTENTS

Chapter **Page**

CHAPTER FIVE: FORMATION COMPARTMENTALIZATION USING ISOTOPIC FINGERPRINTS OF MUDGASES AND MULTILOG QUANTIFICATION

5.1. Introduction 235
5.2. Methodology 236
5.2.1. Examination of inflections in the multi-component geochemical depth profiles 236
5.2.2. Matrix algebra compositional log analysis 237
5.2.2.1. Mineral identification through crossplots 237
5.2.2.2. Matrix algebra compositional log analysis - calculations 241
5.2.3. X-Ray diffractometry analysis (XRD) 249
5.3. Results 254
5.3.1. Foothills region 256
5.3.2. Lloydminster region 261
5.4. Well logs – qualitative uses in mudgas geochemistry 270
5.5. Discussion 272

CHAPTER SIX: HYDRODYNAMICS, FLOW SYSTEMS AND GAS MIGRATION PATHWAYS

6.1. Introduction 275
6.2. Foothills region 277
6.2.1. Flow of formation waters 277
6.2.2. Gas migration mechanisms and pathways in the Foothills region 279
6.3. Lloydminster region 294
6.3.1. Flow of formation waters 294

6.3.2. Gas migration mechanisms and pathways
in the Lloydminster region …………………………………….. 295
6.4. Discussion ………………………………………………………………. 306
6.4.1. Foothills region ………………………………………………… 306
6.4.2. Lloydminster region …………………………………………… 309

CHAPTER SEVEN: THE SCV SOURCE DETECTION
7.1. Introduction ……………………………………………………………… 312
7.2. Surface gas migration and the application of carbon isotopic mud logs
for remediation leaking wells ……………………………………..… 312
7.2.1. The SCV source detection in the Foothills area ……………….….. 313
7.2.2. The SCV source detection in the Lloydminster area ……….….. 324
7.3. Environmental implications …………………………………………….. 344

CHAPTER EIGHT: SUMMARY AND RELATIONSHIPS BETWEEN FOOTHILLS AND HEAVY OIL STUDY AREAS

8.1. Stable isotopes results and discussion…………………………………… 361
8.1.1. $\delta\ ^{13}C$ of Methane …………………………………………….. 362
8.1.1.1. Regional variations ……………………………...… 366
8.1.1.2. Mixing of thermogenic and bacteriogenic methane ….. 368
8.1.2. $\delta\ ^{13}C$ of C2+ hydrocarbons ………………………………..… 369
8.1.2.1. Maturity trends versus source effects versus
biodegradation ……………………………………...… 372
8.1.2.2. Carbon isotope fractionation …………………….…..….. 382
8.1.2.3. Mixing of thermogenic and bacteriogenic ethane …..… 384
8.1.3. Regional migration vs. indigenous sources ……………………. 386
8.2. Isotopic complexity: insights from the stratigraphic framework …..…… 390
8.2.1. Downhole variations …………………………………………… 391
8.2.2. Isotopic shifts and stratigraphic variations ……………..…….393
8.3. Conclusions ……………………………………………………………. 397

CHAPTER NINE: CONCLUSIONS

9.1. Conclusions …………………………………………………………………… 401

9.2. Future work ………………………………………………………………… 412

BIBLIOGRAPHY ………………………………………………………..……. 414

ADDENDUM A

Diffractograms for nine shale samples taken from the Shell Paradise 10-25-047-3W4 core (Figures 5-9 to 5-21)……………….…………………..….……….. 435

*****

APPENDICES

Appendix A: Photographs of cores (Plates 1-122) and their log signatures

- Figures A-1 to A-40 …………………………………………….....… 449
- Plates (1-122) ...…………………………………………………….….…... 489

Appendix B: Well log cross-sections and Composite diagrams ……………... 735

- Appendix I (I-1 to I-5): Foothills region – well log cross-sections …. 735
- Appendix II (II-1 to II-8): Lloydminster region – well log cross-sections ……………………………………………………………. 740
- Appendix III (III-1 to III-7): Composite diagrams: mudlogs–compositional profiles ……………………………………………..…….. 748

LIST OF FIGURES

Figure **Page**

5-1 Neutron – density crossplot for the Mannville Group at Husky A9-15-51-23W3 well location, Lloydminster region …………………… 238

5-2 M – N plot for mineral identification applicable to Mannville Group at Petrovera 1D-25-55-22W3 well location, heavy oil region - Alberta ……………………………………………………... 239

5-3 ROMA - UMA crossplot for lithology identification. Scollard Formation, well Pembina 11-4-49-11W5, Foothills region, Alberta ……... 240

5-4 Example of compositional profile, calculated by a matrix algebra solution ……………………………………………………………… 242

5-5 Shale point defined on a neutron – sonic crossplot. Values are from the Colorado Group, Gilby 15-16-42-4W4, west-central Alberta ………………………………………………….. 245

5-6 Matrix algebra solution for Colorado Group in Gilby 15-16-42-4W5 well, west-central Alberta. The result is shown as a graphic lithology log of the system porosity-shale-quartz …………………………………... 246

5-7 Shale point defined on a neutron – density crossplot. Values are from the Mannville Group, Gilby 15-16-42-4W4, west-central Alberta ….. 247

5-8 Matrix algebra solution for the Mannville Group in Husky 3C-30-47-4W4 well, Lloydminster region. The result is shown as a graphic lithology log of the system porosity-shale-quartz-coal ……… 248

5-9 The resultant diffractogram of sample #2 (538.5m depth) - Shell Paradise 10-25-047-3W4 core. …………………………………………… 436

5-10 The resultant diffractogram of sample #1 (538.9m depth) - Shell Paradise 10-25-047-3W4 core. …………………………………………… 437

5-11 The resultant diffractogram of sample #3 (546m depth) - Shell Paradise 10-25-047-3W4 core …………………………………………… 438

5-12 The resultant diffractogram of sample #4 (567.4m depth) - Shell Paradise 10-25-047-3W4 core …………………………………………… 439

5-13 The resultant diffractogram of sample #5 (576.5m depth) - Shell Paradise 10-25-047-3W4 core ……………………………………………. 440

5-14 The resultant diffractogram of sample #6 (636m depth) - Shell Paradise 10-25-047-3W4 core …………………………………………… 441

5-15 The resultant diffractogram of sample #6 (636m depth) - Shell Paradise 10-25-047-3W4 core – larger intensity scale …………………… 442

5-16 The resultant diffractogram of sample #7 (654.2m depth) - Shell Paradise 10-25-047-3W4 core ……………………………………………. 443

5-17 The resultant diffractogram of sample #7 (654.2m depth) - Shell Paradise 10-25-047-3W4 core - larger intensity scale …………………… 444

5-18 The resultant diffractogram of sample #8 (670m depth) - Shell Paradise 10-25-047-3W4 core ……………………………………………. 445

5-19 The resultant diffractogram of sample #8 (670m depth) - Shell Paradise 10-25-047-3W4 core - larger intensity scale ……………………. 446

5-20 The resultant diffractogram of sample #9 (682m depth) - Shell Paradise 10-25-047-3W4 core ……………………………………………. 447

5-21 The resultant diffractogram of sample #9 (682m depth) - Shell Paradise 10-25-047-3W4 core - larger intensity scale ……………………. 448

5-22 Matrix algebra solution for the Joli Fou - Mannville section in Shell Paradise 10-25-47-3W4 well, Lloydminster region. The result is shown as a graphic lithology log of the system porosity-quartz-shale-smectite ………………………………...…….. 251

5-23 Matrix algebra solution for the Joli Fou - Mannville section in Shell Paradise 10-25-47-3W4 well, Lloydminster region. The result is shown as a graphic lithology log of the system porosity-quartz-shale-illite. Note: the quartz dominated sample #5 from 576.5m depth is also shown in red ………………………………... 252

5-24 Matrix algebra solution for the Joli Fou - Mannville section in Shell Paradise 10-25-47-3W4 well, Lloydminster region.

The result is shown as a graphic lithology log of the system
porosity-quartz-shale-siderite …….....……………………………...… 253

5-25 Wireline data plus mineralogical interpretation for Husky
3C-30-47-4W4 profile …….……………………………………………..255

5-26 “Natural gas plot” showing some of the Paskapoo gases, Ferrier
14-3-42-9W5, Foothills region ……………………………………………. 256

5-27 “Natural gas plot” showing some of the Paskapoo - Scollard gases,
Ferrier 14-3-42-9W5, Foothills region ………………………………... 257

5-28 “Natural gas plot” for some of the Horseshoe Canyon gases, indicating
a single thermogenic generation of the gas and a single
sub-compartment bounded by two effective shale-rich barriers.
Ferrier 14-3-42-9W5, west-central Alberta ……………………………….. 258

5-29 “Natural gas plot” showing two different gases separated by a quartz-rich
shale barrier. Scollard Formation, Ferrier 14-3-42-9W5,
west-central Alberta ……………………………………………………..259

5-30 “Natural gas plot” of the Manville gases from the Gilby profile ………… 260

5-31 C2/C3 diagram for Gilby profile showing δ^{13}C2 – δ^{13}C3 (‰)
versus C2/C3 distinguishes gases generated from the primary
cracking of kerogen, the secondary cracking of oil, and the tertiary
cracking of the wet portion of the gases (after Lorant et al, 1998) ……… 261

5-32 “Natural gas plot” for Colorado gases from Petrovera 1D-25-55-5W4,
showing the difference between two gas sub-compartments separated
by an effective montmorillonite-rich shale barrier ……….…………….. 262

5-33 Stable carbon isotopic profile and the conversion into mineralogy,
Husky 9-15-51-23W3 ……………………………………………….. 263

5-34 Stable carbon isotopic profile and the conversion into mineralogy,
Petrovera 1D-25-55-5W4 ………………………………………………….. 264

5-35 “Natural gas plot” showing two different gas compartments
(Joli Fou gases and Colony Gases) Husky C3-30-47-4W4
separated by an effective montmorillonite-rich shale barrier …………….. 265

5-36 “Natural gas plot” showing some Middle Mannville gases confined

in a single gas sub-compartment at Husky C3-30-47-4W4
profile by two effective barriers: an upper quartz-cemented band
and a lower shale-rich layer ……………………………………………..….266

5-37 "Natural gas plot" for Colorado gases from Husky 9-15-51-23W3,
showing the slight difference between two gas sub-compartments
separated by a partial effective montmorillonite-rich shale barrier ………. 267

5-38 "Natural gas plot" for Second White Speckled Shales gases from
Husky C3-30-47-4W4, showing the slight difference between two
gas sub-compartments separated by a partial effective
montmorillonite-rich shale barrier ……………………………………… 268

***

6-1 C_2/C_1 versus methane $\delta^{13}C$ diagrams showing the basic principle
of their use. Modified from Prinzhofer et al. (2000) ………………………. 277

6-2 Flow patterns (indicated by arrows) in the coal-bearing Upper
Cretaceous-Tertiary strata of the Alberta basin:
(a) Scollard-Paskapoo aquifer; (b) Edmonton aquifer; c) Belly River aquifer.
Modified from Bachu and Michael, 2003. Note: the grey squares indicate
the Foothills area in the present study …………………………………….. 278

6-3 The distribution of the isotopic composition of methane and
physico-chemical parameters of the Scollard gases in the
different mudlog locations in the Foothills region. Only the
mean values are shown ……………………………………………………. 281

6-4 The distribution of the isotopic composition of methane and
physico-chemical parameters of the Horseshoe Canyon gases
in the different mudlog locations in the Foothills region. Only
the mean values are shown ………………………………………………282

6-5 Combination plot of $\delta^{13}C_{CO2}$ and $\delta^{13}C_{CH4}$ with isotope fractionation
lines (Ec). Methanogenesis by carbonate reduction has a larger
$CO_2 - CH_4$ isotope separation than by methyl-type fermentation

(freshwater region), or methane consumption
(modified after Whiticar, 1999) ………………………………………… 283

6-6 Combination plot of $\delta^{13}C_{CO2}$ and $\delta^{13}C_{CH4}$ with isotope fractionation lines (Ec) for the Paskapoo Formation gases (after Whiticar, 1999) ……. 284

6-7 The overall organic maturity trend in the Ferrier-Gilby area, and Lloydminster area for Mannville strata. The values for the mean maximum vitrinite reflectance are from isomaturity maps of Bustin (1991) ………………………………………………….. 285

6-8 The distribution of the isotopic composition of methane and physico-chemical parameters of the Upper Belly River gases in the different mudlog locations in the Foothills region. Only the mean values are shown …………………………………………………..287

6-9 C2/C3 diagram showing δ^{13} C2 – δ^{13}C3 versus C2/C3 distinguishing gases generated from the primary cracking of kerogen, the secondary cracking of oil, and the tertiary cracking of the wet portion of the gases for Ferrier and Gilby profiles (after Lorant et al, 1998) ……………………289

6-10 C2/C3 versus C2/iC4 diagram showing the possible biodegradation of hydrocarbon gases (Prinzhofer, 2000). Ferrier 14-3-42-9W5 ……………………………………………………………… 290

6-11 C2/C3 versus C2/iC4 diagram showing the possible biodegradation of hydrocarbon gases (Prinzhofer, 2000). Gilby 15-16-42-4W5 …………………………………………………….290

6-12 The pattern of ethane δ^{13}C change with depth in the Scollard Formation, Foothills region ………………………………………………...291

6-13 The pattern of ethane δ^{13}C change with depth in the Horseshoe Canyon Formation, Foothills region …………………………..…… 291

6-14 The pattern of ethane δ^{13}C change with depth in the Belly River Group, Foothills region …………………………………………………… 294

6-15 In depth variation of the total abundance of hydrocarbon gases in the Horseshoe Canyon Formation, Foothills region ………………………….. 293

6-16 Spatial distribution of the methane content in Colorado shales,

Lloydminster region ………………………………………………………..…295
6-17 Methane concentration (in vol. %) variability with depth in five mudlog profiles within the Lloydminster region ……….…………….. 296
6-18 Depth profiles of methane $\delta^{13}C$ from gases sampled in Lower Mannville reservoirs, Lloydminster area ……………………………………………298
6-19 The distribution of the isotopic composition of methane and physico-chemical parameters of the Sparky sand gases in the different mudlog locations in the Lloydminster region. Only the mean values are shown ……………………………………………299
6-20 The distribution of the isotopic composition of methane and physico-chemical parameters of the Lloydminster sand gases in the different mudlog locations in the Lloydminster region. Only the mean values are shown ………………………...………………300
6-21 The distribution of the isotopic composition of methane and physico-chemical parameters of the Mannville Group gases in the different mudlog locations in the Lloydminster region. Only the mean values are shown ……………………………………………301
6-22 The distribution of the isotopic composition of methane and physico-chemical parameters of the Colorado Group gases in the different mudlog locations in the Lloydminster region. Only the mean values are shown …………..……………………………302
6-23 Gas wetness distribution within the Lloydminster region …..……………... 303
6-24 Gases from Sparky sandstone plotted on a C1-C2 diagram in linear scale, showing a trend of segregative migration ……………………… 304
6-25 Gases from Lloydminster sandstone plotted on a C1-C2 diagram in logarithmic scale, showing a trend of segregative migration ………………305
6-26 Inferred migration trend of the gas phase through the carrier sandstone beds of the Mannville Group, Lloydminster region ……………………….. 305
6-27 Stable carbon isotope ratios for co-genetic methane and ethane in a natural gas (After Faber, 1987; Whiticar, 1990.) …………….…………..307

***

7-1 Isotope ratios of eight SCV gases superimposed on the mudgas isotopic depth profile from Petro-Canada Ferrier 14-03-042-9W5. Legend for SCV gases is provided in Figure 7-2 ……………………….. 315

7-2 SCV gases from Figure 7-1 and their presumable sources. Petro-Canada Ferrier 14-03-042-9W5……………………………………………….... 316

7-3 Isotope ratios of five SCV gases superimposed on the mudgas isotopic depth profile from Petro-Canada Ferrier 14-03-042-9W5. Legend for SCV gases is provided in Figure 7-4…………………… …… 317

7-4 SCV gases from Figure 7-3 and their presumable sources. Petro-Canada Ferrier 14-03-042-9W5…………………………………………… …… 318

7-5 Isotope ratios of thirteen SCV gases superimposed on the mudgas isotopic depth profile from PC Gilby 15-16-42-04W5. Legend for SCV gases is provided in Figure 7-6…………………………. 319

7-6 SCV gases from Figure 7-5 and their presumable sources. PC Gilby 15-16-42-04W5…………………………………..……….. 320

7-7 Isotope ratios of two SCV gases superimposed on the mudgas isotopic depth profile from IORL Pembina 11-04-049-11W5. Legend for SCV gases is provided in Figure 7-8…………………..…… 321

7-8 SCV gases from Figure 7-7 and their presumable sources. IORL Pembina 11-04-049-11W5…………………………….………… 322

7-9 Chung diagram for 8-24-42-7W5 SCV gas in the Ferrier- Gilby area ….… 322

7-10 Location of wells affected by gas migration (blue dots), which best matched the Ferrier mudlog. Presumable SCV sources are indicated… .… 323

7-11 Location of wells affected by gas migration (blue dots), which best matched the Gilby mudlog. Presumable SCV sources are indicated……… 323

7-12 Location of wells affected by gas migration (blue dots), which best matched the Pembina mudlog. Presumable SCV source is indicated…….. 324

7-13 Isotope ratios of twelve SCV gases superimposed on the mudgas isotopic depth profile from Lindbergh 13-9-056-06W4.

	Legend for SCV gases is provided in Figure 7-14……………………… ..	325
7-14	SCV gases from Figure 7-13 and their presumable sources. Lindbergh 13-09-056-06W4……………………………………………	326
7-15	Isotope ratios of twelve SCV gases superimposed on the mudgas isotopic depth profile from Lindbergh 13-09-056-06W4. Legend for SCV gases is provided in Figure 7-16………………………. .	327
7-16	SCV gases from Figure 7-15 and their presumable sources. Lindbergh 13-09-056-06W4……………………………….……………..	328
7-17	Isotope ratios of ten (10) SCV gases superimposed on the mudgas isotopic depth profile from Lindbergh 13-9-056-06W4. Legend for SCV gases is provided in Figure 7-18, and a close-up view in Figure 7-19………………………………………	329
7-18	SCV gases from Figure 7-17 and their presumable sources. Lindbergh 13-09-056-06W4……………………………………………	330
7-19	Close-up view of SCV gases from Figure 7-17. Lindbergh 13-09-056-06W4 …………………………………… ……..	330
7-20	Isotope ratios of thirteen SCV gases superimposed on the mudgas isotopic depth profile from Lindbergh 13-9-056-06W4 Legend for SCV gases is provided in Figure 7-21. ……………………….	331
7-21	SCV gases from Figure 7-19 and their presumable sources. Lindbergh 13-9-056-06W4……………………………………………..	332
7-22	Isotope ratios of thirteen SCV gases superimposed on the mudgas isotopic depth profile from Petrovera 1D-25-55-5W4. Legend for SCV gases is provided in Figure 7-23, and a close-up view of the SCV gases presumably related to the Viking Fm. in Figure 7-24……….	333
7-23	SCV gases from Figure 7-22 and their presumable sources. Petrovera 1D-25-55-5W4……………………………………………….....	334
7-24	SCV gases from Figure 7-22 and their presumable sources ………………..	334
7-25	Isotope ratios of fifteen SCV gases superimposed on the mudgas isotopic depth profile from Petrovera 1D-25-55-5W4. Legend for SCV gases is provided in Figure 7-26…………………..…….	335

7-26 SCV gases from Figure 7-25 and their presumable sources.
Petrovera 1D-25-55-5W4……………………………………………………..336

7-27 Isotope ratios of fifteen SCV gases superimposed on the mudgas isotopic depth profile from Petrovera 1D-25-55-5W4.
Legend for SCV gases is provided in Figure 7-28 ……………………….. 337

7-28 SCV gases from Figure 7-27 and their presumable sources.
Petrovera 1D-25-55-5W4…………………………………………………… 338

7-29 Isotope ratios of nine SCV gases superimposed on the mudgas isotopic depth profile from Husky C3-30-47-4W4.
Legend for SCV gases is provided in Figure 7-30……………………….. 339

7-30 SCV gases from Figure 7-29 and their presumable sources.
Husky C3-30-47-4W4……………………………………………………. 340

7-31 Isotope ratios of eight SCV gases superimposed on the mudgas isotopic depth profile from Husky C3-30-47-4W4.
Legend for SCV gases is provided in Figure 7-32……………………….. 341

7-32 SCV gases from Figure 7-31 and their presumable sources.
Husky C3-30-47-4W4……………………………………………………. 342

7-33 Isotope ratios of nine SCV gases superimposed on the mudgas isotopic depth profile from Husky C3-30-47-4W4.
Legend for SCV gases is provided in Figure 7-34………………………… 343

7-34 SCV gases from Figure 7-33 and their presumable sources.
Husky C3-30-47-4W4……………………………………………………. 344

7-35 Isotope ratios of nine SCV gases superimposed on the mudgas isotopic depth profile from Husky C3-30-47-4W4.
Legend for SCV gases is provided in Figure 7-36………………………… 345

7-36 SCV gases from Figure 7-35 and their presumable sources.
Husky C3-30-47-4W4…………………………………………………….. 346

7-37 Isotope ratios of sixteen SCV gases superimposed on the mudgas isotopic depth profile from Petrovera 10-17-47-27W3.
Legend for SCV gases is provided in Figure 7-38………………...……. 347

7-38 SCV gases from Figure 7-37 and their presumable sources.

Petrovera 10-17-47-27W3……………………………………………………… 348

7-39 Isotope ratios of thirteen SCV gases superimposed on the mudgas isotopic depth profile from Petrovera 112-/01-04-48-22W3.
Legend for SCV gases is provided in Figure 7-40………………………… 349

7-40 SCV gases from Figure 7-39 and their presumable sources.
Petrovera 112-/01-04-48-22W3…………………………………………… 350

7-41 Isotope ratios of seventeen SCV gases superimposed on the mudgas isotopic depth profile from Petrovera 112-/01-04-48-22W3.
Legend for SCV gases is provided in Figure 7-42………………………… 351

7-42 SCV gases from Figure 7-41 and their presumable sources.
Petrovera 112-/01-04-48-22W3………………………………… …….. 352

7-43 Isotope ratios of fourteen SCV gases superimposed on the mudgas isotopic depth profile from Husky A9-15- 51-23W3.
Legend for SCV gases is provided in Figure 7-44……………………… 353

7-44 SCV gases from Figure 7-43 and their presumable sources.
Petrovera 112-/01-04-48-22W3………………………………………….. 354

7-45 Base map showing the location of the carbon isotope mud gas depth profiles from the heavy oil region, and the presumable sources for the SCV gases in their vicinity. The most prevalent source is indicated with a yellow star beside…………………………………………………………………… 357

7-46 Frequency of presumable sources for the SCV gases in the vicinity of:
a) Lindbergh 13-9-56-6W4 well, and b) Petrovera 1d-25-55-5W4 well …..358

7-47 Frequency of presumable sources for the SCV gases in the vicinity of:
a) Husky A9-15-51-23W3 well, and b) Husky C3-30-47-4W4 well ……... 359

7-48 Frequency of presumable sources for the SCV gases in the vicinity of:
a) Petrovera 1-4-48-27W3 well, and b) Petrovera 10-17-47-27W3 well … 360

***

8-1 Locations of ten carbon isotope mud gas depth profiles in the WCSB …... 361

8-2 Schematic geological cross-section illustrating the relative positions of Ferrier, Gilby, Husky 3C-30, and Lindbergh 13A-9 profiles.

Thermal maturity of the foreland basin strata in the study areas is represented after Bustin, 1991. Isolines represent vitrinite reflectance Romax%. The location of the line of cross section (A-A') is shown in Figure 8-1……………………………………………………………...… 363

8-3 Plots of: (a) Depth - δ ^{13}C values for CH_4; (b) Depth – Wetness index profiles in the WCSB. The data used is derived from the four carbon isotope mudgas profiles plotted along the geological cross section from Figure 8-2. ………………………………………………………………… 365

8-4 Bernard diagram showing the distribution of mudgases from four isotopic mudgas profiles plotted along the geological cross section A-A' from Figure 8-1. Mixtures of bacterial and thermogenic gases appear to be developed in majority of the gases, with a strong migrational component for shallower gases: Paskapoo and Scollar, in the Ferrier profile………...… 367

8-5 Plot of wetness vs. methane δ ^{13}C of the mud gas data of the four isotope depth profiles in Figure 8-2. ……………………………………………..…. 368

8-6 Plot of methane δ ^{13}C vs. ethane δ ^{13}C of the mud gas data of the four isotope depth profiles in Figure 8-2. Published data indicate that cogenetic gases have 5‰< (δ^{13}Cethane - δ^{13}C methane) < 18‰. Mixing with isotopically light bacteriogenic methane shifts gas compositions outside the cogenetic field in the direction shown by the arrow……………………………………… 370

8-7 Plot of ethane δ ^{13}C vs. methane δ ^{13}C of the mud gas data of the four isotope depth profiles in Figure 8-2. Two main clusters are shown: foothills-, and heavy oil gases. Position of the vitrinite reflectance curve for type II kerogen: after Faber (1987), and Whiticar (1990)……………..….. 371

8-8 C2/C3 versus C2/iC4 diagram showing the possible biodegradation of some of the Colorado hydrocarbon gases from the Lloydminster heavy oil area (after Prinzhofer, 2000) …………………………………… 373

8-9 Combination plot of δ^{13}C$_{CO2}$ and δ^{13}C$_{CH4}$ with isotope fractionation lines (Ec) for the Paskapoo Formation gases in the foothills area (after Whiticar, 1999). …………………………………………………… 374

8-10 Plot of ethane δ ^{13}C vs. propane δ ^{13}C of the mud gas data of the four isotope depth profiles in Figure 8-2. The maturity relation (red line) is taken from Faber (1987), and Whiticar (1990)…………………… …. 376

8-11 Plot of ethane $\delta\ ^{13}C$ vs. propane $\delta\ ^{13}C$ of the mud gas data of the four isotope depth profiles in Figure 8-2. Apart from Figure 8-9, here gases are grouped by stratigraphic unit (from oldest to youngest): Sub-Cretaceous (red symbols), Cretaceous Mannville (green symbols), Cretaceous Colorado (blue symbols), Cretaceous Lea Park (purple symbols), Cretaceous Belly River (dark yellow symbols), and Cretaceous-Tertiary Edmonton Gp to Paskapoo (yellow symbols). Two apparent maturity trends are shown: the red dashed line in the foothills area, and the green dashed line in the heavy oil area………………………………………….......... 377

8-12 Graph of ethane $\delta\ ^{13}C$ vs. propane $\delta\ ^{13}C$ for mudgas samples from the Lea Park-, Horseshoe Canyon-, Scollard, and Paskapoo formations – foothills region. Lea Park sediments are dominated by Type III organic matter ((Schröder-Adams et al., 1997), and Horseshoe Canyon – Paskapoo formations contain coal beds throughout. Maturity curves: after Berner and Faber (1996)………………………………………………… 378

8-13 Plot of propane concentration vs. propane $\delta\ ^{13}C$ of the mud gas data of the four isotope depth profiles in Figure 8-2. As in Figure 8-10, effects of maturation and oxidation are distinguished……………………………...… 380

8-14 Plot of ethane concentration vs. ethane $\delta\ ^{13}C$ of the mud gas data of the four isotope depth profiles in Figure 8-2. Arrows indicate maturation trends, and distribution of mixed gases (bacteriogenic and migrated)……. 381

8-15 Carbon isotopic difference between propane and ethane vs. that between ethane and methane for mudgas data of the four isotope depth profiles in Figure 8-2. Maturation arrows are based on the models of James (1983) (black arow), and Sundberg and Bennet (1983) (red arrow)…………….. 383

8-16 Plot of ethane $\delta^{13}C$ vs. Bernard parameter [C1/(C2+C3)] for the Colorado mudgases in Husky 3C-30-47-4W4 and Lindbergh 13A-9-56-6W5……. 384

8-17 Plot of ethane $\delta\ ^{13}C$ vs. propane $\delta\ ^{13}C$ of the Colorado Group mud gas data of the three isotope depth profiles in Figure 8-2. The maturity relation (red line) is taken from Faber (1987), and Whiticar (1990). The deviation of ethane isotopes in sediments above the Second White Specks Shale Fm. in the heavy oil region towards values that indicate an enrichment of ^{12}C can be explained by an admixture of near-surface bacterial ethane to “incipient” (low temperature thermogenic) gases. ……………………………………. 385

8-18 “C1-C2” diagram showing segregative migration among a) Lea Park gases, and b) Colorado gases from Ferrier, Gilby, and Husky – Lindbergh (after Prinzhofer and Pernaton, 1997)……………………………………… 388

8-19 “C1-C2” diagram showing two distinct clusters among Mannville mudgases from Gilby (foothills area), and Husky – Lindbergh (heavy oil area). After Prinzhofer and Pernaton, 1997……………………………………… 389

8-20 Variations in wetness, methane d13C, and ethane d13C in mudgases from the foothills region ……………………………………………………….. 392

8-21 SW to NE stratigraphic cross -section showing carbon isotope depth profiles from four wells across the two study areas in the Western Canada Sedimentary Basin. Datum is Sea Level. The stratigraphic units used in the study are correlated across the four wells. Each well includes isotope profiles for methane, ethane, propane; normal-, and isobutane are added for the two Lloydminster wells……………………………………………………….. 394

8-22 Lindbergh 13A-09-56-6W4 isotopic depth profile plotted together with: a) gas compartments identified using the multilog quantification approach; and b) the simplified litholog of the stratigraphic section, showing main sandstone bodies, siderite concretion , and shale-rich layers. Legend for key stratigraphic surfaces is same as in Figure 8-21 ……………………… 395

8-23 Carbon isotope depth profile for Pembina 11-04-49-11W5 plotted together with a simplified litholog of the stratigraphic section. The arrows on the left side of the profile represent gas compartment boundaries as resulted from the multilog quantification approach. Many inflections on the simplified lithologs appear at the same stratigraphic level as the effective barriers identified using the multilog quantification. The black arrows on the right side of the profile points towards some of the isotopic inflections most probably and most reliably related to physico-chemical contrasts at the shale/sand contacts. Suggested bentonite influence on the isotopic variations is represented with blue circles…………………………………………… 400

LIST OF APPENDICES

<u>Appendix A</u>: Photographs of cores (Plates 1-122) and their log signatures (Figures A-3 to A-40)

Page

Figure A-1 Location map of the Foothills region, showing the core control used in this study ……………………………………………………..……. 449
Figure A-2 Location of the cored well from the heavy - oil region, which penetrates the entire Mannville Group in the Lloydminster area ……… 450

Figure A-3 Core from the Belly River Formation (06-04-042-04W5/0 well) with accompanying wireline log signatures ………………………….…….. 451

Figure A-4 Core from the Lea Park - Belly River formations (02/06-09-046-09W5/0 well) with accompanying wireline log signatures …... 452

Figure A-5 Core from the Lea-Park - Belly River formations (08-02-043-05W5/0 well) with accompanying wireline log signatures …..…. 453

Figure A-6 Core from the Lea-Park - Belly River formations (09-10-044-09W5/0 Well) with accompanying wireline log signatures …….. 454

Figure A-7 Core from the Belly River formation (10-04-049-11W5/0 well) with accompanying wireline log signatures ……………………………..455

Figure A-8 Core from the Lea-Park - Belly River formations (14-28-042-04W5/0 well) with accompanying wireline log signatures …..….. 456

Figure A-9 Core from the Belly River formation (16-11-045-07W5/0 well) with accompanying wireline log signatures …………………...…….. 457

Figure A-10 Core from the Lea-Park - Belly River formations (08-25-042-05W5/0 well) with accompanying wireline log signatures …..….. 458

Figure A-11 Core from the Cardium Formation (02-33-047-07W5/0 well) with accompanying wireline log signatures ……………………….…. 459

Figure A-12 Core from the Cardium Formation (06-12-048-11W5/0 well) with accompanying wireline log signatures ……………………………. 460

Figure A-13 Core from the Cardium Formation (06-14-042-06W5/0 well) with accompanying wireline log signatures ………………...……….. 461

Figure A-14. Core from the Cardium Formation (06-26-048-11W5/0 well) with accompanying wireline log signatures …………………...….…. 461

Figure A-15. Core from the Cardium Formation (06-33-048-11W5/0 well) with accompanying wireline log signatures …………………………… 463

Figure A-16. Core from the Cardium Formation (09-32-043-07W5/0 well) with accompanying wireline log signatures ………………………………..…. 464

Figure A-17. Core from the Cardium Formation (10-11-043-09W5/0 well) with accompanying wireline log signatures …………………………..… 465

Figure A-18. Core from the Cardium Formation (10-14-044-09W5/0 well) with accompanying wireline log signatures ……………………………. 466

Figure A-19. Core from the Cardium Formation (10-16-042-09W5/0 well) with accompanying wireline log signatures ……………………..…………. 467

Figure A-20. Core from the Cardium Formation (10-23-043-09W5/0 well) with accompanying wireline log signatures ……………………………. 468

Figure A-21. Core from the Cardium Formation (10-26-045-09W5/0 well) with accompanying wireline log signatures …………………………………..…. 469

Figure A-22. Core from the Cardium Formation (11-30-045-09W5/0 well) with accompanying wireline log signatures ……………………………. 470

Figure A-23. Core from the Cardium Formation (12-03-042-09W5/0 well) with accompanying wireline log signatures ……………………………. 471
.
Figure A-24. Core from the Cardium Formation (14-01-042-07W5/0 well) with accompanying wireline log signatures ……………………….…… 472

Figure A-25. Core from the Cardium Formation (14-06-047-09W5/0 well) with accompanying wireline log signatures ……………………………….. 473

Figure A-26. Core from the Cardium Formation (16-16-047-10W5/0 well) with accompanying wireline log signatures ……………………….…… 474

Figure A-27. Core from the Colorado Group (06-22-042-09W5/0 well) with accompanying wireline log signatures ……………………...…….. 475

Figure A-28. Core from the Cardium Formation (04-10-042-09W5/2 well) with accompanying wireline log signatures ……………………………. 476

Figure A-29. Core from the Belly River Formation (10-10-042-09W5/0 well) with accompanying wireline log signatures …………………………… 477

Figure A-30. Core from the Viking Formation (06-12-045-07W5/0 well) with accompanying wireline log signatures …………………………….….. 478

Figure A-31. Core from the Viking Formation (07-06-042-07W5/0 well) with accompanying wireline log signatures ………………...……….. 479

Figure A-32. Core from the Viking Formation (07-08-042-05W5/0 well) with accompanying wireline log signatures …………………………… 480

Figure A-33. Core from the Viking Formation (08-11-042-07W5/0 well) with accompanying wireline log signatures ……………………………. 481

Figure A-34. Core from the Viking Formation (10-17-042-04W5/0 well) with accompanying wireline log signatures ……………………………. 482

Figure A-35. Core from the Viking Formation (03/13-13-045-05W5/0 well) with accompanying wireline log signatures …………………………… 483

Figure A-36. Core from the Joli Fou – Mannville contact (03-13-043-05W5/0 well) with accompanying wireline log signatures ……… 484

Figure A-37. Core from the Joli Fou – Mannville contact (10-32-048-06W5/0 well) with accompanying wireline log signatures …...…. 485

Figure A-38. Core from the Joli Fou - Mannville contact (02/11-15-045-07W5/0 well) with accompanying wireline log signatures …... 486

Figure A-39. Core from the Joli Fou – Mannville contact (16-11-045-07W5/0 well) with accompanying wireline log signatures ……… 487

Figure A-40. Core from the Joli Fou – Mannville section (10-25-047-03W4/0 well) with accompanying wireline log signatures ……... 488

PLATES ……………………………………………………………… 490

Appendix B

Page

Appendix I

I-1 Along-dip regional well-log cross-section – Foothills region: Section 1-1' ……… 735

I-2 Along-strike regional well-log cross-section – Foothills region: Section 2-2' …....736

I-3 Along-dip regional well-log cross-section – Foothills region: Section 3-3' ……… 737

I-4 Along-dip regional well-log cross-section – Foothills region: Section 4-4' ……… 738

I-5 Along-strike regional well-log cross-section – Foothills region: Section 5-5' …... 739

Appendix II

II-1 Along-dip regional well-log cross-section – Lloydminster region: Section 1-1' 740

II-2 Along-dip regional well-log cross-section – Lloydminster region: Section 2-2' …741

II-3 Along-dip regional well-log cross-section – Lloydminster region: Section 3-3' …742

II-4 Along-dip regional well-log cross-section – Lloydminster region: Section 4-4' …743

II-5 Along-strike regional well-log cross-section
- Lloydminster region: Section 5-5' ……………………………………..……....744

II-6 Along-strike regional well-log cross-section
- Lloydminster region: Section 6-6' ……………………………..…………745

II-7 Along-strike regional well-log cross-section
- Lloydminster region: Section 7-7' …………………..…………………...… 746

II-8 Along-strike regional well-log cross-section
- Lloydminster region: Section 8-8' ………………………… ………………….. 747

Appendix III

III-1 Composite diagram showing the compositional profile for Ferrier 14-3-42-9W5 together with data that result from the isotope ratio mass spectrometry ………………………………………………………………..….748

III-2 Composite diagram showing the compositional profile for Gilby 15-16-42-4W5 together with data that result from the isotope ratio mass spectrometry ………………………………………………………………….…... 749

III-3 Composite diagram showing the compositional profile for Pembina

11-4-49-11W5 accompanied by data that result from the isotope ratio mass spectrometry ……………………………………………………………………………750
III-4 Composite diagram showing the compositional profile for Lindbergh 4C-16/13-09-56-6W4 together with data that result from the isotope ratio mass spectrometry ……………………………………………………………………………751
III-5 Composite diagram showing the compositional profile for Petrovera 1D-25-55-5W4 together with data that result from the isotope ratio mass spectrometry ……………………………………………………………………………752
III-6 Composite diagram showing the compositional profile for Husky C3-30-47-4W4 together with data that result from the isotope ratio mass spectrometry ……………………………………………………………………………753
III-7 Composite diagram showing the compositional profile for Husky A9-15-51-23W5 together with data that result from the isotope ratio mass spectrometry ……………………………………………………………………………754

CHAPTER FIVE

FORMATION COMPARTMENTALIZATION USING ISOTOPIC FINGERPRINTS OF MUDGASES AND MULTILOG QUANTIFICATION

5.1. Introduction

Starting with the recognition of major gas compartments identified in Chapter Three, and separated by regional stratigraphic boundaries (e.g. the subaerial unconformity at the base of the Scollard Formation, the Lea Park – Colorado Group boundary or the Joli Fou – Mannville Group contact) or major sequence stratigraphic surfaces (marine flooding surfaces, ravinement surfaces or maximum regressive surfaces) – the present approach will try to explain the nature of additional boundaries (either lithological and/or pressure boundaries or isotopic boundaries).

At this point of the study it is recognized that we can consider the existence of two major types of boundaries: ***isotopic boundaries*** and ***stratigraphic boundaries***. In most of the cases, isotopic boundaries coincide with stratigraphic boundaries (see Figures 3-8 to 3-10, Chapter Three). This strong correlation between isotopic and stratigraphic boundaries indicates that the compartmentalization of the gas is strongly influenced by stratigraphic variations. As already concluded in Chapter Three, such boundaries are loci of preferential fluid flow and appear as anomalies on geochemical depth profiles.

In some cases, however, the stratigraphic boundaries do not correspond with any observed inflections or variations in the trends of the isotopic ratios with depth – indicating cross-formational flow across them, and suggesting that they may act as less effective (partial effective) or even ineffective barriers for vertical gas migration.

Other inflections in the trends of the isotopic ratios with depth occur within major stratigraphic formations, suggesting intra-formational compartmentalization of the gas - the presence of sub-compartments within the major compartments identified. These boundaries represent in part isotopic boundaries that are not major stratigraphic boundaries, and whose nature this Chapter will try to explain.

Also related to such of inflections in the trends of the isotopic ratios with depth, which are not coincident with stratigraphic boundaries, one might expect some of the kicks to be correlated to local variations of alteration (biodegradation and/or mixing) or gas generation.

5.2. Methodology

5.2.1. Examination of inflections in the multi-component geochemical depth profiles

The carbon isotope depth profiles for all three locations in the Foothills region (Ferrier 14-3-42-4W5, Gilby 15-16-42-4W5 and Pembina 11-4-49-11W5) and for only four locations (digital logs were available for only four wells) in the Heavy oil region (Husky A9-15-51-23W3, Husky 3C-30-47-4W4, Lindbergh 13-9-56-6W4, and Petrovera 1D-25-55-5W4) were examined based on a simple visual inspection of inflections in the multi-component geochemical depth profiles.

The geochemical parameters mainly used in this visual examination were:

- the absolute values of the carbon isotopic ratio for the various gaseous components ($\delta^{13}C_1$, $\delta^{13}C_2$, $\delta^{13}C_3$, and $\delta^{13}C_4$ ratios) and their trends towards an upward increase or decrease;
- the absolute compositional analyses;
- the isotopic differences $\Delta\delta^{13}C$ ($C_n - C_{n-1}$);
- the concentration ratios: iC_4/nC_4 and C_3/C_2.

Geochemical data from a total of seven isotopic depth profiles from both the Foothills-, and the heavy oil region (see Appendices III-1 to III-7) were integrated with mineralogical profiles derived from gamma-ray, sonic, density, litho-density, and neutron porosity logs. The wireline data have been used to derive mineral fractions and porosity, as it will be further explained.

5.2.2. Matrix algebra compositional log analysis

Formations from all wells with isotopic fingerprints were evaluated using wireline data transformed to generate continuous mineralogical profiles. Sonic transit time, neutron porosity, bulk density, gamma and photoelectric factor wireline data, recorded at 20 cm intervals were made available by IDC Database, Calgary. These data have been used to derive porosity and mineral proportions using methods outlined by Doveton (1994) and Hearst and Nelson (1985).

The mathematics for lithofacies analysis from logs was drawn from simple matrix algebra. However, before considering the theory behind matrix algebra solutions, a most important point must be made: a log crossplot indexed with mineral reference points is an illustration of a matrix algebra system of equations. A matrix algebra solution of component composition is equivalent to a compositional estimation of crossplotted zones.

In order to solve for mineral components, they must be explicitly identified (at least provisionally), and crossplots are invaluable for this phase of diagnosis.

5.2.2.1. Mineral identification through crossplots

Geophysical crossplots are a convenient way to demonstrate how various combinations of logs respond to lithology and porosity (Doveton, 1986; Western Atlas, 1992).

All dual mineral crossplot methods use a minimum of three anchor points to resolve data from two log measurements (Doveton, 1986). One of these points is always the 100% porosity or fluid parameter. The other control points represent the predictable zero porosity value for each of the two measurements and the particular matrices selected (sandstone -, or limestone matrices). For example, if lithology were assumed to be limestone and dolomite, and the two log measurements are bulk density (ρ_b) and compensated neutron porosity (Φ_N), the zero porosity values for limestone and dolomite would be:

$\rho_b = 2.71$ g/cm^3 (limestone) and 2.86 g/cm^3 (dolomite)

$\Phi_N = 0$ Φ units (limestone) and 0.02 Φ units (dolomite).

In this study three or four sets of log data were utilized to determine porosity and a mix of three or four defined rocks or minerals.

Before any compositional log analysis was done, lithology interpretation was facilitated by the use of various geophysical crossplots (sonic – density, neutron – density, neutron- sonic, M-N, Roma-Uma, etc.).

The density – neutron crossplot is the most accurate log analysis method for estimating porosity, as agreed by many of the formation evaluation specialists (Hearst and Nelson, 1985; Doveton, 1986; Western Atlas, 1992). One of such crossplot is shown in Figure 5-1.

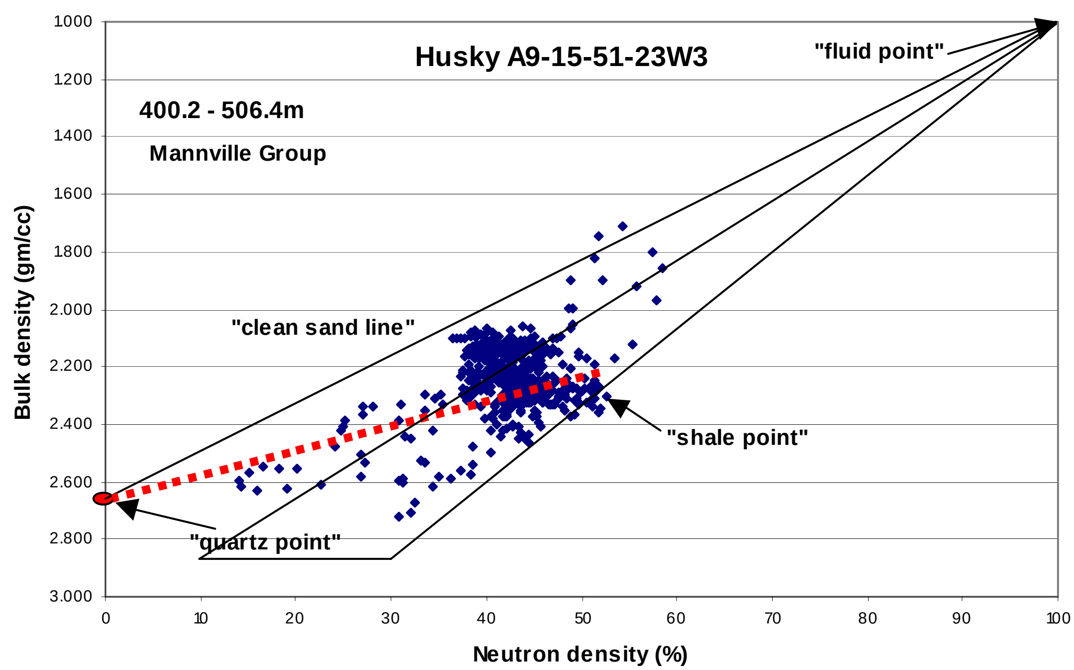

Figure 5-1 Neutron – density crossplot for the Mannville Group at Husky A9-15-51-23W3 well location, Lloydminster region.

Where three porosity logs are available, the ideal crossplot would incorporate all three simultaneously. The M – N plot (Figure 5-2) is a means of combining data from three porosity logs in such a manner that effects due to porosity variation are almost eliminated and those due to matrix changes are maximized. The quantities M and N are defined by:

$$M = 0.01\ (t_f - t)/(\rho_b - \rho_f) \qquad (5.1.)$$

$$N = (\Phi_{Nf} - \Phi_N)/\ (\rho_b - \rho_f), \qquad (5.2.)$$

where t, ρ_b, and Φ_N are log value of sonic travel time (μsec/ft), bulk density (g/cm^3), and neutron porosity (porosity units); and t_f, ρ_f, and Φ_{Nf} are the corresponding values for the pore fluid.

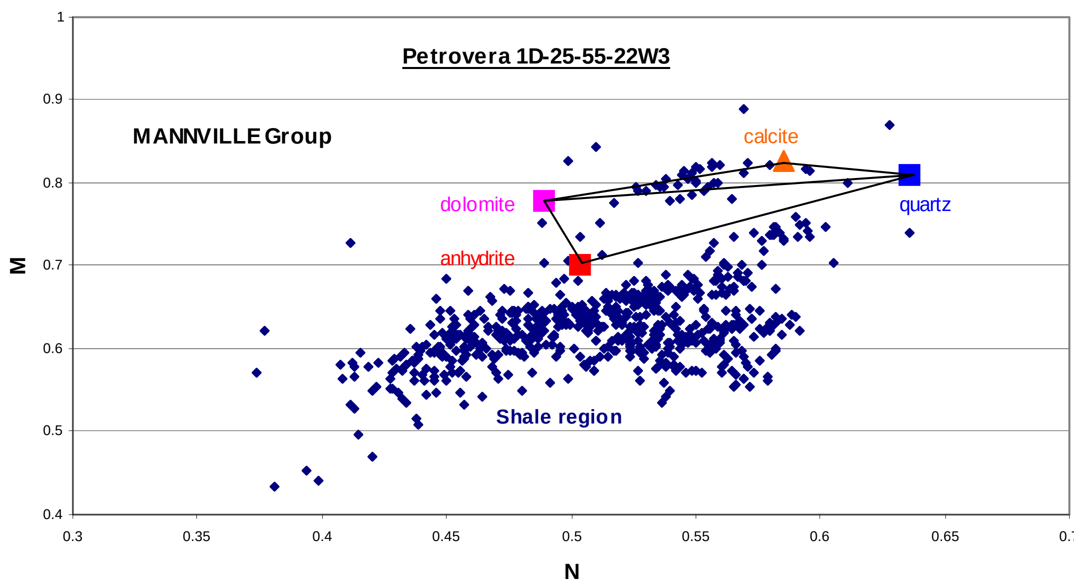

Figure 5-2 M – N plot for mineral identification applicable to Mannville Group at Petrovera 1D-25-55-22W3 well location, heavy oil region - Alberta.

Another crossplot technique for identifying lithology uses data from the Litho-Density log (Figure 5-3). It crossplots the apparent matrix grain density, ρ_{maa}, and the apparent matrix volumetric cross-section, U_{maa}, in barns per cubic centimetre; this plot it is also known as the Roma-Uma crossplot. The apparent matrix grain density has been obtained with the following equation (John Doveton, personal communication):

$$\rho_{maa} = 2.71\text{-}(\rho_b * 1.71/100),$$

where ρ_b is the bulk density from density log. The apparent matrix volumetric cross-section, U_{maa} was computed from the photoelectric cross section index (P_e factor) and the bulk density measurements (John Doveton, personal communication):

$$U_{maa} = P_e * \rho_b$$

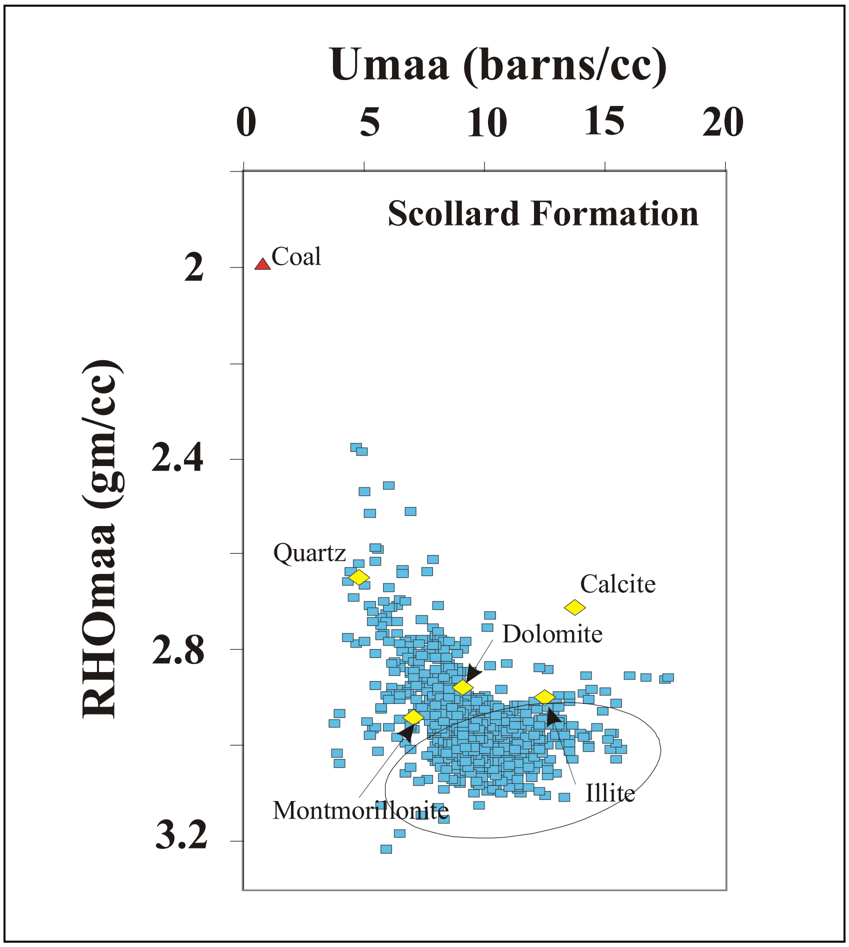

Figure 5-3 ROMA - UMA crossplot for lithology identification. Scollard Formation, well Pembina 11-4-49-11W5, Foothills region, Alberta.

All these crossplots can be used as an initial reconnaissance evaluation that precedes the quantitative solution of porosity, shale content and/or specific mineral content by a matrix algebra solution. Numerous crossplots can be used to manipulate the data, and to verify selected control parameters. It should be mentioned that no crossplot method is completely accurate (Doveton, 1986; Doveton, 2000); every method has advantages and disadvantages. In order to obtain "the best answer", at least three measurements were used in this study and, quite often, several two-way crossplots – for various formations and depth intervals.

5.2.2.2. Matrix algebra compositional log analysis - calculations

A multiple log-transformation approach was used to derive the shale content (or specific clay minerals content), as well as quartz, siderite, K-feldspar, muscovite and coal contents within the foreland basin succession in both foothills and heavy oil regions of Alberta and Saskatchewan.

The signals from the sonic transit time, neutron porosity, gamma, bulk density and PEF (photoelectric factor) logs were integrated and solved for two, three or four ***mineral types*** and ***total porosity*** using matrix algebra compositional analysis of these logs. Each separate log signal at any given depth was related to the solid grain volume using algorithms below (for ***sonic transit time log***):

$$\mathbf{\Delta t = \Delta t_{M1}\, M1 + \Delta t_{M2}\, M2 + \Delta t_{M3}\, M3 + \Delta t_{M4}\, M4 + \Delta t_{\varphi}\, \varphi},$$ where:

Δt sonic transit time recorded by log (μs/ft)

Δt_{Mx} sonic transit time for mineral x (μs/ft)

Mx proportion of mineral x (as fraction of total rock volume)

Φ porosity (as fraction of total rock volume)

Δt_{φ} sonic transit time of fluid in pore space (μs/ft)

Two assumptions are made (Hearst and Nelson, 1985; Doveton, 1986):

1. the sum of the mineral fractions plus porosity equals unity;
2. linear relationships between mineral proportions and their contribution to the petrophysical signal.

A lithological sequence composition (Figure 5-4) could be solved in this way with up to five-six components, provided that a sufficient log number is available (i.e. *n* components will require *n-1* logs for an explicit solution).

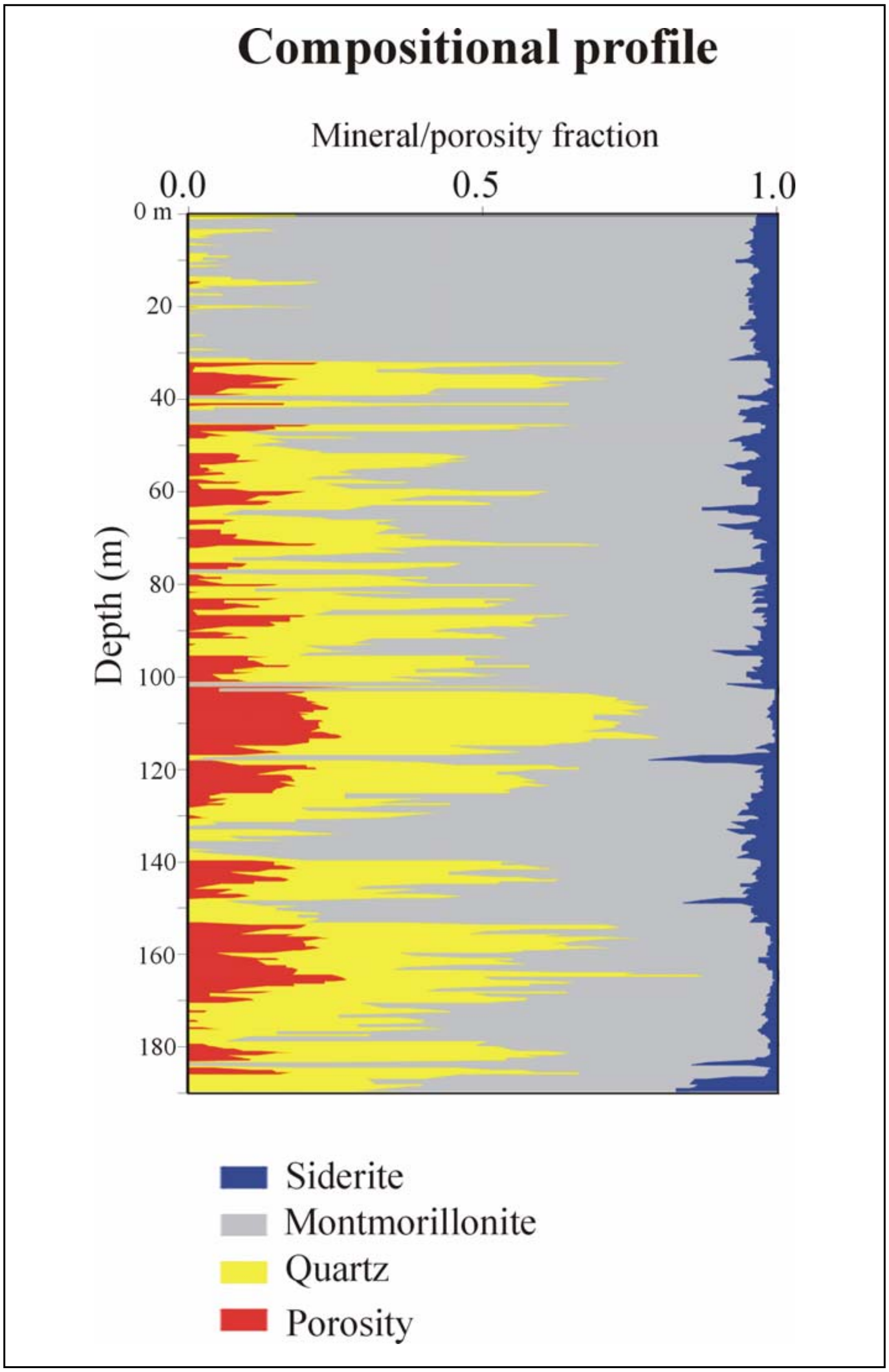

Figure 5-4 Example of compositional profile, calculated by a matrix algebra solution.

For example, with five algorithms and five unknowns (proportions of four minerals M1 to M4, plus porosity), the following set of equations have been solved simultaneously at each depth interval:

$$
\begin{cases}
\Gamma = M1\ \Gamma_1 + M2\ \Gamma_2 + M3\ \Gamma_3 + M4\ \Gamma_4 + \varphi\ \Gamma_\varphi \\
\Phi_N = M1\ \Phi_{N1} + M2\ \Phi_{N2} + M3\ \Phi_{N3} + M4\ \Phi_{N4} + \varphi\ \Phi_{N\varphi} \\
\rho = M1\ \rho_1 + M2\ \rho_2 + M3\ \rho_3 + M4\ \rho_4 + \varphi\ \rho_\varphi \\
\Delta t = M1\ \Delta t_1 + M2\ \Delta t_2 + M3\ \Delta t_3 + M4\ \Delta t_4 + \varphi\ \Delta t_\varphi \\
1 = M1 + M2 + M3 + M4 + \varphi
\end{cases}
$$

The terms used in these equations are:

Mx	proportion of mineral *x* (as fraction of total rock volume)
Φ	porosity (as fraction of total rock volume)
Γ	gamma ray recorded by log (API units)
ΓMx	gamma ray of mineral *x* (API units)
Δt	sonic transit time recorded by log (µsec/ft)
ΔtMx	sonic transit time of mineral *x* (µsec/ft)
Δt_φ	sonic transit time of fluid in pore space (µsec/ft)
ρ	density recorded by log (g/cm^3)
ρMx	density of mineral *x* (g/cm^3)
ρ_φ	density of fluid in pore space (g/cm^3)
Φ_N	neutron density recorded by log (porosity units)
Φ_{NMx}	neutron density of mineral *x* (porosity units)
$\Phi_{N\varphi}$	neutron density of fluid in pore space (porosity units)

Logging parameters (petrophysical responses) for some common rocks and minerals were taken from Hearst and Nelson (1985), and from the Western Atlas and Schlumberger chartbooks.

The analysis of clastic sequences in this study has been somewhat complex owing to the significant content of shale and the wide range possible for clay mineral composition, nature and volumetric content of the silt-sized fraction, and degree of compaction.

Whenever possible, a specific type(s) of clay minerals have been chosen to express the mineralogical content for a certain depth interval and/or formation. Four clay minerals were commonly used to constrain the bulk mineralogy: montmorillonite, illite, smectite and chlorite. However, if any of these four clay minerals did not give a solution for matrix algebra, a "shale point" is empirically defined. The "shale point" is chosen to correspond to the extreme value, but within the supposed shale field.

Shaliness produces a shift of the crossplotted points in a chart in the direction of the "shale point". The "shale point" is found by crossplotting the measured values ($\Phi_{N\ shale}$, ρ_{shale}, Δt_{shale}). Generally, "the shale point" is in the southeast quadrant of neutron-density crossplot and sonic-density crossplot, to the northeast on the neutron-sonic crossplot, and in the lower centre of the density-photoelectric cross-section crossplot (Schlumberger, 1999).

Figures 5-5 and 5-7 demonstrate the use of crossplots in the location of a representative "shale point" as an aid in the qualitative interpretation of the sequences. The shale points on the crossplots specify the log response properties of shales, which can be considered to be typical in the sections. Typically, the shale points typify shales between the sandstones.

In Figure 5-5, the "shale point" is chosen in the northeastern corner on the neutron-sonic crossplot. Its representative logging parameters are as follows: $\Phi_{N\ shale}$ = 40.06, Δt_{shale} = 100.47, ρ_{shale} = 2.37, Γ_{shale} = 214.53, PEF = 3.66. The shale point is located at 1850.4 m depth within the Colorado sequence at Gilby 15-16-42-4W4 well location. The basic mineralogy of the section consists of *quartz*, and a "*shale*" component, which can be resolved by only two logs, the gamma-ray and the neutron density in this case. In the compositional analysis of the Colorado section, these two logs were used to provide the necessary three equations (when adding the unity equation) to solve for the three components (quartz, shale and porosity) at each successive 20 cm increment of depth.

The set of equations would be:

$$\begin{cases} \Gamma = M_{quartz}\,\Gamma_{quartz} + M_{shale}\,\Gamma_{shale} + \varphi\,\Gamma_{\varphi} \\ \Phi_N = M_{quartz}\,\Phi_{Nquartz} + M_{shale}\,\Phi_{Nshale} + \varphi\,\Phi_{N\,\varphi} \\ 1 = M_{quartz} + M_{shale} + \varphi \end{cases}$$

or, introducing the corresponding logging parameters:

$$\begin{cases} \Gamma = M_{quartz} \text{ x } 0 + M_{shale} \text{ x } 214.53 + \varphi \text{ x } 0 \\ \Phi_N = M_{quartz}\,(-1) + M_{shale} \text{ x } 40.06 + \varphi \text{ x } 100 \\ 1 = M_{quartz} + M_{shale} + \varphi \end{cases}$$

The compositional profile of the Colorado Group (1445 – 1966.8 m depth interval) from Gilby 15-16-42-4W5, based on neutron and gamma-ray logs, and calculated by a matrix algebra solution is presented in Figure 5-6.

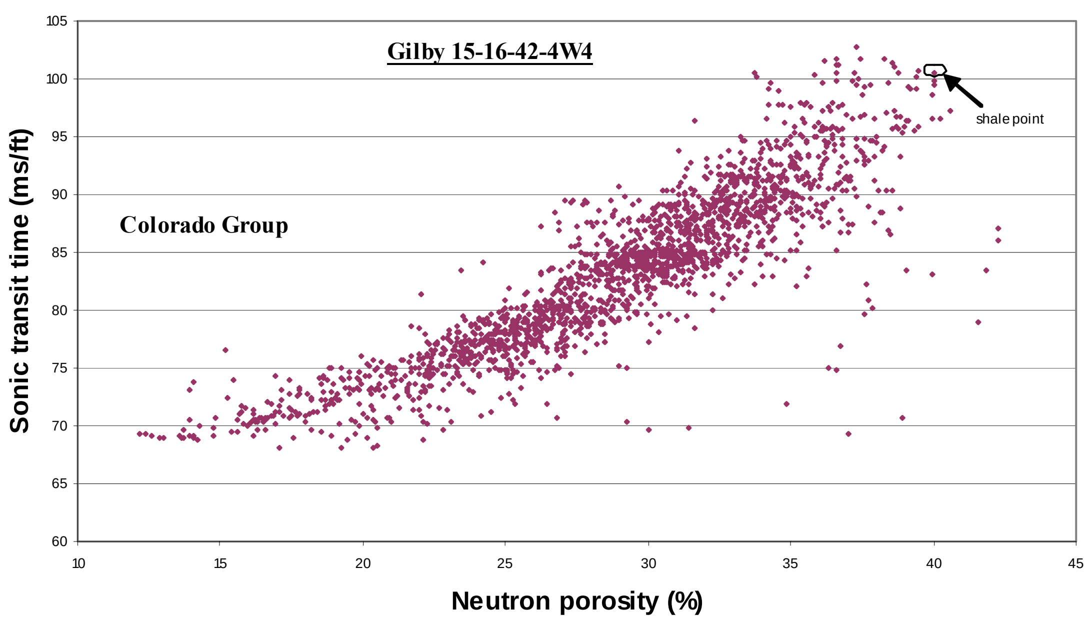

Figure 5-5 Shale point defined on a neutron – sonic crossplot. Values are from the Colorado Group, Gilby 15-16-42-4W4, west-central Alberta.

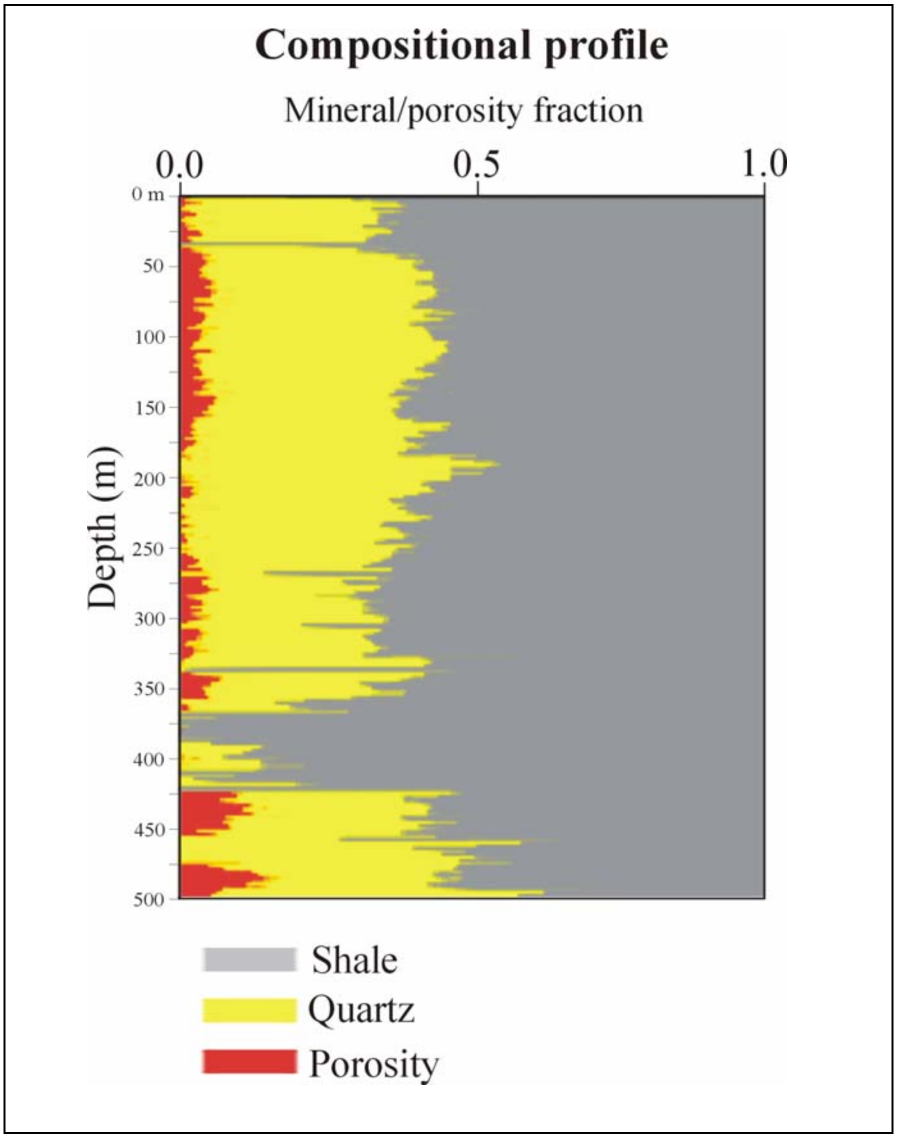

Figure 5-6 Matrix algebra solution for Colorado Group in Gilby 15-16-42-4W5 well, west-central Alberta. The result is shown as a graphic lithology log of the system porosity-shale-quartz.

In Figure 5-7, the "shale point" is chosen in the southeastern corner on the neutron-density crossplot. Its representative logging parameters are as follows: $\Phi_{N\ shale}$ = 40.41, ρ_{shale} = 2.37, Γ_{shale} = 101.24, PEF = 2.28. The shale point is located at 623.8 m depth within the alternating sand-shale-coal sequence of the Mannville Group at Husky 3C-30-47-4W4 well location.

The composition of the section was resolved in terms of the components quartz, shale, coal and pore fluid as calculated by a matrix algebra solution, using the gamma-ray, neutron and density logs.

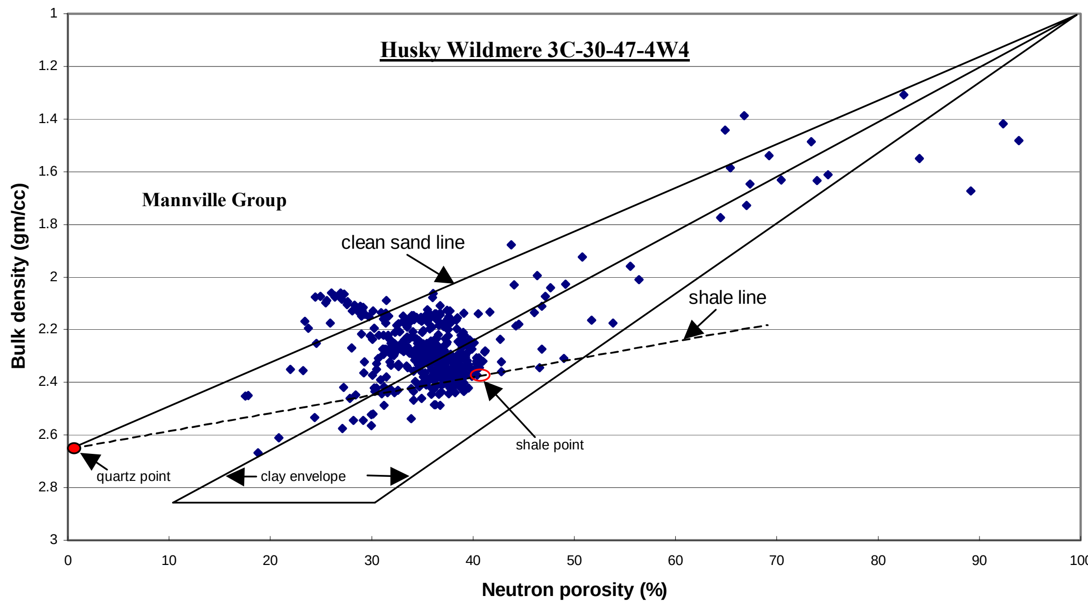

Figure 5-7 Shale point defined on a neutron – density crossplot. Values are from the Mannville Group, Gilby 15-16-42-4W4, west-central Alberta.

The following set of equations would be considered in this case:

$$\begin{cases} \Gamma = M_{quartz}\,\Gamma_{quartz} + M_{shale}\,\Gamma_{shale} + M_{coal}\,\Gamma_{coal} + \varphi\,\Gamma_{\varphi} \\ \Phi_N = M_{quartz}\,\Phi_{Nquartz} + M_{shale}\,\Phi_{Nshale} + M_{coal}\,\Phi_{Ncoal} + \varphi\,\Phi_{N\,\varphi} \\ \rho = M_{quartz}\,\rho_{quartz} + M_{shale}\,\rho_{shale} + M_{coal}\rho_{coal} + \varphi\,\rho_{\varphi} \\ 1 = M_{quartz} + M_{shale} + M_{coal} + \varphi \end{cases}$$

or, introducing the corresponding logging parameters:

$$\begin{cases} \Gamma = M_{quartz} \text{ x } 0 + M_{shale}\, 101.24 + M_{coal} \text{ x } 15 + \varphi \text{ x } 0 \\ \Phi_N = M_{quartz}\,(-1) + M_{shale} \text{ x } 40.41 + M_{coal} \text{ x } 50 + \varphi \text{ x } 100 \\ \rho = M_{quartz} \text{ x } 2.65 + M_{shale} \text{ x } 2.37 + M_{coal} \text{ x } 1.24 + \varphi \text{ x } 1 \\ 1 = M_{quartz} + M_{shale} + M_{coal} + \varphi \end{cases}$$

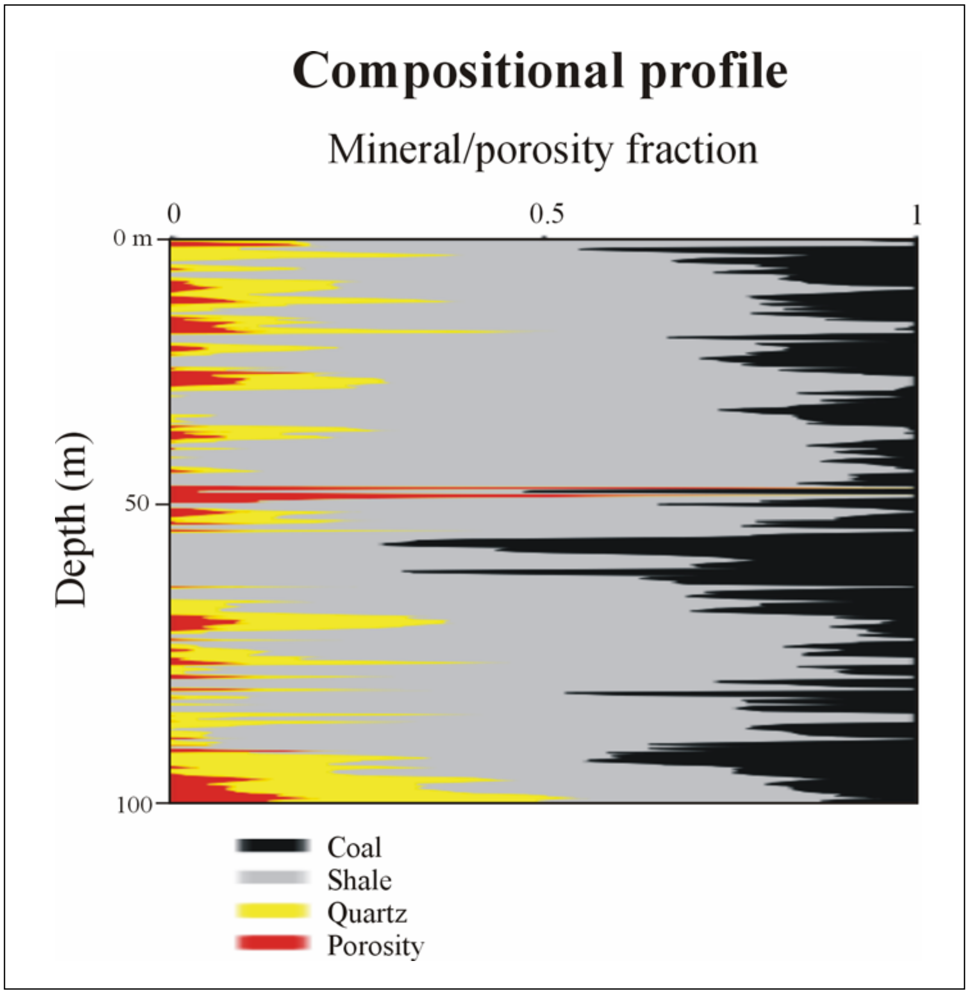

Figure 5-8 Matrix algebra solution for the Mannville Group in Husky 3C-30-47-4W4 well, Lloydminster region. The result is shown as a graphic lithology log of the system porosity-shale-quartz-coal.

The compositional profile of the Mannville Group (541 – 634 m depth interval) from Husky Wildmere 3C-30-47-4W4, based on neutron, bulk density and gamma-ray logs, and calculated by a matrix algebra solution is presented in Figure 5-8.

All the other compositional profiles presented in Appendices III-1 to III-7 were calculated correspondingly, by a matrix algebra solution, and based on various geophysical logs (gamma-ray, bulk density, sonic, neutron density, litho-density).

Although the matrix algebra solutions are not unreasonable representations of the lithology variation in the clastic sequences, they can only be considered as highly generalized results (Doveton, 1986).

5.2.3. X-Ray diffractometry analysis (XRD)

A more definitive interpretation had to be keyed to the types of clay minerals actually observed in the analysed section (from X-ray diffraction, SEM pictures etc.).

In order to check how well the analysis of the wireline data and conversion into mineralogy match the actual stratigraphic section, nine samples were taken from the Shell Paradise 10-25-047-3W4 core, and XRD analyses of the bulk fractions of these samples were performed using an automated powder diffractometer at the University of Alberta (see the litholog of this core, with the XRD sample locations highlighted in red – Figure 2-39, Chapter Two). Unfortunately, these samples were not clay oriented nor ethylene-glycol treated; therefore, the resultant diffracted peaks of radiation (see Figures 5-9 to 5-21, Addendum A, p. 435-448) are formed by addition of the individual patterns. Nevertheless, the dominant mineral phase is still possible to be identified based on its angular position and intensity (Magda C. Ciulavu, geologist CNRL – pers. communication).

The main clay minerals observed in majority of the samples are illite and kaolinite. Also, an interstratification illite/smectite is quite common; a low angle tail of the illite peak identifies its presence. Smectite is the predominant clay mineral in sample #3, and is probably present in sample #1 too. With respect to the sepiolite presence, it is very hard to rule it out from sample #3, as many of sepiolite peaks overlap those of smectite (=beidellite). The second intensity peak in Figure 5-10 (at about 41.2 $^{\theta}$) is not present, which put sepiolite's presence under question mark. Treatment with ethylene-glycol is necessary in order to identify this mineral with certitude. Minor amount of chlorite were identified in samples #4, and #5).

Qualitative analyses of the diffraction data indicate the following dominant clay phase by depth (exceptions: sample #2: siderite, and sample #5: quartz):

- 538.5 m: siderite (sample #2)
- 538.9 m: smectite (=beidellite) (sample #1)
- 546 m: smectite (sample #3)
- 568 m: illite (sample #4)

- 576.5 m: quartz (sample #5)
- 636 m: illite (sample #6)
- 654.2 m: illite (sample #7)
- 670 m: illite (sample #8)
- 682 m: illite (sample #9)

The matrix algebra solution for the Joli Fou - Mannville section in the Shell Paradise 10-25-047-3W4 well, Lloydminster region was additionally performed in order to compare it with the XRD analysis. The results are shown as graphic lithology logs of the porosity-quartz-shale-smectite (Figure 5-22), porosity-quartz-shale-siderite (Figure 5-23), and porosity-quartz-shale-illite (Figure 5-24) systems. The calculated geophysical log inversions match the actual sedimentary section pretty well, and supports the assumptions drawn in the following subchapter, one of them being that some shale-rich, quartz-rich, and/or carbonate - cemented horizons may be acting as barriers (or at least baffles) that have inhibited gas mixing over geological time, or have influenced their vertical migration, and therefore their geochemical depth profiles.

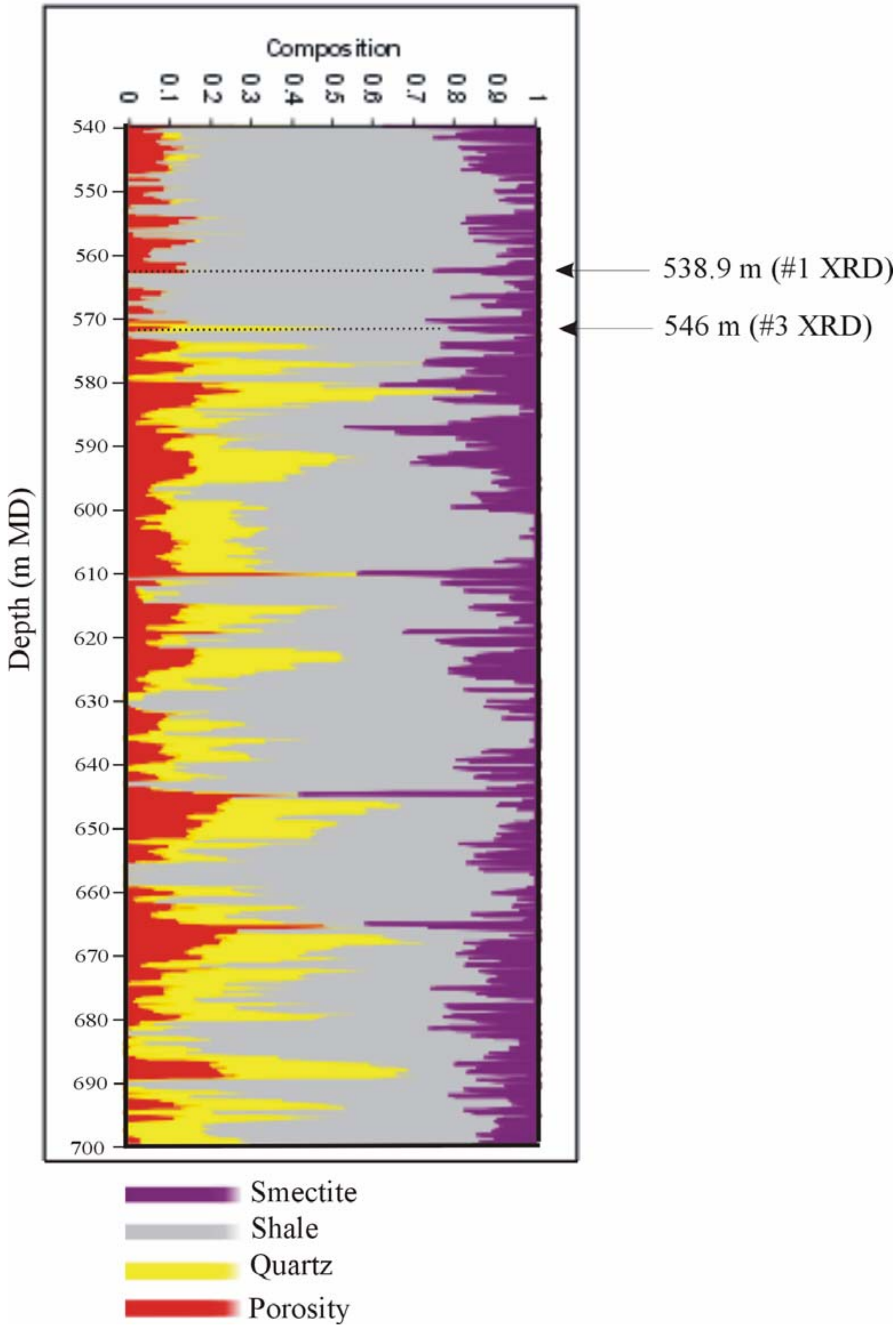

Figure 5-22 Matrix algebra solution for the Joli Fou - Mannville section in Shell Paradise 10-25-47-3W4 well, Lloydminster region. The result is shown as a graphic lithology log of the system porosity-quartz-shale-smectite.

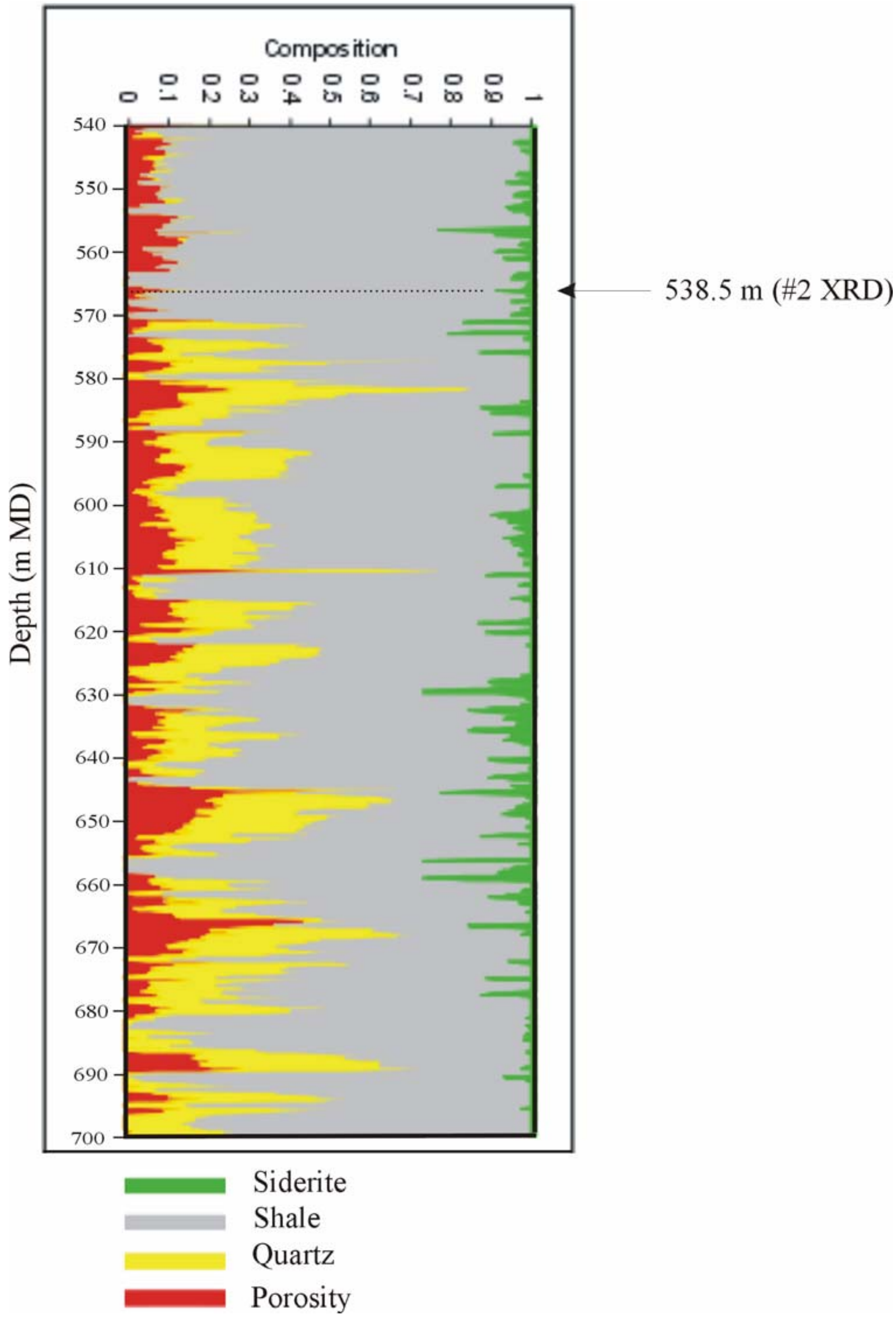

Figure 5-23 Matrix algebra solution for the Joli Fou - Mannville section in Shell Paradise 10-25-47-3W4 well, Lloydminster region. The result is shown as a graphic lithology log of the system porosity-quartz-shale-siderite.

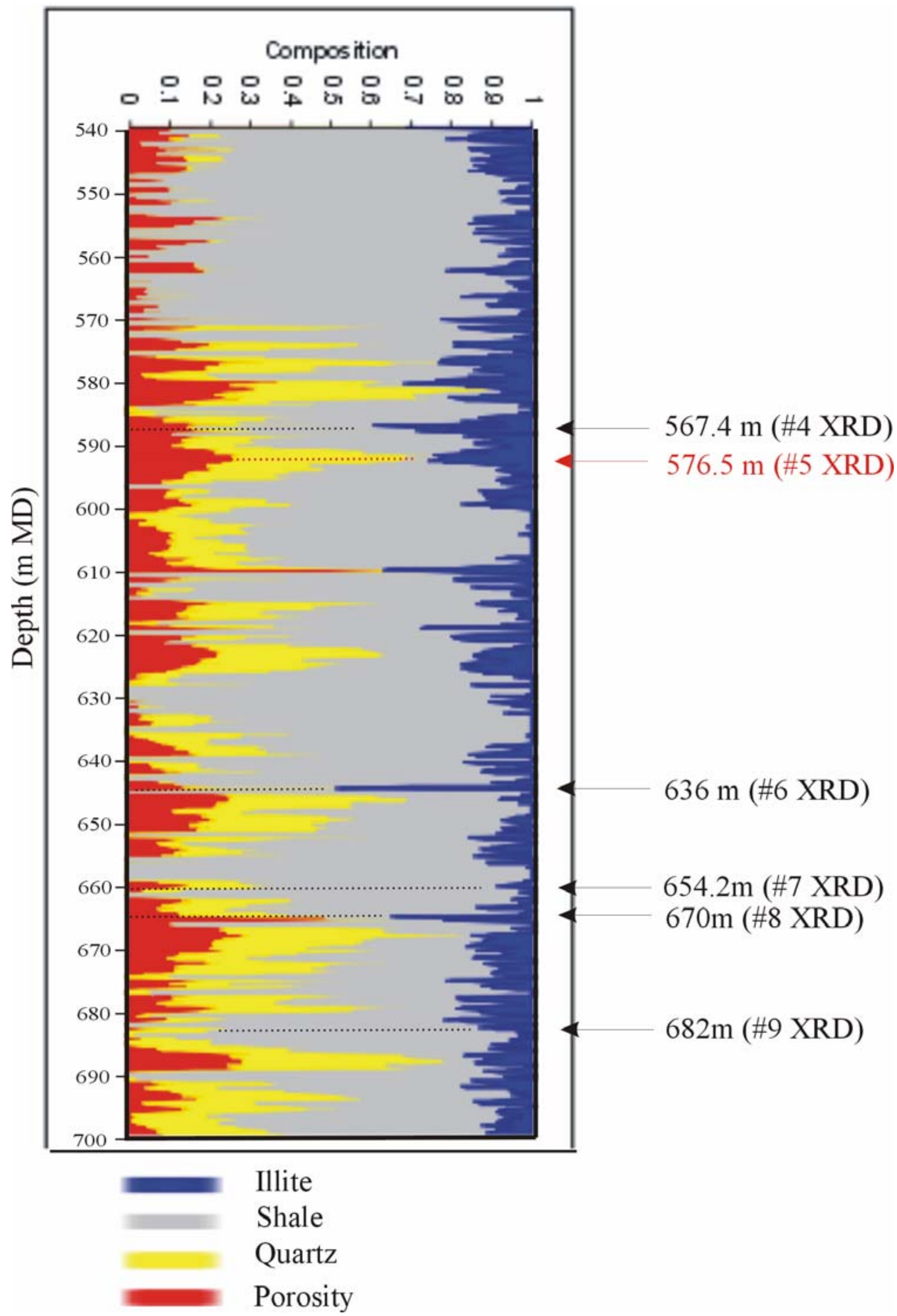

Figure 5-24 Matrix algebra solution for the Joli Fou - Mannville section in Shell Paradise 10-25-47-3W4 well, Lloydminster region. The result is shown as a graphic lithology log of the system porosity-quartz-shale-illite. Note: the quartz dominated sample #5 from 576.5m depth is also shown in red.

5.3. Results

The analysis of the wireline data and conversion into mineralogy (Figure 5-25) shows that the Cretaceous - Tertiary succession in Alberta is represented by a succession of porous-permeable and less permeable strata, across which a number of effective barriers/seals (high-shale content bands, montmorillonite/smectite bands, quartz cemented bands, dolomite cemented bands, siderite cemented bands) serve as boundaries for gas compartments. Major shifts in geochemical mudgas signature are related to the presence of some horizons with sealing properties (high shale content and/or low porosity, diagenetic layer).

The results of inversion of the wireline data into mineralogy for seven mudlog locations, together with their geochemical profiles are presented in Appendices III (III-1 to III-7). Each colored rectangle superimposed on each of the isotopic profiles represents an individual gas sub compartment. This sub-compartmentalization is mainly based on the presence of inferred barriers with sealing properties, and the variation observed in both isotopic mudgas profiles and their related geochemical parameters.

The methodology included a very close and detailed inspection of every gas sample along every profile. The isotopic gas signatures, their molecular composition, in addition to their post-generation history of migration and alteration were intimately integrated with the compositional profiles calculated with matrix algebra solution.

Nor every single gas sub-compartment or every low-permeability barrier will be thoroughly discussed in this Chapter because:

(1) the Appendices III-1 to III-7 (Appendix B) are clear-cut by themselves, and

(2) a detailed argument would exceed the framework of this chapter. Instead, some good examples of low permeability barriers and/or baffles encountered in each of the studied areas will be presented.

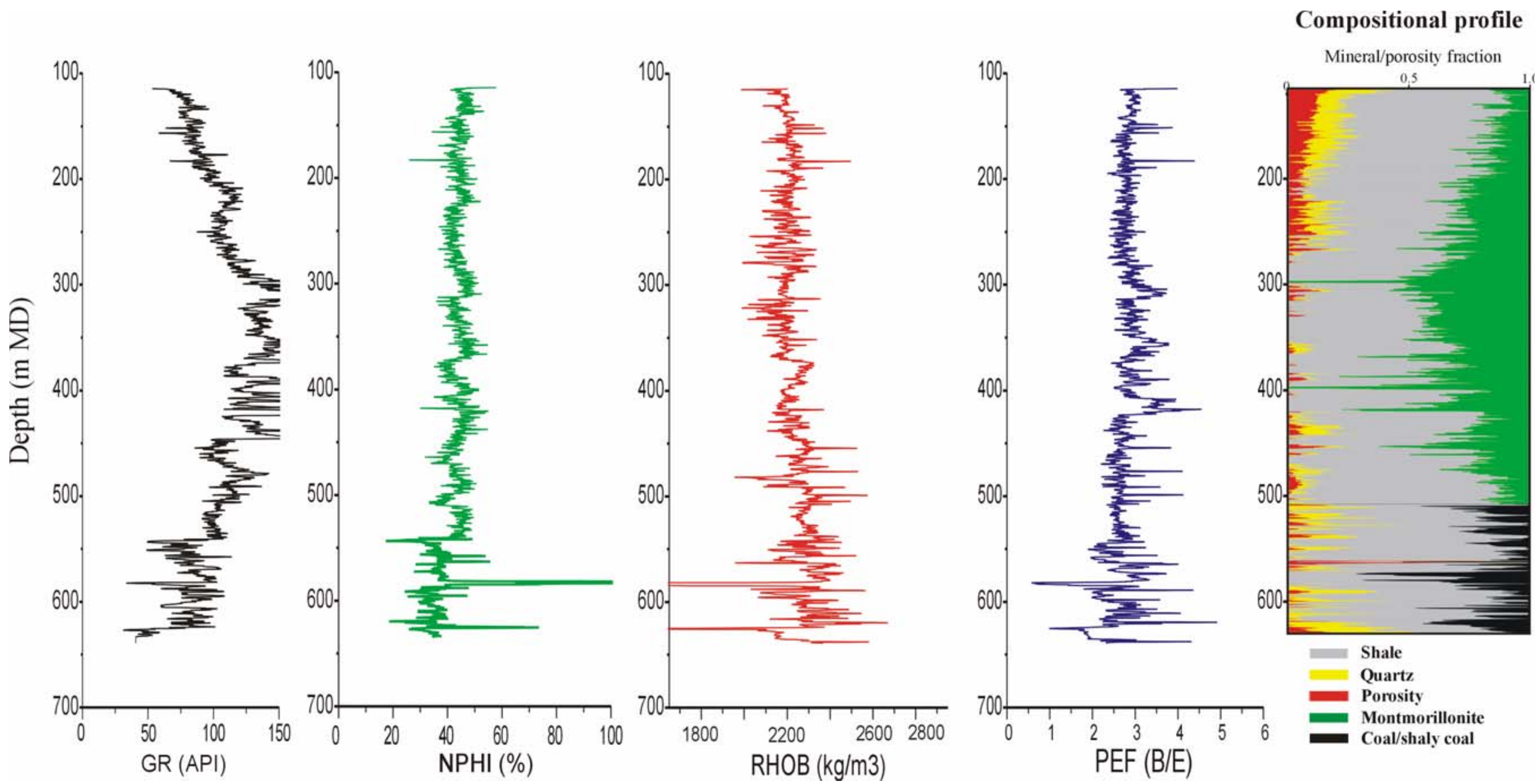

Figure 5-25 Wireline data plus mineralogical interpretation for Husky 3C-30-47-4W4 profile.

5.3.1. Foothills region

In the Foothills region, the majority of the boundaries, which serve as barriers for the gas sub-compartments are represented by shale-rich layers. Only the Mannville Group in the Gilby profile seems to be segregated by local quartz-cementation bands (see Appendix B, III-2). These local quartz-rich layers break up the Mannville Group into several gas sub-compartments (sub-compartments no. 21 to 26 on Appendix B, III-2, between ~ 1980 m – 2160 m measured depth).

In the Ferrier isotope depth profile, the thin shale layer located at approximately 310 m depth (see Appendix B, III-1) separates two different gas compartments, with different styles of biodegradation and probably different mixing histories. Gases above the shale have propane $\delta^{13}C$ heavier than gases below the shale. The carbon isotopic separation for propane is up to 10.70‰. Also, the isotopic separations between propane $\delta^{13}C$ values and n-butane $\delta^{13}C$ values are obviously much lower for the shallower sub-compartment. The different nature of these gases can be seen on a "natural gas plot" in Figure 5-26.

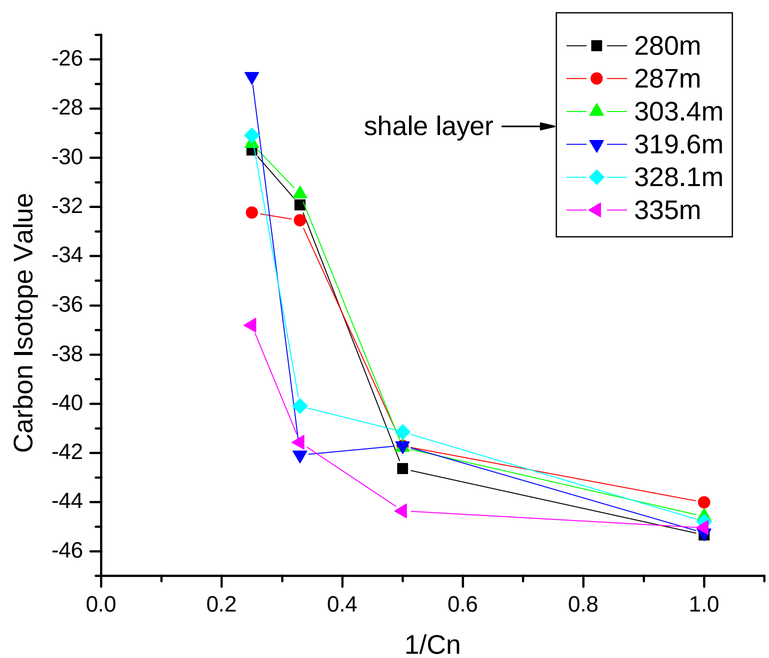

Figure 5-26 "Natural gas plot" showing some of the Paskapoo gases, Ferrier 14-3-42-9W5, Foothills region.

Another example of two different gas sub-compartments separated by effective shale barriers are the sub-compartments labeled no. 6 and no. 7 in Appendix III-1 (Ferrier 14-3-42-9W5). In this case, the boundaries of these sub-compartments are three thin shale-rich layers with very low porosity. The "natural gas plot" from Figure 5-27 identifies also two different gas families.

1004.2 – 1150.6 m interval depth (Figure 5-28) represents a single gas sub-compartment delimited by two effective shale layers and containing thermogenic single-sourced gases (sub-compartment no. 12 on Appendix B, III-1). The extension of the linear trend of these gases to the 1/Cn=0 line is about –24 per mil PDB. This $\delta^{13}C$ value for the source kerogen suggests that the gases were derived from a Type III kerogen homogenous source. The two shale layers delineating the gas sub-compartment do not represent major stratigraphic surfaces, as defined by sequence stratigraphy.

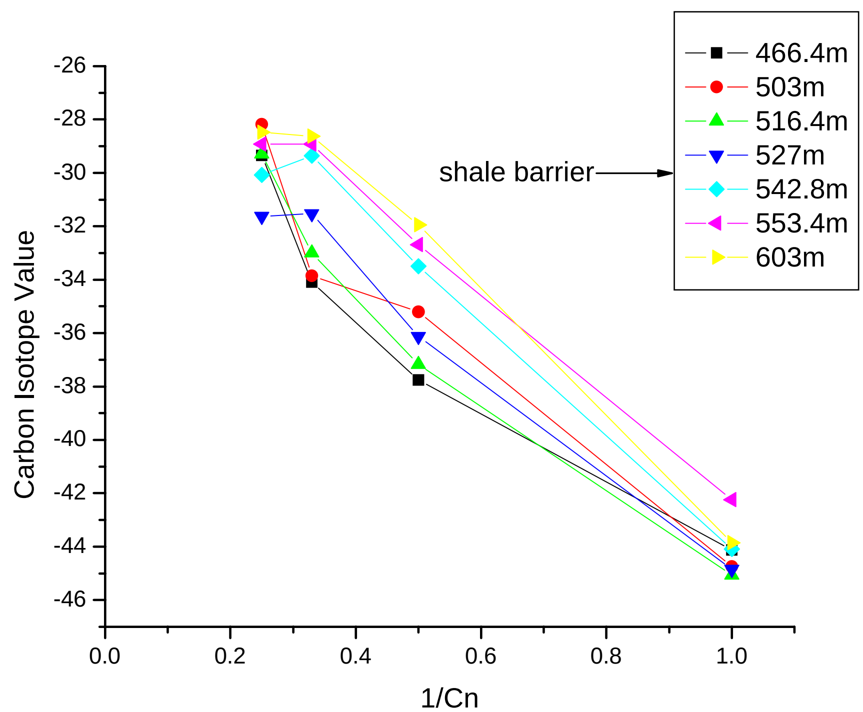

Figure 5-27 "Natural gas plot" showing some of the Paskapoo - Scollard gases, Ferrier 14-3-42-9W5, Foothills region.

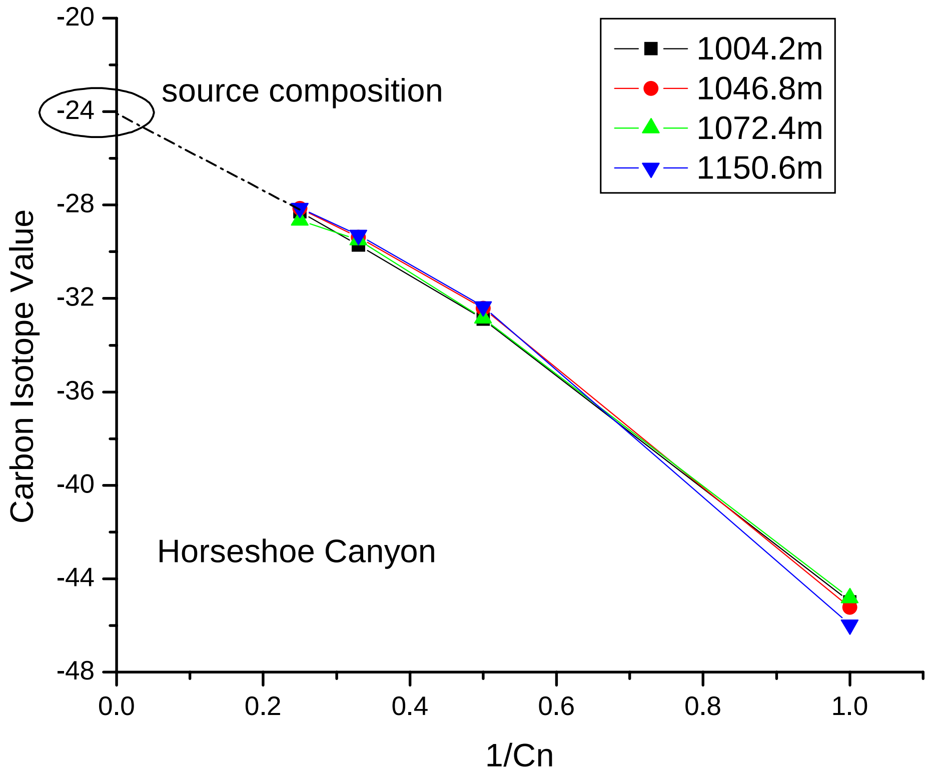

Figure 5-28 "Natural gas plot" for some of the Horseshoe Canyon gases, indicating a single thermogenic generation of the gas and a single sub-compartment bounded by two effective shale-rich barriers. Ferrier 14-3-42-9W5, west-central Alberta.

A number of the gas sub-compartments boundaries are represented by a series of shale layers with variable amounts of associated quartz cement. The effectiveness of such a boundary is controlled by the size and the interconnectivity of its pore space. The lower the porosity, the higher the effectiveness for the shale layer to act as an effective barrier to fluid flow. The quartz-rich layer situated at approximately 730 m depth in the Ferrier profile (see Appendix III-1), and separating sub-compartment no. 8 from sub-compartment no. 9 acts as a barrier and separates a deeper, altered gas from a shallower, less altered gas (Figure 5-29). The gas from 754 m depth has the values for the biodegradation indices higher than the gas from 706.2 m depth.

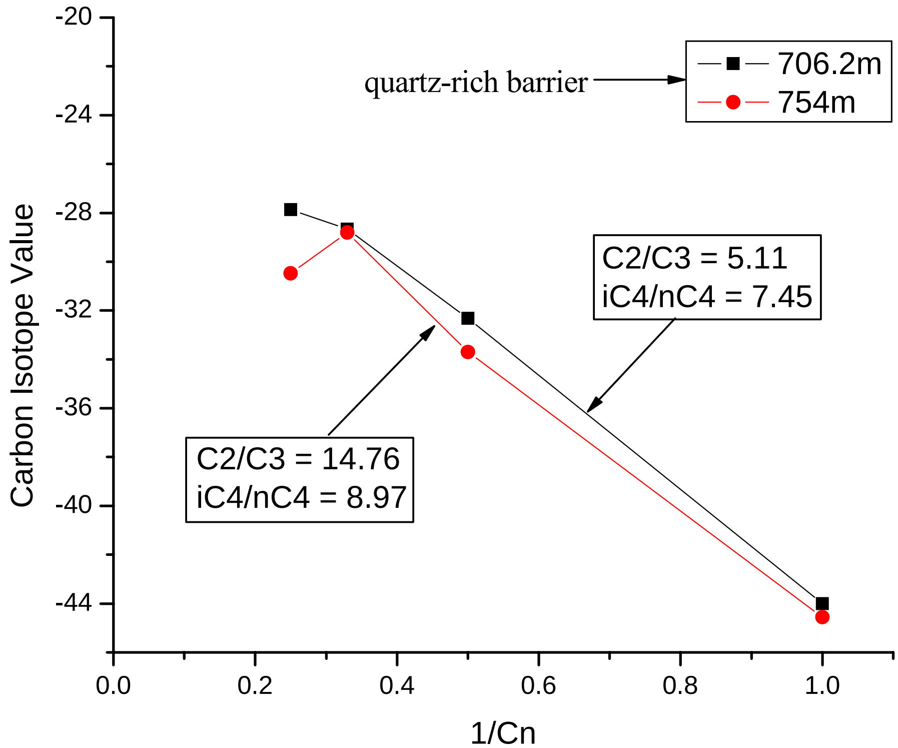

Figure 5-29 "Natural gas plot" showing two different gases separated by a quartz-rich shale barrier. Scollard Formation, Ferrier 14-3-42-9W5, west-central Alberta.

Some of the gas sub-compartments are confined within lithological complexes, which seem to be restricted by overpressured shale layers. Identification of over-, and/or underpressured compartments was done using the acoustic velocity method (Magara, 1978).

Two of such sub-compartments are those labeled no.13 and no. 19 on the Gilby profile (see Appendix B, III-2), which are restricted by overpressured shale layers at the top. In addition, an overpressured shale layer at the bottom restricts sub-compartment no. 13.

Occasionally, the overpressured horizons are confined by the presence of highly compacted layers situated on top of them. In this case, the abnormal pressure within the shales is due to the fact that carbonate-cemented or quartz-cemented horizons carry on the pressure underneath. Two of such situations are shown in Appendix III-2, where the boundary between sub-compartment no. 6 and sub-compartment no. 7, as well as the pressure boundary within the sub-compartment no. 10 mark an upward deflection towards more negative values for propane $\delta^{13}C$ values.

The numerous pockets of isotopically distinct gas sub-compartments in the Gilby profile may indicate a general lack of cross-intraformational flow and the effectiveness of the cementation horizons identified on the compositional profile (see Appendix III-2). Indeed, the Mannville samples plotted on a Chung diagram reveal their individual nature (Figure 5-30). The Mannville gases, based also on the information from Chapter four, represent distinct mixtures of mainly thermogenic-oil associated gases. Their secondary origin through thermal cracking of liquid hydrocarbons is also revealed in Figure 5-31, which presents the so-called "C2/C3 diagram" of Lorant et al. (1998). This diagram distinguishes gases generated from the primary cracking of kerogen, the secondary cracking of oil, and the tertiary cracking of the wet portion of the gases.

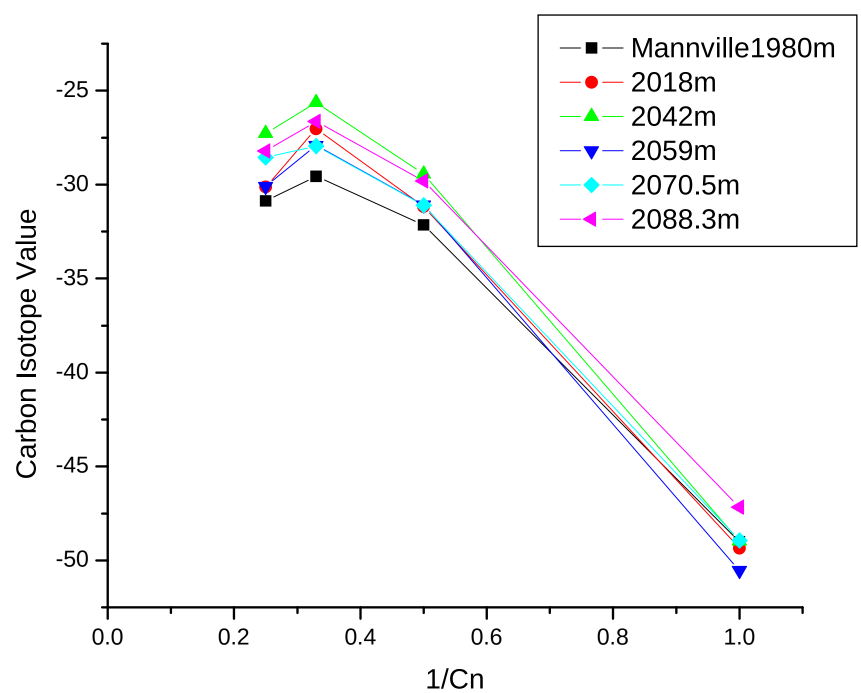

Figure 5-30 "Natural gas plot" of the Manville gases from the Gilby profile.

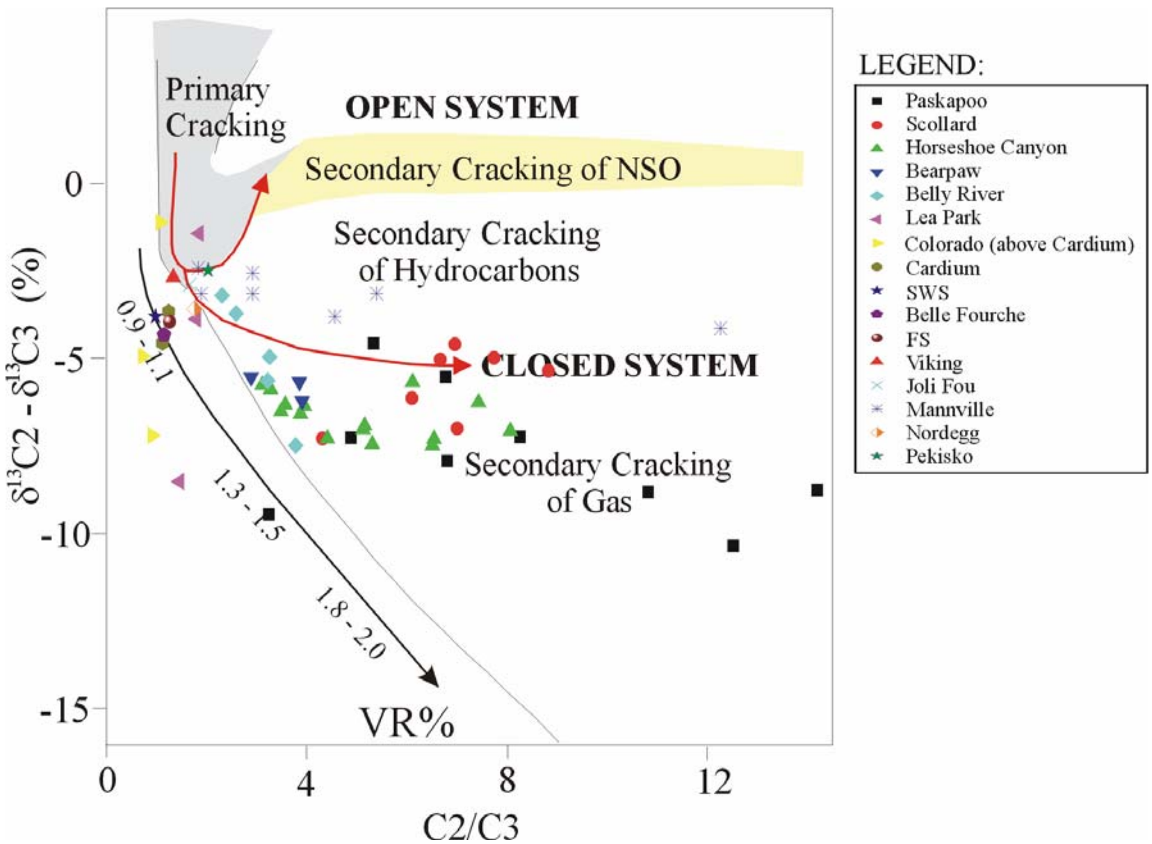

Figure 5-31 C2/C3 diagram for Gilby profile showing $\delta^{13}C2 - \delta^{13}C3$ (‰) versus C2/C3 distinguishes gases generated from the primary cracking of kerogen, the secondary cracking of oil, and the tertiary cracking of the wet portion of the gases (after Lorant et al, 1998)

5.3.2. Lloydminster region

The variation in the concentration ratios (C2/C3, and iC4/nC4) and in the isotopic separations between successive gaseous alkanes ($\Delta\delta^{13}C$ (C2-C1) and $\Delta\delta^{13}C$ (C3-C2)) indicate that the gases above the Joli Fou Formation (see Appendices III-4 to III-7) are separated in compartments with varying degrees and styles of biodegradation (Pallasser, 2000). Indeed, the conversion into mineralogy of the wireline data shows an intrafacies-banding pattern of the Colorado shales based mostly on the presence of the montmorillonite-rich and siderite bands at this stratigraphic level. They serve as boundaries for the gas compartments identified on Appendices III-4 to III-7.

A higher number of carbonate-, and quartz-cemented horizons within the Colorado Group characterize Lindbergh A9-13-56-6W4 and Husky A9-15-51-23W3 (Figure 5-33) profiles in comparison with Husky C3-30-47-4W4 and Petrovera 1D-25-55-5W4. For instance, montmorillonite-rich bands exclusively segregate the Colorado Group at Petrovera 1D-25-55-5W4 location (Figure 5-34). One of such seals is located at ~ 360 m depth and separates two gas sub-compartments characterized by different biodegradation styles (Figure 5-32). This montmorillonite-rich layer overlies the ravinement surface, which marks the onset of the transgressive deposits that cap the Viking Formation in the area.

Although all Mannville gases in the heavy oil region have been identified as biodegraded, different packages of gases are separated by more or less effective seals/barriers and recognized by different characteristics of the biodegradation.

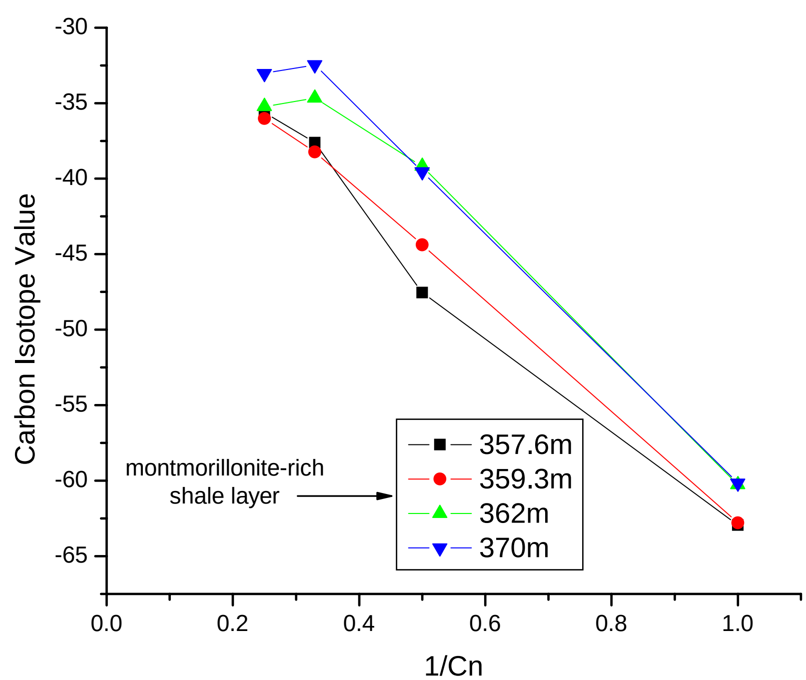

Figure 5-32 "Natural gas plot" for Colorado gases from Petrovera 1D-25-55-5W4, showing the difference between two gas sub-compartments separated by an effective montmorillonite-rich shale barrier.

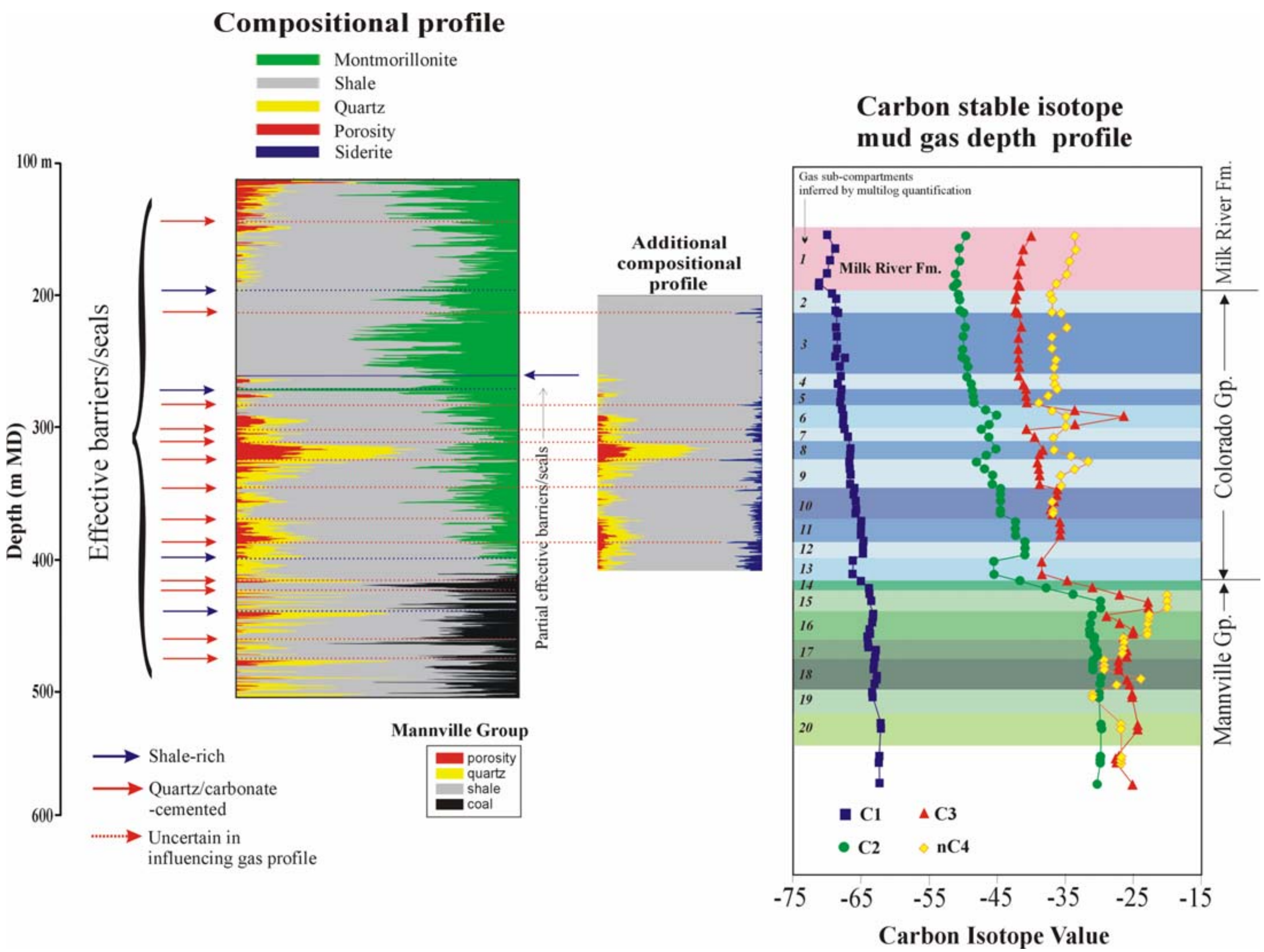

Figure 5-33 Stable carbon isotopic profile and the conversion into mineralogy, Husky 9-15-51-23W3

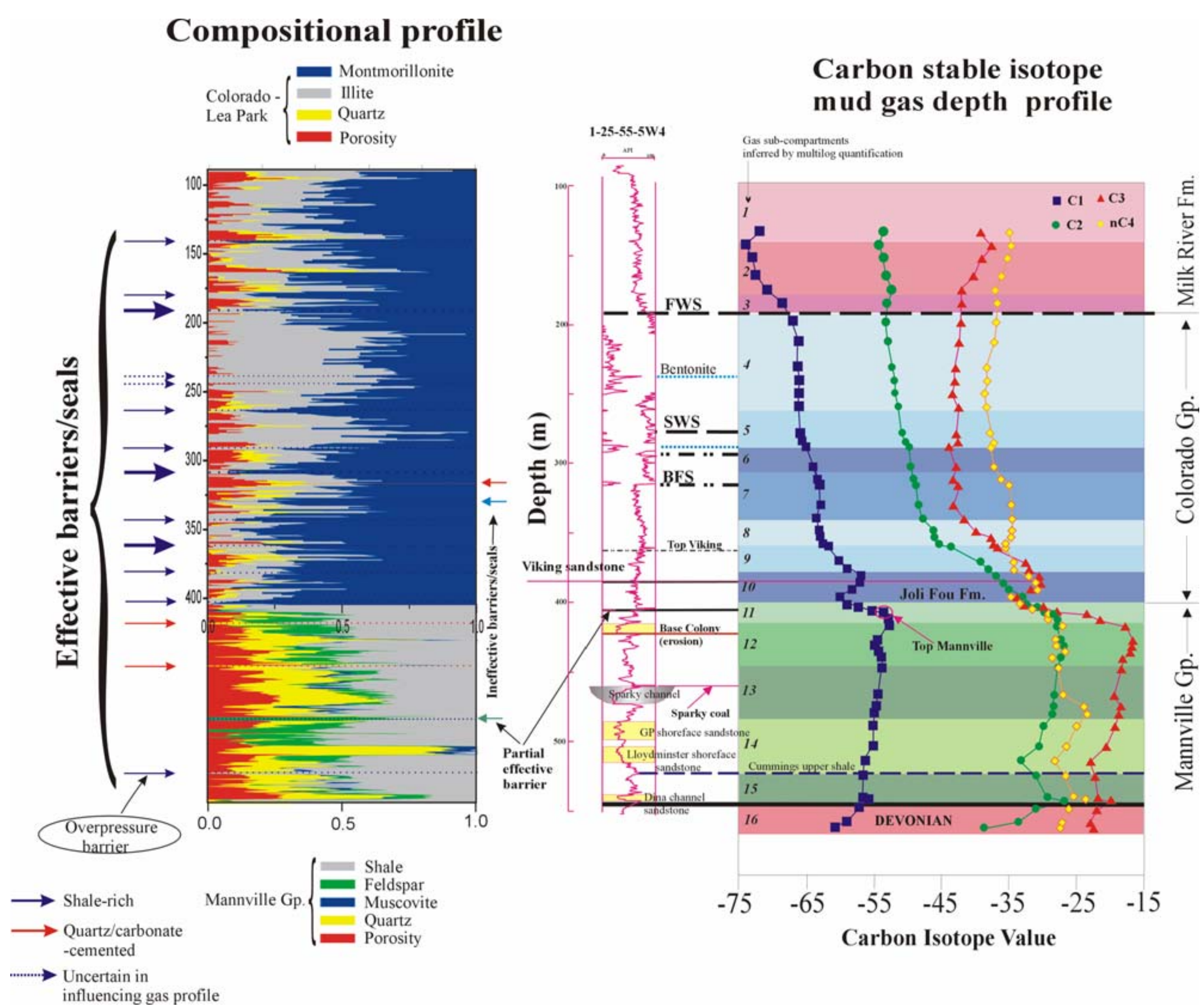

Figure 5-34 Stable carbon isotopic profile and the conversion into mineralogy Petrovera 1D-25-55-5W4.

A good example of a seal composed mainly of clay minerals is represented by a decimetre thick horizon at the Mannville/Joli Fou boundary, Husky C3-30-47-4W4 (Figure 5-35, and Appendix III-6). This horizon effectively acts as a seal for heavier hydrocarbons, which are trapped below and within. For example, the ethane concentrations below and above the seal are 1974.31 ppm and 107.72 ppm respectively. The shale layer influence on the carbon isotope ratio is also obvious: there is a distinct trend of upward increasing $\delta^{13}C_{C3}$, $\delta^{13}C_{iC4}$, and $\delta^{13}C_{nC4}$, in the meantime with an upward decreasing trend for $\delta^{13}C_{C2}$.

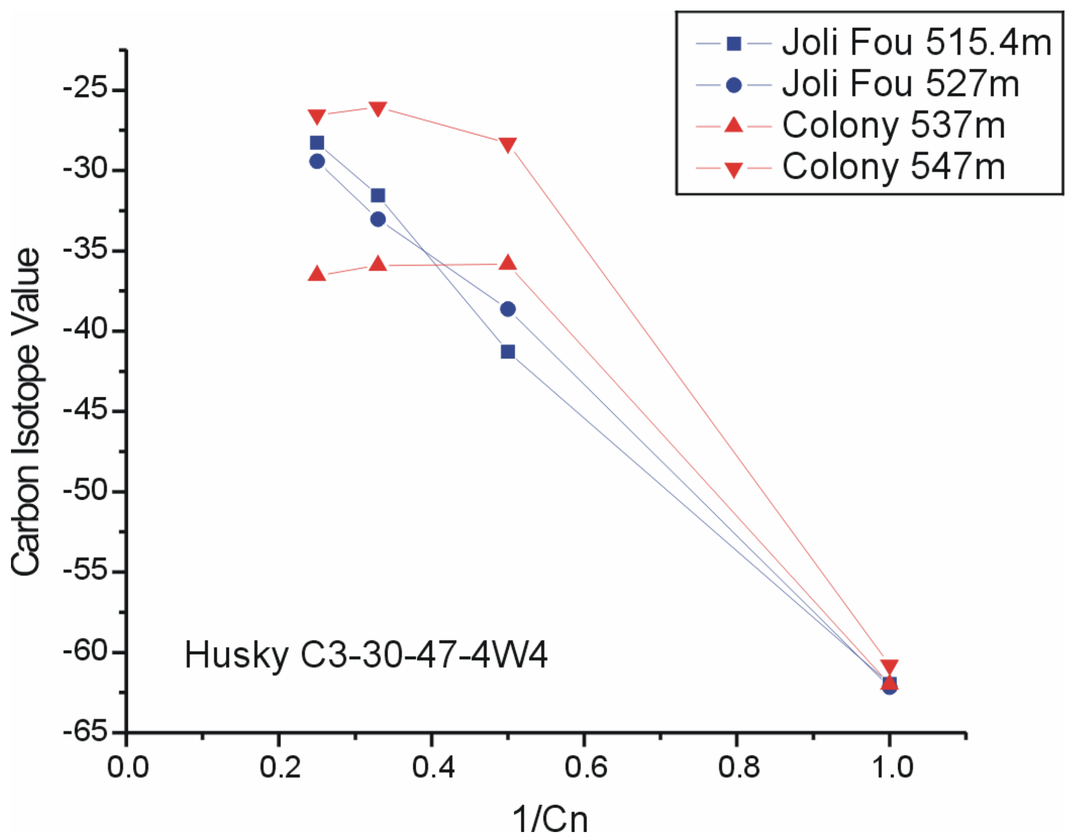

Figure 5-35 "Natural gas plot" showing two different gas compartments (Joli Fou gases and Colony Gases) Husky C3-30-47-4W4 separated by an effective montmorillonite-rich shale barrier.

Mannville Group in the Lloydminster area is characterized by the presence of quartz-cemented bands in alternation with shale-rich layers, which act as effective barrier for gas migration. The lowermost gas sub-compartment in the Husky C3-30-47-4W4 profile (Appendix III-6), labeled no. 17 is confined within a complex, which is restricted by a quartz-cemented horizon at the top and a regional shale marker (Cummings shale) at the bottom. The gas signatures, as they appear on a Chung diagram, are surprisingly similar (Figure 5-36).

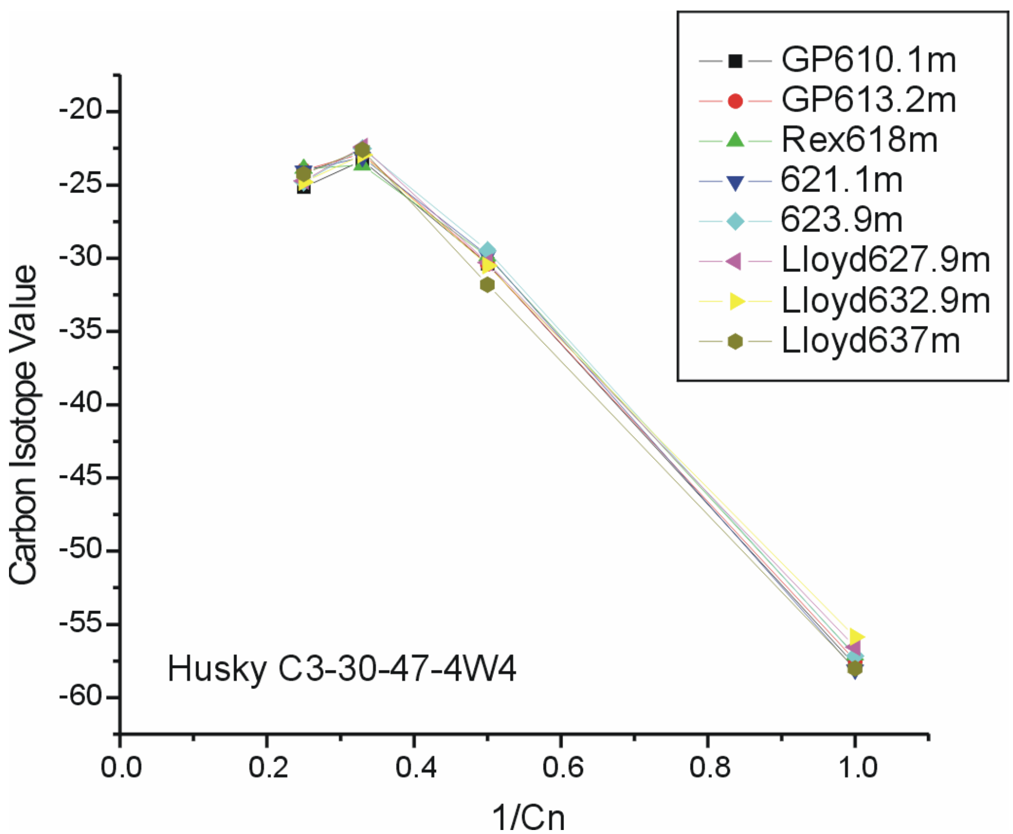

Figure 5-36 "Natural gas plot" showing some Middle Mannville gases confined in a single gas sub-compartment at Husky C3-30-47-4W4 profile by two effective barriers: an upper quartz-cemented band and a lower shale-rich layer.

Except effective barriers, which compartmentalize different types of gases, the presence of partial effective barriers is also shown on the composite diagrams from Appendices III. An example of such partial effective shale-barrier is represented on Husky 9-15-51-23W3 profile by a shale layer situated between sub-compartment no. 3 and no. 4 (Second White Specks Shales). This shale layer, which is montmorillonite-rich, has however, a higher porosity than the other montmorillonite-rich layers. This barrier separates the two gas sub-compartments illustrated in Figure 5-37, for which the only difference was found to be a small variation in the wetness index. All the other geochemical parameters (including carbon isotope ratios) indicate almost no changes across the boundary.

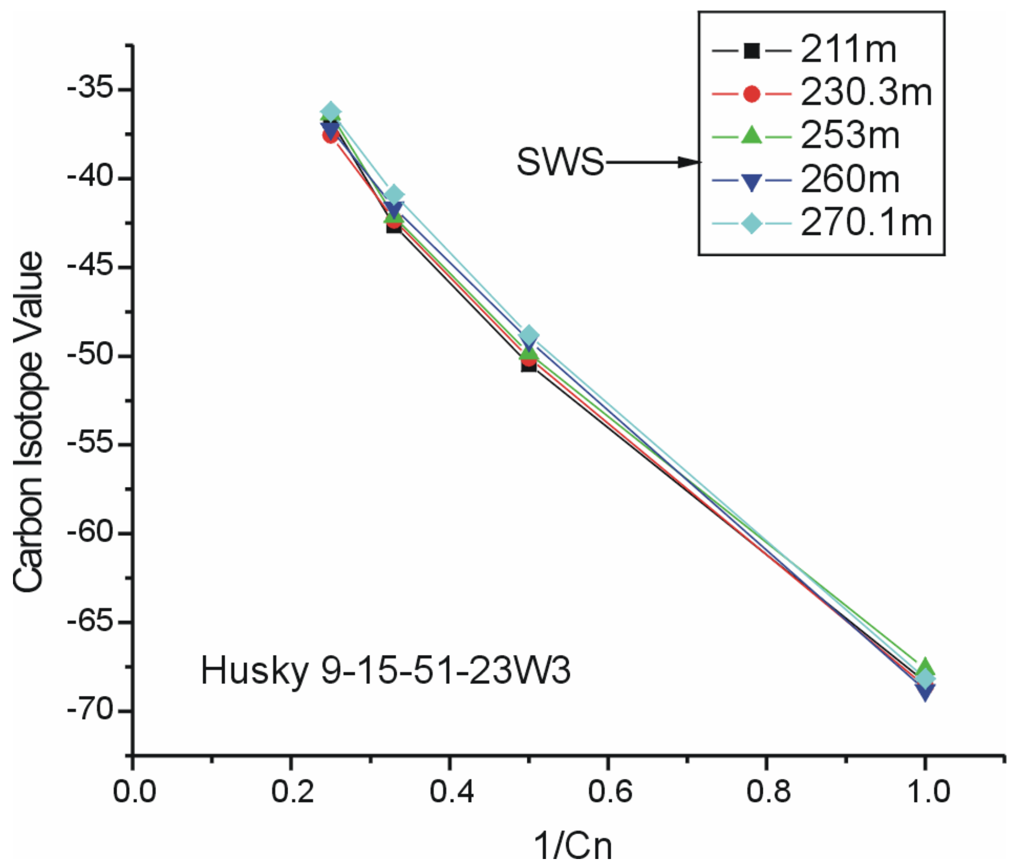

Figure 5-37 "Natural gas plot" for Colorado gases from Husky 9-15-51-23W3, showing the slight difference between two gas sub-compartments separated by a partial effective montmorillonite-rich shale barrier.

Another example of montmorillonite-rich layer (bentonite) acting as a partial effective barrier is represented by the horizon situated within the Second White Specks Formation at Husky C3-30-47-4W4. This shale layer separates the two gases from Figure 5-37, and could be viewed as an effective barrier due to the presence of slight inflections across it in the carbon isotope ratios (see Appendix III-6). However, all the other geochemical parameters do not change across it, and, as can be seen in Figure 5-38, the extension of the lines to 1/Cn=0 predict –25, and respectively –27.5 per mil PDB for the isotopic compositions of the source material. This is interpreted as clear indication of mixing across barriers. Thus, the rock basic properties (porosity and permeability) act as important controlling factors even for shale sequences.

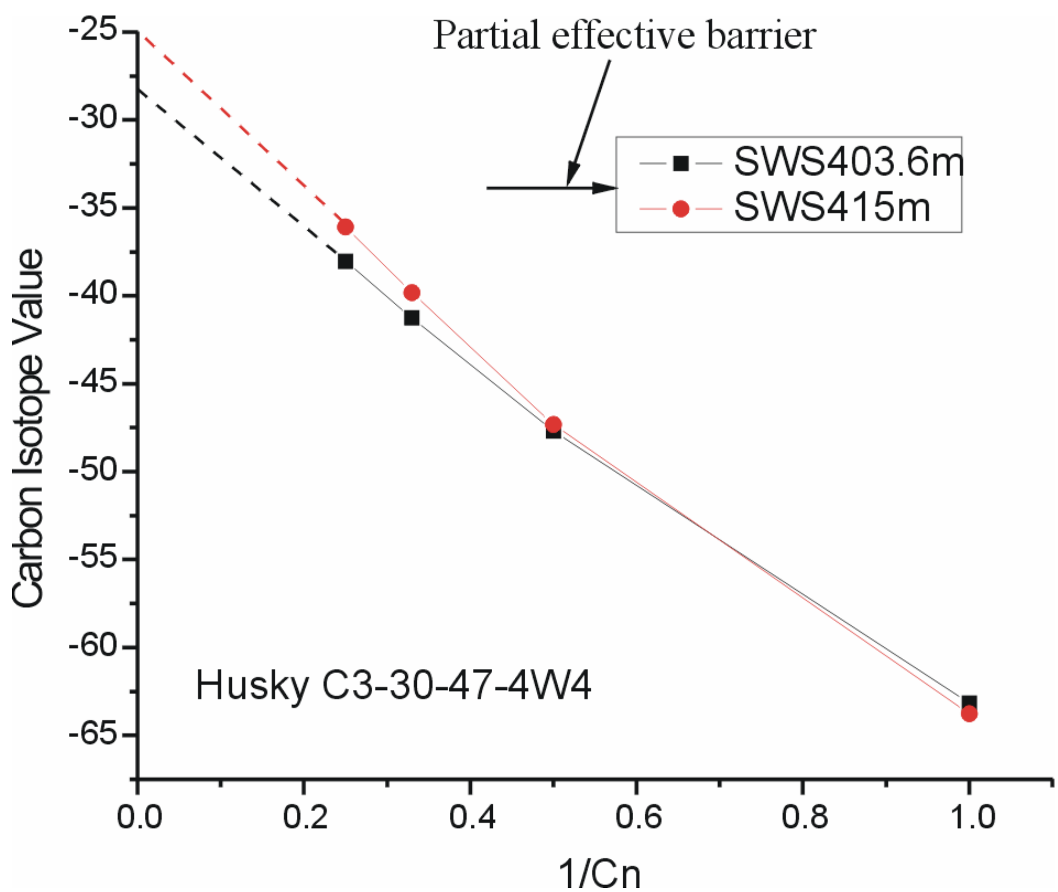

Figure 5-38 “Natural gas plot” for Second White Specks Formation gases from Husky C3-30-47-4W4, showing the slight difference between two gas sub-compartments separated by a partial effective montmorillonite-rich shale barrier.

The presence of any highly porous and permeable zone or fracture system within a shale sequence will reduce both the actual thickness of the rock sequence and its effectiveness as a seal and/or barrier (Nelson and Simmons, 1995). According with Nelson and Simmons (1995), a cap rock porosity of 10% gives nearly five times increase in the diffusion flux of methane and ethane through the shale than a cap rock porosity of only 5%. Consequently, any shale zone or even shale layer with a high porosity will not succeed to act as a seal and /or barrier, in particular for light hydrocarbons.

In the compositional profiles, only the presence of highly compacted, montmorillonite - rich layers, or shales with different composition (mainly illite, montmorillonite, chlorite), but with a very low porosity, seems to influence the trend of the carbon isotope profiles of mudgases. Their presence segregates several packages of gases, with distinct isotopic and molecular composition, and with distinctive biodegradation and/or mixing signatures.

The presence of seal rocks with varying degree of porosity can act either as partial effective barrier or completely ineffective barriers. The rate of diffusive loss through such rocks seems to be higher than in the case of highly compacted, low porosity shale – in spite that diffusive loss through the cap rock (as a migration mechanism) is often not accepted or considered to be so slow, as to be inconsequential (Krooss et al., 1992). However, molecular diffusion is always present if a concentration gradient (chemical potential gradient) exists across the cap rock (Nernst, 1923; Bockris and Reddy, 1970; Nelson and Simmons, 1995).

Nelson and Simmons (1996) showed many and ample physical evidence of leakage from reservoirs and for vertical gas migration. One of the well-known evidence could be observed at the well-site locations. Well-site geologists and mud loggers commonly observe an increase in flow-line background gas as the cap rock above a productive reservoir is drilled. Conversely, there is often no increase above barren reservoirs or where the reservoir rock is not encountered. The observed increase in C1-C4 concentration across the cap rock is exactly what it would be expected if diffusion were occurring. It is the diffusive concentration gradient.

As stated by Nelson and Simmons (1996), no reservoir cap rock has ever been shown to be a perfect seal to hydrocarbon migration. The presence of faults, fractures, microfractures, and porosity of the reservoir cap rock preclude a perfect seal. The cap rock or seal only retards migration.

Migration along faults, fractures, and microfractures, or by capillary action through the pore space, can potentially move large volumes of hydrocarbons, but such bulk migration does not always occur (Hunt, 1996).

5.4. Well logs – qualitative uses in mudgas geochemistry

Resistivity, sonic, and density logs (as well as some others) can give clues to the presence of over- or underpressure. Shale sections are best for analysis of logs for abnormal pore pressure. Because of their low permeabilities, shales do not equilibrate pressure with the mud column in the well bore. Selecting only the purest shales minimizes the effects of mineral variation, multiple phases, fluid composition, and fluid distribution. That leaves only porosity as the major variable within shale sections. Because porosity is related to compaction, porosity measurements from well logs can be calibrated to fluid pressure in the pore system.

In general, there is a gradual increase in shale density with depth, the principal cause being a diminution in shale porosity with increasing overburden (Magara, 1978). However, porosity may increase with depth and those zones are commonly overpressured.

Acoustic velocity can be used to identify over- and underpressure compartments. A plot of shale interval transit times against depth for Petrovera 1D-25-55-5W4 indicates several under-, and overpressure compartments at a very local and very detailed scale (Appendix III-5). Plots of shale interval transit times against depth for Ferrier, and Gilby profiles indicates as well several under-, and overpressure compartments (see Appendices III-1 and III-2)

The isotopic composition of mudgases and their distribution seem to be influenced by the shale compactional effect. The shale above and below the sandstone beds compact normally, but the shales away from the sandstones may become slightly undercompacted and overpressured (Magara, 1981). These slightly undercompacted shales interbedded with sandstones are called ***pressure seals*** (Evans et al., 1975) and seem to retard the vertical movement of fluid. Assuming these pressure seals are entirely developed, the intergranular fluid flow usually occurs laterally, for pressure seals act as semibarriers for vertical fluid movement (Magara, 1981).

In the Petrovera 1D-25-55-5W4 mudgas profile (Appendix B, III-5), slight inflections of the C_1, C_2 and C_3 isotope ratios trend towards higher values (apparently greater maturity) occur below some overcompacted shaly horizons within Mannville Group (below Colony channel, Waseca channel, and within General Petroleum Formation), suggesting these are more effective pressure seals, directing the lateral movement of gases, and serving to concentrate more mature gases.

Furthermore, within General Petroleum shoreface sandstone, the isotope values decrease with depth starting from the maximum regressive surface, which caps the clean sandstone of the prograding nearshore and shoreface facies. This is in good agreement with the presence of the underpressured horizon, allowing gases to move vertically upward.

In Appendix III-1 (Ferrier profile) the ethane concentration seems to increase in compartments situated below overpressured strata, within Belly River and Lea Park formations. On the other hand, two pointed "jumps" in ethane concentration from high to low are observed in one of the highly underpressured compartments of the Mannville Group in Petrovera 1D-25-55-5W4 mudgas profile (Appendix III-5). Taking into account the gas migrational process, it seems that thermogenic gases, generated deep in subsurface are partially retained/concentrated in those more compacted sediments capped by less compacted (or overpressured) shaly sediments. Two other such pressure boundaries, separating sub-compartment no. 6 from sub-compartment no.7 and situated within sub-compartment no. 10 respectively on Gilby profile (Appendix III-2) appear to influence the C2 and C3 isotope ratios trends towards higher values below these boundaries, within the overpressured horizons.

Therefore, it is suggested that, using the general compaction trend it would be possible to estimate diagenetic effects, unconformities, and even small fractures/faults. When compared with general isotopic profile trend, whenever sonic log is available, can give some idea on how the shale compactional behavior influences the isotopic composition of mudgases.

5.5. Discussion

One of the most important aspects of this project's objectives was the ability to relate gas composition and isotope ratios to measurable properties of the rock framework (e.g., permeability, porosity). To assess the degree of compartmentalization (the presence of gas compartments) throughout a stratigraphic section at one well location, the present approach resumed looking essentially at interrelationships between isotopic fingerprints and wireline geophysical well logging suites.

Reservoir compartments and effective seals are easily recognized from inflections in the trends of the geochemical multi-component depth profiles. Even when the seal effect is not obvious on the isotopic profile, it can be observed on related geochemical plots, where there are different characteristics of hydrocarbon concentrations and/or biodegradation indices above and below such of sealing horizons (Appendix III-6, Husky C3-30-47-4W4, the partial effective barrier represented by the montmorillonite-rich layer situated above the Second White Specks Formation - SWS). Shales commonly have some permeability even if the value is quite low and there are vertical and horizontal fluid pressure gradients in most shales (Magara, 1980). In these circumstances, the fluids must be moving all the time, even the rate is commonly quite slow.

The strong correlation between isotopic and stratigraphic boundaries indicates that, in general, compartmentalization of the gas is effectively influenced by major stratigraphic variations. However, the Mannville – Joli Fou (Appendices III-2, III-4, III-5), and the Scollard – Paskapoo boundaries represent examples where the major stratigraphic horizons may act as less effective barriers. The $\delta^{13}C$ values gradually decrease upwards, accompanied by a decrease in the wetness ratio. This trend might be suggestive of gas diffusion from the Mannville upwards through the Joli Fou shales, and from the Scollard upwards in the Paskapoo Formation.

The suggestion that Mannville gases have diffused vertically into the Colorado group, at least locally, is further supported by the fact that there is preservation of the relationship between C_3 and nC_4 components within the Colorado gases (isotopic reversals between the C_3 and nC_4 components; see Chapter Four).

The inference that may be drawn from the data presented in Chapter Five is that some shale-rich, quartz-rich, and/or carbonate - cemented horizons may be acting as barriers (or at least baffles) that have inhibited gas mixing over geological time, or have influenced their vertical migration. In particular, the variation in log properties of shale beds with depth is considered in the analysis of compactional trends and their information concerning the presence of small-scale undercompacted and overcompacted horizons. The erosional rebound of highly compressible and low-permeability shales explains the vertical sealing and the underpressuring observed in the Cretaceous successions (Corbet and Bethke, 1992; Parks and Tóth, 1995; Bekele et al., 2000).

Locally, the underpressuring can help to trap the gas. In these local overcompaction zones, the subnormal pressures have probably resulted from dilatation of pore volume and from a decrease of reservoir temperature associated with uplift and erosion (Barker, 1972). Meanwhile, the reactions that convert organic matter into hydrocarbons during progressive burial can also cause fluid volume increases that result in overpressuring within isolated compartments. Methane generation has been cited as the cause of overpressuring in numerous reservoirs.

Zoning of hydrocarbons has been also observed within the pressure transition zones. It is possible that the transition zones are complicated by local permeability barriers with increasing gas concentration toward the top of each more porous-permeable layer.

Methane tends to focus above the seal, while heavier components predominate below the seal (Gilby, 1238 m depth, Appendix III-2). The compositional profile indicates at this depth a thin shale-rich layer, possibly quartz-cemented, which coincide with a strong overpressured level, indicated on the shale transit time - depth plot.

The barrier/seal presence seems to occur in association with zones of abnormal fluid pressure. The banding consists of alternating layers of different mineralogical composition and/or significantly different porosities (see Appendix III-2, Belly River Group sub-compartments). Thus, these shale-rich and diagenetic bands can act as barriers/baffles for pressure compartments and as traps and/or stoppers for hydrocarbons (mudgases in our case). The existence of a strong overpressure barrier probably inhibited upward migration of light hydrocarbons and argues against a vertical admixture between Cummings and Lloydminster gases (Petrovera 1D-25-55-5W4, Appendix III-5).

The carbon isotope ratios of mudgases from an overpressured to a normal pressured and/or underpressured compartment seem to be likely tracers for prediction of the overpressure, but these preliminary results need further confirmations, as a result of a considerably higher sample density of both DST and mudgas data.

CHAPTER SIX

HYDRODYNAMICS, FLOW SYSTEMS AND GAS MIGRATION PATHWAYS

6.1. Introduction

The flow of formation waters as a factor during the evolution of sedimentary basins and in the generation and accumulation of natural resources has long been established (Anfort et al., 2001). Many basin analysis and numerical models have shown that the flow of formation waters is driven by various mechanisms, such as compaction, tectonic compression, topography, buoyancy and erosional rebound (Bethke and Marshak, 1990; Garvin, 1995).

Flow systems and their directions influence gas migration pathways and accumulations. Flow of formation waters provides the means for long-distance migration to traps and introduces bacteria for generating secondary biogenic gas (Hunt, 1992).

The very high molecular diffusion of the gas – especially methane – in water tends to imply that this process is an important mechanism of primary gaseous hydrocarbon migration as well through the water-impregnated shale series (Leythaueser et al., 1982).

Considering the fractionation processes due to migration, for several decades gas signatures were thought by some of the researchers to be independent of any fractionation due to migration (Schoell, 1980, 1983; Fuex, 1980; Whiticar, 1994; Faber, 1987), whereas some work seemed to demonstrate a more complex behaviour (Hoering and Moore, 1958; Colombo et al., 1965, 1966, 1970; Galimov, 1975; Bondar, 1987). Last decade experimental work (Pernaton et al., 1996; Kross et al., 1998), associated with evidence from natural case studies (Prinzhofer and Pernaton, 1997) presents evidence of isotopic shifts in methane during migration through porous-permeable sandstone bodies. In these study cases, the isotopic composition of methane is believed to be modified during *segregative migration* (Prinzhofer et al., 2000).

In 1980, a paper entitled "*Experimental evidence against any appreciable isotopic fractionation of methane during migration*" by Fuex A.N. convinced many geologists that, indeed, isotopic fractionation during gas migration does not exist. However, not too many geologists know that Fuex's work consisted of three series of experiments, the first two (methane chromatography and volatilization of liquid methane) showing very large isotopic effects, but being considered to be geologically unrealistic. The third series of experiments dealt only with the solubilization of methane in water at thermodynamic equilibrium, and showed little isotopic effect. Also, Fuex (1980) did not evaluate the possible effects of isotopic fractionation related to desorption and diffusion of coalbed gases.

Since 1980, some new experiments involving methane diffusion (Bondar, 1987; Pernaton et al., 1996) dispute Fuex's assessment (not his experimental results!) as did precursor studies (Colombo et al., 1965, 1966; May et al., 1968; Syngayevsky et al., 1978).

Recent experimental results (Pernaton et al., 1996; Prinzhofer et al., 2000) have shown that diffused methane has always a significantly isotopically lighter carbon than the source. As remarked by Prinzhofer et al. (1997), these results can very well raise the issue of extrapolation of these experiments in natural geological cases. As ^{12}C-enriched methane is found in lots of different gas accumulations in the world, two different interpretations are possible: mixing between thermogenic and bacterial gases, and a diffusive trend during migration (Colombo et al., 1965, 1966, 1970; Galimov, 1975; Neglia, 1979; Reitsema et al., 1981).

In order to distinguish isotopically light methane coming from bacterial activity and methane segregated during migration, Prinzhofer and Pernaton (1997) suggested a diagram using C_2/C_1 versus $\delta^{13}C$ of methane (Figure 6-1). In the Prinzhofer-Pernaton diagram (linear plot) a straight line corresponds to mixing of two-end member gases, whereas diffusion processes results in non-linear trends, the curvature of which is determined by the ratio of the diffusion coefficients of ethane vs. methane and $^{13}CH_4$ vs. $^{12}CH_4$, respectively.

The debate about the existence or the importance of isotopic and chemical fractionation of light hydrocarbons during migration still persists.

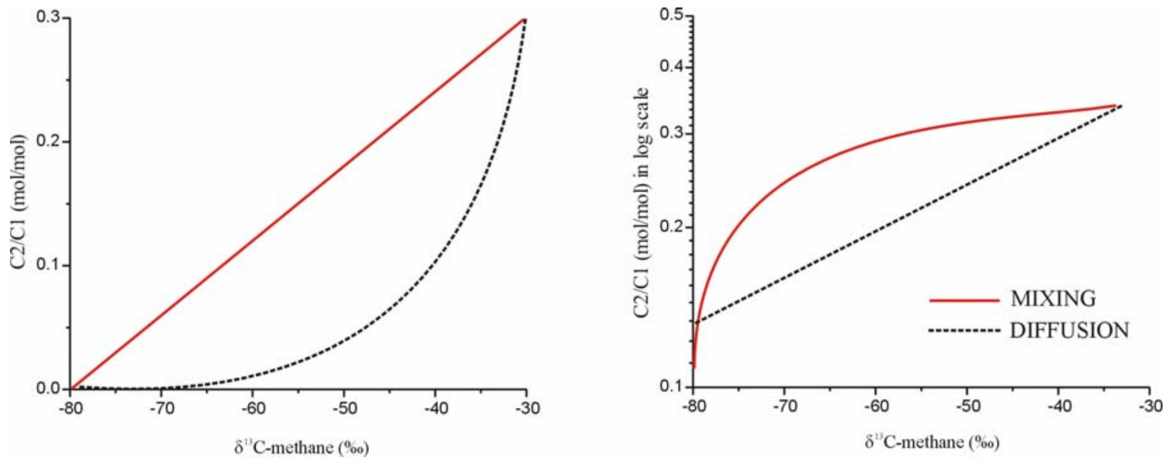

Figure 6-1 C_2/C_1 versus methane $\delta^{13}C$ diagrams showing the basic principle of their use. Modified from Prinzhofer et al. (2000).

6.2. Foothills region

6.2.1. Flow of formation waters

The flow of formation waters in the Upper Cretaceous – Tertiary post Lea Park succession in the Foothills study area, adjacent to the deformation front is quite complex (Bachu and Michael, 2003). The flow is driven by gravity (topography), erosional rebound and reimbibition of gas-saturated sandstones and is controlled by absolute permeability of the rock, and gas generation (Bachu and Michael, 2003).

The Upper Cretaceous – Tertiary post Lea Park succession includes four main aquifers: (1) Basal Belly River; (2) Upper Belly River aquifer, consisting of the sandstones of the Oldman and Dinosaur Park formations; (3) Edmonton aquifer, consisting of the sandstones of the Horseshoe Canyon Formation and (4) Scollard-Paskapoo aquifer, at the top of the succession.

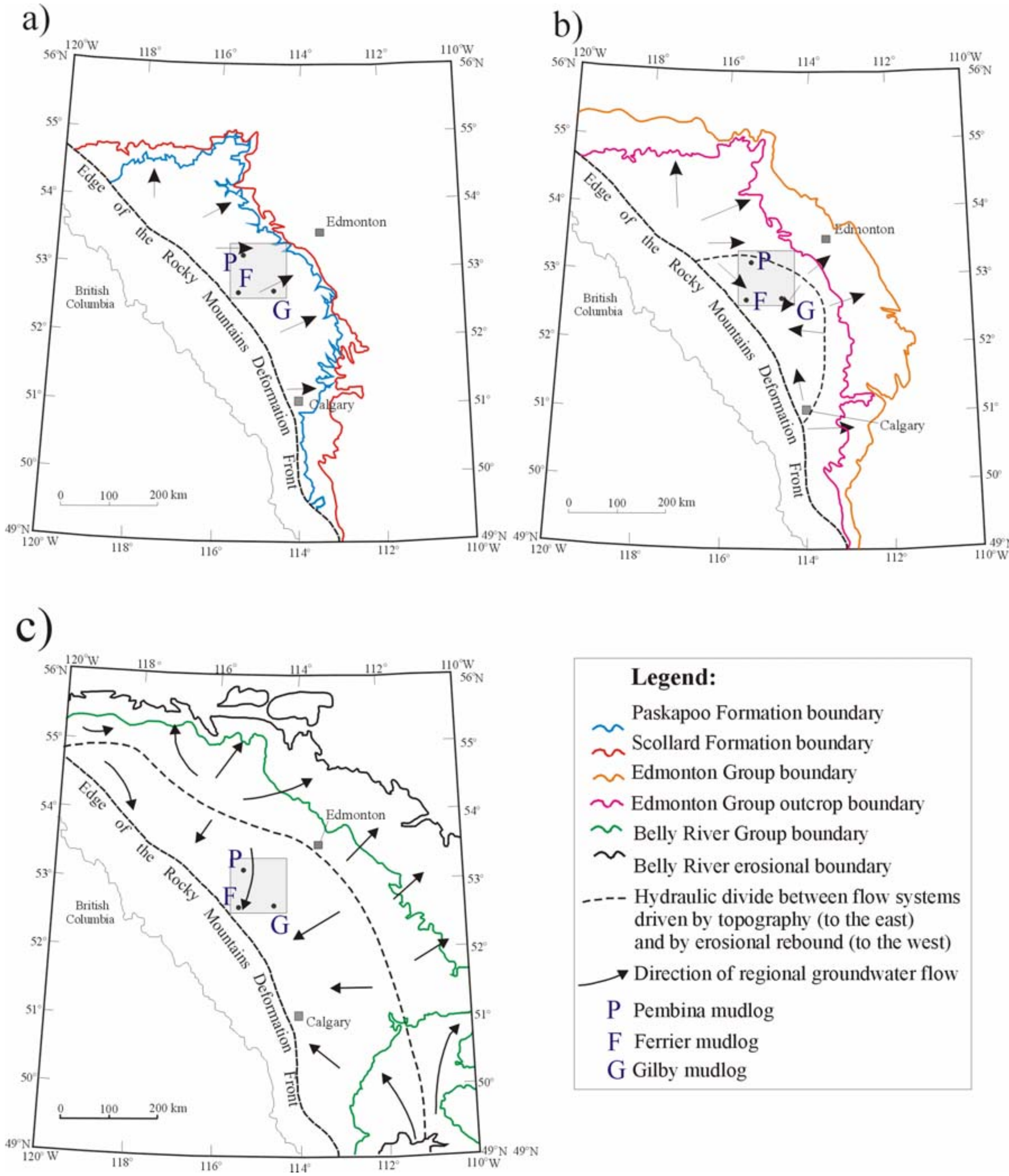

Figure 6-2 Flow patterns (indicated by arrows) in the coal-bearing Upper Cretaceous-Tertiary strata of the Alberta basin: (a) Scollard-Paskapoo aquifer; (b) Edmonton aquifer; c) Belly River aquifer. Modified from Bachu and Michael, 2003. Note: the grey squares indicate the Foothills area in the present study.

This delineation, according with Bachu and Michael (2003) was confirmed by the analysis of the formation waters chemistry and pressure data.

The water table indicates flow in the Scollard-Paskapoo aquifer from high elevations (> 1000 m) near the fold and trust belt in the west to lower elevations (~ 700 m and less) in the northeast. The flow of low-salinity water of meteoric origin in the Scollard-Paskapoo aquifer is in equilibrium with, and driven by topography from recharge areas at high elevations near the fold and trust belt to discharge areas to the east-northeast (Bachu et al., 1998; Bachu and Michael, 2003).

The coals of the Scollard Formation contain the laterally extensive Ardley coal zone. The Ardley coals are subbituminous in rank, and are estimated to contain more than 100 Tcf of methane, of which approximately 25 Tcf could be available in coal seams thicker than 2.5 m (Richardson, 1991).

Coal seams with considerable continuity provide pathways for diffusion and long-distance migration of coal gases. Also, continuous high-permeable coals – like Ardley coals - are major aquifers.

The flow of formation water in the older units, like the Edmonton and Belly River groups is driven by erosional rebound in adjacent confining shales, and is directed inward, downdip, toward the basin foredeep (Bachu, 1995; Bachu and Underschultz, 1995; Parks and Tóth, 1995). The salinity of formation waters is up to 20,000 mg/l in the Belly River Group, and significantly higher (up to 50,000 mg/l) in the Mannville Group.

6.2.2. Gas migration mechanisms and pathways in the Foothills region

The molecular compositions of natural gases as well as the isotope ratios in the hydrocarbons seem to be controlled by the process of lateral migration. According with some authors, (Stahl, 1977; Shamsuddin and Khan, 1991; Leythaeuser et al., 1983; Prinzhofer et al., 2000) there are several *geochemical parameters* indicating the direction of natural gas migration. The distance of migration would be negatively correlated with $\delta^{13}C_1$, volume % C_{2+}, wetness index, and C_2/C_1, and positively correlated with volume % C_1 and ($\delta^{13}C_2$ - $\delta^{13}C_1$) values. In other words, methane $\delta^{13}C$, volume % C_{2+}, C_2/C_1 ratio and the wetness index all decrease – indicating the migration directions and pathways. The methane concentration and the isotopic difference between methane $\delta^{13}C$ and ethane $\delta^{13}C$, on the other hand, increase away from the presumed source.

It is clearly seen from Figure 6-3 and Figure 6-4 that the above-mentioned parameters – $\delta^{13}C1$, volume % C_{2+}, wetness index, C_2/C_1 - decrease from west to east (from Ferrier, through Pembina to Gilby), and increase from west to east {($\delta^{13}C_2$ - $\delta^{13}C_1$) and volume % C_1} respectively.

All these geochemical parameters appear to be consistent with a fractionation due to migration; the migrating gas is isotopically lighter, slightly affected by C2+ fractionation and enriched in methane in comparison with C2+ fraction.

The composition and spatial distribution of gas components in the Scollard formation could also be explained in relationship with the well-established flow of formation waters in this region (topography driven, from west to east).

If we consider the original gas within the Scollard Formation in areas close to the deformation front, this gas, wetter and with isotopically heavier methane, ethane and propane, would represent the residual gas left behind through an effective transport process involving fractionation through diffusion in formation waters.

As already discussed in Chapter Four, coal beds are commonly aquifers where microorganisms can flourish. The topography-driven recharge of meteoric waters at Ferrier location (on the 83B –Rocky Mountain House – Topographical map, 1:250,000 - Ferrier mudlog is located at ~3300 feet above Sea Level, in a local recharge area near the fold and thrust belt) would enhance the chances of aerobic bacteria to enter the shallow aquifer and attack the wet gas components. This is confirmed by the combination plot of $\delta^{13}C_{CO2}$ and $\delta^{13}C_{CH4,}$ with isotope fractionation lines (Ec) – proposed by Whiticar (1999) (Figure 6-5). Figure 6-6 shows the bacterial methane formation and consumption pathways for the Paskapoo gases at Ferrier, Pembina and Gilby locations. As can be observed, the associated carbon dioxide at Ferrier location is isotopically light (<-20 ‰), which is interpreted to be a kinetic isotope effect of oxidation induced by bacterial action, resulting in preferential incorporation of ^{12}C into the CO_2, which leaves the residual light hydrocarbons isotopically heavier. Another key point is that the carbon isotopic fractionation factor between $\delta^{13}C_{CO2}$ and $\delta^{13}C_{CH4}$ remains consistent for, and indicative of

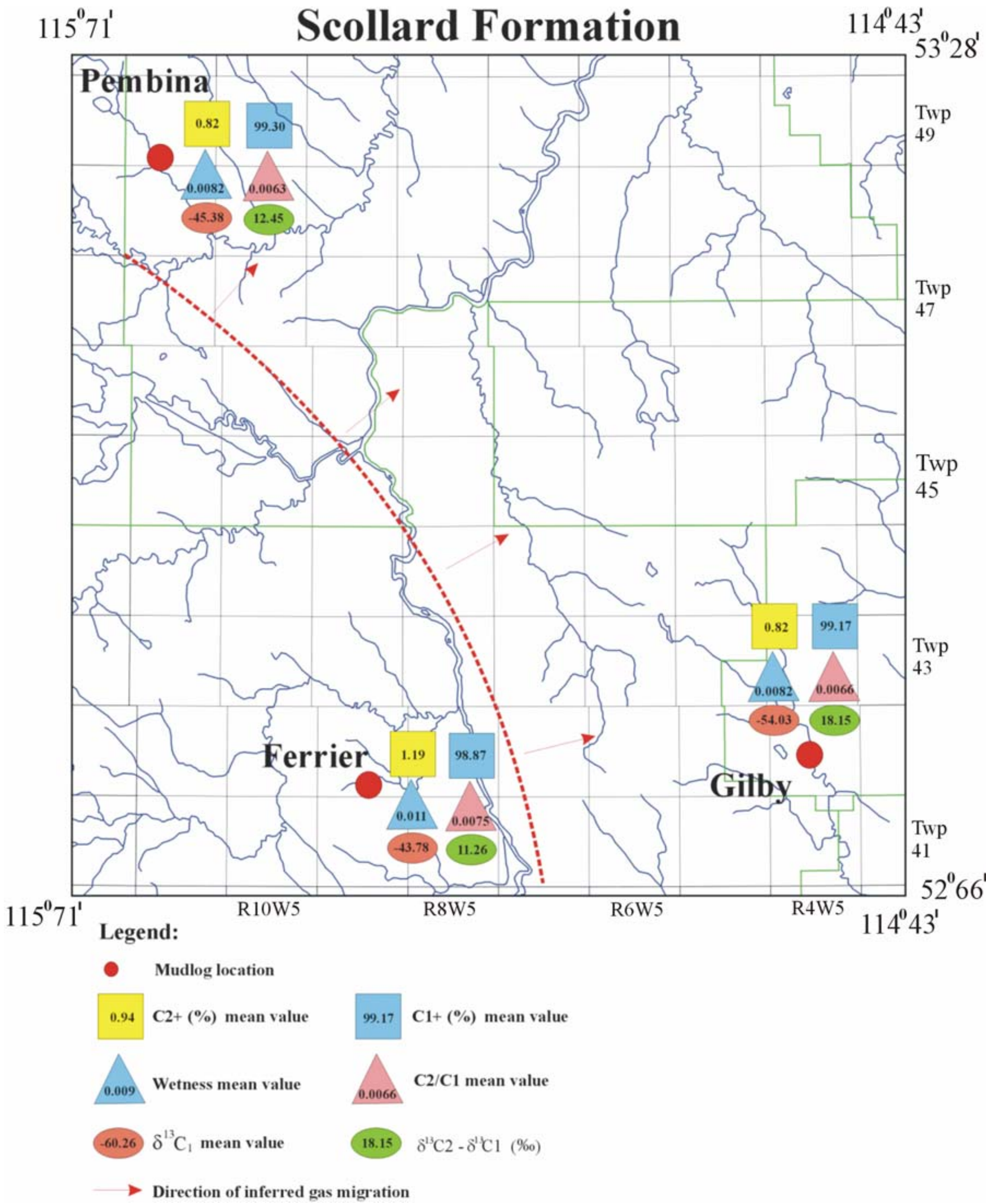

Figure 6-3 The distribution of the isotopic composition of methane and physico-chemical parameters of the Scollard gases in the different mudlog locations in the Foothills region. Only the mean values are shown.

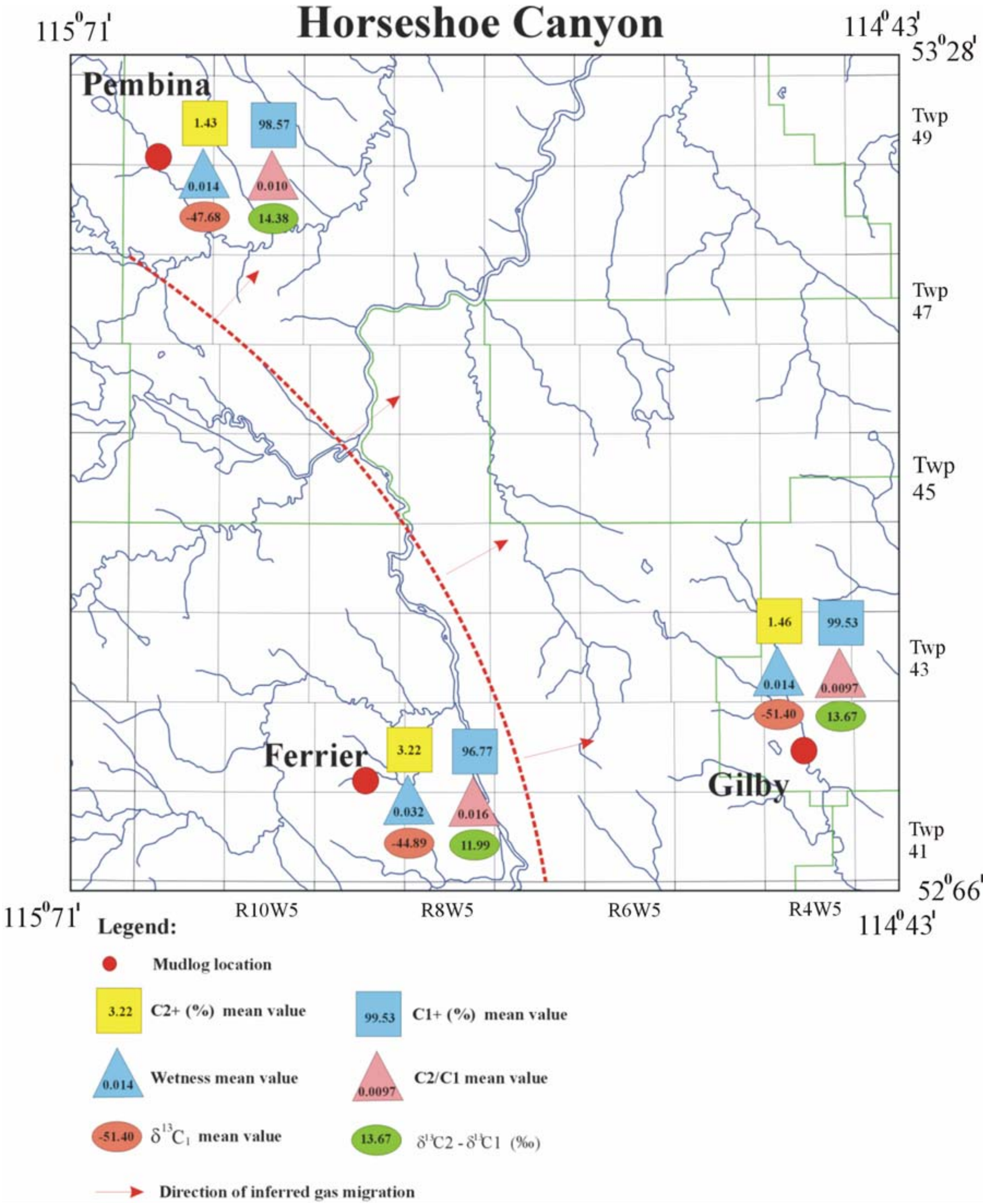

Figure 6-4 The distribution of the isotopic composition of methane and physico-chemical parameters of the Horseshoe Canyon gases in the different mudlog locations in the Foothills region. Only the mean values are shown.

specific setting or diagenetic environment (Whiticar, 1999). CH_4 oxidation causes a strong, clear carbon isotopic separation ($\delta^{13}C_{CO2}$ - $\delta^{13}C_{CH4}$), usually between 5 and 25 towards the latter stages of consumption (Whiticar, 1999).

As a result of the above discussion, the Paskapoo gases at Ferrier location are assumed to be bacterial gases, which suffered the process of methane oxidation by bacteria introduced by meteoric waters. CH_4 bacterial oxidation can lead to difficulties in the interpretation of natural gas sources. As already pointed out in Chapter Four, these gases affected by biodegradation (shallower part of the stratigraphic section in the foothills area), could be misinterpreted as over-mature because they are very dry and chemically resemble thermogenic gases composed of nearly 100% methane (the wetness index ranges between 0.0017 for Scollard and 0.02 for Horseshoe Canyon).

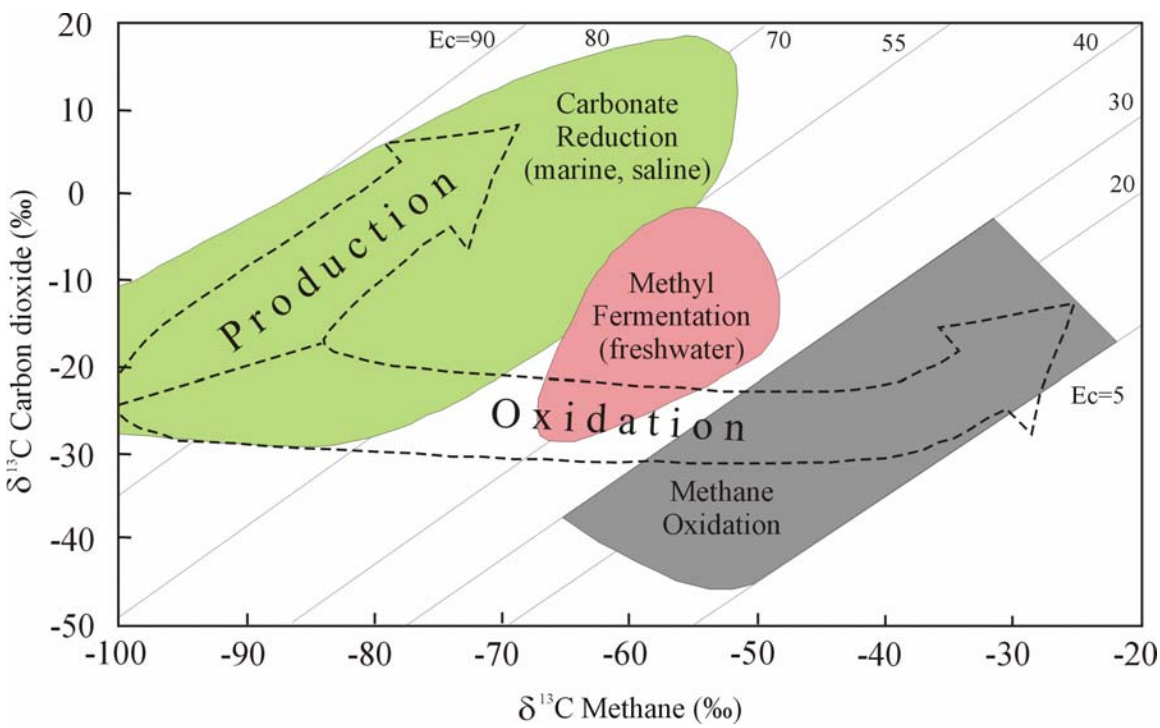

Figure 6-5 Combination plot of $\delta^{13}C_{CO2}$ and $\delta^{13}C_{CH4}$ with isotope fractionation lines (Ec). Methanogenesis by carbonate reduction has a larger CO_2 – CH_4 isotope separation than by methyl-type fermentation (freshwater region), or methane consumption (modified after Whiticar, 1999).

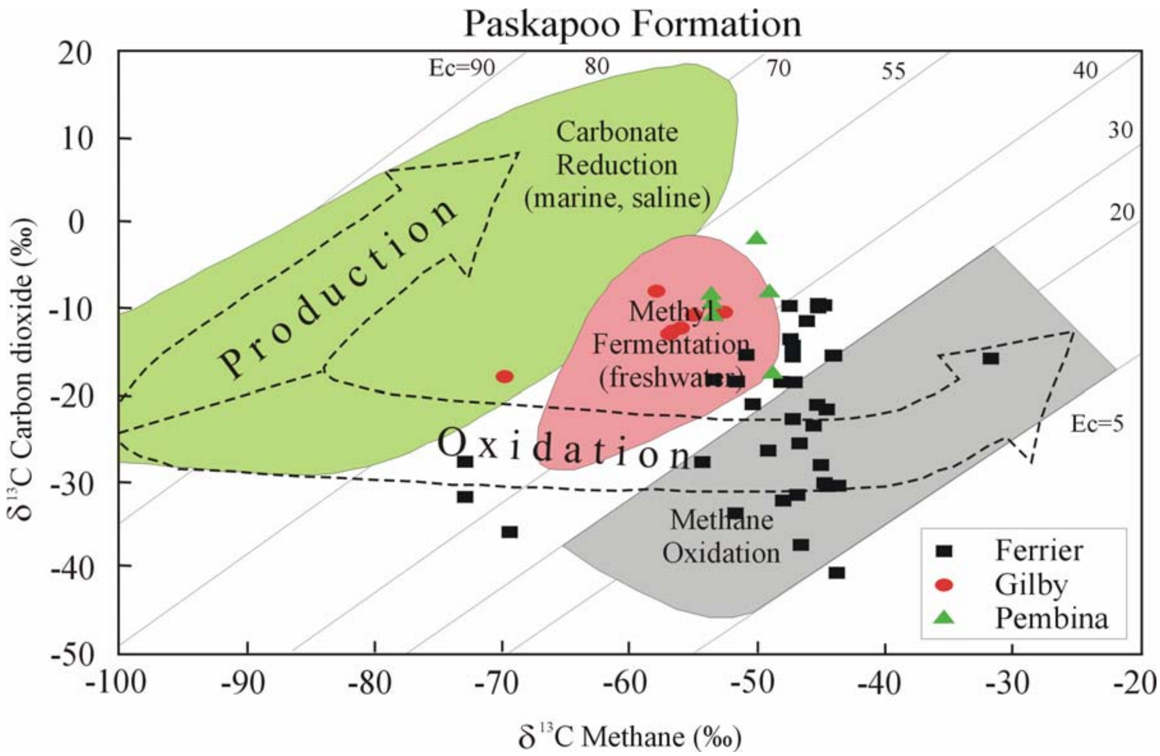

Figure 6-6 Combination plot of $\delta^{13}C_{CO2}$ and $\delta^{13}C_{CH4}$ with isotope fractionation lines (Ec) for the Paskapoo Formation gases (after Whiticar, 1999).

It is also well known that coal preferentially adsorb ^{13}C – methane versus ^{12}C – methane, and ethane relative to methane (Friedrich and Jüntgen, 1972).

Whether adsorption during migration from west – southwest (Ferrier) to east – northeast (Gilby) could actually cause the observed trend must be a function of the volume of rock to which a gas is exposed during migration. As adsorption phenomena (enhanced by bacterial alteration of the wet components of gases) would induce the same kind of fractionation as diffusion, both explanations may be valid in the case of the Scollard gases.

It should be noted, however, that the process of diffusion possibly could be so slow that lateral diffusion over more than a few kilometres would probably take too long, even for Cretaceous-aged traps (Alton Brown, personal communication).

An alternative cause of the increased gas dryness and decreased $\delta^{13}C$ values toward the east (from Ferrier and Pembina locations toward Gilby location) is spatial variation in source maturity. Both the compositional and isotopic trends observed parallels an overall decrease in maturity towards east (Figure 6-7). Although still within the oil window, lower source maturities may impart both a lesser proportion of C2+ alkanes and more negative $\delta^{13}C$ values to generated gases. In this scenario, the wetter gas composition at Ferrier location could be due to increased thermal maturation at greater depth of burial than at Gilby location and thus might not involve gas migration over any substantial distance.

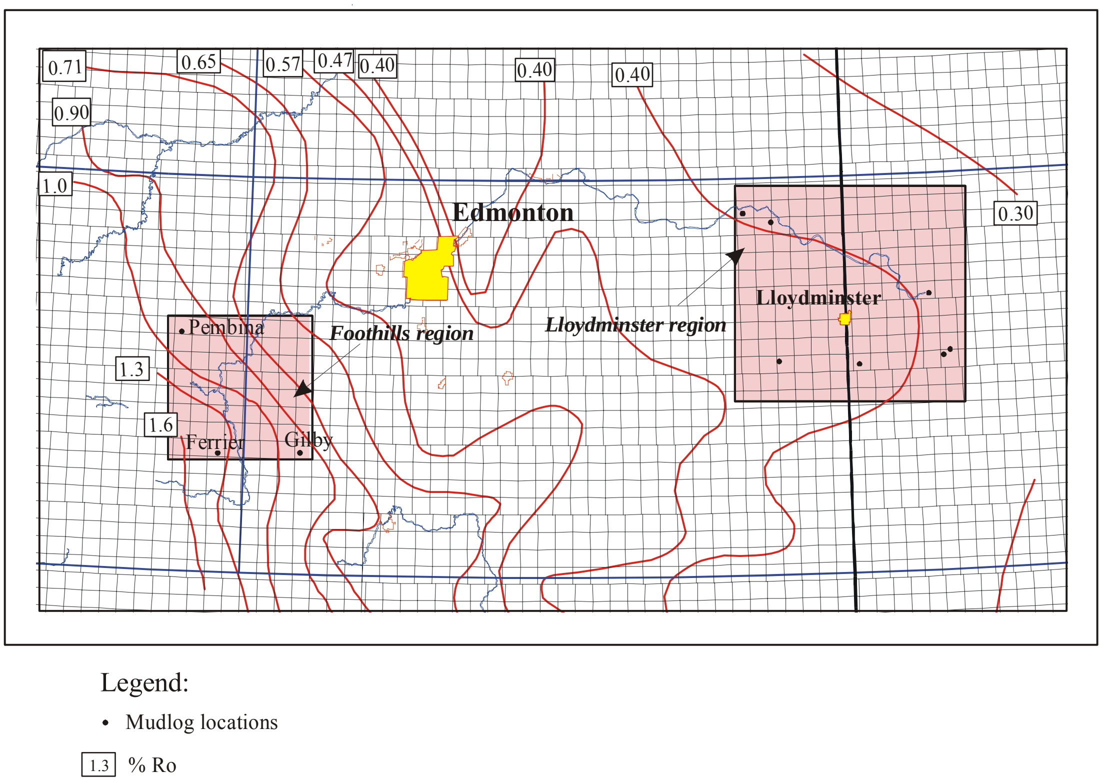

Figure 6-7 The overall organic maturity trend in the Ferrier-Gilby area, and Lloydminster area for Mannville strata. The values for the mean maximum vitrinite reflectance are from isomaturity maps of Bustin, 1991.

Also, if one takes into consideration the Scollard-Horseshoe Canyon data in the Foothills region, the application of the partition function methodology of James (1983) indicates that gas generation at Ferrier location took place at higher levels of maturity than at Gilby location (see Chapter Four).

On the other hand, as already mentioned, the gases sampled at Gilby location are, overall, isotopically relatively lighter than the gases sampled at Ferrier and Pembina locations. They are also dryer. Contradictory, the lighter isotopic ratio of methane cannot be explained by lower maturity because the gases would be wetter in that case, whereas they are dryer.

To state that the isotopic compositions of gases are controlled by the maturity of the source rocks, the tendency of the $\delta^{13}C$ values of being heavy to light should be in accord with the tendency of the wetness index to increase from west to east and with the distributive pattern of higher maturity in the west and lower maturity in the east. This is not the case, at least for the Scollard – Horseshoe Canyon gases. Nevertheless, taking into account the bacterial gas addition to these gases as suggested by the $\delta^{13}C_2$/ $\delta^{13}C_3$, and $\delta^{13}C_2$/ $\delta^{13}C_1$ diagrams (see Chapter Four) – the dryness may be explained by mixing of thermogenic gases with bacterial generated gases.

Upper Belly River gases at Ferrier, and Gilby locations may represent the only case where the maturation effects seem to be dominant. A similar differentiation in $\delta^{13}C$ values is present not only for methane, but also for ethane and propane (more negative values for Gilby relative to Ferrier gases); furthermore, the geochemical parameters indicate a slightly wetter gas at Gilby location (Figure 6-8).

Neither possibility – migration or source maturity control - can be excluded on the basis of the existing data alone.

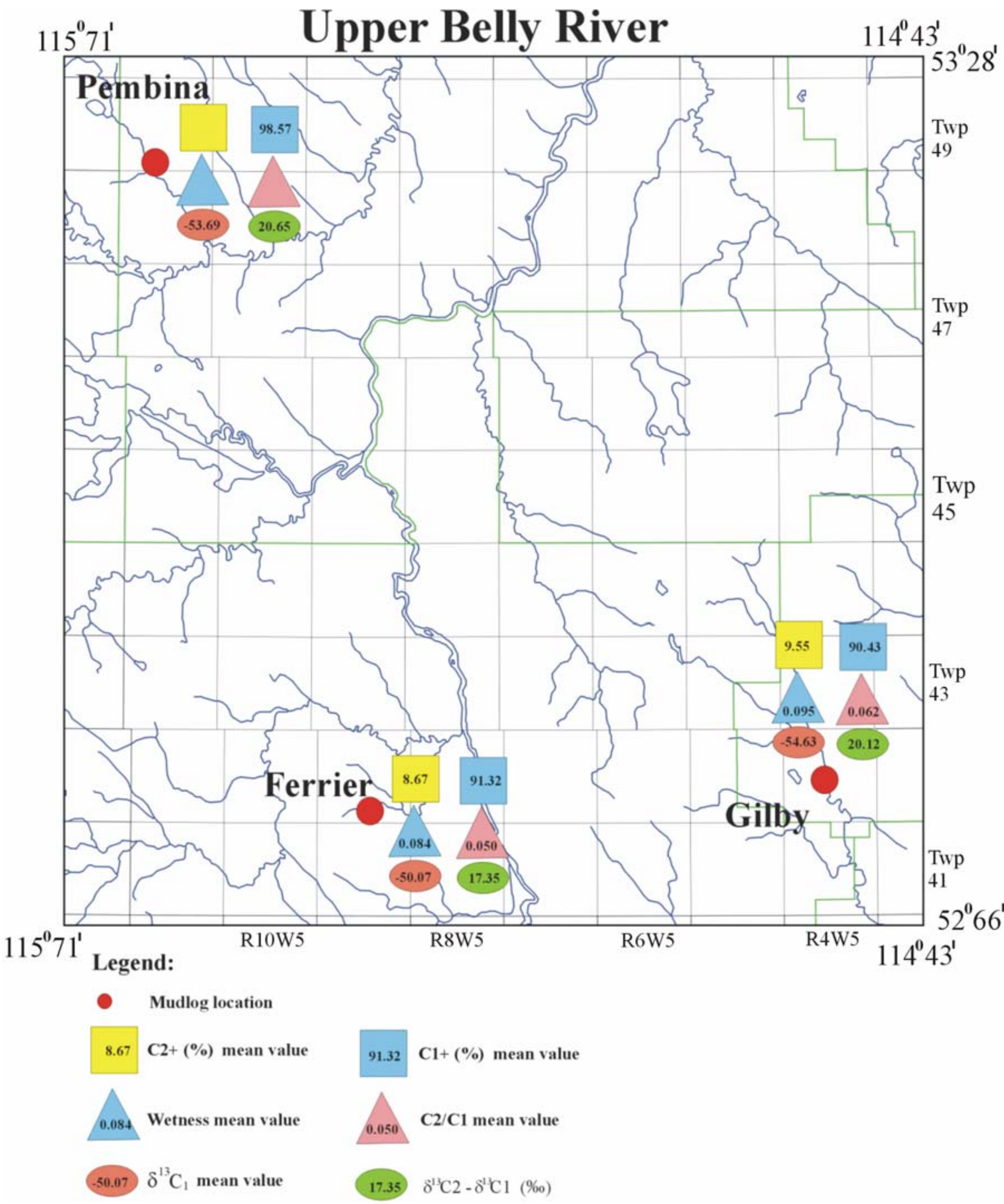

Figure 6-8 The distribution of the isotopic composition of methane and physico-chemical parameters of the Upper Belly River gases in the different mudlog locations in the Foothills region. Only the mean values are shown.

In a ($\delta^{13}C_2$ - $\delta^{13}C_3$) versus C_2/C_3 diagram, where Lorant et al. (1998) modeled the possible trend of maturation for natural gas series, data from Ferrier, Pembina and Gilby indicate secondary cracking from oil for Ferrier-, and secondary cracking from the wet portion of the gases for Gilby samples (Figure 6-9).

This would indicate that the Scollard-Horseshoe Canyon gases have been generated in some later stages of thermal degradation, corresponding to the secondary cracking of the C2+ portion of the gas.

The thermal destruction of C_2 to C_4 gases can happen only at higher maturities, at extremely high temperatures. This is not in good agreement with the geological reality and is further contradicted by two plots of C_2/C_3 versus C_2/iC_4, which enables gases fractionated only through thermal cracking to be distinguished from gases having suffered bacterial alteration (Lorant, 1999, from Prinzhofer et al., 2000). As can be seen from Figure 6-11, Scollard and Horseshoe Canyon gases at Gilby location are obviously more affected by biodegradation than Scollard – Horseshoe Canyon gases at Ferrier location (Figure 6-10). The biodegradation involved here might be the one that degrades wet gas to dry gas. Once again, if this is the situation, the wetter gas composition at Ferrier location might not involve gas migration over any substantial distance.

The ethane isotopic values in the three mudlog locations can be also considered in supporting the idea of different source maturities and/or different isotopic kerogen compositions for the west end (Ferrier, Pembina) and the east end (Gilby) of the Foothills study area.

The ethane $\delta^{13}C$ data for the Scollard gases are represented in Figure 6-12. As can be seen, the ethane isotopic values are significantly similar for the Ferrier and Pembina profiles, but more positive than those for the Gilby profile.

The same relationships can be found with the ethane $\delta^{13}C$ data for the Horseshoe Canyon gases (Figure 6-13), and for the Belly River gases (Figure 6-14) – suggestive for at least two different sources: one for Pembina – Ferrier gases, another one for Gilby gases.

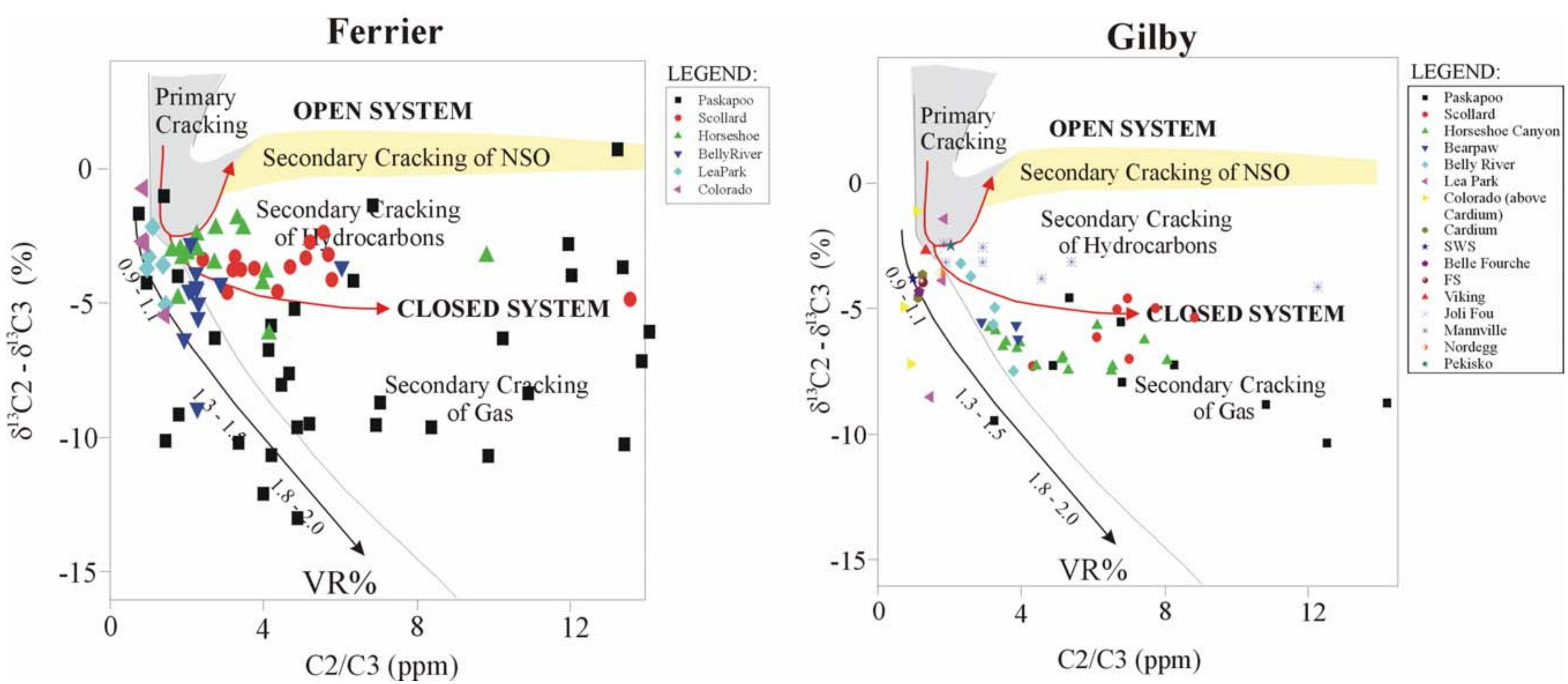

Figure 6-9 C2/C3 diagram showing δ^{13} C2 – δ^{13}C3 versus C2/C3 distinguishing gases generated from the primary cracking of kerogen, the secondary cracking of oil, and the tertiary cracking of the wet portion of the gases for ferrier and Gilby profiles (after Lorant et al, 1998)

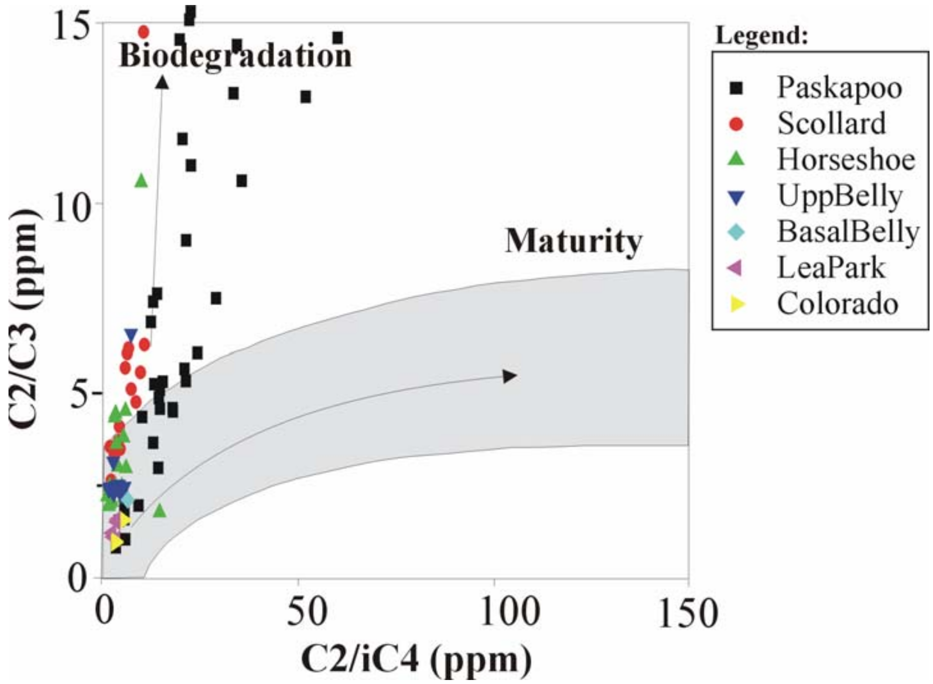

Figure 6-10 C2/C3 versus C2/iC4 diagram showing the possible biodegradation of hydrocarbon gases (Prinzhofer, 2000). Ferrier 14-3-42-9W5

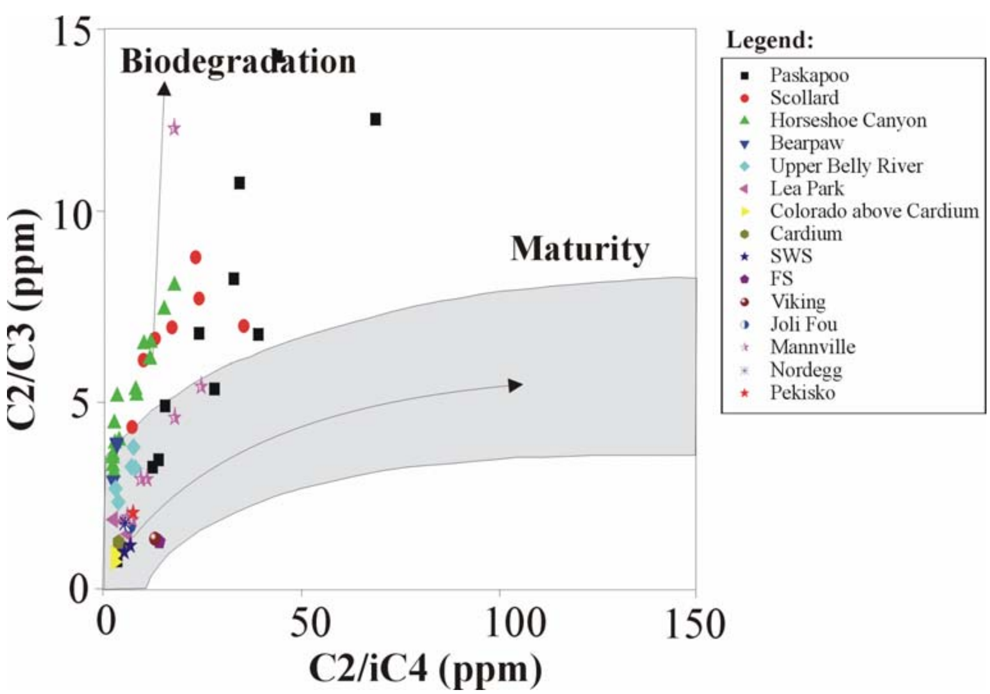

Figure 6-11 C2/C3 versus C2/iC4 diagram showing the possible biodegradation of hydrocarbon gases (Prinzhofer, 2000). Gilby 15-16-42-4W5.

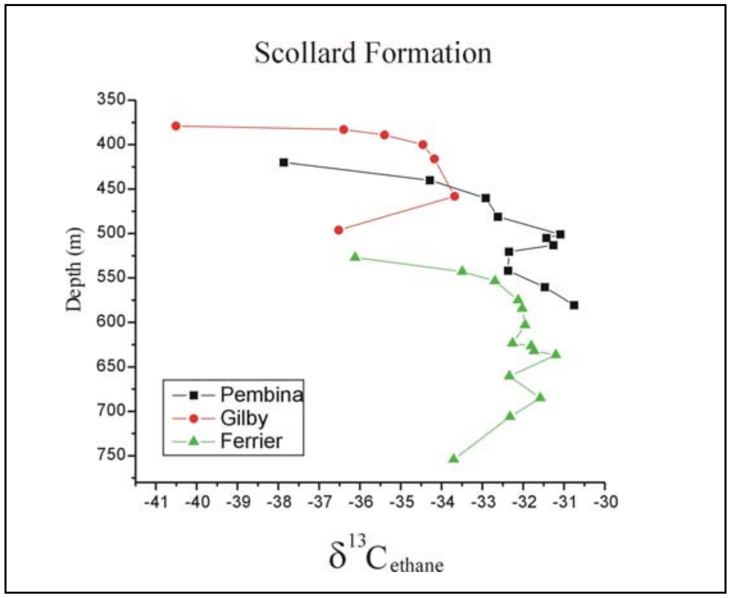

Figure 6-12 The pattern of ethane $\delta^{13}C$ change with depth in the Scollard Formation, Foothills region.

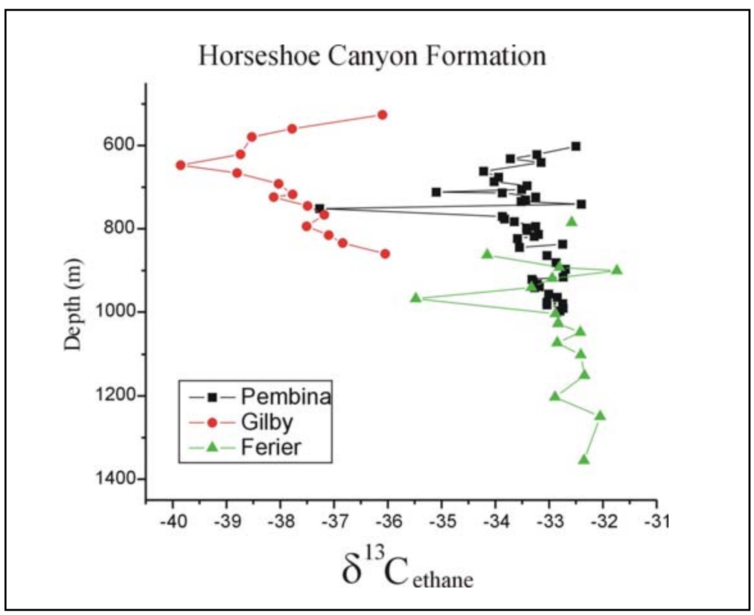

Figure 6-13 The pattern of ethane $\delta^{13}C$ change with depth in the Horseshoe Canyon Formation, Foothills region.

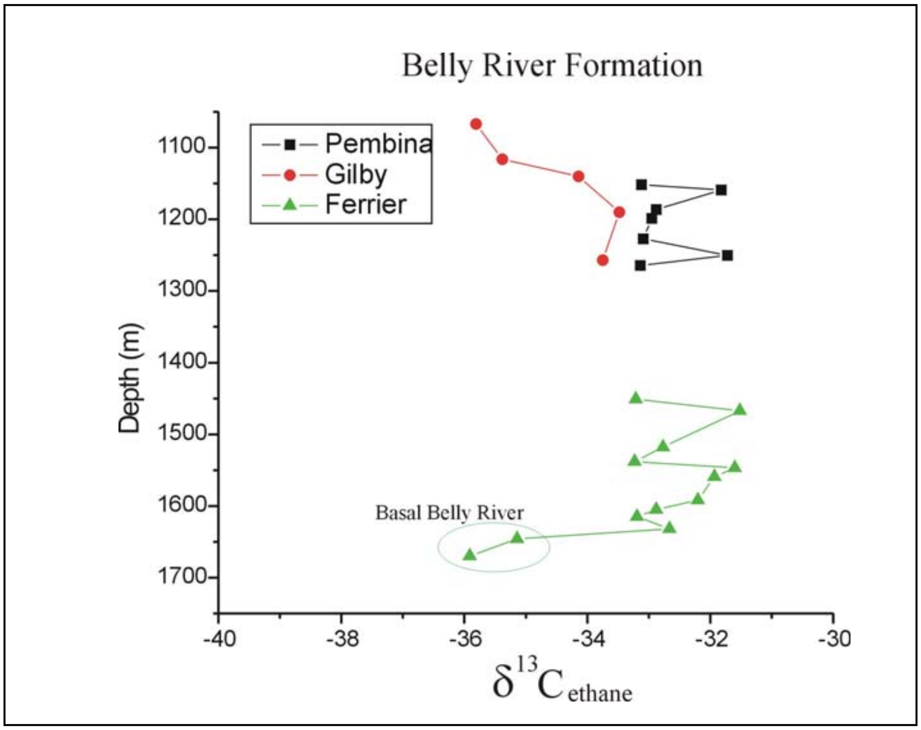

Figure 6-14 The pattern of ethane $\delta^{13}C$ with depth in the Belly River Group, Foothills region.

Since bacteria can be introduced by groundwater flow in recharge areas, microbial activity must be taken into consideration since this activity can affect the composition of shallow gases. Significant amounts of late-stage anaerobic biogenic gas can be generated that either can be mixed with previously generated thermogenic gas or can fill degassed coal-bearing strata. Biogenic gas is composed of isotopically light methane (Rice and Claypool, 1981; Schoell, 1983; Rice, 1992) and its mixing with earlier generated thermogenic gas could account for the compositional changes observed in shallow coal-bearing strata.

Increased gas abundance at Gilby location (Figure 6-15) could be explained in terms of its position close to the outcrop boundary of the Edmonton Group, in recharge areas (see Figure 6-2). Here, the meteoric water driven by regional topography, may penetrate the coals of the Horseshoe Canyon Formation and create favourable conditions for the production of late stage biogenic methane (Bachu and Michael, 2003). This amount of late-stage bacteriogenic gas, being mixed with earlier or original gas, may account as well for the increased dryness at Gilby location.

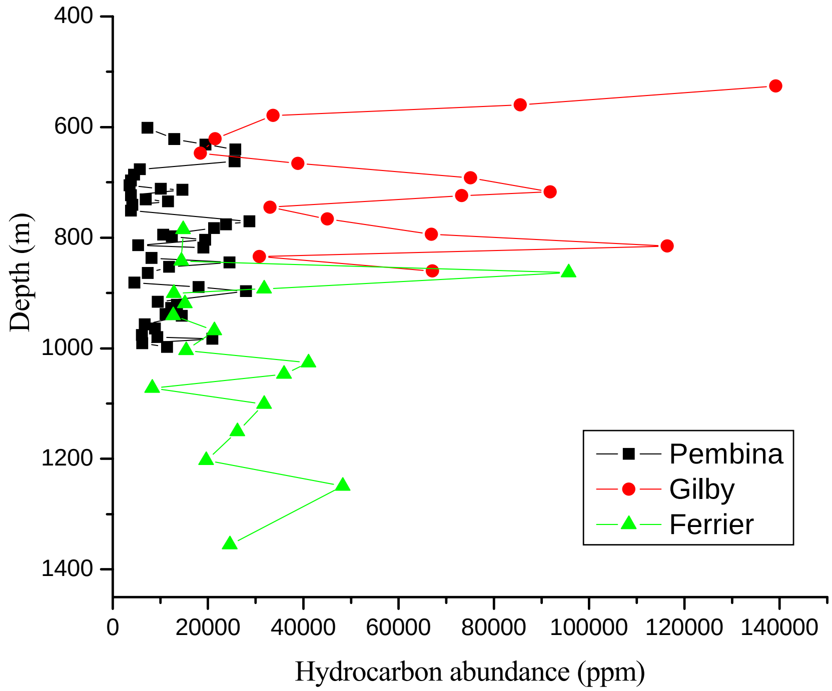

Figure 6-15 In depth variation of the total abundance of hydrocarbon gases in the Horseshoe Canyon Formation, Foothills region.

6.3. Lloydminster region

6.3.1. Flow of formation waters

The Cretaceous hydrostratigraphic succession in east-central Alberta comprises sandy aquifers and shaly aquitards of the Mannville Group, Colorado Group and Lea Park Formation (Roston and Tóth, 1997).

A hydrological study focused in the Chauvin area of east-central Alberta (Holysh, 1989) revealed the regional ground water flow pattern in this part of the Western Canada Sedimentary Basin, between Townships 36 and 57. This study suggests that in east-central Alberta two opposing flow systems meet in the Mannville Group. Waters flowing downward from the surface meet waters that are moving upwards, through the Mannville Group, from the Devonian strata. Water flow is then redirected laterally to the northwest (Holysh, 1989, Holysh and Tóth, 1996).

Bachu et al. (1998) come up to the same conclusion, stating that, in the eastern part of the Alberta Basin, the flow of formation waters in the Belly River Group is driven by local topography. The salinity of formation waters in the shallow part of the basin is low (< 10,000 mg/l).

Groundwater flow conditions in the east-central Alberta can be summarized as follows (Holysh and Tóth, 1996):

"1. Groundwater flow is adjusted to the relief of the water table in the glacial drift and shallow bedrock, that is, to less than the depth of the Ribstone Creek Member of the Belly River Formation. The discharge areas receive water from recharge areas in adjacent highlands.

2. Groundwater flow is descending regionally through the Lea Park Formation and Colorado Group shales into the Mannville Group.

3. The Mannville receives deep formation waters from the underlying Devonian strata.

4. Descending meteoric waters and waters rising from the Devonian strata mix in the Mannville Group and move north-eastward into subcrop or outcrop regions in Saskatchewan."

6.3.2. Gas migration mechanisms and pathways in the Lloydminster region

The distribution of the hydrocarbon gas components shows a varied pattern in the area. In the Lea Park – Colorado series, methane content tend to increase from the surface down to the approximate lower limit of the Second White Specks Formation, and then to decrease towards the top of the Mannville Group. Within the Mannville Group, the methane abundance shows a puzzling trend of increasing and decreasing values.

On the basis of the available data we can conclude also that the methane concentration increase toward the eastern and southeastern part of the study area (Figure 6-16 and Figure 6-17).

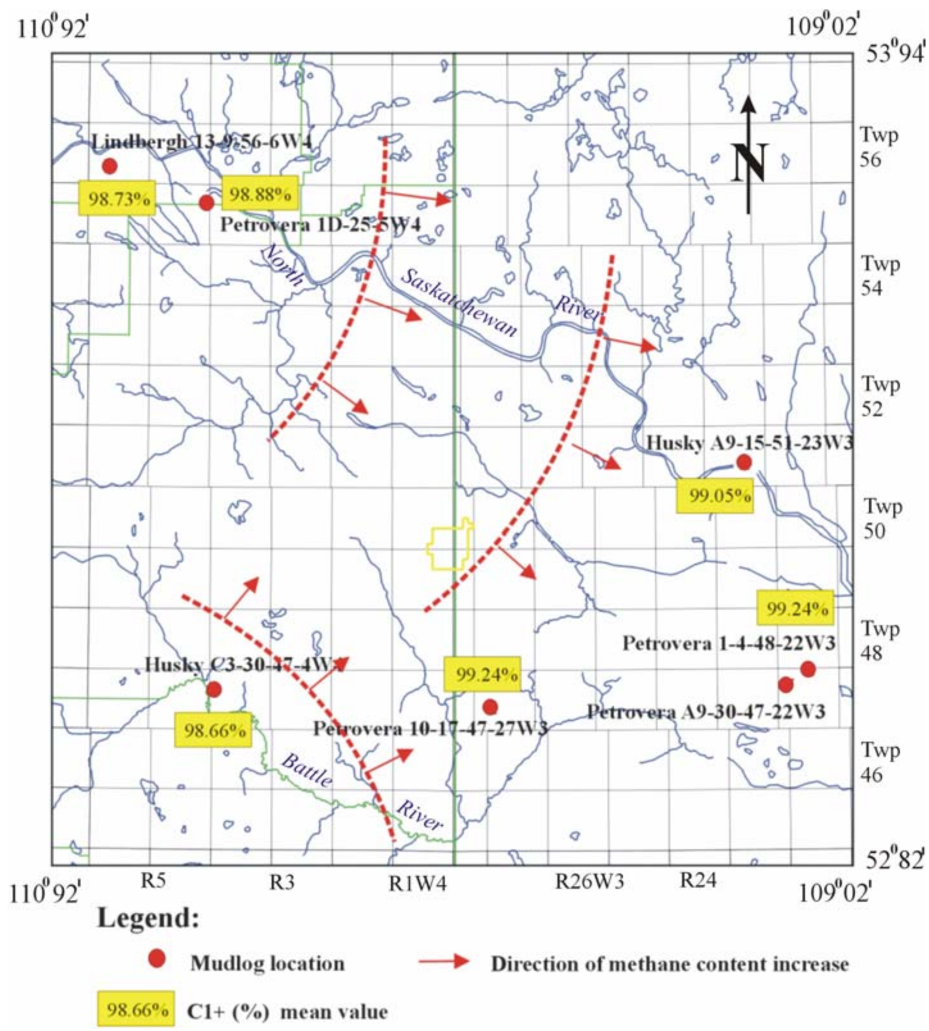

Figure 6-16 Spatial distribution of the methane content in Colorado shales, Lloydminster region.

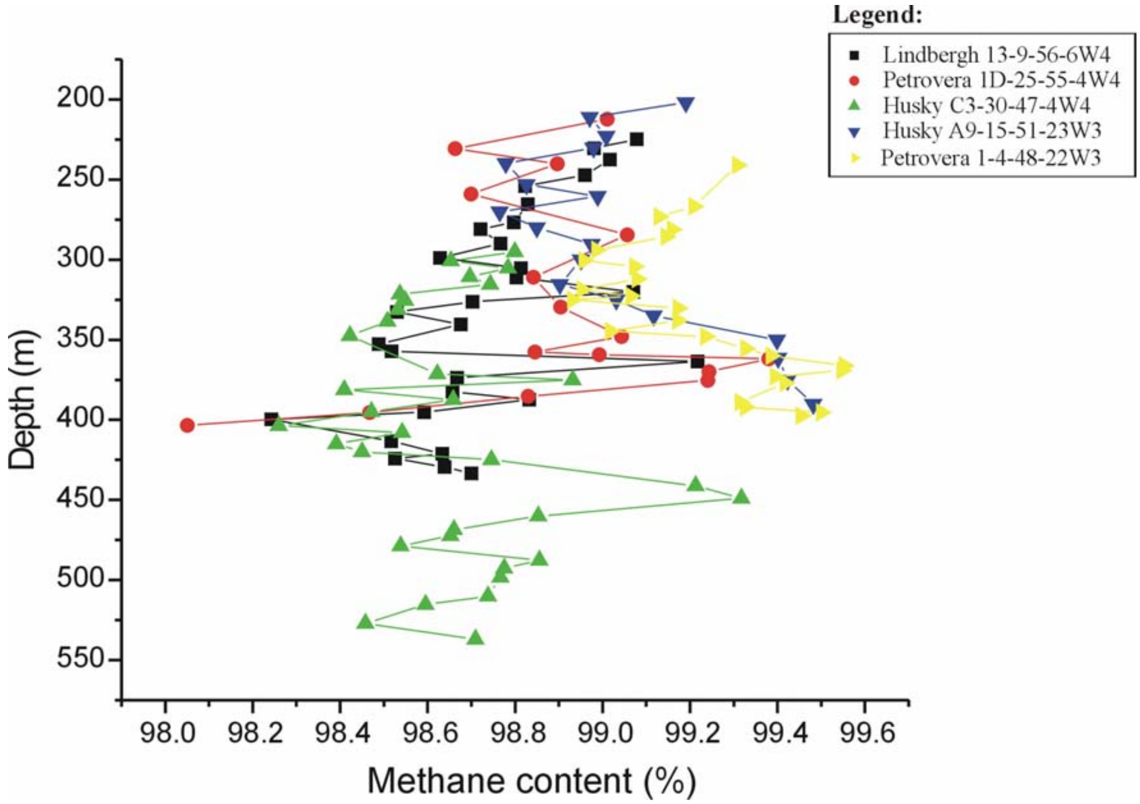

Figure 6-17 Methane concentration (in vol. %) variability with depth in five mudlog profiles within the Lloydminster region.

The spatial distribution suggests a linkage with the groundwater recharge that might affect the total composition of the gas. It is possible that the pattern of decreased methane content from Petrovera 1-4-48-23W3 to Husky 3C-30-47-4W4, or from Husky 9-15-51-27W3 to Lindbergh A9-13-56-6W4 could be related to regional recharge in the west- northwest. It is believed that this phenomenon is attributable to downward moving waters carrying dissolved methane away from recharge areas.

Another similarity to groundwater/surface water distribution is that the areas with high methane content also correspond to the current downstream positions of the two main river systems (W-NW ⟶ E-SE flowing) into the study area: North Saskatchewan River (to the north) and Battle River (to the south) (Figure 6-16).

Considering one or more gas systems migrating through solubilization/diffusion in formation waters, the migrating part of the gas will be enriched in methane and this methane will be enriched in ^{12}C (Galimov, 1975; Pernaton et al., 1996; Prinzhofer and Pernaton, 1997). Taking this into account, one can say, as in the Scollard – Horseshoe Canyon gases, that $\delta^{13}C$, volume % C2+, wetness index, and C2/C1 may be strongly affected by migration. As a result, the distance of migration will be negatively correlated with all these four parameters.

The lighter isotope having the greater solubility, $\delta^{13}C$ is expected to decrease in the direction of the groundwater flow. This direction of isotopic change means that loss of the very soluble isotope through the groundwater system should result in the ^{13}C enrichment of the remaining gas.

Looking only at the methane $\delta^{13}C$ variation within the main sandstone carrier beds (Figure 6-18) contained by the Mannville Group (Sparky, General Petroleum and Lloydminster), and then observing independently the pattern of the other migration parameters (Figures 6-19 to 6-21), a southwest to northeast and a northwest to southeast direction of migration can be observed.

The remaining gas fraction seems to be enriched by about 8–14 ‰ PDB (Lloydminster sand), and 9 - 10 ‰ PDB (Sparky sand).

Looking specifically at Colorado gases (Figure 6-22), for which two more mudlog information were taken into consideration – Husky Wainwright 2A-05-046-06W4 and Husky Standard Hill A14-16-49-22W3 – the data for the migration parameters are more scattered. However, the migration directions are consistent too with the regional trend, toward east-northeast and toward the discharge area associated with the North Saskatchewan River valley.

Additionally, in a graphic columnar representation (Figure 6-23) used to compare the magnitudes of frequencies distribution of the wetness index in the Lloydminster region, it can be easily observed the lower values toward the eastern end of the study area – indicative of migration direction.

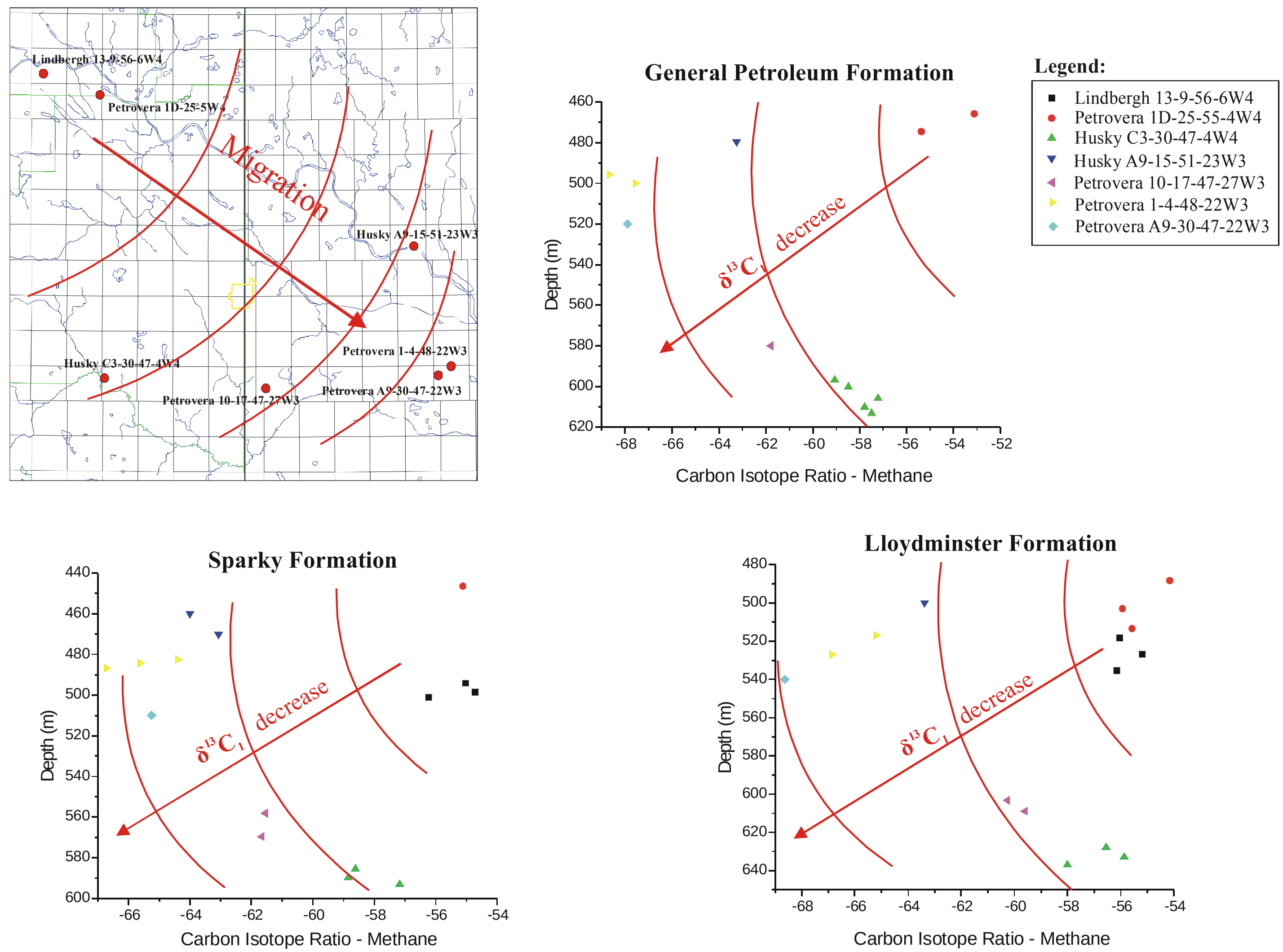

Figure 6-18 Depth profiles of methane $\delta^{13}C$ from gases sampled in Lower Mannville reservoirs, Lloydminster area.

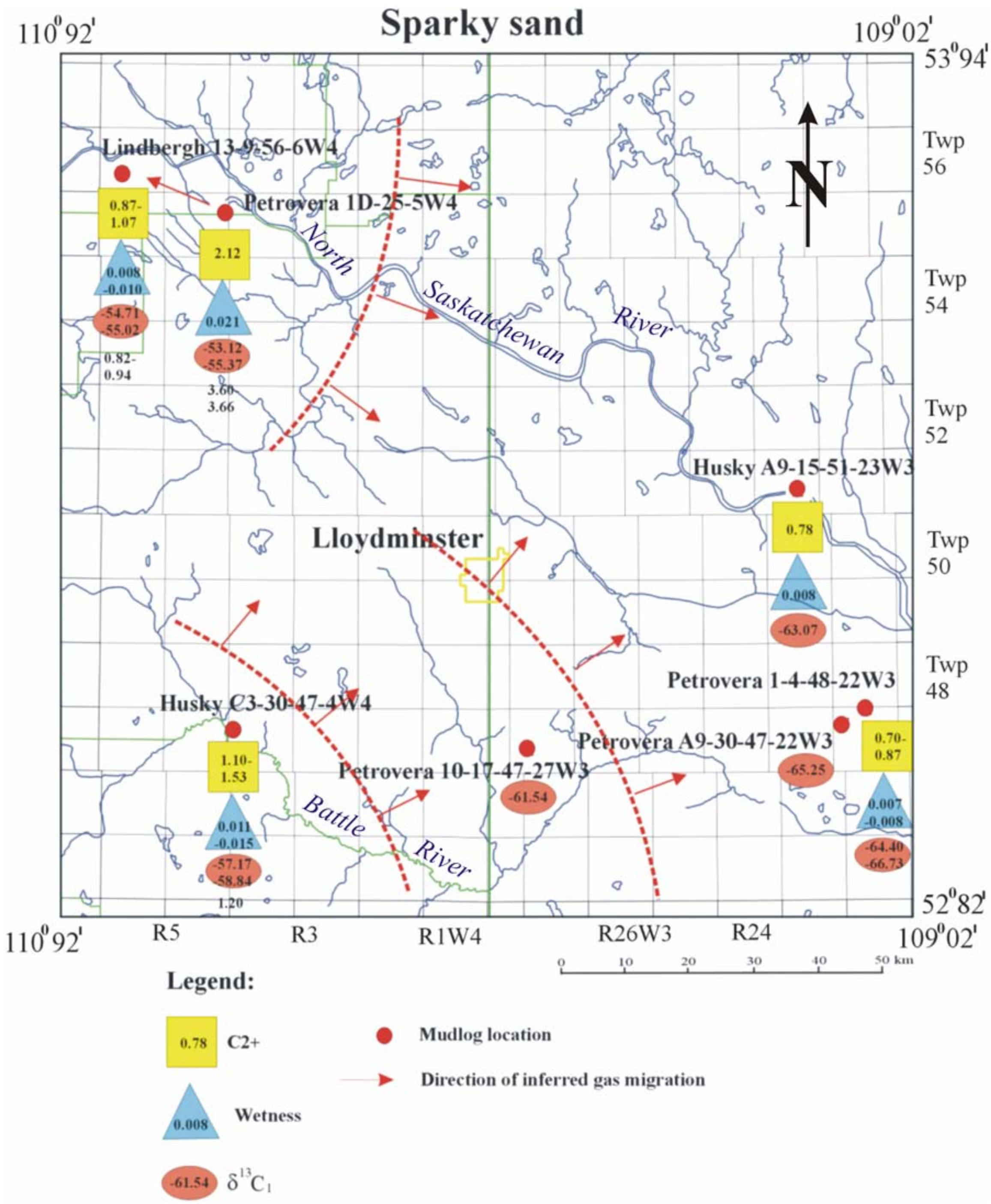

Figure 6-19 The distribution of the isotopic composition of methane and physico-chemical parameters of the Sparky sand gases in the different mudlog locations in the Lloydminster region. Only the mean values are shown.

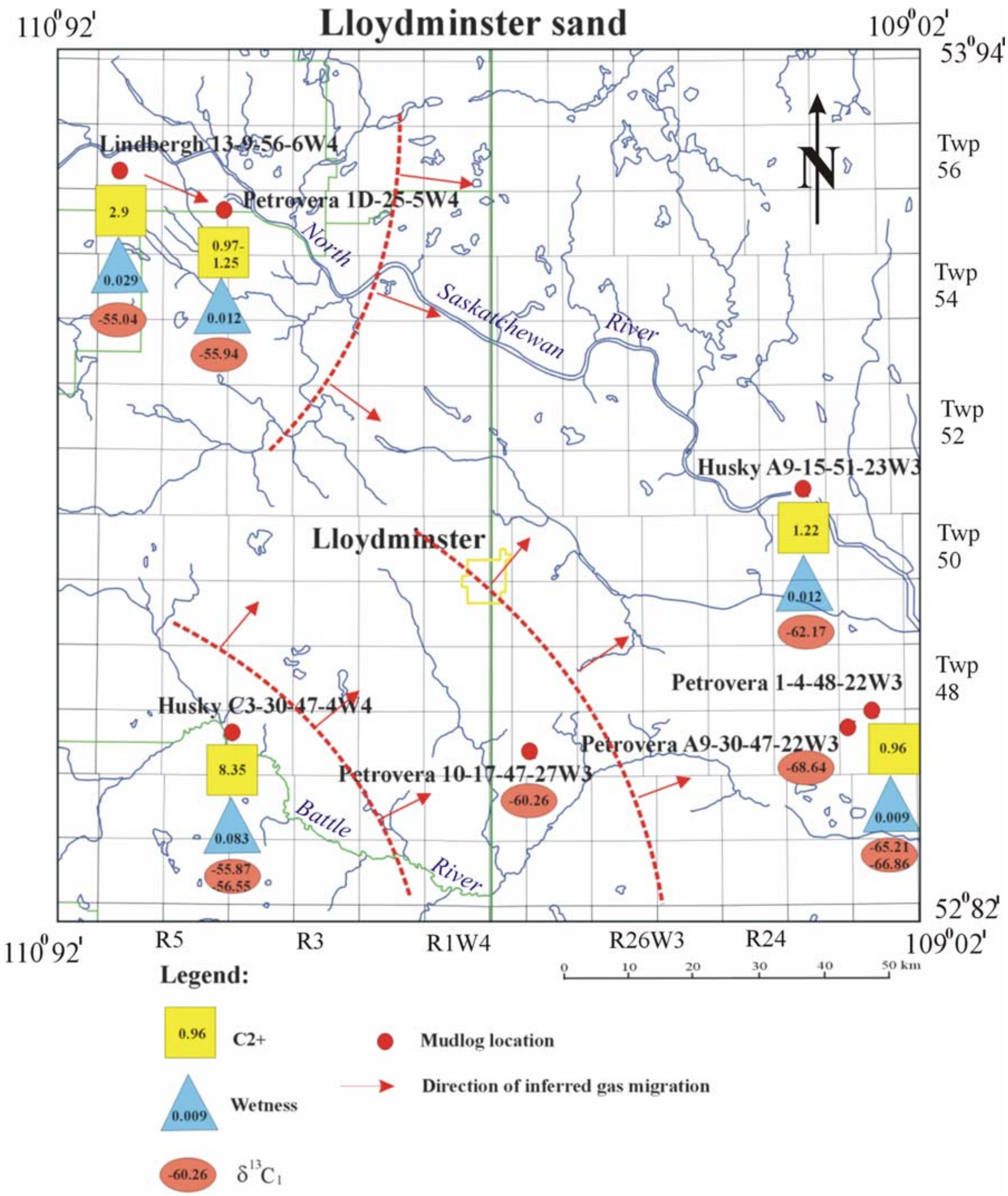

Figure 6-20 The distribution of the isotopic composition of methane and physico-chemical parameters of the Lloydminster sand gases in the different mudlog locations in the Lloydminster region. Only the mean values are shown.

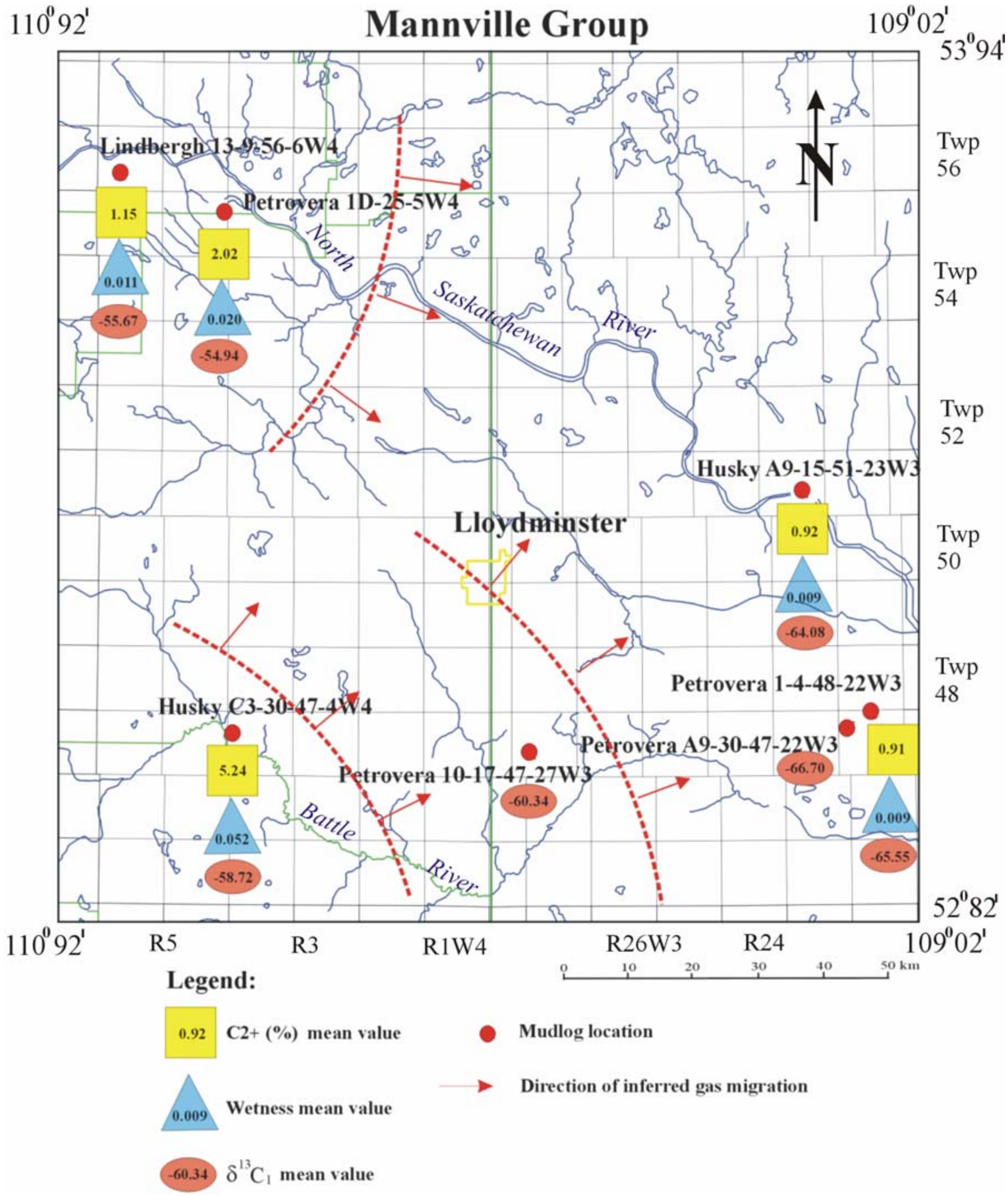

Figure 6-21 The distribution of the isotopic composition of methane and physico-chemical parameters of the Mannville Group gases in the different mudlog locations in the Lloydminster region. Only the mean values are shown.

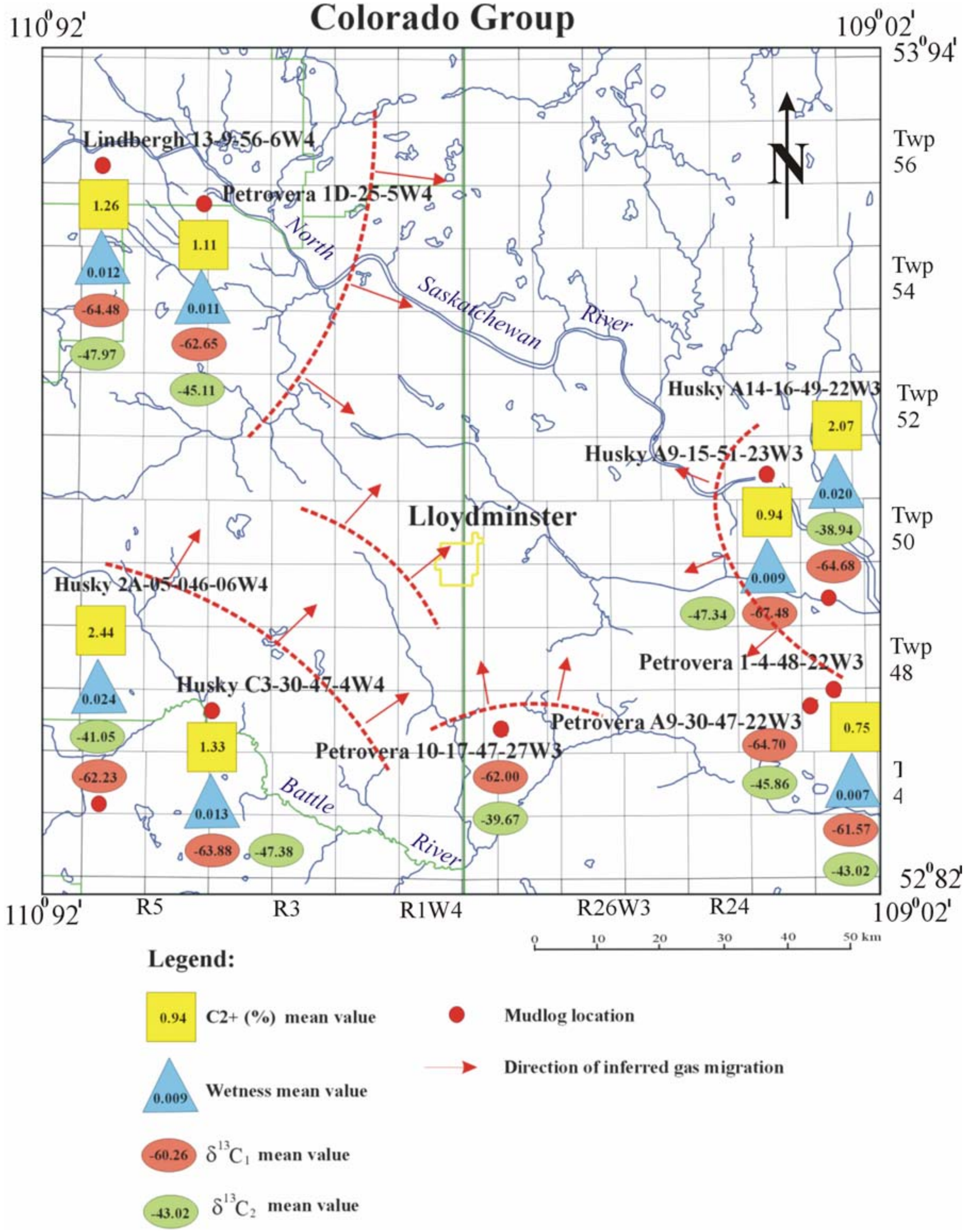

Figure 6-22 The distribution of the isotopic composition of methane and physico-chemical parameters of the Colorado Group gases in the different mudlog locations in the Lloydminster region. Only the mean values are shown.

Although the regional groundwater flow is toward the northeast, local convergences and channelling are indicated by several deep re-entrants of the hydraulic head contours (Holysh and Tóth, 1996). These features are attributed to variations in permeability caused by lithologic changes.

The difficulty in interpretation evolving from the Colorado Group data distribution may be due to the influence of several factors:

- sudden changes in flow directions, where hydrocarbon gases cross lateral permeability barriers;
- local presence of areas with relative low energy potential, and thus with a sudden decrease in pore pressure;
- *in-situ* gas generation around the wellbores of the steamed wells;
- local biodegradation effects.

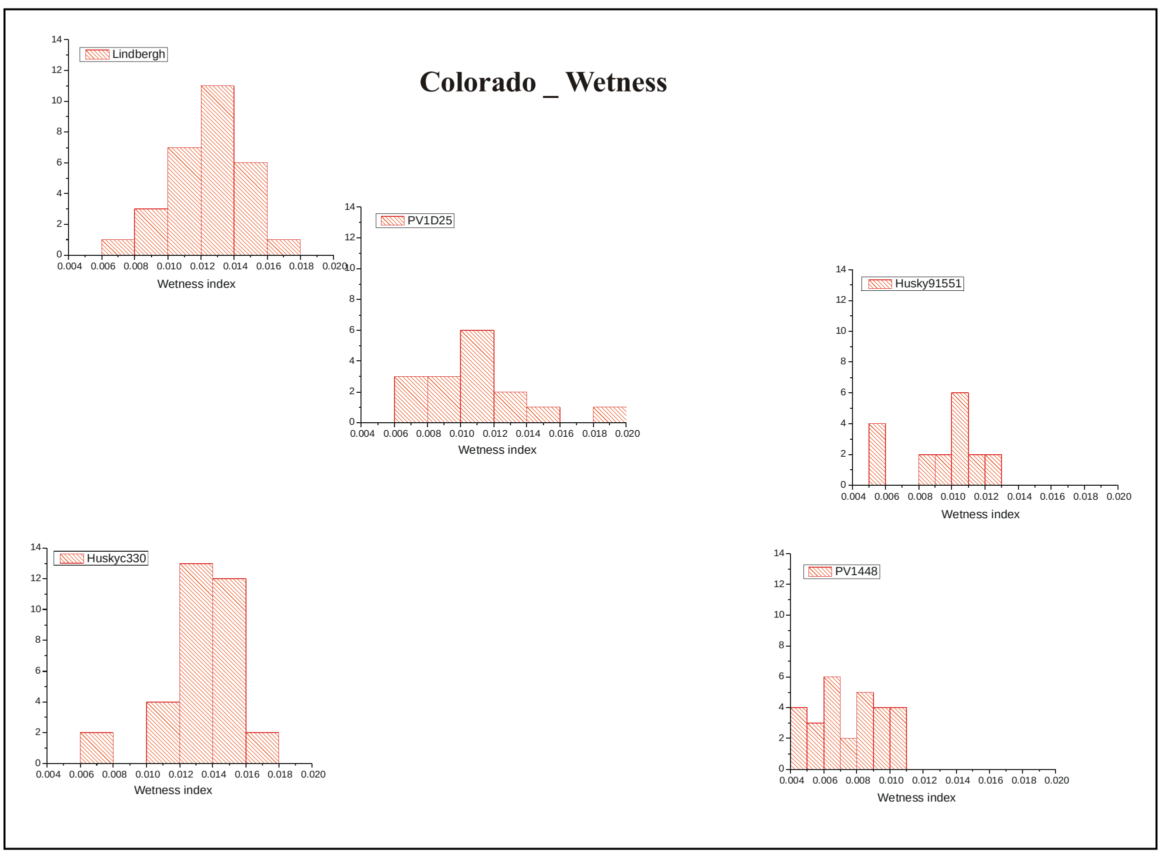

Figure 6-23 Gas wetness distribution within the Lloydminster region.

All these findings presented above suggest that lateral long-distance migration might have occurred through the sandstone carrier beds within the Mannville Group.

To prove that segregative migration might be the process induced here, a diagram using C_2/C_1 versus $\delta^{13}C$ of methane for Lloydminster sands and for Sparky sands show a clear trend of chemical and isotopic fractionation during migration. This is shown by the shape of the trend, which is curved on a linear scale (Figure 6-24) and straight on a logarithmic scale (Figure 6-25).

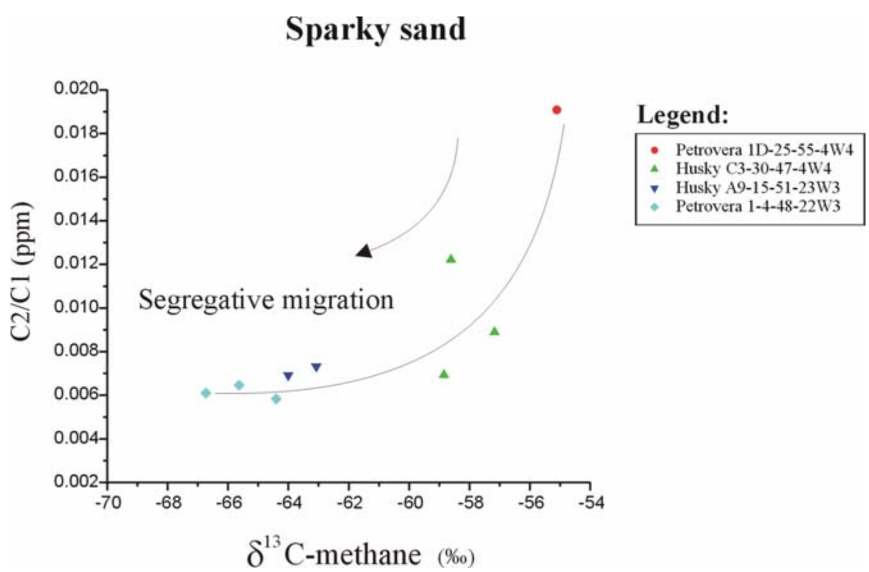

Figure 6-24 Gases from Sparky sandstone plotted on a C1-C2 diagram in linear scale, showing a trend of segregative migration.

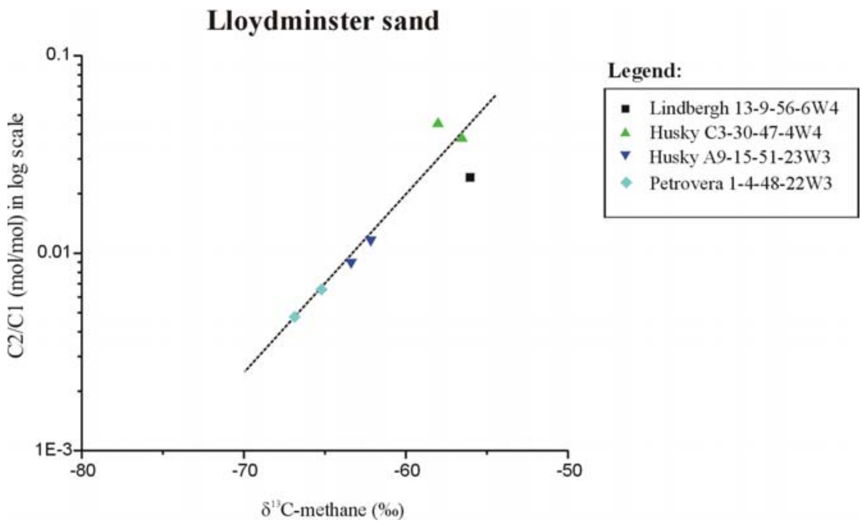

Figure 6-25 Gases from Lloydminster sandstone plotted on a C1-C2 diagram in logarithmic scale, showing a trend of segregative migration.

The inferred migration trend of the gas phase (at least for methane) through the carrier sandstone beds, as deduced from these segregative trends would be that presented in Figure 6-26.

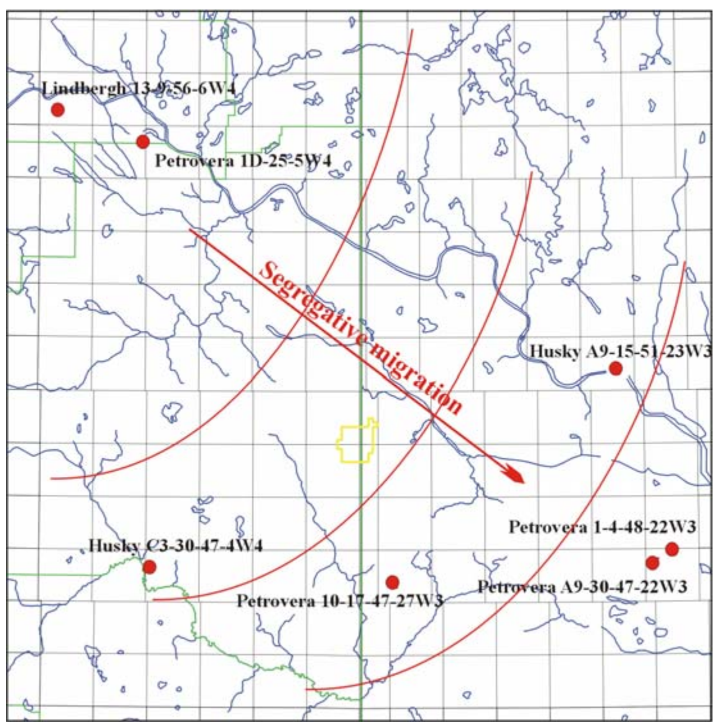

Figure 6-26 Inferred migration trend of the gas phase through the carrier sandstone beds of the Mannville Group, Lloydminster region.

6.4. Discussion

6.4.1. Foothills region

Results from the analyses of the regional hydrology (Parks and Tóth, 1995; Bachu and Underschultz, 1995; Bachu and Michael, 2003) show the following:

1) differences in water chemistry across the basin suggest there are distinct hydraulic flow regimes present;
2) variations in water chemistry play a significant role in hydrodynamics in the basin;
3) groundwater evolution in the basin is controlled by a complicated set of factors;
4) methane – generating bacteria are introduced by groundwater in recharge areas. The flux of fresh meteoric waters in the recharge areas enhances the potential for bacteriogenic methane generation.

The distribution of freshwater hydraulic heads in Scollard-Paskapoo aquifer (Bachu and Michael, 2003) suggests potential for fluid flow is from the west to the northeast. The higher salinity and low hydraulic heads in the Foothills study region indicate flow driven inward by erosional rebound in both Edmonton and Belly River aquifers.

The position of the Pembina mudlog profile very close to the location of the hydraulic divide between flow systems driven by topography (to the east) and by erosional rebound (to the west) (see Figure 6-2) may explain its carbon isotopic signatures. The vertical trends observed in a methane $\delta^{13}C$ versus ethane $\delta^{13}C$ plot (Figure 6-27) are interpreted as a strong evidence for mixing between thermogenic and microbial gas, because the methane is greatly affected, whereas the ethane is unaffected. This is consistent with the typical very low ethane concentrations in microbial gases.

Since Belly River and Bearpaw gases are the most affected by mixing with bacterial gas, the entire hydrostratigraphic system down to the Lea Park Formation may be in hydrodynamic equilibrium with the present topography. Water of meteoric origin recharges in this case all the aquifers, from Paskapoo-Scollard down to Belly River. The recharge areas could be either the Rocky Mountain deformation front to the west or the topographic highs at the Swan Hills to the north.

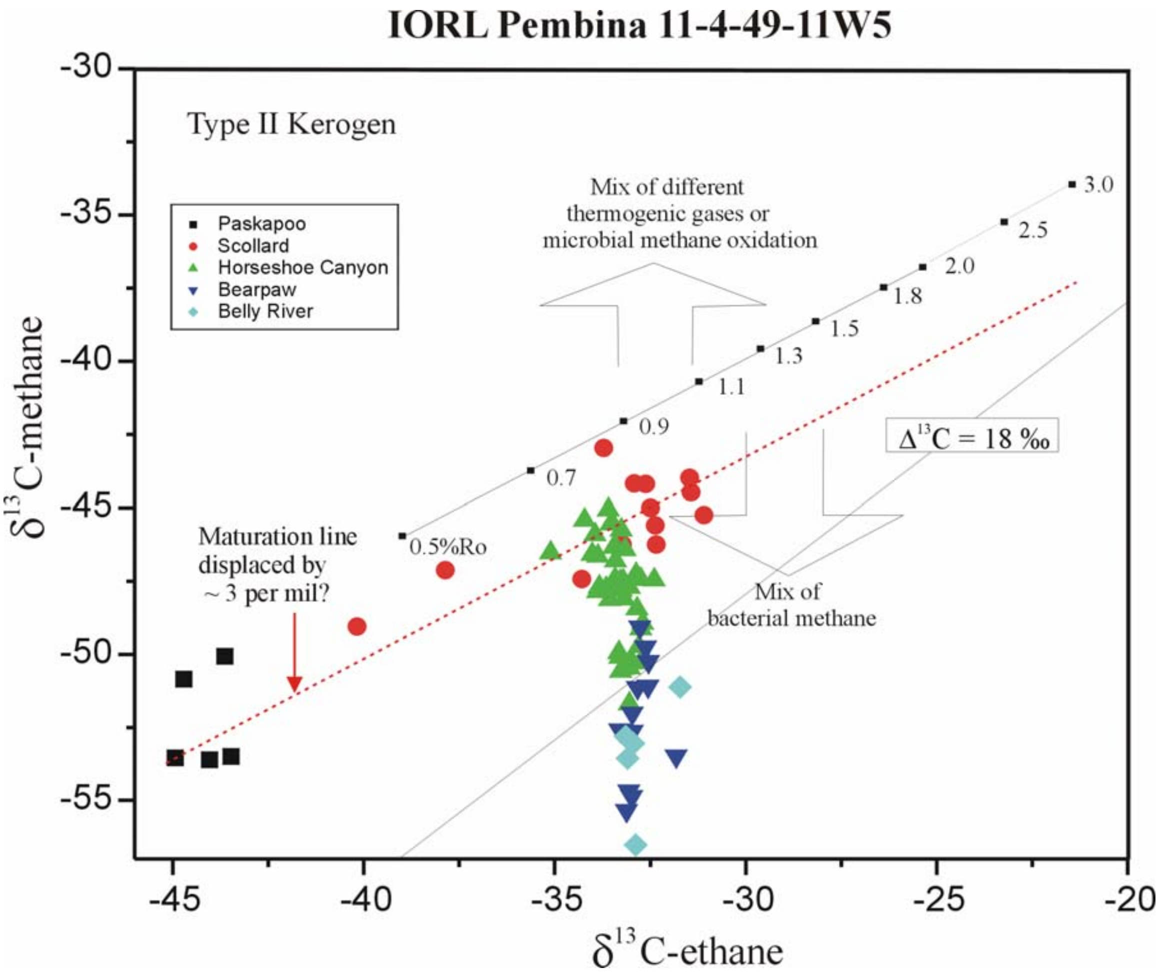

Figure 6-27 Stable carbon isotope ratios for co-genetic methane and ethane in a natural gas (After Faber, 1987; Whiticar, 1990.)

The ground water flow association with the gas composition in the Foothills region may be strictly related to the introduction of methane generating bacteria down to the Belly River aquifer. The ways in which flow systems and their directions influence gas migration pathways in this region seem to be more difficult to interpret.

An effective transport process involving fractionation through diffusion in formation waters may refer only at Scollard-Horseshoe Canyon gases. The inferred migration direction would be from west to east, from Ferrier to Gilby, as wetter and isotopically heavier methane, ethane and propane from Ferrier profile, would represent the residual gas left behind.

Another situation exhibiting a connection with the inward flow of formation waters in the Foothills study region refer to the Belly River Formation. As discussed above, the geochemical parameters indicate a slightly wetter gas at Gilby location. If we take into consideration the volume % C2+, the wetness index, and the C2/C1 ratio at both Gilby and Ferrier locations, the inferred migration direction would be from Gilby to Ferrier, since all these parameters decrease in this direction. However, this process is not supported by isotopic data. If the Belly River gas at Gilby location would be the source for the Belly River gas at Ferrier location, this gas would be heavier, whereas it is lighter (see Figure 6-7).

The interference in the Foothills study area of several highly opposing flow systems may give rise to a much more complicated flow pattern – not possible to be solved on the basis of the existing data alone. The correct interpretation of the data may be difficult to interpret at the present stage, with the available data.

Two more likely and simpler mechanisms to explain the observed isotopic and compositional data in the Foothills study area are: (1) that gas migrates through buoyancy and diffusion accompanied by compositional fractionation, eastward and away from the Rocky Mountain deformation front, and (2) a source maturity control.

In the first case, as described by Leythaeuser et al. (1980, 1984), such a process would tend to lead to a progressive enrichment in methane near the migration front. Although this process explains the compositional variations observed, it might not be supported by isotopic data, in concurrence with the experimental results observed by Fuex (1980), which states that no carbon isotopic shift would be anticipated. If we consider, however, the last decade experimental work, providing evidence for significant isotopic shifts in methane during migration, carbon isotope ratios of mudgases may be related to migration in this basin, with little effect from maturity levels and bacterial contamination.

In the second case, as already described in Chapter Four and above, the wetter gas composition at Ferrier location, as well as its heavier carbon isotopic composition could be due simply to increased thermal maturation at greater depth of burial than at Gilby location and thus might not involve gas migration over any substantial distance. The increased dryness at Gilby location, thus away from the deformation front, could be explained by bacterial contamination.

6.4.2. Lloydminster region

One explanation of the observed compositional and isotopic variations over the area may involve the groundwater flow. In this part of the Western Canada Sedimentary Basin, where the carrier beds and the entire Cretaceous succession is relatively flat bedded (see Appendices II-1 to II-8), the role of capillary forces, buoyancy, and relative permeability may have played a more significant role than previously envisaged (Adams et al., 2004), and the water flow systems must have strongly influenced hydrocarbon migration.

One can presume that water flowing through the basin continually took gases into solution until saturation was reached. Most probably, more than one gas generation process forced methane and probably ethane into solution of pore water into Cretaceous aquifers, both at a regional scale and at a more local scale, related to the local recharge areas.

Even during migration through a shale body, as the gas goes into solution with groundwater, the solution-dissolution process will fractionate the more soluble components (Neglia, 1979). As a result, the low-potential discharge zones will consist of almost pure methane.

The existence of a strong pressure gradient forced the water to flow and may also help in the continuous degassing of the water. The presence of a large difference in hydraulic pressure between the western part and the eastern part of the study area is supported by a potentiometric surface map of the Mannville Group in Saskatchewan (Christopher, 1980). This map shows a regional discharge in the area adjoining the Lloydminster region of Alberta, between latitudes 52 and 54. Christopher (1980) suggest that deep Mannville brines are moving upwards to the near surface in the North Saskatchewan River valley, where the bottom of the bedrock channel is lower than the hydraulic head values of the Mannville waters.

After a long-distance lateral migration, the gas dissolved in water may be released due to pressure drop in the eastern part of the area.

The higher abundance of total hydrocarbons at the Golden Lakes location can result from either generation of methanogenic gas (either bacteriogenic or early thermogenic) in excess of the solubility or exsolution of gas brought about by a reduction in hydrostatic pressure.

Exsolution by reduction of hydrostatic pressure seems to be a more plausible possibility, as both uplift and erosion and upward migration of gas-bearing waters to zones of lower hydrostatic pressure can claim as being the reason for it. Nevertheless, taking into account some of the gas signatures within the Colorado shales in this area, one can observe that they fit the calculated curves on James diagram extremely well (Petrovera A9-30-47-22W3). These gases appear to be potential thermogenic gas sources, as demonstrated as well by their linear slopes on "natural gas plots" (see Chapter Four).

A possibility to explain the progressive increase in gas dryness toward the eastern limit of the Lloydminster study area is that thermogenic gas generated deeper and in the western part of the area (e.g. Husky 3C-30-47-4W4, Cummings shales) is mixing with a bacterial and/or early thermogenic gas end member reservoired to the east.

This could be the case of the Golden Lakes field (southeastern part of the heavy oil study area), where the total gas abundance recovered at Petrovera 1-4-48-22W3 usually exceed 150,000 ppm, and can reach even 260,000 ppm (within the Second White Specks Formation). Therefore, another possibility to explain some of the complexity of the Lloydminster Mannville gases is a direct result of in place biogenic destruction of the 'sweet oil', loss of ethane, propane, butane and simultaneous generation of methane. The process may still be going on and the variations we see may reflect the degree or extent of alteration. Therefore, from a static point of view, the current geochemical and hydrogeological data in the Lloydminster region indicate a variable degree of gas alteration, and generation, but there is also evidence to indicate the potential for long distance gas migration to the northeastern outcrop edge of the Alberta basin.

In conclusion, two more likely mechanisms to explain the distribution of chemical proportion and carbon isotopic ratios for mudgases sampled from the Lloydminster region involves: (1) the regional and local groundwater flow [significant to note here that the downward flowing of the groundwater may obstruct the rise of the upward-moving hydrocarbon gases or can cause these gases to shift laterally from the recharge zones - as suggested by Holysh and Tóth (1995)], and/or (2) an in-situ gas generation and biodegradation.

CHAPTER SEVEN

THE SCV SOURCE DETECTION

7.1. Introduction

Isotopic fingerprints of mud-gases can be used to determine both the gas generation mechanism and their alteration and migration. By comparing them with the isotopic ratios of gas components from soil and surface gases, in the same field, it is possible to provide an accurate estimate of the source depth of the migrating gases. This ability to determine the source depths of shallow gases is particularly useful for the remediation of leaking heavy-oil wells in the Western Canadian Sedimentary basin (Rowe and Muehlenbachs, 1999).

7.2. Surface gas migration and the application of carbon isotopic mud logs for remediation leaking wells.

A significant number of conventional wells in Northeastern Alberta and Saskatchewan (Lloydminster area) are affected by gas migration (Erno and Schmitz, 1994, Rowe, 1998). These gases migrate vertically from depth along the wellbores, and are primarily manifested as surface casing vent (SCV) flows (gas rising inside the surface casing), and/or soil gas bubbles around the wellbores. The SCV gases functions as a bleed-off valve, allowing built-up gases to vent directly into atmosphere. The SVC flow rates range from 0.01m^3/day to 200 m^3/day (Schmitz et al., 1993; Erno and Schmitz, 1994). Although gas migration through soils tend to occur at much lower rates (0.01 m3/day) than SCV flows. Soil gases can often be observed bubbling through ponded water around wellbores. The gas migrating through soil frequently kills or stuns vegetation growth within a radius of several meters surrounding the well (Rich, 1995). These gas flows constitute both a regulatory and an environmental concern, representing:

- risk to ground water;
- fire or explosion hazard;
- environmental damage;
- source of odor;
- waste of the resource.

The "mud-gas" isotopic depth profile (or isotopic fingerprint) can be used to estimate the source of a leaking gas. Isotope ratios of migrating gases from a leaking well are compared to the isotopic fingerprint for that well. By matching the isotopic separation of the C_1 to C_4 components with the fingerprint, the source depth of the leaking gases can be determined with a fair degree of confidence. The use of isotopic fingerprints to determine gas-source depths in the Lloydminster area had greatly reduced well-remediation costs (Rowe and Muehlenbachs, 1999): rather than re-cementing the wells at the nominal producing depths, remediation efforts were done at depths indicated through isotopic fingerprinting.

7.2.1. The SCV source detection in the Foothills area

Ninety (90) surface casing vent samples were made available from the University of Alberta data base in the Foothills study area, and investigated for gas sources, based on comparison to mud logs at:

1. Pembina 00/11-04-049-11W5-0,
2. Ferrier 00/14-03-042-09W5-0, and
3. Gilby 00/15-16-042-04W5-0.

Each SCV data set has been superimposed on the isotopic profile of the formations penetrated from that field. The best fit of each data set was found by sliding the data vertically until the isotope ratios of the C_{2+} components best matched the underlying isotopic fingerprint. This allowed the presumable source(s) to be estimated from the vertical axis. As can be observed in Figure 7-1 and Figure 7-3 Ferrier Field, Alberta), the SCV gases likely come from the Paskapoo Formation, from various depths. The majority of the SCV gases (4 out of 14 samples) around the Gilby profile appear to come as well from the Paskapoo Formation (Figure 7-5) For the Pembina field, only two SCV datasets matched the isotopic fingerprint, indicating the upper part of the Scollard Formation as a leaking source, related probably to the Nevis coal zone (Figure 7-7).Other presumable sources (see Figures 7-10 to 7-12) for the leaking gases can be determined being roughly:

- Belly River and Horseshoe Canyon formations (Ferrier field) (Figure 7-1);
- Pekisko Fm., Nordegg Fm., Rock Creek Fm., Mannville Gp., Westgate Fm., Lea Park Fm., and Belly River Fm. (Gilby field).

Interesting to note is the fact that one SCV gas matched both Ferrier and Gilby profiles in the same presumable source formation: Belly River Formation (6-20-42-6W5 SCV gas). On the other hand, 8-24-42-7W5 SCV gas indicates either Horseshoe Canyon Fm. (Ferrier) or Nordegg Fm. (Gilby). Compared with Horseshoe Canyon gases in the Gilby profile, the SCV gas at 8-24-42-7W5 seems to be more mature – raising the following questions:

- how far apart from an isotopic mudlog profile can the fingerprinting really work?
- is this an indication that a more mature Horseshoe Canyon formation gas has been migrated eastward, from Ferrier to Gilby? The gas illustrates the linear trend, which is indicative of a thermogenic, single sourced gas from kerogen Type III (Figure 7-9). The most likely cause of its low methane δ^{13}C value is an influx of biogenic methane mixed with the thermogenic gas. On the other hand, the remarkably heavy ethane and propane δ^{13}C-values (-32.32 and –29.12‰, respectively) may indicate a gas prone OM source.

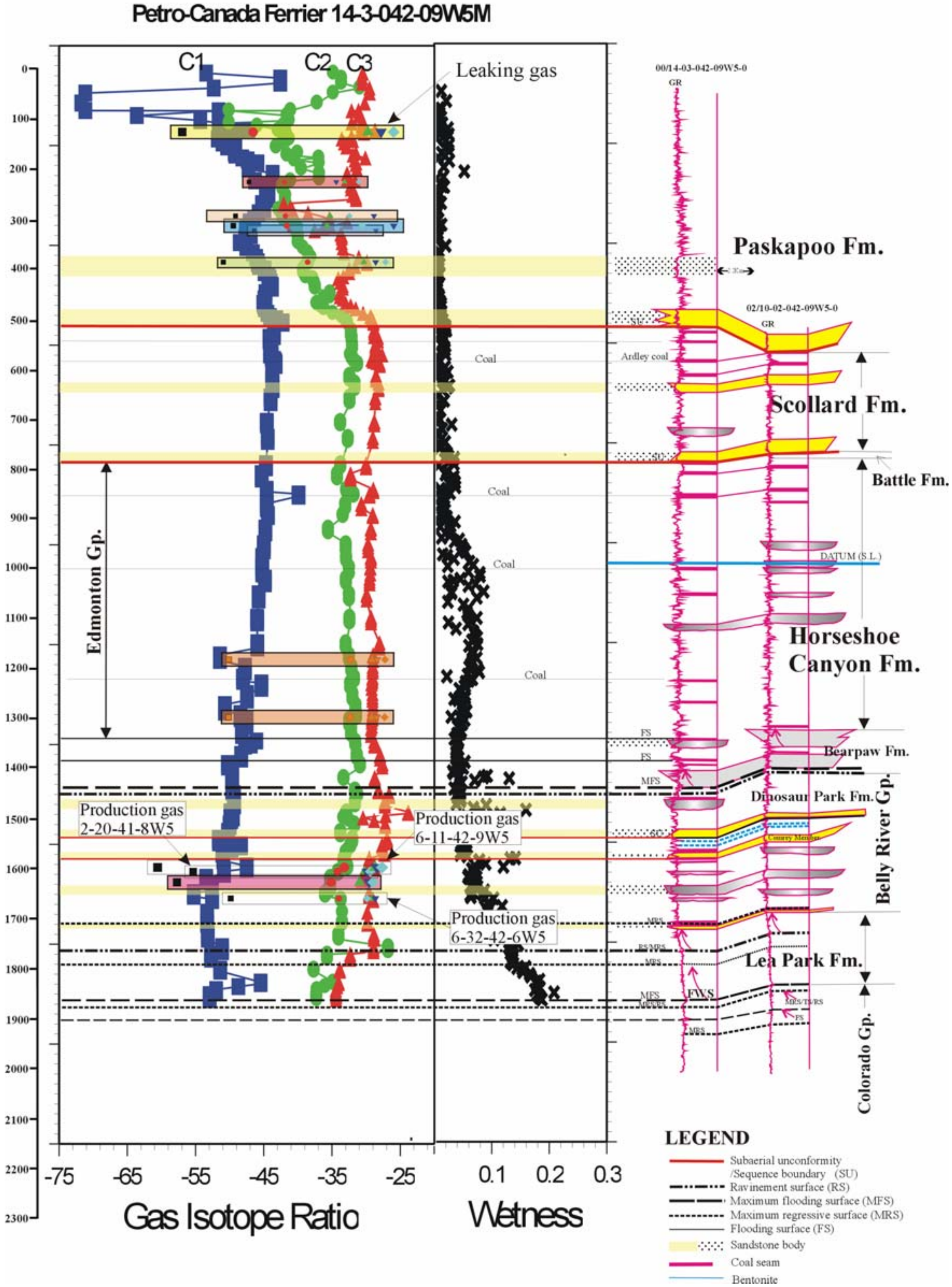

Figure 7-1 Isotope ratios of eight SCV gases superimposed on the mudgas isotopic depth profile from Petro-Canada Ferrier 14-03-042-9W5. Legend for SCV gases is provided in Figure 7-2.

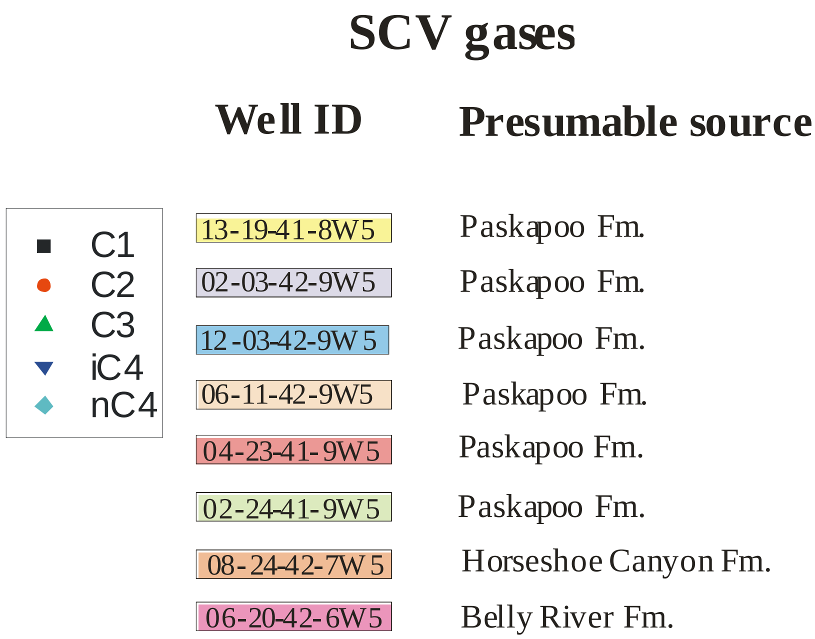

Figure 7-2 SCV gases from Figure 7-1 and their presumable sources. Petro-Canada Ferrier 14-03-042-9W5.

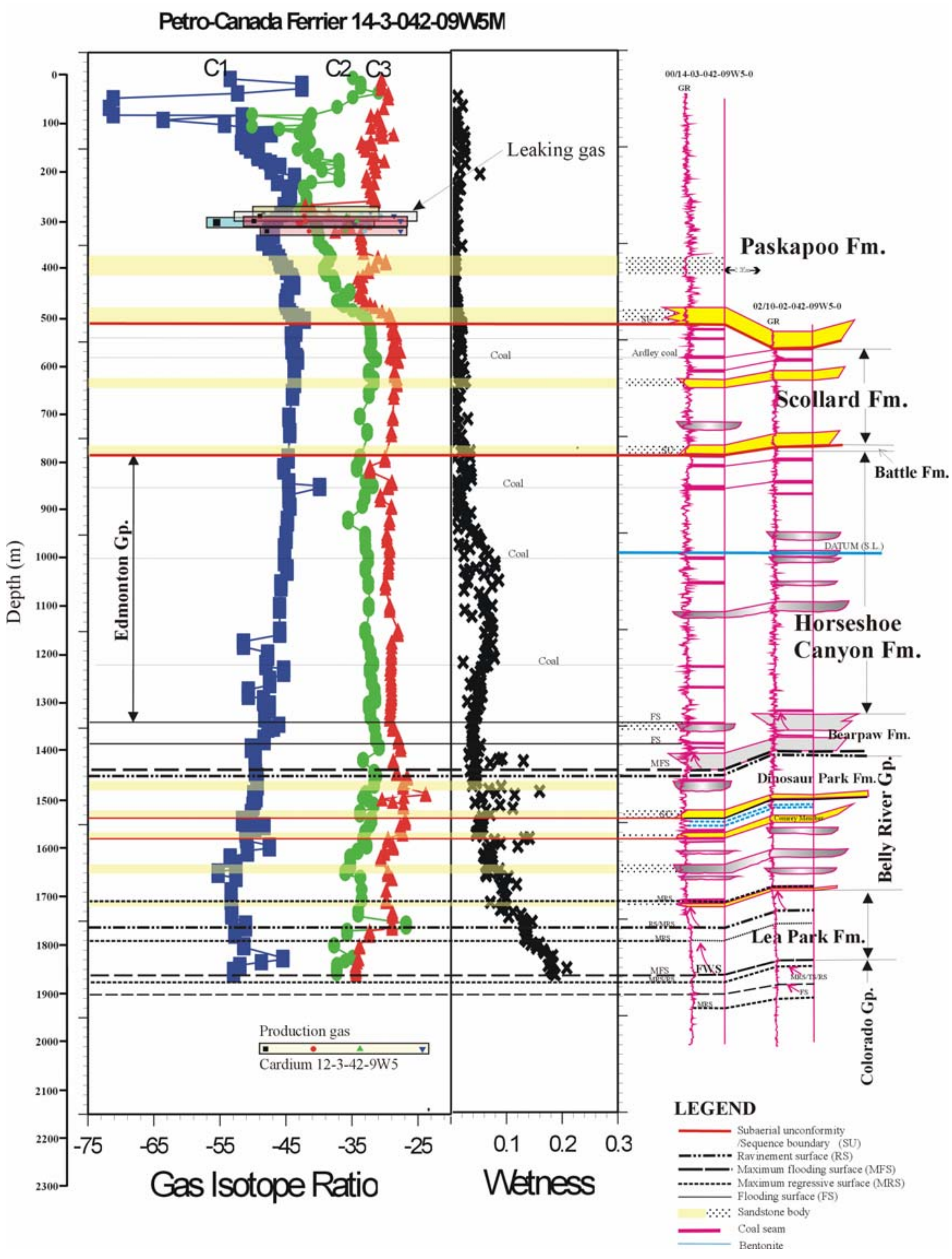

Figure 7-3 Isotope ratios of five SCV gases superimposed on the mudgas isotopic depth profile from Petro-Canada Ferrier 14-03-042-9W5. Legend for SCV gases is provided in Figure 7-4.

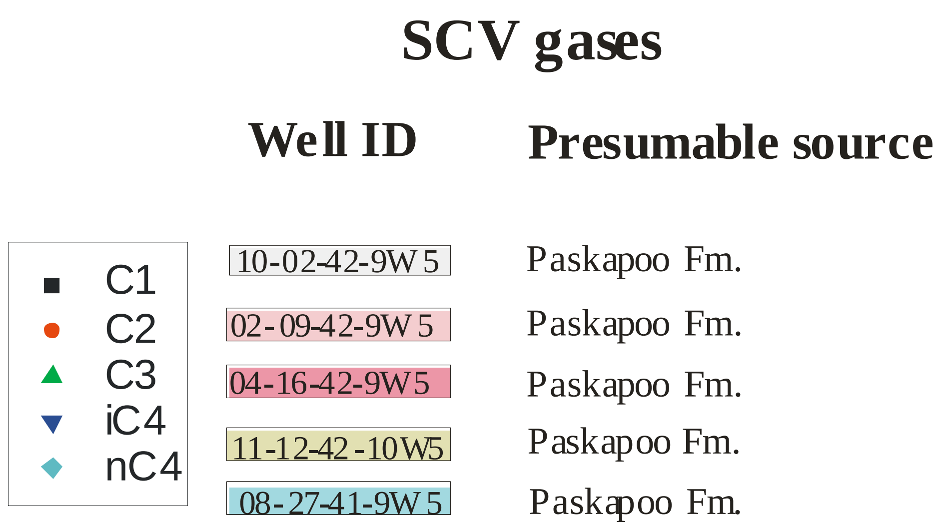

Figure 7-4 SCV gases from Figure 7-3 and their presumable sources. Petro-Canada Ferrier 14-03-042-9W5.

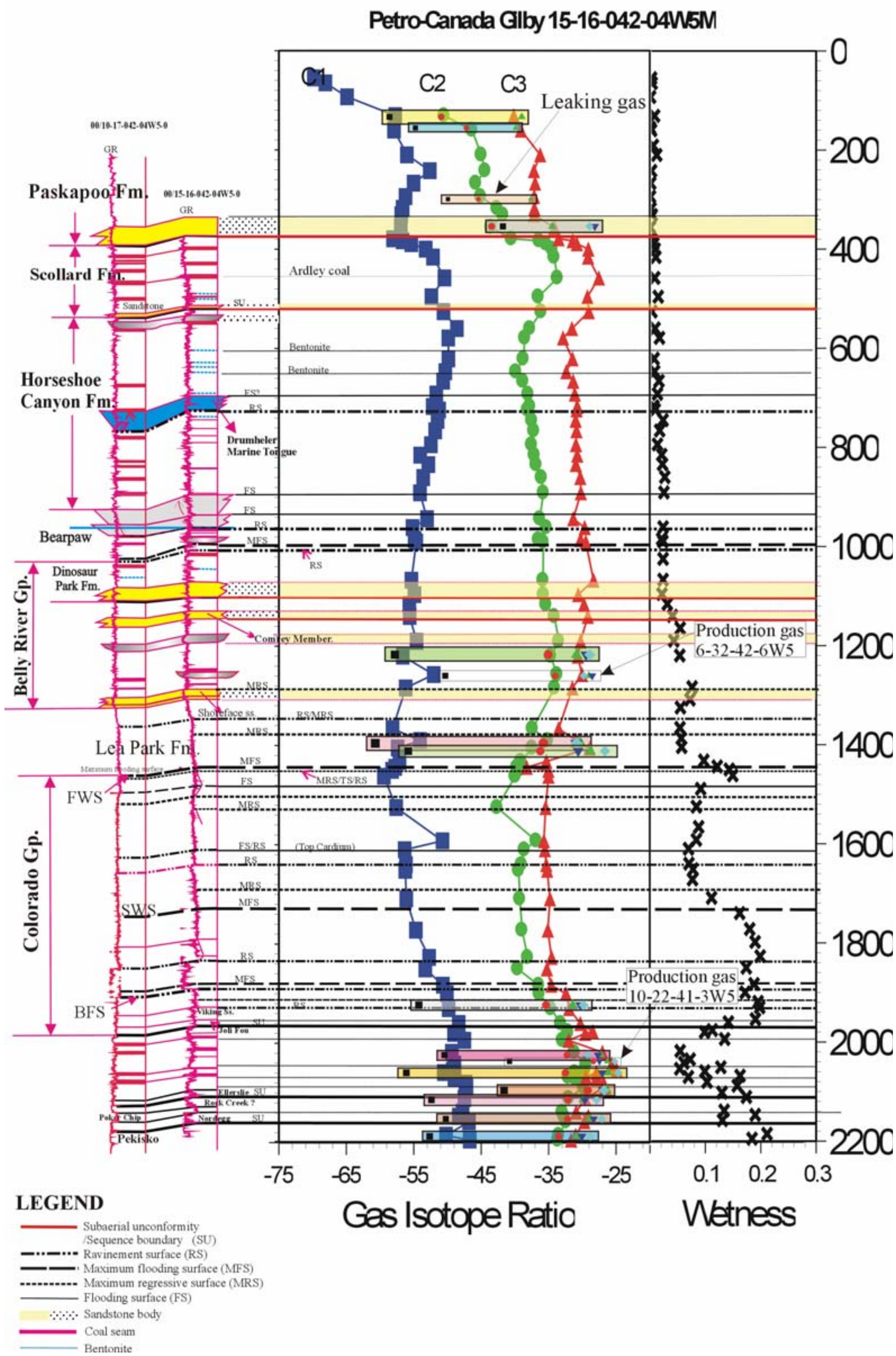

Figure 7-5 Isotope ratios of thirteen SCV gases superimposed on the mudgas isotopic depth profile from PC Gilby 15-16-42-04W5. Legend for SCV gases is provided in Figure 7-6.

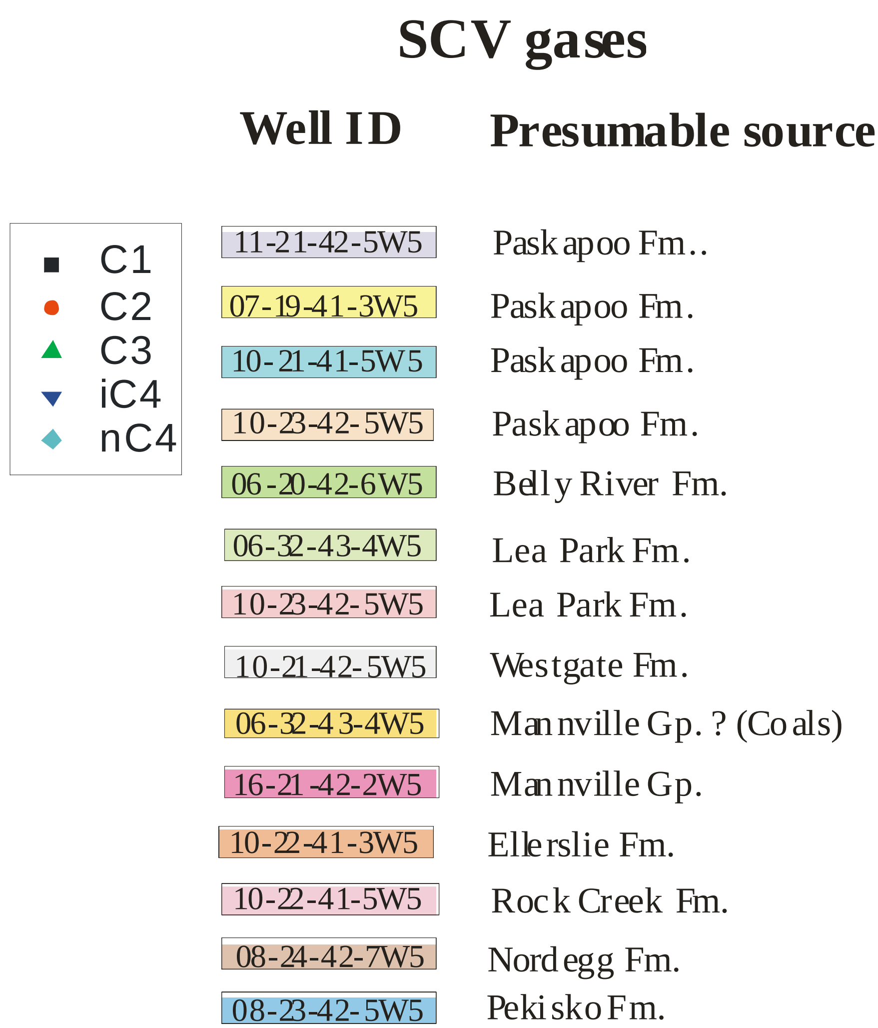

Figure 7-6 SCV gases from Figure 7-5 and their presumable sources. PC Gilby 15-16-42-04W5.

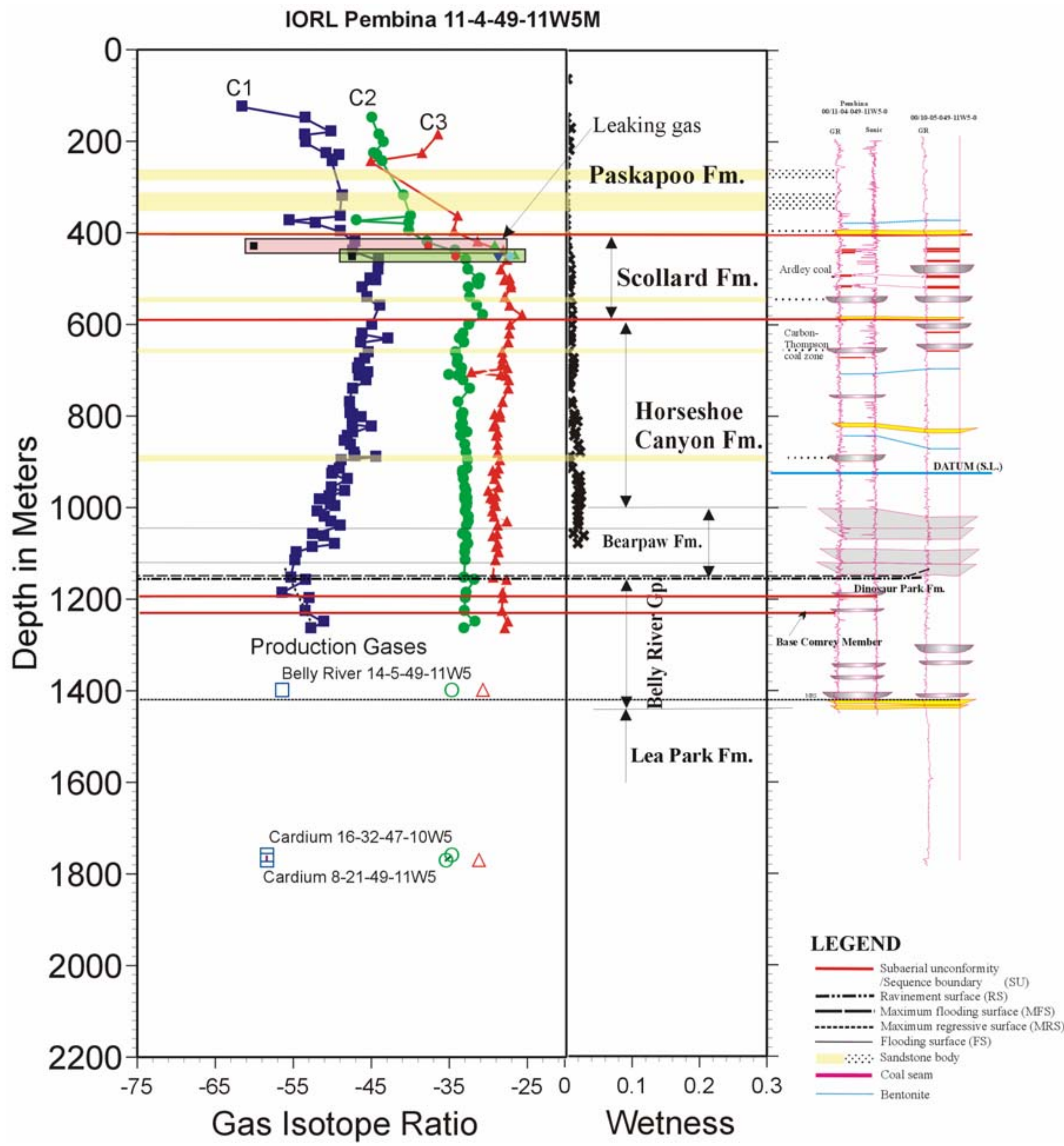

Figure 7-7 Isotope ratios of two SCV gases superimposed on the mudgas isotopic depth profile from IORL Pembina 11-04-049-11W5. Legend for SCV gases is provided in Figure 7-8.

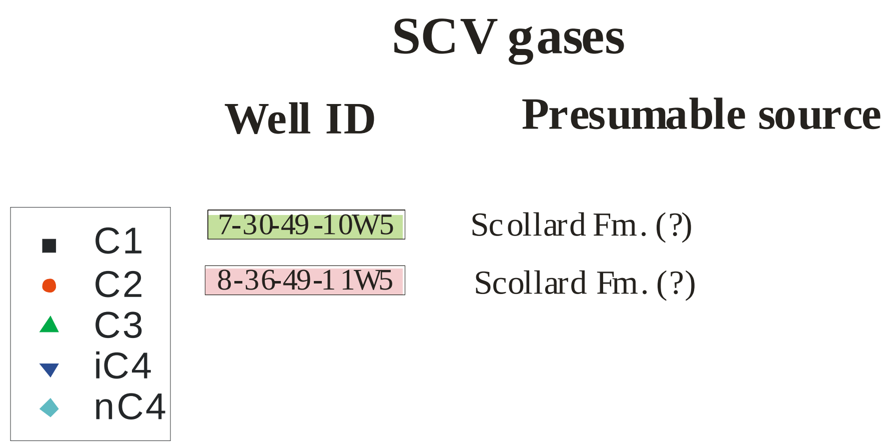

Figure 7-8 SCV gases from Figure 7-7 and their presumable sources. IORL Pembina 11-04-049-11W5.

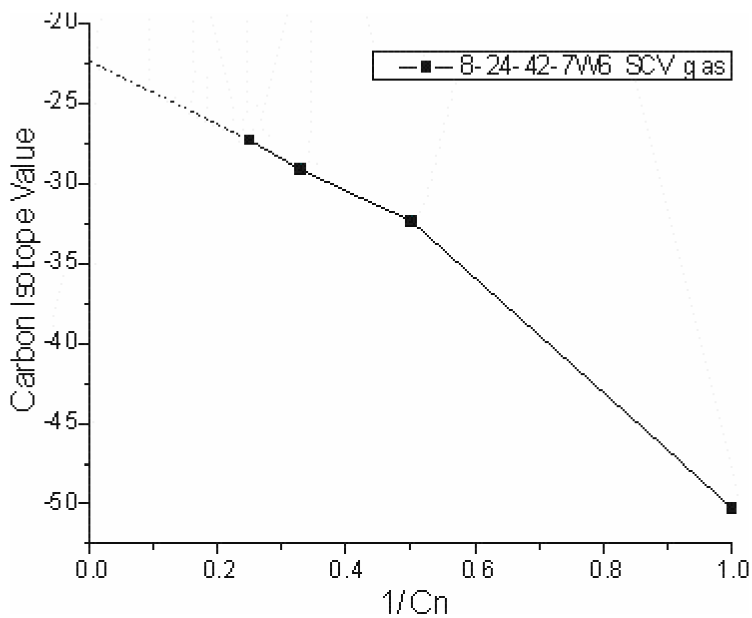

Figure 7-9 Chung diagram for 8-24-42-7W5 SCV gas in the Ferrier- Gilby area.

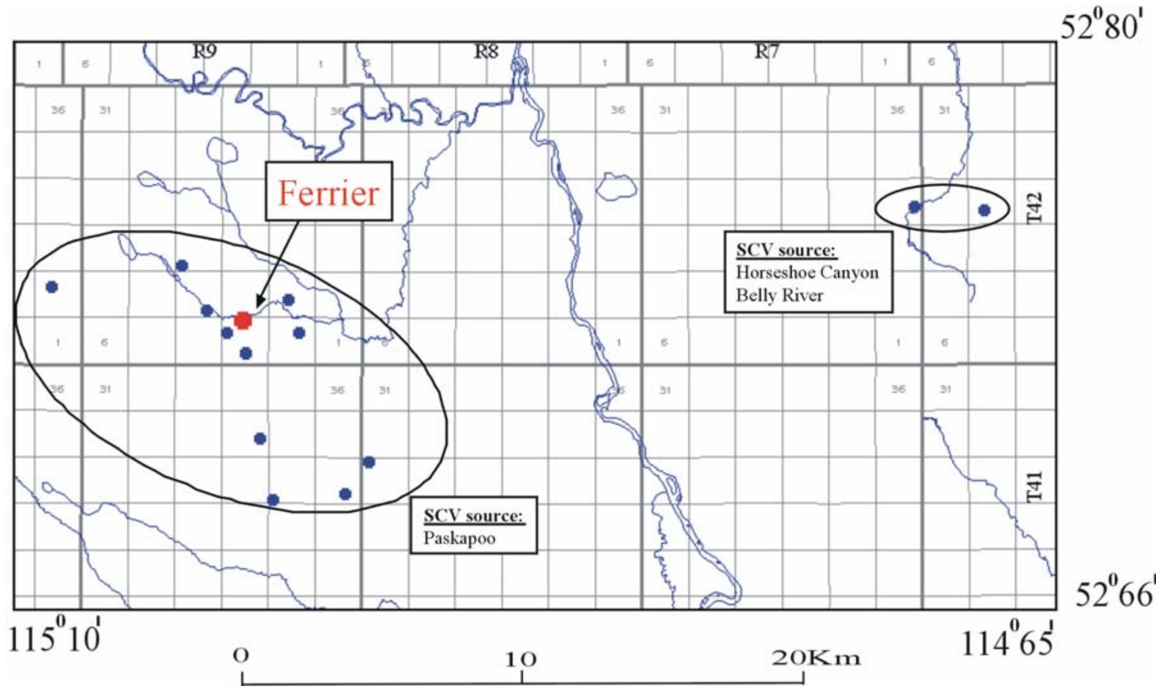

Figure 7-10 Location of wells affected by gas migration (blue dots), which best matched the Ferrier mudlog. Presumable SCV sources are indicated.

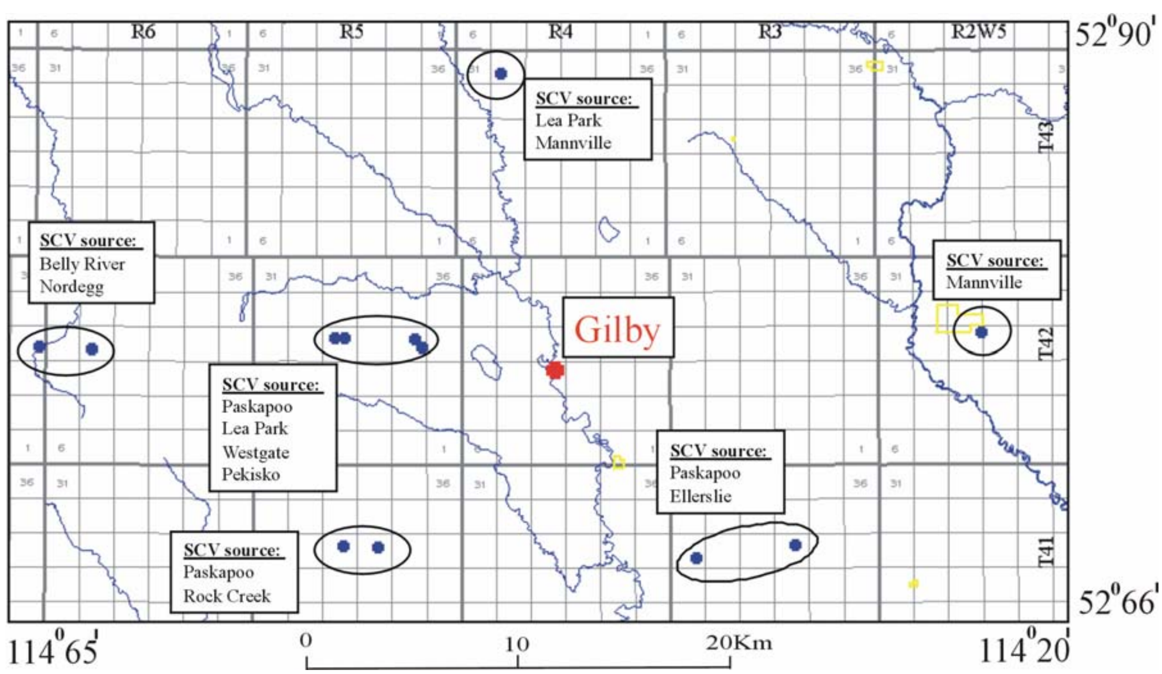

Figure 7-11 Location of wells affected by gas migration (blue dots), which best matched the Gilby mudlog. Presumable SCV sources are indicated.

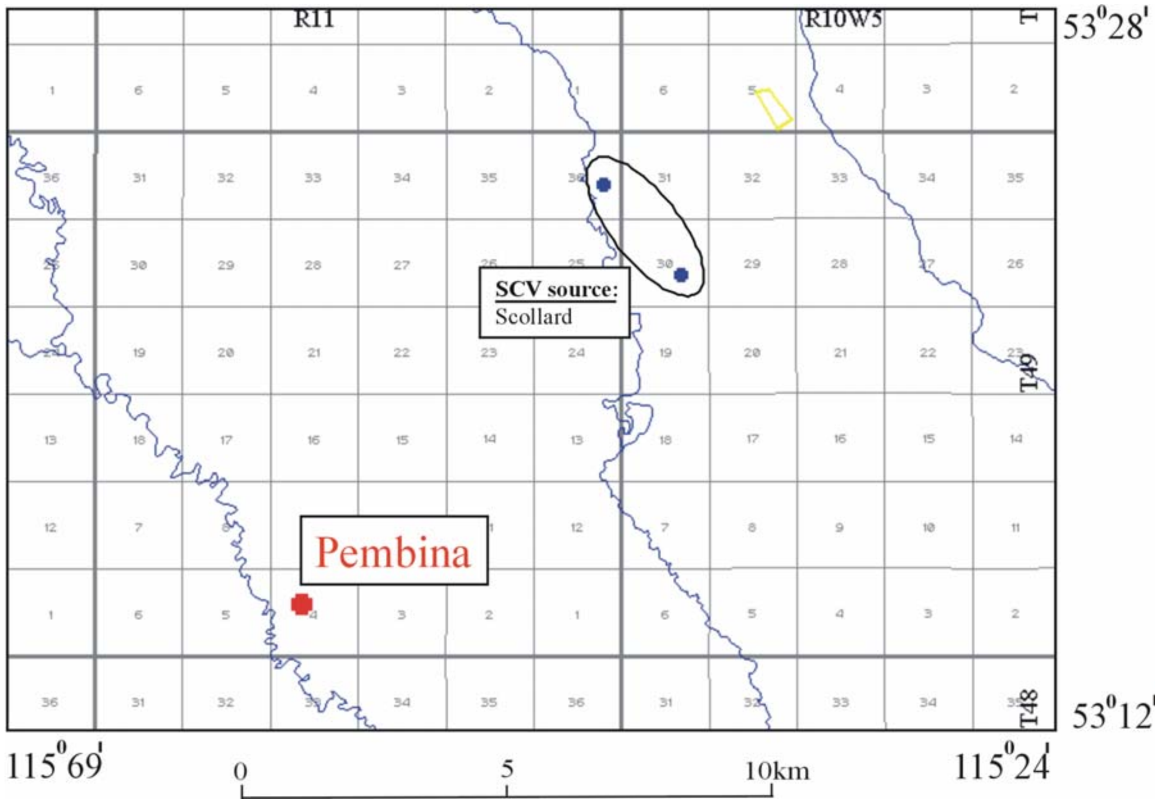

Figure 7-12 Location of wells affected by gas migration (blue dots), which best matched the Pembina mudlog. Presumable SCV source is indicated.

7.2.2. The SCV source detection in the Lloydminster area

Six hundred twenty three (623) surface casing vent (SCV) samples were made available from the University of Alberta data base in the Lloydminster study area, and investigated for gas sources, based on comparison to mud logs at:

1. Petrovera 00/01-25-055-05W4-0
2. Husky C0/03-30-047-04W4-0
3. Husky 11/09-15-051-23W3-0
4. Lindbergh 00/13-09-056-06W4-0
5. Petrovera 11/10-17-047-27W3-1
6. Petrovera 1A1-04-048-22W3-0
7. Petrovera 11/09-30-047-22W3-1

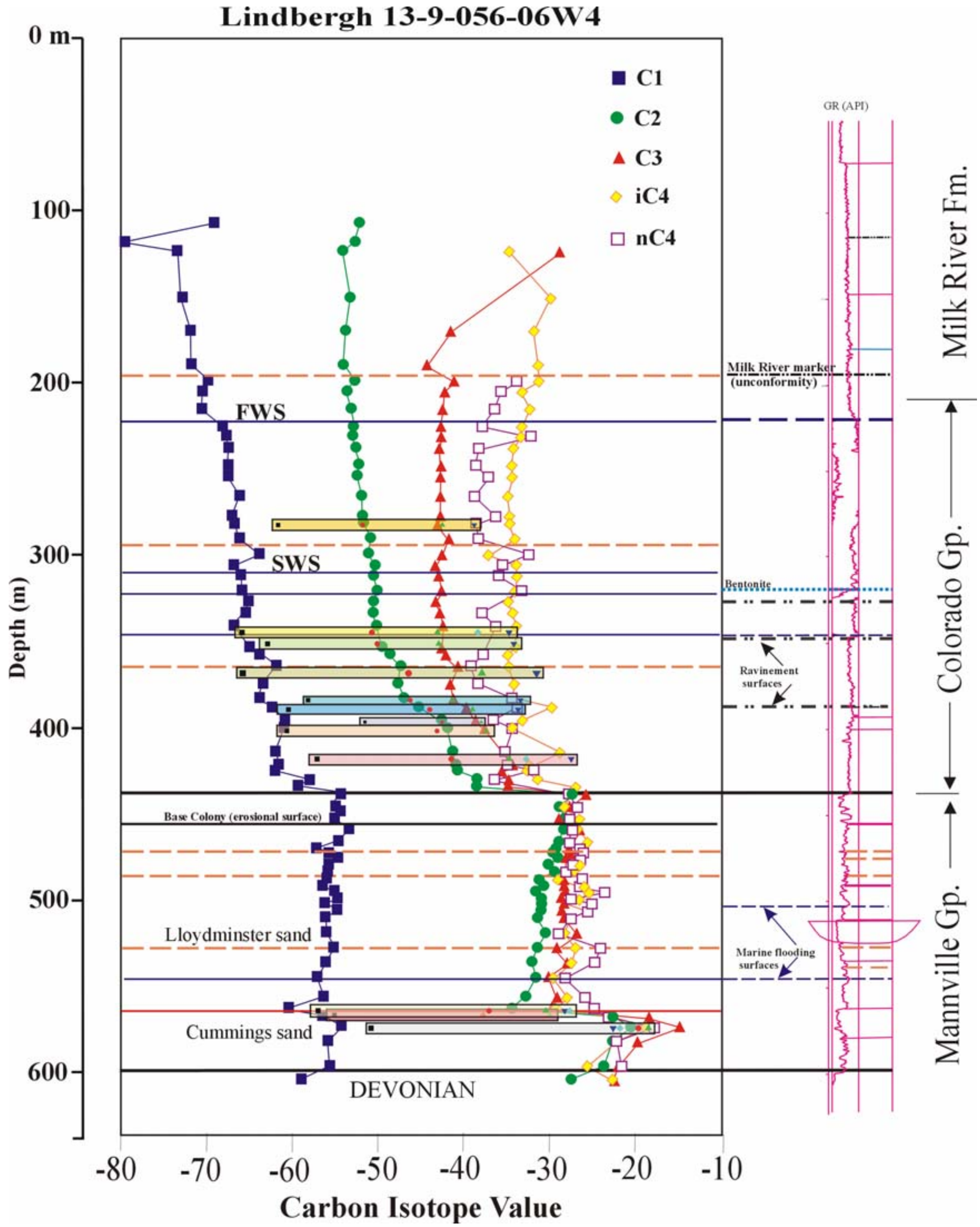

Figure 7-13 Isotope ratios of twelve SCV gases superimposed on the mudgas isotopic depth profile from Lindbergh 13-9-056-06W4. Legend for SCV gases is provided in Figure 7-14.

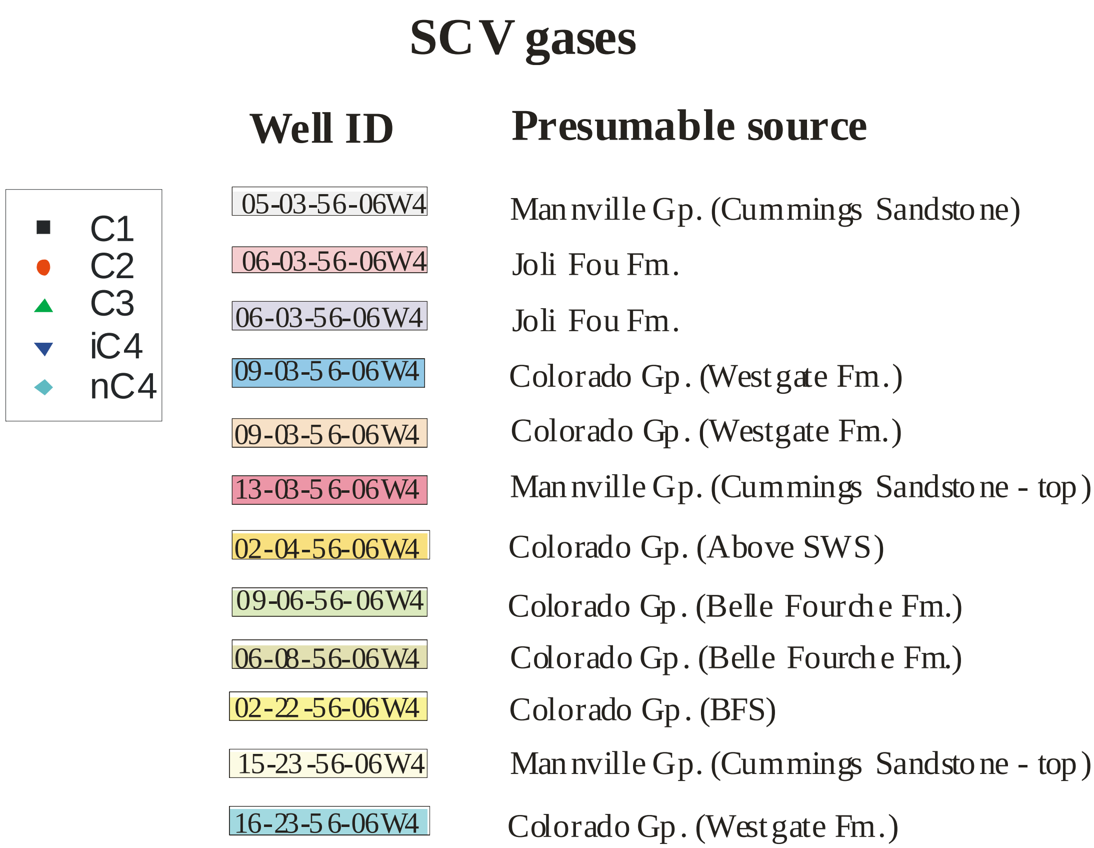

Figure 7-14 SCV gases from Figure 7-13 and their presumable sources.
Lindbergh 13-09-056-06W4.

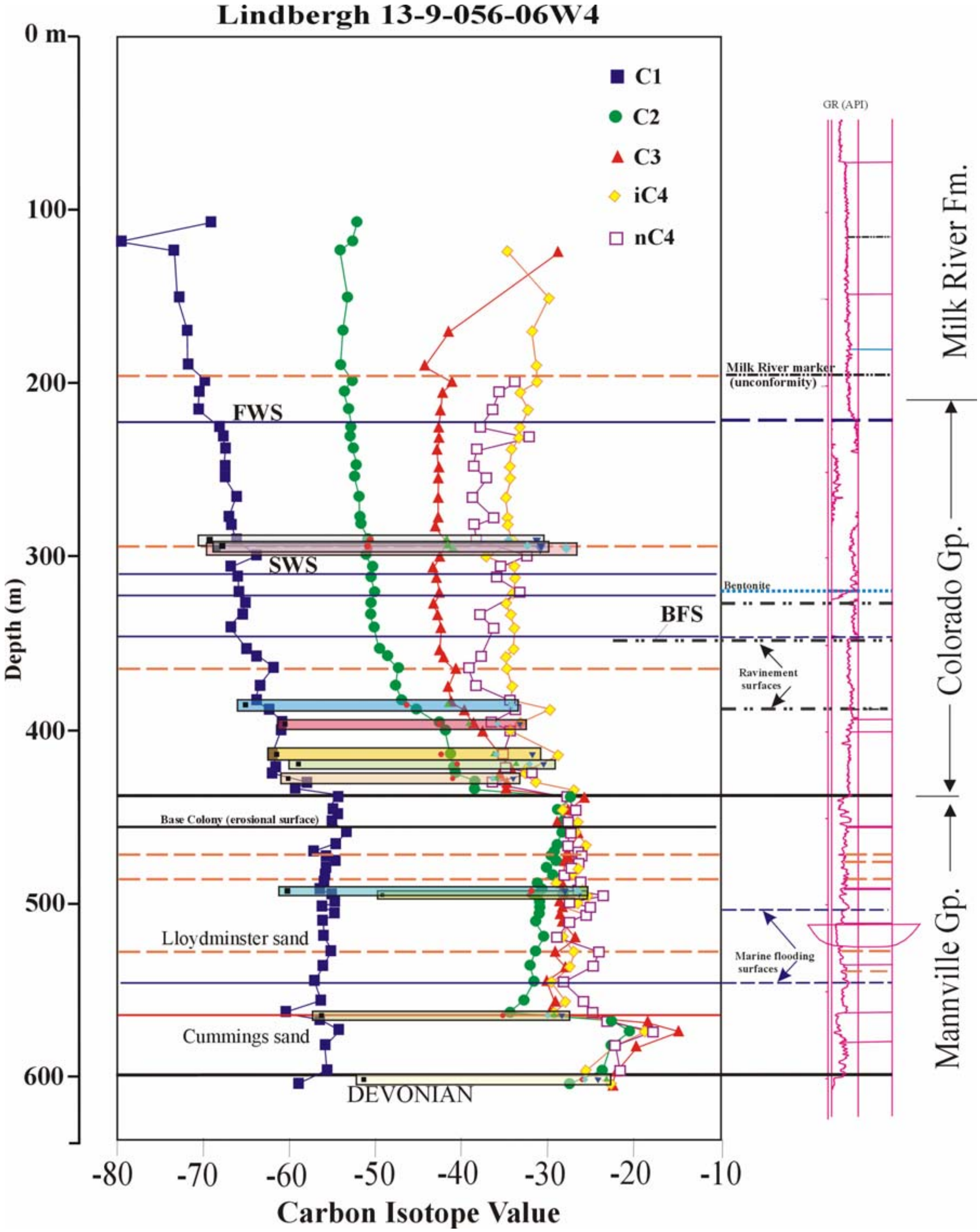

Figure 7-15 Isotope ratios of twelve SCV gases superimposed on the mudgas isotopic depth profile from Lindbergh 13-09-056-06W4. Legend for SCV gases is provided in Figure 7-16.

SCV gases

■ C1
● C2
▲ C3
▼ iC4
◆ nC4

Well ID	Presumable source
13-15-57-07W4	Colorado Gp. (Above SWS)
13-15-57-07W4	Colorado Gp. (Above SWS)
13-15-57-07W4	Colorado Gp. (Above SWS)
13-20-57-06W4	Colorado Gp. (Westgate Fm.)
13-20-57-06W4	Joli Fou Fm.
14-20-57-06W4	Colorado Gp. (Viking Fm.)
06-25-57-06W4	Joli Fou Fm.
06-25-57-06W4	Joli Fou Fm.
06-25-57-06W4	Mannville Gp. (Cummings Sandstone - top)
06-25-57-06W4	Mannville Gp. (Sparky Fm.)
02-29-57-06W4	Devonian ?
16-34-57-07W4	Mannville Gp. (Sparky Fm.)

Figure 7-16 SCV gases from Figure 7-15 and their presumable sources. Lindbergh 13-09-056-06W4.

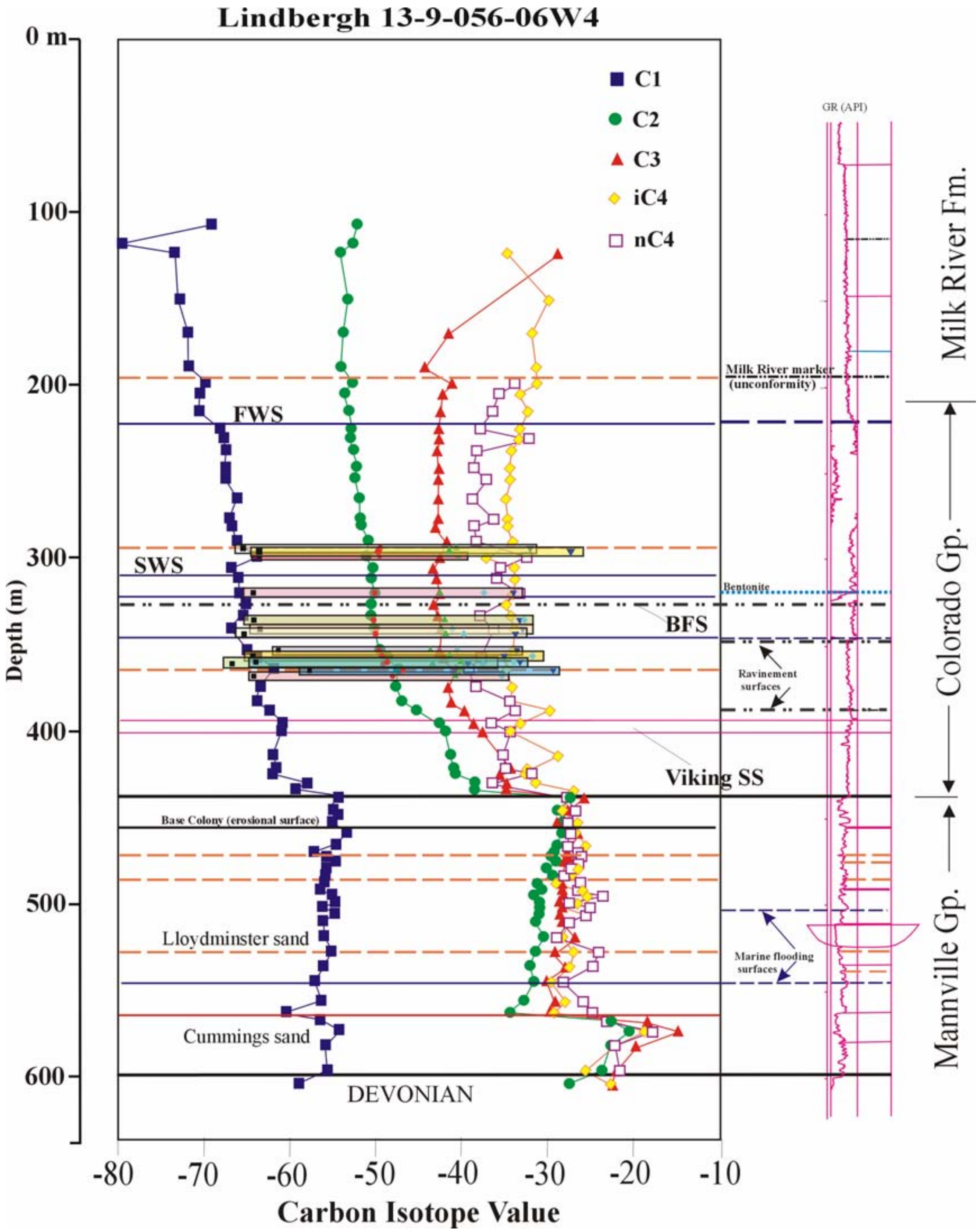

Figure 7-17 Isotope ratios of ten (10) SCV gases superimposed on the mudgas isotopic depth profile from Lindbergh 13-9-056-06W4. Legend for SCV gases is provided in Figure 7-18, and a close-up view in Figure 7-19.

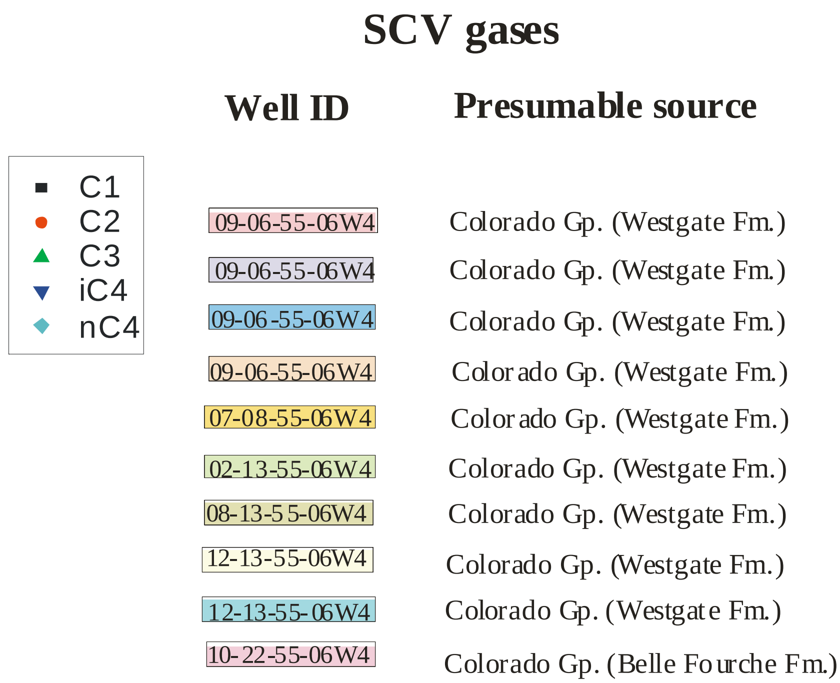

Figure 7-18 SCV gases from Figure 7-17 and their presumable sources. Lindbergh 13-09-056-06W4.

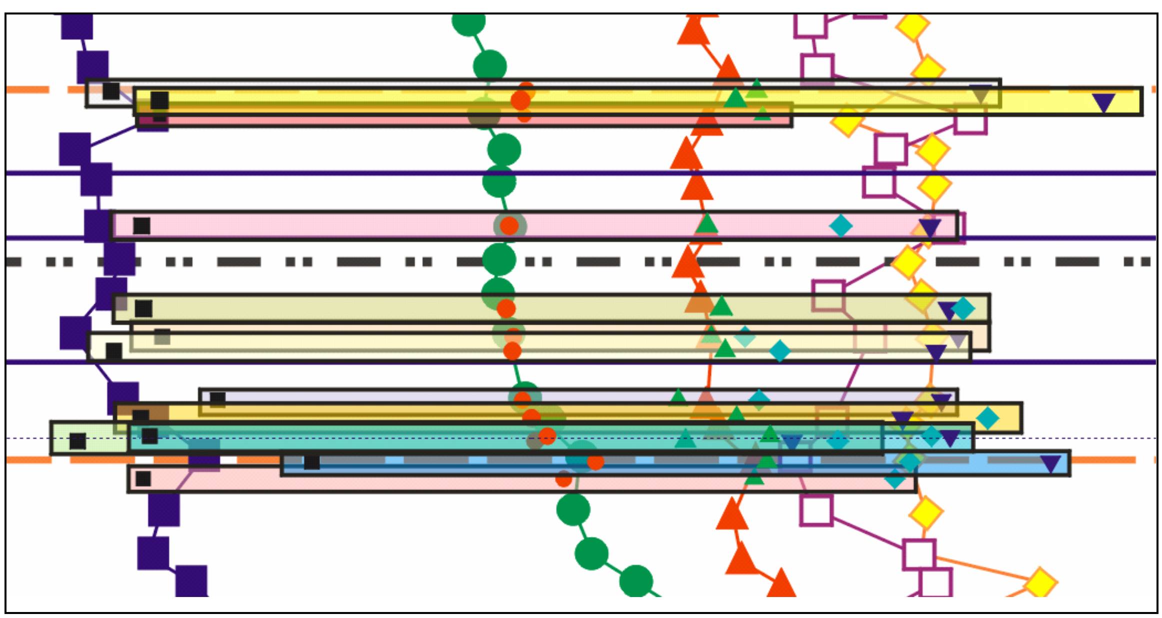

Figure 7-19 Close-up view of SCV gases from Figure 7-17. Lindbergh 13-09-056-06W4.

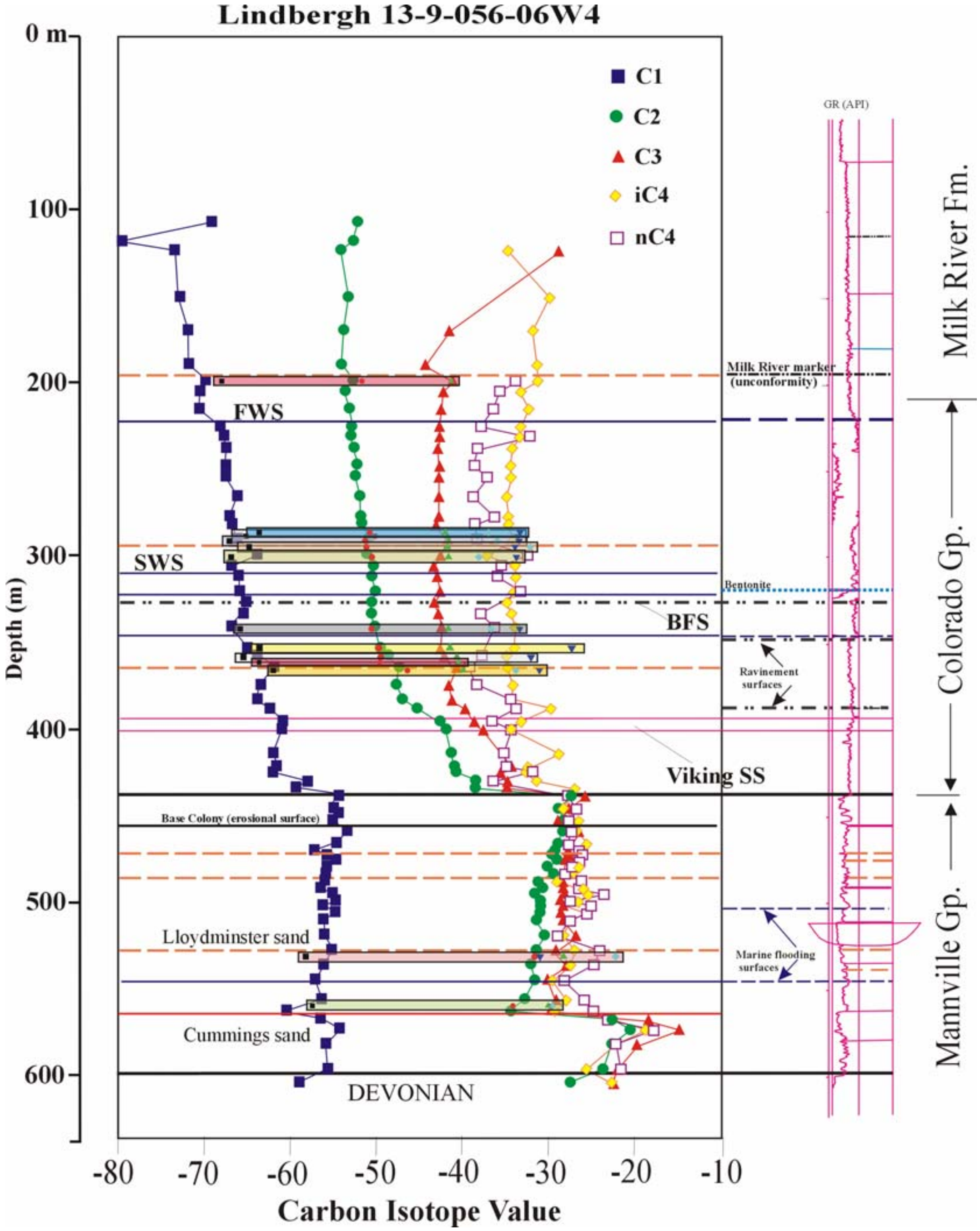

Figure 7-20 Isotope ratios of thirteen SCV gases superimposed on the mudgas isotopic depth profile from Lindbergh 13-9-056-06W4. Legend for SCV gases is provided in Figure 7-21.

SCV gases

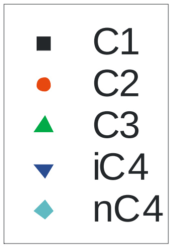

Well ID	Presumable source
11-22-55-06W4	Colorado Gp. (Belle Fourche Fm.)
01-23-55-06W4	Mannville Gp. (Lloydminster Fm.)
14-23-55-06W4	Colorado Gp. (Above SWS)
14-23-55-06W4	Colorado Gp. (Above SWS)
14-23-55-06W4	Colorado Gp. (Above SWS)
01-27-55-06W4	Milk River Fm.
11-28-55-06W4	Colorado Gp. (Westgate Fm.)
08-35-55-07W4	Mannville Gp. (Cummings Fm.)
13-36-55-07W4	Colorado Gp. (Above SWS)
13-36-55-07W4	Colorado Gp. (Westgate Fm.)
02-04-55-06W4	Colorado Gp. (Westgate Fm.)
09-06-55-06W4	Colorado Gp. (Westgate Fm.)
08-13-55-06W4	Colorado Gp. (Westgate Fm.)

Figure 7-21 SCV gases from Figure 7-19 and their presumable sources. Lindbergh 13-9-056-06W4.

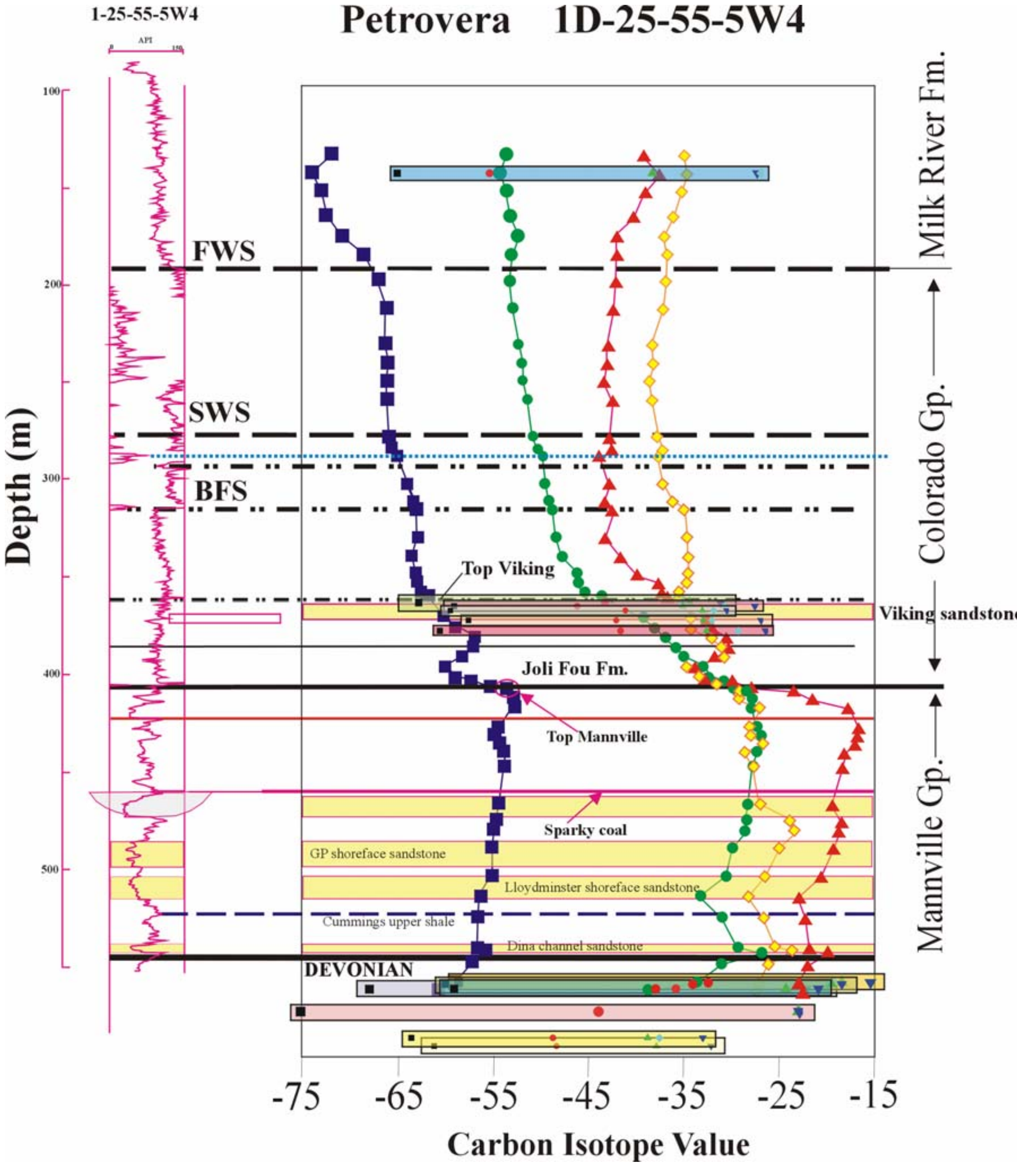

Figure 7-22 Isotope ratios of thirteen SCV gases superimposed on the mudgas isotopic depth profile from Petrovera 1D-25-55-5W4. Legend for SCV gases is provided in Figure 7-23, and a close-up view of the SCV gases presumably related to the Viking Fm. in Figure 7-24.

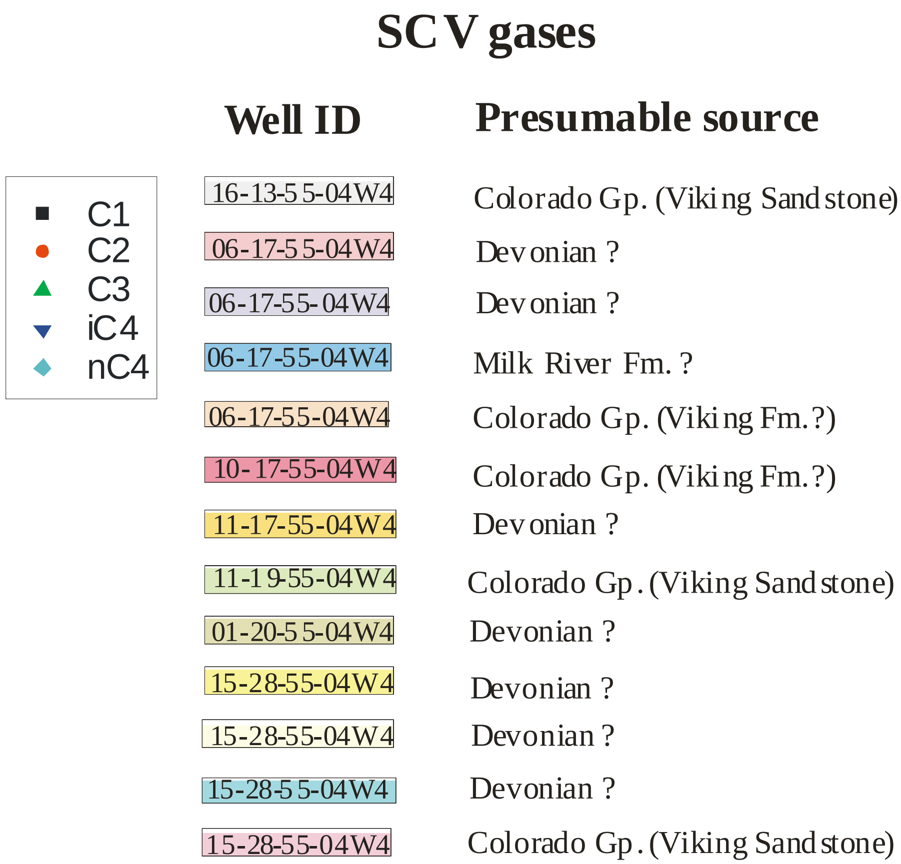

Figure 7-23 SCV gases from Figure 7-22 and their presumable sources.
Petrovera 1D-25-55-5W4.

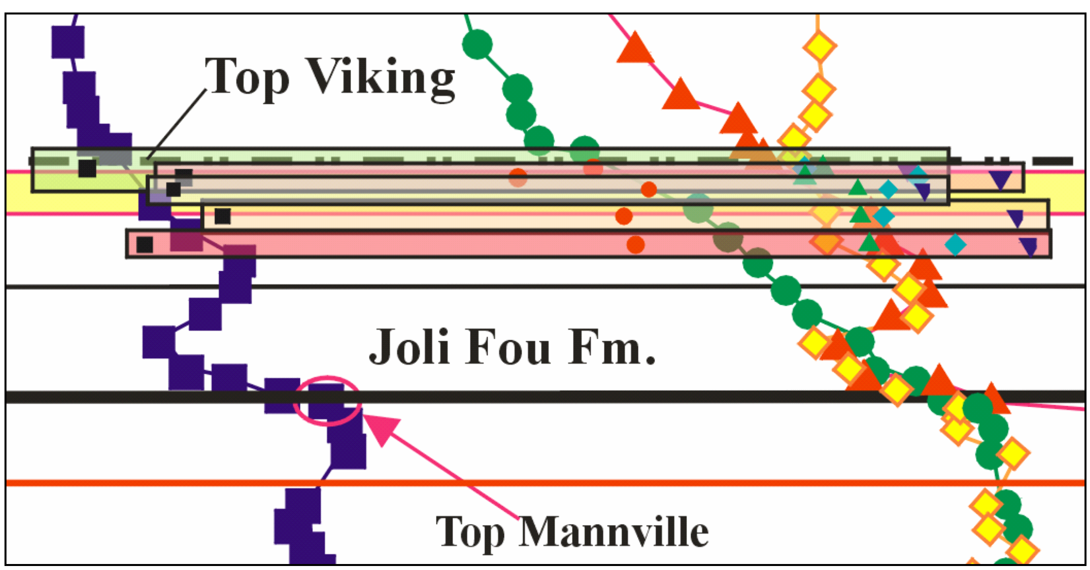

Figure 7-24 SCV gases from Figure 7-22 and their presumable sources.

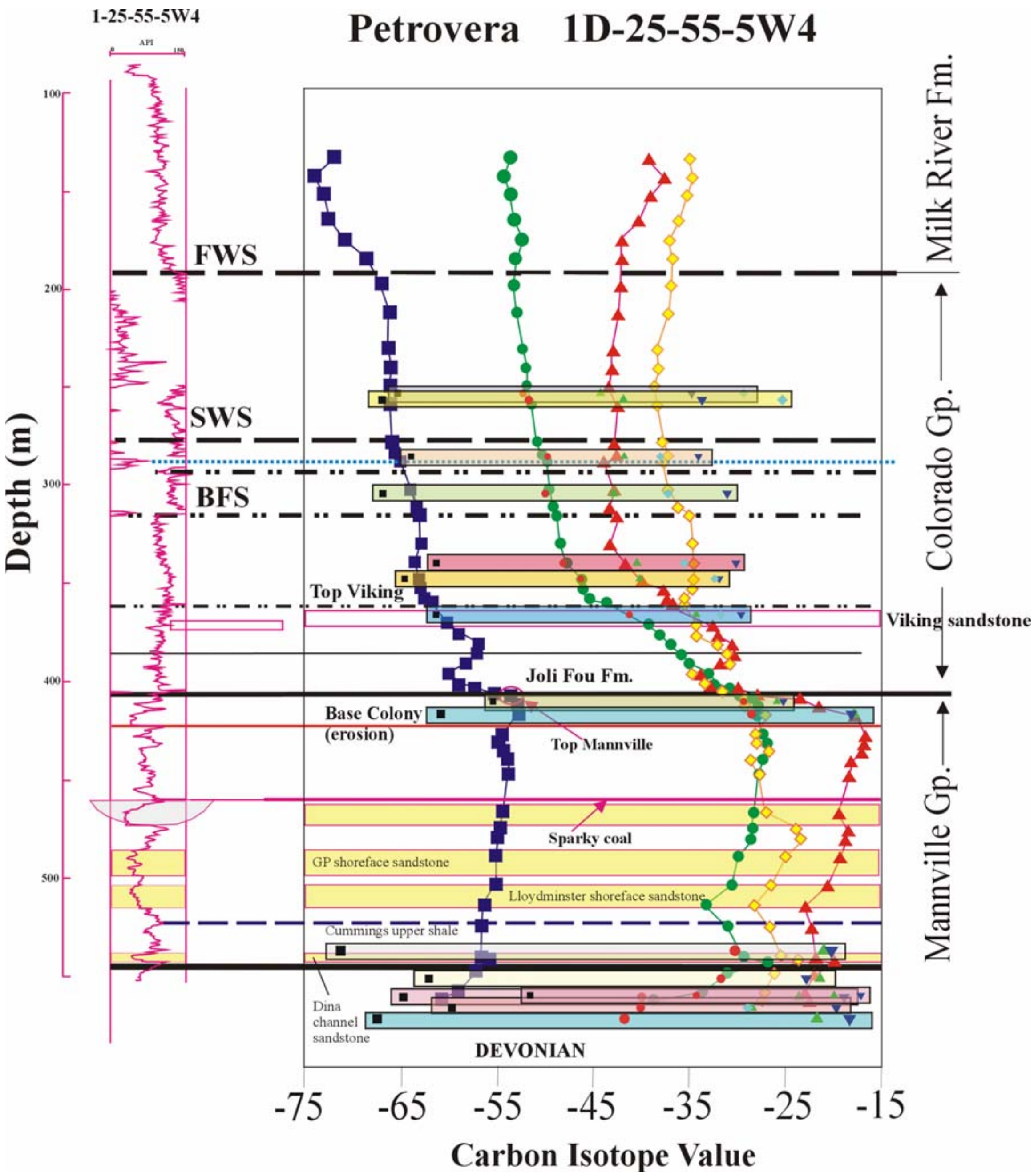

Figure 7-25 Isotope ratios of fifteen SCV gases superimposed on the mudgas isotopic depth profile from Petrovera 1D-25-55-5W4. Legend for SCV gases is provided in Figure 7-26.

SCV gases

- ■ C1
- ● C2
- ▲ C3
- ▼ iC4
- ◆ nC4

Well ID	Presumable source
01-29-55-04W4	Mannville Gp. (Dina Sandstone)
06-31-55-04W4	Devonian ?
06-31-55-04 W4	Colorado Gp. (Above SWS)
16-32-55-04W4	Colorado Gp. (Viking Sandstone)
03-07-55-05W4	Colorado Gp. (SWS)
03-07-55-05W4	Colorado Gp. (Westgate Fm.)
04-07-55-05W4	Colorado Gp. (Westgate Fm.)
06-07-55-05W4	Colorado Gp. (Belle Fourche Fm.)
11-07-55-05W4	Mannville Gp. (Colony Fm.)
15-07-55-05 W4	Colorado Gp. (Above SWS)
04-09-55-05W4	Devonian
02-18-55-05W4	Devonian
02-18-55-05W4	Devonian
02-18-55-05W4	Mannville Gp. (Colony Fm.)
02-18-55-05 W4	Devonian ?

Figure 7-26 SCV gases from Figure 7-25 and their presumable sources. Petrovera 1D-25-55-5W4.

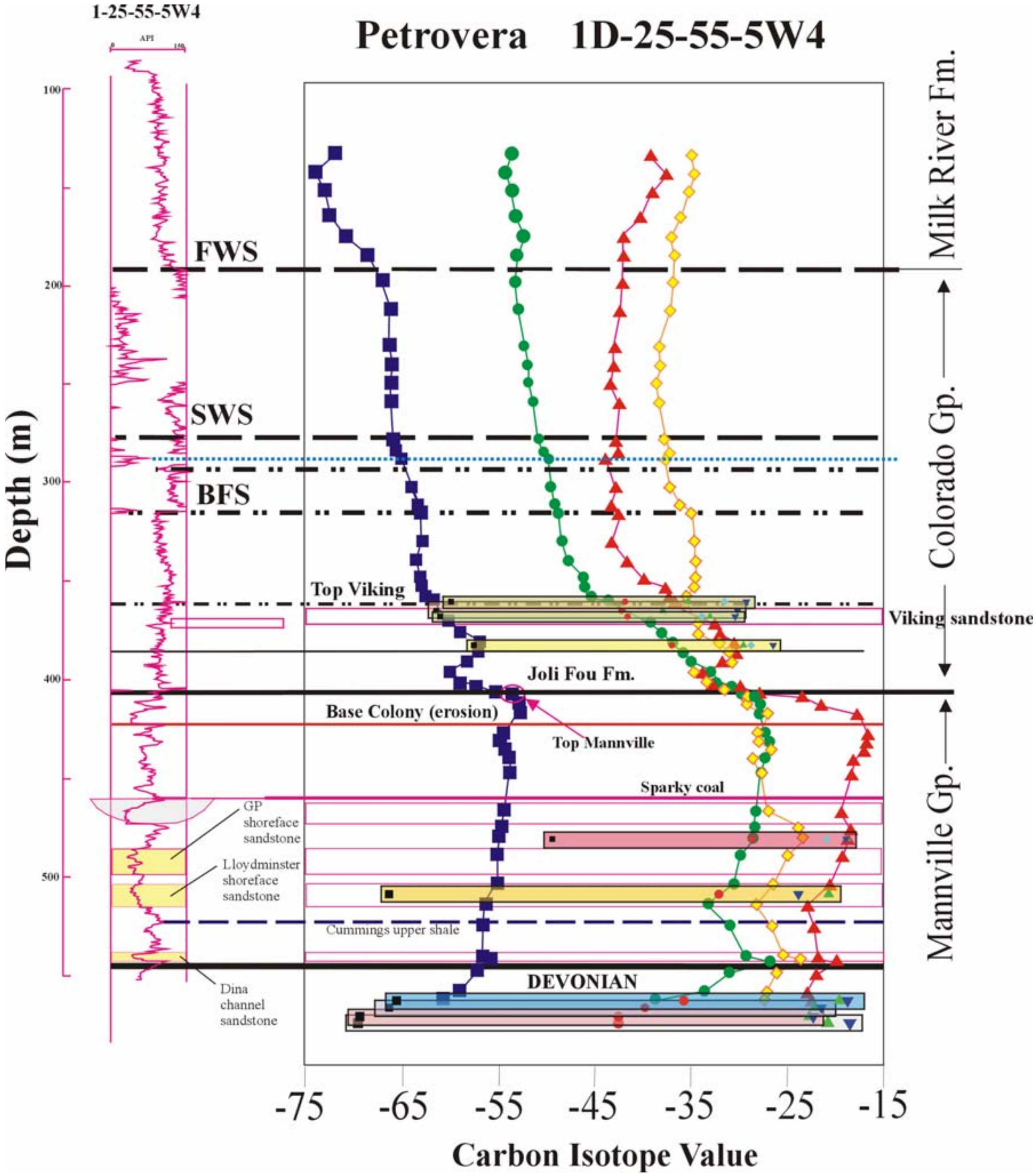

Figure 7-27 Isotope ratios of fifteen SCV gases superimposed on the mudgas isotopic depth profile from Petrovera 1D-25-55-5W4. Legend for SCV gases is provided in Figure 7-28

SCV gases

■ C1
● C2
▲ C3
▼ iC4
◆ nC4

Well ID	Presumable source
15-18-55-05W4	Devonian
15-18-55-05W4	Devonian
15-18-55-05W4	Devonian
15-18-55-05W4	Devonian
13-21-55-05W4	Colorado Gp. (Viking Sandstone)
11-23-55-05W4	Mannville Gp. (Rex - Sparky Fm.)
08-24-55-05W4	Mannville Gp. (Lloydminster Fm.)
16-33-55-05W4	Colorado Gp. (Viking Sandstone)
12-34-55-05W4	Colorado Gp. (Viking Sandstone)
11-35-55-05W4	Colorado Gp. (Viking Fm.)

Figure 7-28 SCV gases from Figure 7-27 and their presumable sources. Petrovera 1D-25-55-5W4.

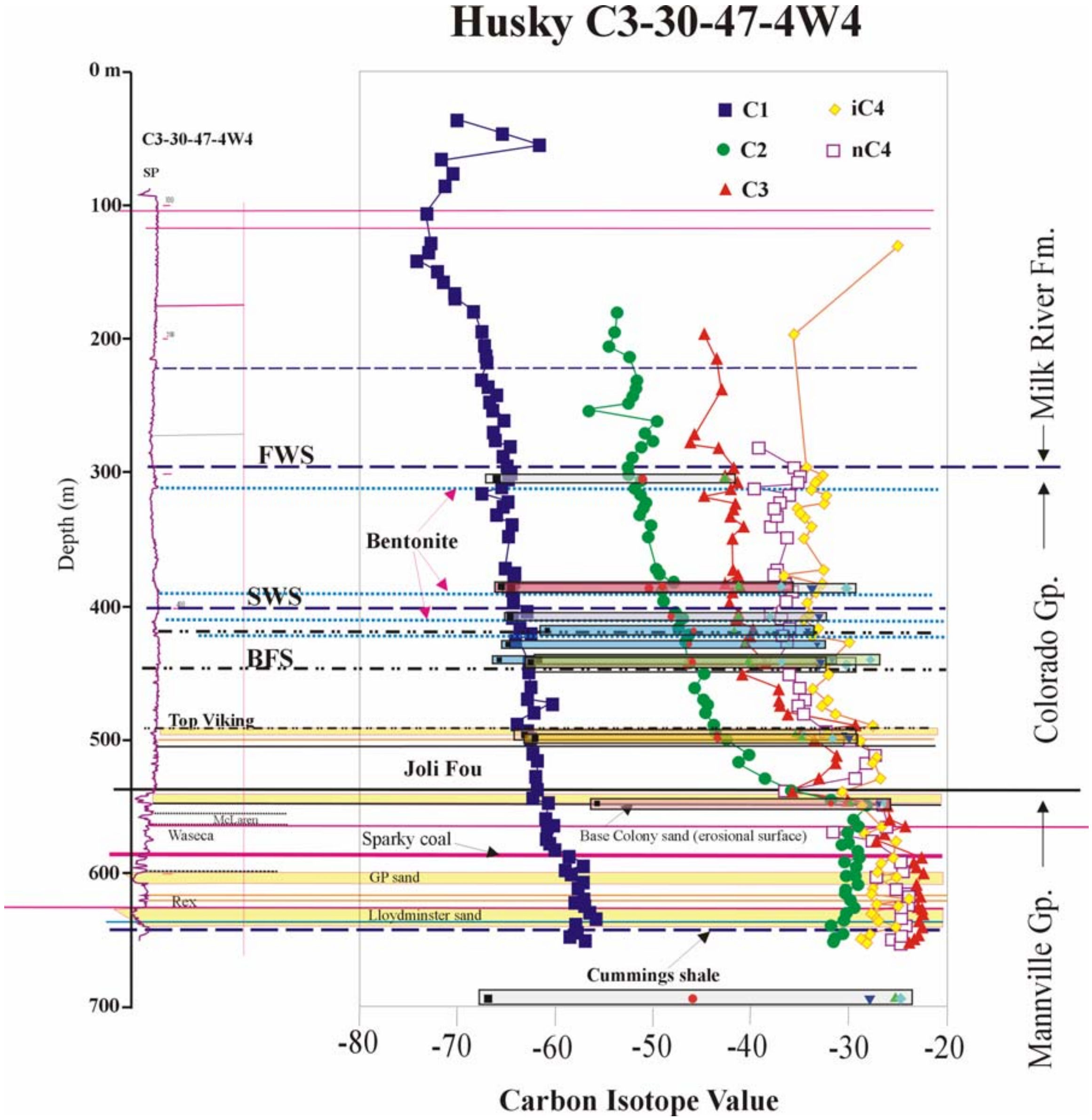

Figure 7-29 Isotope ratios of nine SCV gases superimposed on the mudgas isotopic depth profile from Husky C3-30-47-4W4. Legend for SCV gases is provided in Figure 7-30.

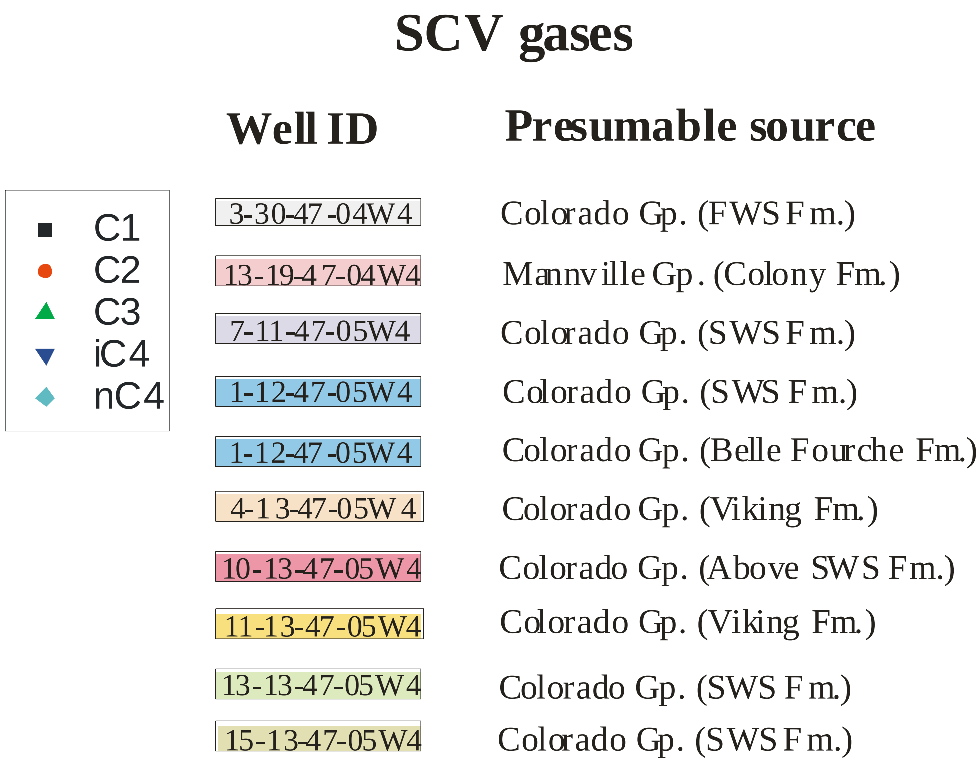

Figure 7-30 SCV gases from Figure 7-29 and their presumable sources. Husky C3-30-47-4W4.

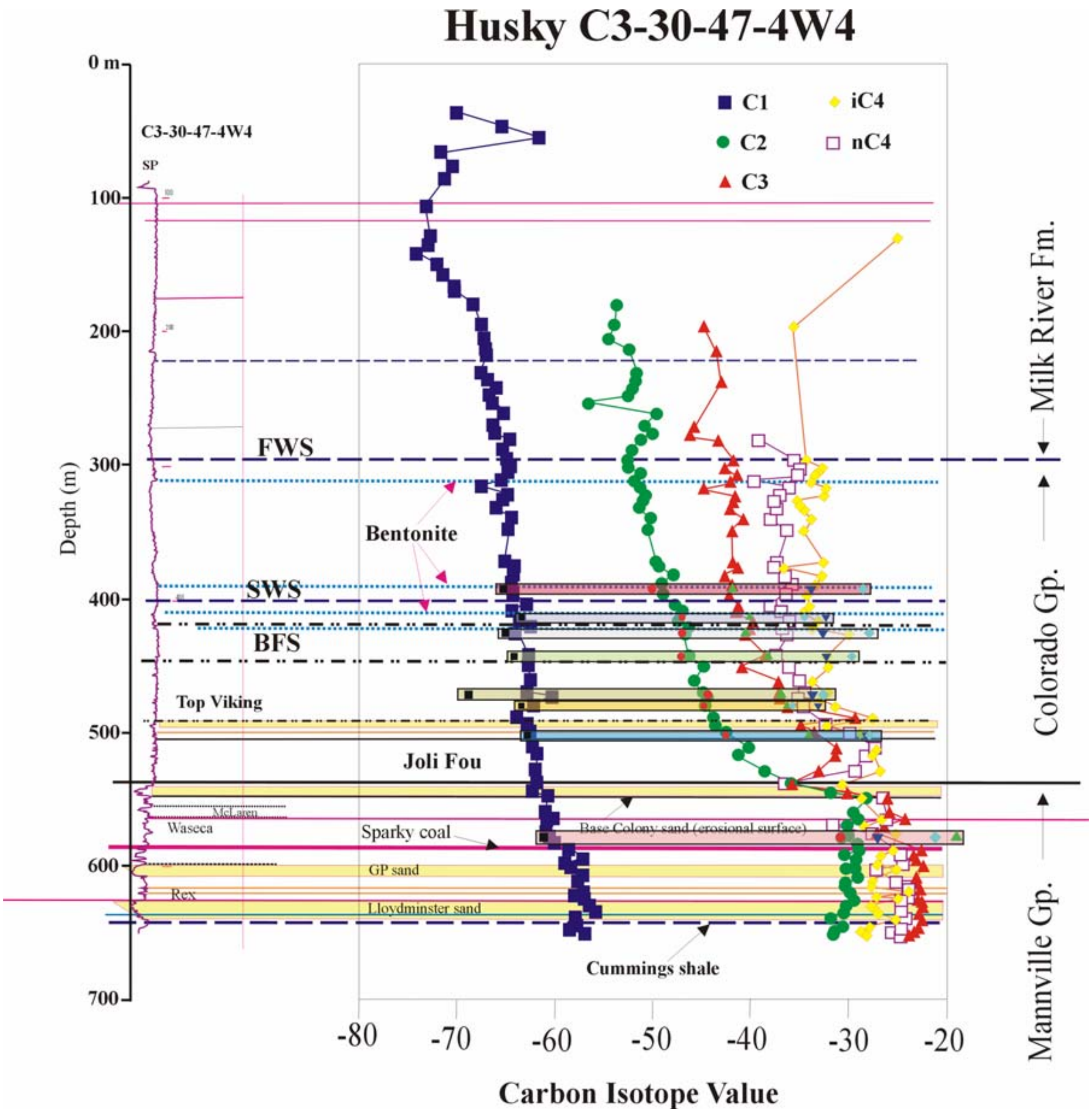

Figure 7-31 Isotope ratios of eight SCV gases superimposed on the mudgas isotopic depth profile from Husky C3-30-47-4W4. Legend for SCV gases is provided in Figure 7-32.

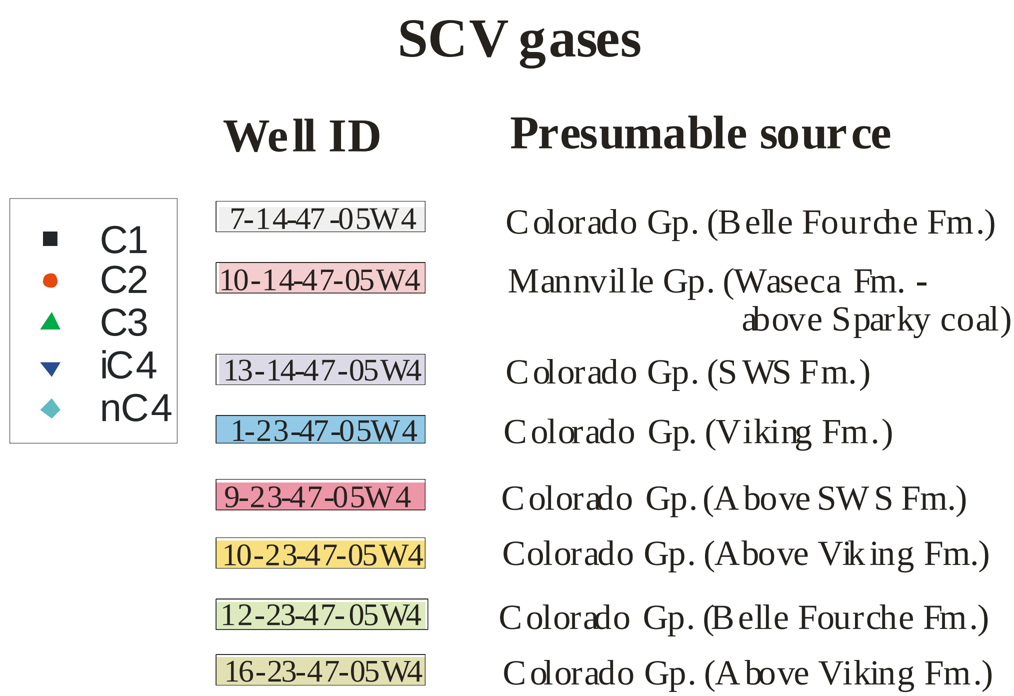

Figure 7-32 SCV gases from Figure 7-31 and their presumable sources. Husky C3-30-47-4W4.

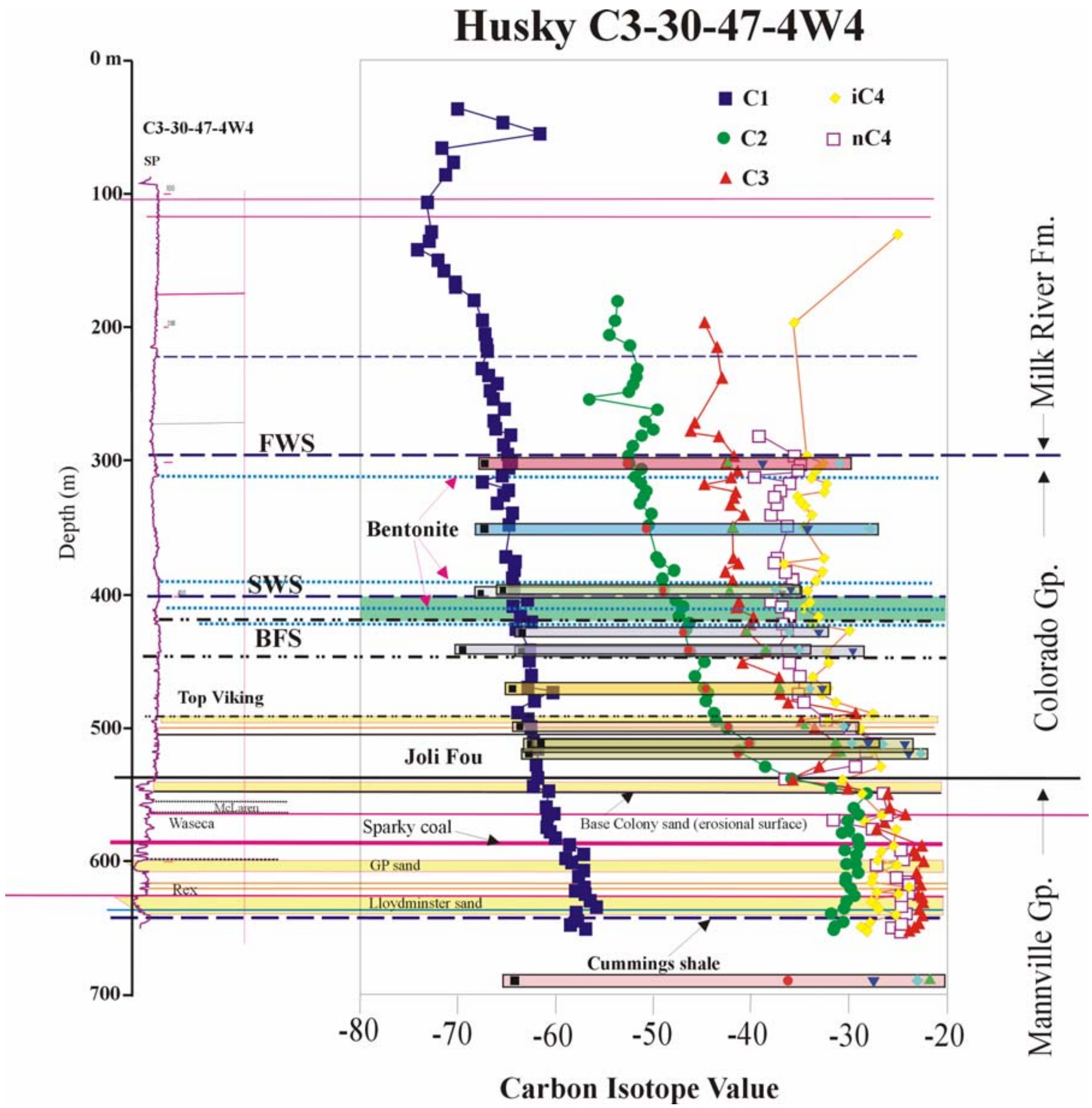

Figure 7-33 Isotope ratios of nine SCV gases superimposed on the mudgas isotopic depth profile from Husky C3-30-47-4W4. Legend for SCV gases is provided in Figure 7-34.

SCV gases

C1
C2
C3
iC4
nC4

Well ID	Presumable source
2-24-47-05W4	Colorado Gp. (SWS Fm.)
3-24-47-05W4	Mannville Gp.?
7-24-47-05W4	Colorado Gp. (Belle Fourche Fm.)
10-24-47-05W4	Colorado Gp. (Viking Fm.)
11-24-47-05W4	Colorado Gp. (Above SWS Fm.)
12-24-47-05W4	Colorado Gp. (FWS Fm.)
13-24-47-05W4	Colorado Gp. (Above Viking Fm.)
4-25-47-05W4	Colorado Gp. (SWS Fm.)
16-23-47-05W4	Colorado Gp. (Joli Fou Fm.)

Figure 7-34 SCV gases from Figure 7-33 and their presumable sources. Husky C3-30-47-4W4.

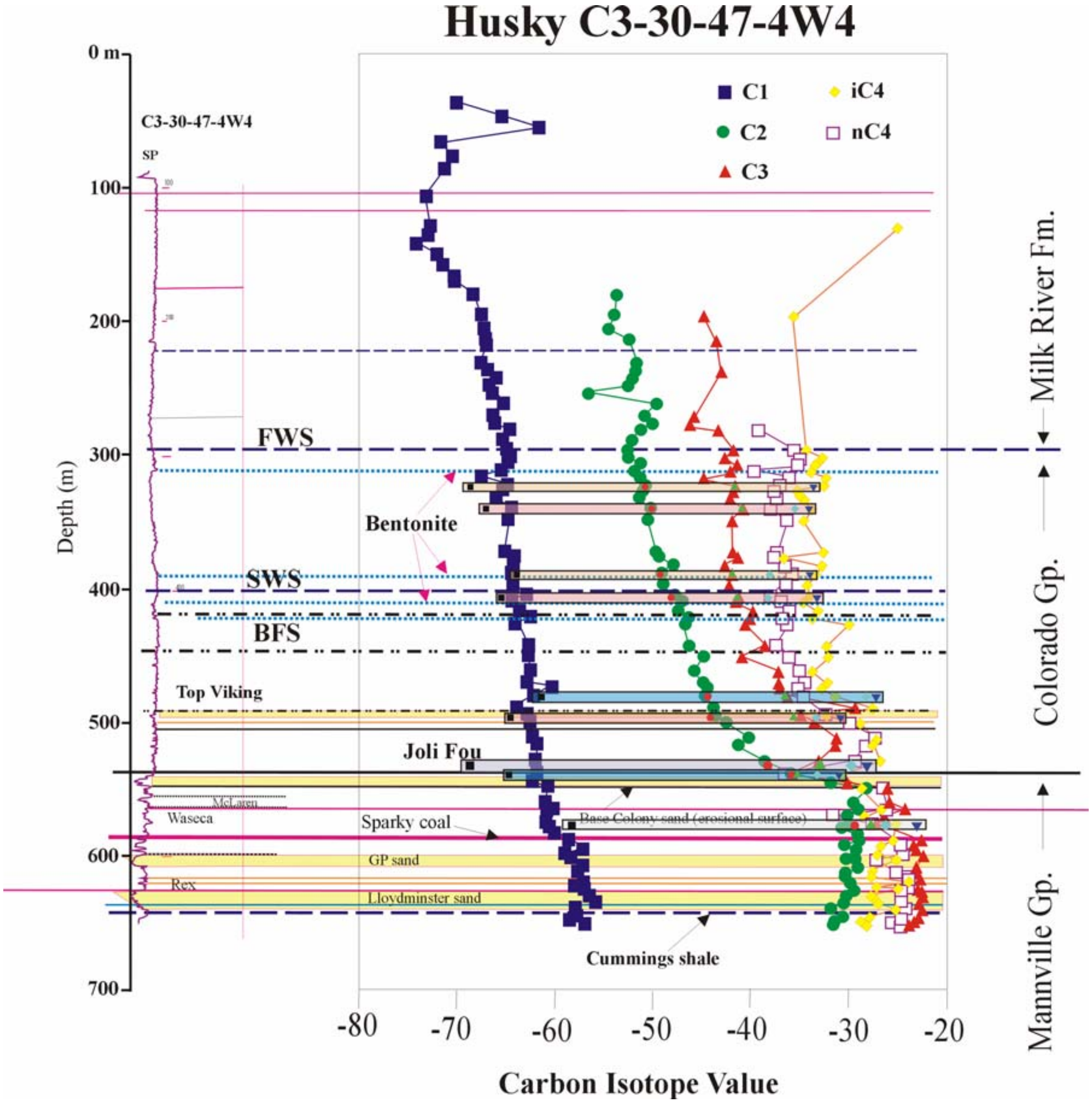

Figure 7-35 Isotope ratios of nine SCV gases superimposed on the mudgas isotopic depth profile from Husky C3-30-47-4W4. Legend for SCV gases is provided in Figure 7-36.

SCV gases

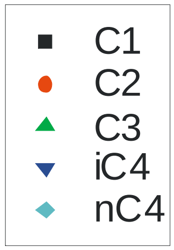

Well ID	Presumable source
9-25-47-05W4	Mannville Gp.(above Sparky coal)
10-25-47-05W4	Colorado Gp. (SWS Fm..)
10-25-47-05W4	Colorado Gp. (Viking Fm.)
10-25-47-05W4	Colorado Gp. (Below SWS Fm.)
11-25-47-05W4	Colorado Gp. (Base Joli Fou Fm.)
10-29-47-05 W4	Colorado Gp. (Above Viking Fm.)
10-29-47-05W4	Colorado Gp. (Base Joli Fou- top Mannville)
1-36-47-05W4	Colorado Gp. (Below FWS Fm.)
1-36-47-05W4	Colorado Gp. (Above SWS Fm.)

Figure 7-36 SCV gases from Figure 7-35 and their presumable sources. Husky C3-30-47-4W4.

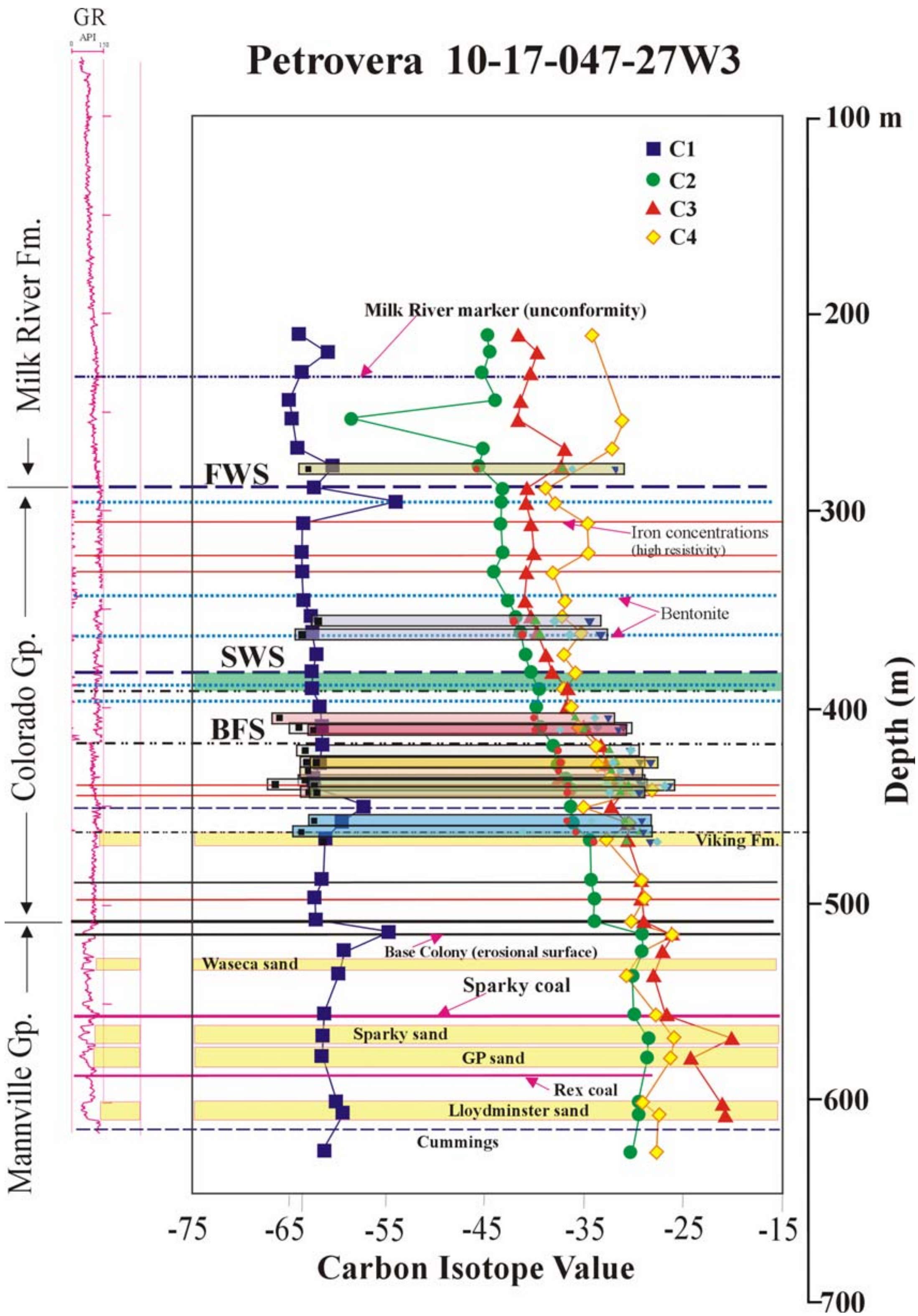

Figure 7-37 Isotope ratios of sixteen SCV gases superimposed on the mudgas isotopic depth profile from Petrovera 10-17-47-27W3. Legend for SCV gases is provided in Figure 7-38.

SCV gases

- ■ C1
- ● C2
- ▲ C3
- ▼ iC4
- ◆ nC4

Well ID	Presumable source
6-11-47-23W3	Colorado Gp. (Belle Fourche Fm.) - 1 sample
6-11-47-23W3	Colorado Gp. (Westgate Fm.) - 4 samples
5-11-47-23W3	Colorado Gp. (Belle Fourche Fm.) - 1 sample
2-10-47-23W3	Colorado Gp. (Above SWS) - 2 samples
2-06-47-23W3	Colorado Gp. (Westgate Fm.) - 2 samples
4-04-47-23W3	Colorado Gp. (Westgate Fm.) - 1 sample
3-03-47-23W3	Colorado Gp. (Belle Fourche Fm.) - 1 sample
3-11-47-23W3	Colorado Gp. (Westgate Fm.) - 1 sample
4-11-47-23W3	Colorado Gp. (Westgate Fm.) - 2 samples
9-11-47-23W3	Milk River Fm. - 1 sample

Figure 7-38 SCV gases from Figure 7-37 and their presumable sources. Petrovera 10-17-47-27W3.

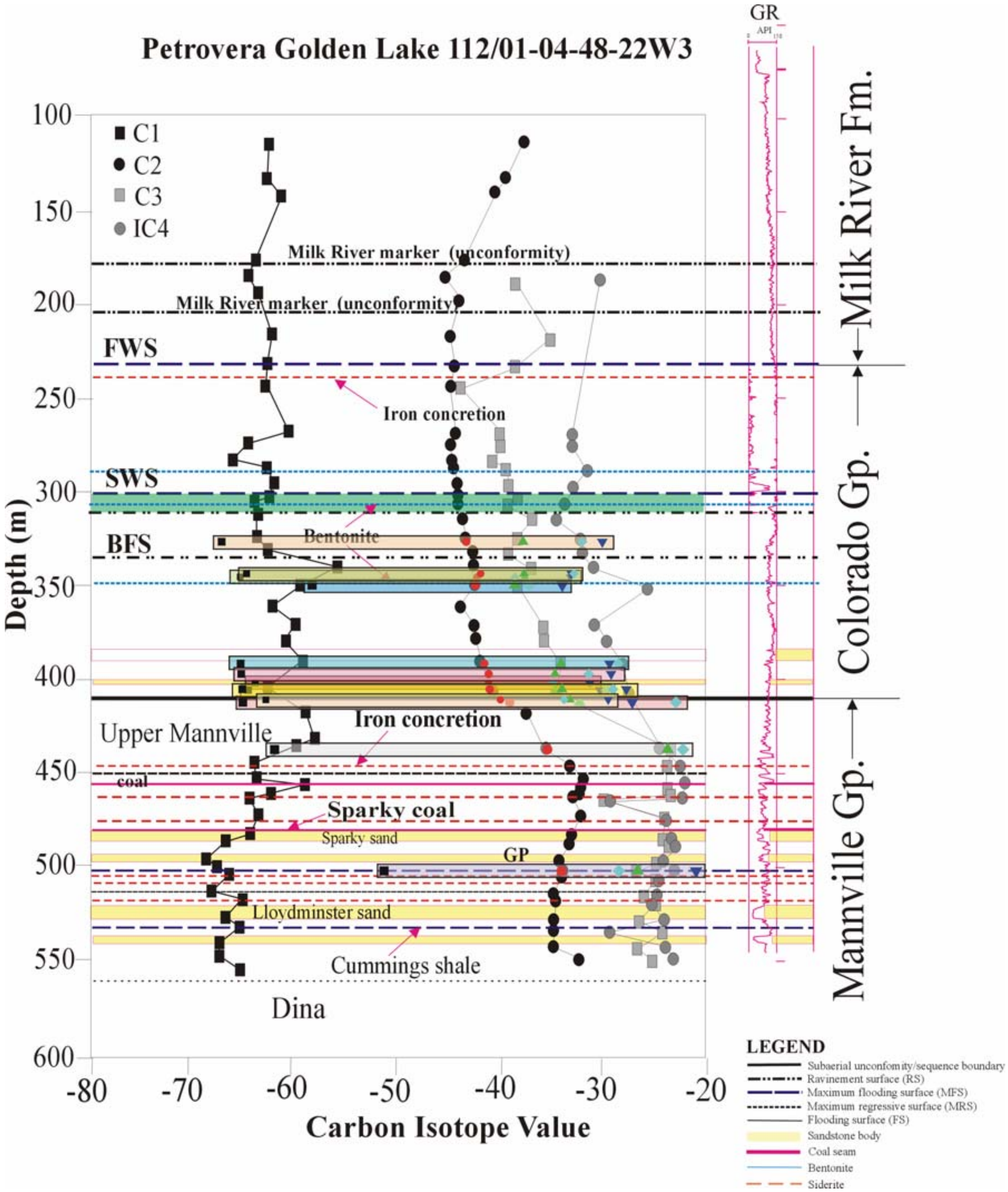

Figure 7-39 Isotope ratios of thirteen SCV gases superimposed on the mudgas isotopic depth profile from Petrovera 112-/01-04-48-22W3. Legend for SCV gases is provided in Figure 7-40.

SCV gases

C1
C2
C3
iC4
nC4

Well ID	Presumable source
1-04-48-22W3	Mannville Gp. (Colony Fm.)
2-10-48-22W3	Mannville Gp. (GP Fm. - marine shales)
4-20-48-22W3	Colorado Gp. (Westgate Fm.)
8-10-48-23W3	Mannville Gp. (Colony Fm.)
1-11-48-23W3	Colorado Gp. (Belle Fourche Fm.)
1-11-48-23W3	Spinney Hill Sandstone.
8-11-48-23W3	Joli Fou Fm.
9-11-48-23W3	Colorado Gp. (Westgate Fm.)
10-11-48-23W3	Colorado Gp. (Westgate Fm.)
13-11-48-23W3	Joli Fou Fm.
13-11-48-23W3	Joli Fou Fm. - Mannville Gp.
14-11-48-23W3	Joli Fou Fm.
16-11-48-23W3	Joli Fou Fm.

Figure 7-40 SCV gases from Figure 7-39 and their presumable sources. Petrovera 112-/01-04-48-22W3.

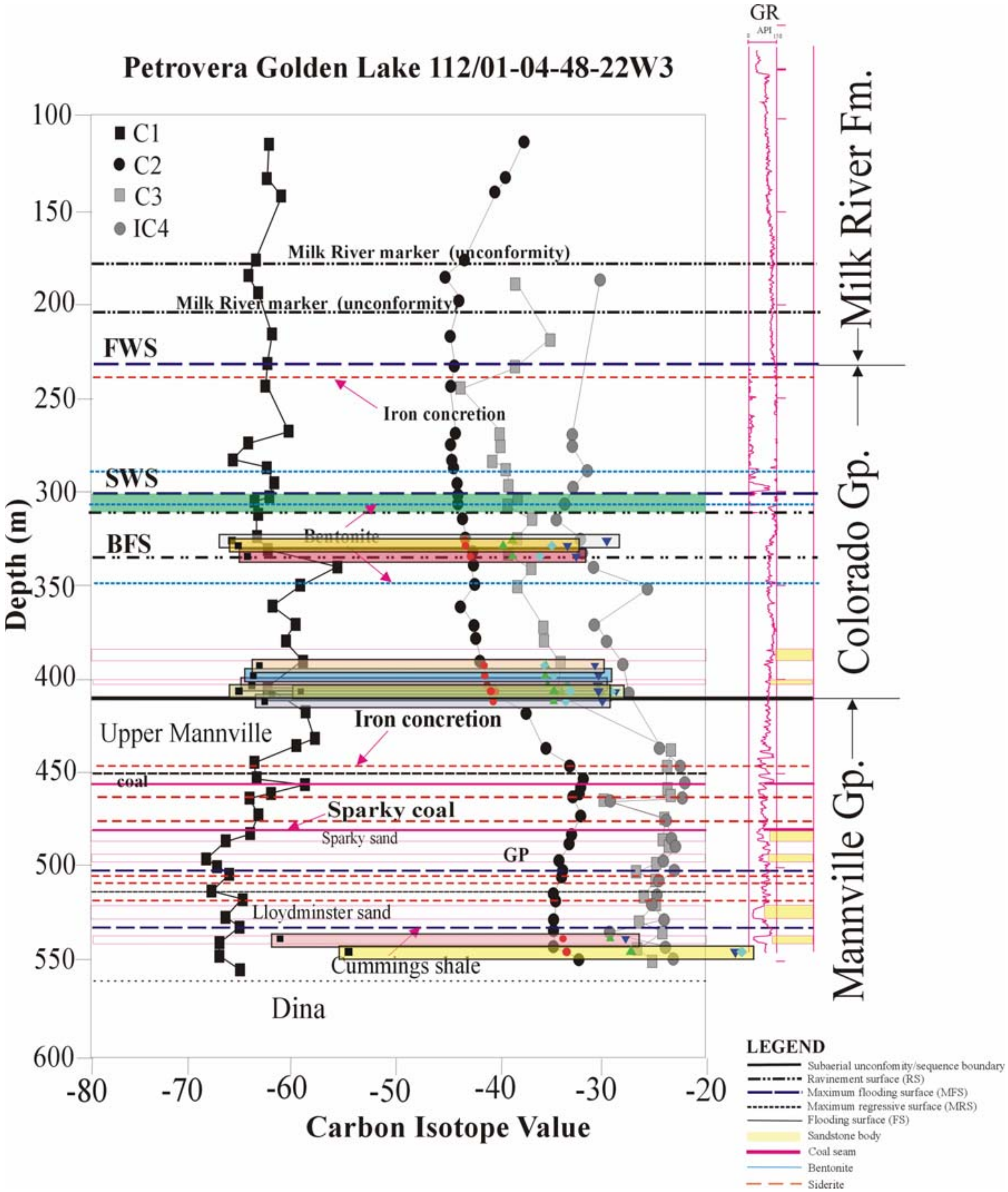

Figure 7-41 Isotope ratios of seventeen SCV gases superimposed on the mudgas isotopic depth profile from Petrovera 112-/01-04-48-22W3. Legend for SCV gases is provided in Figure 7-42.

SCV gases

- ■ C1
- ● C2
- ▲ C3
- ▼ iC4
- ◆ nC4

Well ID	Presumable source
01-12-48-23W3	Colorado Gp. (Belle Fourche Fm.)
03-12-48-23W3	Joli Fou Fm.
04-12-48-23W3	Joli Fou Fm. - Spinney Hill - 3 samples
04-12-48-23W3	Mannville Gp. (Lloydminster Fm.)
05-12-48-23W3	Joli Fou Fm. - 4 samples
05-12-48-23W3	Colorado Gp. (Fish Scale)
12-12-48-23W3	Colorado Gp. (Fish Scale)
13-12-48-23W3	Joli Fou Fm.
11-14-48-23W3	Joli Fou Fm.
06-14-48-23W3	Mannville Gp. (Cummings Fm.?)
03-11-48-23W3	Joli Fou Fm.
14-11-48-23W3	Joli Fou Fm. - Spinney Hill

Figure 7-42 SCV gases from Figure 7-41 and their presumable sources. Petrovera 112-/01-04-48-22W3.

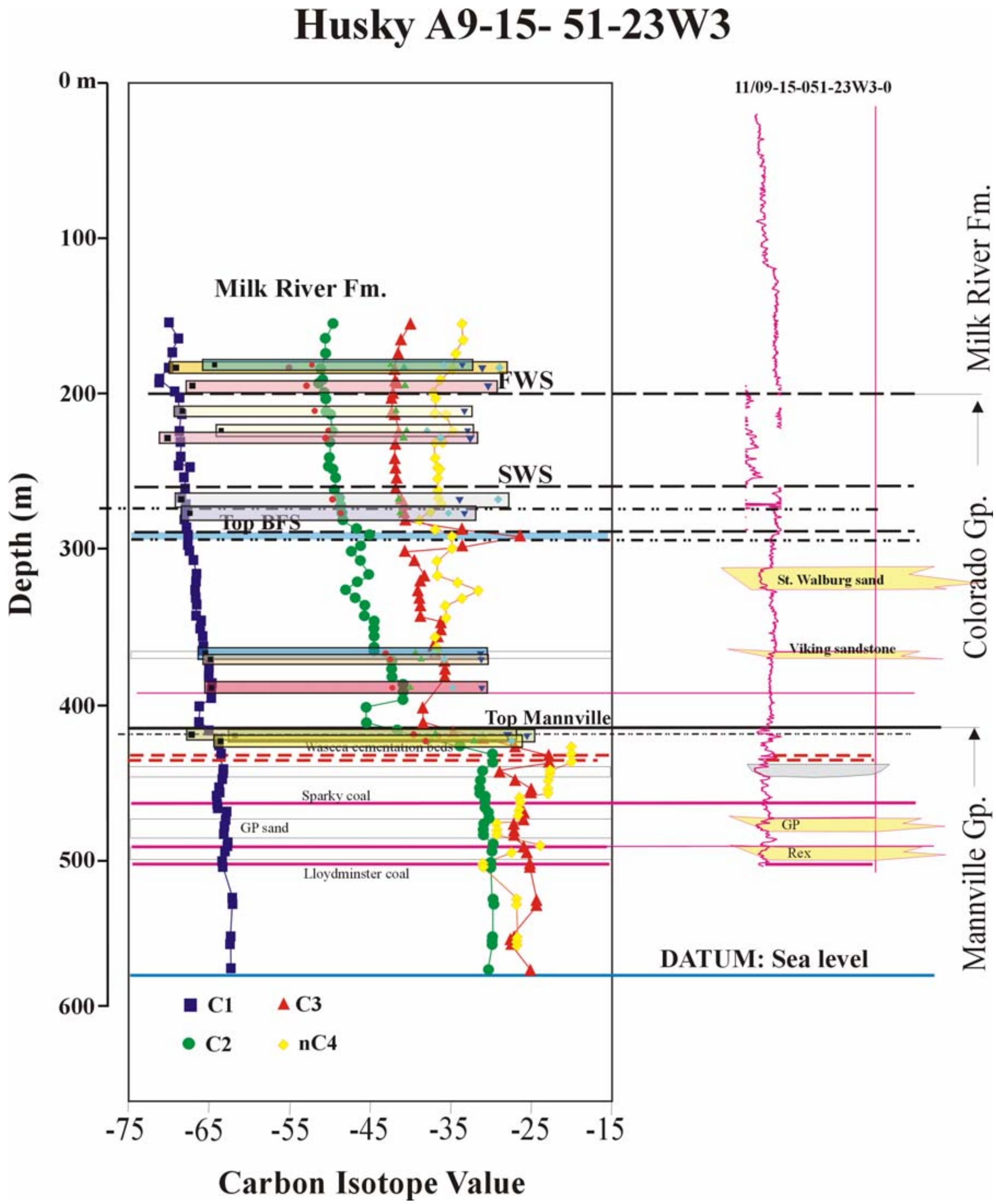

Figure 7-43 Isotope ratios of fourteen SCV gases superimposed on the mudgas isotopic depth profile from Husky A9-15- 51-23W3. Legend for SCV gases is provided in Figure 7-44.

SCV gases

C1
C2
C3
iC4
nC4

Well ID	Presumable source
09-33-51-23 W3	Colorado Gp. (SWS)
01-21-51-23W3	Milk River Fm. ?
09-33-51-23 W3	Colorado Gp. (SWS)
05-36-51-23W3	Colorado Gp. (Viking Sandstone)
12-36-51-23W3	Colorado Gp. (Viking Sandstone)
12-36-51-23W3	Colorado Gp. (Viking Fm.?)
05-06-51-23W3	Milk River Fm. ?
05-10-52-23W3	Mannville Gp. (Colony Fm.)
07-10-52-23W3	Mannville Gp. (Colony Fm.)
02-10-52-23W3	Mannville Gp. (Colony Fm.)
03-20-51-24W3	Colorado Gp. (Below FWS)
03-20-51-24W3	Milk River Fm. ?
03-20-51-24W3	Colorado Gp. (Below FWS)
03-20-51-24W3	Colorado Gp. (Below FWS)

Figure 7-44 SCV gases from Figure 7-43 and their presumable sources. Petrovera 112-/01-04-48-22W3.

As for the Foothill study area, each data set has been superimposed on the isotopic profile of the formations penetrated from that field. The best fit of each data set was found by sliding the data vertically until the isotope ratios of the C_{2+} components best matched the underlying isotopic fingerprint. This allowed the presumable source(s) to be estimated from the vertical axis (Figures 7-13 to 7-44).

As can be seen in Figure 7-45, the sources for SCV gases in the Lloydminster region are more diversified than those in the Foothills region. For each mudlog, the most presumable sources have been indicated. These are mainly Colorado Group, and Mannville Group, but a both deeper Devonian source (see Figures 7-15, 7-22, 7-25, 7-27) and a shallower Milk River source seem to be as well present, in the northwest corner of the study area, and in the south eastern corner of the study area respectively. When the source horizon lies in the deeper strata, the SCV gases likely come from the producing horizons in the area: different Mannville reservoir sandstones (Dina, Lloydminster, Colony) and/or Sparky coal related, - and Viking Formation, from various depths. Majority of the SCV gases coming from the Colorado Group appear to be related to the shaly Westgate, Belle Fourche, Fish Scale, Second White Specks and First White Specks formations - pointing again to the early thermogenic gas generation in this stratigraphic section. Figures 7-46 to 7-48 show a detailed distribution per formation of the number of SCV gases identified in presumable sources.

The prevalence of SCV from the Second White Specks Formation and Belle Fourche Formation can be explained mostly by their source rock potential. Second White Specks Formation has been identified as an effective source rock since 1984 (Macauley, 1984), and gas production from the Belle Fourche Formation has been reported in the Southeast Alberta, Southwest Saskatchewan, and Montana (Ridgley et al., 2001). East of 114^0 longitude the Second White Specks Formation is a potential source rock and is the source of produced bacteriogenic gas in southern Saskatchewan (Stasiuk and Goodarzi, 1988). The Westgate, Belle Fourche, and Fish Scales formations are also potential source rocks, but of lesser quality (Bloch et al., 1999).

In the studied Lloydminster heavy oil area, the Second White Specks Formation map of Bloch et al. (1999) shows the highest total organic carbon (TOC) content (an average value of 6.5 wt %) among the lower Colorado Group formations. Linked with the fact that at Petrovera 1D-25-55-5W4, a local overpressure within the Second White Specks Formation has been suggested using the acoustic velocity method of Magara (1978), the prevalent SCV gases are most likely sourced from within the surrounding SWS shales.

7.3. Environmental implications

Carbon Isotope Fingerprint of ethane (C_2), and propane (C_3) is a proven, cost effective method used to compare and fingerprint known formation gases, identify the gas source in order to isolate it and block the flow. The ability to determine source depths of shallow gases is particularly useful for the remediation of numerous leaking heavy-oil wells in the Western Canada Sedimentary Basin (Rowe and Muehlenbachs, 1999b).

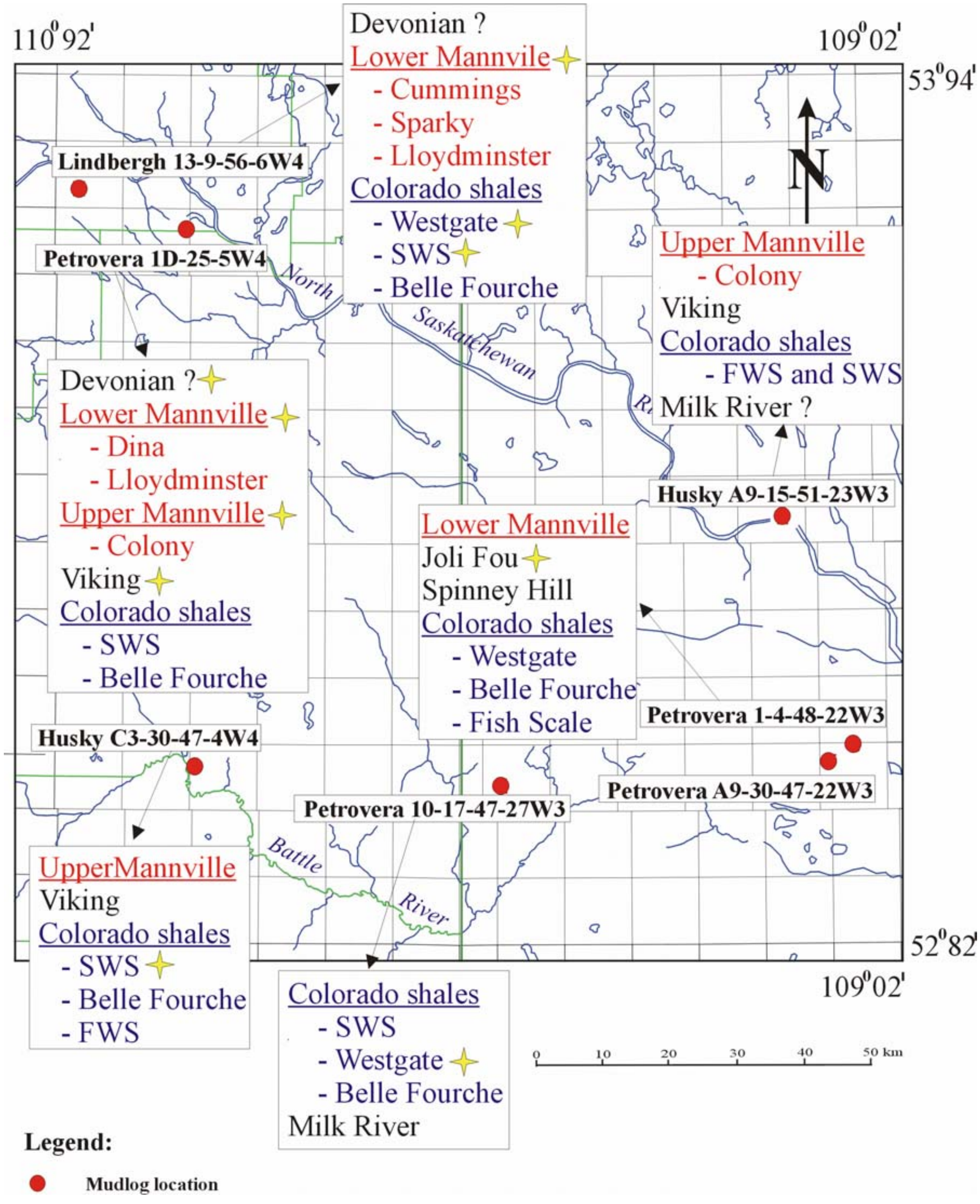

Figure 7-45 Base map showing the location of the carbon isotope mud gas depth profiles from the heavy oil region, and the presumable sources for the SCV gases in their vicinity. The most prevalent source is indicated with a yellow star beside.

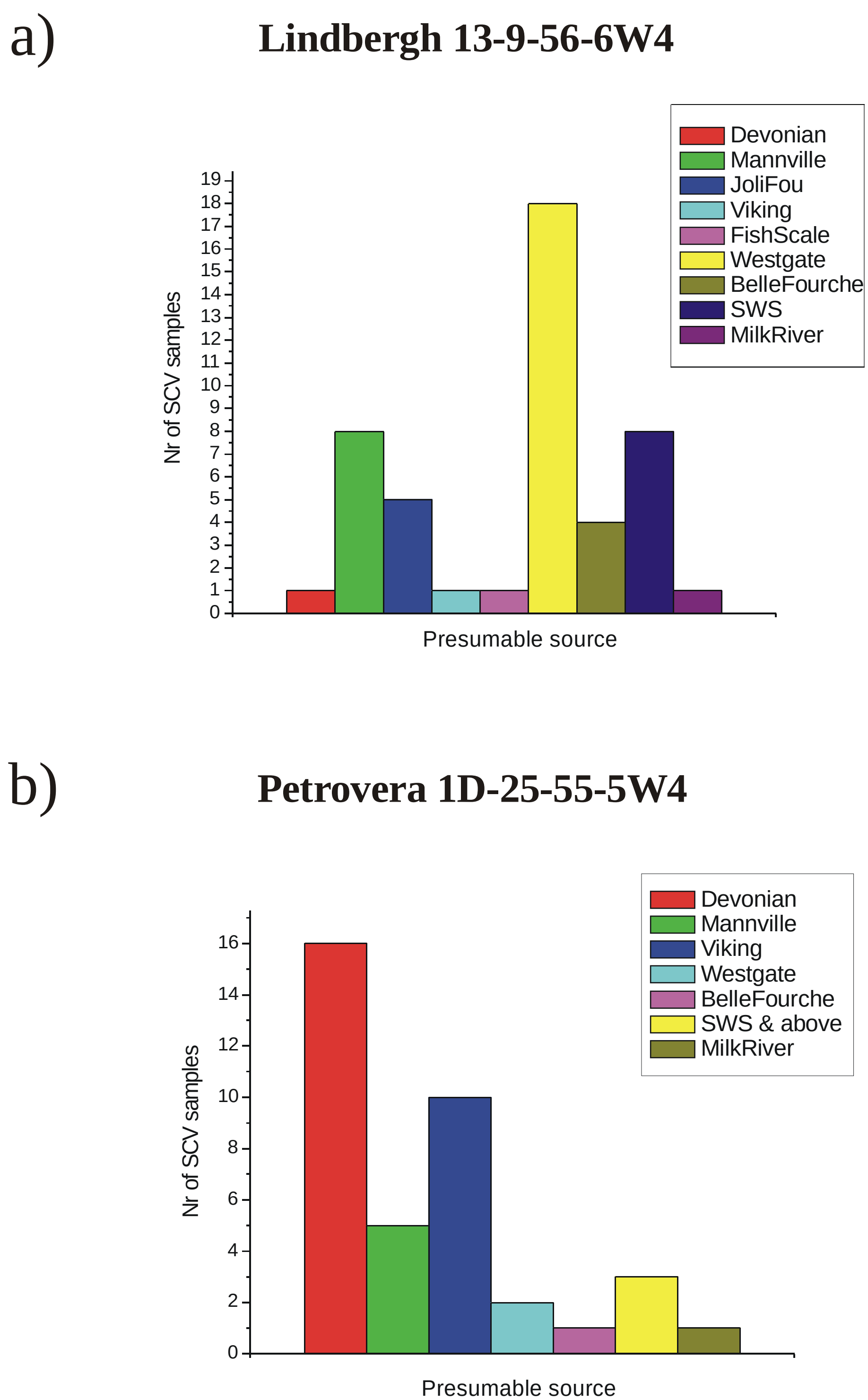

Figure 7-46 Frequency of presumable sources for the SCV gases in the vicinity of: a) Lindbergh 13-9-56-6W4 well, and b) Petrovera 1d-25-55-5W4 well.

a)

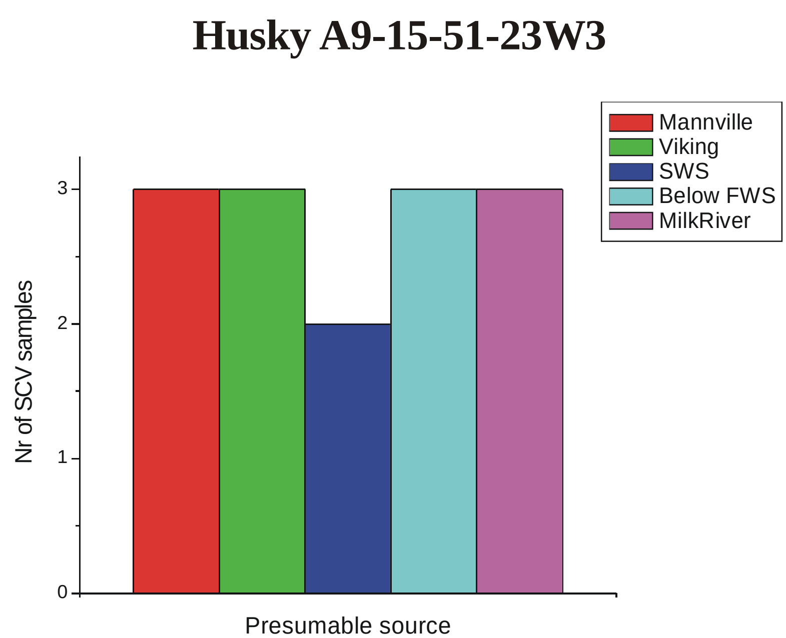

b)

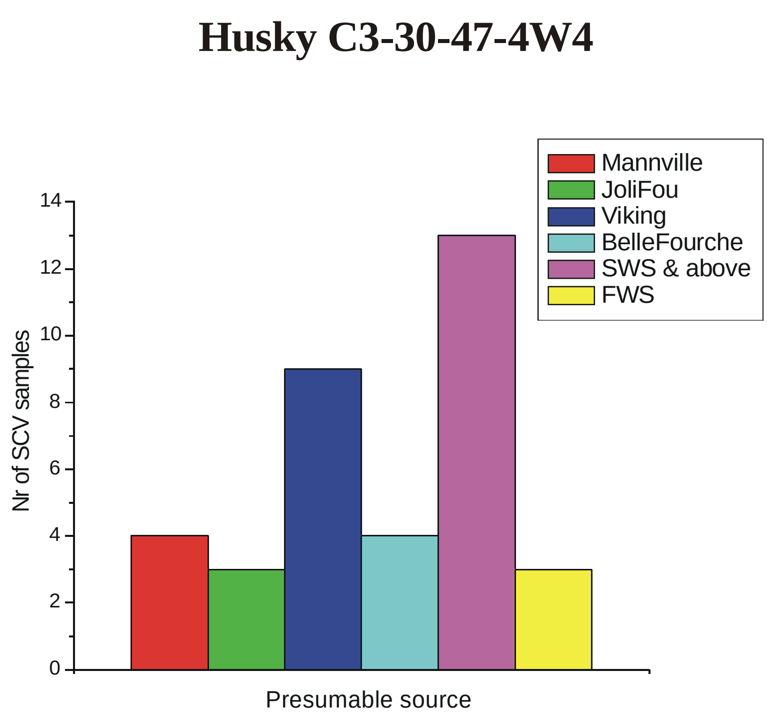

Figure 7-47 Frequency of presumable sources for the SCV gases in the vicinity of: a) Husky A9-15-51-23W3 well, and b) Husky C3-30-47-4W4 well.

a)

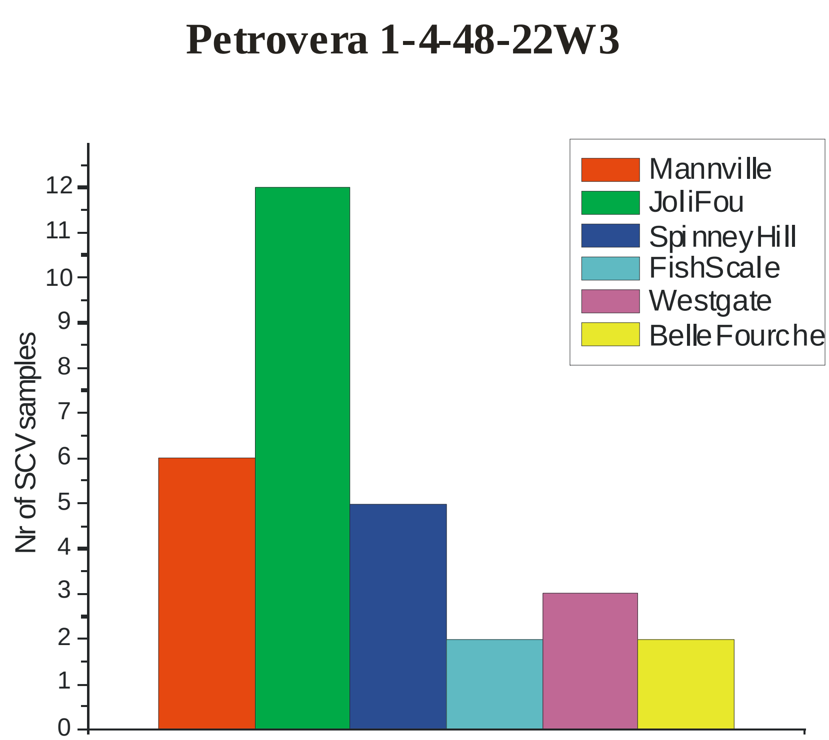

b)

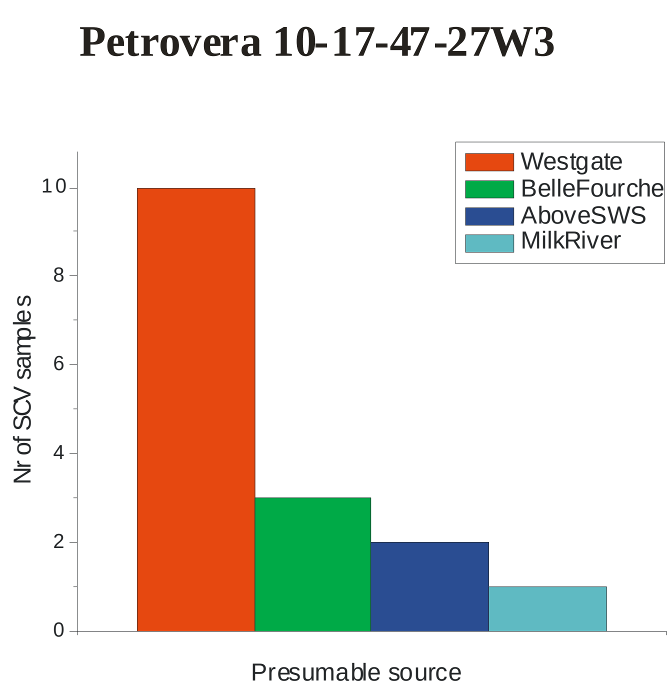

Figure 7-48 Frequency of presumable sources for the SCV gases in the vicinity of: a) Petrovera 1-4-48-27W3 well, and b) Petrovera 10-17-47-27W3 well.

CHAPTER EIGHT: SUMMARY AND RELATIONSHIPS BETWEEN FOOTHILLS AND HEAVY OIL STUDY AREAS

8.1. Stable isotopes results and discussion

Carbon isotope and molecular compositions of Cretaceous - Tertiary mudgases have been examined from ten isotopic depth profiles from two areas in the Western Canada Sedimentary Basin (WCSB): foothills-, and heavy-oil regions. The locations of the ten carbon isotopes mud gas depth profiles are shown in Figure 8-1, with respect to the approximate present gas window and oil window within the basin.

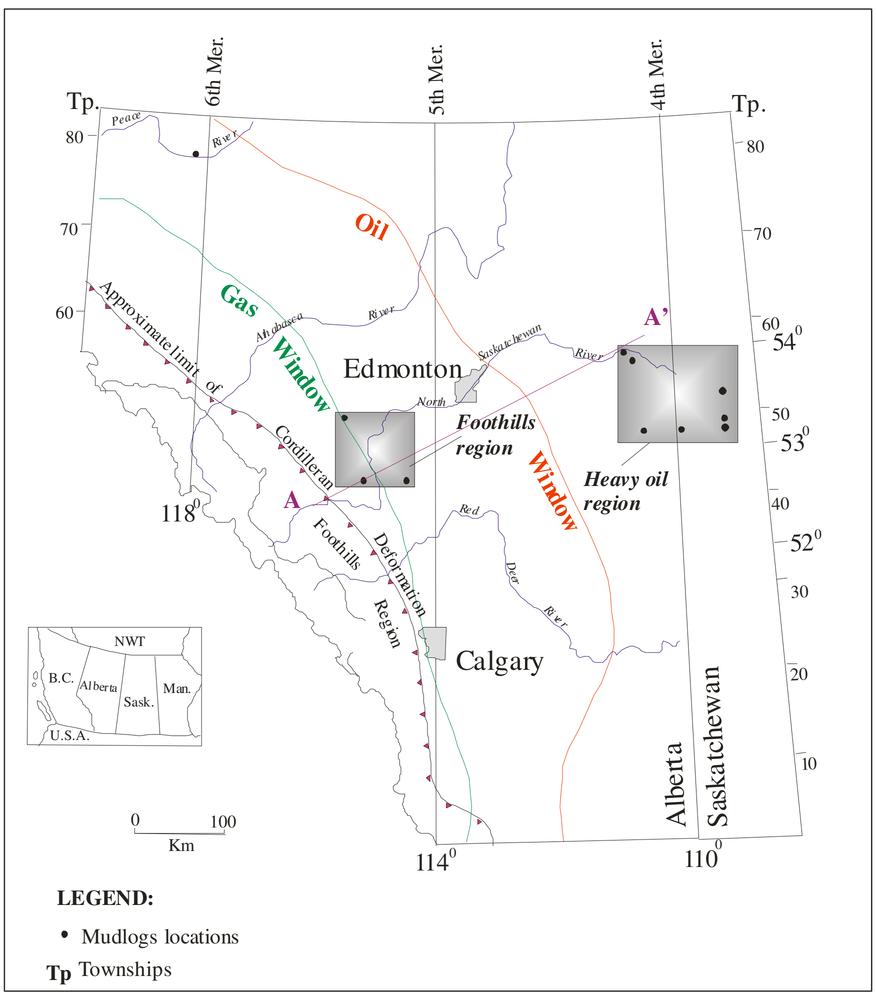

Figure 8-1 Locations of ten carbon isotope mud gas depth profiles in the WCSB

Chemical and stable isotope data were acquired from the University of Alberta database. The majority of the mudgases collected for this study were acquired from the Cretaceous sedimentary section (the only exceptions being Gilby profile, extending down into Mississippian, and two profiles at Lindbergh field – heavy oil area, extending down into Devonian). The schematic geological cross-section A-A' in Figure 8-2 illustrates the relative position of four of these mudgas profiles in the sedimentary basin. Ferrier profile is located in the westernmost part of the Alberta foreland basin, close to the approximate limit of the disturbed belt, and Lindbergh profile is located in the Cold Lake – Lloydminster heavy oil area.

The analyzed mudgases are dominated by methane and the higher hydrocarbons (C2+) gases, the later ranging from less than 1% (~0.08% - Paskapoo and Scollard gases, in the Foothills area; ~0.13% - Lea Park gases in the heavy oil region) to more than 30% by volume (Belly River sandstones – Foothills region). Of the non-hydrocarbon gases, carbon dioxide is either non-detectable or does not exceed 0.78% by volume, with a mean value of ~ 0.022% (very few exceptions have values between 3-4% at the Lindbergh field –heavy oil region).

8.1.1. $\delta\,^{13}C$ of Methane

Methane is the dominant component in the natural gas samples analyzed in this study. Its relative concentration ranged from 66.67% in the Lower Belly River gas (Foothills region) to 99.91% in the Paskapoo gas samples (Foothills region). Majority of the gases have a relatively light-, and very light isotopic compositions [$\delta\,^{13}C_{methane}$ = -39.9 ‰ (Horseshoe Canyon gas, Ferrier profile) to – 79.46‰ (Lea Park gas, Lindbergh profile].

Methane in natural gases may be formed via biological processes (bacteriogenic CH_4), thermal degradation of kerogen and oil (thermogenic CH4), or methamorphic reactions and degassing of the Earth's mantle (Schoell, 1988). Methane from the methamorphic reactions and degassing of the earth's mantle shows a considerably

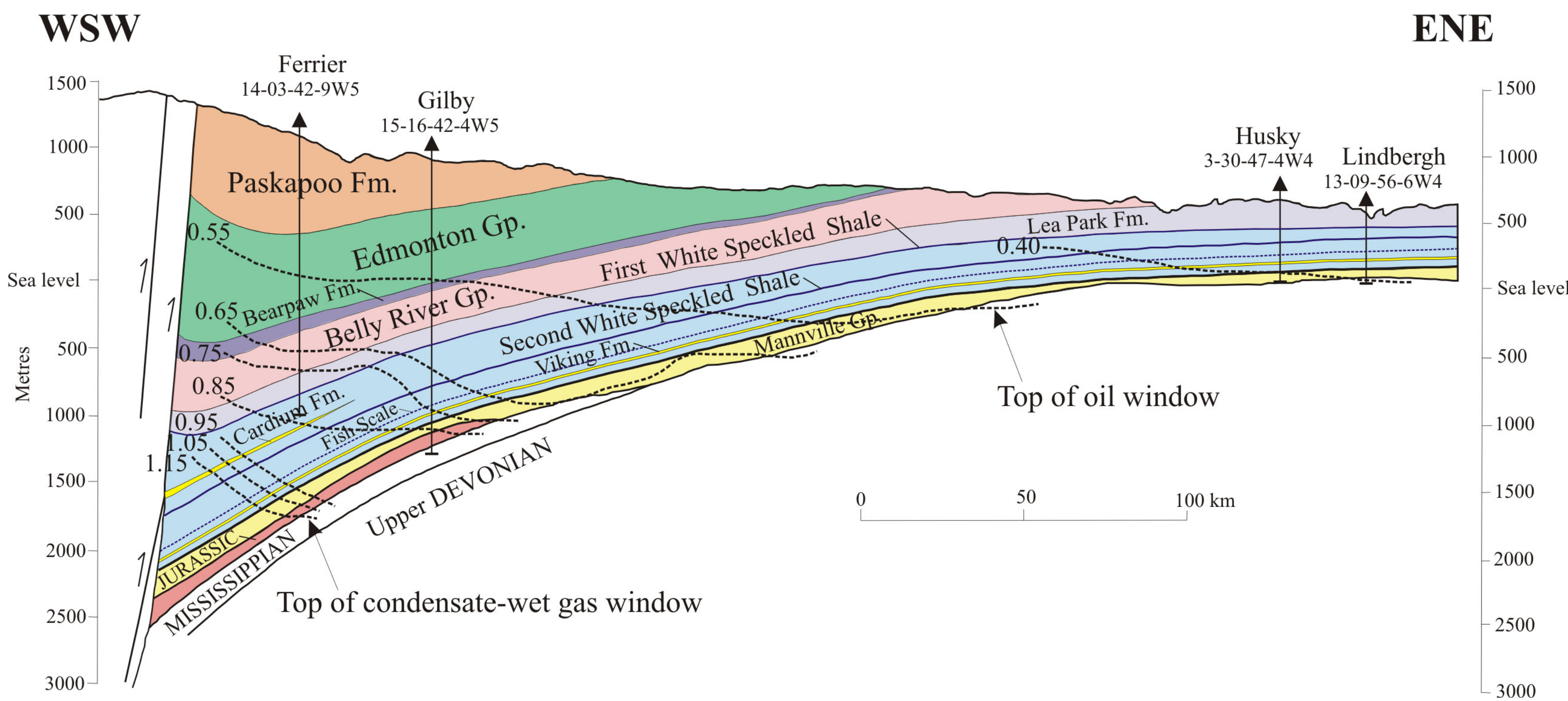

Figure 8-2. Schematic geological cross-section illustrating the relative positions of Ferrier, Gilby, Husky 3C-30, and Lindbergh 13A-9 profiles Thermal maturity of the foreland basin strata in the study areas is represented after Bustin, 1991. Isolines represent vitrinite reflectance Romax%. The location of the line of cross section (A-A') is shown in Figure 8-1.

heavier isotopic signature compared to those for the WCSB gases, therefore, this source of CH_4 will not be discussed further. Nevertheless, CH_4 from any of these various sources may possibly contribute to the natural gases and thus influence their overall composition.

It is generally accepted that depending on the geothermal gradient of the area, the depth and temperature limit for bacteriogenic CH_4 occurrence is about 2000 m and 70-80^0 C, respectively (Gűrgey et al., 2005). The maximum recorded borehole temperatures in the examined profiles were 56^0 C (Foothills region) and 25^0 C (Heavy oil region). Figure 8-2 shows that all of the mudgases depths (and corresponding temperatures) are suitable for bacteriogenic CH_4 formation. It is demonstrated in Figure 8-3 (a) that $\delta\ ^{13}C$ values for WCSB CH_4 gases show a good correlation with depth (towards heavier composition) eastward, in the Lloydminster area, but a puzzling trend for the foothills area. In the foothills area, in both Ferrier and Gilby profiles $\delta\ ^{13}C_{methane}$ values increase with depth from surface downward, to Scollard Formation, decrease down to ~ 600 m Sub Sea level (equivalent to the lower part of Belly River Formation in the Ferrier profile, and uppermost part of the Colorado Group in the Gilby profile), and then increase again to total depth.

Bacteriogenic gases are generally very dry [$(C_2$-$C_5)/C_1$-$C_5) < 0.5$], and composed almost entirely of methane (95-99% CH_4; Rice and Claypool, 1981). Schoell (1980) proposed that thermogenic and bacteriogenic gases can be separated based on their ^{13}C composition, and that $\delta\ ^{13}C_{methane}$ of ~ -55‰ separates the two groups; values less than -55‰ indicate a biogenic source and values greater than -55‰ indicate a thermogenic origin. Although a value of -55‰ provides a general guideline, bacteriogenic methane can have isotopic values ranging from less than -100‰ to -40‰ (Jenden and Kaplan, 1986; Whiticar et al., 1986) but thermogenic methane is rarely lighter than -55‰ (Schoell, 1980; Rice and Claypool, 1981; Barker and Fritz, 1981). As already mentioned, the methane analyzed in the present study ranges from -39.9‰ to – 79.46‰. The wetness index against depth diagram shown in Figure 8-3 (b) suggest that the majority of the gases sampled within the first 1150 metres are very dry, with one exception: the Lower Mannville gases from Husky profile (Lloydminster region). This is

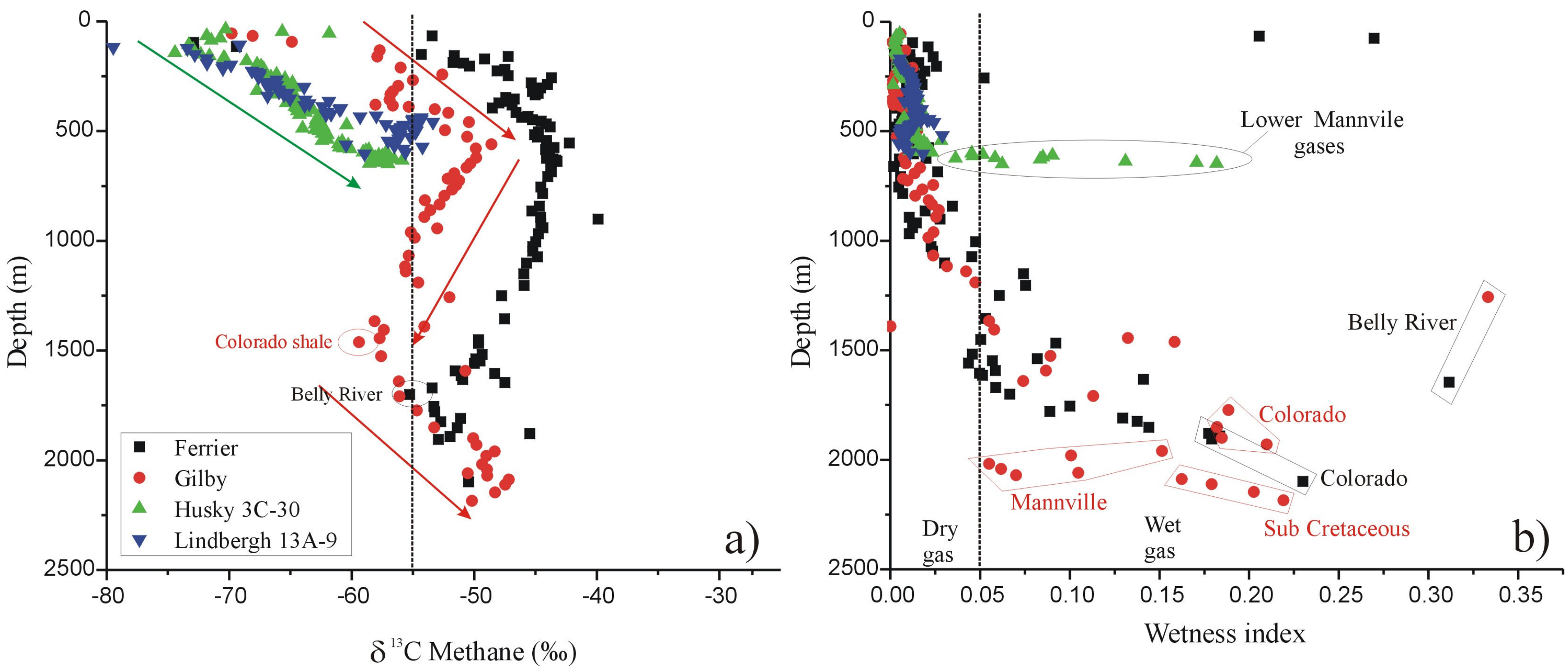

Figure 8-3 Plots of: (a) Depth - δ ^{13}C values for CH_4; (b) Depth – Wetness index profiles in the WCSB. The data used is derived from the four carbon isotope mudgas profiles plotted along the geological cross section from Figure 8-2.

not consistent with the results derived from Figure 8-3 (a), which show an overall isotopic composition heavier than -55‰. However, it must be remembered that the C2-C5 gases are preferentially dissolved in oil, leaving the gas phase enriched in CH_4. The gas phase released from this oil will be dry and rich in CH_4 and may result in misinterpretation (Clayton, 1981).

Referring to a modified Bernard's (1978) diagram (Figure 8-4), the analyzed methane gases could be classified mostly as thermogenic, and a mixture of bacteriogenic and thermogenic gases. A bacteriogenic component presence is clearly indicated by the molecular and isotopic composition of methane, and is additionally supported by the conclusions of a regional hydrogeological assessment done recently in the Alberta Basin (Harrison et al, 2006). The assessment has focused in the Interior Plains of Alberta (Township 35 to Township 52 and Range 25 W4M to Range 19 W5M), and points to the presence of "microbially derived gas" within the upper parts of the Scollard (Ardley)-Paskapoo formations. Moreover, previous studies which have incorporated isotope data and the hydrogeology of coal basins have demonstrated that secondary bacteriogenic methane can be produced in economic quantities at any coal rank (Scott, 1993; Scott et al., 1994).

8.1.1.1. Regional variations

Figure 8-5, a plot of wetness vs. methane $\delta^{13}C$, readily distinguishes between mudgases sampled in the Foothills region below a present day depth of approximately 400-500 m subsea (Lower Horseshoe Canyon – Ferrier, Lea Park – Gilby) from those sampled in the shallower part of the foothills profiles and in the heavy oil region (the only exception are the Lower Mannville gases from Husky profile). The wetness of the gases from the first group ranges from ~ 4.3% to 33%. In contrast, the wetness of the gases from the second group does not exceed 3.4%. Gases from the first group have also a relatively restricted range of methane $\delta^{13}C$ values. The wetness and the methane $\delta^{13}C$ data indicate a source within the oil window (Schoell, 1983) for the first group of gases.

Based on the classification in Figure 8-4 and Figure 8-5, and on conclusions from Chapter Four, most of the gases plot in the mixed gas field, and may have a dual bacteriogenic and thermogenic origin. However, Mannville gases from the Lloydminster

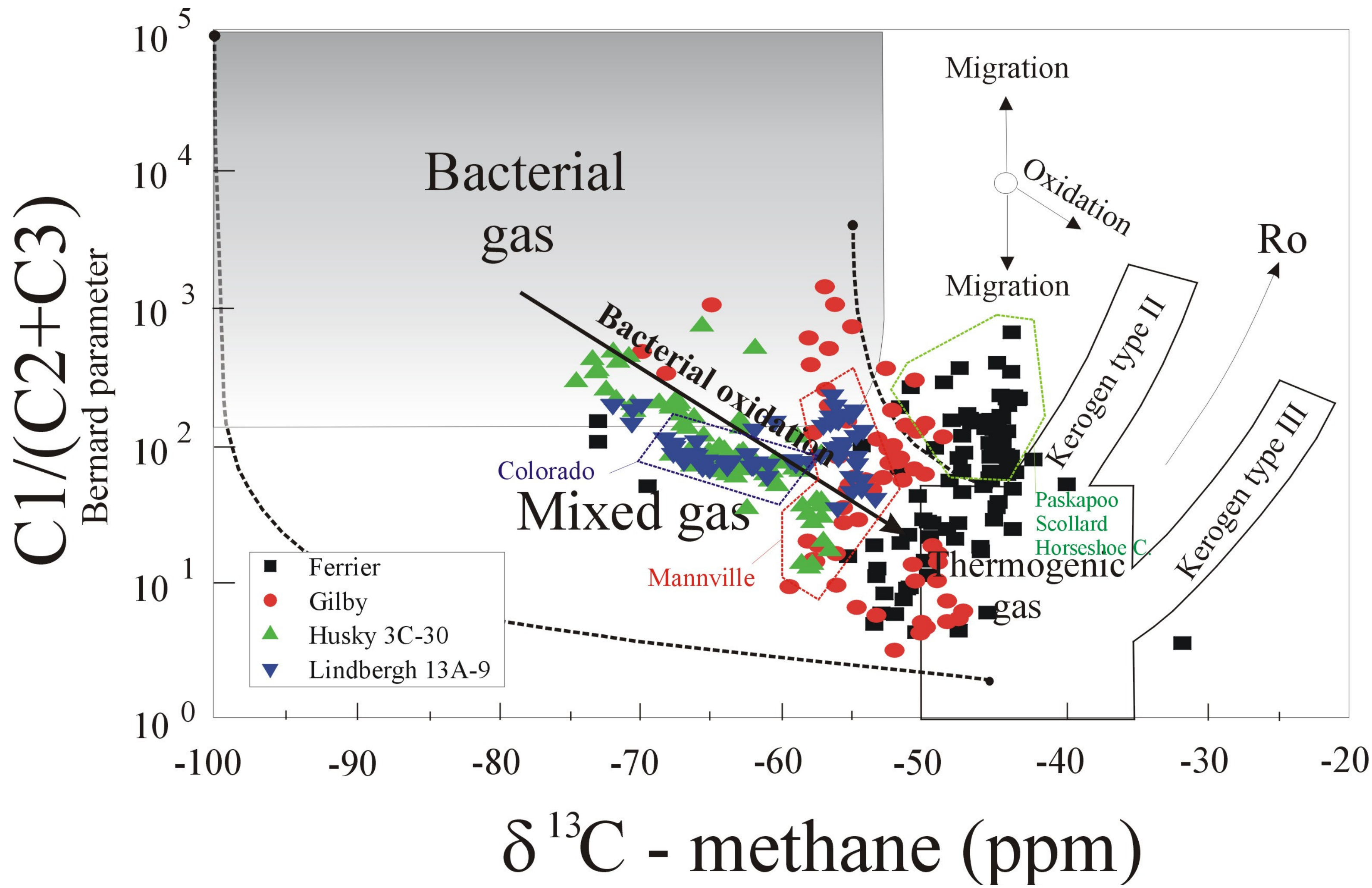

Figure 8-4 Bernard diagram showing the distribution of mudgases from four isotopic mudgas profiles plotted along the geological cross section A-A' from Figure 8-1. Mixtures of bacterial and thermogenic gases appear to be developed in majority of the gases, with a strong migrational component for shallower gases: Paskapoo and Scollar, in the Ferrier profile.

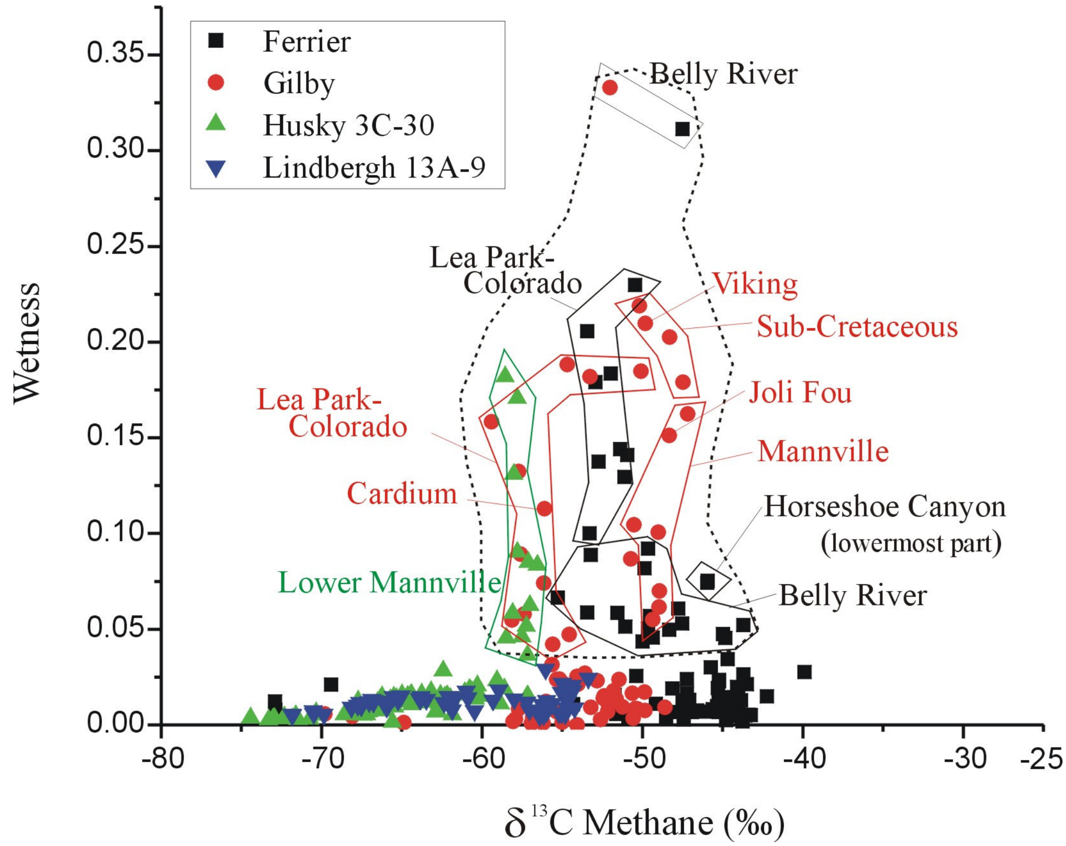

Figure 8-5 Plot of wetness vs. methane $\delta^{13}C$ of the mud gas data of the four isotope depth profiles in Figure 8-2.

heavy oil region plotted outside of the thermogenic gas field in Figure 8-4 (the red dashed boundary zone) could also be regarded as early thermogenic gases which have lost their C2+ hydrocarbon components during migration into shallow stratigraphic section. In the same way, Colorado Group gases from the same region, plotted in the mixed gas field as well (the blue dashed boundary zone in Figure 8-4) could also be regarded, as already discussed (Chapter Four), as immature thermogenic gases.

8.1.1.2. Mixing of thermogenic and bacteriogenic methane

Support for bacteriogenic and thermogenic gas mixing in many of the WCSB analyzed gases is also suggested by a plot of methane $\delta^{13}C$ vs. ethane $\delta^{13}C$ (Figure 8-6). Published data suggest that for cogenetic gases, (δ^{13}Cethane - δ^{13}Cmethane) probably does not exceed 18‰ and rarely is less than 5‰ except in supermature gases (Sundberg and Bennett, 1983; Jenden and Kaplan, 1988). Figure 8-6 shows that with some exceptions, gases from WCSB plot within these limits. However, many of the eastern WCSB gases (Lloydminster area), and even some of the foothills gases plot well outside the cogenetic region in the direction expected for mixing with isotopically light bacteriogenic methane. One of the Lea Park gas, for example, has (δ^{13}Cethane - δ^{13}C methane) equal to 26.76‰.

8.1.2. δ ^{13}C of C2+ hydrocarbons

Ethane values range from -58.98‰ (Lea Park Formation, Lloydminster region) to -20.47‰ (Cummings Formation, Lindbergh field, Lloydminster region). Propane values range from -47.14‰ (upper Colorado shales, Lloydminster region) to -14.91‰ (Cummings Formation, Lindbergh field, Lloydminster region). Normal butane values range from -44.96‰ (Colorado shales, Lloydminster region) to -17.87‰ (Cummings Formation, Lindbergh field, Lloydminster region). Isobutane values range from -48.10‰ (Paskapoo Formation, foothills region) to -16.95‰ (Waseca Formation, Lloydminster region).

Compared to methane, relatively few δ^{13}C data for the C_{2+} hydrocarbons have been published (Colombo et al. 1965; Galimov et al., 1970; Smith et al. 1971; Stahl and Carey, 1975; Rigby and Smith, 1981; James, 1983; Schoell, 1984). Published ethane δ ^{13}C data for natural gases are generally less negative than -45‰ and range up to -20‰.; most propane δ^{13}C data range from -35‰ to -20‰.

Very light values for ethane (-50‰ to -70‰) might be due to reduction of two carbon carboxylic acids, such as acetic and oxalic acid, in a process analogous to bacterial methanogenesis (Claypool, 1999). One of the most depleted value for ethane δ ^{13}C (-73.9‰) has been reported for the Judith River Formation in Western Canada Sedimentary Basin (Taylor et al., 2000). According to these authors, ethane δ^{13}C values provide an important diagnostic parameter for differentiating bacteriogenic from thermogenic natural gases. Following the approach of Bernard et al. (1977), they

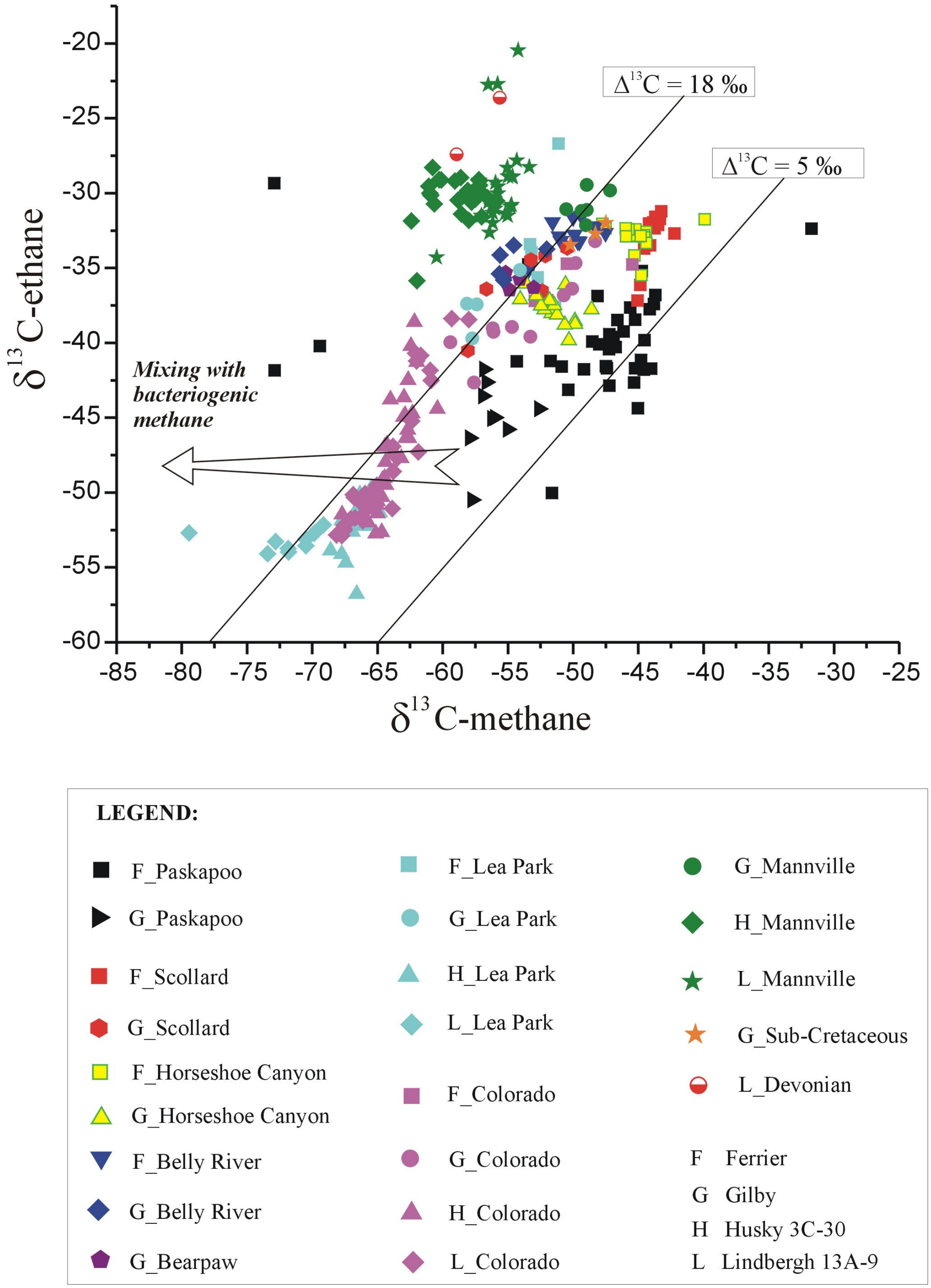

Figure 8-6 Plot of methane $\delta\,^{13}C$ vs. ethane $\delta\,^{13}C$ of the mud gas data of the four isotope depth profiles in Figure 8-2. Published data indicate that cogenetic gases have 5‰< (δ^{13}Cethane - δ^{13}C methane) < 18‰. Mixing with isotopically light bacteriogenic methane shifts gas compositions outside the cogenetic field in the direction shown by the arrow.

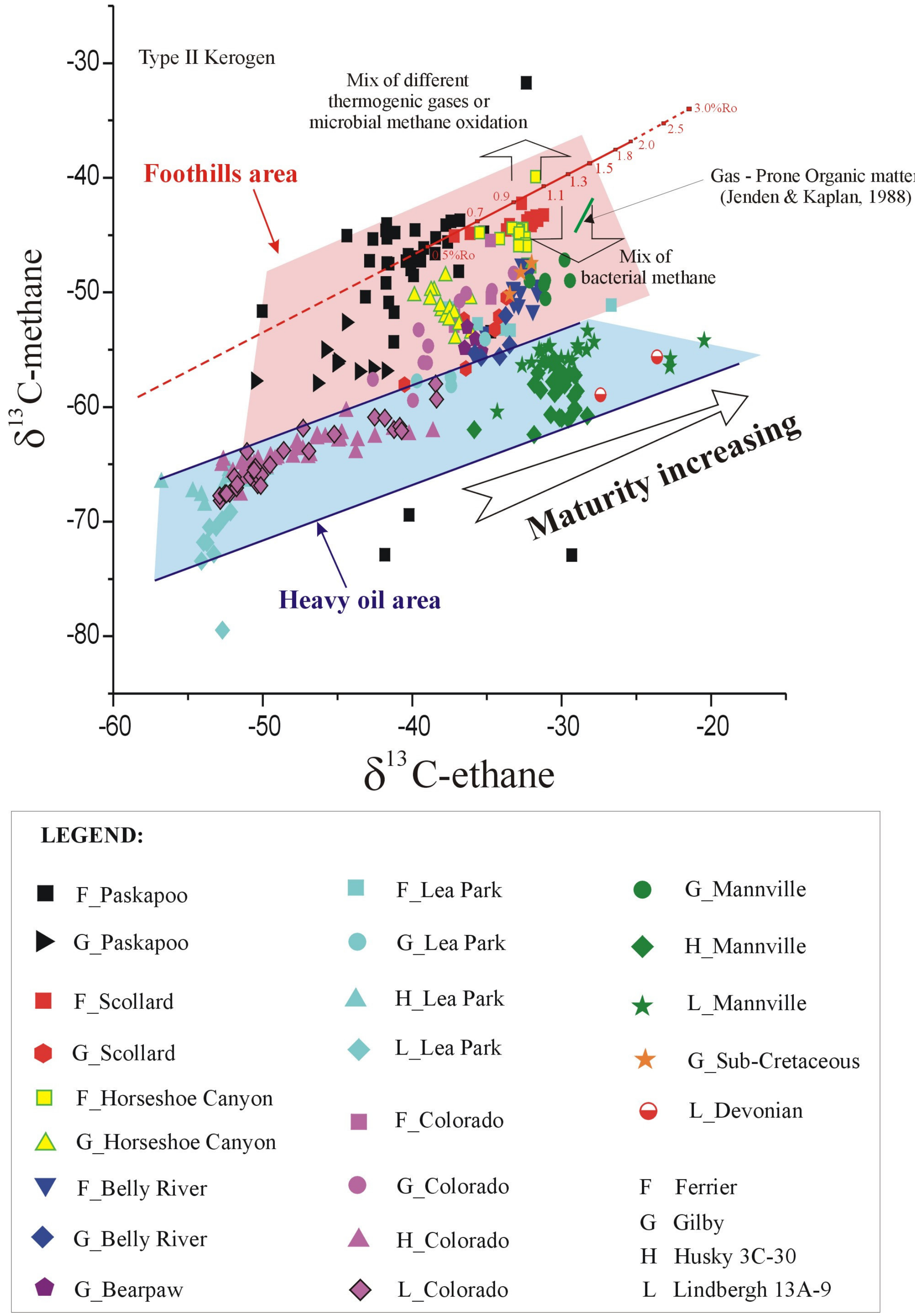

Figure 8-7 Plot of ethane δ ^{13}C vs. methane δ ^{13}C of the mud gas data of the four isotope depth profiles in Figure 8-2. Two main clusters are shown: foothills-, and heavy oil gases. Position of the vitrinite reflectance curve for type II kerogen: after Faber (1987), and Whiticar (1990).

propose a value of -45‰ for ethane $\delta^{13}C$ in order to discriminate deeper thermogenic from near-surface bacteriogenic gas.

In contrast to most published values, the WCSB mudgas data analyzed in this study seems more broadly distributed. The methane vs. ethane isotope diagram of natural gases from the four representative isotope profiles across WCSB is illustrated in Figure 8-7, which shows two main clusters: foothills gases and heavy oil gases. The heavy oil gases have a characteristic increase of methane isotopes as ethane isotope value increase, demonstrating a maturity trend and an apparent genetic relationship between them. The foothills group gases appear to be a mixture of at least two distinct components: a dry low maturity gas and a wet, more mature thermogenic gas. The low maturity gas, composed of bacterial methane and isotopically light ethane (as low as -50.49‰) is inferred to be indigenous to the shallow part of the basin, and generated in the Paskapoo – Scollard formations. The more mature thermogenic gas has presumably been generated from deeper buried source rocks along the basin axis and has migrated both vertically (Belly River sandstones) and updip to the east. This gas is best characterized by natural gases from the Mississippian Pekisko Formation, Jurassic "Nordegg" Member of the Fernie Group, Lower Cretaceous Glauconitic Member of the Mannville Group, Cretaceous Belly River Group, and Cretaceous Horseshoe Canyon Formation. This hypothetical two-component mixing model can help explain the distribution of the Foothills gas data and their deviation from the expected ethane $\delta\ ^{13}C$ vs, methane $\delta\ ^{13}C$ maturation trend. Because the dry gas mixing end member is generated well past the oil window (see Figure 8-2), it contains much less ethane than the wet gas mixing end member.

8.1.2.1. Maturity trends versus source effects versus biodegradation

Figure 8-7 shows the comparison of carbon isotope ratio of methane vs. ethane for hydrocarbons generated from kerogen type II. Points of isomaturation (%Romax) are indicated on the figure. As the degree of maturation increases for the single source, the $\delta\ ^{13}C_{methane}$ and $\delta\ ^{13}C_{ethane}$ will follow along the empirical line. Departures from colinearity are strong indicators of secondary effects such as the admixtures of a bacterial gas or of a different thermogenic gas (Whiticar, 1996). Methane oxidation would also shift the methane-ethane isotope pair off the line because methane is preferentially consumed by bacteria, and the microbial uptake is associated with an isotope effect which enriches the residual methane in ^{13}C (Whiticar and Faber, 1986). It is obvious that measured isotope data of both methane and ethane deviate significantly from the calculated empirical values. As already proposed, this deviation of methane and ethane isotopes from the model towards values that indicate an enrichment of ^{12}C can be explained by an admixture of bacteriogenic gases to thermal gases.

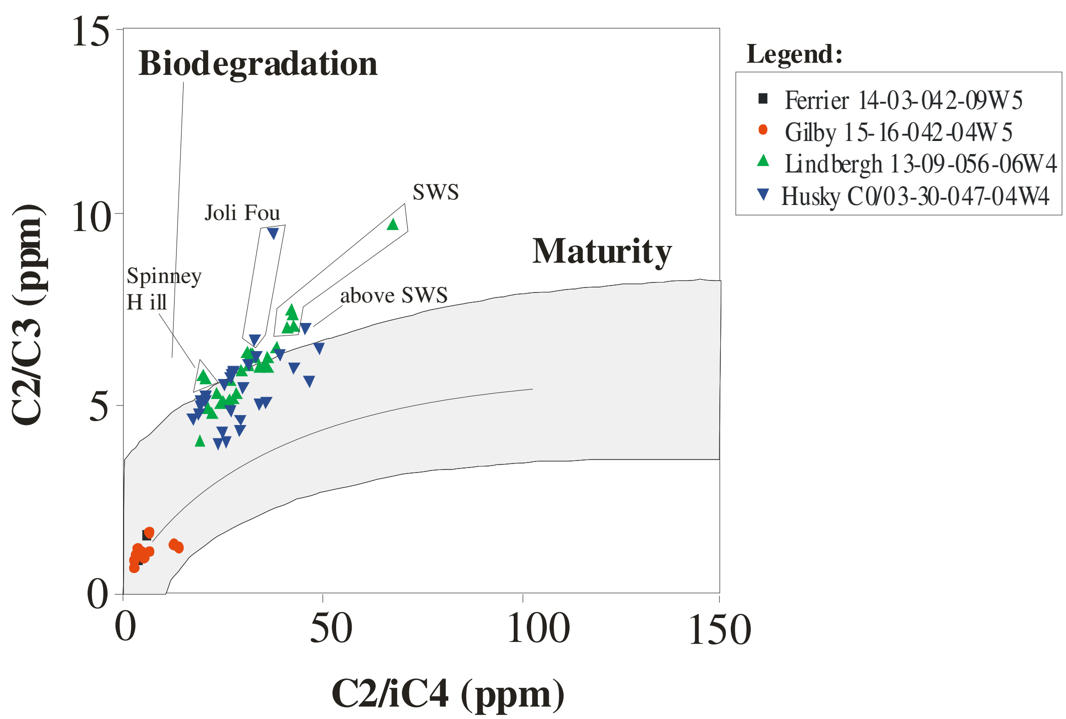

Figure 8-8 C2/C3 versus C2/iC4 diagram showing the possible biodegradation of some of the Colorado hydrocarbon gases from the Lloydminster heavy oil area (after Prinzhofer, 2000)

According to Jenden et al. (1988) it is very difficult to try to estimate gas maturities using methane and ethane data. The correlation between $\delta\ ^{13}C_{methane}$ and $\delta\ ^{13}C_{ethane}$ is surprisingly poor ($R^2 = 0.3892$; Figure 8-7). A better correlation exists between ethane $\delta\ ^{13}C$ and propane $\delta\ ^{13}C$ ($R^2 = 0.8469$; Figure 8-10). Regression of propane $\delta\ ^{13}C$ on ethane $\delta\ ^{13}C$ gives a line with slope 0.7327. However, Faber's line is displaced by ~

2‰ towards lighter propane δ ^{13}C values. A number of gases plot above the maturation line and may be oxidized. The oxidation trends illustrated in Figure 8-10 by red rectangles are defined by samples from Colorado Gp. (Lloydminster heavy oil area), Paskapoo Formation (Ferrier profile), and Mannville Gp. (Lloydminster heavy oil area).

Figure 8-8 shows a plot of C2/C3 versus C2/iC4 diagram which enables gases fractionated through thermal cracking to be distinguished from gases having suffered bacterial alteration (Prinzhofer et al., 2000). Except Ferrier and Gilby gases (Foothills region), all the analyzed Colorado gases in the Lloydminster region show trace of bacterial alteration (Joli Fou in Husky, and SWS in Lindbergh). One of the Joli Fou sample (527m depth, Husky) presents as well a very high Δ δ ^{13}C (C2-C1) value (>20), which indicate biodegradation as well (Pallaser, 2000).

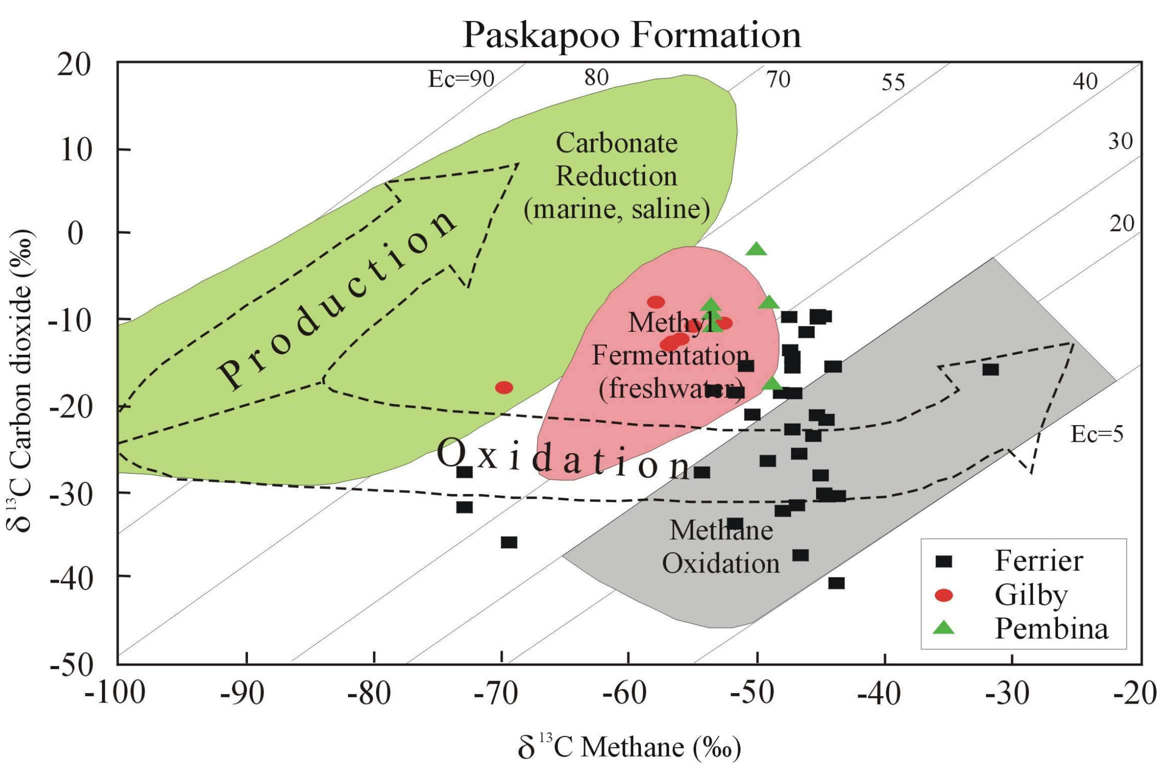

Figure 8-9 Combination plot of $\delta^{13}C_{CO2}$ and $\delta^{13}C_{CH4}$ with isotope fractionation lines (Ec) for the Paskapoo Formation gases in the foothills area (after Whiticar, 1999).

Regarding Paskapoo gases at Ferrier location, they are believed to be bacterial gases, which suffered the process of methane oxidation by bacteria introduced by meteoric waters. This is confirmed by the combination plot of $\delta^{13}C_{CO2}$ and $\delta^{13}C_{CH4,}$ with isotope fractionation lines (Ec) – proposed by Whiticar (1999). Figure 8-9 shows the bacterial methane formation and consumption pathways for the Paskapoo gases at Ferrier, Pembina and Gilby locations. As can be observed, the associated carbon dioxide at Ferrier location is isotopically light (<-20 ‰), which is interpreted to be a kinetic isotope effect of oxidation induced by bacterial action, resulting in preferential incorporation of ^{12}C into the CO_2, which leaves the residual light hydrocarbons isotopically heavier. Another key point is that the carbon isotopic fractionation factor between $\delta^{13}C_{CO2}$ and $\delta^{13}C_{CH4}$ remains consistent for, and indicative of specific setting or diagenetic environment (Whiticar, 1999). CH_4 oxidation causes a strong, clear carbon isotopic separation ($\delta^{13}C_{CO2}$ - $\delta^{13}C_{CH4}$), usually between 5 and 25 towards the latter stages of consumption (Whiticar, 1999).

From carbon isotope values of ethane and propane it appears that Foothills gases were generated from both immature source rocks (Romax < 0.5 %) and source rocks that reached maturities in the oil window and wet gas window between 0.55% and a maximum of ~1.5% Romax (in the Mannville Gp. – at Gilby).

On the cross-plots in Figure 8-7, 8-10 and 8-11, Cretaceous Colorado Gp. and Lea Park Formation gases from Lloydminster heavy oil region, identified by Rowe and Muehlenbachs (1999a) as low temperature thermogenic gases occur at the lowest ethane $\delta\ ^{13}C$ vs. propane $\delta\ ^{13}C$ values. These very low maturity gases occur in sediments with estimated Ro values as low as 0.25% (Rowe and Muehlenbachs, 1999b).

In addition to maturity, however, Figure 8-10 probably also reflect variations in source of the organic matter. Pyrolysis experiments have shown that $\delta^{13}C$ of methane derived from gas-prone organic matter is isotopically heavier than $\delta^{13}C$ of methane formed from the cracking of long chain hydrocarbons and oil-prone organic matter (Frank et al. 1974; Chung, 1976; Chung and Sackett, 1980; Rohrback et al., 1984). It seems reasonable to assume that organic matter type could exert an important influence on ethane and propane $\delta\ ^{13}C$ values also. Some of the Horseshoe Canyon and Scollard gases in the foothills area may be an example of gas generation from kerogen type III.

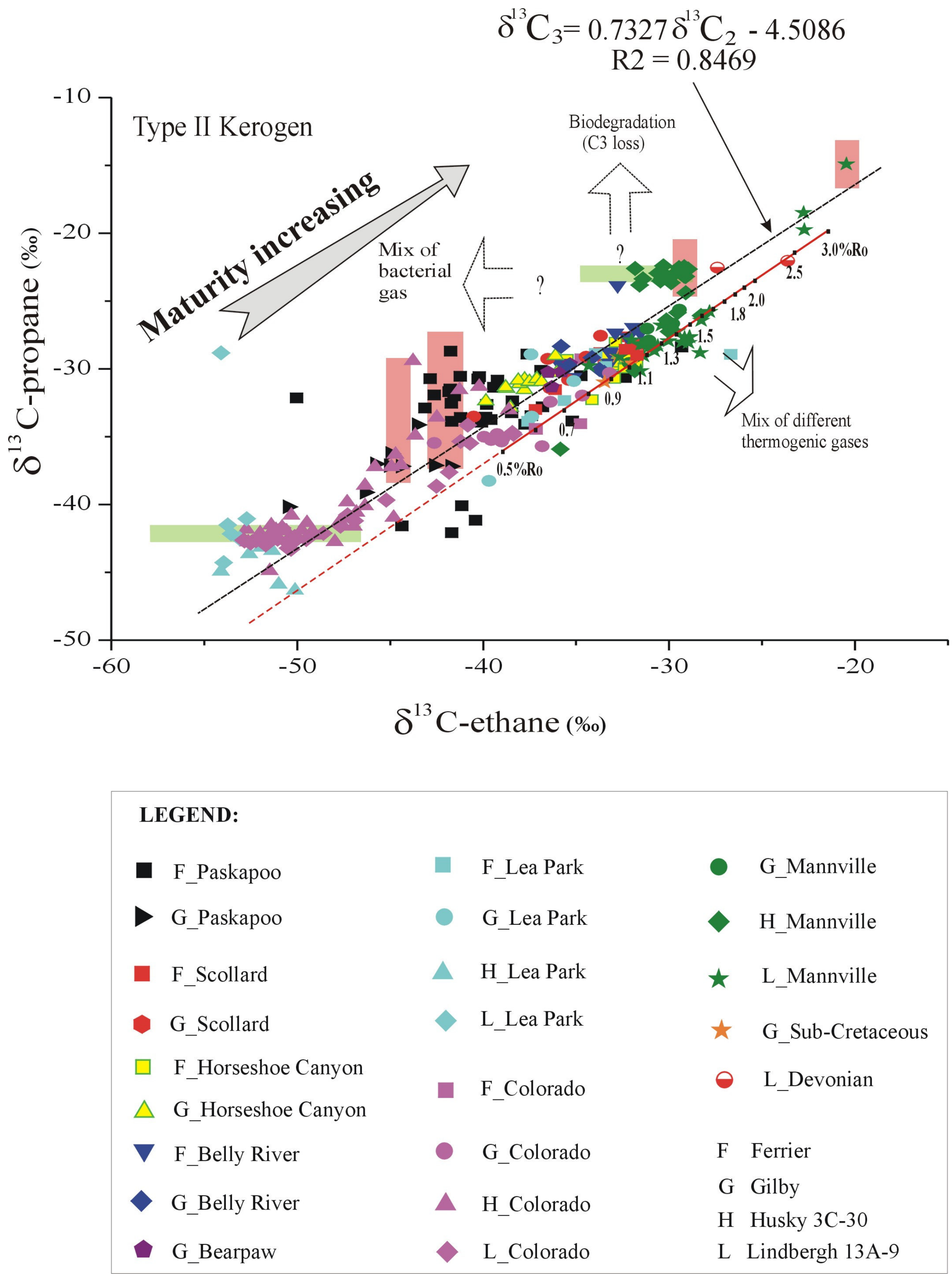

Figure 8-10 Plot of ethane δ ^{13}C vs. propane δ ^{13}C of the mud gas data of the four isotope depth profiles in Figure 8-2. The maturity relation (red line) is taken from Faber (1987), and Whiticar (1990).

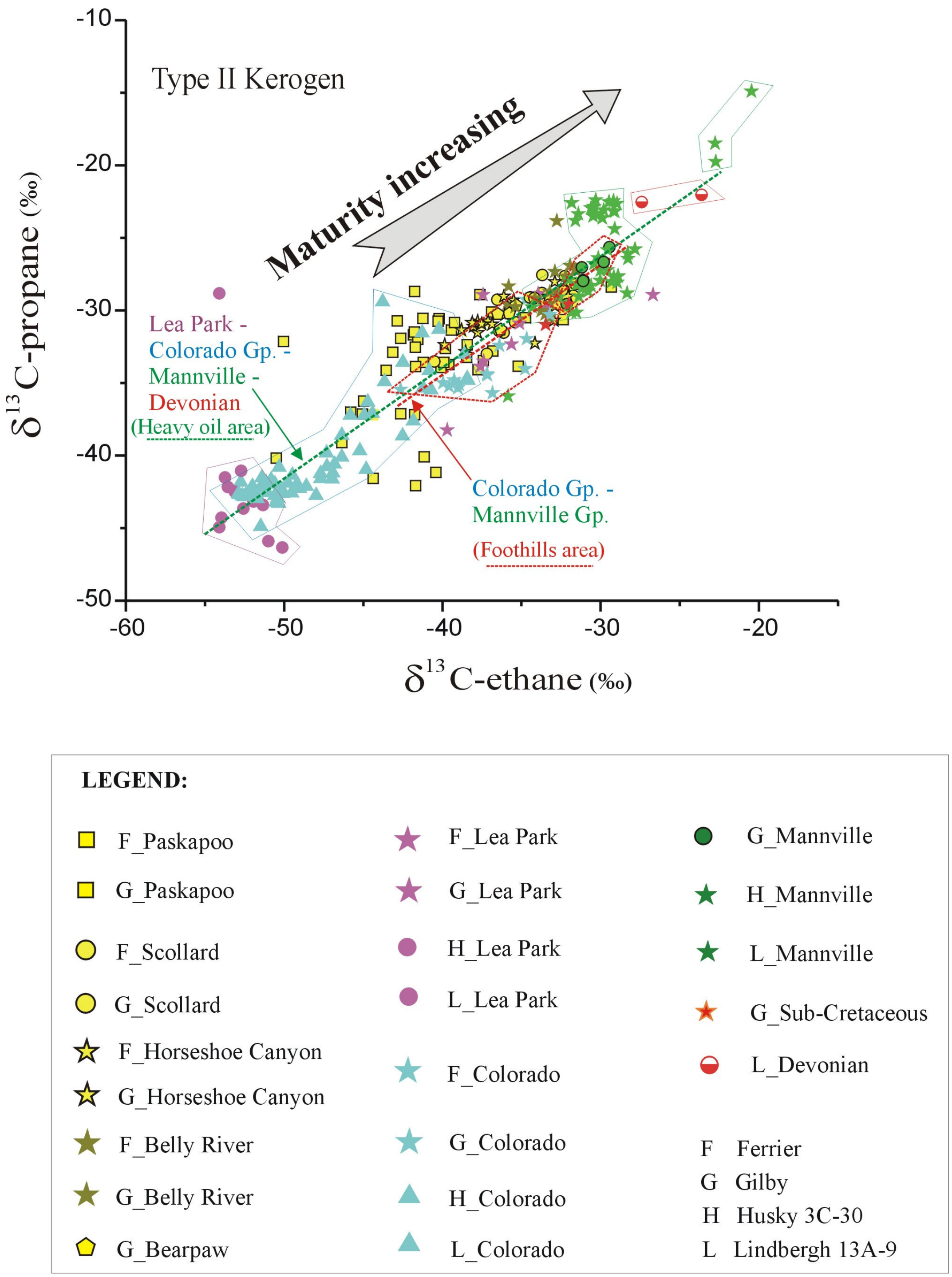

Figure 8-11 Plot of ethane δ ^{13}C vs. propane δ ^{13}C of the mud gas data of the four isotope depth profiles in Figure 8-2. Apart from Figure 8-9, here gases are grouped by stratigraphic unit (from oldest to youngest): Sub-Cretaceous (red symbols), Cretaceous Mannville (green symbols), Cretaceous Colorado (blue symbols), Cretaceous Lea Park (purple symbols), Cretaceous Belly River (dark yellow symbols), and Cretaceous-Tertiary Edmonton Gp to Paskapoo (yellow symbols). Two apparent maturity trends are shown: the red dashed line in the foothills area, and the green dashed line in the heavy oil area.

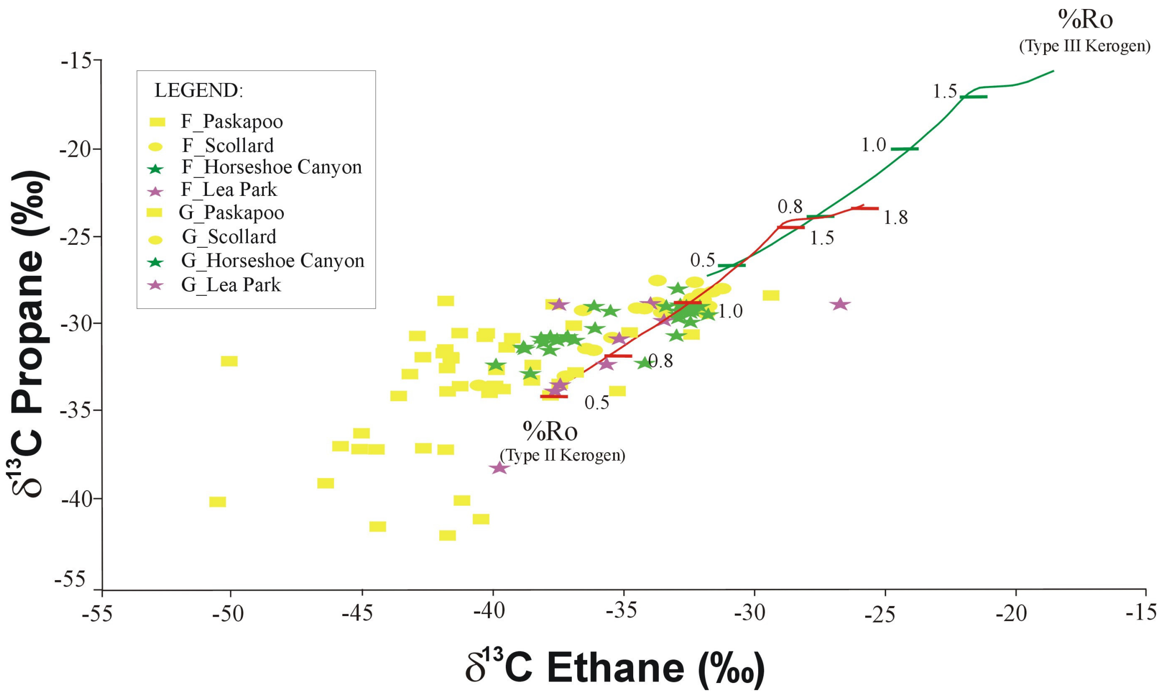

Figure 8-12 Graph of ethane δ ^{13}C vs. propane δ ^{13}C for mudgas samples from the Lea Park-, Horseshoe Canyon-, Scollard, and Paskapoo formations – foothills region. Lea Park sediments are dominated by Type III organic matter ((Schröder-Adams et al., 1997), and Horseshoe Canyon – Paskapoo formations contain coal beds throughout. Maturity curves: after Berner and Faber (1996).

As illustrated in Figure 8-7, these gases plot closer to the ethane δ ^{13}C versus methane δ ^{13}C relation for gas – prone organic matter in the Sacramento basin (Jenden and Kaplan, 1988). Moreover, if instantaneous isotope/maturity models of Berner and Faber (1996) for gases of Type II and Type III source rocks are applied to these gases (Figure 8-12) – it appears that gases plotting closer to the terrestrial line (and the inferred extension of it) can be explained through generation from huminitic precursors, whereas samples closer to the line of gases from exinitic substances may be explained as such. Gases plotting in between the maturity lines can be explained as mixtures of the two sources.

Obviously, what looked as single maturity trends in Figure 8-11, now can be interpreted as at least three different ones, related to two different types of organic precursors:

- a clear Cretaceous gas maturity trend from the foothills area (Colorado-, to Mannville Group);

- a Cretaceous to Devonian gas maturity trend from the heavy oil area (Lea Park-, to Colorado Group, to Mannville Group, to Devonian);
- a Cretaceous – Tertiary gas maturity trend from the foothills area, related to a predominant Type III organic precursor (Paskapoo-, to Scollard-, to Horseshoe Canyon Formation).

Interestingly, predicted maturities for huminitic precursors appear to match the maturities that occur at the depth level at which the samples were collected (see Figure 8-2 for reference). The Paskapoo – Scollard gases were collected from host sediments where Ro max < 0.5% (Bustin, 1991). For gases that presumably were generated from both huminitic and exinitic sources (e.g. Lea Park, and lowermost Horseshoe Canyon gases) the correlation suggest that the gases were generated from sources that occur at the depth level at which the samples were collected.

Using this approach, the Lea Park – Paskapoo gases from foothills region seem to share a common maturity level (%Ro = <0.5 - ~0.9), which corresponds to an early and very early mature stage within the oil window. Within this region, although there seems to be a general correlation between the maturity of the gas (related to two different types of organic precursors) and maturity of the host sediments, at least one notable exception stands up: gas from younger Belly River Group in the foothills area seems more mature (Romax = 0.8 – 1.3) than gas from the underlying Lea Park and Colorado Group (Romax = 0.6 - 0.95). This suggests that gas migrated updip within the permeable near-shore and fluvial sandstones of the Belly River Group from deeper in the basin (the most probable source being the Jurassic – Mississippian strata; see Figure 8-13 and 8-14).

The main biodegradation trends in Figure 8-10 (red rectangles) are defined by the Mannville gases and some of the Colorado Group gases (Joli Fou, Spinney Hill, and Viking gases) - in the heavy oil region, and Paskapoo gases at Ferrier location. These trends are understood as the result of microbial oxidation. Microbial oxidation of natural gas enriches the residual hydrocarbons in ^{13}C, resulting in less negative $\delta\ ^{13}C$ values (Barker and Fritz, 1981; Coleman et al., 1981). In systems containing a mixture of hydrocarbon gases, microbes may attack the longer chain hydrocarbons more rapidly than

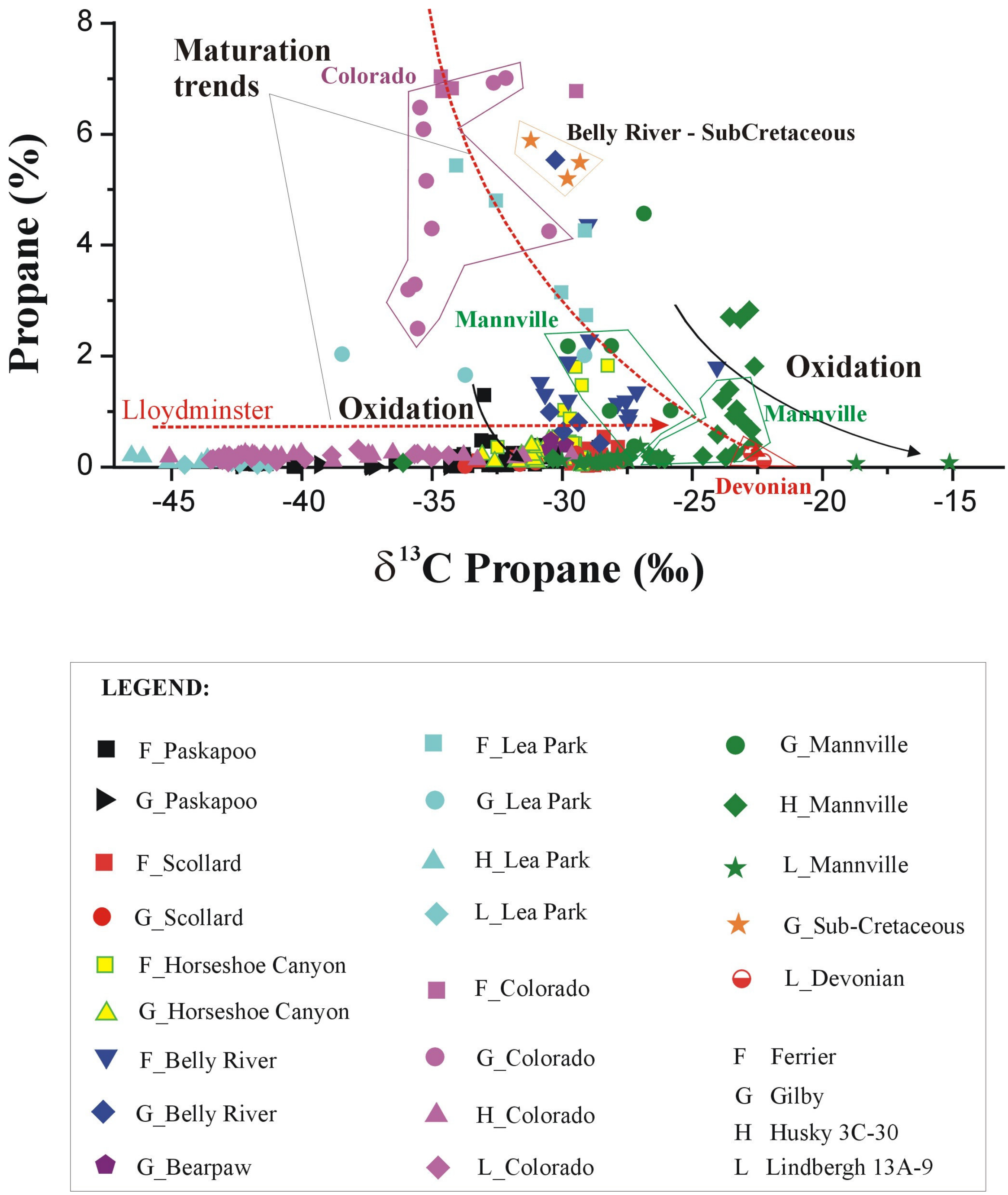

Figure 8-13 Plot of propane concentration vs. propane δ ^{13}C of the mud gas data of the four isotope depth profiles in Figure 8-2. As in Figure 8-10, effects of maturation and oxidation are distinguished.

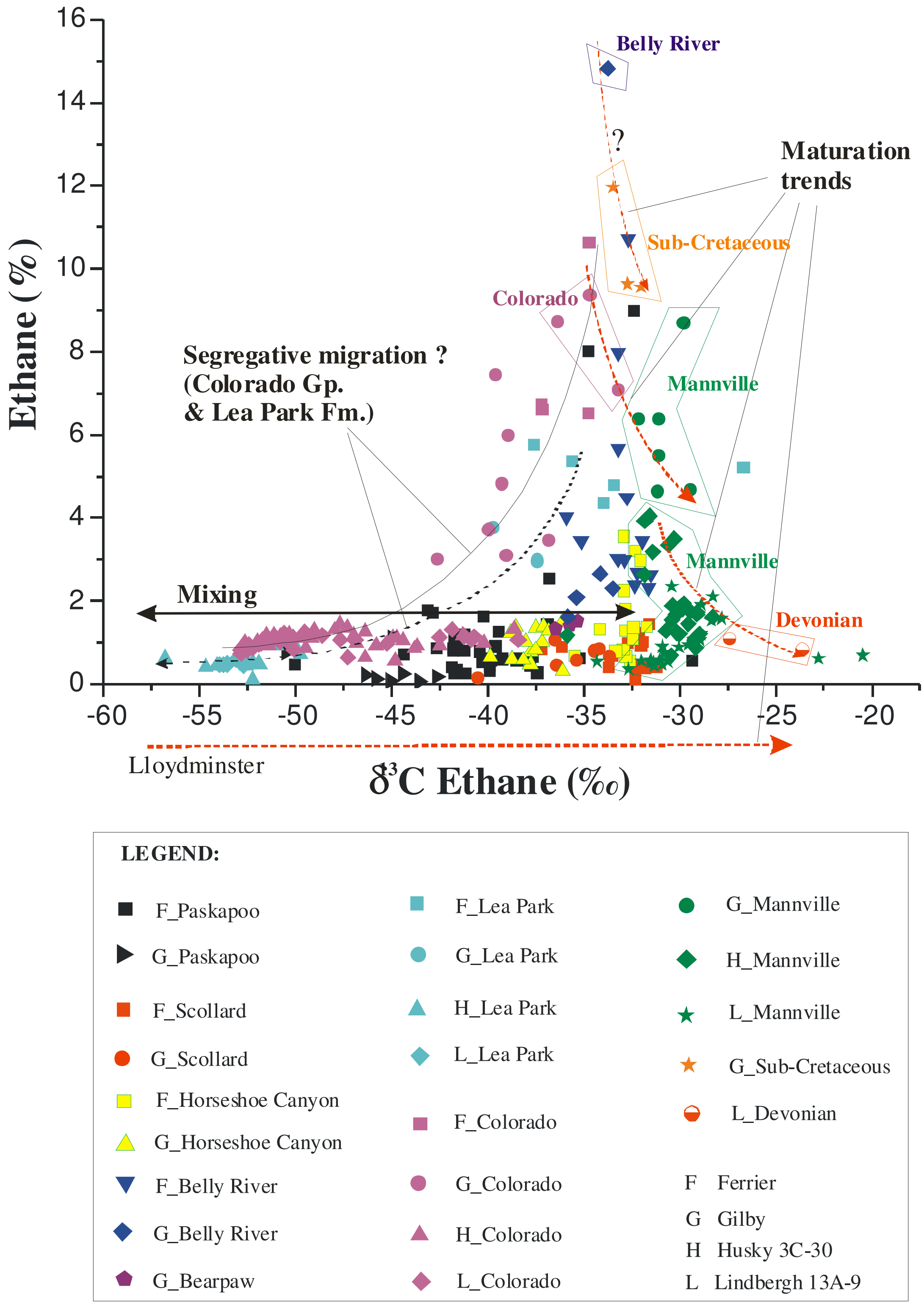

Figure 8-14 Plot of ethane concentration vs. ethane $\delta^{13}C$ of the mud gas data of the four isotope depth profiles in Figure 8-2. Arrows indicate maturation trends, and distribution of mixed gases (bacteriogenic and migrated).

the short-chain hydrocarbons (Stahl, 1980). During the earliest stages of oxidation, however, propane appears to be selectively removed (James and Burns, 1984). In Figure 8-10 propane $\delta^{13}C$ values increases from ~ -35‰ to -29‰ (Colorado Gp.) with little change in ethane $\delta^{13}C$. After more extensive alteration, ethane also appears to be attacked; as propane $\delta^{13}C$ values increases from ~ -25‰ to -15‰, ethane increases from -29‰ to -21‰ (Mannville Gp., - heavy oil area).

Figure 8-13 shows that the concentration of propane in the altered gases does decrease with increasing propane $\delta^{13}C$. Like Figure 8-10, this plot also indicates that the effects attributed to oxidation are quite distinct from those of maturation. The effects of oxidation are not easily recognized in Figure 8-14; among the altered gases, only two Mannville samples have anomalously heavy ethane values.

8.1.2.2. Carbon isotope fractionation

James (1983) and Sundberg and Bennett (1983) have noted that with increasing maturity the carbon isotope fractionations between ethane and propane and between ethane and methane decrease for cogenetic hydrocarbons. The models developed by these authors are illustrated in Figure 8-15. They are attractive because they offer a means of estimating source rock maturities and distinguishing cogenetic hydrocarbons from gas mixtures. The WCSB mudgas data plot well off the maturation lines, and the effect of gas mixing can be clearly seen. As already discussed, many of these WCSB mudgases are mixtures of thermogenic and bacteriogenic gases and should not be expected to fit. These samples will be shifted to the right and above any of the maturation line. Due to the selective removal of propane, biodegraded gases may often plot above the maturation line, at high $\delta^{13}C$ (propane – ethane) values.

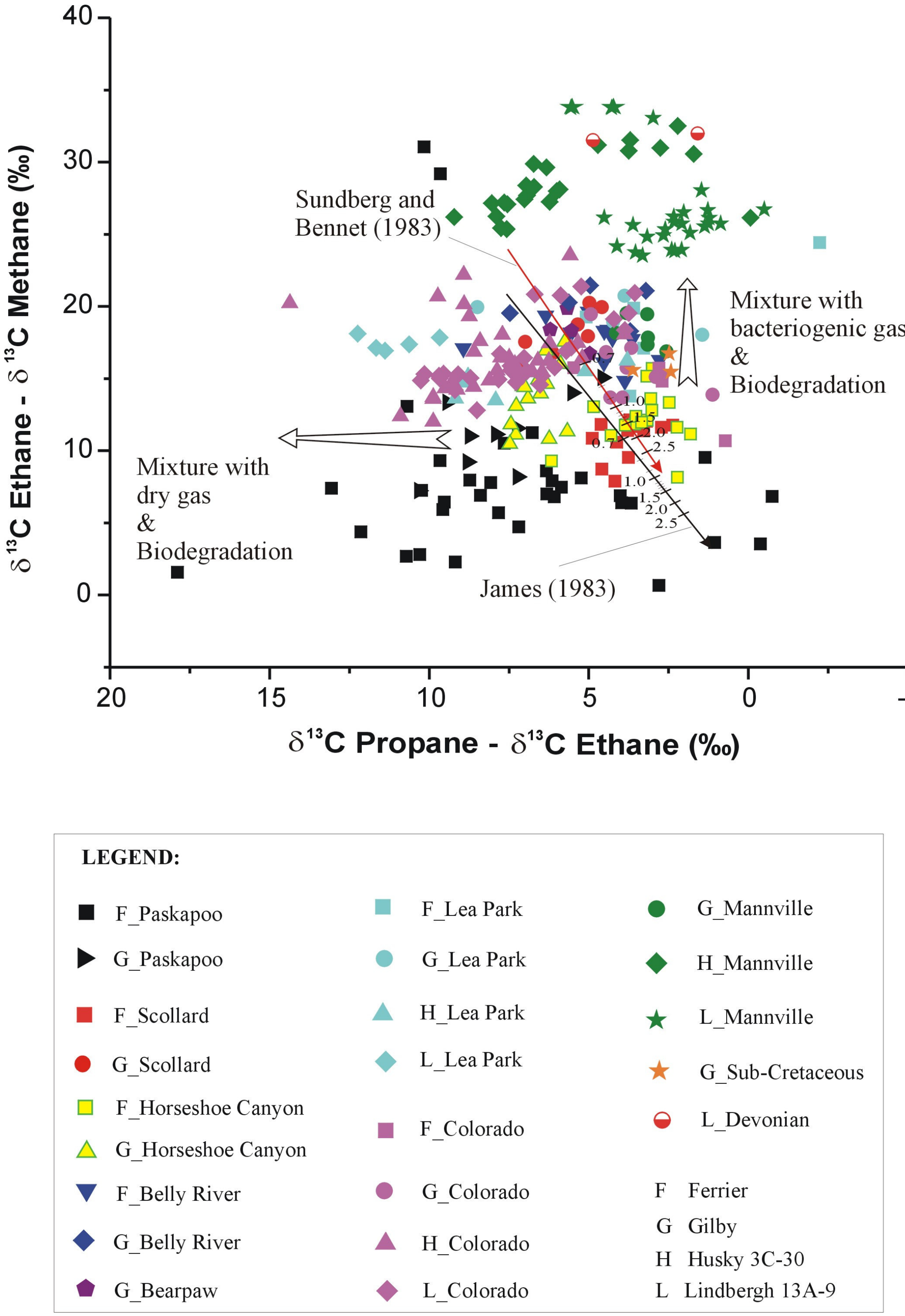

Figure 8-15 Carbon isotopic difference between propane and ethane vs. that between ethane and methane for mudgas data of the four isotope depth profiles in Figure 8-2. Maturation arrows are based on the models of James (1983) (black arow), and Sundberg and Bennet (1983) (red arrow).

8.1.2.3. Mixing of thermogenic and bacteriogenic ethane

As already mentioned, the origin of ethane with $\delta^{13}C$ less than -45‰ is still uncertain. In the Lloydminster heavy oil area, ethane $\delta^{13}C$ values as negative as -58.98‰ have been measured in the Lea Park Formation, and as low as -53.05‰ in the Colorado Group shales. In order to resolve for the uncertainty concerning the isotopic signature of bacteriogenic ethane and to distinguish between bacteriogenic and thermogenic hydrocarbon gases, a natural gas classification scheme based on CH_4/C2+ versus ethane $\delta^{13}C$ can be used (Taylor et al. 2000). As illustrated in Figure 8-16, a value of -45‰ for ethane isotopic signature demarcates an empirical bacteriogenic and thermogenic field for Colorado Group gases in two of the mudgas depth profiles from the Lloydminster region.

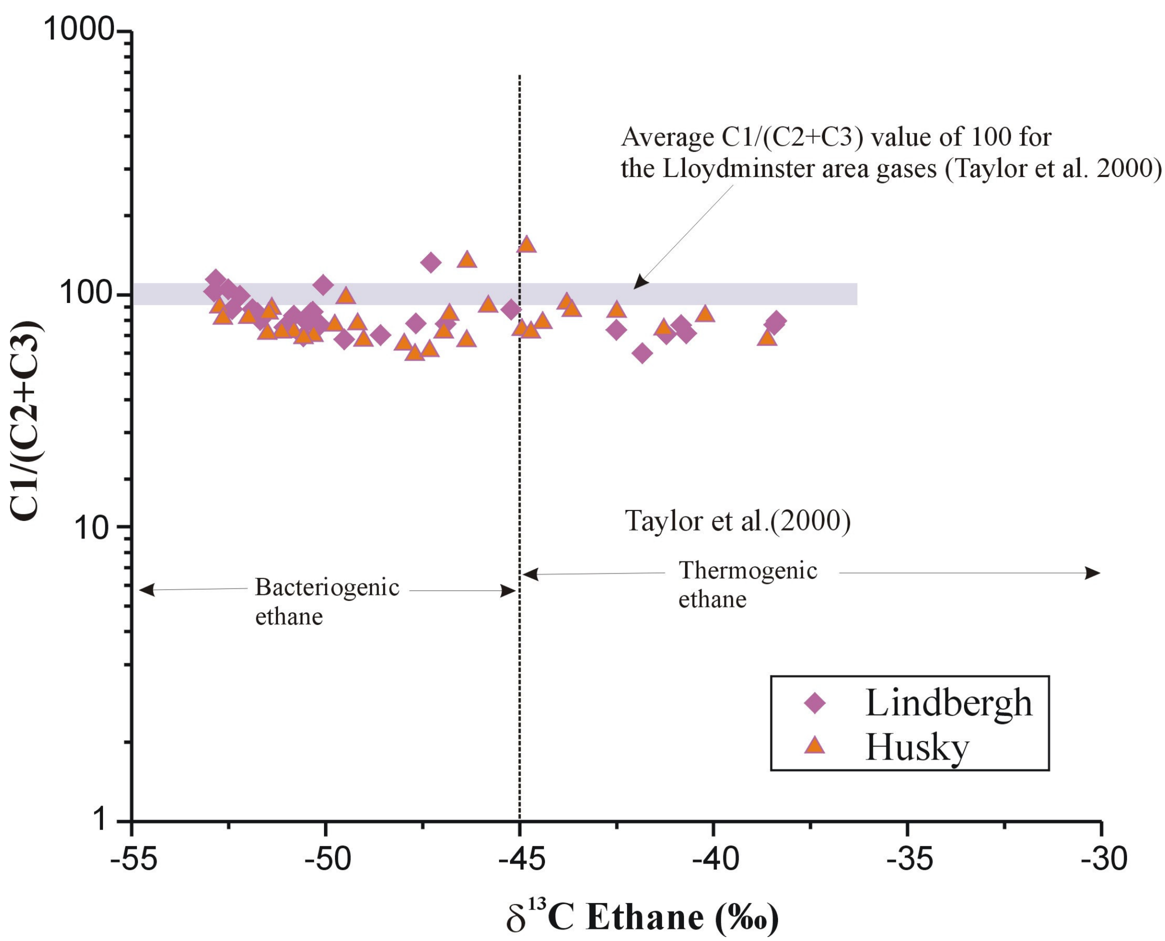

Figure 8-16 Plot of ethane $\delta^{13}C$ vs. Bernard parameter [C1/(C2+C3)] for the Colorado mudgases in Husky 3C-30-47-4W4 and Lindbergh 13A-9-56-6W5.

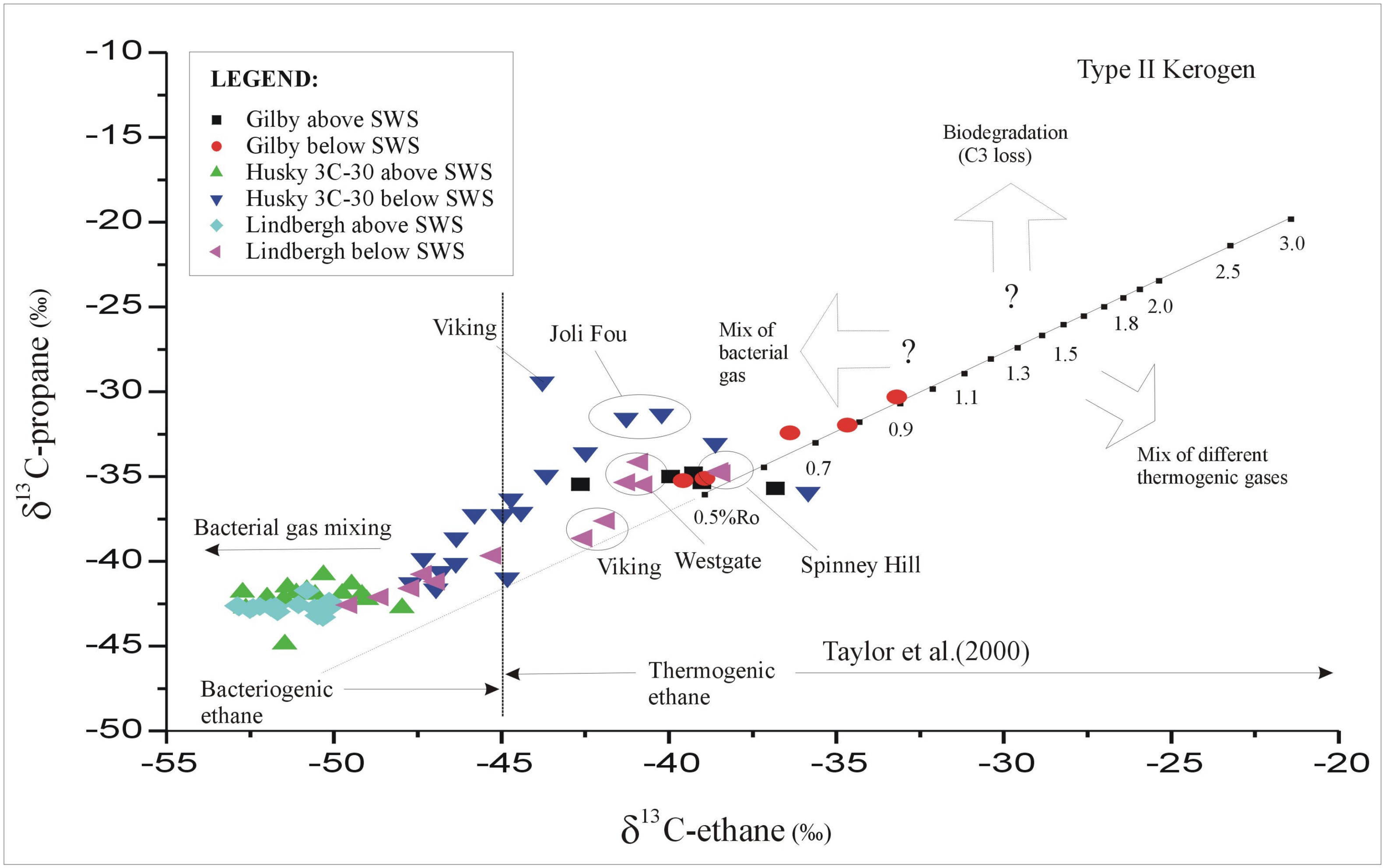

Figure 8-17 Plot of ethane δ ^{13}C vs. propane δ ^{13}C of the Colorado Group mud gas data of the three isotope depth profiles in Figure 8-2. The maturity relation (red line) is taken from Faber (1987), and Whiticar (1990). The deviation of ethane isotopes in sediments above the Second White Specks Shale Fm. in the heavy oil region towards values that indicate an enrichment of ^{12}C can be explained by an admixture of near-surface bacterial ethane to "incipient" (low temperature thermogenic) gases.

The increasingly negative carbon isotope values of ethane from sediments above the Second White Specks Shale Fm. (SWS) - up to -53.08‰ for the $\delta^{13}C$ in Petrovera 1D-25-55-5W4 - and the deviation of ethane isotopes towards values that indicate an enrichment of ^{12}C (Figure 8-17) can be easily explained by an admixture of near-surface bacterial ethane to “incipient” (low temperature thermogenic) gases. The implication of this aspect is an awareness that the presence of considerable reserves of low temperature gas associated with shallow, low maturity shales in the Rocky Mountain basins and Western Canada Sedimentary Basin, are not necessarily and entirely thermogenic in origin, but they can be as well bacteriogenic, or mixtures of thermogenic with bacteriogenic gases. Bacteriogenic ethane was found elsewhere by Waseda and Didyk (1995) and Paull et al. (2000). Oremland et al. (1988) detected, in gas from anoxic sediments, bacterial ethane with values up to -55‰.

8.1.3. Regional migration vs. indigenous sources

One of the most important constraints upon the origin of WCSB mudgases is the distribution of source rocks in the basin. According to Riediger (2006) the most important active source rocks for the Alberta petroleum systems are: Devonian Duvernay and Keg River formations, Mississippian Exshaw Formation, Triassic Doig Formation, Jurassic Fernie Group (“Nordegg” Member), Lower Cretaceous Nanton Formation, and Upper Cretaceous Colorado Group. Regionally distributed active source rocks for the studied areas are Duvernay, Exshaw, Nordegg, and Colorado (Riediger, 2006).

Upper Devonian Woodbend Group (Duvernay Formation) has a TOC up to 16%, type II organic matter, and charged the Upper Devonian reefs in Alberta (Riediger, 2006). Exshaw Formation, with a TOC of 8-14%, and type II organic matter, is a proven prolific source rock for conventional oils and heavy oil in the Alberta basin (Riediger, 2006). Nordegg Member of Fernie Group has TOC up to 30%, type II organic matter, and is a proven source for a few oil pools in subcropping units (Charlie Lake; Belloy), and overlying Mannville at Manola field (Creaney and Allan, 1992). Upper Cretaceous Colorado Group has TOC up to 8%, dominantly type II organic matter, and is a proven source for oils at Pembina Cardium field, and numerous other Upper Cretaceous Cardium, Viking reservoirs (Riediger, 2006).

Local maturity data from Bustin (1991) is compiled in Figure 8-2. As expected, rocks from the stratigraphic section are immature (<0.55% Romax) to over mature (>1.15% Romax, probably entering the dry gas generation window, within the Upper Devonian strata) – in the foothills area. On the eastern side of the basin, in the Lloydminster heavy oil area, Cretaceous rocks have vitrinite reflectance values less than ~0.4% Romax. This translates into an overall east to west increase in maturation. Chemical and stable carbon isotope data from the analysed mudgases indicate not only that they have multiple sources, but the fact that they may have been derived from the above described source rocks within the gas and oil windows.

Although there is a general correlation between maturity of the gases and maturity of the host sediments, there are some exceptions with respect to regional, lateral variations. On a basinal scale, in order to compare Foothills study area with the Lloydminster heavy oil area, three main stratigraphic units were examined for the ultimate migration pathways of the hydrocarbons: Lea Park Formation, Colorado Group and Mannville Group. These stratigraphic units were selected because they are common to both study areas.

Lower Cretaceous Mannville, Jurassic Fernie, and Mississippian samples from the foothills area provide a reasonable fit to the James diagram (see Figure 4-30, Chapter four), indicating a maturity range of 0.7 to ~1% vitrinite reflectance for generation of the majority of samples. Maturity estimates derived using the carbon isotope ratios of Colorado mudgases from the foothills area are also valid, with a resultant range of less than 0.7 to ~1.0 %vitrinite reflectance. Placement of measured $\delta^{13}C$ values for mudgases sampled in the eastern side of the basin (heavy oil area) on the James maturity diagrams indicates that the maturity range over which the Lea Park - Colorado gases were generated extends from approximately 2 to 7 LOM (equivalent with a vitrinite reflectance less than 0.5%). However, the positions of the wet gas components from a few Lea Park Formation gases (e.g. Petrovera 10-17, Husky C3-30), and several Colorado Group gases [e.g. Belle Fourche (Petrovera A9-30, Petrovera 1-4), Viking and Spinney Hill

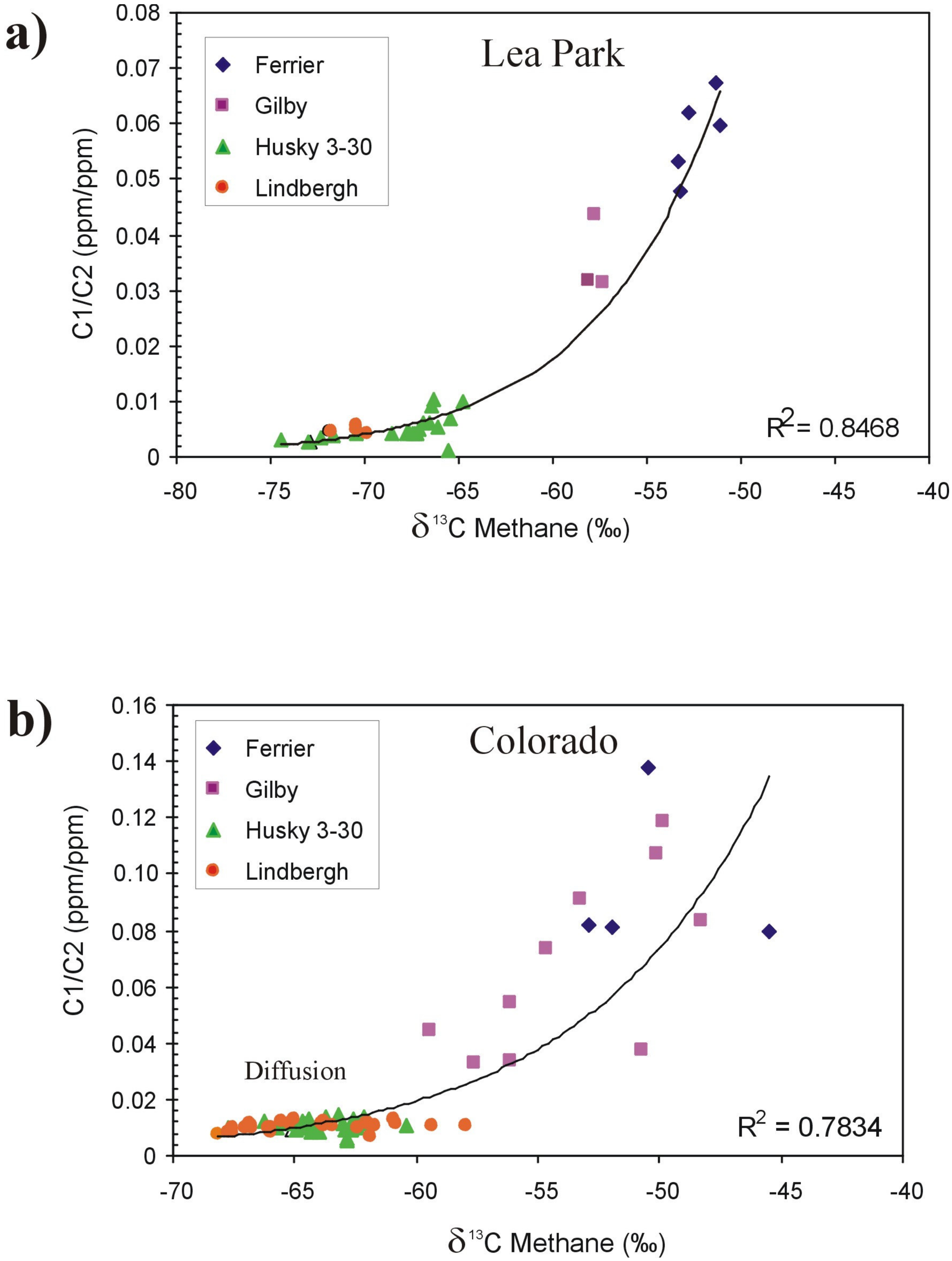

Figure 8-18 "C1-C2" diagram showing segregative migration among a) Lea Park gases, and b) Colorado gases from Ferrier, Gilby, and Husky – Lindbergh (after Prinzhofer and Pernaton, 1997).

sandstones (Lindbergh)] suggest that the mature components of these gases have been generated at maturity levels higher than 0.4% Romax, up to ~ 0.7% Romax, similar to "foothills" gases. All of the heavy oil mudgas depth profiles are located in the immature portion of the basin, at an equivalent of < 0.4% Romax.

The majority of the Lea Park and Colorado Group gases from the heavy oil region, with very dry chemical values and with light isotope signatures of methane (< 58‰) are probably derived, as already discussed, from low temperature thermogenic generation and from bacterial generation. However, some authors have proposed that isotopically light methane may also correspond to thermogenic gases affected by segregation during their migration (Pernaton et al., 1996; Prinzhofer and Pernaton, 1997). Using the diagrams described by Prinzhofer and Pernaton (1997) it is thus possible to check whether the isotopic signatures of the Lea Park and Colorado gases, at least partially, could result from post-genetic fractionation.

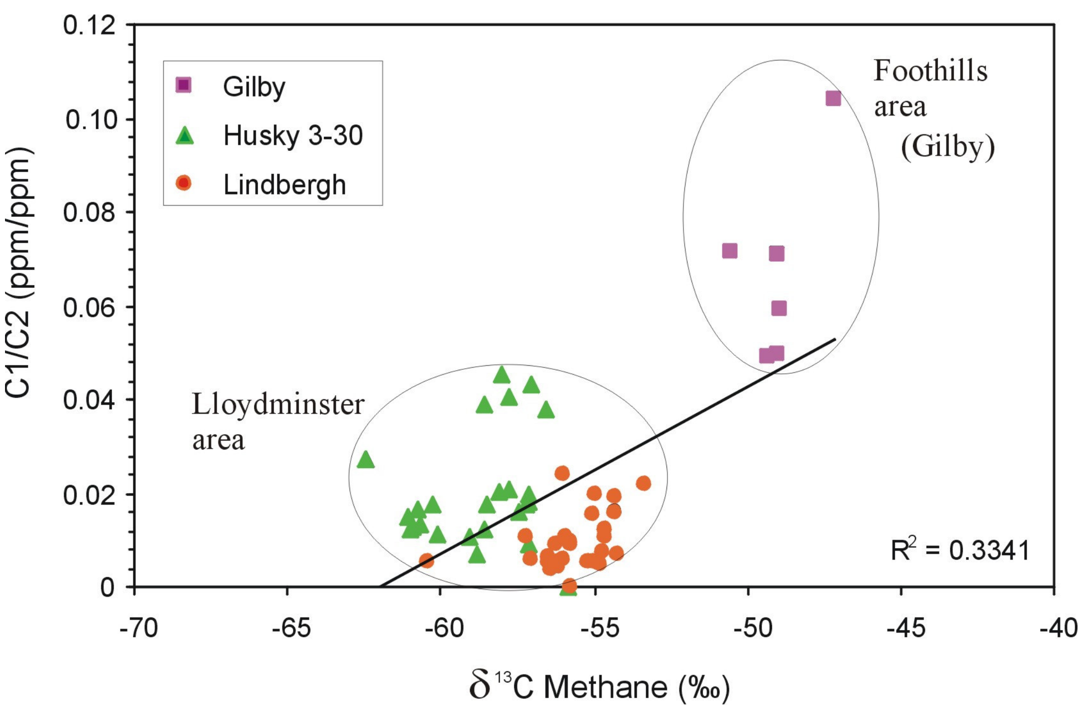

Figure 8-19 "C1-C2" diagram showing two distinct clusters among Mannville mudgases from Gilby (foothills area), and Husky – Lindbergh (heavy oil area). After Prinzhofer and Pernaton, 1997.

In a diagram δ^{13}Cmethane versus ln C2/C1, which allows differentiating mixing processes from diffusion/adsorption processes (Prinzhofer and Pernaton, 1997), the data from the Lea Park Formation and Colorado Group indicate a segregative migration control for both Lea Park and Colorado gases. This is shown by the shape of the trends, which are curved on the linear scale (Figure 8-18). One can argue that the lighter isotopic ratios of methane in the eastern side of the basin could be explained entirely by mixing with bacteriogenic gas. However, in that case, the trend in the C1/C2 versus $\delta^{13}C_1$ diagram would show a straight line on the linear scale (Prinzhofer and Pernaton, 1997), which is not the case. On the other side, plotting the Mannville data in the "C1-C2" diagram, it is not possible to support the hypothesis of a mixing trend or a segregative one, as the gas data plot essentially in two distinct clusters (Figure 8-19). A segregation process should induce the existence of gases with intermediate values between the two clusters – hypothesis which in fact should not be overlooked until new mudgas data will become available from a tectonic setting situated between the two compared areas (foothills and heavy oil). Long distance lateral gas migration in excess of 100 km, up to >320km is generally accepted and documented (Nelson and Simmons, 1995; Jenden et al., 1988). If the long distance migration in the WCSB is regarded as a working hypothesis, then the natural gases, pervasive throughout the marine section of the Colorado Group appear to have migrated to some extent from source rocks 200 - 250 km to the west – southwest, towards the updip margin of the basin. Migration must have occurred not only along bedding planes, but probably also through porous zones associated with the Colorado – Mannville unconformity, and with the coarser-grained sections (e.g. Westgate Formation) of the Colorado Group "shales". Migration up section would have been accompanied by mixing with bacteriogenic methane and ethane, indigenous to the eastern margin of the basin.

8.2. Isotopic complexity: insights from the stratigraphic framework

A simplified scheme of the stratigraphic column of the Western Canada Sedimentary Basin is given in Figure 2-40 (Chapter 2). Stratigraphic relationships between the formations along a geological cross-section line connecting the two study areas are illustrated in Figure 8-2. A rather limited number of cores were examined to verify observations and to confirm the nature of significant surfaces (i.e. maximum flooding surfaces, and major erosional surfaces). Correlations along dip-and strike oriented cross-sections were the main tool used to understand the stratigraphic relationships and to reach many of the conclusions presented here.

8.2.1. Downhole variations

The three isotopic depth profiles from the Foothills region show that there is variability with depth, but there are several major features apparent:

- there is a trend towards heavier isotopic values in the Scollard Formation, Lea Park Formation and Mannville Group (Gilby profile);
- there is a relative invariability within the Horseshoe Canyon Formation;
- there is a trend towards lighter isotopic values for methane from base Scollard to top Colorado Group;
- there is a trend towards heavier isotopic values from top Colorado Group downward.

Figure 8-20 illustrates relationships between gas composition and stratigraphy in the foothills region. Perhaps the most notable observation is the decrease in the isotopic compositional variability of the gases at the Colorado – Mannville boundary (~ 1900 m depth), as well as the spreading out and the significant increase in gas wetness values from top Colorado Group downward.

Carbon isotopes of methane and ethane are strongly correlated in gases derived from a common source (Schoell, 1983; Faber, 1987). In Figure 8-20, however, ethane $\delta^{13}C$ values are more broadly distributed, and show no consistent variation with depth/age. As already discussed, the apparent inconsistency between wetness, methane $\delta^{13}C$, and ethane $\delta^{13}C$ can be solved if many of the samples are interpreted as mixtures of gases derived from source rocks of significantly different maturity, and type organic matter.

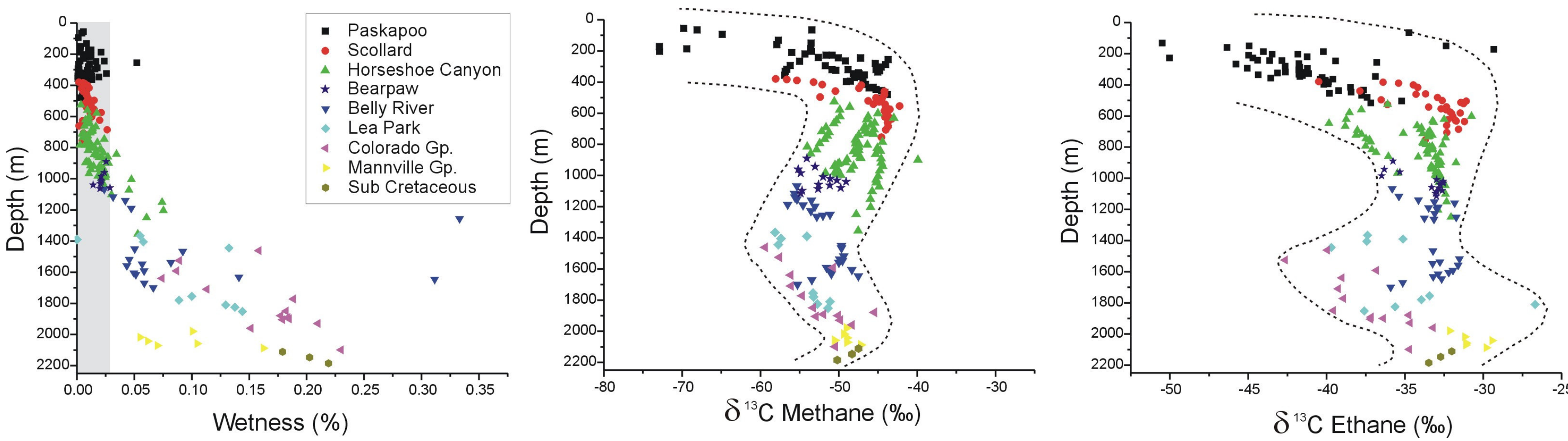

Figure 8-20 Variations in wetness, methane d13C, and ethane d13C in mudgases from the foothills region

In the Lloydminster area, both methane and C_{2+} compounds typically have increasing $\delta^{13}C$ values with depth through the Lea Park/Milk River - Colorado Group sequence, and show a marked increase near the top of the Mannville Group (see Figure 8-21). This observation accentuates once again the strong influence of the Colorado-Mannville boundary as a regional, basin-scale sequence stratigraphic surface, which controlled the long-distance migration of fluids within WCSB. The distribution of the isotopic compositions within alkane gases of the Mannville Group can be area specific, with $\delta^{13}C$ values remaining somewhat similar or even decreasing slightly with depth. Thus, it is demonstrated that there is a systematic variation in carbon isotopic compositions of alkanes gases with stratigraphic depth.

8.2.2. Isotopic shifts and stratigraphic variations

Carbon isotope values show a strong correspondence to stratigraphic position: major shifts in their trends occur at significant sequence stratigraphic surfaces: subaerial unconformities, ravinement surfaces, maximum flooding surfaces (Figure 8-21). This observation is in agreement with what Bohacs already remarked in 1993: petrophysical and geochemical sediment variations do not necessarily change gradually, but have significant shifts at lithofacies boundaries, sequence boundaries and flooding surfaces (Bohacs, 1993).

In a large number of cases, however, the stratigraphic boundaries do not correspond with any observed inflections or variations in the trends of the isotopic ratios with depth – indicating cross-formational flow across them, or their stand-in positions as less effective (partial effective) or even ineffective barriers for vertical gas migration. As demonstrated by the analysis of the wireline data and conversion into mineralogy by a matrix algebra solution, a number of shifts in geochemical signature appear to be related to the presence of some horizons with sealing properties (high shale content and/or low porosity, diagenetic layers). Among shales, only the presence of highly compacted, montmorillonite - rich layers, or shales with different composition (mainly illite, montmorillonite, chlorite), but with a very low porosity, seems to influence the trend of

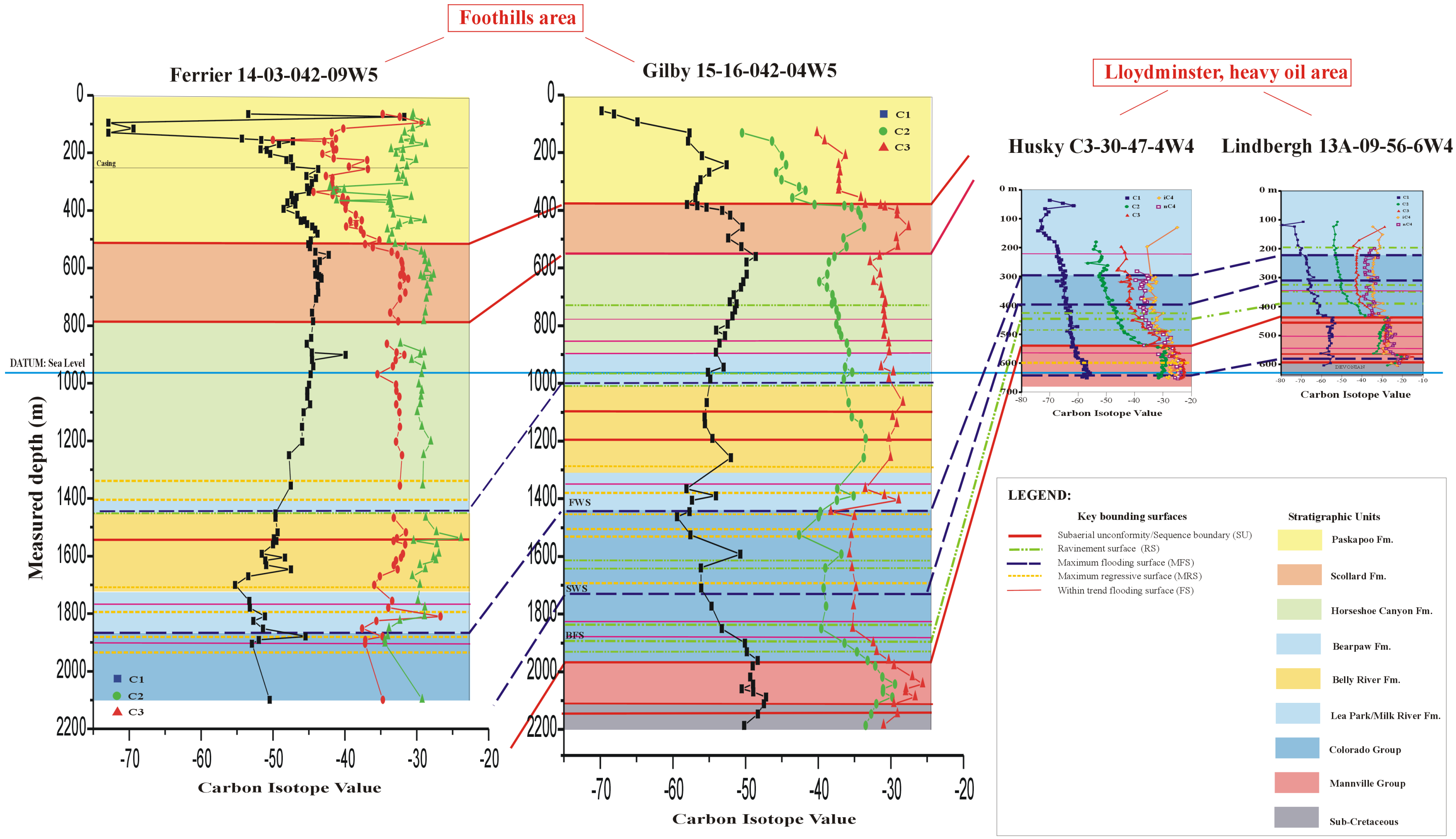

Figure 8-21 SW to NE stratigraphic cross -section showing carbon isotope depth profiles from four wells across the two study areas in the Western Canada Sedimentary Basin. Datum is Sea Level. The stratigraphic units used in the study are correlated across the four wells. Each well includes isotope profiles for methane, ethane, propane; normal-, and isobutane are added for the two Lloydminster wells.

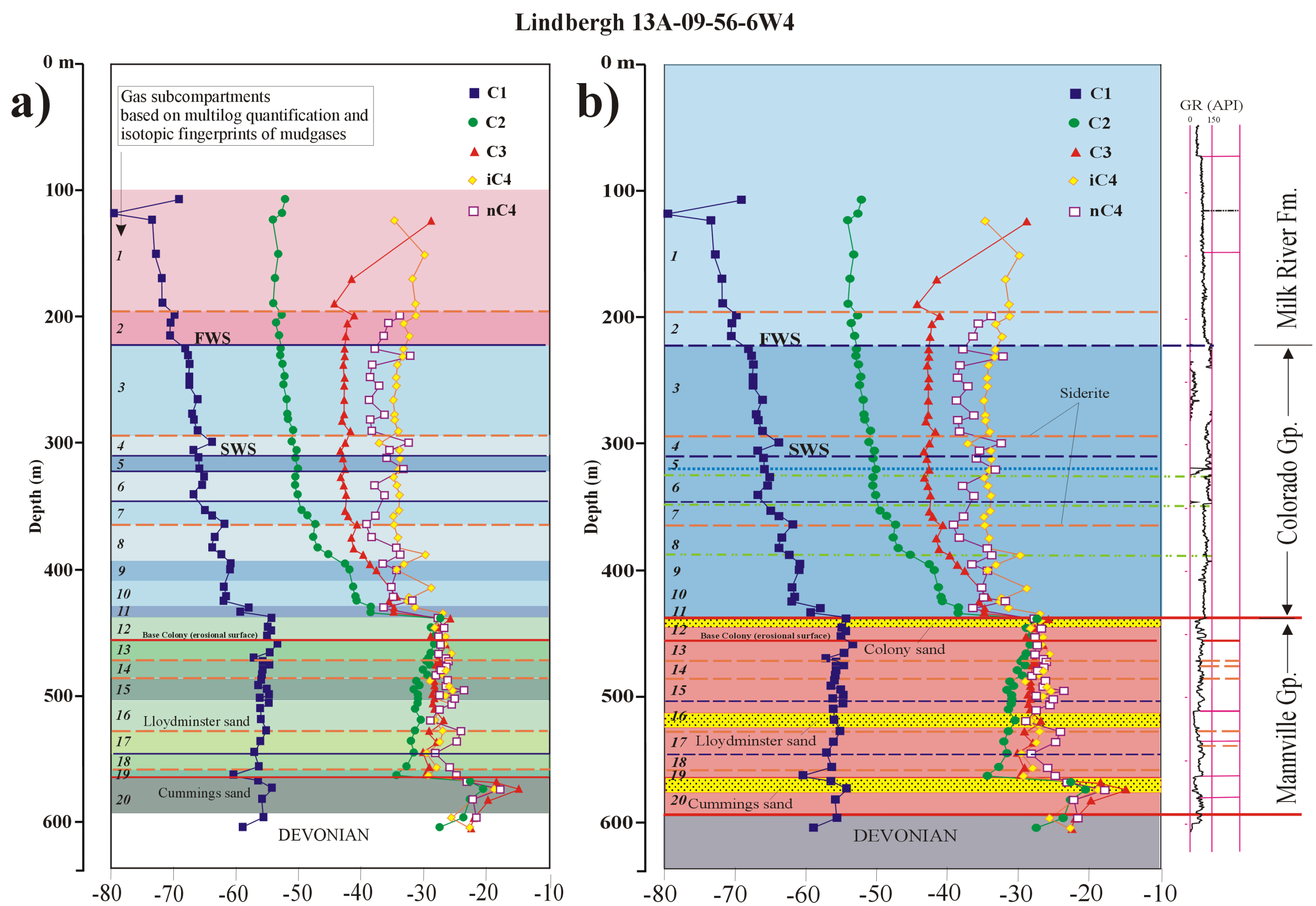

Figure 8-22 Lindbergh 13A-09-56-6W4 isotopic depth profile plotted together with: a) gas compartments identified using the multilog quantification approach; and b) the simplified litholog of the stratigraphic section, showing main sandstone bodies, siderite concretion , and shale-rich layers. Legend for key stratigraphic surfaces is same as in Figure 8-21.

the carbon isotope ratios on mudgas profiles (see Appendix III for details). Their presence segregates several packages of gases, with distinct isotopic and molecular composition, and with distinctive biodegradation and/or mixing signatures.

Although it is impossible to indicate precisely, many inflections on the simplified lithologs appear at the same stratigraphic level, similar to the effective barriers/seals identified using the multilog quantification approach (Figure 8-22). To further illustrate this statement, one of the carbon isotope depth profiles with a higher mudgas sampling density is used: Pembina 11-04-49-11W5 (Figure 8-23). In Figure 8-23, the stratigraphic section penetrated by the Pembina well was plainly subdivided into packages of sandstones, and silty shales bounded by through-going thin layers of coal seams and shales, including bentonite beds. In the Cretaceous section of the WCSB, bentonite beds, which are composed of montmorillonitic clays derived from volcanic ash, are numerous and extensive in both marine sequences of the Colorado Group and the non-marine strata of the Belly River and Edmonton groups. Even though the image (Figure 8-23) seems rather complicated, it is worth noting some obvious digressions of the stable isotope values at the sandstone/shale contacts, within shaly sections, and at the bentonite/other type shale contacts. A shift in the $\delta^{13}C$ values towards isotopically lighter ethane, propane, and sometimes methane occurs at the sandstone/shale contacts. As already documented by Leythaeuser et al. (1983), and Leythaeuser et al. (1984), these sand/shale digressions can be explained considering diffusion and assuming a slightly lower diffusion rate of the heavy isotope species. The better drained portions of the finer-grained rock units close to the sandstone bodies may have lost a significant part of their alkanes, and have preferentially retained the higher molecular weight material. The more mobile front-end portion of the gas probably represents the migrated/diffused part that accumulated in the reservoir sandstones, or coarser grained units of the sedimentary section.

As for both shales and coals, adsorption on sedimentary organic matter should be considered. Their sorption capacity is a function of the total organic content (TOC), and the pore structure (Ross and Bustin, 2007). Relative to organic-rich shales and coals, organic-poor shales (bentonites) have a low sorption capacity. The low sorption capacities of shales relate to the affinity of water to their negatively charged surfaces

(Chiou and Rutherford, 1997). Hydrophobic layers (e.g. bentonites) will pass methane, while hydrophilic ones will pass water more easily. Thus, molecular sizes, as well as polarity of the shale layer are critical. For example, a bentonite layer not 100% water saturated, will be able to absorb some ^{12}C hydrocarbon gases, will pass others, and the majority of the ^{13}C hydrocarbon gases will concentrate in a free state below the seal (bentonite layer). Due to a relatively low sample density in the studied mudlog profiles, the only two reliable examples of such of bentonite impact on carbon isotope ratios shifts are indicated in Figure 8-23 with blue arrows, at ~ 790 m, and 1250 m depth respectively. In the case of no sorbed gas capacity in a moisture-equilibrated sample, the isotopic fractionation above and below the seal is possible to be more evident. This cannot be decided on the basis of available data.

The diffusion of gases through pore throats to adsorption sites is also dependant on the kinetic diameter of the gas (Ross and Bustin, 2007). For example, the smaller kinetic diameter of ^{12}C, compared with ^{13}C would manifest in higher diffusivity of ^{12}C hydrocarbon gases than for ^{13}C hydrocarbon gases.

Kerogen, which is generally hydrophobic, more or less retains the mobile materials in the matrix of its complex structure (Jeong et al., 2003). Therefore, adsorption of ^{12}C-rich molecules is suggested as one of the reasons for the higher retention of ^{12}C hydrocarbon gases within the Scollard Formation, Lea Park, or Westgate formations.

In conclusion, complexly interbedded, diverse lithologies of the WCSB form the source, seal, and reservoir of its hydrocarbon system. Even the finer-grained rocks of the Colorado Group do not form a simple layer-cake stratigraphy, but record an active setting, with deposition, non-deposition, and erosional events.

8.3. Conclusions

The occurrence of bacteriogenic gas, widespread mixing between migrated and indigenous thermogenic gases, and variations in organic matter source, make the origin of WCSB gases very difficult to interpret. Methane $\delta^{13}C$ values are probably the most reliable indicator of thermogenic gas maturity, but cannot be used where bacteriogenic gas mixing has occurred (Jenden et al., 1988). Due to variations in source organic matter, ethane and propane $\delta^{13}C$ values appear even less reliable. Despite these difficulties, carbon isotopic ratios of gases analyzed in this study have been shown to be related to local and regional maturity levels, demonstrating the presence of maturity trends, and a genetic relationship between them. Deviations from the typical patterns are suggested to be caused by:

- mixing between indigenous thermogenic gases and vertically or laterally migrated post-mature gases from deeper in the section ;
- admixture of bacteriogenic gases;
- bacterial degradation;
- physical (porosity and permeability contrasts) and geochemical (organic richness, clay mineralogy) attributes of the surfaces separating the gas compartments.

Indigenous bacterial gas seems to be present in immature to marginally mature Upper Cretaceous-Tertiary rocks close to the Cordilleran deformation front of WCSB, and in the Upper Cretaceous Colorado-Lea Park section of the eastern side of the basin.

Thermogenic gases are present throughout the entire stratigraphic section, in both studied areas – as indigenous, mixed, and migrated gases. Indigenous thermogenic gas (source rocks $Ro<0.65\%$) is present in the entire Cretaceous sedimentary section, from Mannville Group up to Scollard Formation. Migrated thermogenic gases can be recognized particularly in shallow reservoirs where contributions from local sources appear small (e.g. Belly River gases).

The gas migration mechanisms are suggested to be related to free gas phase passage through porous media, diffusion, and solution/exsolution processes related to the presence and influence of groundwater flow systems. When information about migration at the basin scale and the field scale are compared, it appears that the general trend of migration is from west-southwest to east-northeast. However, it seems that at the field scale, local disturbances may be due to preferential pathways created by local geology, topography and hydrogeology.

Based on a rather sparse data set, this thesis suggests that isotopic variability of WCSB gases is only partly induced by maturity at one single location. The strong correlation between isotopic and stratigraphic boundaries indicates that compartmentalization of the gas is strongly influenced by stratigraphic variations. This implies that the majority of stratigraphic boundaries act as effective barriers to gas migration so that one can say that each gas package retains its distinct isotopic character. Starting with separation of gases in several compartments based on major stratigraphic boundaries, it has been demonstrated that many more horizons act as barriers/baffles, significantly inflecting carbon isotopic depth profiles and creating local sub-compartments. Even most indications of compartmentalization might be related to pore-fluid pressures, numerous chemical parameters may also infer or confirm compartmentalization. The hydrocarbon chemistry may show similar variations. The mineralogy may also reflect the variations in water chemistry. The mudgas compositions may also differ between compartments.

The main shifts of carbon isotope ratios, as suggested by these preliminary data and thesis, are likely to be related to the physical properties of the rocks, differences between organic precursors (type II versus type III kerogen), total organic carbon (TOC) content, gas biodegradation and mixing.

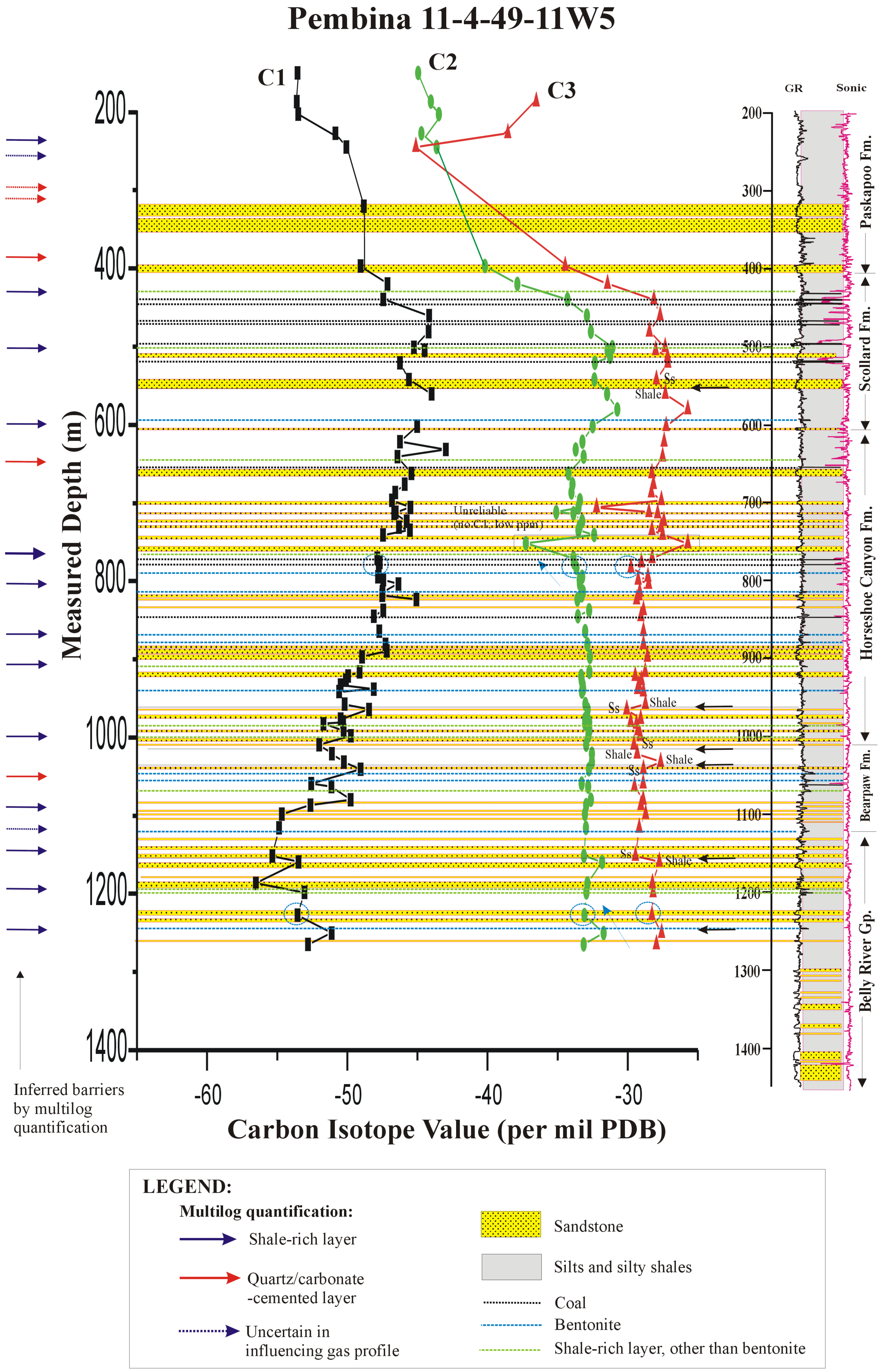

Figure 8-23 Carbon isotope depth profile for Pembina 11-04-49-11W5 plotted together with a simplified litholog of the stratigraphic section. The arrows on the left side of the profile represent gas compartment boundaries as resulted from the multilog quantification approach. Many inflections on the simplified lithologs appear at the same stratigraphic level as the effective barriers identified using the multilog quantification. The black arrows on the right side of the profile points towards some of the isotopic inflections most probably and most reliably related to physico-chemical contrasts at the shale/sand contacts. Suggested bentonite influence on the isotopic variations is represented with blue circles.

9.1. Conclusions

A number of conclusions may be drawn from this integrated approach.

1.) **Carbon isotope depth profiles provide a significant contribution to the geological understanding of a region**

Recent analytical advances in carbon isotopes of natural gases (methane to butane) due mainly to the use of GC-CF-IRMS technique make possible the analysis of trace amounts of higher hydrocarbon homologues recovered from the drilling fluids (mudgases), and allows us to reconstruct some of the physico-chemical processes which affect these *in-situ* natural gases. These reconstructions provide important information on both the origins and the dynamic behavior of hydrocarbon fluids between the source rocks and the accumulation sites.

Correlating this methodology with other geological and geophysical disciplines increases the understanding of hydrocarbon history in sedimentary basins.

From an exploration point of view, the isotopic composition of mudgases can be used to provide an indication of the maturity level at which that gas was generated; whether there are multiple sources of gas in the basin, and whether there has been a contribution from bacteriogenic gas. Information on the maturity and composition of the gases could be extremely important for predicting areas of maximum gas generation in a basin. Furthermore, delineation of gas migration pathways may indicate exploration potential in areas that are currently under-explored.

From a production point of view stable isotopes can be used to fingerprint sources of leaking gases, and to determine communication between wells, presence of barriers/baffles within a producing horizon, and constrain the basin geometry and fluid compartments present in the field area.

2.) **Key stratigraphic surfaces reveal geochemically significant rock packages**

The sequence stratigraphic approach consisted of looking at the geological record as composed of rock packages bounded by physical surfaces formed by distinct events. The stacking of the depositional environments, along with the physical attributes of the surfaces separating the environments, reveals the sequence stratigraphic framework. The Western Canada foreland section was analyzed and correlated at a regional scale in an attempt to both gain a much better understanding of lateral and vertical changes in the layers making up the basin fill and to disclose the critical significance of sequence stratigraphic surfaces on carbon isotope ratios.

The key bounding surfaces that separate geochemically significant rock packages are:

- the unconformable portions of the sequence boundaries (subaerial unconformities and/or ravinement surfaces, which have eroded through a subaerial unconformity);
- the ravinement surfaces, and
- the maximum flooding surfaces.

The well-log cross-sections constructed throughout the foreland basin succession summarize the regional facies distribution and thickness, and reveal a series of key bounding surfaces and local facies successions. Carbon isotope values show a strong correspondence to stratigraphic position: the major shifts in their trends occur at significant sequence stratigraphic surfaces, being in fact controlled by the lithology. The major shifts in the carbon isotope ratios of mudgases occur at sequence boundaries (either subaerial unconformities or ravinement surfaces) and maximum flooding surfaces. The presence of the subaerial unconformities on mudgas profiles seems to mark a transition from more negative values (within overlying deposits) to more positive values (within underlying deposits) of the carbon isotope ratios. These discontinuities serve mainly as lateral migration pathways. The coarse grained deposits above the unconformities illustrate in general a slight decrease in isotope ratios upwards.

The presence of maximum flooding surfaces seems to mark a transition from overlying immature gases towards more mature underlying gases; flooding surfaces act as regional seals that control the long-distance migration of gases. Along them there is a porosity and permeability decrease, related to an increase in shale content.

Ravinement surfaces are related to greater wetness index values, and mark inflections towards more negative values for ethane $\delta^{13}C$ and propane $\delta^{13}C$ values. They could serve as partially effective hydrodynamic isolation.

The coal seams within the coal bearing strata (Mannville-, Belly River-, and Edmonton groups, and Scollard Formation) represent a potential source of isotopically enriched organic matter. The carbon isotopic values are obviously more positive at the coal stratigraphic levels, due to both desorption/diffusion processes and alteration in conjunction with groundwater flow.

3.) **Post-generation history of the gases from WCSB is very complex**

Consideration of gas composition and carbon isotope data for mudgases with empirically derived genetic classification of gases permitted greater insight into the factors controlling the compositional and isotopic variations described. Regional and in depth variations in molecular and isotopic composition of mudgases were closely considered in the present study in order to determine genetic characterization and maturity of the source rock of the gases, their alteration and migration history, as well as to distinguish between various gas packages.

a.) Application of established gas typing procedures indicates that the majority of the gases the Foothills region were generated in conjunction with liquid hydrocarbons in the oil-window of source maturity. Gases are characterized by thermogenic $\delta^{13}C$ signatures, and a variable proportion of ethane and higher alkanes of any of the gases sampled. However, a mixture of thermogenic gases with bacteriogenic gases represents the bulk majority of the gases sampled within the Foothills region. A characteristic of methane isotopic composition is that in all three isotopic profiles more and more isotopically light methane is admixed with increasing depth from surface down to the top of the Colorado Group. From here down into pre-Cretaceous sediments, the trend is reversed in an expected position (increasing values with increasing depth). Two situations may be taken into account to explain the reversed trend in the relationship of the isotopic composition of methane with depth: (1) early generation of thermogenic gas, isotopically light methane being added to heavy methane which formed from mature organic matter; and (2) methane derived from oil destruction in reservoirs, thus separated from source organic matter.

Anomalously carbon isotope ratios documented within the Scollard, Paskapoo, and Horseshoe Canyon formations suggest near-surface degradation related to the shallow depth, and to the presence of coal-bearing strata. This type of degradation effect has been documented mostly for methane, ethane, and propane, where the carbon isotopes have been altered to values that appear to be more mature than they are expected. These oxidation-related changes could easily be misinterpreted as being more mature than they really are without the additional supporting data.

Bacterial contamination is an important issue when characterizing the gas origin and migration when using stable isotopes, as the correct interpretation of the data may be difficult to interpret. Bacterial oxidation of bacterial gas may give a residual gas showing a thermogenic signature, whereas diffusive processes during migration may give a bacterial signature to a thermogenic gas.

Significant deviations in gas composition in a direction perpendicular to the Rocky Mountain range are noted, given that an increase in the relative proportion of methane is observed from Ferrier – Pembina to Gilby location, accompanied by a ^{12}C enrichment in the same direction. A reasonable explanation is either that progressive ^{13}C enrichment westward is a consequence of a Rayleigh distillation effect or that the isotopic compositions of gases are controlled by the maturity of the source rocks. The gas composition near the deformation front (Ferrier) is controlled by active gas generation and source maturity. The gas composition in an eastward direction (Gilby) is controlled by mixing with bacteriogenic methane and/or oxidation of heavy gases.

b.) Within the Lloydminster - heavy oil study area, the majority of the Colorado gases are in-situ thermogenic gases, partially affected by biodegradation and/or mixed with late-generation biogenic gas. Occasionally, the C2+ components of the shallow gases in the Lloydminster region are found to be more mature, migrated gases, and could have been sourced in deeper Mannville Group. Petrophysical evidence (weak permeability barriers) and the presence of isotopic reversals between C3 and C4 components - diagnostic of the Mannville gases – do occur in the Colorado shale gases as well.

The heavier n-alkanes molecules typically have increasing $\delta^{13}C$ values with depth through the shales of the Colorado Group and show a marked increase near the top of the Mannville Group. The distribution of the isotopic compositions within the Mannville Group can be area specific, with $\delta^{13}C$ values remaining somewhat similar (Husky 3C-30-47-4W4) or even decreasing slightly with depth.

Thus, it is demonstrated that there is a systematic variation in carbon isotopic signature of alkane gases with stratigraphic depth.

Methane $\delta^{13}C$ values as well as the compositional range provide strong evidence that the bulk majority of the gas collected within the Lloydminster region is affected by mixing with light gas, both biogenic and early thermogenic. The higher $\delta^{13}C$ value for the methane in this area is –52.83 ‰ (Colony Member, Mannville Group, at Lindbergh A9-16-56-6W4 location). The lower value is –79.46 ‰, provided by a gas sample collected in the Lea Park Formation in the Golden Lakes area.

In the western part of the Lloydminster region, the coexistence of isotopically heavy ethane (ethane $\delta^{13}C$ values in the range of –20‰ to –28‰) with methane having $\delta^{13}C$ values in the range of –52‰ to –61‰ indicate the mixing of thermogenic gas with some quantities of biogenic methane – probably late-generated.

The likely source for the bacteriogenic gas is found in the uppermost part of the stratigraphic section, within the Lea Park Formation (which contain gases having the lightest isotope ratios), at Lindbergh-, and Wildmere fields – in the western part of the study area.

Lower Cretaceous Mannville gases have apparently mixed with large amounts of bacterial methane, which accounts for very negative $\delta^{13}C_{C1}$ values (up to -77.97‰, Waseca Member, Petrovera 1-4-48-22W3). Moreover, Mannville gases associated with the heavy oils have migrated long distances, and biodegradation has significantly altered their isotope ratios from the patterns established in deeper, unaltered gases. Bacterial alteration of Mannville gases has led to characteristic isotopic reversals between the $\delta^{13}C_{C3}$ and $\delta^{13}C_{nC4}$ values and fairly positive propane $\delta^{13}C$ values. The highest degree of bacterial oxidation seems to be related to the position of the actual recharge areas in western-, and northwestern part of the Lloydminster area. Thus, information on the mudgases composition could allow the prediction of where the biodegradation can occur or where the biodegradation is expected to be more significant.

4.) **The trend of the carbon isotope ratios on mudgas profiles appears to be influenced by a number of smaller scale lithological barriers/baffles**

The analysis of the wireline data and conversion into mineralogy by a matrix algebra solution showed that the Cretaceous - Tertiary succession in both of the study areas of the Alberta basin is represented by a succession of porous-permeable and less permeable strata, across which a number of effective barriers/seals (high-shale content bands, montmorillonite bands, quartz cemented bands, dolomite cemented bands, siderite cemented bands) serve as boundaries for gas compartments. The Cretaceous – Tertiary stratigraphic succession is extremely heterogeneous, and vertical gas migration appears to be controlled by (often small) zones of high or low permeability.

Major shifts in geochemical mudgas signature, including those related to major stratigraphic boundaries, are related to the presence of some horizons with sealing properties (high shale content and/or low porosity, diagenetic layer). Among shales, only the presence of highly compacted, montmorillonite - rich layers, or shales with different composition (mainly illite, montmorillonite, chlorite), but with a very low porosity, seems to influence the trend of the carbon isotope ratios on mudgas profiles. Their presence segregates several packages of gases, with distinct isotopic and molecular composition, and with distinctive biodegradation and/or mixing signatures.

It was demonstrated that different gas geochemistry characterizes distinct flow units potentially separated by permeability contrasts. Each isotopic mudgas profile presents evidence of several packages of thermogenic gases, mixed-, and biodegraded gases, which are segregated by effective seals. As a consequence, isotopic compositions and variations of mudgases are best employed in conjunction with wireline analysis for defining details of transition zones and reservoir compartments. Reservoir compartments and effective seals are easily recognized from inflections in the isotopic depth trends.

The combination of petrophysical approach and the isotopic fingerprinting technique can also be used to constrain the basin geometry and fluid compartments present in the field area.

5.) **Correlation between groundwater flow directions and gas-geochemical parameters appears factual, but needs further investigation**

Carbon isotopic gas signatures were combined with an evaluation of the regional hydrogeology to outline prospective gas migration routes in the Foothills and Lloydminster areas.

Mechanisms controlling secondary gas migration within the two study areas of the Western Canada Sedimentary Basin involve hydrodynamics, buoyancy, diffusion, segregative fractionation and permeability heterogeneities. Regional ground water flow seems to have mostly influenced the gas migration pathways within Cretaceous section at the northeastern edge of the Alberta basin. The gas is suggested to have migrated through solubilization/diffusion in formation waters. The migration process seems to have been accompanied by compositional and isotopic fractionations.

The interference in the Foothills study area of several highly opposing groundwater flow systems may give rise to a much more complicated flow pattern (involving gas, water and fluid - rock matrix interactions) – not possible to be solved on the basis of the existing data alone. Water of meteoric origin recharges in this case all the Upper Cretaceous aquifers, from Paskapoo-Scollard down to Belly River. The correct interpretation of the data may be difficult to deduce at the present stage, with the available data.

Two more likely and simpler mechanisms to explain the observed isotopic and compositional data in the Foothills study area are: (1) that gas migrates through buoyancy and diffusion accompanied by compositional fractionation, eastward and away from the Rocky Mountain deformation front, and (2) a source maturity control.

The most reasonable explanation for the distribution of chemical proportion and carbon isotopic ratios for mudgases sampled from the Lloydminster region involves the regional and local groundwater flow. As suggested also by Holysh and Tóth (1995), the downward flowing of the groundwater may obstruct the rise of the upward-moving hydrocarbon gases or can cause these gases to shift laterally from the recharge zones.

Therefore, the current geochemical and hydrogeological evidence indicate the potential for long distance gas migration to the northeastern outcrop edge of the Alberta basin. The molecular and isotopic composition of gases at the eastern edge of the Alberta basin is inferred to represent the discharge of regional gas migration systems of 10's to 100's of kilometres in length.

The combination of regional hydrogeology and mudgas isotope geochemistry would allow for more accurate mapping of gas migration pathways, which can be used for prospect risking and for the ranking of exploration plays.

Considering that the carbon isotopes help to trace the so-called major "degassing fluxes" through geological times (Ballentine et al., 1996) delineation of migration pathways may indicate exploration potential in areas that are currently underexplored.

6.) **Conclusions drawn from the geochemical characterization of mudgases might have significance for unconventional gas exploration**

Unconventional gas deposits, such as those produced from coal beds and shale, are an important hydrocarbon resource. Many of these unconventional deposits contain a mix of thermogenic and bacteriogenic gas. In these types of plays, the origin of gas is fundamental to assessing a natural gas reservoir and in guiding exploration strategies.

According to our findings, two models on the generation of the gas in the Colorado Group – Lloydminster area are the bacterial gas generation and early thermogenic gas generation. The presence of bacterial methane in this area may increase its economical potential, therefore identifying zones where conditions are favorable for active microbial methanogenesis is very important. Isotopic and compositional data from mixed microbial/thermogenic gas fields must be carefully examined, and microbial activity must be identified using additional data (dissolved inorganic carbon, and CO_2 geochemistry in the associated water).

7.) **Carbon isotopic depth profiles can serve for gas migration mitigation**

Carbon isotope fingerprints of ethane (C2), and propane (C3) is a proven, cost effective method used to compare and fingerprint known formation gases, and to identify the leaking gas (SCVF) sources in order to isolate them and block the flow. The ability to determine source depths of shallow gases is particularly useful for the remediation of numerous leaking heavy-oil wells in the Western Canada Sedimentary Basin.

Isotope ratios of couple of tens of migrated gases superimposed on the isotopic profiles of the formations penetrated in various fields, both in Lloydminster and Foothills regions have been used to estimate the source of leaking gases.

The majority of migrating gases in the Foothills study area seem to be sourced in the shallow Paskapoo and Scollard formations, but occasionally the source horizon lies in the deeper strata (Mannville Group, Fernie Group or Pekisko Formation). In those cases, the migrating gas sampled at surface is very similar to the typical production gas from that field (e.g. 10-22-41-3W5: Lower Mannville/Nordegg/Banff production in Gilby field; 6-32-42-6W5: Belly River production in both Gilby and Ferrier fields; 2-20-41-8W5: Belly River production in Ferrier field; 6-11-42-9W5: Belly River production in Ferrier field).

In the Lloydminster area, the SCV source is mainly related to the Mannville and Colorado groups. The SCV Manville gases are very similar to the typical production gases from producing fields. Majority of the SCV gases coming from the Colorado Group appear to be related to the shaly Westgate, Belle Fourche, Fish Scale, Second White Specks, and First White Specks formations – aiming again to the early thermogenic gas generation in this stratigraphic section.

8.) **Regional mudgas variations**

Although both the foothills gases and the heavy oil gases analyzed in this thesis are mostly mixtures of thermogenic and bacteriogenic gases, they usually form separate clusters when plotted on various diagrams: the heavy oil gases have a characteristic increase of methane isotopes as ethane isotope value increase, demonstrating a maturity trend and an apparent genetic relationship between them. The foothills group gases appear to be a mixture of at least two distinct components: a dry low maturity gas and a wet, more mature thermogenic gas. The low maturity gas, composed of bacterial methane and isotopically light ethane (as low as -50.49‰) is inferred to be indigenous to the shallow part of the basin, and generated in the Paskapoo – Scollard formations. The more mature thermogenic gas has presumably been generated from deeper buried source rocks along the basin axis and has migrated both vertically (Belly River sandstones) and updip to the east. This gas is best characterized by natural gases from the Mississippian Pekisko Formation, Jurassic “Nordegg” Member of the Fernie Group, Lower Cretaceous Glauconitic Member of the Mannville Group, Cretaceous Belly River Group, and Cretaceous Horseshoe Canyon Formation. This hypothetical two-component mixing model can help explain the distribution of the Foothills gas data and their deviation from the expected ethane $\delta^{13}C$ vs, methane $\delta^{13}C$ maturation trend.

Carbon isotopic ratios of gases analyzed in this study have been shown to be related to local and regional maturity levels, demonstrating the presence of maturity trends, and a genetic relationship between them. Deviations from the typical patterns are suggested to be caused by:

- mixing between indigenous thermogenic gases and vertically or laterally migrated post-mature gases from deeper in the section ;
- admixture of bacteriogenic gases;
- bacterial degradation;
- physical (porosity and permeability contrasts) and geochemical (organic richness, clay mineralogy) attributes of the surfaces separating the gas compartments.

Indigenous bacterial gas seems to be present in immature to marginally mature Upper Cretaceous-Tertiary rocks close to the Cordilleran deformation front of WCSB, and in the Upper Cretaceous Colorado-Lea Park section of the eastern side of the basin.

Thermogenic gases are present throughout the entire stratigraphic section, in both studied areas – as indigenous, mixed, and migrated gases. Indigenous thermogenic gas (source rocks Ro<0.65%) is present in the entire Cretaceous sedimentary section, from Mannville Group up to Scollard Formation. Migrated thermogenic gases can be recognized particularly in shallow reservoirs where contributions from local sources appear small (e.g. Belly River gases).

The gas migration mechanisms are suggested to be related to free gas phase passage through porous media, diffusion, and solution/exsolution processes related to the presence and influence of groundwater flow systems. When information about migration at the basin scale and the field scale are compared, it appears that the general trend of migration is from west-southwest to east-northeast. However, it seems that at the field scale, local disturbances may be due to preferential pathways created by local geology, topography and hydrogeology.

9.) **Isotopic variability of WCSB gases is only partly induced by maturity at one single location**

The main shifts of carbon isotope ratios (sharp inflections and deviations towards increasing and decreasing $\delta^{13}C$ values), as suggested by this thesis, are likely to be related to the physical properties of the rocks, differences between organic precursors (type II versus type III kerogen), total organic carbon (TOC) content, gas biodegradation and mixing.

*****

In summary, the present thesis demonstrates that the carbon isotopic mud gas profiles represent a powerful tool that provides information about the compartmentalization of the gas, the effectiveness of low permeability barriers, the origin, alteration and maturity of gases, and the regional gas dynamics. However, this geochemical information is but one part of the puzzle in the investigation of regional gas dynamics, and should be integrated with geological information, lithostratigraphic-, and sequence stratigraphic information, petrographic information and geophysical data.

These results may have important implications for understanding the role of gas geochemistry in characterization of actual prospects. Hydrocarbon exploration and production operations in the Western Canada Sedimentary Basin could benefit from this new picture of the regional hydrochemistry of the basin. This allows for more accurate mapping of likely oil and gas migration pathways, which can be used for prospect risking and for the ranking of exploration plays.

9.2. Future work

1.) The number of mudgas profiles used in this thesis was limited and should be increased in future studies (more densely spaced isotopic depth profiles including other areas in the Western Canada Sedimentary Basin).

2.) Further detailed well log cross-sections are required to assess a more comprehensive lateral and vertical distribution of depositional environments, facies change and variability of the sequence stratal units and their bounding surfaces within the Western Canadian Sedimentary Basin. A re-interpretation of stratal elements that reflect fourth to fifth order phases of regional deposition, while collecting even a higher density mud gas samples will engage a more creative framework, allowing to focus on small details.

Integration of geological, geophysical, biostratigraphical and geochemical data would constitute a useful contribution to the understanding of depositional environments and stratigraphic architecture at regional scale, and interpretation of mud gas carbon isotope data in the Alberta basin.

3.) More experimental controls and geological case studies are necessary in order to better establish the constraints on the concepts of the isotopic profiles of mudgases, specifically with regard to the influence of the type and maturity of organic matter. Carbon isotopic analyses of kerogen from potentially source rocks should be performed, on both sapropelic-, and humic organic matter.

4.) $\delta^{13}C$ analysis of the dissolved gases in formation waters is another possible future research to be performed, considered in conjunction with carbon isotopic composition of mudgases.

5.) In addition to mudgases, the use of adsorbed gases (i.e., those gases released from cuttings upon acid treatment) may be also considered. The adsorbed gases tend to provide more of an integrated value for gas that has been present in the pore space over time, whereas the mudgases gases are more constrained to the gases that have entered the pore space recently. The use of both gas types would provide a powerful tool.

6.) The integration of several isotope tracers would give a much more accurate reconstruction of light hydrocarbon history, from their generation to their latter sites of accumulation and/or dissipation and ultimate oxidation. Noble gas isotopes (helium - ^{4}He, ^{40}Ar - argon) may be the new frontier exploration tools, as their chemical inertia allows us to use them as precise tracers of sources and of simple associated physical processes (phase states, migration, leakage).

7.) Due to the complexity of isotopic profiles in sedimentary sequences, further research in well-defined geological systems with higher density and good quality samples combined with experimental measurements is required to improve the understanding of all the processes and factors controlling the variability of the carbon isotope ratios of mudgases.

BIBLIOGRAPHY

Adams, J.J., Rostron, B.J., and Mendoza, C.A., 2004 - Coupled fluid flow, heat and mass transport, and erosion in the Alberta basin: implications for the origin of the Athabasca oil sands. Can. J. Earth Sci., vol. 41, p. 1077-1095.

Anfort, S., Bachu, S., and Bentley, L.R., 2001 – Regional scale hydrogeology of the Upper Devonian-Lower Cretaceous sedimentary succession, south-central Alberta, Canada. AAPG Bulletin, v. 85, p. 637-660.

Arkadakskiy, S.V., 2006 - Fate of leaking natural gas in soil near oil and gas wells in Western Canada. Ph.D. Thesis, University of Alberta.

Bachu, S., 1995 – Synthesis and model of formation water in the Alberta basin, Canada, AAPG Bulletin, v. 79, p. 1159-1178.

Bachu, S. and Underschultz, J.R., 1995 – Large-scale erosional underpressuring in the Mississippian-Cretaceous succession, southwestern Alberta basin, AAPG Bulletin, v. 79, p. 989-1004.

Bachu, S., Dawson, F.M., Richardson, R.J.H., 1998 – Regional-Scale Characterization of Coal-Bed Methane Reservoirs in the Alberta Basin in Comparison with Other Rocky Mountain Basins, AAPG Annual Convention Abstracts, Salt Lake City, Utah.

Bachu, S. and Michael, K., 2003 – Possible controls of hydrological stress regimes on the producibility of coalbed methane in Upper Cretaceous – Tertiary strata of the Alberta basin, Canada, AAPG Bulletin, v. 87, p. 1729-1754.

Ballentine, C.J., O'Nions, R.K., Coleman, M.L., 1996 – A magnus opus: helium, neon and argon isotopes in a North Sea oilfield. Geochim. Cosmochim. Acta, v. 60, p. 831-849.

Barker, C., 1972 - Aquathermal Pressuring; Role of Temperature in Development of Abnormal-Pressure Zones. AAPG Bulletin v. 56, p. 2068-2071.

Barker, J.F., Fritz, P., 1981 – Carbon isotope fractionation during microbial methane oxidation. Nature, v. 293, p. 289-291.

Bekele, E.B., Person, M.A., Rostron, B.J., and Barnes, R., 2000 – Modeling secondary oil migration with core-scale data: Viking Formation, Alberta basin. AAPG Bulletin, v.86, p. 55-74.

Bernard, B.B., 1978 – Light hydrocarbons in marine sediments, Ph.D. dissertation, Texas A&M University, 144 pp.

Bernard, B.B., Sackett J.M., 1977 – Offshore Technology Conference, Ninth, Houston, TX, p. 435-438.

Bernard, B.B., Brooks, J.M., Sackett J.M., 1978 – Light hydrocarbons in recent Texas continental shelf and slope sediments. Journal of Geophysical Research, vol. 83, p. 4053-4061.

Berner, U., and Faber, E., 1987 – Maturity related mixing model for methane, ethane and propane, based on carbon isotopes. Organic Geochemistry, Vol. 13, p. 67-72.

Bethke, C.M., and Marshak, S, 1990 – Brine migration across North America – the plate tectonics of groundwater. Annual Reviews, Earth Planetary Sciences, v.18, p. 287-315.

Bethke, C.M., Reed, J.D., and Oltz, D.F., 1991 – Long-range petroleum migration in the Illinois basin, AAPG Bulletin, v. 75, p. 925-945.

Bhattacharya, J., and Walker, R.G., 1991 - Allostratigraphic subdivision of the Upper Cretaceous Dunvegan, Shaftesbury and Kaskapau formations, northwestern Alberta subsurface. Bulletin of Canadian Petroleum Geology, v. 39, p. 145-164.

Bloch, J.D., Schröder-Adams, C.J., Leckie, D.A., McIntyre, D.J., Craig, J., and Staniland, M. 1993. Revised stratigraphy of the lower Colorado Group (Albian to Turonian), Western Canada. Bulletin of Canadian Petroleum Geology, v. 42, p. 325.

Bloch, J.D., Schröder-Adams, C.J., Leckie, D.A., Craig, J., and McIntyre, D.J. 1999. Sedimentology, micropaleontology, geochemistry, and hydrocarbon potential of shale from the Cretaceous Lower Colorado Group in Western Canada. Geological Survey of Canada Bulletin 531, 185 pp.

Bloch, J.D, Schroder-Adams, C.J., and Leckie D.A., 2002 – The Petrology of Late Cretaceous Colorado Group Shales from the Pasquia Hills, East-central Saskatchewan: Preliminary Results. *In*: Summary of Investigations 2002, vol. 1, Saskatchewan Geological Survey, Saskatchewan Energy and Mines Miscellaneous Report 2002-4.1, p. 126-133.

Bohacs, K.M., 1993 – Source quality variations tied to sequence development in the Monterey and associated formations, Southwestern California. *In:* Katz, B.J., and Pratt, L.M. (Eds.) Source Rocks in a Sequence Stratigraphic Framework. AAPG Studies in Geology # 37, p. 177-204.

Bockris, J.O., Reddy, A.K.N., 1970 – Modern electro-chemistry, v. 1, New York, Plenum, 622p.

Bondar, A.D., 1987 - Role of diffusion in differentiation of carbon isotopes of methane of the earth's crust (in Russian). Geokhimiya, v.9, p.1274-1283.

Boreen, T. and Walker, R.G. 1991 - Definition of allomembers and their facies assemblages in the Viking Formation, Willesden Green area, Alberta. Bulletin of Canadian Petroleum Geology, v. 39, no. 2, p. 123-144.

Boreham, C.J., Hope, J.M., Hartung-Kagi, B., 2001 - Understanding source distribution and preservation of Australian natural gas: a geochemical perspective. APPEA J. 41 (1 200), p. 523–547.

Braman, D.R. and Sweet, A.R. 1990 - Overview of Campanian to Paleocene stratigraphy, southern Alberta Foothills. *In* Field guide to Uppermost Cretaceous Strata in Southern Saskatchewan and Alberta, D.R Braman and A.R. Sweet (eds.). Canadian Society of Petroleum Geologists, Annual Convention Fieldtrip Guide, p. 66-70.

Brand, W.A. 1996 - High precision isotope ratio monitoring techniques in mass spectrometry. Journal of Mass Spectrometry, v. 31, p. 225-235.

Bruun, P., 1962. Sea-level rise as a cause of shore erosion. American Society of Civil Engineers Proceedings, Journal of the Waterways and Harbors Division 88, p. 117–130.

Bustin, R.M., 1991 – Organic maturation of the Western Canada sedimentary basin. International Journal of Coal Geology, v. 19, p. 319-358.

Cadrin, A.A.J., Kyser, T.K., Caldwell, W.G.E., and Longstaffe, F.J., (1995) – Isotopic and chemical compositions of bentonites as paleoenvironmental indicators of the

Cretaceous Western Interior Seaway; Paleogeo., Paleoclim., Paleoecol., v.119, p. 301-320.

Caldwell, W.G.E, and Kauffman, E.G. (editors) 1993. Evolution of the Western Interior Basin. Geological Association of Canada. Special Paper 39, 680 pp.

Cant, D.J., and Stockmal, G.S. 1989. The Alberta foreland basin: Relationship between stratigraphy and Cordilleran terrane-accretion events. Canadian Journal of Earth Sciences, v. 26, p. 1964-1975.

Cattaneo, A., and Steel, R.J., 2003 - Transgressive deposits: a review of their variability. Earth-Science Reviews, Vol. 62, Issues 3-4, p. 187-228.

Chiou, C.T., and Rutherford, D.W., 1997 – Effects of exchanged cation and layer charge on the sorption of water and EGME vapors on montmorillonite clay. Clay and Clay Minerals, v. 45, p. 8-22.

Christopher, J.E., 1980 – The Lower Cretaceous Mannville Group of Saskatchewan – A tectonic overview. In: L.S. Beck, J.E. Christopher and D.M. Miller (Eds.), Lloydminster and beyond: geology of Mannville hydrocarbon reservoirs. Sask. Geol. Surv., Special Publication no.5, p.3-32.

Chung, H.M., 1976 – Isotope fractionation during the maturation of organic matter. Ph.D. Dissertation, Texas A&M University, College Station, Texas, 139 pp.

Chung, H.M., and Sackett, W.M., 1980 – Carbon isotope effects during the pyrolytic formation of early methane from carbonaceous materials. In: A.G. Douglas and J.R. Maxwell (Editors), Advances in Organic Geochemistry 1979. Pergamon, Oxford, p. 705-710.

Chung, H.M., Gormly, J.R., and Squires, R.M., 1988 - Origin of gaseous hydrocarbons in subsurface environments: theoretical considerations of carbon isotope distribution; Chem. Geol. V. 71, p. 97-103.

Claypool, G.E., and Kaplan, I.R., 1974 – The origin and distribution of methane in marine sediments. In: I.R. Kaplan (Ed.) Natural gases in marine sediments, Plenum Publishing, p. 99-139.

Claypool, G.E., 1999 – American Association of Petroleum Geologists Hedberg Research Conference – Natural gas formation and occurrence, Durango, CO, p. 27-29.

Clayton, C., 1991 – Effect of maturity on carbon isotope ratios of oils and condensates. Organic Geochemistry, v. 17, p. 887-899.

Coleman, D.D., Risatti, J.B., Schoell, M, 1981 – Fractionation of carbon and hydrogen isotopes by methane-oxidizing bacteria. Geochimica et Cosmochimica Acta, v. 45, p. 1033-1037.

Coleman, D.D., Liu, C.L., and Riley, K.M., 1988 – Microbial methane in the shallow Paleozoic sediments and glacial deposits of Illinois, U.S.A., Chem. Geol., v. 71, p. 23-40.

Colombo, U., Gazzarrini, F.,, Sironi, G., Gonfiantini, R., Tongiorgi, E., 1965. Carbon isotope composition of individual hydrocarbons from Italian natural gases. Nature, v.205, p.1303-1304.

Colombo, U., Gazzarrini, F., Gonfiantini, R., Sironi, G., Tongiorgi, E., 1966 - Measurement of $^{13}C/^{12}C$ isotope ratios on Italian natural gases and their geochemical interpretation fractionation. In: P.A. Schenck and I. Havenar (Eds.) Advances in organic geochemistry, 1964, Oxford, Pergamon Press, p. 279-292.

Colombo, U., Gazzarrini, F., Gonfiantini, R., Tongiorgi, E., and Caflish, L., 1969 – Carbon isotopic study of hydrocarbons in Italian natural gases. *In:* Schenk, P.A. and Havenaar, I. (Eds.), Advances in Organic geochemistry 1968, Oxford, Pergamon Press, 1969.

Colombo, U., Gazzarrini, F., Gonfiantini, R., Kneuper, G., Teichmuller, M., Teichmuller, R., 1970 - Carbon isotope study on methane from German coal deposits. In: G.D. Hobson and G.C. Speers (Eds.) Advances in organic geochemistry, 1966. Oxford, Pergamon Press, p. 1-26.

Corbet, T.F., and Bethke, C.M., 1992 – Disequilibrium fluid pressures and groundwater flow in the Western Canada sedimentary basin. Journal of Geophysical Research, v. 97, no. B5, p. 7203-7217.

Cramer, B., Poelchau, H. S., Gerling, P., Lopatin, N. V., and Littke, R., 1999. Methane released from groundwater: the source of natural gas accumulations in northern West Siberia. Marine and Petroleum Geology, 16, p. 225–244.

Davis, J.B., Yarborough, H.F., 1966 – Anaerobic oxidation of hydrocarbons by Desulfovibrio desulfuricans. Chemical Geology, v.1, p. 137-144.

Dawson, F.M., Evans, C.G., Marsh, R., and Richardson, R. 1994. Uppermost Cretaceous and Tertiary strata of the Western Canada Sedimentary Basin. *In* Geological Atlas of the Western Canada Sedimentary Basin. G.D. Mossop and I. Shetsen (comps.), Calgary. Canadian Society of Petroleum Geologists and Alberta Research Council, p. 387-406.

Dimitrakopoulos, R., and K. Muehlenbachs, 1987, Biodegradation of petroleum as a source of ^{13}C enriched carbon dioxide in the formation of carbonate cements: Chemical Geology, v. 65, p. 283-291.

Dominguez, J.M.L., Wanless, H.R., 1991 - Facies architecture of a falling sea-level strandplain, Doce River coast, Brazil. In: Swift, D.J.P., Oertel, G.F., Tillman, R.W., Thorne, J.A. (Eds.), Shelf Sand and Sandstone Bodies: Geometry, Facies and Sequence Stratigraphy, vol. 14. International Association of Sedimentologists Special Publication, pp. 259–281.

Doveton, J.H., 1986 – Log analysis of subsurface geology. Concepts and computer methods. John Wiley and Sons, Inc., 273 pp.

Doveton, J.H., 2000 – Spreadsheet log analysis of subsurface geology. The Compass, v.75, no. 2 & 3, p. 57-67.

Eberth, D.A. and Hamblin, A.P., 1993 - Tectonic, stratigraphic, and sedimentologic significance of a regional discontinuity in the upper Judith River Group (Belly River wedge) of southern Alberta, Saskatchewan, and northern Montana. Canadian Journal of Earth Sciences, 30, p. 174-200.

Embry, A.F., 1993 - Transgressive–regressive (T–R) sequence analysis of the Jurassic succession of the Sverdrup Basin, Canadian Arctic Archipelago. Canadian Journal of Earth Sciences 30, 301–320.

Emery, D., Myers, K., Bertram, G.T., 1996 - Sequence stratigraphy. Oxford ; Cambridge, Mass. : Blackwell Science, 297 pp.

Erno, B., and Schmitz, R., 1994 – Measurements of soil migration around oil and gas wells in the Lloydminster area. Technical meeting of the Petroleum Society of the CIM, 94, paper #73.

Evans, C.R., McIvor, D.K., and Magara, K., 1975 – Organic matter, compaction history, and hydrocarbon occurrence – Mackenzie delta, Canada; 9-th World Petroleum congress, Tokyo, Proc., v.3, p.149-157.

Faber, E., 1987 – Zur Isotopengeochemie gasformiger Kohlenwasserstoffe. Erdol Erdgas Kohle Zeitschrift 103, p. 210-218.

Frank, D.J., Gormly, J.R., and Sackett, W.M., 1974 – Revaluation of carbon-isotope compositions of natural methanes. AAPG Bulletin, 58, p. 2319-2325.

Friedrich, H.U., Jüntgen, H., 1972 – Some measurements on the $^{12}C/^{13}C$ in methane or ethane desorbed from hard coal or released by pyrolysis. *In:* Gaertner, H.r., Wehner, H. (Eds.), Advances in organic geochemistry, 1971, Pergamon, Oxford, p. 639-646.

Fuex, A.N., 1980 - Experimental evidence against an appreciable isotopic fractionation of methane during migration. *In:* A.G. Douglas and J.R. Maxwell (Eds.) Advances in organic geochemistry, 1979, London, Pergamon Press, p. 725-732.

Fuglem, M.D., 1970 – Use of core in evaluation of productive sands, Lloydminster area. *In:* Mesozoic Core Seminar, Saskatchewan Geological Society and Department of Mineral resources, Oct. 29-30, 1970, Regina, 12 pp.

Galimov, E.M., Ivlev, A.A., Kuznetsova, N.G., 1970 – Carbon isotope composition of gaseous hydrocarbons in petroleum and the problem of their origin, Geochem. Int., v. 7, p. 594-603.

Galimov, E.M., 1975. Carbon isotopes in oil-gas geology. In: NASA technical translation, NASA TT F-682, Washington, D.C., U.S. Government Printing Office.

Galloway, W.E., 1989. Genetic stratigraphic sequences in basin analysis. I. Architecture and genesis of flooding-surface bounded depositional units. American Association of Petroleum Geologists Bulletin 73, 125–142.

Garven, G. 1985. The role of regional fluid flow in the genesis of the Pine Point deposit, Western Canada Sedimentary Basin. Economic Geology, vol. 80, p. 307–324.

Gibson, D.W. 1977. Upper Cretaceous and Tertiary coal-bearing strata in the Drumheller-Ardley region, Red Deer River Valley, Alberta. Geological Survey of Canada, Paper 76-35, 41p.

Glass, D.J. (ed.). 1990. Lexicon of Canadian Stratigraphy, Volume 4, Western Canada. Canadian Society of Petroleum Geologists, 772p.

Gregor, V.A., 1997. Mannville linears in the Lloydminster heavy oil area and their relationship to fractures and fluid flow in the western Canada sedimentary basin. *In:* Petroleum geology of the Cretaceous Mannville Group, Western Canada. S.G. Pemberton and D.P. James (eds.). Canadian Society of Petroleum Geologists, Memoir 18, p. 428-474.

Gűrgey, K., Paul Philp A., Clayton, C., Emiroğlu, H., and Siyako, M., 2005. Geochemical and isotopical approach to maturity/source/mixing estimations for natural gas and associated condensates in the Thrace Basin, NW Turkey. Applied Geochemistry 20, p. 2017-2037.

Hacquebard,P.A., 1977. Rank of coal as an index of organic metamorphism for oil and gas in Alberta. *In* The origin and migration of petroleum in the Western Canadian sedimentary basin, Alberta: Geological Survey of Canada Bulletin 262, p. 11-22.

Hamblin, A.P. 1995. Stratigraphic architecture of the Campanian Belly River (Judith River) Group, southern Alberta plains, surface and subsurface. Geological Survey of Canada, Open File 3058, p. 33-38.

Hamblin, A.P. and Lee, P.J. 1997. Uppermost Cretaceous, Post-Colorado gas resources of the Western Canada Sedimentary Basin, Interior Plains. Geological Survey of Canada Bulletin 518, 88p.

Harrison, S.M., Gentzis, T., Labute, G., Seifert, S., Payne, M., 2006 – Preliminary hydrological assessment of Late Cretaceous-Tertiary Ardley coals in part of the Alberta Basin, Alberta, Canada. International Journal of Coal Geology, v. 65, p. 59-78.

Hearst, J.R., Nelson, P.H., 1985 – Well logging for physical properties. McGraw-Hill Book Company, New York, 571pp.

Hoering, T.C., and Moore, H.E., 1958 – The isotopic composition of nitrogen in natural gases and associated crude oils, Geochimica et Cosmochimica acta, v., p. 225-232.

Holysh, S., 1989 – Regional groundwater flow and petroleum related geochemical signatures, Chauvin area, east-central Alberta. MSc thesis, Univ. of Alberta, 208 pp.

Holysh, S., Tóth, J., 1996 – Flow of formation waters: likely cause for poor definition of soil gas anomalies over oil fields in east-central Alberta, Canada. *In:* D. Schumacher and M.A. Abrams (Eds.) Hydrocarbon migration and its near-surface expression, AAPG Memoir 66, p. 255-277.

Ingerson, E., 1953 – Nonradiogenic isotopes in geology: a review. Bulletin of the Geological Society of America, v. 64, p. 301-373.

Issler, D.R., S.D.Willett, S.D., Beaumont, C. and Grist, A.M., 1999. Paleotemperature history of two transects across the Western Canada Sedimentary Basin: Constraints from apatite fission track analysis. Bulletin of Canadian Petroleum Geology, v.47, p. 475-486.

Jackson, P.C., 1984 – Paleogeography of Lower Cretaceous Mannville Group of Western Canada. In: Masters, J.A. (Ed), Elmworth – Case study of a Deep Basin Gas Field. AAPG Mem 38. p. 49-77.

James, A.T., 1983 - Correlation of natural gas by use of carbon isotope distribution between hydrocarbon components: AAPG Bulletin, v. 67, p. 1176-1191.

James, A.T., 1990 - Correlation of reservoired gases using the carbon isotopic compositions of wet gas components: AAPG Bulletin, v. 74, p. 1441-1458.

James, A.T., and Burns, B.J., 1984 – Microbial alteration of subsurface natural gas accumulations. AAPG Bull., v.68, p.957-960.

Jeong, S., Werth, K.J., and Wander, M.M., 2003 – Sorption of hydrophobic organic contaminants to glacially deposited sediments of central Illinois. Geophysical Research Abstracts, Vol. 5, 06245. European Geophysical Society, 2003.

Jenden, P.D., and Kaplan, I.R., 1986 – Comparison of microbial gases from the Middle America Trench and Scripps Submarine Canyon: Implications for the origin of natural gas, Appl. Geochem., v.1, p. 631-646.

Jenden, P.D., and Kaplan, I.R., 1989 – Origin of natural gas in Sacramento basin, California, AAPG Bulletin, v. 73, p. 431-453.

Jenden, P.D., Newell, K.D., Kaplan, I.R., and Watney, W.L., 1988 – Composition and stable-isotope geochemistry of natural gases from Kansas, Midcontinent, U.S.A., Chem. Geol., v. 71, p. 117-147.

Jenden, P.D., Drazan, D.J., and Kaplan, I.R., 1993 – Mixing of thermogenic natural gases in northern Appalachian basin, AAPG Bulletin, v. 77, p. 980-998.

Jerzykiewicz, T. 1995 - Stratigraphy of the Saunders Group in the central Alberta Foothills – a progress report. Geological Survey of Canada, Paper 85-1B, p. 247-258.

Kalkreuth,W. and McMechan, M.E., 1984 - Regional pattern of thermal maturation as determined from coal-rank studies, Rocky Mountain foothills and front ranges north of Grande Cache, Alberta – implications for petroleum exploration. Bulletin of Canadian Petroleum Geology, v.32, p. 249-271.

Kalkreuth,W. and McMechan, M.E., 1988 – Burial history and thermal maturity, Rocky Mountain front ranges, foothills and foreland, east-central British Columbia and adjacent central Alberta, Canada. AAPG Bull., vol 72, p. 1395-1410.

Kauffman, E.G., and Caldwell, W.G.E. 1993. The Western Interior Basin in Space and Time. In W.G.E. Caldwell and E.G. Kauffmann (eds.) Evolution of the Western Interior Basin. Geological Association of Canada, Special Paper 39, p.1-30.

Krause, F.F., and Nelson, D.A. 1984. Storm event sedimentation: Lithofacies association in the Cardium Formation, Pembina area, west-central Alberta, Canada. *In*: D.F. Stott and D.J. Glass (eds.), The Mesozoic of Middle North America. Canadian Society of Petroleum Geologists, Memoir 9, p. 485-511.

Krooss, B.M., Leythaeuser, D., Schaefer, R.G., 1992 – The quantification of diffusive hydrocarbon losses through cap rocks of natural gas reservoirs – a reevaluation. AAPG Bull., v. 76, no. 3, p. 403-406.

Krooss, B.M., Schlomer, S., Gaschnitz, R., Littke, R., 1998. Aspects of natural gas generation and migration in sedimentary systems, Mineralogical Magazine, v. 62A, p. 818-819.

Leckie, D.A., Rosenthal, L., and James, D. 1996. Sedimentology of clastic reservoirs in southern Alberta: the Blaimore-Mannville groups and bounding strata. Geological Survey of Canada, Open File 3322, 108p.

Lerbekmo, J.F., Demchuk, T.D., Evans, M.E., and Hoye, G.S. 1992. Magnetostratigraphy and biostratigraphy of the continental Paleocene of the Red Deer valley, Alberta, Canada. Bulletin of Canadian Petroleum Geology, v. 40, p. 24-35.

Letourneau, J., Rostron, B., and K. Muehlenbachs, K., 2002. Geochemical and Hydrogeological Correlation of Active Gas Macro-seeps in Alberta. AAPG Hedberg Conference. April 7-10, 2002, Vancouver, BC, Canada.

Leythaeuser, D., Schaefer, R.G., and Yükler, A., 1980 – Diffusion of light hydrocarbons through near-surface rocks. Nature, v. 284, p. 522-525.

Leythaeuser, D., Schaefer, R.G., and Yükler, A., 1982 – Role of diffusion in primary migration of hydrocarbons. AAPG Bulletin, v. 66, p. 408-429.

Leythaeuser, D., Schaefer, R.G., and Pooch, H., 1983 – Diffusion of light hydrocarbons in subsurface sedimentary rocks. AAPG Bulletin, v. 67, p. 889-895.

Leythaeuser, D., Mackenzie, A., Schaefer, R.G., and Bjorøy, 1984 – A novel approach for recognition and quantification of hydrocarbon migration effects in shale-sandstone sequences. AAPG Bulletin, v. 68, p. 196-219.

Littke, R., Cramer, B., Gerling, P., Lopatin, N. V., Poelchau, H. S., Schaefer, R. G., and Welte, D. H., 1999. Gas generation and accumulation in the West Siberian Basin. AAPG Bulletin, 83, p. 1642–1665.

Lorant, F., Prinzhofer, A., Behar, F, and Huc, A.Y., 1998 – Carbon isotopic and molecular constraints on the formation and the expulsion of thermogenic hydrocarbon gases; Chem. Geol., v. 147, p. 240-264.

Macauley, G., 1984 – Geology of the oil shale deposits of Canada. Geological Survey of Canada, Paper 81-25, 65 pp.

Macdonald, D.E., Ross, T.C., McCabe, P.J., and Bosman, A., 1987. An evaluation of the coal resources of the Belly River Group to a depth of 400 m in the Alberta plains. Alberta Research Council, Open File Report 1987-8, 76pp.

MacEachern, J.A., Raychaudhuri, I., and Pemberton, S.G. 1992. Stratigraphic applications of the Glossifungites ichnofacies: delineating discontinuities in the rock record. *In* S.G. Pemberton (ed). Applications of ichnology to petroleum exploration, a core workshop: SEPM Core Workshop 17, p. 169-198.

MacEachern, J.A., and Hobbs, T.W., 2004. The ichnological expression of marine and marginal marine conglomerates and conglomeratic intervals, Cretaceous Western Interior Seaway, Alberta and northeastern British Columbia. Bulletin of Canadian Petroleum Geology, v. 52, p. 77-104.

Macqueen, R., and Leckie, D.A. (editors) 1992. Foreland Basins and Foldbelts. AAPG Memoir 55, 460pp.

Magara, K., 1981 – Mechanisms of natural fracturing in a sedimentary basin. AAPG Bull., p. 123-132.

Magara, K., 1978 – Compaction and fluid migration. Dev. in Petrol. Sci., 9, Elsevier, Amsterdam.

Martini, A., Budai, A., Walters, L., and Schoell, M., 1996 – Economic accumulation of biogenic methane, Nature, v. 383, p. 153-158.

Mathison, J.E., 1988 – Upper Mannville tidal creek and incised fluvial channel reservoirs at the Fort Kent Thermal Project of east-central Alberta. *In:* D.P.James and D.A. Leckie (Eds.) Sequences, Stratigraphy, Sedimentology, Surface and Subsurface. Canadian Society of Petroleum Geology Memoir 15, p. 331-350.

May, F., Freund, W., Peter Müller, E., 1968 – Modellversuche über Isotopen-fraktionierung von Erdgaskomponenten während der Migration, Z. Angew. Geol. Vol. 14, no. 7.

McCabe, P.J., Strobl, R.S., Macdonald, D.E., Nurkowski, J.R., and Bosman, A. 1989. An evaluation of the coal resources of the Horseshoe Canyon Formation and laterally equivalent strata, to a depth of 400 m, in the Alberta Plains area. Alberta Research Council, Open File Report 1989-07, 75 pp.

Meyboom, P. 1960. Geology and groundwater resources of the Milk River sandstones in southern Alberta. Research Council of Alberta, Memoir 2, 89 pp.

Mossop, G., and Shetsen, I. (compilers) 1994. Geological Atlas of the Western Canada Sedimentary Basin. Canadian Society of Petroleum Geologists and the Alberta Research Council, 510 pp.

Murray, A.P., Summons, R.E., Boreham, C.J., and Dowling, L.M., 1994. Biomarker and n-alkanes isotope profiles for Tertiary oils: relationship to source rock depositional setting. Organic Geochemistry, 22, p. 521-542.

Neglia, S., 1979 – Migration of fluids in sedimentary basins, AAPG Bulletin, v. 63, p. 573-597.

Nelson, J.S, Simmons, E.C., 1995 – Diffusion of methane and ethane through the reservoir cap rock: implications for the timing and duration of catagenesis. AAPG Bull., v. 79, no. 7, p. 1064-1074.

Nelson, J.S, Simmons, E.C., 1996 – Diffusion of methane and ethane through the reservoir cap rock: implications for the timing and duration of catagenesis: Reply. AAPG Bull., v. 80, no. 9, p. 1486-1488.

Nernst, W., 1923 – Theoretical chemistry from the standpoint of Avogadro's rule and thermodynamics, revised in accordance with the eight-tenth German edition by L.W. Codd. London, MacMillan, 922 pp.

Nummedal, D. and Swift, D.J.P. 1987. Transgressive stratigraphy at sequence-bounding unconformities: some principles derived from Holocene and Cretaceous examples. *In* D. Nummedal, O.H. Pilkey, and J.D. Howards (eds.). Sea-level fluctuation and coastal evolution: SEPM Special Publication 41, p. 241-260.

Nurkowski, J.R., 1984. Coal quality, coal rank variation and its relation to reconstructed overburden, Upper Cretaceous and Tertiary Plains coals, Alberta, Canada, AAPG Bulletin v. 68, p. 285-295.

Oremland, R.S., Whiticar, M.J., Strohmaier, F.E., and Kiene, R.P., 1988 – Bacterial ethane formation from reduced ethylated sulfur compounds in anoxic sediments. Geochimica et Cosmochimica Acta, v. 52, p. 1895-1904.

Pallasser, R.J., 2000 – Recognizing biodegradation in gas/oil accumulations through the $\delta^{13}C$ compositions of gas components. Organic Geochemistry, v. 31, p. 1363-1373.

Parks, K.P., and Tóth, J., 1995 – Field evidence for erosion-induced underpressuring in the Upper Cretaceous and Tertiary strata, west central Alberta, Canada. Bulletin of Canadian Petroleum Geology, v. 43, p. 281-292.

Pattison, S.A.J. 1991. Sedimentology and allostratigraphy of regional, valley-fill, shoreface and transgressive deposits of the Viking Formation (Lower Cretaceous), Central Alberta. Unpublished Ph.D. Thesis, McMaster University, Hamilton, Ontario, 380 pp.

Pattison, S.A.J., and Walker, R.G., 1998. Multiphase transgressive filling of an incised valley and shoreface complex, Viking Formation, Sundance-Edson area, Alberta. Bulletin of Canadian Petroleum Geology, v. 46, p. 89-105.

Paull, C.K., Lorenson, T.D., Borowski, W.S., Usler III, W., Olsen, K., Rodriguez, N.M., 2000 – Isotopic compositions of CH4, CO2 species, and sedimentary organic matter within samples from the Blake Ridge: gas source implications. In: Paull, C.K., Matsumoto, R., Wallace, P.J., Dillon, W.P., et al. (Eds.), Proceedings of the Ocean Drilling Program, Scientific Results 164, College Station, TX, p. 67-78.

Pemberton, S.G., and MacEachern, J.A. 1995. The sequence stratigraphic significance of trace fossils: Example from the Cretaceous Foreland Basin of Alberta, Canada. *In* AAPG Memoir 64, p. 429-475.

Pernaton, E., Prinzhofer, A., Schneider, F., 1996. Reconsideration of methane signature as a criterion for the genesis of natural gas: influence of migration on isotopic signature, Revue de l'IFP, v. 51, p.635-651.

Plint, A.G., 1988. Sharp-based shoreface sequences and offshore bars in the Cardium Formation of Alberta; their relationship to relative changes in sea level. In: Wilgus, C.K., Hastings, B.S., Kendall, C.G.St.C., Posamentier, H.W., Ross, C.A., Van Wagoner, J.C. (Eds.), Sea Level Changes—An Integrated Approach, vol. 42. SEPM Special Publication, p. 357–370.

Plint, A.G., Walker, R.G., and Duke, W.L. 1988. An outcrop to subsurface correlation of the Cardium Formation in Alberta. *In* D.P.James and D.A. Leckie (eds.) Sequences, Stratigraphy, Sedimentology, Surface and Subsurface. Canadian Society of Petroleum Geology Memoir 15, p. 167-184.

Plint, A.G., Nummedal, D., 2000. The falling stage systems tract: recognition and importance in sequence stratigraphic analysis. In: Hunt, D., Gawthorpe, R.L. (Eds.), Sedimentary Response to Forced Regression, vol. 172. Geol. Soc. London Special Publ, p. 1–17.

Posamentier, H.W., Jervey, M.T., Vail, P.R., 1988. Eustatic controls on clastic deposition. I. Conceptual framework. In: Wilgus, C.K., Hastings, B.S., Kendall, C.G.St.C., Posamentier, H.W., Ross, C.A., Van Wagoner, J.C. (Eds.), Sea Level Changes—An Integrated Approach, vol. 42. SEPM Special Publication, p. 110–124.

Power, B, and Walker, R.G., 1996 – Allostratigraphy of the Upper Cretaceous Lea Park-Belly River transition in central Alberta, Canada. Bull. Can. Petrol. Geol., v.44, no.1, p.14-38

Price, R.A. 1994. Cordilleran tectonics and the evolution of the Western Canada Sedimentary Basin. In Geological Atlas of the Western Canada Sedimentary Basin. G.D. Mossop and I. Shetsen (comps.), Calgary. Canadian Society of Petroleum Geologists and Alberta research Council, p. 13-24.

Prinzhofer, A., Huc, A.Y., 1995 – genetic and post-genetic molecular and isotopic fractionations in natural gases; Chemical Geology, v. 126, p. 281-290.

Prinzhofer, A., Pernaton, E., 1997. Isotopically light methane in natural gas: bacterial imprint or segregative migration?, Chemical Geology, v. 3-4, p. 193-200.

Prinzhofer, A., Mello, M.R., da Silva Freitas, L.C., Takaki, T., 2000 (a) - New geochemical characterization of natural gas and its use in oil and gas evaluation. In: M.R. Mello and B.J. Katz (Eds.) Petroleum systems of South Atlantic margins. AAPG Memoir 73, p. 107-119.

Prinzhofer, A., Mello, M.R., and Takaki, T., 2000 (b) – Geochemical characterization of natural gas: a physical multivariable approach and its applications in maturity and migration estimates, AAPG Bulletin, v. 84, p. 1152-1172.

Putnam, P.E., 1982 – Aspects of the petroleum geology of the Lloydminster heavy oil fields, Alberta and Saskatchewan. Bull. of Can. Petrol. Geol., v. 30, p. 81-111.

Rayleigh, J.W.S., 1896 – Theoretical considerations respecting the separation of gases by diffusion and similar processes. Philos. Mag. 42, p.493-499.

Reinson, G.E., Warters, W.J., Cox, J., and Price P.R. 1994. Cretaceous Viking Formation of the Western Canada Sedimentary Basin. *In:* Mossop, G., and Shetsen, I. (compilers), Geological Atlas of the Western Canada Sedimentary Basin. Canadian Society of Petroleum Geologists and the Alberta Research Council, Chapter 21.

Reitsema, R.H., Kaltenback, A.J., and Lindberg, F.A., 1980. Source and migration of light hydrocarbons indicated by carbon isotopic ratios. AAPG Bull., 65, p. 1536-1542

Reynolds, A.D., 1996. Paralic successions. *In*: Emery, D., and Myers, K.J. (eds.) Sequence stratigraphy. Applications to Depositional Systems, p. 134-177.

Rice, D.D., 1992 – Controls, habitat and resource potential of ancient bacterial gas. *In:* R. Vially (Ed.) Bacterial gas, Editions Technip, Paris, p. 91-118.

Rice, D.D., 1993 – Composition and origins of coalbed gas. In: B.E. Law and D.D. Rice (Eds.), Hydrocarbons from coal. AAPG Studies in Geology 38, p. 159-184.

Rice, D.D. and Claypool, G.E., 1981 - Generation, accumulation, and resource potential of biogenic gas. AAPG Bulletin, v. 65; no. 1; p. 5-25

Rich, K., 1995. Determination of the source of migrating gas from oil and gas wells in the Lloydminster area using stable isotope analyses. M.Sc.thesis, University of Alberta.

Richards, M.T., 1996. Fluvial Systems. *In*: Emery, D., and Myers, K.J. (Eds.) Sequence stratigraphy. Applications to Depositional Systems, p.111-133.

Richardson, R.J.H., 1991 – Coal resources and coalbed methane potential of a major Alberta coal zone. In Coalbed Methane of Western North America, Guidebook for the Rocky Mountain Association of Geologists Fall Conference and Field Trip (Schwochow, S.D., D.K. Murray and M.F. Fahy (Eds.), Denver, CO, p.255-263.

Riediger, C., Aronson J., Meyer E. and Asgar-Deen M., 2006 - K-Ar dating of diagenetic illite in K-bentonites, with implications for charge in the Western Canada Foreland Basin. Abstract, Integrated Charge Evaluation, Fluid Properties, and Geochemistry Workshop, Denver, Colorado, October 9-13, 2006.

Ridgley, J.L., Hester, T.C., Condon, S.M., Cook, T., Anna, L.O., Lillis, P.G., Rowan, E.L., and Snyder, G.T., 2001 – Assessment of Shallow Biogenic Gas Resources in Montana. *In:* Abstracts of Technical Talks, Posters and Core Displays. Canadian Society of Petroleum Geologists, page no. 045-1 to 045-6.

Rigby, D. and Smith, J.W., 1981 – An isotopic study of gases and hydrocarbons in the Cooper basin. Australian Petroleum Exploration Association Journal, v.21, p.222-229.

Rohrback, B.G., Peters, K.E, and Kaplan, I.R., 1984 – Geochemistry of artificially-heated humic and sapropelic sediments, II. Oil and Gas generation. AAPG Bulletin, 68, p. 961-970.

Rooney, M. A., Claypool, G. E., and Chung, E. M., 1995. Modelling thermogenic gas generation using carbon isotope ratios of natural gas hydrocarbons. Chemical Geology, 126 (3/4), p.219–232.

Ross, D.J.K., Bustin, R. M., 2007 – Impact of mass balance calculations on adsorbtion capacities in microporous shale gas reservoirs. Submitted to the Bulletin of Canadian Petroleum Geology, *in review*. Fuel (2007), doi: 10.1016/j.fuel.2007.02.036

Rostron, B.J., Tóth, J., 1997 – Cross-formational fluid flow and the generation of a saline plume of formation waters in the Mannville Group, West-Central Alberta. In: Petroleum Geology of the Cretaceous Mannville Group, Western Canada, S.G. Pemberton and D.P. James (Eds.), CSPG Memoir 18, p. 169-190.

Rowe, D.M., 1998 – Determination of the origin of migrating gases in the heavy oil fields of Alberta and Saskatchewan using carbon isotope analyses. MSc thesis, University of Alberta, 85 pp.

Rowe, D.M. and Muehlenbachs A., 1999 (a). Low-temperature thermal generation of hydrocarbon gases in shallow shales. Nature, v. 398, p. 61-63.

Rowe, D.M. and Muehlenbachs K., 1999 (b). Isotopic fingerprint of shallow gases in the Western Canadian Sedimentary Basin: tools for remediation of leaking heavy oil wells. Organic Geochemistry, v. 30, p. 861-867.

Russell, L.S. 1983. Evidence for an unconformity at the Scollard-Battle contact, Upper Cretaceous strata, Alberta. Canadian Journal of Earth Sciences, v. 20, p. 1219-1231.

Sandberg, K.R., and Bennet C.R., 1983 - Carbon isotope thermomethry of natural gas. In: M. Bjoroy, P. Albrecht, C. Cornford, et al. (Eds.) Advances in organic geochemistry, Chicester, England, John Wiley and Sons, p. 769-774.

Schlumberger, 1999 – Log Interpretation Principles/Applications. Eight printing, Schlumberger Wireline and Testing, Texas.

Schmitz, R., Carlson, P.B., Lorenz, G.D., Watson, M.D., and Erno, B.P. 1993 – Husky Oil's gas migration research effort- an update. In: 10th heavy oil and oil sands technical symposium, Canadian Heavy oil Association.

Schoell, M., 1977 – Die Erdgase der Süddeutschen Molasse, Erdoel-Erdgas-Zeitschrift, v. 93, p. 311-322.

Schoell, M., 1980. The hydrogen and carbon isotopic composition of methane from natural gas of various origin. Geochimica Cosmochimica Acta, v.44, p. 649-661.

Schoell, M., 1983. Genetic characterization of natural gases, AAPG Bull., v. 67, no. 12, p. 2225-2238.

Schoell, M., 1988 – Multiple origins of methane in the earth. Chemical Geology, v. 21, p. 1-10.

Schoell, M., McCaffrey, M.A., Fago, F.J., and Moldowan, J.M. 1992. Carbon isotope compositions of 28,30-bisnorhopanes and other biological markers in a Monterey crude oil. Geochemica et Cosmochimica Acta, 56, p. 1391-1399.

Schoell, M., Simoneit, B.R.T., and Wang, T.G., 1994. Organic geochemistry and coal petrology of Tertiary brown coal in the Zhoujing mine, Baise Basin, South China – 4. Biomarker sources inferred from stable carbon isotope compositions of individual compounds. Organic Geochemistry, 21, p. 713-719.

Schröeder-Adams, C.L., Bloch, J.D., Leckie, D.A., Craig, J, McIntyre, D.J., and Adams, P.J. 1996. Paleoenvironmental changes in the Cretaceous (Albian to Turonian) Colorado group of western Canada: microfossil, sedimentological and geochemical evidence. Cretaceous Research, v. 17, p. 311-365.

Schröeder-Adams, C.L., Adams, P., Leckie, D., Bloch, J., Craig, J., and Seif El_Dein, S.A., 1997 – Upper Cretaceous Medicine Hat Formation and First White Speckled Shale in southeastern Alberta: evidence for localized shallow water deposits. CSPG Bull., vol 45, no.3, p. 356-376.

Scott, A.R., 1993 - Composition and origin of coalbed gases from selected basins in the United States. 1993 International Coalbed Methane Symposium Proceedings. University of Alabama, Tuscaloosa, Alabama, p. 207– 222.

Scott, A.R., Zhou, N., and Ayers, W.B., 1994 – Thermogenic and secondary biogenic gases, San Juan basin, Colorado and New Mexico – implications for coal bed gas producibility, AAPG Bull., vol. 78, p. 1186- 1209.

Shurr, G.W., and Ridgley, J.L., 2002 – Unconventional shallow biogenic gas systems. AAPG Bull., v. 86, p.1939-1970.

Sloss, L.L. 1963. Sequences in the cratonic interior of North America. Geological Society of America Bulletin, v. 74, p. 93-113.

Sloss, L.L., Krumbein, W.C., Dapples, E.C., 1949. Integrated facies analysis. In: Longwell, C.R. (Ed.), Sedimentary Facies in Geologic History, vol. 39. Geological Society of America Memoir, pp. 91–124.

Smith, J.E., Erdman, J.G., and Morris, D.A., 1971 – Migration, accumulation and retention of petroleum in the earth. *In*: 8th World Petroleum Congress Proceedings, v.2. London, Applied Science Publishers, p.13-26.

Smith, S.R., vanHulten, F.F.N., and Young, S.D., 1984 – Distribution of the Sparky formation heavy oil fields within Lloydminster sub-basin. In: Lorsong, J.A. and Wilson, M.A. (Eds.), Saskatchewan Geological Society, Spec. Publ. 7, p. 149-168.

Smith, J.W., Rigby, D., Gould, K.W., and Hart, G., 1985 - An isotopic study of hydrocarbon generation processes. Org. Geochem., v. 8, p. 341-347.

Southard, J.B., 1971. Representation of bed configurations in depth-velocity-size diagrams. Journal of Sedimentary Petrology, v. 41, p. 903-915.

Stahl, W., Carey, B.D., 1975 – Source-rock identification by isotope analyses of natural gases from fields in the Val Verde and Delaware basins, West Texas, Chem. Geol., v. 16, p. 257-267.

Stahl, W., 1977 – Carbon and nitrogen isotopes in hydrocarbon research and exploration. Chem. Geol., v. 20, p. 121-149.

Stahl, W.J., 1978, Source rock – crude oil correlation by isotopic type-curves: Geochimica et Cosmochimica Acta, v. 42, p. 1573-1577.

Stahl, W.J., 1980 – Compositional changes and $^{13}C/^{12}C$ fractionation during the degradation of hydrocarbons by bacteria. Geochimica et Cosmochimica Acta, v. 44, p. 1903-1907.

Stasiuk, L.D., and Goodarzi, F., 1988 – Organic petrology of Second White Speckled Shale, Saskatchewan, Canada – possible link between bituminite and biogenic gas? Bull. of Canadian Petroleum Geology, v. 36, p. 397-406.

Stott, D.F., and Aitken, J. D. (editors) 1993. Sedimentary cover of the craton in Canada. In the collection: The geology of North America. 826p.

Syngayevsky, Y.D., Lebedev, V.S., Safrona, T.P., Sushilin, A.V., 1978 – Study of fractionation of carbon isotopes during migration of hydrocarbons in the gas phase through rocks, Geol. Nefti Gaza 1, p. 53-59.

Szatkowski, B., Whittaker, S., Johnston, B., 2002 – Identifying the Source of Migrating Gases in Surface Casing Vents and Soils Using Stable Carbon Isotopes, Golden Lake Pool, west-central Saskatchewan. In: Summary of Investigations 2002, Volume 1, Saskatchewan Geological Survey, Sask. Industry and Resources, Misc. Rep.2002-4.1, p. 118-125.

Taylor, S.W., Sherwood Lollar, B., and Wassenaar, L.I., 2000 – Bacteriogenic ethane in near-surface aquifers: implications for leaking hydrocarbon well bores. Environ. Sci. Technol., 34, p. 4727-4732.

Tilley, B.J., Muehlenbachs, K., 2006. Gas maturity and alteration systematics across the Western Canada Sedimentary Basin from four mud gas isotope depth profiles. Organic Geochemistry 37, p.1857–1868.

Tilley, B.J., Muehlenbachs, K., and Szatkowski, B.J., 2001. Compartmentalization of gas reservoirs: insights from carbon isotope ratios. *In* Abstracts of Technical Talks, Posters and Core Displays. Canadian Society of Petroleum Geologists, p. 336-339.

Tissot, B.P, and Welte, D.H., 1994 – Petroleum formation and occurrence, Springer-Verlag, Berlin, 699 pp.

Tompkins, B.G., 1989 – An integrated core-well log study and stratigraphic correlation of the Lower Cretaceous Mannville Group, Lloydminster sub-basin, west-central Saskatchewan and east-central Alberta. MSc Thesis, Univ. of Calgary.

Van Krevelen, D.W., 1961 – Coal. Elsevier, Amsterdam – London - New York, 514 pp.

Van Wagoner, J.C., Posamentier, H.W., Mitchum, R.M., Vail, P.R., Sarg, J.F., Loutit, T.S., Hardenbol, J., 1988. An overview of sequence stratigraphy and key definitions. In: Wilgus, C.K., Hastings, B.S., Kendall, C.G.St.C., Posamentier, H.W., Ross, C.A., Van Wagoner, J.C. (Eds.), Sea Level Changes—An Integrated Approach, vol. 42. SEPM Special Publication, pp. 39–45.

Van Wagoner, J.C., Mitchum, R.M., Campion, K.M., and Rahmanian, V.D. 1990. Siliciclastic sequences, stratigraphy in well logs, cores, and outcrops: concepts for high-resolution correlation of time and facies. AAPG Methods in Exploration 7, 55p.

Vigrass, L.W., 1977 – Trapping of oil at the intra-Mannville (Lower Cretaceous) disconformity in the Lloydminster area, Alberta and Saskatchewan. AAPG Bull., v. 61, p. 1010-1028.

Walker, R.G., and Plint, A.G. 1992 - Wave- and shallow-marine systems. *In:* R.G. Walker and James N. (Eds.) Facies models: response to sea level change. Geological Association of Canada, p. 47-72.

Waseda, A., Didyk, B.M., 1995 – Isotope composition of gases in sediments from the Chile continental margin. In: Lewis, S.D., Behrmann, J.H., Musgrave, R.J., Candy, S.C., et al. (Eds.), Proceedings of the Ocean Drilling Program, Scientific Results 141, College Station, TX, p. 307-312.

Western Atlas, 1992 – Introduction to wireline log analysis. Western Atlas International, Houston, Texas.

Whiticar, M.J., 1990 – A geochemical perspective of natural gas and atmospheric methane, Org. Geochem., v. 16, p. 531-547.

Whiticar, M.J., 1994 – Correlation of natural gases with their sources. *In:* Magoon L.B. and W.G. Dow (Eds.), The petroleum systems – from source to trap. AAPG Memoir 60, p. 261-283.

Whiticar, M.J., 1996 – Stable isotope geochemistry of coals, humic kerogens and related natural gases. International Journal of Coal Geology 32, p. 191-215.

Whiticar, M.J., 1999 – Carbon and hydrogen isotope systematics of bacterial formation and oxidation of methane, Chemical Geology, v. 161, p. 291-314.

Whiticar, M.J., Faber, E., 1986 – Methane oxidation in sediment and water column environments – isotope evidence. Organic Geochemistry, v.10, p. 759-786.

Whiticar, M.J., Faber, E., Schoell, M., 1986 – Biogenic methane formation in marine and fresh water environments: CO2 reduction vs. acetate fermentation-isotope evidence. Geochimica et Cosmochimica Acta, v. 65 1(6), p. 2723-2742.

Zengler, K., Richnow, H.H., Rossello´-Mora, R., Michaelis, W., Widdel, F., 1999 - Methane formation from long-chain alkanes by anaerobic microorganisms. Nature 401, p. 266–269.

Zheng L., and Yapa, P.D., 2002 - Modeling gas dissolution in deepwater oil/gas spills. Journal of Marine Systems, Volume 31, Issue 4, p. 299-309.

Addendum A

Diffractograms for 9 (nine) shale samples taken from
the Shell Paradise 10-25-047-3W4 core (**Figures 5-9 to 5-21**)

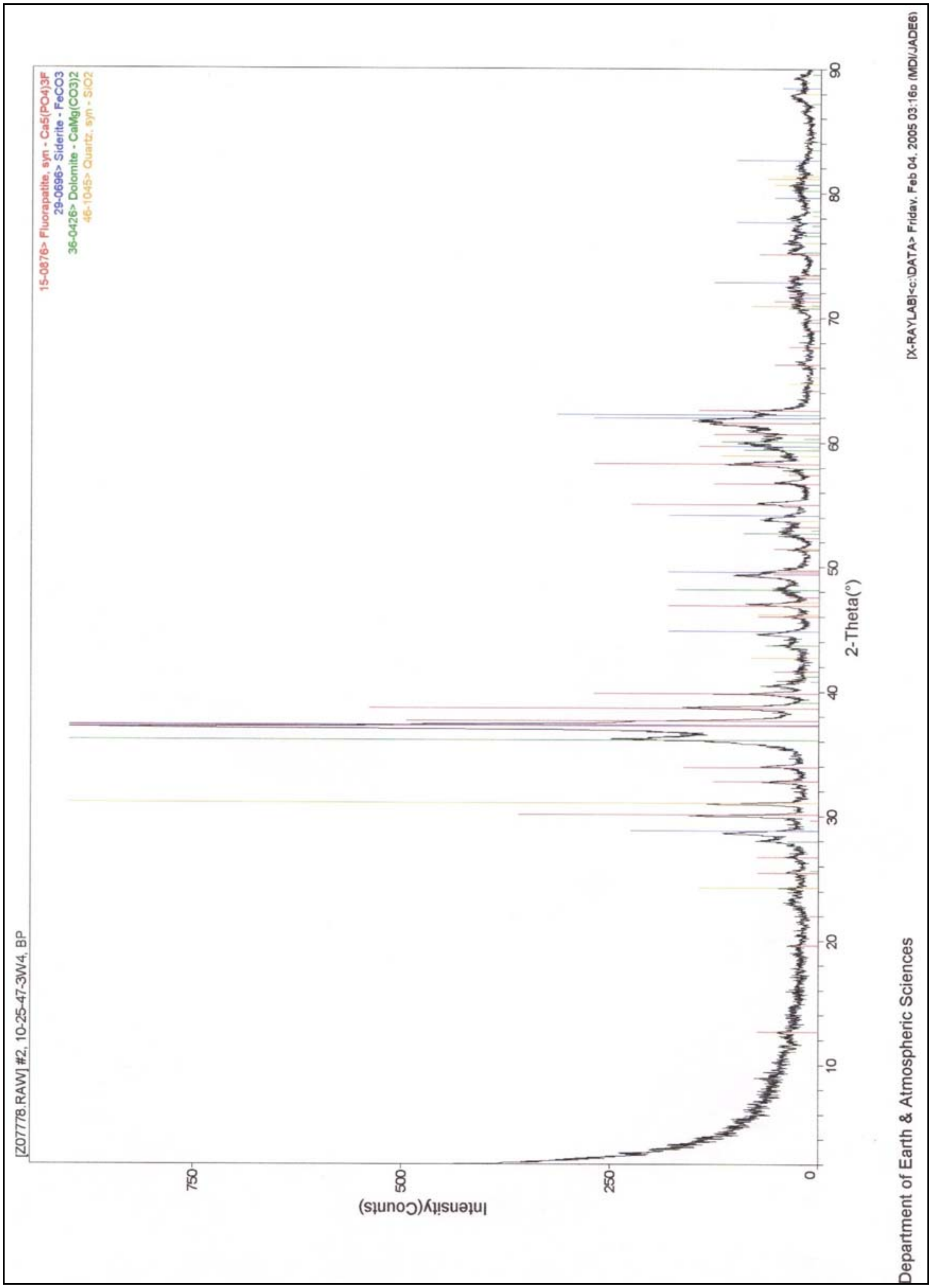

Figure 5-9 The resultant diffractogram of sample #2 (538.5m depth) - Shell Paradise 10-25-047-3W4 core.

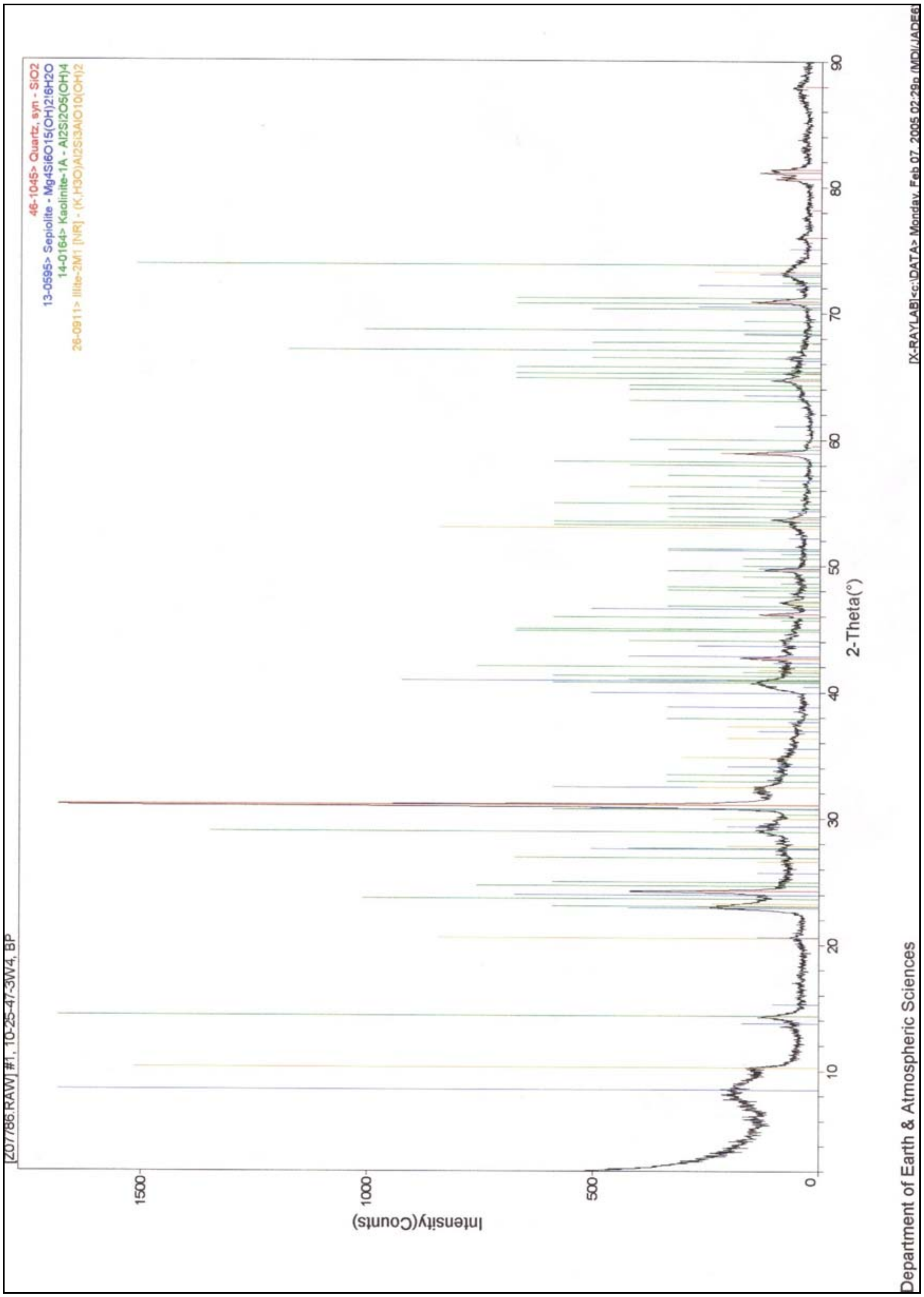

Figure 5-10 The resultant diffractogram of sample #1 (538.9m depth) - Shell Paradise 10-25-047-3W4 core.

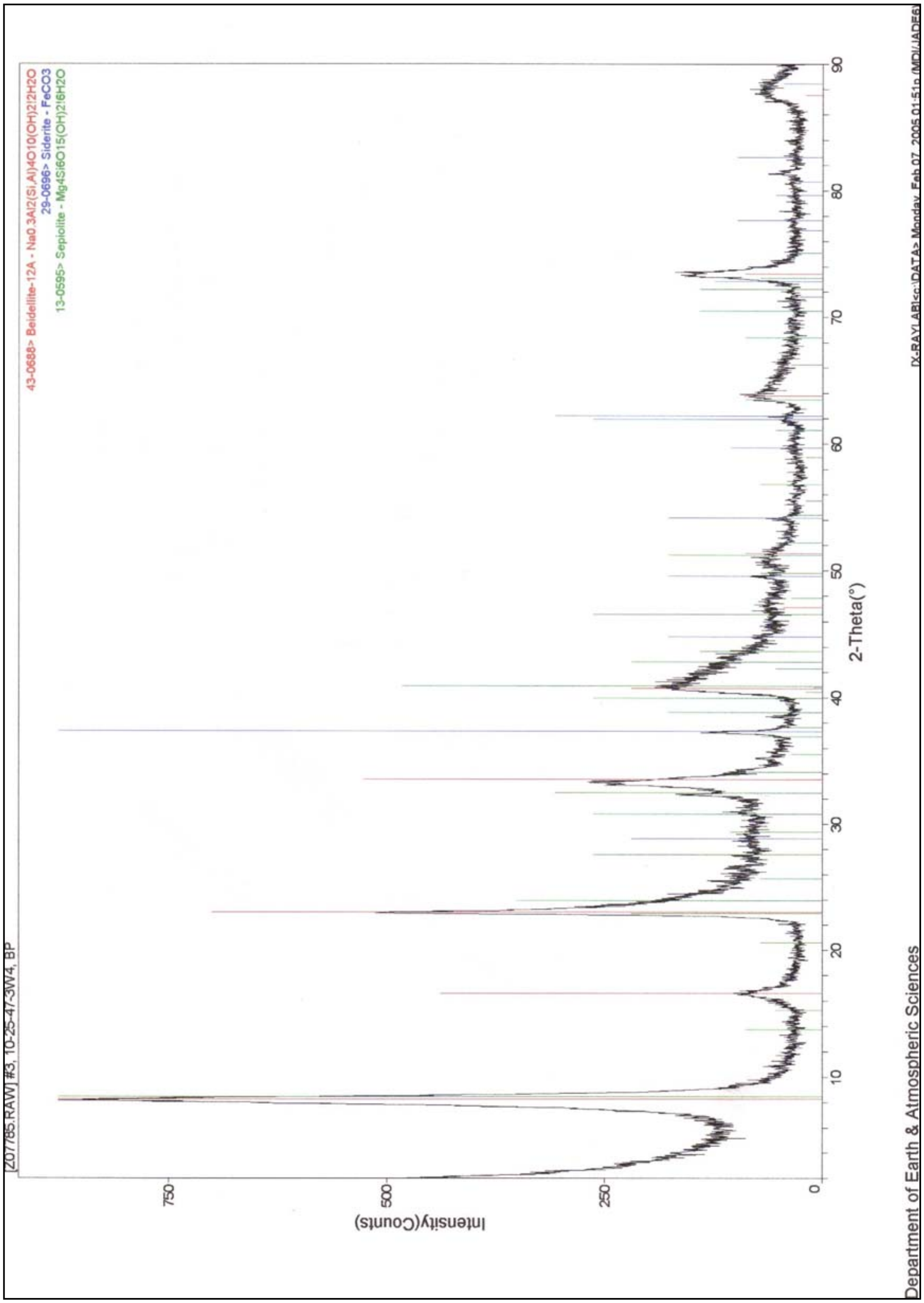

Figure 5-11 The resultant diffractogram of sample #3 (546m depth) - Shell Paradise 10-25-047-3W4 core.

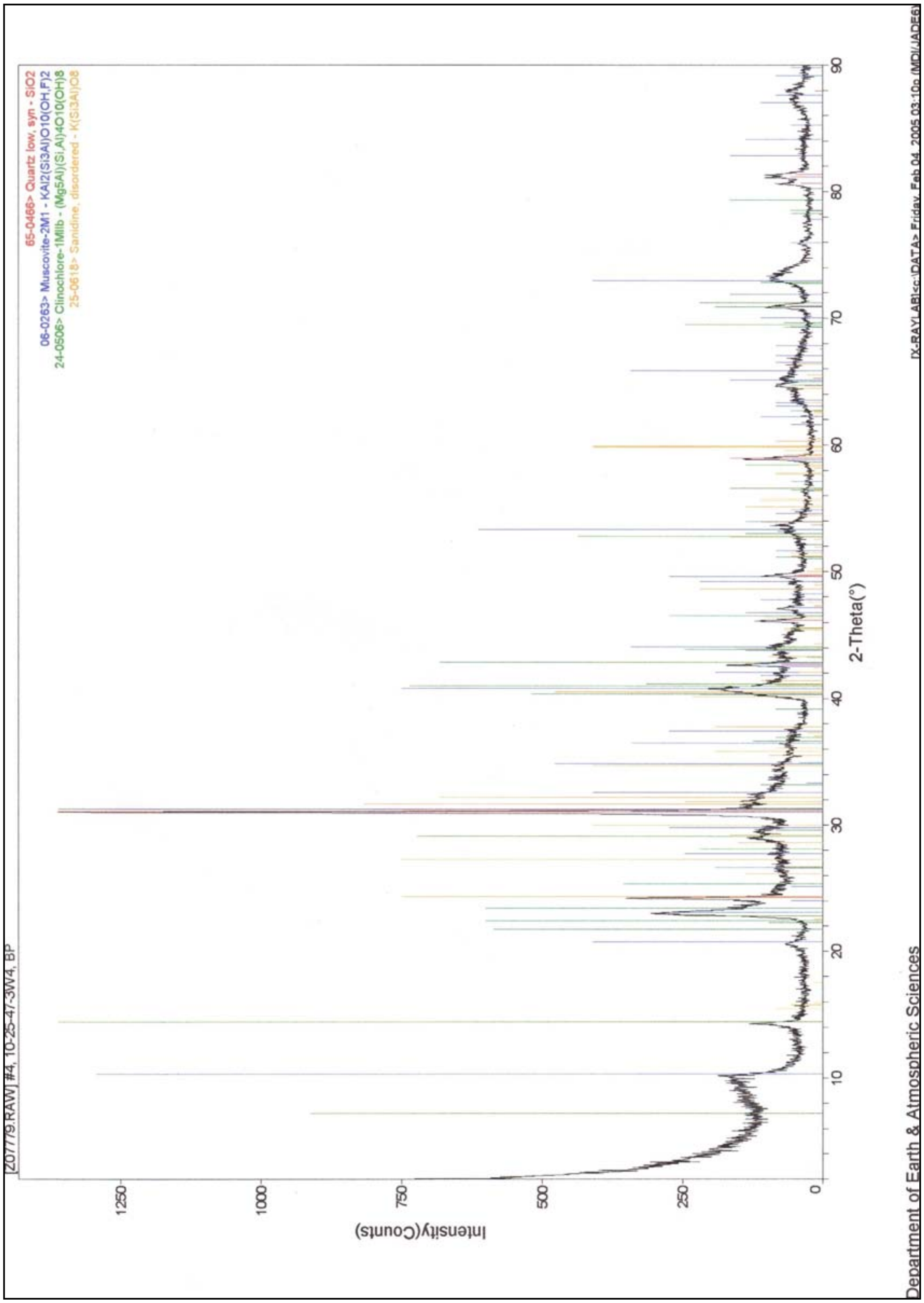

Figure 5-12 The resultant diffractogram of sample #4 (567.4m depth) - Shell Paradise 10-25-047-3W4 core.

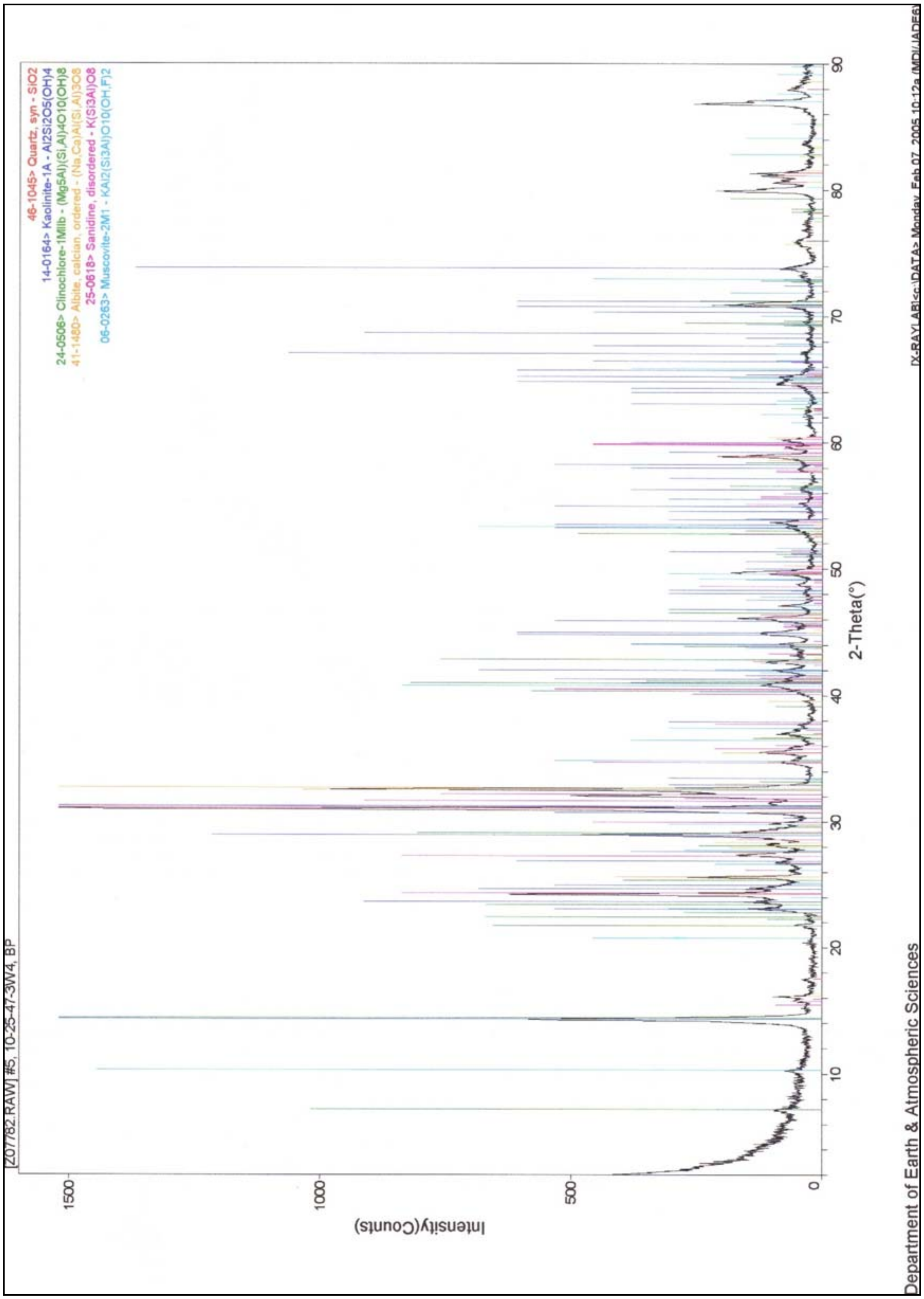

Figure 5-13 The resultant diffractogram of sample #5 (576.5m depth) - Shell Paradise 10-25-047-3W4 core.

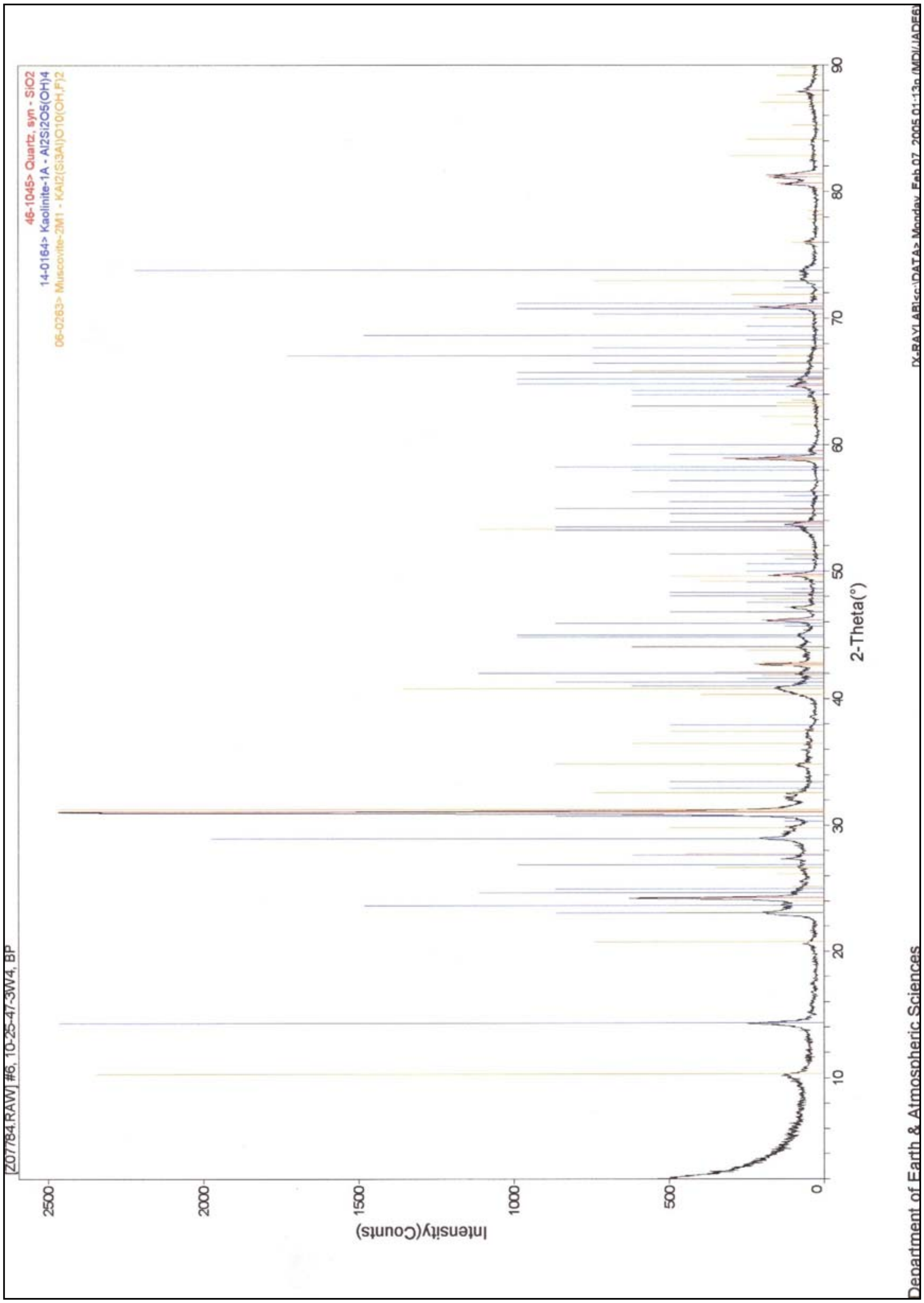

Figure 5-14 The resultant diffractogram of sample #6 (636m depth) - Shell Paradise 10-25-047-3W4 core.

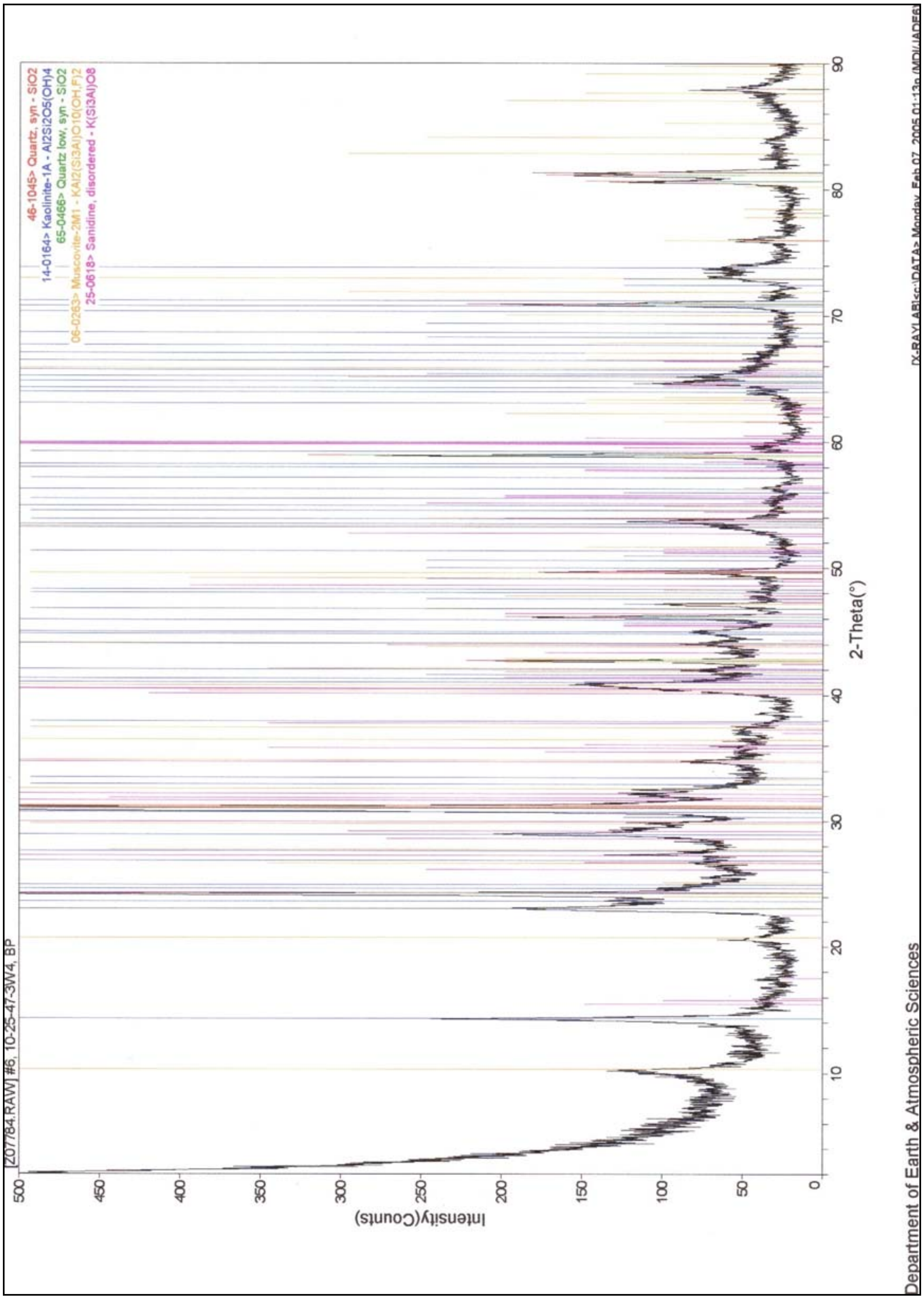

Figure 5-15 The resultant diffractogram of sample #6 (636m depth) - Shell Paradise 10-25-047-3W4 core – larger intensity scale.

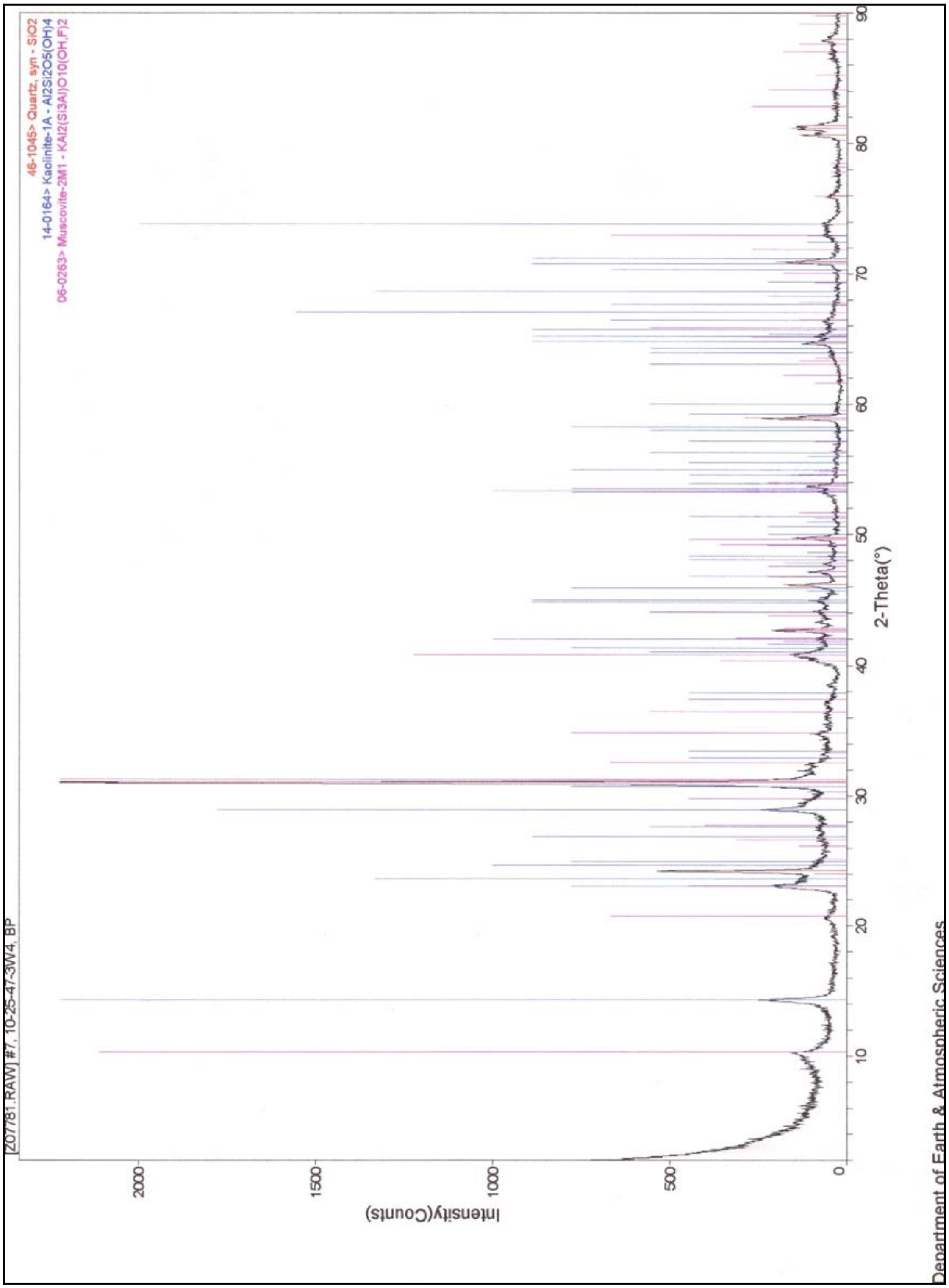

Figure 5-16 The resultant diffractogram of sample #7 (654.2m depth) - Shell Paradise 10-25-047-3W4 core.

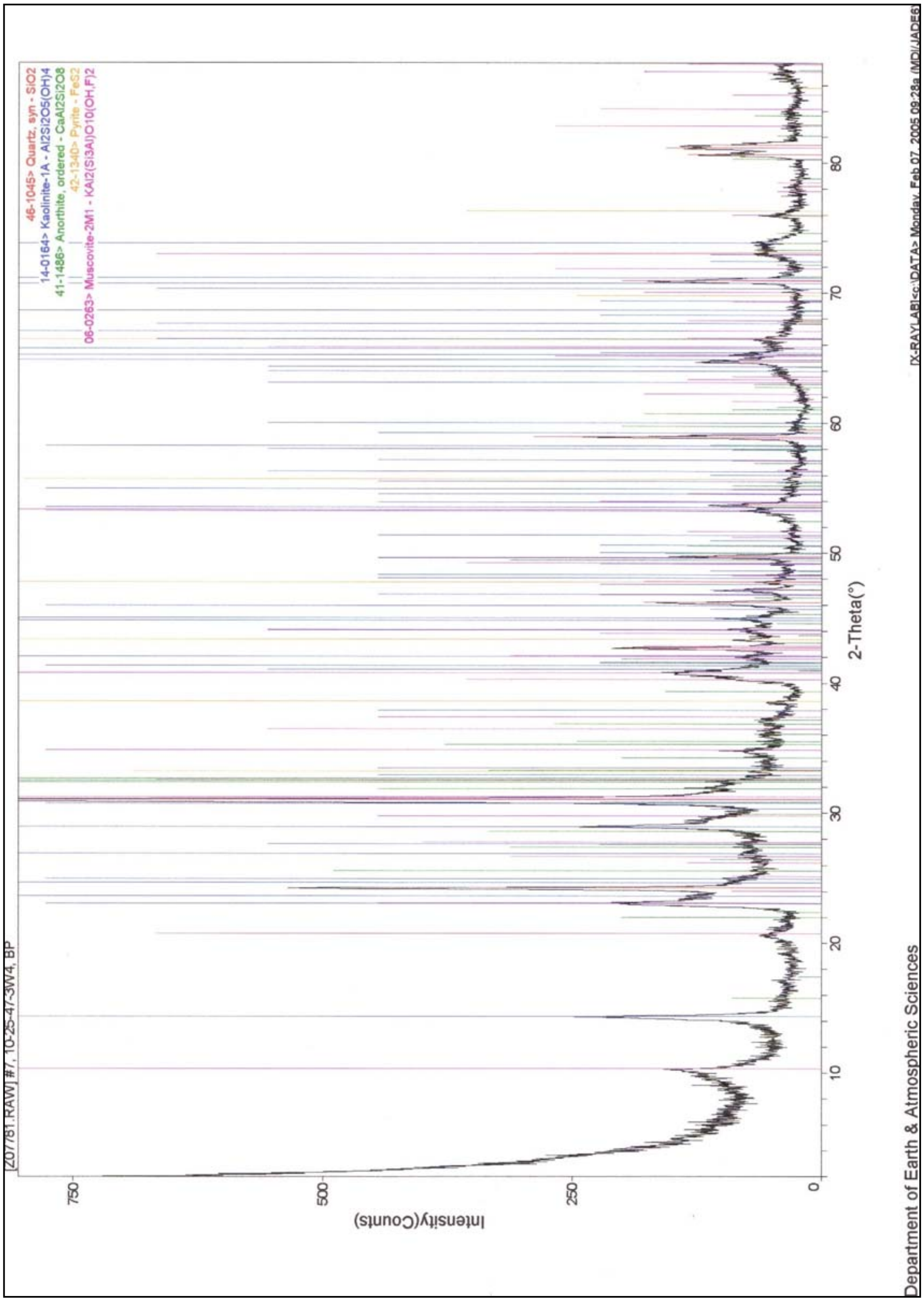

Figure 5-17 The resultant diffractogram of sample #7 (654.2m depth) - Shell Paradise 10-25-047-3W4 core - larger intensity scale.

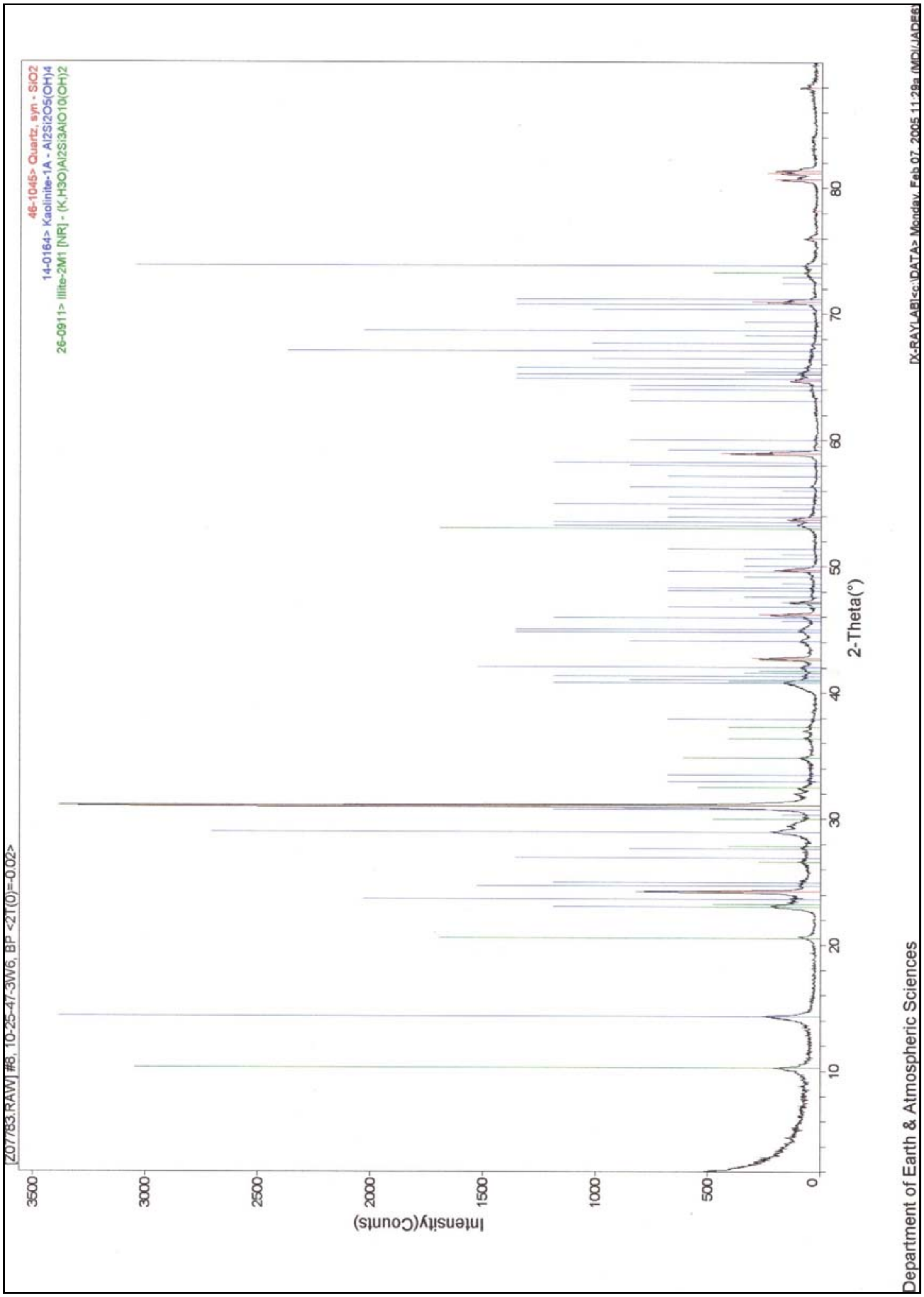

Figure 5-18 The resultant diffractogram of sample #8 (670m depth) - Shell Paradise 10-25-047-3W4 core.

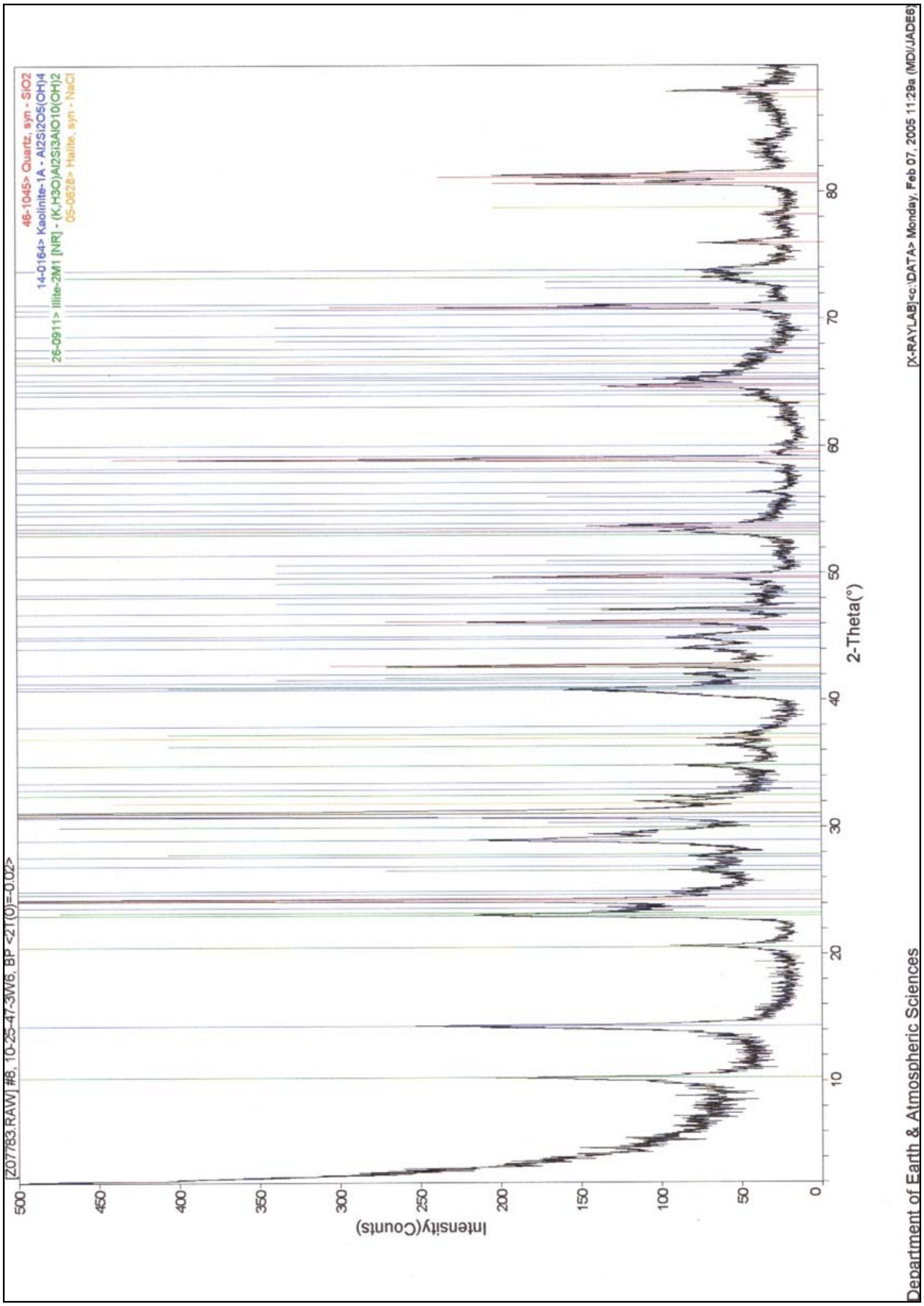

Figure 5-19 The resultant diffractogram of sample #8 (670m depth) - Shell Paradise 10-25-047-3W4 core - larger intensity scale.

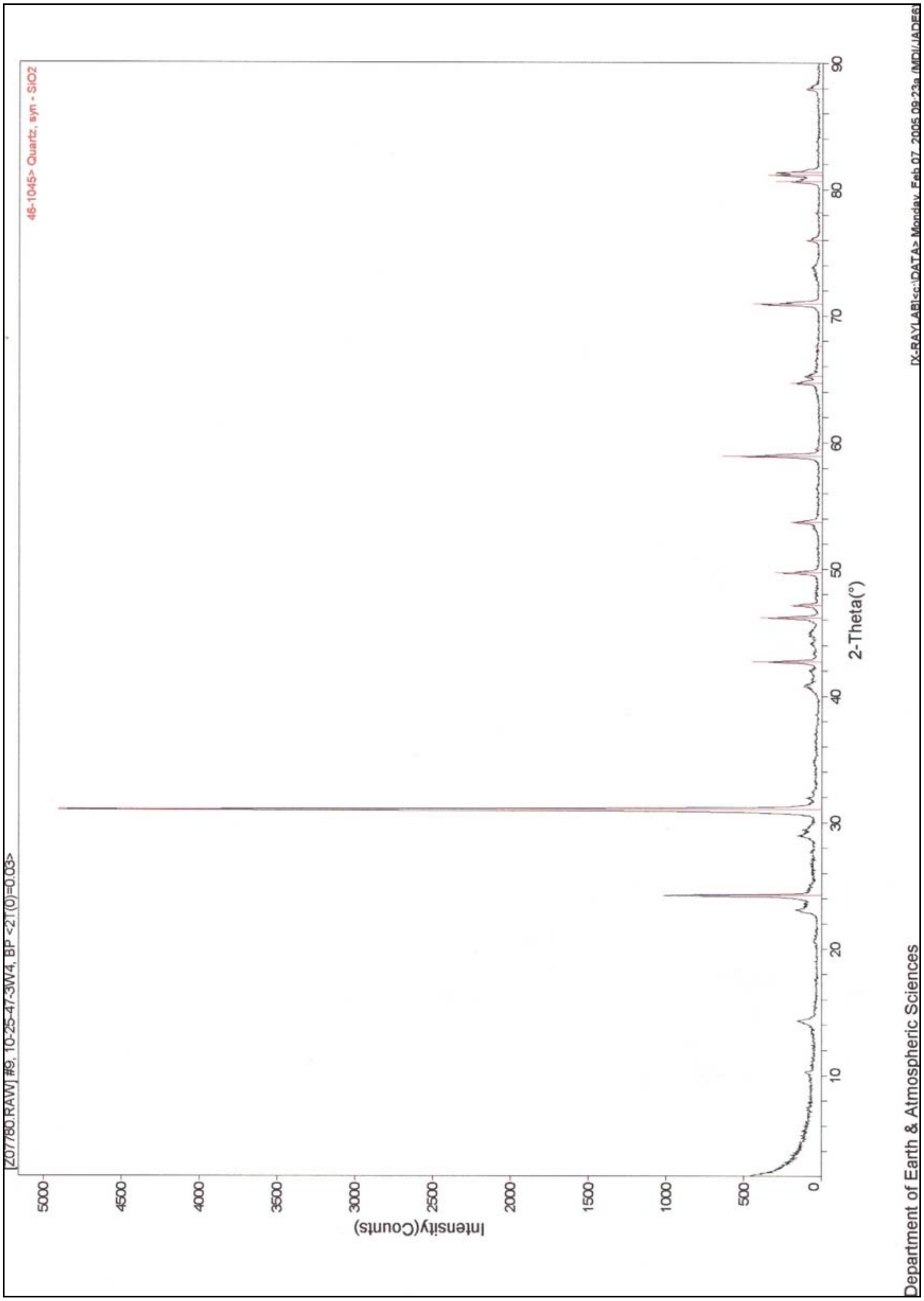

Figure 5-20 The resultant diffractogram of sample #9 (682m depth) - Shell Paradise 10-25-047-3W4 core.

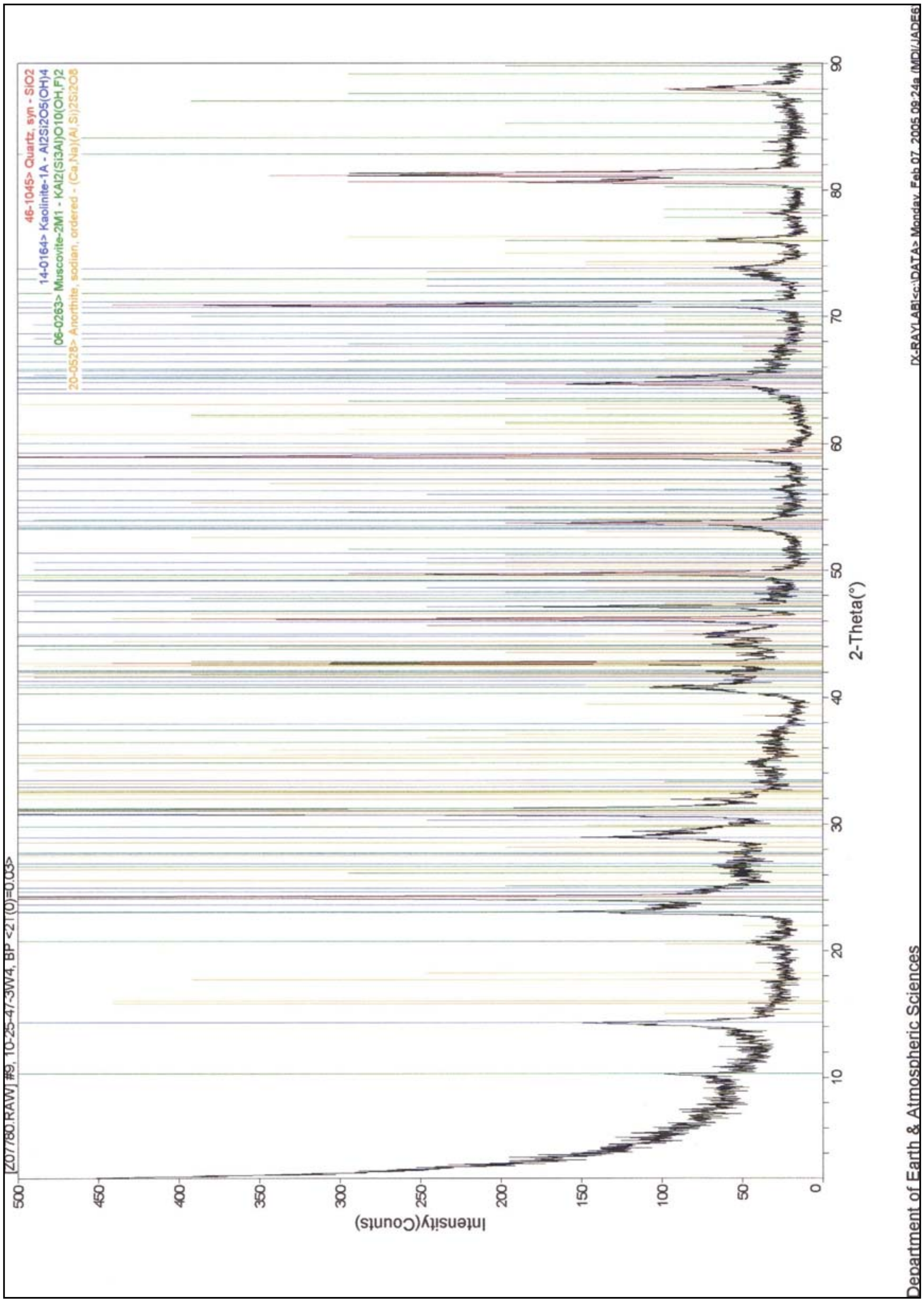

Figure 5-21 The resultant diffractogram of sample #9 (682m depth) - Shell Paradise 10-25-047-3W4 core - larger intensity scale.

University of Alberta

MUDGASES GEOCHEMISTRY AND FACTORS CONTROLLING THEIR VARIABILITY

APPENDIX A

by

DANIELA VLAD

A thesis submitted to the Faculty of Graduate Studies and Research
in partial fulfillment of the requirements for the degree of

Doctor of Philosophy

Department of Earth and Atmospheric Sciences

Spring 2010
Edmonton, Alberta

Appendix A:

Photographs of cores (Plates 1-122) and their log signatures

Page

Figure A-1 Location map of the Foothills region, showing the core control used in this study ………………………………………………………...……. 449

Figure A-2 Location of the cored well from the heavy - oil region, which penetrates the entire Mannville Group in the Lloydminster area ……… 450

Figure A-3 Core from the Belly River Formation (06-04-042-04W5/0 well) with accompanying wireline log signatures ……………………………….…….. 451

Figure A-4 Core from the Lea Park - Belly River formations (02/06-09-046-09W5/0 well) with accompanying wireline log signatures …... 452

Figure A-5 Core from the Lea-Park - Belly River formations (08-02-043-05W5/0 well) with accompanying wireline log signatures …...…. 453

Figure A-6 Core from the Lea-Park - Belly River formations (09-10-044-09W5/0 Well) with accompanying wireline log signatures …….. 454

Figure A-7 Core from the Belly River formation (10-04-049-11W5/0 well) with accompanying wireline log signatures ……………………………..455

Figure A-8 Core from the Lea-Park - Belly River formations (14-28-042-04W5/0 well) with accompanying wireline log signatures …..….. 456

Figure A-9 Core from the Belly River formation (16-11-045-07W5/0 well) with accompanying wireline log signatures ……………………...…….. 457

Figure A-10 Core from the Lea-Park - Belly River formations (08-25-042-05W5/0 well) with accompanying wireline log signatures …..….. 458

Figure A-11 Core from the Cardium Formation (02-33-047-07W5/0 well) with accompanying wireline log signatures …………………………….… 459

Figure A-12 Core from the Cardium Formation (06-12-048-11W5/0 well) with accompanying wireline log signatures ……………………………. 460

Figure A-13 Core from the Cardium Formation (06-14-042-06W5/0 well) with accompanying wireline log signatures …………………...……….. 461

Figure A-14. Core from the Cardium Formation (06-26-048-11W5/0 well) with accompanying wireline log signatures …………………...….…. 462

Figure A-15. Core from the Cardium Formation (06-33-048-11W5/0 well) with accompanying wireline log signatures …………………………… 463

Figure A-16. Core from the Cardium Formation (09-32-043-07W5/0 well) with accompanying wireline log signatures …………………………...…. 464

Figure A-17. Core from the Cardium Formation (10-11-043-09W5/0 well) with accompanying wireline log signatures …………………………..… 465

Figure A-18. Core from the Cardium Formation (10-14-044-09W5/0 well) with accompanying wireline log signatures ……………………………. 466

Figure A-19. Core from the Cardium Formation (10-16-042-09W5/0 well) with accompanying wireline log signatures ……………………..…………. 467

Figure A-20. Core from the Cardium Formation (10-23-043-09W5/0 well) with accompanying wireline log signatures ……………………………. 468

Figure A-21. Core from the Cardium Formation (10-26-045-09W5/0 well) with accompanying wireline log signatures …………………………...…. 469

Figure A-22. Core from the Cardium Formation (11-30-045-09W5/0 well) with accompanying wireline log signatures ……………………………. 470

Figure A-23. Core from the Cardium Formation (12-03-042-09W5/0 well) with accompanying wireline log signatures ……………………………. 471
.

Figure A-24. Core from the Cardium Formation (14-01-042-07W5/0 well) with accompanying wireline log signatures …………………………..…… 472

Figure A-25. Core from the Cardium Formation (14-06-047-09W5/0 well) with accompanying wireline log signatures ………………………………….. 473

Figure A-26. Core from the Cardium Formation (16-16-047-10W5/0 well) with accompanying wireline log signatures …………………………..…… 474

Figure A-27. Core from the Colorado Group (06-22-042-09W5/0 well) with accompanying wireline log signatures …………………...…….. 475

Figure A-28. Core from the Cardium Formation (04-10-042-09W5/2 well) with accompanying wireline log signatures ……………………………. 476

Figure A-29. Core from the Belly River Formation (10-10-042-09W5/0 well) with accompanying wireline log signatures ……………………………. 477

Figure A-30. Core from the Viking Formation (06-12-045-07W5/0 well) with accompanying wireline log signatures …………………………………..…. 478

Figure A-31. Core from the Viking Formation (07-06-042-07W5/0 well) with accompanying wireline log signatures …………………...……….. 479

Figure A-32. Core from the Viking Formation (07-08-042-05W5/0 well) with accompanying wireline log signatures …………………………..… 480

Figure A-33. Core from the Viking Formation (08-11-042-07W5/0 well) with accompanying wireline log signatures ……………………………. 481

Figure A-34. Core from the Viking Formation (10-17-042-04W5/0 well) with accompanying wireline log signatures ……………………………. 482

Figure A-35. Core from the Viking Formation (03/13-13-045-05W5/0 well) with accompanying wireline log signatures ……………………………. 483

Figure A-36. Core from the Joli Fou – Mannville contact (03-13-043-05W5/0 well) with accompanying wireline log signatures ……… 484

Figure A-37. Core from the Joli Fou – Mannville contact (10-32-048-06W5/0 well) with accompanying wireline log signatures …..…. 485

Figure A-38. Core from the Joli Fou - Mannville contact (02/11-15-045-07W5/0 well) with accompanying wireline log signatures …... 486

Figure A-39. Core from the Joli Fou – Mannville contact (16-11-045-07W5/0 well) with accompanying wireline log signatures ……… 487

Figure A-40. Core from the Joli Fou – Mannville section (10-25-047-03W4/0 well) with accompanying wireline log signatures ……... 488

PLATES ……………………………………………………………………. 489

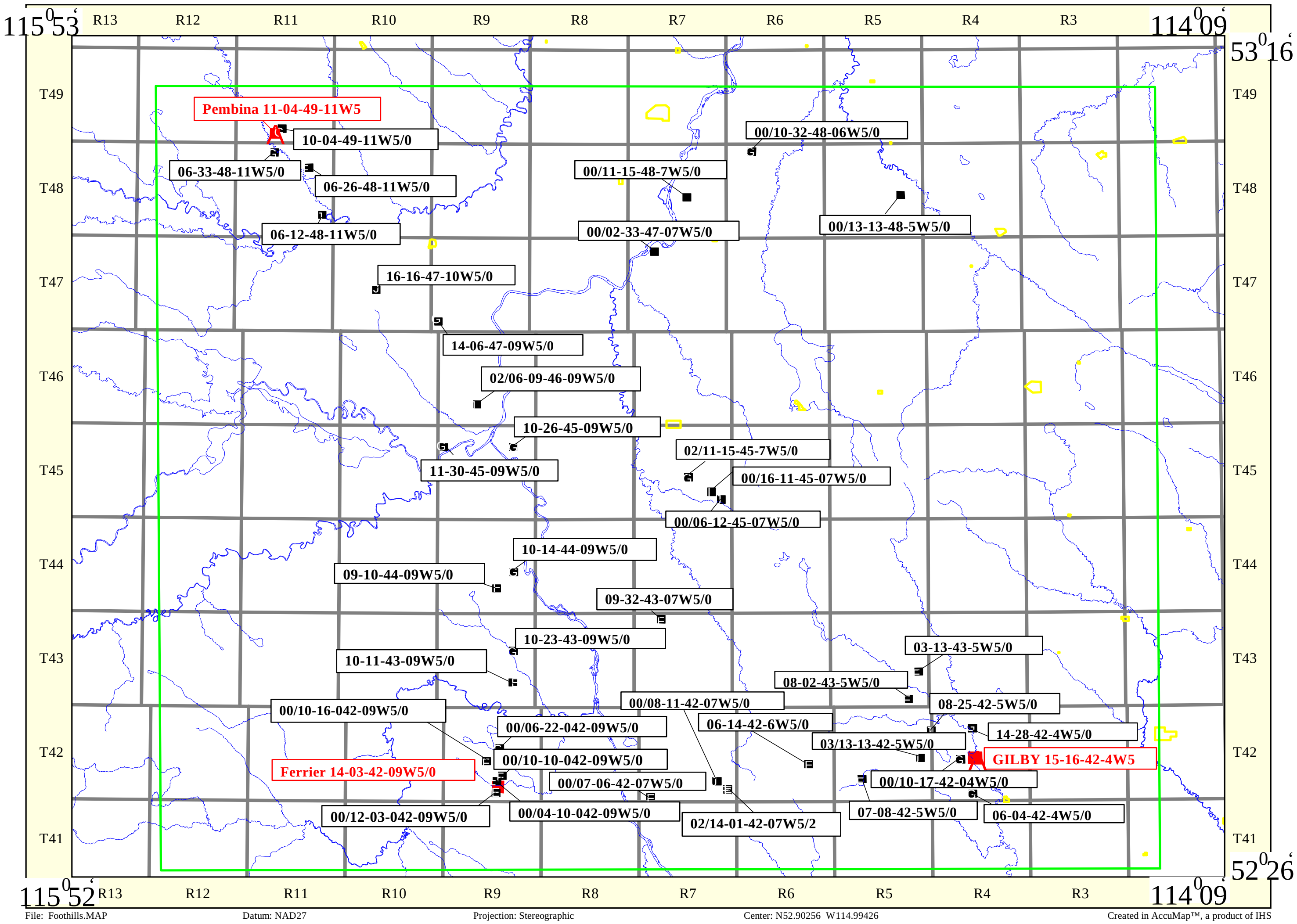

Figure A-1 Location map of the Foothills region, showing the core control used in this study.

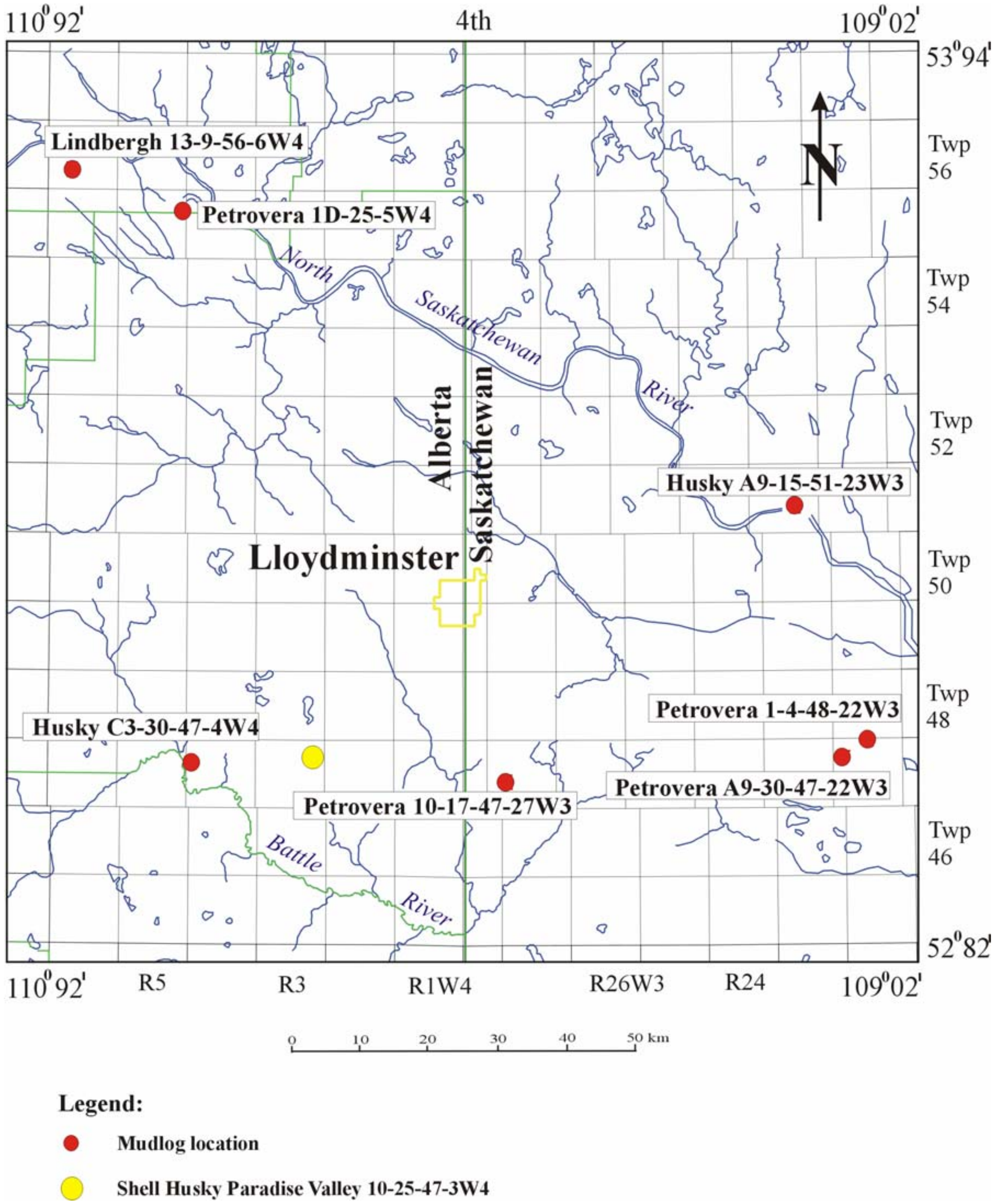

Figure A-2 Location of the cored well from the heavy - oil region, which penetrates the entire Mannville Group in the Lloydminster area.

06-04-042-04W5/0

1266 – 1269.5m & 1269.5 – 1274.5m

Porosity-Bulk Density

Resistivity-Induction

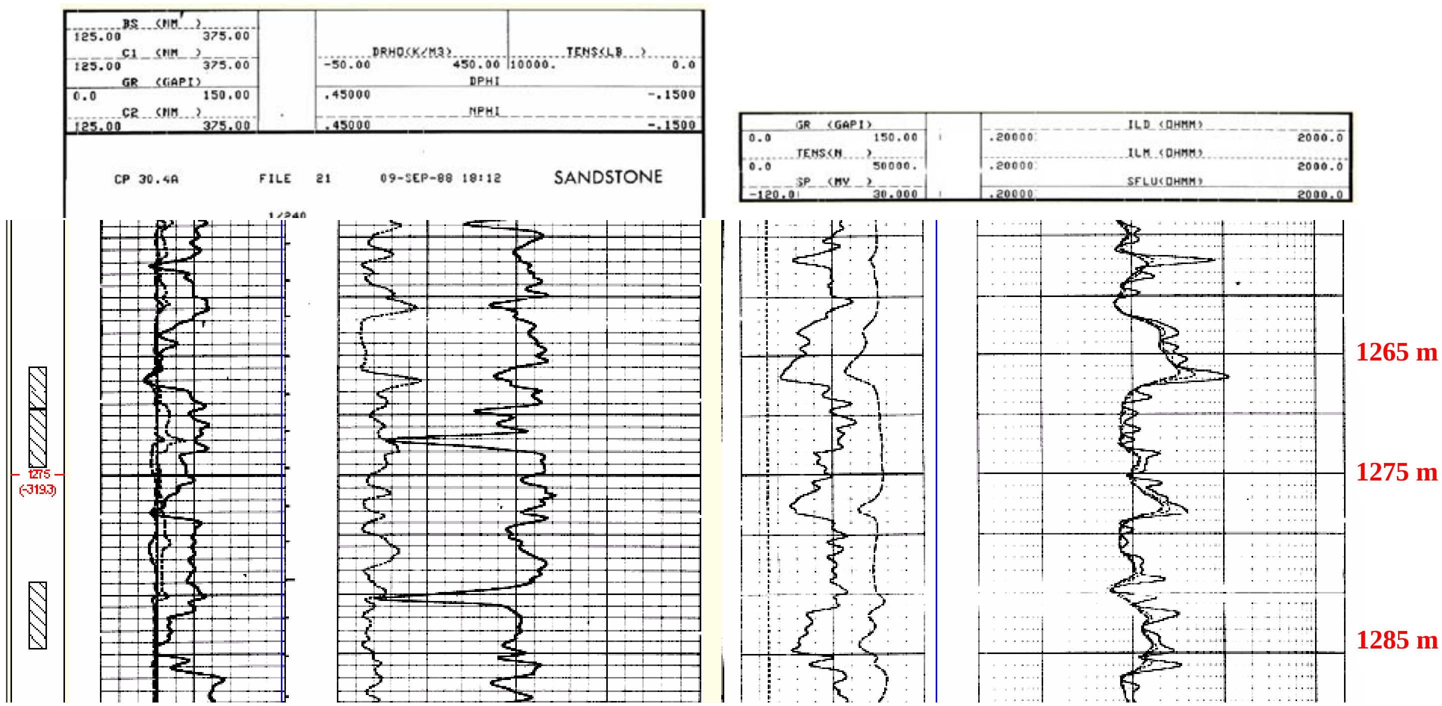

Figure A-3. Core from the Belly River Formation (06-04-042-04W5/0 well) with accompanying wireline log signatures.

02/06-09-046-09W5/0

1432 – 1453m

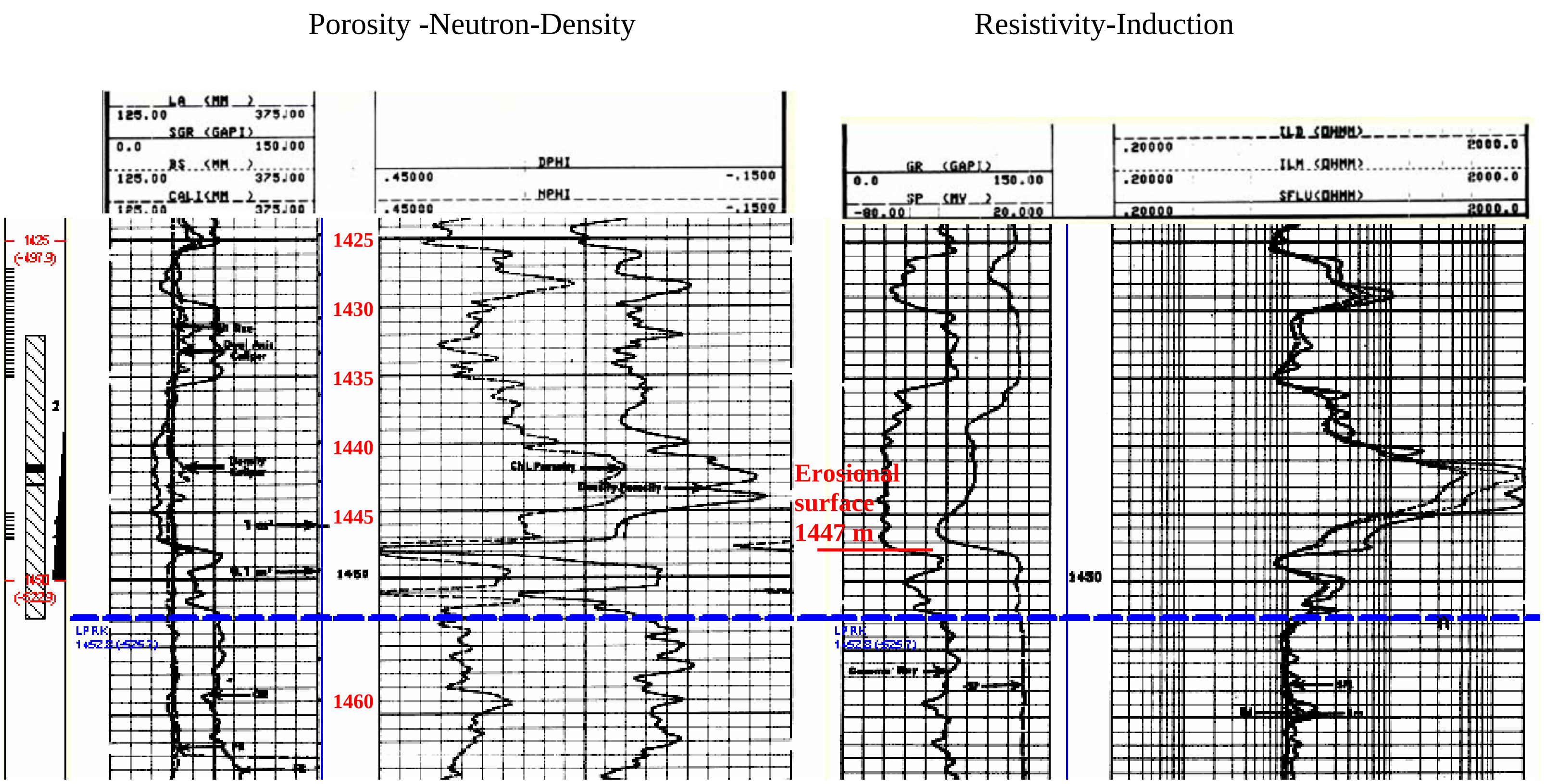

Figure A-4. Core from the Lea Park - Belly River formations (02/06-09-046-09W5/0 well) with accompanying wireline log signatures.

08-02-043-05W5/0

1310 – 1328 m

Porosity-Neutron-Density

Resistivity-Induction

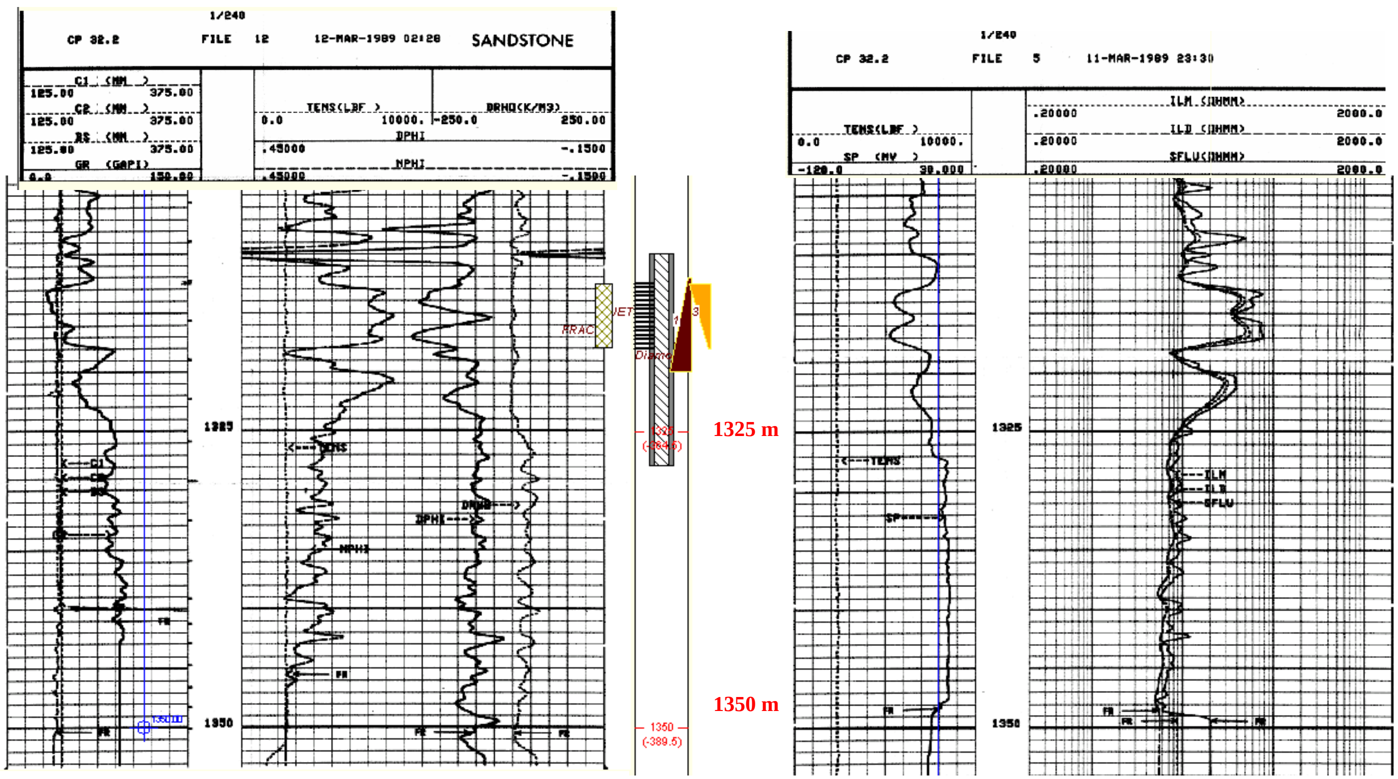

Figure A-5. Core from the Lea-Park - Belly River formations (08-02-043-05W5/0 well) with accompanying wireline log signatures.

09-10-044-09W5/0

1545 – 1563m

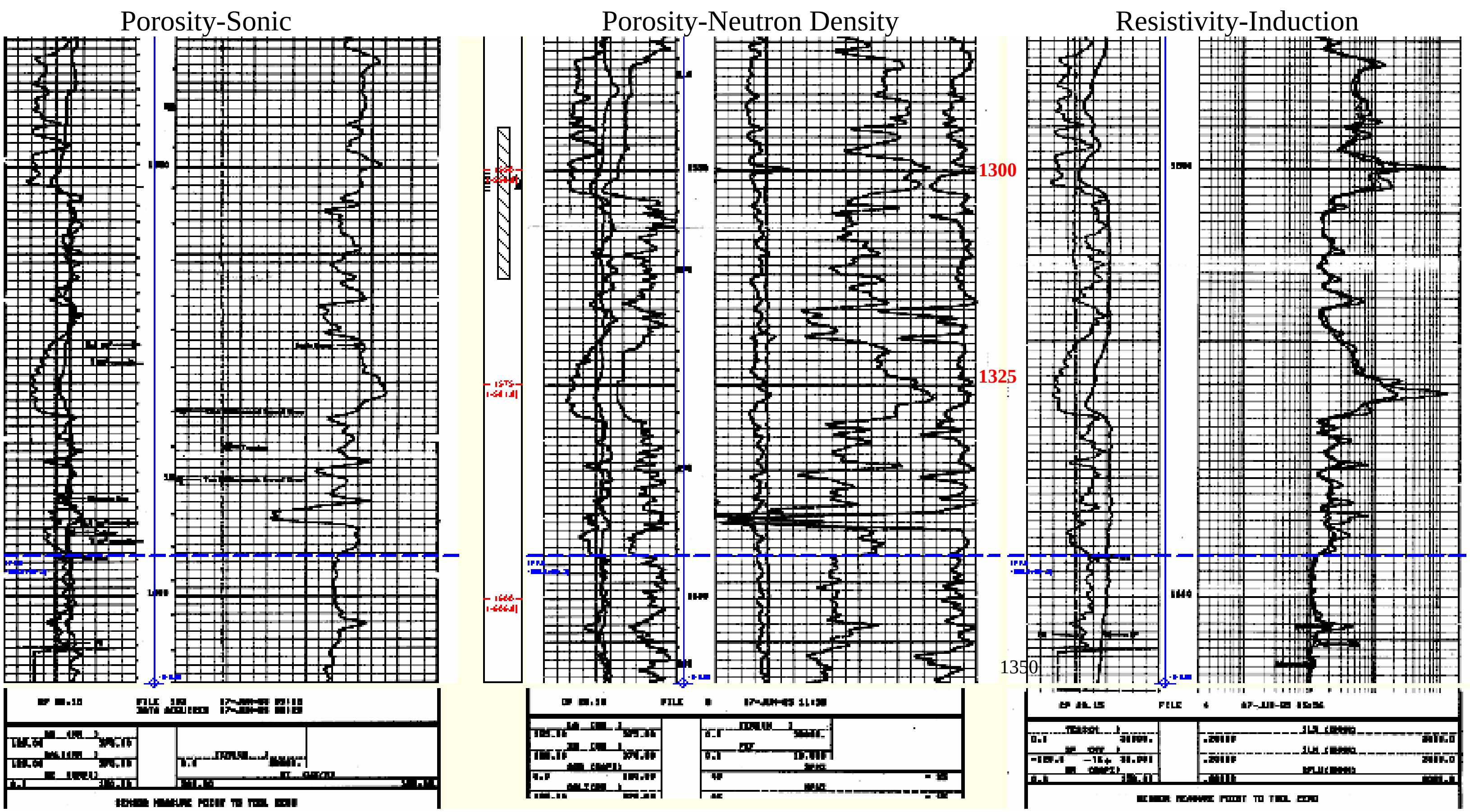

Figure A-6. Core from the Lea-Park - Belly River formations (09-10-044-09W5/0 well) with accompanying wireline log signatures.

10-04-049-11W5/0

1417 – 1435m

Porosity-Neutron-Density

Resistivity-Induction

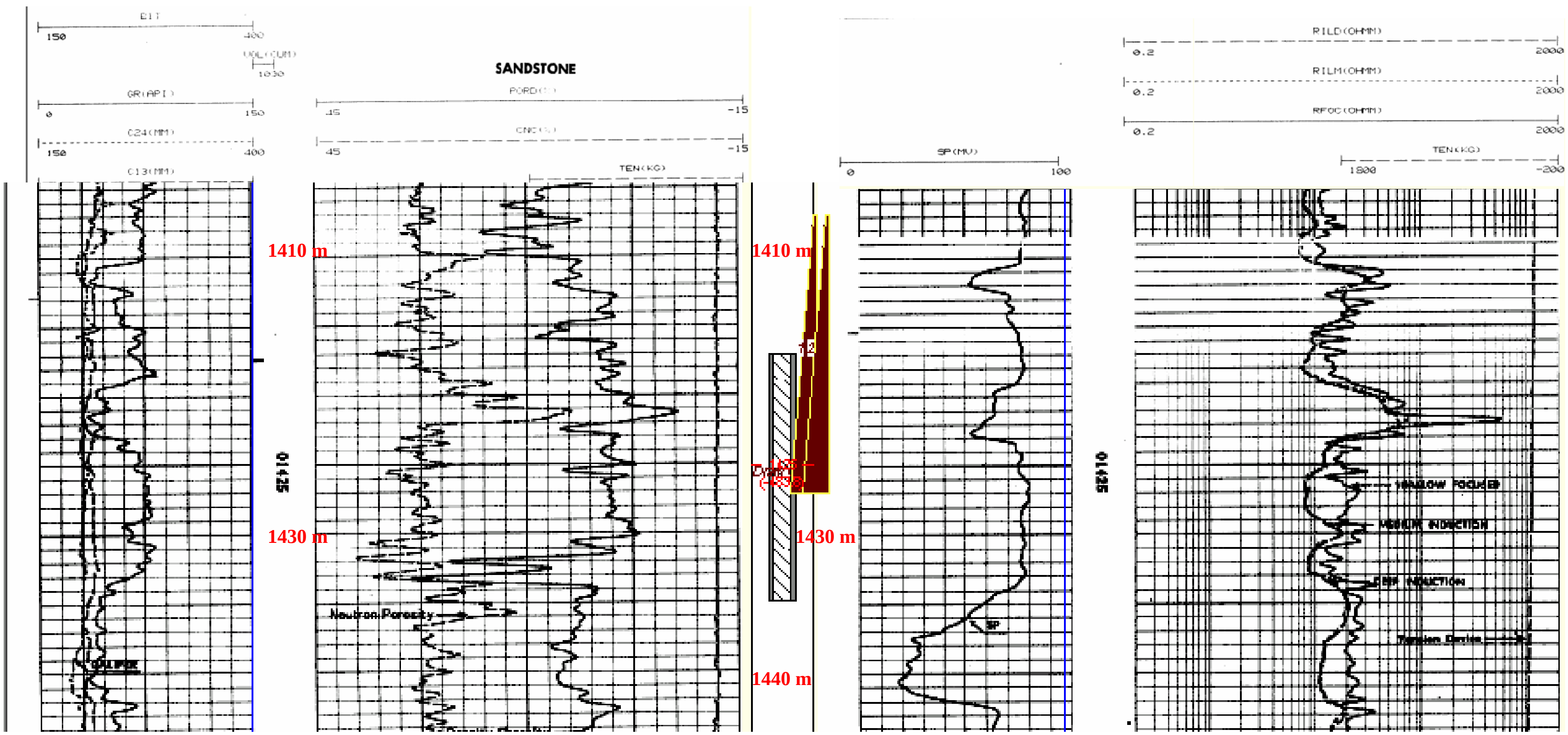

Figure A-7. Core from the Belly River formation (10-04-049-11W5/0 well) with accompanying wireline log signatures.

14-28-042-04W5/0

1277 – 1295m

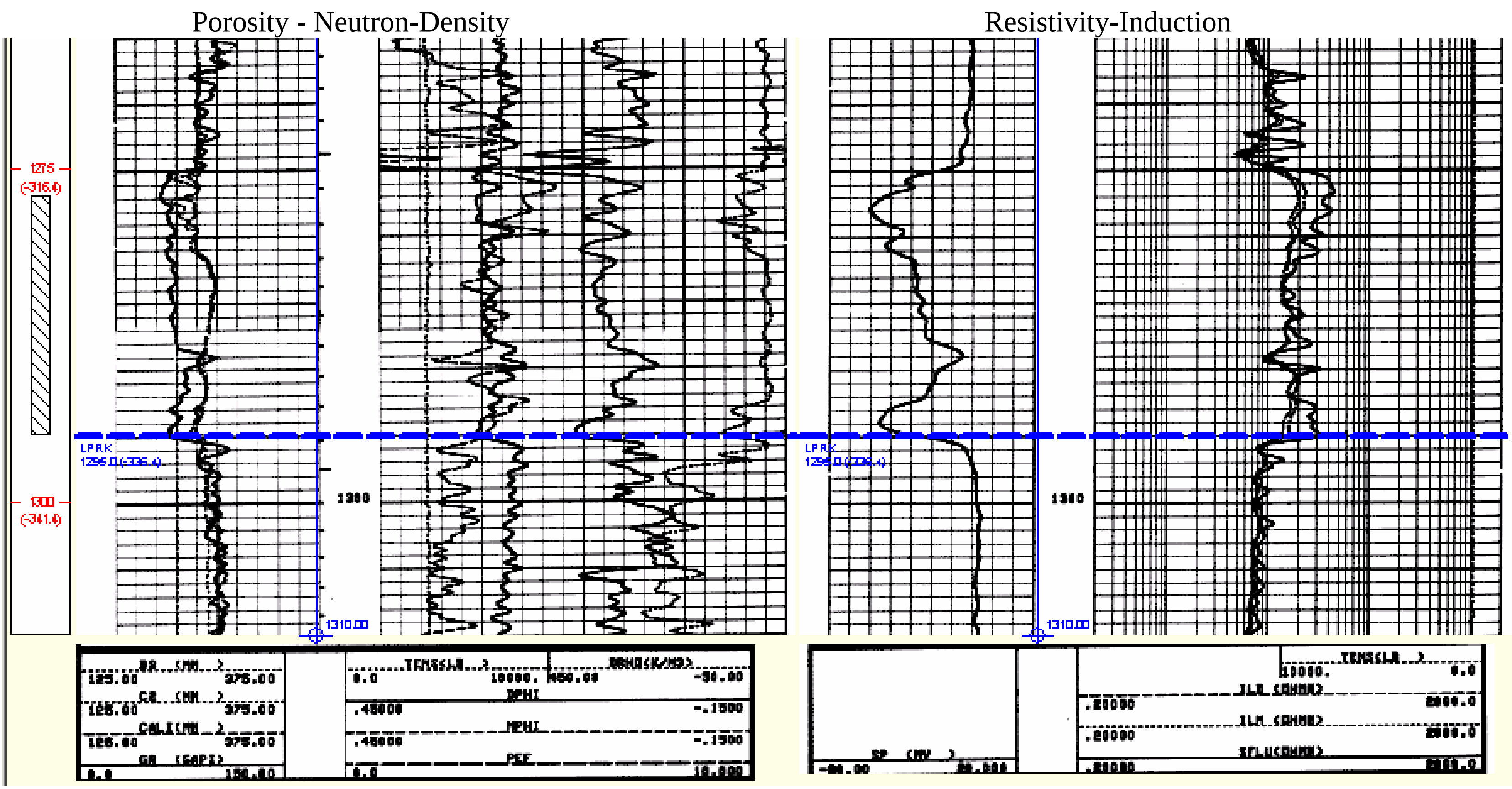

Figure A-8. Core from the Lea-Park - Belly River formations (14-28-042-04W5/0 well) with accompanying wireline log signatures.

16-11-045-07W5/0

1300 – 1329m

Porosity - Neutron-Density

Resistivity-Induction

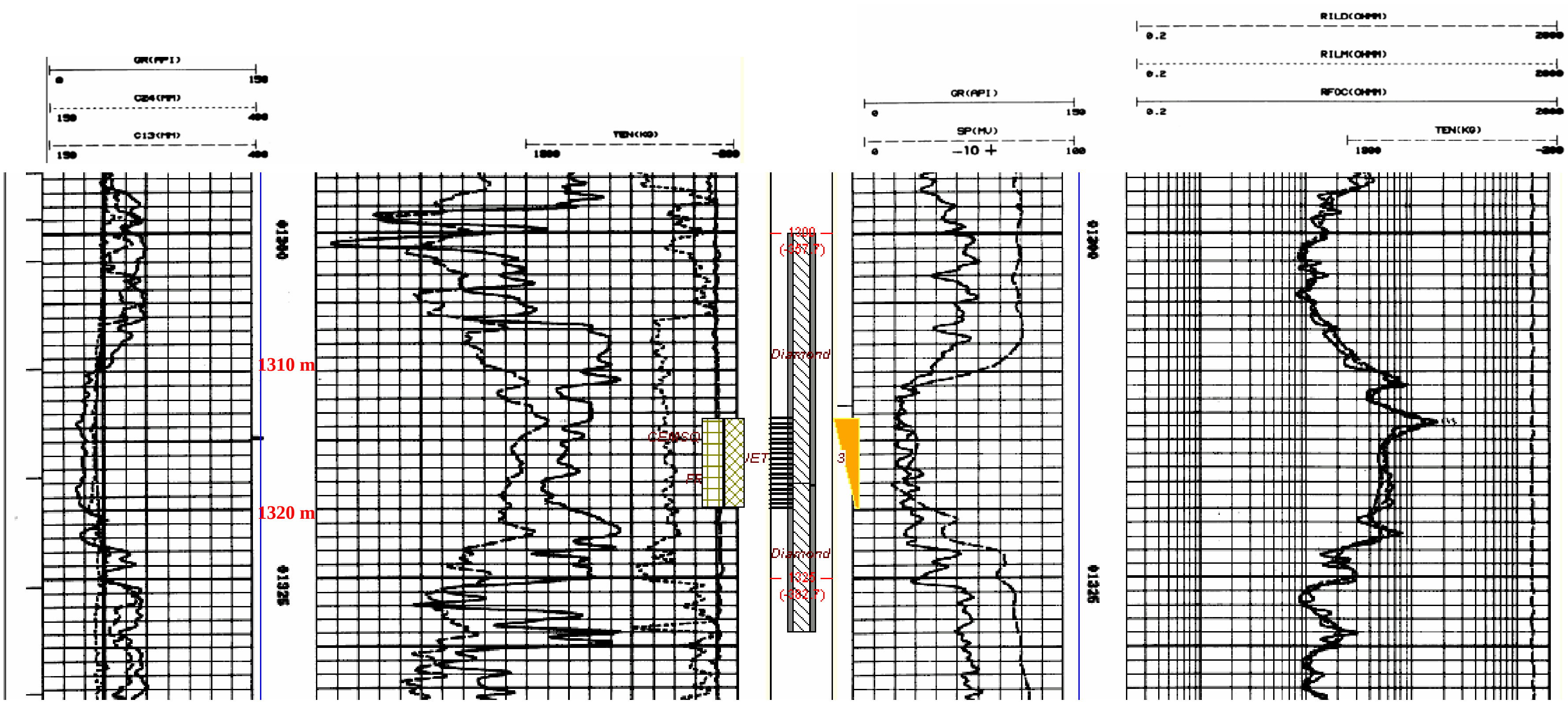

Figure A-9. Core from the Belly River formation (16-11-045-07W5/0 well) with accompanying wireline log signatures.

08-25-042-05W5/0

1312 - 1324m

Porosity-Neutron-Density

Resistivity-Induction

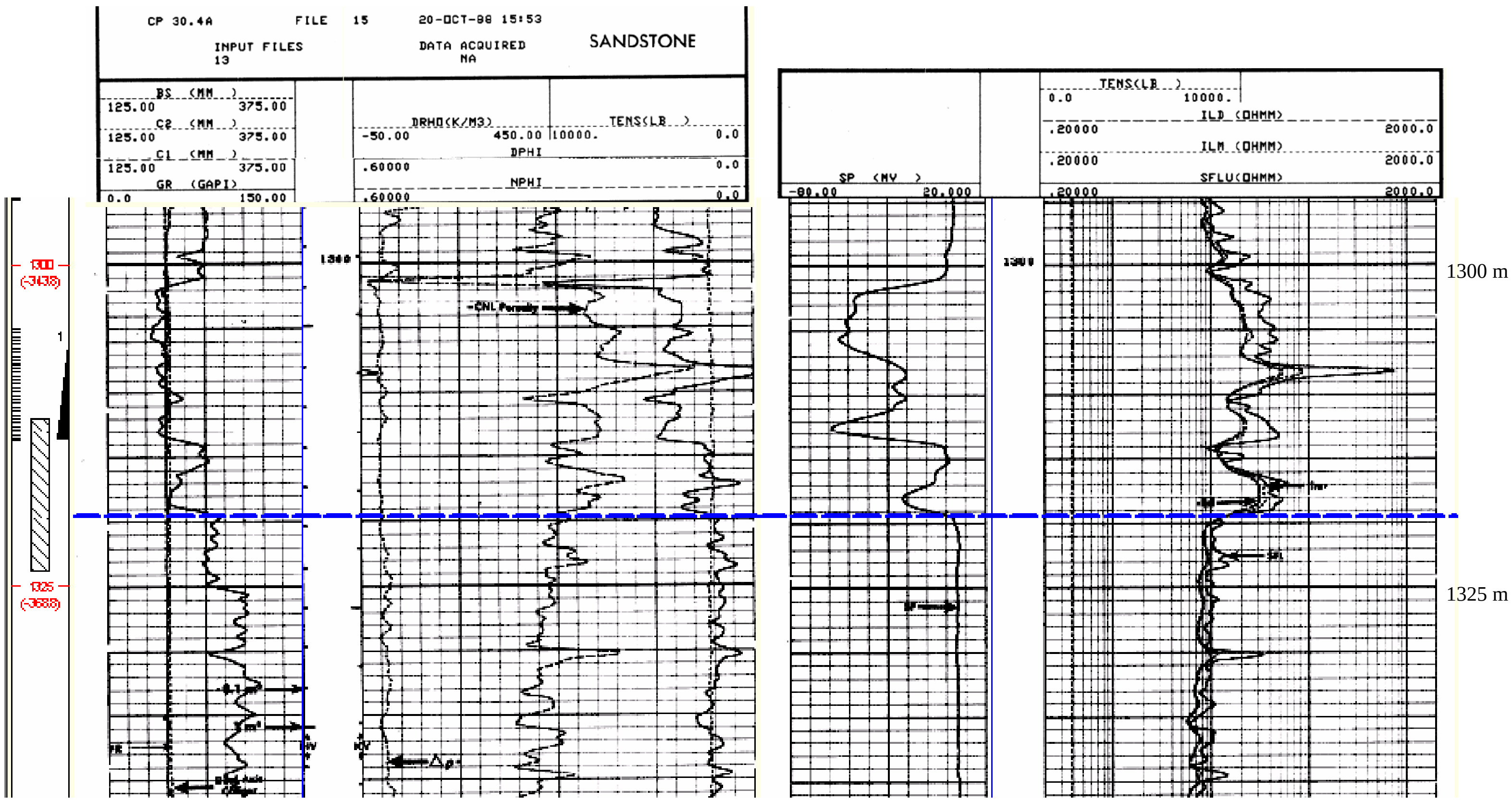

Figure A-10. Core from the Lea-Park - Belly River formations (08-25-042-05W5/0 well) with accompanying wireline log signatures.

02-33-047-07W5/0

1462.4 – 1502m

Resistivity - Micro

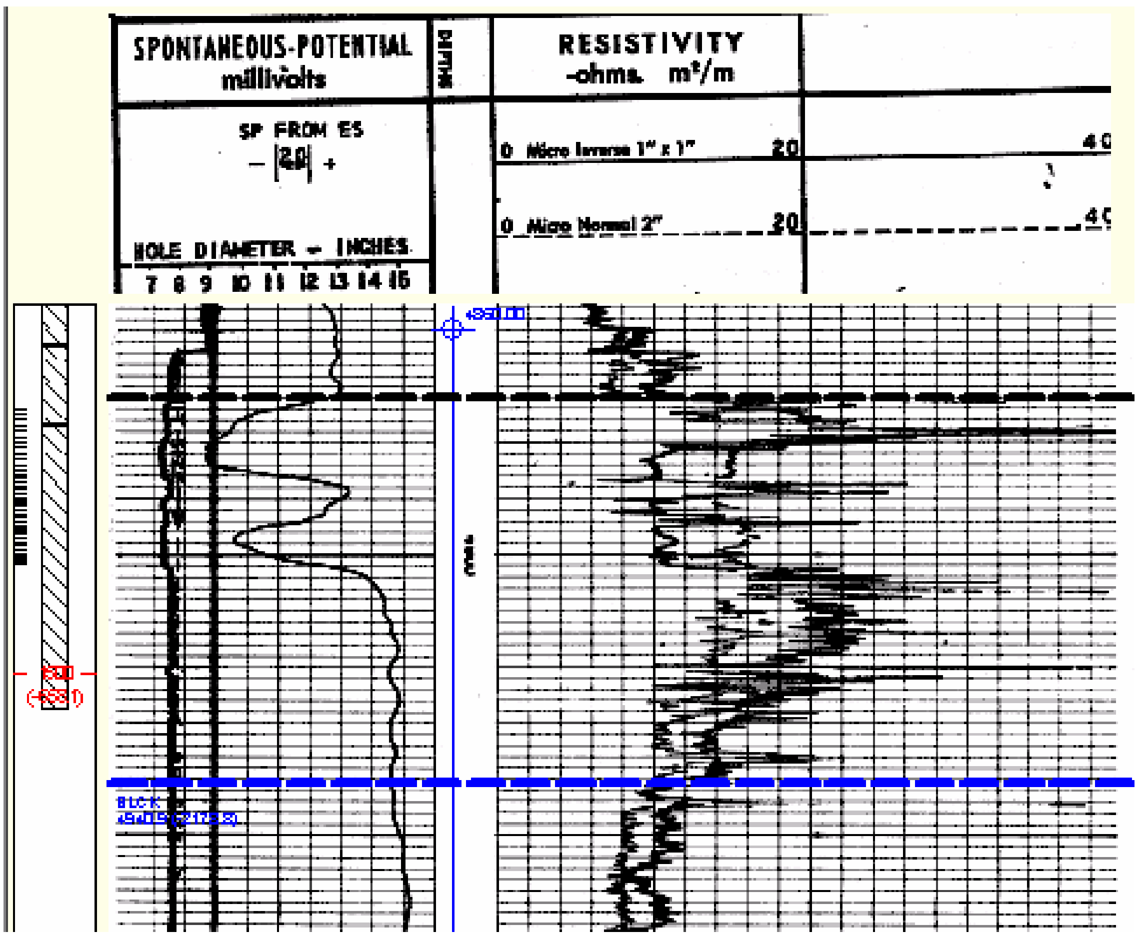

Figure A-11. Core from the Cardium Formation (02-33-047-07W5/0 well) with accompanying wireline log signatures.

06-12-048-11W5/0

1765 – 1774m

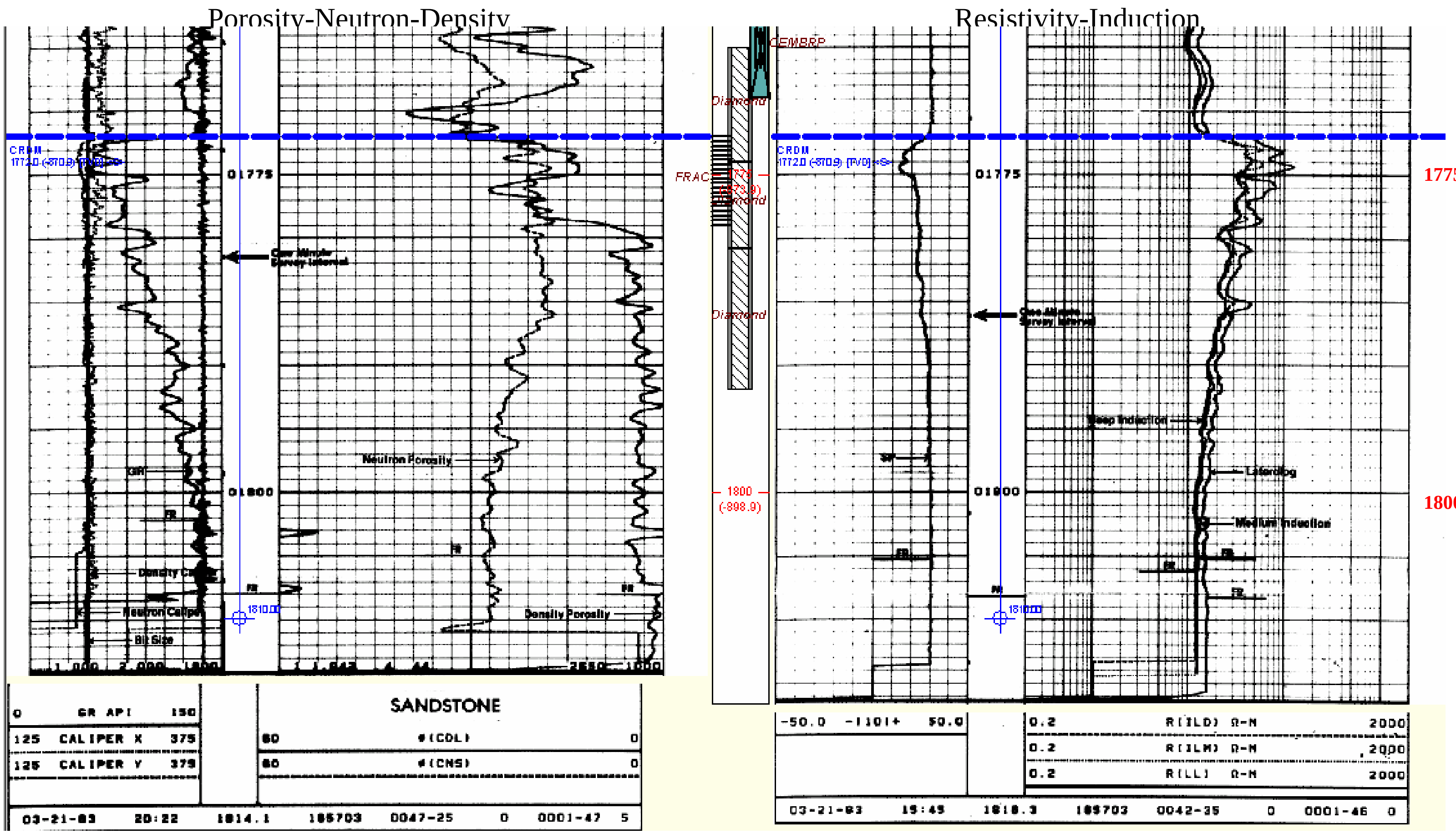

Figure A-12. Core from the Cardium Formation (06-12-048-11W5/0 well) with accompanying wireline log signatures.

06-14-042-06W5/0

1907.4 – 1916.6m

Resistivity-Induction

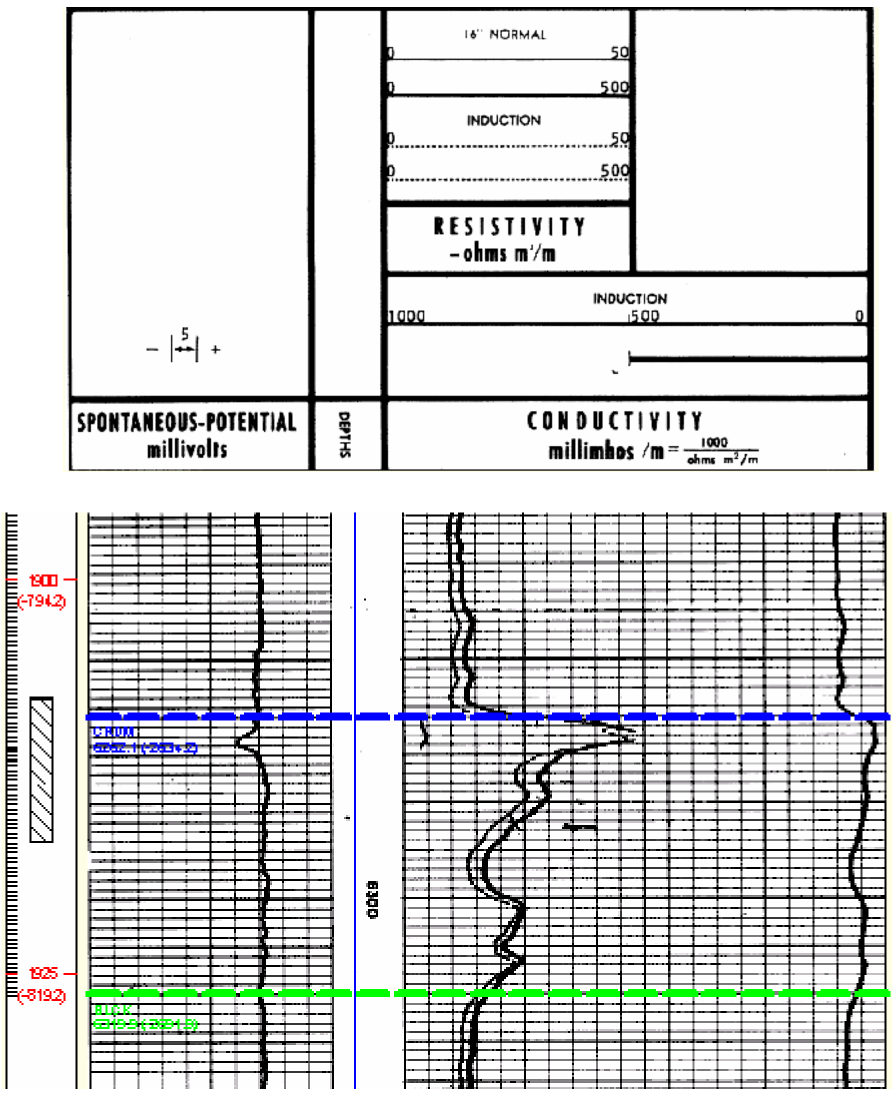

Figure A-13. Core from the Cardium Formation (06-14-042-06W5/0 well) with accompanying wireline log signatures.

06-26-048-11W5/0

1770.9 – 1789.2m

Porosity-Neutron-Density | Resistivity-Induction

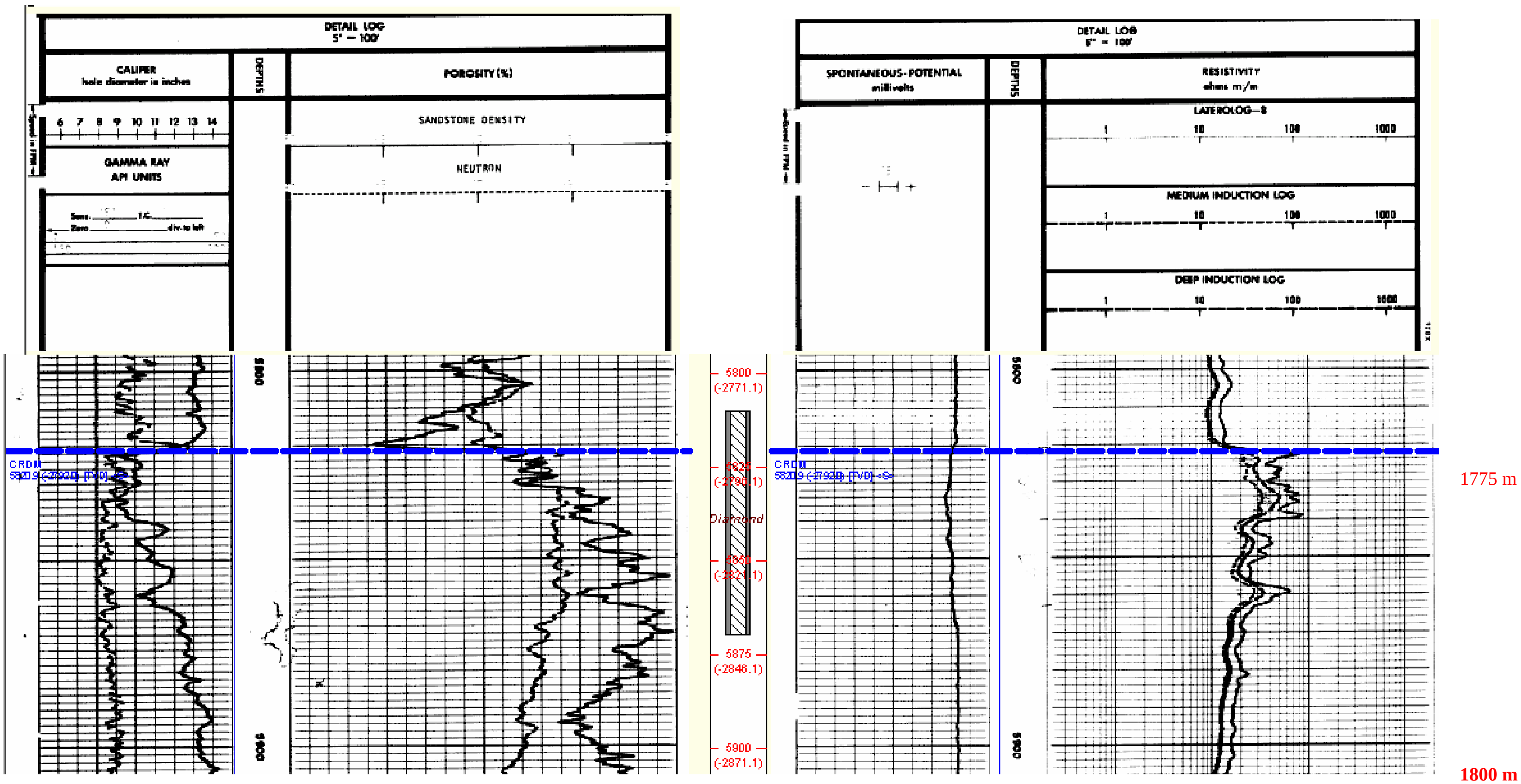

Figure A-14. Core from the Cardium Formation (06-26-048-11W5/0 well) with accompanying wireline log signatures.

06-33-048-11W5/0

1760.5 – 1778.8m

Porosity – Bulk Density | Resistivity - Lateral

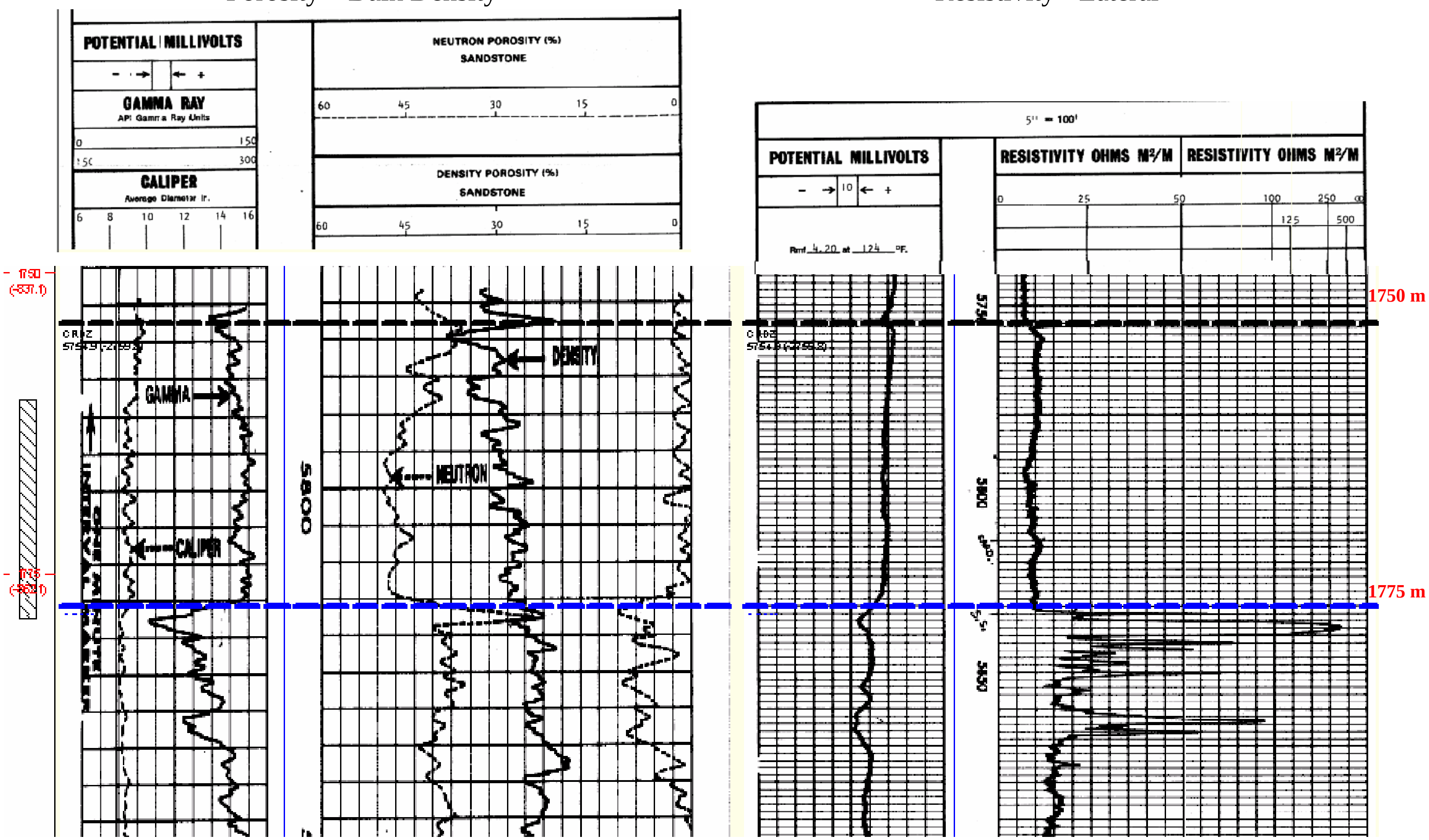

Figure A-15. Core from the Cardium Formation (06-33-048-11W5/0 well) with accompanying wireline log signatures.

09-32-043-07W5/0

1867 – 1885.3m

Porosity-Bulk Density

Resistivity-Induction

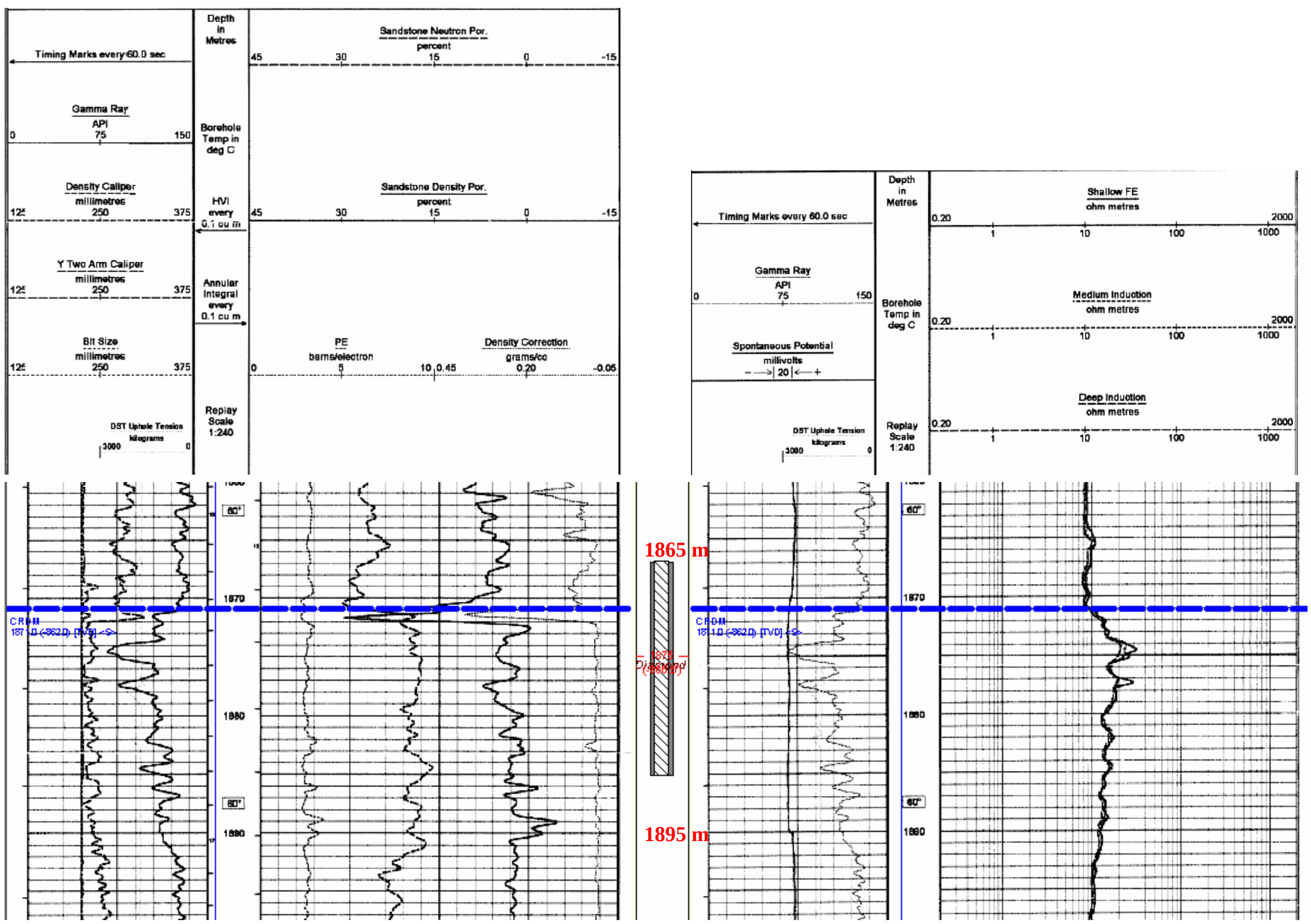

Figure A-16. Core from the Cardium Formation (09-32-043-07W5/0 well) with accompanying wireline log signatures.

10-11-043-09W5/0

2017 – 2035m

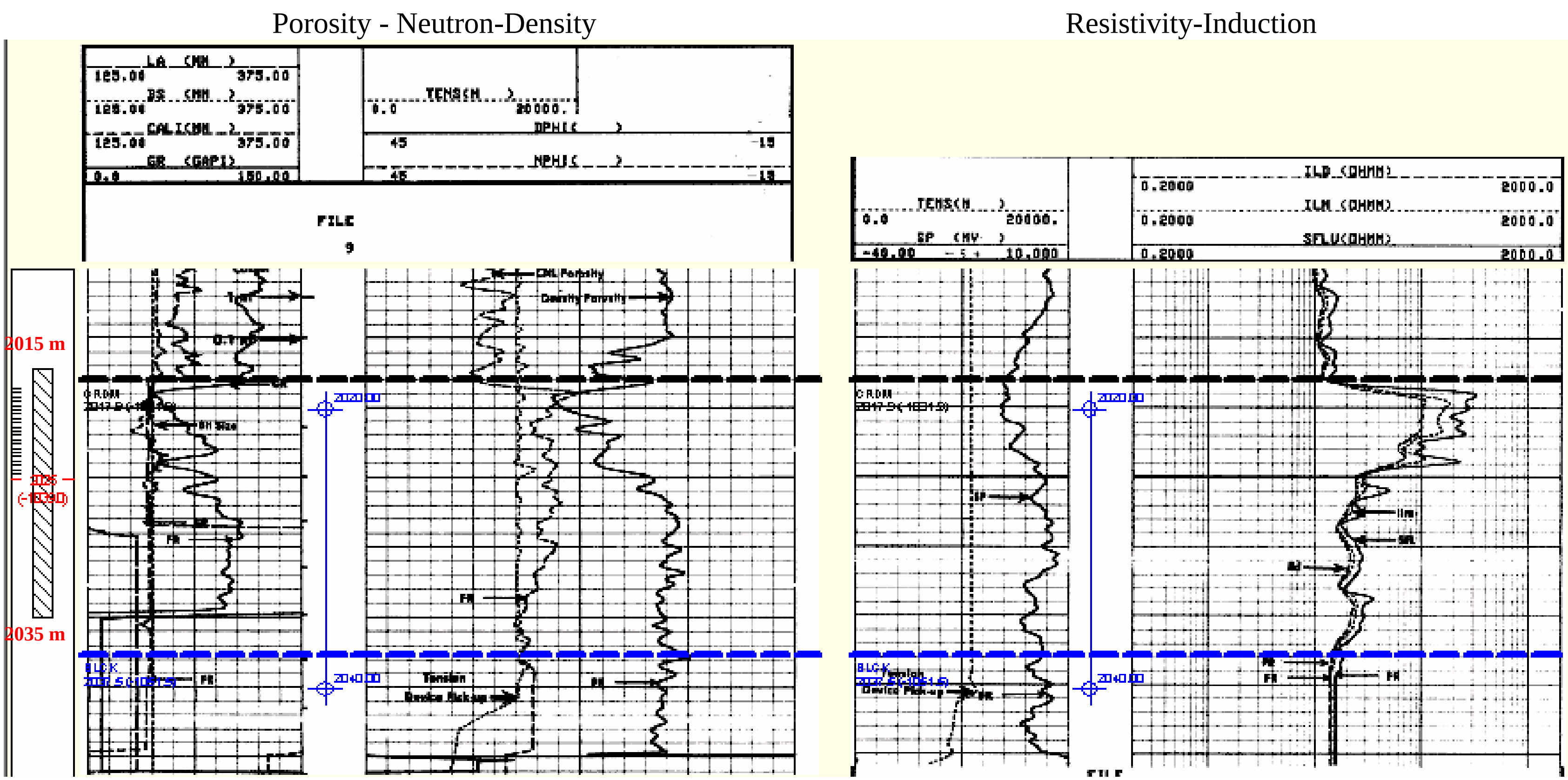

Figure A-17. Core from the Cardium Formation (10-11-043-09W5/0 well) with accompanying wireline log signatures.

10-14-044-09W5/0

1898.9 – 1917.8m

Resistivity - Lateral

Porosity-Bulk Density

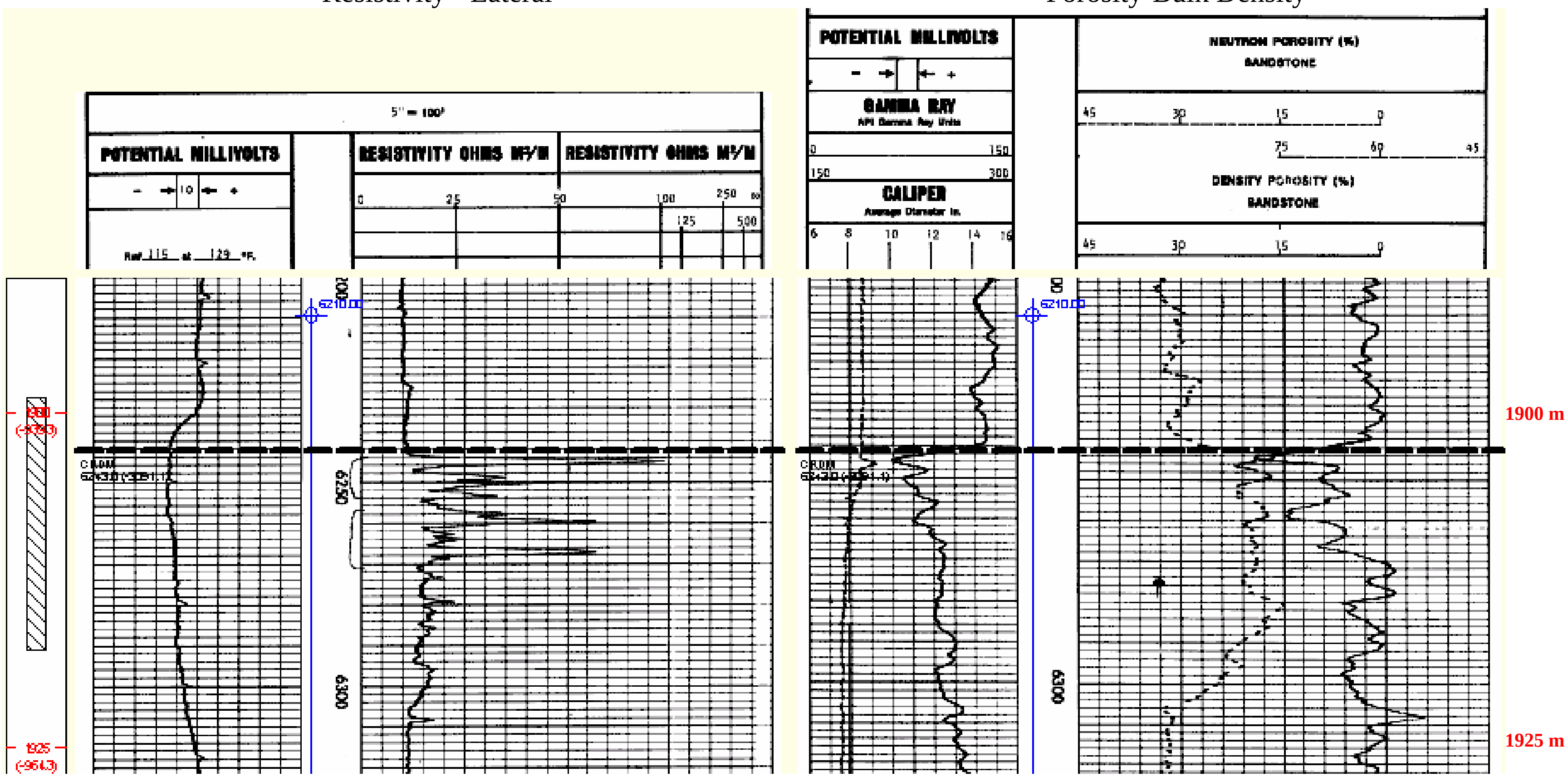

Figure A-18. Core from the Cardium Formation (10-14-044-09W5/0 well) with accompanying wireline log signatures.

10-16-042-09W5/0

2077 - 2093m

Porosity-Sonic

Resistivity-Induction

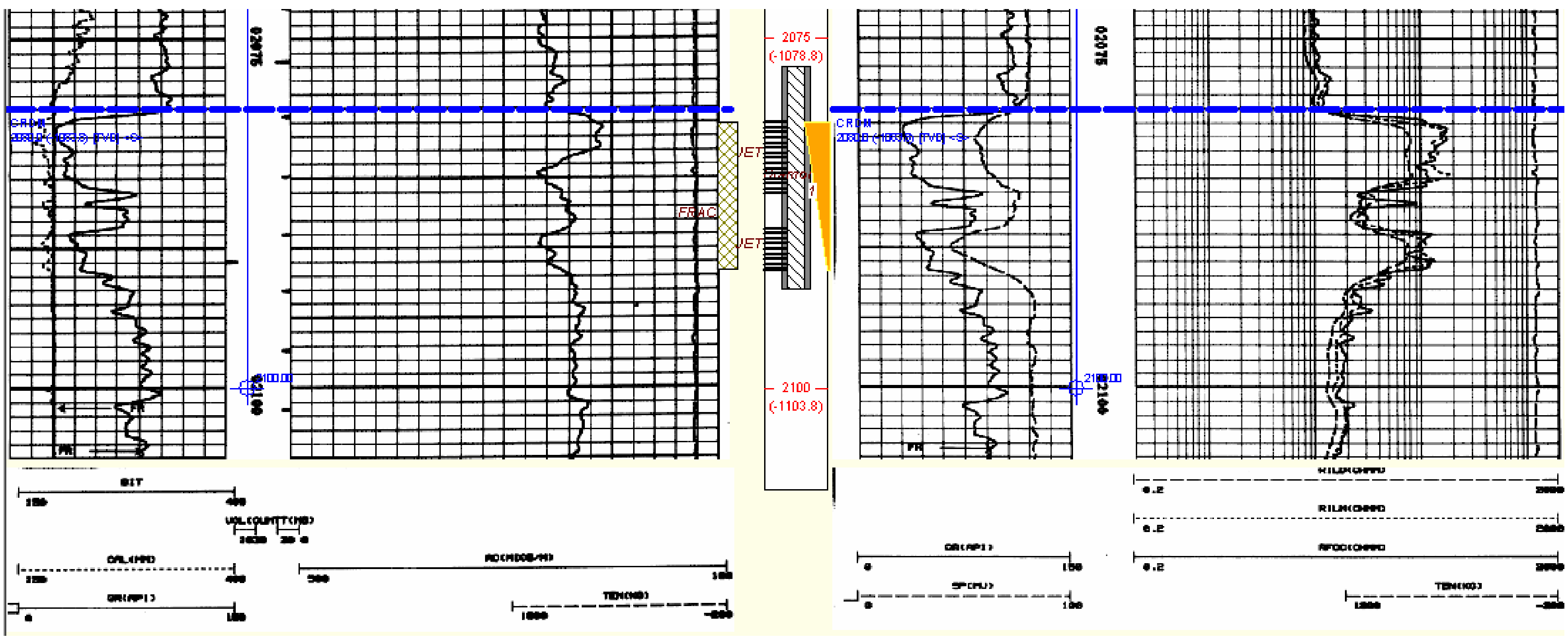

Figure A-19. Core from the Cardium Formation (10-16-042-09W5/0 well) with accompanying wireline log signatures.

10-23-043-09W5/0

1980.3 – 1995.2m
1995.2 – 2018.1m

Resistivity-Induction

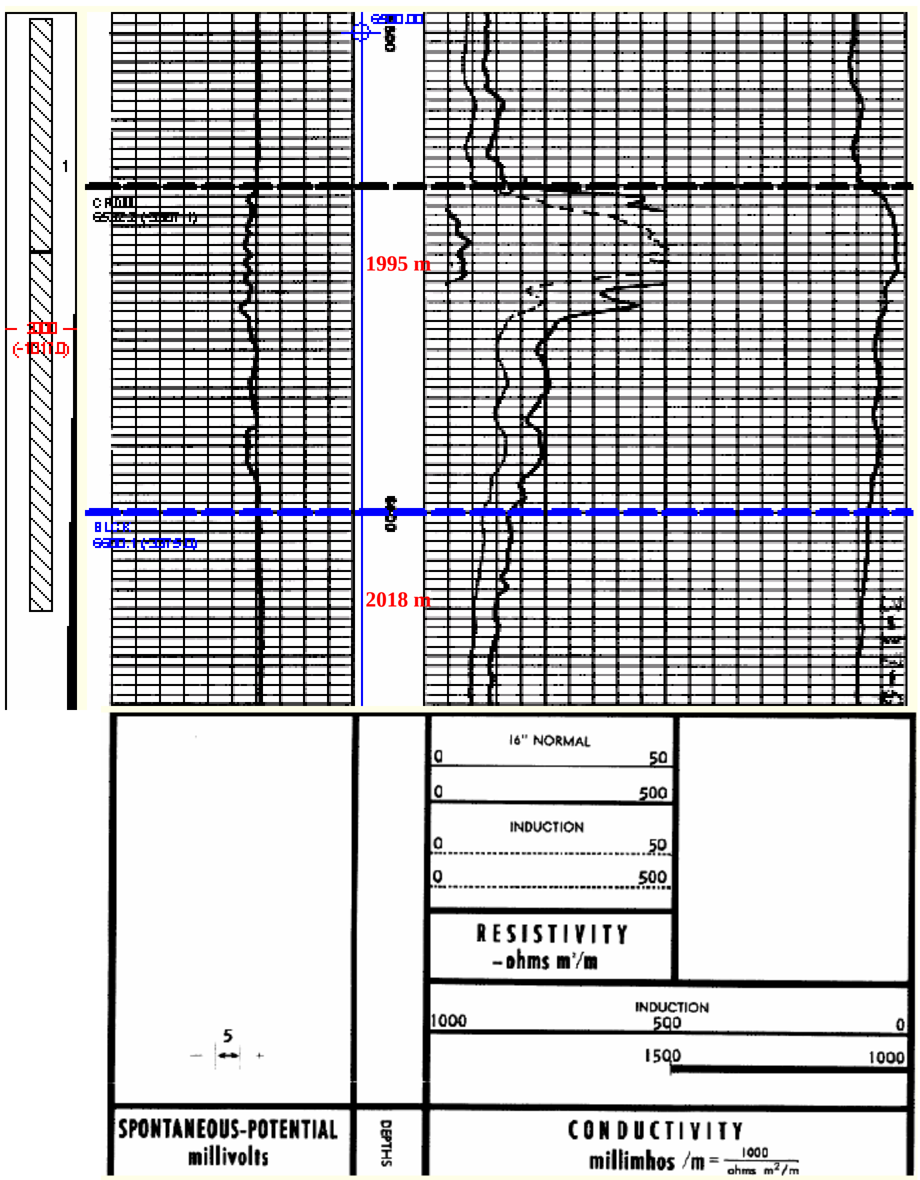

Figure A-20. Core from the Cardium, and Blackrock formations (10-23-043-09W5/0 well) with accompanying wireline log signatures.

10-26-045-09W5/0

1743.8 – 1762m

Porosity-Bulk Density

Resistivity-Lateral

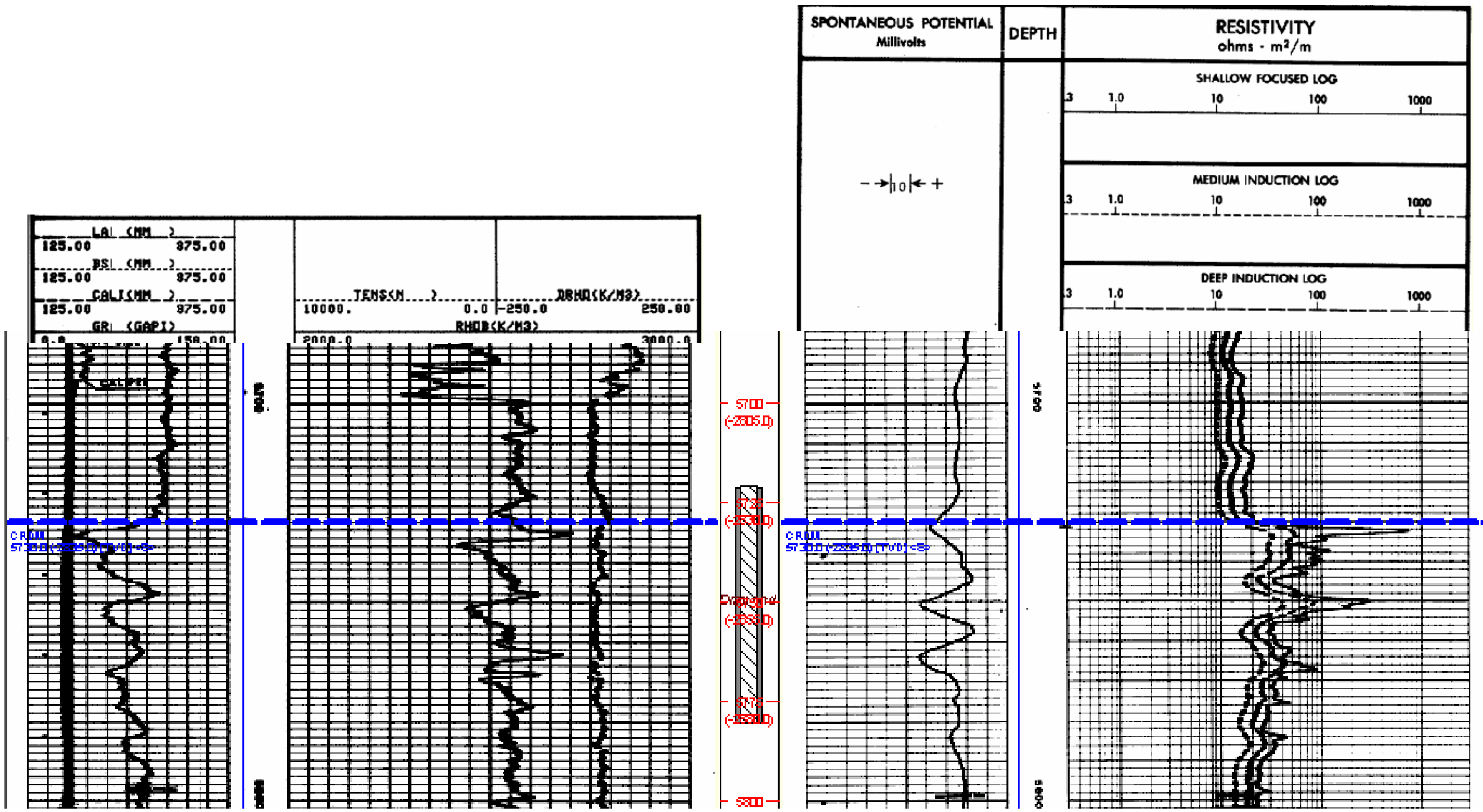

Figure A-21. Core from the Cardium Formation (10-26-045-09W5/0 well) with accompanying wireline log signatures.

11-30-045-09W5/0

1822 – 1840 m

Porosity-Bulk Density

Resistivity-Induction

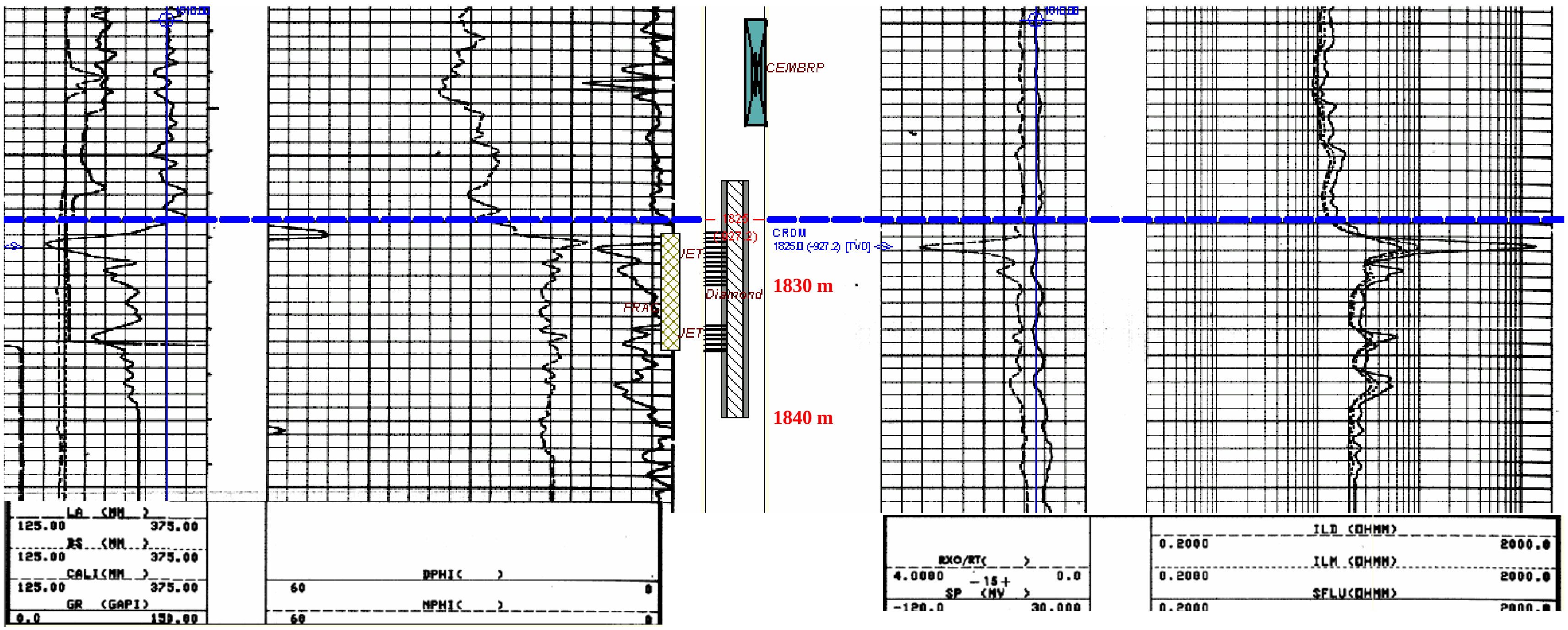

Figure A-22. Core from the Cardium Formation (11-30-045-09W5/0 well) with accompanying wireline log signatures.

12-03-042-09W5/0

2116 – 2134.2 m & 2134.2 – 2136 m

Porosity-Sonic

Resistivity-Induction

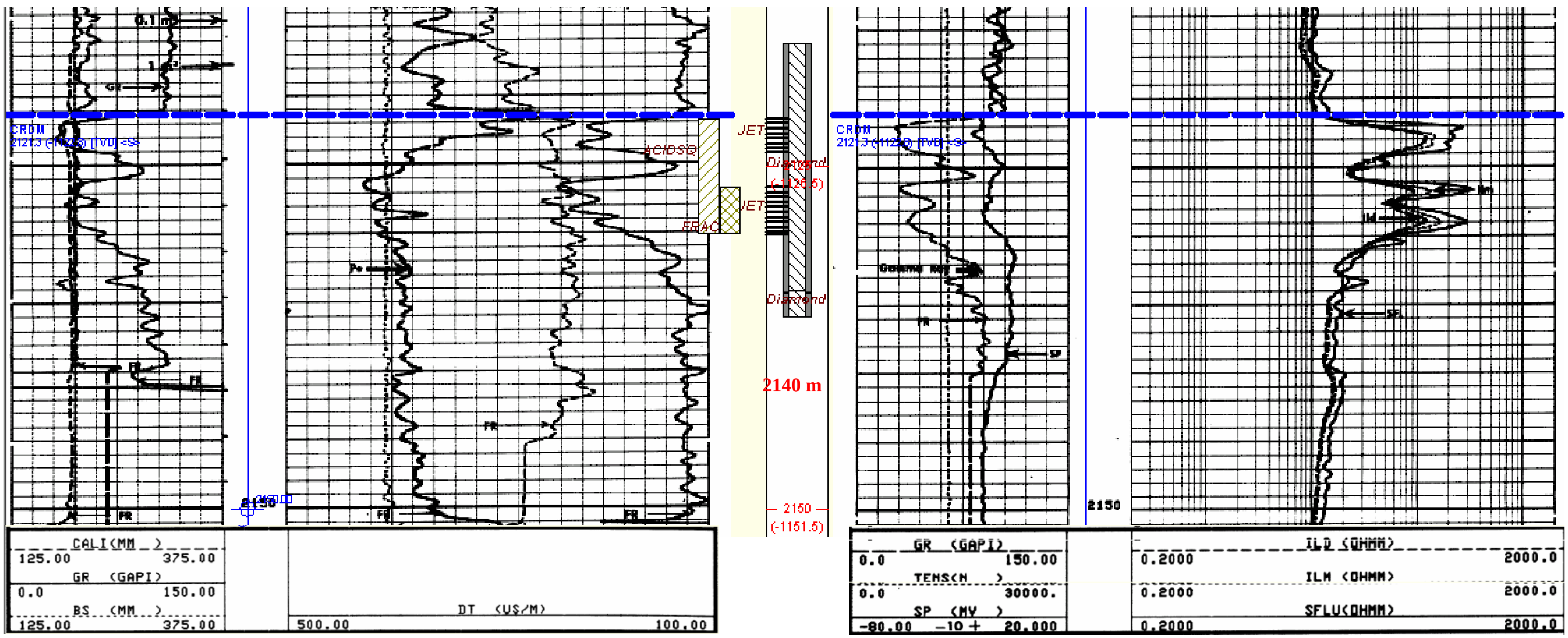

Figure A-23. Core from the Cardium Formation (12-03-042-09W5/0 well) with accompanying wireline log signatures.

14-01-042-07W5/0

1992.8 – 2008.9m

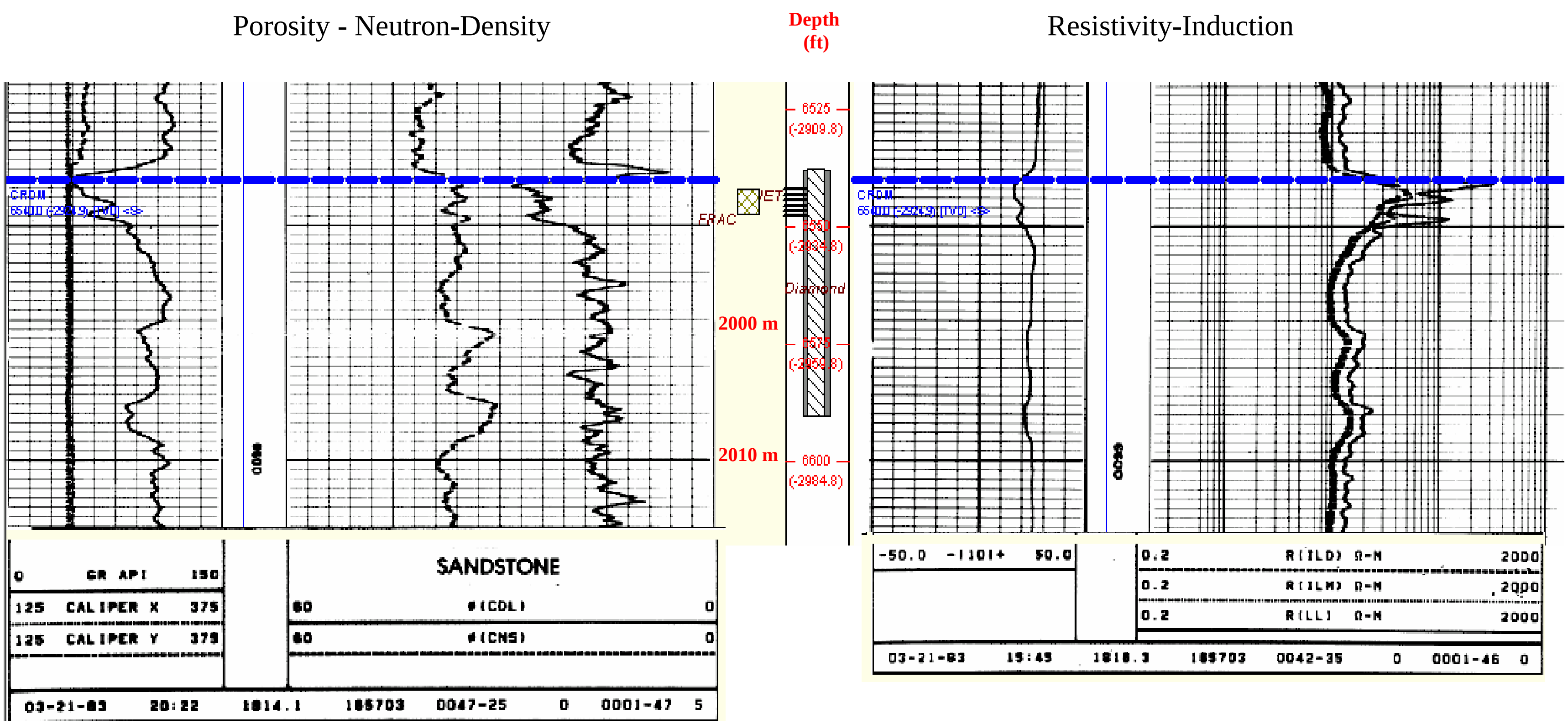

Figure A-24. Core from the Cardium Formation (14-01-042-07W5/0 well) with accompanying wireline log signatures.

14-06-047-09W5/0

1787.7 – 1802.6 m

Resistivity-Induction

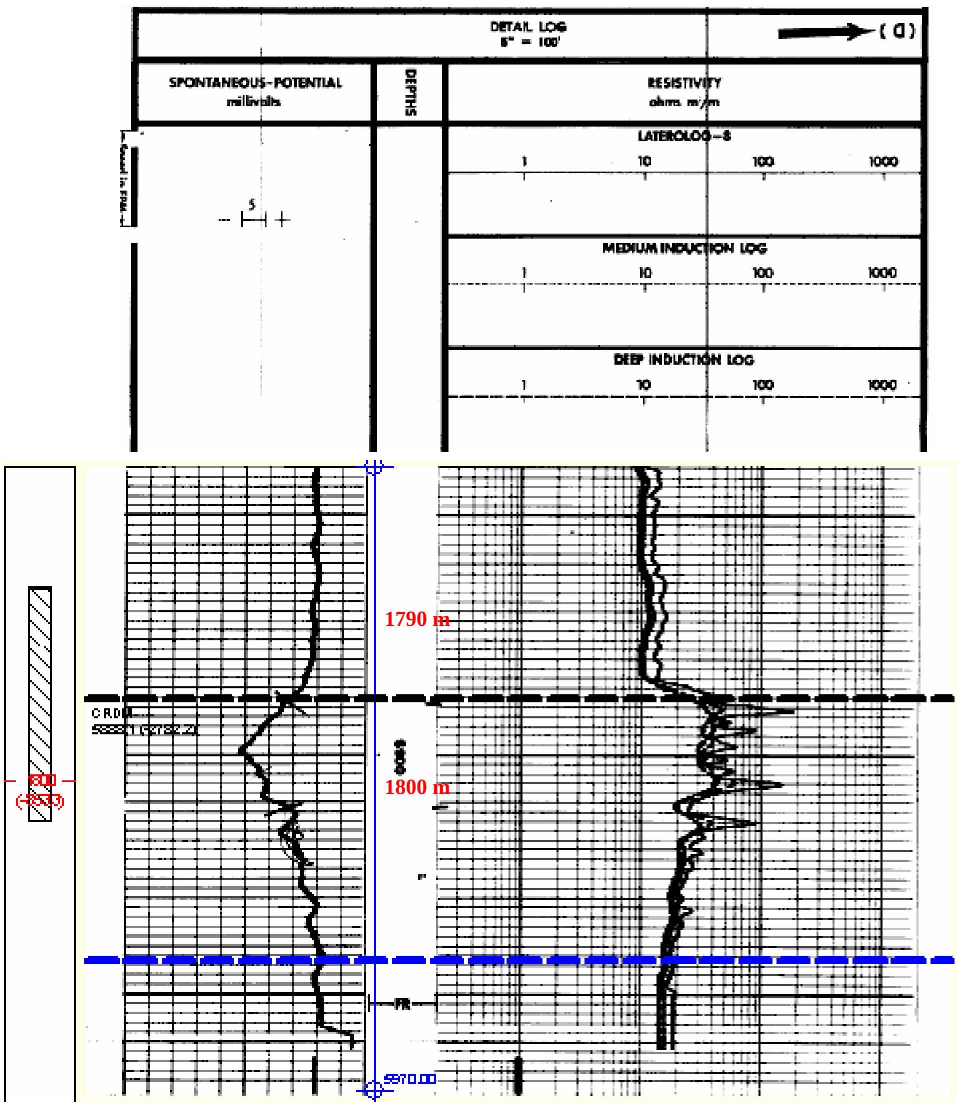

Figure A-25. Core from the Cardium Formation (14-06-047-09W5/0 well) with accompanying wireline log signatures.

16-16-047-10W5/0

1901 – 1919m

Lithology – Gamma-Ray

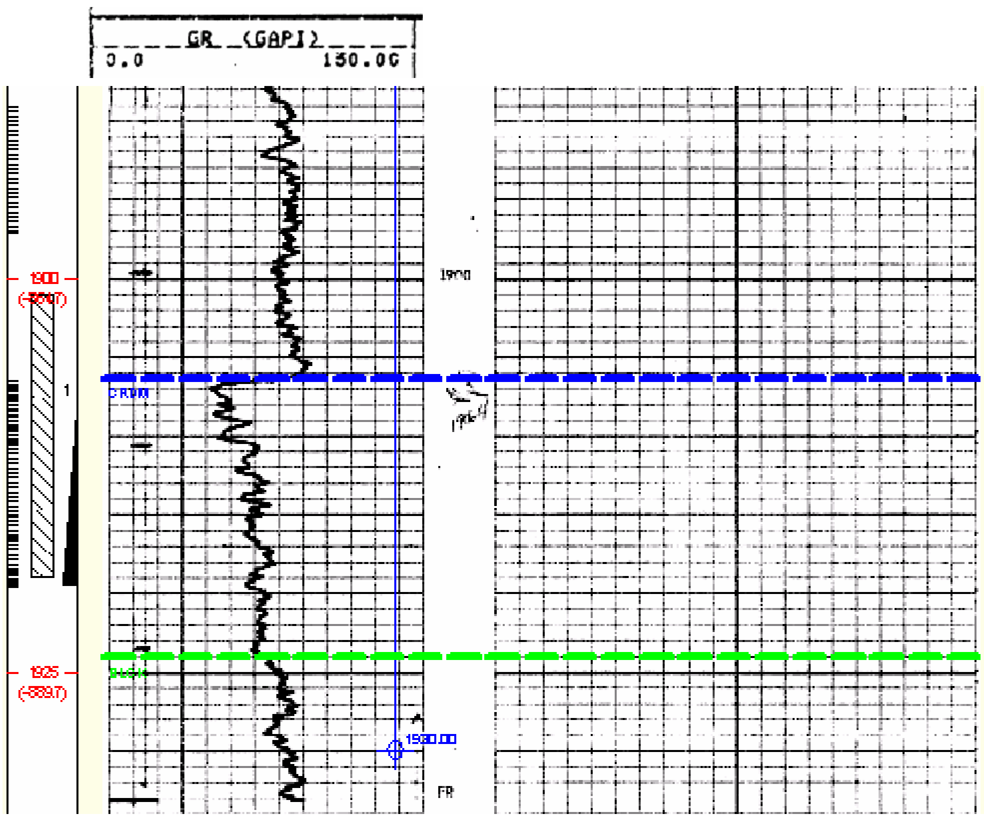

Figure A-26. Core from the Cardium Formation (16-16-047-10W5/0 well) with the only available wireline log signature (lithology gamma-ray).

06-22-042-09W5/0

2074.5 – 2089.7 m

Porosity – Sonic　　　　Resistivity-Induction

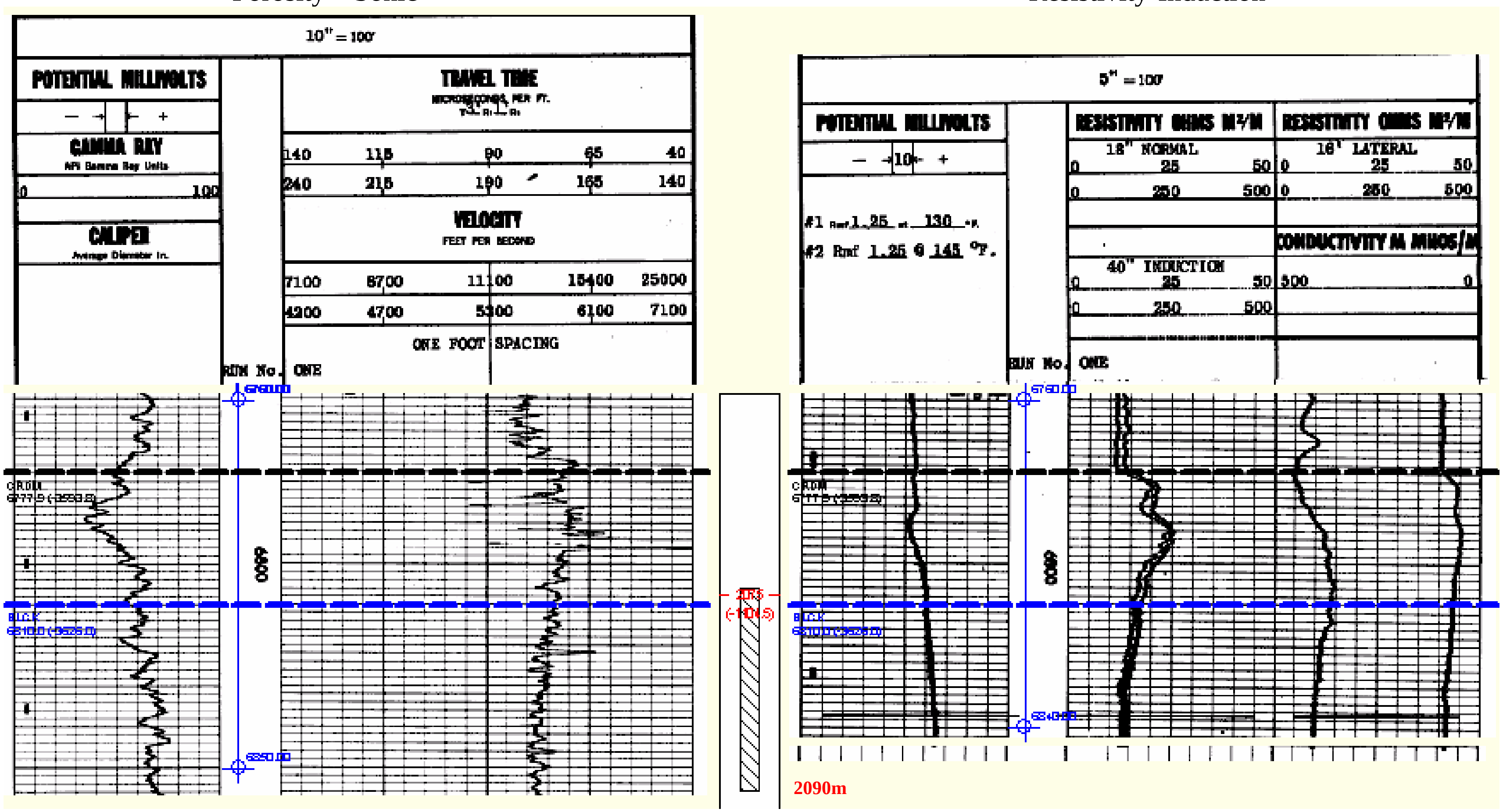

Figure A-27. Core from the Colorado Group (06-22-042-09W5/0 well) with accompanying wireline log signatures.

04-10-042-09W5/2

2097 – 2110.7 m

Porosity – Neutron-Density

Resistivity-Induction

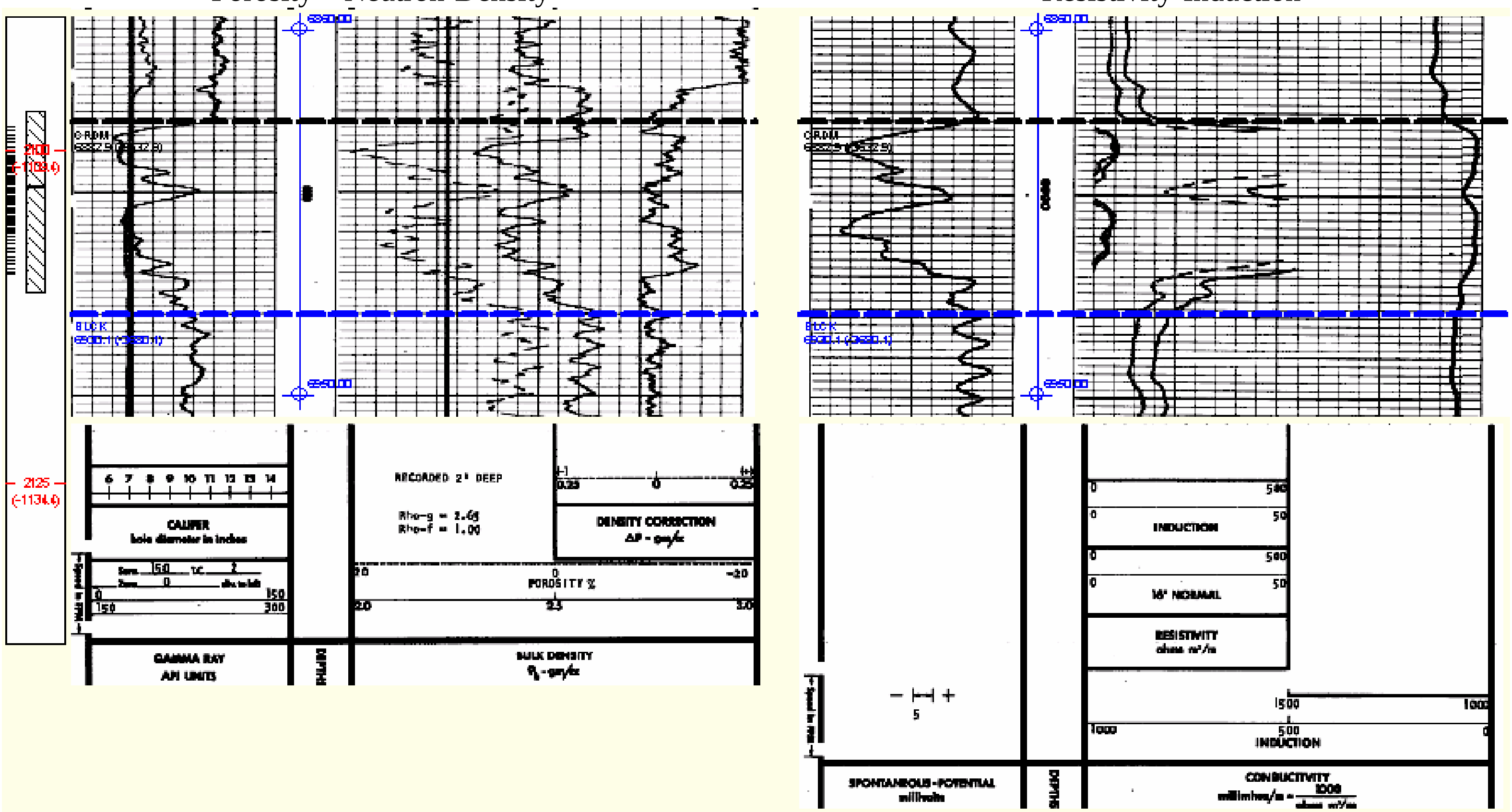

Figure A-28. Core from the Cardium Formation (04-10-042-09W5/2 well) with accompanying wireline log signatures.

10-10-042-09W5/0

2058.3 – 2073.3 m

Resistivity-Induction

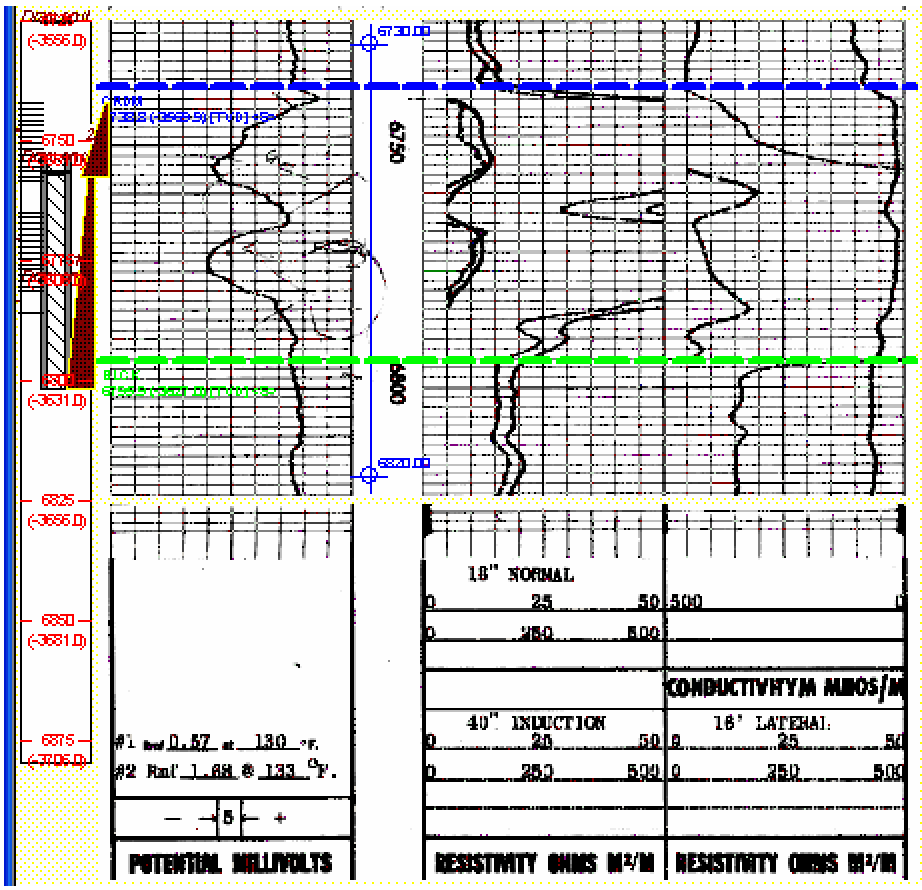

Figure A-29. Core from the Belly River Formation (10-10-042-09W5/0 well) with accompanying wireline log signatures.

06-12-045-07W5/0

1980 – 1985m
1985 – 2001m

Porosity - Neutron-Density

Resistivity-Induction

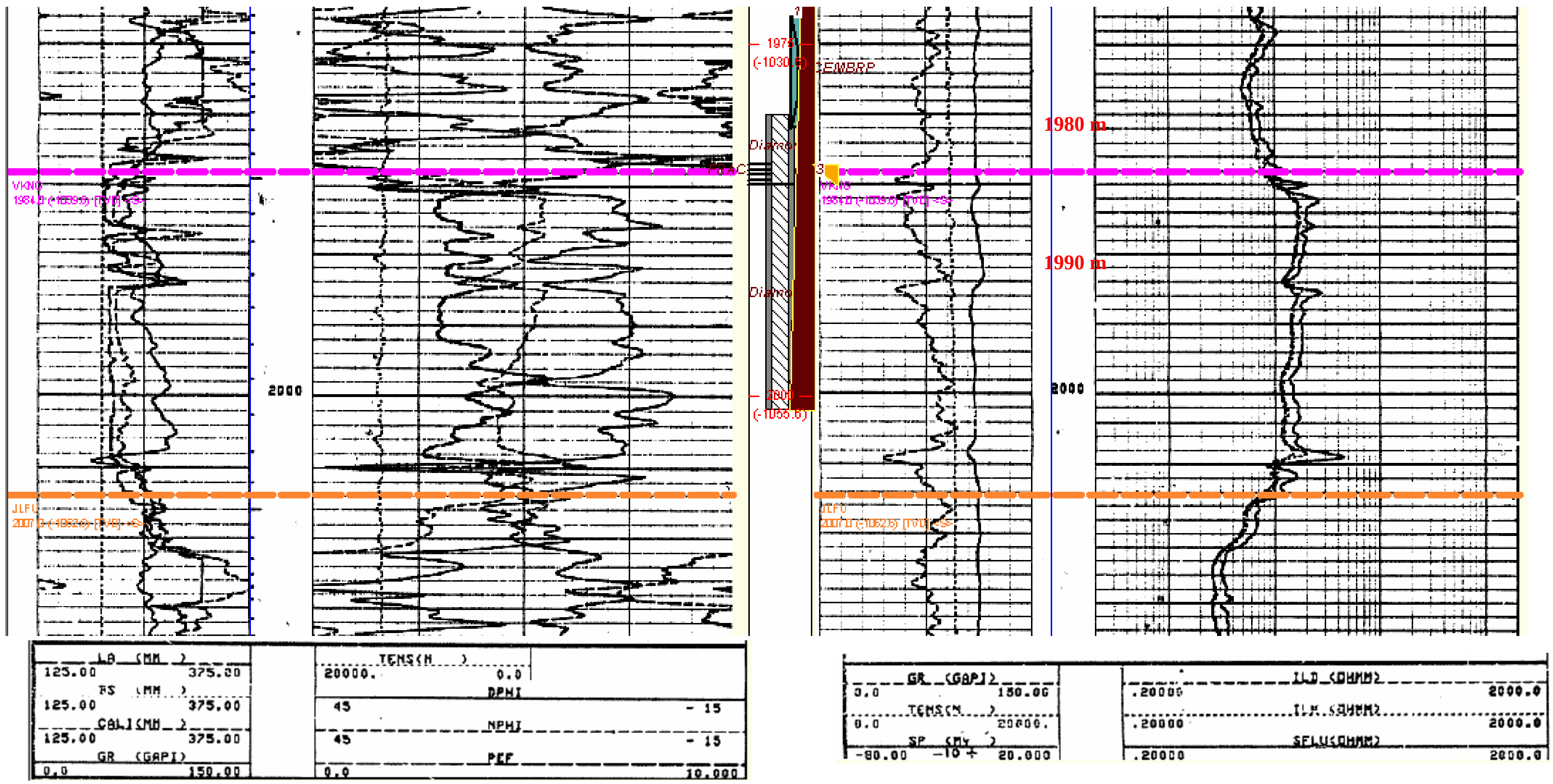

Figure A-30. Core from the Viking Formation (06-12-045-07W5/0 well) with accompanying wireline log signatures.

07-06-042-07W5/0

2271 – 2289.2 m

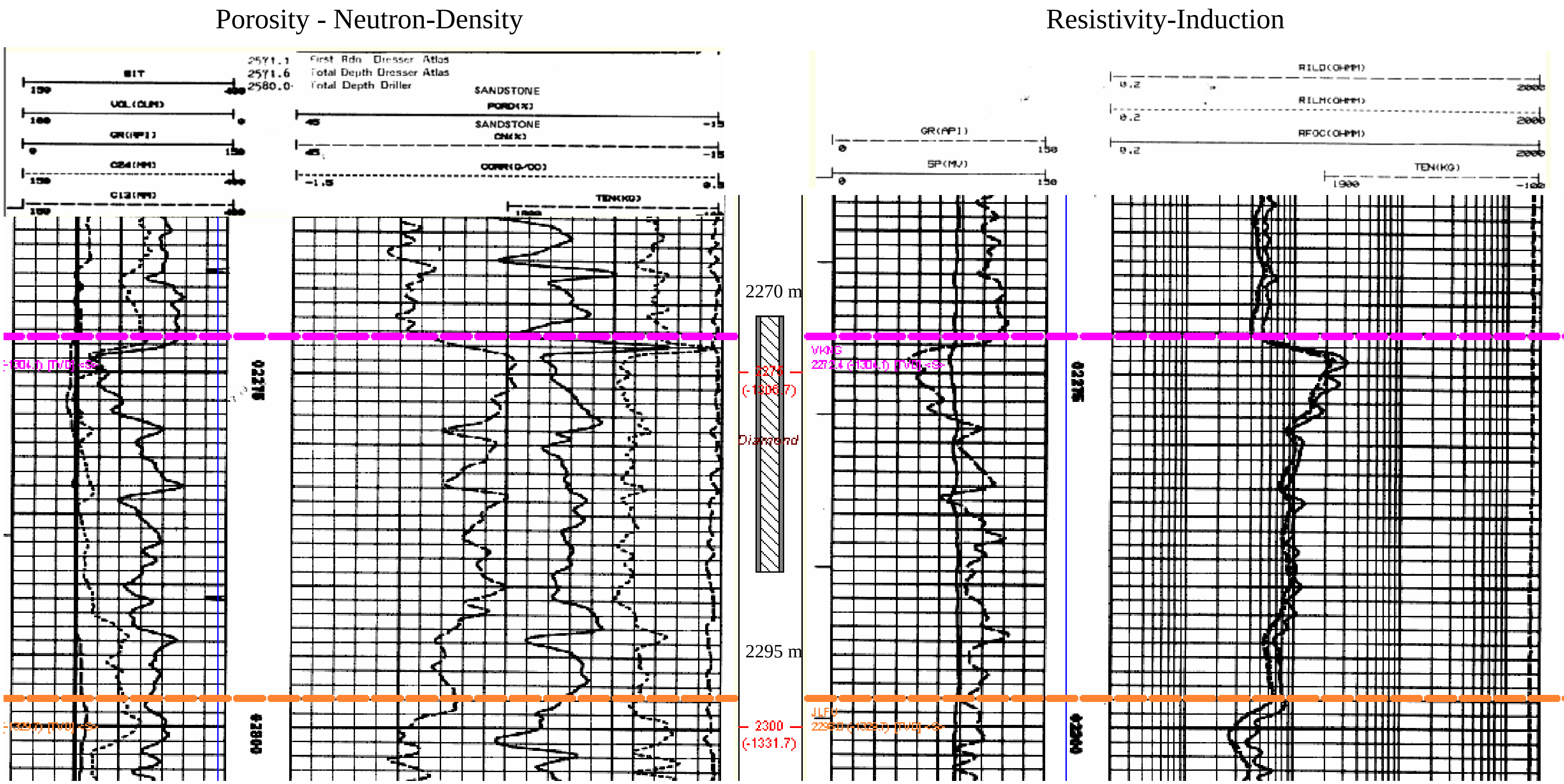

Figure A-31. Core from the Viking Formation (07-06-042-07W5/0 well) with accompanying wireline log signatures.

07-08-042-05W5/0

2051 – 2069 m

Porosity – Sonic Porosity - Resistivity

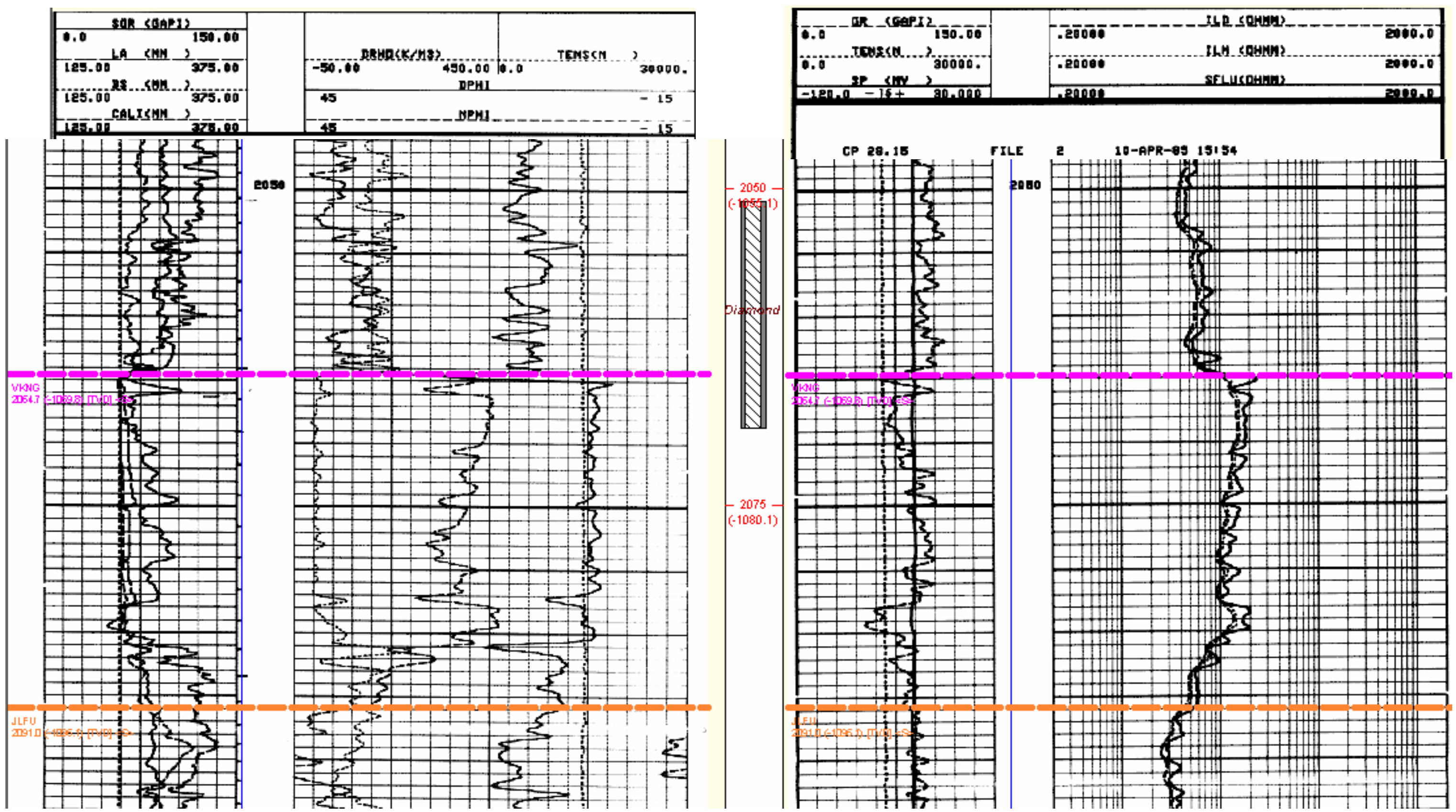

Figure A-32. Core from the Viking Formation (07-08-042-05W5/0 well) with accompanying wireline log signatures.

08-11-042-07W5/0

2271 – 2278.1 m & 2278.3 – 2289.2 m

Porosity - Neutron-Density | Resistivity-Induction

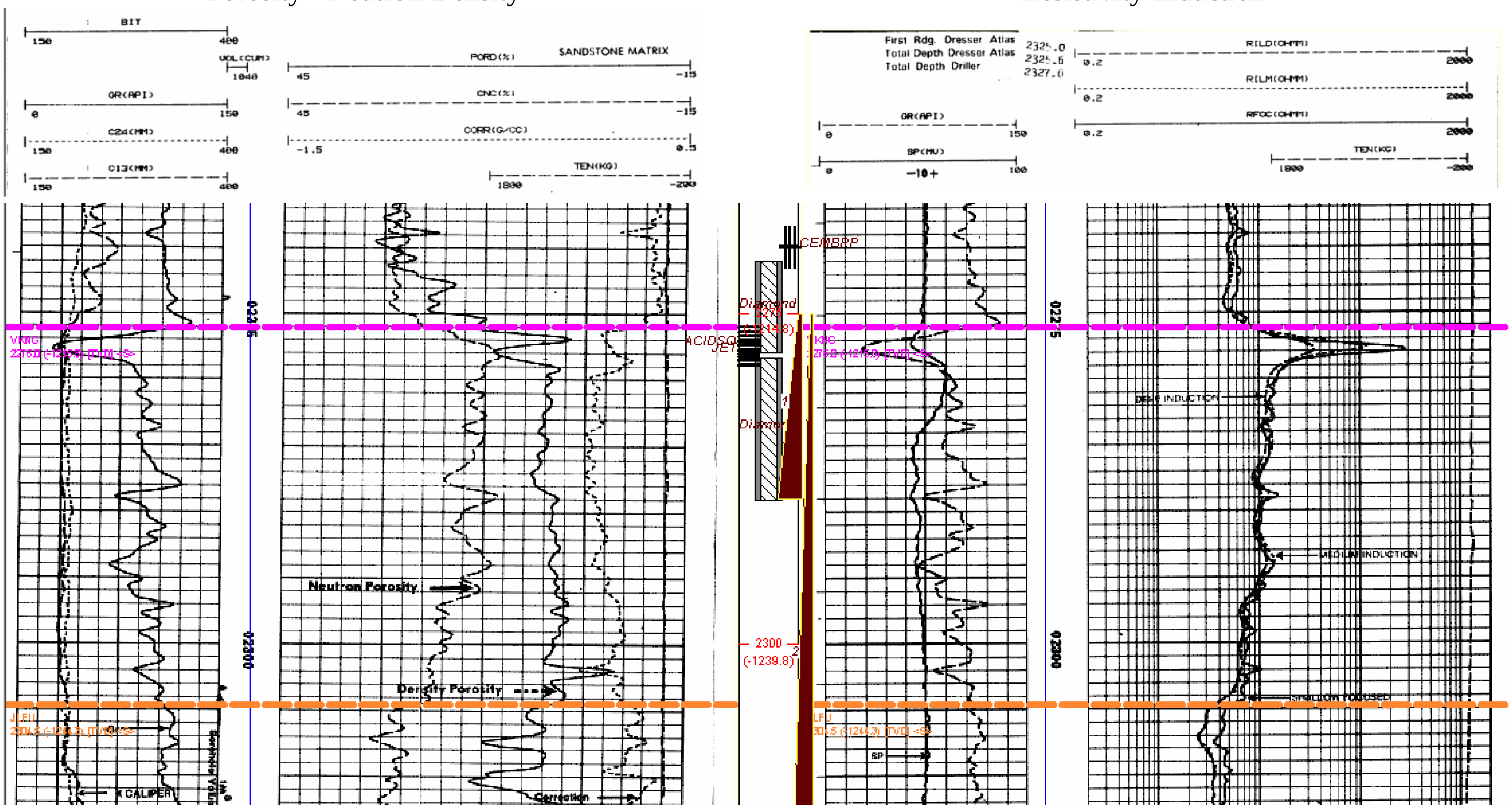

Figure A-33. Core from the Viking Formation (08-11-042-07W5/0 well) with accompanying wireline log signatures.

10-17-042-04W5/0

1934 – 1952m

Porosity - Neutron-Density

Resistivity-Induction

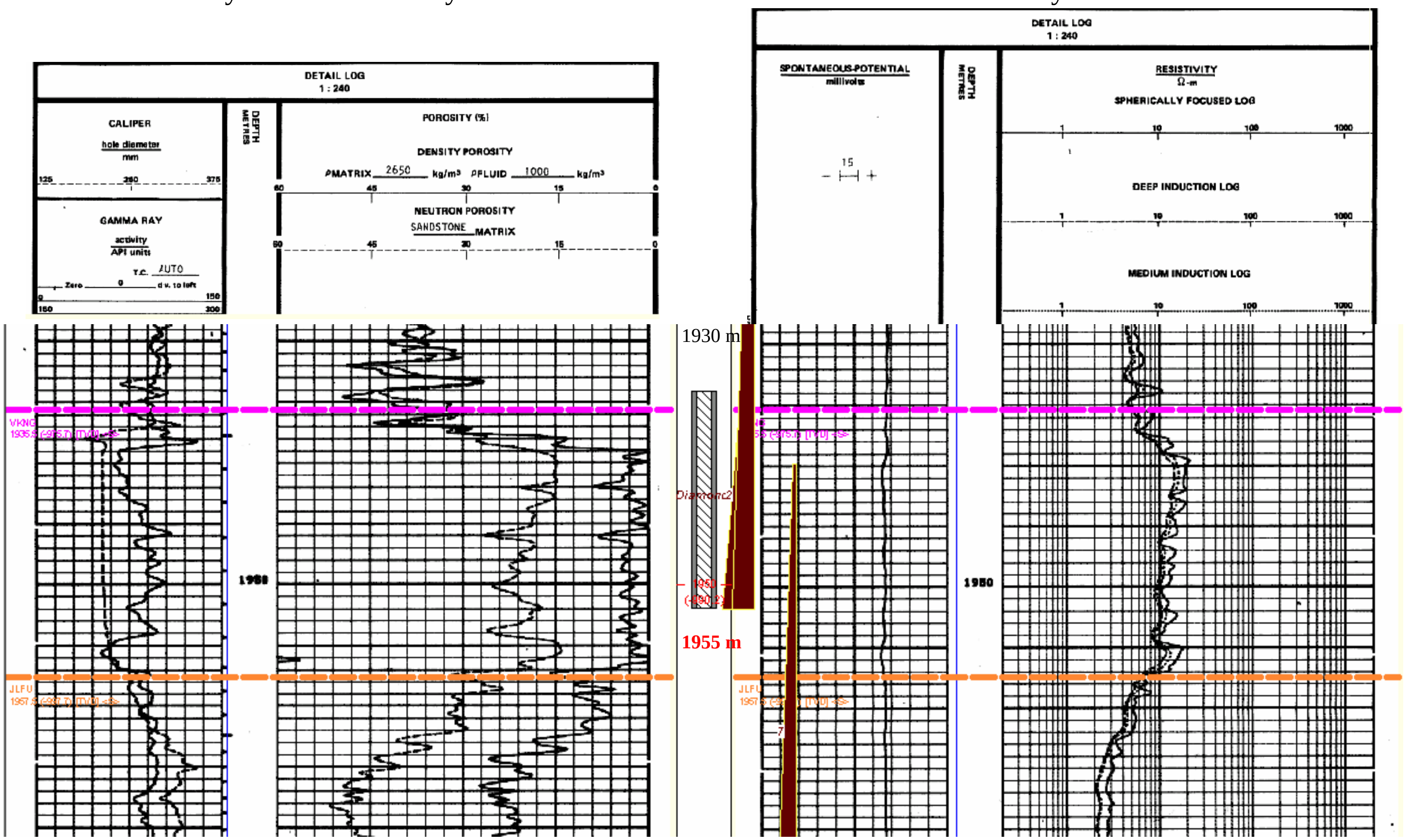

Figure A-34. Core from the Viking Formation (10-17-042-04W5/0 well) with accompanying wireline log signatures.

03/13-13-042-05W5/0

1974 – 1980 m

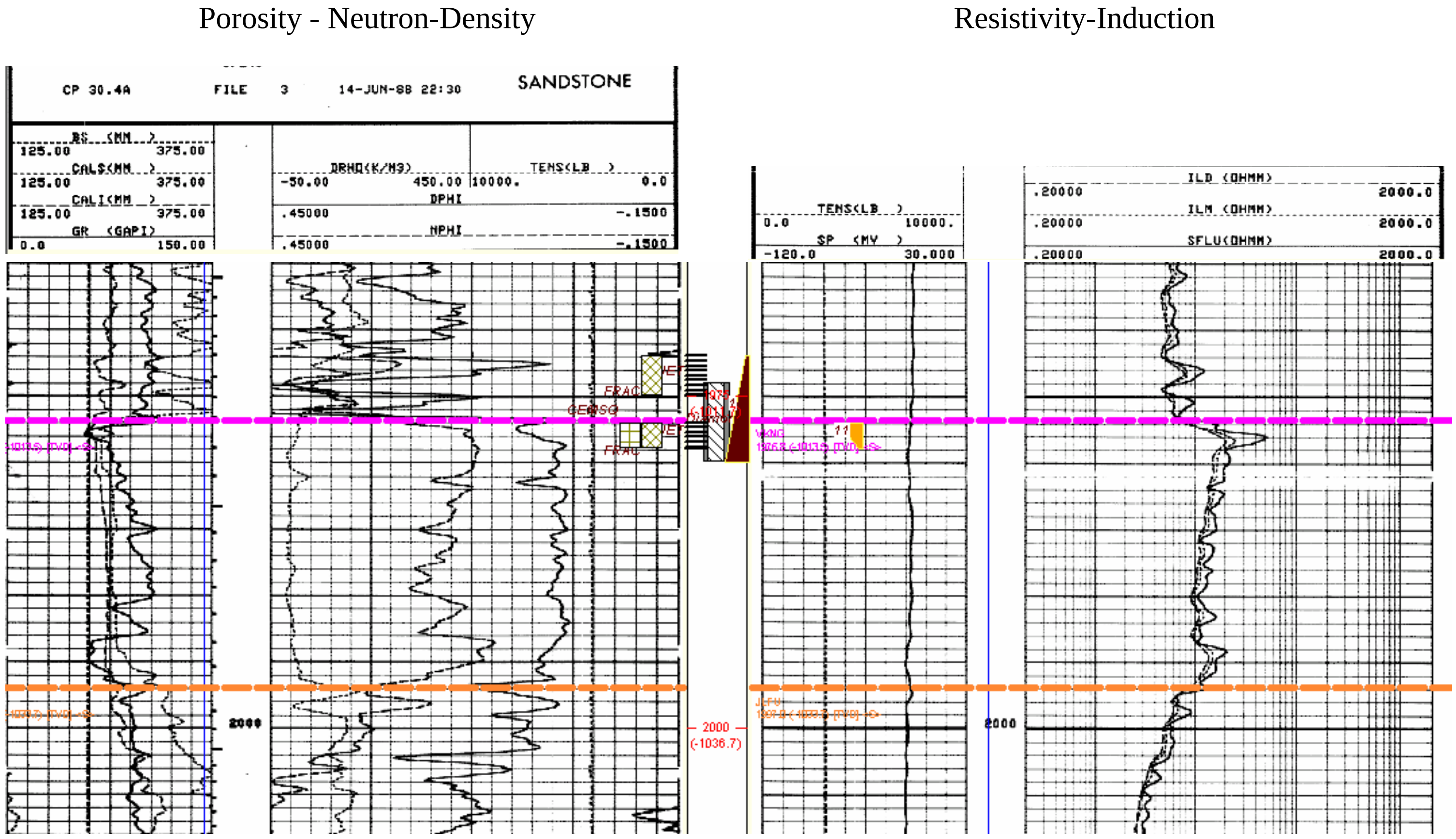

Figure A-35. Core from the Viking Formation (03/13-13-045-05W5/0 well) with accompanying wireline log signatures.

03-13-043-05W5/0

1986.5 – 2004.7 m

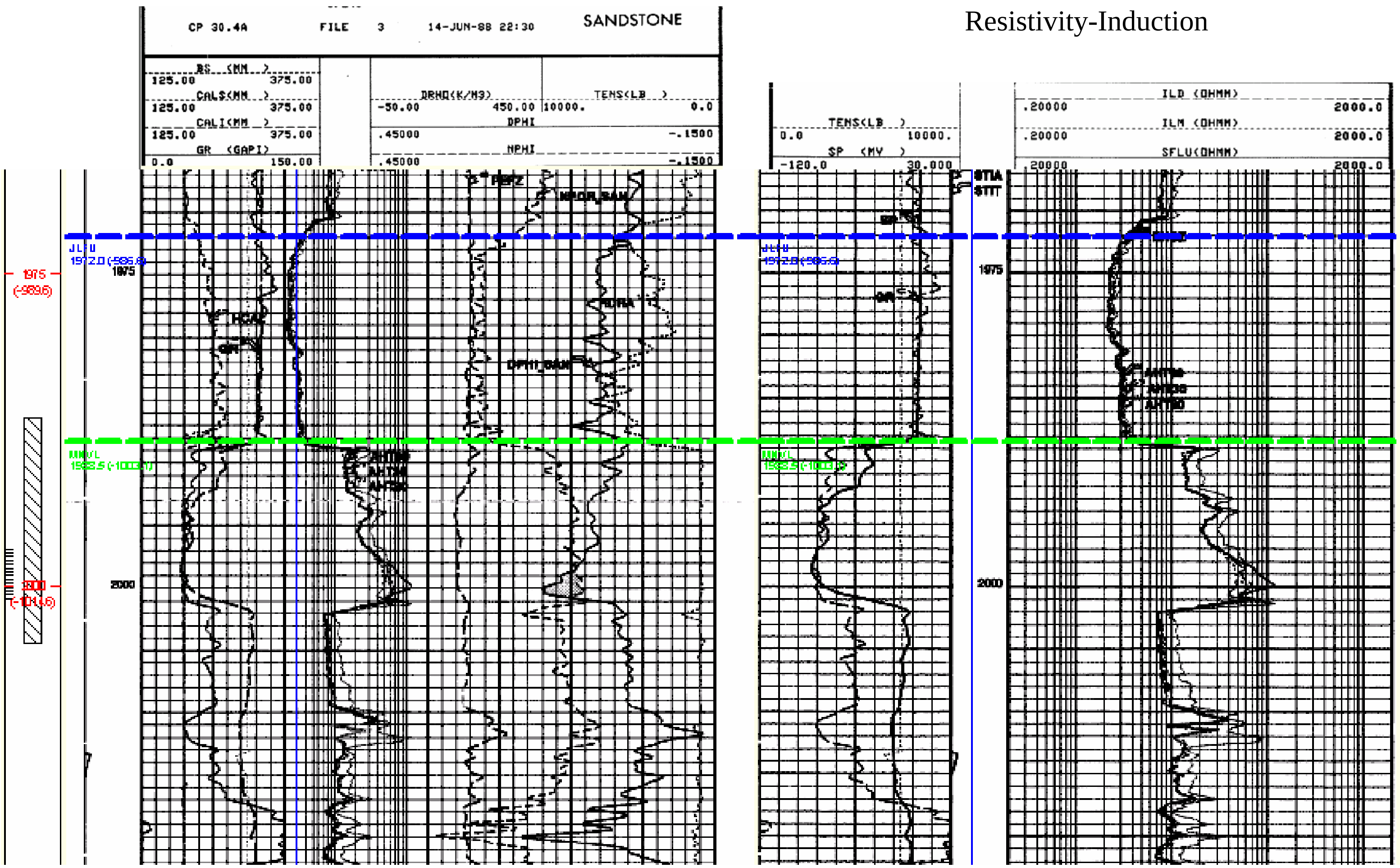

Figure A-36. Core from the Joli Fou – Mannville contact (03-13-043-05W5/0 well) with accompanying wireline log signatures.

10-32-048-06W5/0

1721 – 1730.1 m

Porosity - Neutron-Density

Resistivity-Induction

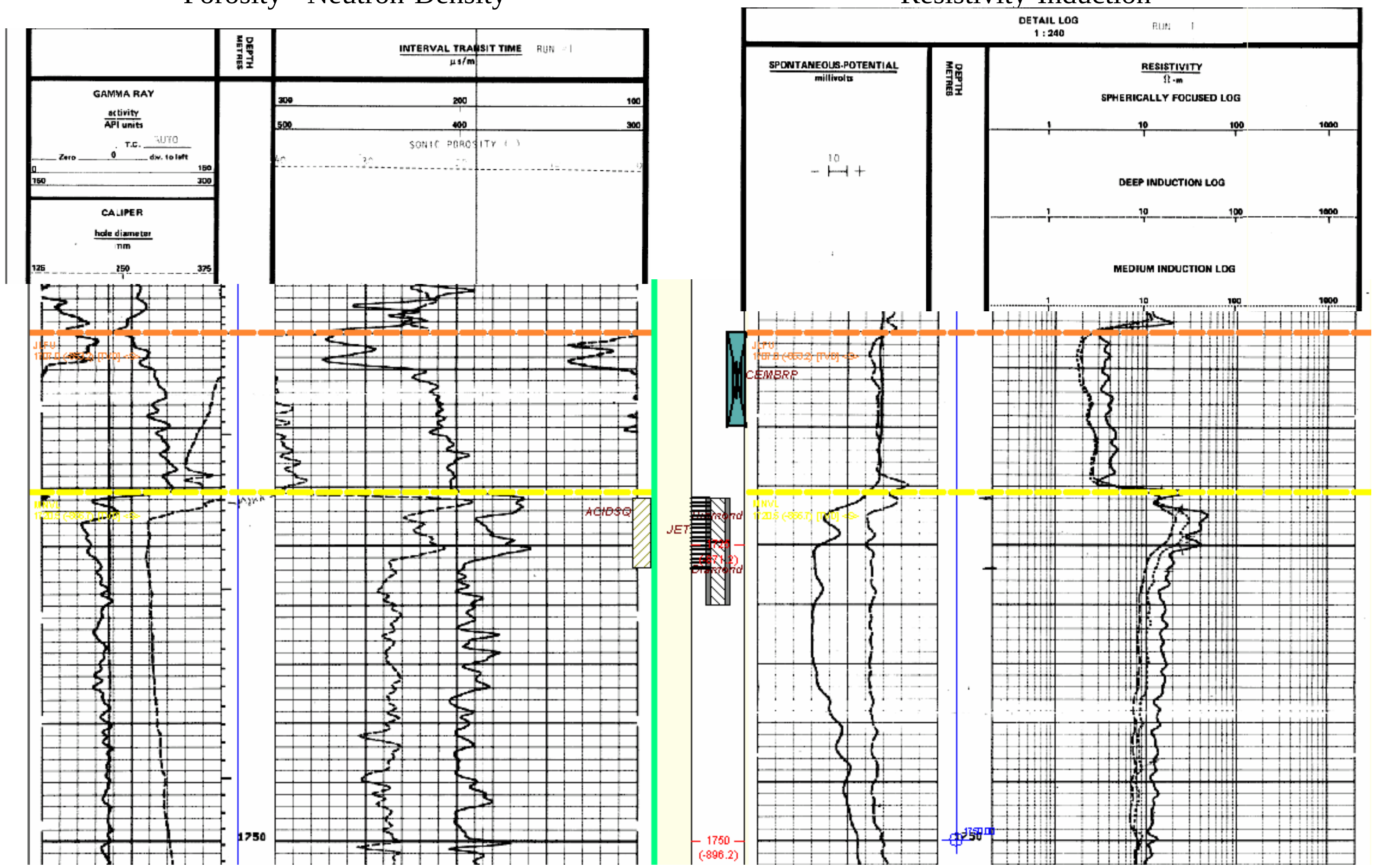

Figure A-37. Core from the Joli Fou – Mannville contact (10-32-048-06W5/0 well) with accompanying wireline log signatures.

02/11-15-045-07W5/0

2012.3 – 2024.5m

Porosity - Neutron-Density

Resistivity-Induction

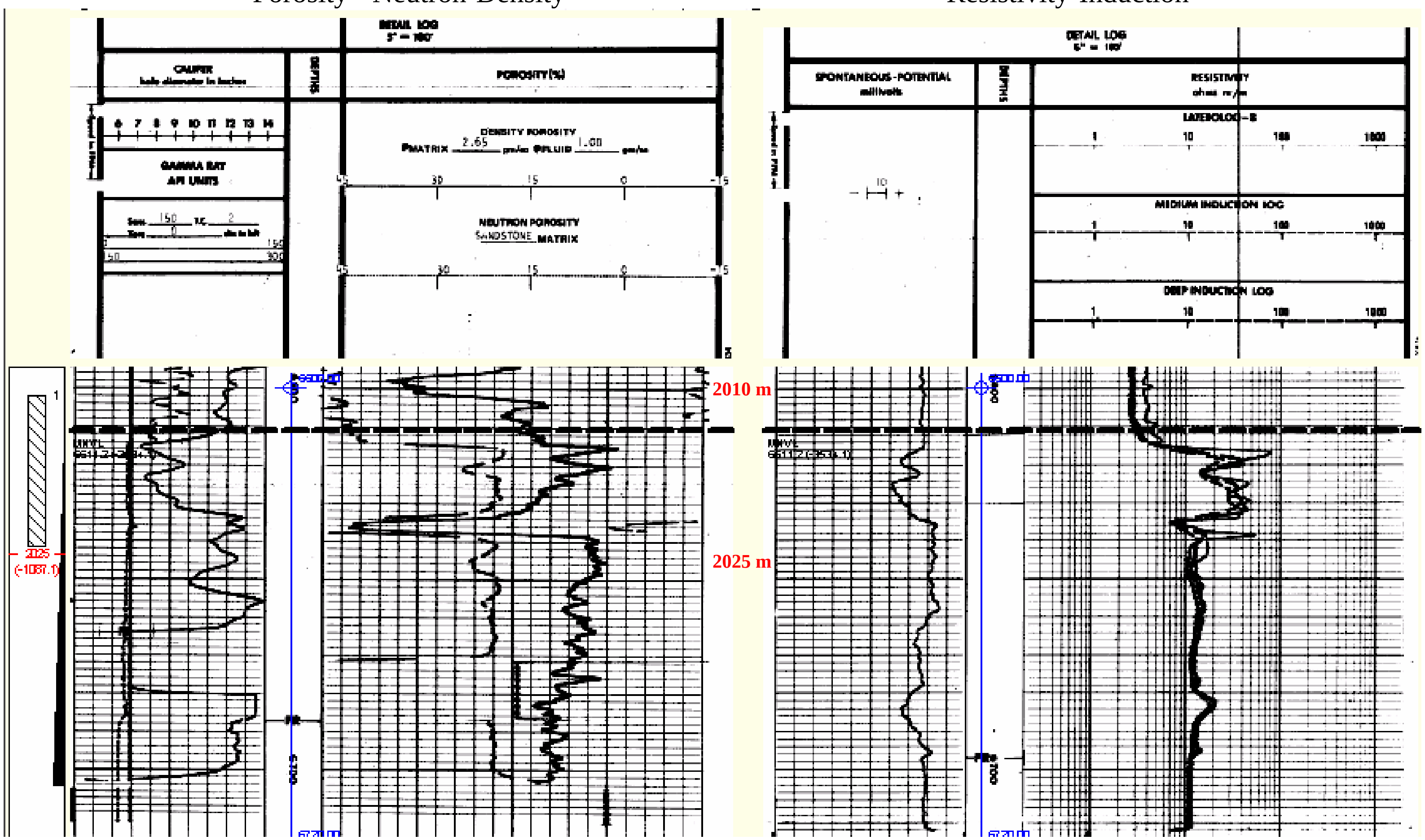

Figure A-38. Core from the Joli Fou - Mannville contact (02/11-15-045-07W5/0well) with accompanying wireline log signatures.

16-11-045-07W5/0

2015 – 2028.8 m

Porosity - Neutron-Density

Resistivity-Induction

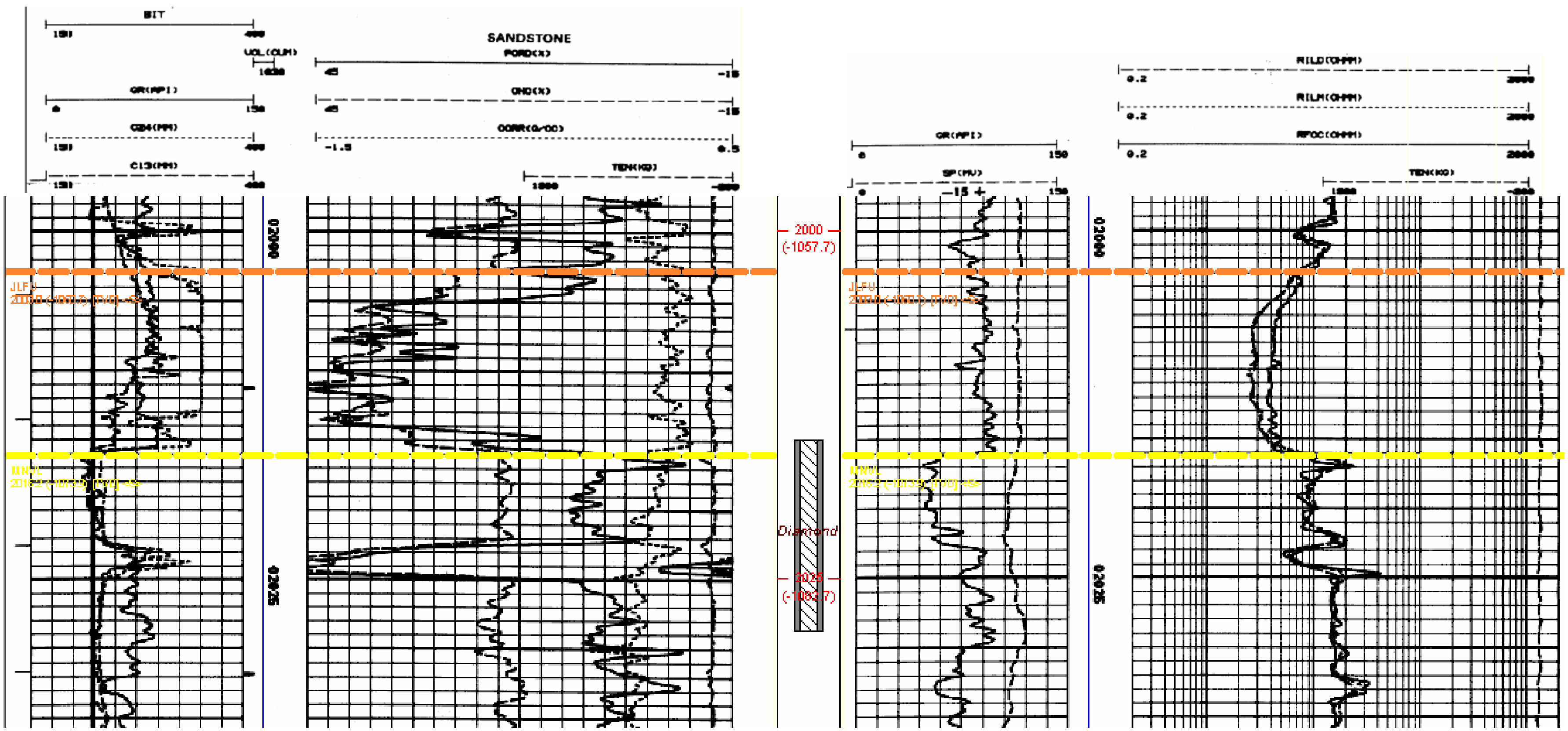

Figure A-39. Core from the Joli Fou – Mannville contact (16-11-045-07W5/0 well) with accompanying wireline log signatures.

10-25- 047-03W4/0

538 – 699 m

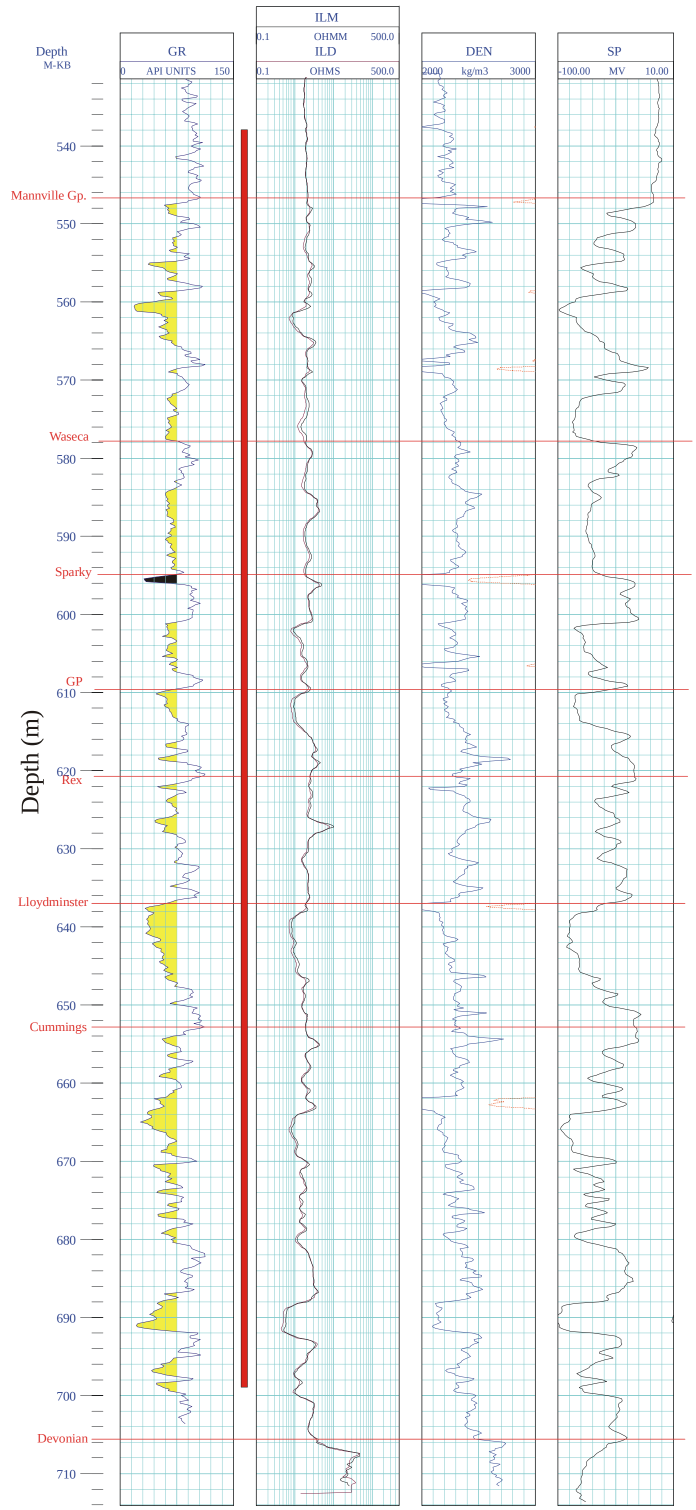

Figure A-40. Core from the Joli Fou – Mannville section (10-25- 047-03W4/0 well) with accompanying wireline log signatures.

PLATES

PLATE 1

Core photographs of 06-04-042-04W5/0
Belly River Fm.

Whole core interval is 1266 - 1274.5 m. Base of core (Base), top of core (Top).

White arrows point to the base channel surface (depth ~ 1267 m), which is erosive and defines the sharp transition between a fine-grained facies and a coarse-grained facies in fluvial environments. The insets A and B are reproduced as close-ups in PLATE 3. Note gamma-ray or resistivity well-log signature associated with erosion surface in non-marine environments (see Fig. A-3).


Top
1266 m
Base
1269.5 m
15 cm
Coal
Alluvial plain sediments
Channel sandstone
A
B

PLATE 1

PLATE 2

Channel base of 06-04-042-04W5/0
Belly River Fm.

Whole core interval is 1266 - 1274.5m. Base of core (b), top of core (t).

Depth 1267m: close-up view from PLATE 1 of the boundary between a fluvial channel sandstone and the underlying fine-grained sediments (Belly River Formation).
This type of stratigraphic boundary seems to influence the carbon isotopic mudgas profiles, acting as a flow unit boundary.

Note: the pencil in the photograph is 15 cm long.

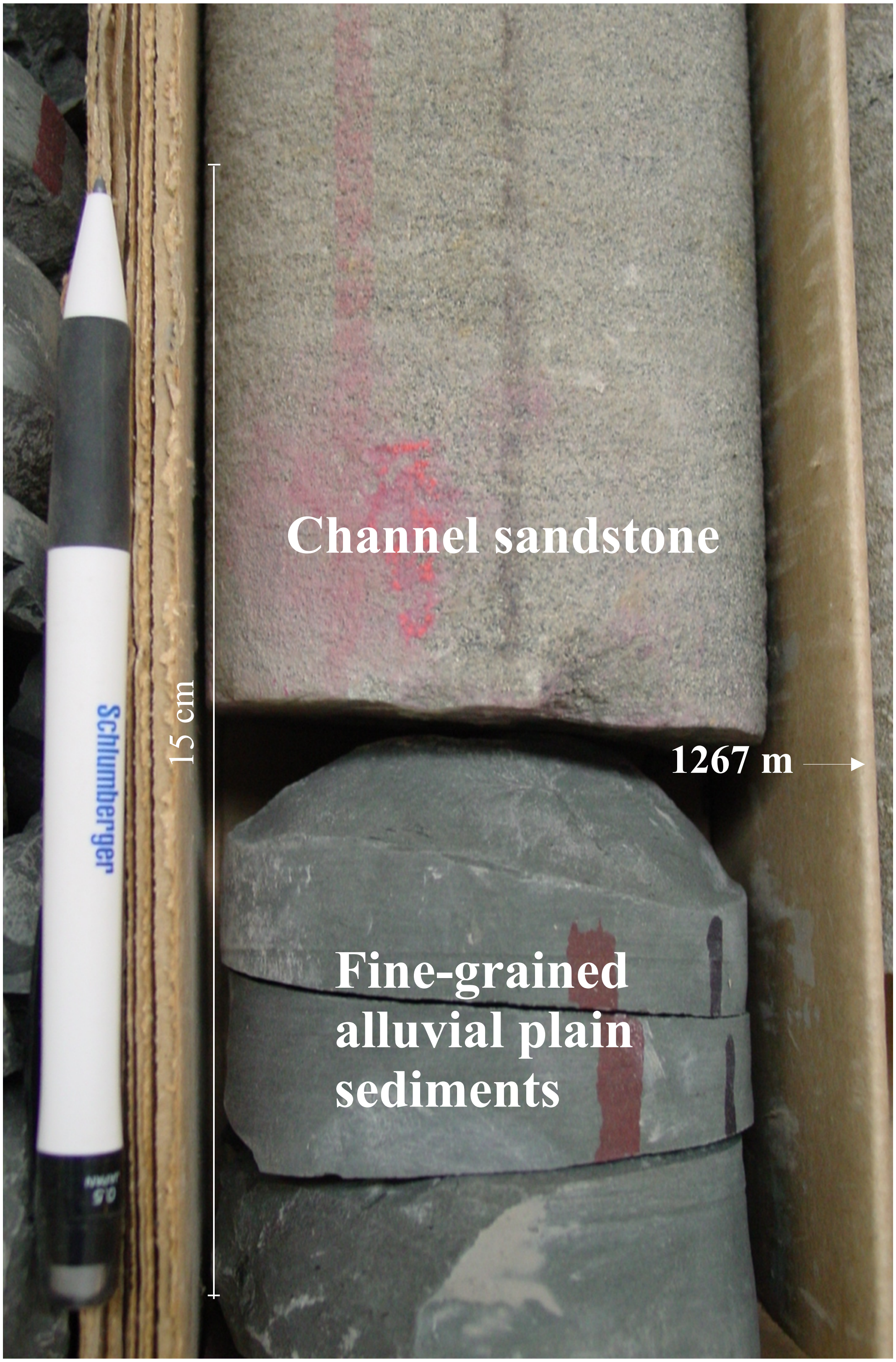
Channel sandstone
15 cm
Schlumberger
1267 m
Fine-grained
alluvial plain
sediments

PLATE 2

PLATE 3

Core photographs of 06-04-042-04W5/0
Belly River Fm.

A) Close-up from PLATE 1: fine-grained (silts, shales) alluvial plain sediments

B) Close-up from PLATE 1: contact between a channel sandstone and the underlying fine-grained sediments

Whole core interval is 1266 - 1274.5m.

PLATE 3

PLATE 4

Core photographs of 02/06-09-046-09W5/0
Lea Park Fm. - Belly River Fm.

Whole core interval is 1432 - 1453 m. Base of core (b), top of core (t).

(A) Lea Park Formation: fine-grained sandstone, siltstone, shale and coal facies
White arrow indicates the erosional base of a regressive sandstone body cutting one of the coal seams found on top of a coarsening-upward sequence of the Lea Park Fm.

(B) Contact between Lea Park Fm. and Basal Belly River.
This facies, representing fluvial channel sediments, is bounded by an erosional surface at its base and overlain by a poorly sorted conglomerate, and coarse-grained sandstone grading upward into finer sandstones and then siltstones.
See PLATE 6 for a close-up view of the basal conglomerate.
Note: the black arrow points towards the uppermost part of the shoreface sandstone capped by non-marine facies. The surface is known as a maximum regressive surface (MRS), and seems to act as a flow unit boundary, influencing the carbon isotopic mudgas profiles.

Lea Park Fm.
Coal and carbonaceous shale
Belly River Fm.
t
B
Base Belly River Fm.

b
Lea Park Fm.
15 cm
Coal and carbonaceous shale
A

PLATE 4

PLATE 5

Core photograph of 02/06-09-046-09W5/0
Lea Park Fm.

Whole core interval is 1432 - 1453 m

White arrow indicates the erosional base of a regressive sandstone cutting the fine-grained sediments found on top of a coarsening-upward sequence of the Lea Park Fm. Depth: 1451.9 m.
This sharp contact (also known as a regressive surface of erosion - RSE - cf. Power and Walker, 1996) demarcates one of the stratigraphic surfaces capable of influence the carbon isotope signature.

PLATE 5

PLATE 6

Core photograph of 02/06-09-046-09W5/0
Belly River Fm.

Whole core interval is 1432 - 1453 m. Base of core (b), top of core (t)

A) Sharp contact between Belly River conglomerate and the underlying sediments of the regressive Lea Park Formation, demarcated by sideritized rip-up clasts (white arrow).

B) Close-up view of the erosional surface. Depth: 1447m
See Figure A-4 for the association with wireline log signatures.

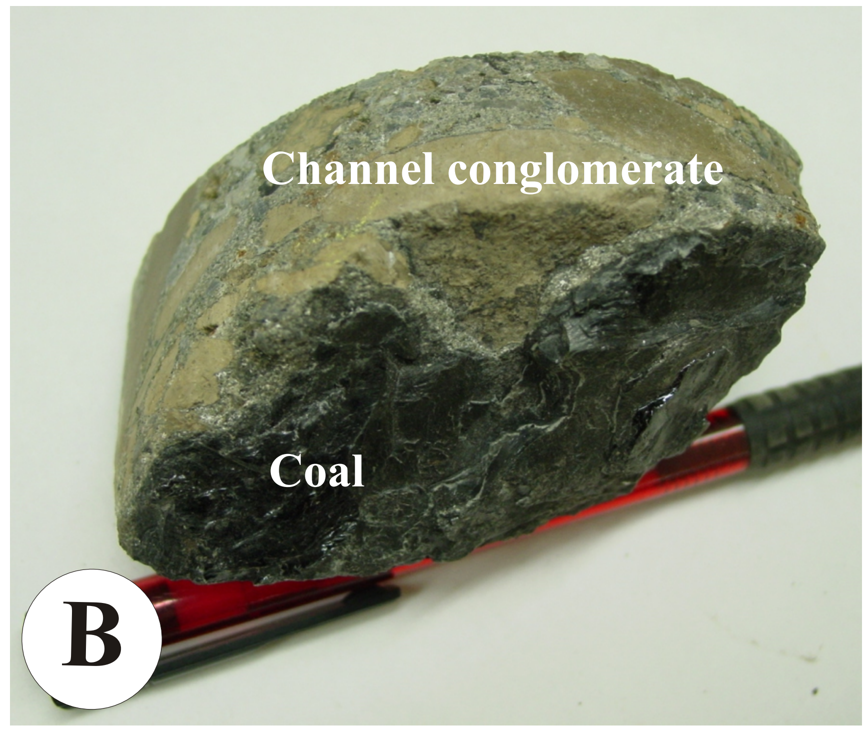

PLATE 6

PLATE 7

Core photographs of 08-02-043-05W5/0
Lea Park - Belly River formations

Whole core interval is 1310 - 1328 m

Fully developed shoreline succesion of the Lea Park - Belly River transition. The white arrow is pointing to an erosional surface underlying shoreface sediments.
Depth 1317.5m
Note the complete lack of transitional interval between the offshore shelf mudstones and the shoreface sandstones.

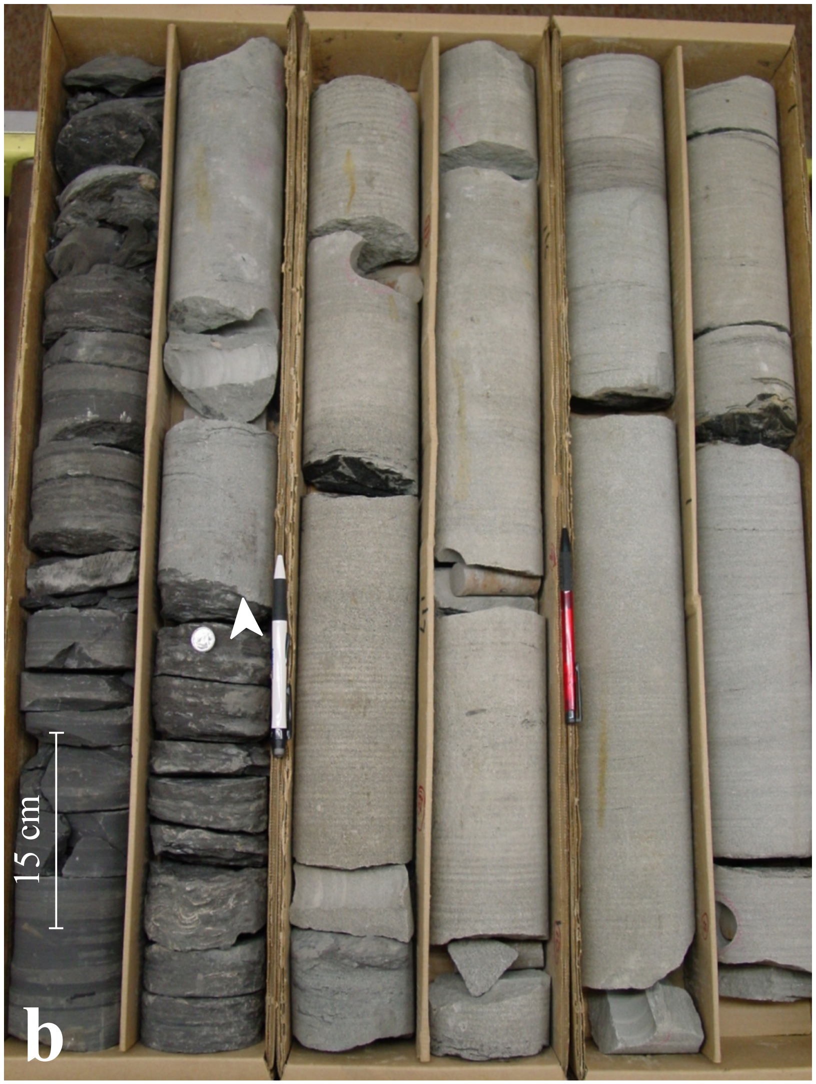

PLATE 7

PLATE 8

Core photograph of 08-02-043-05W5/0
Lea Park -Belly River transition

Close-up of an erosional base of a shoreface sandstone (white arrow). Depth 1317.5m. Note the nature of the contact, which is angular and sharp.

PLATE 8

PLATE 9

Core box photographs of 09-10-044-09W5/0
Belly River Fm.

Whole core interval is 1545 - 1563 m. Base of core in bottom left photograph, top of core in top right photograph. Base of core (b), top of core (t).
The insets A and B are reproduced as close-ups in PLATE 11.

Black arrow points towards the base of a fluvial channel of the Belly River Fm. Depth: 1552.5m.

PLATE 9

PLATE 10

Fluvial channel scour of 09-10-044-09W5/0
Belly River Fm.

Close-up of the erosional base of a fluvial channel fill within the Lea Park - Belly River transition. Coarse grained fluvial deposits are separated from parallel- laminated, fine to medium grained sandstones by an irregular, erosional contact. Note the rip-up clasts in the overlying conglomerate.
Depth 1552.5 m

PLATE 10

PLATE 11

Fluvial channel facies of 09-10-044-09W5/0
Belly River Fm.

Close-ups from PLATE 9:

(A) Depth 1551 m: coarse fluvial sandstone

(B) Depth 1541 m: finer grained sandstone, part of an upward-coarsening cycle.

PLATE 11

PLATE 12

Core photographs of 10-04-049-11W5/0
Belly River Fm.

Whole core interval is 1417 - 1435 m. Base of core (Base), top of core (Top).

The core photographs cover only the 1421-1424 m interval, showing fluvial channel and flood plain deposits.
White arrows point towards the base of the channel. Depth: 1423 m.
The insets A and B are reproduced as close-ups in PLATE 14.

PLATE 12

PLATE 13

Fluvial channel base of 10-04-049-11W5/0
Belly River Fm.

Whole core interval is 1417 - 1435 m

Close-up of the erosional base of a fluvial channel sandstone within the Belly River Fm.

Base channel is at 1423 m depth

PLATE 13

PLATE 14

Core photographs of 10-04-049-11W5/0
Belly River Fm.

Close-up view from Plate 12:
A) Massive structure, parallel laminations, and rip-up clasts of the Belly River fluvial channel sandstone.
B) Wavy, contorted and parallel laminations of the flood plain deposits.

Whole core interval is 1417 - 1435 m

PLATE 14

PLATE 15

Basal Belly River sandstone of 14-28-42-4W5

Whole core interval: 1277 - 1295 m

A) shoreface sandstone of the Lea Park - Belly River transition. Depth: 1294 m

B) shoreface sandstone of the Lea Park - Belly River transition. Depth: 1292 m

C) Fluvial channel sandstone.Depth: 1283 m

D) Fluvial channel sandstone. Depth: 1279 m

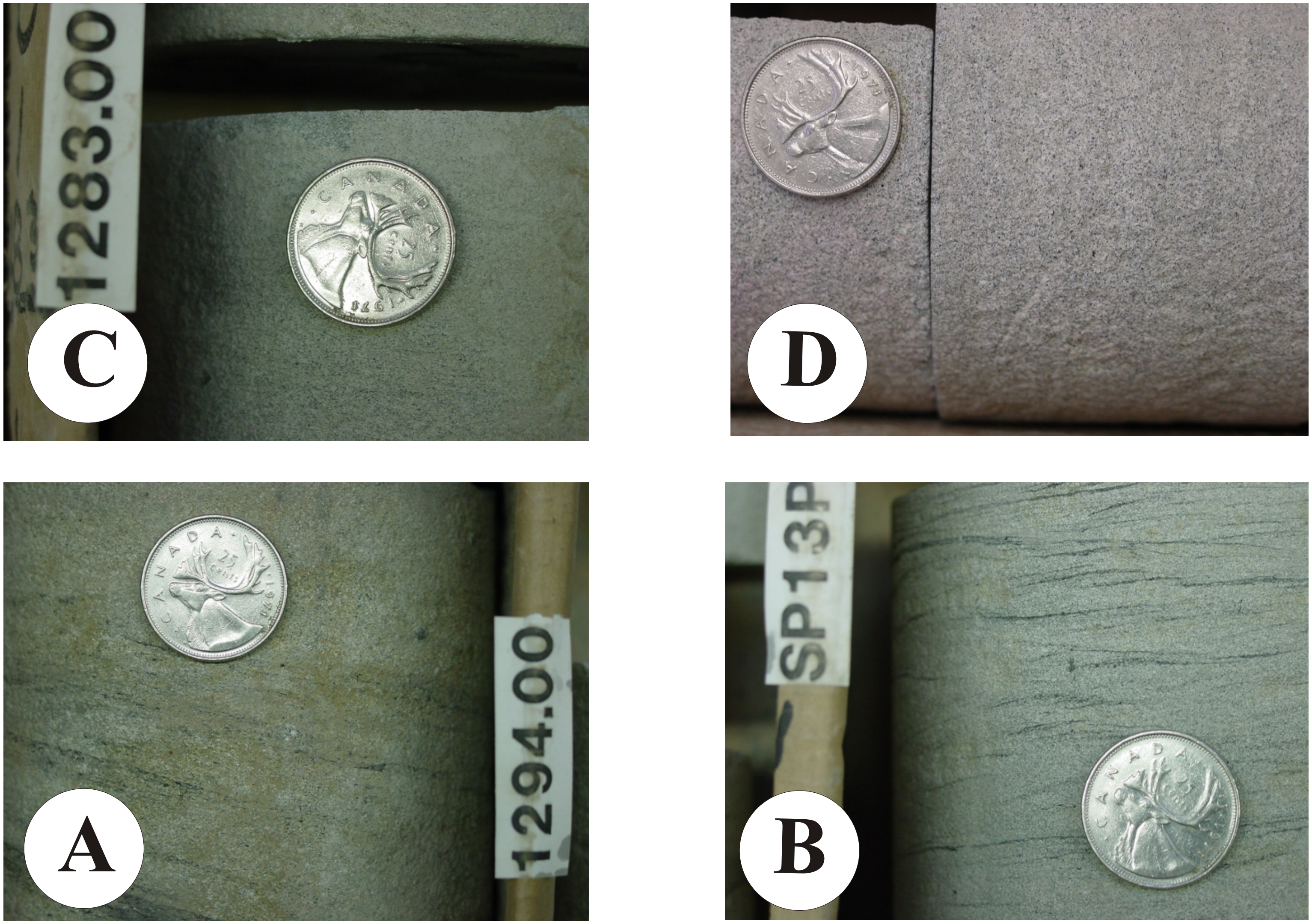

PLATE 15

PLATE 16

Belly River channel 16-11-45-7W5

Whole core interval: 1300-1329 m

A) Pebbly sandstones exhibiting trough cross-bedding. Depth 1316 m.

B) Coarse-grained pebbly sandstone facies. Depth 1319 m.

C) Poorly sorted chert conglomerate interbedded with coarse-grained pebbly sandstone in the Belly River channel. May be part of a braided river deposit. Depth 1314.5 m.

D) Scour surface mantled by mudstone rip-up clasts found near the top of the Belly River channel. Depth 1310 m.

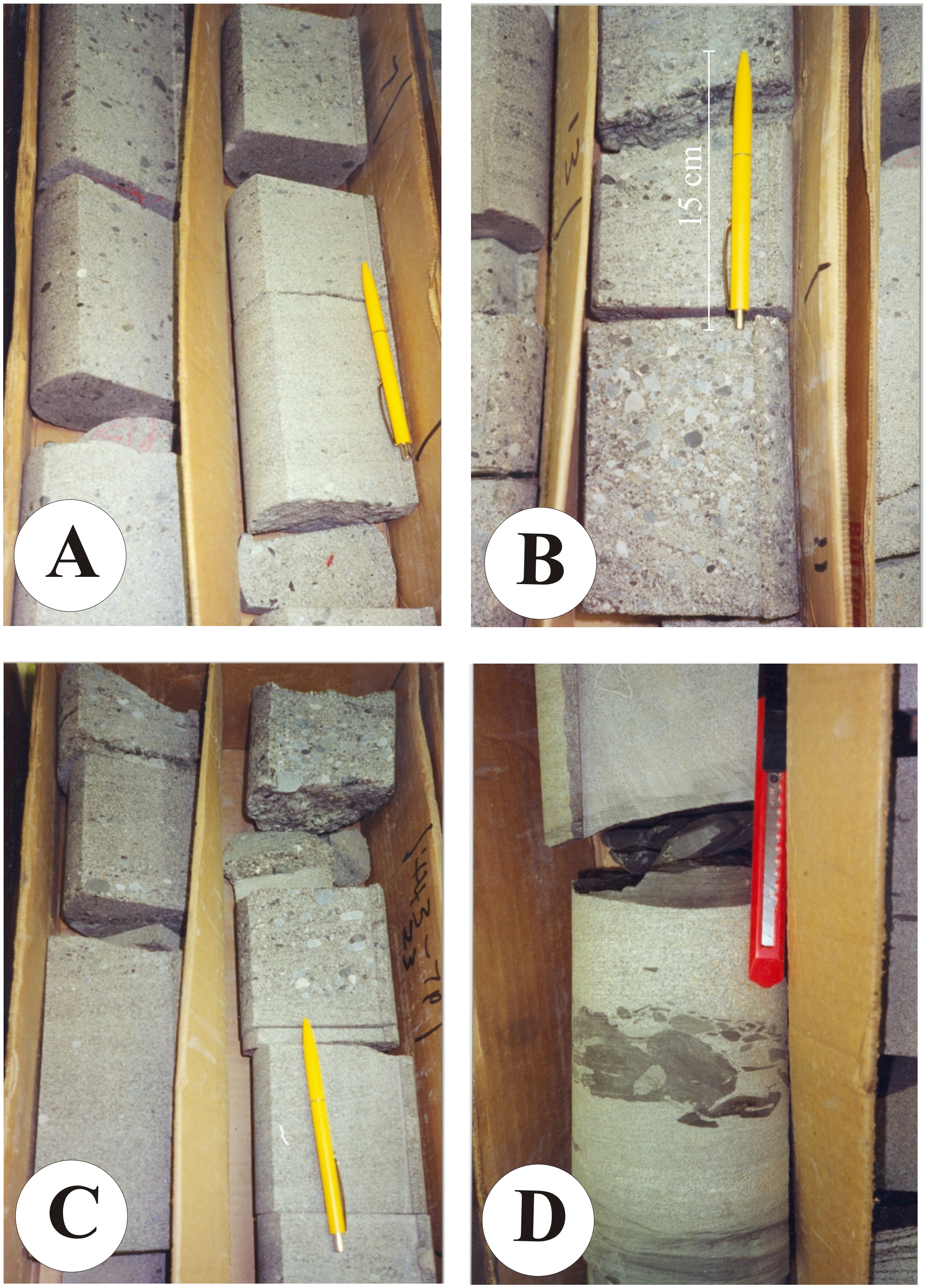

PLATE 16

PLATE 17

Core photographs of 08-25-042-05W5/0
Lea Park - Belly River Fm.

Box photographs showing the prograding shoreface facies of the Lea Park - Belly River transition.
Whole core interval is 1312-1324 m. Only the 1315-1321 m core interval is covered here.

PLATE 17

PLATE 18

Core photographs of 08-25-042-05W5/0
Belly River Fm.

Whole core interval is 1312 - 1324 m

Sharp-based fining upward fluvial sequence within the Belly River Fm. The bedset consists almost entirely of cross-laminated sandstones.
White arrows indicate the base of a fluvial channel cutting the coarsening-upward sequence of the Lea Park Fm. Depth 1313.7 m

PLATE 18

PLATE 19

Ravinement shoreface of 02-33-047-07W5/0
Cardium Fm.

A) Sharp, erosional contact (white arrows), demarcated by conglomeratic lag, between conglomerates and underlying sandstone facies. Whole core interval is 1462.4 - 1502 m.

B) Close-up view of the erosional contact, interpreted as a ravinement surface (RS) (transgressive surface of erosion). Depth: 1487.2 m

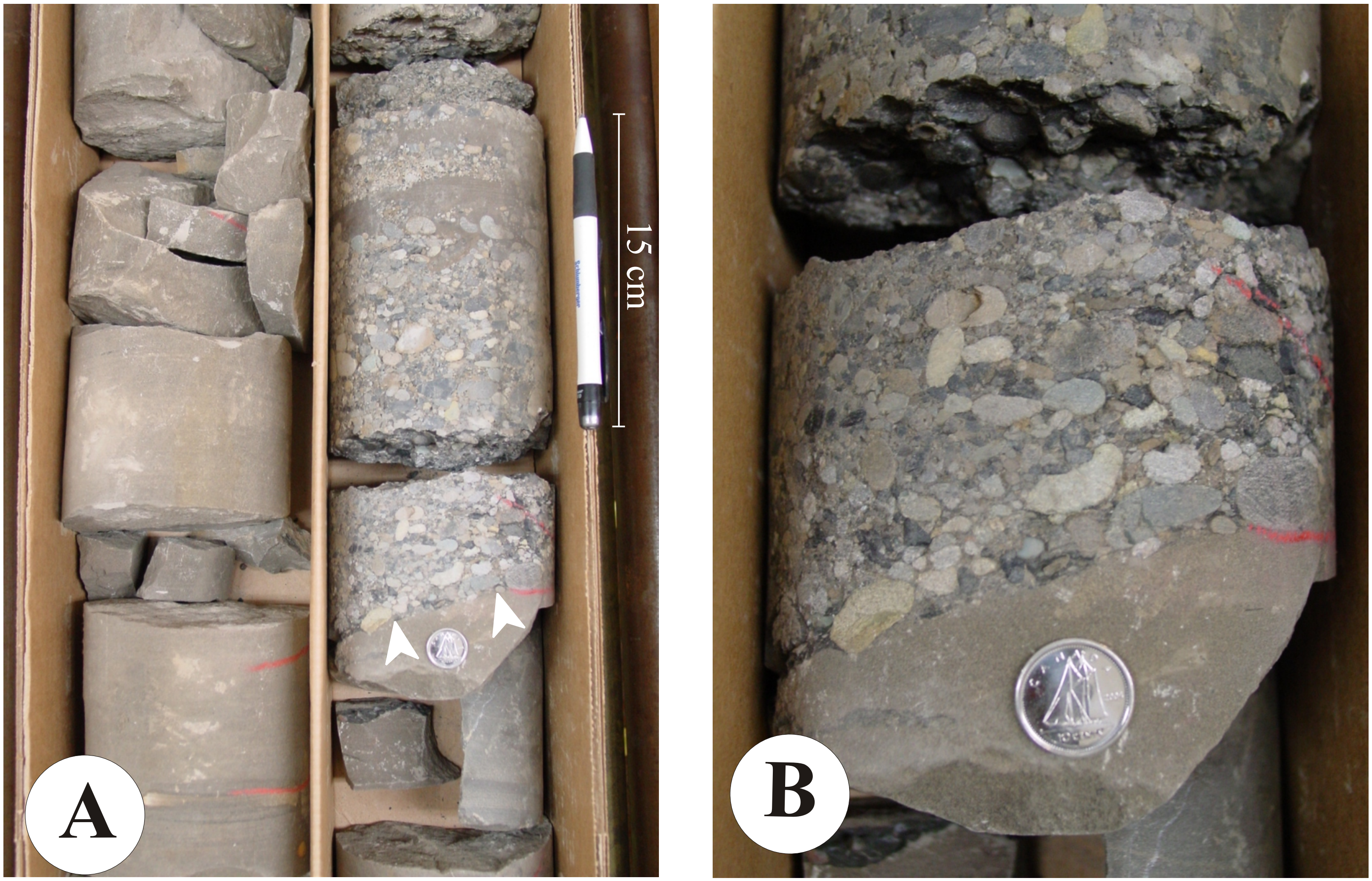

PLATE 19

PLATE 20

Conglomeratic facies of 02-33-047-07W5/0
Cardium Fm.

Conglomeratic shoreface of the Cardium Fm. at Pembina field, Alberta. White arrows point towards the contact between Colorado shales and the underlying conglomeratic shoreface of the Cardium Formation. Depth: 1486.5 m.
The insets A and B are reproduced as close-ups in PLATE 21.
Whole core interval is 1462.4 - 1502 m. Base of core (Base), top of core (Top).

PLATE 20

PLATE 21

Conglomeratic facies of 02-33-047-07W5/0
Cardium Fm.

(A) Close-up view of the conglomeratic shoreface of the Cardium Fm. Depth: 1487 m

(B) Close-up view of the contact between Colorado shales and the underlying conglomeratic shoreface of the Cardium Fm. Depth: 1488 m.

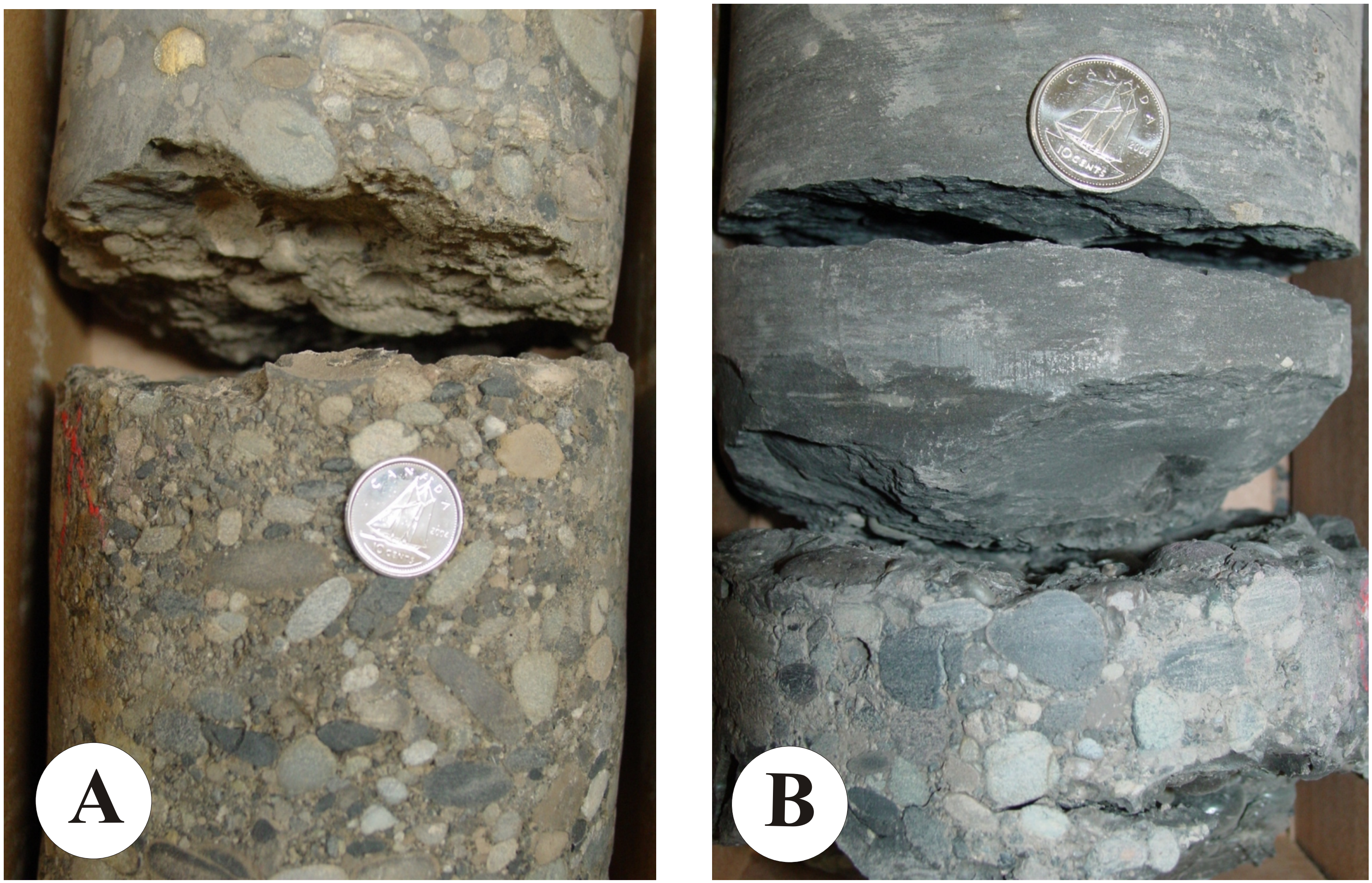

PLATE 21

PLATE 22

Core photographs of 06-12-048-11W5/0
Cardium Fm.

Whole core interval is 1765 - 1780.8 m

Interbedded sandstone, siltstones and shales facies association of the Cardium Fm. (Pembina field) characterized by: bioturbated silty mudstones, sharp contacts between facies, cross-bedded (HCS?), fine-medium grained sandstones.
White arrow points towards the conglomeratic lag which defines an erosional contact with the underlying cross-bedded sandstone facies, and marks the top of the Cardium Sand Zone, as defined in oil and gas industry subsurface (Depth: 1772.15 m).
Setting: upper offshore, lower-upper shoreface.

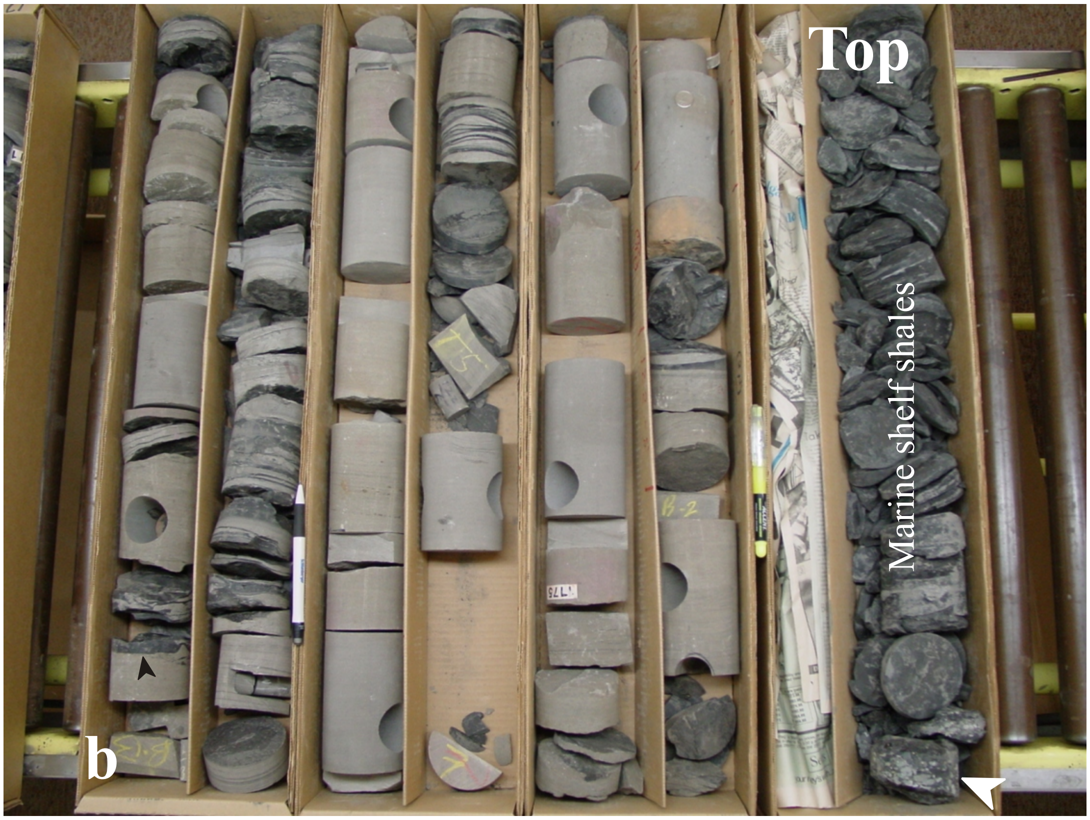

PLATE 22

PLATE 23

Ravinement surface of 06-12-048-11W5/0
Cardium Fm.

Close-up view of the contact between Colorado shales (white arrow) and underlying conglomerates pebbly sandstone. Depth: 1771.9 m.

Whole core interval is 1765 - 1780.8 m

PLATE 23

PLATE 24

Core photographs of 06-14-042-06W5/0
Cardium Fm.

Whole core interval is 1907.4 - 1916.6 m. Base of core (Base), top of core (Top).

Sandier-upward sequence of the Cardium Fm. at Willesden Green field.

White arrows (A, B, and C) point towards close-up views presented in Plate 25.

PLATE 24

PLATE 25

Core photographs of 06-14-042-06W5/0
Cardium Fm.

Close-up views from Plate 24:

A) Pervasively bioturbated muddy sandstones, underlying the facies above, which consists of interbedded sandstones and mudstones; the interbedded nature of later facies association, the sharp-based beds, and the ripple cross-lamination, probably of wave origin - suggest deposition below fair-weather wave base.

B) Hummocky cross-stratified (HCS) sandstone.

C) Interbedded sandstones and mudstones. Note the sharp tops on sandstone beds - which may be interpreted as episodically emplaced sands during storm flows.


Base
15 cm
Schlumberger
HIGHLIGHTER · SURLIGNEUR · RESALTADOR
SANFORD
ACCENT
Top

A B C

PLATE 25

PLATE 26

Core photographs of 06-26-048-11W5/0
Cardium Fm.

Sandier-upward sequences of the Cardium Fm. at Pembina field. Note the cutting out of individual facies and the entire sequence the base of the conglomerate (black arrow). Whole core interval is 1770.9 - 1789.2 m.

Black arrow points towards the so-called E5 erosion surface defined by Plint et al. (1986, 1987), which marks the top of the Raven River allomember (”Cardium Sand”).

The base of the conglomerate (E5) has been interpreted as a transgressive surface of erosion (ravinement surface) and can be better identified on resistivity logs (see Fig. 3 in Bergman and Walker, 1988).

PLATE 26

PLATE 27

Ravinement surface of 06-26-048-11W5/0
Cardium Fm.

Close-up view of the erosion surface (E5) from Plate 26. Depth 1774 m.

PLATE 27

PLATE 28

Core photographs of 06-33-048-11W5/0
Cardium Fm.

Whole core interval is 1760.5 - 1778.8 m.
White arrow points towards the E5/T5 log marker, recognized as the top of a coarsening-upward sequence. Note the lag conglomerate abruptly overlain by laminated mudstones. Depth: 1778 m.
Field: Pembina.

The erosional discontinuity (white arrow), interpreted as a surface of initial transgression, marks a boundary between two different lithologies, influencing the gas composition and signatures along the mudgas profiles.

PLATE 28

PLATE 29

Ravinement surface of 06-33-048-11W5/0
Cardium Fm.

Close-up view of the E5/T5 marker from Plate 28 (Cardium Fm., Pembina field)
Depth 1778 m.

PLATE 29

PLATE 30

Core photographs of 09-32-043-07W5/0
Cardium Fm.

Coarsening-upward sequences of the Cardium Fm. at Willesden Green field. Whole core interval is 1867 - 1885.3 m. Bottom of core (Bottom), top of core (Top). Note the two erosional surfaces demarcated by lag conglomerates, and which can be associated with a distinct gamma-ray and/or resistivity deflection (see Fig. A-16).

The insets A and B are reproduced as close-ups in PLATE 31.

PLATE 30

PLATE 31

Core photographs of 09-32-043-07W5/0
Cardium Fm.

Whole core interval is 1867 - 1885.3 m. Bottom of core (b), top of core (t).

(A) Close-up view of the lower sharp contact (from Plate 30) demarcating one of the erosional discontinuities of the Cardium Fm. Depth: 1875.5 m.

(B) Close-up view of the upper sharp contact (from Plate 30) demarcating one of the erosional discontinuities of the Cardium Fm. Depth: 1874.6 m

Both contacts are recognized by strong deflections on gamma-ray and resistivity logs (see Fig. A-16).

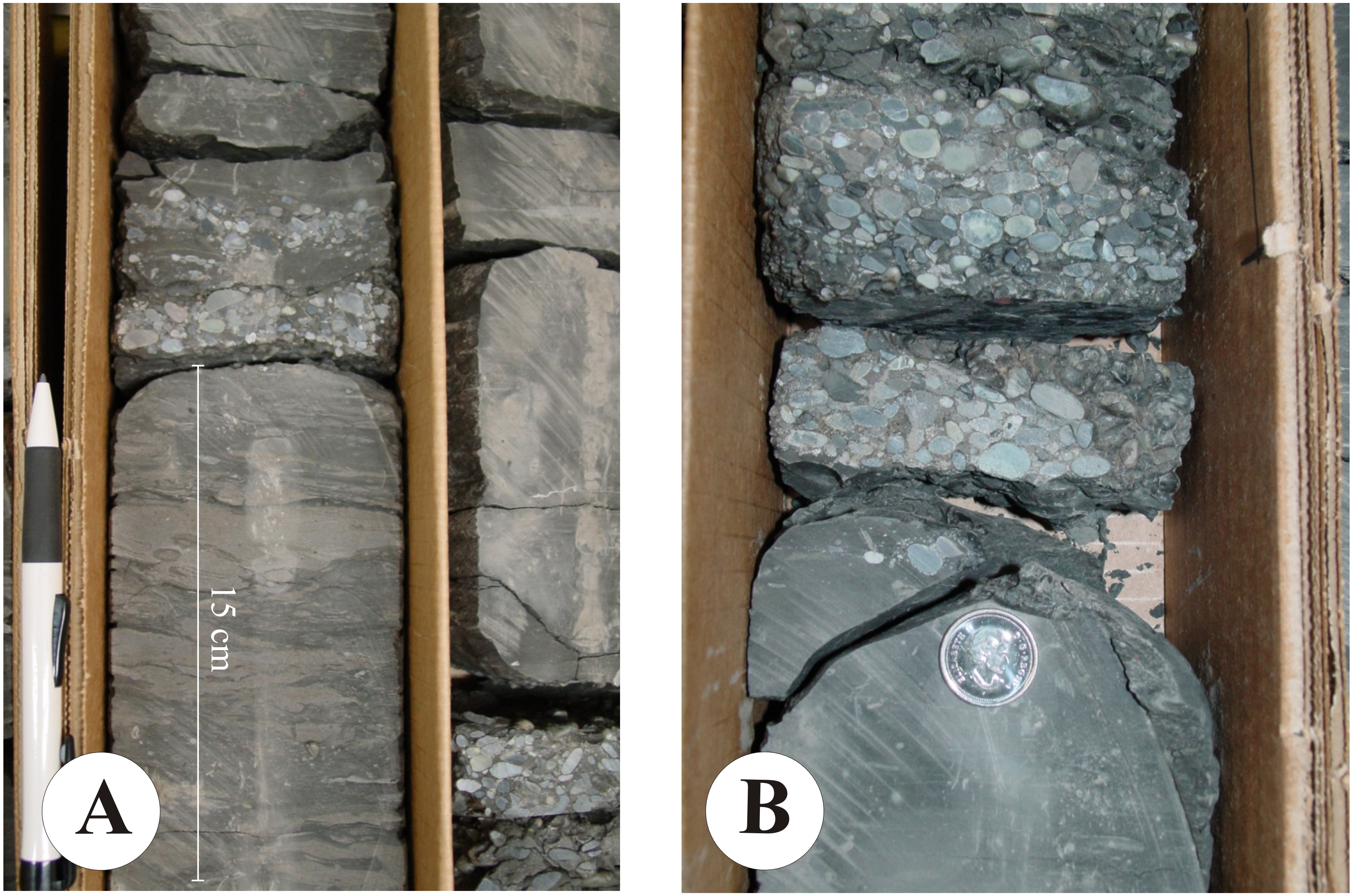

PLATE 31

PLATE 32

Lower shoreface of 09-32-043-07W5/0
Cardium Fm.

Close-up view of the lower shoreface facies of the Cardium Fm. Depth 1878.5 m. Whole core interval is 1867 - 1885.3 m.

PLATE 32

PLATE 33

Core photographs of 10-11-043-09W5/0
Cardium Fm.

Sandier-upward sequences of the Cardium Fm. at Willesden Green field, Alberta. Whole core interval is 2017 - 2035 m. Bottom of core (b), top of core (t).

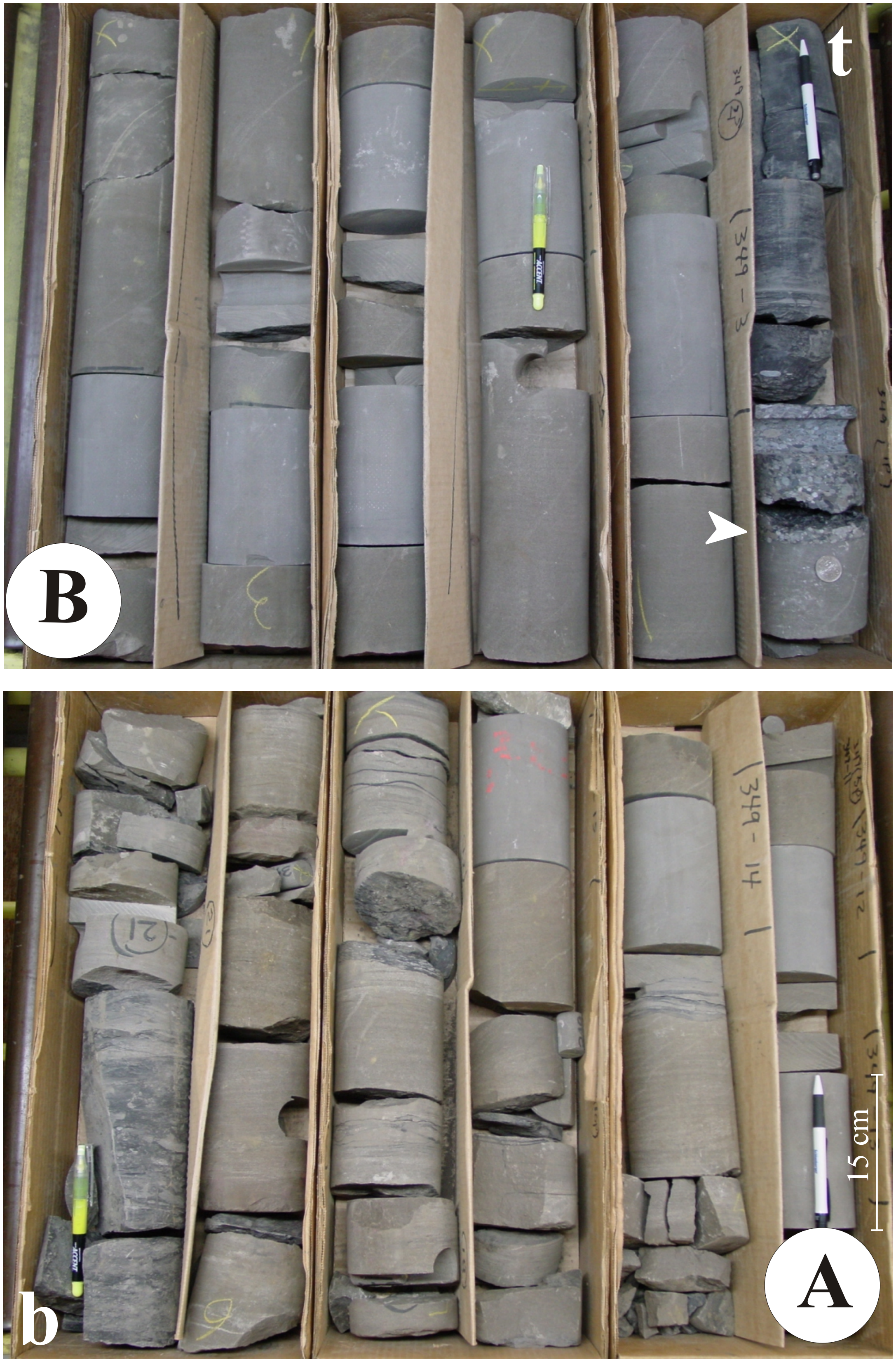

PLATE 33

PLATE 34

Ravinement surface of 10-11-043-09W5/0
Cardium Fm.

Close-up view of one of the most important event markers in the Cardium Fm. at Willesden Green field, the erosional surface E5 of Plint et al. (1986, 1987). Depth: 2018.4 m.

Whole core interval is 2017 - 2035 m.

Note: see Eyles and Walker, 1988, Fig. 3 and Fig. 5 for reference.


Clast-supported conglomerate
Erosional surface (RS)
Non-bioturbated sandstones

PLATE 34

PLATE 35

Core photographs of 10-11-043-09W5/0
Cardium Fm.

Whole core interval is 2017 - 2035 m. Bottom of core (b), top of core (t).

(A) Lower shoreface: bioturbated muddy sandstones .
Depth: 1227 m

(B) Upper shoreface: non-bioturbated sandstones, sharp based and with preserved structures (low-angle stratification, cross-cutting stratification). Depth: 1219.5 m.

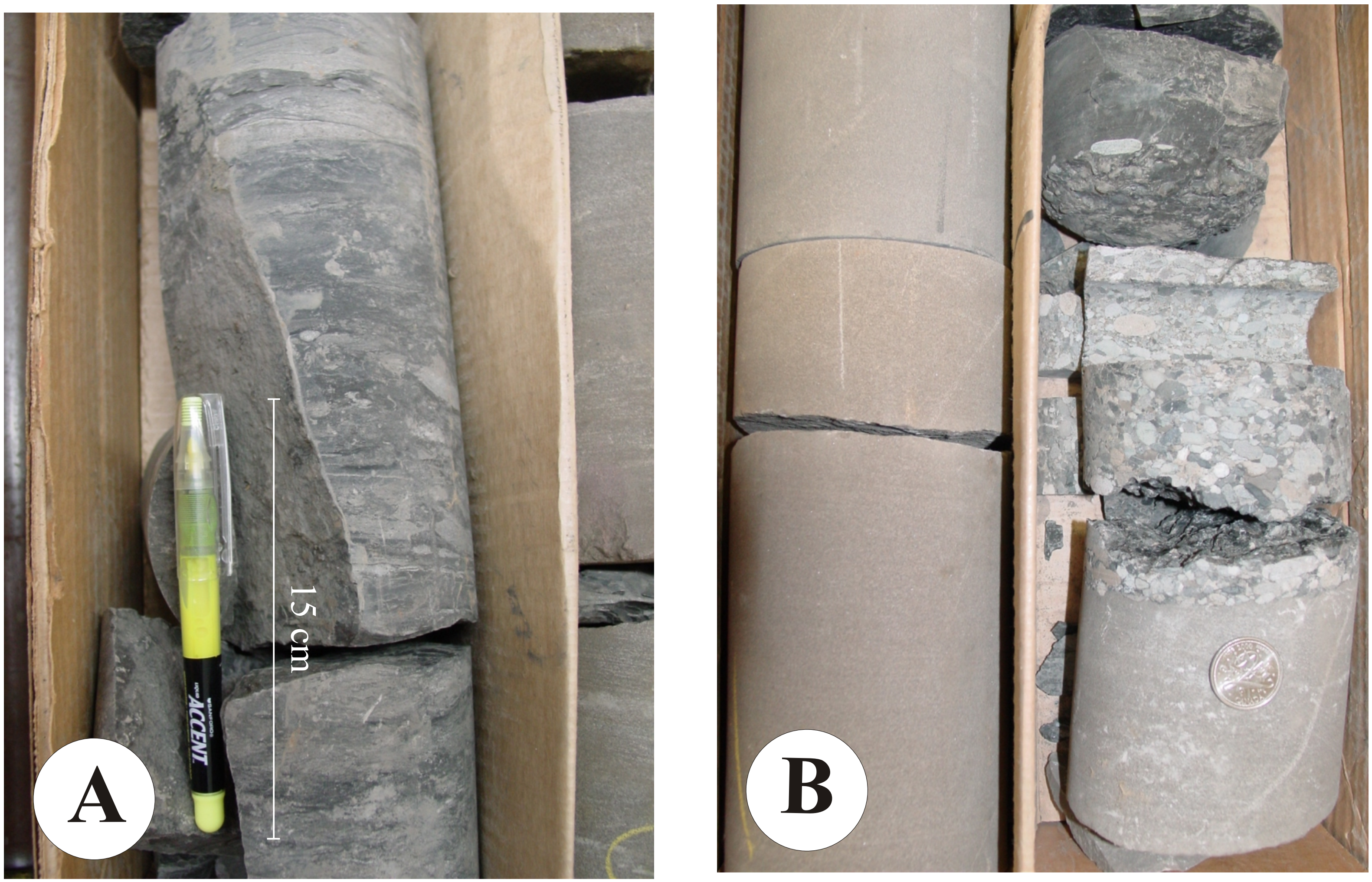

PLATE 35

PLATE 36

Core photographs of 10-14-044-09W5/0
Cardium Fm.

Sandier-upward sequence of the Cardium Fm. at Willesden Green field, Alberta. Whole core interval is 1898.9 - 1917.8 m. Bottom of core (b), top of core (t). White arrow points towards an erosional surface (transgressive surface of erosion) defined by a thin grit horizon occurring at the top of the sandier-upward sequence. Depth: 1903.5 m

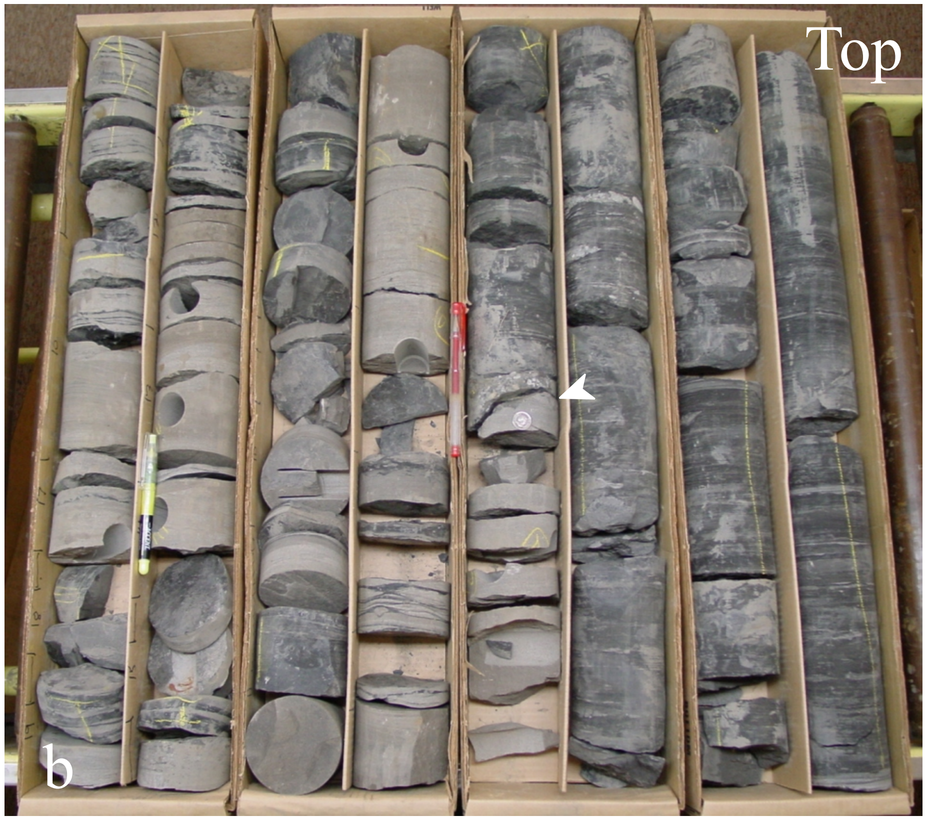

PLATE 36

PLATE 37

Ravinement surface of 10-14-044-09W5/0
Cardium Fm.

Close-up view of the erosional surface from previous Plate. Depth 1903.5 m
Whole core interval is 2017 - 2035 m.

Note: The erosional surface (RS) is associated with a distinct gamma-ray and resistivity deflection (see Fig. A-18).

PLATE 37

PLATE 38

Core photographs of 10-16-042-09W5/0
Cardium Fm.

Sandier-upward sequences of the Cardium Fm. at Ferrier field, Alberta.
Whole core interval is 2077 - 2093 m.
Note the knife-sharp base of the conglomerate facies (white arrows, depth: 2081.4 m) associated with gamma-ray, sonic, and resistivity deflections (see Fig. A-19).
The sandstone-conglomerate contact has been interpreted as a transgressive surface of erosion (RS), the surface being coated with a transgressive lag of pebbles derived from the upper shoreface.

The insets A,B, and C are reproduced as close-ups in PLATE 40.

PLATE 38

PLATE 39

Ravinement surface of 10-16-042-09W5/0
Cardium Fm.

Whole core interval is 2077 - 2093 m. Base of core (b), top of core (t).

Close-up of the erosional surface (black arrows) defined by the presence of the conglomerate cutting the non-burowed sandstones. This erosional surface defines one of the most prominent subsurface marker of the Cardium Formation: the E5 surface of Plint et al. (1986, 1987).
Note: for reference and analogies see Bergman and Walker, 1988.

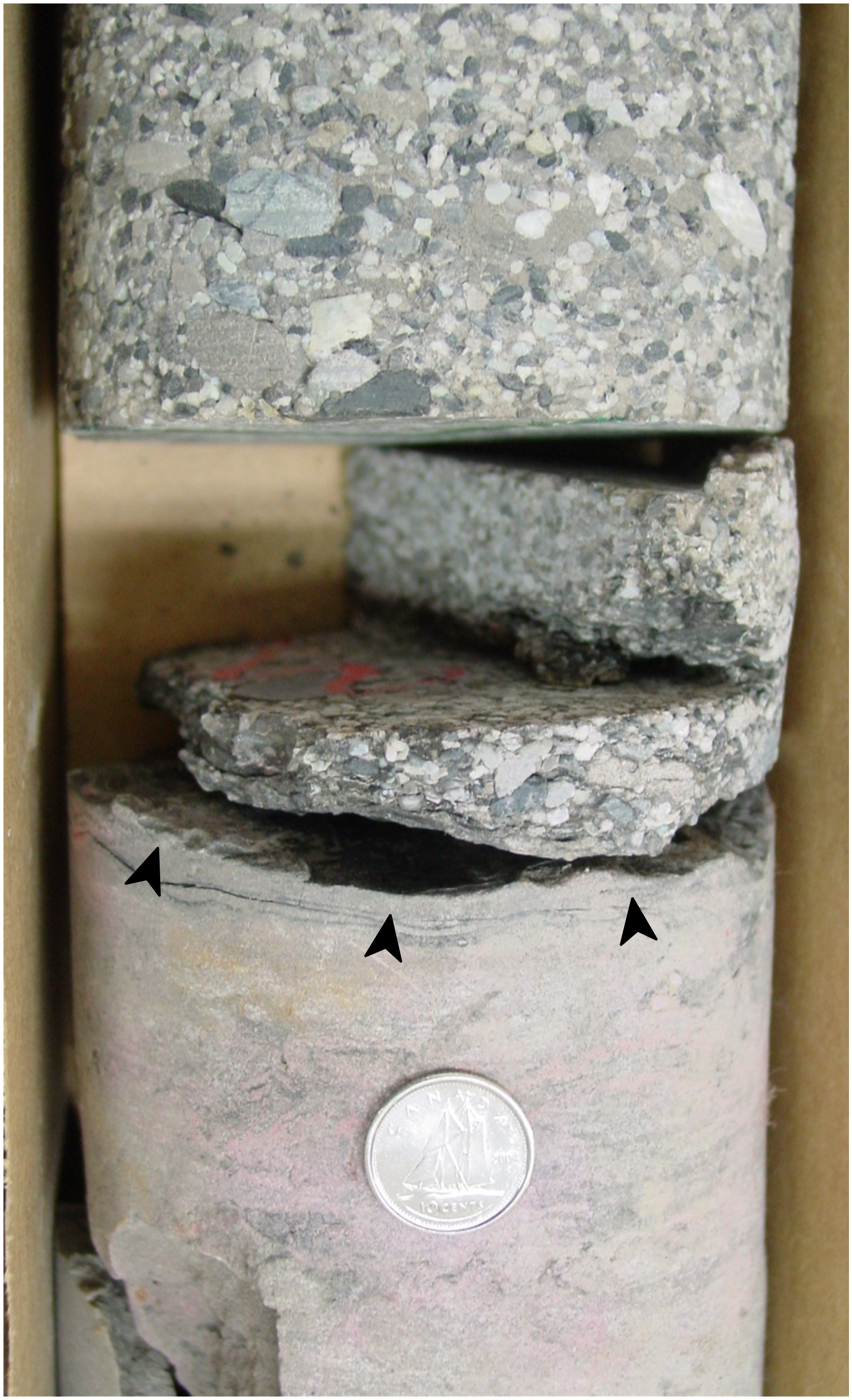

PLATE 39

PLATE 40

Core photographs of 10-16-042-09W5/0
Cardium Fm.

Plate’s 38 details (stratigraphic order):

A) Hummocky cross-stratified sandstones interbedded with muddy sandstones of the lower shoreface succesion.

B) Close-up of the conglomerate facies.

C) The conglomerate facies and its sharp top of transgressive marine mudstones.

Whole core interval is 2077 - 2093 m

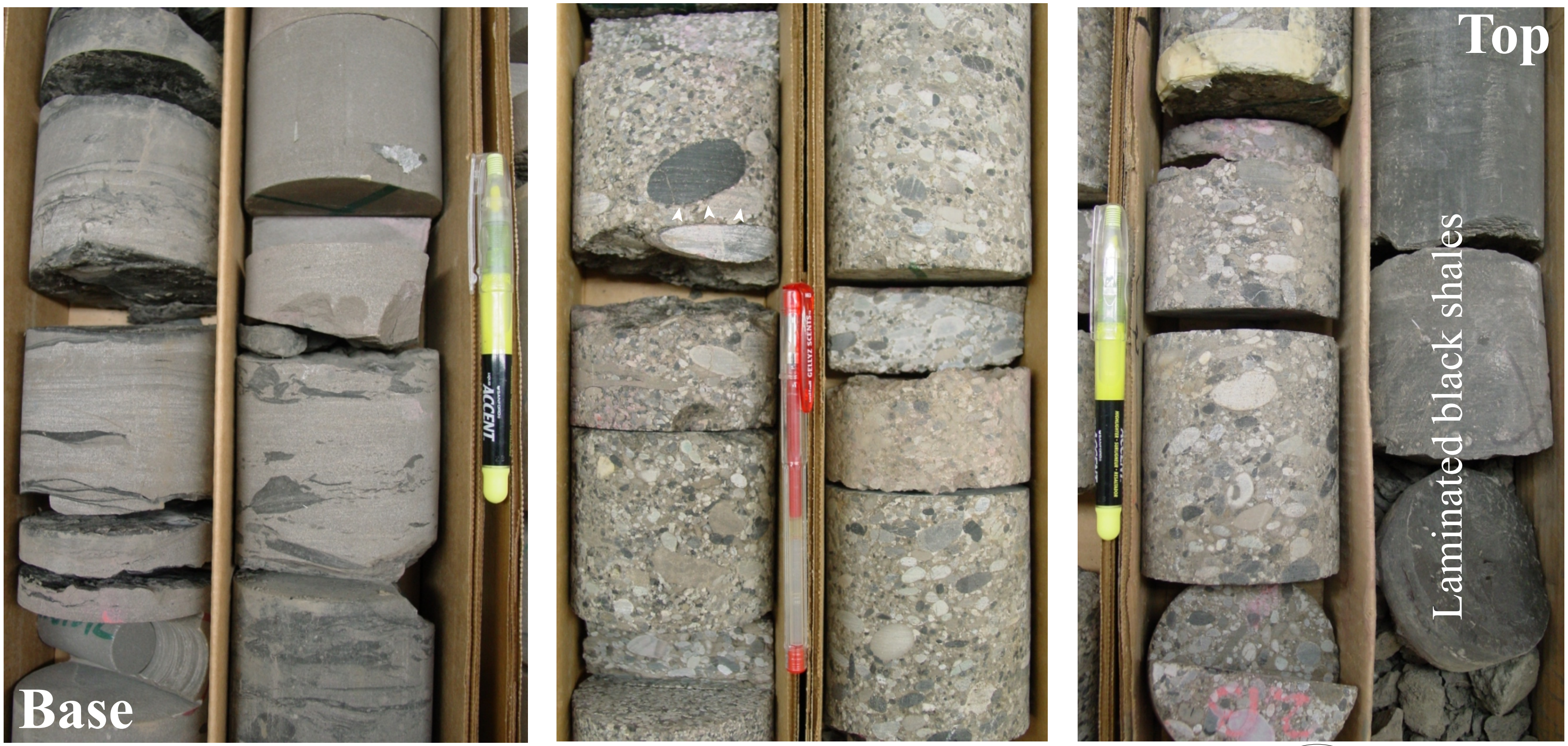

A B C

PLATE 40

PLATE 41

Core box photograph of 10-23-043-09W5/0
Cardium Fm.

Whole core interval is 1980.3 - 2018.1 m. Base of core (b), top of core (t).

Sharp contact with conglomeratic lag (black arrow) between shale facies association above and the underlying interbedded shale and sandstone facies association of the Cardium shoreface. The conglomeratic lag defines the top of the Cardium Sand, which is erosive, and interpreted as being a ravinement surface (RS).


Slightly bioturbated sandstones and mudstones
Laminated dark mudstones
15 cm

PLATE 41

PLATE 42

Core box photograph of 10-23-043-09W5/0
Cardium Fm. - erosional surface

Whole core interval is 1980.3 - 2018.1 m.

Close-up view of the chert pebble conglomerate forming a transgressive surface of erosion over a hummocky cross-bedded sandstone, which defines the top of the Cardium Sand (black arrow) in PLATE 41.
The fine-grained sandstone overlain by the poorly sorted conglomerate may represent the beach environment.
The erosion surface is associated with a resistivity deflection (see Fig. A-20).
Depth: 1993.8 m

PLATE 42

PLATE 43

Core box photograph of 10-26-045-09W5/0
Cardium Fm.

Whole core interval is 1743.8 - 1762 m. Base of core (b), top of core (t).

Sandier-upward sequence of the Cardium Fm. at Willesden Green field, Alberta. Black arrows point to erosional surface E5 (Plint, 1988). Evidence of erosion for this discontinuity is supplied by the conglomeratic lag that immediately overlie this surface.
The top of the Cardium Sand shoreface in the study area is capped by a regionally extensive flooding surface and the marine shale deposits of the Colorado Group.

PLATE 43

PLATE 44

Core box photograph of 10-26-045-09W5/0
Top Cardium Sand

Contact between laminated dark mudstones and underlying deposits of the lag conglomerate, which defines the transgressive surface of erosion of the Cardium Sand (see PLATE 43).
Whole core interval is 1743.8 - 1762 m. Base of core (b), top of core (t).
Depth 1747.8 m.

PLATE 44

PLATE 45

Core box photographs of 11-30-045-09W5/0
Cardium Fm.

Whole core interval is 1822 - 1840 m. Base of core (b), top of core (t).

Sandier-upward sequence of the Cardium Fm.
White arrow points to the sharp contact (ravinement surface - RS), demarcated by the conglomeratic lag between conglomerates pebbly sandstones and shale facies association and the underlying sharp-based sandstones with low angle, cross-cutting stratification.

PLATE 45

PLATE 46

Core box photograph of 11-30-045-09W5/0
Cardium Fm.

Whole core interval is 1822 - 1840 m. Base of core (b), top of core (t).

Close-up of the conglomerate pebbly sandstone and shale facies association, which drapes the surface correlated with erosion surface E5 of Plint et al. (1986, 1987)
A) Depth: 1826.5 m
B) Depth: 1825.7 m (above the red pen in Plate 45).

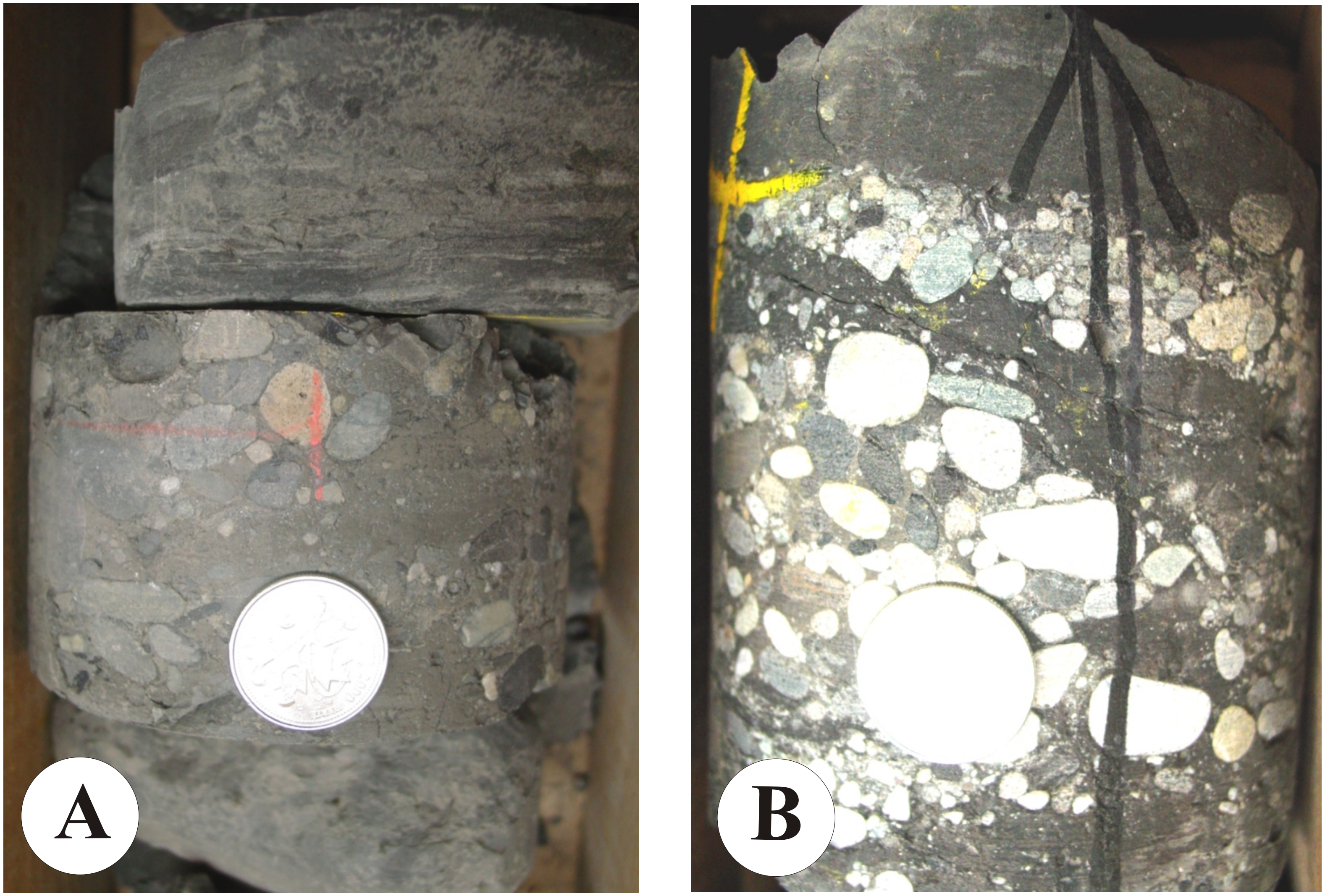

PLATE 46

PLATE 47

Core photograph of 11-30-045-09W5/0
Cardium Fm. - Lower shoreface facies

Pebbly, black, burrowed interbedded shale and fine- to medium-grained sandstone. Bioturbation has obliterated most sandstone beds, leaving only ponds and lenses of sandstones that are discontinuous on the scale of the core.
Depth 1836.2 m

PLATE 47

PLATE 48

Core photographs of 12-03-042-09W5/0
Cardium Fm.

Sandier-upward sequences of the Cardium Fm. at Ferrier field, Alberta.
White arrow points towards an erosion surface demarcated by a conglomeratic lag, which corresponds with a gamma-ray and resistivity deflection on wireline logs (see Fig. A-23, Depth: 2122.8 m).
Whole core interval is 2116 - 2136 m.

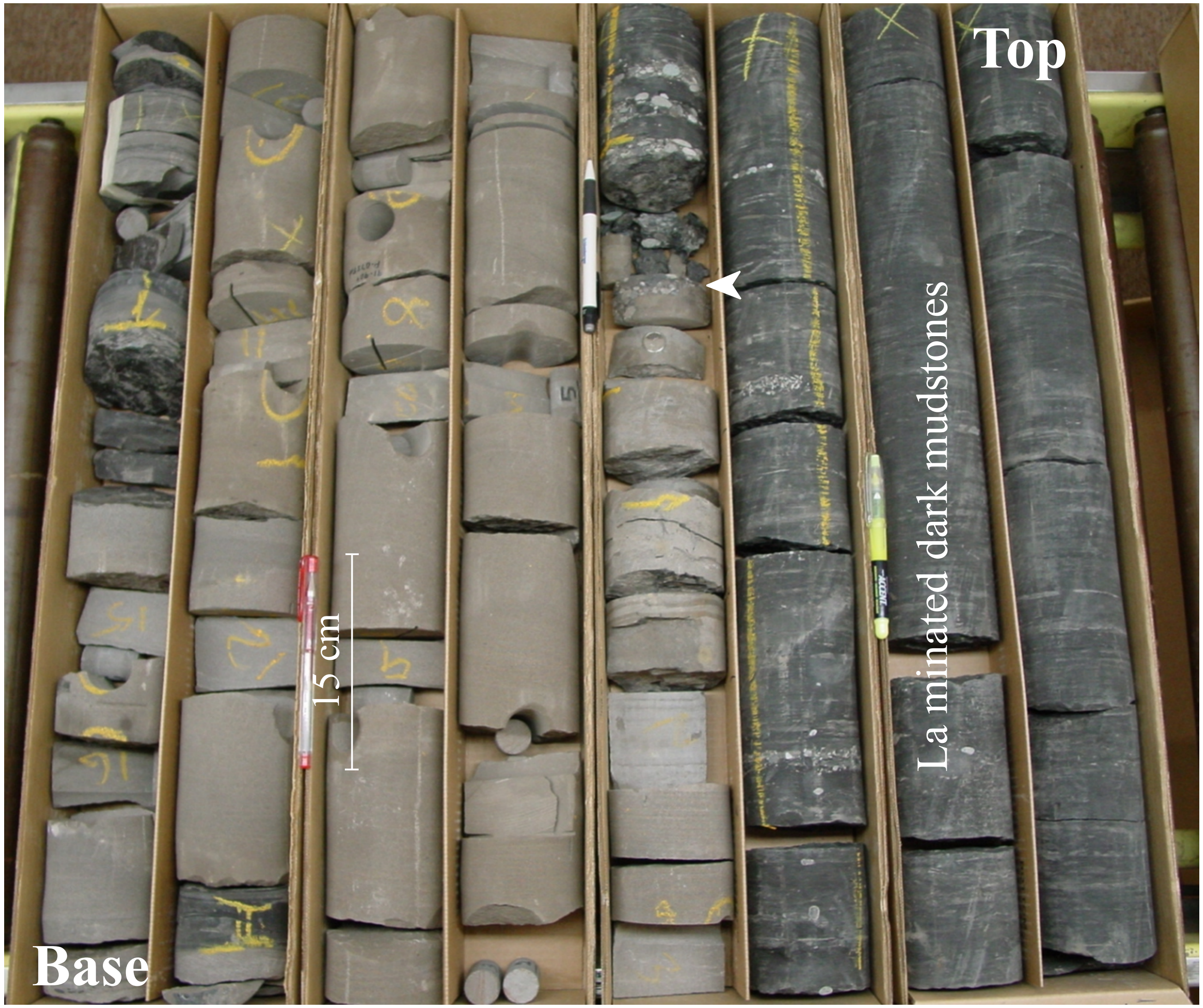

PLATE 48

PLATE 49

Ravinement surface of 12-03-042-09W5/0
Cardium Fm.

Whole core interval is 2116 - 2136 m.
Close-up view of the *Glossifungites*-demarcated erosional discontinuity, which is interpreted as a ravinement surface, and corresponds to the E5 surface of Plint et al. (1986, 1987). Depth: 2122.8 m
Note: in both A and B photos, the white arrow points towards the same feature.

PLATE 49

PLATE 50

Core photographs of 14-01-042-07W5/0
Cardium Fm.

Whole core interval is 1992.78 - 2008.93 m. Base of core (b), top of core (t).

A) Core sequence in the Cardium Fm. at Willesden Green field, Alberta, representing progressively shallower water sediments deposited on deeper water material as a result of shoreline progradation.

B) Poorly sorted conglomerate representing a transgressive surface of erosion near the top of the Cardium Sand zone. The conglomerate overlies fine-grained sandstones of the middle-, to upper shoreface

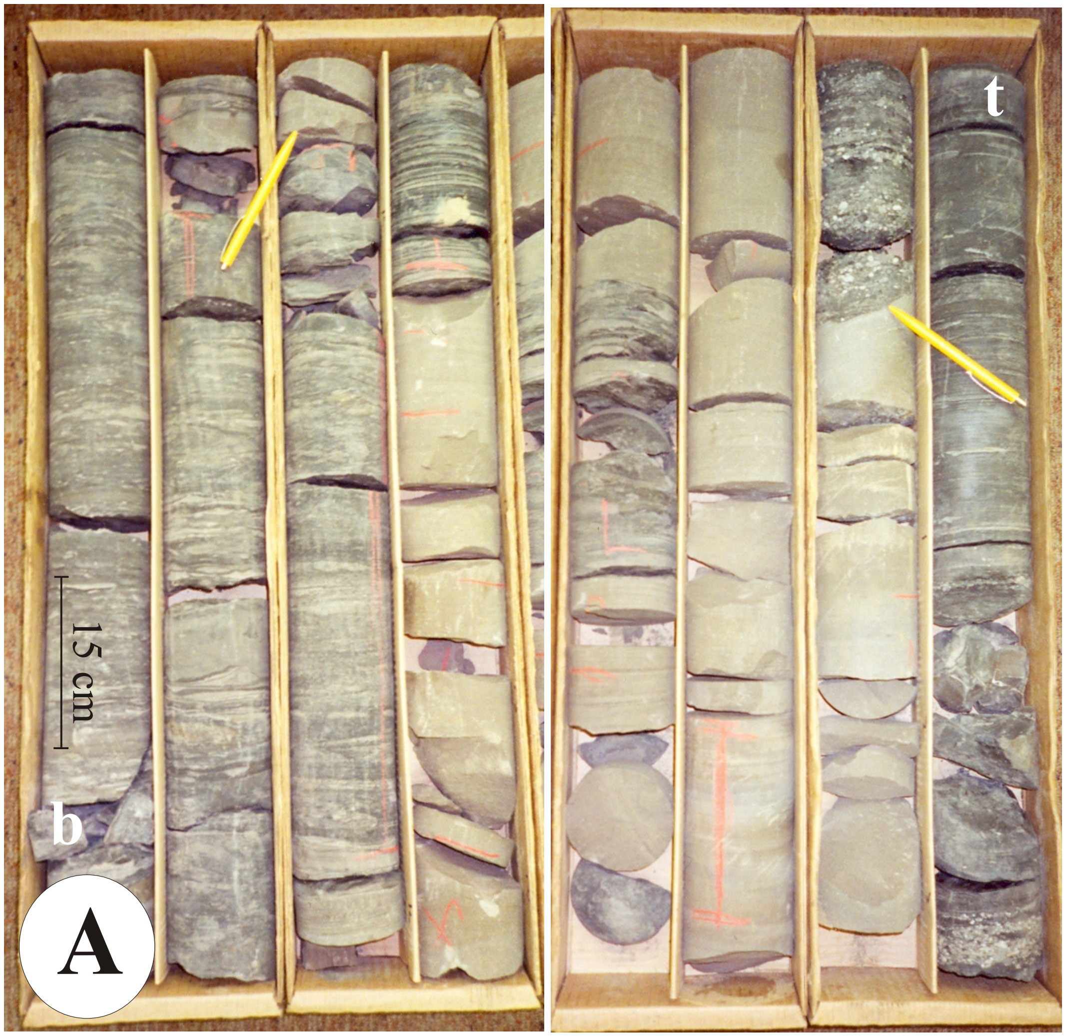

PLATE 50

PLATE 51

Core photographs of 14-06-047-09W5/0
Cardium Fm.

Whole core interval is 1787.7 - 1802.6 m

The offshore-transition zone and the lower shoreface facies association of the Cardium Fm. at Pembina field, Alberta. The interbedded sandstone (with flat parallel lamination, wavy parallel lamination, and massive) siltstone and shale facies association is light to moderate bioturbated (*Planolites*, *Asterosoma*, *Chondrites*).

PLATE 51

PLATE 52

Erosional surface of 14-06-047-09W5/0
Cardium Fm.

Whole core interval is 1787.7 - 1802.6 m

Close-up view of the erosional contact (white arrow) demarcated by the conglomeratic lag, which truncates silty and sandy shales containing a *Glossifungites* assemblage. Depth: 1795.2 m.

PLATE 52

PLATE 53

Core photographs of 14-06-047-09W5/0
Cardium Fm.

Whole core interval is 1787.7 - 1802.6 m

Close-up view of two of the Cardium Fm. facies associations:
(A) interbedded shale and sandstones facies association. Depth: 1797.4 m.
(B) flat parallel laminated sandstones. Depth: 1796.8 m.

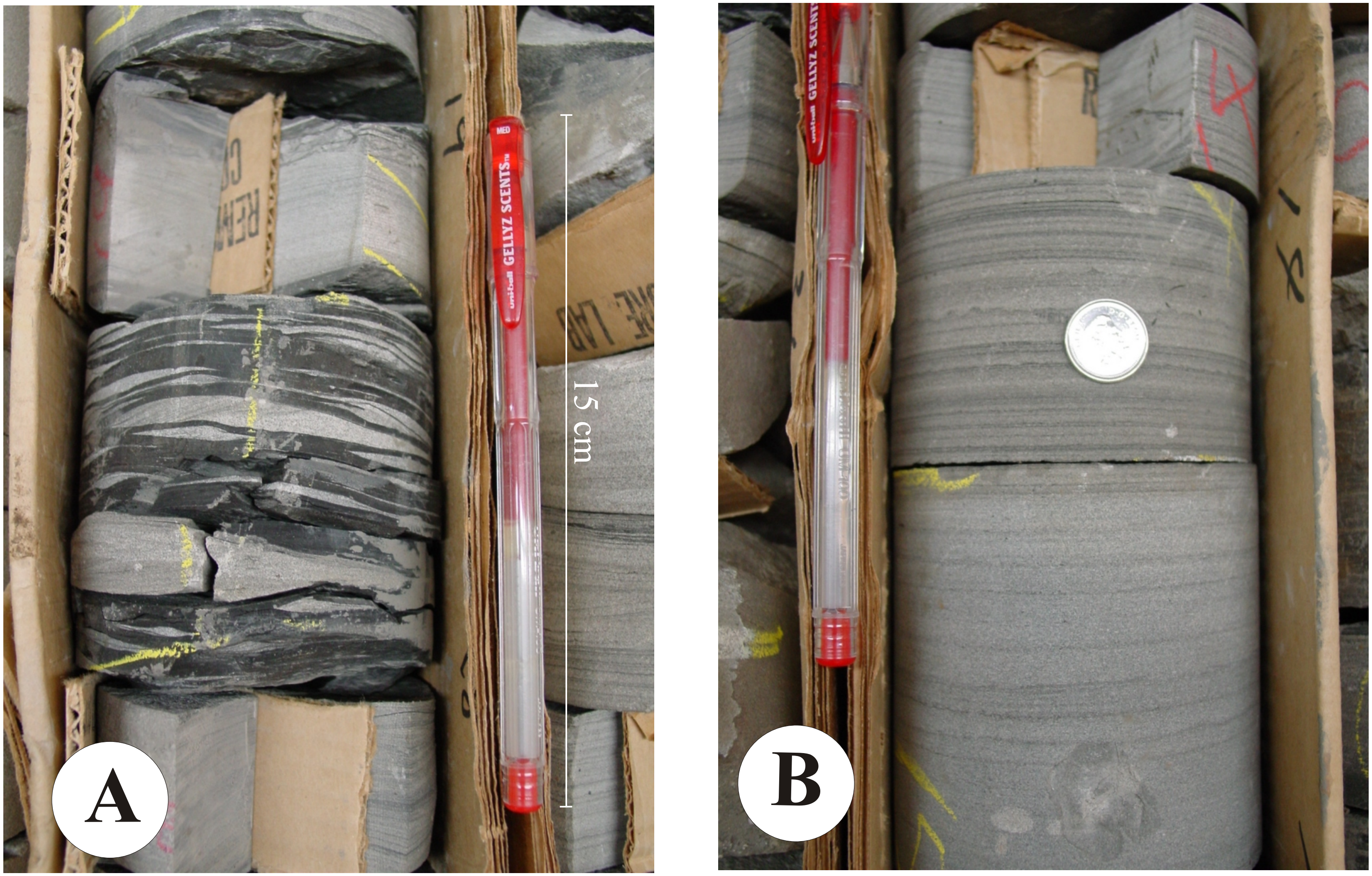

PLATE 53

PLATE 54

Core photographs of 16-16-047-10W5/0
Cardium Fm.

Whole core interval is 1901 - 1919 m. Bottom of core (b), top of core (t). Sandier-upwards sequence of the Cardium Fm. at Pembina field, Alberta. Note the upward facies change from bioturbated muddy siltstones, through bioturbated muddy sandstones, and non-bioturbated sandstones. White arrow points towards the cutting of an individual facies, and suggests the presence of a transgressive surface of erosion (RS).

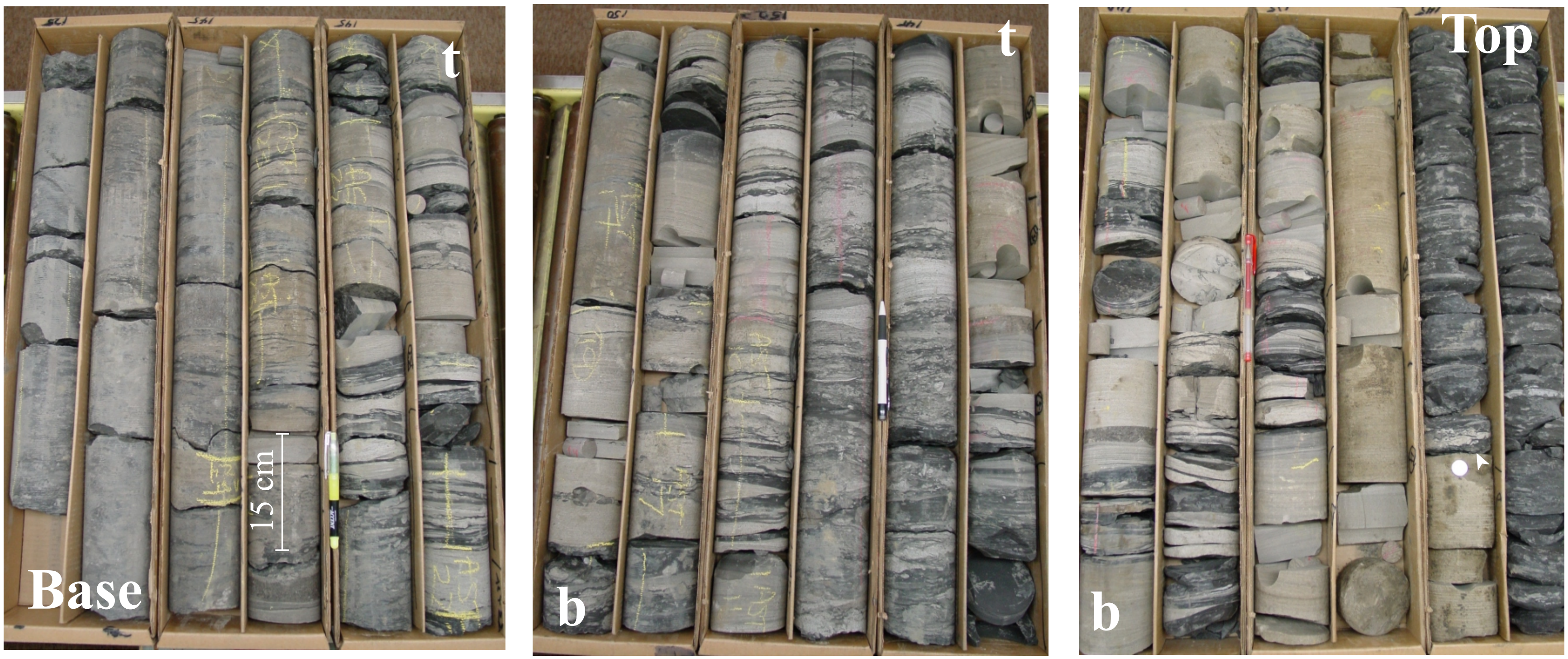

PLATE 54

PLATE 55

Core photographs of 16-16-047-10W5/0
Cardium Fm.

Whole core interval is 1901 - 1919.75 m.
Close-up view of the erosional discontinuity, which marks the top of the Cardium Sand.
Note the sharp contact between fine-grained hummocky cross-stratified sandstones and the overlying pebbly, interbedded shale and sandstone facies association.
Interpretation: distal equivalent of ravinement processes.
Depth: 1906 m.

PLATE 55

PLATE 56

Core photographs of 16-16-047-10W5/0
Cardium Fm.

Whole core interval is 1901 - 1919.75 m.
Close-up view of some of the facies associations of the Cardium Formation:
A) Moderately burrowed interval with thin hummocky cross-stratified (HCS) beds (tempestites?).
B) Interbedded silty sandstones, bioturbated muddy sandstone and black mudstone, displaying a high burrowing intensity.
C) *Lockeia* ? (L), current ripples, and wavy parallel laminated sandstone beds in an example of interbedded silty sandstone, bioturbated muddy sandstone, and black mudstone facies association, displaying a low burrowing intensity.

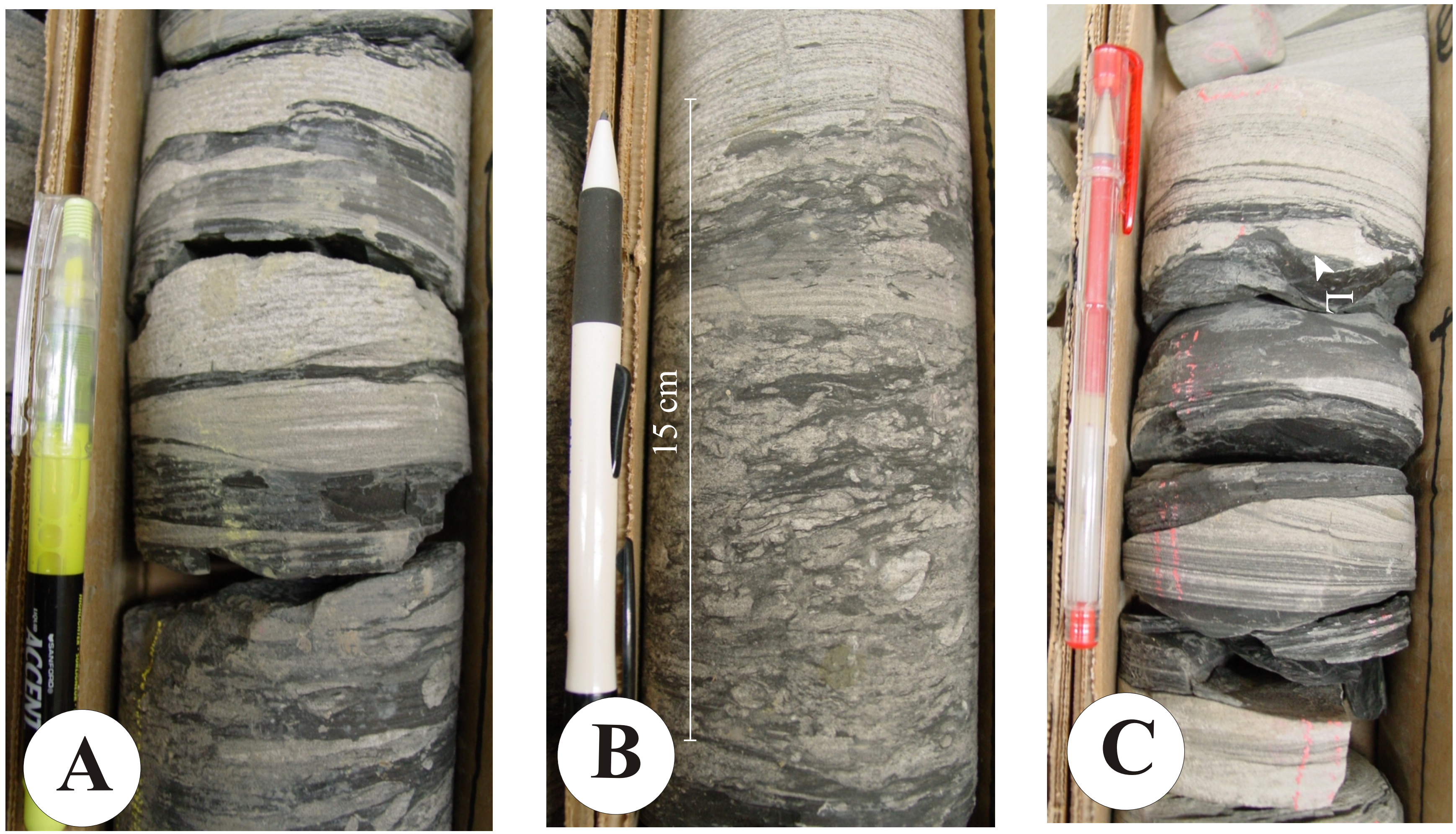

PLATE 56

PLATE 57

Colorado shales of 06-22-42-9W5
Core #2
2074.5 - 2089.7m

Various views of the marine shale mudstones of the Colorado Group at Ferrier field, Alberta
Depth: ~ 2086 m.

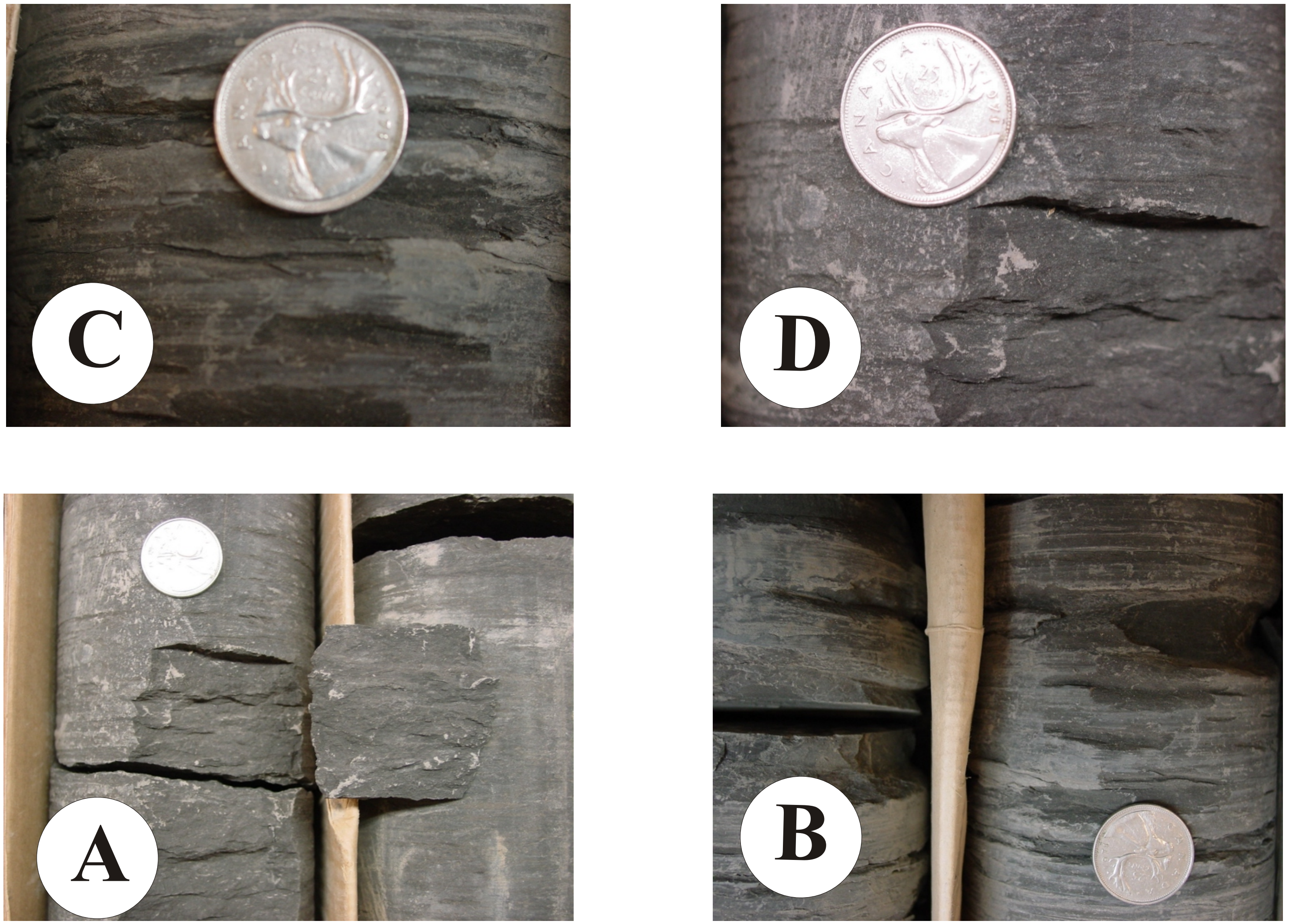

PLATE 57

PLATE 58

Core photographs of 04-10-042-09W5/2
Cardium Fm.

The uppermost three meters (2097 - 2100 m interval) of a sandier-upward sequence of the Cardium Fm. at Ferrier field, Alberta, capped by the marine shales of the Colorado Group.
Whole core interval is 2097 - 2110.7 m. Base of core (Base), top of core (Top).

PLATE 58

PLATE 59

Core photographs of 04-10-042-09W5/2
Cardium Fm.

A) Close-up view of the sharp contact defined by the presence of the conglomerate (Cgl.) cutting the non-bioturbated sandstones (Ss.); this contact, associated with wireline log deflections at ~ 2099.6 m depth (see Fig. A-28), is interpreted as an erosional surface produced in a transgressive shoreface environment.

B) Close-up view of the contact (white arrow) between marine shale deposits of the Colorado Gp. and underlying lag conglomerate; depth: 2098.3 m.

Whole core interval is 2097 - 2110.7 m. Base of core (b), top of core (t).

PLATE 59

PLATE 60

Core photographs of 04-10-042-09W5/2
Cardium Fm.

Core photographs (2103.5 - 2110.7 m core interval) showing, from lower left to upper right, sandier - upward cycles in the Cardium Fm. at Ferrier field, Alberta, showing a progressive vertical change from burrowed interbedded shale and fine - medium grained sandstones (1), through non-bioturbated sandstones and mudstones (2) to hummocky cross-stratified and low-angle laminated, non-bioturbated sandstones (3). Whole core interval is 2097 - 2110.7 m. Base of core (Base), top of core (Top).

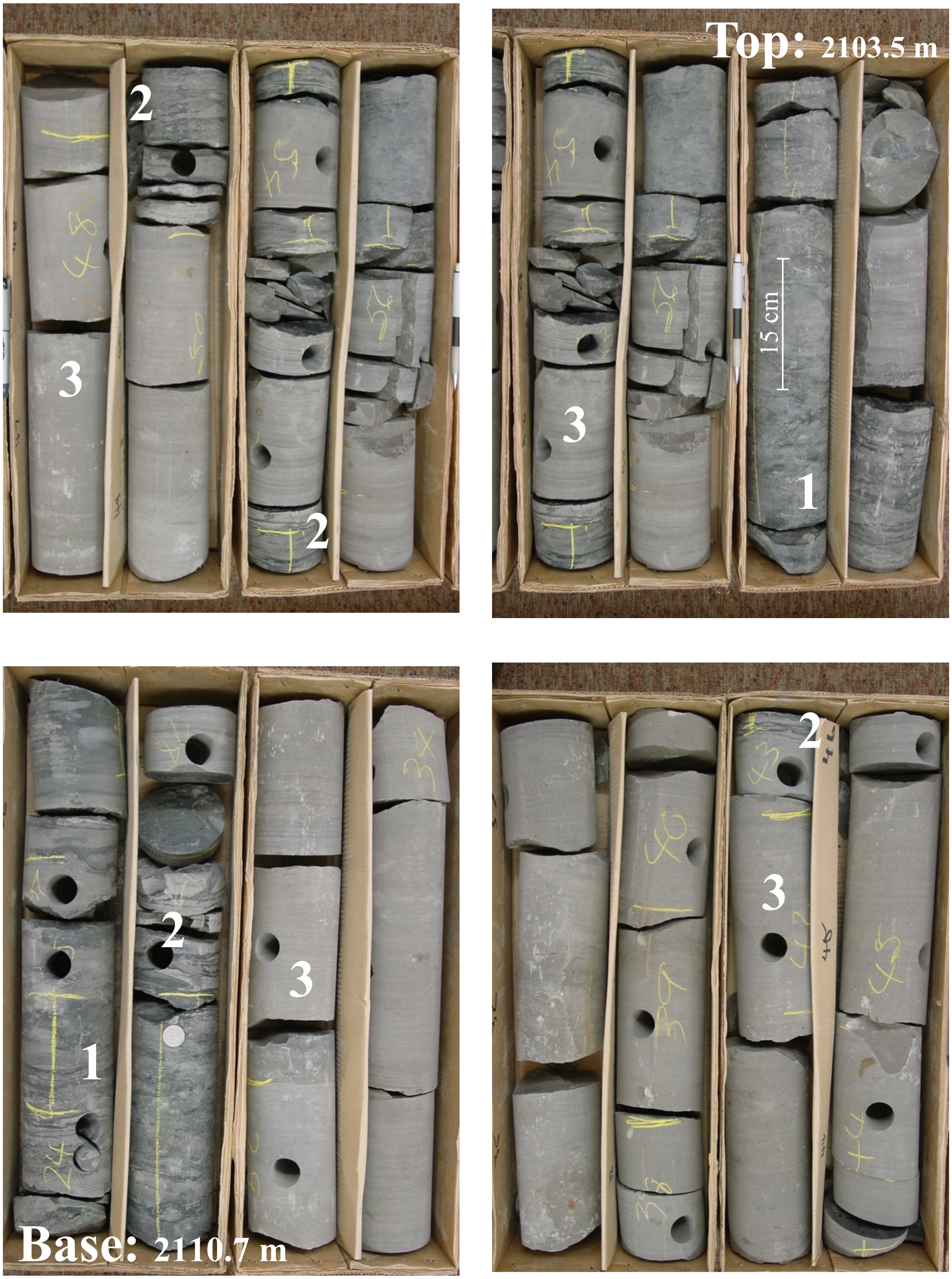

PLATE 60

PLATE 61

Core photographs of 04-10-042-09W5/2
Cardium Fm.

A) and B) Close-up view of the pale gray, throughly bioturbated muddy sandstone and sandstone facies association. The assemblage of trace fossils belongs to the *Cruziana* ichnofacies. Depths: 2103 m, and 2103.6 m.

C) and D) Close-up view of the non-bioturbated sandstone facies association, with preserved structures (flat parallel lamination). Depths: 2107.2 m and 2108 m.

Whole core interval is 2097 - 2110.7 m. Base of core (b), top of core (t).

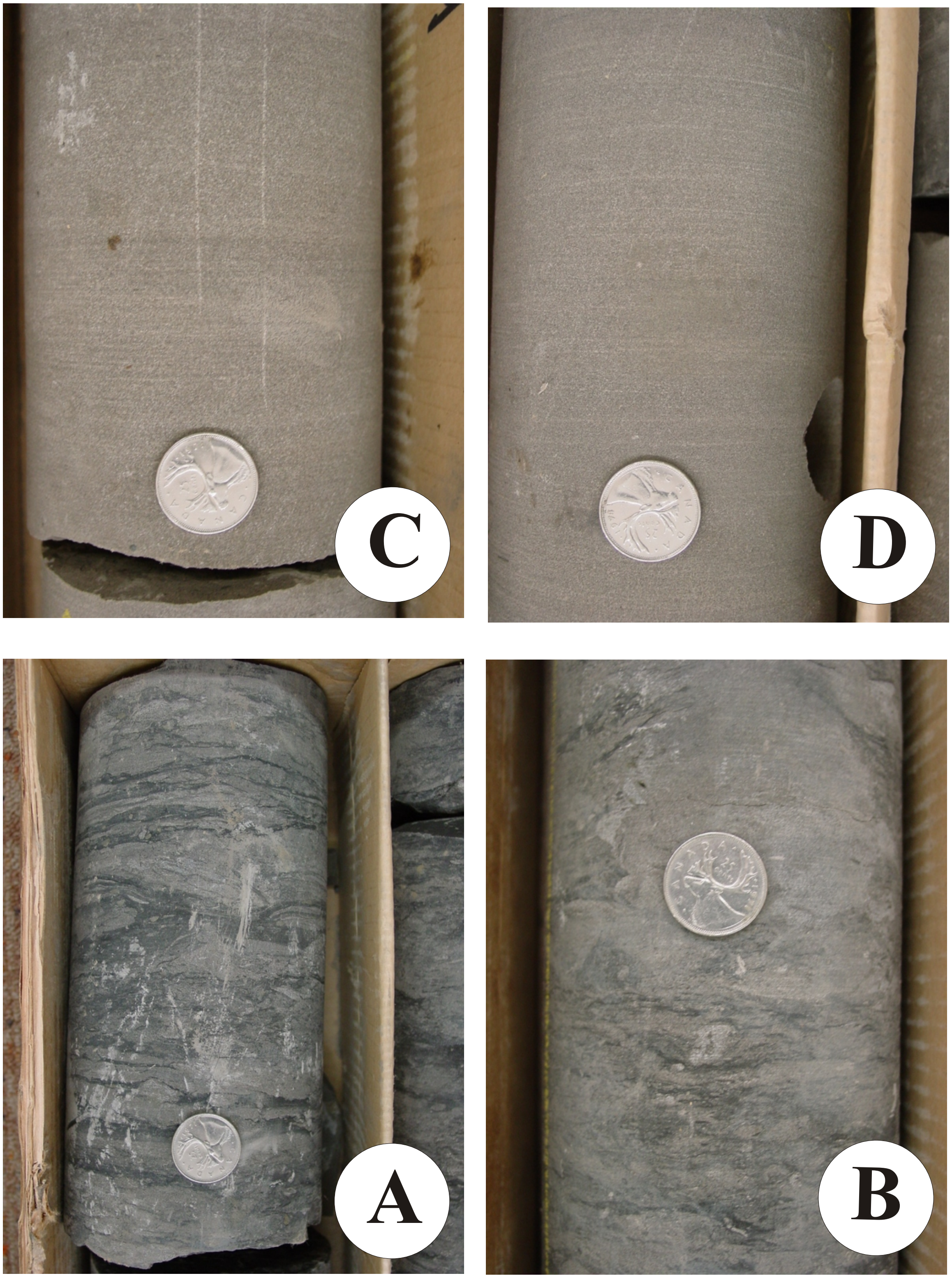

PLATE 61

PLATE 62

Core photographs of 04-10-042-09W5/2
Cardium Fm.

A) and B) Close-up view of the non-bioturbated sandstone facies association, with preserved structures (flat parallel lamination). Depths: 2108.7 m and 2108.9 m.

C) and D) Close-up views of the pale gray, throughly bioturbated muddy sandstone and sandstone facies association. The assemblage of trace fossils belongs to the *Cruziana* ichnofacies (*Teichechnus* and *Thalassinoides*). Depths: 2109.5 m, and 2110 m.

Whole core interval is 2097 - 2110.7 m. Base of core (b), top of core (t).

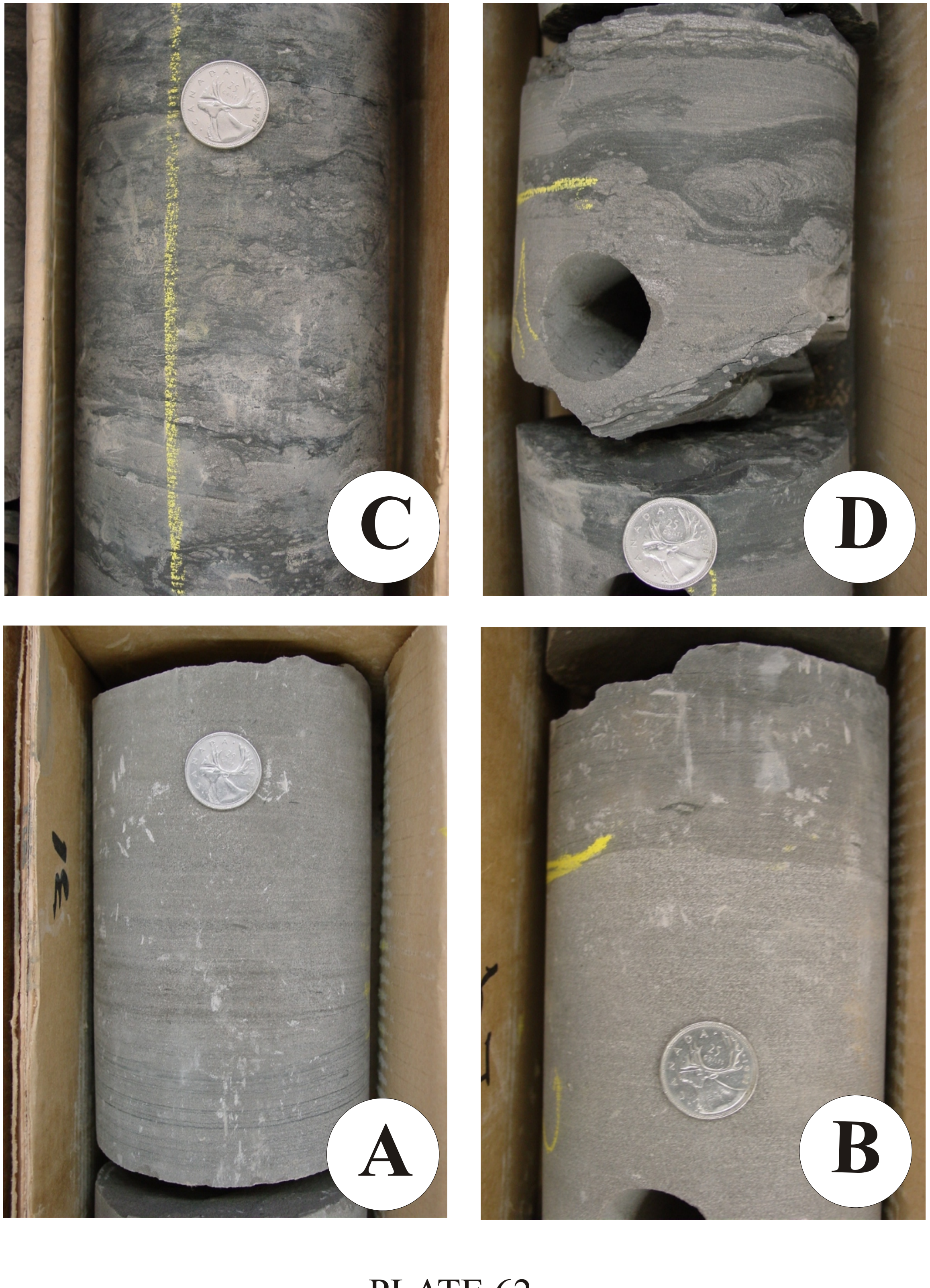

PLATE 62

PLATE 63

Core photographs of 06-012-045-07W5/0
Viking Fm.

Whole core interval is 1980 - 2001 m. Base of core (b), top of core (t).

Core interval 1980 - 1985 m within the Viking Formation showing the transgressive lag (interbedded mudstone, sandstone and conglomerate facies association) on top of the formation.
At this location, the conglomerate stringers are interpreted as veeners on transgressive ravinement surfaces; picking which one has the regional stratigraphic significance is difficult.

PLATE 63

PLATE 64

Core photographs of 07-06-042-07W5/0
Westgate - Viking formations

Whole core interval is 2271- 2289.2 m. Base of core (b), top of core (t).

The Viking Formation estuarine valley fill deposits (VF) truncated by a bounding discontinuity (lower black arrow), identified with VE3 of Boreen and Walker (1991), which is overlain by an interbedded silty sandstone and bioturbated mudstone facies association (lower shoreface). This is in turn truncated by VE4 (upper black arrow), demarcated by the presence of a transgressive lag (TL).
The insets A and B are reproduced as close-ups in PLATE 65.

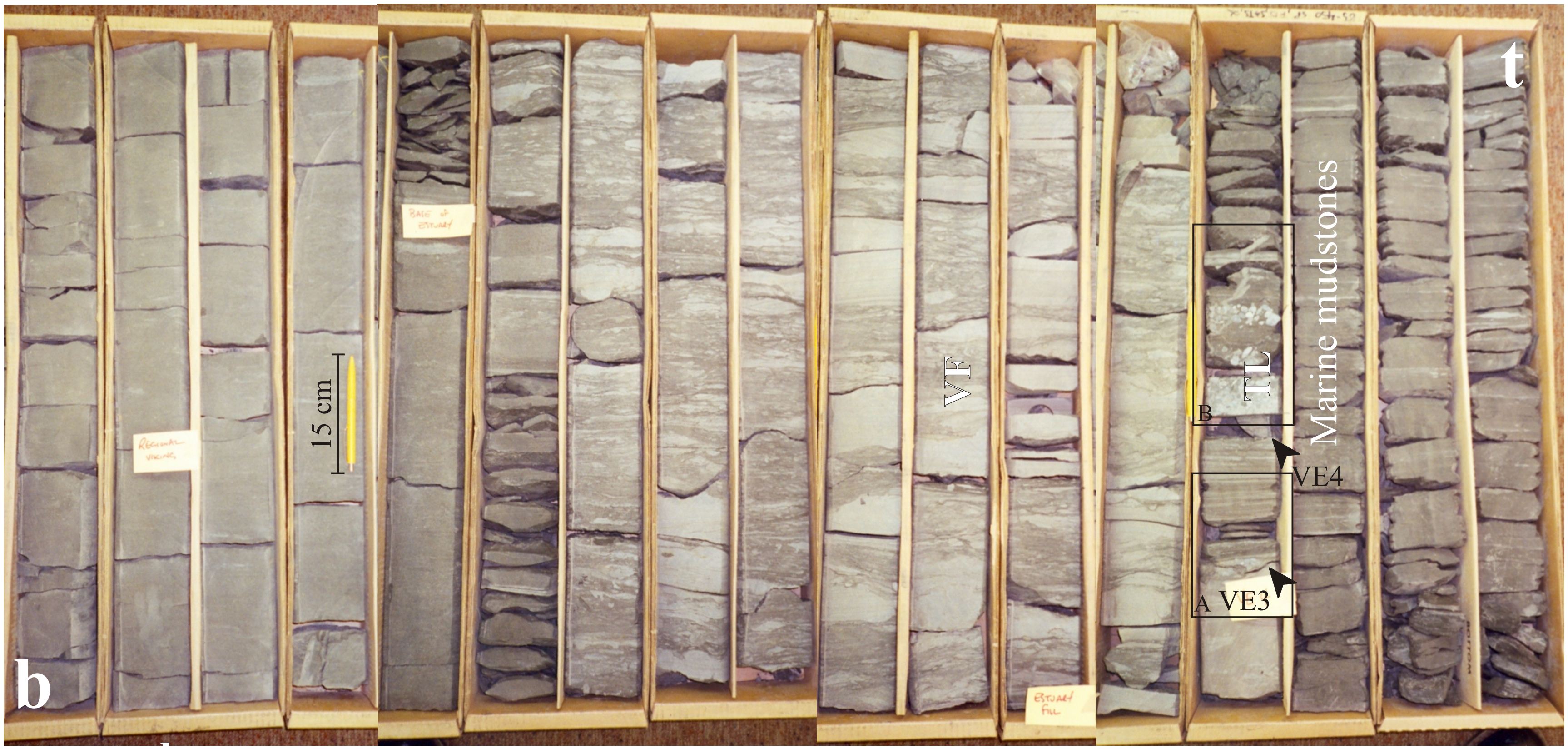

PLATE 64

PLATE 65

Core photographs of 07-06-042-07W5/0
Westgate - Viking formations

Whole core interval is 2271- 2289.2m. Base of core (b), top of core (t).

Close-up view of the transgressive lags on top of the Viking Fm. The lags are characterized by a sharp base, the *Glossifungites* surface, and the thin, but coarse overlying facies.

A) Close-up view of the erosion surface VE3: black arrow points towards the sharp contact of the conglomeratic lag with the underlying deposits of a prograding shoreface. Depth 2274.25 m.
Note the wireline log deflections associated with this discontinuity (see Fig. A-30).

B) Close-up view of the VE4 erosion surface: sharp and mantled by the interbedded mudstone, sandstone and conglomerate facies association, which represents the transgressive lag on top of the Viking Fm. The pebble lag and the marine black shales indicate that this erosion surface (RS) was modified during subsequent marine transgression. Depth 2274.10 m.
Note: for reference and analogies see Fig.3 and Fig.18 from Boreen and Walker (1991).

PLATE 65

PLATE 66

Core photographs of 07-08-042-05W5/0
Viking Fm.

Whole core interval is 2051 - 2069 m. Bottom of core (b), top of core (t).

The upper portion of the Viking Formation, showing at least four different pebble stringers (white arrows) interpreted as being associated with transgressive surfaces of erosion. The surfaces are demarcated by the *Glossifungites* ichnofacies.
The uppermost conglomeratic lag (depth: 2065 m) could be picked as the one with regional stratigraphic significance, due to its association with the wireline log deflections (see Fig. A-31).

PLATE 66

PLATE 67

Core photographs of 07-08-042-05W5/0
Viking Fm.

Whole core interval is 2051 - 2069 m

Close-up view of two of the sharp-based lag conglomerates in the uppermost part of the Viking formation at Gilby field:
(A) Depth: 2065 m.
(B) Depth: 2066.2 m.

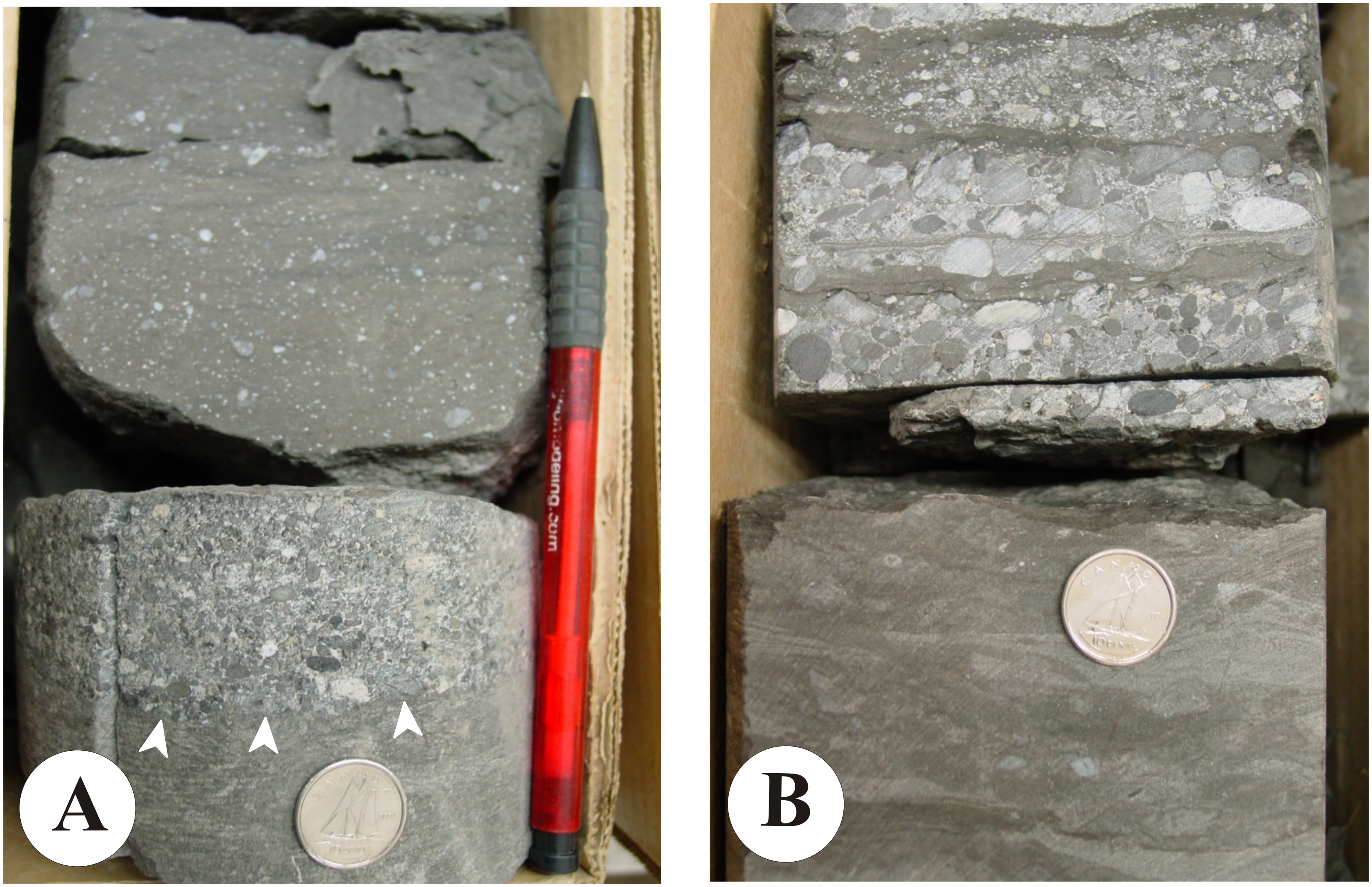

PLATE 67

PLATE 68

Core photographs of 07-08-042-05W5/0
Viking Fm.

Whole core interval is 2051 - 2069 m.

Upper offshore to lower shoreface deposits of the Viking Formation at Gilby field: pale gray, thoroughly bioturbated siltstones and fine-grained sandstones.

PLATE 68

PLATE 69

Core photograph of 07-08-042-05W5/0
Viking Fm.

Whole core interval is 2051 - 2069 m

Close-up view (from Plate 68) of the lower shoreface facies association of the Viking formation.
Depth: 2068 m.

PLATE 69

PLATE 70

Core photographs of 08-11-042-07W5/0
Viking Fm.

Whole core interval is 2271 - 2289.2 m. Base of core (b), top of core (t).

The upper portion of the Viking formation (2271 - 2278.1 m), showing two lag conglomerates (white arrows) interpreted as being associated with transgressive surfaces of erosion. The surfaces are demarcated by the *Glossifungites* ichnofacies. The uppermost conglomeratic lag (depth: 2277.8 m) could be picked as the one with regional stratigraphic significance, due to its association with resistivity and gamma-ray log deflections (see Fig. A-32).

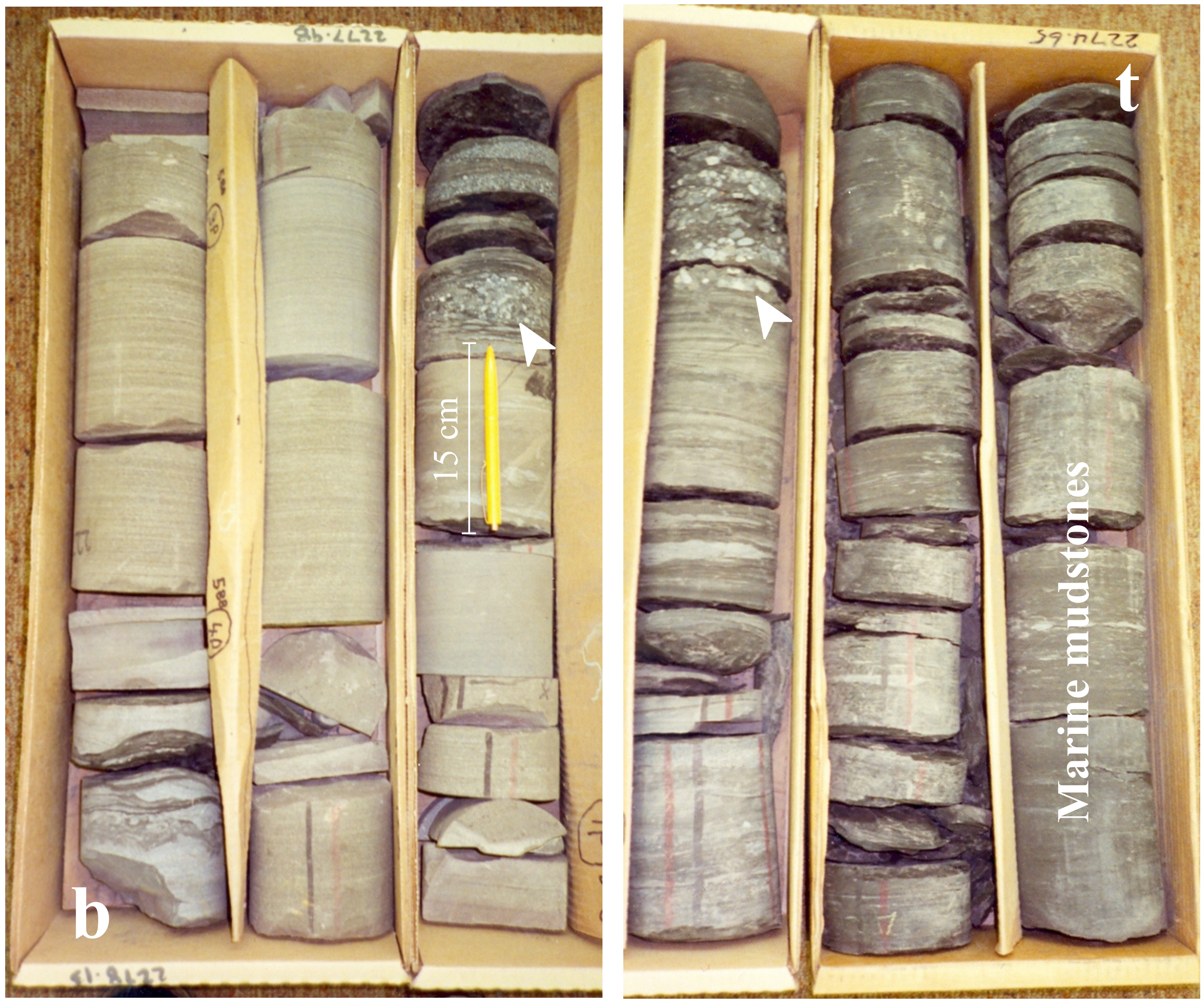

PLATE 70

PLATE 71

Core photographs of 08-11-042-07W5/0
Viking Fm.

Whole core interval is 2271 - 2278 m. Base of core (b), top of core (t).

A) Close-up view of the regional Viking Formation: pale - grey, throughly bioturbated, silty sandstone and fine sandstone (upper offshore to lower shoreface).
Depth: 2280.5 m.

B) Close-up view of the two lag conglomerates at the top of the Viking Formation. Note the sharp contact between the stacked wavy parallel laminated sandstones and oscillation rippled sandstone defining repetitive storm bed deposition, underlying the upper conglomeratic lag. This contact is recognized as the VE4 regionally extensive erosive surface as described by Pattison (1991); Boreen and Walker (1991).

C) Close-up view of the contact between fine-grained, parallel laminated sandstones, with a low degree of bioturbation (the valley fill deposits of the Viking Formation) and the overlying facies association of interbedded conglomerates, sandstones and mudstones. This contact is interpreted as a discontinuity related as well with ravinement processes.

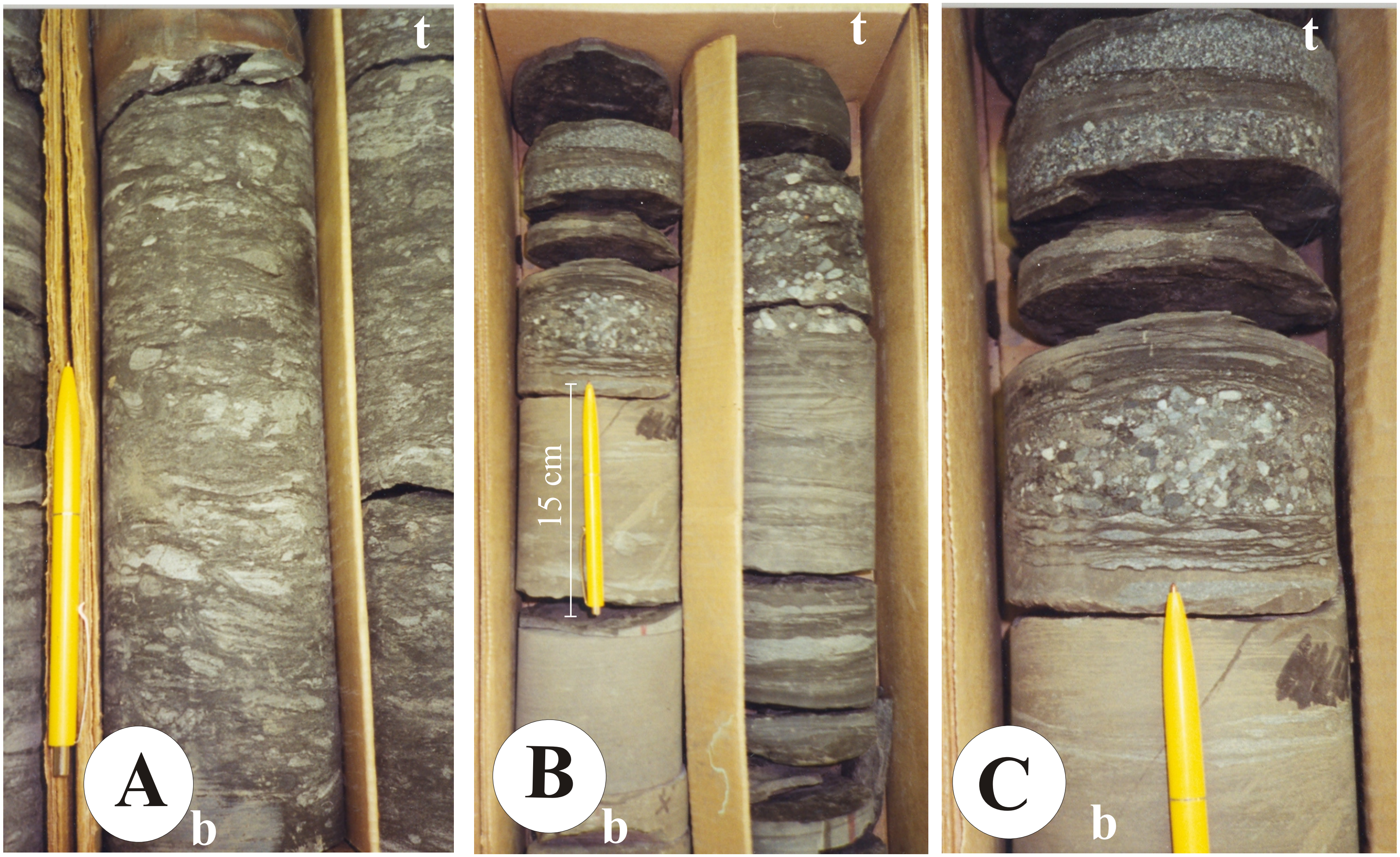

PLATE 71

PLATE 72

Core photographs of 10-17-042-04W5/0
Viking Fm.

Whole core interval is 1934 - 1952.20 m. Base of core (b), top of core (t).

The upper portion of the Viking Formation at Gilby field, showing a pebble stringer (above yellow pencil) interpreted as being associated with a transgressive surface of erosion. The surface (depth: 1939.6 m) is demarcated by the *Glossifungites* ichnofacies, and is associated with wireline log deflections (see Fig. A-33).

PLATE 72

PLATE 73

Core photographs of 13-13-048-05W5/0
Westgate - Viking formations

Whole core interval is 1974 - 1980m. Base of core (b), top of core (t).

Sandier-upward sequence of the Viking formation , north of Willesden Green field, Alberta. Black arrow (depth: 1976.4 m) points to the contact surface, which is erosive and defines the onset of the Westgate transgression. Yellow pencil points towards the Colorado flooding surface.
Note the evidence of repetitive transgressive ravinement processes (the presence of sharp-based pebble stringers and conglomerates).

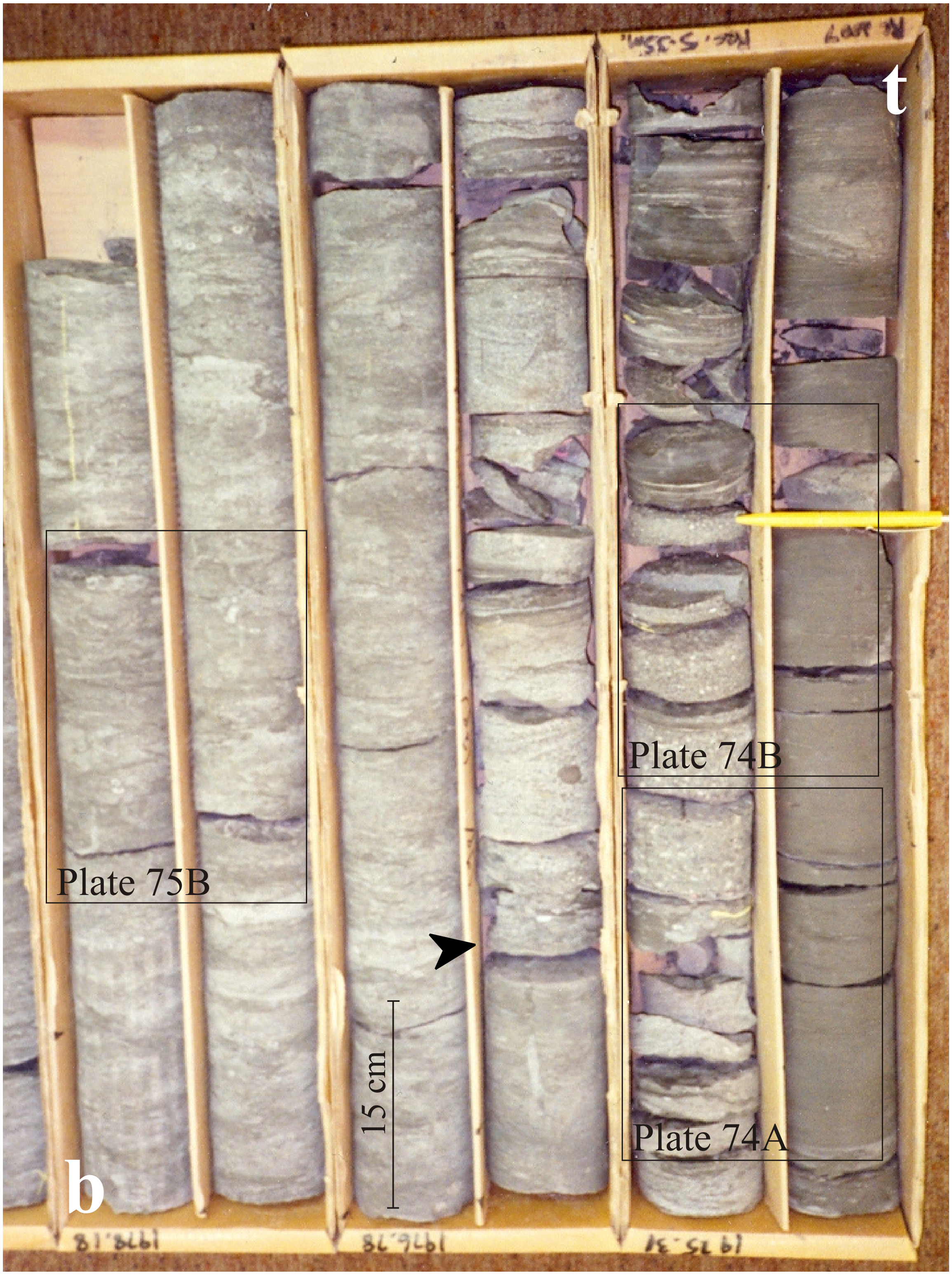

PLATE 73

PLATE 74

Core photograph of 13-13-048-05W5/0
Westgate - Viking formations

Whole core interval is 1974 - 1980 m. Base of core (b), top of core (t).

Close-up view of the uppermost conglomeratic lag of the Viking Fm.
A) Yellow pencil points towards the base of the lag conglomerate. Depth: 1975 m.
B) Yellow pencil point towards the top of the conglomerate, which represents the contact between Westgate and Viking formations. Depth: 1974.7 m.

PLATE 74

PLATE 75

Core photographs of 13-13-048-05W5/0
Westgate - Viking formations

Whole core interval is 1974 - 1980 m. Base of core (b), top of core (t).

A) Close-up view of the uppermost part of the Viking Fm. The black arrow points towards the sharp contact between Westgate Fm. and Viking Fm. The yellow pencil points towards medium-grained, cross-bedded sandstones, with mudstone rip-up clasts, interpreted as embayment deposits of the Viking Fm. Depth: 1975.6 m.
B) Close-up view of the upper offshore to lower shoreface deposits of the Viking Fm.: pale gray, thoroughly bioturbated siltstones and fine-grained sandstones.
Depth: 1977.5 m.

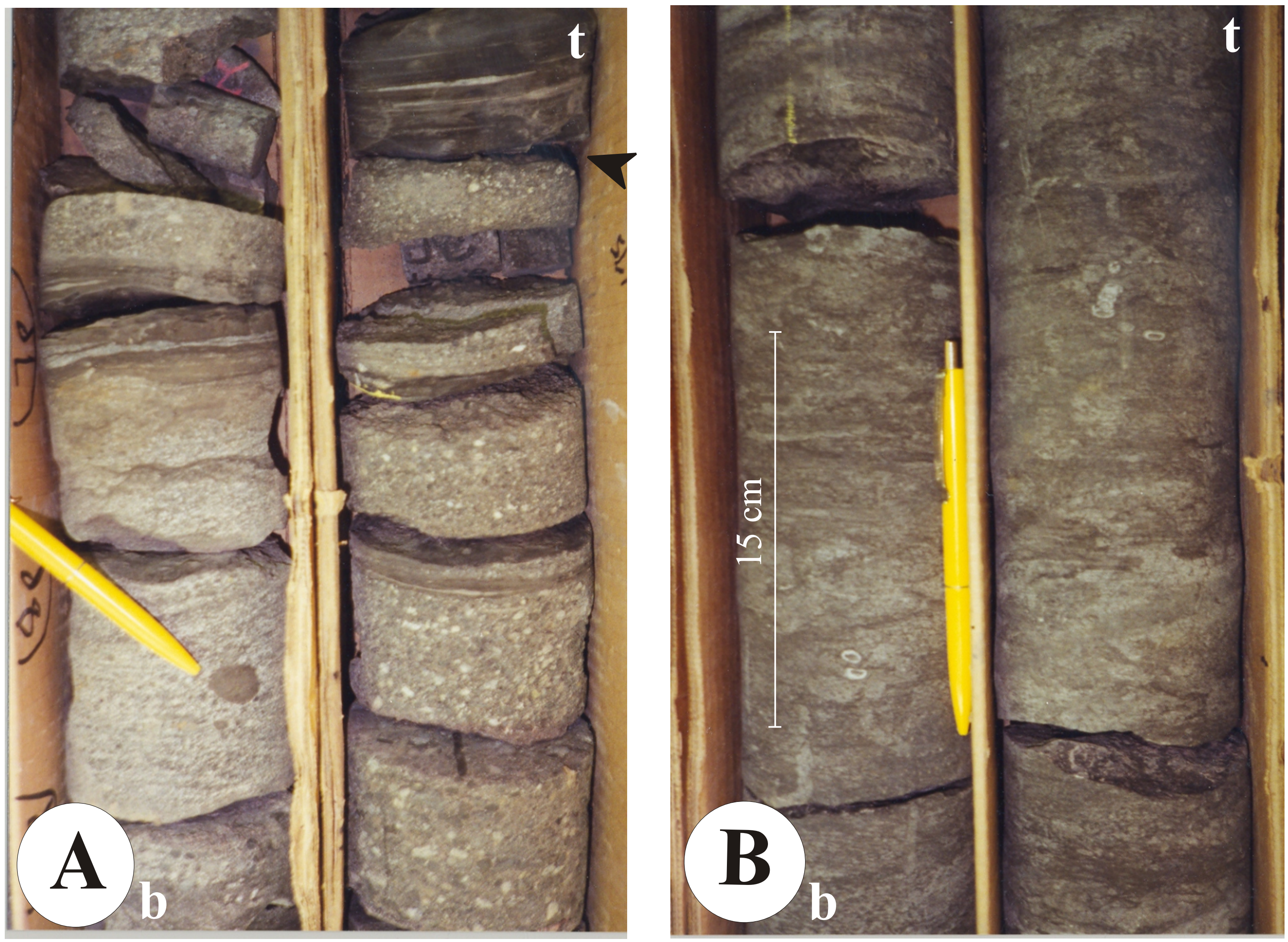

PLATE 75

PLATE 76

Core photographs of 03-13-43-05W5/0
Mannville Fm.

Whole core interval is 1986.5 -2004.7 m. Base of core (b), top of core (t).

Upper part of the Mannville Group, showing transition from non-marine alluvial plain deposits (1), to sharp-based (white arrows), pebble-sandstone, and cross-bedded medium to coarse grained sandstones of a channel deposit (2).

PLATE 76

PLATE 77

Core photographs of 03-13-43-05W5/0
Joli Fou - Mannville contact

Whole core interval is 1986.5 -2004.7 m. Base of core (b), top of core (t).

Close-up view of the Joli-Fou Formation - Mannville Group contact, delineated by the presence of a thin lag conglomerate with siderite-cemented clasts. The overlying silty shales contain a distal *Cruziana* (Planolites, Chondrites) trace fossil assemblage.

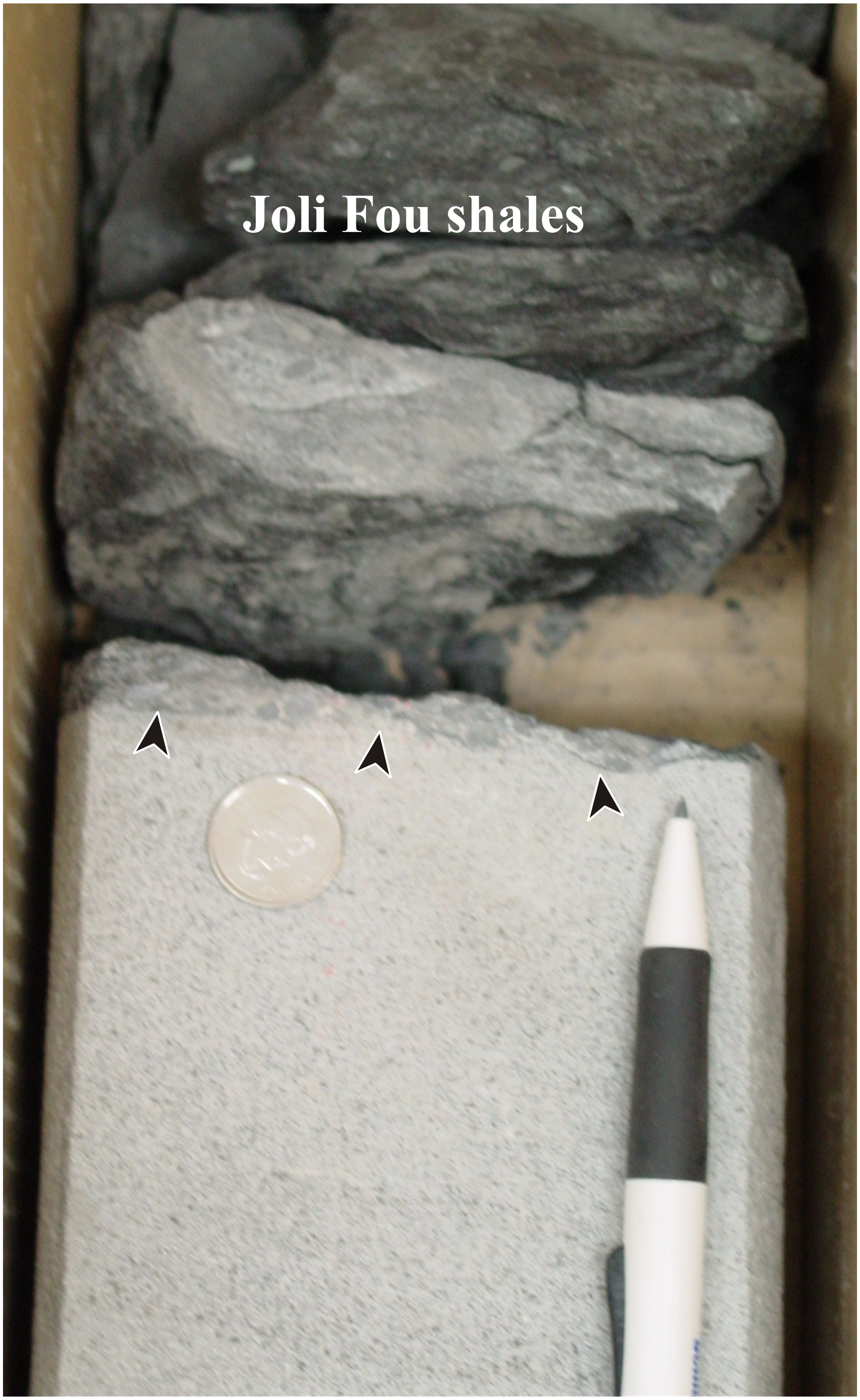

PLATE 77

PLATE 78

Core photographs of 03-13-43-05W5/0
Joli Fou- Mannville contact

Whole core interval is 1986.5 -2004.7 m

Close-up view of the thin conglomeratic lag associated with the Joli-Fou flooding surface, which is erosive and defines the top of the Manville Group.
Depth 1988.5 m.

PLATE 78

PLATE 79

Core photographs of 03-13-043-05W5/0
Joli Fou - Mannville contact

Whole core interval is 1986.5 -2004.7 m. Base of core (b), top of core (t).

A) Close-up view of the base fluvial channel facies identified in the uppermost part of the Mannville Group. Depth: 2000.8 m.

B) Close-up view of the medium-coarse grained sandstone, found on top of the Upper Mannville Group, and interpreted as a channel-fill deposit. This is suggested by the overall fining-upward sandstone body with a lower erosional contact. The absence of marine trace fossils and marine fauna, as well as the absence of any evidence of tidal processes such as flaser bedding, bi-directional cross-beds, and tidal bundles, suggest that the channel fill is fluvial dominated.
Depth: 1998.8 m.

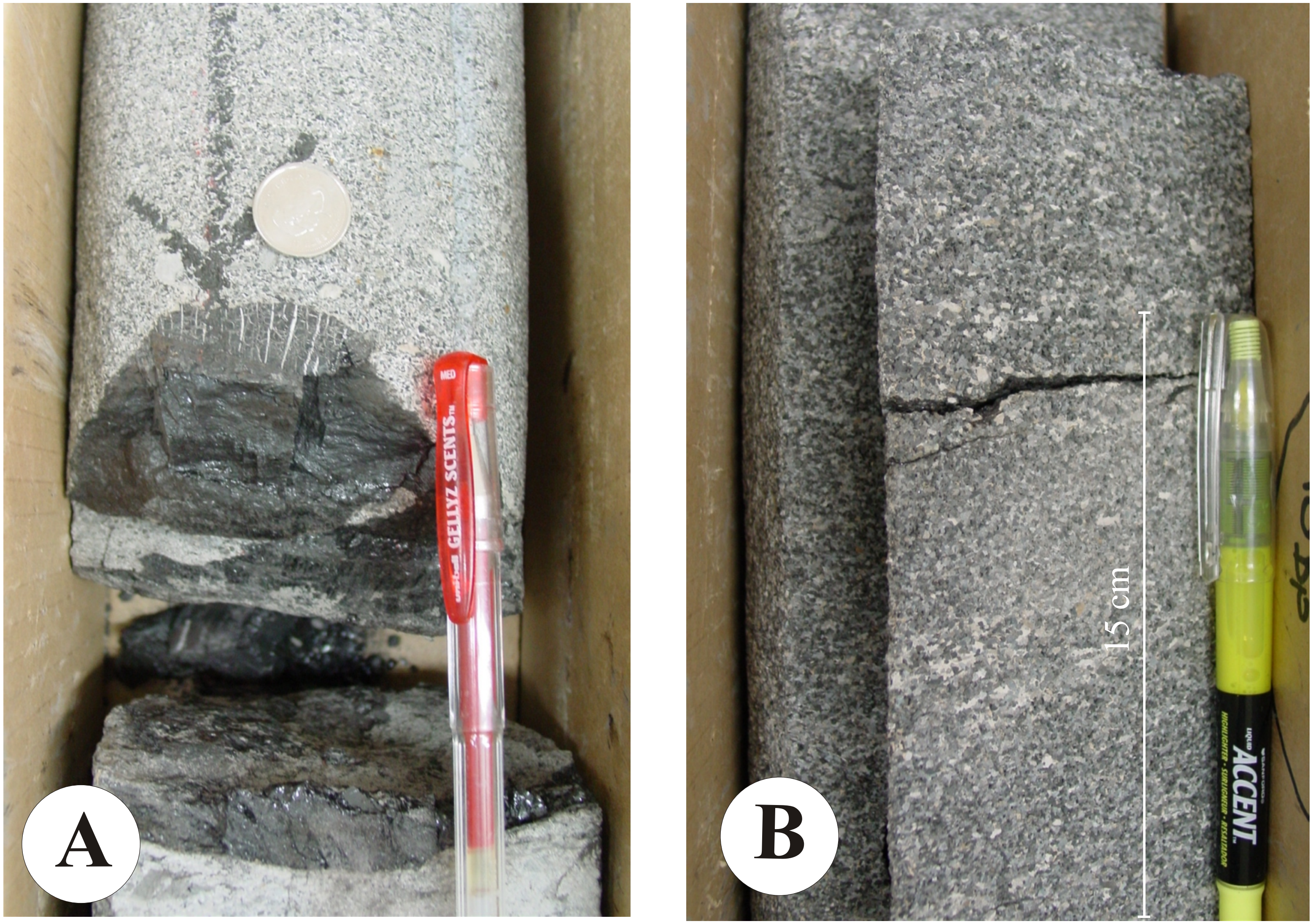

PLATE 79

PLATE 80

Core photograph of 10-32-048-06W5/0
Joli Fou - Mannville formations

Whole core interval is 1720.90 - 1730.10 m Base of core (b), top of core (t).

Black arrow points to the Mannville sandstone - Joli Fou shales contact surface, which is erosive and defines the onset of the Joli Fou transgression.
Depth: 1722.1 m.

PLATE 80

PLATE 81

Core photograph of 10-32-048-06W5/0
Joli Fou - Mannville formations

Whole core interval is 1720.90 - 1730.10 m Base of core (b), top of core (t).

Close-up view of the Mannville sandstone - Joli Fou shales contact surface, which is interpreted as a flooding surface, defining the onset of the Joli Fou transgression. Depth: 1720.95 m.

PLATE 81

PLATE 82

Core photographs of 11-15-045-07W5/0
Joli Fou Fm. and Mannville Gp.

Upper part of the Mannville Group, showing transition from non-marine alluvial plain deposits (1), to sharp-based (white arrows), cross-bedded medium to coarse grained sandstones of a channel deposit, devoid of ichnofossils (2), to medium grained sandstone with carbonaceous and coaly fragments (3), to interbedded shale and fine - grained sandstones, bioturbated and ripple cross-laminated (4), and ending up with the dark, parallel laminated marine shale of the Joli Fou Formation.
Note: white arrow points towards the sharp, erosional base of the Mannville fluvial channel (see PLATE 82 cont.).

Whole core interval is 2012.3 - 2024.5 m. Base of core (Bottom), top of core (Top)

PLATE 82

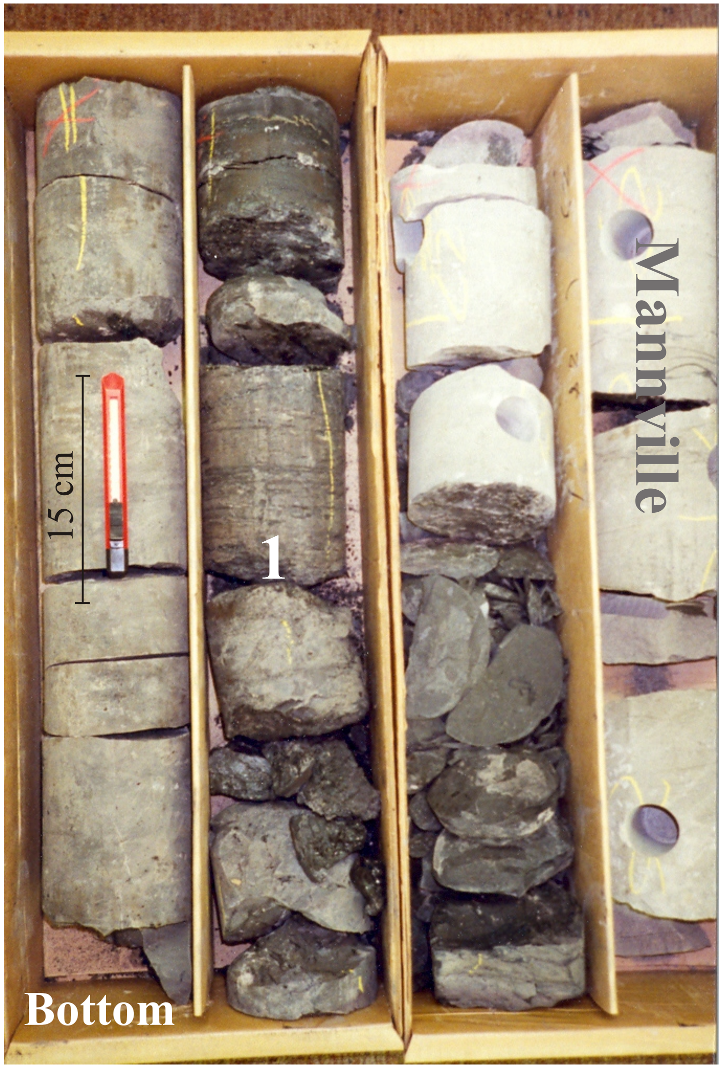

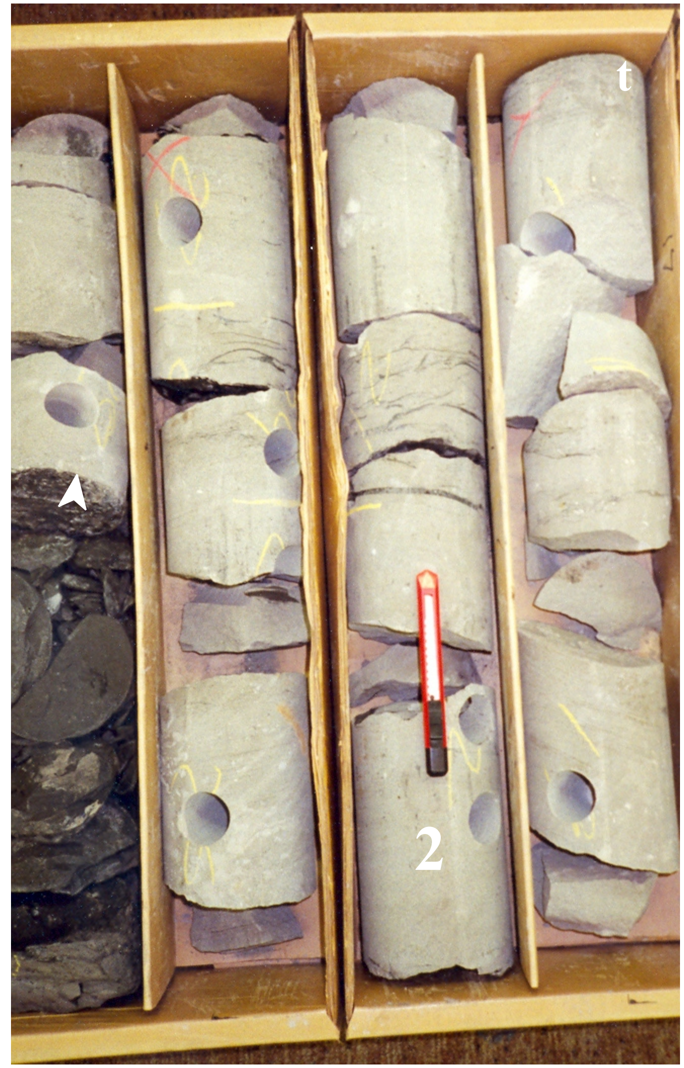

PLATE 82 cont.

PLATE 83

Core photograph of 11-15-045-07W5/0
Joli Fou Fm. and Mannville Gp.

Whole core interval is 2012.3 - 2024.5 m.

Black arrow points to the Mannville sandstone - Joli Fou shales contact surface, which is erosive and defines the onset of the Joli Fou transgression. Depth 2015 m.

PLATE 83

PLATE 84

Core photograph of 16-11-045-07W5/0
Joli Fou Fm. and Mannville Gp.

Whole core interval is 2015 - 2023.60 m. Base of core (b), top of core (t).

Black arrow points to the Mannville sandstone - Joli Fou shales contact surface, which is erosive and defines the onset of the Joli Fou transgression.
Note the gamma-ray and resistivity well-log signatures associated with this key stratigraphic surface (Fig. A-38).
Depth 2016.3 m.

PLATE 84

PLATE 85

Shell Husky Paradise Valley 10-25-47-3W4
Core #1 Joli Fou Fm.
538 - 547.25 m

Core photographs of the Joli Fou Formation. Laminated dark shales of the Joli Fou Formation have an easily identifiable log signature: high gamma-ray, positive SP, very low resistivity, and a high interval transit time (see Fig. A-39). The formation may contain sideritized mudstones and bentonite layers (white arrows; sample #2, and respectively # 1for XRD).

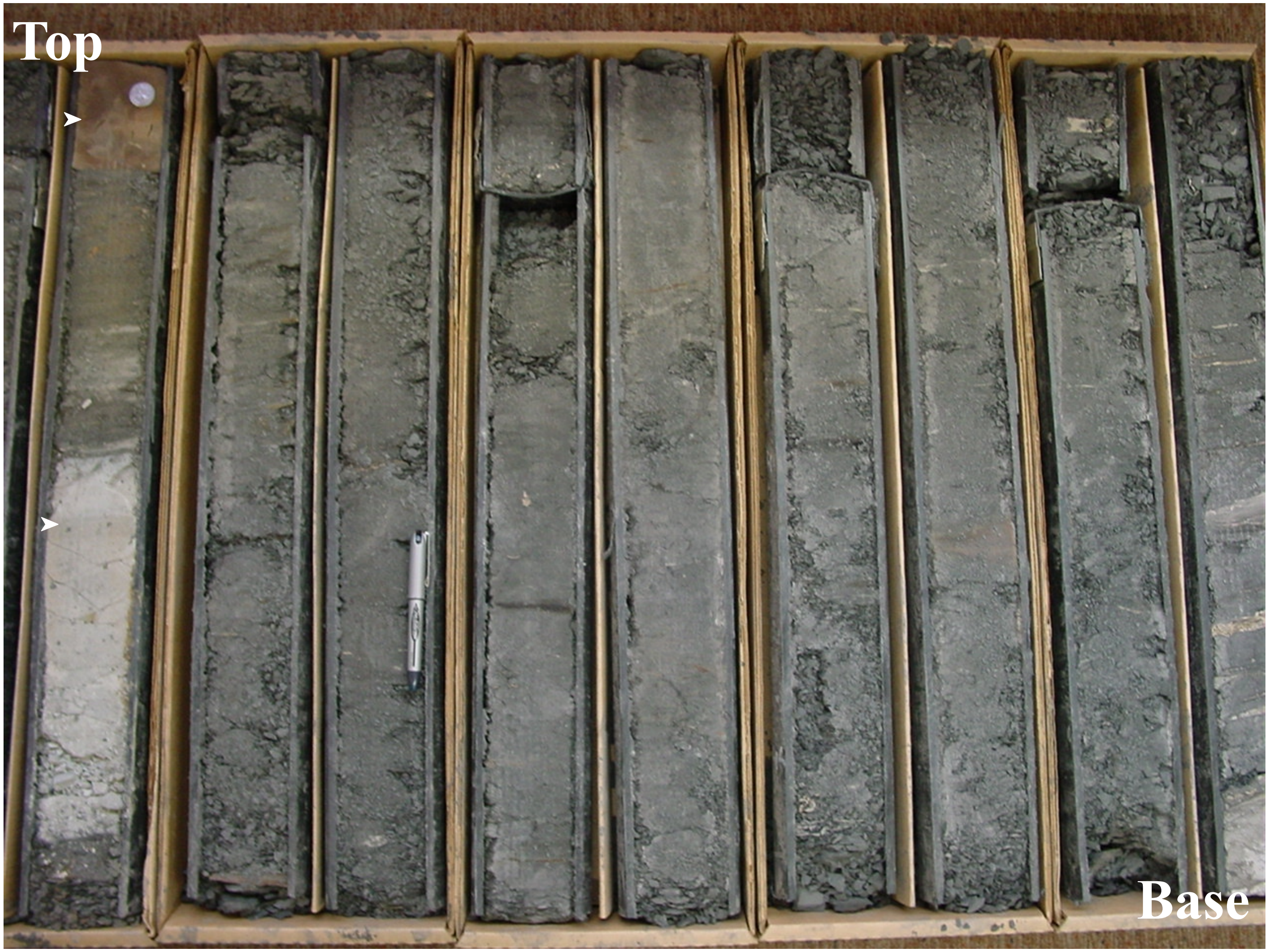

PLATE 85

PLATE 86

Shell Husky Paradise Valley 10-25-47-3W4
Core #1 Joli Fou Fm.
538 - 547.25 m

Close-up views of the Joli Fou shales:
A) Laminated dark grey mudstone and bentonite layer. Depth: 538.9 m for bentonite.
B) Sideritized mudstone. Depth: 538.5 m

PLATE 86

PLATE 87

Shell Husky Paradise Valley 10-25-47-3W4
Core #2
547.25 - 556 m

Colony Fm.

Core photographs of the upper part of the Colony Formation. Facies association is dominated by wavy to ripple cross-laminated (current-ripple laminations?) interbedded shale and fine - grained sandstone. Degree of bioturbation increases towards top. Lenticular and flaser bedding has been as well observed.
Setting: progradational tidal sequence (subtidal/intertidal?).

PLATE 87

PLATE 88

Shell Husky Paradise Valley 10-25-47-3W4
Core #2
547.25 - 556 m

Colony Fm.

A) Sideritized mudstone. Depth: 546.2 m.

B) Ripple cross-laminated to flaser bedded sandstone. Depth: 552.5 m.

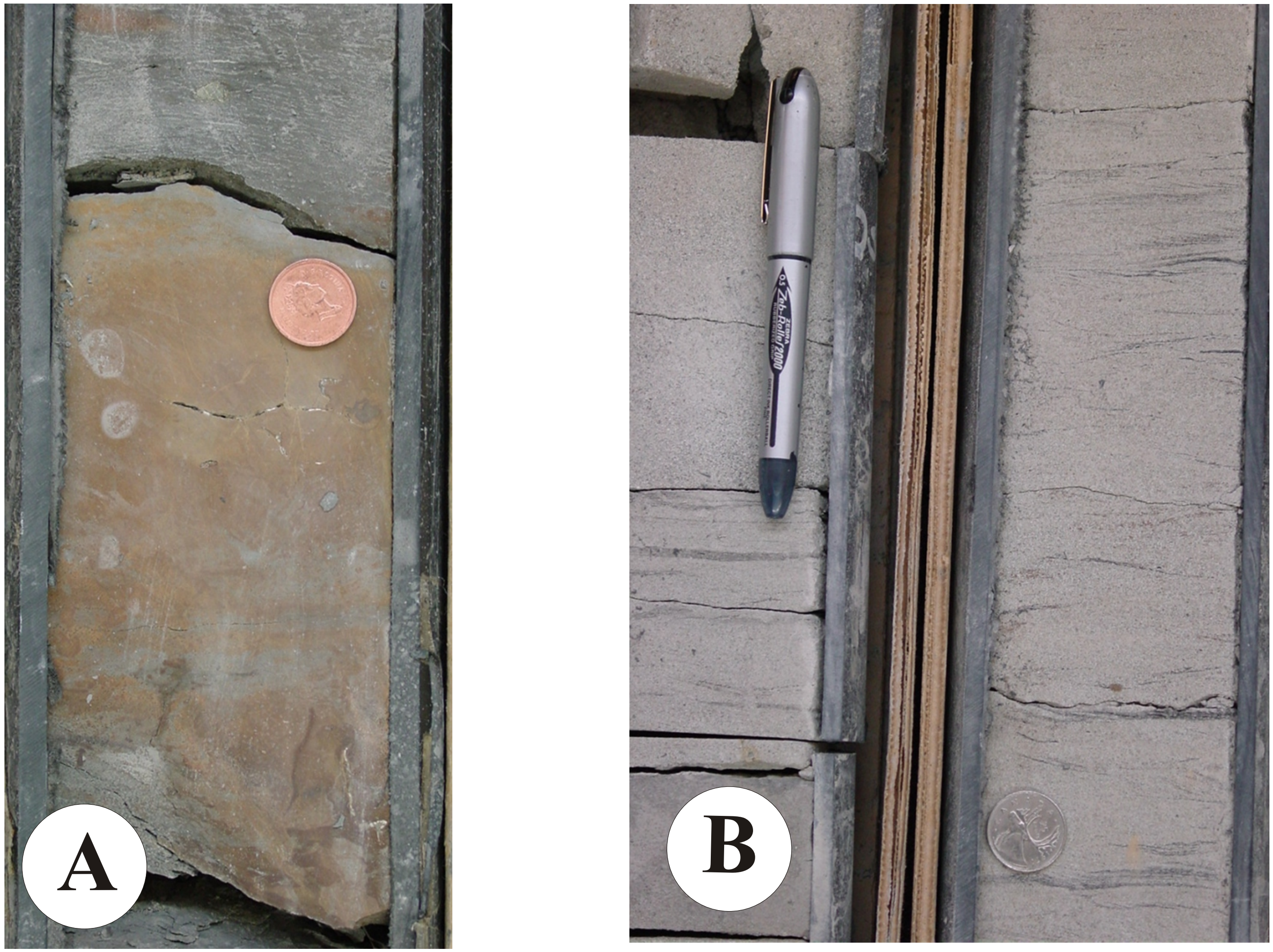

PLATE 88

PLATE 89

Shell Husky Paradise Valley 10-25-47-3W4
Core #3
Whole core interval: 556 -563 m
Recovered: 556 - 559 m

Colony Fm.

Core photographs of the lower part of the Colony Formation. Facies association is dominated by wavy to horizontal planar laminated and ripple cross-laminated interbedded shale and fine - grained sandstone. Lenticular bedding has been as well observed.
Note: open black rectangles show the location of the close-up views presented in Plate 90.

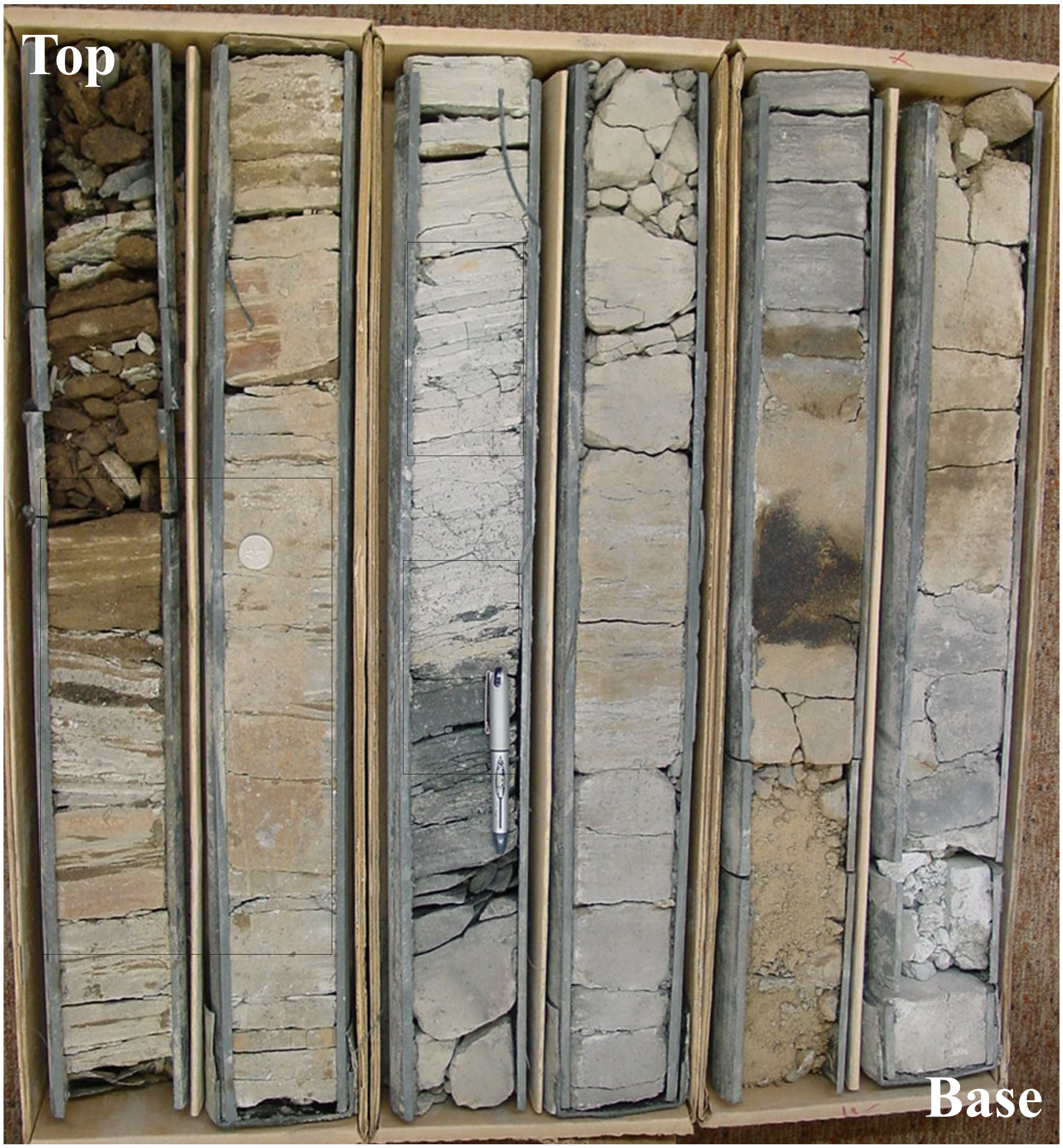

PLATE 89

PLATE 90

Shell Husky Paradise Valley 10-25-47-3W4
Core #3
Whole core interval: 556 -563 m
Recovered: 556 - 559 m

Colony Fm.

Close-up views of the coarsening-upward (prograding tidal ?) deposits of the Colony Formation:
A) Thin coal bed interlaminated within the sandy sequence. Depth: 557.6 m.
B) Wavy to horizontal planar laminated and ripple cross-laminated fine-grained sandstone. Depth: 557.4 m.
C) Interbedded shales with interbedded shales and silty fine- grained sandstones. Depth: 556-557 m.

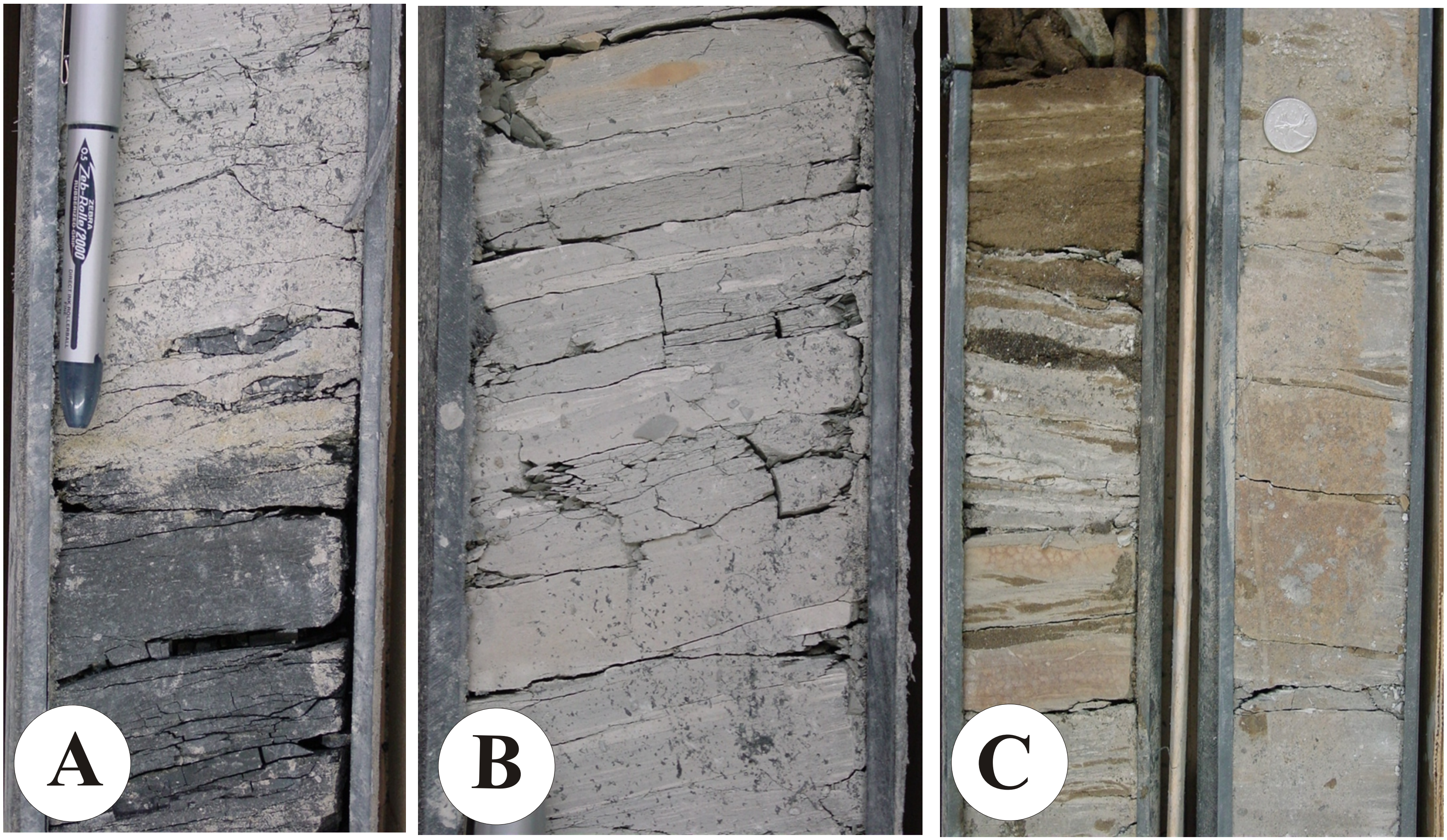

PLATE 90

PLATE 91

Shell Husky Paradise Valley 10-25-47-3W4
Core #5
564.25 - 573 m

(McLaren Fm.)

Core photographs of the coastal plain and prograding shallow marine cycle of the McLaren Fm.
The uppermost part of the fining upward fluvial channel sequence (see Plate 93) is characterized by rootlets and horizontal burrowing within interbedded shale and siltstones. This coastal plain sediments are gradationally overlain by a sandier-upward interval characterized by lenticular and ripple cross-lamination, as well as by the presence of flaser bedding.
Note: open black rectangles show the location of the close-up views presented in Plate 92.

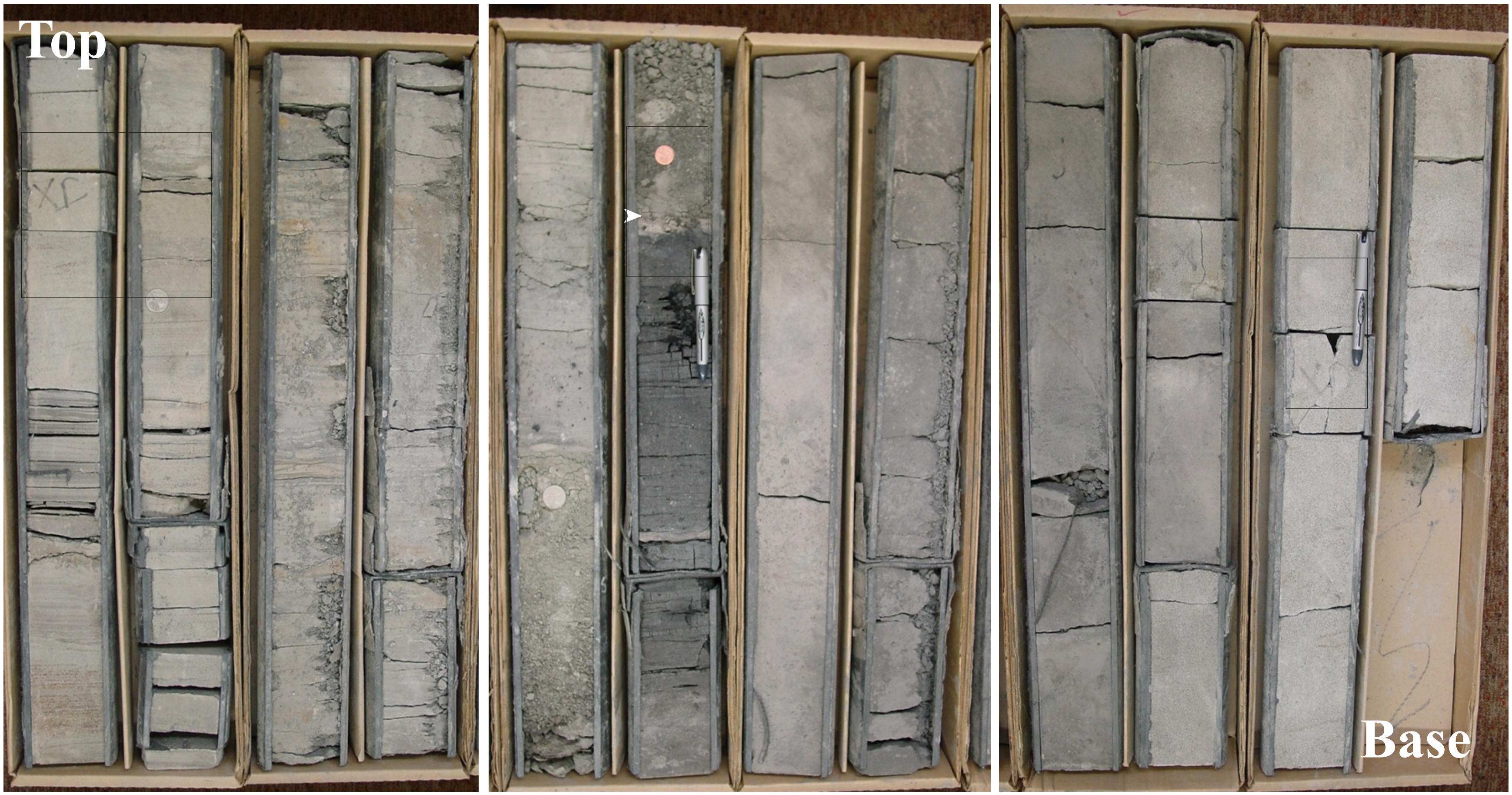

PLATE 91

PLATE 92

Shell Husky Paradise Valley 10-25-47-3W4
Core #5
564.25 - 573 m

(McLaren Fm.)

Close-up views from previous plate (Plate 91):

A) Fine-grained , shallow marine sandstone, exhibiting horizontal parallel lamination, flaser lamination, and organic laminae dispersal. Depth: 565 m.

B) Marine shale on coastal plain coal (shale sample no.4 for XRD). Depth: 568 m.

C) Massive fluvial channel sandstone. Depth: 572.2 m.

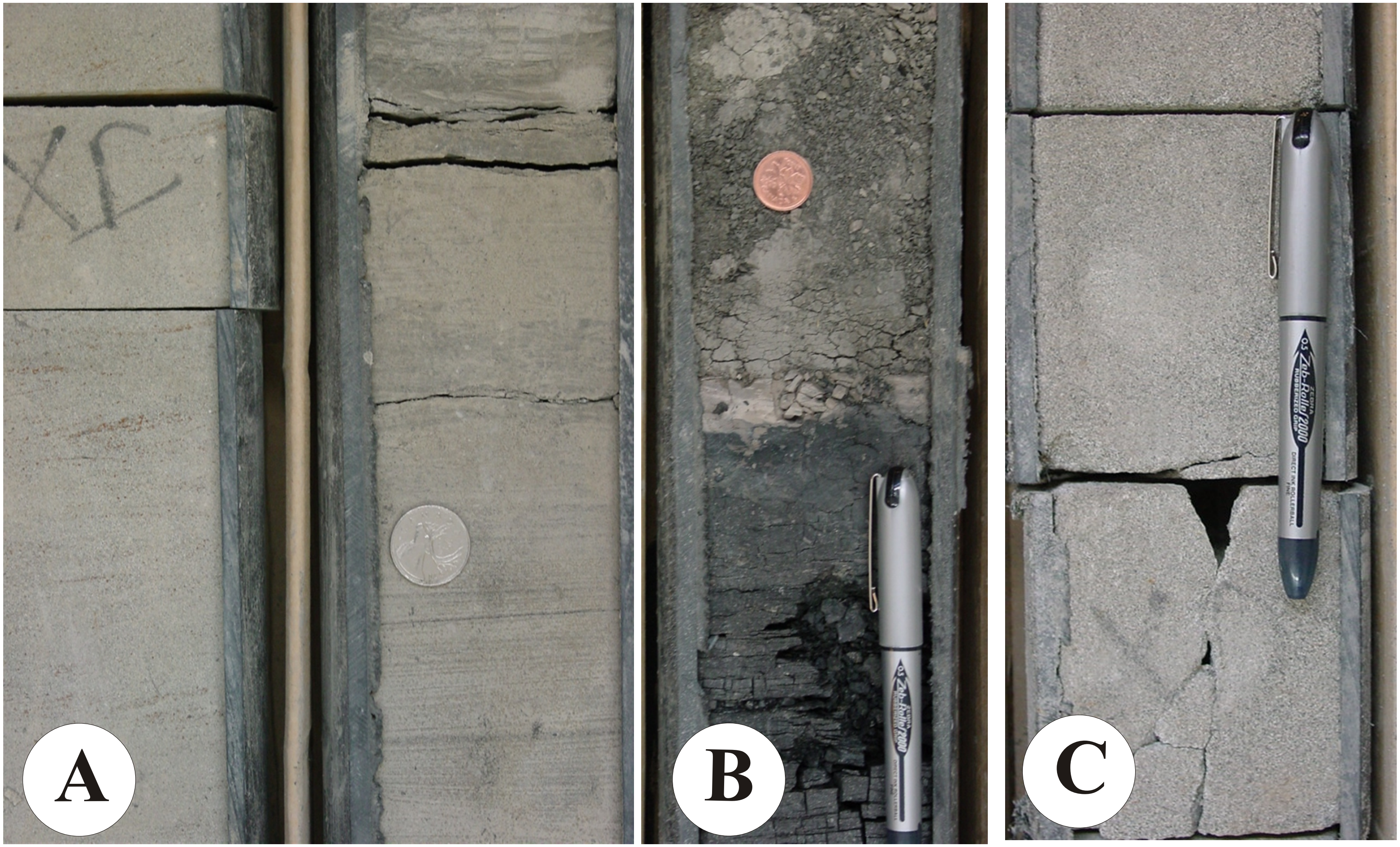

PLATE 92

PLATE 93

Shell Husky Paradise Valley 10-25-47-3W4
Core #6
573 - 582 m

(Waseca Fm. - McLaren Fm.)

Core photographs of the Waseca Formation - McLaren Formation erosional contact. The interbedded shale and thin fine-grained sandstone interval of the upper Waseca is dominated by small sand filled horizontal burrowing as the preserved primary sedimentary structures are wavy to horizontal planar bedding. A McLaren lithic sandstone channel (massive and with low angle parallel lamination) incises down to the Waseca coastal plain sediments.

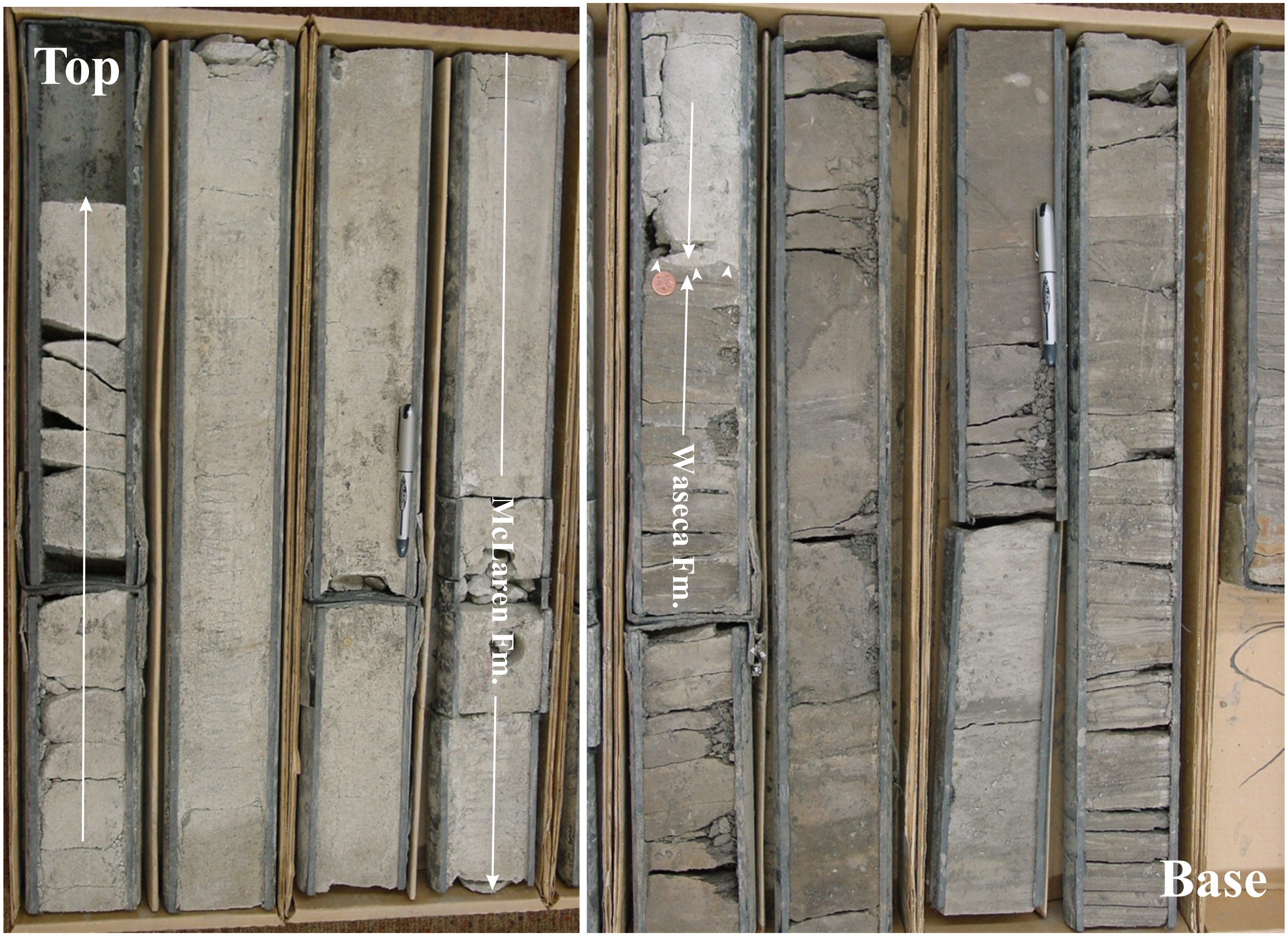

PLATE 93

PLATE 94

Shell Husky Paradise Valley 10-25-47-3W4
Core #6
573 - 582 m

(Waseca Fm. - McLaren Fm.)

Close-up view of the erosional contact: coastal plain - fluvial channel sandstone (white arrows) Mannville Gp.
Depth: 578 m
Note: see the association with wireline log deflections (Fig. A-39).

PLATE 94

PLATE 95

Shell Husky Paradise Valley 10-25-47-3W4
Core #8
591 - 600 m

(Sparky Fm. - Waseca Fm.)

Sparky Formation - Waseca Formation contact. Sparky upper cycle consists of interbedded sandstones and shales reflecting additional shallow water, possibly intertidal deposition (mud drapes on top of ripples), which is capped by the development of the Sparky coal. A Waseca lithic sandstone channel (massive) incises down to the Sparky coal level.
Note: open black rectangles show the location of the close-up views presented in Plate 97.

PLATE 95

PLATE 96

Shell Husky Paradise Valley 10-25-47-3W4
Core #8
591 - 600 m

(Sparky Fm. - Waseca Fm.)

Close-up view of the Sparky Fm. - Waseca Fm. contact. White arrows point towards the erosional base of a fluvial channel, which, given the local conditions on most coastal environments (sedimentation, relative sea level changes, wave and tidal action) may be regarded as a subaerial unconformity/sequence boundary.

PLATE 96

PLATE 97

Shell Husky Paradise Valley 10-25-47-3W4
Core #8
591 - 600 m

(Sparky Fm. - Waseca Fm.)

Close-up view of the Sparky upper cycle:

A) Wavy laminated and rippled sandstones interbedded with shale layers. Depth: 597.8 m.

B) Wavy laminated and rippled sandstones interbedded with shale layers. Depth: 597.6 m.

C) Thoroughly sideridized mudstone beds.. Depth: 599.2 m.

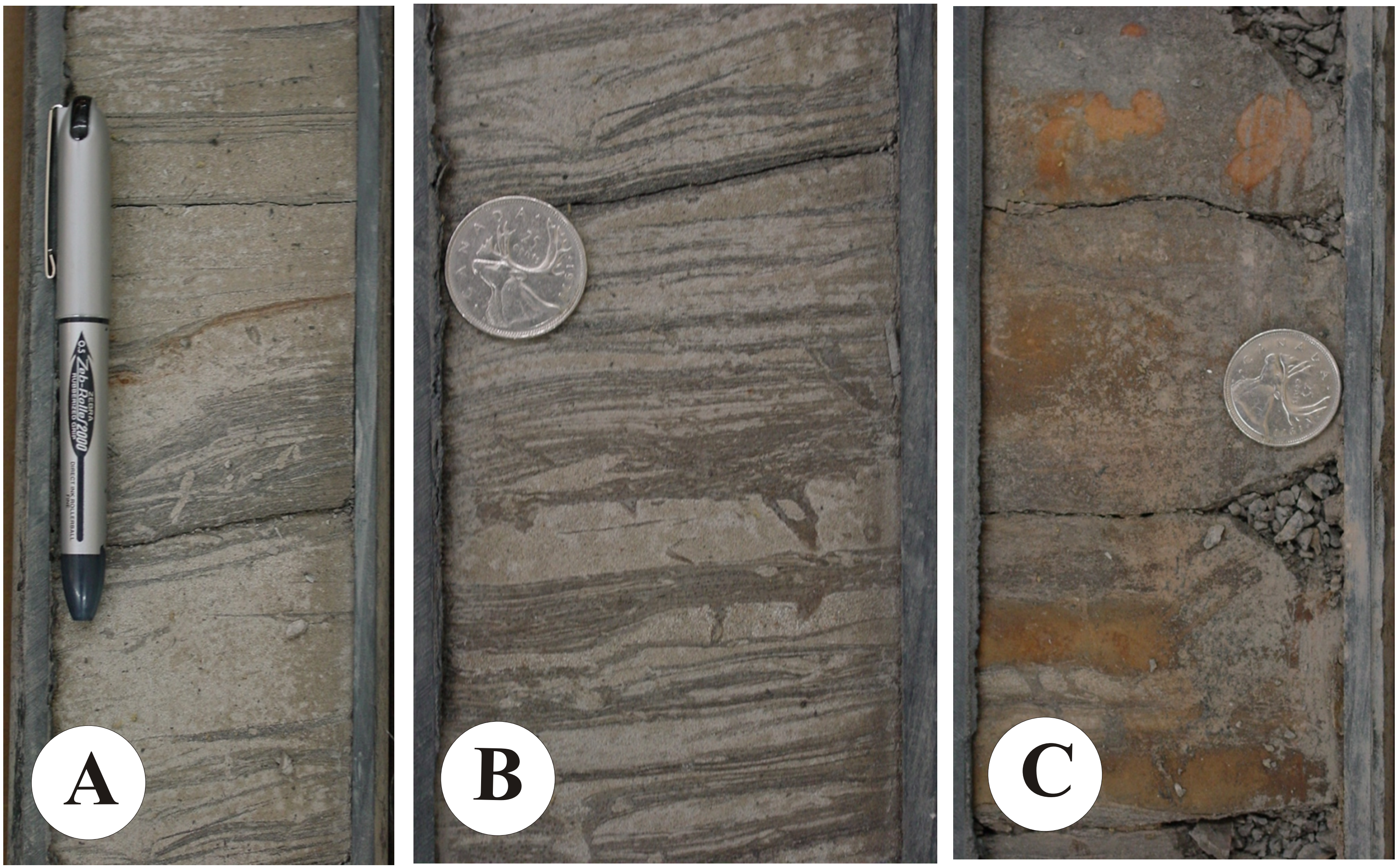

PLATE 97

PLATE 98

Shell Husky Paradise Valley 10-25-47-3W4
Core #9
600 - 609 m

Sparky Fm.

Core photographs of the Sparky sandier-upward cycle.
The basal Sparky is dominated by bioturbated, dark shale which subtlycoarsens upwards as thin centimetre thick wavy laminated to faintly ripple cross laminated very fine-grained sandstone lenses. Nondescript horizontal burrowing is evident throughout the interval.
Note: open black rectangles show the location of the close-up views presented in Plate 99.

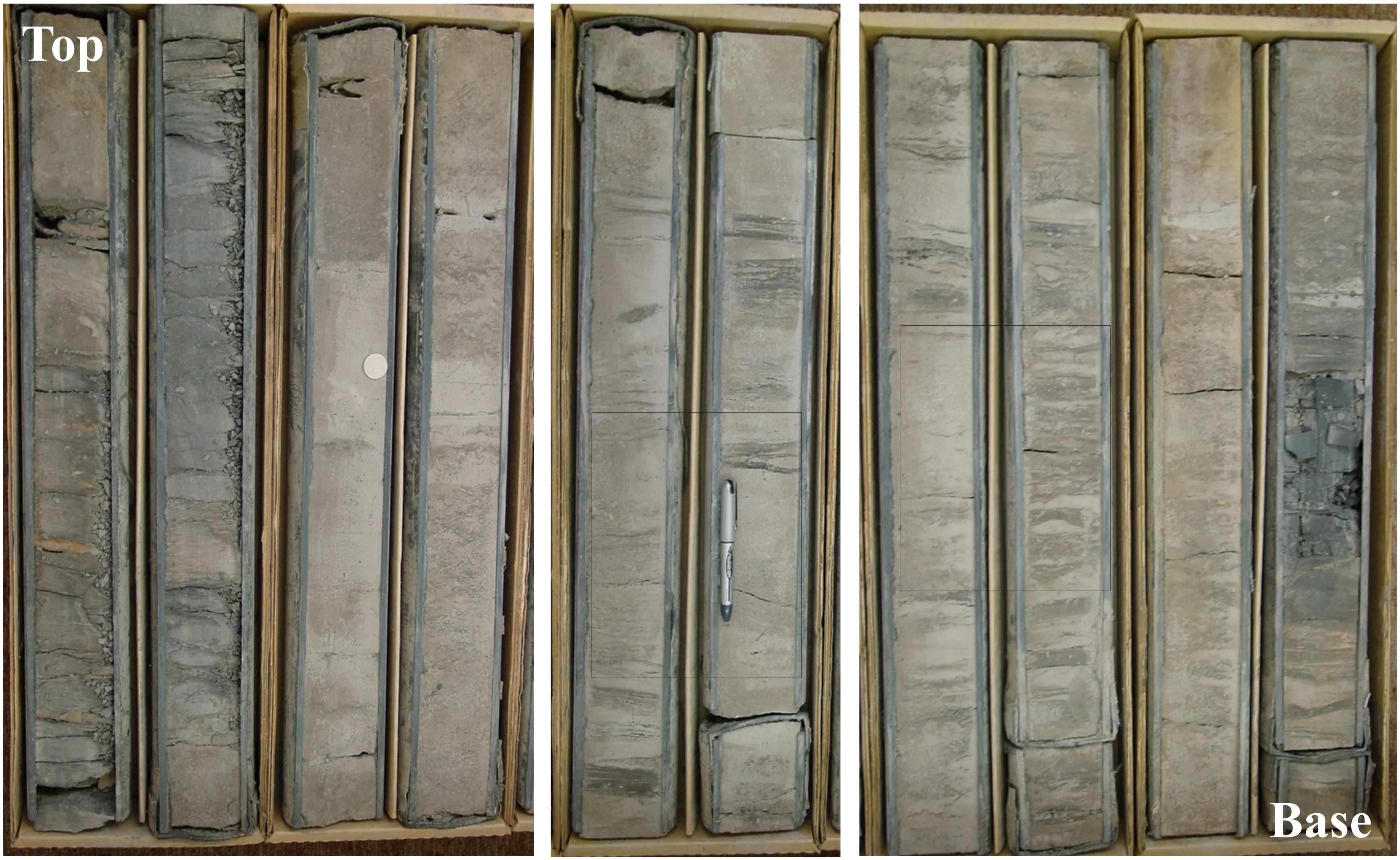

PLATE 98

PLATE 99

Shell Husky Paradise Valley 10-25-47-3W4
Core #9
600 - 609 m

Sparky Fm.

Close-up views of the Sparky sandstones from previous plate (Plate 98). Note the slightly coarsening upward fine-to medium-grained sandstone displaying a massive appearance within the upper portion of the sandstone.

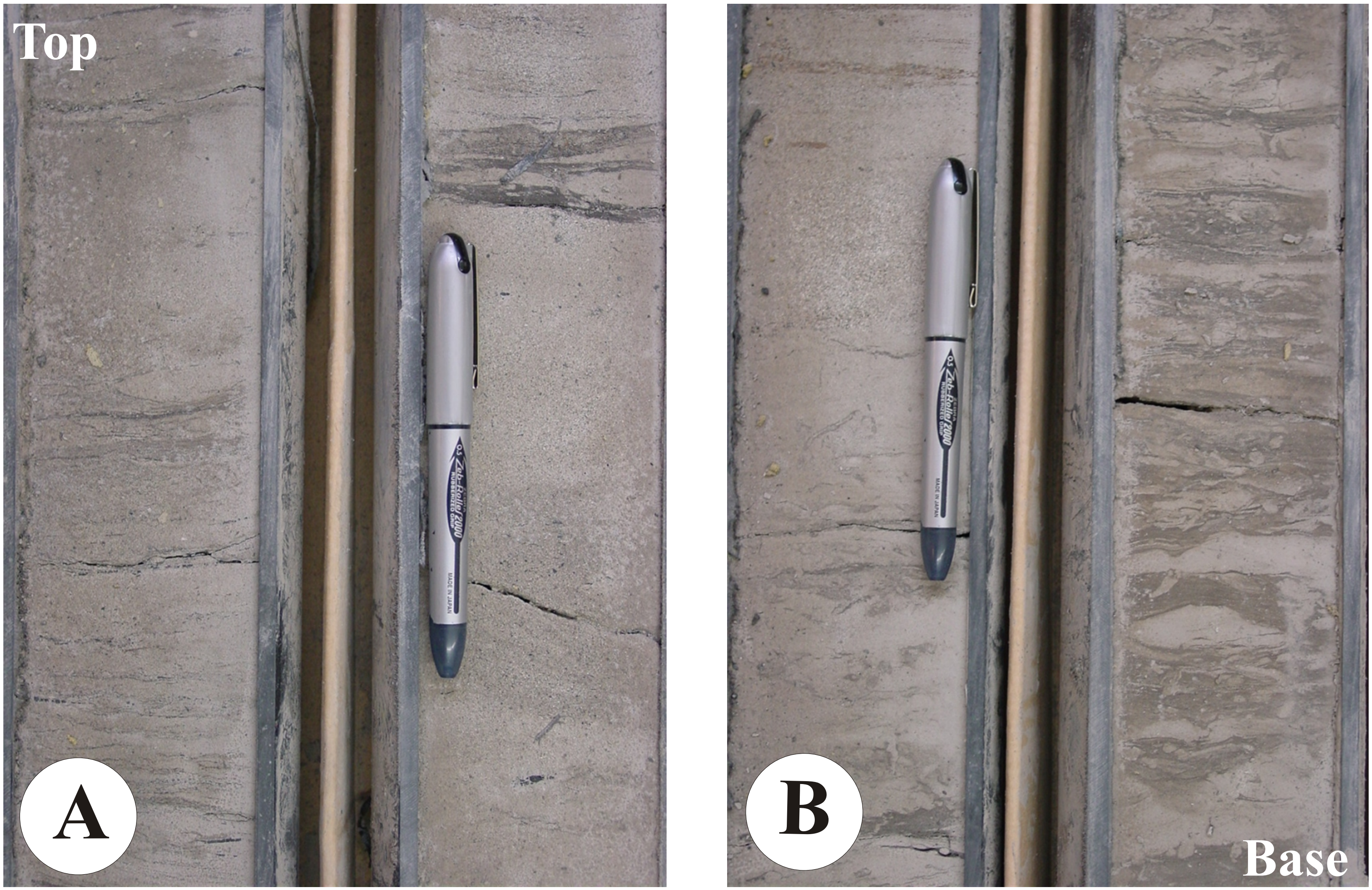

PLATE 99

PLATE 100

Shell Husky Paradise Valley 10-25-47-3W4
Core #10
609 - 618 m

General Petroleum Fm.

Core photographs of the General Petroleum Fm. sandier-upward cycle, delineated by a correlatable dark shale to shale with thin sandstone interbeds (white arrow).
The coarsening upward cycle consists of ~ 1 metre of intensely bioturbated shales with thin ripple laminated fine-grained sandstone lenses, and sand percent increasing upward. The upper sandy interval within the coarsening upward cycle is characterized by high angle trough cross-stratification, and ripple cross-lamination.
Note: open black rectangles show the location of the close-up views presented in PLATE 101.

PLATE 100

PLATE 101

Shell Husky Paradise Valley 10-25-47-3W4
Core #10
609 - 618 m

Grand Rapid Fm.

Close-up views of the G.P. lower shoreface facies assemblage from previous plate (Plate 100). Note the pale gray, thoroughly bioturbated (*Cruziana* ichnofacies) silty sandstones and fine sandstones.
A) Depth: 615.6 m.
B) Depth: 612.4 m.
C) Depth: 611.8 m.

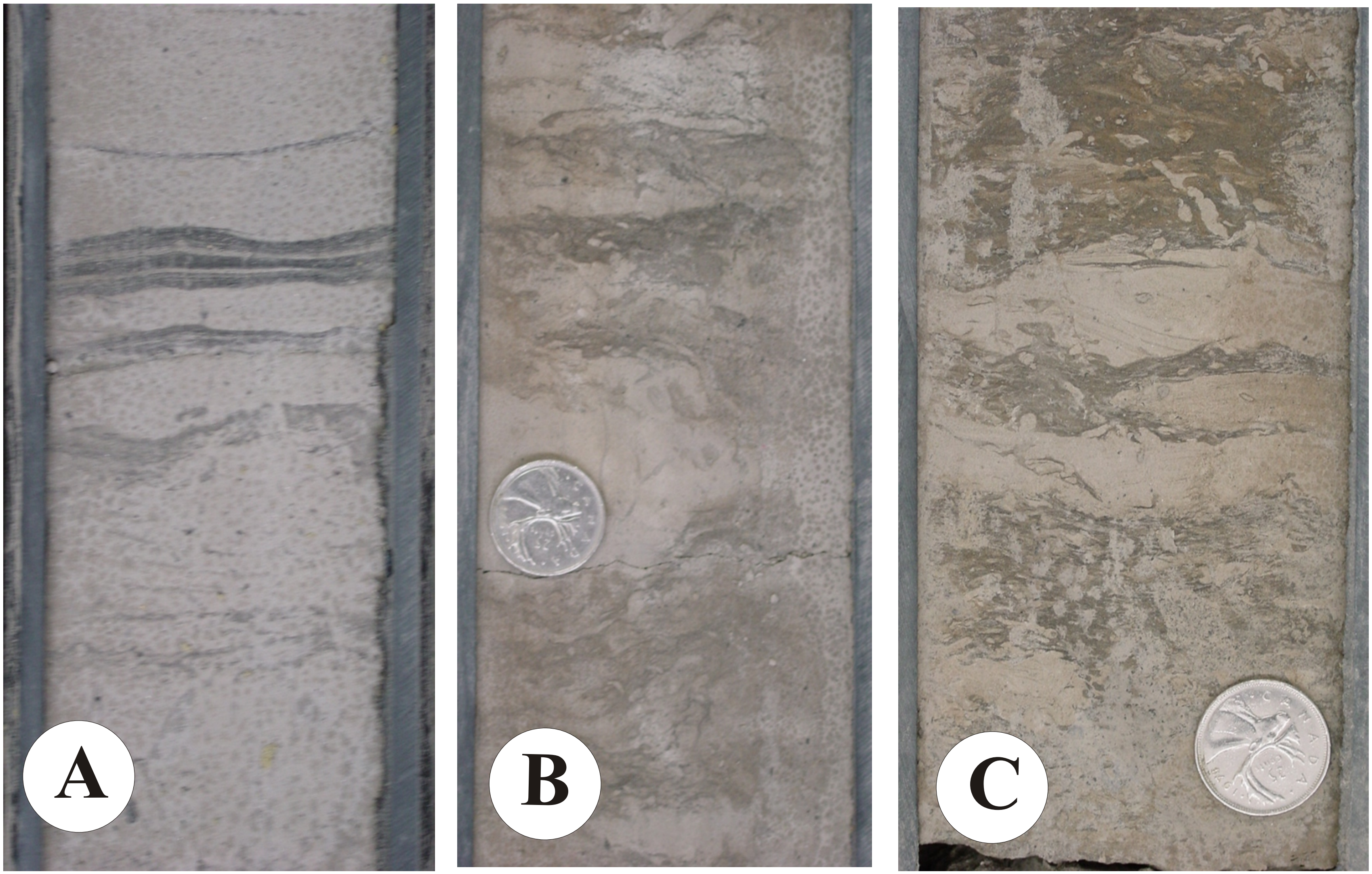

PLATE 101

PLATE 102

Shell Husky Paradise Valley 10-25-47-3W4
Core #11

Rex Fm. - General Petroleum Fm.

Rex Formation - General Petroleum Formation contact. Rex Formation coastal plain sediments grade into General Petroleum sandier-upwards sequence marked by General Petroleum dark marine shale (white arrow).
Rex channel sandstone is fine to medium grained, characterized by low angle cross stratification at the base, and ripple cross lamination and flaser bedding throughout. The lower part of the General Petroleum Formation seen in this core is represented by an interbedded shale and fine sandstone sequence, with wavy-, and ripple cross laminations.

PLATE 102

PLATE 103

Shell Husky Paradise Valley 10-25-47-3W4
Core #11

Rex Fm.

Close-up views of the Rex channel sandstone from previous plate (Plate 102).
A) Depth: 626.5 m.
B) Depth: 625.4 m.
C) Depth: 625.1 m.

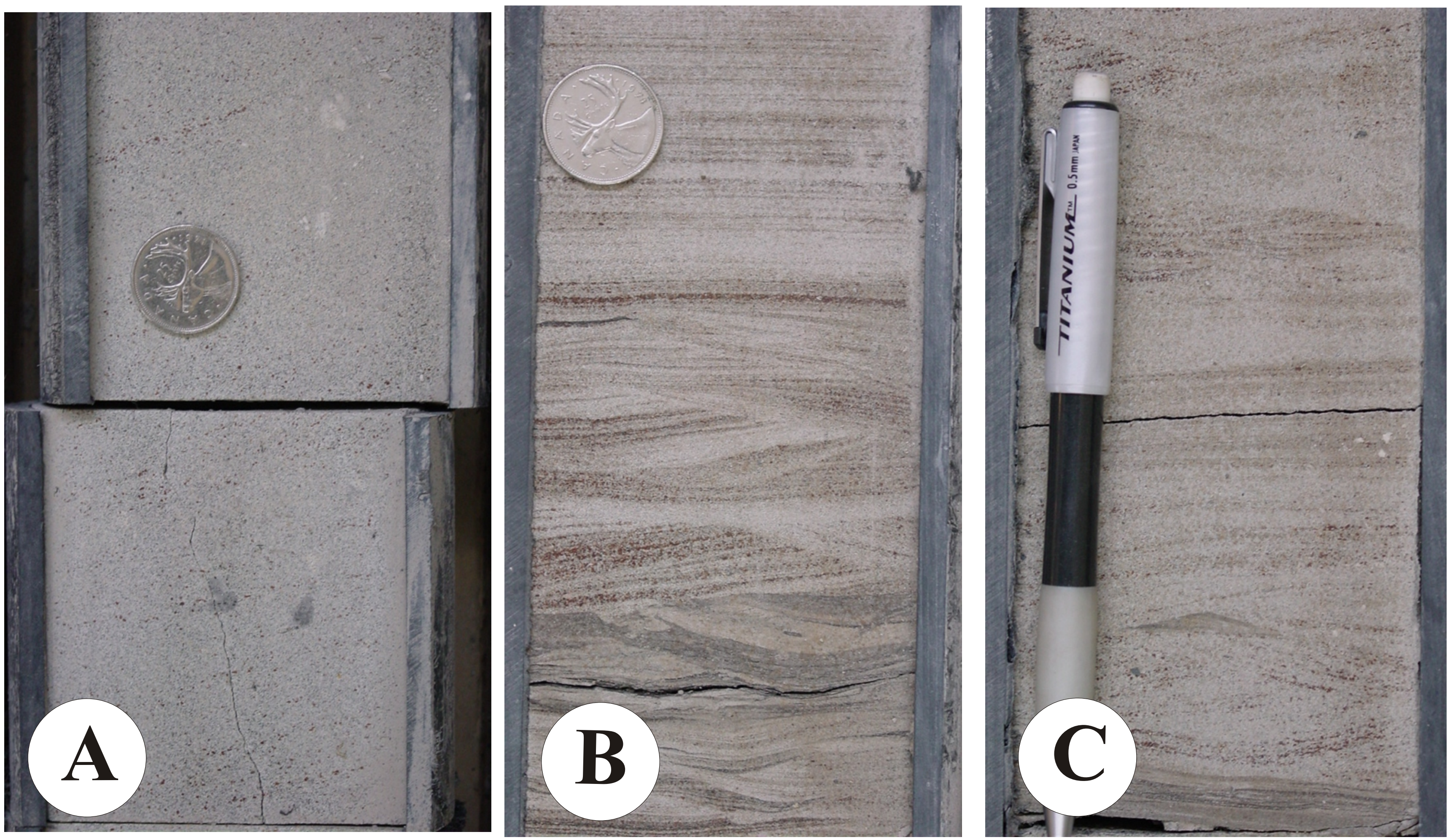

PLATE 103

PLATE 104

Shell Husky Paradise Valley 10-25-47-3W4
Core #11

General Petroleum Fm.

Close-up views of the General Petroleum Fm. from PLATE 102.
A) Depth: 621 m. Bioturbated (*Cruziana* ichnofacies) medium grained sandstone.
B) Depth: 619.2 m. Wavy laminations with mud breaks
C) Depth: 618.6 m. Dark grey shale alternating with gray sandstone exhibiting ripples.

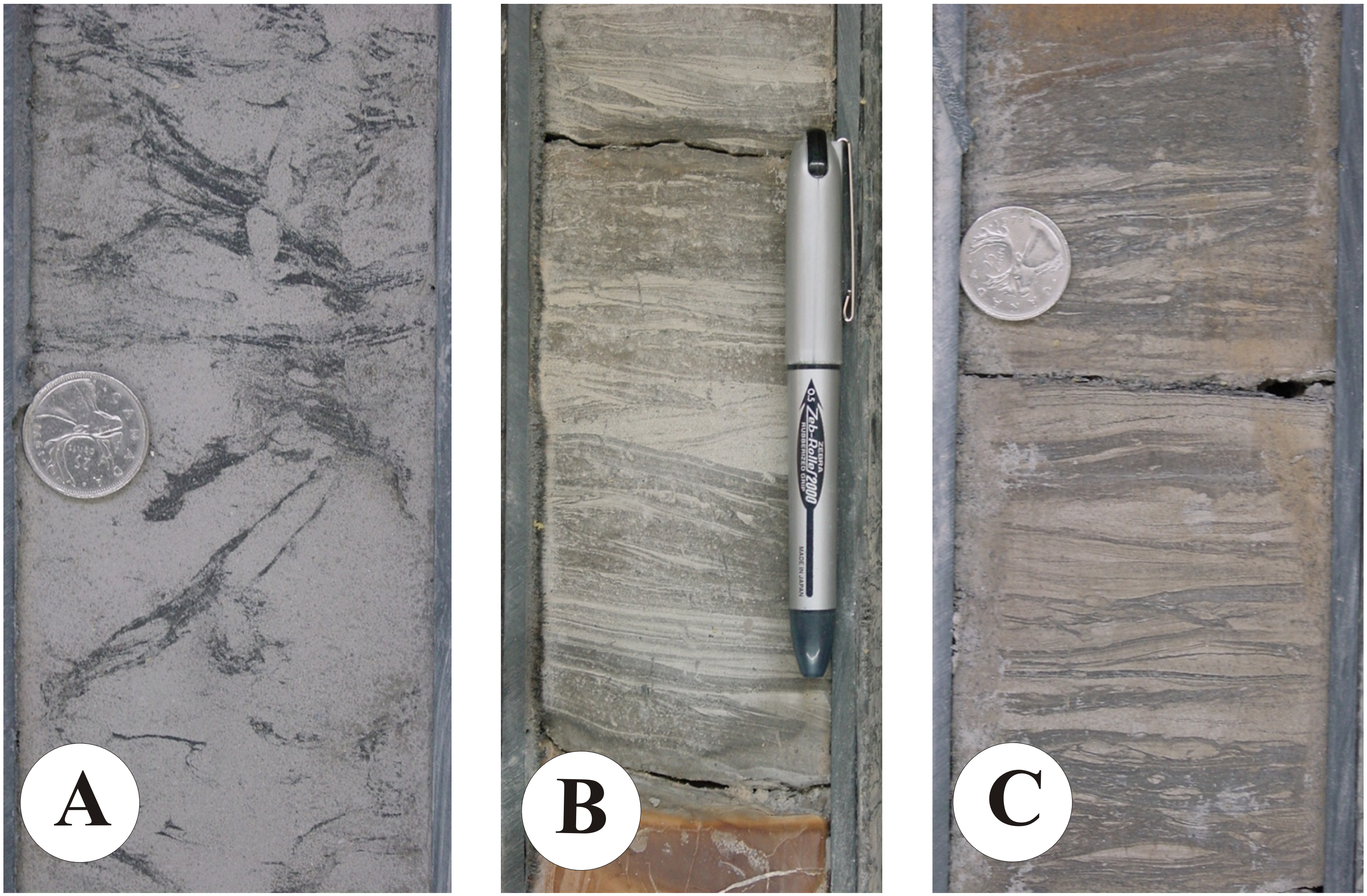

PLATE 104

PLATE 105

Shell Husky Paradise Valley 10-25-47-3W4
Core #12

Rex Fm.

Coarsening-upward sequence of the Rex Fm. cut by a channel (white arrow points to the channel base). The basal 3-4 m thick fine-grained portion is composed of dominantly dark shale interbedded with fine-to medium- grained sandstone interlaminae. Diverse bioturbation (*Teichichnus, Planolites, Cylindrichnus,* and *Asterosoma)*, along with nondescript vertical burrows is characteristic of the trace fossil assemblage within the interval.
Note: open black rectangles show the location of the close-up views presented in Plates 106 and 107.

PLATE 105

PLATE 106

Shell Husky Paradise Valley 10-25-47-3W4
Core #12

Rex Fm.

Close-up views of the lower part of the Rex Formation from previous plate (Plate 105). The basal shale dominant portion of the Rex shallowing cycle was deposited in shallow marine, probably subtidal setting with bioturbation and wave generated structures (ripple lamination and wavy bedding), being dominant. Flaser bedding has been observed as well.

A) Depth: 635.6 m.
B) Depth: 634.8 m.
C) Depth: 630.7 m.

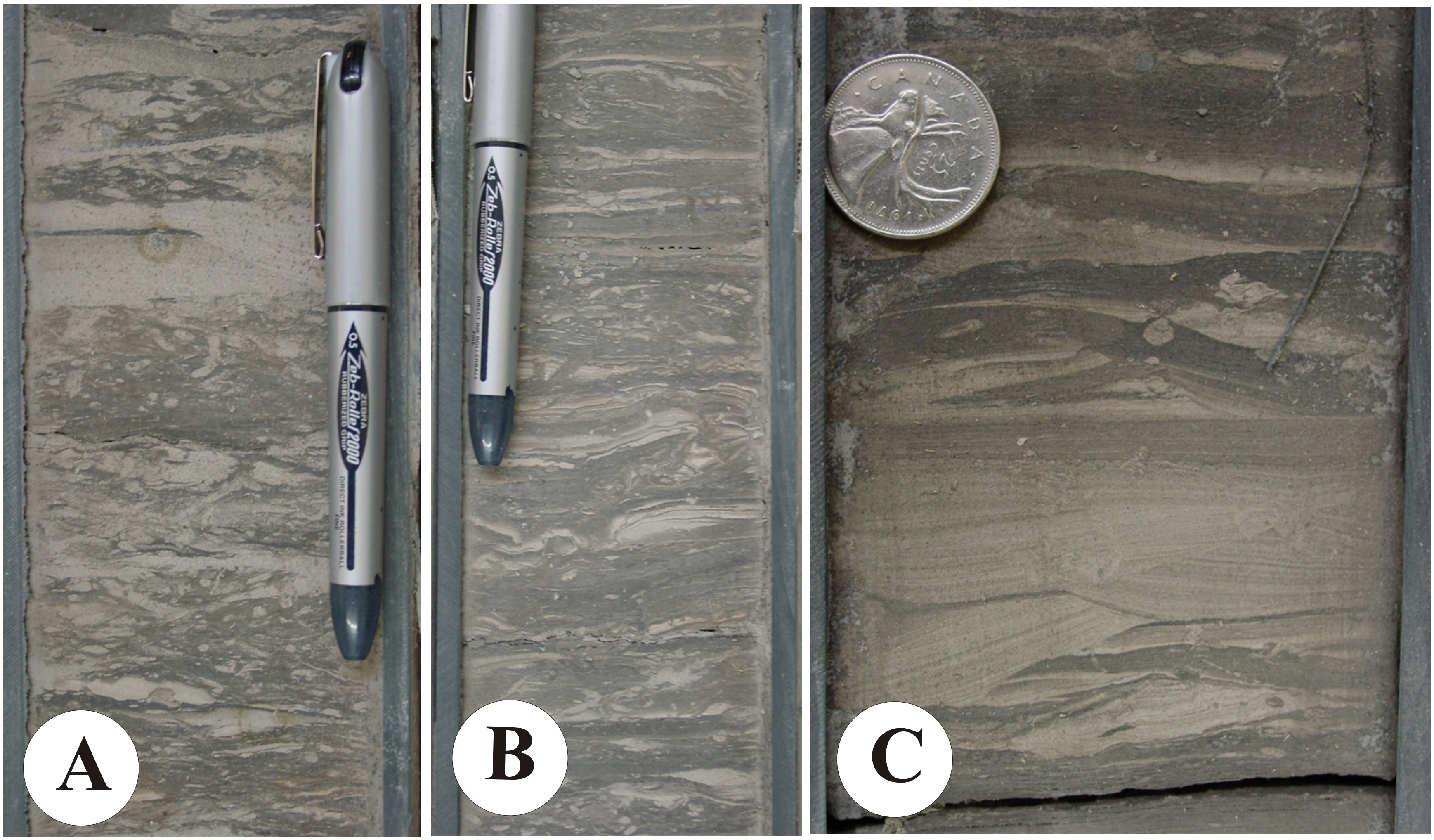
A
B
C
ZEBRA
0.5 Zeb-Roller 2000
RUBBERIZED GRIP
DIRECT INK ROLLERBALL
FINE
CANADA
25 cents

PLATE 106

PLATE 107

Shell Husky Paradise Valley 10-25-47-3W4
Core #12

Rex Fm.

Close-up views of the upper part of the Rex Formation from Plate 105.
The medium grained, massive channel sandstone (possibly estuarine) cuts into underlying shallowing upward sequence,characterized by abundant medium scale low angle cross- laminations (hummocky beds?), flaser bedding and climbing ripple laminations.
A) Depth: 630.1 m.
B) Depth: 629 m.
C) Depth: 628.6 m.

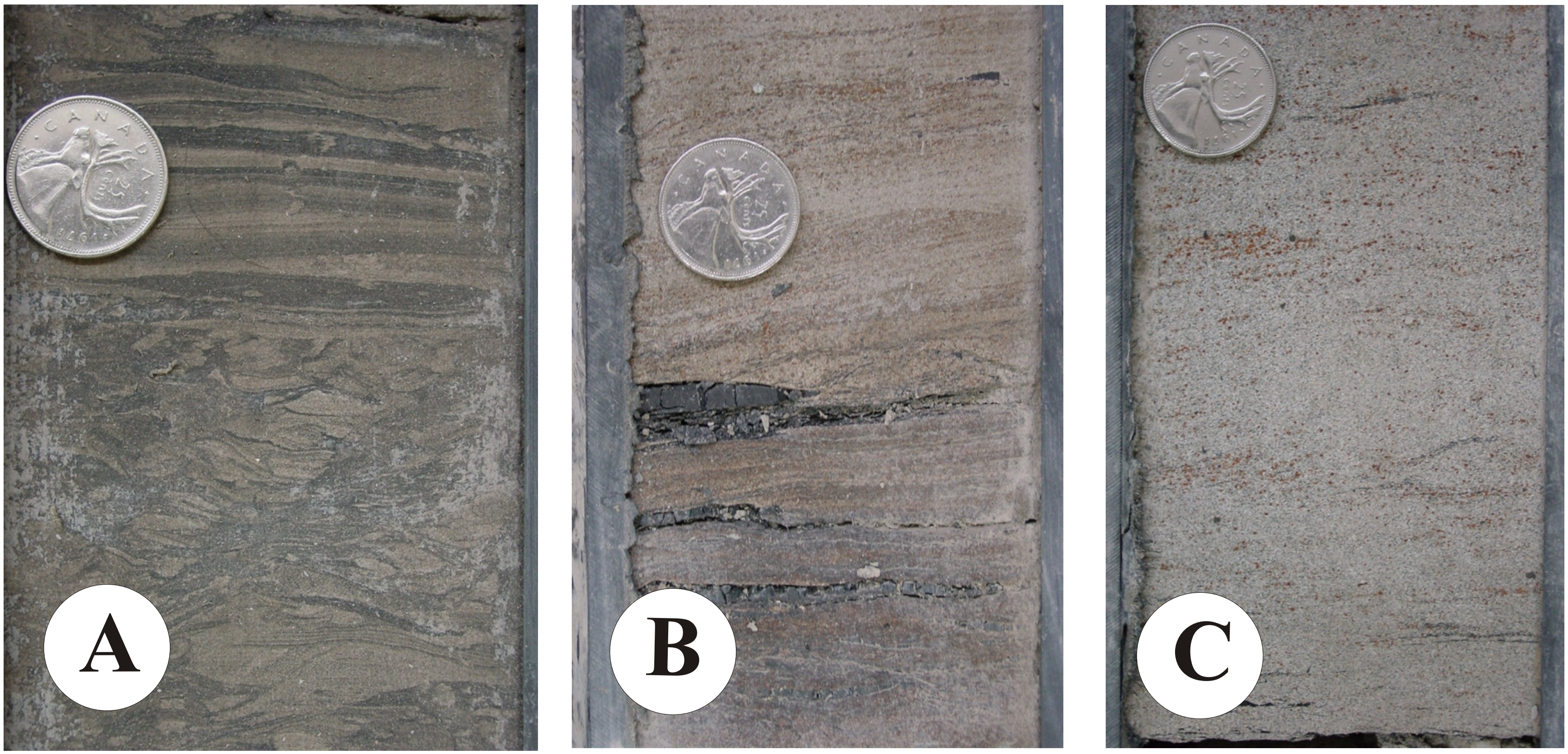

PLATE 107

PLATE 108

Shell Husky Paradise Valley 10-25-47-3W4
Core #13
636 - 645 m

Lloydminster Fm.

Progradational, lower to upper shoreface sandstone of the Lloydminster Formation, capped by coastal plain sediments (coals and fine silty shales). The uppermost quartzose sandstone is medium scale low angle cross-stratified, horizontal planar laminated to massive. Ripple cross-lamination and climbing- ripple lamination also occur. Sparse bioturbation was observed within the interval.

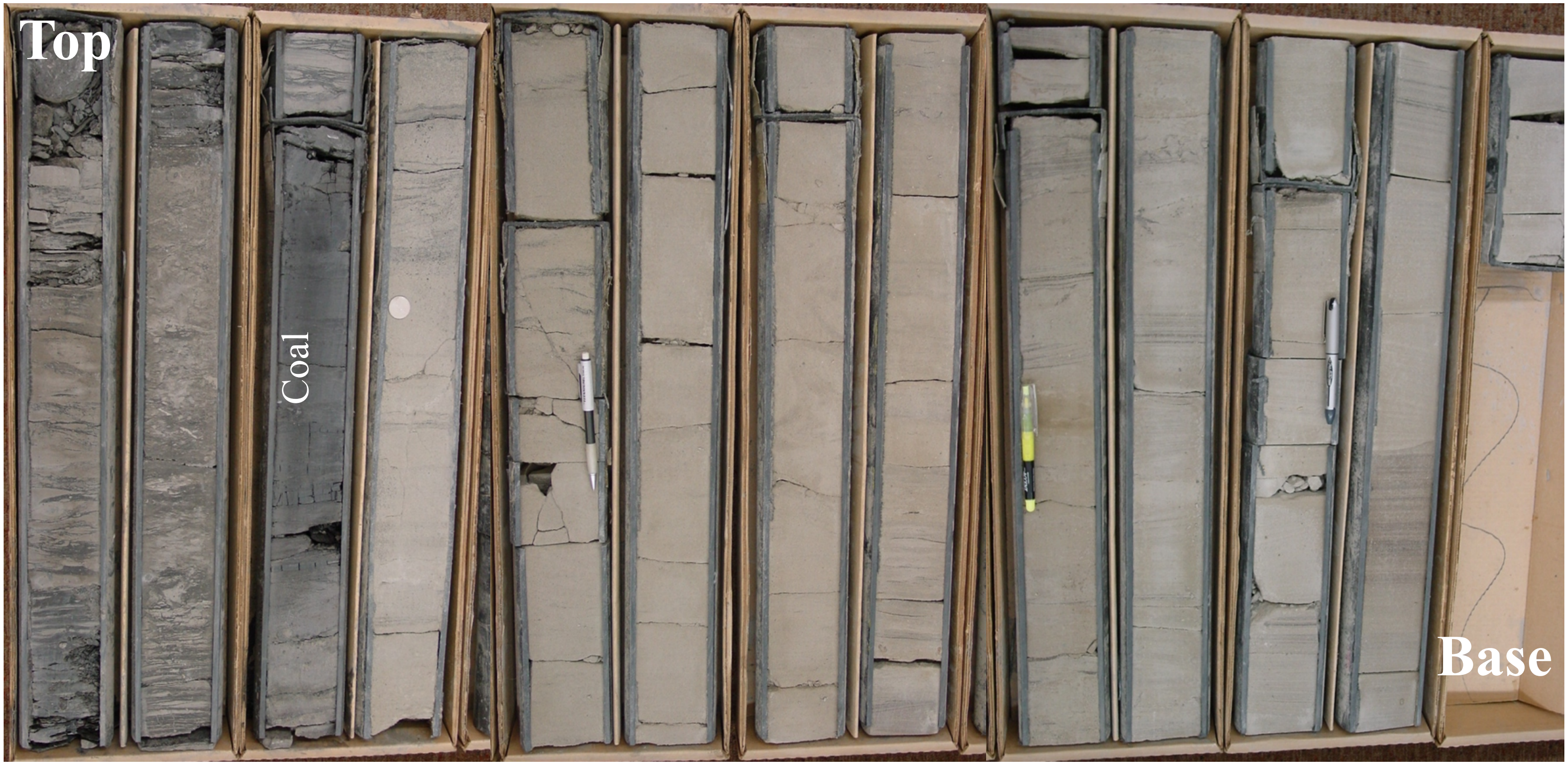

PLATE 108

PLATE 109

Shell Husky Paradise Valley 10-25-47-3W4
Core #13
636 - 645 m

Lloydminster Fm.

A) Close-up view of the upper shoreface sandstone of the Lloydminster Fm., capped by a coal seam.

B) Close-up view of the coastal plain sediments

PLATE 109

PLATE 110

Shell Husky Paradise Valley 10-25-47-3W4
Core #13
636 - 645 m

Lloydminster Fm.

Close-up view of the fine quartzose sandstone, which completes the coarsening upward sequence of the progradational shoreface of the Lloydminster Fm.

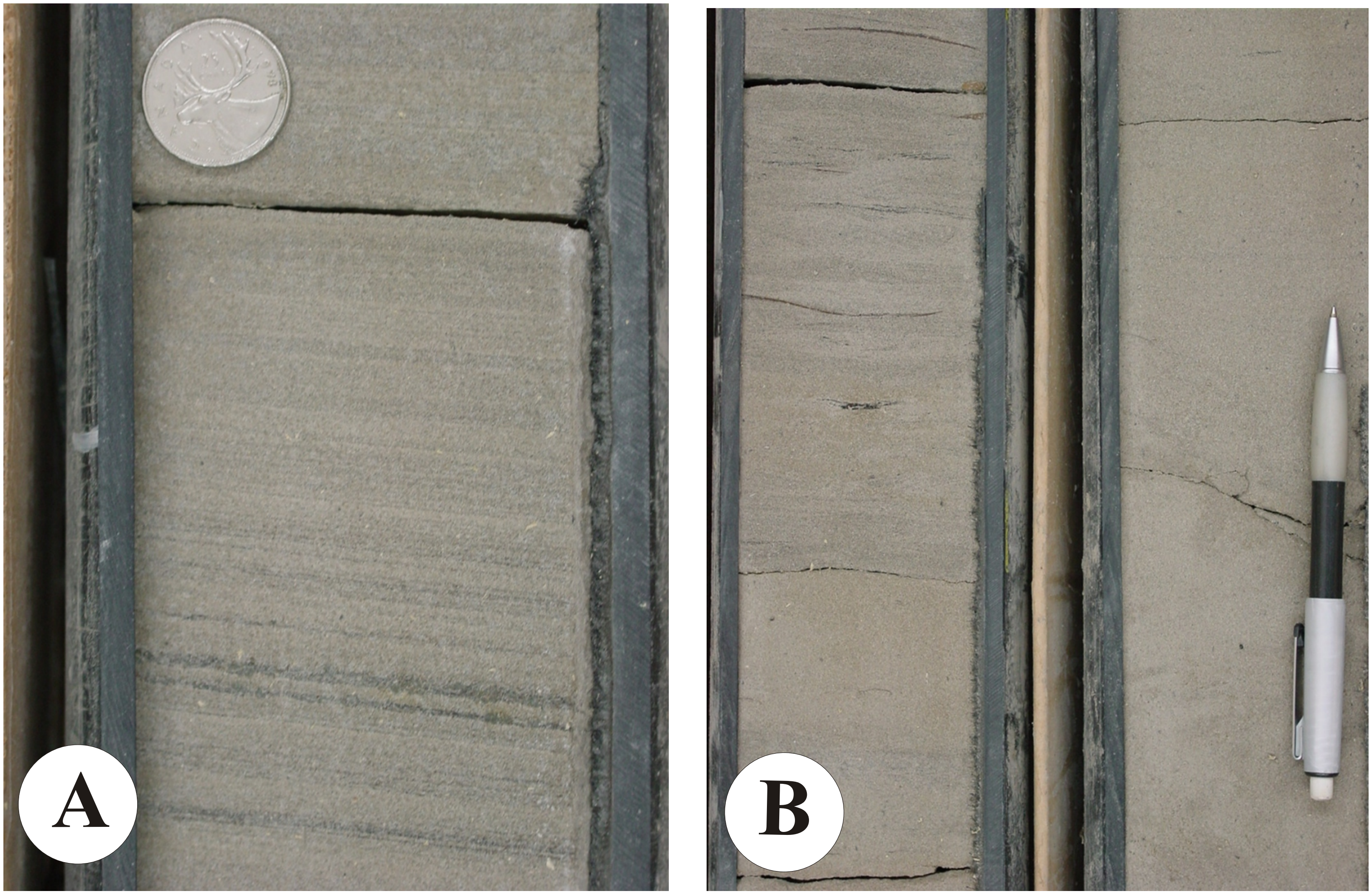

PLATE 110

PLATE 111

Shell Husky Paradise Valley 10-25-47-3W4
Core #14
645 - 654.2 m

Lloydminster Fm.

Coarsening-upward sequence of the Lloydminster Formation, from offshore marine shales through interbedded sandstones, siltstones and shales to hummocky cross-stratified sandstones.
The basal dark shale is horizontal-planar laminated with abundant ripple-laminated millimetre-scale light brown siltstone to very fine sandstone interbeds.

PLATE 111

PLATE 112

Shell Husky Paradise Valley 10-25-47-3W4
Core #14
645 - 654.2 m

Lloydminster Fm.

A) Close-up view of the laterally persistent dark shale of the Lloydminster Formation.

B) Lower offshore facies association of the Lloydminster Formation: interbedded sandstones, siltstones and shales.

C) Upper offshore facies association of the Lloydminster Formation: interbeded sandstones, siltstones and shales. Sandstones are sharp based, very fine to fine grained, with flat parallel lamination, wavy parallel lamination, and hummocky cross-stratification.

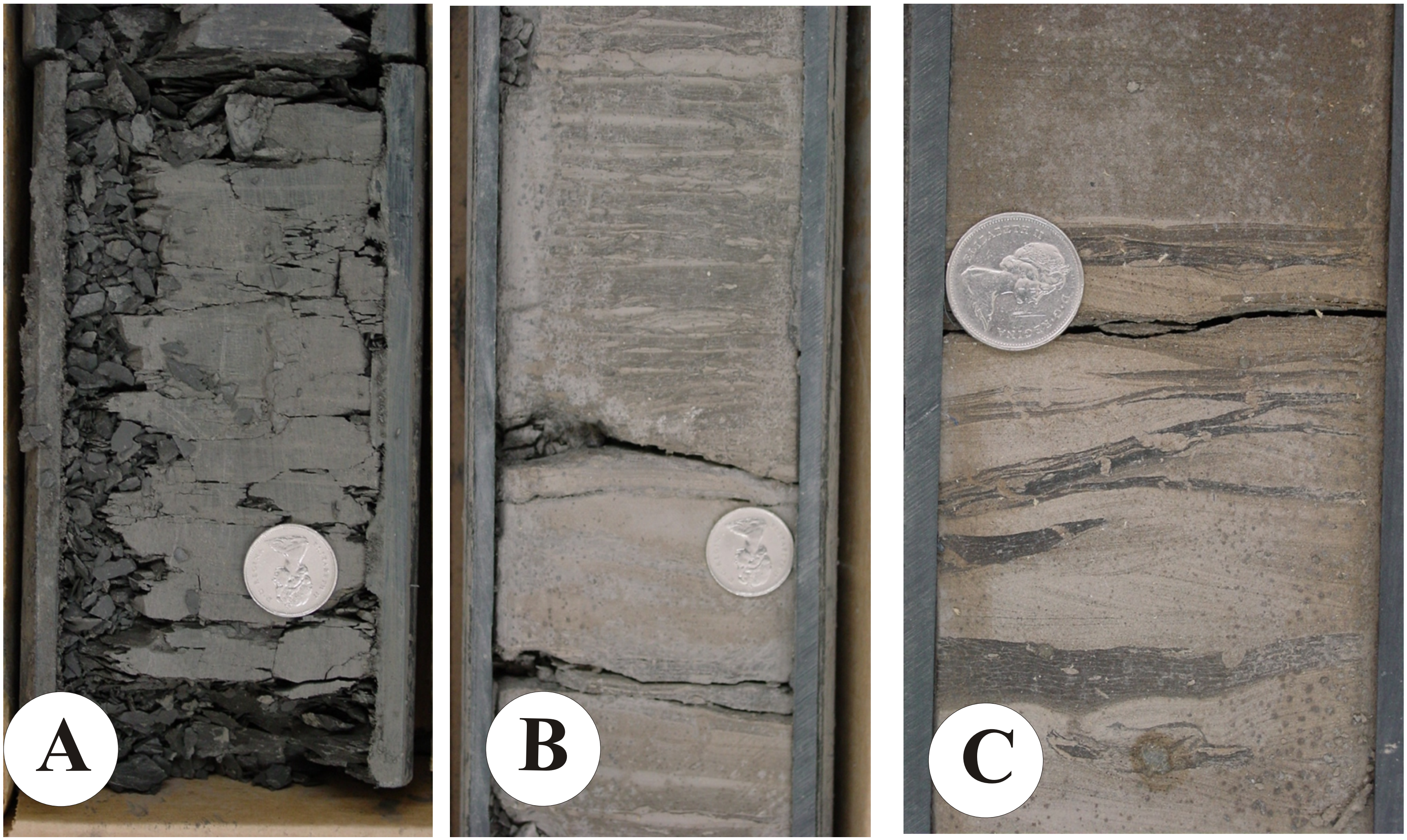

PLATE 112

PLATE 113

Shell Husky Paradise Valley 10-25-47-3W4
Core #14
645 - 654.2 m

Lloydminster Fm.

Close-up view of the hummocky cross-stratified sandstones of the lower shoreface of the Lloydminster Formation. The sandstones are very fine grained, moderately sorted. There is no bioturbation.
Setting: this facies was deposited in the lower shoreface of a progradational shoreline dominated by waveprocesses. The absence of bioturbation implies very high sedimentation rates and/or very high energy conditions.

PLATE 113

PLATE 114

Shell Husky Paradise Valley 10-25-47-3W4
Core #15
645 - 654.2m

Cummings Fm.

8 m succession of interbedded, sandstones and shales and coal present in an overall fining-upwards sequence. Wavy ripple laminations to lenticular bedding and flaser bedding characterize the interbedded sequence. Moderate amounts of horizontal burrowing can be observed.
Setting: coastal plain sediments grading to shallow marine (tidal influence).

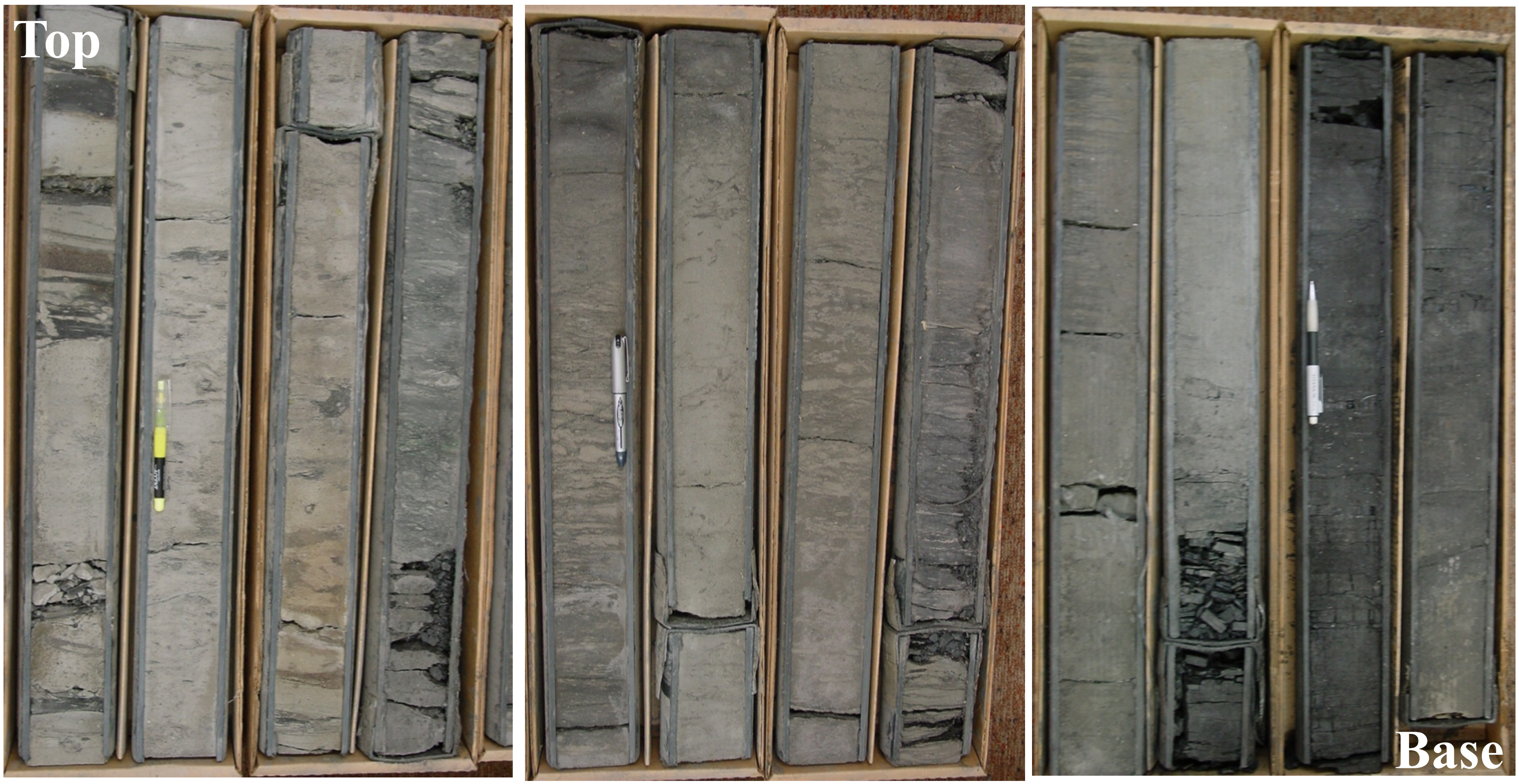

PLATE 114

PLATE 115

Shell Husky Paradise Valley 10-25-47-3W4
Core #16
663 - 672m

Cummings Fm.

Sandier -upward sequence of the Cummings Formation, consisting mostly of a sandy interval made up of well sorted subrounded lithic-quartzose sandstone. The sandstone laminae are ripple laminated, flaser bedded with an overall wavy character to the beds.
Setting: progradational marine shoreface sandstone.
Note: open black rectangles show the location of the close-ups presented in Plate 116.

PLATE 115

PLATE 116

Shell Husky Paradise Valley 10-25-47-3W4
Core #16
663 - 672m

Cummings Fm.

Close-up views from previous plate (Plate 115):

A) Contact between a fine grained shallow marine sandstone and shales above.

B) Apparently massive fine grained sandstone.

C) Remnants of stacked, wavy parallel laminated sandstone, sedimentary structures being obliterated by bioturbation.

D) Massive, blocky sandstone

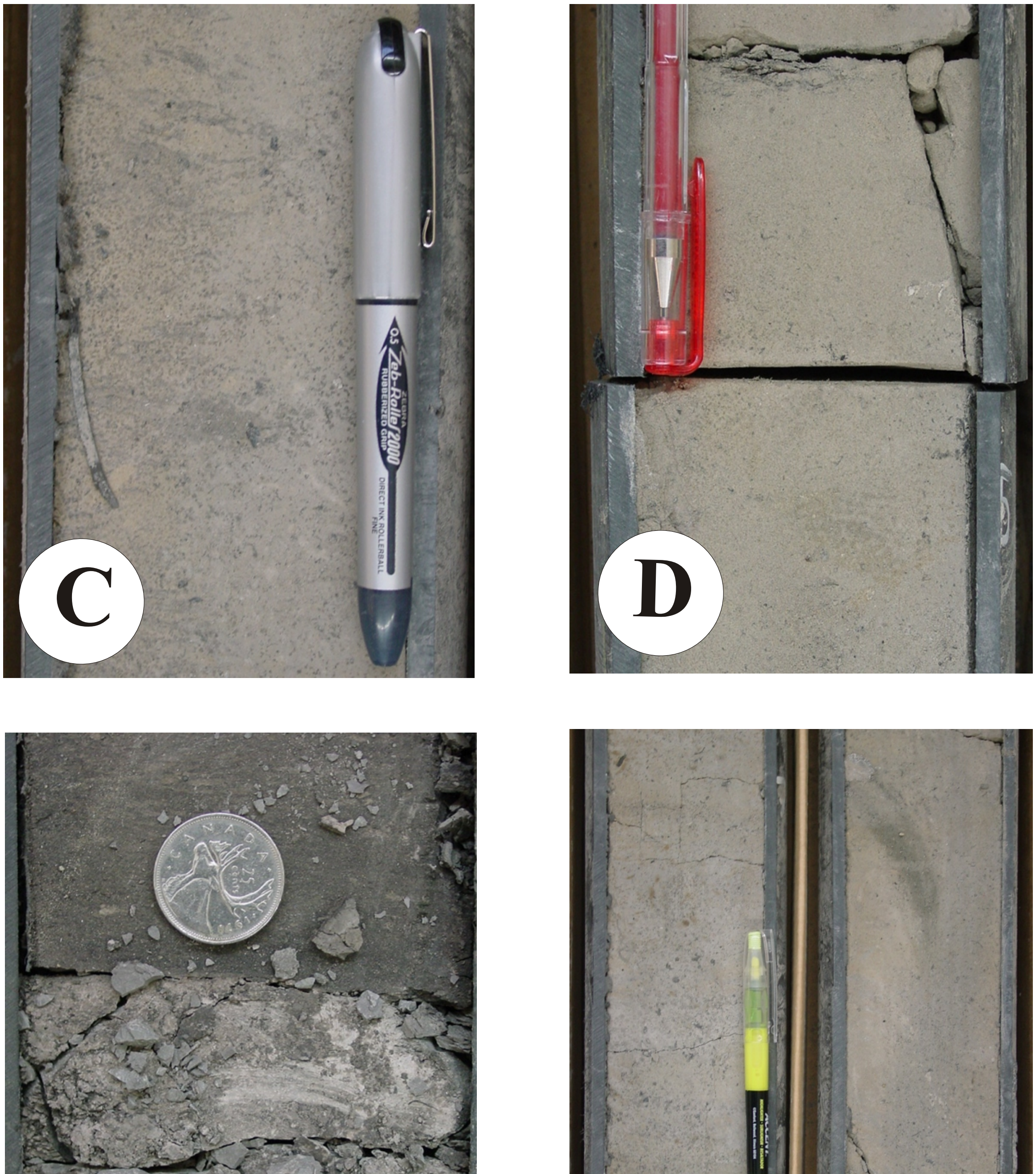
C
D
A
B
Zeb-Roller 2000
RUBBERIZED GRIP
DIRECT INK ROLLERBALL
FINE
CANADA

PLATE 116

PLATE 117

Shell Husky Paradise Valley 10-25-47-3W4
Core #17
672 - 681m

Cummings Fm.

Coastal plain to shoreface sediments of the Cummings Formation: transition from the thick coal, capping the underlying progradational sequence, to interbedded siltstones and fine grained sandstones. Initial evidence of bioturbation within the Lower Cretaceous section is present at this stratigraphic level, coincident with the change from Dina sandstone to interbedded sandstone and shale. The low abundance, low-diversity ichnological suite is characterized by nondescript horizontal burrowers.

PLATE 117

PLATE 118

Shell Husky Paradise Valley 10-25-47-3W4
Core #17
672 - 681m

Cummings Fm.

Coastal plain sediments of the Cummings Formation:

A) Lenticular bedded, and ripple cross-laminated fine sandstones interbedded with shales. Sideritized beds are present (white arrow).

B) Intensely bioturbated, massive to lenticular bedded sandstones and shales.

PLATE 118

PLATE 119

Shell Husky Paradise Valley 10-25-47-3W4
Core #18
681 - 690m

Dina - Cummings Fm.

Gradational transition from the basal Dina sandstone to the overlying interval of shales and interbedded sandstones and shale beds. The shales are massive to horizontal laminated and gray-brown in colour with scattered organic detritus and pyrite where the massive sandstone grades up into interbedded sandstone and mudstone. The interbedded interval contains wavy, lenticular flaser bedding and ripple cross- lamination. Abundant organic laminae and rootlets are present locally.
Note: open black rectangles show the location of the close-ups from Plate 120.

PLATE 119

PLATE 120

Shell Husky Paradise Valley 10-25-47-3W4
Core #18
681 - 690m

Dina - Cummings Fm.

A) Ripple cross-laminated fluvial channel sandstone.
Depth: 689 m.

B) Dark gray to blak mudstones and silty mudstones.
Depth: 682.7 m.

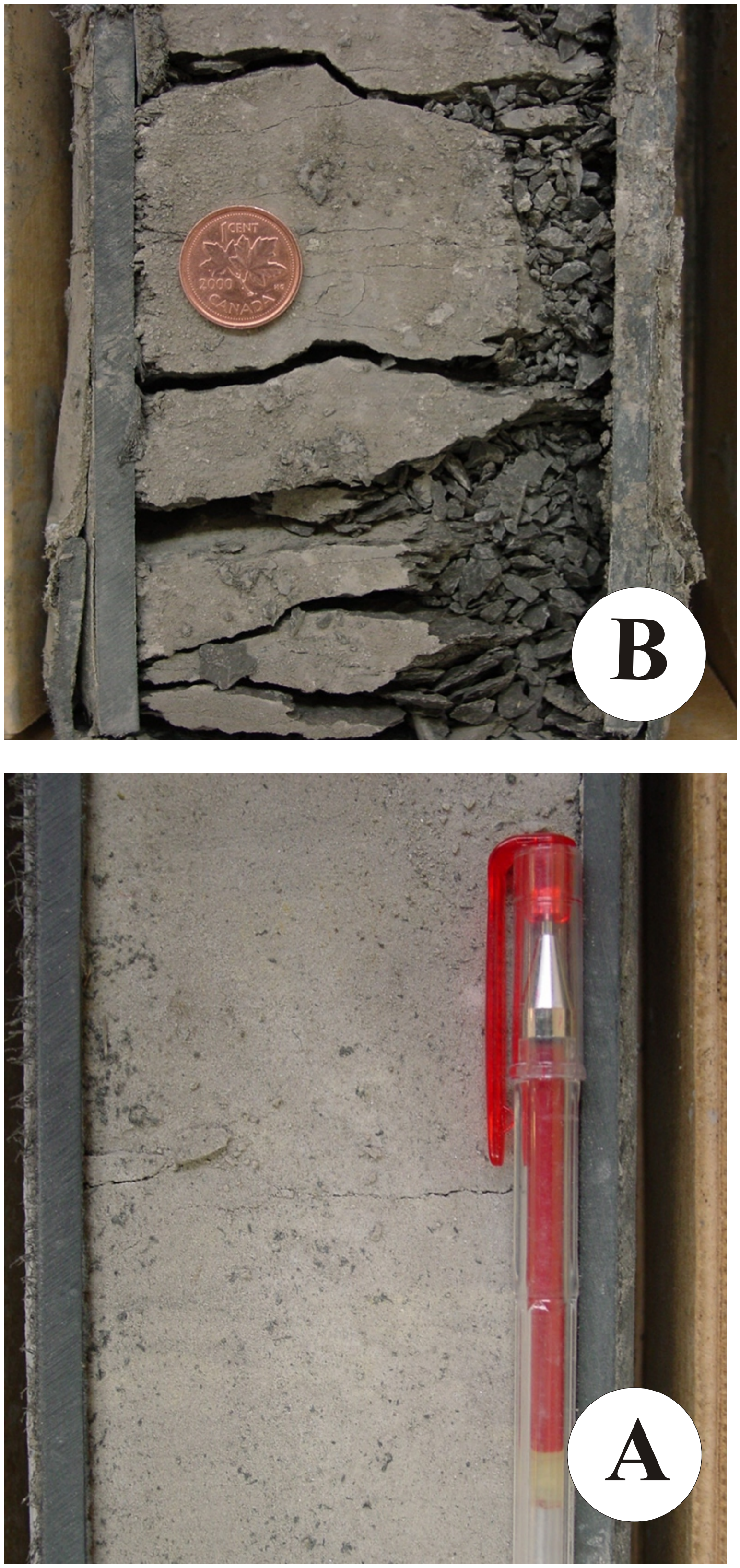

PLATE 120

PLATE 121

Shell Husky Paradise Valley 10-25-47-3W4
Core #19
690 - 670m

Shallow marine (tidal) sediments of the Dina Formation, capped by the massive, fining upward, fluvial Dina sandstone. The sandstone is part of a larger-scale overall fining-upward sequence into the overlying shally interval. This sequence is represented by both core #18 and core #19.
Note: open black rectangles show the location of the close-ups presented in Plate 122.

PLATE1 121

PLATE 122

Shell Husky Paradise Valley 10-25-47-3W4
Core #19
690 - 670m

Dina - Cummings formations

A) Wavy cross-laminated sandstone of the basal Dina Fm.
Depth: 699.4 m.

B) Close-up view of the fluvial channel Dina sandstone: medium-grained, with large scale trough cross-lamination.
Depth: 690 m.

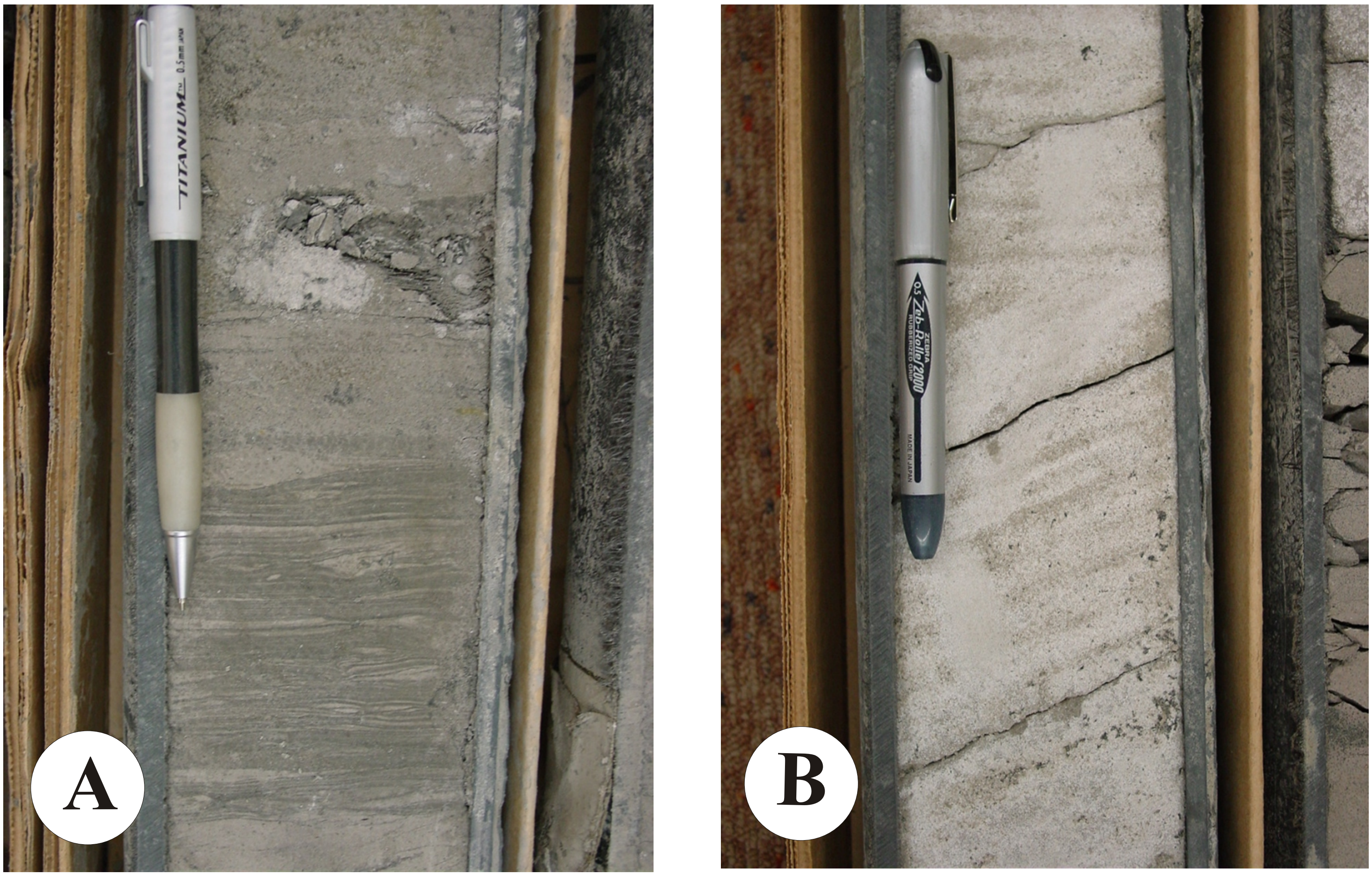

PLATE 122

University of Alberta

MUDGASES GEOCHEMISTRY AND FACTORS CONTROLLING THEIR VARIABILITY

APPENDIX B

by

DANIELA VLAD

A thesis submitted to the Faculty of Graduate Studies and Research
in partial fulfillment of the requirements for the degree of

Doctor of Philosophy

Department of Earth and Atmospheric Sciences

Spring 2010
Edmonton, Alberta

Appendix B

Well log cross-sections and Composite diagrams

Page

Appendix I

I-1 Along-dip regional well-log cross-section – Foothills region: Section 1-1' ……… 735

I-2 Along-strike regional well-log cross-section – Foothills region: Section 2-2' …......736

I-3 Along-dip regional well-log cross-section – Foothills region: Section 3-3' ……… 737

I-4 Along-dip regional well-log cross-section – Foothills region: Section 4-4' ……… 738

I-5 Along-strike regional well-log cross-section – Foothills region: Section 5-5' ….... 739

Appendix II

II-1 Along-dip regional well-log cross-section – Lloydminster region: Section 1-1' 740

II-2 Along-dip regional well-log cross-section – Lloydminster region: Section 2-2' …741

II-3 Along-dip regional well-log cross-section – Lloydminster region: Section 3-3' …742

II-4 Along-dip regional well-log cross-section – Lloydminster region: Section 4-4' …743

II-5 Along-strike regional well-log cross-section
- Lloydminster region: Section 5-5' ………………………………………..……....744

II-6 Along-strike regional well-log cross-section
- Lloydminster region: Section 6-6' ……………………………………..…………745

II-7 Along-strike regional well-log cross-section
- Lloydminster region: Section 7-7' ……………………..……………………...… 746

II-8 Along-strike regional well-log cross-section
- Lloydminster region: Section 8-8' ………………………… …………………... 747

Appendix III

III-1 Composite diagram showing the compositional profile for Ferrier 14-3-42-9W5 together with data that result from the isotope ratio mass spectrometry …………………………………………………………………………...….748

III-2 Composite diagram showing the compositional profile for Gilby 15-16-42-4W5 together with data that result from the isotope ratio mass spectrometry …………………………………………………………………………….….. 749

III-3 Composite diagram showing the compositional profile for Pembina
11-4-49-11W5 accompanied by data that result from the isotope ratio mass
spectrometry ………………………………………………………………………………750

III--4 Composite diagram showing the compositional profile for Lindbergh
4C-16/13-09-56-6W4 together with data that result from the isotope ratio mass
spectrometry ………………………………………………………………………………751

III-5 Composite diagram showing the compositional profile for Petrovera
1D-25-55-5W4 together with data that result from the isotope ratio mass
spectrometry ………………………………………………………………………………752

III-6 Composite diagram showing the compositional profile for Husky
C3-30-47-4W4 together with data that result from the isotope ratio mass
spectrometry ……………………………………………..………….……….753

III-7 Composite diagram showing the compositional profile for Husky
A9-15-51-23W5 together with data that result from the isotope ratio mass
spectrometry …………………………………………………….…….………..754

ALONG -DIP REGIONAL WELL-LOG CROSS - SECTION - Foothills region

Appendix I-1
Section 1 - 1'

Appendix I-2

Section 2 -2'

ALONG - DIP REGIONAL WELL-LOG CROSS-SECTION - Foothills region

Appendix I-3

Section 3 -3'

Appendix I-4
Section 4 -4’

SW ALONG - DIP REGIONAL WELL-LOG CROSS - SECTION - Foothills region NE

Appendix I-5

Section 5- 5'

ALONG - STRIKE REGIONAL WELL-LOG CROSS - SECTION: PEMBINA - FERRIER (Foothills region)

Along dip well log cross section - *Lloydminster region*

Appendix II-2
Section 2 - 2'

Along dip well-log cross-section - *Lloydminster region*

Along dip well-log cross-section - *Lloydminster region*

Appendix II-3
Section 3 - 3'

Along dip well-log cross-section - *Lloydminster region*

Along strike well log cross-section - *Lloydminster region*

5 (N) 5' (S)

Along strike cross-section - *Lloydminster region*

Along strike well-log cross-section - *Lloydminster region*

Along strike cross-section - *Lloydminster region*

Appendix II-8
Section 8 - 8'

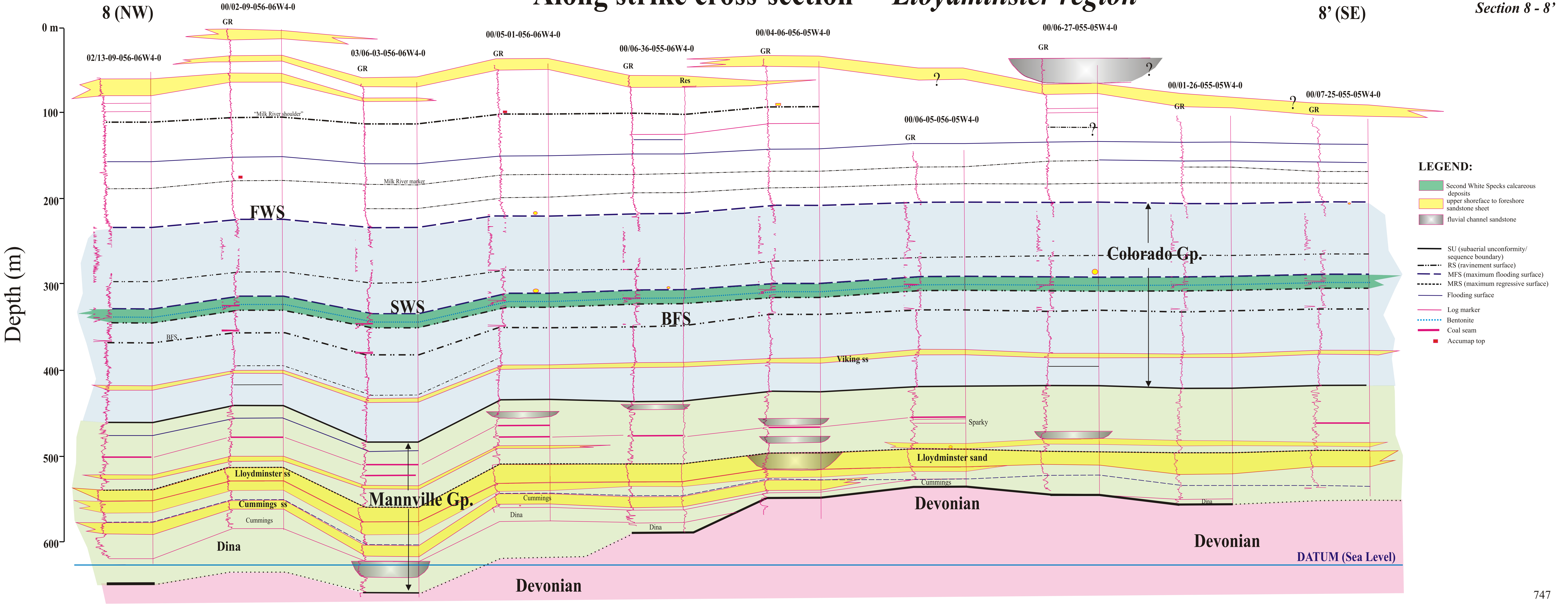

Composite diagram showing the compositional profile for Ferrier 14-3-42-9W5 together with data that result from the isotope ratio mass spectrometry.

Gilby 15-16-42-4W5

Composite diagram showing the compositional profile for Gilby 15-16-42-4W5 together with data that result from the isotope ratio mass spectrometry.

Pembina 11-4-49-11W5

Composite diagram showing the compositional profile for Pembina 11-4-49-11W5 accompanied by data that result from the isotope ratio mass spectrometry.

Ranger/Murphy Lindbergh 4C-16/13-09-56-6W4

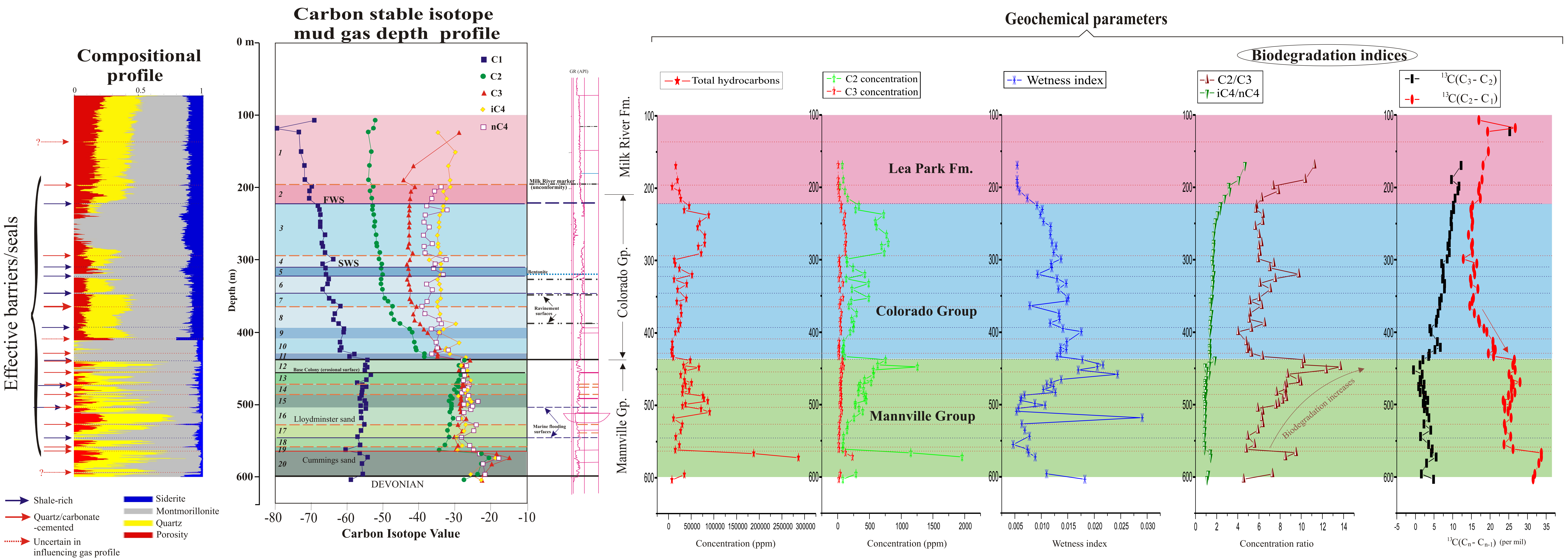

Composite diagram showing the compositional profile for Lindbergh 4C-16/13-09-56-6W4 together with data that result from the isotope ratio mass spectrometry.

Composite diagram showing the compositional profile for Petrovera 1D-25-55-5W4 together with data that result from the isotope ratio mass spectrometry.

Husky C3-30-47-4W4

Composite diagram showing the compositional profile for Husky C3-30-47-4W4 together with data that result from the isotope ratio mass spectrometry.

Composite diagram showing the compositional profile for Husky A9-15-51-23W3 together with data that result from the isotope ratio mass spectrometry.